

Bangor University

DOCTOR OF PHILOSOPHY

Novel Isoforms and Functions of the *S.pombe* Rad9 Checkpoint Protein

Janes, Simon

Award date:
2012

Awarding institution:
Bangor University

[Link to publication](#)

General rights

Copyright and moral rights for the publications made accessible in the public portal are retained by the authors and/or other copyright owners and it is a condition of accessing publications that users recognise and abide by the legal requirements associated with these rights.

- Users may download and print one copy of any publication from the public portal for the purpose of private study or research.
- You may not further distribute the material or use it for any profit-making activity or commercial gain
- You may freely distribute the URL identifying the publication in the public portal ?

Take down policy

If you believe that this document breaches copyright please contact us providing details, and we will remove access to the work immediately and investigate your claim.

Download date: 02. Apr. 2025



DISEASE AND DEVELOPMENT RESEARCH CLUSTER

GENOME BIOLOGY RESEARCH GROUP

"Novel Isoforms & Functions of the S. pombe Rad9 Checkpoint Protein"

Cell Cycle Regulation & DNA Repair Research Team

In Association With and Sponsored By
Cancer Research Wales



By
Simon Janes

ACKNOWLEDGEMENTS

My sincerest thanks and gratitude are extended to my principal Ph.D. supervisor and mentor Dr. Thomas Caspari – whom I also continue to hold in the utmost highest regard as a true friend and colleague, for his inspirational enthusiasm, support and advice on the progressive development of a challenging project with versatile scope and exciting future potential as a novel investigative field in the context of cancer research.

I am also indebted to the Cancer Research Wales charity organisation for the generous provision of essential sponsorship finance to adequately cover the incurred laboratory, academic and living expenditure – without which engagement in this Ph.D. project would have proven to be an impossible undertaking.

Many thanks are also extended to key research staff members Dr. Edgar Hartsuiker, Dr. David Pryce, Dr. Mikhaleva-Harrison and Prof. Simon Webster for their invaluable advice, assistance and critical input on particular practical aspects of the research and I would also like to express my thanks and gratitude to Dr. Adam T. Watson (based at the Genome Damage and Stability Research Centre, School of Life Sciences, University of Sussex) for the generous donation of the unmodified/”empty” pAW1 and pAW8 plasmids utilised in the Cre-RMCE transformation system for the preparation of the necessary experimental *S. pombe* strains constructed in this research study.

My appreciative thanks are also extended to a key group of supportive undergraduate and postgraduate personnel – BSc. (Hons) project students, MSc. project students, Ph.D. project students and research placement experience trainees, jointly supervised by Thomas and myself, for their collaborative efforts on essential “detailed follow-up” work on specific diverse facets of the research into novel Rad9 protein functions – namely; Mr Mohamed Abeda, Mr. Mustafa Al-Belazi, Mrs Muneera Alghannami, Mrs Besma Jasmin Al-Kinani, Ms. Susanna Concilio, Ms. Susan Davies, Mr. Karim Garrido, Ms. Maria Hauswald, Ms. Anna Isermann, Mr. Dylan Jones, Ms. Simrath Karwal, Mrs Widad Mansour, Ms. Amber Maltby, Mr. Herbert Mtetwa, Ms. Nadja Ney, Mr. Rabiaa Oun, Ms. Ulrike Schmidt and Mr. H.M. Syfuddin.

In addition, I would also like to thank Prof. Wolfgang Wuster in his supportive role as the designated Senior Postgraduate Tutor and Ph.D. Student Assessment Co-Ordinator, along with Prof. Deri Tomos, Dr. Anil Shirshat for taking on the extra responsibilities and incurred workload duties in the respective roles of Chairperson, Independent Internal Assessor within the serving capacity of my Ph.D. Supervisory and Assessment Committee.

I would also like to express my sincere gratitude to Dr. Felicity Watts, (based at the Genome Damage and Stability Research Centre, School of Life Sciences, University of Sussex) for taking on the incurred workload and responsibilities in the respective role of external examiner.

Appreciative thanks are also extended to the Pro Vice Chancellor Prof. Colin Baker for his friendly patient advice, support and understanding with regard to my extenuating personal difficulties/circumstances incurred whilst in the critical final stages of the Ph.D. thesis preparation and submission.

My appreciative thanks and gratitude are also conveyed to the concerted daily efforts of the administrative and technical support staff which facilitated key aspects my Ph.D. research studies with regard to provision of information on progressive assessment report submissions, meetings and seminars, ordering of reagents/equipment, conference accommodation booking arrangements and “in- house” maintenance/repair of vital laboratory equipment – namely; Dr. Pat Gadstone, Mrs Karen Goodwin, Mrs Gemma Jones, Ms. Debbie Henderson, Mr. Alan Jones, Mrs Tracey Johnstone, Ms. Denice McKibbin, Mr. Emlyn Roberts, Mrs Jane Smith, Mrs Louise Thurlow and Mrs Sally Wells.

I would also like to express my sincere appreciation and gratitude for the overwhelming encouragement, sustained patience and unwavering support of a multitude of family members and friends over the past four years, all of whom have seen me through some particularly difficult times – notably; my parents Mr Peter Janes and Mrs June Janes, my sister Ms. Caroline Janes, Ms. Alex Aiken, Ms. Katherine Burnup, Ms. Susan Davies, Ms. Clary Dewing, Mr Li Fan, Mr. Ron Greeff, Ms. Jackie Griffiths, Ms. Catherine Elaine Jones, Mrs Marion Norbury, Mr. Tom O’Donoghue, Ms. Tracy Perkins, Mr. Darren Rowlands, Mr. David Rowlands, Ms. Rebecca Tennant, Mr. Dave Smith, Mr. Mark Smith, Ms. Rebecca Williams and last, but by no means least, Dr. Ian Wilson, Mrs Carole Wilson, Ms. Lisa Wilson and the late Mr. Lewis Wilson (along with many others too numerous to list by name).

Finally, I wish to dedicate this Ph.D. thesis to past, present and future cancer patients and their families worldwide (including personal family members and friends), in the sincere hope that progressive continuation of the research may culminate in the potential development of novel chemotherapeutic strategies which will contribute significantly to the clinical management and treatment of this complex and debilitating range of diseases that claim so many lives each year.

ABSTRACT

Cancer is of paramount medical concern as an increasingly major contributor of disease-related fatalities of significant prevalence – particularly in the context of current statistical/stochastic epidemiological studies which predict that one in three people will contract cancer at some stage of their lives, whilst one in four of these patients will die as a consequence of their particular neoplastic-associated condition.

The human Rad9 protein exists in two full-length isoforms (termed Rad9A and Rad9B) whose respective differentially-elevated levels and related expression profiles are distinctive for specific tumour cell tissue types.

Most known functions of the DNA damage response protein Rad9 are executed via the well-characterised Rad9-Rad1-Hus1 (“9-1-1”) protein complex, which is loaded onto chromatin in close vicinity to DNA lesion sites.

The chromatin-loaded “9-1-1” complex functions as both a DNA damage “sliding-clamp” sensor and a recruitment platform which modulates and co-ordinates the activities of a wide variety of different proteins implicated in cell cycle checkpoint signalling, steroidal nuclear receptor signalling, protein chaperoning and DNA repair – via associative protein-protein interactions with the C-terminal tail domain of the Rad9 sub-unit.

This toroidal, heterotrimeric “9-1-1” DNA sliding-clamp complex is highly conserved and its recently resolved crystal structure shows a functional similarity to the homotrimeric PCNA DNA sliding-clamp complex.

Associative ring formation amongst the individual Rad9, Rad1 and Hus1 sub-units is limited, via stringent steric and thermodynamic parameters, to the heterotrimeric type “9-1-1” DNA sliding-clamp complex configuration.

Recent clinical data strongly indicate that over-expression of Rad9, but not Hus1 or Rad1, also promotes tumour growth.

Aside from the well-documented phenomena of the modulation of apoptotic signalling and pyrimidine nucleobase biosynthesis activities, comparatively little is known about the “9-1-1” complex-independent functions of the human Rad9 protein – whose dysfunctional activities may be implicated in the development and progression of carcinogenesis.

The initial research emphasis of this Ph.D. project was focused on the elucidation on the mechanism of expression and potential functional roles of a novel N-Terminal truncated (“short”) variant of the Rad9 protein – termed “Rad9-S”, which is expressed in the experimental eukaryotic cell cycle model organism *Schizosaccharomyces pombe*.

Expression of relatively low levels of a constitutive form of Rad9-S were detected in *S. pombe* cells under normal conditions, whilst significantly increased levels of an expressed inducible form of the protein were detected in *S. pombe* cells as part of an exclusive response to heat shock.

In addition to Rad9-S, the constitutive expression of two shorter truncated Rad9 variants – termed Rad9-VS and Rad9-T (“very-short” and “tiny”), was also detected in *S. pombe* cells.

This experimental observation indicates that *S. pombe* may prove to be a useful homologous eukaryotic model organism, in future research studies, for the elucidation of the unknown functions of the four truncated isoform variants of human Rad9B which may be implicated in novel mechanisms of carcinogenic development and progression.

The mechanism of expression of the Rad9-S, Rad9-VS truncated protein variants was postulated to involve alternative translation at the alternative AUG start-codon sites at Methionine 50 (M50) and Methionine 74 (M74) within the *S. pombe rad9* gene, in which leaky ribosomal scanning is implicated.

Heat shock may increase the frequency of leaky ribosome scanning, exclusive to the M50 alternative AUG start-codon site, via alterations of the secondary topological configuration of the *rad9* mRNA, in which *rad9* mRNA-protein associative interactions with heat-shock proteins, RNA chaperones and/or RNA stabilisers may also be implicated.

The *rad9* mRNA region spanning the codon region M1 to M50 inclusive may also function as a novel type of *cis*-acting hypothermic suppressor element that induces a supramolecular configurational rearrangement of the mRNA secondary structure in response to cold shock which blocks leaky ribosome scanning at the alternative M50 AUG start-codon site with consequential suppression of Rad9-S expression under low (16°C) and moderate temperatures (25-30°C).

Expression of the Rad9-T truncated protein variant was postulated to involve a limited proteolytic cleavage mechanism in which metacaspase-mediated and/or COP9 signalosome-mediated limited proteolytic processing may be implicated.

In *silico* sequence alignment analyses identified a potential metacaspase target-site motif within the *S. pombe* Rad9 protein and comparative modelling indicated that key residues at the focal cleavage-site of this motif were situated at the Rad9:Rad1 interface of the “9-1-1” DNA sliding-clamp complex.

In silico multiple sequence alignment analyses also indicated that the *S. pombe* Rad9 protein contained two sequences, flanking the identified potential metacaspase target-site motif, which exhibited significant homology with the two alternative C-termini of the *H. sapiens* Rad9B paralogue and its truncated isoforms.

Distinctive phosphorylation-type post-translational modifications of Rad9-S were also found to influence the expression of the respective two smaller truncated protein variants; Rad9-VS and Rad9-T.

It was postulated that a variety of potential Rad9 phospho-isoforms may be implicated in a interactive “activity-modulatory feedback” mechanism, in which they function as transcriptional and/or translational regulators of the expression of the Full-length Rad9, N Δ 49-Rad9 (“Rad9-S”) and N Δ 73-Rad9 (“Rad-VS”).

Whilst kinase-mediated phosphorylation of several key residues, identified within a conserved potential metacaspase site in the full-length Rad9, Rad9-S and Rad9-VS protein isoforms, may inhibit proteolytic-cleavage formation of the detected Rad9-T truncated protein variant.

Taken together, these data indicated that specific checkpoint kinase-mediated phosphorylation of the *S. pombe* Rad9 protein may constitute part of a “feedback” signalling network for the regulation of metacaspase-mediated processing of the *S. pombe* Rad9 protein which may be implicated in novel checkpoint responses that suppress the formation and/or alter specific functional activities of the Rad9-Rad1-Hus1 (“9-1-1”) DNA sliding-clamp and promote the proteolytic expression of two truncated Rad9 isoforms whose functions are unknown, but may elicit alternative regulatory cell cycle signalling pathways under particular genotoxic and/or environmental stress conditions.

Whilst confirmation of the existence of these two postulated metacaspase-generated truncated Rad9 isoforms and elucidation of their roles in cell cycle checkpoint signalling remains to be established, their potential novel functions may be analogous to those of the *H. Sapiens* Rad9B isoforms which are as yet unknown.

S. pombe cells “Cre-Lox”– engineered for the exclusive expression of the Rad9-S protein variant exhibited a high degree of cytotoxic sensitivity towards a wide range of different types of genotoxic agents.

This supported the initial hypothesis which postulated that deletion of the first 49 N-terminal amino acid residues in the truncated Rad9-S protein variant would sterically suppress the formation of the constrained ring configuration of the Rad9-Rad1-Hus1 heterotrimeric DNA sliding-clamp complex and thus render the engineered cells unable to elicit the appropriate cell cycle checkpoint responses to various types of induced DNA damage.

An unanticipated, exceptional experimental observation was the partial resistance of engineered Rad9-S cells (~30% retained cell viability) towards acute exposure to the Topoisomerase I (Topo I) inhibitor drug camptothecin (~30% retained cell viability) – which transiently traps the enzyme on the DNA in S-phase.

Consequential collision of DNA replication forks with the resultant duplex-immobilised DNA-CPT-Topo I ternary complex leads to the formation of one-sided double-stranded breaks which are subsequently detected by the G2-M DNA damage checkpoint.

Five key phosphorylation sites were identified within the truncated Rad9-S protein variant which were critical for the partial resistance of engineered Rad9-S cells towards camptothecin-induced DNA damage – notably; Y12 and Y62 (potential Mph1 kinase target sites) and T176, T363, S374 (equivalent Rad3 kinase target sites to those found in the full-length Rad9 protein at positions T225, T412 and S423 respectively).

A potential DNA-binding domain, spanning residues M50 – M74 Rad9, was also identified within the truncated Rad9-S protein that may possess additional functions as a nuclear translocation signal responsive element, a nuclease recruitment-site and/or exonuclease catalytically-active site which are implicated in the co-ordinated repair of camptothecin-induced DNA double-stranded breaks.

Subsequent genetic and biochemical experimental data indicated that the truncated Rad9-S protein variant may mediate a co-ordinated cell cycle arrest signal and DNA repair response to camptothecin-induced DNA damage, that functions outside of the canonical Rad9-Rad1-Hus1 complex, which is channelled into a novel pathway that interacts independently of both the G2-M and mitotic checkpoints.

Comparative acute survival assays performed on cultures of the *S. pombe* cells engineered for the exclusive expression of the truncated Rad9-S protein variant, under induced osmotic stress conditions, rendered the cells hyper-sensitive to camptothecin-induced DNA damage and hyper-resistant to heat shock.

Comparative acute survival assays also indicated that deletion of the Sty1 kinase, but not Wis1 kinase, within an exclusive Rad9-S expression type genetic background also increased the sensitivity of the cells to camptothecin-induced DNA damage.

Whilst comparative bioinformatics-based *in silico* sequence alignments of the Rad9-S, Sty1 and Wis1 indicated that both Rad9-S and Sty1 contained potential interactive motifs for the Rad3 kinase, which were absent in the Wis1 protein.

Taken together, these data indicated that the truncated Rad9-S protein variant may be implicated in two novel separate differential signalling responses upon exposure to either heat shock or camptothecin, in which appropriate pathway selection is dictated via the suppression or induction of Rad9:Sty1-mediated co-operative activation of the Rad3 kinase.

Comparative acute survival assays indicated that deletion of *rad1* within an exclusive Rad9-S expression type genetic background rendered the engineered cells hypersensitive to heat shock, but had no adverse impact on their observed partial resistance to camptothecin-induced DNA damage.

Comparative acute survival assays also indicated that deletion of *hus1* within an exclusive Rad9-S expression type genetic background rendered the engineered cells hypersensitive to both hyperthermic- and camptothecin- induced genotoxic cytological stresses.

Experimental genetic studies also indicated that the Rad17 clamp-loader protein is unlikely to be directly implicated in these Rad9-S-mediated checkpoint responses to hyperthermic- or camptothecin- induced genotoxic stresses.

Taken together, these experimental observations indicate that the Rad9-S-mediated response to camptothecin-induced DNA damage proceeds via formation of a heterodimeric, “open-ring”, Rad9-S:Hus1 C-clamp type complex, whilst the Rad9-S-mediated response to hyperthermic stress proceeds via formation of an alternative heterotrimeric Rad9-S:Rad1:Hus1 toroidal clamp complex and that these respective checkpoint pathways are novel functions of Rad9 which operate outside of the canonical full-length Rad9-Rad1-Hus1 heterotrimeric DNA sliding-clamp complex.

It was also postulated that the shorter truncated isoform variants Rad9-VS and Rad9-T may be implicated in a feedback regulatory mechanism for modulatory control of the respective functional activities of the Rad9-S protein-mediated responses to both heat shock- and camptothecin- induced types of DNA damage – which may also be analogous to those of the human Rad9B paralogue and its respective truncated isoforms.

Future experimental studies into the identified *S. pombe* Rad9-S-modelled checkpoint response to camptothecin-induced genotoxicity may offer potential new insights into the reasons for the exclusive elevated expression of Rad9, but neither Rad1 or Hus1, in aggressive breast tumours and/or novel mechanisms of acquired tumour drug resistance to camptothecin-based anti-cancer chemotherapeutics.

Whilst future experimental investigation of the identified *S. pombe* Rad9-S–modelled checkpoint response to hyperthermic stress may advance knowledge of the complex mechanisms of action implicated in the combinatorial hyperthermic-enhanced efficacy of chemo- and/or radio-therapeutic adjuvant clinical anti-cancer regimens and provide useful information of the acquired mechanisms of tumour resistance to these types of treatments.

Taken together, in summarised context, progressive research into the initial “pilot data” acquired from this Ph.D. project may provide vital information for the future treatment of chronic breast cancer patients administered camptothecin-derivatised agents, in combination with adjuvant hyperthermotherapy and/or radiotherapy, to combat the metastatic spread of refractory tumours which have developed multiple drug resistance to the “conventional arsenal” of chemotherapeutic drugs utilised in standard clinical practice – such as taxols and anthracyclics.

LIST OF FIGURES

CHAPTER 1

Fig 1.1: Key Factors Implicated in the Promotion of Carcinogenesis	P.5
Fig 1.2: Summarised Overview of Human Rad9 Functions	P.8
Fig 1.3: <i>hRad9A</i> and <i>hRad9B</i> Gene Locus Sites & Protein Sequences	P.9
Fig 1.4: <i>hHUS1</i> and <i>hHus1B</i> Gene Locus Sites & Protein Sequences	P.10
Fig 1.5: Alternative Complex Isoforms of the “9-1-1” Clamp	P.11
Fig 1.6: <i>hRad17</i> Gene Locus Site and Isoform Protein Sequences	P.12
Fig 1.7: Tissue-Specific Expression Profiles for the <i>hRAD9A</i> Gene	P.13
Fig 1.8: Tissue-Specific Expression Profiles for the <i>hRAD9B</i> Gene	P.14
Fig 1.9: Summarised Biochemical Roles of Rad9 in Carcinogenesis	P.16
Fig 1.10: Key Structural Features of the Rad9-Rad1-Hus1 Complex	P.24
Fig 1.11: Interactive Domains of “9-1-1” Clamp-Loading Proteins	P.25
Fig 1.12: Mechanistic Overview of “9-1-1” Clamp Loading Onto DNA	P.28
Fig 1.13: DNA Polarity-Specific Models of “9-1-1” Clamp-Loading	P.30
Fig 1.14: Mechanistic Models of “9-1-1” DNA Sliding-Clamp Motion	P.31
Fig 1.15: 1D and 3D “9-1-1–DNA” Lesion Site Translocation Pathways	P.32
Fig 1.16: hRadA – Key Checkpoint Signalling Domains & Residues	P.52
Fig 1.17: Key Features of ATR- and Chk1- Activation Proteins	P.53
Fig 1.18: “9-1-1” Clamp-Orchestrated Chk1 Activation	P.54
Fig 1.19: Constitutive and Inducible Models of ATR Activation	P.55
Fig 1.20: “9-1-1” Clamp-Intercommunicative Chk1 Signal Network	P.56
Fig 1.21: “9-1-1” Clamp Influences on G1/S Checkpoint Activation	P.57
Fig 1.22: “9-1-1” Clamp Influences on Intra-S Checkpoint Activation	P.58
Fig 1.23: “9-1-1” Clamp Influences on G2/M Checkpoint Activation	P.59
Fig 1.24: “9-1-1” Clamp-Induced p38-MAPK Checkpoint Signalling	P.60
Fig 1.25: “9-1-1” Clamp Influences on the Circadian Checkpoint	P.61

LIST OF FIGURES (continued)

CHAPTER 1(continued)

Fig 1.26: “9-1-1” Clamp-Induced G2-Decatenation Model	P.62
Fig 1.27: “9-1-1” Clamp Influences on Intra-M Phase Checkpoints	P.63
Fig 1.28: Asymmetric Kinetochores Spindle Attachment Rectification	P.64
Fig 1.29: Mechanistic Overview of the Mitotic Spindle Checkpoint	P.65
Fig 1.30: Mechanistic Overview of Androgen Receptor Activity	P.70
Fig 1.31: Functional Domain Map of the Androgen Receptor	P.71
Fig 1.32: “9-1-1” Clamp Suppression of Androgen Receptor Activity	P.72
Fig 1.33: TPR2 Modulation of Hsp90 Chaperone Complex Activity	P.80
Fig 1.34: Rad9-Modulated TPR2 Activity – Key Domain Interactions	P.82
Fig 1.35: DNA Damage Types and Sources – A Biochemical Overview	P.89
Fig 1.36: Types of DNA Conformer-Induced Replicative Inhibition	P.90
Fig 1.37: Classification Review of DNA Damage Repair Mechanisms	P.91
Fig 1.38: Functional Roles of the “9-1-1” Clamp in DNA Repair	P.98
Fig 1.39: A Mechanistic Overview of Global Genomic DNA Repair	P.100
Fig 1.40: A Mechanistic Overview of Transcription-Coupled Repair	P.101
Fig 1.41: “9-1-1” Co-Ordination of the BER Repairosome Activities	P.102
Fig 1.42: “9-1-1” Clamp Modulation of SP-BER & LP-BER Activities	P.103
Fig 1.43: A Mechanistic Overview of Base-Mismatch DNA Repair	P.104
Fig 1.44: “9-1-1” Clamp Influences on MMR-Apoptotic Induction	P.105
Fig 1.45: Mechanistic Overview of the “GO System” Repair Network	P.106
Fig 1.46: Modulatory “9-1-1” Clamp-MYH1 Activity Interactions	P.107
Fig 1.47: “9-1-1” Clamp Modulation of Oxidative Mismatch Repair	P.108
Fig 1.48: Mechanistic Overview of DNA dsBreak Repair Pathways	P.109
Fig 1.49: “9-1-1” Clamp Modulation of DSB-Induced Quiescence	P.110
Fig 1.50: “9-1-1” Clamp Modulation of Metnase Functional Activities	P.111

LIST OF FIGURES (continued)

CHAPTER 1(continued)

Fig 1.51: “9-1-1” Clamp Modulation of TLS & Template-Switching	P.112
Fig 1.52: “9-1-1” Clamp Modulation of TLK1 Activity-Mediated TLS	P.117
Fig 1.53: Phospho-Regulated “9-1-1” Clamp DNA Repair Activities	P.118
Fig 1.54: Biochemical Overview of CAD- Catalysed Reactions	P.124
Fig 1.55: CAD Activity Regulation – Key Domains & Residues	P.125
Fig 1.56: Associative Rad9-CAD Domain Interactions	P.126
Fig 1.57: Independent hRad9-Mediated Apoptotic-Induction Model	P.130
Fig 1.58: Rad1-Modulated “9-1-1” Clamp Stability and Translocation	P.135
Fig 1.59: Jab1 Proteosomal Functions & CSN Interactions	P.136
Fig 1.60: Rad1-Jab1 Associative “9-1-1” Clamp Degradation Model	P.137
Fig 1.61: Jab1-Targeted “9-1-1” Clamp Proteolysis – CSN Regulation	P.138
Fig 1.62: Jab –“9-1-1” Complex-Coupled Cell Cycle Regulation	P.139
Fig 1.63: Overview of the Fission Yeast <i>S. pombe</i> Life Cycle	P.143
Fig 1.64: Examples of Key Conserved Checkpoints in <i>S. pombe</i>	P.144
Fig 1.65: SDS-PAGE and HPLC-SEC Fractionation Analyses	P.147
Fig 1.66: Comparative SDS-PAGE Western Blot Analyses	P.148

LIST OF FIGURES (continued)

CHAPTER 2

Fig 2.1: PCR Protocols for the Generation of the pAW1Plasmid-Derived <i>loxP-Ura4⁺-loxM3 rad9</i> Gene Locus-Targeted Fragment and the pAW8 Donor Plasmid Sph1-<i>rad9</i>-SpeI Gene Cassette Inserts	P.171
Fig 2.2: Basic Essential Components of the Cre-Recombinase-Mediated Cassette Exchange System	P.172
Fig 2.3: Mechanistic Overview of the Cre-RMCE System for Generation of Rad9/Rad9-S Strains	P.173
Fig 2.4: Base-Strain Plasmid pAW1 PCR Modification Primers: Sequences and Targets	P.174
Fig 2.5: PCR Primers for Generation of Full-Length <i>rad9</i> Gene pAW8 Plasmid Cassette Inserts	P.175
Fig 2.6: Fusion PCR Protocol for the Generation of pAW8 Plasmid Experimental Mutated <i>rad9</i> Gene Cassette Inserts	P.176
Fig 2.7: Summarised PCR Reaction Mixtures and Thermocycler Parameters	P.193
Fig 2.8: Summarised Details of DNA Sequencing Primers and ddNTP Terminators	P.195
Fig 2.9: Models of Conserved and Adaptable Protein Conformers	P.264
Fig 2.10: DisCon – Program Operational System Flow Diagram	P.265
Fig 2.11: metaPrDOS – Program Operational System Flow Diagram	P.266
Fig 2.12: Vienna RNAfold Analysis of <i>S. pombe rad9</i> Intron 2	P.268

LIST OF FIGURES (continued)

CHAPTER 3

Fig 3.1: Constitutive and Heat-Inducible “Rad9-S” Expression	P.286
Fig 3.2: Experimental <i>S. pombe rad9</i> Gene Constructs	PP.289-290
Fig 3.3: Overview of the Adapted Cre-RMCE System	P.291
Fig 3.4: $\Delta rad9$ “Cre-Lox Base-Strain” Genotype Verification	PP.296-297
Fig 3.5: pAW8-<i>rad9</i> Plasmid Construction	P.300
Fig 3.6: pAW8-<i>rad9-c3xHA</i> Plasmid Construction	P.301
Fig 3.7: pAW8-<i>rad9</i>Δ<i>Intron1-c3xHA</i> Plasmid Construction	P.302
Fig 3.8: pAW8-<i>rad9-M50L-c3xHA</i> Plasmid Construction	P.303
Fig 3.9: pAW8-<i>N</i>Δ49-<i>rad9-c3xHA</i> Plasmid Construction	P.304
Fig 3.10: pAW8-<i>N</i>Δ73-<i>rad9-c3xHA</i> Plasmid Construction	P.305
Fig 3.11: pAW8-<i>N</i>Δ311-<i>rad9-c3xHA</i> Plasmid Construction	P.306
Fig 3.12: pAW8-<i>N</i>Δ357-<i>rad9-c3xHA</i> Plasmid Construction	P.307
Fig 3.13: Plate Selection of Cre-RMCE-Generated <i>S. pombe</i> Strains	P.311
Fig 3.14: Comparative <i>rad9</i>-Specific PCR Genotype Analysis	P.312
Fig 3.15: <i>rad9</i>-Specific Gene Expression Profile Analysis	P.313
Fig 3.16: metaPrDOS Analysis of Rad9, M50A & M50L Mutants	P.317
Fig 3.17: metaPrDOS Analysis of Rad9, “Rad9-S” & “M74” Variants	P.318
Fig 3.18: metaPrDOS Analysis of Rad9, “M311”, “M312” & “M358”	P.319
Fig 3.19: Site Map of SpRad9 Protein Stability Modulation Motifs	P.328
Fig 3.20: Comparative Map of SpRad9 Stability Modulation Motifs	PP.329-330
Fig 3.21/3.22: Transmembrane-Spanning Domain Modelling of SpRad9	PP.335-336
Fig 3.23: Hydropathy Profile Analyses of the <i>S. pombe</i> Rad9 Protein	PP.337-338
Fig 3.24: <i>In Silico</i> Identification of a Conserved 29 Residue-Spanning Potential Non-Cytoplasmic ATR^{Rad3} Kinase Activation Motif	P.339
Fig 3.25: Secondary Structure Repeat Motif Analysis of SpRad9	PP.345-346

LIST OF FIGURES (continued)

CHAPTER 3 (continued)

- | | |
|---|-------------------|
| Fig 3.26: Coiled-Coil Motif Analysis of the <i>S. pombe</i> Rad9 Protein | PP.347-348 |
| Fig 3.27: Kinase Site and Aggregative Modulatory Motif Analyses of the REPPER-Identified Coiled-Coil Repeat Domain Sequences Within the <i>S. pombe</i> Rad9 Protein | PP.349-350 |
| Fig 3.28: Secondary Structural Motif Profile Analysis of SpRad9 | P.353 |
| Fig 3.29: Stability Profiling of the <i>S. pombe</i> Rad9 Protein Isoforms | PP.356-357 |

LIST OF FIGURES (continued)

CHAPTER 4

Fig 4.1: Postulated Intron 1 Retention Model of “Rad9-S” Expression	P.361
Fig 4.2: Internal Intron Sequences Within the <i>S. pombe rad9</i> Gene	P.362
Fig 4.3: Intron1 RNA Aptamer-Mediated “Rad9-S” Expression Model	P.363
Fig 4.4: Intron 1 RNA Aptamer Model of Heat Shock “Rad9-S” Induction	P.364
Fig 4.5: Experimental Induction of <i>S. pombe</i> “Rad9-S” Expression	PP.368-370
Fig 4.6: Heat-Specific Induction of <i>S. pombe</i> “Rad9-S” Expression	P.373
Fig 4.7: Vienna RNAfold Analysis of the Intron1 mRNA Sequence of the <i>S. pombe rad9</i> Gene	P.374
Fig 4.8: Vienna RNAfold Analysis of the 5’-UTR Sequence of the <i>S. pombe rad9</i> Gene	P.377
Fig 4.9: Vienna RNAfold Analysis of the 3’-UTR Sequence of the <i>S. pombe rad9</i> Gene	P.378
Fig 4.10: Hypothermic Suppression of “Rad9-S” Expression	P.384
Fig 4.11: Vienna RNAfold Analysis (“Raw Data” Output) of the Encoded M1-S49 Sequence Within the Transcribed <i>S. pombe rad9</i> mRNA	PP.385-386
Fig 4.12: Vienna RNAfold Analysis (“Processed Data” Output) of the Encoded M1-S49 Sequence Within the Transcribed <i>S. pombe rad9</i> mRNA	PP.387-388
Fig 4.13: Structural Component Analysis of the Encoded M1-S49 Sequence Within the Transcribed <i>S. pombe rad9</i> mRNA	P.389
Fig 4.14: Comparative Secondary RNA Structural Conformer Analyses of the Isolated and M1-S49-Incorporated T18-C40 Encoded Sequences Within the Transcribed <i>S. pombe</i> mRNA	P.390
Fig 4.15: Hypothermic Inhibition Model of “Rad9-S” Suppression	P.391
Fig 4.16: Temporal Assay of Heat-Induced “Rad9-S” Expression	P.393
Fig 4.17: Perturbed “9-1-1” Complex-Induced Expression of a Novel Truncated <i>S. pombe</i> Rad9 Variant – “Rad9-VS”	P.396
Fig 4.18: 2D-PAGE Analytical Detection of spRad9 Isoforms	P.399
Fig 4.19: Kinase Site Modulation of Rad9 Isoform Expression	P.400
Fig 4.20: 2D-PAGE Alignment Analyses of “Rad9-S” Phosphoisoforms	P.401

LIST OF FIGURES (continued)

CHAPTER 4 (continued)

Fig 4.21: <i>rad9</i> Intronic RNA Folding Analyses – “Raw Data”	P.405
Fig 4.22: <i>rad9</i> Intronic RNA Folding Analyses – “Processed Data”	P.406
Fig 4.23: COP9-Directed Rad9 Partial Proteosomal Processing Model	P.413
Fig 4.24: Rad9-Targeted Metacaspase Cleavage Processing Model	P.414
Fig 4.25: <i>In Silico</i> Identification of Potential Caspase Cleavage Sites Within the <i>S. pombe</i> Rad9 Protein	P.415
Fig 4.26: Comparative In Silico Alignment Analyses of the Potential Metacaspase Target Motif Sequences Identified Within the <i>S. pombe</i> Rad9 Protein	P.416
Fig 4.27: Possible Identity of the 2D-PAGE-Detected spRad9 Isoforms	P.417
Fig 4.28: metaPrDOS Analyses of Detected spRad9 Isoforms	P.420
Fig 4.29: metaPrDOS Analyses of spRad9 Cleavage Products	P.421
Fig 4.30: Site Map of spRad9 Isoform Stability Modulation Motifs	P.424
Fig 4.31: Zygggregator Analysis of the Postulated Rad9 Isoforms	PP.425-426
Fig 4.32: YASPIN Analysis of the Postulated Rad9 Isoforms	P.429
Fig 4.33: Stability Profiling of the Truncated SpRad9 Isoforms	PP.433-434
Fig 4.34: Rad9 Isoformic-Modulated “Feed-Back” Expression Model	P.439

LIST OF FIGURES (continued)

CHAPTER 5

Fig 5.1: Comparative Modelling of Engineered Rad9 Isoforms	P.446
Fig 5.2: Eukaryotic Linear Motif (ELM) Analysis of <i>S. pombe</i> Rad9	P.447
Fig 5.3: Comparative Analysis of the Relative Abundance of Localised Functional Protein Motif Types Within the Full-Length and Truncated <i>S. pombe</i> Rad9 Protein Variants	P.451
Fig 5.4: Phosphorylation Site Analysis of the <i>S. pombe</i> Rad9 Protein	P.452
Fig 5.5: Relative Numbers of Kinase Sites in Rad9 Variants	P.454
Fig 5.6: Predictive Genotoxic Responsive Models for Rad9 Isoforms	P.460
Fig 5.7: Comparative “Solvent Control” Acute Survival Assays	P.461
Fig 5.8: Comparative Heat and Osmotic Stress Acute Survival Assays	P.462
Fig 5.9: Comparative Acute Oxidative Stress Survival Assays	P.463
Fig 5.10(i): Acute Survival Assays with Adduct-Forming/Cross-Linking Agents	P.464
Fig 5.10(ii): Acute Survival Assays with Adduct-Forming/Cross-Linking Agents	P.465
Fig 5.11(i): Acute Survival Assays with Topoisomerase Inhibitors	P.466
Fig 5.11(ii): Acute Survival Assays with Topoisomerase Inhibitors	P.467
Fig 5.12: Acute Survival Assays with Caffeine, HU and TBZ	P.468
Fig 5.13: Comparative Analyses of the Relative Degree of Enhanced Sensitivity of <i>S. pombe</i> Strains, Engineered for the Exclusive Expression of Specific Truncated Rad9 Variants, to Different Types of Induced Genotoxic Stresses	PP.469-470
Fig 5.14: 2D-PAGE Data – Genotoxic Type Rad9-S Modifications	P.473
Fig 5.15: Rad9-S Responses to Different Types of Induced DSBs	P.474
Fig 5.16: Identification of a Novel Functional Domain in Rad9	P.479
Fig 5.17: Comparative Modelling of the M50-M74 Functional Domain Within the Full-Length <i>S. pombe</i> Rad9 Protein	P.480
Fig 5.18: 2D-PAGE Data – Localisation of Rad9-S Phosphoisoforms	P.481

LIST OF FIGURES (continued)

CHAPTER 6

Fig 6.1: Summarised Cytotoxic Mode of Action of Camptothecin	P.484
Fig 6.2: <i>rad9-S Δtop1</i> x “Wild-Type” Back-Crossed Strain Isolation	P.487
Fig 6.3: Comparative <i>rad9-S Δtop1</i> Acute CPT Survival Assays	P.488
Fig 6.4: Overview of the <i>S. pombe</i> G2/M Checkpoint Pathway	P.492
Fig 6.5: CPT Survival Assays – Clamp & Clamp-Loader Sub Units	P.505
Fig 6.6: Comparative Rad9 and Hus1 Isoformic Protein Analyses	PP.506-507
Fig 6.7: Comparative Analyses of “Rad9-S”:Hus1 Interactions	P.508
Fig 6.8: Functional Domain Map of the “Rad9-S”:“Hus1-C” Complex	P.509
Fig 6.9: CPT, HU and 2D-PAGE Assays – “Hus1-Binding” Mutants	P.510
Fig 6.10: CPT and 2D-PAGE Assays – “Hus1-Binding” Mutants and “DNA-Binding Phosphorylation Site Knock-Out” Mutants	P.511
Fig 6.11: Evidence for Novel “Rad9-S”, “Hus1-C” & Mph1 Interactions	P.512
Fig 6.12: “Rad9-S” Mutants – Comparative Cellular Localisation Assays	P.513
Fig 6.13: Differential Phosphoisoformic Localisation of “Rad9-S”	P.514
Fig 6.14: Functional Model for the “Rad9-S”:Hus1 Heterodimer	P.515
Fig 6.15: Acute CPT Survival Assays – Proximal Transducer Kinases	P.523
Fig 6.16: CPT Assays – Rad3 Kinase Ala “Knock-Out” Point Mutants	P.524
Fig 6.17: CPT Assays – Ala and Glu Rad3 Kinase-Site Point Mutants	PP.525-526
Fig 6.18: Rad3 Kinase-Initiated T176 Target-Site “Priming” Model	P.527
Fig 6.19: Comparative Western Blot Analyses of Full-Length Rad9 and Truncated “Rad9-S” Isoform Expression in the Absence and Presence of CPT-Induced DNA Damage with <i>rad3</i> and <i>rad26</i> Gene Deletions	PP.528-529
Fig 6.20: Comparative Lactose Synchronisation Assays	PP.530-531
Fig 6.21: Functional Roles of the <i>S. pombe</i> “Scaffold/Mediator” Proteins Crb2, Mrc1 and Rad4 in Chk1 Activation-Mediated Checkpoint Signalling Responses to DNA Damage	PP.535-537
Fig 6.22: Acute CPT Survival Assays – Scaffold Proteins/Mediators	P.538

LIST OF FIGURES (continued)

CHAPTER 6 (continued)

- Fig 6.23: Acute CPT Survival Assays – Distal Transducer Kinases** P.543
- Fig 6.24: 2D-PAGE Analyses of Potential “Rad9-S”-Cds1 Interactions** P.544
- Fig 6.25: Hypothetical Model of Rad3- and Tel1- Differential Phosphorylation-Mediated Modulation of Functional Mrc1-“Rad9-S” Interactive Activities Which May Influence Specific Checkpoint Pathway Selective Activation Initiated Via the Heterodimeric “Rad9-S”：“Hus1-C” “Open-Ring/C-Clamp” Complex** PP.545-546
- Fig 6.26: Evidence for Potential Functional Roles of the Truncated “Rad9-VS” Isoform and Hhp1 Kinase in the Temporal Regulation of Functional “Rad9-S” Activities** PP.549-550
- Fig 6.27: Comparative Acute CPT Survival Assays and 2D-PAGE-Coupled Western Blot Analyses – Effectors and Regulators** PP.554-555
- Fig 6.28: Overview of DNA Damage and Cell Cycle Stress Responses** P.563
- Fig 6.29: Acute CPT Survival Assays – Mitogen-Activated Kinases** P.564
- Fig 6.30: 2D-PAGE Analyses of Potential MPA Kinase Interactions** P.565
- Fig 6.31: Osmotic Stress Responses I: Drop-Plate (Chronic) Assays** P.566
- Fig 6.32: Osmotic Stress Responses II: Acute Cell Survival Assays** P.567
- Fig 6.33: Acute CPT and TBZ Assays – Bub1, Mad2 and Mph1 Mutants** P.575
- Fig 6.34: 2D-PAGE Analyses of “Rad9-S”：Mph1 Interactions** P.576
- Fig 6.35: HPLC-SEC and Co-Immunoprecipitation Analyses** PP.577-578
- Fig 6.36: Collated Genetic and Biochemical Evidence for “Rad9-S”-Mph1-Hus1 Interactions** P.579
- Fig 6.37: Collated *In Silico* and Biochemical Evidence for** P.580
- Fig 6.38: Data Evidence for “Rad9-S”-Mph1-Cds1 Interactions
“Rad9-S”-Mph1-Hus1 Interactions** P.581
- Fig 6.39: 2D-PAGE Resolved Cds1 & Mph1 Phosphoisoform Profiles** P.582
- Fig 6.40: Mph1-Cds1 Complementary Kinase-Site Activation Model** P.583
- Fig 6.41: Acute CPT Survival Assays – FEAR Network Mutants** P.587
- Fig 6.42: Model for the “Rad9-S” Signal Response to Camptothecin** PP.592-593

LIST OF FIGURES (continued)

CHAPTER 6 (continued)

- Fig 6.43: Model for the “Rad9-S” Signal Response to Thermal Stress** **PP.594-595**
- Fig 6.44: Epigenetic and Proteomic Differential Pathway Model** **PP.596-597**
- Fig 6.45: Acute Cell Survival Assays – Caffeine and Camptothecin** **P.618**
- Fig 6.46: Acute Cell Survival Assays – Caffeine and Heat Shock** **P.619**
- Fig 6.47: Comapartive 2D PAGE-Coupled Western Blot Analyses of Differential Phosphoisoform Modulation of the Truncated “Rad9-S” Protein Variant Implicated in Cytological Checkpoint Signalling Responses to Camptothecin-Induced Genotoxicity and Hyperthermic Stress** **PP.620-622**
- Fig 6.48: Potential Biochemcial Targets Implicated in Caffeine-Mediated Potentiation of the Cytotoxic Effects of Hyperthermic Stress and Camptothecin-Induced DNA Damage in *S. pombe* Cells “Cre-Lox” Engineered for the Exclusive Expression of the “Rad9-S” Truncated Protein Variant** **P.623**
- Fig 6.49: Hypothetical Human Rad9B-Mediated Checkpoint Pathway Signalling Models Which May Be Implicated in the Development of Metastatic Tumour Resistance to the Combinatorial Adjuvant Hyperthermic- and Caffeine- Potentiated Anti-Neoplastic Cytotoxic Efficacy of Polychemotherapeutic and Radiotherapeutic Treatments** **P.625**

LIST OF FIGURES (continued)

CHAPTER 7

Fig 7.1: Data Evidence for a Nuclease-Like Domain in <i>S. pombe</i> Rad9	P.668
Fig 7.2: Mph1-Activation of the “Rad9-S” “Nuclease-Like” Domain	P.669
Fig 7.3: Key Proteins Implicated in the Repair of CPT-Induced DSBs	P.674
Fig 7.4: Acute CPT Survival Assays – Nuclease and Ligase IV Mutants	P.675
Fig 7.5: Pro- and Anti- Recombination Functions of the Rqh1 Helicase	P.678
Fig 7.6: Regression-Coupled Recombination-Initiated Fork Recovery	P.679
Fig 7.7: Acute CPT Survival Assays – <i>rqh1</i>-Deletion Mutants	P.680
Fig 7.8: Model of Rad9-S “Nuclease-Mediated” Chk1 Suppression	P.687
Fig 7.9: “Rad9-S” Co-Ordinated Chk1 Suppression & DNA Repair	PP.688-689

LIST OF TABLES

Table 1.1: Characteristic Features of Benign & Malignant Tumours	P.3
Table 1.2: <i>hRAD9</i> Gene Expression – Neoplastic Correlations	P.15
Table 1.3: Potential Rad9-Mediated Tumour Resistance to Novel Therapeutics	P.21
Table 1.4: “9-1-1” Clamp-Modulated DNA Repair Protein Activities	P.99
Table 1.5: <i>H. sapiens</i> and <i>S. pombe</i> Functional Protein Homologues	P.143
Table 2.1: Gene Marker-Based Replica Plate Selection of <i>S. pombe</i> “Cross-Strain” Colonies	P.198
Table 3.1: Identified SpRad9 Protein Stability Modulation Motifs	P.327
Table 5.1: ELM-Identified Functional Sequences in <i>S. pombe</i> Rad9	PP.448-450
Table 5.2: Potential Number of Kinase Target Sites in Rad9 Variants	P.453
Table 5.3: Predicted Number of Kinase Target Sites in Rad9 Variants	P.453
Table 6.1: Comparative Summary of Functionally-Equivalent Homologous Protein Targets in <i>S. pombe</i> and <i>H. sapiens</i> Implicated in Caffeine-Induced Potentiation of the Cytotoxic Effects of Hyperthermic Stress and Camptothecin-Induced DNA Damage	P.624

LIST OF APPENDICES

Appendix 2.11.1: pAW1 Cre-Lox Non-Essential Gene Replacement Plasmid Maps	PP.269 – 271
Appendix 2.11.2: pAW8 Cre-Lox Donor Gene Exchange Plasmid Maps	PP.272 – 275
Appendix 2.11.3: PCR Primers – Sequence and Function	P.276
Appendix 2.11.4: pAW1 Plasmid PCR Fragment-Integrated <i>rad9</i> Gene Locus Map	P.277
Appendix 2.11.5: pAW8 Cre-Lox Donor <i>rad9</i> Gene Exchange Plasmid Constructs	P.278
Appendix 2.11.6: Pre-Constructed (Pre-Supplied) <i>S. pombe</i> Strains Utilised in this Study	P.279
Appendix 2.11.7: Constructed Full-Length, Truncated and Point-Mutated <i>rad9</i> Strains	P.280
Appendix 2.11.8: Cre-Lox Double-Mutant <i>S. pombe</i> Strains Constructed for this Study	P.281
Appendix 6.1: Journal of Cell Science Publication (Editor and Referee Panel Accepted – <i>In Press</i>)	PP.626-663
“Heat Induction of a Novel Rad9 Variant From a Cryptic Translation Initiation Site Reduces Mitotic Commitment”	
Simon Janes, Ulrike Schmidt, Nadja Ney, Susanna Concilio, Mohamed Zekri and Thomas Caspari	
[Electronic Publication Ahead of Print 13th July 2012]	

CONTENTS

Declaration and Consent Statement: i – iii

Acknowledgements: iv – v

Abstract: vi – xiv

List of Figures: xv – xxvii

List of Tables: xxviii

List of Appendices: xxix

Contents: xxx – xxxxi

Abbreviations: xxxiii – xxxix

<u>CHAPTER</u>	<u>PAGE No.</u>
1. INTRODUCTION	1 – 150
1.1 Human Rad9: A Viable Cancer Chemotherapeutic Target	2 – 22
1.2 Associative “9-1-1” Complex-Dependent Rad9 Functions	23 – 118
1.2.1 Physico-Biochemical Properties of the Rad9-Rad1-Hus1 DNA Sliding Clamp: Loading and Sensory Motion Dynamics	23 – 32
1.2.2 DNA Damage Checkpoint Signal Activation and Modulation	33 – 65
1.2.3 Androgen Nuclear Receptor Activity Modulation	66 – 74
1.2.4 Modulation of TPR2 Activity-Influenced Protein Folding	75 – 85
1.2.5 DNA Repair Pathway Selection and Activity Modulation	86 – 118
1.3 “9-1-1” Complex-Independent Rad9 Functions	119 – 130
1.3.1 Pyrimidine Nucleobase Biosynthetic Activity Modulation	119 – 126
1.3.2 Intrinsic Apoptotic Signal Activity Modulation	127 – 130
1.4 COP9 Signalosomal Regulation of Functional Rad9 Activities	131 – 139

<u>CHAPTER</u>	<u>PAGE No.</u>
1. INTRODUCTION (Continued)	
1.5 Project Brief: Research Background Aims and Objectives	140 – 150
1.5.1 <i>S. pombe</i>: A Versatile Eukaryotic Model Organism	140 – 144
1.5.2 The Initial Discovery of “spRad9-S”: A Novel spRad9 Variant	145 – 148
1.5.3 Ph.D. Experimental Aims and Objectives	149 – 150
2. MATERIALS AND METHODS	151 – 281
2.1 Sourced Materials – Purchase Details	152 – 161
2.2 Buffer Solutions – Composition and Function	162 – 166
2.2.1 Buffer Solution Details I: DNA Extraction, Purification and Analytical Sample Reagents	162
2.2.2 Buffer Solution Details II: TCA-Precipitated & Soluble Protein Sample Preparations	163
2.2.3 Buffer Solution Details III: 1D-PAGE, 2D-PAGE and Western Blot Analyses	164
2.2.4 Buffer Solution Details IV: Enzyme Storage and Reaction Media Compositions	165
2.2.5 Buffer Solution Details V: <i>S. pombe</i> Cre-Lox Base-Strain Transformation Reagents	166
2.2.6 Hoechst-Calcofluor Dual Fluorescence Stain Preparation	166
2.3 Media Composition and Function	167 – 168
2.3.1 Liquid Media Composition and Function: Broth Culture Preparations	167
2.3.2 Solid Media Composition and Function: Agar Culture Plate Preparations	168
2.4 <i>S. pombe</i> Genomic DNA Extraction Protocol	169 – 170

<u>CHAPTER</u>	<u>PAGE No.</u>
2. MATERIALS AND METHODS (Continued)	
2.5 Cre-Recombinase-Mediated Cassette Exchange Protocols	171 – 196
2.5.1 PCR Product Gel Purification Protocol	177 – 178
2.5.2 Donor pAW8-Experimental Rad9 Cassette Insert Plasmid Construction Protocols	179 – 187
2.5.2.1 Sph1 and SpeI Restriction Enzyme Digest Protocol	179
2.5.2.2 Ligation Protocol	180
2.5.2.3 α -Competent <i>E. coli</i> Cell Transformation Protocol	181
2.5.2.4 Miniprep Protocols	182 – 185
2.5.2.5 Restriction Digest Assay Verification of pAW8- <i>rad9</i> Plasmid Constructs	186 – 187
2.5.3 <i>S. pombe</i> Transformation Protocol	188 – 191
2.6 Initial “Cre-Lox”-Engineered <i>S. pombe</i> Strain Verification Assays	192 – 196
2.6.1 Selective Agar Media Phenotyping Assays	192
2.6.2 PCR Genotyping Assays	192
2.6.2.1 PCR Genotypic Verification of the $\Delta rad9$ Cre-RMCE “Base-Strain”	192
2.6.2.2 PCR Genotypic Verification of pAW8- <i>rad9</i> Base-Strain Cre-RMCE Transformants	192
2.6.3 DNA Sequence Verification of the “Cre-Lox” Engineered <i>S. pombe</i> Strains	193 – 195
2.6.4 Engineered <i>rad9</i> Gene Expression Verification	196
2.7 Preparation of <i>S. pombe</i> Genetic “Cross-Strain” Mutants	197 – 199

<u>CHAPTER</u>	<u>PAGE No.</u>
2. MATERIALS AND METHODS (Continued)	
2.8 Protein Sample Preparation and Analysis Protocols	200 – 233
2.8.1 Preparation and Analysis of TCA-Precipitated Total Protein Extracts	200 – 202
2.8.2 Preparation of Soluble Total Protein Extracts	203 – 213
2.8.2.1 Preparation and Analysis of Cytosolic and Nuclear Fractionated Protein Samples	206 – 208
2.8.2.2 Preparation and Analysis of Total Soluble Protein HPLC-SEC Fractionated Samples	209 – 210
2.8.2.3 Preparation and Analysis of Total Soluble Protein Co-IP “Pull-Down” Samples	211 – 213
2.8.3 Preparation of Total Protein Extracts for 2D-PAGE Analyses	214 – 222
2.8.3.1 Preparation of TCA-Precipitated Total Protein 2D-PAGE Samples	214 – 217
2.8.3.2 Preparation of Comparative Alkaline Phosphatase Digested 2D-PAGE Samples	218 – 222
2.8.4 1D SDS-PAGE Analytical Protocol	223 – 224
2.8.5 2D-PAGE Analytical Protocol	225 – 230
2.8.5.1 IPG Strip Rehydration : Active Protein Sample Uptake	225
2.8.5.2 IEF-PAGE: 1st Dimension Gel Electrophoresis	226 – 227
2.8.5.3 SDS-PAGE: 2nd Dimension Gel Electrophoresis	228 – 230
2.8.6 Western Blot Analytical Protocol	231 – 233
2.9 Acute and Chronic Survival Assay Protocols	234 – 252
2.9.1 Chronic Survival Assays – “Drop-Plate” Protocols	234 – 235
2.9.2.2 Acute Survival Assays	236 – 252
2.9.2.2(i) Acute U.V. Survival Assay	236 – 238
2.9.2.2(ii) Acute Survival Assays with Different Types of Genotoxic Compounds	239 – 252

<u>CHAPTER</u>	<u>PAGE No.</u>
2. MATERIALS AND METHODS (Continued)	
2.9.3 Lactose Synchronisation Assays	253 – 257
2.10 <i>In Silico</i> Analyses – Bioinformatics Software Tools Utilised	258 – 268
2.10.1 Protein Physico-Biochemical Property Estimations	258
2.10.2 Protein Secondary Structural Conformation Analyses	258
2.10.3 Protein Transmembrane-Spanning Domain Analyses	258
2.10.4 Protein Coiled-Coil Repeat Motif Analyses	259
2.10.5 Comparative Protein Sequence and Functional Motif Homology Alignments	259
2.10.6 Kinase-Specific Protein Phosphorylation Site Target Residue Predictions	260
2.10.7 Protein Aggregate Potential Motif Sequence Predictions	260
2.10.8 Protein Intrinsic Disorder Sequence Predictions	261 – 266
2.10.9 RNA Secondary Structure Folding Predictions	267 – 268

2.11 Materials and Methods Supplementary Appendices	269 – 281
Appendix 2.11.1: pAW1 Cre-Lox Non-Essential Gene Replacement Plasmid Maps	269 – 271
Appendix 2.11.2: pAW8 Cre-Lox Donor Gene Exchange Plasmid Maps	272 – 275
Appendix 2.11.3: PCR Primers – Sequence and Function	276
Appendix 2.11.4: pAW1 Plasmid PCR Fragment-Integrated <i>rad9</i> Gene Locus Map	277
Appendix 2.11.5: pAW8 Cre-Lox Donor <i>rad9</i> Gene Exchange Plasmid Constructs	278
Appendix 2.11.6: Pre-Constructed (Pre-Supplied) <i>S. pombe</i> Strains Utilised in this Study	279
Appendix 2.11.7: Constructed Full-Length, Truncated and Point-Mutated <i>rad9</i> Strains	280
Appendix 2.11.8: Cre-Lox Double-Mutant <i>S. pombe</i> Strains Constructed for this Study	281

<u>CHAPTER</u>	<u>PAGE No.</u>
<u>RESULTS CHAPTERS</u>	
3. Construction of Initial Experimental <i>S. pombe</i> Strains: Genotypic and Phenotypic Verification	282 – 357
3.1 Introduction	283 – 286
3.2 Creation of Experimental <i>S. pombe</i> Strains	280 – 307
3.2.1 Construction and Genotypic Verification of the “Cre-Lox” $\Delta rad9$ Base-Strain	292 – 297
3.2.2 Construction and Restriction Digest Verification of the pAW8 Donor Plasmid Set	298 – 307
3.3 Genotypic and Phenotypic Analyses of the Constructed Strains	308 – 313
3.4 <i>In Silico</i> Protein Stability Assessment of the Engineered <i>S. pombe</i> Rad9 Protein Variants	314 – 357
3.4.1 Intrinsic Structural Disorder Analyses	315 – 319
3.4.2 Anti- and Pro- Aggregation Functional Motif Analyses	320 – 330
3.4.3 Secondary Supra-Molecular Structural Motif Analyses	331 – 353
3.4.3.1 Transmembrane-Spanning Domain Analyses	332 – 339
3.4.3.2 Secondary Structural Repeat Motif Domain Analyses	340 – 350
3.4.3.3 Helix, Strand and Coil Secondary Structural Motif Analyses	351 – 353
3.4.4 Correlated <i>In Silico</i> Data Analyses: A Comparative Review of the Critical Structure-Stability Relationships Identified Within the Engineered Full-Length and Truncated <i>S. pombe</i> Rad9 Isoformic Variants	354 – 357

<u>RESULTS CHAPTERS (Continued)</u>	<u>PAGE No.</u>
4. Supportive Experimental Evidence for the Expression of Novel Truncated Type Variants of the <i>S. pombe</i> Rad9 Protein	358 – 439
4.1 Introduction	359 – 364
4.2 Induced Expression of “Rad9-S” is a Specific Cytological Response to Hyperthermic Stress	365 – 370
4.3 The Truncated “Rad9-S” Protein Variant is an Alternative Translational Product that Originates From the Internal AUG Initiation Codon Situated at Methionine 50 and Whose Expression is Independent of Intron1 Retention Within the Transcribed <i>S. pombe rad9</i> mRNA	371 – 374
4.4 <i>In Silico</i> RNA Folding Analyses of the Untranslated Regions Within the <i>S. pombe rad9</i> Gene Reveal that the 3’-UTR May Be Implicated in Hyperthermically-Induced Expression of The Truncated “Ra9-S” Protein Variant	375 – 378
4.5 The Amino Acid Encoded mRNA M1-S49 Spanning Region of the <i>S. pombe rad9</i> Gene May Be Implicated in the Hypothermic Suppression of Truncated “Rad9-S” Protein Variant Expression	379 – 391
4.6 Heat Induction of “Rad9-S” is Restricted to Actively Cycling Cells	392 – 393
4.7 Impaired Formation and DNA Clamp-Loading of the “9-1-1” Complex Does Not Induced Expression of the “Rad9-S” Truncated Protein Variant	394 – 396
4.8 Comparative 2D PAGE-Coupled Western Blot Analyses Reveal the Expression of Additional Novel Truncated Rad9 Isoforms Within <i>S. pombe</i>	397 – 401
4.9 <i>In Silico</i> Elucidation of Hypothetically Feasible Mechanisms of Expression of the Truncated “Rad9-VS” and “Rad9-T” Isoforms	402 – 417
4.9.1 Intron-Retained <i>S. pombe rad9</i> mRNA Transcripts are Unlikely to be Implicated in the Expression of the “Rad9-T” Truncated Isoform	404 – 406
4.9.2 A Limited-Proteolytic Cleavage Mechanism May Be Implicated in the Expression of the Truncated “Rad9-T” Isoform	407 – 417
4.10 <i>In Silico</i> Protein Stability Assessment of the Hypothetically Predicted Amino Acid Sequences of the Detected <i>S. pombe</i> Rad9 Isoforms – “Rad9-S”, “Rad9-VS” and “Rad9-T” and Undetected Metacaspase-Mediated Limited-Proteolytic Rad9 Cleavage Products	418 – 434

<u>RESULTS CHAPTERS (Continued)</u>	<u>PAGE No.</u>
4. Supportive Experimental Evidence for the Expression of Novel Truncated Type Variants of the <i>S. pombe</i> Rad9 Protein (continued)	358 – 439
4.10.1 <i>In Silico</i> Predictive Intrinsic Structural Disorder Analyses	419 – 421
4.10.2 <i>In Silico</i> Predictive Aggregation and Protease Susceptibility	422 – 426
4.10.3 <i>In Silico</i> Predictive Coil, Helix and Strand Secondary Structural Sub-Type Motif Content	427 – 429
4.10.4 Correlated <i>In Silico</i> Data Analyses: A Comparative Review of the Critical Structure-Stability and Potential Functional Viability Relationships Identified Within the Full-Length Rad9 Protein and Truncated <i>S. pombe</i> Rad9 Isoforms	430 – 434
4.11 A Complex Signalling Network May Regulate the Levels of Expression and Functional Activities of the <i>S. pombe</i> Rad9 Isoforms in Selective Checkpoint Responses to Specific Types of Genotoxic and Environmental Cytological Stresses	435 – 439

<u>RESULTS CHAPTERS (Continued)</u>	<u>PAGE No.</u>
5. Functional Viability Assessment of the Engineered <i>S. pombe</i> Rad9 Protein Variants	440 – 481
5.1 Introduction	441
5.2 Comparative <i>In Silico</i> Functional Viability Analyses of the Engineered Full-Length and Truncated <i>S. pombe</i> Rad9 Protein Variants	442 – 454
5.3 Exclusive Expression of the Engineered Truncated Rad9 Variants Enhances Cellular Sensitivity to Various Types of Induced Genotoxic and Environmental Stresses	455 – 470
5.4 Distinctive Phosphoisoform Profiles of the “Rad9-S” Truncated Protein Variant are Generated in Cellular Responses to Specific Types of Induced Genotoxic Stresses	471 – 474
5.5 The Identification of the M50-M74 Domain as a Potential Key Functional Component of Protective “Rad9-S”- Mediated Cellular Responses Against Camptothecin-Induced DNA Damage	475 – 481

<u>RESULTS CHAPTERS (Continued)</u>	<u>PAGE No</u>
6. Genetic and Biochemical “Deciphering” of Differential “Rad9-S” – Initiated Checkpoint Responses to Camptothecin-Induced DNA Damage and Hyperthermic Thermal Stress	482 – 663
Introduction	483 – 484
6.1 The top1 Gene is Not Suppressed Within Engineered <i>S. pombe</i> Cells that Exclusively Express the Truncated “Rad9-S” Protein Variant	485 – 488
6.2 Component G2-M Cell Cycle Checkpoint Pathway Inputs	489 – 555
6.2.1 Hus1 is a Critical Clamp Protein Sub-Unit Component of the “Rad9-S”-Mediated Checkpoint Response to Camptothecin-Induced DNA Damage, in Which Rad1 and Rad17 are Not Implicated	493 – 515
6.2.2 The Rad3:Rad26 Heterodimeric DNA-Associated Complex is a Critical Functional Component of the “Rad9-S”-Mediated Checkpoint Response to Camptothecin-Induced Genotoxicity	516 – 531
6.2.3 Mrc1 is a Critical Mediator Component of the “Rad9-S”-Initiated Response to Camptothecin-Induced DNA Damage in Which Neither Crb2 or Rad4 are Implicated	532 – 538
6.2.4 Cds1 is a Critical Secondary (Distal) Transducer/Effector Kinase Component of the “Rad9-S”-Mediated Checkpoint Response to Camptothecin-Induced DNA Damage, in Which the Suppression of Chk1 Functional Activity May Be Implicated	539 – 546
6.2.5 Hhp1 is a Critical Effector Kinase Component Which May Be Implicated in the Temporal Cell Cycle Phasic Co-Ordination and Functional Activity Regulation of the “Rad9-S”-Mediated Checkpoint Response to Camptothecin-Induced Genotoxicity	547 – 550
6.2.6 Cdc25 and Rad24 May Modulate the Phosphoisoform-Specific Functional Activities of the Truncated “Rad9-S” Protein	551 – 555
6.3 Component MAP Kinase Cell Cycle Checkpoint Pathway Inputs	556 – 567
6.4 Component Spindle Checkpoint Inputs	568 – 583
6.5 Component FEAR Network Pathway Inputs	584 – 587
6.6 Differential Checkpoint Responses to Camptothecin-Induced DNA Damage and Hyperthermic Stress are Initiated by “Rad9-S”	588 – 597

<u>RESULTS CHAPTERS (Continued)</u>	<u>PAGE No</u>
6. Genetic and Biochemical “Deciphering” of Differential “Rad9-S” – Initiated Checkpoint Responses to Camptothecin-Induced DNA Damage and Hyperthermic Thermal Stress (continued)	482 – 663
6.7 Caffeine Significantly Potentiates the Sensitivity of <i>S. pombe</i> Cells “Cre-Lox” Engineered for the Exclusive Expression of the truncated “Rad9-S” variant to Camptothecin-Induced DNA Damage and Hyperthermic Stress: Potential Indications of Equivalent Novel Human Rad9B Functional Checkpoint Checkpoint Signalling Responses	598 – 625
Appendix 6.1: Journal of Cell Science Publication (Editor and Referee Panel Accepted – <i>In Press</i>)	626 – 663
“Heat Induction of a Novel Rad9 Variant From a Cryptic Translation Initiation Site Reduces Mitotic Commitment”	
Simon Janes, Ulrike Schmidt, Nadja Ney, Susanna Concilio, Mohamed Zekri and Thomas Caspari	
[Electronic Publication Ahead of Print 13th July 2012]	

<u>RESULTS CHAPTERS (Continued)</u>	<u>PAGE No</u>
7. Experimental Evidence for Functional Roles of “Rad9-S” in DNA Repair	664 – 689
7.1 Introduction	665 – 669
7.2 Rad16 Endonuclease and DNA Ligase IV are Critical Components that are Functionally-Implicated in the DNA Repair Mechanism Mediated by the Heterodimeric “Rad9-S”：“Hus1-C” Complex in Response to Camptothecin-Induced Genotoxicity	670 – 675
7.3 Rqh1 Helicase is Not Functionally Implicated in the DNA Repair Mechanism Mediated by the Heterodimeric “Rad9-S”：“Hus1-C” Complex in Response to Camptothecin-Induced Genotoxicity	676 – 680
7.4 The Heterodimeric “Rad9-S”：“Hus1-C” Complex May Elicit a Novel DNA Repair Pathway for the Rectification of Double-Stranded Breaks Induced by Camptothecin	681 – 689
8. Evaluative Discussion	690 – 697
8.1 Critical Appraisal of the Experimental Data	691 – 692
8.2 Future Implications in the Clinical Management of Cancer	693 – 697
REFERENCES	698 – 790
Journal and Bibliographical Citations	698 – 785
Utilised Internet Website Resources	786 – 790

ABBREVIATIONS

A = Adenine

ACS = American Cancer Society

Amp = Ampicillin

APC/C = Anaphase Promoting Complex/Cyclosome

APE1 = Apurinic/Apyrimidinic Endonuclease 1

APS = Ammonium Persulphate

AP-1 = Transcription Factor

Aq = Aqueous

AR = Androgen Receptor

ATM = Ataxia Telangiectasia Mutated

ATR = ATM and Rad3-Related

ATRIP = ATR-Interacting Protein

ATRMBC = Anthracycline- and Taxane- Refractory Metastatic Breast Cancer

BER = Base Excision Repair

BRCA1 = Breast Cancer Associated Protein 1

BRCT = BRCA1 C-Terminus Domain

Bub = Budding Uninhibited by Benzimidazoles

CAD = Carbamoyl Phosphate Synthetase/Aspartate Transcarbamoylase/Dihydroorotase

CAFF = Caffeine

CDK = Cyclin-Dependent Kinase

CDKI = Cyclin-Dependent Kinase Inhibitor

CENP-E = Centromere Protein E

CHK1 = Centrosome-Associated Checkpoint Kinase 1

CHK2 = Centrosome-Associated Checkpoint Kinase 2

CHX = Cycloheximide

c-Jun = Oncoprotein and Sub-Unit of the AP-1 Transcription Factor

Co-IP = Co-Immunoprecipitation

cMet = MET or MNNG HOS Transforming Gene

CPC= Chromosomal Passenger Complex

CPT = Camptothecin

Cre-RMCE = Cre-Recombinase Mediated Cassette Exchange

CSN = COP9 Signalosome Complex

CSN5 = COP9 Signalosome Complex Sub-Unit 5 (also known as Jab1)

dATP = 2'-Deoxyadenosine-5'-Triphosphate

dCTP = 2'-Deoxycytidine-5'-Triphosphate

DDK = Dbf4-Dependent Kinase

ddH₂O = Distilled/Deionised H₂O

ddNTPs = 2', 3'-Dideoxyribonucleotide-5'-Triphosphates

dGTP = 2'-Deoxyguanine-5'-Triphosphate

DMSO = Dimethylsulphoxide

DNAJC7 = (also known as TPR2)

dNTPs = 2'-Deoxyribonucleotide-5'-Triphosphates

DSB's = Double-Stranded DNA Breaks

DsDNA = Double-Stranded DNA

dTTP = 2'-Deoxythymidine-5-Triphosphate

EDTA = Ethylenediaminetetraacetate

ELP = Ellipticine

EMM = Edinburgh Minimal Medium

EtOH = Ethanol

ETP = Etoposide

EUROSCARF = EUROpean Saccharomyces Cerevisiae ARchive for Functional analysis

FEAR = Cdc-Fourteen Early Anaphase Release

FEN 1 = Flap Endonuclease 1

5-FOA = 5-Fluoro-orotic Acid

GC = Gene Conversion

GGR = Global Genomic Repair

HA = Haemagglutinin Epitope Affinity Tag

HGFR = Hepatocyte Growth Factor Receptor

hMYH1 = Human Mut Y Glycosylase Homologue 1

hOGG1 = Human 8-Oxoguanine Glycosylase I

hRad1 = Human Rad1 Protein

hRad9 = Human Rad9 Protein

H₂O₂ = Hydrogen Peroxide

HPLC = High-Performance Liquid Chromatography

HPLC-SEC = High-Performance Liquid Coupled Size-Exclusion Chromatography

HR = Homologous Recombination

HRP = Horse Radish Peroxidase

HRR = Homologous Recombination Repair

HSP = Heat-Shock Protein

HU = Hydroxyurea

Hus = Hydroxyurea Sensitive

hHus1 = Human Hus1 Protein

IARC = International Agency for Research on Cancer

IEF = Isoelectric Focusing

INCENP = Inner Centromere Protein

IRES = Internal Ribosome Entry Segment

I.R. = Ionising Radiation

IUPred = Intrinsically-Unstructured Prediction

Jab1 = Jun-Activating Binding Protein 1 (also known as CSN5)

JNK = c-Jun N-Terminal Kinase

[XXXXV]

kBp = Kilobase-pair

kDa = Kilodalton

Lact = Lactose

LB = Luria Base Medium

Leu = Leucine

LFA1 = Integrin/Adhesion Receptor 1

LHR = G-Coupled Lutropin Choriogonadotropin Receptor

LiAc = Lithium Acetate

LiAc-TE = Lithium Acetate-Tris-EDTA

Lig I = DNA Ligase I

Lig IV = DNA Ligase IV

LP-BER = Long-Patch Base Excision Repair

Mad = Mitotic Arrest Deficient

MAPK = Mitogen-Activated Protein Kinase

MCC = Mitotic Checkpoint Complex

MDN = Menadione

MEN = Mitotic Exit Network

MeOH = Methanol

MIF1 = Cytokine Macrophage Migration Inhibitory Factor 1

Mit C = Mitomycin C

MLH1 = Mut L Homologue 1

MMEJ = Microhomology-Mediated End-Joining

MMR = Base Mis-Match Repair

MMS = Methylmethanesulphonate

MNNG = 4-Methyl-N'-Nitro-N-Nitrosoguanidine

Mps1 = Monopolar Spindle Kinase 1

MRN = Mre11-Rad50-Nbs1 Complex

MSH2 = Mut S Homologue 2

MSH3 = Mut S Homologue 3

MSH6 = Mut S Homologue 6

MW = Molecular Weight

NΔX-Rad9-c3xHA = Rad9 1st X N-Terminal Amino Acids Deleted HA Epitope-Tagged

NEIL1 = Endonuclease VIII-Like Protein 1

NEKs = Never-in-Mitosis *Aspergillus*-Like Kinases

NER = Nucleotide Excision Repair

NES = Nuclear Exclusion Signal Sequence

NHEJ = Non-Homologous End-Joining

NLS = Nuclear Localisation Signal Sequence

4-NQO = 4-Nitroquinoline-1-Oxide

PAGE = Polyacrylamide Gel Electrophoresis

2D-PAGE = Two-Dimensional Polyacrylamide Electrophoresis

PCNA = Proliferating Cell Nuclear Antigen

PEG = Polyethyleneglycol

Ph = Phenol

Phleo = Phleomycin

Phos = Phosphorylated

pI = Isoelectric Point

PIP = PCNA-Interacting Peptide Motif

PLK1 = Polo-Like Kinase 1

Polβ = DNA Polymerase β

Polδ = DNA Polymerase δ

Polε = DNA Polymerase ε

Polη = DNA Polymerase η

Polζ = DNA Polymerase ζ

prDOS = Predicted Disorder of Structure

PRMT5 = Protein Arginine Methyltransferase 5

PR = Progesterone Receptor

p27/Kip1 = p27/Kip1 CDK Inhibitor

Rad = Radiation Sensitive

Rad9 = Full-Length Rad9 Protein

Rad9-3xHA = C-terminal (HA)₃-Tagged Full-Length Rad9

Rad9 Δ Intron1-3xHA = C-terminal (HA)₃-Tagged Deleted Intron1 Full-Length Rad9

Rad9-(M50A)-c3xHA C-terminal (HA)₃-Tagged Alanine 50 Full-Length rad9 Mutant

Rad9-(M50L)-c3xHA C-terminal (HA)₃-Tagged Leucine 50 Full-Length rad9 Mutant

Rad9-S = N-Terminal Truncated Short Rad9 Protein Variant

Rad9-S-3xHA = C-terminal (HA)₃-Tagged N-Terminal Truncated Short Rad9 Protein Variant

RHINO = Rad9-Rad1-Hus1 Interacting Orphan Protein

RNR = Ribonucleotide Reductase

RPA = Replication Protein A

SAC = Spindle Assembly Checkpoint

SDS = Sodium Dodecylsulphate

SEC = Size-Exclusion Chromatography

SNP = Sodium Nitroprusside

Skp1 = S-Phase Kinase-Associated Protein 1

Sorb = Sorbitol

SP-BER = Short-Patch Base Excision Repair

SRC-1 = Steroid Receptor Co-Activator 1

SSA = Single-Stranded Annealing

SSB's = Single-Stranded DNA Breaks

ssDNA = Single-Stranded DNA

STS = Sodium Thiosulphate

TAE = Tris-Acetic Acid-EDTA

TAOs = Thousand-and-One Kinases

TBE = Tris-Boric Acid-EDTA

TBH = Tert-Butyl-Hydroperoxide

TBZ = Thiabendazole

TCA = Trichloroacetic Acid

TCR = Transcription-Coupled Repair

TDG = Thymine Dimer Glycosylase

TE = Tris-EDTA

TEMED = N,N,N',N' – Tetramethylethylenediamine

TIM1 = Timeless 1

TIPIN = TIM1-Interacting Protein

TLK1 = Tousled-Like Kinase 1

TLK1B = Tousled-Like Kinase 1B

TLS = Translesion Synthesis

TPR = Tricopeptide Repeat Peptide Motif

TPR2 = Tricopeptide Repeat Protein 2 (also known as DNAJC7)

TopBP1 = Topoisomerase II Binding-Protein 1

Top1 = Topoisomerase I

Top2 = Topoisomerase II

Topo II = Topoisomerase II

U = Uracil

UTR = Un-Translated Region

U.V. = Ultra-Violet

WHO = World Health Organisation

WRN = Werner Syndrome Protein

YEA = Yeast Extract Adenine-Rich Medium

Chapter 1

Introduction

[1]

1.1 Human Rad9: A Viable Anti-Cancer Chemotherapeutic Target

Cancer is of paramount medical concern as an increasingly major contributor of disease-related fatalities throughout the world, which has prompted extensive research focused upon the progressive development of novel therapeutics with significantly improved pharmacological efficacy and markedly reduced toxicity-related side-effects.

Statistical and stochastic analyses of clinical data, derived from a variety of epidemiological studies, indicate that one in three people will be diagnosed with cancer at some stage of their lives and one in four of these patients will die as a consequence of their particular neoplastic-associated condition. (American Cancer Society, 2011; IARC, 2011; WHO, 2011).

The pathophysiological aetiology of cancer encompasses a diverse collection of systemically-related disease conditions, ranging through a progressive series of pre-, intermittent- and post-neoplastic cytological states and origins with distinctive “biochemical signatures” (defined in Fig 1.1, p.5; Fig 1.9, p.16), which culminate in the manifestation of specific benign and malignant tumour sub-types – defined in Table 1.1, p.3 (Pecorino L., 2008; Weinberg R.A., 2006).

The mechanism of carcinogenesis, implicated in the pathophysiological transformation from normal, to relatively benign and later aggressive, malignant cytological status, may be fundamentally regarded as an integral, systemic multi-stage process comprised of four key phases, notably; Initiation, Promotion, Progression through to Evolution to metastatic and/or multiple drug resistant morphological phenotypes (Fig 1.9, p.16).

These four key phases are orchestrated via a cumulative complex interactive network of genetic, epigenetic and proteomic biochemical events (Fig 1.1, p.5; Fig 1.9, p.16) which are triggered via adverse combinations of acute and chronic lifestyle risk-related factors.

Typical carcinogenic-associated risk factors include; age, sex, genetic/biochemical pre-dispositions, diet, metabolism, obesity, smoking, alcohol/drug abuse and relative acute/chronic exposure to various genotoxic and epigenetic toxins, ionising and non-ionising radiation sources which may be manifested in the form of pollutants, food additives, drugs/xenobiotics, household and a wide variety of different types of industrial/workplace-related materials/products – to name but a few examples! (Boelsterli U.A., 2007; Janes S.R.C., 2006; Klaassen C.D., 2008; Matzke M.A. *et al.*, 1999; Simons J.W., 1999; Sugimara T. and Ushijima T., 2000; Timbrell J.A., 2008).

[2]

Table 1.1: Characteristic Features of Benign & Malignant Tumours

[Compiled via Collated Information From: Pecorino L., 2008; Weinberg R.A., 2006]

BENIGN	MALIGNANT
Often encapsulated	Rarely encapsulated and encapsulation is often incomplete when present
Non-invasive and remain localised absence of metastatic capability	Invasive with tendency to form secondary bodies with latent metastatic potential
Well differentiated with retained close resemblance to the cells of origin	Poorly differentiated with diminished resemblance to cells of origin and in some cases completely undifferentiated
Cells/nuclei of uniform size/appearance	High incidence of variance in cell size and nuclei appearance Nuclei often hyperchromatic
Mitotic figures relatively rare or absent	Prevalent incidence of mitotic figures
Low or absent incidence of anaplasia	High incidence of varying degrees of anaplasia
Relatively rare incidence of degenerative transformations	Relatively high incidence of degenerative transformations
Relatively slow/passive growth	Relatively rapid/aggressive growth

Benign tumours are not regarded as truly cancerous, in the strictest medical sense, as a consequence of the fact that they are typically comprised of relatively restrictive, slow-growing groups of well-differentiated cells which only proliferate locally within well-defined boundary edges, often encapsulated in fibrous sheath type matrices which limits their invasive capacity (Pecorino L., 2008; Weinberg R.A., 2006).

[In the majority of benign cases it is possible to accomplish complete eradication of the manifested neoplastic pathophysiological condition via surgical removal of the tumour in conjunction with “follow-up” radio and/or chemo-therapeutic treatments]

Conversely, malignant tumours are clinically defined as truly cancerous conditions as a consequence of the fact that they are typical comprised of poorly-differentiated, rapidly-dividing cells which possess the capability to metastasise and invade neighbouring tissues (Pecorino L., 2008; Weinberg R.A., 2006).

[In the majority of malignant cases it is relatively difficult to accomplish complete eradication of the manifested neoplastic pathophysiological condition as a consequence of the aggressive morphological nature of the tumour cells concerned, which enables them develop multiple drug resistance to a wide range of chemotherapeutics and to eventually spread throughout the body via the lymphatic system with consequential fatal prognosis for the patient]

The human Rad9 protein exists in two main forms, designated Rad9A and Rad9B (Dufault V.M. *et al.*, 2003; Ishikawa K. *et al.*, 2006; Leloup C. *et al.*, 2010; Lieberman H.B. *et al.*, 2006; Lieberman H.B. *et al.*, 2011) – which can also be expressed as several smaller isoforms (Fig 1.3, p.9).

Elevated levels of expression of the human Rad9 protein isoforms A and B (Fig 1.3, p.9) have also been identified in tumour cells originating from a variety of different tissue types, which in some cases has been demonstrated to strongly correlate with hypermethylation of introns 1 and/or 2 within the *hRAD9* gene (Fig 1.7, p.13; Fig 1.8, p.14; Table 1.2, p.15).

Suppressed expression of human Rad9A has also been correlated directly with the increased incidence and progressive development of a variety of different childhood and independent secondary cancers (Weis E. *et al.*, 2011).

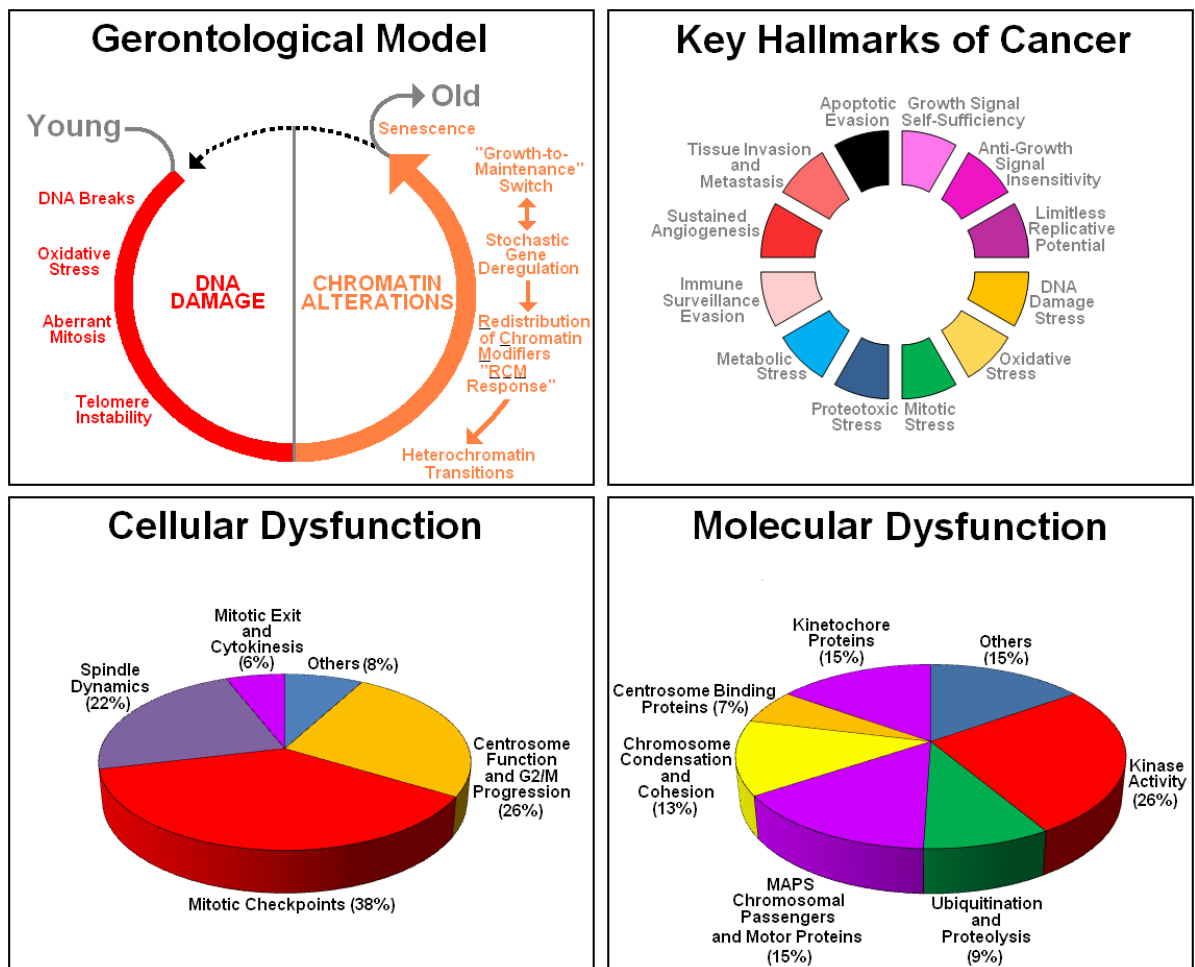
The human Rad9 protein exhibits a versatile array of functions which modulate the activity of specific cell cycle genetic, epigenetic and proteomic biochemical events (Broustas C.G. and Lieberman H.B., 2012; Ishikawa K. *et al.*, 2006; Lieberman H.B., 2006; Lieberman H.B. *et al.*, 2011; Marquardt J.U. *et al.*, 2012) and may thus also impinge upon the four key developmental phases of carcinogenesis - Fig 1.1, p.5; Fig 1.2, p.8; Fig 1.9, p.16.

The “Rad1/Hus1-Dependent” functions of human Rad9 rely critically upon the formation of the Rad9-Rad1-Hus1 toroidal, heterotrimeric PCNA-like DNA sliding clamp which acts as both a DNA damage sensor and a recruitment platform for various signalling proteins and DNA repair factors whose respective docking interactions involve the highly flexible C-terminal tail domain of the Rad9 protein which is situated outside of the Rad9-Rad1-Hus1 complex (Ishikawa K. *et al.*, 2006; Lieberman H.B. *et al.*, 2006; Lieberman H.B. *et al.*, 2011) – Fig 1.2, p.8.

In addition to DNA damage detection, a variety of other key “Rad1/Hus1-Dependent” human Rad9 functions have been identified – notably; DNA Damage Checkpoint Activation, Specific DNA Repair Pathway Selection and Activity Modulation, Cell Cycle Phase-Specific Activity Modulation, Androgen Receptor Activity Modulation and Protein Chaperone Activity Modulation, via specific Rad9-Tpr2 regulatory protein interactions (Ishikawa K. *et al.*, 2006; Lieberman H.B. *et al.*, 2006; Lieberman H.B. *et al.*, 2011; Wang L. *et al.*, 2004; Xiang S-L. *et al.*, 2001) – Fig 1.2, p.8.

Fig 1.1: Key Factors Implicated in the Promotion of Carcinogenesis

[Compiled via Collated Information from: Chiarugi V. *et al*, 1994; Luo J. *et al*, 2009; Perez de Castro *et al*, 2007; Sinclair D.A. and Oberdoerffer P., 2009



“Nucleocentric” mechanisms of carcinogenic induction are encompassed in the gerontological model (Top Left Figure), in which initial DNA damage-driven alterations in chromatin supra-molecular structure promote senescence and ageing, in conjunction with propagated accumulation of further genotoxic and/or epigenetic events which are amplified during successive cell cycle rounds (Sinclair D.A. and Oberdoerffer P., 2009)

Reversible chromatin alterations implicated in the gerontological model, which are not a consequence of genomic aberrations, may “re-program” the “epigenomic clock” to a younger cytological transformation status (Sinclair D.A. and Oberdoerffer P., 2009).

There are 12 essential hall-marks of cancer (Top Right Figure) which may be classified into three major categories, notably; Dysregulated Cellular Growth, Stress Factor-Induced Genomic Instability (Metabolic Stress, Oxidative Stress, Proteotoxic Stress, Mitotic Stress, DNA Damage Stress and DNA Replication Stress) and Dysfunctional Immunosurveillance (Denoyelle C. *et al*, 2006; Hanahan D. and Weinberg R.A., 2000; Hanahan D. and Weinberg R.A., 2011; Kroemer G. and Pouyssegur J., 2008; Luo J. *et al*, 2009; Papp B. *et al*, 2003; Whitesell L. and Linqvist S.L., 2005).

Mitotic alterations implicated in carcinogenesis may be classified in two major categories, notably; Dysfunctional Cellular Events (Bottom Left Figure) and Dysfunctional Biomolecular Events (Bottom Right Figure) that constitute the main “biochemical triggers” which initiate the progressive transformation to neoplastic cytological status – centrosomal and checkpoint protein kinases are of particular prevalence in this context (Perez de Castro L. *et al*, 2007).

The human Rad9 protein has multi-functional roles which impinge on the regulated activity of the majority of the cellular events summarised in the figures above and thus may also exert significant oncogenic potential (Broustas C.G. and Lieberman H.B., 2012; Lieberman H.B. *et al*, 2011).

Several “Rad1/Hus1” – Independent functions of human Rad9, which do not require formation of the Rad9-Rad1-Hus1 complex, have also been identified – notably; Apoptotic Activity Modulation and Pyrimidine Nucleotide Biosynthetic Activity Modulation, via specific regulatory Rad9-CAD protein interactions (Komatsu K. *et al*, 2000; Lieberman H.B. *et al*, 2011; Lee M.W. *et al*, 2003; Lindsey-Boltz L.A. *et al*, 2004; Yin Y. *et al*, 2004; Yoshida K. *et al*, 2002) – Fig 1.2, p.8.

Whilst the multiple functions of the human Rad9A protein have been extensively studied, comparatively little is known about the specific functions of the human Rad9B protein paralogue and its smaller isoforms (Fig 1.3, p.9).

However, very recent experimental studies indicate that the human RadB protein paralogue may be functionally implicated in novel phasic G1-S transitional arrest type cell cycle checkpoint responses to nucleolar stress, which are mediated via both ATR- and JNK- kinase signalling cascade pathways (Pérez-Castro A.J. and Friere R., 2012).

Two isoforms of the human Hus1 protein, designated Hus1A and Hus1B (Hang H. *et al*, 2002), have also been identified (Fig 1.4, p.10) which has led to the deductive hypothesis that four potential Rad9-Rad1-Hus1 complex isoforms may exist that perform critically distinctive functional roles in specific cellular responses to replication stress and DNA damage (Dufault V.M. *et al*, 2003) – Fig 1.5, p.11 .

Loading of The Rad9-Rad1-Hus1 complex onto DNA is accomplished via the Rad17:Rfc2-5 complex (discussed later in detail in Section 1.2.1, pp.23-32).

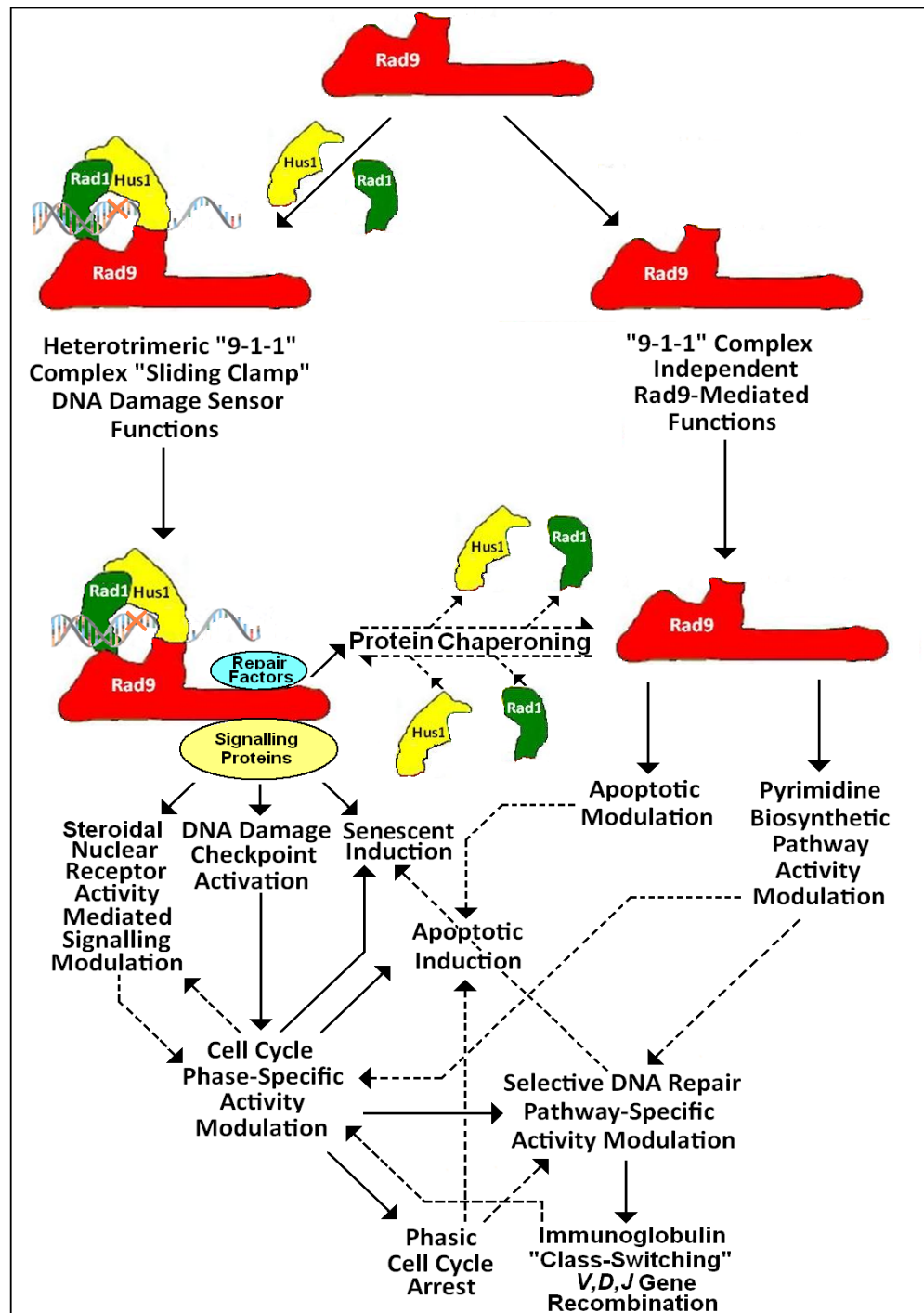
Intriguingly, four isoforms of the human Rad17 protein have also been identified (Fig 1.6, p.12) and thus it is conceivable to hypothesise that four isoforms of the Rad17:Rfc2-5 clamp-loading complex may exist, each of which interacts with and loads a specific isoform of the Rad9-Rad1-Hus1 complex onto DNA in response to distinctive types of replication stress and/or DNA damage (Fig 1.5, p.11).

Human Rad9 is considered to be a particularly valid choice of potential anti-cancer chemotherapeutic target by the advantageous virtue of the fact that it acts both as a key interactive DNA damage sensory initiator component at the very start of various cell cycle checkpoint signalling cascades and as a multi-functional associative recruitment platform which modulates the activity of a diverse range of different proteins and repair factors implicated in the DNA damage response and other related biological processes (Broustas C.G. and Lieberman H.B., 2012; Ishikawa K. *et al.*, 2008; Lieberman H.B., 2008; Lieberman H.B. and Zhu A., 2010; Lieberman H.B. *et al.*, 2011) – Fig 1.2, p.8.

Thus, the respective pharmacological efficacies of Rad9 activity-targeted anti-cancer chemotherapeutic strategies (discussed at the end of this section, pp.17-22) are far less likely to be negated/circumvented via alternative pathway selection by-pass effects (Broustas C.G. and Lieberman H.B., 2012; De Palma M. and Hanahan D., 2012; Ishikawa K. *et al.*, 2008; Lieberman H.B., 2008; Lieberman H.B. and Zhu A., 2010; Lieberman H.B. *et al.*, 2011).

As is the case for specific checkpoint kinase inhibitors due to the fact that the pharmacologically-targeted proteins are functionally-implicated in a wide variety of down-stream cell cycle signalling cascades which comprise a number of complex, inter-communicative “cross-talk” regulatory pathways (Garrett M.D. and Workman P., 1999; Workman P., 2004; Yap T.A. *et al.*, 2010).

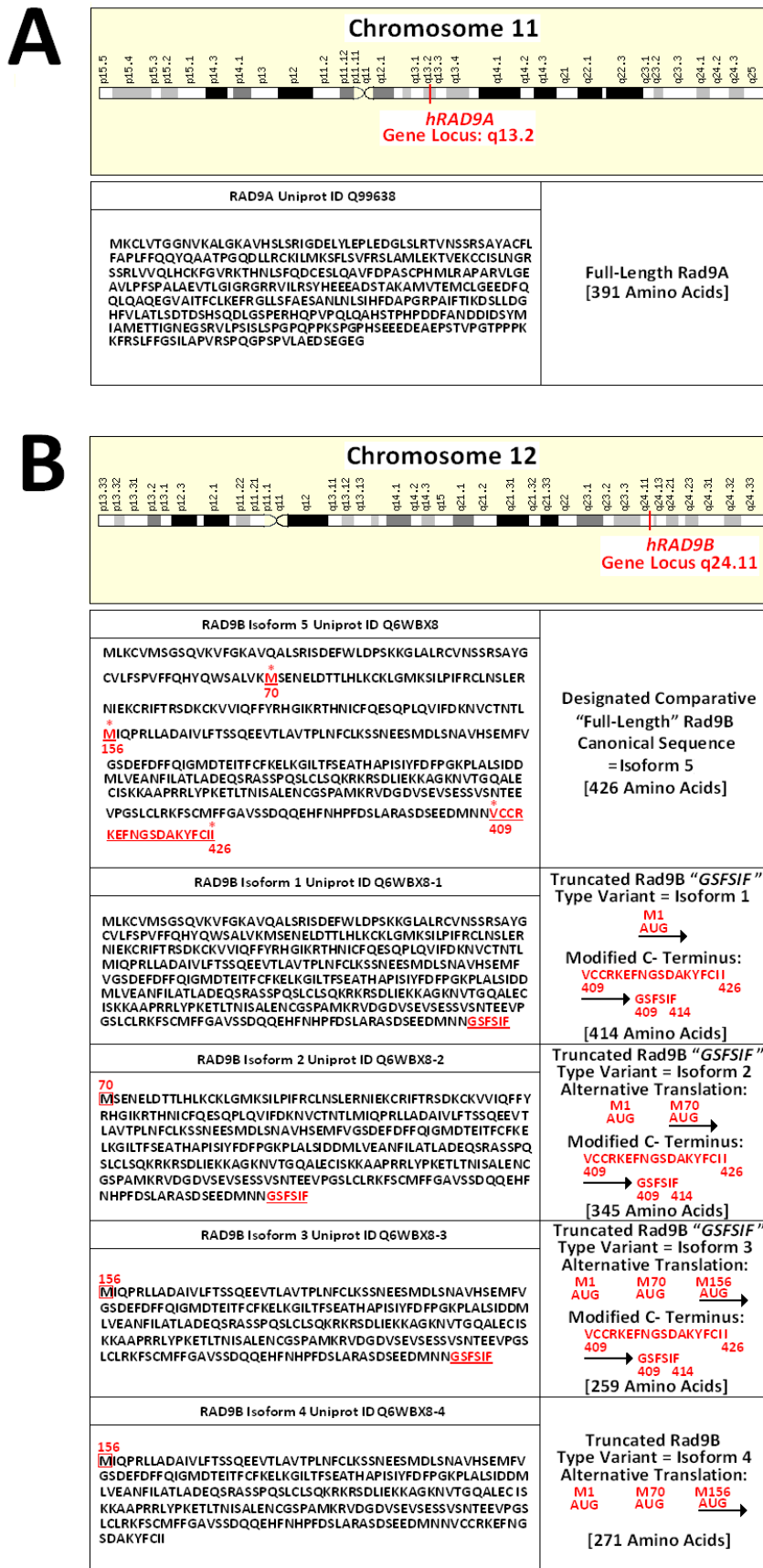
Fig 1.2: Summarised Overview of Human Rad9 Functions



Human Rad9 is an evolutionary conserved, multi-functional protein which spans a diverse range of activity-modulatory roles in a variety of fundamental biomolecular processes that can be categorized into two major groups – notably; “9-1-1” Complex-Dependent Functions & “9-1-1” Complex-Independent Functions (An L. *et al*, 2010; Broustas C.G. and Lieberman H.B., 2012; Deshpande A.M. *et al*, 2011; Ishikawa K. *et al*, 2006; Komatsu K. *et al*, 2000; Lee M.W. *et al*, 2003; Lieberman H.B. *et al*, 2006; Lieberman H.B. *et al*, 2011; Lindsey-Boltz L.A. *et al*, 2004; Saberi A. *et al*, 2008; Wang L. *et al*, 2004; Xiang S-L. *et al*, 2001; Yin Y. *et al*, 2004; Yoshida K. *et al*, 2002).

[Solid arrows denote the specific “9-1-1” Complex-Dependent & “9-1-1” Complex-Independent Functions, whilst dashed arrows denote the potential inter-communicative pathways between the various functions which may act as an additional “cross-talk” network for regulation of specific free- and Rad1/Hus1-associated Rad9 activities implicated in the preservation of cellular genomic integrity]

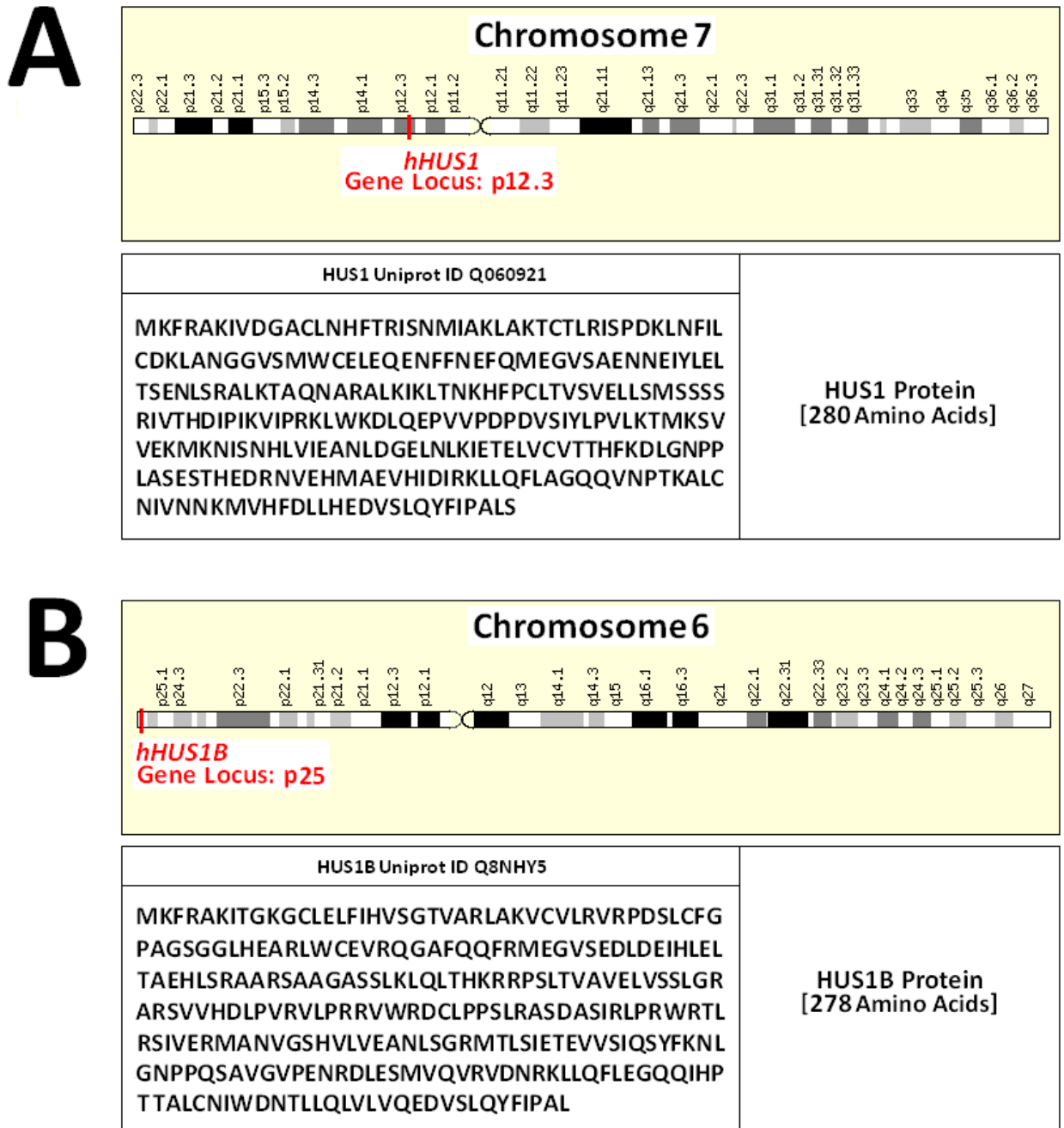
Fig 1.3: *hRAD9A* and *hRAD9B* Gene Locus Sites & Protein Sequences



A: *hRAD9A* Genetic Data Resource: <http://www.uniprot.org/uniprot/Q99638>

B: *hRAD9B* Genetic Data Resource: <http://www.uniprot.org/uniprot/Q6WBX8>

Fig 1.4: *hHUS1* and *hHUS1B* Gene Locus Sites & Protein Sequences

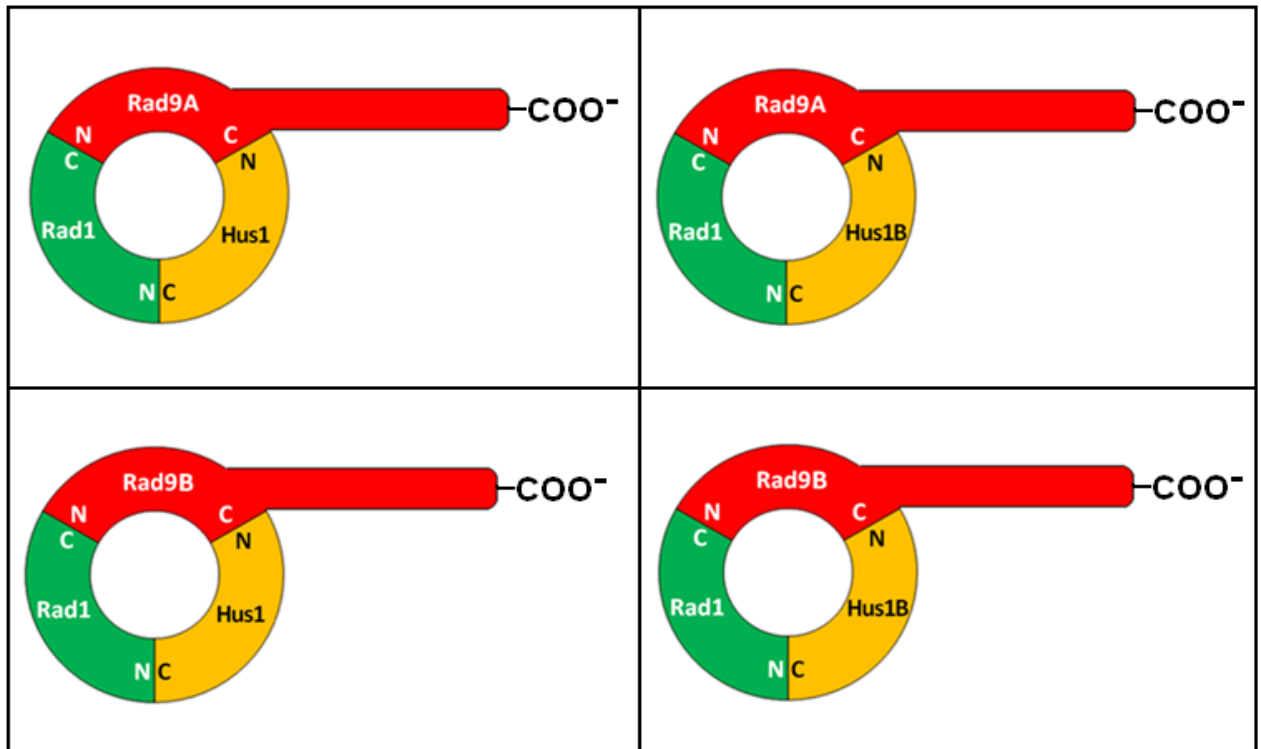


A: *hHUS1* Genetic Data Resource: <http://www.uniprot.org/uniprot/Q060921>

B: *hHUS1B* Genetic Data Resource: <http://www.uniprot.org/uniprot/Q8NH5>

Fig 1.5: Alternative Complex Isoforms of the “9-1-1” Clamp

[Taken and Adapted From: Dufault V.M. *et al*, 2003)



Various experimental studies have established that both the human Rad9A protein and the paralogue protein, Rad9B (Fig 1.3, p.9) can associate with human Rad1, Hus1 and/or the Hus1B protein paralogue (Fig 1.4, p.10), along with the human Rad17 protein component of DNA clamp-loader complex (Fig 1.6, p.12).

It has therefore been postulated that formation of four isoformic “9-1-1” DNA sliding-clamps is feasible and that each respective complex may possess distinctive biological functions in specific types of DNA damage and/or cellular replication stress responses (Dufault V.M. *et al*, 2003).

Somewhat intriguingly, the human Rad17 protein component of the hRad17:RFC2-5 complex (which loads the “9-1-1” clamp onto the DNA – discussed in detail in Section 1.2.1, pp.23-32) also exists as four different isoforms (Fig 1.6, p.12).

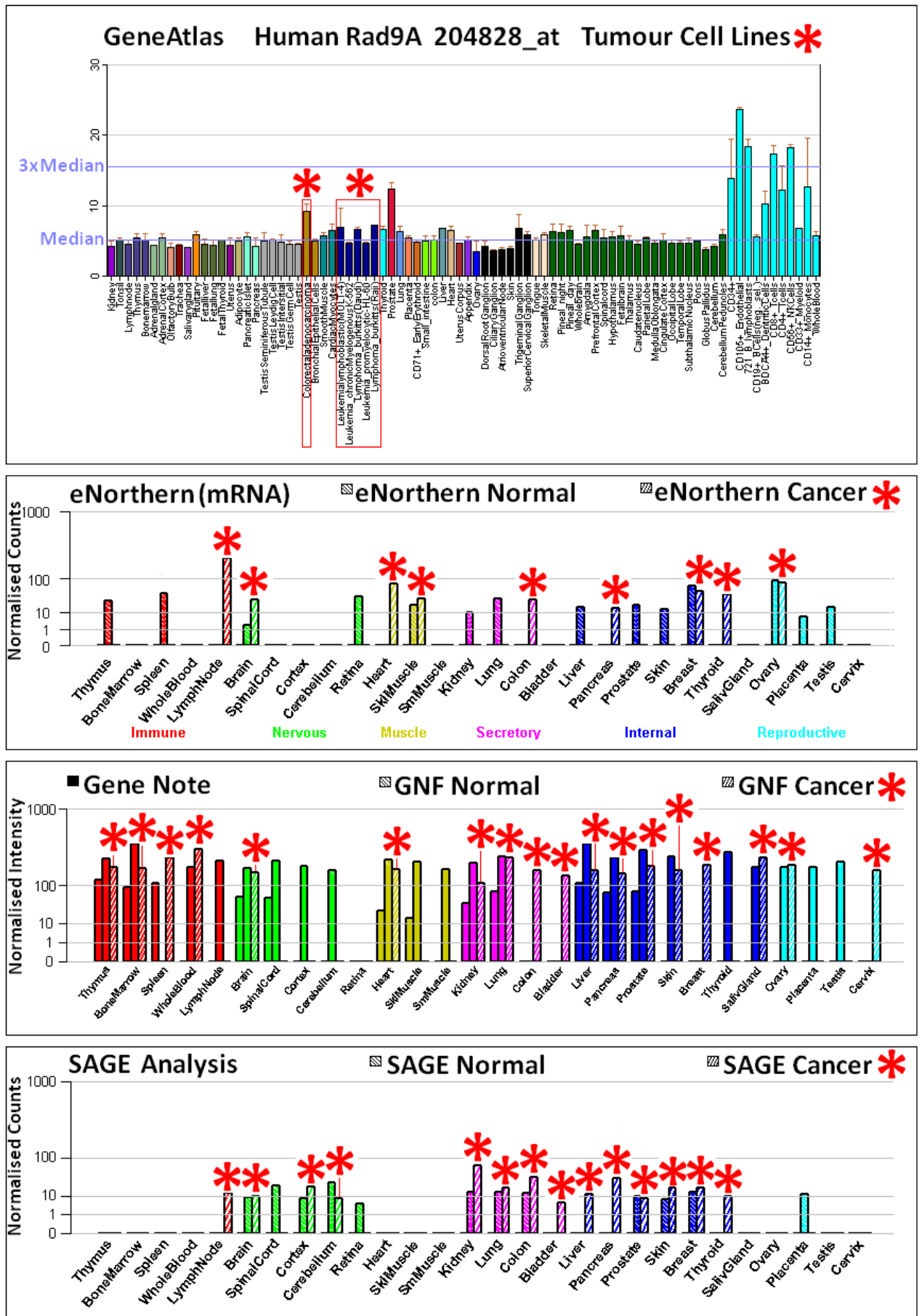
It is also therefore feasible to hypothesise the potential existence of four isoformic hRad17:RFC2-5 complexes, each of which associates with and loads a specific “9-1-1” clamp isoform onto DNA - dictated by the type of structural DNA damage/lesion, in conjunction with the appropriate cell cycle checkpoint signalling response.

Fig 1.6: *hRAD17* Gene Locus Site and Isoform Protein Sequences



hRAD17 Genetic Data Resource: <http://www.uniprot.org/uniprot/Q75943>

Fig 1.7: Tissue-Specific Expression Profiles for the *hRAD9A* Gene



Expression Data Resource: <http://www.genecards.org/cgi-bin/carddisp.pl?gene=RAD9A>

Fig 1.8: Tissue-Specific Expression Profiles for the *hRAD9B* Gene

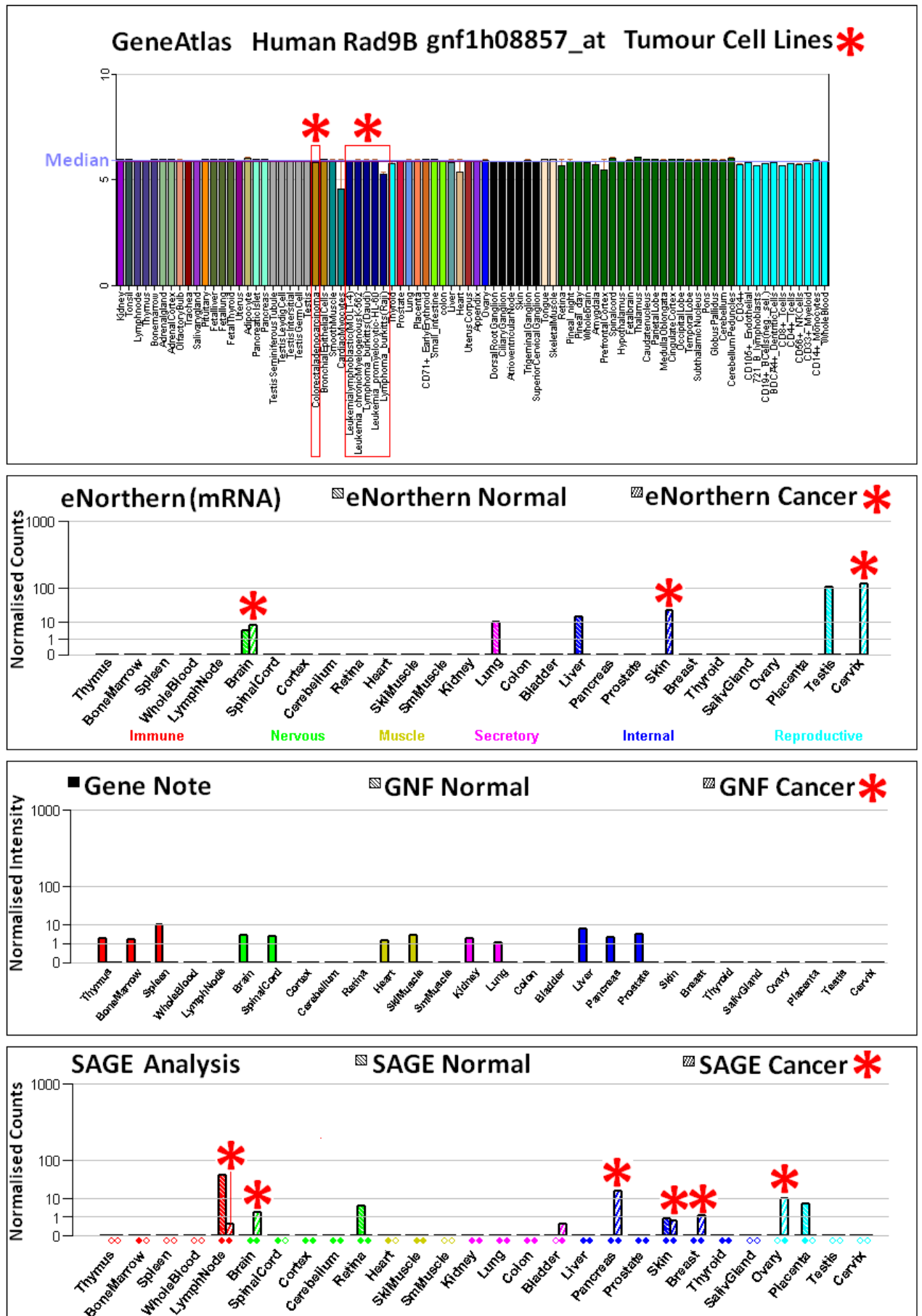


Table 1.2: *hRAD9* Gene Expression – Neoplastic Correlations

Tumour Tissue Type	Correlated hRad9 Experimental Observations	Reference
Breast	Activation and over-expression of the <i>hRAD9</i> gene at the chromosomal 11q13 locus DNA hypermethylation at Intron 1 and Intron 2 of the <i>hRAD9</i> gene	Chan V. <i>et al</i> , 2008 Cheng C.K. <i>et al</i> , 2005
Ovary	High significance of over-expression of the <i>hRAD9</i> gene in both mitotic and apoptotic indices within epithelial ovarian tumour cells	de La Torre J. <i>et al</i> , 2008
Prostate	Elevated cytological levels of the hRad9 protein as as consequence of aberrant amplification and/or hypermethylation at CpG islands within the 3' end of Intron 2 of the <i>hRAD9</i> gene	Rao K.V. <i>et al</i> , 2012 Zhu A. <i>et al</i> , 2008
Testicular	* Elevated cytological levels of the hRad9B protein isoform within testicular seminoma cells	Hopkins K.M. <i>et al</i> , 2003
Lung	High cumulative cytological levels of the hRad9 protein expressed within the nuclei of non-small cell lung carcinoma cells	Maniwa Y. <i>et al</i> , 2005
	Non-synonymous H239R SNP within the <i>hRAD9</i> gene expressed in relatively high cytological levels within non-small cell lung adenocarcinoma cells	Maniwa Y. <i>et al</i> , 2006 Tanaka Y. <i>et al</i> , 2010 Yuki T. <i>et al</i> , 2008
Thyroid	Elevated cytological levels of the hRad9 protein expressed in thyroid tumours and significant expression of higher levels of hRad9 in malignant thyroid tumours cells in comparative analyses with benign tumour cells	Kebebew E. <i>et al</i> , 2006
Gastric	Critical hRad9 functional requirement for G2/M checkpoint signal-transduction identified within gastric cancer cells	Hayashi K. <i>et al</i> , 2002

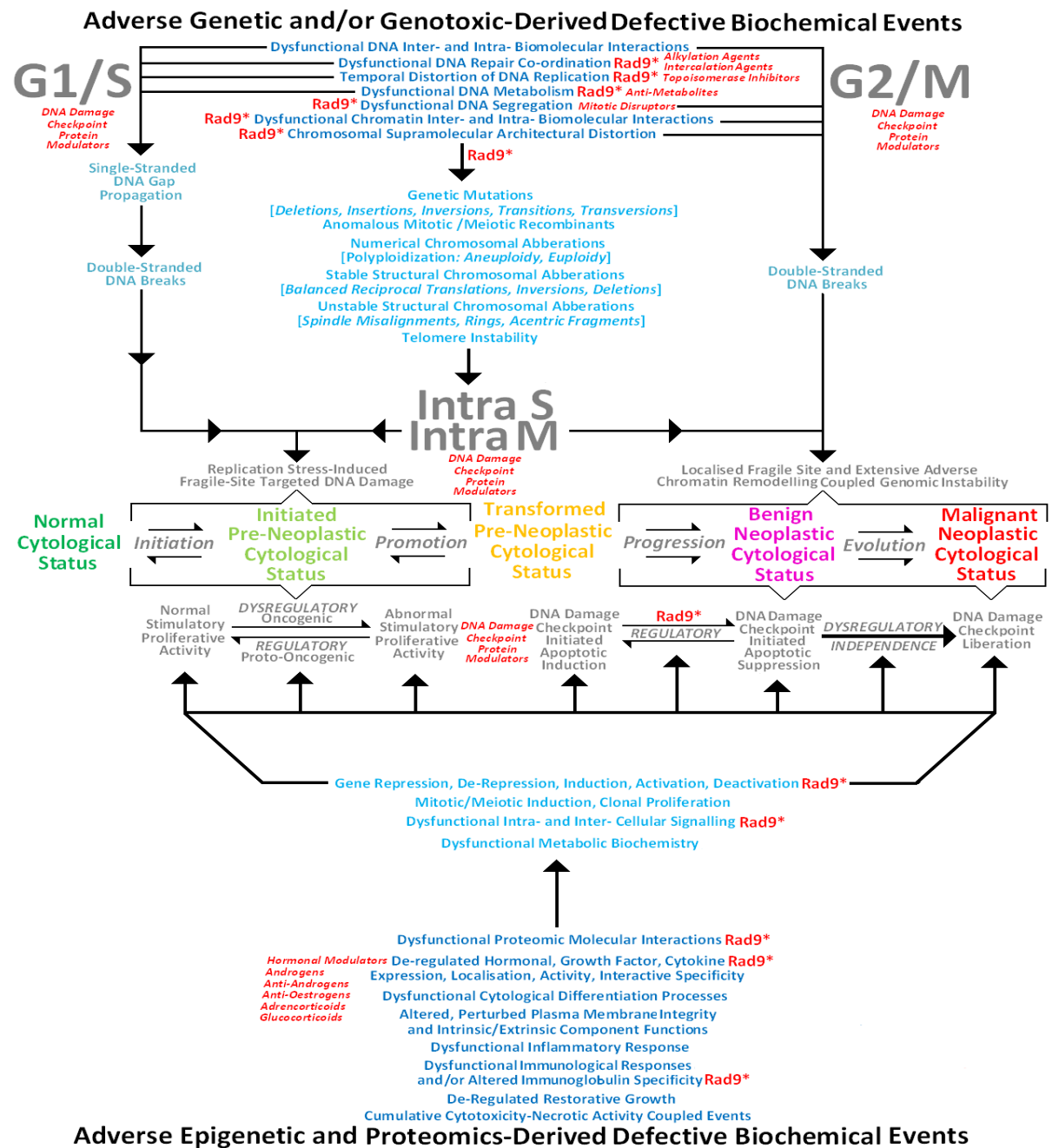
* **NOTE:** Whilst the biological functions of the human Rad9A protein are well-documented, comparatively little is known about distinctive functions of the human Rad9B protein paralogue.

The equivalent mouse homologue, mRad9b, has been demonstrated to function as an essential interactive protein component in embryonic development and in cell cycle checkpoint signalling response-mediated resistance to γ -irradiation- and Mitomycin C-induced types of DNA damage (Leloup C. *et al*, 2010).

Both *hRAD9A* and *hRAD9B* genes exhibit distinctive expression profiles in different normal and cancerous tissue types (Fig 1.7, p.13; Fig 1.8, p.14), in which the human Rad9B paralogue may also serve as a specific biomarker for testicular seminomas (Hopkins K.M. *et al*, 2003).

Fig 1.9: Summarised Biochemical Roles of Rad9 in Carcinogenesis

[Constructed via Collated Information From: Bartek J. *et al*, 1999; Bartkova J. *et al*, 2006; Gorgoulis V.G. *et al*, 2005; Janes S.R.C., 1999; Janes S.R.C, 2006; Matzke M.A. *et al*, 1999; Simons J.W.,1999; Sugimura T. and Ushijima T.,2000; Timbrell J.A., 2008; Yamasaki H. *et al*, 1999]



*Rad9 = Dysfunctional Rad9 Interactions Which May Potentially be Implicated in Biochemical Activity Modulation of Specific Genotoxic, Epigenetic & Proteomic Carcinogenic Initiation, Promotion, Progression & Evolution Events (Broustas C.G. and Lieberman H.B., 2012; Lieberman H.B. *et al*, 2011)

Specific Rad9-Modulated activities may also contribute to acquired tumour multiple drug resistance against different types of anti-cancer chemotherapeutics - *named classes of drugs* are provided in italic notation alongside their targeted biomolecular processes (Larsen I.K. and Kastrop J.S, 2002).

Pharmacological ligand and/or peptidomimetic manipulation of specific types of protein-protein hRad9-domain interactive associations, via specific targeting of particular functional-associated N-Terminal terminal and C-Terminal Tail Domain recognition sites (discussed in detail in later sections of this chapter), may be feasible approaches for the future development of novel anti-cancer chemotherapeutics with enhanced pharmacological efficacies and reduced toxic side-effects.

Such treatments would potentially enable appropriate biochemical rectification of specific Rad9-dysfunctional mechanisms (Fig 1.2, p.8) implicated in the various cytological states of tumourigenic propagation, progression and multiple drug resistance (Fig 1.9, p.16).

A. priori, in order to avoid potentially severe, catastrophic toxicological side-effects, each member of this novel class of pharmaceuticals would have to possess a sufficiently high degree of specificity against its intended hRad9-protein interactive functional target.

However, with the exception of enzymatic active-site targeted approaches (as in the case of kinase-and/or phosphatase-type regulatory post-translational modification of hRad9 functional protein activities – <http://www.freepatentsonline.com./7384761.html>), the design of such pharmacological ligands/peptidomimetics presents a difficult, challenging task as a consequence of several key factors (Yin H. and Hamilton A.D., 2005) – notably;

- (i) The majority of critical interactive residues within the endogenous specific protein-protein interactive targets and/or respective protein ligands are relatively ambiguously-defined and only provide indirect correlative data with respect to rational small-molecule drug design.

- (ii) Relatively large associative intrafacial supramolecular regions ($\sim 1600\text{\AA}$ / ~ 170 atoms of “buried” biomolecular interactive surface area) are implicated in the stable formation of the protein-protein complexes, which impose a severe competitive capacity limitation with regard to small-molecule drug specificity-targeted design.
- (iii) The supramolecular structural architecture of the interfacial protein-protein associative regions display relatively flat/featureless topological surface characteristics, which impose severe limitations on the selectivity of the designed small-molecule drug ligands.
- (iv) Ineffective design of simple peptide analogue-based ligand modulation of critical binding domain motifs located within the individual protein components, implicated in the specificity of the interactive complex formation, as a consequence of the non-contiguous nature of their physio-biochemical properties.

Nevertheless, advances in the development and implementation of various approaches for the design of effective and highly-specific small-molecule, peptide and peptidomimetic-based modulatory ligands of protein-protein interactions continue to progress (Cai Z. *et al*, 2008; Chu L-H. and Chen B-S, 2008; Follis A.V. *et al*, 2012; Glanzer J.G. *et al*, 2011; Sillerud O. and Larson R.S., 2005) with subsequent successful practical applications.

Significant progression into this field has been further augmented via the burgeoning new discipline of Chemical Biology, in conjunction with the experimental application of “Forward” and “Reverse” types of “Chemical Genetics” approaches.

One such key example, is the recent development of novel experimental anti-cancer pharmacological agents which specifically perturb p53-MDM2 type protein-protein interactions for selective induction of apoptosis in neoplastic cells (Dukina A.S. and Lindsley C.W., 2007).

Therefore, it is not entirely inconceivable that progressive research advancements into this field may be applied to the potential future design and development of a novel range of specific hRad9 function-targeted anti-cancer chemotherapeutics (of the type discussed previously – p.17).

An alternative feasible macromolecular-based approach, which may be adopted in the near future, would focus upon the design and development of novel anti-sense oligonucleotide strategies for suppression of aberrant *hRAD9A/hRADB* tumorigenic gene expression (Fig 1.3, p.9; Fig 1.7, p.13; Fig1.8, p.14; Table 1.2, p.15) and therapeutic anti-body conjugates targeted against oncogenic-associated, elevated levels of expressed hRad9 protein variants (Broustas C.G. and Lieberman H.B., 2012; Ishikawa K. *et al*, 2008; Lieberman H.B., 2008; Lieberman H.B. and Zhu A., 2010; Lieberman H.B. *et al*, 2011) and/or Rad9-Rad1-Hus1 DNA clamp isoforms Fig 1.5, p.11).

In summarised conclusion, the Rad9 protein is a potentially valid and versatile pharmacological target for the future design and development of at least seven potential different classes of novel anti-cancer chemotherapeutics – with respect to their specific biochemical modulatory modes of action, which may comprise;

- (i) Selective DNA damage checkpoint response hRad9/“9-1-1” complex-targeted apoptotic induction in neoplastic cells.
- (ii) Perturbance of hRad9/ “9-1-1”-complex-mediated enhanced error-prone types of DNA repair mechanisms for selective suppression of perpetuated genomic errors implicated in the cytological initiation, promotion and progression phases of carcinogenesis.
- (iii) Suppression/reversal of elevated DNA repair pathways implicated in the mechanisms of tumour cell acquired multiple drug resistance to various DNA–damaging types of anti-proliferative conventional chemotherapeutics in current clinical use.

- (iv) Suppression of aberrant, dysfunctional hRad9/"9-1-1"-complex-modulatory hormonal nuclear receptor-DNA interactions, which may be implicated in cytological neoplastic growth hormone-mediated progression events, for suppression of tumour cell metastatic proliferation and/or acquired multiple drug resistance to steroid-based modulatory types of anti-cancer chemotherapeutics in current clinical use.

- (v) Perturbance of adverse hRad9/"9-1-1"-complex-induced recombinant *V, J, D* gene type immunoglobulin "class-switching" conversions for suppression of tumour cell-specific immune signalling responses, resistance to anti-body conjugate- and/or viral construct-based therapeutics.

- (vi) Suppression of adverse oncogenic protein mis-folding events via specific modulation of hRad9-TPR2 associative protein activities.

- (vii) Therapeutic modulation of specific levels of free- and Rad1/Hus1-ring complexed- hRad9 isoforms, which may be implicated in tumourigenic progression, via appropriate pharmacological targeting of hRad9-Jab1-interactive COP9 signalosome-coupled proteosomal pathways and/or anti-sense *hRAD9A/B* gene expression manipulation.

Specific pharmacological manipulation of the aforementioned hRad9 protein functions may also be utilised in combination with the current "conventional arsenal" of anti-cancer drugs in use, including the progressive development and clinical implementation of "3rd generation therapeutics", for enhanced efficacy via suppression of potential novel hRad9-mediated biochemical mechanisms of acquired tumour multiple cross-resistance to a wide range of different agents (Table 1.3, p.21).

Table 1.3: Potential Rad9-Mediated Tumour Resistance to Novel Therapeutics

Therapeutic Agent/Type Classification	Examples	Potential Mechanism(s) of "Rad9-Propagated" Tumour Resistance
Photodynamic Therapeutics (PDTs)	eg Levulinic Acid-Based Derivatives eg Porphyrin-Based Derivatives	Modulatory MAP Kinase Pathway Activity in Response to PDT Oxidative/Free-Radical-Induced DNA Damage and/or Elevated DNA Repair Activity
p13-Kinase Inhibitors	eg Wortmanin eg Demethoxyviridin Derivatives	Modulatory Alternative Checkpoint Kinase Activity and/or Associated Pathway Inhibitory "By-Pass" via "Checkpoint Signal-Responsive Switching"
Cyclin-Dependent Kinase Inhibitors (CDKIs)	eg Synthetic Flavones eg Tri-Substituted Purines eg Paullones eg Purvalanols	
Ras-Raf-Mek-Erk Pathway Receptor Tyrosine Kinase Inhibitors	eg CAAX-Box Mimetics eg Farnesyl Transferase Inhibitors	
mTor Pathway Inhibitors	eg Rapamycin Derivatives	
p53-G2 Checkpoint Kinase Inhibitors	eg Methylxanthine Derivatives eg 7-Hydroxystaurosporine eg Pifithrin- α	
p21/CIP/WAF1 Inhibitors	eg p21 Gene-Targeted Anti-Sense Oligonucleotides	Rad9- p21 Gene Promoter Interactions
Telomerase Inhibitors	Catalytic Active Site Inhibitors eg Oxadiazole-Derivatised Chloropyridines G-Quadruplex Substrate Binding Inhibitors eg Carbazole Derivatives eg Triethylene Tetramine Derivatives	Associative Rad9-Induction of Elevated Telomerase Activity
Nucleosomal Histone Acetylase/Deacetylase Modulators/Inhibitors	eg Trichostatin eg Trapoxin eg Depudecin eg Synthetic Benzamide Derivatives	Chromatin Re-Modelling By-Pass Activities Mediated via: Rad9-HDAC/MYH1 Interactions Rad9-Metnase Interactions Rad9-TLK1/1B Interactions
Hsp90 Inhibitors	eg Radicol eg Geldanamycins	Chaperone Protein Folding Pathway Activity By-Pass Mediated via Rad9-TPR2 Interaction
Ubiquitination-Coupled Proteosomal Pathway Inhibitors	eg Peptide Aldehydes eg Lactocystin Derivatives eg Dipeptide Boronic Acids	COP9 Signalosome-Mediated Proteolytic Pathway Activity Modulation By-Pass via Rad9-Jab1 Interactions
Angiogenesis Inhibitors	Anti-Angiogenic Factors - eg Endostatin VEGF Receptor Antagonists - eg SU5416 VEGF Release Inhibitors - eg Marimistat	Interactive Rad9-Hormonal Receptor Activity Modulation By-Pass
	Anti-VEGF Anti-Bodies - eg Avastin	Rad9-Mediated Immunoglobulin V, D, J Recombinant Gene Conversion By-Pass
Conjugated Anti-Body (Ab) Therapeutics	eg Pro-Drug Enzyme-Ab Conjugates ["ADEPT"-Specific Cytotoxic Targeting] eg Ricin-Conjugated Immunotoxic Ab's eg Radioisotope-Conjugated Ab's eg Polymeric Ab Conjugates	eg Immunoglobulin-Targeting of Ab-Based Therapeutics eg Immunoglobulin-Targeting of Anti-Tumour Viral-Based Therapeutics
Anti-Tumour Viral-Based Therapeutics	eg "GDEPT" Viral Constructs eg Oncolytic Viral Constructs	eg Modulation of Regulatory Immune Response "Cross-Talk" Activities

Summarised examples of "3rd generation" cancer chemotherapeutics in current development and their efficacious biochemical mode(s) of action which may be countered via potential Rad9-mediated mechanisms of tumour multiple drug resistance.

[Compiled via Collated Information From: An L. *et al.*, 2010; Canfield C. *et al.*, 2009; Carmeliet P. and Jain R.K., 2000; Chang D-Y *et al.*, 2011; Cortajarena A.L. *et al.*, 2008; Davids L.M. and Kleemann B., 2011; De Haro L.P. *et al.*, 2010; Denny W.A., 2004; Fan Y. *et al.*, 2003; Francia S., *et al.*, 2006; Francia S. *et al.*, 2007; Garrett M.D. and Workman P., 1999; Govinden S.V. and Goldenberg D.M., 2010; Hu J.C. *et al.*, 2006; Huang J. *et al.*, 2007; Ishikawa K. *et al.*, 2006; Kristeliet R. *et al.*, 2004; Lieberman H.B., 2006; Lieberman H.B., 2008; Lieberman H.B. *et al.*, 2011; Liu J. *et al.*, 2008; McDonald E. *et al.*, 2006; McLaughlin F. and La Thangue N.B., 2004; Maloney A. and Workman P., 2002; O'Shea C.C., 2005; Pommier Y. and Kohn K.W., 2003; Ronald S. *et al.*, 2011; Ruoslahti E. and Rajotte D., 2000; Saberi A. *et al.*, 2008; Schellmann N. *et al.*, 2010; Sunavala-Dossabhoy G. and De Benedetta A., 2009; Wang L. *et al.*, 2004; Workman P., 2002; Workman P., 2003a; Workman P., 2003b; Workman P., 2004; Workman P., 2005; Workman P., 2010; Xiang S-L *et al.*, 2001; Yang D-Y. *et al.*, 2007; Yap T.A. *et al.*, 2010; Yin Y. *et al.*, 2004; Zawacka-Pankau J. *et al.*, 2008; Zheng Q.Z. *et al.*, 2010]

A significant proportion of the “conventional arsenal” of anti-cancer drugs which are utilised in current clinical practice may be regarded as strictly anti-proliferative chemotherapeutics which elicit their cytotoxic pharmacological efficacy via DNA damage induction and/or perturbation of DNA replicative processes (Larsen I.K. and Kastrup J.S., 2002; Pecorino L.,2008) – Fig 1.9, p.16.

Consequently, such drugs are only capable of targeting actively cycling cells and are relatively ineffective against dormant neoplastic cells in the latent/quiescence G₀ phase of the cell cycle.

Thus, there is serious post-treatment potential for the re-emergence and proliferation of surviving dormant tumour cells if they later undergo cytological transition from G₀ to active phases of the cell cycle (Pecorino L., 2008; Weinberg R.A., 2006).

This necessitates regular monitoring of the patient after an apparently successful chemotherapeutic regimen, typically over a 5 year “remission” period, for early detection and appropriate clinical management in the case of a possible relapse of their respective neoplastic pathophysiological condition (Larsen I.K. and Kastrup J.S., 2002; Pecorino L., 2008; Weinberg R.A., 2006).

Recent experimental studies have indicated that Rad9 may be implicated in mechanisms of alternate sensory DNA damage-mediated suppression of cell cycle checkpoint adaptations to cyclic re-switching between DNA re-section and DNA double-strand break-like structural formation events, which act “in concert” to maintain a senescent/”dormant” cytological status (Deshpande A.M. *et al*, 2011).

Future potential research and development of novel “anti-Rad9 senescence-abrogative” type pharmacological agents could be employed for the targeted biochemical enforcement of dormant tumour cells back into active phases of the cell cycle to ensure their eradication, via polychemotherapeutic regimens, thereby circumventing the clinical problem of remission.

1.2 Associative “9-1-1” Complex-Dependent Rad9 Functions

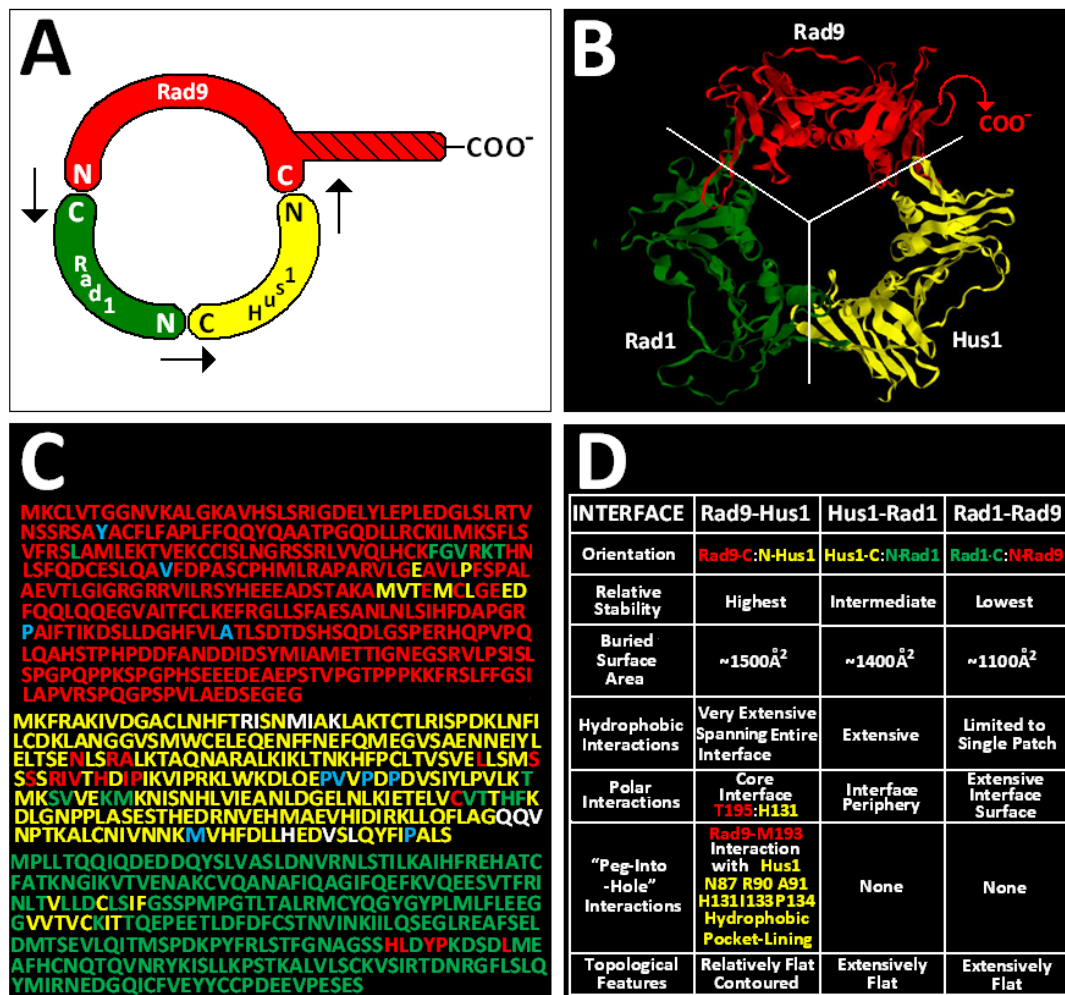
1.2.1 Sensory Sliding-Clamp Physico-Biochemical Dynamics

A wide variety of different types of biophysical- and/or biochemical- mediated structural distortions of DNA topology, may stall DNA polymerases and induce helicase-dissociation at the duplex replication fork, with consequential formation of large tracts of single-stranded DNA (ssDNA) at the damaged sites, which then become coated with Replication Protein A (RPA) – Fig 1.11A, p.25 (Byun T.S. *et al*, 2005; Delacroix S. *et al*, 2007; Namiki Y. and Zou L., 2006; Walter J. and Newport J., 2000; Xu X. *et al*, 2008).

The resultant ssDNA.RPA tract complexes function as protein-interactive recognition substrates for the independent recruitment of the PCNA-like toroidal, heterotrimeric Rad9-Rad1-Hus1 DNA sliding-clamp complex (referred to commonly as the “9-1-1” complex – Fig 1.10, p.24), along with the primary/proximal transducer DNA damage response cell signalling kinases ATM and ATR (Fig 1.11D, p.25) in complex-association with its binding partner ATRIP (Fig 1.11C, p.25), to the respective chromatin-localised DNA damage sites (Alderton G.K. *et al*, 2004; Byun T.S. *et al*, 2005; Cortez D. *et al*, 2001; Delacroix S. *et al*, 2007; Kondo T. *et al*, 2001; Namiki Y. and Zou L., 2006; Unsul-Kacmaz K. and Sancar A., 2004; Walter J. and Newport J., 2000; Zou L. and Elledge S.J., 2003).

Initial loading of the Rad9-Rad1-Hus1 complex (Fig 1.10, p.24) onto the resultant DNA polymerase α -RPA-ssDNA tract complexes at the stalled replication forks is accomplished via co-associative recruitment of the Replication Factor C (RFC)-like “9-1-1” clamp-loader complex, termed “RSR” (Fig 1.12B, P.28) – which is comprised of the major Rad17 sub-unit (Fig 1.11E, p.25) in association with the smaller sub-units; Rfc2, Rfc3, Rfc4 and Rfc5 respectively (Byun T.S. *et al*, 2005; Griffith J.D. *et al*, 2002; Kanoh Y. *et al*, 2006; Kondo T. *et al*, 2001; Lee J. *et al*, 2003; Wu X. *et al*, 2005; You Z. *et al*, 2002; Zou L. *et al*, 2003), discussed on pp.25-26 with Fig 1.12, p.28.

Fig 1.10: Key Structural Features of the Rad9-Rad1-Hus1 Complex



A: Absolute Anti-Clockwise N→C Stereochemical Configuration of the Rad9-Rad1-Hus1 Toroidal PCNA-like Heterotrimeric DNA Sliding-Clamp Complex (Bermudez V.P. *et al.*, 2003; Bylund G.O. *et al.*, 2006; Doré A.S. *et al.*, 2009; Griffith J.D. *et al.*, 2002; Venclovas C. and Thelen M.P., 2000; Xu M. *et al.*, 2009).

Unlike the Rad1 and Hus1 Sub-Units, Rad9 also possess a highly mobile, unstructured C-Terminal Tail Domain which protrudes outside of the “9-1-1” ring and engages with variety of DNA Damage Checkpoint and Repair Proteins (Lieberman H.B. *et al.*, 2011; Singh K.K. *et al.*, 2007).

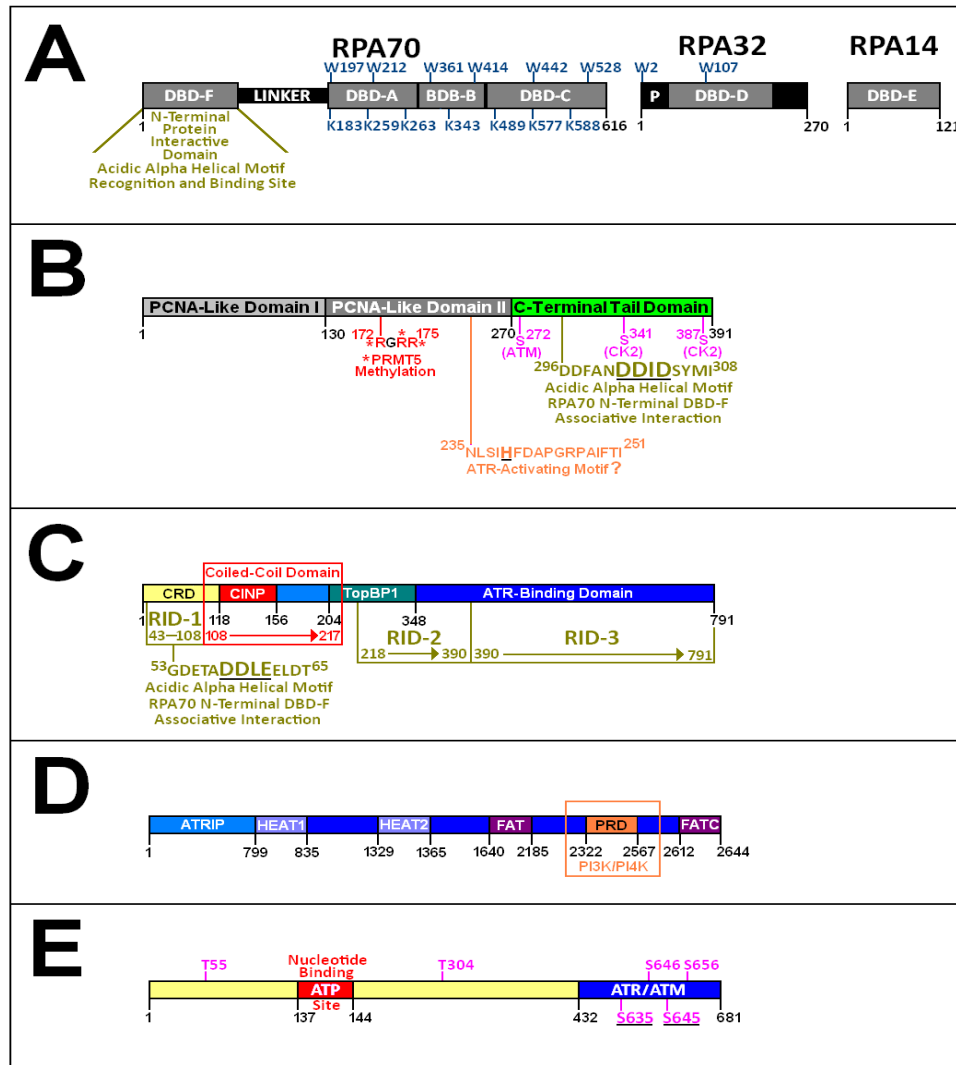
B: X-Ray Crystallographic Resolution of the Protein Structure of the Rad9-Rad1-Hus1 Toroidal Complex (Doré A.S. *et al.*, 2009), this image was generated from the appropriate PDB file via utilisation of the *Polyview 3D* software tool (PDB ID: 3G65) – the approximate location of the Rad9 C-Terminal Tail Domain is depicted (which is non-crystallisable as a consequence of its relatively high, unstructured Mobility/Intrinsic Disordered Propensity and is thus evasive to X-Ray crystallographic resolution).
http://www.genome.jp/dbget-bin/www_bget?.pdb.3G65
<http://polyview.cchmc.org/polyview3d.html>

C: Key Amino Residues, within the Rad9, Rad1 and Hus1 Sub-Units, which are implicated in various “9-1-1” Complex N→C Interface Associations and other Protein/DNA-Interactions (Doré A.S. *et al.*, 2009; Gilljam K.M. *et al.*, 2009; Sohn S.Y. and Cho Y., 2009; Warbrick E., 1998; Xu M. *et al.*, 2009)

XXXXXX = Rad9 Interface-Associative Amino Acid Residues
 XXXXXX = Rad1 Interface-Associative Amino Acid Residues
 XXXXXX = Hus1 Interface-Associative Amino Acid Residues
 XXXXXX = PIP Box-Binding Pocket Amino Acid Residues (Absent in Rad1) – p.96
 XXXXXX = Hus1 Single DNA Nucleobase-Binding Pocket Amino Acid Residues

D: Summarised Comparison of the Key Structural Features of the Rad9:Hus1, Hus1:Rad1 and Rad9:Rad1 Associative Interfaces within the “9-1-1” DNA Sliding-Clamp Complex (Doré A.S. *et al.*, 2009; Sohn S.Y. and Cho Y., 2009; Xu M. *et al.*, 2009).

Fig 1.11: Interactive Domains of “9-1-1” Clamp-Loading Proteins



- A:** Human Replication Protein A (RPA) is an ssDNA-binding, heterotrimeric toroidal complex comprised of three subunits; RPA70, RPA32 and RPA14 (named according to their respective molecular weights – 70 kDa, 32 kDa and 14 kDa). The DNA-Binding-Domains (DBDs) are indicated, along with key amino acid residues implicated in ssDNA associations and the N-terminal recognition motif in the RPA70 sub-unit which binds to specific motifs within the Human Rad9A protein (Fig B) and ATR-Interacting Protein (ATRIP – Fig C) (Binz S.K. and Wold M.S., 2008; Liu Y. *et al.*, 2005; Oakley G.G. and Patrick S.M., 2010; Shell S.M. *et al.*, 2005; Xu X. *et al.*, 2008 [Uniprot: P27694, P15927 and P35244])
- B:** Key Structural Domains and Functional Motifs within the human Rad9A protein, of particular note; the C-terminal tail domain motif which binds to the N-terminal RPA70 sub-unit recognition site, the “HFD” motif implicated in enhanced activation of the human ATR kinase (Fig D) and methylation of three key Arginine residues (R172, R174 and R175) by the PRMT5 methylase enzyme which is implicated in human Rad9-mediated activation of the human Chk1 cell cycle checkpoint kinase. [Uniprot: Q99638] (He W. *et al.*, 2011; Navadgi-Patil V.M. and Burgers P.M., 2009; Xu X. *et al.*, 2008).
- C:** Key Structural Domains and Functional Motifs within the human ATR-Interacting Protein (ATRIP) partner of the human ATR cell cycle checkpoint kinase (Fig D), of particular note; the three RID domains (RPA-Interacting Domains), the N-Terminal Checkpoint Recruitment Domain (CRD), the ATR-binding domain, the TopBP1 checkpoint mediator protein-binding domain and the CDK2-Interacting Protein Domain (CINP) (Lovejoy C.A. *et al.*, 2009; Mordes D.A. and Cortez D., 2008; Nakaya R. *et al.*, 2010; Namiki Y. and Zou L., 2006; Xu X. *et al.*, 2008). [Uniprot: QW8XE1]
- D:** Key Structural Domains and Functional Motifs within the human ATR cell cycle checkpoint kinase protein, of particular note; the N-terminal ATRIP-binding domain, the two “HEAT” domain motifs (Huntingdon, Elongation Factor 3, PP2A Substrate and TOR1), the “FAT/FAT-C” motif domains (FRAPP, ATM, TRAPP) and the “PRD” (PIKK, PI3K/PI4K Regulatory Domain) which possesses kinase catalytic activity (Mordes D.A. and Cortez D., 2008). [Uniprot: Q13535]
- E:** Key Structural Domains and Functional Motifs within the human Rad17 Protein, of particular note; the ATP Nucleotide Binding Site, the C-Terminal proximal/primary cell checkpoint ATR/ATM kinase interactive C-Terminal Domain and key phosphorylated amino acids residues which modulate the functional activity of the protein (Bao S. *et al.*, 2001; Medhurst A.L. *et al.*, 2008; Post S. *et al.*, 2001; Xu M. *et al.*, 2009). [Uniprot O75943]

The biochemical mechanism of deployment of the Rad9-Rad1-Hus1 complex onto large tracts of RPA-coated ssDNA (Fig 1.10, p.24) is thermodynamically-driven via a hydrolytic ATP-coupled protein-interactive process, analogous to that implicated in loading of the homotrimeric PCNA clamp onto replicative sites of the duplex (Bermudez V.P. *et al*, 2003; Bloom L.B., 2009; Ellison V. and Stillman B., 2003; Xu M. *et al*, 2009) – which may be defined in terms of 6 key co-operative, sequential steps (Fig 1.12, p.28), notably;

- (i) Initial associative formation of the ternary [RSR clamp-Loader-“9-1-1”-clamp-RPA.ssDNA] complex is elicited via ATP-binding to a specific nucleotide acceptor “pocket” within the Rad17 sub-unit (Fig 1.11E, p.25) of the RSR clamp-loading complex.

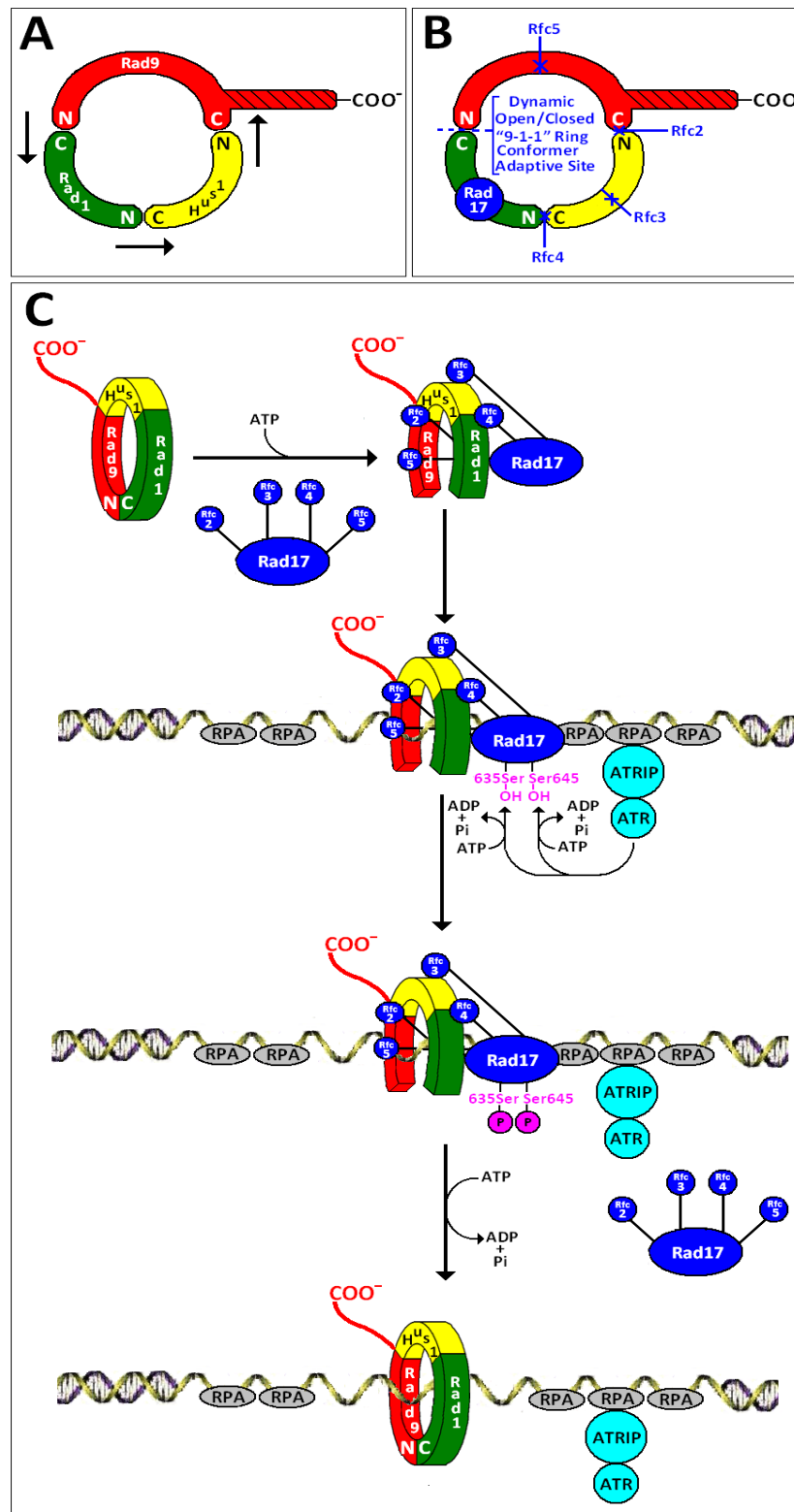
- (ii) The resultant ATP-bound Rad17 sub-unit triggers supra-molecular conformational changes in the modified [RSR clamp-Loader-“9-1-1”-clamp-RPA.ssDNA] ternary complex which induce conversion of the “Rad9-Rad1-Hus1” complex from the “closed” conformer state to the partial “open-ring” conformer state via thermodynamic promotion of non-covalent bond dissociation events at the Rad9-Rad1 interface (Fig 1.10, p.24).

[This localised specificity of “9-1-1” ring-opening is attributed to the physico-biochemical properties of the Rad9-Rad1 interface which is extensively flat with the lowest surface area span, has fewer associative interactions and is the least energetically stable – Fig 1.10D, p.24 (Doré A.S. *et al*, 2009; Xu M. *et al*, 2009)]

- (iii) Transient passage of the duplex through the dissociated Rad9-Rad1 “interfacial slot” enables the Rad9-Rad1-Hus1 complex to encircle and associate with the DNA.

- (iv) Simultaneous phosphorylation of the ATP-bound Rad17 sub-unit at Ser635 and Ser645 (Fig 1.11E, p.25) by the primary ATR checkpoint transducer kinase (in the form of a proximal ATR-ATRIP-RPA.ssDNA type independently-loaded complex) induces supra-molecular conformational changes within the ternary [RSR clamp-Loader-“9-1-1”-clamp-RPA.ssDNA] which enhance the thermodynamic stability of the established open-ring conformer state-type Rad9-Rad1-Hus complex-DNA associative interactions, prior to ring-closure of the “9-1-1” clamp around the duplex (Bao S. *et al*, 2001; Bloom L.B, 2009; Medhurst A.L. *et al* 2008; Post S. *et al*, 2001; Xu M. *et al*, 2009).
- [The Rad9 sub-unit of the “9-1-1” clamp also contains a potential “HFD” ATR-activation motif, located within its PCNAII-like domain – Fig 1.11B, p.25 (Navadgi-Patil V.M. and Burgers P.M., 2009; Navadgi-Patil V.M. and Burgers P.M., 2011), which may facilitate ATR phosphorylation of the Rad17 sub-unit component of the RSR clamp-loader complex]
- (v) Stabilised duplex-association of the Rad9-Rad1-Hus1 open-ring conformer state induces supra-molecular conformational modifications within the ternary [RSR clamp-Loader-“9-1-1”-clamp-RPA.ssDNA] complex which trigger hydrolysis of the ATP molecule bound within the nucleotide-specific acceptor pocket of the Rad17 sub-unit (Fig 1.11E, p.25) of the RSR clamp-loader complex (Kano H. *et al*, 2006; Xu M. *et al*, 2009).
- (vi) Hydrolytic conversion of the Rad17-bound ATP molecule to Rad17-bound ADP, within the RSR component, induces supra-molecular conformational alterations within the ternary [RSR clamp-Loader-“9-1-1”-clamp-RPA.ssDNA] complex which thermodynamically promote Rad9-Rad1 interfacial re-association (thereby affecting “9-1-1” ring-closure around the duplex) and dissociation of the Rad17:Rfc2-5 clamp-loader complex from the ssDNA.RPA substrate. (Bloom L.B, 2009; Kano H. *et al*, 2006; Xu M. *et al*, 2009).

Fig 1.12: Mechanism of “9-1-1” Clamp-Loading Onto DNA



A: Absolute Anti-Clockwise N→C Termini-Interfacial Stereochemical Configuration of the Toroidal, Heterotrimeric Rad9-Rad1-Hus1 PCNA-Like DNA Sliding-Clamp Complex (Burtelow M.A. *et al*, 2001; Doré A.S. *et al*, 2009; Xu M. *et al*, 2009)

B: Co-Operative Binding-Site Locations of the Individual RSR “9-1-1” Clamp-Loader Complex Sub-Units; Rad17, Rfc2, Rfc3, Rfc4 and Rfc5, within the Rad9-Rad1-Hus1 Complex (Doré A.S. *et al*, 2009)

C: Summarised Co-ordinated Biochemical Mechanism of RSR Complex-Mediated Loading of the “9-1-1” Clamp onto DNA (Bloom L.B., 2009; Shiomi Y. *et al*, 2002; Xu M. *et al*, 2009) – Discussed in Detail on pp.26-27.

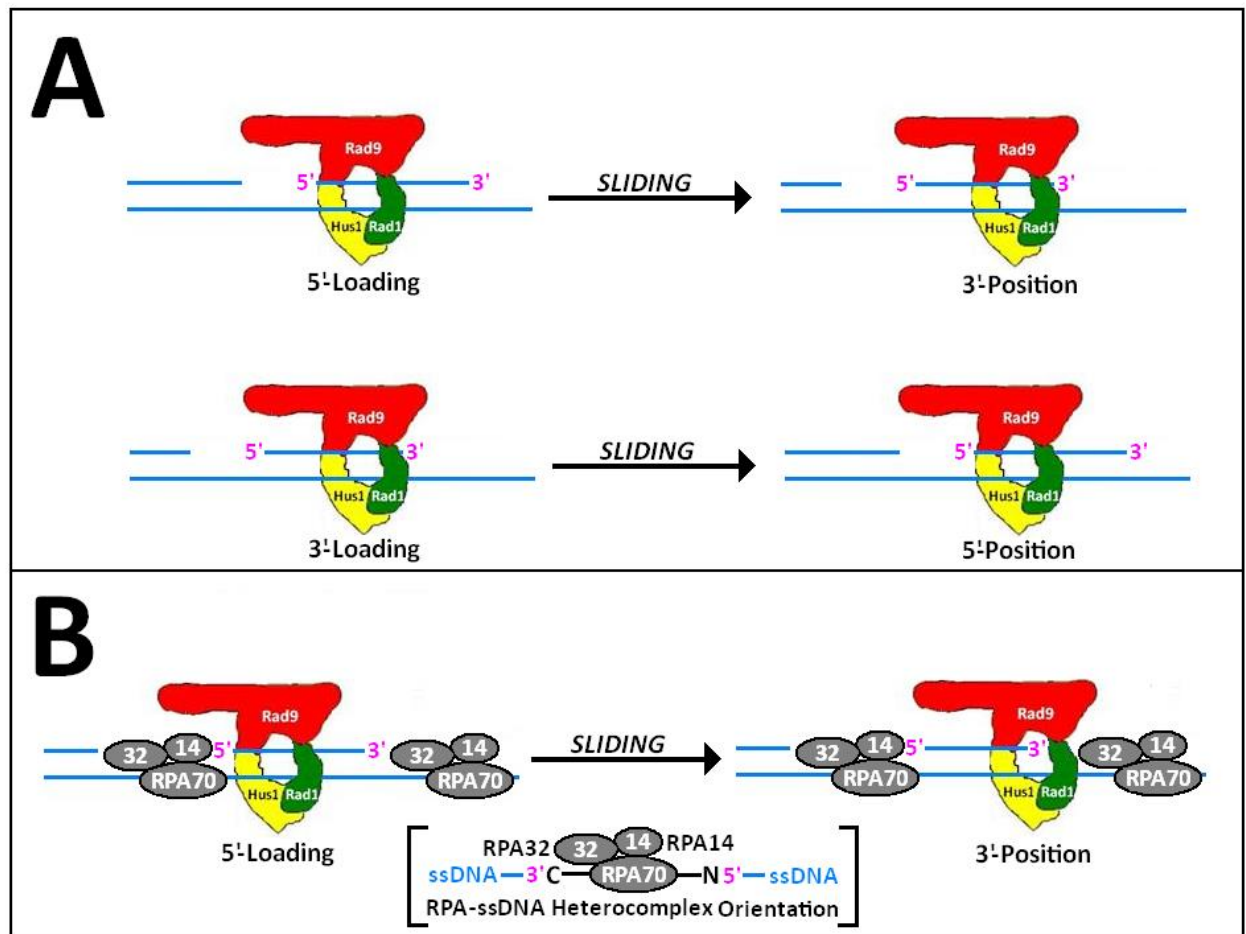
Initial polarity-specific loading of the Rad9-Rad1-Hus1 PCNA-like sliding-clamp complex onto the DNA may proceed via either 5'- or 3'- orientated junctions proximal to the lesion site(s), determined via the supra-molecular, topological architecture of the localised area of damaged chromatin (Majka J. *et al*, 2006) – described summarily in Fig 1.13, p.30.

The motion of the Rad9-Rad1-Hus1 complex along the DNA may proceed via alternative “nut and bolt” or “washer and bolt” type mechanisms (Fig 1.14, p.31), which are determined, selectively via the physico-biochemical structural characteristics of the respective DNA lesion site(s), that in turn may modulate nucleosomal-based chromatin supra-molecular architecture re-modelling events (Beck S. and Olek A., 2003; Morales V. *et al*, 2001; Strahl B.D. and Allis D., 2000; Turner B.M., 2002), which may later impinge sterically upon the traversal duplex progression of the loaded “9-1-1” sliding-clamp (Adelman J.L. *et al*, 2010; Blanco F.J. and Montoya G., 2011; Bloom L.B., 2009; Bowman G.D. *et al*, 2005; Georgescu R.E. *et al*, 2008; Ivanov I. *et al*, 2006; Kazmirski S.L., *et al*, 2005; Laurence T.A. *et al*, 2008; Yao N.Y. *et al*, 2000; Yao N.Y. and O'Donnell M., 2008).

Translocation of the loaded Rad9-Rad1-Hus1 complex, to proximal DNA lesion sites within localised regions of chromatin, may proceed via 1D or 3D mechanistic pathways (Fig 1.15, p.32), which may be determined, selectively by the specific types of encountered DNA damage which may exert influential effects upon chromatin supra-molecular architecture and/or topological re-modelling alterations (Bloom L.B., 2009; Gowers D.M. and Halford S.E., 2003; Gowers D.M. *et al*, 2005; Halford S.E., 2009; Halford S.E. and Marko J.F., 2004; Laurence T.A. *et al*, 2008; Yao N.Y. *et al*, 2000).

Fig 1.13: DNA Polarity-Specific Models of “9-1-1” Clamp-Loading

[Taken and Adapted From: Majka J. *et al*, 2006]



The Rad9-Rad1-Hus1 toroidal heterotrimeric complex is postulated to function as a DNA damage scanner, which may slide back and forth along DNA-associated chromatin supramolecular structural complexes, thereby acting as a continual “pro-active monitoring system” of genomic integrity (Burtelow M.A. *et al*, 2000; Roos-Mattjus P. *et al*, 2002).

The functional polarity, with respect to 5'- or 3'- junction-specific orientated “9-1-1” complex-loading, may be dictated by a variety of interactive, chromatin supramolecular architecture-related physico-biochemical parameters – including; clamp-loading site localisation, DNA lesion type and/or proximal/distal associative influences of DNA damage responsive proteins implicated in cell cycle checkpoint signalling and DNA repair (Majka J. *et al*, 2006).

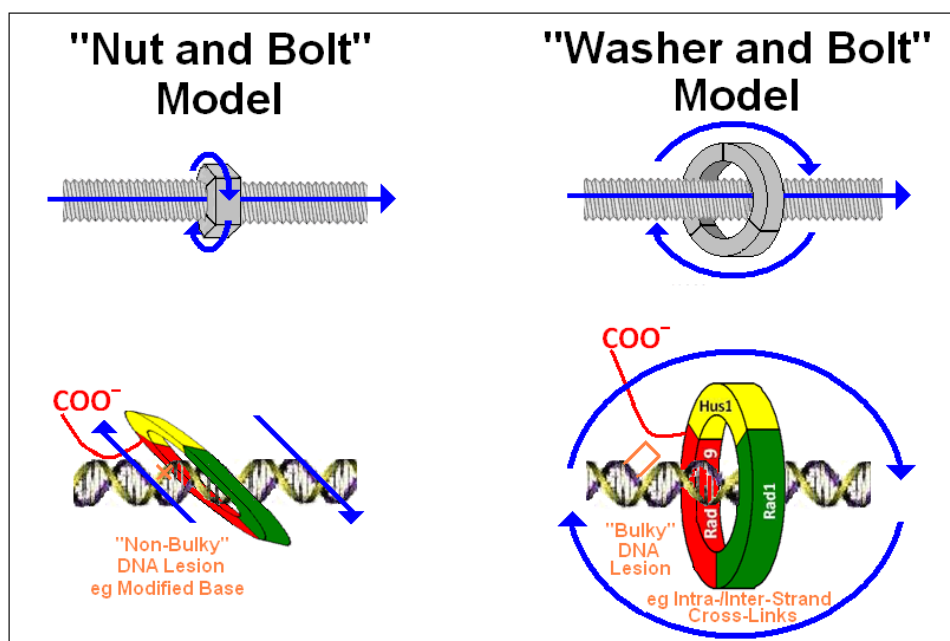
A: In the case of naked DNA, initial functionalized “9-1-1” complex-loading may be accomplished via equivalent selective prevalence at either 5'- or 3'- junction termini prior to clamp-sliding to a neighbouring junction site (Majka J. *et al*, 2006).

B: RPA-coated DNA restricts initial functionalized “9-1-1” complex-loading onto 5'-junction termini, in which 3'-junction terminal “9-1-1” complex-functionality may be elicited via 5'→ 3' type clamp-sliding to a neighbouring junction site (Majka J. *et al*, 2006).

Different types of “9-1-1” clamp polarity-loading orientation may serve as a selective biochemical mechanism for the initiation of particular sensory-signals towards different types of DNA damage which are “translated” into Rad9 C-terminal tail domain-mediated functional interactions with specific target proteins implicated in the appropriate cell cycle checkpoint and/or DNA repair responses respectively (Majka J. *et al*, 2006).

Fig 1.14: Mechanistic Models of “9-1-1” DNA Sliding-Clamp Motion

[Compiled via Collated Information From: Adelman J.L. *et al*, 2010; Blanco F.J. and Montoya G., 2011; Bowman G.D. *et al*, 2005; Georgescu R.E. *et al*, 2008; Ivanov I. *et al*, 2006; Kazmirski S.L. *et al*, 2005; Laurence T.A. *et al*, 2008; Yao N. *et al*, 2000; Yao N.Y. and O'Donnell M., 2008]



The relative sliding velocity of the Rad9-Rad1-Hus1 heterotrimeric complex along the DNA, which may be critical to the detection of different types of DNA damage, is “biochemically governed” via the differential counter-strengths of repulsive (DNA-dissociative) and attractive (DNA-associative) interactions between the DNA molecule, amino acid residues and/or functional motifs within the three sub-units of the “9-1-1” toroidal clamp.

DNA-dissociative interactions serve to reduce the frictional forces between the “9-1-1” clamp and DNA, thereby increasing the relative “sliding-velocity” of the complex along the DNA molecule.

These DNA-dissociative interactions comprise electrostatic repulsion between negatively-charged acidic amino acid residues and the DNA phosphodiester groups, in conjunction with exclusion of hydrophobic amino acid residues from the extended “hydration spine” that is derived from the proximal chain of water molecule shells which surround the phosphodiester groups of the DNA.

DNA-attractive interactions serve as braking forces between the “9-1-1” clamp and the DNA, thereby decreasing the relative “sliding-velocity” of the complex along the DNA molecule.

These DNA-attractive interactions comprise electrostatic attraction between positively-charged basic amino acid residues and the DNA phosphodiester groups, in conjunction with hydrogen-bonding between hydrophilic amino acid residues and the extended DNA “hydration spine” and possibly π -electron stacking/intercalative interactions between aromatic amino acid residues and DNA nucleobases.

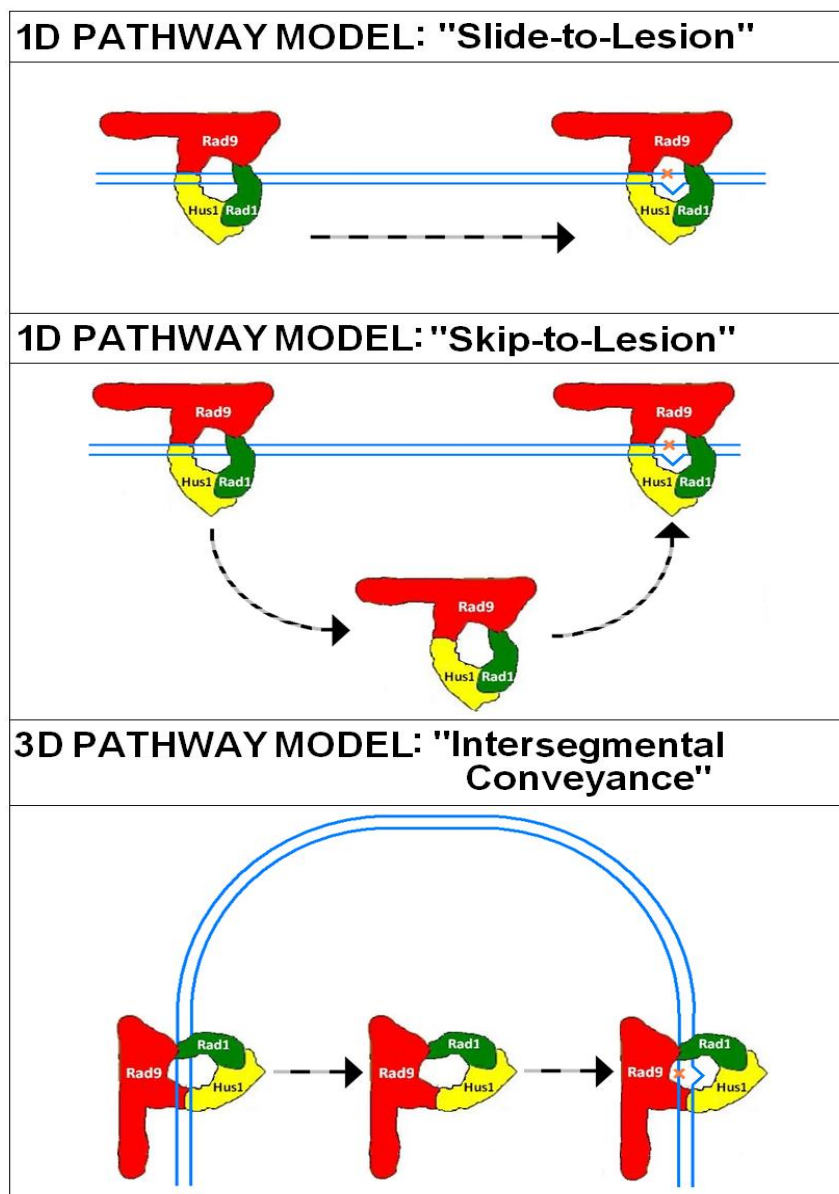
The Hus1 sub-unit of the “9-1-1” clamp also contains a hydrophobic pocket which can bind a single DNA nucleobase and may function as a component detector of modified base type DNA lesions.

In the “*Nut and Bolt*” model, the “9-1-1” complex slides progressively along the DNA in a rotating type motion which follows the “helical contour” of the duplex, via the central elliptical hole of the complex which facilitates passage of the DNA in a tilted orientation “in-plane” with the nucleobases.

In the “*Washer and Bolt*” model, the “9-1-1” clamp slides progressively along the DNA in a “straddling/out-of-plane” motion, which does not adhere to the conventional “helical contour” of the duplex and may be implicated in the detection and by-pass of bulky DNA lesions in special cases, such as PCNA- and “9-1-1”-clamp-mediated template-switching in Translesion Synthesis (TLS) mechanisms of DNA damage-site avoidance and repair (discussed later in detail – Section 1.2.5, pp.112-116; Fig 1.51, p.112).

Fig 1.15: 1D & 3D “9-1-1–DNA” Lesion Site Translocation Pathways

[Compiled via Collated Information From: Bloom L.B., 2009; Gowers D.M. and Halford S.E., 2003; Gowers D.M. *et al*, 2005; Halford S.E., 2009; Halford S.E. and Marko J.F.,2004; Laurence T.A. *et al*, 2008; Yao N.Y. *et al*, 2000]



Sliding clamps, including the Rad9-Rad1-Hus1 toroidal, heterotrimeric complex, typically move along the DNA in a continuous manner, via a direct one-dimensional diffusion type process, between adjacent, non-specific localities to the lesion in the absence of any transient dissociation of the respective protein complex from the DNA molecule.

The “9-1-1” sliding clamp may also adopt a one-dimensional “skip-to-lesion” motional pathway mechanism, in which the complex may be simultaneously moved through three-dimensional space along the one-dimensional duplex contour to the lesion site within the same DNA molecule, mediated via transient DNA dissociation/re-association events co-ordinated via “inter-communicative” physico-biochemical events between adjacent Rad17:RFC2-5 clamp-loading complexes and the chromatin supramolecular architecture.

Alternatively, the “9-1-1” sliding clamp may also adopt a three-dimensional “inter-segmental conveyance” motional pathway mechanism, mediated via transient DNA dissociation/re-association events co-ordinated via “inter-communicative” physico-biochemical events between adjacent Rad17:RFC2-5 clamp-loading complexes and local/global changes within the chromatin supramolecular architecture as a consequence of “bent-DNA” configurations induced by certain types of “bulky” types of DNA lesions (eg inter- and intra- strand cross-linkages).

1.2.2 DNA Damage Checkpoint Signal Activation and Modulation

As discussed previously, DNA damage and genotoxic events play key significant roles in a variety of mechanisms associated with the cytological initiation, promotion and progression phases of carcinogenesis (Fig 1.9, p.16).

The high fidelity of DNA replication, with regard to precision co-ordinated chromosomal segregation and accurate transmission of genetic information to daughter cells during mitotic or meiotic processes, is critical to the propagation of normal cytological status and functions.

The vital requirement for accurate maintenance of genomic integrity and stability during mitotic and meiotic processes, under the constant evolutionary pressure of daily exposure to a wide variety of endogenous and exogenous inductive sources of DNA damage (discussed later in Section 1.2.5, pp.86-118), has culminated in the cytological establishment of a highly conserved, well-developed intercommunicative network of protein-protein associative signal transduction cascades which function collectively in cell cycle regulatory DNA damage response checkpoint pathways (Boye E. *et al*, 2009; Dasika G.K. *et al*, 1999; Houtgraaf J.H. *et al*, 2006; Kaufmann W.K. 1995; Latif C. *et al*, 2001; Mercer W.E., 1998; Sancar A. *et al*, 2004; Smith J. *et al*, 2010).

The overall “cytological reaction” to DNA damage essentially comprises three main types of response, notably; the transient phase-specific cessation of cell cycle progression, the initiation of appropriate DNA repair mechanisms and/or induction of apoptotic pathways (Boye E. *et al*, 2009; Chiarugi V. *et al*, 1994; Houtgraaf J.H. *et al*, 2006; Humpal S.E., 2009; Kaufmann W.K., 1995; Sancar A. *et al*, 2004; Smith J. *et al*, 2010).

Selection of the most appropriate response is dictated via specific protein-protein interactive signalling events within the checkpoint pathways whose elicitation is governed by several key factors, notably; cytological phenotype/morphology, biochemical type, nature/origin, severity/relative abundance and/or combinations of DNA lesion(s) concerned and respective point(s) within the cell cycle at which DNA damage has occurred .

Large tracts of ssDNA, generated as a consequence of stalled DNA polymerases during DNA replication at sites of DNA damage-induced lesions and resultant helicase dissociation at the advanced duplex replication fork, are coated with Replication Protein A (RPA) – which serves as a recognition trigger signal for the independent recruitment-activation of the “Rad9-Rad1-Hus1”, ATM and ATR/ATRIP complexes respectively (Byun T.S. *et al*, 2005; Delacroix S. *et al*, 2007; Richard D.J. *et al*, 2009; Walter J. and Newport J., 2000; Shin M.H. *et al*, 2012; Zou Y. *et al*, 2006).

The primary (proximal) transducer component proteins ATM (Ataxia Telangiectasia Mutated) and ATR (ATM and Rad3 Related) are members of the Phosphatidylinositol-3-OH Kinase-Related-Kinase (PIKK/PI3K) family, activated in early checkpoint responses upon binding to the end sites of DNA damage (Abraham R.T., 2001; Brown K.D. *et al*, 2003; Matsuoka S. *et al*, 1998; Savitsky K. *et al*, 1995; Smith G.C. *et al*, 1999; Smith J. *et al*, 2010).

These “proximal” transducer kinases specifically recognise and phosphorylate specific Ser and Thr residues within the “SQ/TP” phosphorylation-target motifs, displayed on their respective protein substrates, comprised of the characteristic consensus sequence; Ser-Thr-Gln-Glu (Kim S.T. *et al*, 1999).

ATM is a 350 kDa oligomeric protein which incorporates a myriad of “HEAT” (Huntingdon, Elongation Factor 3, PP2A substrate and TOR1) type sequence motifs (Bakkenist C.J. and Kastan M.B., 2003; Perry J. and Kleckner N., 2003) and possesses significant homology to phosphoinositide 3-kinases, but with the notable exception of an absence of lipid kinase activity respectively (Savitsky K. *et al*, 1995; Shiloh Y., 1997).

Under normal cytological conditions, the specific kinase activity of ATM is maintained at a regulatory suppressed minimal level in which the protein exists predominantly in its inactive heterodimeric complex state (Niida H. and Nakanishi M, 2006).

Conversion of the inactive homodimeric form of ATM, that exists predominantly within the normal, unstressed cytological environment, to the active monomeric species is triggered via protein-DNA interactions as a consequence of detected alterations in higher level chromatin supramolecular architecture which are induced via ionising radiation-induced duplex double-stranded breaks in conjunction with the formation of linear DNA substrates (Bakennist C.J. and Kastan M.B., 2003; Finn K. *et al*, 2012; Ira G. and Hastings P.J., 2012; Niida H. and Nakanishi M., 2006; Quevedo O. *et al*, 2012; Shin M.H. *et al*, 2012).

These associative ATM-DNA interactions induce supramolecular conformational rearrangements within the ATM homodimeric complex that thermodynamically-facilitate intermolecular autophosphorylation of a critical Ser1981 target residue within the kinase domain of each ATM monomer (Bakennist C.J. and Kastan M.B., 2003; Finn K. *et al*, 2012; Ira G. and Hastings P.J., 2012; Niida H. and Nakanishi M., 2006p; Shin M.H. *et al*, 2012).

Autophosphorylation of the ATM subunits at Ser 1981, within the ATM homodimer, functions as a sensitive/rapid “switch mechanism” for the induction of further supramolecular conformational changes within the homodimeric complex that promote dissociative formation of the active ATM monomeric species respectively and also expose the kinase active site of the protein to enable it to phosphorylate its “down-stream” transducer and effector targets (Bakennist C.J. and Kastan M.B., 2003; Finn K. *et al*, 2012; Ira G. and Hastings P.J., 2012; Niida H. and Nakanishi M., 2006; Shin M.H. *et al*, 2012) – Figs 1.21-1.27, pp.57-63.

The precise mechanism of activation of ATM, in response to ionising radiation type DNA damage-induced alterations of higher level chromatin supramolecular structure, remains to be elucidated.

Recent experimental studies have demonstrated that the implicated changes in chromatin conformational architecture may be detected by ATM at a considerable distance away from the originating double-stranded DNA break-site (DSB), in support of previous observations that have inferred that the initial early phase activation of ATM does not appear to involve association of ATM in close proximity and/or directly with the DSB site respectively (Niida H. and Nakanishi M., 2006; Finn K. *et al*, 2012; Ira G. and Hastings P.J., 2012; Quevedo O. *et al*, 2012).

Associative MRE11 protein interactions have also been demonstrated, *in vitro*, to enhance the catalytic kinase activity of post-activated ATM monomer and promote the cumulative recruitment of activated ATM to DSB-type DNA lesion sites within damaged chromatin (Finn K. *et al*, 2012; Ira G. and Hastings P.J., 2012; Lee J.H. and Paull T.T., 2004; Longhese M.P. *et al*, 2009; Niida H. and Nakanishi M., 2006).

The MRE11 protein is also a key component of the MRN complex, which is comprised of MRE11-RAD50-NBS1 associated proteins and participates in DSB type damage-site recognition/targeting events implicated in Homologous Recombination (HR) and Non-Homologous End-Joining (NHEJ) DNA repair pathways respectively (Carney J.P. *et al.*, 1998; Christmann M. *et al.*, 2003; Finn K. *et al.*, 2012; Ira G. and Hastings P.J., 2012) – discussed later in Section 1.2.5, p.109; Fig 1.48, p.109.

The primary (proximal) transducer ATM kinase also phosphorylates Ser residues, at positions 278 and 343, located within the NBS1 protein (Lim D.S. *et al.*, 2000) – Figs 1.21-1.24, pp.57-60.

These ATM-mediated post-translational phosphorylation events induce supramolecular conformational changes within NBS1 which serve as a critically favourable thermodynamic prerequisite for promotive associative participation of the protein in the formation of MRN complex foci at DSB-type DNA lesion sites within damaged chromatin (Zhao S. *et al.*, 2000).

ATM-mediated phosphorylation of BRCA1 is also a critical pre-requisite for the initiated formation of the BRCA1 Associated Surveillance Complex (BASC), which is comprised of a multi-functional interactions between various associative protein constituents that encompass; ATM, BLM, BRCA1, MLH1, MSH2 and MSH6 and the MRN complex respectively (Cortez D. *et al.*, 1999; Finn K. *et al.*, 2012; Foray N. *et al.*, 2003; Ira G. and Hastings P.J., 2012; Niida H. and Nakanishi M., 2006; Wang Y. *et al.*, 2000).

The BASC protein components MLH1 and MSH2 are also implicated in the direct activation of ATM in response to ionising radiation (I.R.)-induced DNA damage via two distinctive types of intrinsically-co-ordinated biochemical signalling events which are comprised of associative protein-protein binding interactions between ATM-MLH1 and MSH2-CHK2 (Brown K.D. *et al.*, 2003)

These ATM-MLH1 and MSH2-CHK2 associative protein interactions may also constitute a synergistic molecular scaffold mechanism for ATM-induced phosphorylation of CHK2 at Thr68 for activation of the S-phase cell-cycle checkpoint (Fig 1.21, p.57) and consequential initiation of DNA base mis-match repair (MMR) recognition of I.R.-induced DNA lesions respectively. (Matsuoka S. *et al*, 2000; Zhou B.B. *et al*, 2000; Christmann M. *et al*, 2003).

ATM-activated CHK2 kinase-induced phosphorylation of the histone 2AX protein (H₂AX), in close proximity to chromatin dsDNA breaks, may also constitute a biochemical sensory trigger for “downstream” signal recognition of these DNA lesions (Burma S. *et al*, 2001).

ATM phosphorylated-inactivation of the NF κ B kinase inhibitor (I κ B kinase) also triggers activation of the NF κ B kinase protein in response to dsDNA breakage events (Li N. *et al*, 2001).

In addition to ATM activation, as discussed previously (pp.35-37), the Mre11-Rad50-Nbs1 (MRN) complex also provides tracts of ssDNA substrate-binding sites for Replication Protein A (RPA), which are generated via MRN complex-mediated re-section of duplex dsDNA breakages (Jazayeri A. *et al*, 2006; Myers J.S. and Cortez D., 2006).

The resultant stretches of RPA-coated DNA, formed via the MRN complex-mediated rectification of DSB lesion sites, also act as recruitment substrates for activation of the ATR/ATRIP complex respectively. (Zou L. and Elledge S.J., 2003).

ATR exists predominantly in the form of a stable complex associated with its regulatory protein counterpart “ATRIP” – ATR-Interacting Protein (Cortez D. *et al*, 2001; Alderton G.K. *et al*, 2004; Unsal-Kacmaz K. and Sancar A., 2004) – Fig 1.17B, p.51; Fig 1.17C, p.53.

ATR is a 303 kDa protein, which shares significant sequence homology with the *H. sapiens* ATM and *S. pombe* Rad3 proteins respectively – hence its designated abbreviated name; ATR and Rad3-related protein (Cimprich K.A. *et al.*, 1996) – Fig 1.17B, p.53.

Previous experimental studies have indicated no measurable change in the overall kinase activity for ATR and thus it may be biochemically-primed to phosphorylate protein substrates in a constitutive manner in response to DNA damage (Abraham R.T., 2001; Finn K. *et al.*, 2012; Ira G. and Hastings P.J., 2012; Niida H. and Nakanishi M., 2006) – Fig 1.19, p.55.

Whilst more recent research work has established that the kinase activity of ATR may be induced via TopBP1-independent and TopBP1-dependent type mechanistic interactions with other proteins, such as FEM1B, MTA1 and RHINO, whose associative recruitment is co-ordinated via the sensory DNA sliding clamp Rad9-Rad1-Hus complex-coupled detection of DNA damage lesion sites within the chromatin supramolecular architecture (Cotta-Ramusino C. *et al.*, 2011; Li D.Q. *et al.*, 2010; Lin S.J. *et al.*, 2012; Navadgi-Patil V.M. and Burgers P.M., 2009; Pfander B. and Diffley J.F., 2011; Qu M. *et al.*, 2012; Smits V.A. *et al.*, 2010; Sun T.P. and Shieh S.Y., 2009) – Fig 1.19, p.55.

Experimental studies have also demonstrated that the ATR/ATRIP complex is implicated in the phosphorylated-modulation of a range of protein activities which initiate a variety of different DNA damage checkpoint response pathways, including; RAD9, H2AX, CHK1, CHK2 and p53 (Tibbetts R.S. *et al.*, 1999; Ward I.M. and Chen J., 2001; Liu Q. *et al.*, 2004) – Figs 1.20-1.27, pp. 56-63.

Taken together, the experimental evidence indicates that the ATR primary (proximal) transducer checkpoint kinase may exist in both constitutive and inducible forms whose respective functional activities are dependent upon its sub-cellular translocation in response to environmental stresses and/or genotoxic type cytological events which adversely impinge upon DNA replication.

In contrast to ATM, activation of ATR is also triggered via associative interactions of the protein with various ssDNA-protein complexes in response to bulky DNA base adducts/lesions – notably; U.V.-induced pyrimidine dimers, large base-adducts, DNA cross-links and stalled replication forks (Unsal-Kacmaz K. *et al*, 2002).

The overall major principle function of the primary (proximal) transducer proteins ATM and ATR, implicated in the initiation of various DNA damage response pathways, may be considered to be the phosphorylated activation of the secondary (distal) transducer type centrosome-associated checkpoint kinase proteins CHK1 (at Ser317 and Ser345), CHK2 at Thr68 and Ser123) and the p38 Mitogen-Activated Kinase (MAPK).

These three secondary (distal) transducer/effector kinases are implicated in the phosphorylation-mediated regulation of the activity of various “down-stream target” effector protein components that initiate the appropriate cell cycle checkpoint responses (Abraham R.T. *et al*, 2001; Brown A.L. *et al*, 1999; Bulavin D.V. *et al*, 2001; Bulavin D.V. *et al*, 2002; Chaturvedi P. *et al*, 1999; Matsuoka S. *et al*, 1998; Nyberg K.A. *et al*, 2002; Shieh S.Y. *et al*, 2000; Zhao H. and Piwnicka-Worms H., 2001), discussed summarily in Figs 1.21 – 1.27, pp.57-63.

Co-ordinated biochemical orchestration of orderly cell cycle progression is normally regulated via the modulated activity of Cyclin-Dependent Kinases (CDKs), which are inactive in the phosphorylated form and require appropriate temporal activation via CDC25 phosphatase-mediated dephosphorylated-induction of transient conformational changes within the CDK protein supramolecular structure, to enable the associative formation of the pre-requisite CDK-cyclin complexes that trigger specific sequential phases of the cell cycle (Nurse P., 1997; Morgan D.O., 1997; Sherr C.J. and Roberts J.M., 1999; Stewart Z.A. *et al*, 2003).

A core critical function of the CHK1, CHK2 and p38-MAPK kinase proteins is the phosphorylation of the CDC25 effector class of protein phosphatases (A, B and C) – which induce supramolecular conformational changes within the respective CDC25 protein which abrogate its functional interactions with its Cyclin-Dependent Kinase (CDK) effector target(s) via three main biochemical mechanisms (Banin S. *et al*, 1998; Canman C.E. *et al*, 1998; Niida H. and Nakanishi M., 2006), notably;

- (i) Promotion of thermodynamically-favoured complex formations between the CDC25 protein and the 14-3-3 class of proteins (eg 14-3-3 σ) and subsequent translocation of the resultant CDC25-14-3-3 protein complexes from the nucleus to the cytosol, where they are sequestered – with consequential inhibition of CDC25-CDK associative interactions. (Dalal S.N. *et al*, 1999; Hermeking H. *et al*, 1997; Peng C.Y. *et al*, 1997).
- (ii) Promotion of CDC25 protein ubiquitination events, prior to subsequent degradative destruction of the CDC25 protein (Mailand N. *et al*, 2000).
- (iii) Inactivation of the phosphatase catalytic active-site within the CDC25 protein with resultant inhibition of CDC25-mediated de-phosphorylation-activation of CDK targets and consequential perturbed formation of critical CDK-cyclin signaling complexes implicated in cell cycle progression (Niida H. and Nakanishi M., 2006).

CHK1- and CHK2- phosphorylated abrogation of the critical biochemical pre-requisite CDC25A-mediated dephosphorylation of Thr14 and Tyr15 of CDK2 inhibits the functional formation and activities of the CDK2-Cyclin A and CDK2-Cyclin E complexes with consequential initiated G1/S cell cycle arrest. (Falck J. *et al*, 2001a; Falck J. *et al*, 2001b; Mailand N. *et al*, 2000; Niida H. and Nakanishi M., 2006; Peng C.Y. *et al*, 1997; Sanchez Y. *et al*, 1997) – Fig 1.21, p.57.

Whilst p38-MAPK-phosphorylated abrogation of CDC25A phosphatase activity inhibits the functional formation and activity of the CDK4-Cyclin D and CDK6-Cyclin D complexes with consequential initiation of G1/S cell cycle arrest (Lavoie J.N. *et al*, 1996; Yee A.S. *et al*, 2004; Thornton T.M. and Rincon M., 2009) – Fig 1.24, p.60.

CHK1- and CHK2- phosphorylated abrogation of the the critical biochemical pre-requisite CDC25C-mediated dephosphorylated-activation of CDK1 (also known as Cdc2) inhibits the function formation and activities of the CDK1-Cyclin A and CDK1-Cyclin B complexes with consequential induction of G2/M cell cycle phase arrest (Abraham R.T. *et al*, 2001; Niida H. and Nakanishi M., 2006) – Fig 1.23, p.59.

Protein phosphatase CDC25B-targeted dephosphorylation of CDK1 induces supramolecular conformational changes within the activated Cyclin-Dependent Kinase protein which promote the associative formation of the CDK1-Cyclin B1 complex (Schmitt E. *et al*, 2006).

The CDK1-Cyclin B1 heterodimeric complex is a key functional biochemical signaling component in the mechanistic regulation of centrosomal microtubule nucleation events which are implicated in the modulatory control of the G2/M interphase transitional progression of the cell cycle prior to initiation of early mitotic phase commitment (Schmitt E. *et al*, 2006; Trovesi C. *et al*, 2011).

Unlike the CDC25A and CDC25C phosphatases, the CDC25B phosphatase functions as both a constitutive effector protein in the absence of DNA damage and an inducible effector protein under cytological conditions of genotoxic stress (Schmitt E. *et al*, 2006).

In the absence of DNA damage, constitutive CHK1-mediated phosphorylated-inactivation of the CDC25B phosphatase (at N-terminus Ser151 and Ser230 residual sites) is a key negative feedback biochemical regulatory mechanism which serves two critical purposes; the cytological prevention of catastrophic premature cell division and premature apoptotic induction (Schmitt E. *et al*, 2006).

Phosphorylation of Ser230 within the CDC25B phosphatase is an essential pre-requisite for the centrosomal localisation of protein to enable it to elicit the progressive duration of early S-phase through to mitosis (Schmitt E. *et al*, 2006) – Fig 1.24, p.60.

Whilst phosphorylation of both Ser151 and Ser230 N-Terminal Domain residues, within the CDC25B phosphatase protein, is an essential pre-requisite for the associative formation of the dimerised 14-3-3 σ :CDC25B complex – which is then translocated out of the nucleus and sequestered in the cytoplasm with consequential inhibition of CDK1-Cyclin B functional activities and initiated G2/M arrest (Schmitt E. *et al*, 2006) – Fig 1.24, p.60.

Inducible CHK1- and CHK2-mediated phosphorylated-inactivation of the CDC25B phosphatase (at Ser151, Ser230 and Ser563 residual positions), in response to upstream DNA damage signal transduction, triggers the G2 Checkpoint and subsequent G2/M phase cell-cycle arrest as a consequence of the inhibited formation and functional activities of the CDK1-Cyclin B complex (Dalal S.N. *et al*, 1999; Schmitt E. *et al*, 2006) – Fig 1.24, p.60.

Phosphorylation of Ser563, situated in close proximity to the CDK1 substrate-binding domain contained within the catalytic active-site of the CDC25B phosphatase protein, induces supramolecular conformational changes within the enzyme which inhibit its dephosphorylation of CDK1 with consequential abrogation of associative formation and functional activities of the CDK1-Cyclin B heterodimeric complex and initiation of G2/M cell cycle arrest (Schmitt E. *et al*, 2006) – Fig 1.24, p.60.

Phosphorylated-inactivation of the CDC25B protein, independent of “downstream” CHK1 and CHK2 biochemical cell-cycle modulatory signal transduction events, is also elicited via the p38 α MAPK/MAPKAP2 pathway in response to U.V.-induced DNA damage (Bulavin D.V. *et al*, 2001; Bulavin D.V. *et al*, 2002; Nyberg K.A. *et al*, 2002) – Fig 1.24, p.60.

In this case, phosphorylated-activation of the p38 α Mitogen Activated Kinase (p38 α MAPK) protein, via MAPK Activating Protein Kinase 2 (MAPKAP2), enables it to phosphorylate CDC25B at residual position Ser309 (Bulavin D.V. *et al*, 2001; Bulavin D.V. *et al*, 2002; Nyberg K.A. *et al*, 2002) – Fig 1.24, p.60.

p38-MAPK-mediated phosphorylation of Ser309 within CDC25B induces supramolecular conformational changes in the CDK phosphatase protein that thermodynamically promote associative binding interactions with 14-3-3 proteins resulting in cytoplasmic sequestration of the CDC25B–14-3-3 protein complex with consequential inhibition of CDK1 activation, perturbed associative formation and activities of the CDK1-Cyclin B complex, culminating in G2 checkpoint activation and G2/M cell-cycle phase arrest (Bulavin D.V. *et al*, 2001; Bulavin D.V. *et al*, 2002; Nyberg K.A. *et al*, 2002) – Fig 1.24, p.60.

The expression of Cyclin-Dependent Kinases (CDKs) is constitutive throughout the entire cell cycle and their respective activity levels are also regulated via two main families of Cyclin-Dependent Kinase Inhibitors (CDKIs), in addition to interactions with CDC25 phosphatases, which are implicated collectively in the modulatory control of the cell cycle checkpoints, namely;

(i) The INK4-type class of CDKIs, which include; p16INK4A (p16), p15INK4B (p15), p18INK4C and p19INK4D (p19).

(ii) The Cip/Kip-type class of CDKIs, which include; p21/Waf1/Cip1 (p21), p27/Kip1 (p27) and p57/Kip2 (p57).

The INK4-type CDKIs inhibit the activity of the CDK4 and CDK6 proteins and are G1-phase specific, whilst the Cip/Kip-type CDKIs possess a greater degree of versatility with respect to their capability to inhibit a range of CDKs throughout all phases of the cell cycle (Fig 1.20, p.56; Fig 1.21, p.57; Fig 1.24, p.60; Fig 1.27, p.63).

Cytological control of the relative levels and activities of cyclins during cell cycle progression is elicited via regulatory transcriptional mechanisms which result in the induction or suppression of cyclin-encoding genes and via polyubiquitination-type post-transcriptional modification cyclin-targeted proteosomal degradation events (Knoepp D.M. *et al*, 1999; Stewart Z.A. *et al*, 2003).

Both primary and secondary DNA damage checkpoint signal transducer kinase proteins; ATM, ATR/ATRIP, CHK1, CHK2 and p38-MAPK, are also implicated in the phosphorylation-enhanced stabilisation and activation of the effector “downstream” tumour-suppressor protein p53.

The p53 protein is a versatile sequence-specific inductive transcriptional regulator which binds to the promoter-target domains of a range of modulatory genes that are implicated in the control and initiation of cell cycle progression, apoptosis, cell-cycle phase-specific arrest and DNA repair respectively (Shieh S.Y. *et al*, 2000; Kim M.Ae. *et al*, 2007) – Fig 1.21, p.57 and Fig 1.24, p.63.

In addition, the p53 protein also self-regulates its own turn-over rate and relative transcriptional activity via a negative feedback mechanism upon binding to the promoter region of the *MDM2* gene with consequential elevated expression of the “ring-finger” ubiquitin ligase protein.

The resultant enhanced expression of the MDM2 protein and consequential formation of the associative MDM2-p53 heterodimeric complex, targets the p53 protein for ubiquitination-mediated proteosomal degradation (Chen B.J. *et al*, 1994; Chehab N.H. *et al*, 1999; Kastan M.B., 1999; Unger T. *et al*, 1999; Hirao A. *et al*, 2000; Vogelstein B. *et al*, 2000; Maya R. *et al*, 2001).

The Rad9-Rad1-Hus1 complex is currently postulated to function as a DNA damage scanner which may slide back and forth along DNA-associated chromatin supramolecular structural complexes, thereby acting as a continual “early-warning safe-guard monitoring system” of genomic integrity. (Burtelow M.A. *et al*, 2000; Roos-Mattjus P. *et al*, 2002) – discussed previously in Section 1.2.1, pp.23-32.

The C-Tail terminal domain of the Rad9 sub-unit, which protrudes out of the “9-1-1” sliding-clamp sensory complex (Fig 1.10B, p.24; Fig 1.17A, p.53), possesses a high degree of disordered structure propensity which enables the polypeptide chain to adopt a wide array of transient supramolecular configurations that facilitate its associative interactions with a variety of different cell cycle signalling and repair factor proteins in response to detected DNA damage lesion sites.

The Rad9 C-Terminal Tail domain also contains SQ/TP type kinase and phosphatase target motifs which engage in transient residue-specific constitutive and inducible phosphorylated/de-phosphorylated types of protein-interactive events that are implicated in the modulation of various ATR → Chk1 and ATR → p38MAPK signal transduction-initiated cell cycle checkpoint pathway responses to replication stress and genotoxic events (Chen M-J. *et al*, 2001; Fujinaka Y. *et al*, 2012; Roos-Mattjus P. *et al*, 2003; St Onge R.P. *et al*, 2001; St. Onge R.P. *et al*, 2003), discussed summarily in Figs 1.20 – 1.29, pp.56-65.

Both ATM and ATR primary (proximal) transducer checkpoint kinases phosphorylate specific residues within the C-tail terminal domain of the Rad9 protein sub-unit in response to replication stress- and/or genotoxic event- induced DNA damage lesions which are detected by the “9-1-1” sensory DNA sliding-clamp complex (Chen M-J *et al*, 2001; Fujinaka Y. *et al*, 2012; Shin M.H. *et al*, 2012; St. Onge R.P. *et al*, 2001; St. Onge R.P. *et al*, 2003) – Fig 1.16, p.52.

Methylation of the Rad9 sub-unit, at specific arginine residues R172, R174 and R175, is a critical post-translational modification pre-requisite for the induction of supramolecular conformational changes within the protein which may be implicated in initial ATR activation (via associative “HFD” motif interactions) and promote engagement of its C-Terminal Tail Domain with the ATM, ATR and CK2 kinases (Dai Y. and Grant S., 2010; He W. *et al*, 2011; Nadvadgi-Patil V.M. and Burgers P.M., 2009; Shangary S. *et al*, 2000) – Fig 1.16, p.52; Fig 1.17A, p.53.

Induction of supramolecular changes within the C-terminal tail domain of Rad9, mediated via Casein Kinase 2 (CK2)- and ATR-mediated phosphorylation of the Ser387 side-chain (Fig 1.17A, p.53), enables it to associate with the Topoisomerase II β Binding Protein 1 (TopBP1) N-terminal BRCT I and BRCT II domains. (Delacroix S. *et al*, 2007) – Fig 1.17D, p.53; Fig 1.18, p.54.

ATM phosphorylation of the Rad9 C-terminal domain at Ser272 (Shangary *et al*, 2000; Shin M.H. *et al*, 2012), may also be implicated in the induction of supramolecular conformational changes within the protein which serve to enhance the associative ATR/ATRIP-TopBP1-“9-1-1”-BRCA1 ternary complex interactions that initiate CHK1 activation (Rappas M. *et al*, 2010; Shangary S. *et al*, 2000; Shin M.H. *et al*, 2012) – Fig 1.17A, p.53; Fig 1.18, p.54.

From a biochemical mechanistic overview of CHK1 activation, TopBP1 may be considered as a BRCT-domain interactive biomolecular co-ordinator of the associative “9-1-1”, ATR-ATRIP and BRCA1 complex integral functions which are implicated in the mediation of Chk1 kinase-initiated cell cycle checkpoint responses to replication stress and genotoxic cytological events (Delacroix S. *et al*, 2007; Lee J. *et al*, 2007) – Figs 1.18-1.20, pp.54-56.

The resultant “Rad-Rad1-Hus1 DNA sliding-clamp complex – TopBP1” interaction-induced supramolecular conformational changes within the TopBP1 protein permit access and binding of the ATR-ATRIP complex to the ATR-Activating Domain (AAD), located between BRCT VI and BRCT VII domains of the TopBP1 protein, accompanied by consequential “positive-feedback” activation of the ATR kinase (Delacroix S. *et al*, 2007).

Additional “TopBP1 – ATR/ATRIP” complex-induced supramolecular conformational changes enable formation of associative interactions between the Breast Cancer Susceptibility Protein (BRCA1) and the BRCT domains of TopBP1 (Delacroix S. *et al*, 2007; Foray N. *et al*, 2003) – Figs 1.21-1.24, pp.57-60.

Each respective associative BRCT domain-protein complex interaction, within the TopBP1 protein, is formed via a “head-to-tail” supramolecular α - β - α anti-parallel dimerised tandem (BRCT)₂ configuration in which the N-terminal face of one BRCT domain is orientated opposite the two C-terminal α -helices of the other BRCT domain via an extended “inter-BRCT-bridging” hairpin polypeptide loop (Kilkenny M.L. *et al*, 2008; Manke I.A. *et al*, 2003; Rodriguez M. *et al*, 2003).

The resultant tandem (BRCT)₂ configurations form phosphopeptide motif sub-domain binding pockets for specific phosphorylated proteins (such as Rad9 and BRCA1), which are stabilised via an intricate symmetrical self-complementary inter- and intra- hydrogen-bonding network of side-chain and main-chain Ser residues and peptide-backbones of A, L, T, E residues which is “thermodynamically-reinforced” via hydrophobic C, H, L, P, R, S, Y residual interactions (Kilkenny M.L. *et al*, 2008; Manke I.A. *et al*, 2003; Rodriguez M. *et al*, 2003).

The adaptor protein Claspin is also currently postulated to be essential for the correct orientation of the ATR protein and the “9-1-1” complex in a specific protein-protein interactive supramolecular complex configuration to enable ATR to phosphorylate the C-terminal tail domain of the hRad9 protein at Ser 387 (Chini C.C. and Chen J., 2003; Sar F. *et al*, 2004; Sorensen C.S. *et al*, 2004; Liu S. *et al*, 2012).

[As discussed previously (p.46), phosphorylation of the Ser387 residue within the C-Terminal Tail Domain of Rad9, which protrudes out of the sensory “9-1-1” DNA sliding-clamp complex, is an essential post-translational modification pre-requisite for associative interactions with the TopBP1 protein (Delacroix S. *et al* , 2007) – Figs 1.17, p.53 and Fig 1.18, p.54.

This hypothesis is based upon investigative experimental observations that have indicated that the “ring-like” supermolecular structure of Claspin binds to stalled DNA replication forks with a high degree of specificity in which the protein may participate in direct associative interactions with various branched DNA structures (Sar F. *et al*, 2004).

In this respect, Claspin is also postulated to function as a critical associative detector element for ATR/ATRIP complex-recognition of stalled DNA replication forks and co-ordination of ATR phosphorylated-activation of CHK1-initiated checkpoint pathways which elicit the delayed origin-firing of DNA replication forks (Shechter D. *et al*, 2004) – Figs 1.17, p.53 and Fig 1.18, p.54.

Claspin is predominantly localised within the cell nucleus and its phosphorylation, in response to DNA damage and replicative stress, is an essential post-translational modification-induced supramolecular conformational transitional pre-requisite which enables the protein to interact with the associative ATR/ATRIP/“9-1-1” complexes and the secondary (distal) transducer protein kinase CHK1 respectively (Chini C.C. and Chen J., 2003) – Fig 1.18, p.54.

Claspin-enhanced synergistic interaction of CHK1 with the ATR/ATRIP and “9-1-1” complexes facilitates maximal ATR phosphorylated-activation of CHK1 (triggered via initial formation of ATR- and Rad9 C-terminal tail domain- TopBP1 associative complexes) with consequential amplified transduction of the DNA damage response signal to various down-stream biochemical effector targets (Chini C.C. and Chen J., 2003; Delacroix S. *et al*, 2007) – Figs 1.17, p.53 and Fig 1.18, p.54.

In conclusive summary, the Rad9-Rad1-Hus1 complex both senses DNA damage and triggers ATR/ATRIP-initiated downstream cell-signalling cascades (Fig 1.20, p.56) that elicit the appropriate G1/S, Intra-S, G2/M (Figs 1.21-1.26, pp.57-62) and Intra-M phase (Figs 1.27-1.29, pp.63-65) types of checkpoint-mediated cell cycle arrest, apoptosis and/or DNA repair responses (Dai Y. and Grant S., 2010).

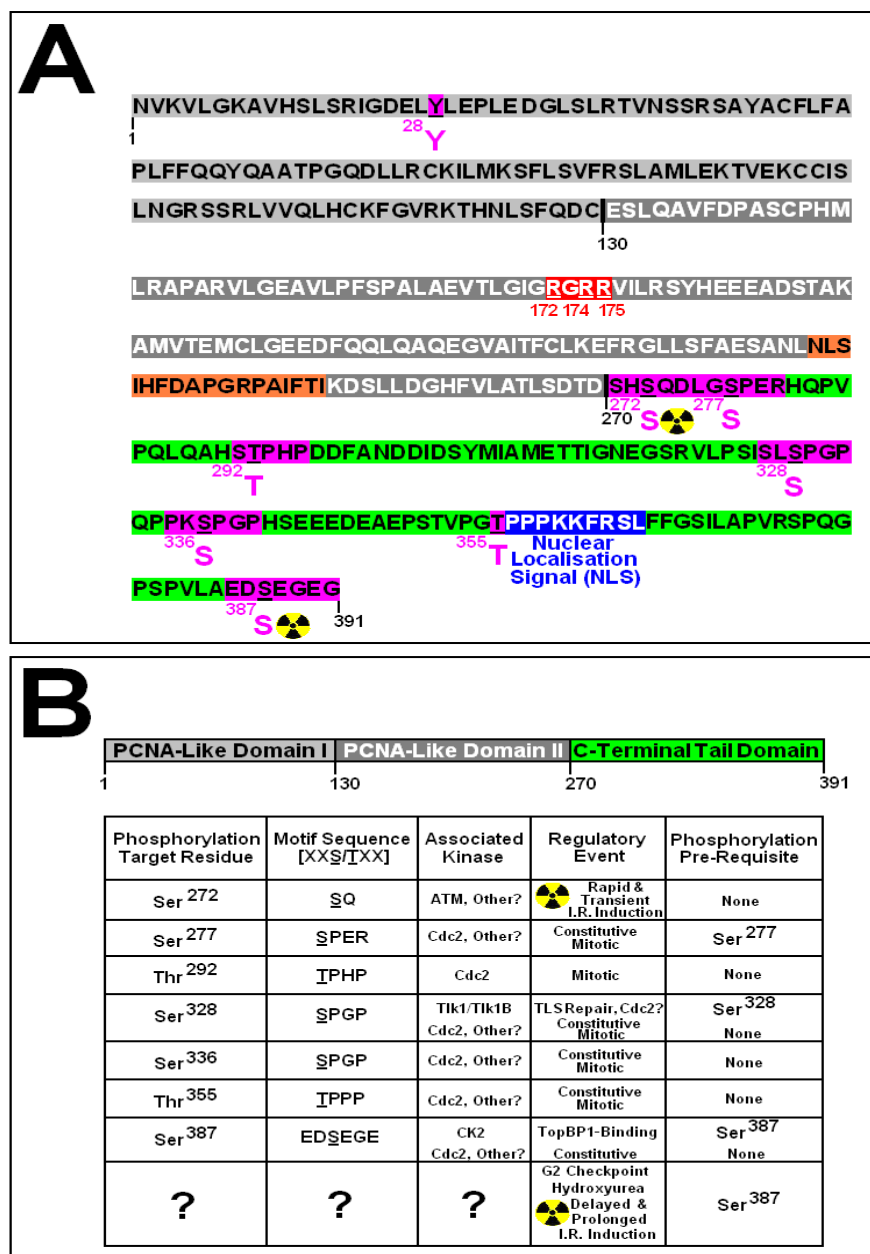
Protein Kinase C δ is also known to be implicated in the constitutive and genotoxic-induced phosphorylation of Rad9 (Yoshida K. *et al*, 2003).

At least 9 potential Protein Kinase C δ phosphorylated target sites have been identified within the Rad9 protein, which may be implicated in the post-translational generation of differential phosphorylation-state isoforms of Rad9 that may elicit specific modulatory functions on cell cycle checkpoint-mediated signalling responses to different types of DNA damage and/or replication stress (Yoshida K. *et al*, 2003).

Selection of these checkpoint responses may in turn be “biochemically-governed” via the nature and extent of DNA damage, in conjunction with the temporal point(s) within the cell cycle where specific genotoxic and/or replication stress events occur (Matsuoka S. *et al*, 1998; Brown A.L. *et al*, 1999; Chaturvedi P. *et al*, 1999; Shieh S.Y. *et al*, 2000; Abraham R.T. *et al*, 2001; Zhao H. and Piwnicka-Worms H., 2001).

Additional PCNA-Rad9-Hus1 interactions may also mediate biochemical “cross-talk” signals between the various cell cycle checkpoint pathways, to elicit inhibition of DNA replication in response to particular genotoxic and/or replication stress events, as an additional level of control which serves as “back-up/safe-guard” mechanism for the cytological preservation of genomic integrity. (Komatsu K. *et al*, 2000c).

Fig 1.16: hRad9A – Key Checkpoint Signalling Domains & Residues



A: Elementary Functional Proteomic Signalling Domain Map of the hRad9A Protein [Uniprot: Q99638]

R172, R174, R175 = PRMT5 Methylase-Targeted Arginine Residues Implicated in DNA Damage Checkpoint Signalling (He W. *et al.*, 2011).

XXXX = Potential “HFD” Functional Motif Implicated in Associative Enhancement of ATR Kinase Activity (Navadgi-Patil V.M. and Burgers P.M., 2009).

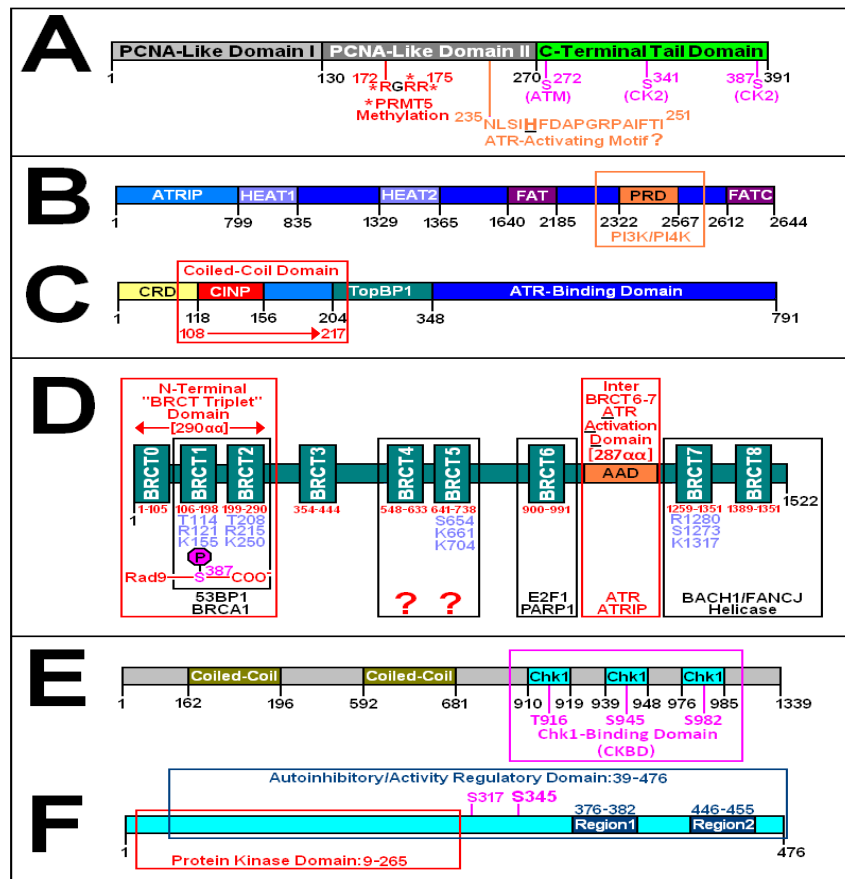
XXXX = Kinase/Phosphatase Target Motif Sites Implicated in Cell Cycle DNA Damage Checkpoint Signalling (Canfield C. *et al.*, 2009; Chen M. *et al.*, 2001; St. Onge R.P. *et al.*, 2001; St. Onge R.P. *et al.*, 2003; Ueda S. *et al.*, 2012; Yoshida K. *et al.*, 2002).

XXXX = Nuclear Localisation Signal Motif (Hirai I. and Wang H-G., 2002; Kadir R. *et al.*, 2012).

B: hRad9A C-Terminal Tail Protein Kinase/Phosphatase Interactive Phosphorylation Target Motif Sites Implicated in Cell Cycle Checkpoint Modulatory Signal-Mediated DNA Damage Response Type Pathways. (Compiled via Collated Information From: Canfield C. *et al.*, 2009; Chen M.J. *et al.*, 2001; St. Onge R.P. *et al.*, 2003).

[NOTE: Phosphorylation sites at Y28 (located within the N-terminal domain) and the C-Terminal tail domain of hRad9 are also implicated in critical S/M checkpoint control events with regard to signal transduction-mediated inhibition of premature chromosomal condensation events throughout the entire duration of the S-phase of the cell cycle, prior to M-phase initiation (Zhang C. *et al.*, 2008).]

Fig 1.17: Key Features of ATR- and Chk1- Activation Proteins



A: Key Checkpoint Signalling Residues and Motifs within the human Rad9A protein, of particular note; the C-terminal tail domain residues phosphorylated by ATM and Casein Kinase 2 (CK2), the “HFD” motif implicated in enhanced activation of the human ATR kinase (Fig B) and methylation of three key Arginine residues (R172, R174 and R175) by the PRMT5 methylase enzyme, all of which are implicated in human Rad9-mediated activation of the human Chk1 cell cycle checkpoint kinase (Dai Y. and Grant S.; 2010; He W. *et al.*, 2011; Navadgi-Patil M. and Burgers P.M., 2009). [Uniprot: Q99638]

B: Key Structural Domains and Functional Motifs within the human ATR cell cycle checkpoint kinase protein, of particular note; the N-terminal ATRIP-binding domain, the two “HEAT” domain motifs (Huntingdon, Elongation Factor 3, PP2A Substrate and TOR1), the “FAT/FAT-C” motif domains (FRAPP, ATM, TRAPP) and the “PRD” (PIKK, PI3K/PI4K Kinase Domain) – whose catalytic activity may be enhanced via associative allosteric interactions of the ATR protein with the “HFD” motif situated within the human Rad9A protein (Fig A). (Mordes D.A. *et al.*, 2008; Mordes D.A. and Cortez D., 2008; Navadgi-Patil M. and Burgers P.M., 2009) [Uniprot: Q13535]

C: Key Structural Domains and Functional Motifs within the human ATR-Interacting Protein (ATRIP) partner of the human ATR cell cycle checkpoint kinase (Fig B), of particular note; the N-Terminal Checkpoint Recruitment Domain (CRD), the ATR-binding domain, the TopBp1 checkpoint mediator protein-binding domain and the CDK2-Interacting Protein Domain (CINP) (Lovejoy C.A. *et al.*, 2009; Mordes D.A. and Cortez D., 2008). [Uniprot: QW8XE1]

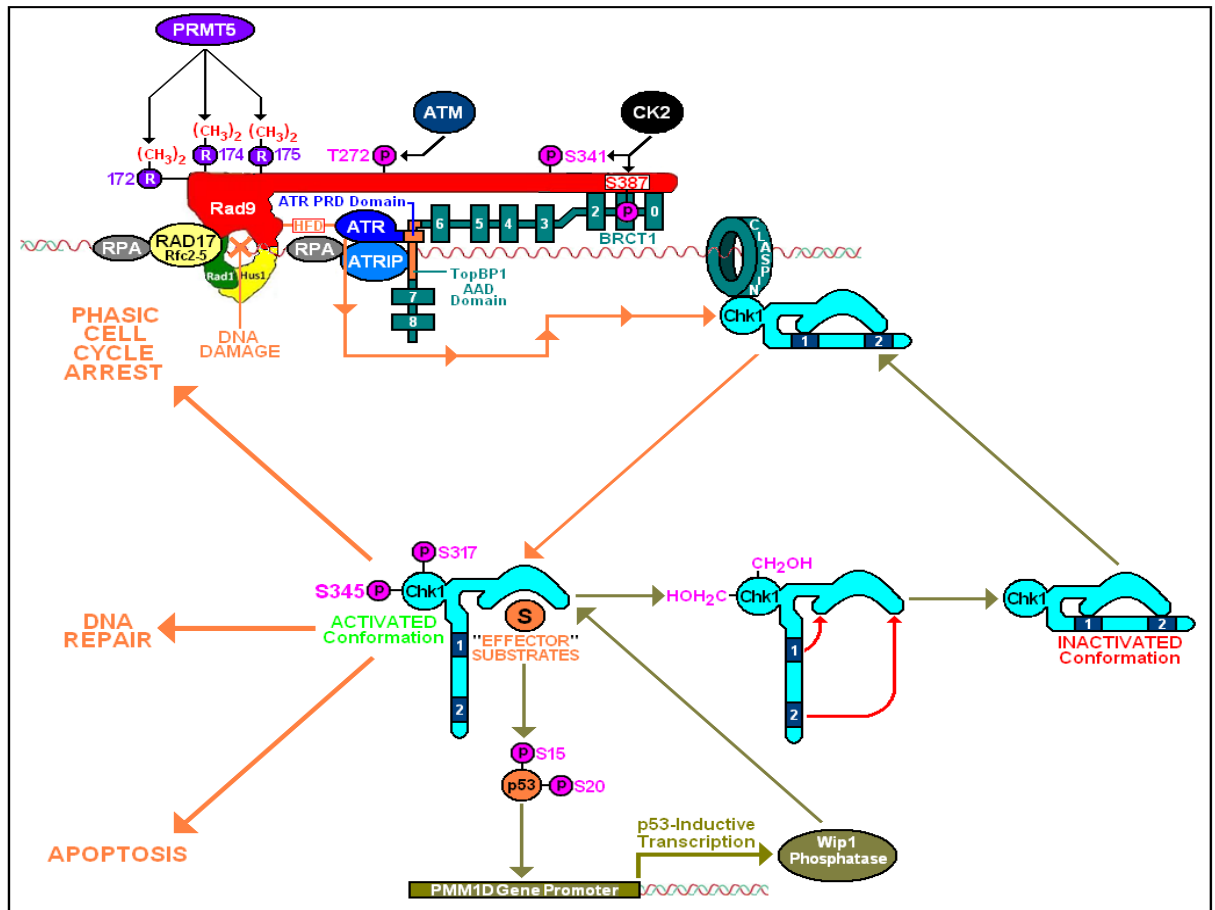
D: Key Functional BRCT Domains and Amino Acid Residues of the TopBP1 Mediator/“Scaffold” protein, of particular note; The N-Terminal BRCT Triplet Domain which associates with the human Rad9A protein (Fig A) via BRCT1 sub-domain interactions with the ATR (Fig B)-phosphorylated Ser387 residue of the human Rad9A C-Terminal Tail Domain and the ATR Activation Domain (AAD) which associates with the PRD Domain of ATR and allosterically enhances its kinase catalytic activity (Fig B) (Huo Y.G. *et al.*, 2010; Mordes D.A. *et al.*, 2008; Rappas M. *et al.*, 2010; Yan S. and Michael W.M., 2009a; Yan S. and Michael W.M., 2009b). [Uniprot: Q92547]

E: Key Functional Domains of the Claspin Mediator/“Scaffold” ring protein, of particular note; the coiled-coil domains which are implicated in associative DNA interactions and the three Chk1 (Fig F) interactive sites and their key phosphorylated Ser residues within the Chk1-Binding Domain (CKBD) (Sierant M.L. *et al.*, 2010; Tanaka K., 2010). [Uniprot: Q9HAW4]

F: Key Functional Domains of the Chk1 Checkpoint Signal Transducer protein, of particular note; The N-Terminal Catalytic Kinase Domain and Key Phosphorylation Sites and Associative Kinase Active Site Lid Sub-Domains (Regional Motifs 1 and 2) within the Autoinhibitory/Activity Regulator Domain (Tapia-Alveal C. *et al.*, 2009). [Uniprot: O14757]

Fig 1.18: “9-1-1” Clamp-Orchestrated Chk1 Activation

[Collated via Adapted Information Taken From: Canton D.A. and Scott J.D., 2010; Cimprich K.A. & Cortez D., 2008; den Elzen N. *et al.*, 2004; Fujinaka Y. *et al.*, 2012; He W. *et al.*, 2011; Leung- Pineda V. *et al.*, 2006; Mordes D.A. and Cortez D., 2008; Navadgi-Patil V.M. & Burgers P.M., 2009; Navadgi-Patil V.M. & Burgers P.M., 2011; Palermo C. *et al.*, 2008; Rappas M. *et al.*, 2010; Tanaka K., 2010; Sierant M.L. *et al.*, 2010; Smith J. *et al.*, 2010; Yan S. & Michael W.M., 2008a; Yan S. & Michael W.M., 2008b; Tapia-Alveal C. *et al.*, 2009; Ueda S. *et al.*, 2012; Warmerdam D.O. *et al.*, 2010]



Essential post-translational modifications of the Rad9 protein for “9-1-1” clamp complex-initiation of the ATR→Chk1 DNA damage response pathways are PRMT5-mediated methylation of Rad9 at Arg172, Arg174 and Arg175), ATM-mediated phosphorylation at Thr272 residue and Casein Kinase 2 (CK2) –mediated phosphorylation of Ser341 and Ser387 (Dai Y. and Grant S., 2010; He W. *et al.*, 2011) – Fig 1.17A, p.53.

Interactions between the Rad9 “HFD” ATR-activation motif and ATR, in conjunction with association of the ATR catalytic PRD domain with the TopBP1 AAD domain, which is facilitated via the proximal association of the TopBP1 protein with the Rad9 C-terminal tail domain (via the TopBP1 BRCT Domain – Rad9-S387 Casein Kinase 2 (CK2)-phosphorylated residue) activates the ATR kinase (Mordes D.A. *et al.*, 2008; Mordes D.A. and Cortez D., 2008; Navadgi-Patil V.M. and Burgers P.M., 2009; Rappas M. *et al.*, 2010) – Figs 1.17A, 1.17B, 1.17D, p.53.

Subsequent “9-1-1” clamp-complex recruitment of claspin, facilitates its phosphorylation by ATR (at Thr919, Ser945 and Ser982) which induces supramolecular configurational changes that mediate associative interactions of the secondary (distal) checkpoint kinase Chk1 within the Chk1-binding domain of the adaptor protein (Sierant M.L. *et al.*, 2010; Tanaka K., 2010) – Fig 1.17E, p.53.

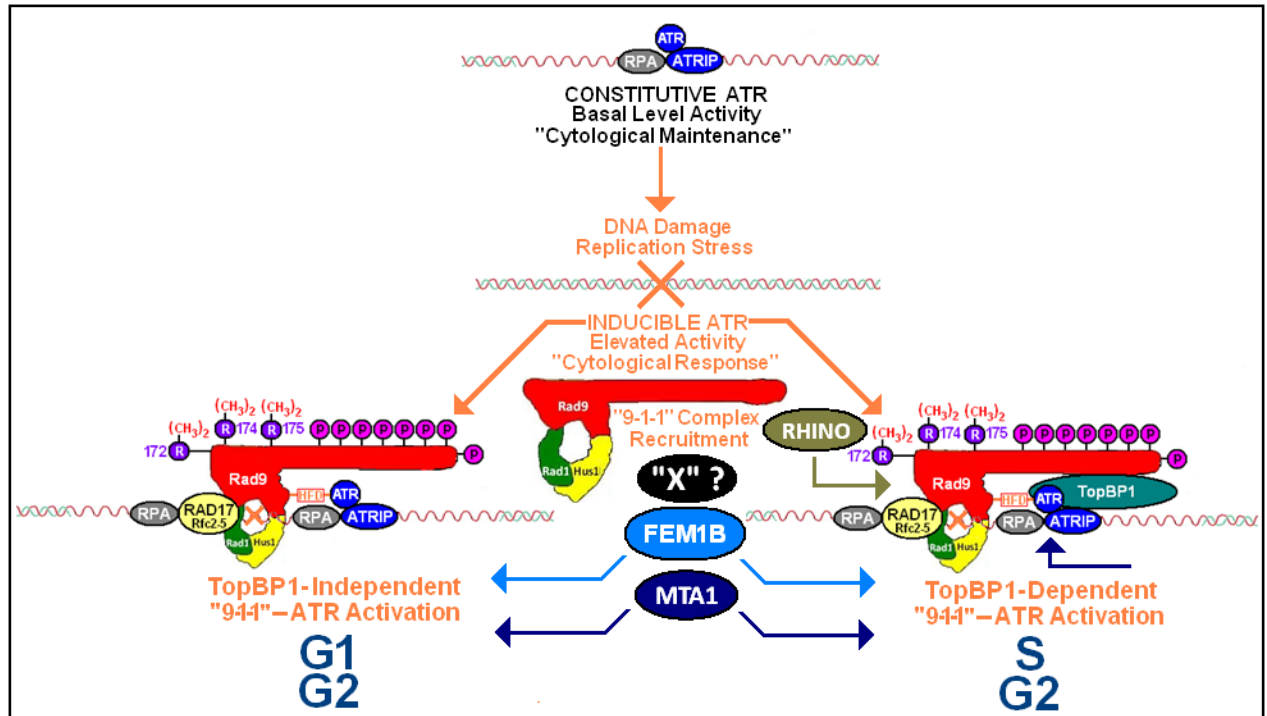
Subsequent ATR-mediated phosphorylation-activation of Chk1 (at Ser317 and Ser345) induces supramolecular configurational changes within the secondary (distal) transducer checkpoint kinase which promote domain lid-dissociation from the catalytic active site and thus enable Chk1 to phosphorylate its downstream protein effector targets for elicitation of the appropriate cytological responses to the “9-1-1” clamp sensor-detected genotoxic- and/or replication stress- induced DNA damage lesions (Tapia-Alveal C. *et al.*, 2009; Warmerdam D.O. *et al.*, 2010) – Fig 1.17F, p.53.

Chk1-mediated phosphorylation-activation of the p53 protein, enables it to associate with the *PMM1D* gene promoter and induce expression of the Wip1 protein phosphatase, which also targets and dephosphorylates Chk1 (at Ser317 and Ser345), with consequential initiation of supramolecular conformational changes within the checkpoint kinase which promote re-association of the lid domains 1 and 2 with the catalytic site for Chk1 inactivation – thereby providing a negative feedback mechanism for regulation of Chk1-mediated DNA damage signalling (den Elzen N. *et al.*, 2004; Leung-Pineda V. *et al.*, 2006) – Fig 1.17F, p.53.

Regulation of Chk1 activity is also mediated via associative interactions with the 14-3-3σ for cytosolic sequestration of the resultant Chk1:14-3-3σ complex, thereby preventing Chk1 from phosphorylating its nuclear-localised protein effector targets (Canton D.A. and Scott J.D., 2010; Dunaway S. *et al.*, 2005).

Fig 1.19: Constitutive and Inducible Models of ATR Activation

[Compiled via Collated Information Adapted From: Cotta-Ramusino C. *et al.*, 2011; Fujinaka Y. *et al.*, 2012; Li D.Q. *et al.*, 2010; Lin S.J. *et al.*, 2012; Mordes D.A. *et al.*, 2008; Mordes D.A. and Cortez D., 2008; Pfander B. and Diffley J.F., 2011; Qu M. *et al.*, 2012; Smith J. *et al.*, 2010; Smits V.A. *et al.*, 2010; Sun T.P. and Shieh S.Y., 2009



Under normal cytological conditions, a basal level of associative RPA:ATRIP-mediated constitutive ATR activity is sufficient for maintenance of genomic integrity (Smits V.A. *et al.*, 2010).

Genotoxic cytological conditions of DNA damage, replication stress and/or other environmental stresses induce elevated levels ATR activity via TopBP1-independent and TopBP1-dependent mechanisms which are mediated via associative Rad9 functional C-Terminal Tail Domain protein interactions within the “9-1-1” clamp complex (Smits V.A. *et al.*, 2010).

The TopBP1-independent mechanism of “9-1-1” clamp complex-enhanced ATR activation may proceed via allosteric modulation of the catalytic kinase activity of the PRD domain of ATR (Fig 1.17B, p.53) via Rad9 “HFD” motif domain interactions with the ATR checkpoint kinase protein and elicits G1 and G1 cell cycle phasic arrest in response to genotoxic events (Navadgi-Patil V.M. and Burgers P.M., 2009; Smits V.A. *et al.*, 2010)

The TopBP1-dependent mechanism of “9-1-1” clamp complex-enhanced ATR activation, discussed previously in Fig 1.18, p.54, elicits S and G2 cell cycle phasic arrest in response to genotoxic events (Smits V.A. *et al.*, 2010).

The FEM1B protein (human homologue of the *Caenorhabditis elegans* sex determination fem1 protein) may also be implicated in functional associative Rad9 C-terminal tail domain interactions which elicit the “9-1-1” clamp complex-mediated TopBP1-independent and TopBP1-dependent mechanisms of elevated ATR checkpoint kinase-mediated phosphorylated-activation of Chk1-initiated cell cycle checkpoint responses to DNA damage and replication stress (Sun T.P. and Shieh S.Y., 2009).

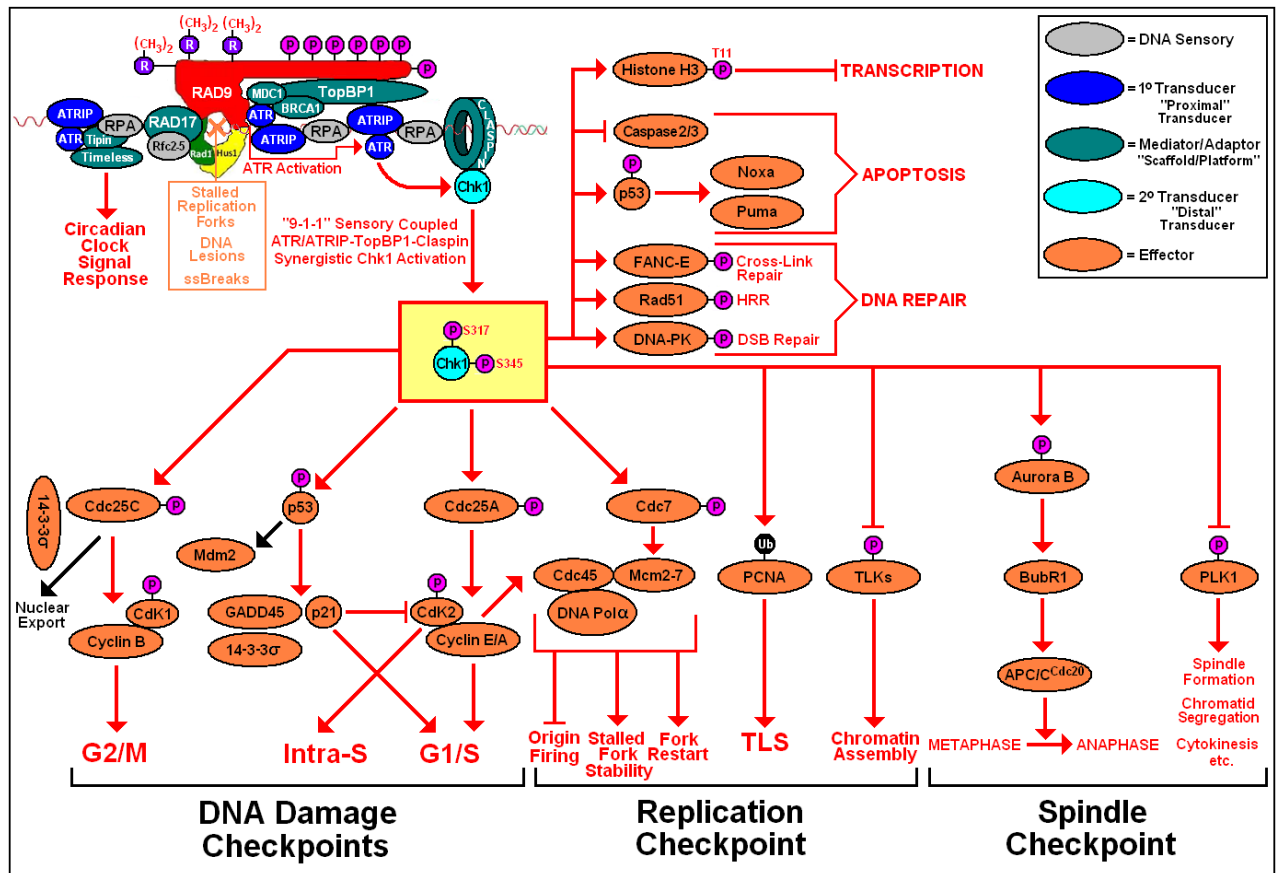
A recently discovered novel protein, “RHINO” (“Rad9-Rad1-Hus1 Interacting Orphan”) has also been demonstrated to associate with both Rad9 and TopBP1 and may therefore be implicated in the TopBP1-dependent mechanism of elevated ATR checkpoint kinase-mediated phosphorylated-activation of Chk1-initiated cell cycle checkpoint responses to DNA damage and replication stress (Cotta-Ramusino C. *et al.*, 2011).

The MTA1 protein (Metastasis-Associated Protein 1) has been demonstrated to be required for activation of ATR-Claspin-Chk1-initiated checkpoint responses to both U.V.- and Ionising Radiation- induced forms of DNA damage and double-stranded duplex breaks and thus may also be functionally implicated in TopBP1-independent and/or TopBP1-dependent “9-1-1” clamp complex-mediated mechanisms of enhanced ATR activity (Li D.Q. *et al.*, 2010).

Other unidentified associative protein interactions (designated “X” in the figure above) may also be implicated in the Rad9-Rad1-Hus1 complex-mediated TopBP1-independent and TopBP1-dependent mechanisms of enhanced ATR activity in response to genotoxic events (Smits V.A. *et al.*, 2010).

Fig 1.20: “9-1-1” Clamp-Intercommunicative Chk1 Signal Network

[Taken and Adapted From: Dai Y. and Grant S., 2010; He W. *et al*, 2011]



Rad9-Rad1-Hus1 complex-initiated ATR-Chk1 kinase activation triggers a variety of key “downstream” protein signalling protein component “cross-talk” activities which are implicated in regulatory cell cycle DNA damage response checkpoint pathways (Dai Y. and Grant S., 2010; Sancar A. *et al*, 2004; Smith J. *et al*, 2010).

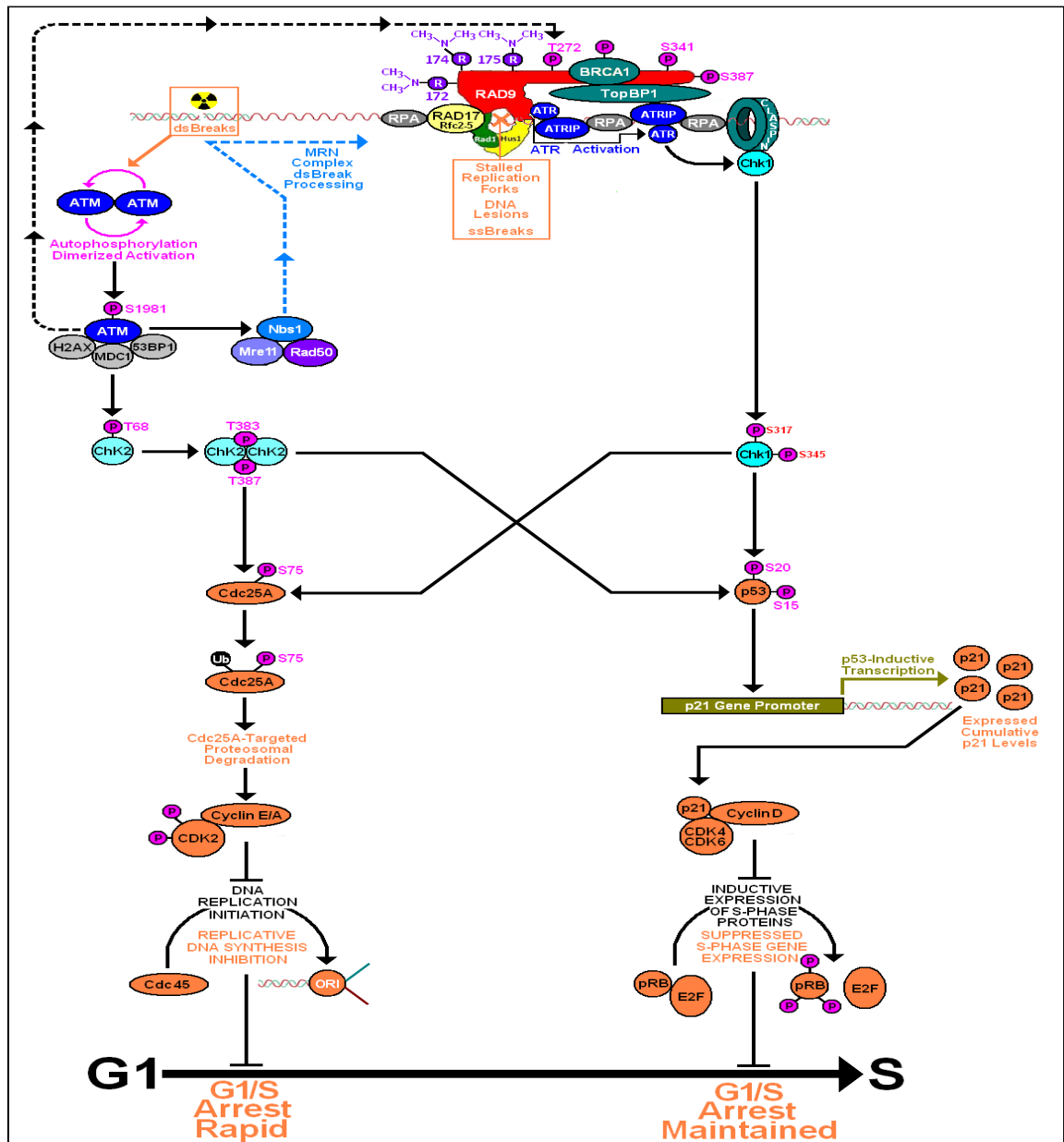
These pathways are comprised of complex protein inter-communicative “downstream” sequential signalling cascades of DNA Damage Sensors, Mediator/Adaptor “Scaffold” Platforms, Primary (Proximal) Transducers, Secondary (Distal) Transducers and Effectors whose respective function/activities are regulated via specific transient types of associative phosphorylation and dephosphorylation post-translational modifications mediated via various types of kinase and phosphatase catalytic events which also modulate protein-specific associative 14-3-3 protein-sequestration events respectively (Christmann M. *et al*, 2003; Dai Y. and Grant S., 2010; Dunaway S. *et al*, 2005; Niida H. and Nakanishi M., 2006; Smith J. *et al*, 2010).

The human Rad9A protein component of the “9-1-1” clamp functions collectively in the initiation of 7 key Chk1-Activated DNA Damage Checkpoint Pathways – notably; the G1/S Checkpoint (Fig 1.21, p.57), The Intra-S Phase Checkpoint (Fig 1.22, p.58), the G2/M Checkpoint (Fig 1.23, p.59), the p38-MAPK Checkpoint (Fig 1.24, p.60), the Circadian Checkpoint (Fig 1.25, p.59), the G2-Decatenation Checkpoint (Fig 1.26, p.60) and the Intra-M Phase Spindle Checkpoint (Figs 1.27-1.29, pp.63-65) (Boye E. *et al*, 2009; Dai Y. and Grant S., 2010; Houtgraaf J.H. *et al*, 2006; Sancar A. *et al*, 2004; Smith J. *et al*, 2010; Thornton T.M. and Rincon M., 2009).

Rad9-Rad1-Hus1 complex-initiated ATR/Chk1 activation of apoptotic signalling pathways may also impinge upon the functional activity of “9-1-1” clamp-independent Rad9-mediated modulation of apoptotic signal DNA damage checkpoint responses (discussed later in Section 1.3.2, pp.127-130).

Associative human Rad9A C-Terminal Tail Domain protein-interactive signalling functions, coupled with ATR-initiated Chk1-Activation, also mediate “9-1-1” clamp-modulation of the activities of particular DNA repair pathways – most notably; Base-Excision Repair (BER), Chromatin Re-Modelling/Assembly, Double-Strand Breakage (DSB) Repair Mechanisms, Replicative Senescence and Translesion Synthesis (TLS) Repair (discussed in detail later in Section 1.2.5, pp.86-118).

Fig 1.21: “9-1-1” Clamp Influences on G1/S Checkpoint Activation



Rad9-Rad1-Hus1 complex-induced ATR→Chk1 activation initiates both a rapid G1/S arrest and a sustained G1/S via two distinctive subsequent Chk1 kinase-mediated biochemical interactions (Bartek J. and Lukas J., 2001a; Bartek J. and Lukas J., 2001b; Sancar A. *et al.*, 2004; Smith J. *et al.*, 2010).

Chk1 kinase phosphorylation-mediated inactivation of Cdc25A phosphatase initiates its ubiquitination-targeted proteolytic degradation, with consequential inhibition of Cdc25A-mediated Thr14 and Tyr15 dephosphorylation-activated CDK2 and maintenance of the S-phase promoting Cyclin E/CDK2 complex in its inactive phosphorylated state which prevents loading of Cdc45 onto the replication origin with consequential inhibition of progressive replication origin firing (Falck J. *et al.*, 2001a; Falck J. *et al.*, 2001b; Mailand N. *et al.*, 2000; Niida H. and Nakanishi M., 2006; Peng C.Y. *et al.*, 1997; Sancar A. *et al.*, 2004; Sanchez Y. *et al.*, 1997; Smith J. *et al.*, 2010).

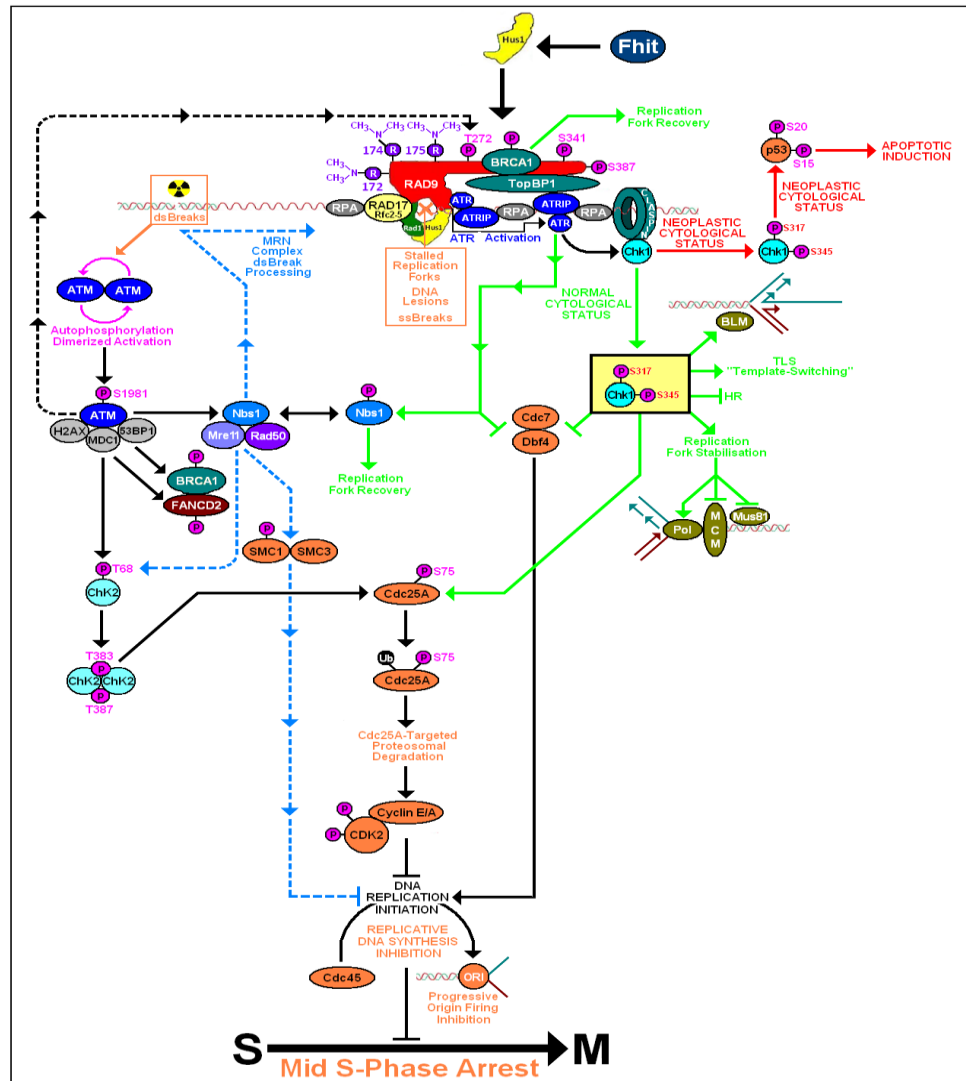
Chk1 kinase phosphorylation-mediated activation of p53 enables it to bind to the p21 gene promoter with enhancement p21 transcriptional activity and consequential elevated expression of the p21 protein, which then binds to the CDK4/6:Cyclin D complex and perturbs CDK4/6:Cyclin D complex-mediated phosphorylation-activated of the retinoblastoma protein (Rb) with subsequent inhibition of Rb-mediated E2F transcription factor release with resultant suppressed transcription of S-phase genes, culminating in sustained G1/S arrest.

The p21 protein also associates with and inhibits the activity of the CDK2:CyclinE/A complex for secured maintenance of G1/S cell cycle checkpoint arrest (Sancar A. *et al.*, 2004; Smith J. *et al.*, 2010)

ATM kinase-mediated phosphorylation-induced conversion of Chk2 to its autophosphorylation-activated dimeric kinase form also results in Chk2-mediated phosphorylation of Cdc25A with consequential Rapid G1/S arrest or Chk2-mediated phosphorylation of p53 with consequential sustained G1/S arrest (Falck J. *et al.*, 2001a; Falck J. *et al.*, 2001b; Mailand N. *et al.*, 2000; Niida H. and Nakanishi M., 2006; Peng C.Y. *et al.*, 1997; Sanchez Y. *et al.*, 1997; Smith J. *et al.*, 2010).

Co-operative parallel pathway “cross-talk redundancy” between the respective “9-1-1” complex-activated and ATM-activated secondary (distal) transducer kinases Chk1 and Chk2, that phosphorylate both Cdc25A and p53, ensures the initiation of an appropriate degree of sustained G1/S arrest response which is dependent upon the biochemical nature and extent of the DNA damage (Abraham R.T., 2001; Niida H. and Nakanishi M., 2006; Sancar A. *et al.*, 2004; Smith J. *et al.*, 2010).

Fig 1.22: “9-1-1” Clamp Influences on Intra-S Checkpoint Activation



Rad9-Rad1-Hus1 complex-induced ATR→Chk1 activation initiates Intra-S Phase arrest via subsequent Chk1 kinase phosphorylation and inactivation of Cdc25A phosphatase which is then subject to ubiquitination-targeted proteolytic degradation, with consequential inhibition of Cdc25A-mediated Thr14 and Tyr15 dephosphorylation-activated CDK2 and abrogated CDK2:CyclinE/A complex activities (Falck J. *et al.*, 2001a; Falck J. *et al.*, 2001b; Falck J. *et al.*, 2002; Mailand N. *et al.*, 2000; Niida H. and Nakanishi M., 2006; Peng C.Y. *et al.*, 1997; Sanchez Y. *et al.*, 2007; Smith J. *et al.*, 2010).

Single-stranded DNA gaps may also be detected via associative “9-1-1” clamp ATR/ATRIP-activation which, together with activated Chk1, can perturb the catalytic activity of the Cdc7/Dbf4 protein kinase with consequential inhibition of DNA replication initiation (Sancar A. *et al.*, 2004; Smith J. *et al.*, 2010).

In addition to perturbed replication origin firing, the “9-1-1” clamp-triggered ATR→Chk1 pathway also elicits several other key functional influences on DNA damage responses – notably; inhibition of homologous recombination (HR) DNA repair factors, induction of replication fork stability (via associative retention of DNA polymerases within the replication machinery via inhibition of MCM DNA helicase, Mus81 endonuclease-mediated fork cleavage activities and/or fork reversal DNA lesion by-pass via modulation of BLM DNA helicase activity) and promotion of alternative DNA repair pathways to HR such as Translesion Synthesis (TLS)-coupled “Template-Switching” (Christmann M. *et al.*, 2003; Jansen J.G. *et al.*, 2007; Sancar A. *et al.*, 2004; Taylor M. *et al.*, 2011).

ATM kinase-mediated phosphorylation-induced conversion of Chk2 to its autophosphorylation-activated dimeric kinase form also results in phosphorylation of Cdc25A and consequential Intra-S-Phase arrest of the cell cycle (Falck J. *et al.*, 2001; Mailand N. *et al.*, 2000; Niida H. and Nakanishi M., 2006; Peng C.Y. *et al.*, 1997; Sancar A. *et al.*, 2004; Sanchez Y. *et al.*, 2007; Smith J. *et al.*, 2010).

In either case, ubiquitin-targeted proteolytic removal of Cdc25A phosphatase maintains the S-phase-promoting Cyclin E/Cdk2 complex in its phosphorylated, inactive state which perturbs loading of Cdc45 onto the replication origin with consequential inhibition of progressive replication origin firing (Sancar A. *et al.*, 2004; Smith J. *et al.*, 2010).

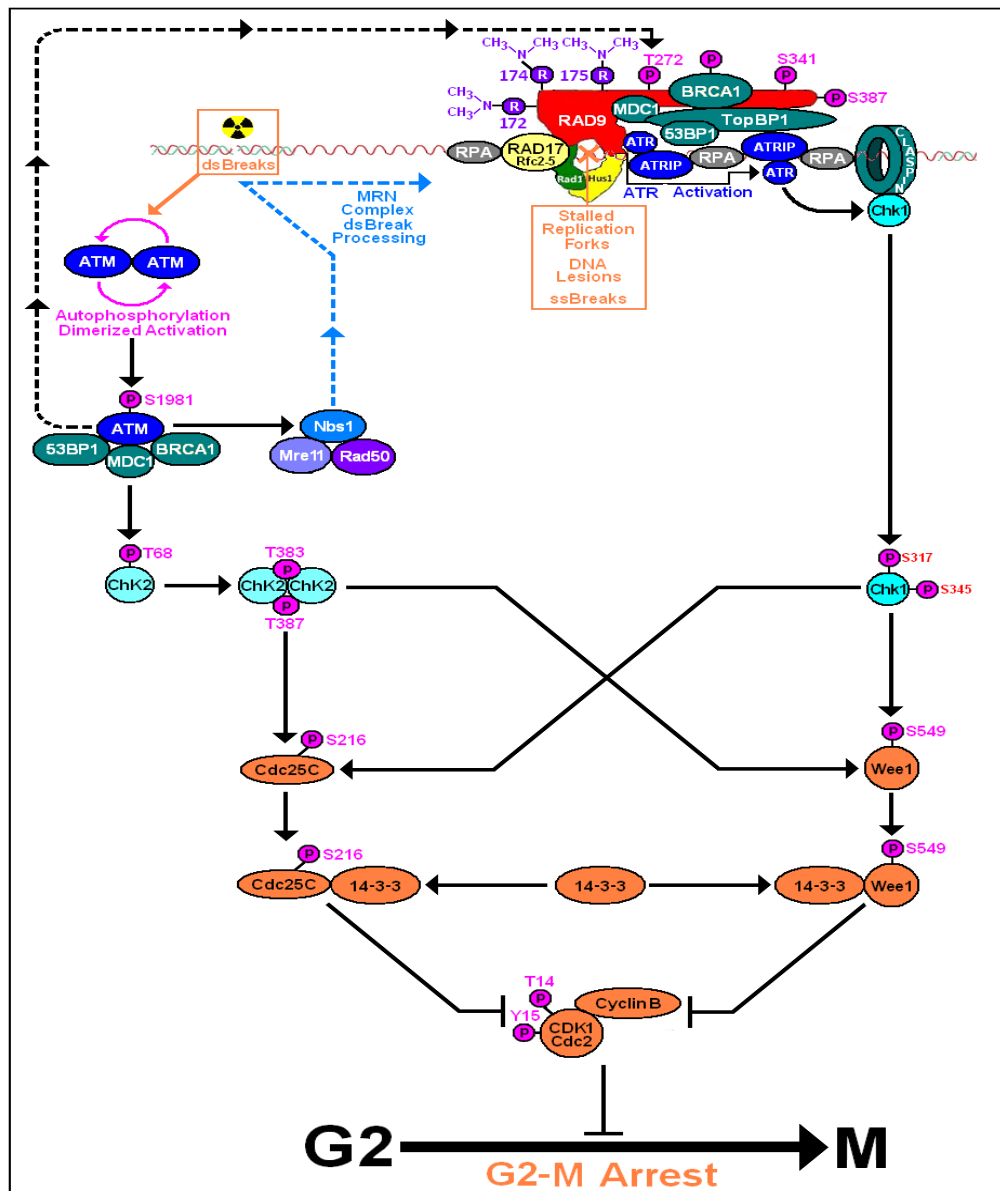
Both ATR- and ATM- kinase-mediated phosphorylation of Nbs1 impinge upon formation and associative activities of the Mre11-Rad50-Nbs1 (“MRN”) complex for the orchestrated co-ordination of MRN complex-mediated repair of DNA double-stranded breaks and stalled DNA replication fork recovery, in conjunction with inhibition of DNA replication initiation via downstream interactions of the MRN complex with the SMC1/SMC3 heterodimeric complex (Christmann M. *et al.*, 2003; Sancar A. *et al.*, 2004; Smith J. *et al.*, 2010).

ATM kinase-mediated phosphorylation of BRCA1 and FANCD2, with consequential formation of the BRCA1:FANCD2 complex may also impinge upon the activity of associative Rad9 C-terminal tail domain BRCA1:TopBP1 ternary complex activities which initiate the recovery of stalled DNA replication forks (Christmann M. *et al.*, 2003; Sancar A. *et al.*, 2004; Smith J. *et al.*, 2010).

Interactive association of Fhit (Fragile Histidine Triad Transcription Protein) with the Hus1 sub-unit, within the “9-1-1” clamp complex, is an essential prerequisite for the co-ordinative coupling of Chk1 activation with cell cycle arrest to enable sufficient time for DNA repair in mid-S phase (Ishii H. *et al.*, 2006; Pichiorri F. *et al.*, 2008)

In Fhit-defective cells, inappropriate Chk1-initiated DNA damage responses are elicited with consequential uncoupling of cell cycle arrest and impaired DNA repair processes which culminate in the propagation of genomic instability and promotion of carcinogenesis (Cirombella R. *et al.*, 2010; Ishii H. *et al.*, 2006)

Fig 1.23: “9-1-1” Clamp Influences on G2/M Checkpoint Activation



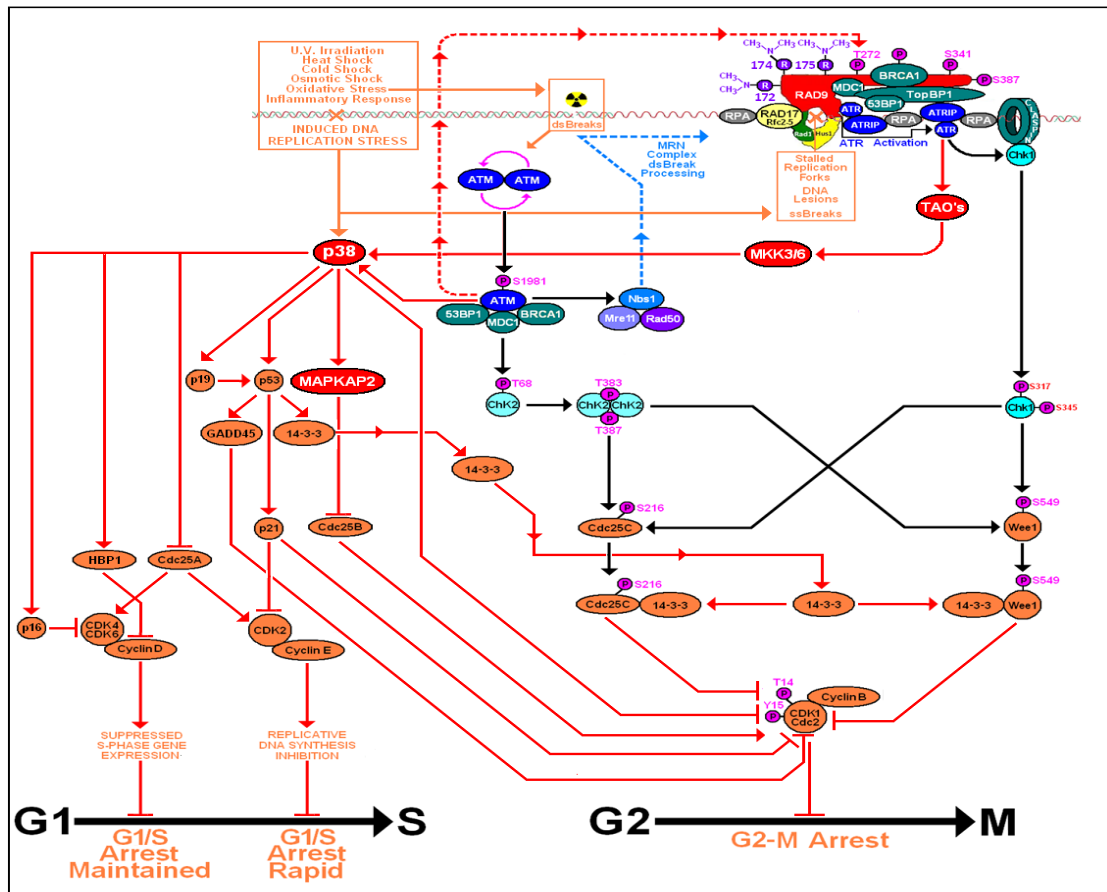
Rad9-Rad1-Hus1 complex-induced ATR→Chk1 activation initiates G2-M arrest via subsequent Chk1 kinase phosphorylation of the Wee1 kinase (at Ser 549) which enables formation of the Wee1-14-3-3 σ complex with subsequent enhancement of the inhibitory Cdc2-targeted Wee1 kinase activity, which phosphorylates CDK1 at Thr14 and Tyr15 with consequential abrogation of functional CDK1 associative CDK1/Cdc2:Cyclin B complex-mediated signalling activities which are required for G2 cell cycle progression into the mitotic (“M”) phase (Lee J. *et al.*, 2001; Nyberg K. *et al.*, 2002; Sancar A. *et al.*, 2004; Smith J. *et al.*, 2010; Stewart Z.A. *et al.*, 2003).

ATM kinase-mediated phosphorylation-induced conversion of Chk2 to its autophosphorylation-activated dimeric kinase form also results in phosphorylation of the Cdc25C phosphatase which initiates the associative formation and subsequent nuclear translocation/cytoplasmic sequestration of the resultant Cdc25C:14-3-3 σ complex with consequential inhibition of Cdc25C-mediated Thr14 and Tyr15 dephosphorylation-activation of CDK1/Cdc2 and abrogated CDK2/Cdc2:Cyclin B complex-mediated signalling activities (Abraham R.T., 2001; Niida H. and Nakanishi M., 2006; Sancar A. *et al.*, 2004; Smith J. *et al.*, 2010).

Co-operative parallel pathway “cross-talk redundancy” between the respective “9-1-1” complex-activated and ATM-activated secondary (distal) transducer kinases Chk1 and Chk2, that phosphorylate both Cdc25C and Wee1, ensures the initiation of an appropriate degree of sustained G2-M arrest response which is dependent upon the biochemical nature and extent of the DNA damage (Abraham R.T., 2001; Niida H. and Nakanishi M., 2006; Sancar A. *et al.*, 2004; Smith J. *et al.*, 2010).

Induction of the G2 checkpoint may also be initiated via direct associative interactions of the 14-3-3 σ protein with the CDK1/Cdc2-Cyclin B complex, with consequential nuclear translocation/cytoplasmic sequestration of the resultant CDK1/Cdc2:14-3-3 σ ternary complex and thus perturbed CDK2/Cdc2:Cyclin B complex-mediated signalling activities (Chan T.A. *et al.*, 1999; Nyberg K.A. *et al.*, 2002; Sancar A. *et al.*, 2004; Smith J. *et al.*, 2010).

Fig 1.24: “9-1-1” Clamp-Induced p38-MAPK Checkpoint Signalling



Autophosphorylation-activated ATM and “9-1-1” clamp-activated ATR primary (proximal) transducer kinases may also activate the p38-MAPK kinase isoforms in response to DNA damage and/or perturbed DNA replication induced by various cytological stress factors including; U.V. irradiation, cold shock, heat shock, cold shock, osmotic shock, oxidative stress and inflammatory biochemical signalling events (Bulavin D.V. *et al.*, 2001; Casanovas O. *et al.*, 2000; Denoyelle C. *et al.*, 2006; Faust D. *et al.*, 2005; Ito K. *et al.*, 2006; Kishi H. *et al.*, 2001; Reinhardt H.C. *et al.*, 2007; Reinhardt H.C. and Yaffe M.B., 2009; Reiser V. *et al.*, 2006; Thornton T.M. and Rincon M., 2009; Zhou B.B. and Elledge S.J., 2000).

Activation of the p38-MAPK isoforms may proceed via direct ATM-mediated phosphorylation and/or via an indirect pathway involving ATR-phosphorylation of Thousand-and-One Kinases (TAO's) which then initiate phosphorylated-activation of Map Kinase Kinases 3 and 6 (MKK3/6) which in turn phosphorylate and thereby activate the p38 MAPK kinases (Raman M. *et al.*, 2007; Reinhardt H.C. *et al.*, 2007; Reinhardt H.C. and Yaffe M.B., 2009; Thornton T.M. and Rincon M., 2009; Wang X. *et al.*, 2000; Zhou B.B. and Elledge S.J., 2000).

p38 MAPK kinase isoforms both stabilise and phosphorylate p53 (at Ser15, Ser389 and Ser392) with consequential induction of p21, which is also stabilised by p38 MAPK's, which culminates in the induction of rapid G1/S arrest, Mid-S phase arrest and G2/M arrest (Bulavin D.V. *et al.*, 1999; el-Deiry W.S. *et al.*, 1993; Han J. and Sun P., 2007; Huang C. *et al.*, 1999; Hui L. *et al.*, 2007; Kim Y.G. *et al.*, 2002; She Q.B. *et al.*, 2000; She Q.B. *et al.*, 2001) – via the respective cell cycle checkpoint pathways discussed previously (Figs 1.21 – 1.23, pp.57 – 59).

p38 MAPK phosphorylation-mediated activation of p53-induced elevated transcriptional expression of the GADD45 proteins (Growth Arrest DNA Damage) also results in the cumulative formation of GADD45:CDK1(Cdc2) complex with consequential inhibition of CDK1(Cdc2)/Cyclin B activity and initiation of G2/M cell cycle arrest (Zhan Q. *et al.*, 1999; Thornton T.M. and Rincon M., 2009).

p38 MAPK kinase isoforms are also implicated in the phosphorylation-inactivation and subsequent 14-3-3σ protein-mediated cytosolic sequestration of the phosphatases Cdc25A and Cdc25B (via p38 MAPK-induced activation of the MAPKAP2 kinase which then phosphorylates and inactivates Cdc25B), in conjunction with p38 MAPK phosphorylation-mediated activation of p53-induced elevated transcriptional expression of 14-3-3σ, with consequential initiation of maintained G1/S arrest and G2/M arrest (Goloudina A. *et al.*, 2003; Hermeking H. *et al.*, 1997; Lemaire M. *et al.*, 2006; Lopez-Girona A. *et al.*, 1999; Manke I.A. *et al.*, 2005; Morris M.C. *et al.*, 2005) – via the respective cell cycle checkpoint pathways discussed previously (Figs 1.21 - 1.23, pp.57 – 59).

p38 MAPK kinase isoforms also target and modulate the transcriptional activity of the *INK4a/ARF* gene locus, with consequential elevated expression of the encoded p16 (INK4a) and p19 (ARF) proteins which regulate the G1/S checkpoint via two distinctive mechanistic pathways (Bulavin D.V. *et al.*, 2004; Faust D. *et al.*, 2005; Ito K. *et al.*, 2006; Roussel M.F., 1999; Thornton T.M. and Rincon M., 2009).

The p16 protein inhibits Cyclin-Dependent Kinase CDK4/6 activation and initiates a maintained G1/S arrest, whilst the p19 protein enhances the functional stability of the p53 protein (via cytosolic sequestration of the MDM2 protein which targets p53 in the nucleus for ubiquitin-mediated proteolysis) with consequential elevated expression of p21 which culminates in rapid G1/S arrest and G2/M arrest (Weber J.D. *et al.*, 1999; Tao W. and Levine A.J., 1999) – via the respective cell cycle checkpoint pathways discussed previously (Figs 1.21 – 1.23, pp.57 – 59).

p38 MAPK kinase isoforms also inactivate Cyclin D1 via direct targeted phosphorylation and/or phosphorylation-stabilisation of the HMG-Box transcriptional protein HBP1 which suppresses the transcriptional activity of the *Cyclin D1* gene, with consequential initiation of a maintained G1/S cell cycle arrest (Lavoie J.N. *et al.*, 1996; Yee A.S. *et al.*, 2004; Thornton T.M. and Rincon M., 2009).

Fig 1.25 “9-1-1” Clamp Influences on the Circadian Checkpoint

[Compiled via Collated Information Taken and Adapted From: He W. *et al.*, 2011;

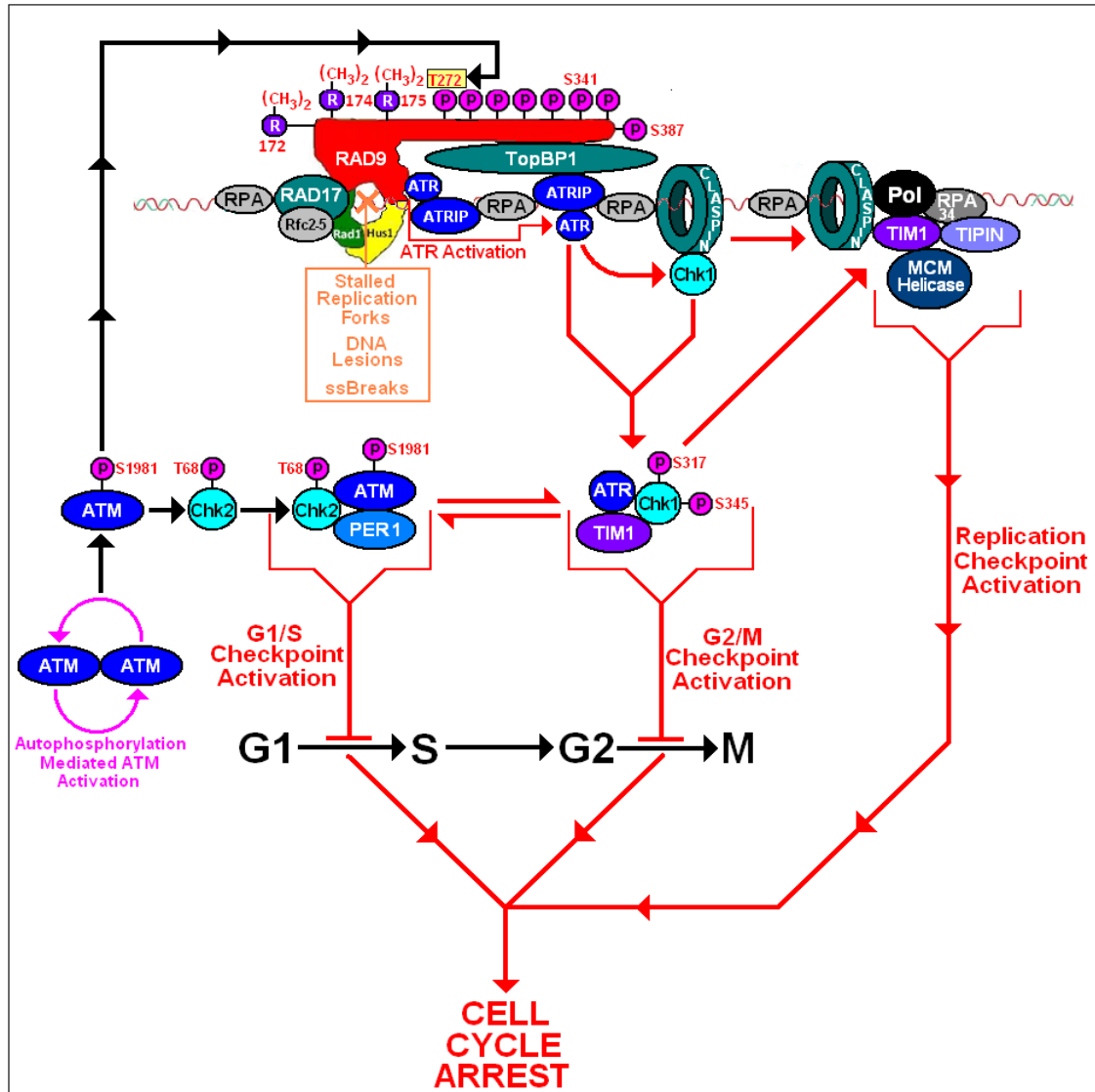
Kondratov R.V. and Antoch M.P., 2007;

Kondratov R.V. *et al.*, 2007;

Levi F. and Schibler U., 2007;

Morgan D.O., 1997;

Zhou B.B. and Elledge S.J., 2000]



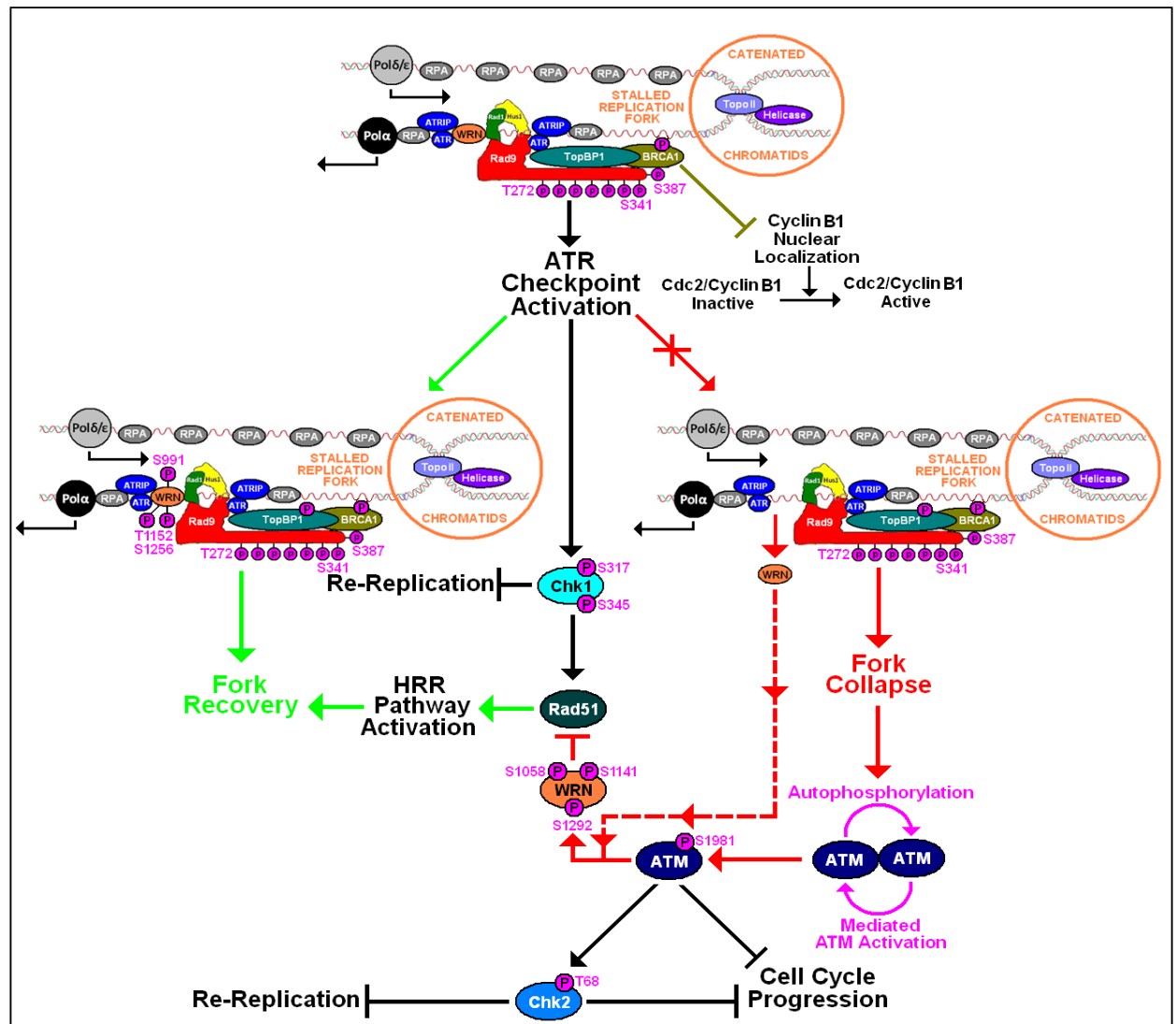
The core circadian clock proteins PER1 (Period 1) and TIM1 (Timeless), together with its non-circadian partner TIPIN (TIM1-Interacting Protein), are also implicated in the activation of the primary (proximal) transducer kinases Chk1 and Chk2 in response to genotoxic damage and/or DNA replication stress for the regulatory temporal co-ordination of the G1/S (ATM→Chk2 pathway) and G2/M (“9-1-1” clamp-initiated ATR→Chk1 pathway) cell-cycle checkpoints with DNA metabolism (Antoch M.P. and Kondratov R.V., 2010; Chen C. and McKnight S.L., 2007; Collis S.J. and Bolton S.J., 2007; Duffield G.E. *et al.*, 2002; Gauger M.A. and Sancar A., 2005; Hong C.I. *et al.*, 2009; Unsul-Kacmaz K. *et al.*, 2005; Zhou B.B. and Elledge S.J., 2000) – Figs 1.21 - 1.24, pp.57-60.

The Chk2-ATM-PER1 heterotrimeric complex initiates the G1/S checkpoint arrest and the ATR-TIM1-Chk1 heterotrimeric complex initiates the G2/M checkpoint arrest, in which TIM1 may also be implicated in the ATM-dependent activation of the Chk2-initiated G2/M arrest (Antoch M.P. *et al.*, 2005; Kemp M.G. *et al.*, 2010; Yang X. *et al.*, 2010) – discussed previously in Fig 1.21, p.57 and Fig 1.23, p.59.

TIM1, in heterodimeric complex association with its non-circadian partner TIPIN, may also interact with ClaspIN, DNA polymerases, the Replication Protein A sub-unit RPA34 and MCM helicase in a collectively protein assembly which travels with the DNA replication fork and may initiate an Intra-S phase-type replication checkpoint arrest for temporal co-ordination of transient oscillatory DNA replication and DNA recombination events which are induced under both normal and genotoxic/replication stress-related cytological conditions (Gotter A.L., 2003; Gotter A.L. *et al.*, 2007; Loros J.J. *et al.*, 2007; Unsul-Kacmaz K. *et al.*, 2007; Yoshizawa-Sugata N. and Masai H., 2007).

Fig 1.26: “9-1-1” Clamp-Induced G2-Decatenation Checkpoint Model

[Compiled via Colated Information Adapted From: Greer Card D.A. *et al.*, 2010; He W. *et al.*, 2011; Pichierri P. *et al.*, 2003; Pichierri P. *et al.*, 2011; Pichierri P. *et al.*, 2012; Sancar A. *et al.*, 2004



The Rad9-Rad1-Hus1 complex is loaded onto RPA-coated stalled replication forks, whose induction may be mediated via a variety of different genotoxic- and/or replication-stress- related cytological events which culminate in adverse DNA topological rearrangements within the chromatin supramolecular architecture (discussed later in Section 1.2.5, pp.86-118; Fig 1.35, p.89 and Fig 1.36, p.90) – as in the case of the impairment of Topoisomerase II activity with resultant formation of catenated chromatids that may promote double-strand breakage (DSB) events. (Dillon L.W. *et al.*, 2010; Greer Card D.A. *et al.*, 2010).

Human Rad9A, acting in associative concert with TopBP1 (which also binds Topoisomerase II), ATR and BRCA1, within the “9-1-1” clamp complex, may trigger a G2-Decatenation checkpoint in which ATM-mediated phosphorylation of Rad9A at Thr272 within its C-Terminal Tail Domain and Thr68 within Chk2 is also implicated with consequential prevention of cut-like cytological phenotypes, suppression of re-replication events and phasic arrest of cell cycle progression to provide time for stalled fork recovery and/or appropriate rectification of DSBs via the Homologous Recombination Repair (HRR) pathway (discussed later in Section 1.2.5, p.109; Fig 1.48, p.109) – which is initiated via Chk1-phosphorylated-activation of the Rad51 DNA repair factor (Enders G.H., 2008; Greer Card D.A. *et al.*, 2010).

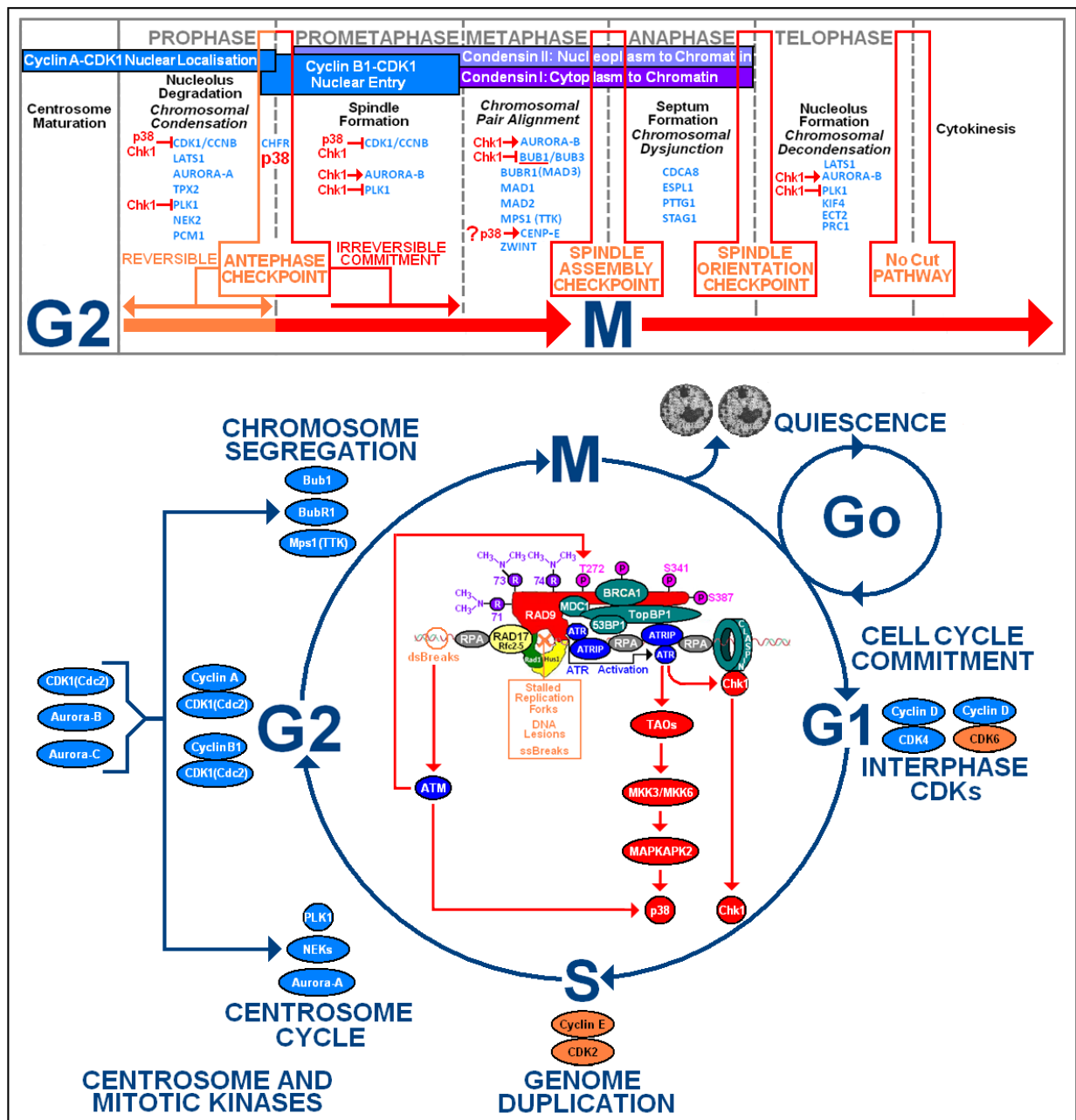
Both ATM and ATR primary (proximal) transducer checkpoint kinases are also implicated in the differential phosphorylation of the Werner Syndrome protein (WRN) which possesses 3'-5'-exonuclease and helicase domain activities and catalyses the unwinding of secondary DNA structures such as hairpins, DNA forks, resolution of recombination intermediates via Holliday Junction Branch migration and induction of D-loop dissociation and degradative removal of bubbles, stem-loops, and 3-way or 4-way DNA junctions (Ammazzalorso F. *et al.*, 2010; Oshima J., 2000; Pichierri P., 2003; Pirzio L.M. *et al.*, 2008; Rossi M.L. *et al.*, 2010; Salk D., 1985; Sidorova J.M., 2008).

ATR phosphorylated-activation of WRN (at Ser991, Thr1152 and Ser1256), via “9-1-1”-complex associative WRN-Rad1 interactive recruitment of WRN in association with RPA at nuclear foci of stalled replication fork sites and in close proximity to the primary transducer checkpoint kinase, initiates WRN-catalysed repair of the stalled DNA fork and thus prevents formation of DSBs to enable replication fork recovery (Ammazzalorso F. *et al.*, 2010; Gray M.D. *et al.*, 2005; Pichierri P. *et al.*, 2007; Rossi M.L. *et al.*, 2010).

Collapsed replication fork degeneration-induced DSB formation is prevented via ATM-mediated phosphorylation of WRN (at Ser1058, Ser1141 and Ser1292) which induces supramolecular conformational changes within the WRN protein which promote its dissociation from RPA and the Rad1 sub-unit of the “9-1-1” clamp, prior to appropriate rectification of the collapsed replication fork via the alternative Chk1-activated Rad51-Mediated HRR repair pathway (Ammazzalorso F. *et al.*, 2010; Pichierri P. *et al.*, 2007; Pichierri P. *et al.*, 2011).

Fig 1.27: "9-1-1" Clamp Influences on Intra-M Phase Checkpoints

[Compiled via Collated Information Taken and Adapted From: Chin C.F. and Yeong F.M., 2010
Malumbres M. and Barbacid M., 2007
Musacchio A. and Hardwick K.G., 2002]



The cytological regulation of the centrosome cycle and appropriate temporal chromosomal segregation is tightly choreographed via a series of sequential Intra-M Phase checkpoints for the prevention of propagated chromosomal aberrations during mitosis (Fig 1.9, p.16), thereby acting as a further "safe-guard" against potential neoplastic transformation and progression (Chin C.F. and Yeong, 2010; Malumbres M. and Barbacid M., 2007; Musacchio A. and Hardwick K.G., 2002).

Cyclin-Dependent Kinases (eg CDK1/Cdc2, CDK4), NIMA (Never-In-Mitosis *Aspergillus*-like Kinases (NEKs), Polo-Like Kinases (eg PLK1) and Aurora Kinases (Aurora-A, Aurora-B, and Aurora-C) function as transducers and/or effectors of various signalling pathways which control appropriate co-ordination of centrosome cycle progression in conjunction with mitotic spindle formation and activation of the Anaphase Promoting Complex/Cyclosome (APC/C) (Chin C.F. and Yeong, 2010; Chung I. *et al.*, 2011; Longhese M.P. *et al.*, 2006; Malumbres M. and Barbacid M., 2007; Musacchio A. and Hardwick K.G., 2002). – Fig 1.28, p.64.

The functional activity of the Spindle Assembly Checkpoint (SAC), which "monitors" and ensures the correct symmetrical bipolar attachment orientation of the mitotic spindle microtubules to the sister chromatids, is regulated by the Bub Kinases (Bub1, BubR1), Aurora B kinase and a dual-specificitySer/Thr/Tyr kinetochore kinase known as the Monopolar Spindle Kinase 1 (MPS1/TTK1) that are key components of the Mitotic Checkpoint Complex (MCC) (Chin C.F. and Yeong, 2010; Malumbres M. and Barbacid M., 2007; Musacchio A. and Hardwick K.G., 2002) – Fig 1.28, p.64; Fig 1.29, p.65.

Co-ordinated ATM and associative "9-1-1" clamp-ATR ternary complex functions culminate in the activation of the distal transducer kinases Chk1 and p38 (Fig 1.24, p.60) which in turn may impinge upon the regulation of various Intra-M phase checkpoints, including in particular the Spindle Checkpoint (Fig 1.20, p.56; Fig 1.28, p.64; Fig 1.29, p.65), via phosphorylation-mediated alteration of the functional activities of specific kinases such as Aurora B, BUB1, CDK1/CCNB, PLK1 and the Kinesin-Like Plus-End Directed Motor protein – termed "CENP-E" (Chin C.F. and Yeong, 2010; Malumbres M. and Barbacid M., 2007; Musacchio A. and Hardwick K.G., 2002).

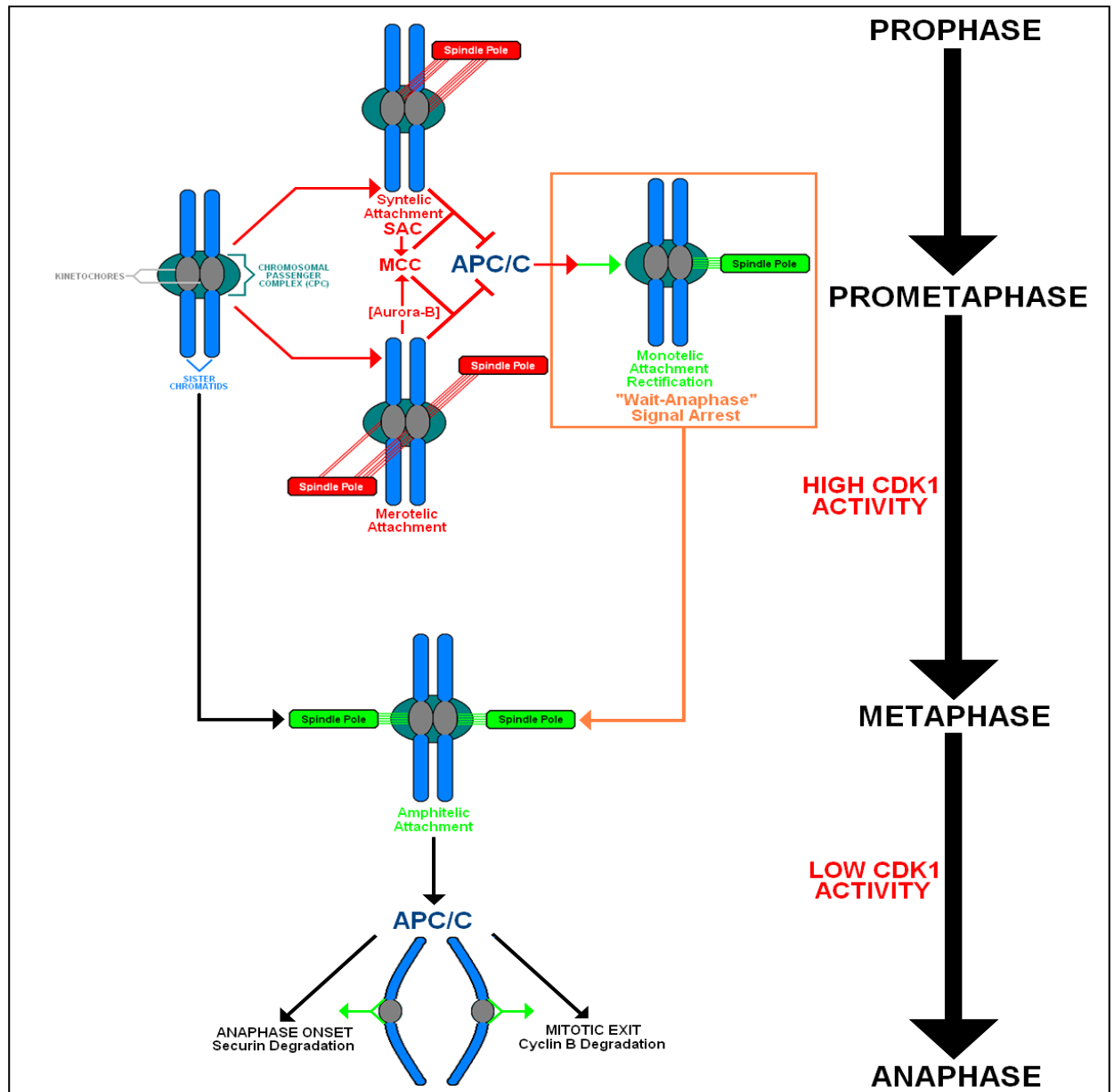
Fig 1.28: Asymmetric Kinetochores Spindle Attachment Rectification

[Compiled via Collated Information Taken and Adapted From: Acquaviva C. and Pines J., 2006

Chan G.K. and Yen T.J., 2003

Fuller B.G. and Stukenberg P.T., 2009

Maresca T.J. and Salmon E.D., 2010



During Prometaphase (Fig 1.27, p.63), formation of asymmetrical types of kinetochores-mitotic spindle attachments (ie Syntelic or Merotelic) triggers activation of the Spindle Assembly Checkpoint (SAC) in conjunction with the soluble Mitotic Checkpoint Complex (MCC), which inhibits the Anaphase Promoting Complex/Cyclosome (APC/C) and initiates a “Wait Anaphase” signal arrest to provide time for the dissociative removal of misaligned kinetochores-mitotic spindle attachments and completion of Monotelic kinetochores-mitotic spindle reattachment-directed formation of the correct symmetrical bi-polar Amphitelic kinetochores-mitotic spindle attachments, prior to separation of the sister chromatids (Acquaviva C. and Pines J., 2006; Chan G.K. and Yen T.J., 2003; Longhese M.P. *et al.*, 2008; Quevedo O. *et al.*, 2012; Tan A.L.C. *et al.*, 2005) – Fig 1.29, p.65.

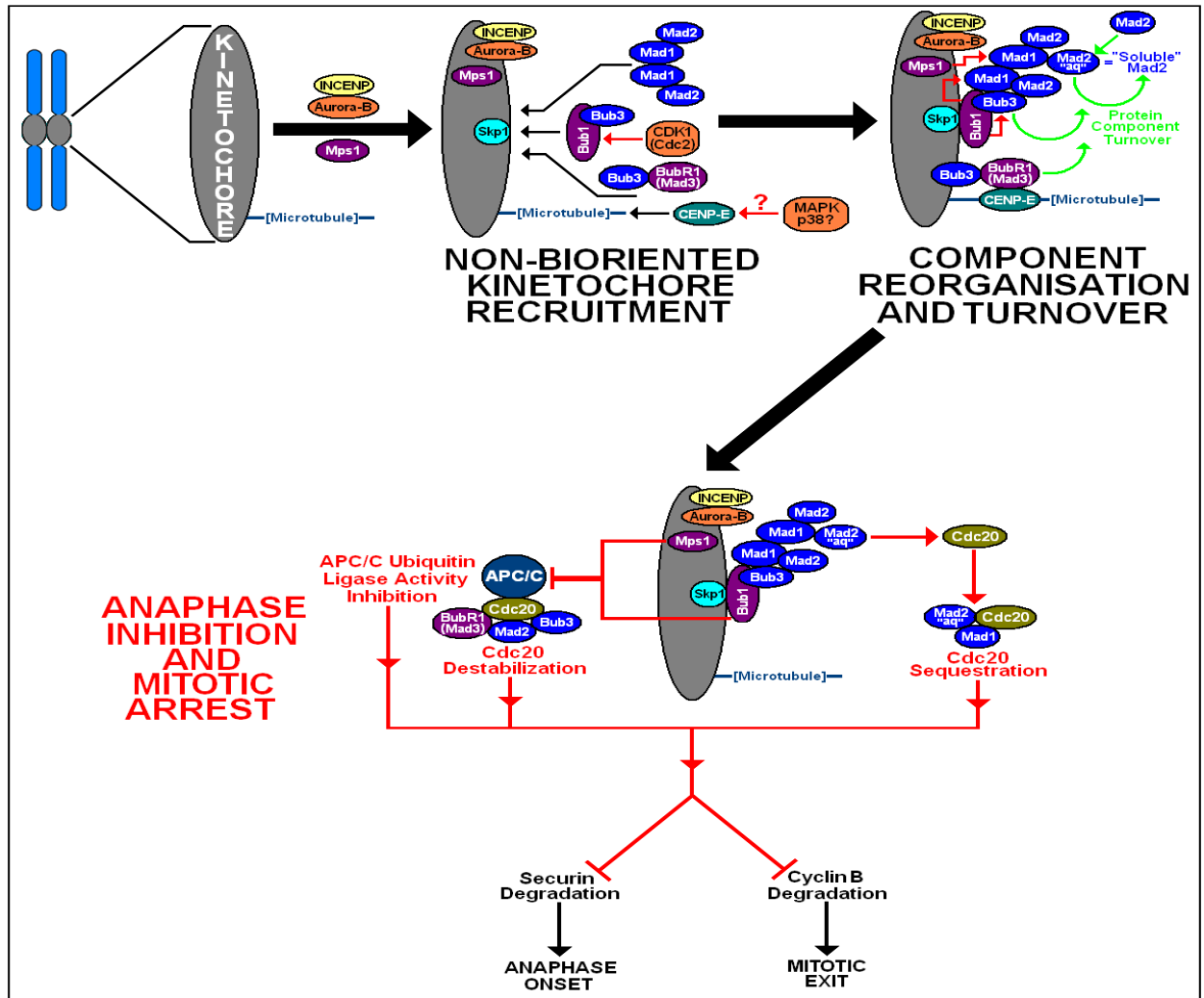
Cytokinetic activity within the mitotic spindle “mid-zone” is regulated by the Chromosomal Passenger Complex (CPC), which is implicated in the co-ordination of APC/C specificity factor Cdc20-mediated inhibition of mitotic checkpoint activation with sister chromatid disjunction during Anaphase (Maresca T.J. and Salmon E.D., 2010; Tseng B.S. *et al.*, 2010; Tsukahara T. *et al.*, 2010).

Progression from metaphase to anaphase is mediated via the Cdc20 specificity factor component of the APC/C complex, which suppresses CDK1 activity via induction of Cyclin B degradation and induction of Securin degradation to liberate the protein Separase required for the catalytic separation of sister chromatids during Anaphase via hydrolysis of the protein Cohesin – which maintains associated sister chromatid pairs during Metaphase. (Maresca T.J. and Salmon E.D., 2010; Tan A.L.C. *et al.*, 2005) – Fig 1.29, p.65.

Consequential loss of CDK1 activity, in conjunction with dephosphorylation of the INCENP protein and relocation of the CPC complex from the centromeres to the spindle mid-zone, prevents inappropriate/catastrophic activation of the mitotic checkpoint during Anaphase in response to loss of kinetochores-mitotic spindle attachment tension as a consequence of normal sister chromatid separation. (Maresca T.J. and Salmon E.D., 2010; Tan A.L.C. *et al.*, 2005; Vázquez-Novelle M.D. *et al.*, 2010) – Fig 1.29, p.65.

Fig 1.29: Mechanistic Overview of the Mitotic Spindle Checkpoint

[Compiled via Collated Information Taken and Adapted From: Grimison B. *et al.*, 2006; Kitagawa K. *et al.*, 2003; Liu J. *et al.*, 2007; Maresca T.J. & Salmon E.D., 2006; Longhese M.P. *et al.*, 2006; Maresca T.J. and Salmon E.D., 2010; Tan A.L.C. *et al.*, 2005; Vigneron S. *et al.*, 2004



INCENP and Aurora B kinase are key functional components of the chromosomal tension sensory apparatus which detects anomalous asymmetrical/non-bipolar kinetochore-mitotic spindle attachments (Fig 1.28, p.64) and initiates formation of the spindle checkpoint-mediated signalling cascade complex (Liu S.T. *et al.*, 2003; Tan A.L.C. *et al.*, 2005; Tseng B.S. *et al.*, 2010; Vigneron S. *et al.*, 2004).

CDK1-mediated phosphorylation of Bub1 promotes formation of the Bub1:Bub3 heterodimeric complex, which is recruited to the kinetochore via associative Skp1-Bub1 interactions, with consequential kinetochore recruitment of the Mad1:Mad2 heterodimeric complex via associative Bub3 interactions within the resultant kinetochore-Skp1-Bub1-Bub3 ternary complex (Yamaguchi S. *et al.*, 2003).

p38-MAP Kinase-mediated phosphorylation of CENP-E may also promote its association with kinetochore-bound microtubules for activated kinetochore-mitotic spindle-CENP-E ternary complex-mediated recruitment of the Bub3:BubR1/Mad3 heterodimeric complex via associative CENP-E – BubR1/Mad3 interactions (Ditchfield C. *et al.*, 2003; Howell B.J. *et al.*, 2001; Huang Y. *et al.*, 2009; Maia A.F. *et al.*, 2010).

Mps1 kinase-mediated hyperphosphorylation of Mad1 and Bub1, in conjunction with Bub1 kinase-mediated phosphorylation of Mad1 and Bub3 (denoted by red arrows), induce transient sub-complex conformational changes within the associative kinetochore-mitotic checkpoint ternary complex that promote protein component associative re-organisation and turn-over (denoted by green arrows) events with consequential release of soluble Mad2 – termed “Mad2(aq)” which forms Cdc20-inhibitory type soluble complexes (Brady D.M. and Hardwick K.G., 2000; Hewitt L. *et al.*, 2010; Seeley T.W. *et al.*, 1999; Wassmann K. *et al.*, 2003).

The heterodimeric Mad2(aq):Mad1 complex sequesters the Ubiquitin Ligase APC/C complex specificity factor Cdc20 with consequential inhibition of APC/C-Cdc20 complex-mediated ubiquitin-targeted proteasomal degradation of Securin and Cyclin B, thereby blocking Anaphase progression and mitotic exit (Enre D. *et al.*, 2011; Fava L.L. *et al.*, 2011; Maldonado M. and Kapoor T.M., 2011; Orth M. *et al.*, 2011).

Mps1 kinase- and Bub1 kinase-mediated phosphorylation of the APC/C-Cdc20 complex may also elicit its associative transfer to the heterotrimeric BubR1/Mad3-Mad2-Bub3 complex, which promotes Cdc20 destabilisation with consequential inhibition of proteasomal degradative removal of Securin and Cyclin B for maintained Anaphase arrest and blocked mitotic exit (Yudkovsky Y. *et al.*, 2000).

Both BubR1/Mad3 and Mad2 also abrogate associative interactions between the APC/C complex and Cdc20 protein within the resultant BubR1/Mad3-APC/C-Cdc20 -Mad2-Bub3 ternary complex (Morrow C.J. *et al.*, 2005; Hewitt L. *et al.*, 2010).

1.2.3 Androgen Nuclear Receptor Activity Modulation

The C-terminal domain of the hRad9 protein, acting within the hHus1/hRad1 associative heterotrimeric toroidal 9-1-1 DNA sliding-clamp complex, has also been observed to interact with the C-terminal Ligand Binding Domain (LBD) of nuclear Androgen Receptor (AR) in a co-regulatory capacity which suppresses its transactivation in prostate tumour cells. (Wang L. *et al*, 2004) – Summarised in Fig 1.32, p.72.

The nuclear Androgen Receptor protein (AR) is essentially comprised of four domains, namely; the N-Terminal Transactivation Domain (TTD), the DNA Binding Domain (DBD), the Hinged-Region Domain and the C-Terminal Ligand Binding Domain (LBD) respectively. (Chang C.S. *et al*, 1988a; Chang C.S. *et al*, 1988b; Chang C. *et al*, 1995; He B. and Wilson E.M., 2002; Lee D.K. and Cheng C., 2003; Manglesdorf D.J. *et al*, 1995) – Fig 1.31, p.71.

The inactive nuclear AR is sequestered in the cytosol in stable associative complexation with heat shock proteins, such as Hsp70 and Hsp90, respectively – Fig 1.30, p.70.

Initial activation of the nuclear AR is triggered via endogenous ligand associative interactions of the steroid hormone substrates; testosterone and 5 α -dihydroxytestosterone, with the AR C-terminal LBD, which induce supramolecular configurational alterations within the AR protein that thermodynamically-favour heat shock complex dissociation, promote AR phosphorylation and translocation to the nucleus. (Manglesdorf D.J. *et al*, 1995; Lee D.K. and Cheng C., 2003) – Fig 1.30, p.70 and Fig 1.31, p.71

Ligand-activated AR dimerisation, mediated via anti-parallel associative interactions between the two respective individual AR protein sub-units, then proceeds within the nuclear environment (Bledsoe R.K. *et al.*, 2002; He B. and Wilson E.M., 2002; Langley E. *et al.*, 1995) – Fig 1.30, p.70.

The supramolecular configuration of the AR dimer enables it to recognise and bind to specific DNA response element sequences within target gene promoters, via duplex major groove intercalation associations with the two DNA Binding Domains (DBDs), prior to subsequent recruitment of a variety of endogenous selective type I steroid co-regulators which contain specific sequence motifs that interact with the N- and C- termini of the AR dimer, for consequential enhancement of gene transcription. (Heinlein C.A. and Chang C., 2002) – Fig 1.30, p.70 and Fig 1.31, p.71.

For example, protein ligands of the p160/Steroid Receptor Coactivator family – which include; SRC1, SRC-2/TIF2, SRC3/A1B1/pCIP/RAC3 interact with the DNA-AR dimer complex via induction of a supramolecular configurational realignment of helix 12 within the AR dimer sub-units to expose a small hydrophobic binding pocket within the AR C-Terminal LBD – to which the small α -helical LXXLL motif (Fig 1.31, p.71), contained within the coactivator protein ligand, is docked. (Heery D.M. *et al.*, 1997; Darimont B.D. *et al.*, 1998; Feng W. *et al.*, 1998; Glass C.K. and Rosenfeld M.G., 2000; Llopis J. *et al.*, 2000; McInery E.M. and O'Malley B.W., 2002).

Conversely, other AR protein co-activator ligands, such as ARA54 and ARA70 interact with the DNA-AR dimer complex via targeted recognition and docking with the FXXLF motif (Fig 1.31, p.71) - which is also a ligand-dependent AR-associated peptide motif, located within the AR N-Terminal Transactivation Domain (N-TTD), that mediates interactions between the AR N-TTD and AR C-LBD terminal domains which optimise maximal nuclear AR transactivation. (Yeh S. and Chang C., 1996; Chang C. *et al.*, 1999; Kang H.Y. *et al.*, 1999, Hsu C.L. *et al.*, 2003).

AR co-regulatory ligands such as; ARA54, ARA67, ARA70N, Gelsolin and SRC-1, modulate AR transactivation via subtle, transient differential alterations of the supramolecular configuration of the AR N-C termini interaction respectively. (Hsu C.L. *et al*, 2005) – Fig 1.31, p.71.

In this respect, AR co-activators such as; ARA54, ARA70N, Gelsolin and SRC1 induce enhancement of AR transactivation, whilst ARA67 acts as an AR co-repressor via induced enhancement of a particular supramolecular AR N-C termini interactive configuration which results in steric inhibition of AR transactivation. (Hsu C.L. *et al*, 2005).

The C-terminal domain of hRad9 also contains an FXXLF motif of similar functional homology sequence to the FXXLF motif situated within the N-terminal transactivation domain (N-TTD) of the AR (He B. *et al*, 2002; Wang L. *et al*, 2004) – Fig 1.32, p.72 and possesses a relatively strong associative interactive affinity for the C-terminal AR-LBD as a consequence of several key features related to the thermodynamically-favourable amino acid sequence side-chain physico-chemical properties present within and/or in flanking proximal relative positions to the FXXLF motif which closely match the optimal binding criteria model (proposed by He B. and Wilson E.M., 2003) with regard to interaction of the AR-TDD N-terminal FXXLF motif with the C-terminal AR-LBD - notably;

- (i) The presence of two positively-charged/protonated amino group Lys side-chain residues, at positions K359 at positions K360 within the hRad9 C-terminal domain (Fig 1.32, p.72) – situated directly adjacent to the end of the N-terminus of the residual FXXLF motif. (He B. and Wilson E.M., 2003; Wang L. *et al*, 2004).
- (ii) The absence of positively-charged/protonated-basic group side-chain amino acid residues at the end of the C-terminus of the residual FXXLF motif within the hRad9 C-terminal tail domain. (He B. and Wilson E.M., 2003; Wang L. *et al*, 2004) – Fig 1.32, p.72.

- (iii) The absence of potential α -helical conformer-distortional types of amino acid side-chains (such as glycine and proline) within the FXXLF motif located in the hRad9 C-terminal tail domain. (He B. *et al.*, 2002; Wang L. *et al.*, 2004) – Fig 1.32, p.72.
- (iv) The critical location of a phenylalanine residue (F366) to the FXXLF motif C-terminus (Fig 1.32, p.72) within the hRad9 C-terminal tail domain (He B. *et al.*, 2002; Wang L. *et al.*, 2004).

The hRad9 protein, acting within the hHus1/hRad1 associative heterotrimeric toroidal 9-1-1 DNA sliding-clamp complex, is currently hypothesised to possess an anti-carcinogenesis role with regard to the suppression of functional AR transactivation as a consequence of inhibitory disruption of the AR N-C termini interactions – Fig 1.32, p.72.

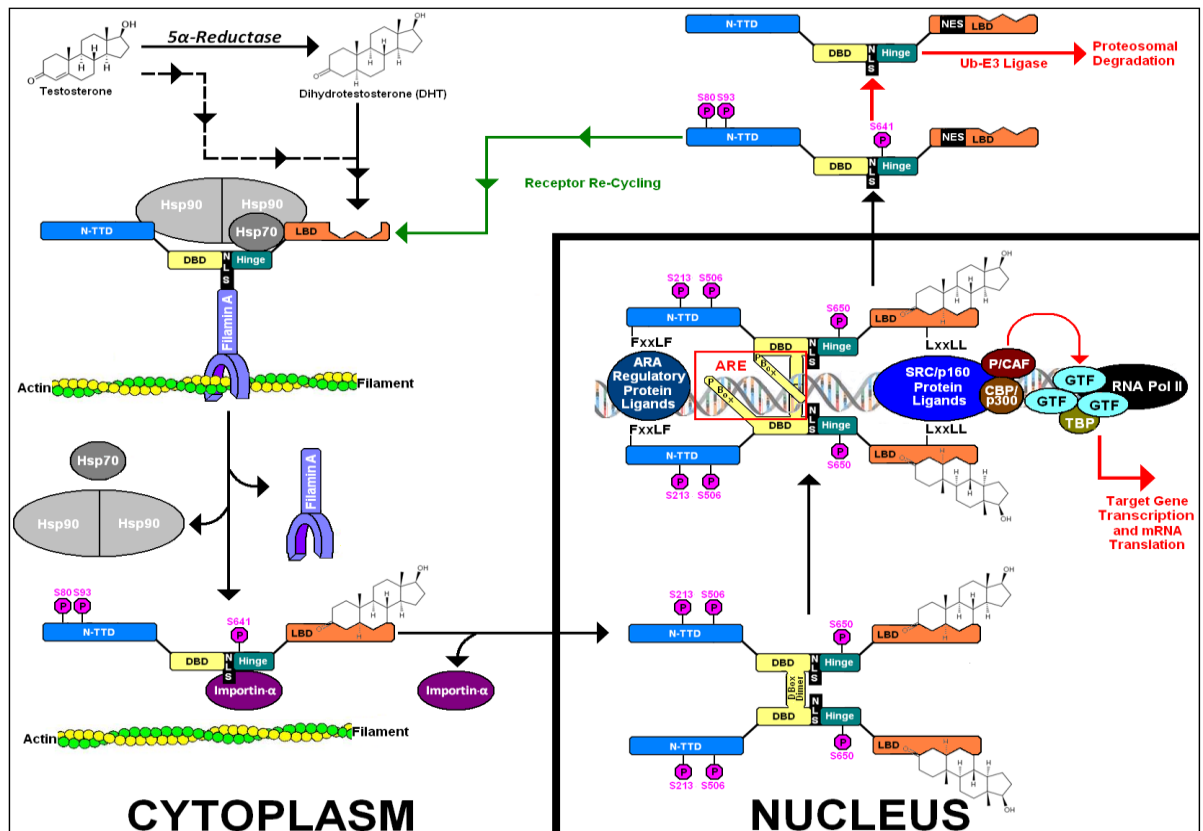
These inhibitory interactions are mediated through associative binding interactions between the AR C-terminal LBD and the FXXLF motif within the protruding C-terminal tail domain of the hRad9 protein, which are initially triggered via formation of DNA damage lesions within the AR target promoter response elements, for prevention of un-regulated AR Dimer-induced dysfunctional enhanced gene transcription of steroidal growth factors. (Wang L. *et al.*, 2004) – Fig 1.32, p.72.

The AR also modulates the transcriptional activity of a range of genes which are implicated in a range of different cytological processes, including; apoptosis, ATP-coupled ion transport, differentiation, development, genotoxic responses, inter-cellular signalling, metabolism, morphogenesis, replication stress responses (Bolton E.C. *et al.*, 2007; Massie C.E. *et al.*, 2007).

The AR also has non-genomic type functions within various plasma membrane- and kinase-mediated signalling pathways (Bennett N.C. *et al.*, 2010), which may impinge upon other Rad9-modulated activities such as checkpoint activation, DNA repair and nucleotide biosynthesis.

Fig 1.30: Mechanistic Overview of Androgen Receptor Activity

[Compiled via Collated Information From: Bennett N.C. *et al*, 2010; Centenera M.M. *et al*, 2008]



Binding of the steroidal substrates testosterone, or DHT (dihydrotestosterone – synthesised via conversion of testosterone to DHT via the enzyme 5- α -Reductase), to the Ligand Binding Domain (LBD) of the AR monomer (AR) induces supra-molecular configurational changes within the protein, that initiate its phosphorylated activation at residues Ser80 and Ser93 (situated within the N-Terminal Transactivation Domain – NTTD) and Ser641 (situated within the Hinge Domain), which in turn induces further supra-molecular configurational changes that promote dissociation from the AR Hinge-Domain-Filamin A-Actin Filament and (Hsp90)₂:Hsp70 protein chaperone interactions which maintain the AR in the cytosol in an inactive state (Bennett N.C. *et al*, 2010; Brinkmann A.O. *et al*, 1989; Brinkmann A.O. *et al*, 1999; Centenera M.M. *et al*, 2008; Gioeli D. *et al*, 2002; Marcelli M. *et al*, 2006)

Subsequent associative interactions between the hinge-domain and nuclear localisation site (NLS) domain within the released AR-Steroid Substrate complex and the transporter protein Importin- α mediate nuclear translocation of the monomeric AR-Steroid Substrate complex (Bennet N.C. *et al*, 2010; Lamont K.R. and Tindall D.J., 2010).

Dissociation of Importin- α , within the nuclear microenvironment, promotes dimerisation of the AR-Steroid Substrate complex (Bennet N.C. *et al*, 2010; Centenera M.M. *et al*, 2008; Lamont K.R. and Tindall D.J., 2010).

The resultant dimeric AR complex, (AR)₂, then binds to sequence-specific Androgen Response Elements (AREs) situated within the DNA of various genes, via Zinc-Finger Motifs (Fig 1.31, p.71), which induce proximal site configurational changes within the local chromatin supra-molecular architecture that facilitate access of the transcriptional protein machinery to the gene promoters with consequent enhancement of gene expression (Beato M., 1989; Bolton E.C. *et al*, 2007; Chen T., 2008; Claessens F. *et al*, 2001; Cleutjens C.B. *et al*, 1997; Funder J.W., 1993; Lambert J.R. and Nordeen S.K., 1998).

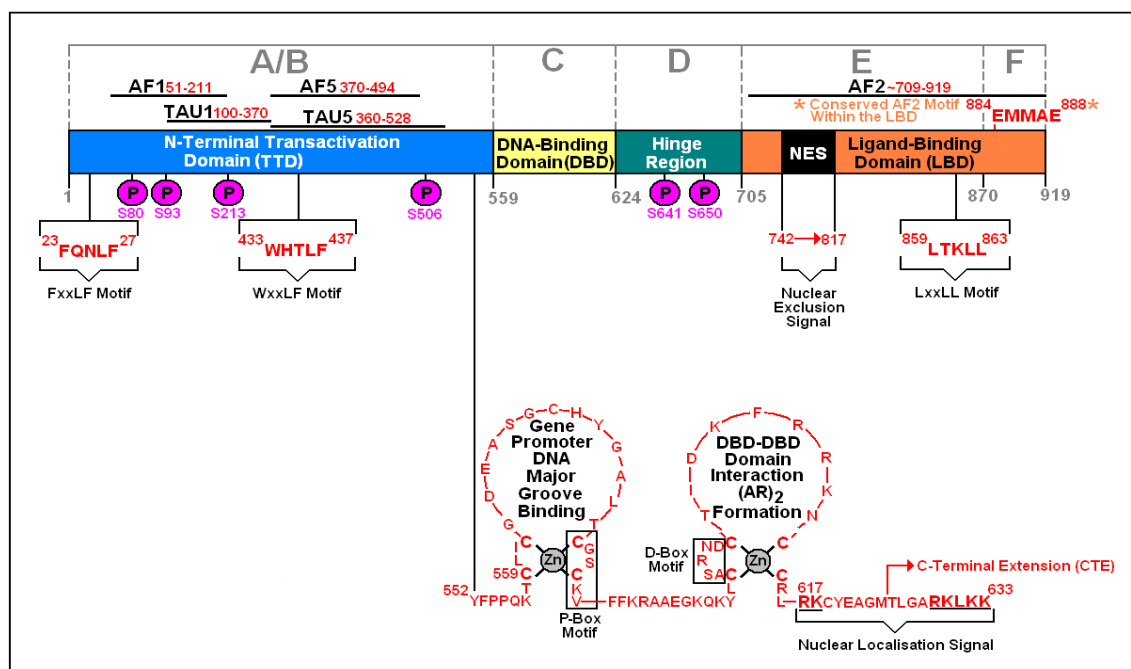
The gene transcriptional-induction activity of the dimeric Androgen Receptor Complex, (AR)₂ is regulated via interactions with a variety of two main classes of Co-Activator and Co-Repressor proteins – notably; The “ARA-type” ligands which associate with F/WxxLF motifs situated in the NTTD Domain and the “SRC/p160-type” ligands which associate with the LxxLF motif situated in the LBD Domain (Bennett N.C. *et al*, 2010; Chang C-Y. and McDonnell D.P., 2005; Chen T., 2008; Glass C.K. and Rosenfeld M.G., 2000; Kempainen J.A. *et al*, 1999; Rosenfeld M.G. *et al*, 2006) – discussed in detail on pp.67-68.

Subsequent DNA-transcriptional and translational protein machinery interactions induce further conformational changes within the chromatin supra-molecular architecture which promote dissociation of the Androgen Receptor Dimer, from the ARE binding-site, into the monomeric form which is then exported out of the nucleus and re-cycled via re-associative formation of the cytoskeletal-bound (Hsp90)₂:Hsp70-AR-FilaminA-Actin ternary complex (Bennett N.C. *et al*, 2010)

Phosphorylation at Ser80, Ser93 and Ser641 residues within the nuclear-exported monomeric form of Androgen Receptor stabilises and protects the protein from proteasomal degradation, prior to re-cycling (Bennett N.C. *et al*, 2010).

Fig 1.31: Functional Domain Map of the Androgen Receptor

[Compiled via Collated Information From: Bennett N.C. *et al*, 2010; Centenera M.M. *et al*, 2008
Koochekpour S, 2010; Nguyen D. *et al*, 2001



The Androgen Nuclear Receptor Monomer is classified into 5 main domain-containing segments – notably; A or B (designated for each of the respective 2 isoforms of the AR which are expressed – A = Full-Length Isoform, B= Truncated N-Terminus Isoform, both containing the “N-TTD” Domain Isoform), C (containing the DNA Binding Domain – “DBD”), D (Containing the “Hinge Region”), E (containing the Nuclear Exclusion Signal – “NES” and comprising the major portion of the “LBD” Domain) and F (containing the Nuclear Localisation Signal – “NLS” and comprising the minor C-terminal portion of the LBD) (Adler A.J. *et al*, 1993; Beato M. *et al*, 1995; Ham J. *et al*, 1988).

Phosphorylation of residues Ser80, Ser93 and Ser641 enhances the stability of the Androgen Receptor monomer and protects the protein from proteasomal degradation (Bennett N.C. *et al*, 2010; Block L.J. *et al*, 1998).

Phosphorylation of residues Ser213, Ser506 and Ser650 is a critical pre-requisite for induction of the transcriptional activity of the Androgen Receptor dimer (Bennett N.C. *et al*, 2010; Rochette-Egly C., 2003).

The N-Terminal Transactivation Domain (“N-TTD”) contains FxxLF and WxxLF motifs, the Activation Function protein-interactive surface sub-domains AF1 and AF5 and the Transactivation Unit sub-domains TAU1 and TAU5 (Jenster G. *et al*, 1995).

The C-Terminal Ligand-Binding Domain (“LBD”) contains the LxxLL motif, and the Activation Function protein-interactive sub-domain AF2 (Bennett N.C. *et al*, 2010).

The AF2 sub-domain possesses a higher affinity for FxxLF and WxxLF motifs within the N-Terminal Transactivation Domain (NTTD), than the FxxLL-like motifs contained within the “SRC/p160 type” co-regulatory protein ligands which associate with the Ligand-Binding Domain (He B. *et al*, 2004; He B. *et al*, 1999; He B. *et al*, 2000; He B. *et al*, 2001; Bennett N.C. *et al*, 2010; Matias P.M. *et al*, 2000; Nazareth L.V. *et al*, 1999; Sack J.S. *et al*, 2001).

The FxxLF and WxxLF motifs within the N-TTD associatively interact with the “ARA-type” co-regulatory protein ligands (Heery D.M. *et al*, 1997; Hur E. *et al*, 2004).

The N/C-Termini interactions between the NTTD and LBD domains, mediated via the FxxLF, WxxLF and LLxxL motifs, are implicated in the DNA-dependent formation of the active Androgen Receptor dimer (He B. and Wilson E.M., 2002; Li J. *et al*, 2006).

Thus the TAU1 and TAU5 sub-domains, “in concert” with the AF1 and AF5 sub-domains, function collectively as the major NTTD domain regulatory sites for modulation of the transcriptional activity of the Androgen Receptor (Bennett N.C. *et al*, 2010; Wong C.I. *et al*, 1993).

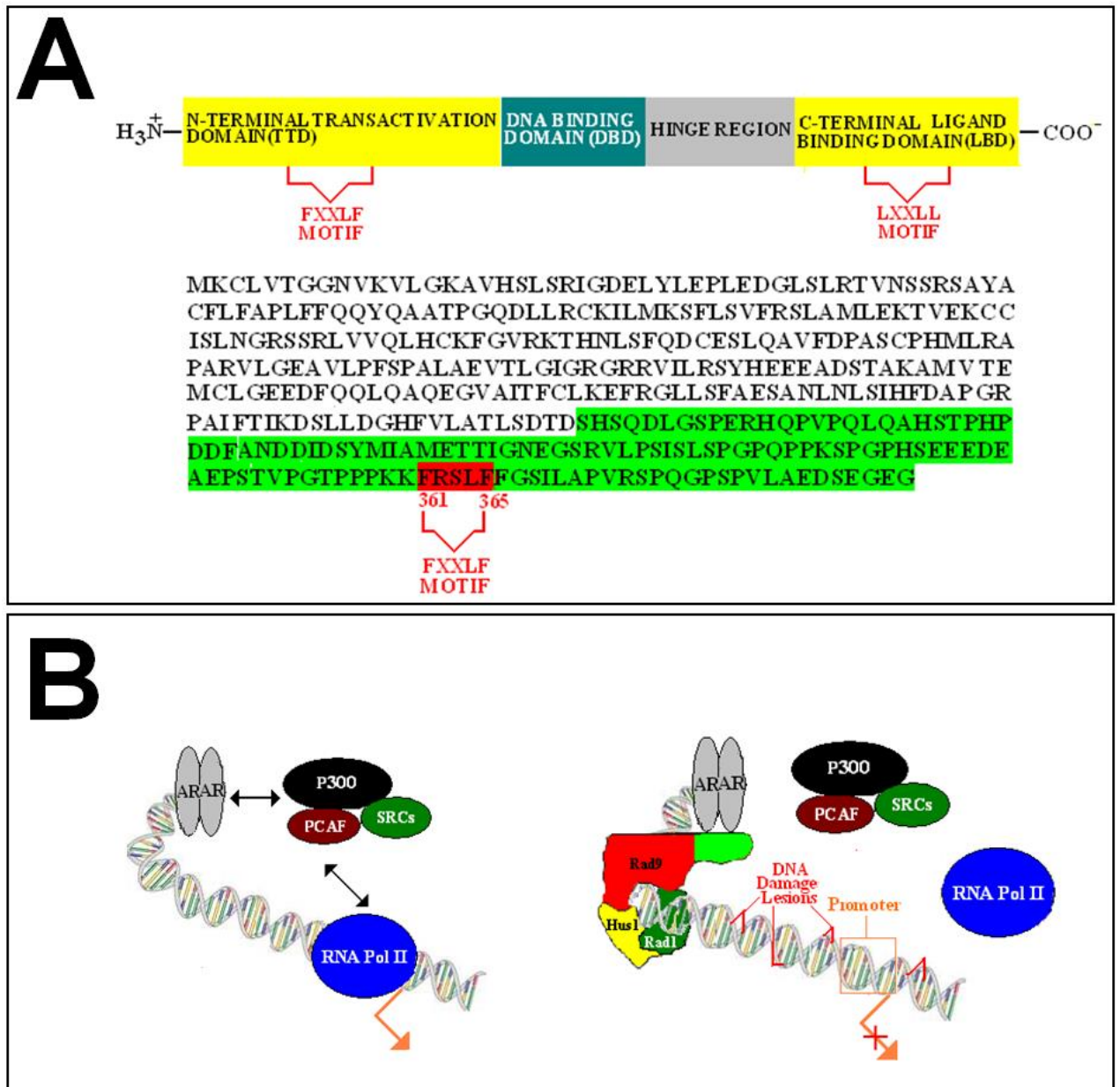
The DNA-Binding Domain (DBD) is comprised of the three α -helical domains of the respective Zinc-Fingers and the C-Terminal Extension (Freedman L.P. *et al*, 1988; Remerowski M.L. *et al*, 1991; Schoenmakers E. *et al*, 2000; Truss M. and Beato M. 1993)

The first Zinc-Finger contains a D-box motif comprised of 5 key residues which are implicated in DNA base-sequence recognition of the Androgen Response Element (ARE) and engage in associative AR-binding interactions with the major groove of the duplex, the 2nd Zinc Finger contains a D-Box Motif comprised of 5 key residues which engage in DNA-dependent AR dimerisation (Bennett N.C. *et al*, 2010; Centenera M.M. *et al*, 2008; Dahlman-Wright K. *et al*, 1991; Roche P.J. *et al*, 1992; Schoenmakers E. *et al*, 1999).

Proximal polypeptide sequences flanking the D-box and P-box motifs effect additional associative interactions which enhance the stability and DNA binding affinity of the Androgen Receptor dimer (Haelens A. *et al*, 2001; Tsai S.Y. *et al*, 1988; Umesono K. *et al*, 1989).

The C-Terminal Extension (CTE) motif effects additional DBD domain associations, “in synch.” with adjacent residues within the 2nd Zinc Finger Motif, which enhance the DNA-binding affinity and specificity of the Androgen Receptor dimer to the ARE within the target gene (Bennett N.C. *et al*, 2010; Schoenmakers E. *et al*, 1999; Verrijdt G. *et al*, 2006).

Fig 1.32: "9-1-1" Clamp Suppression of Androgen Receptor Activity



A: The human RAD9A protein C-terminal tail domain (highlighted in green) contains an FXXLF motif (spanning positions 361 to 365) which resembles similar functional sequence homology to the FXXLF motif located in the androgen receptor N-Terminal transactivation domain respectively. (Wang L. *et al*, 2004).

B: Associative-DNA response element sequence interactions with the ligand-activated dimerised nuclear Androgen Receptor (AR)₂ result in enhanced gene transcription under normal conditions. (Heinlein C.A. and Chang C., 2002).

Recruitment of the heterotrimeric toroidal "9-1-1" DNA sliding-clamp complex to sites of chromatin damage in proximity to the AR dimer target response element sequence also results in inhibitory associative interactions between the AR C-Terminal Ligand Binding Domain and the FXXLF motif within the protruding C-Terminal Tail Domain of the Rad9 protein with consequential suppression of functional AR transactivation for prevention of potential inappropriate/dysfunctional, unregulated expression of steroidal growth factor-mediated cytological neoplastic transformation and/or carcinogenesis. (Wang L. *et al*, 2004).

An androgen response element (ARE) has also been identified within the human *RAD9A* gene, of specific target sequence: 5'-CCAAGGCTCTGGTAGTTCCTTGGA-3', to which the zinc finger motifs of the AR dimer bind (interactive DNA base sequence recognition target motifs are indicated in bold, underlined italics above) with consequential elevation of expressed Rad9A protein levels (Moehren U. *et al.*, 2008).

The human Rad9A protein may therefore also auto-modulate its cellular levels and functional activities in a potential regulatory feedback mechanism, mediated via Rad9A protein-AR interactions, which impinge upon *RAD9A* gene-AR transcriptional activity.

The plasma membrane-localised estrogen receptor-substrate complex, 17 β -estradiol/Estrogen Receptor α (E(2)/ER), has also been demonstrated to suppress genotoxic-initiated ATR cell cycle checkpoint responsive activities via E(2)/ER induction of rapid PI3K/AKT signalling which suppresses associative TopBP1-ATR interactions (Pedram A. *et al.*, 2009).

The resultant E(2)/ER-activated AKT kinase perturbs associative interactions between ATR and TopBP1, via phosphorylation of Ser1159 within the TopBP1 protein and also inhibits associative interactions between Chk1 and Claspin via targeted phosphorylation of Chk1, with consequential suppression of ATR-Chk1-initiated DNA damage response checkpoint signalling pathways (Pedram A. *et al.*, 2009).

Since the Rad9-Rad1-Hus1 complex is a fundamental sensory/adaptive mediator of various ATR-Chk1-initiated genotoxic signalling responses (discussed in detail previously – Section 1.2.2, pp.46-65) it is conceivable that additional complex “feedback” mechanisms of cell cycle checkpoint pathway regulation may be elicited via associative indirect and/or direct “9-1-1” clamp-modulation of Androgen and/or other steroidal receptor activities which impinge upon E(2)/ER-mediated PI3K/AKT kinase signalling.

Other experimental studies have demonstrated that all three sub-units of the Rad9-Rad1-Hus1 complex can associate with the TPR2 protein, in which the functional activity of TPR2 is modulated exclusively via protein domain-specific Rad9-TPR2 interactions (Xiang S-L. *et al*, 2001) – discussed in detail in Section 1.2.4, pp.75-85.

The key function of the TPR2 protein is the modulation of the activity of the Hsp90-mediated chaperone protein-folding pathway (Brychzy A. *et al*, 2003; D’Andrea L.D. and Regan L., 2003; Li J. *et al*, 2011; Moffatt N.S. *et al*, 2008; Wandlinger S.K. *et al*, 2008; Young J.C. *et al*, 1998) – discussed in detail in Section 1.2.4, pp.75-85.

As discussed previously, the (Hsp90)₂Hsp70 protein chaperone complex apparatus is also implicated in the cytosolic sequestration and stabilisation of the androgen receptor monomer in its unphosphorylated, inactive form (Fig 1.30, p.70).

Thus it is possible that associative “9-1-1” complex-mediated regulation of TPR2 activity, via Rad9-TPR2 functional domain interactions, may be implicated in a separate feedback mechanism which impinges upon androgen receptor activity via modulation of Hsp90 and Hsp70 activities.

1.2.4: Modulation of TPR2 Activity-Influenced Protein Folding

Post-translational re-modelling of immature client protein/nascent polypeptides into the correct supramolecular conformational forms of the functional mature proteins is performed by the protein folding machinery which is comprised of a number of key interactive chaperone, co-chaperone and co-factor type component complexes (Fink A.L., 1999; Mahalingham D. *et al*, 2009; Goetz M.P. *et al*, 2003; Wandlinger S.K. *et al*, 2008) – Fig 1.33B, p.80.

Associative complex interactions of the Hsp70 and Hsp90 chaperone components, with the client nascent protein/polypeptide substrate, are mediated via their respective ATPase-coupled activities which constitute a cyclical ADP-ATP exchange regulatory mechanism (Grenert J.P. *et al*, 1999; Johnson J.L. and Brown C., 2009; Riggs D.L. *et al*, 2004) – Fig 1.33B, p.80.

The Hsp70:ATP complex exhibits rapid “on/off” switching kinetics for targeted client nascent protein/polypeptide substrates, in which Hsp70-mediated hydrolysis of ATP is initiated via associative interactions between the homologous DNAJ domains of the related co-chaperone components Hsp40 and p23 (Karagöz G.E. *et al*, 2011; Ohtsuka K. and Hata M., 2000; Wandlinger S.K. *et al*, 2008; Wegele H. *et al*, 2004) – Fig 1.33B, p.80.

The resultant ADP-bound–Hsp70 complex induces further supramolecular conformational changes within the Hsp70 chaperone component which enhance the strength of its associative binding interactions with the client nascent protein/polypeptide substrate (Johnson J.L. and Brown C., 2009; Wegele H. *et al*, 2006) – Fig 1.33B, p.80.

The ATP-bound–Hsp90 complex induces supramolecular conformational changes within the Hsp90 chaperone component which enhance the strength of its associative binding interactions with the client nascent protein/polypeptide substrate (Grenert J.P. *et al*, 1999; Johnson J.L. and Brown C., 2009) – Fig 1.33B, p.80.

Whilst Hsp90-mediated ATP hydrolytic formation of the ADP-bound–Hsp90 complex induces supramolecular conformational changes within the Hsp90 protein which disrupt its associative binding interactions with the client nascent protein/polypeptide substrate (Grenert J.P. *et al*, 1999; Johnson J.L. and Brown C., 2009; Wandlinger S.K. *et al*, 2008) – Fig 1.33B, p.80.

The adaptor protein Hop/p60, in conjunction with the co-factors Aha1, Cdc37 and p23, regulates the transient stability of the supramolecular conformational complex states implicated in the Hsp70/Hsp90-mediated folded conversion of the immature client protein/nascent polypeptide substrates to mature functionally-configured protein products (Carrigan P.E. *et al*, 2006; Harst A. *et al*, 2005; Johnson B.D. *et al*, 1998; Karagöz G.E. *et al*, 2011; Wandlinger S.K. *et al*, 2008; Wegele H. *et al*, 2004; Wegele H. *et al*, 2006) – Fig 1.33B, p.80.

Associative Hop-Hsp70 interactions are relatively weak, in contrast to the tight binding of Hop to Hsp90 and p23 (Harst A. *et al*, 2005; Johnson B.D. *et al*, 1998; Johnson J.L. and Brown C., 2009; Karagöz G.E. *et al*, 2011; Wegele H. *et al*, 2004; Wegele H. *et al*, 2006) – Fig1.33B, p.80.

Hop1 also stabilises the nucleotide-free transition state of Hsp90 and inhibits its ATPase activity to elicit release of the folded mature protein product from the Hsp70/Hsp90 chaperone complex machinery and facilitate the associative loading transfer of another immature client protein/nascent polypeptide substrate from Hsp70 to Hsp90 which is required for initiation of a fresh cycle of the folding pathway mechanism (Carrigan P.E. *et al*, 2006; Li J. *et al*, 2011; Southwood D.R. and Agard D.A, 2011; Wegele H. *et al*, 2006; Yi F. *et al*, 2010 – Fig 1.33B, p.80.

Associative Cdc37-Hsp90 complex interactions are responsive towards ADP- and ATP- bound nucleotide transition states (discussed on pp.73-74) and also elicit further supramolecular conformational changes which promote the associative recruitment of other co-factors such as p23 (Gaiser A.M. *et al*, 2010; Harst A. *et al*, 2005; Mandal A.K. *et al*, 2007)– Fig 1.33B, p.80.

Subsequent associative interactions between the N-terminus of Hsp90 and the co-chaperone p23 enhance the ATPase-driven release of the folded mature protein product from the Hsp70/Hsp90 chaperone complex machinery (Eustace B.K. and Jay D.G, 2004; Harst A. *et al*, 2005; Karagöz G.E. *et al*, 2011 Wegele H. *et al*, 2004; Wegele H. *et al*, 2006) – Fig 1.33B, p.80.

Tetratricopeptide Repeat Protein 2 (TPR2), also known as DNAJC7 (DNA J Homologue Sub-Family C, Member 7), is a Type III member of the DNAJ Hsp40 protein family (Brychzy A. *et al*, 2003; Moffatt N.S. *et al*, 2008; Murthy A.E. *et al*, 1996) – Fig 1.33A, p.80.

The TPR2 protein, in conjunction with Hop/p60, is capable of replacing the component functional activities of of Type I and Type II J-Proteins within the Hsp70/Hsp70 chaperone machinery, but cannot perform this task in the absence of Hop/p60 (Brychzy A. *et al*, 2003; Moffatt N.S. *et al*, 2008; Ramsey A.J. *et al*, 2007; Ramsey A.J. *et al*, 2009) – Fig 1.33B, p.80.

Independent TPR2-mediated protein chaperoning of nascent client protein/polypeptide substrates in the absence of other J-proteins is a temporally unstable mechanism which maintains an optimal level of regulated TPR2 activity and thus prevents prolonged TPR2-mediated inhibition of Hsp90 which would otherwise culminate in abrogated protein folding (Brychzy A. *et al*, 2003; Moffatt N.S. *et al*, 2008; Ramsey A.J. *et al*, 2007; Ramsey A.J. *et al*, 2009).

Analogous to Hop/p60, TPR2 also contains two TPR motifs (designated Tpr1 and Tpr2) which can bind simultaneously to Hsp70 and Hsp90 via an associative mechanism which requires ATP to promote binding interactions between Hsp70 and the J-domain within TPR2 (Brychzy A. *et al*, 2003; Moffatt N.S. *et al*, 2008; Ramsey A.J. *et al*, 2007; Ramsey A.J. *et al*, 2009) – Fig 1.33A, p.80.

However, the interactive mechanisms of the associative Hop–Hsp70/Hsp90 and TPR2–Hsp70/Hsp90 complexes are different (Brychzy A. *et al*, 2003; Moffatt N.S. *et al*, 2008; Ramsey A.J. *et al*, 2007; Ramsey A.J. *et al*, 2009).

In the absence of ATP, TPR2 is capable of engaging in associative interactions with only one of the proteins at a time – ie Hsp70 or Hsp90 (Brychzy A. *et al*, 2003; Moffatt N.S. *et al*, 2008; Ramsey A.J. *et al*, 2007; Ramsey A.J. *et al*, 2009).

Unlike Hop/p60, TPR2 specifically induces the ATP-independent dissociation of Hsp90 from the nascent client protein/polypeptide substrate within the Hsp70/Hsp90 chaperone complex machinery, but has no disruptive effect on associative Hsp70 interactions (Brychzy A. *et al*, 2003; Liu F-H. *et al*, 1999; Moffatt N.S. *et al*, 2008; Ramsey A.J. *et al*, 2007; Ramsey A.J. *et al*, 2009) – Fig 1.33B, p.80.

This exclusive specificity of TPR2 for Hsp90 is mediated via associative interactions between a critical Asp residue within the C-Terminal EEVD motif of the Hsp90 protein and the dicarboxylate clamp motifs contained within the Tpr1 and Tpr2 domains of the TPR2 protein (Prasad B.D. *et al*, 2010; Moffatt N.S. *et al*, 2008; Young J.C. *et al*, 1998) – Fig 1.33A, p.80.

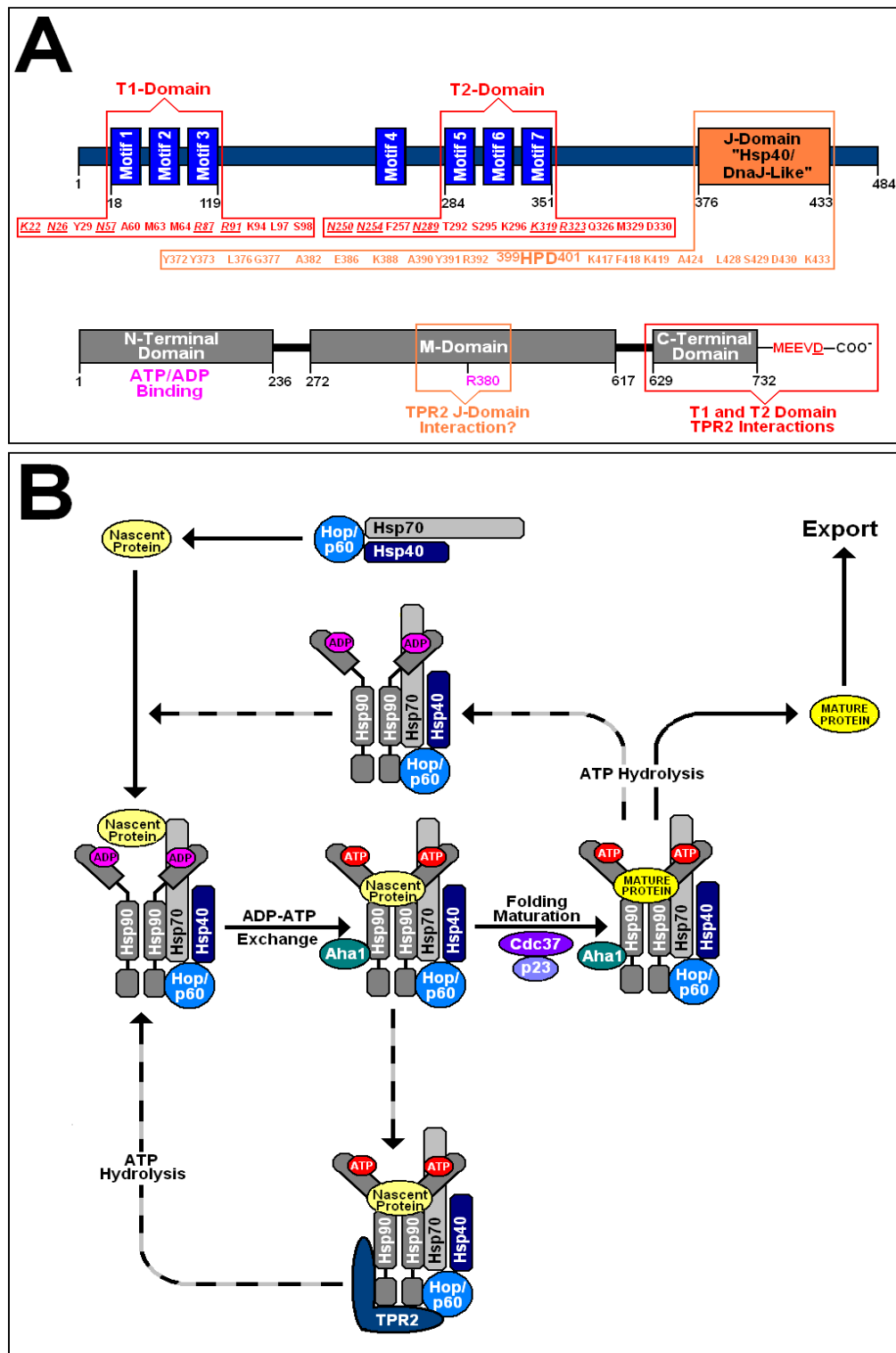
The binding specificity of TPR2 for Hsp90 is also enhanced via extensive Van der Waal's contacts between neighbouring hydrophobic residues situated in flanking positions which surround the dicarboxylate clamp motifs within the Tpr1 and Tpr2 domains of the TPR2 protein (Prasad B.D. *et al*, 2010; Moffatt N.S. *et al*, 2008; Young J.C. *et al*, 1998) – Fig 133A, p.80.

The Tpr1 and Tpr2 domains within the TPR2 protein are also functionally implicated in the disruption of the Hsp90 – nascent client protein/polypeptide substrate binding interactions, whilst the TPR2 Hsp40-Like J-domain induces ATP hydrolysis and formation of associative interactions between Hsp70 and the resultant Hsp90-liberated nascent client protein/polypeptide substrate interactions (Brychzy A. *et al*, 2003; Liu F-H. *et al*, 1999; Moffatt N.S. *et al*, 2008; Ramsey A.J. *et al*, 2007; Ramsey A.J. *et al*, 2009) – Fig 1.33A and Fig 1.33B, p.80.

Thus the principle function of TPR2 is the transient associative retro-conversion of incorrectly folded nascent client protein/polypeptide substrates from the later predominant Hsp90 complexes to the earlier predominant Hsp70 complexes within the Hsp70/Hsp90 chaperone machinery (discussed previously on pp.) and consequential rectification of the respective anomalous substrate supramolecular configurations via initiation of further fresh cycles of the mechanistic folding pathway interactions (Brychzy A. *et al*, 2003; Liu F-H. *et al*, 1999; Moffatt N.S. *et al*, 2008; Ramsey A.J. *et al*, 2007; Ramsey A.J. *et al*, 2009) – Fig 1.33B, p.80.

A. priori, TPR2 may be regarded as a critical regulatory “safe-guard” component of the Hsp70/Hsp90 chaperone protein folding system for the prevention of cumulative levels of misfolded/dysfunctional proteins and thus suppression of proteotoxic-types of induced carcinogenesis (discussed previously in Section 1.1 in Fig 1.1, p.5 and Fig 1.9, p.16).

Fig 1.33: TPR2 Modulation of Hsp90 Chaperone Complex Activity



A: Domain map of the TPR2 protein (Key residues implicated in dicarboxylate clamp formation are indicated in red and underlined; Key residues implicated in Hsp90 protein binding specificity are indicated in red; Key J-Domain residues, including the critical “HPD” functional motif, which bears significant sequence homology to the Hsp40 protein and are implicated in associative Hsp90 interactions are indicated in orange) – Top Figure.

Key functional domains of the Hsp90 protein are N-Terminal ATP/ADP binding-site, the M-domain (containing an Arg residue which is critical for associative interactions with the J-Domain of the TPR2 protein) and a C-Terminal Domain (containing a critical EEVD motif which mediates associative T1 and T2 TPR domain interactions with the TPR2 protein and is implicated in the selective specificity of Hsp90 interactions within the chaperone pathway) – Bottom Figure.

B: Summarised mechanism of the regulatory role of TPR2 within the chaperone protein-folding pathway (discussed in detail on pp.75-79).

The Tpr1 and Tpr2 domains of the TPR2 protein also associatively interact with the N-termini of each of the sub-units of the heterotrimeric, toroidal Rad9-Rad1-Hus1 DNA sliding-clamp complex (Xiang S-L. *et al.*, 2001) – Fig 1.34, p.82.

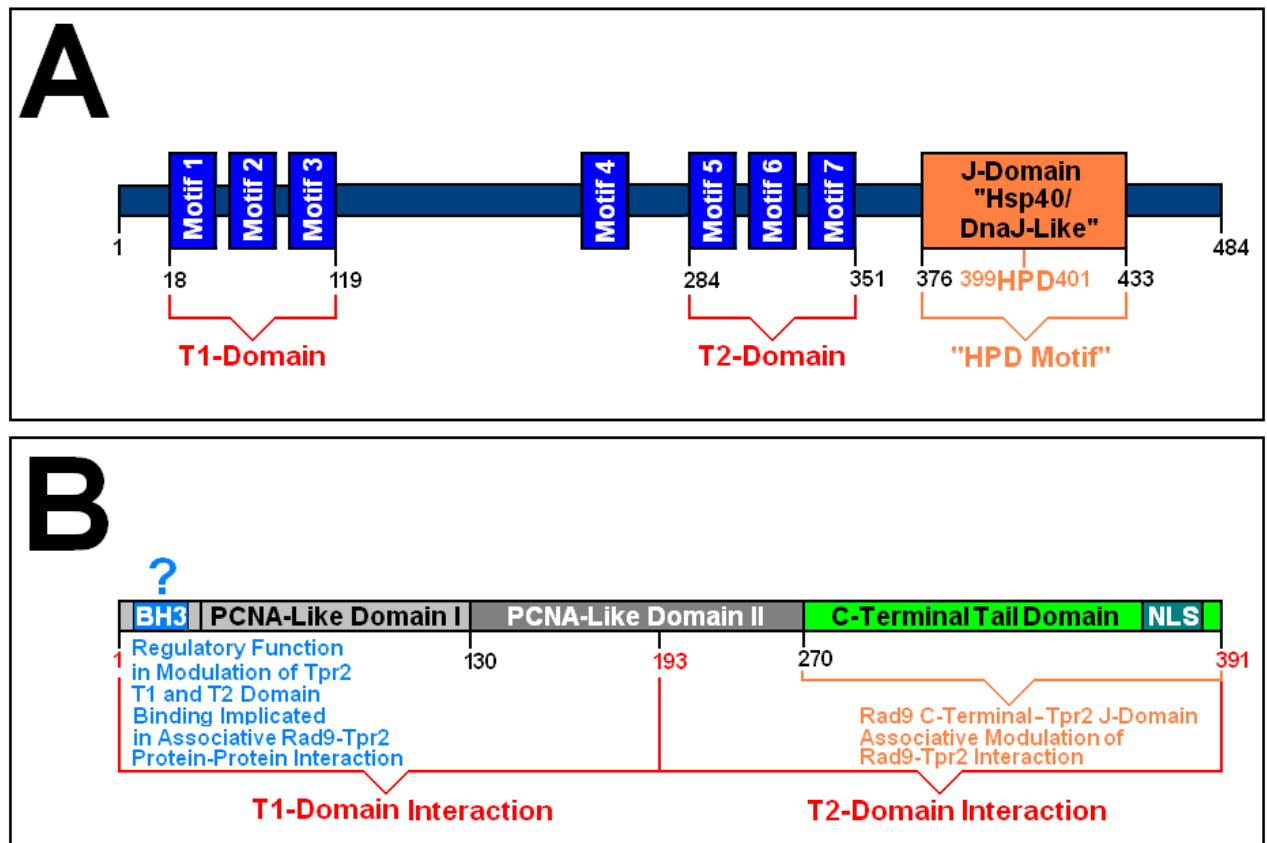
Unlike the respective TPR2-Rad1 and TPR2-Hus1 interactions, the TPR2 J-domain is also implicated in the association with Rad9, in which it modulates the cellular localisation of both the TPR2 and Rad9 proteins (Xiang S-L. *et al.*, 2001) – Fig 1.34, p.82.

As discussed previously, the “9-1-1” complex suppresses the transcriptional activity of the AR via specific Rad9-AR interactions (Section 1.2.3, pp.66-74), whilst TPR2 is known to be implicated in the modulation of Hsp70/Hsp90 chaperone complex machinery-mediated functional maturation-folding of nascent client steroid receptor protein substrates such as the progesterone receptor (Blatch G.L. and Lässle M., 1999; Felts S.J. *et al.*, 2007; Goebel M. and Yanagida M., 1991; Schülke P. *et al.*, 2010; Smith D.F., 2004).

The (Hsp90)₂Hsp70 protein chaperone complex apparatus is also implicated in the cytosolic sequestration and stabilisation of the AR and other steroid nuclear receptor monomers in their respective unphosphorylated, inactive forms (discussed previously in Section 1.2.3, pp.66-74; Fig 1.30, p.70).

Taken together, these experimental observations indicate additional “9-1-1” complex-mediated “feed-back” mechanisms that may regulate nuclear steroidal receptor functional activities via associative “9-1-1” complex–TPR2 interactions (Fig 1.34, p.82) and thus also impinge upon the “9-1-1” complex-mediated suppression of the transcriptional activity of the AR (discussed previously in Section 1.2.3, pp.66-74; Fig 1.32, p.72).

Fig 1.34: Rad9-Modulated TPR2 Activity – Key Domain Interactions



A: Elementary domain map of the TPR2 protein with highlighted T1, T2 and “HPD” domains (discussed in detail previously in Fig 1.33, p.77).

Individual Tricopeptide Repeat (TPR) motifs are comprised of the characteristic, conserved ~34 amino acid acid (generalised) sequence: [WLF]-X(2)-[LIM]-[GAS]-X(2)-[YCF]-X(8)-[ASE]-X(3)-[FYI]-X(2)-[ASL]-X(4)-[PKE]

<http://www.ncbi.nlm.nih.gov/structure/cdd/cddsrv.cgi?uid=194311> PubMed Protein Conserved Domains Archive clo2429: TPR Superfamily PSSM Id: 1943911 Name: TPR [Update 5th May 2011]

[d’Andrea L.D. and Regan L., 2003; Goebel M. and Yanagida M., 1991; Lamb J.R. *et al.*, 1995]

TPR2 interacts with all three protein sub-units of the Rad9-Rad1-Hus1 complex via N-Terminal T1 domain associative interactions, whilst additional C-Terminal T2 domains and J Domain interactions are required for both Hus1 and Rad9 association and TPR2 homodimerization (Xiang S-L. *et al.*, 2001).

B: The human Rad9A protein contains N-Terminal and C-Terminal interactive domains which associate with the T1 and T2 domains of the TPR2 (Fig A) protein respectively (Xiang S-L. *et al.*, 2001).

The N-Terminal BH3-like domain within the human Rad9A protein may also be implicated in the modulation of the associative strength of the respective Rad9A N-Terminal – TPR2-T1 and Rad9A C-Terminal – TPR2-T2 domain interactions (Xiang S-L. *et al.*, 2001).

Residue-specific Kinase-mediated phosphorylation and/or Phosphatase-mediated dephosphorylation of the human Rad9A C-Terminal domain may induce transient supramolecular configurations which modulate the associative strength of its interaction with the TPR2 T2-domain (Xiang S-L. *et al.*, 2001).

The associative strength of the respective interactions between Rad9A and the T1 and T2 domains of TPR2 are also regulated by the J-domain of TPR2, unlike the other two sub-units of the “9-1-1” clamp complex; Rad1 and Hus1 (Xiang S-L. *et al.*, 2001).

The presence of ATP has also been demonstrated, *in Vitro*, to inhibit the aforementioned associative Rad9A-TPR2 protein-protein interactions – in which TPR2 J-domain-mediated regulation of Hsp70 chaperone functionality, via stimulation of its ATPase catalytic activity, may thus enhance Rad9A-TPR2 associative interactions as a consequence of the elevated induction of hydrolytic conversion of ATP to ADP (Xiang S-L. *et al.*, 2001).

The mechanism of Hsp70/Hsp90 chaperone complex machinery-mediated functional maturation-folding of the nascent secondary (distal) transducer checkpoint protein kinase Chk1 client protein substrate is equally dependent upon TPR2 and Hop/p60, but does not require the p23 co-chaperone (Felts S.J. *et al*, 2007; Redlak M.J. and Miller J.A., 2011) – Fig 1.33B, p.80.

Other research studies have also demonstrated that Swe1 and Wee1 effector checkpoint kinase-mediated phosphorylation of Hsp90 is implicated in the modulation of the functional activities of Hsp70/Hsp90 chaperone complex machinery (Mollapour M. *et al*, 2010; Redlak M.J. and Miller J.A., 2011).

As discussed previously, the heterotrimeric toroidal Rad9-Rad1-Hus1 complex is implicated in the initiation of various ATR/ATRIP→Chk1-activated regulatory cell cycle checkpoint pathways in response to genotoxic and/or DNA replication stresses (Section 1.2.2, pp.33-65).

Taken together, these experimental observations indicate additional “9-1-1” complex-mediated “feed-back” mechanisms that may regulate cell cycle checkpoint activities via associative “9-1-1” complex–TPR2 interactions (Fig 1.34, p.80), which may also be implicated in the appropriate modulation of the Rad9-Rad1-Hus1 complex-mediated ATR/ATRIP→Chk1 activation (discussed previously in Section 1.2.2, pp.33-65) in response to proteotoxic types of induced DNA damage and/or DNA replication stress.

In this context, associative “9-1-1” complex–TPR2 interactions may be implicated in the suppression of proteotoxic-induced carcinogenesis events (discussed previously in Section 1.1 in Fig 1.1, p.5 and Fig 1.9, p.16).

Various research studies have also indicated that the Hsp70 chaperone protein mediates several key functional activities which are implicated in the negative regulation of pro-apoptotic pathways, notably; the inhibition of Procaspase-9 recruitment to Apaf-1 proteosome (Beere H.M. *et al*, 2000), suppression of Asp1-1 apoptoproteosomal activity (Saleh A. *et al*, 2000), suppression of the catalytic activity of N-terminal kinase domain of c-Jun – which is implicated in the development of tolerance to caspase-independent mechanisms of induced apoptosis (Gabai V.L. *et al*, 2000) and protection against stress-induced apoptosis (Mosser D.D. *et al*, 2000).

Full-length human Rad9A is also cleaved by Caspase-3, at specific proteolytic target motifs within the PCNA-like II domain and C-Terminal Tail domain, to yield N-terminal BH3-like domain-retained truncated fragments which bind and inhibit the functional activities of BH3-type apoptotic suppressor proteins such as BCL-xL and BCL-2 with consequential promotion of apoptosis (Earnshaw W.C. *et al*, 1999; Komatsu K. *et al*, 2000a; Komatsu K. *et al*, 2000b; Le M.W. *et al*, 2003; Nicholson D.W. *et al*, 1999) – discussed in detail later in Section 1.3.2, pp.127-130.

The C-Tail Terminal Tail domain of full-length human Rad9 has also been demonstrated to interactively associate with the *p21* gene promoter and enhance its transcriptional activity with consequential elevated p21 protein activity-mediated induction of apoptosis (Yin Y. *et al*, 2004).

Taken together, these experimental observations indicate additional “9-1-1” complex-mediated “feed-back” mechanisms that may regulate Hsp70-mediated proapoptotic suppression activities and “9-1-1” complex-independent Rad9-mediated apoptotic modulatory functions via associative “9-1-1” complex–TPR2 interactions (Fig 1.34, p.82) – which in turn may impinge upon the functional activities of the TPR2-regulation of the Hsp70/Hsp90 chaperone protein-folding complex machinery (Fig 133., p.80).

The protein chaperone components Hsp70, Hsp90 and TPR2, within the multi-functional protein-folding complex machinery (Fig 1.34, p.82), have also been demonstrated to interact with U-Box Type Ubiquitin Protein Ligases (E3s) and it has been postulated that these interactions may be implicated in a sensory mechanism which targets irreversible mis-folded proteins for proteosomal degradation (Hatakeyama S. *et al*, 2004).

Associative Jab1 (CSN5) interactions with the Rad1 sub-unit component of the “9-1-1” DNA sliding-clamp are also known to be required for its targeted ubiquitination, mediated via E3 Ubiquitin Protein Ligases, which constitutes as key pre-requisite step for the initiation of the sequential proteolytic degradation of the heterotrimeric, toroidal Rad9-Rad1-Hus1 complex (Hirai I. *et al*, 2004; Huang J. *et al*, 2007) – discussed later in Section 1.4, pp.131-139.

Taken together, these experimental observations indicate additional “9-1-1” complex-mediated “feed-back” mechanisms that may regulate the activities of both the Rad9-Rad1-Hus1 complex and independent Rad9 functions (summarised previously in Fig 1.2, p.8), via associative “9-1-1” complex–TPR2 interactions (Fig 1.34, p.82) which modulate the level of “9-1-1” complex proteolytic degradation and/or may also be implicated in the proteolytic-specific targeting of the respective individual Rad1, Hus1 and Rad9 sub-units in response to different types of proteotoxic-induced DNA damage and/or DNA replication stress.

Such mechanisms may also be implicated in the modulation of the levels and activities of the individual isoforms of the Rad9, Hus1 and Rad17 proteins (Fig 1.3, p.9; Fig 1.4, p.10; Fig 1.6, p.12) for regulation of the functional activities of each of four potential “9-1-1” DNA sliding-clamp isoforms (Fig 1.5, p.11) and individual Rad9A and Rad9B isoforms (Fig 1.3, p.9) respectively.

These plausible potential functions of Rad9-TPR2 interactions are strictly hypothetical at present since the precise roles of Rad9 in the regulation of TPR2 activity are unknown.

1.2.5 DNA Repair Pathway Selection and Activity Modulation

DNA in every cell is subjected to a myriad of different types of damage-orientated molecular insult via exposure to a diverse variety of endogenous biochemical reactions and exogenous/environmental genotoxic agents which proceed via spontaneous and/or inductive events that can be sub-categorised into several defined classifications in the context of their respective biomolecular interactive mechanisms (Pallis A.G. and Karamouzis M.V., 2010; Tuteja N. and Tuteja R., 2001) – depicted summarily in Fig 1.35, p.89.

The relative severity and impact of the resultant structural DNA alterations on the perturbation of the continuity of genetic information is variable and dependent to a large extent upon the precise biochemical nature of the respective lesion (Pallis A.G. and Karamouzis M.V., 2010; Tuteja N. and Tuteja R., 2001).

Negligible disruptive effects are manifested via alkylation of a single DNA base, whilst minor disruptive effects are associated with the hydration/loss of a DNA base and consequential apurinic/apyrimidinic site formation (Pallis A.G. and Karamouzis M.V., 2010; Tuteja N. and Tuteja R., 2001).

Major disruptive effects are manifested in the case of formation of large/sterically bulky base adduct insertions, DNA base-dimers, intra-/inter-strand cross-linkages within the DNA molecule and/or with a large biomolecular species such as a protein and single-/double-stranded breakages within the duplex (Caldecott K.W., 2008; McKinnon P.J. and Caldecott K.W., 2007; Pallis A.G. and Karamouzis M.V., 2010; Tuteja N. and Tuteja R., 2001).

The culminative physio-biochemical effect of these genotoxic events, particularly in the case of large/steric bulk DNA lesions, is the promotion of stalled replication forks as a consequence of induced topological alterations within the DNA (Dillon L.W. *et al.*, 2010) – Fig 1.36, p.90.

Each cell also experiences approximately 10,000 – 50,000 single-strand DNA breaks and 50 – 200 double-stranded DNA breaks per day as a consequence of acute and chronic exposure to a wide variety of genotoxic biophysical and biochemical insults (Caldecott K.W. *et al*, 2008; McKinnon P.J. and Caldecott K.W., 2007; Speit G. *et al*, 1984) – depicted summarily in Fig 1.35, p.89.

In particular, genotoxic events which induce double-stranded breakage type DNA lesions (DSB's) are considered to be the most potent promoters of carcinogenesis as a consequence of the fact that rectification of DSB's is accomplished via the cytological employment of various recombinational repair pathways (Fung H. and Weinstock D.M., 2011; Tuteja N. and Tuteja R., 2001 – depicted summarily in Fig 1.37, p.91 and Fig 1.48, p.109.

With the notable exception of Gene Conversion, these recombinational pathways possess an inherent degree of mechanistic error-prone DNA repair potential which may compromise genomic integrity. (Christmann M. *et al*, 2003; Fung H. and Weinstock D.M., 2011; McKinnon P.J. and Caldecott K.W., 2007; Pastink. A. *et al*, 2001; Povik L.F., 2006; Tuteja N. and Tuteja R., 2001).

Induction of DNA replication stress may also result in DSB repair-induced formation of cis- and/or trans- type chromosomal hybrid proto-oncogene-fusion type translocation constructs which are expressed as carcinogenic-promoting chimeric type oncogenic proteins (Dillon L.W. *et al*, 2010; Hegyi H. *et al*, 2009; Huang M. *et al*, 2002a; Longhran T.P. *et al*, 2000; Okuya M. *et al*, 2010; Povirk L.F., 2006; Rabkin C.S. and Janz S., 2008) – Fig 1.36, p.90.

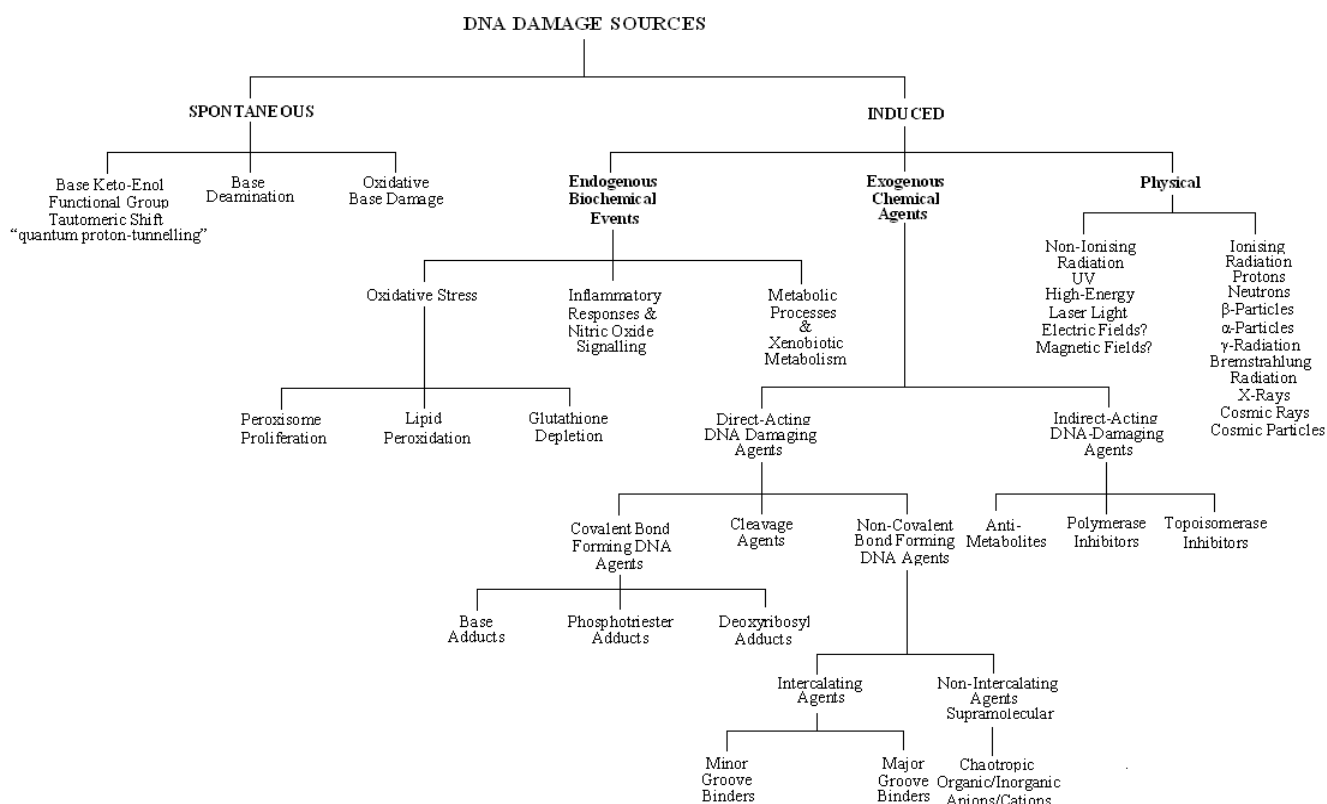
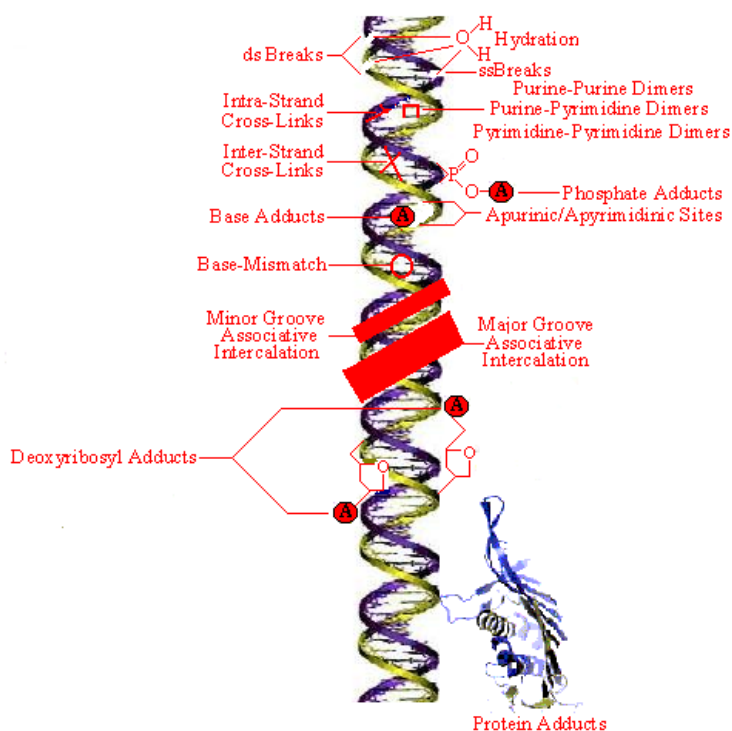
The accumulation of chromosomal breaks in response to DNA replication stress, as a consequence of defective repair of DSB type lesions, is also a well-documented early indicator of carcinogenesis (Bartkova J. *et al*, 2005; Bryant P.E., 2004; Fung H. and Weinstock D.M., 2011; Pallis A.G. and Karamouzis M.V., 2010).

The Intra-/Inter- Cross-Link Repair (ICL) and Translesion Synthesis Repair (TLS) pathways, which are implicated in the cytological rectification and/or by-pass of large/sterically bulky DNA lesions (Fig 1.37, p.91; Fig 1.39, p.100; Fig 1.40, p.101; Fig 1.51, p.112), also exhibit error-prone mechanistic potential which may contribute to compromised genomic integrity (Christmann M. *et al*, 2003; Pallas A.G. and Karamouzis M.V., 2010; Tuteja N. and Tuteja R., 2001).

Mutation-induced disproportionate dysregulation of the dynamically-balanced equilibrium between replicative DNA lesions and selective DNA repair pathway activation responses may culminate in the promotion of carcinogenesis (Bartkova J. *et al*, 2005; Dillon L.W. *et al*, 2010) – Fig 1.36, p.90.

Tumourigenic pre-disposition may also be a consequence of manifested expression of dysfunctional mutations within genes that encode DNA damage checkpoint and/or DNA repair proteins, including Rad9 (Bartek J. *et al*, 2007a; Bartek J. *et al*, 2007b; Branzie D. and Foiani M, 2008; Dillon L.W. *et al*, 2010) – Fig 1.36, p.90.

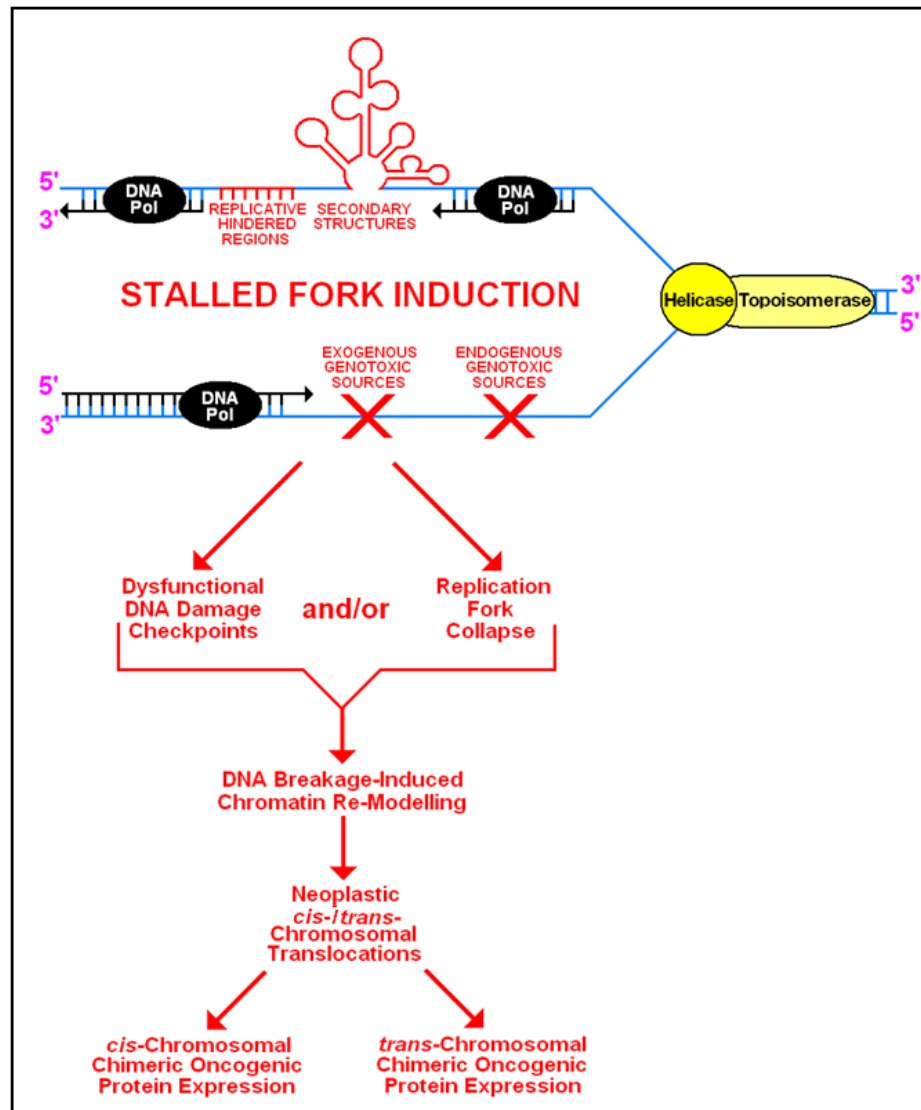
Fig 1.35: DNA Damage Types and Sources – A Biochemical Summary



[Compiled via Collated Information From: Ashby J. *et al.*, 1994; Barnes D.E. and Lindahl T., 2004; Becker M.M. and Wang Z., 1989; Beukers R. *et al.*, 2008; Blank M. and Goodman R., 1999; Behari J. and Paulraj R., 2007; Boucher D. *et al.*, 2006; Chan S.W. and Dedon P.C., 2010; Cooper W.G., 1993; Cooper W.G., 1996; Crumpton M.J. and Collins A.R., 2004; Falone S. *et al.*, 2007; Fang Y.Z. *et al.*, 2002; Farver O., 2000; Ferguson L.R. and Denny W.A., 2007; Hall D.B. *et al.*, 1996; Hemnani and Parihar M.S., 1998; Hill M.A., 1999; Horton A.A. and Fairhurst S., 1987; Kelly S.O. and Barton J.K., 1999; Kim G.Y., 2002; Kundrat P. and Stewart R.D., 2006; Larson I.K. and Kastrop J.S., 2002; Maranon J. and Sorraín O.M., 1978; Marnett L.J. *et al.*, 2003; Marnett L.J. and Plastaras J.P., 2001; Matsumoto H. *et al.*, 2007; McCann J. *et al.*, 1993; Mishra P.C. and Mishra R.N., 1976; Nair U. *et al.*, 2007; Nakagawa H. *et al.*, 2006; Nickens K.P. *et al.*, 2010; Nikjoo H. *et al.*, 1998; Nunez M.L. *et al.*, 1999; Olsson G. *et al.*, 2004; Prise K.M. *et al.*, 1998a; Prise K.M. *et al.*, 1998b; Rao M.S. and Reddy J.K., 1991; Reddy J.K. and Rao M.S., 1989; Rein R. and Harris F.E., 1964; Roots R. *et al.*, 1990; Schulte-Frohlinde D. *et al.*, 1990; Sharma R.A. *et al.*, 2001; Simko M., 2007; Slupphaug G. *et al.*, 2003; Teoule R., 1987; Wolffe A.P. and Hayes J.J., 1999; Zheng R. *et al.*, 2010]

Fig 1.36: Types of DNA Conformer-Induced Replicative Inhibition

[Taken and Adapted From: Dillon L.W. *et al*, 2010]



Different types of DNA damage and/or replication stress may promote dissociation of the DNA polymerases, Pol α , Pol δ and Pol ϵ , from the helicase/topoisomerase replicative complex to generate long tracts of ssDNA which possess the potential to fold into a variety of topological secondary structures within the duplex.

These topological secondary structures may stall the replication fork with consequential activation of the ATR-dependent DNA damage response checkpoint pathways.

[A variety of different types of associative protein interactions within the C-terminal tail domain of the Rad9 sub-unit, which protrudes outside of the Rad9-Rad1-Hus1 PCNA-like DNA sliding-clamp sensory complex, are also implicated in ATR-Chk1-activated DNA damage response checkpoint pathways – discussed previously in Section 1.2.2, pp.33-65]

Fragile sites within the chromatin supra-molecular architecture, in proximity to localised ssDNA topological secondary structures, may be particularly susceptible to spontaneous types of replication fork reversal and/or erratic polymerase “associative-dissociative hopping” progression at regions of secondary structure along the DNA.

Dysfunctional activation and/or suppression of these secondary structure-induced ATR-dependent checkpoint pathways may compromise appropriate regulatory cell cycle responses to DNA damage and/or replication stress with consequential propagation of DNA breakage events and chromosome translocational aberrations, which in turn may promote carcinogenesis (Rabkin C.S. and Janz S., 2008) – Fig 1.9, p.16.

Fig 1.37: Classification Review of DNA Damage Repair Mechanisms

[Compiled via Collated Information From: Christmann M. *et al*, 2003; Barnes D.E. and Lindahl, 2004; Foustari M. and Mullenders L.H., 2008; Friedberg E.C., 2005; Hakem R., 2008; Li G.M., 2008; Verbeek B. *et al*, 2008

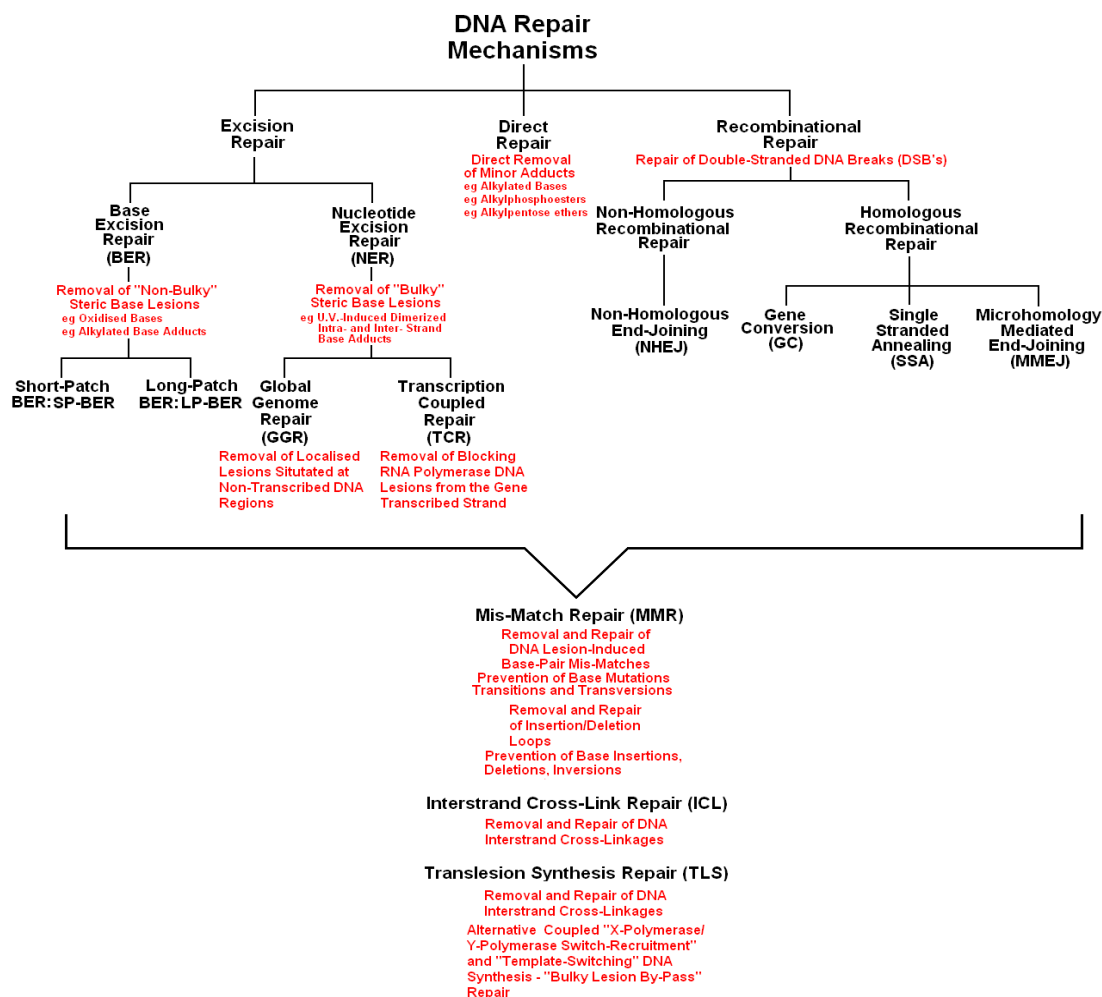


Table 1.5: Summarised DNA Repair Mechanism Responses

DNA DAMAGE RESPONSE	MECHANISM
Direct-Repair Reversal	Enzymatic Repair of: O^6 -Alkyl-Guanine O^4 -Alkyl-Thymine Alkylphosphotriesters Ligation of DNA Strand Breaks
Excision of DNA Damage	Base Excision Repair (BER) Nucleotide Excision Repair (NER) Mis-Match Repair (MMR) and/or ICL/TLS
Tolerance of DNA Damage	Replicative By-Pass of Template Strand Damage via Gap Formation and Recombination (HRR), NHEJ and/or ICL/TLS

Note: The most important damage response is probably excision-mediated repair of the DNA, whilst the direct-reversal repair is somewhat limited to removal of small alkylation DNA lesions and direct ligation of single-stranded and double-stranded phosphodiester bond lyses.

An associative mutagenic risk of cumulative error-prone replicative potential exists in the case of DNA damage tolerance responses elicited via NHEJ, SSA and MMEJ by-pass repair mechanisms.

Although the majority of biochemical pathways associated with DNA repair are primarily constitutive, various experimental studies have also identified a number of inter-communicative modulatory DNA damage response pathway interactions implicated in the selective induction and regulatory control of specific DNA repair mechanisms respectively. (Hwang B.J. *et al*, 1998; Bartek J. *et al*, 2001; D'Amours D. and Jackson S.P., 2002; Lee S.H. and Kim C.H., 2002; Venkitaraman A.R., 2002; Christmann M. *et al*, 2003).

The homotrimeric PCNA clamp has also been demonstrated, experimentally, to interact with the Rad9 and Hus1 sub-units of the heterotrimeric Rad9-Rad1-Hus1 (“9-1-1”) complex in response to genotoxic events and/or perturbed DNA replication (Komatsu K. *et al*, 2000c).

Under normal cytological conditions, PCNA-DNA interactions may enhance the topological flexibility of the lagging strand of the replication fork for the facilitated access of the associative protein complexes which are implicated in the synthesis, assembly and ligation of the base sequence complementary okazaki fragments (Querol-Audí J. *et al*, 2012).

In contrast to the PCNA clamp, “9-1-1” complex-DNA interactions may enhance the transient topological stability of localised DNA damage sites to provide sufficient time for the targeted recruitment and assembly of protein complexes which are implicated in the rectification of specific genotoxic lesions, thereby facilitating their recognition and repair (Querol-Audí J. *et al*, 2012).

Taken together, these phenomena may indicate that the differential DNA-interactive functions of the PCNA and “9-1-1” DNA “sliding clamp” complexes could serve as a critical component of a variety of checkpoint-coupled mechanisms which are responsible for the sequential co-ordination of cell cycle arrest, DNA repair and re-initiation of DNA replication in response to specific genotoxic and/or environmental cytological stresses.

The Rad9-Rad1-Hus1 heterotrimeric toroidal PCNA-like DNA “sliding clamp” complex also performs several key integral functions in the biochemical modulation of various DNA repair mechanisms (Fig 1.37, p.91; Fig 1.38, p.98; Table 1.4, p.99), thus providing an inter-communicative link with the respective “downstream” signal transductional “cross-talk” effector responses of the regulatory cell cycle DNA-damage checkpoint pathways (Fig 1.38A, p.98) – notably;

- (i) Protection of recessed 5' end DNA substrates, generated as *in situ* transient intermediates in various biochemical mechanisms of DNA repair/maintenance pathways, from extensive exonuclease degradation and promoted resolution of the resultant “9-1-1”-complex-stabilised structures back to their respective native supramolecular duplex topological configurations (Ellison V. and Stillman B., 2003) – Fig 1.38B, p.98.

- (ii) Associative Rad9 C-Terminal Tail Domain interactions with DNA polymerase ϵ , within the “9-1-1” sliding-clamp complex may also be implicated in the recognition and repair of DNA gaps and/or single-stranded DNA breaks – SSBs (Sukhanova M.V. *et al*, 2011).
[In this context, it has also been postulated that Rad9-SSB interactions, within the “9-1-1” sliding-clamp complex, may provide a regulatory signal link which couples DNA damage checkpoint responses with the appropriate selection of the Base Excision Repair and Single-Stranded Break DNA repair pathway activities (Sukhanova M.V. *et al*, 2011)]

- (iii) The “9-1-1” sensory complex has also been elucidated to be a critical biochemical trigger for initiation of “downstream” DNA-damage checkpoint signal transductional responses to DNA replication fork arrest (Longhese M.P. *et al*, 1997), dsDNA breaks (Kondo T. *et al*, 2001; Melo J.A. *et al*, 2001) and perturbed telomere maintenance (d'Adda di Fagagna F. *et al*, 2004; Garvik B. *et al*, 1995; Lydall D., 2009; Lydall D. and Weinert T, 1995; Longhese M.P. *et al*, 2000; Nabetani A. *et al*, 2004; Slijepcevic P., 2006; Slijepcevic P. and Al-Wahiby S., 2005) – Fig 1.38A and Fig 1.38B, p.98.

- (iv) Various experimental studies have demonstrated that the human Rad9 protein (hRad9), acting within the Rad1-Hus1 associative PCNA-like toroidal heterotrimeric DNA “sliding-clamp”, is implicated in the enhancement of the catalytic activity of particular enzymes implicated in DNA repair pathway and/or maintenance mechanisms (Table 1.4, p.99).
- (v) The biochemical mechanisms of the “9-1-1” complex-stimulated DNA repair nuclease type enzymatic activities (Table 1.4, p.99) may also involve associative interactions between an identified potential nuclease-binding/nuclease catalytic activity type domain motif within the hRad9 protein (Bessho T. and Sancar A., 2000 – discussed summarily in Fig 1.44B, p.105).
- (vi) The “9-1-1” clamp has been postulated to be implicated in a biochemical feedback type of mechanism which co-ordinates the recruitment and regulation of the enzymatic activities of APE1, FEN1, LigI and Pol β in SP-BER and LP-BER DNA repair pathways (Balakrishnan L. *et al.*, 2009; Collura A. *et al.*, 2012) – discussed summarily in Fig 1.41, p.102 and Fig 1.42, p.103.
- (vii) Rectification of oxidised DNA base adducts, via co-ordinated interactions between the BER and MMR repair pathways, may also involve “9-1-1” clamp-mediated recruitment and activity modulation of the APE1, FEN1, hOGG1, Lig I, MLH1, MSH2, MSH3, MSH6, MYH1, NEIL1, Pol β and TDG proteins (Bai H. *et al.*, 2010; Balakrishnan L. *et al.*, 2009; Chang D-Y. *et al.*, 2011; Germann M.W. *et al.*, 2010; Guan X. *et al.*, 2007b; He W. *et al.*, 2008; Park M.J. *et al.*, 2009; Luncsford P.J. *et al.*, 2010; Reha-Kranz L.J. *et al.*, 2011; Taricani L. *et al.*, 2010; Zheng L. *et al.*, 2010); described summarily in Figs 1.41-1.47, pp.102-108.

[Note: Differential ATR/ATRIP and TopBP1 associative cross-talk signalling with the Rad9-Rad1-Hus1 and MSH2:MSH6 complexes, which are independently recruited to the DNA lesion sites, may also serve as a regulatory activation mechanism for the Chk1-initiated and Chk2-initiated DNA damage checkpoint pathways – Fig 1.44, p.105]

(viii) Epigenetic nucleosomal post-translation modification-based chromatin re-modelling of histones H3 and H4, via Rad9-associative enzymatic activity regulation of histone Deacetylase (Fig 1.46B, p.107), Metnase (Fig 1.50, p.111) and TLK1/TLK1B (Fig 1.52, p.117) within the “9-1-1” clamp, may be implicated in specific signal response-mediated modulation of the SP-BER (Fig 1.42, p.103), LP-BER (Fig 1.42, p.103), MMR (Fig 1.43, p.104), HR (Fig 1.48, p.109), NHEJ (Fig 1.48, p.109) and TLS-Coupled “Template-Switching” DNA repair pathways (Fig 1.51, p.112 – discussed in detail on pp.113-116) (Canfield C. *et al*, 2009; Chang D-Y. *et al*, 2011; De Benedetti A. *et al*, 2010; De Haro L.P. *et al*, 2010).

[In this context, the selective activation/modulation of specific DNA repair pathways may be dependent upon the type and physio-biochemical structure of the DNA damage site which is “sensed” via distinctive transient conformer associations between the Rad9-Rad1-Hus1 complex and “lesion-fixed” DNA topological alterations of the chromatin supramolecular architecture]

The heterotrimeric toroidal Rad9-Rad1-Hus1 complex may also be implicated in the sequential recruitment and modulation of DNA repair factor functions that propagate recurring cycles of DNA re-section and DNA re-synthesis which activate different DNA damage checkpoints in an alternate manner with consequential maintained quiescent/dormant cytological status (Deshpande A.M. *et al*, 2011) – Fig 1.49, p.110.

This DNA repair-mediated mechanism of perpetuated quiescent cytological status may also be implicated in the observed multi-drug resistance of dormant tumour cells to a wide variety of different types of anti-proliferative chemotherapeutics (Deshpande A.M. *et al*, 2011; Essers M.A. and Trumpp A., 2010; Trumpp A. and Wiestler O.D., 2008).

Dbf-Dependent Kinase (DDK, also known as Cdc7)-mediated phosphorylation of the Ser319, Ser320 and Ser321 residues, situated within the C-Tail Terminal Domain of the Rad9 Sub-unit, are postulated to induced supra-molecular conformational changes within the “9-1-1” sliding-clamp complex which promote its dissociation from the DNA after elicited genotoxic detection and initiation of appropriate cell cycle checkpoint responses in order to facilitate access of various protein components of the DNA repair machinery to the lesion site (Furuya K. *et al*, 2010; Paek A.L. and Weinert T., 2010) – Fig 1.53, p.118.

Somewhat paradoxically, other experimental studies have indicated that the “9-1-1” sliding-clamp complex also has a function in the recruitment of various DNA repair proteins to the DNA damage lesion site via associative interactions with the C-Tail Terminal Domain of the Rad9 sub-unit – which also enhances some of their respective activities (discussed previously and summarised in Table 1.4, p.99).

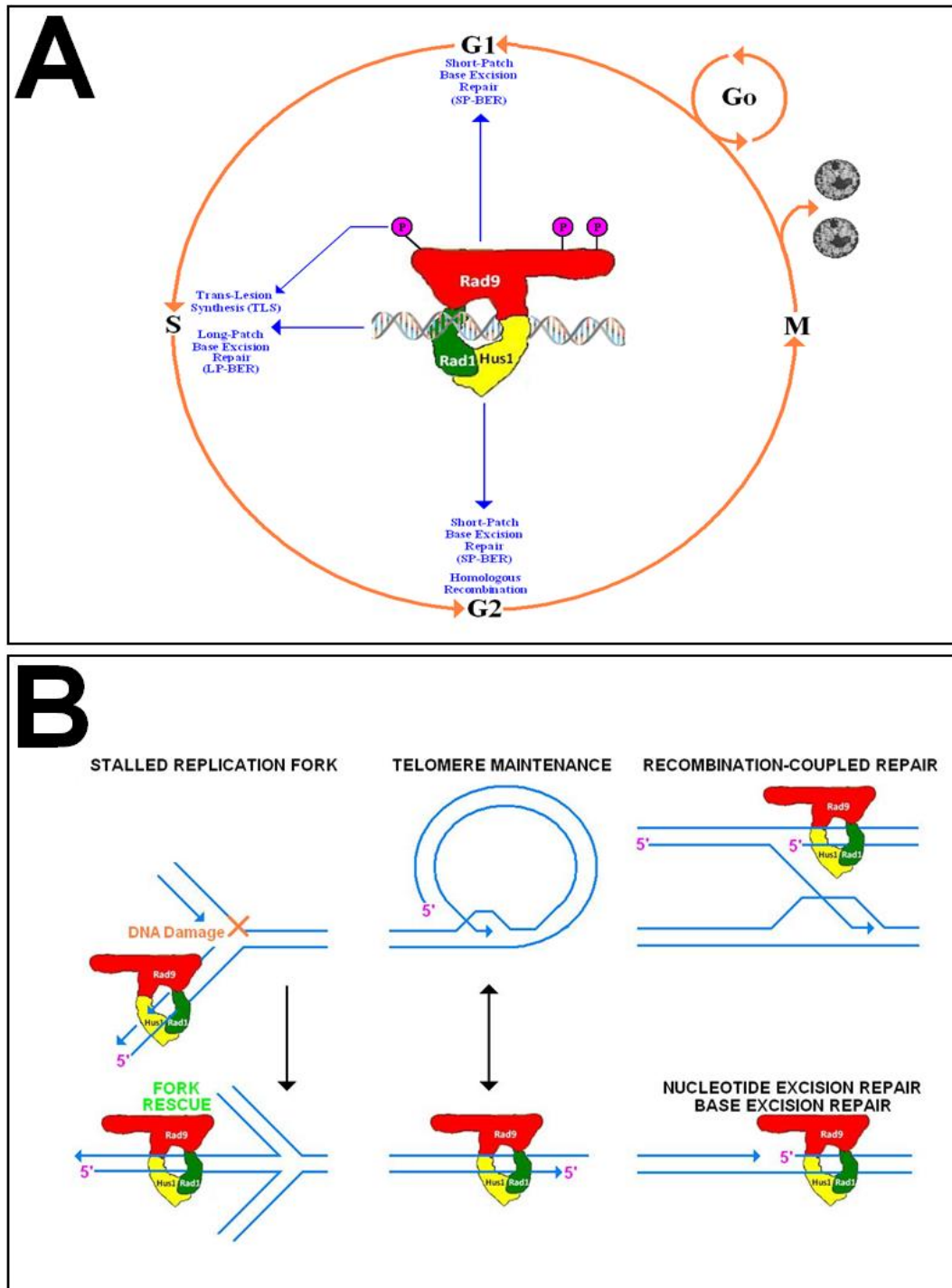
Phosphorylation of the DDK/Cdc7 kinase by the secondary (distal) transducer kinase Chk1 occurs within the Intra-S phase cell cycle DNA Damage Checkpoint – which is also initiated via associative “9-1-1” complex interactions (discussed previously in Section 1.2.2, pp.33-65; Fig 1.20, p.56 and Fig 1.22, p.58).

Taken together, these different experimental observations may indicate that the DNA repair prerequisite for dissociation or retention of the heterotrimeric toroidal Rad9-Rad1-Hus1 complex may be dictated by the biochemico-physical nature of the encountered DNA lesion in conjunction with the appropriate selected type of mechanism(s) for its rectification – which in turn may be “governed” via “9-1-1” complex-initiated Chk1-mediated cell cycle checkpoint signal-specific events (discussed previously in Section 1.2.2, pp.33-65).

Dissociation of the “9-1-1” sliding-clamp complex from the DNA lesion, via DDK/Cdc7 kinase-mediated phosphorylation of the C-Terminal Tail Domain of the Rad9 sub-unit, may also be constitute a DNA damage checkpoint response to extensive and/or very severe DNA damage.

In this context, the function of the DDK/Cdc7 kinase would be the prevention of inappropriate DNA lesion site-recruitment of Y-polymerases and/or other repair factors implicated in error-prone mechanisms of DNA repair, which would otherwise result in a catastrophic loss of genomic integrity in the surviving cell with consequential promotion of carcinogenesis.

Fig 1.38: Functional Roles of the “9-1-1” Clamp in DNA Repair



A: Summarised modulatory roles of hRad9, acting within “9-1-1” sensory complex-initiated checkpoint DNA damage response-repair pathways at various phases of the cell-cycle – LP-BER and SP-BER are phase-specific, whilst other pathways are comparatively non-cell cycle phase-specific (López-Contreras A.J. and Fernandez-Capetillo O., 2010).

NOTE: A critical phosphorylation site at T225, identified in the homologous eukaryotic *S.pombe* PCNA-like domain of the spRad9 protein, is hypothesised to be implicated in kinase-mediated type interactive regulation and/or selection of particular DNA damage repair pathways - for example, via integral template-switching between BER/NER and TLS pathways via ubiquitin-coupled determinant utilisation of X-type or Y-type DNA polymerases respectively (Jansen J.G. *et al.*, 2007; Kai M. *et al.*, 2007) – Figs 1.39 - 1.42, pp.100-103; Fig 1.51, p.112.

[Homologous functional phosphorylation site(s) may also exist in the case of the human hRad9 protein]

B: Associative interactions of “9-1-1” complex with various DNA structural substrate intermediates, generated via DNA maintenance and/or DNA damage repair pathway processes, are postulated to be essential for both the prevention of catastrophic extensive exonuclease degradation of the resultant 5'-recessed ends and enhanced promotional rectification of these transient supramolecular conformational forms back to reconstituted duplex DNA (Taken and Adapted From: Ellison V. and Stillman B., 2003; Nabetani A. *et al.*, 2004).

Table 1.4: “9-1-1” Clamp-Modulated DNA Repair Protein Activities

DNA Repair-Implicated Protein Factor/Enzyme	Specific Rad9-Rad1-Hus1 Complex Protein-Interactive Modulated DNA Repair Pathway Activity Function(s)	Referenced Citation Sources
ENDONUCLEASES	APE1 (Apurinic/Apyrimidinic Endonuclease 1)—BER (pp.102-103)	Balakrishnan L. <i>et al.</i> , 2009
	FEN1 (Flap Endonuclease I)—BER (pp.102-103) —GC, SSA, MMEJ, NHEJ (p.109)	Balakrishnan L. <i>et al.</i> , 2009 Guo Z. <i>et al.</i> , 2008 Querol-Audí J. <i>et al.</i> , 2012 Wu X. <i>et al.</i> , 1999 Zheng L. <i>et al.</i> , 2010
GLYCOSYLASES	hMYH1 (Human MutY Glycosylase Homologue)— BER/MMR Coupled "Go System" (pp.102-108)	Chang D.Y. <i>et al.</i> , 2011 Chang D.Y. and Lu A.L., 2005 Luncsford P.J. <i>et al.</i> , 2010 Lu A.L. <i>et al.</i> , 2001 Lu A.L. <i>et al.</i> , 2006 Shi G. <i>et al.</i> , 2006
	hOGG1 (Human 8-Oxoguanine Glycosylase 1) — BER/MMR Coupled "Go System" (pp.102-108)	Dianov G.L. <i>et al.</i> , 2011 Park M.J. <i>et al.</i> , 2009
	NEIL 1 (Endonuclease VIII-Like Protein 1) — BER/MMR Coupled "Go System" (pp.102-108)	Guan X. <i>et al.</i> , 2007a Taricani L. <i>et al.</i> , 2010
	TDG Glycosylase (Thymine Dimer Glycosylase)-BER (pp.102-103) -NER (pp.100-101) -GGR (p.100) -TCR (p.101)	Guan X. <i>et al.</i> , 2007b
LIGASES	DNA Ligase I — Various DNA Repair Pathways (pp.100-116)	Balakrishnan L. <i>et al.</i> , 2009 Helt C.E. <i>et al.</i> , 2005 Rodriguez M. <i>et al.</i> , 2003 Smirnova E. <i>et al.</i> , 2005 Song W. <i>et al.</i> , 2007 Song W. <i>et al.</i> , 2009 Wang W. <i>et al.</i> , 2006
POLYMERASES	DNA Pol β — Various DNA Repair Pathways (pp.100-116)	Balakrishnan L. <i>et al.</i> , 2009 Gembka A. <i>et al.</i> , 2007 Touelle M. <i>et al.</i> , 2004
	DNA Pol δ — Various DNA Repair Pathways (pp.100-116)	Jansen J.G. <i>et al.</i> , 2007
	DNA Pol ϵ — Various DNA Repair Pathways (pp.100-116)	Deshpande A.M. <i>et al.</i> , 2011 Puddu F. <i>et al.</i> , 2011 Sukhanova M.V. <i>et al.</i> , 2011
	DNA Pol η — "Template-Switch"- Mediated TLS (pp.111-117)	Jansen J.G. <i>et al.</i> , 2007
	DNA Pol ζ — "Template-Switch"- Mediated TLS (pp.111-117)	Jansen J.G. <i>et al.</i> , 2007
TELOMERASES	Regulatory Maintenance of Telomere Integrity (p.98; p.107)	Khair L. <i>et al.</i> , 2010 Francia S. <i>et al.</i> , 2006 Francia S. <i>et al.</i> , 2007 Michaelson R.J. <i>et al.</i> , 2005 Slijepcevic P., 2006
METHYLASES	Metnase — Chromosomal Decatenation (p.111) — HR (p.109; p.111) — NHEJ (p.109; p.111) — "Template-Switch"- Mediated TLS (pp.111-116)	De Haro L.P. <i>et al.</i> , 2010
KINASES	ATR (ATM and Rad3-Related Kinase)—Rad9 Phosphorylation Induced "9-1-1" Clamp DNA Repair Pathway Selection (p.98; p.105)	Kai M. <i>et al.</i> , 2007
	DDK (Dbf4-Dependent Kinase)/Cdc7—Rad9 Phosphorylation Induced "9-1-1" Clamp DNA Dissociation to Enable Access of DNA Repair Proteins to the Lesion Site (p.118)	Furuya K. <i>et al.</i> , 2010 Paek A.L. & Weinert T., 2010
	TLK1/TLK1B (Tousled-Like Kinase 1/1B) — "Template-Switch" Mediated TLS (pp.112-117)	Canfield C. <i>et al.</i> , 2009 De Benedetti A. <i>et al.</i> , 2009 De Benedetti A. <i>et al.</i> , 2010 Ronald S. <i>et al.</i> , 2011 Sunvala-Dossabhoy G. & De Benedetti A., 2009
MMR-IMPLICATED PROTEIN FACTORS	MLH1 (MutL Homologue 1)—MMR (p.104)	He W. <i>et al.</i> , 2008
	MSH2 (MutS Homologue 2)—MMR (pp.104-105; p.108)	Bai H. <i>et al.</i> , 2010
	MSH3 (MutS Homologue 3)—MMR (pp.104-105; p.108)	
	MSH6 (MutS Homologue 6)—MMR (pp.104-105; p.108)	

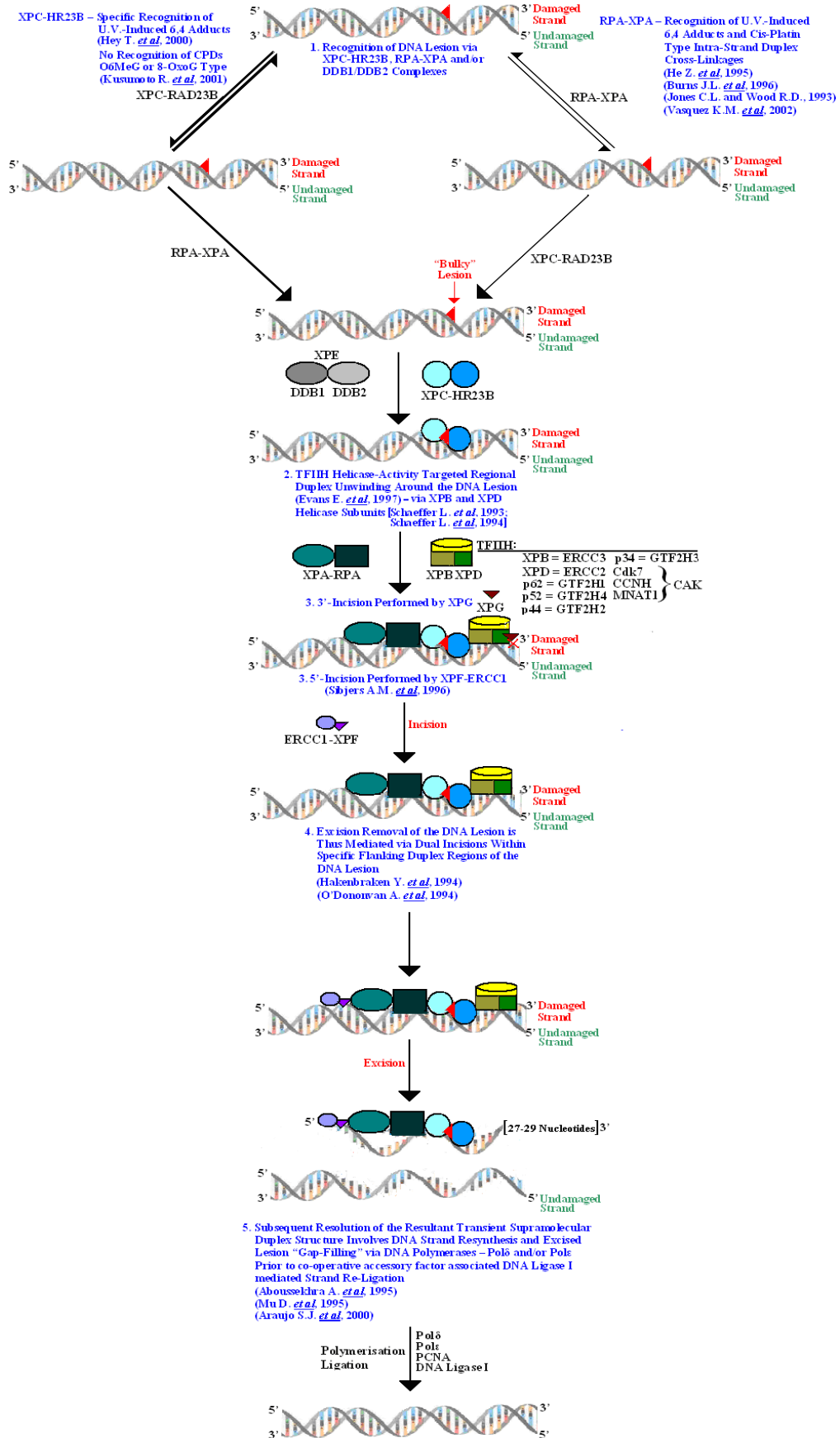
NOTE: The Rad9 and Hus1, but not Rad1, sub-units of the “9-1-1” DNA sliding-clamp complex contain binding pockets for the PCNA-Interacting Peptide (PIP) box motif (Doré A.S. *et al.*, 2009; Eichinger C.S. and Jentsch S., 2011; Komatsu K. *et al.*, 2000c; Sohn S.Y. and Cho Y., 2009; Xu M. *et al.*, 2009) – Highlighted in Fig 1.10C, p.24 (Section 1.2.1).

The PIP Box motif is of general consensus sequence: QxxL/I/MxxHF/DF/Y and is contained in a variety of different proteins including DNA polymerases and other associated DNA repair proteins (Gilljam K.M. *et al.*, 2009; Warbrick E., 1998; Warbrick E., 2000; Warbrick E., 2006).

Thus, in addition to Rad9 C-Terminal Tail domain associations, the “9-1-1” complex may modulate the functional activities of the various proteins (tabulated above) via Rad9 and Hus1 sub-unit PIP box-binding interactions.

Fig 1.39: A Mechanistic Overview of Global Genomic Repair

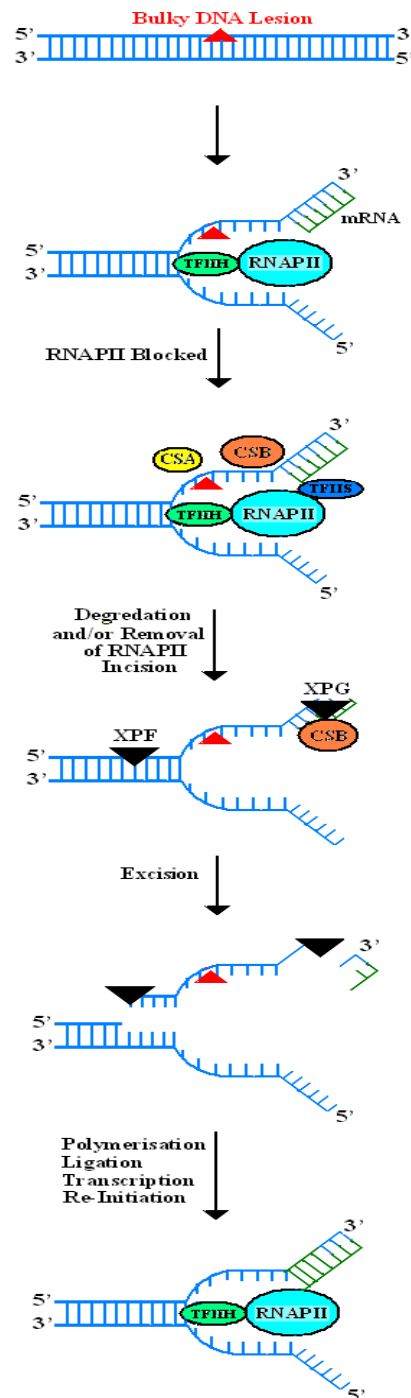
[Taken and Adapted From: Christmann M. *et al.*, 2003; Shuck S.C. *et al.*, 2008]



GGR is mainly a transcription-independent NER pathway for removal of DNA lesions of non-transcribed genomic domains and non-transcribed regions of transcribed DNA strands for predominantly favoured, rapid and efficient removal of highly duplex-distortive lesions (Balajee A.S. *et al.*, 1997; Hanawalt P.C., 2002; Mullenders L.H. and Berneburg M., 2001)

Fig 1.40: A Mechanistic Overview of Transcription-Coupled Repair

[Taken and Adapted From: Christmann M. *et al*, 2003; Fousteri M. and Mullenders L.H.F., 2008]



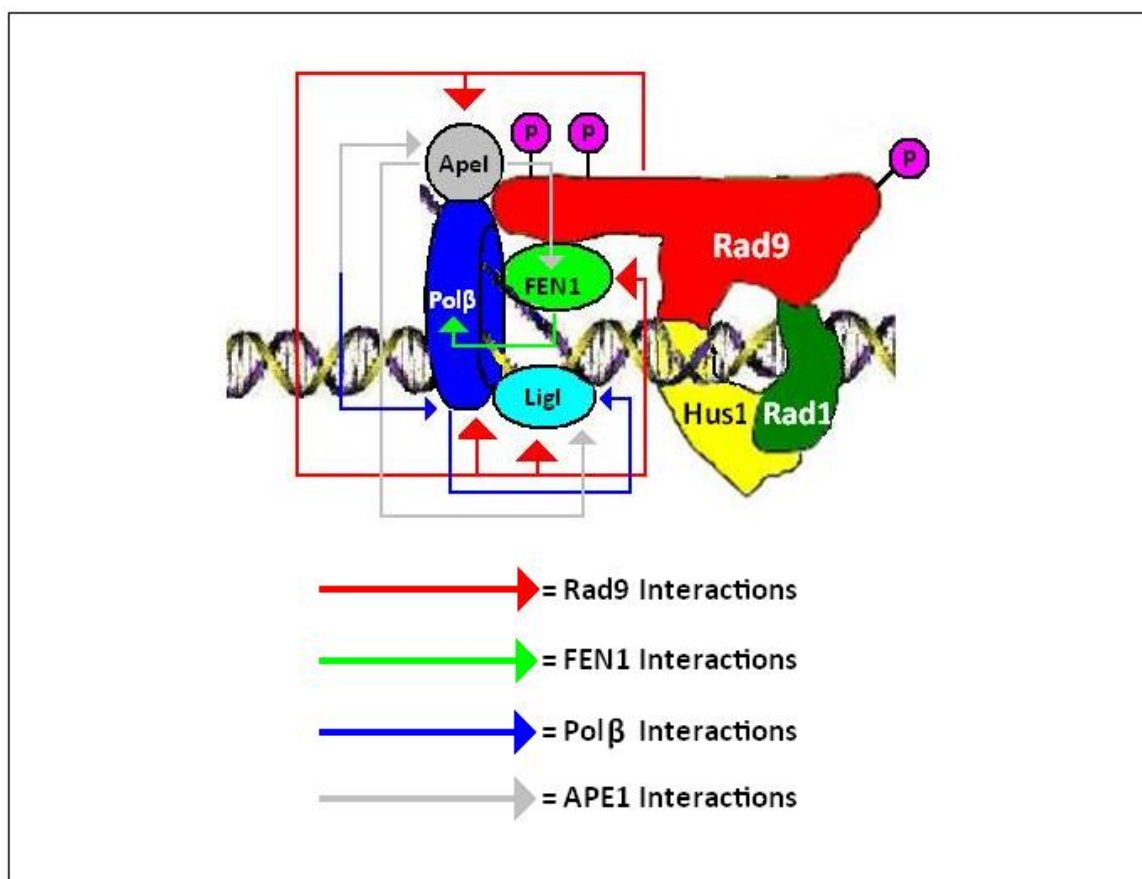
Transcription-Coupled Repair (TCR) is an alternative NER-pathway which is cytologically-utilised for the removal of various RNA-polymerase blocking lesions within transcribed strands of active genes (Bohr V.A. *et al*, 1985; Mellon I. *et al*, 1987)

DNA lesion-induced conformational changes within the supramolecular duplex structure inhibit the transcriptional process of RNA Polymerase II (RNAPII) with consequential displacement of RNAPII mediated via CSA, CSB and/or TFIIIS assembly at the lesion site, initiated facilitative recruitment access of the exonucleases XPF-ERCC1 and XPG for subsequent cleavage removal of the DNA lesion-containing strand and strand re-synthesis via DNA polymerases Pol δ and/or Pol ϵ prior to strand-annealing performed by DNA Ligase I (Christmann M. *et al*, 2003).

In contrast to the GGR-NER DNA repair pathway (Fig 1.39, p.100), the TCR-NER pathway is also predominantly more efficient at removal of U.V.-induced CPD type DNA lesions (Christmann M. *et al*, 2003).

Fig 1.41: “9-1-1” Co-Ordination of the BER Repairosome Activities

[Taken and Adapted From: Balakrishnan L. *et al*, 2009]



A variety of experimental studies have indicated that the “9-1-1” complex stimulates APE1, FEN1, DNA Ligase I and DNA Polymerase β enzymatic activities via direct associative interactions with the C-Tail Terminal Domain of the Rad9 component sub-unit (Collura A. *et al*, 2012; Gembka A. *et al*, 2007; Guo Z. *et al*, 2008; Helt C.E. *et al*, 2005; Rodriguez M. *et al*, 2003; Smirnova E. *et al*, 2006; Song W. *et al*, 2007; Song W. *et al*, 2009; Toueille M. *et al*, 2004; Wang W. *et al*, 2006; Wu X. *et al*, 1999; Zheng L. *et al*, 2010).

In the above model, structural interactions between FEN1 and DNA Pol β stimulate the cleavage activity of FEN1, whilst maximal stimulation DNA Ligase I activity is mediated via APE1 and DNA Pol β interactions, whilst Rad9 is not considered to be implicated in the direct stimulation of these respective enzymatic activities (Balakrishnan L. *et al*, 2009).

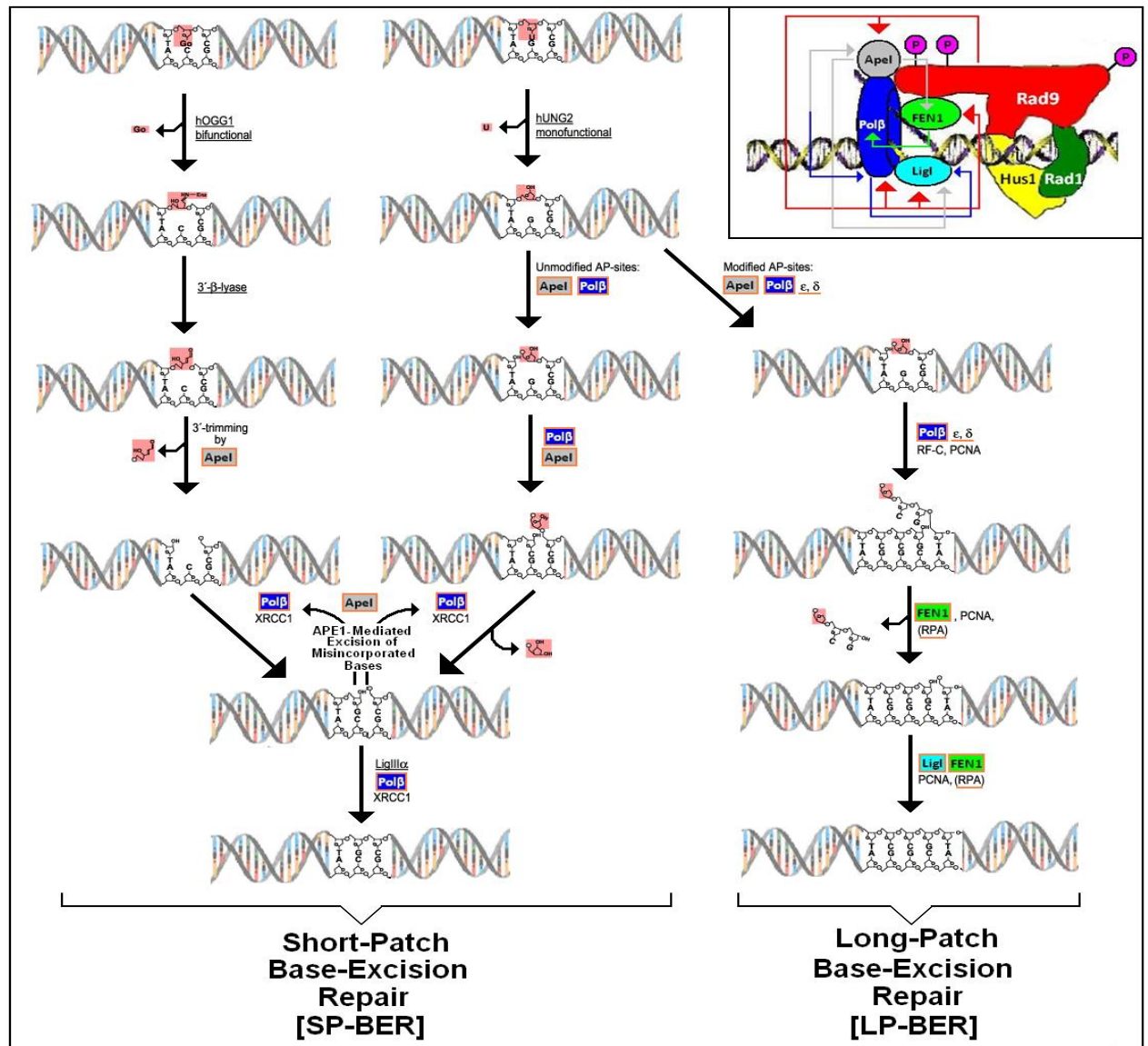
Thus, the primary function of the “9-1-1” clamp is to act as a mediator for the sequential recruitment of the respective protein components of the Base Excision Repairosome and co-ordination of their “synergy-orchestrated” enzymatic activities via specific Rad9 C-Terminal Tail Domain interactions (Balakrishnan L. *et al*, 2009).

Arrows pointing in a single direction denote a specific stimulatory interaction between one particular protein with another protein (Balakrishnan L., *et al*, 2009).

Arrows pointing in both directions denote potential stimulatory and counter-stimulatory interactive protein activities within the Base Excision Repairosome complex (Balakrishnan L. *et al*, 2009).

The respective of SP-BER and LP-BER mechanistic DNA repair pathways are summarily discussed on the following page (Fig 1.42, p.103) together with the above model (inset) to indicate the associated functional roles of the respective enzymes whose activities are modulated by the “9-1-1” clamp.

Fig 1.42: “9-1-1” Clamp Modulation of SP-BER & LP-BER Activities



Base Excision Repair (BER) Pathways may proceed via utilisation of a range of different Type I and Type II N-glycosylase enzymes, dependent upon the nature of the base modification – typically for the repair of oxidised or alkylated DNA bases, for example hOGG1 (repair of oxidatively-modified Guanine – Fig A) or hUNG1 (for repair of oxidatively-deaminated Cytosine conversion to Uracil – Fig B) (Christmann M. *et al.*, 2003; Schärer O.D. and Jiricny J., 2001).

[Type I glycosylases excise modified bases to generate an apurinic/apyrimidinic (AP) within the DNA, whilst Type II glycosylases excise modified bases and also effect cleavage of the resultant AP site via their 3'-endonuclease activity with consequential formation of a single-stranded DNA breakage (Christmann M. *et al.*, 2003; Wilson D.M. 3rd and Barsky D., 2001).

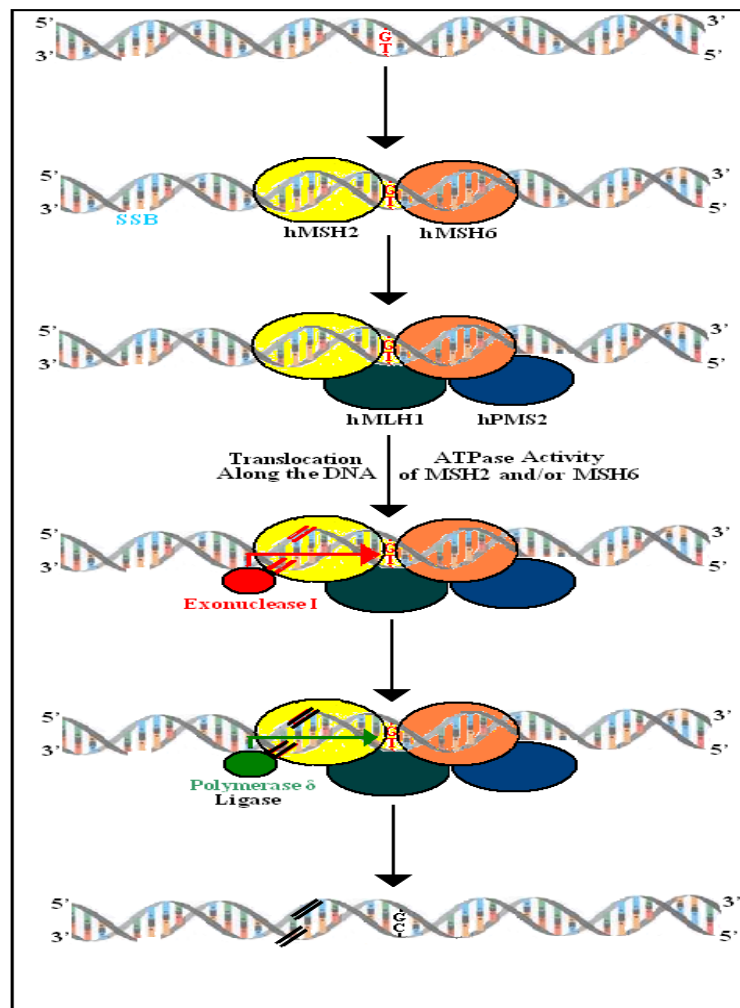
Selection of either the Short-Patch or Long-Patch BER pathway is critically pre-determined via the propensity of the DNA polymerase β (Polβ) catalytic lyase activity towards 5'-cleavage of the generated Apurinic/Apyrimidinic intermediate – which is dependent upon the biochemical nature of the AP-site. (Matsumoto Y. and Kim K., 1995; Prasad R. *et al.*, 1998; Sobol R.W. *et al.*, 2000)

The Short-Patch BER (SP-BER) pathway proceeds via a sequential mechanism that is “triggered” via initial recognition and hydrolytic cleavage excision of the modified base lesion (via a DNA N-glycosylase enzyme) and removal of the resultant AP site via 3'-end excision - mediated by Apurinic/Apyrimidinic Endonuclease I (APE1) and 5'-displacement mediated via the catalytic lyase activity of Polβ (that targets the hemi-acetal form of the AP-site 5'-deoxyribose residual form) which also subsequently inserts the appropriate one-nucleotide repair patch, into the resultant DNA strand “gap”, followed by direct annealing/“gap” sealing of the inserted one-nucleotide repair patch via the cooperative interaction of DNA Ligase IIIα, XRCC1, Polβ and Poly(ADP-Ribose) Polymerase I (PARP). (Dianov G.L. *et al.*, 1992; Kubota Y. *et al.*, 1996; Sobol R.W. *et al.*, 1996; Wiebauer K. and Jiricny J., 1990)

The Long-Patch BER (LP-BER) pathway proceeds via an alternative sequential mechanism that is “triggered” via PCNA-complex recognition of SP-BER-generation of reduced of oxidised AP sites (eg 3'-unsaturated aldehydes or 3'-phosphates), that are resistant to Polβ catalytic lyase-mediated hydrolytic β-elimination, in which cooperative interactions between PCNA and its RFC-loading complex in conjunction with DNA polymerase δ (Polδ) and/or DNA polymerase ε (Polε) invoke strand-dissociation at the AP DNA lesion site, followed by Flap Endonuclease I (FEN1)-mediated excision of the displaced deoxyribosephosphate strand intermediate and subsequent Polδ/Polε-mediated synthesis and insertion of a longer oligonucleotide repair patch (typically ~ 2-10 nucleotides) into the resultant “gap” – prior to “gap-filled long-patch annealing/sealing” by DNA Ligase I for completion of DNA repair (Klugland A. and Lindahl T., 1997; Nakamura J. *et al.*, 2000; Prasad R. *et al.*, 1996; Srivastava D.K. *et al.*, 1998; Stucki M. *et al.*, 1998)

Fig 1.43: A Mechanistic Overview of Base-Mismatch DNA Repair

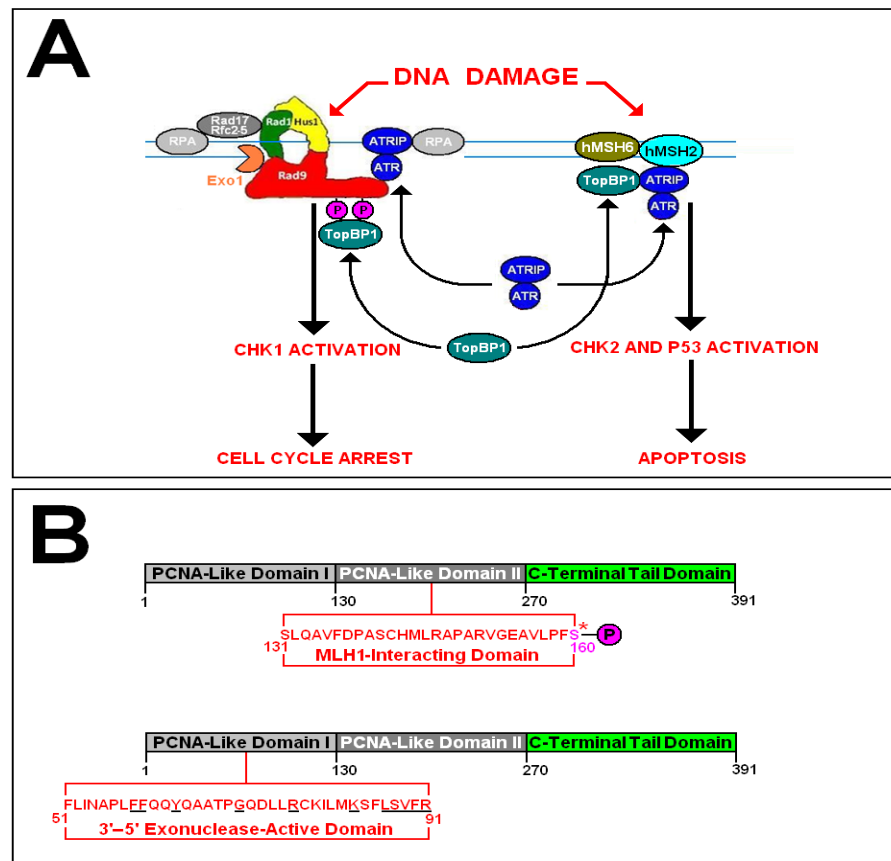
[Taken and Adapted From: Christmann M. *et al*, 2003]



The Base-Mismatch DNA Repair (MMR) pathways consist of several sequential key steps which are initiated via DNA base-pair anomalous site recognition of base-base mismatches, insertions/deletion frameshift-induced mismatches via the MutS α complex (comprised of hMSH2 and hMSH6 sub-units) and/or alternative loop-specific insertion/deletion frameshift-induced mismatches via the MutS β complex (comprised of hMSH2 and hMSH3 sub-units – not shown) respectively (Acharya S. *et al*, 1996; Christmann M. and Kaina B., 2000; Fishel R. *et al*, 1993; Genschel J. *et al*, 1998; Leach F.S. *et al*, 1993; Palombo F. *et al*, 1995; Palombo F. *et al*, 1996; Umar A. *et al*, 1994) – notably;

1. Phosphorylation of the hMSH2:hMSH6 protein sub-units of the MutS α complex and/or hMSH2:hMSH3 protein sub-units of the MutS β complex induces transient conformational changes within the supramolecular structure which converts them to the respective “active state” MutS α -ATP and/or MutS β -ATP complexes that are able to recognise and associate with the DNA base mismatch lesion site (Christmann M. *et al*, 2003; Fishel R., 1998; Gradia S. *et al*, 1997) .
2. Consequential conversion of ADP→ATP within the adenosine nucleotide binding-sites of the MutS α and/or MutS β complex, initiated via binding of the MutS α -ADP and/or MutS β -ADP complexes to the DNA mismatch lesion site, also induces conformational changes within the respective supramolecular complexes structures which stimulate their intrinsic ATPase catalytic domain activities with consequential hydrolysis of ATP which induces further conformational alterations within the supramolecular MutS complex isoform structures that enables them to associate with the heterodimeric MutL α complex (comprised of hMLH1 and hPMS2 protein sub-units), whilst the energy released from ATP hydrolysis is “thermodynamically-coupled” to active translocated assembly of the resultant multimeric complex along the duplex from the origin of the mismatch lesion site to an SSB signal site implicated in DNA strand-specificity identification (Alani E. *et al*, 1997; Blackwell L.J. *et al*, 1998a; Blackwell L.J. *et al*, 1998b; Blackwell L.J. *et al*, 2001; Christmann M. *et al*, 2003; Li G.M. and Modrich P., 1995; Nicolaides N.C. *et al*, 1994; Papadopoulos N. *et al*, 1994).
3. MMR multimeric complex recruitment of exonuclease I to the anomalous base-pair duplex site elicits hydrolytic cleavage excision removal of the base mismatch prior to MMR multimeric complex-mediated sequential recruitment of DNA polymerase δ and DNA ligase enzymes for subsequent corrective base-replacement oligonucleotide synthesis and “gap-sealing”/reannealing of the resolved duplex region (Christmann M. *et al*, 2003; Genschel J. *et al*, 2002; Longley M.J. *et al*, 1997).
4. Intrinsic MMR multimeric complex ATPase activity, “triggered” via the biophysico-chemical mechanism described in step 2 above, also initiates binding of ATP to the hMSH sub-unit adenosine nucleotide binding sites with consequential inducement of other types of transient conformational rearrangements within the supramolecular MMR multiplex complex structure which result in the formation of an ATP hydrolysis-independent DNA “sliding clamp” that diffuses away from the repaired base mismatch site and functions as a signal for “inactive-state” MMR protein sub-unit dissociation from the rectified DNA duplex structure (Alani E. *et al*, 1997; Christmann M. *et al*, 2003; Berardini M. *et al*, 2000; Gradia S. *et al*, 1999; Gradia S. *et al*, 2000).

Fig 1.44: “9-1-1” Clamp Influences on MMR-Apoptotic Induction



A: ATR-activated DNA damage checkpoint signalling responses may be initiated via two independent TopBP1 adaptor protein-mediated pathways (Fig A taken and adapted from Pabla N. *et al.*, 2011).

The “9-1-1” clamp-TopBP1-ATR/ATRIP-RPA ternary complex activates Chk1 kinase signal-mediated DNA damage checkpoint responses which culminate in cell cycle arrest (discussed previously in Section 1.2.2, pp.33-65).

The hMSH2:hMSH6-TopBP1-ATR/ATRIP-RPA ternary complex activates Chk2 kinase and p53 signal-mediated DNA damage checkpoint responses which culminate in cell cycle arrest and apoptotic induction (discussed previously in Section 1.2.2, pp.33-65).

The Rad9 sub-unit of the “9-1-1” clamp complex contains a conserved “HFD” motif which may interact with ATR and enhance its catalytic kinase activity (Navadgi-Patil M. and Burgers P.M., 2009) – discussed previously in Section 1.2.2, pp.33-65; Fig 1.17A, p.53; Fig 1.18, p.54; Fig 1.19, p.55.

Thus, it is possible that biochemical “cross-talk” between the two independent pathways may take place via Rad9-modulated activity of ATR, which in turn may impinge upon the regulation of the MMR DNA repair pathway (Reha-Krantz L.J. *et al.*, 2011).

A p53 binding-site consensus sequence has also been identified within the transcriptional promoter of the *hMSH2* gene (Christmann C. *et al.*, 2003; Sherer S.J. *et al.*, 2000; Warnick C.T. *et al.*, 2001).

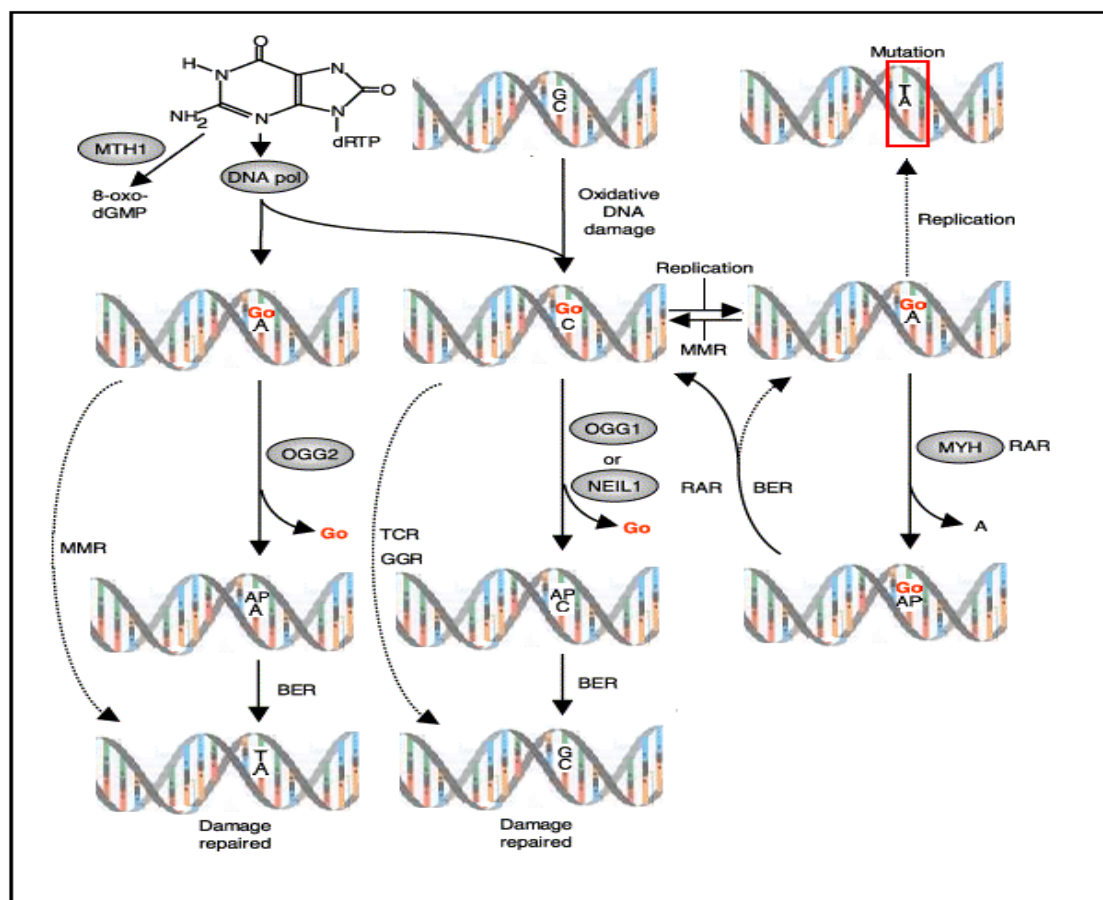
The hMSH2, hMSH3, hMSH6 proteins also interact with the three sub-units of “9-1-1” clamp (Bai H. *et al.*, 2010; Liu Y. *et al.*, 2010) and the Rad9-Rad1-Hus1 complex also enhances the G/T DNA substrate-binding activity of the MutSa protein component of the DNA Mis-Match Repair (MMR) pathway (Bai H. *et al.*, 2010; Liu Y. *et al.*, 2010) – discussed summarily in Fig 1.43, p.104.

Thus, these two independent pathways may act in a synergistic mechanism which regulates the overall activity of the MMR pathway via Rad9-modulation of ATR catalytic activity and hMSH2:hMSH6-TopBP1-ATR/ATRIP-RPA-activated “feedback” p53-mediated transcriptional modulation of hMSH2 activity levels – that in turn may regulate the MMR pathway via stoichiometric alteration of the relative levels of hMSH2:hMSH3 and hMSH2:hMSH6 dimers (discussed summarily in Fig 1.43, p.104).

B: The human Rad9 protein also contains an MLH1 interactive domain (He W. *et al.*, 2008), which may mediate “9-1-1” clamp-modulation of the MLH1-PMS2 interactive functions within the MMR DNA repair pathway (Fig 1.43, p.104) and a conserved catalytic 3'-5' exonuclease motif (Bessho T. and Sancar A., 2000) which may also associate with and modulate the activity of other nucleases implicated in various repair pathways.

Fig 1.45: Mechanistic Overview of the “GO-System” Repair Network

[Taken and Adapted From: Slupphaug G. *et al*, 2003]



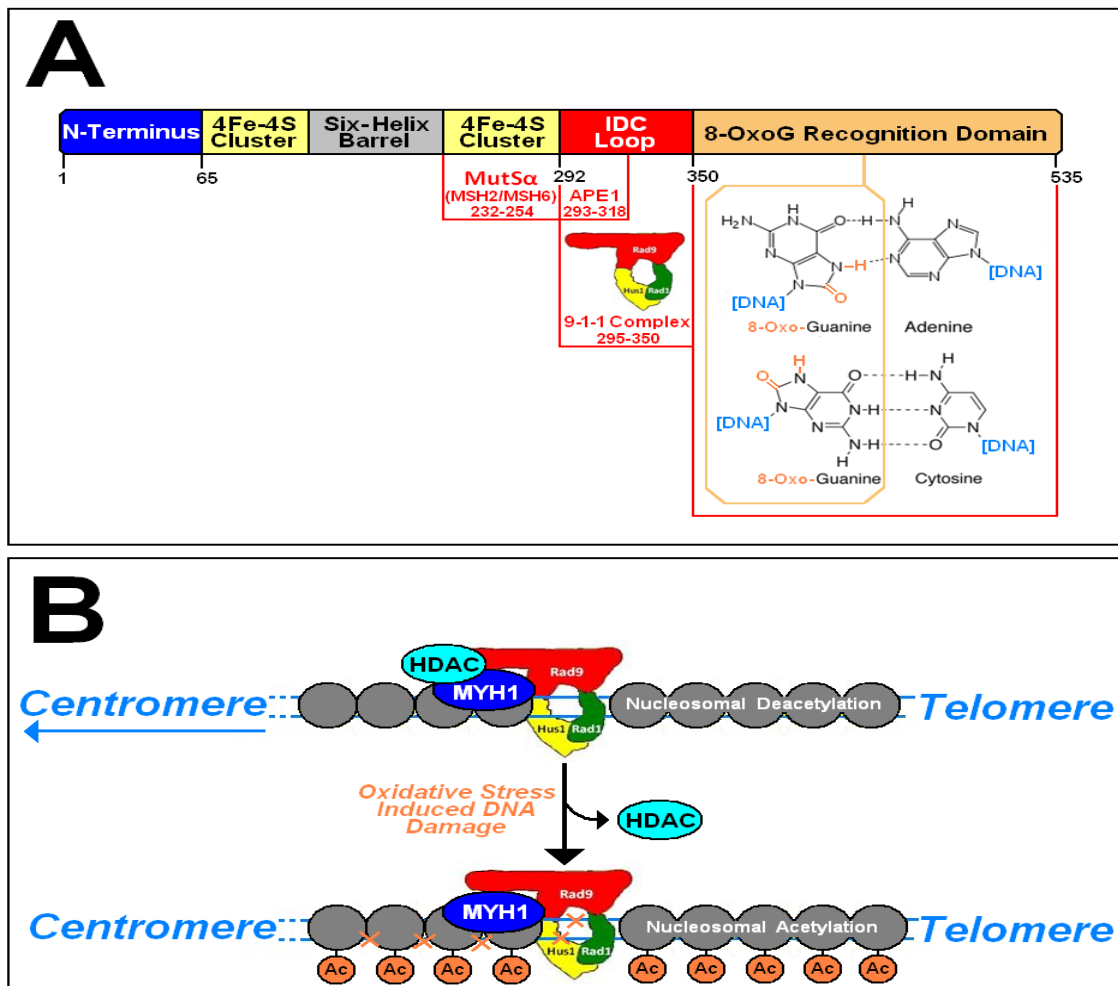
Collaborative “alternative-switching” between various DNA repair pathways may be utilised in the form of additional levels of cytological “back-up safe-guards” for the preservation of replicative genomic integrity – as illustrated in the above example of the “Go System”, which exploits mutual synergistic DNA repair mechanisms for prevention of perpetuated oxidative-modified-Guanine-base-mediated mutagenic effects (such as 8-Oxoguanine – “Go”-induced base-pair mismatches) via several alternative interacting pathways which prevent and/or remove mis-incorporated Go lesions from newly-synthesised DNA daughter-strands during DNA replication (Slupphaug G. *et al*, 2003), notably;

- (i) Human Mut T Homologue 1 (MYH1)-mediated hydrolytic-reduction of 8-Oxo-dGTP (Fujikawa K. *et al*, 1999; Sakai Y. *et al*, 2002; Sukami K. *et al*, 1993).
- (ii) BER- and/or MMR-initiated Oxoguanine Glycosylase 2 (OGG2)-mediated repair of 8-OxoG:A mismatches (Slupphaug G. *et al*, 2003).
- (iii) BER-, GGR- and/or TCR-initiated OGG2-mediated repair of 8-OxoG:C mismatches (Christmann M. *et al*, 2003; Slupphaug G. *et al*, 2003)
- (iv) BER-initiated NEIL1 glycosylase-mediated repair of 8-OxoG:C mismatches (Slupphaug G. *et al*, 2003).

Thus potential mutagenic propagation of A:8-OxoG via successive rounds of DNA replication, as a consequence of initial circumvented C:8-OxoG repair, is prevented via cytological employment of either individual or combined versions of these respective pathways (Slupphaug G. *et al*, 2003).

Fig 1.46: Modulatory "9-1-1" Clamp-MYH1 Activity Interactions

[Taken and Adapted From: Cai R.L., 2000; Chang D.Y. *et al*, 2011; Luncsford P.J. *et al*, 2010]



A: The heterotrimeric Rad9-Rad1-Hus1 PCNA-like DNA Sliding-Clamp complex, modulates the activity of the human MutY homologue (hMYH1) via associative Rad9 C-Terminal Tail domain interactions with the IDC loop/"hinge-domain" of the DNA glycosylase enzyme, thereby regulating the MMR pathways implicated in excision and replacement of oxidised-type nucleobase adducts (Luncsford P.J. *et al*, 2010).

[The C-Tail Terminal domain of the Rad9 sub-unit of the "9-1-1" clamp also interacts with and enhances the activity of the Apurinic Endonuclease DNA repair enzyme APE1 – which also associates within the IDC loop/"hinge-domain" of the hMYH1 DNA Glycosylase repair enzyme (Luncsford P.J. *et al*, 2010).

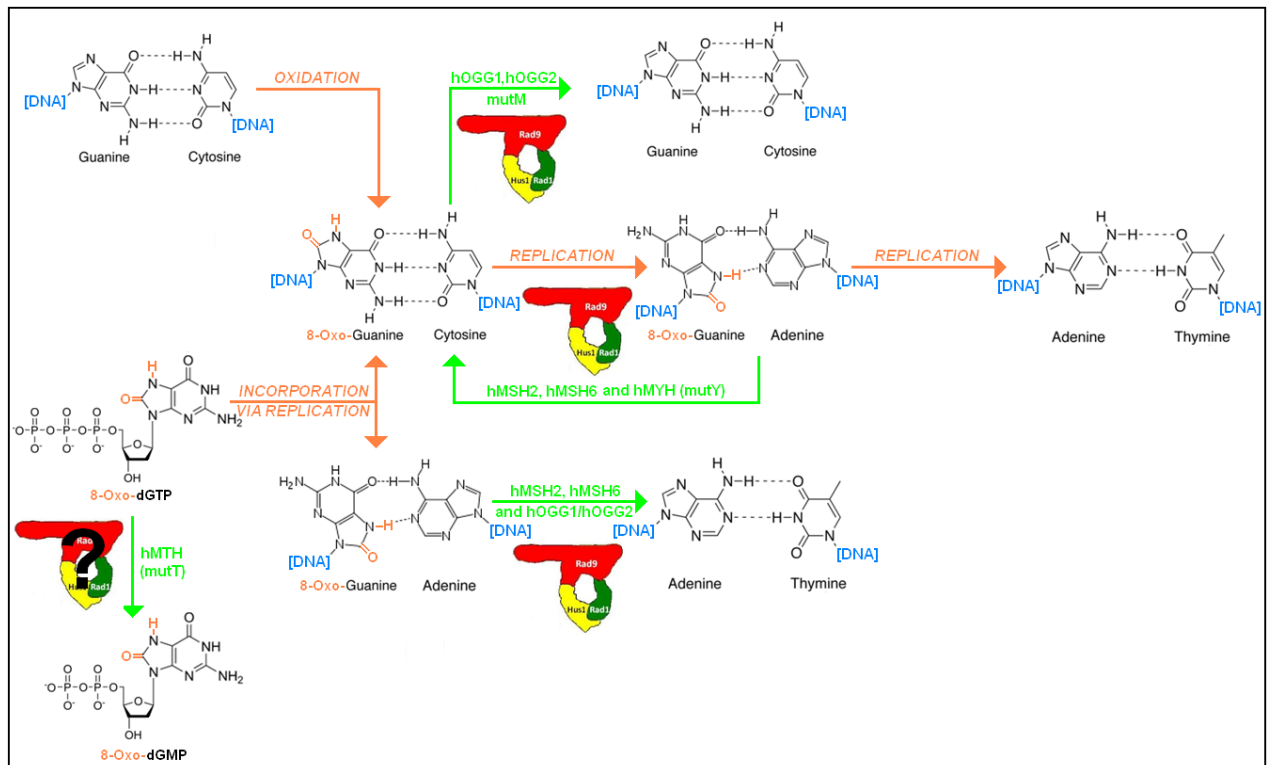
B: In *S. pombe*, the heterotrimeric Rad9-Rad1-Hus1 PCNA-like DNA sliding-clamp complex also modulates chromatin re-modelling in response to oxidative stress induced DNA damage, via co-operative regulation of histone deacetylase spHst4 (HDAC) and spMyh1 Activity mediated via associative interaction of each respective enzyme with the spRad9 C-Terminal Tail domain (Chang D.Y. *et al*, 2011).

In *S. pombe*, under normal cytophysiological conditions, the histone deacetylase spHst4 is complex-associated with both spMyh1 and the heterotrimeric "9-1-1" clamp complex, in which spHst4, spMyh1 and spHus1 sub-unit are physically bound to telomeres (Chang D.Y. *et al*, 2011)

Oxidative stress-induced DNA damage triggers an spMyh1-dependent decrease in spHst4 protein levels with consequential hyperacetylation of histone 3 at Lys56 which in turn induces alterations in chromatin supra-molecular structure that promote telomeric dissociation of spHst4 and the spHus1 sub-unit of the "9-1-1" clamp complex and telomeric association of spMyh1 – whose DNA glycosylase activity is enhanced via associative interactions with the C-Terminal Tail domain of the spRad9 subunit in responsive preparation for MMR-mediated excision-replacement of oxidised nucleobase adducts (Chang D.Y. *et al*, 2011; Luncsford P.J. *et al*, 2010).

Fig 1.47: “9-1-1” Clamp Modulation of Oxidative Mismatch Repair

[Taken and Adapted From: Germann M.W. *et al*, 2010



Integrative repair pathway model for the co-ordinated recification of the DNA-incorporated oxidized-base adduct 8-Oxoguanine (Germann M.W. *et al*, 2010).

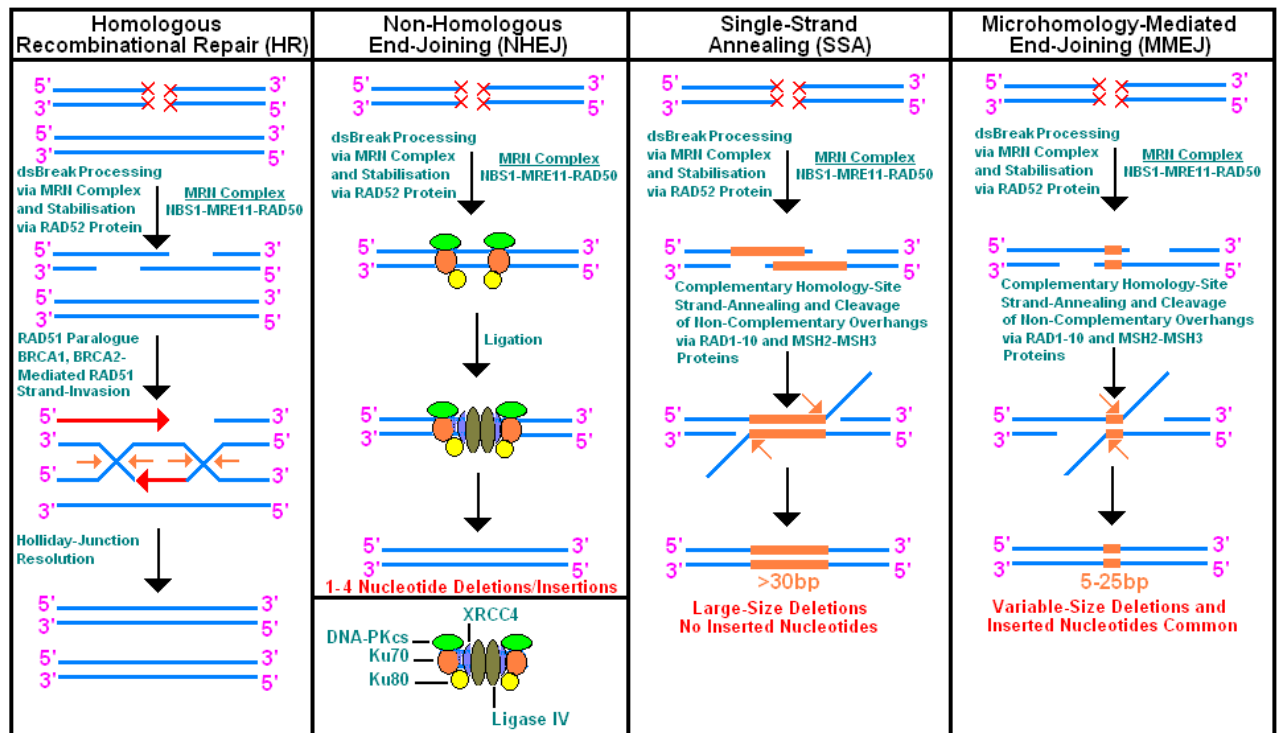
[**Note:** Corrective Pathways are indicated in green; Detrimental Pathways are indicated in orange]

The “9-1-1” clamp may also modulate of the respective activities of the implicated hOGG1, MSH2, MSH3, MSH6, and MYH1, via associative interactions with the C-Tail Terminal Domain of the Rad9 component sub-unit, for selective regulation of the respective pathways implicated in this integrative repair network (Bai H. *et al*, 2010; Chang D-Y. *et al*, 2011; Germann M.W. *et al*, 2010; Luncsford P.J. *et al*, 2010; Park M.J. *et al*, 2009).

Uncertainty remains as to whether or not similar “9-1-1” clamp-associative interactions modulate the activity of the hMTH protein, which may also be implicated in regulation of this integrative DNA repair network.

Fig 1.48: Mechanistic Overview of DNA dsBreak Repair Pathways

[Taken and Adapted From: Christmann M. *et al*, 2003; McHugh P.J. *et al*, 2001; Longhese M.P. *et al*, 2010]



The heterotrimeric “MRN” complex, comprised of Mre11-Rad50-Nbs1, is a key multi-functional component of both the HR (Homologous Recombinational Repair –HRR and Single-Stranded Annealing – SSA) and the Non-Homologous End Joining (NHEJ) pathways implicated in the repair of double-stranded DNA breaks (DSBs) – that possesses endonuclease, exonuclease, helicase enzymatic activities and forms associative interactions with FEN1 for removal of the excess terminal 3'- and 5'- DNA “overhangs”/“flaps” which are *in situ*-generated “by-products” of these respective DNA mechanisms (Christmann P. *et al*, 2003; Dion V. *et al*, 2012; Trovesi C. *et al*, 2011).

Homologous Recombinational Repair (HRR), also termed “Gene Conversion” (GC), is an error-free mechanism of DSB-repair as a consequence of utilisation of the “daughter-strand region” of DNA in the undamaged chromosome, which shares sequence homology with that of the damaged DNA strand region in the corresponding chromosomal partner, as a template for exchange of genetic information during repair of the respective DSB lesion (Christmann M. *et al*, 2003; Fujinaka Y. *et al*, 2012; George C.M. *et al*, 2011; Sonada E. *et al*, 2001) – mediated via the following steps:

- (i) MRN complex-mediated 5' → 3' directional re-section of the DSB lesion sites results in the formation of a 3'-single-stranded DNA, which is effectively “shielded” from 3'exonucleolytic degradation via association with the heptameric RAD52 protein (Stasiak A.Z. *et al*, 2000) and 5' exonucleolytic degradation via association with the Rad9-Rad1-Hus1 heterotrimeric “9-1-1” complex respectively (Ellison V. and Stillman B., 2003).
- (ii) Associative interactions between the resultant 3'-ssDNA-complex-bound RAD52 heptamer with the Replication Protein A (RPA) and RPA and RAD51 proteins initiate DNA strand-exchange activity with the DSB homologous DNA sequence region of the undamaged corresponding chromosome (Benson F.E. *et al*, 1994; Siggurdson S. *et al*, 2001) – mediated via RAD51-catalysed damaged-DNA “strand invasion” complementary base sequence “D-loop” displacement of the undamaged DNA duplex homologous template region (Baumann P. and West S.C., 1997; Gupta R.C. *et al*, 1998).
- (iii) Completion of DSB repair is then accomplished via DNA synthesis, ligation and holliday junction branch migration, mediated via associative functional interactions between the RAD51 multi-paralogue nucleoprotein assembly (comprised of RAD51B, RAD51C, RAD51D, XRCC2 and XRCC3 proteins), DNA polymerase and DNA ligase proteins respectively (Eggler A.L. *et al*, 2002; Christmann M. *et al*, 2003; Liu N. *et al*, 2002; Masson J.Y. *et al*, 2001; Schild D. *et al*, 2000; Takata M. *et al*, 2000; Wiese C. *et al*, 2002).

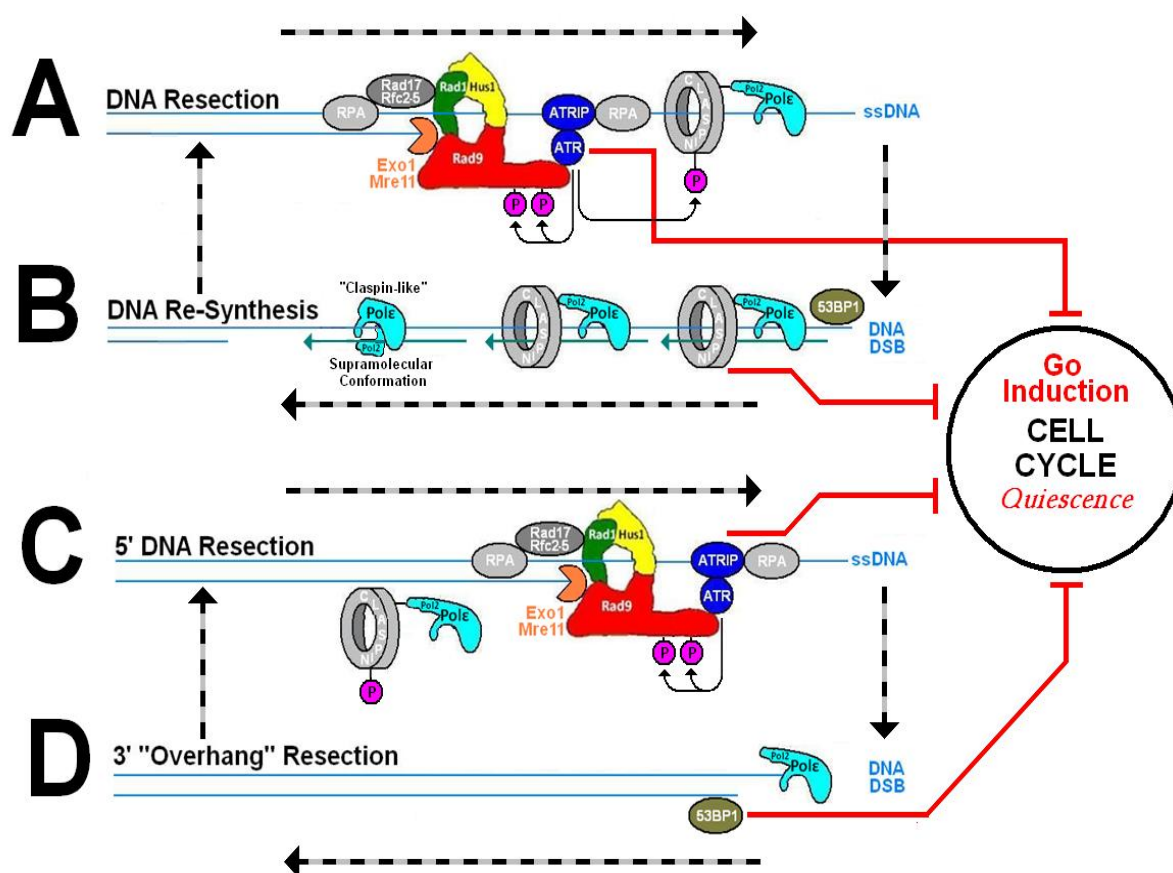
Single-Stranded Annealing (SSA) and Microhomology-Mediated End-Joining (MMEJ) are error-prone mechanisms of DNA repair implicated in the repair of DSB sites which are flanked by repeat sequences in which the complementary strands of the respected homologous regions are re-annealed via DNA ligases whilst the generated excess overhang tails are subsequently cleaved via the exonuclease activity of the MRN complex - with consequential loss of the intermediate sequences situated between the respective ligated homologous ends (Christmann M. *et al*, 2003; Carney J.P. *et al*, 1998; Crespan E. *et al*, 2012; Decottignies A., 2007; McHugh P.J. *et al*, 2001; McVey M. and Lee S.E., 2008; Taylor E.M. *et al*, 2009; Trujillo K.M. *et al*, 1998; Yu A.M. and McVey M., 2010).

Non-Homologous End Joining (NHEJ) is an alternative error-prone mechanism of DNA repair in which Ku70-Ku80 dimeric complex-mediated DSB site-recognition is also required for recruitment of the catalytic subunit of the DNA-Dependent Protein Kinase (DNA-PKcs) to the DNA ds breakage lesion with consequential formation of DNA-PK holoenzyme – which is implicated in phosphorylated-activation of the single-stranded specific exonuclease protein Artemis and activation of the XRCC4 DNA Ligase IV protein (Christmann M. *et al*, 2003; Mc Hugh P.J. *et al*, 2001).

The NHEJ-repair mechanism consists of initial 5'- and 3'- single-strand flap and hairpin loop degradation – mediated via the interactive functional associative multi-enzyme complex comprised of MRN, Artemis and FEN1 proteins, prior to subsequent re-ligation of the processed DNA ends via the XRCC4 DNA Ligase IV enzyme respectively (Christmann M. *et al*, 2003; McHugh P.J. *et al*, 2001).

Fig 1.49: “9-1-1” Clamp Modulation of DSB-Induced Quiescence

[Taken and Adapted From: Carneiro T. *et al*, 2010; Deshpande A.M. *et al*, 2011]



DNA damage checkpoints may exhibit impaired adaptation to replicative senescence as a consequence of transient, interchangeable signal responses to double-stranded DNA breaks (Deshpande A.M. *et al*, 2010).

Generation of long 3' ssDNA overhangs at the DSB sites, via Exo1 and/or other nuclease activity-mediated DNA re-section of the shortest telomeric termini, may trigger “9-1-1” clamp-initiated checkpoint signalling responses (depicted in Figures A and C).

Recruitment of the DNA polymerases Polε and Pol2 to the “nuclease-processed” DSB lesion sites, via the claspin and “9-1-1” ring-complexes, may then enable re-synthetic conversion of the long 3'-ssDNA overhangs back to dsDNA (Fig B).

[Polε and Pol2 may also form a claspin-like DNA polymerase catalytic heterodimeric complex which elicits the re-synthesis conversion of ssDNA to dsDNA – Fig B]

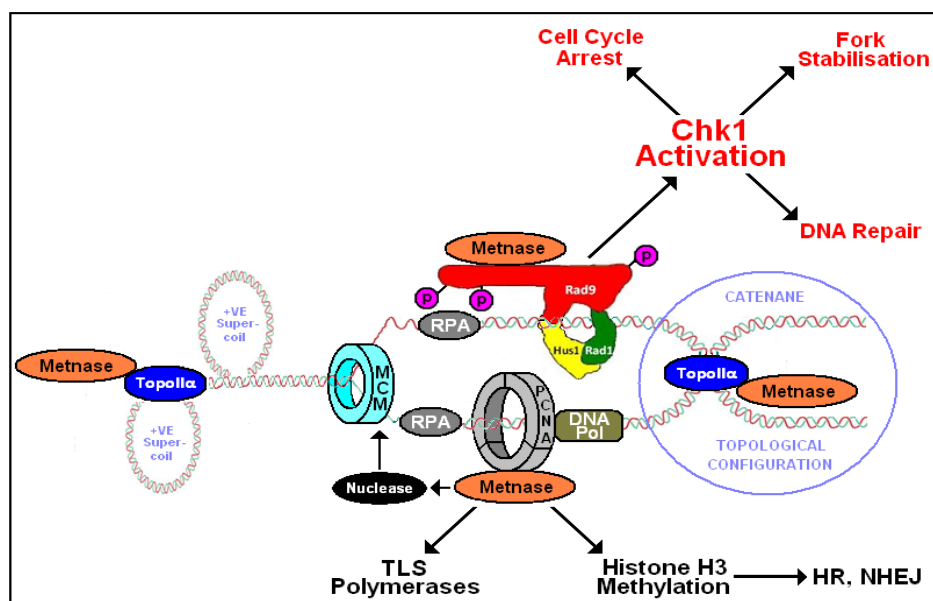
Alternatively, the resultant long 3'-ssDNA overhangs may be cleaved to truncated DSB-like structures via 53BP1-induced nuclease re-section activities (Fig D).

[The Rad9 sub-unit of the “9-1-1” complex possesses a potential 3'-5' exonuclease catalytic motif (Bessho T. and Sancar A., 2000), which may also associatively co-ordinate and/or modulate the activity of other nucleases implicated in the generation and conversion of these long 3' ss-DNA overhangs at the DSB lesion sites]

Continual “3'-ssDNA Re-Section – Re-Synthesis” cycling may occur at each dysfunctional truncated telomeric terminus site, via generation of fresh ssDNA and DSB-like substrates which trigger alternate checkpoint responses (Fig A and Fig B; Fig C and Fig D) with consequential suppression of checkpoint signalling and perpetuation of DNA damage, culminating in maintained cell cycle quiescence (Deshpande A.M. *et al*, 2010).

Fig 1.50: “9-1-1” Clamp Modulation of Metnase Functional Activities

[Taken and Adapted From: De Haro L.P. *et al*, 2010]



Metnase is a multi-functional human protein that contains catalytic methylase (“SET”), nuclease and transposase domains which are implicated in the regulation of specific activities of several key DNA metabolic processes – notably; Non-Homologous End-Joining (NHEJ – Fig 1.48, p.109), DNA Integration, Chromosomal Decatenation and Chromosomal Translocation (Beck B.D. *et al*, 2008; Hromas R. *et al*, 2008; Jiang H.Y. *et al*, 2002; Lee S.H. *et al*, 2005; McClendon A.K. *et al*, 2005; Williamson E.A. *et al*, 2008; Wray J. *et al*, 2010).

Over-expression and correlated activity enhancement of Metnase in leukaemic and breast tumour cells has been implicated in their acquired multiple drug resistance towards several classes of Topoisomerase II inhibitory-type anti-cancer chemotherapeutics (Wray J. *et al*, 2009a; Wray J. *et al*, 2009b) – notably; Anthracycline Antibiotics (eg Daunorubicin, Doxorubicin) and Epipodophyllotoxins (eg Etoposide, Teniposide).

Metnase has been demonstrated to interact with and stimulate the enzymatic activity of Topoisomerase II α , thereby promoting relaxation of positive DNA supercoils and resolution of DNA catenanes for prevention of stalled DNA replication forks (De Haro L.P. *et al*, 2010).

Metnase-mediated methylation of nucleosomal Histone H3 sub-units, at lysine residues K4 and K36, induces conformational changes within the chromatin supramolecular architecture which facilitate access of repair proteins to damaged DNA lesion sites and thereby enhance the efficiency of Homologous Recombination (HR) and NHEJ DNA repair processes (Fnu S. *et al*, 2011) – discussed in Fig 1.48, p.109.

Metnase Histone H3 methylation-induced chromatin “re-modelling” may also impinge upon the functional mechanism of “9-1-1” clamp-modulated TLK1/1B activity which is implicated in TLS regulation (Canfield C. *et al*, 2009) – discussed summarily in Fig 1.52, p.117.

Metnase has also been demonstrated to enhance the enzymatic activity of DNA Ligase IV, which may contribute to the enhanced efficiency of HR and NHEJ DNA repair (De Haro L.P. *et al*, 2010) – discussed summarily in Fig 1.48, p.109.

Metnase also interacts with and stimulates the enzymatic activity of Topoisomerase II α , thereby promoting relaxation of positive DNA supercoils and resolution of DNA catenanes for prevention of stalled DNA replication forks (De Haro L.P. *et al*, 2010), which may also constitute a regulatory mechanism for the modulation of G2-Decatenation Checkpoint activities (discussed previously in Fig 1.26, p.62).

Metnase may be implicated in the promotion of co-ordinated stalled replication fork recovery and re-start mechanisms, mediated via its SET domain conserved PIP box interactions with the Rad9 and PCNA monomer sub-units, which modulate specific functional activities of the respective homotrimeric PCNA and heterotrimeric “9-1-1” DNA sliding-clamp complexes, however the enzyme does exhibit any influential regulation of replication fork progression. (De Haro L.P. *et al*, 2010).

In addition to its automethylation-mediated activity regulation, Metnase may also modulate specific functional activities of the homotrimeric PCNA and heterotrimeric “9-1-1” clamp complexes via specific methylation-type post-translational modifications of the respective PCNA and Rad9 sub-units respectively (De Haro L.P. *et al*, 2010).

These PCNA- and “9-1-1” clamp- Metnase interactions may also be implicated in enhancement of the enzymatic activities of Translesion Synthesis (TLS) DNA Polymerases which mediate replicative “template-switch” by-pass of “bulky” DNA lesions, such as U.V.-induced Thymine Dimers (De Haro L.P. *et al*, 2010; Livnah Z. *et al*, 2010; Jansen J.G. *et al*, 2007; Zhuang and Ai Y., 2010) – discussed summarily in Fig 1.51, p.112.

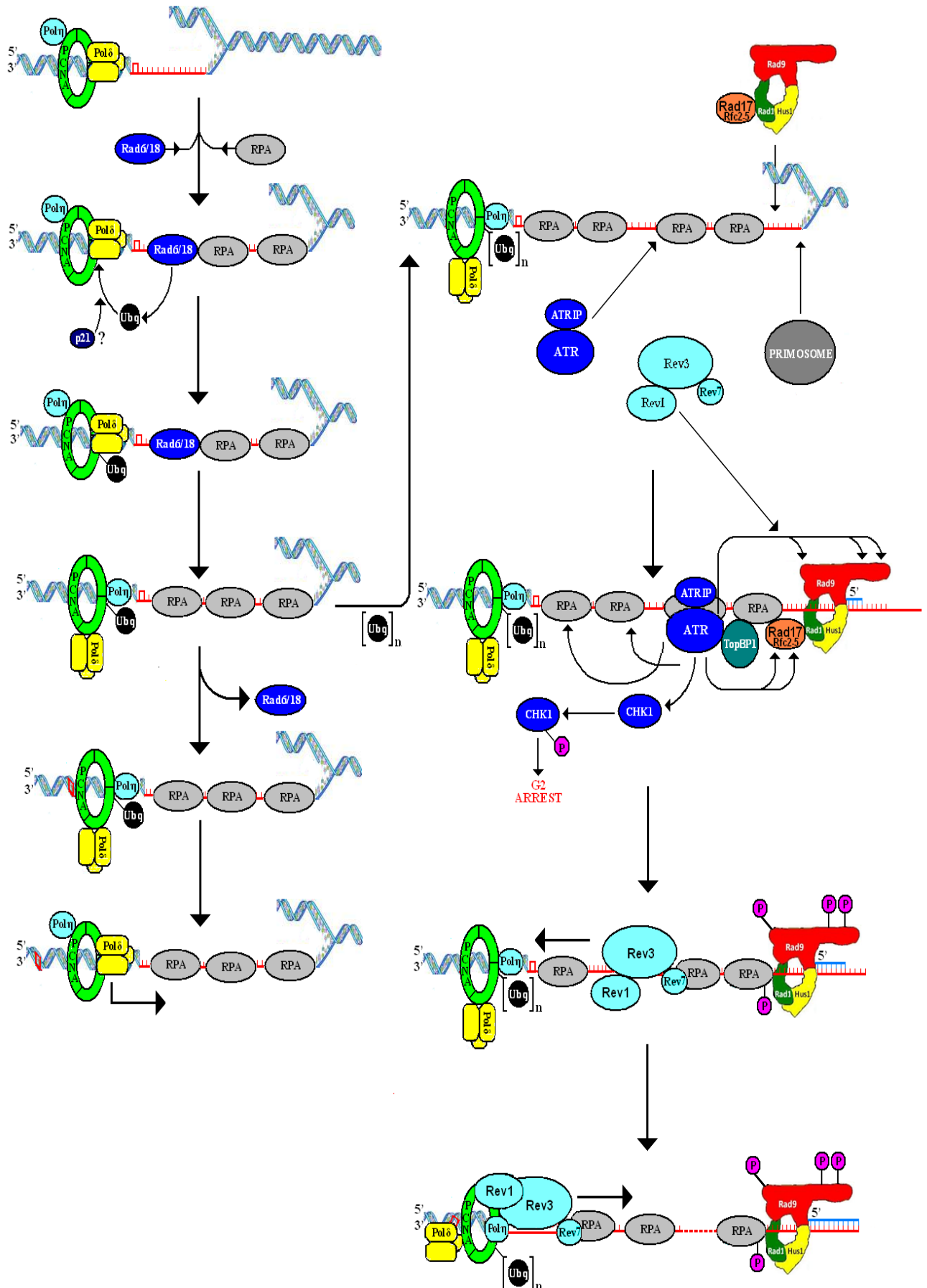
Metnase-mediated Rad9 methylation may also be implicated in the modulation of “9-1-1” clamp-ATR/ATRIP-RPA ternary complex activation of Chk1 kinase-initiated DNA damage checkpoint responses via a similar mechanism to that of PRMT5 methylation of Rad9 (He W. *et al*, 2011) – discussed previously in Section 1.2.2, pp.33-65; Fig 1.18, p.54.

The “9-1-1” clamp complex may modulate Metnase functional activities, via “Rad9 C-terminal Tail Domain – SET Domain PIP box” type associative interactions (De Haro L.P. *et al*, 2010).

Taken together, these Rad9-Metnase interactions could constitute an intricate “feedback network” mechanism of co-ordinated regulation of the functional activities of the Rad9-Rad1-Hus1 complex and the enzyme which in turn modulate chromatin re-modelling, stalled replication fork recovery/re-start and HR, NHEJ and TLS-coupled “Template-Switching” DNA repair pathway activities.

Fig 1.51: "9-1-1" Clamp Modulation of TLS & Template-Switching

[Taken and Adapted From: Livneh Z. *et al*, 2010; Jansen J.G. *et al*, 2007; Zhuang Z. and Ai Y., 2010]



Bulky DNA lesions are primarily removed via nucleotide excision repair pathways (Fig 1.39, p.100 and Fig 1.40, p.101) – but these may also be effectively “by-passed” via alternative translesion synthesis and/or template-switching DNA repair pathways in which full-length Rad9 protein associative functioning within the “9-1-1” complex is a critical mechanistic component (Jansen J.G. *et al.*, 2007) – Fig 1.51, p.112.

In these instances selection of the translesion synthesis or template switching mechanism, for effective DNA repair and/or by-pass of the bulky lesion site for unhindered continuation of DNA replication, is biochemically determined via the relative extent of ubiquitination of the PCNA complex (Jansen J.G. *et al.*, 2007) – Fig 1.51, p.112.

Monoubiquitination of the PCNA complex initiates the translesion synthetic pathway which utilises the stringent proof-reading DNA polymerases (eg Pol δ and Pol ϵ), whereas polyubiquitination of the PCNA complex initiates the template-switching pathway which utilises the Y-family of DNA polymerases and associative catalytic sub-units respectively (Chang D.J. and Cimprich K.A., 2009; Jansen J.G. *et al.*, 2007; Lee K.Y. and Myung K., 2008; Masuda Y. *et al.*, 2010).

In the hypothetical model postulated by Jansen J.G. and co-workers (Fig 1.51, p.112), translesion synthesis is triggered via stalled enzymatic activity of Pol δ at DNA lesion sites which only mildly perturb the functional configuration of the duplex supramolecular structure with consequential recruitment of RPA and Rad6/Rad18 to the template strand and subsequent Rad6/Rad18 complex-mediated p21-regulated ubiquitination of PCNA (Fig 1.51, p.112).

Transient substitution of Pol δ for Pol η (a “non-stringent proof-reading” Y-polymerase) enables synthesis of a relatively short oligonucleotide template for utilisation by Pol δ , which is then re-positioned at the primer terminus past the DNA lesion site via a secondary polymerase switching event prior to re-initiation of replicative progression (Jansen J.G. *et al.*, 2007) – Fig 1.51, p.112.

The hypothetical model proposed by Jansen J.G. and co-workers also postulates that severe DNA lesion-induced alterations of the functional conformation of the duplex supramolecular structure, result in stall replication forks as a consequence of suppressed Pol η (and/or other selected DNA Y-polymerases)-mediated incorporation of bases that is limited to the region opposite the 3'-nucleotide of the DNA lesion site (Fig 1.51, p.112).

This “replication-inhibitory” site acts as a polyubiquitination “trigger” for “9-1-1” clamp recruitment to the alternative downstream 5'-primer site from the DNA lesion and independent loading of the ATR/ATRIP complex to the RPA-coated ssDNA region, prior to Rad9-recruited TopBP1-activation of the ATR kinase and subsequent phosphorylation of CHK1 with resultant initiation of the G2 checkpoint and G2/M phase cell-cycle arrest (Jansen J.G. *et al*, 2007) – discussed previously in detail in Section 1.2.2, pp.33-65; Fig 1.23, p.59.

In this secondary TLS-repair pathway, the checkpoint DNA damage response is “silenced” via ATR/ATRIP complex displacement and “9-1-1” complex-mediated promoted recruitment and interactive assembly of the Rev1 sub-unit in association with the Pol ζ sub-units Rev3 and Rev7 (Jansen J.G. *et al*, 2007) – Fig 1.51, p.112.

Polk, in association with Rev1-Rev3-Rev7 ternary complex, acts a functional pre-requisite for subsequent translocation of the resultant Rev1-Pol ζ (Rev3/Rev7)-Polk ternary complex to the PCNA-Pol δ -Pol η ternary complex (Jansen J.G. *et al*, 2007) – Fig 1.51, p.112.

Rev1-polyubiquinated-PCNA association-mediated Pol η displacement-exchange of binding of the Rev1-Pol ζ (Rev3/Rev7)-Pol κ polymerase complex at the 3'-terminus of the DNA lesion site then proceeds, prior to Pol ζ -mediated 5'-nucleotide incorporation within the distorted duplex region, followed by subsequent Y-polymerase-mediated DNA strand gap-filling synthesis and annealing performed via DNA Ligase-recruitment – mediated via the “9-1-1” complex respectively (Jansen J.G. *et al*, 2007) – Fig 1.51, p.112.

Recruitment of the Y-polymerases for the template switching pathway is potentially error-prone, due to the relative low proof-reading stringency of these enzymes and somewhat paradoxically, this is also an essential functional feature of the Y-polymerases which enables these enzymes to perform DNA synthesis even in the presence of base-lesions/mismatches which would hinder the progress of high fidelity proof-reading polymerases (eg Pol δ) respectively (Jansen J.G. *et al*, 2007).

In these circumstances, associative protein kinase/phosphatase interactive Rad9 functions/signalling within the “9-1-1” complex (discussed previously in Section 1.2.2, pp.33-65; Fig 1.16, p.52) may serve to enhance the DNA replicative fidelity of the Y-polymerases to preserve genomic integrity (Jansen J.G. *et al*, 2007) – Fig 1.51, p.112.

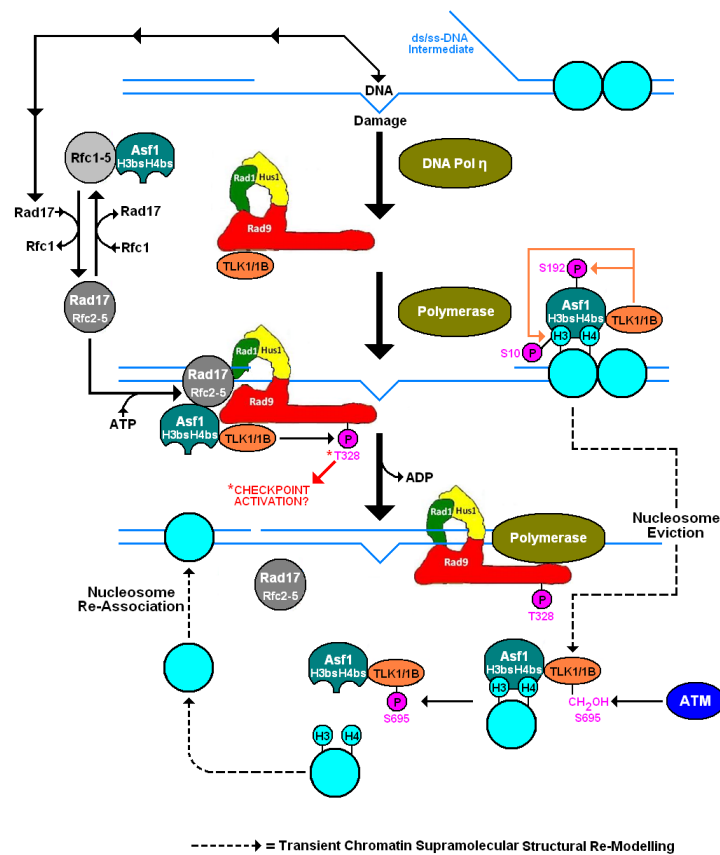
The “9-1-1” sliding-clamp complex may also modulate the activities of the Tausled-Like Kinase TLK1 and/or its isoform TIK1B, via Rad9 associative TLK1/TLK1B interactions, which are implicated in the co-ordinated removal of nucleosomes from the chromatin for facilitated access of the TLS repair machinery to the bulky DNA lesion site and subsequent reassociation of the displaced nucleosomes at the location of the rectified duplex distortion (Canfield C. *et al*, 2009; De Benedetti A. *et al*, 2009; Sunavala-Dossabhoy G. and De Benedetti A., 2009) – Fig 1.52, p.117.

The co-ordinated modulation of Metnase functional activities, mediated via associative Rad9 C-Terminal Tail domain interactions within the “9-1-1” sliding-complex and PCNA-Metnase heterodimeric complex interactions, may also be implicated in the co-ordinated regulation of TLS polymerase activities and removal of nucleosomes at the bulky DNA lesion site via methylation of histone H3 sub-units (De Haro L.P. *et al.*, 2010) – Fig 1.50, p.111.

Initiated recruitment of DNA base-mismatch repair pathways (Fig 1.43, p.104; Fig 1.45, p.106; Fig 1.47, p.108) may also be implicated in both the TLS and template-switching mechanisms within the integrative hypothetical model (Fig 1.51, p.112) as an additional “safe-guard” against the low proof-reading fidelity of Y-polymerases for preservation of genomic integrity (Jansen J.G. *et al.*, 2007).

Fig 1.52: “9-1-1” Clamp Modulation of TLK1 Activity-Mediated TLS

[Taken and Adapted via Collated Information From: Canfield C. *et al.*, 2009; De Benedetti A. *et al.*, 2009; Jiao Y. *et al.*, 2012; Sunavala-Dossabhoy G. & De Benedetti A., 2009]



Asf1 is a histone H3-H4 chaperone implicated in chromatin re-modelling for promotion of nucleosomal assembly onto newly replicated DNA and nucleosomal disassembly from activated promoter sites or damage lesion sites within the DNA for facilitated, unhindered access of the respective transcriptional, translational or repairosome protein machinery (Adkins M.W. and Tyler J.K. 2004; Linger J.K. and Tyler J.K., 2007).

TLK1 (Tousled-Like Kinase) is a Serine/Threonine Kinase which may act as a chaperone for Asf1 and modulate its activity via residue-specific post-translation phosphorylation modifications at Ser10 and Ser192 (De Benedetti A. *et al.*, 2009; De Benedetti A. *et al.*, 2010; Sillje H. and Nigg E., 2001).

The nascent mRNA transcript of the *TLK1* gene is alternatively-spliced and translated into two isoformic proteins, TLK1 and TLK1B, which possess similar functional activities and are often referred to collectively as TLK1/1B (Shalom S. and Don J., 1999; Canfield C. *et al.*, 2009).

Initial associative exchange of Asf1 from the Rfc1 sub-unit of the PCNA clamp-loader (Rfc1-5) to the Rad17 sub-unit of the “9-1-1” clamp-loader (Rad17:Rfc2-5) may occur, in response to DSB and/or “Bulky” DNA damage lesions (eg U.V.-induced Thymine-Dimer formation), followed by loading of the Rad9-Rad1-Hus1 complex onto the DNA damage site (Canfield C. *et al.*, 2009; Ronald S. *et al.*, 2011)

TLK1/1B kinase may then be recruited resultant Asf1-Rad17:Rfc2-5-“9-1-1”-clamp-DNA ternary complex, via associative Rad9 sub-unit interactions – which may also modulate the catalytic activity of TLK1/1B, with consequential phosphorylation of the Rad9 C-tail terminal domain at Thr328 which triggers ATM-mediated checkpoint activation-induced cell cycle arrest to enable DNA repair to take place (Canfield C. *et al.*, 2009; Sunavala-Dossabhoy G. and De Benedetti A., 2009).

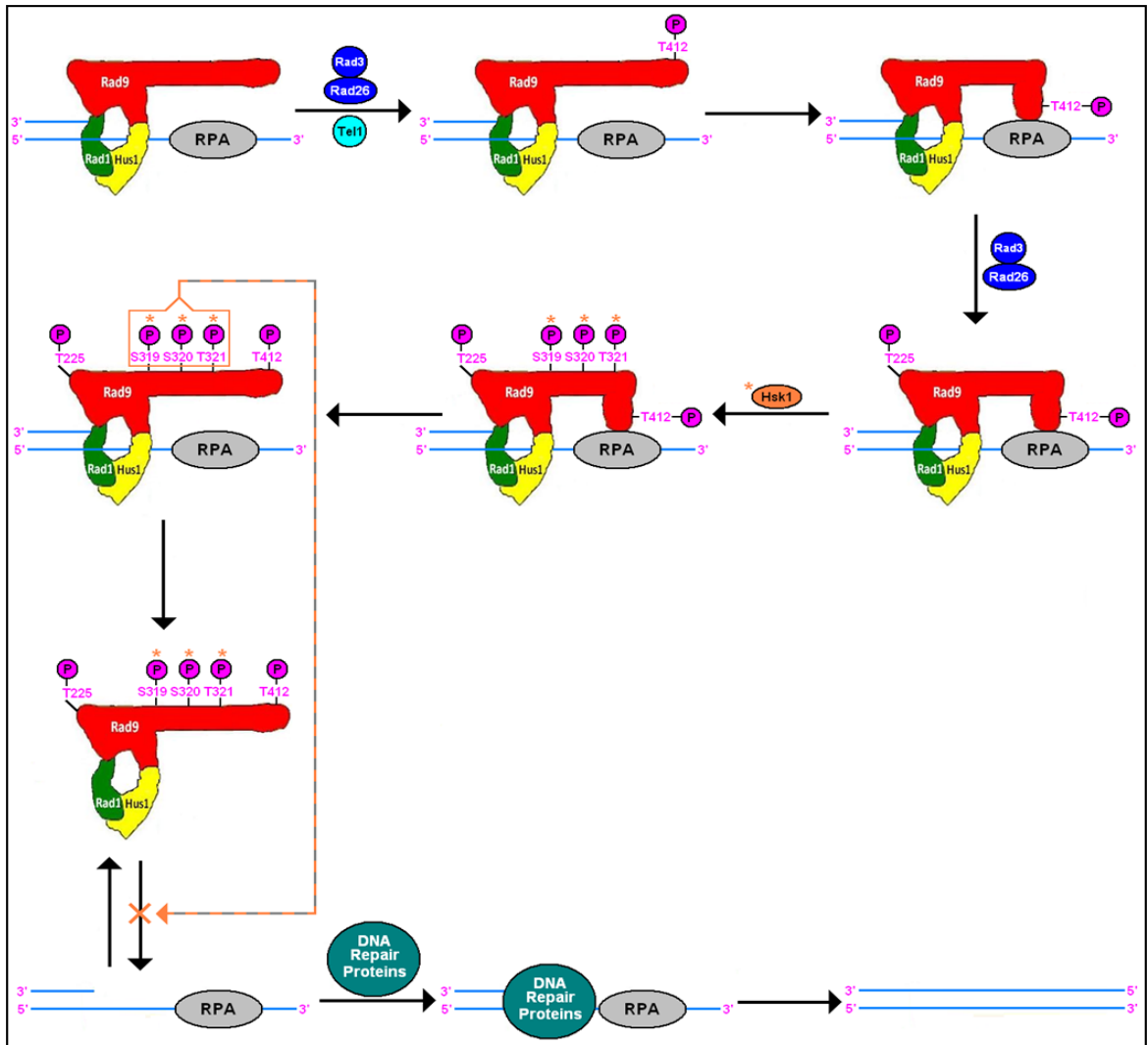
Phosphorylation of the Rad9 C-Terminal Tail Domain at Thr328, via TLK1/1B, also induces supra-molecular configurational changes within the ternary complex which trigger dissociation of the Rad17:Rfc2-5 clamp-loader, associative exchange of TLK1/1B from the Rad9 sub-unit to Asf1 and dissociative nucleosomal translocation of the dimeric Asf1-TLK1/1B complex (Canfield C. *et al.*, 2009)

TLK1/1B phosphorylation of Asf1, at Ser10 and Ser192, may induce supra-molecular configurational alterations within the protein which enhance the associative affinity of the Asf1 histone H3 and H4 binding-sites (“H3bs” and “H4bs”) and promote dissociation of the resultant Asf1:Nucleosome:TLK1/1B complex, thereby effecting the removal of nucleosomes to enable unhindered access of “9-1-1” clamp-recruited DNA polymerases and other repair proteins to the DNA lesion site (via associative Rad9 C-Tail Terminal Domain Interactions) for DSB repair and/or TLS-mediated by-pass of “bulky” DNA lesions (Canfield C. *et al.*, 2009; De Benedetti A. *et al.*, 2009; De Benedetti A. *et al.*, 2010; Sunavala-Dossabhoy G. *et al.*, 2003; Sunavala-Dossabhoy G. *et al.*, 2005).

ATM checkpoint kinase-mediated phosphorylation of the TLK1/1B sub-unit, at Ser695, suppresses its kinase activity and induces supra-molecular conformational changes within the “DNA-free”/unbound TLK1/1B:Asf1-Nucleosome complex promote dissociation of the Asf1:TLK1/1B dimer to enable nucleosomal re-association with the DNA, mediated via RSC protein mobilization – which also serves as a co-ordinative trigger signal for cell cycle resumption after DNA repair has been accomplished (Canfield C. *et al.*, 2009; Groth A. *et al.*, 2003; Shim E.Y. *et al.*, 2007).

Fig 1.53: Phospho-Regulated “9-1-1” Clamp DNA Repair Activities

[Taken and Adapted From: Furuya K. *et al*, 2010; Paek A.L. and Weinert T., 2010]



In the above *S. pombe* model (proposed by Furuya K. *et al*, 2010), the Rad9 sub-unit component of the “9-1-1” clamp co-ordinates the transitional equilibrium between Rad9-Rad1-Hus1 complex-association to the DNA damage lesion site, activation of Chk1 kinase-initiated DNA damage checkpoint responses and subsequent Rad9-Rad1-Hus1 complex-dissociation for facilitated recruitment of repair proteins to the DNA damage lesion site (Paek A.L. and Weinert T., 2010).

Initial spRad3/Rfc2-5 complex-loading of the “9-1-1” clamp onto the DNA and subsequent phosphorylation of spRad9 at T225, T412 and S423 by the primary/proximal transducer kinase, spRad3, triggers activation of the secondary/distal transducer kinase, spChk1, which initiates DNA damage checkpoint responses (discussed previously in detail in Section 1.2.2, pp.33-65).

The initial spRad3- and/or spTel1- phosphorylation of spRad9, at T412, may also enhance Rad9 C-Terminal Tail Domain interactions with Replication Protein A (RPA) and thus promote stabilisation of the “9-1-1” clamp-DNA association at the lesion site of DNA damage (Furuya K. *et al*, 2004; Furuya K. *et al*, 2010).

Rad3-phosphorylation of spRad9 at T225 also induces supra-molecular conformational alterations within the heterotrimeric “9-1-1” clamp which sterically weaken associative interactions at the spRad9-spHus1 interface via disruption of a critical hydrogen bond between spRad9-T225 and spHus1-H125 (Furuya K. *et al*, 2010).

Subsequent spChk1 kinase-initiated DNA damage checkpoint responses also activate the Dbf4-Dependent Kinase (DDK) homolog spHsk1 which phosphorylates the Rad9 C-Terminal Tail Domain at residue positions Ser319, Ser320 and Ser321 (Furuya K. *et al*, 2010).

DDK phosphorylation-mediated post-translational modification of spRad9 induces further supra-molecular conformational changes within the heterotrimeric “9-1-1” clamp which disrupt spRad9 C-Terminal Tail Domain-spRPA associative interactions and promote disengagement of the Rad9-Rad1-Hus1 complex from the DNA, thereby facilitating unimpeded access of DNA repair proteins to the DNA damage site for the correct, efficient repair of the DNA lesion (Furuya K. *et al*, 2010).

An equivalent mechanism may occur in human cells, involving the equivalent functional protein homologues hsATR (spRad3), hsATM (spTel1), hsChk1 (spChk1), hsRad9-hsRad1-hsHus1 (spRad9-Rad1-Hus1) and hsCdc7 (spHsk1) respectively – in the case of the *H. sapiens* “9-1-1” complex weakened associative interactions at the hsRad9-hsHus1 interface would occur via equivalent ATR (spRad3) phosphorylation of the hsRad9 T195 residue and disruption of the critical hsRad9-T195-hsHus1-H131 hydrogen bond (Doré *et al*, 2009).

1.3 “9-1-1” Complex-Independent Rad9 Functions

1.3.1 Pyrimidine Nucleobase Biosynthesis Activity Modulation

The hRad9 protein has also been experimentally observed to directly modulate the activity of the CAD (C_{arbamoyl}phosphate synthetase/A_{spartate} Transcarbamoylase/D_{ihydroorotase}) multi-enzymatic protein complex, a key component of the pyrimidine biosynthetic pathway (Lindsey-Boltz L.A. *et al.*, 2004) – Fig 1.54, p.124 and Fig 1.55, p.125.

Associative interactions between the CSPaseII domain within the multi-enzymatic protein CAD and the N-terminus and PCNA-liked domains I and II within the human Rad9A protein induce supramolecular conformational changes within the CAD protein which result in a two-fold enhancement of the V_{max} value of the CSPaseII catalytic activity (Lindsey-Boltz L.A. *et al.*, 2004) – Fig 1.56, p.126.

Negative regulatory control of the Rad9A-enhanced CSPaseII catalytic activity of the CAD protein is mediated via allosteric cooperative effects of transitional Rad9A C-Terminal tail domain dephosphorylation/phosphorylation site-induced supramolecular configurational modifications which promote dissociation of the N-terminal-PCNAI-PCNAII-CSPaseII interactions within the bound Rad9A-CAD ternary complex (Lindsey-Boltz L.A. *et al.*, 2004) – Fig 1.56, p.126.

The biochemical mechanism implicated in Rad9A associative enhancement of the activity of the CSPaseII domain of the CAD multi-enzymatic complex remains to be elucidated, although several hypothetical have been proposed (Lindsey-Boltz L.A. *et al.*, 2004), notably;

- (i) The bound CAD-Rad9A complex may induce supramolecular configurational changes within the CSPaseII domain which enhance affinity for its substrates; Glutamine, bicarbonate and ATP respectively (Lindsey-Boltz L.A. *et al.*, 2004).

- (ii) The bound CAD-Rad9A complex may induce supramolecular configurational changes within the CSPaseII domain which enhance its glutaminase activity with a consequential increase in V_{max} with no resultant alteration of substrate affinity.

However, this hypothesis is contradicted by previous experimental studies which indicated that the two-fold enhancement in V_{max} of CPSaseII in the CAD-Rad9A complex was unperturbed when ammonia was substituted as a nitrogen donor in place of glutamine (Lindsey-Boltz L.A. *et al.*, 2004).

- (iii) Associative interactions between CAD and the Rad9A complex may result in the induction of supramolecular conformational changes which promote a thermodynamically-favourable shift towards oligomeric assembly of CAD to its hexameric enzymatically-active form with enhancement of hexameric conformational stability and/or suppression of hexameric sub-unit dissociation respectively. (Lindsey-Boltz L.A. *et al.*, 2004).

Previous experimental studies indicate that dissociation of the active CAD hexameric form to its monomeric form had negligible effect on CSPaseII domain activity but did result in a significant decrease in the ATCase activity respectively (Carrey E.A. *et al.*, 1985; Qiu Y. and Davidson J.N., 2000).

Taken together initially, these experimental observations appeared to indicate that Rad9A associative binding interactions with CAD might possibly promote enhancement of the ATCase V_{max} value (Lindsey-Boltz L.A. *et al.*, 2004)

However, previous studies have established that the activity of the CPSaseII domain within the CAD is the actual rate-limiting step (Coleman P.F. *et al.*, 1977) such that enhancement of ATCase catalytic activity via Rad9A would have negligible effect on the overall activity of the CAD protein (Lindsey-Boltz *et al.*, 2004).

An alternative hypothetical transition-state intermediate mechanism may account for the experimentally observed two-fold increase of the CSPaseII V_{max} value in CAD which is mediated via associative Rad9A-CAD complex interactions.

The critical step in this mechanism could involve the promotional formation of a thermodynamically-favourable transition-state with significantly lowered activation energy via discrete supramolecular conformational alterations within the active site of the CSPaseII domain of the CAD protein which are induced via specific co-operative non-covalent associative interactions within the Rad9A N-terminus and PCNA-like I and II domains respectively.

To date, this type of postulated mechanism does not appear to have been considered in the current research literature and may warrant future experimental investigation.

In contrast, no similar binding interactive effect has been experimentally observed between CAD and hRad9 acting within the associative hHus1/hRad1 heterotrimeric toroidal 9-1-1 DNA sliding-clamp complex, indicative that hRad9 may possess independent functions related to the modulation of pyrimidine biosynthesis coupled to DNA damage responses and checkpoints implicated in regulatory cell cycle biochemical signalling processes respectively (Lindsey-Boltz L.A. *et al*, 2004).

Enhanced activity of ribonucleotide reductase via transcriptional and/or post transcriptional mechanisms in response to DNA damage is a well-documented phenomenon (Elledge S.J. *et al*, 1993).

Modulation of CSPaseII activity via proteolytic degradation with the apoptotic protein caspase-3 (Huang M. *et al.*, 2002b) and/or via associative phosphorylation interactive events with Protein Kinase A and MAP kinase components of the signalling cascade pathways implicated in cell growth and cell cycle regulation have also been experimentally demonstrated (Graves L.M. *et al.*, 2000; Sigoillot F.D. *et al.*, 2002a; Sigoillot F.D. *et al.*, 2002b; Sigoillot F.D. *et al.*, 2003) – Fig 1.55, p.125.

Enhanced CSPaseII activity has also been observed in comparative experimental studies performed on tumour cells (Reardon M.A. and Weber G., 1985; Sigoillot F.D. *et al.*, 2004) which may be correlated with elevated levels of Rad9 expression in specific cancerous tissue types – discussed previously in Section 1.1, pp.2-22; Fig 1.7, p.13; Fig 1.8, p.14; Table 1.2, p.15.

The original hypothetical assumption postulated that alterations in the relative concentration levels of ribonucleotide triphosphate (rNTP) pools would have little affect on the relative concentration levels of deoxyribonucleotide triphosphate (dNTP), on the basis that rNTP pool levels are approximately 100 fold higher than those of the dNTP pool levels respectively with insignificant consequential modulatory effects on DNA damage response pathways in relation to cell survival and mutation frequency (Lindsey-Boltz L.A. *et al.*, 2004).

However there is currently no experimental evidence to support this hypothetical assumption, whilst alterations in rNTP levels may be of significance with regard to RNA damage and RNA synthesis associated genotoxic stress responses (Feyzi E. *et al.*, 2007), implicated in cellular recovery mechanisms which may promote induction of pyrimidine biosynthesis via functionally-interactive CAD-Rad9A complex formation respectively (Linsey-Boltz L.A. *et al.*, 2004).

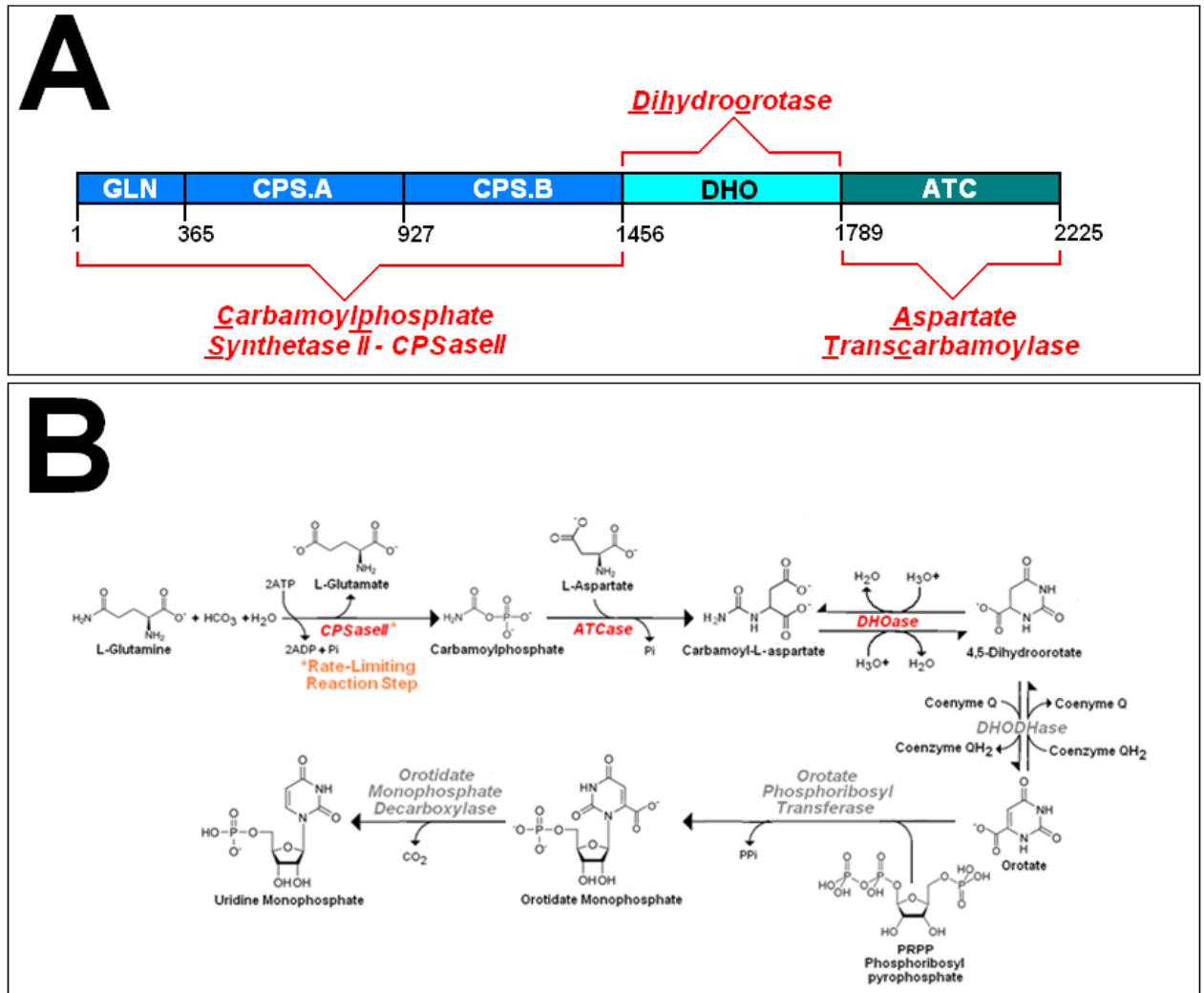
In addition to nucleic acid synthesis, pyrimidine biosynthesis is also a critical biochemical prerequisite for the synthesis of UDP-carbohydrates and CDP-lipids which are utilised in a versatile range of different cellular functions (Huang M. and Graves L.M., 2003).

Other experimental studies have also revealed that whilst CAD is mainly localised in the cytosol, a minor proportion of this multi-enzyme protein complex appears to be localised within the nucleus (Angeletti P.C. and Engler J.A., 1998; Carrey E.A. *et al*, 2002; Sigoillot F.D. *et al*, 2003).

Thus, Rad9 may potentially function in a range of complementary versatile roles with regard to cytological maintenance and integrity within regulatory cell cycle signalling pathways in addition to those implicated in DNA damage response checkpoints respectively.

Fig 1.54: Biochemical Overview of CAD-Catalysed Reactions

[Compiled via Collated Information From: Coleman P.F. *et al.*, 1977; Evans D.R. & Guy H.I., 2004; Jones M.E., 1980; Levine R.L. *et al.*, 1971; Mori M. *et al.*, 1976; Shoaf W.T. & Jones M.E., 1973; Sigoillot F.D. *et al.*, 2002a; Sigoillot F.D. *et al.*, 2002b; Tatibana M. and Ito K., 1969]

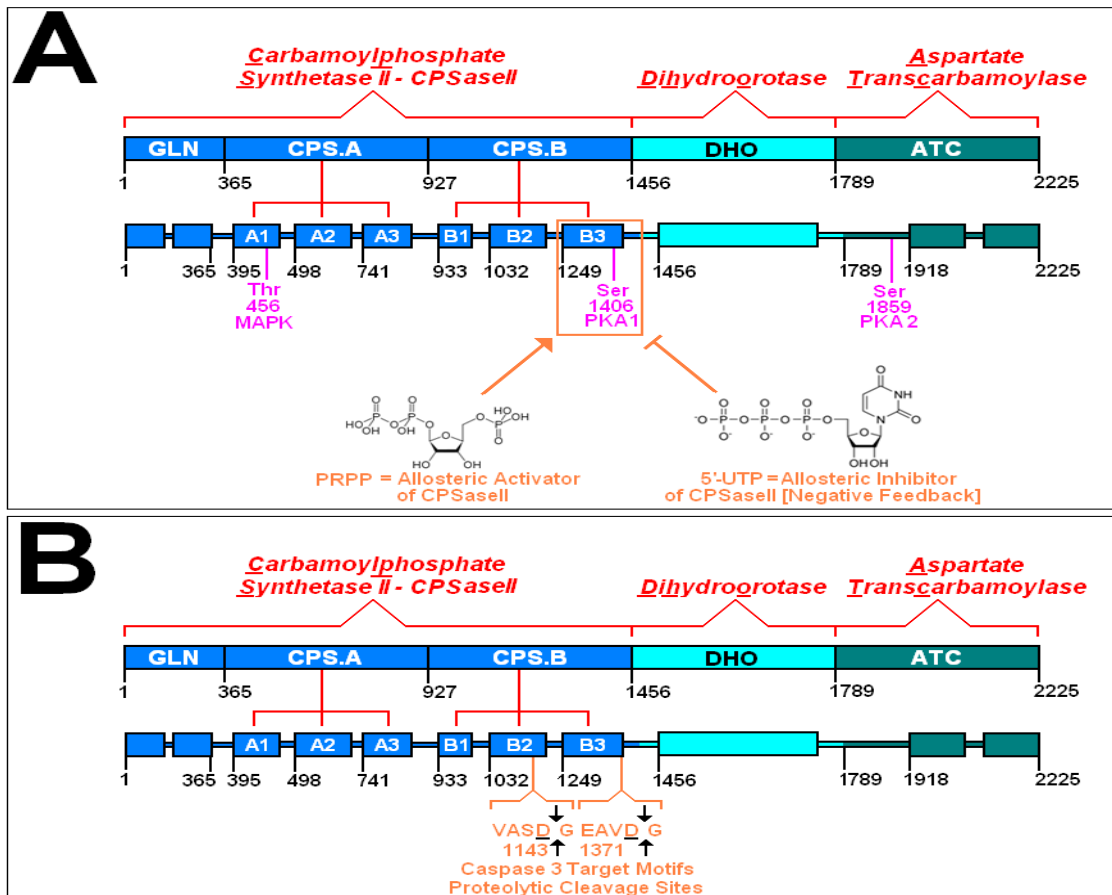


A: CAD is protein with multi-enzymatic functions containing Carbamoylphosphate Synthetase II (CSPaseII), Dihydroorotase (DHO) and Aspartate Transcarbamoylase (ATCase) type catalytic domains.

B: The CAD multi-enzymatic protein is implicated in the catalysis of first three key steps within the pyrimidine biosynthetic pathway, in which the rate-limiting step is determined by the relative activity of the CSPaseII domain within the CAD complex respectively (Coleman P.F. *et al.*, 1977; Hager S.E. and Jones M.E., 1967; Jones M.E., 1980).

Fig 1.55: CAD Activity Regulation – Key Domains & Residues

[Compiled via Collated Information From: Sigoillot F.D. *et al.*, 2002b; Sigoillot F.D. *et al.*, 2005]



A: Allosteric regulation of the relative activity of the CSPaseII domain within CAD is mediated via 5'-UTP (uridine nucleotide) negative feedback inhibition and positive feedback activation via PRP (phosphoribosylpyrophosphate) respectively (Carrey E.A. and Hardy D.G., 1988)

PKA1-mediated phosphorylation of Ser1406 induces supramolecular conformational changes within the CSP.B sub-domain which desensitize the CSPaseII catalytic domain towards 5'-UTP negative feedback allosteric inhibition and PRPP positive feedback allosteric activation (Sigoillot F.D. *et al.*, 2002b; Sigoillot F.D. *et al.*, 2005).

MAPK-mediated phosphorylation of Thr456 induces supramolecular conformational changes within the CSP.A sub-domain which desensitize the CSPaseII catalytic domain towards 5'-UTP negative feedback allosteric inhibition and enhance the CSPIIase catalytic domain towards PRPP positive feedback allosteric activation (Graves L.M. *et al.*, 2000).

The MAPK and cAMP-dependent kinase (PKA1 and PKA2) signalling pathways are implicated in the control of cell growth via cell-cycle phase-specific sequential phosphorylation-mediated modulation of CAD catalytic activities (Robinson M.J. and Cobb M.H., 1997; Sigoillot F.D. *et al.*, 2002b; Sigoillot F.D. *et al.*, 2005).

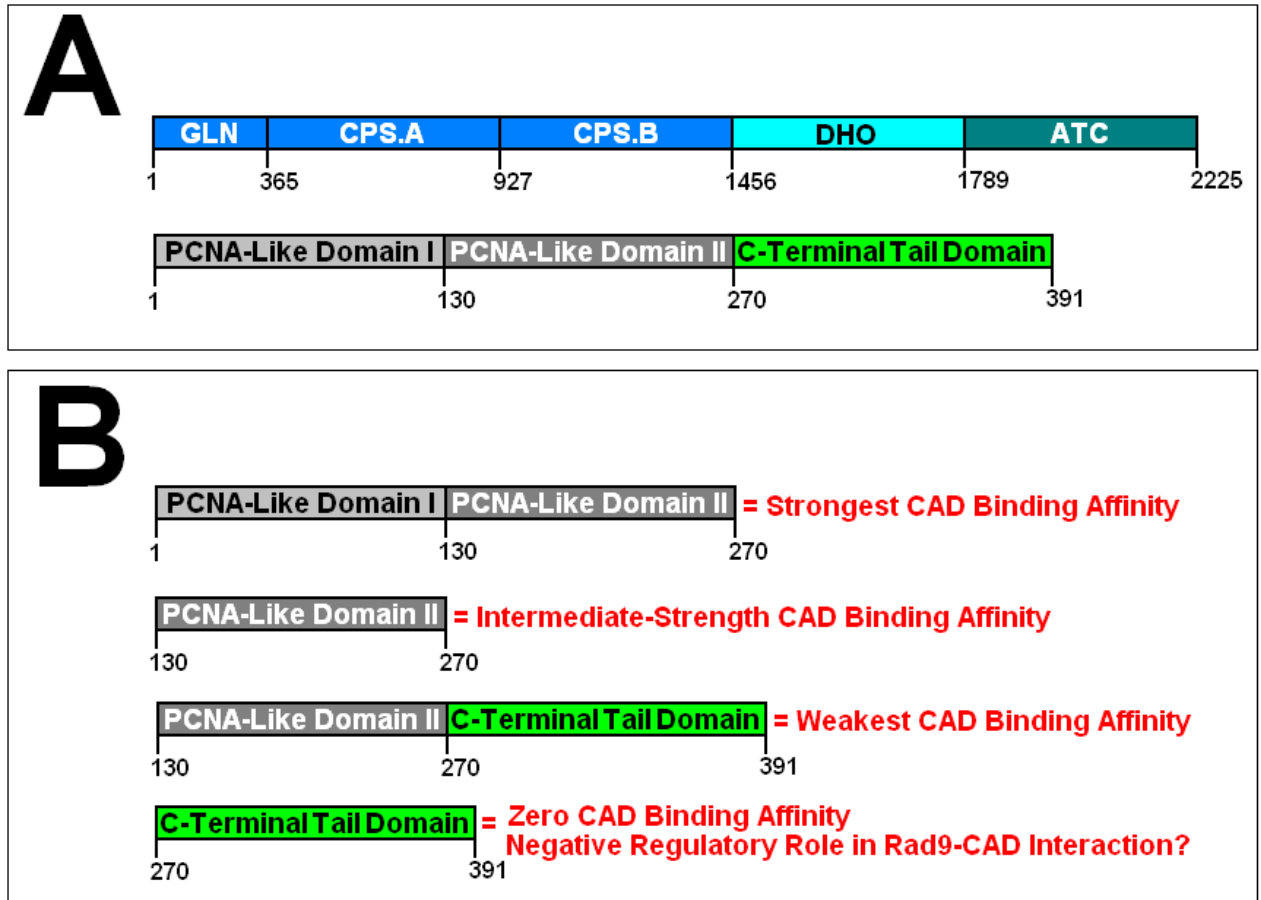
MAPK-mediated phosphorylation of Thr456 occurs immediately prior to cell cycle S-Phase initiation, with consequential enhancement of PPRP-stimulated CSPaseII catalytic activity and conversion of 5'-UTP from an allosteric inhibitor to an allosteric activator of CSPaseII catalytic activity, thereby providing the necessary metabolic precursors for the required biosynthesis of DNA, RNA and glycoproteins (Sigoillot F.D. *et al.*, 2002b; Sigoillot F.D. *et al.*, 2003; Sigoillot F.D. *et al.*, 2007).

Cell cycle progression and exit from S-phase initiates Thr456 dephosphorylation and PKA1-mediated phosphorylation of Ser1406 reverts the enhanced PPRP-stimulation of CSPaseII activity to the basal activity level with consequential down-regulation of CAD catalytic activities (Kotsis D.H. *et al.*, 2007; Sigoillot F.D. *et al.*, 2002b; Sigoillot F.D. *et al.*, 2003).

B: Apoptotic suppression of pyrimidine biosynthesis is mediated via Caspase 3 site-specific proteolytic cleavage of CAD at two target substrate motifs situated within the B2 and B3 sub-units of the CPS.B sub-domain of the CSPaseII catalytic domain (Huang M. *et al.*, 2002b; Larsen B.D. and Megoney L.A., 2010).

Fig 1.56: Associative Rad9-CAD Domain Interactions

[Compiled via Collated Information From: Lindsey-Boltz L.A. *et al*, 2004
Sigoillot F.D. *et al*, 2002b
Sigoillot F.D. *et al*, 2005]



A: Basic component map of the multi-functional protein CAD protein indicating the CSPaseII (GLN-CPSA-CPSB), DHOase and ATCase catalytic domains (Top Figure).

Basic component map the human Rad9A protein indicating the PCNA-like domain I, PCNA-like Domain II and the C-Tail Terminal Domain (Bottom Figure).

B: Comparative CAD Co-immunoprecipitation studies with human Rad9A fragments indicate that the N-Terminus and PCNA-like I and II domains are implicated in the associative CAD-Rad9A interactions which elevate the overall activity of the CAD protein via enhanced CSPase II domain catalytic activity (Lindsey-Boltz L.A. *et al*, 2004).

These comparative CAD Co-immunoprecipitation studies also indicate that the C-Terminal Tail domain of the human Rad9A protein could be implicated in the negative regulation of the Rad9A-PCNA I/II-domain-CAD associative interactions and thus serves as a potential mechanism for modulatory control of the Rad9A-enhanced CSPaseII catalytic activity of the CAD protein (Lindsey-Boltz L.A. *et al*, 2004) – discussed on p.119.

1.3.2 Intrinsic Apoptotic Signalling Activity Modulation

The hRad9 protein is hypothetically postulated to play a key modulatory role at the crux of the delicate balance of regulatory cell cycle check-point biochemical signalling determinants which enable cytological survival, via induction of DNA repair and/or by-pass of minor DNA damage or initiate apoptotic responses and trigger programmed cell death respectively, on the basis of noted observations in several experimental studies (Komatsu K. *et al*, 2000a; Komatsu K. *et al*, 2000b; Lee M.W. *et al*, 2003; Yin Y. *et al*, 2004; Yoshida K. *et al*, 2002;) – notably;

- (i) Associative interactions of the hRad9 protein with the p21 promoter consensus DNA-binding sequence have been observed to directly induce expression of the pro-apoptotic p21 protein in the absence of hHus1 and hRad1 proteins respectively (Yin Y. *et al*, 2004).

- (ii) Associative interactions of the hRad9 C-terminus with the cAbl kinase have been observed to result in subsequent cAbl-mediated phosphorylation of a specific Tyrosine residue (Y28) situated within BH3-like domain of the hRad9 N-Terminus, which has been demonstrated to be a critical modification pre-requisite that triggers supramolecular conformational type alterations within hRad9 N-terminal BH3-like domain to enable it to engage with and inactivate apoptotic suppressor proteins such as Bcl-x1 and Bcl-2 via binding interactions between the respective BH3 domains of the proteins (Komatsu K. *et al*, 2000a; Komatsu K. *et al*, 2000b; Yoshida K. *et al*, 2002).

(iii) The hRad9 protein has also been observed to be proteolytically processed by the apoptotic enzymatic protein Caspase-3 at several specific identified sequence motifs within the hRad9 protein (Fig 1.57, p.130) with consequential eradication of the functional capability of the protein to form the associative hHus1/hRad1 heterotrimeric toroidal 9-1-1 DNA sliding-clamp complex and generation of hRad9 N-terminal fragments with retained BH3-like binding domains which may possess the ability to associate with and inactivate various BH3-type apoptotic suppressor proteins, such as Bcl-2 and Bcl-xl, with subsequent promotion of apoptosis (Lee M.W. *et al.*, 2003).

On the basis of these observed experimental phenomena, a hypothetical model has been postulated for cytological apoptotic induction signalling in response to extensive/irreparable DNA damage (Fig 1.57, p.130) in which hRad9 is implicated as a critical determinant component (Lee M.W. *et al.*, 2003).

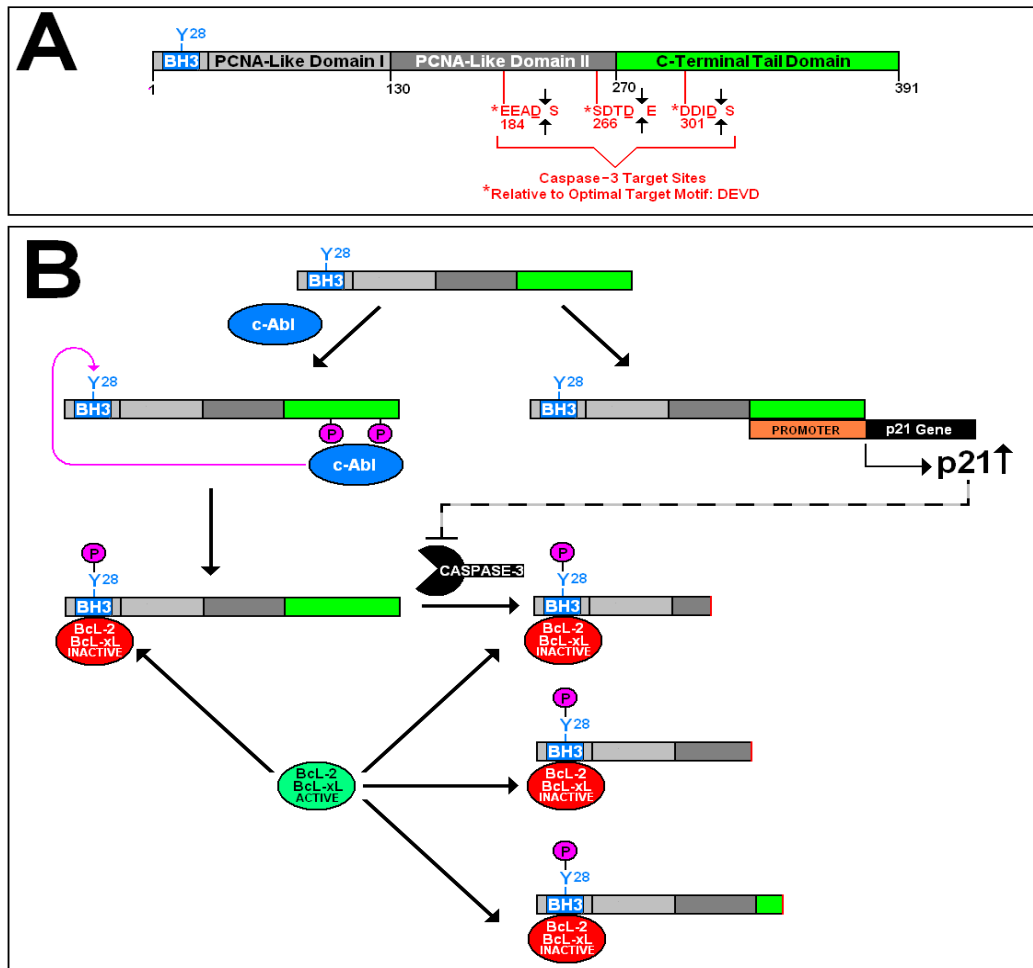
Intriguingly, both ATRIP and Rad9 contain potential Caspase-3 cleavage sites within their respective acidic α -helical motifs which associate with the N-Terminal DNA-Binding-Domain F (DBD-F) of the 70kDa Replication A protein sub-unit (RPA70) – Fig 1.11A, p.25, notably;

- (i) The **DIDD** Caspase-3 proteolytic target motif situated within the C-Terminal Tail Domain of Rad9 (Fig 1.57, p.127), which also comprises part of its RPA70 DBD-F associative acidic α -helical motif: DDFAN **DIDDSYMI** (Fig 1.11B, p.25).
- (ii) The potential **DDLE** Caspase-3 proteolytic target motif situated within the ATR-Interacting Protein (ATRIP), which comprises part of its RPA70 DBD-F associative acidic α -helical motif: GDETA **DDLEELDT** (Fig 1.11C, p.25).

A feasible postulate of this observation is that Caspase-3 cleavage of these sites within ATRIP and Rad9 may serve to inhibit their associative RPA-protein interactions and thus prevent both constitutive and induced Rad9-mediated activation of ATR with consequential suppression of ATR-Chk1 initiated cell cycle checkpoints (discussed previously in Section 1.2.2, pp.33-65) and promotion of proapoptotic signalling-mediated events.

Fig 1.57: Independent hRad9-Mediated Apoptotic Induction Model

[Compiled via Collated Information From: Earnshaw W.C. *et al.*, 1999; Nicholson D.W., 1999; Komatsu K. *et al.*, 2000; Yoshida K. *et al.*, 2002; Lee M.W. *et al.*, 2003; Yin Y. *et al.*, 2004]



Activation of the BH3-like binding domain, triggered via associative interactions with the c-Abl kinase at the C-terminal tail domain and subsequent phosphorylation of Y28 by the kinase within the full-length hRad9 protein N-Terminus, enables it to bind and inactivate BH3-type apoptotic suppressor proteins such as Bcl-xl and Bcl-2 with consequential induction of apoptosis (Komatsu K. *et al.*, 2000; Yoshida K. *et al.*, 2002), whilst additional phosphosphorylation of Rad9 by Protein Kinase C δ is also required for binding of the Rad9 BH3-like domain to the Bcl-2 protein (Yoshida K. *et al.*, 2003) – Fig B.

The full-length hRad9 protein is also implicated in direct associative interactions with the p21 promoter DNA-binding consensus sequence which results in elevated inductive expression of the p21 protein in an hHus1/hRad1-independent mechanism (Yin Y. *et al.*, 2004) – p21 protein phosphorylation associative-interactions are also implicated in the inhibition of pro-caspase 3 activation, CDK and DNA replicative processive activities respectively (Suzuki A. *et al.*, 1998; Suzuki A. *et al.*, 1999; Child E.S. and Mann D.J., 2006) – Fig B.

Caspase-3 is also implicated in proteolytic cleavage inactivation of a range of other proteins including; polyADPribose polymerase, ATM, RAD51, the DNA-PK catalytic sub-unit, CAD (discussed previously in Section 1.3.1, pp.119-126; Fig 1.55B, p.125) and possibly ATRIP (discussed on pp.128-129) – all of which participate in DNA damage checkpoint response and/or repair pathways respectively (Nicholson D.W., 1999).

Caspase-3 cleavage of the full-length hRad9 protein abrogates associative hHus1/hRad1 heterotrimeric toroidal 9-1-1 DNA sliding-clamp complex formation and functions, that may serve a regulatory purpose under cytological conditions of extensive DNA damage in which DNA repair would be inappropriate due to enhanced error-prone probability and/or when DNA repair is no longer thermodynamically favourable. (Lee M.W. *et al.*, 2003) – Fig A and Fig B.

Caspase-3 proteolytic processing of full-length hRad9 also generates several intact N-terminal fragments with the retained activated BH3-like protein binding-domain, which are subsequently translocated from the nucleus to the cytosolic environment where they bind and inactivate BH3-type apoptotic suppressor proteins such as Bcl-xl and Bcl-2 with consequential induction of apoptosis. (Lee M.W. *et al.*, 2003) – Fig A and Fig B.

Thus, the hRad9 protein may have potential distinctive modulatory functions within the penultimate decisive end-point “signalling crux” of DNA repair and cell survival versus apoptotic programmed cell death respectively.

1.4 COP9 Signalosomal Regulation of Rad9 Functional Activities

Experimental investigations have indicated that the Rad1 sub-unit of the “9-1-1” DNA sliding-clamp complex may also possess a chaperone-like function which may serve to stabilise and protect the Hus1 sub-unit from ubiquitin-targeted proteolytic degradation, via formation of the heterodimeric Rad1:Hus1 complex, within the cytoplasm (Hirai I. *et al*, 2004) – discussed summarily in Fig 1.58, p.135.

The “9-1-1” complex has also been demonstrated to interact with the Jab1 (CSN5) sub-unit of the COP9 signalosome complex, via associative Jab1-Rad1 interactions, which may serve as a signal trigger for the sub-cellular translocation of the resultant Rad9-Rad1:Jab1-Hus1 ternary complex out of the nucleus to the cytoplasm (Huang J. *et al*, 2007).

The Jab1 protein (Jun-Activating Binding Protein 1), also known as CSN5 (COP9 Signalosome Sub-Unit 5), is a critical associative component of the COP9 signalosome complex (CSN) which is required for mediation of the functional CSN activities (Adler A.S. *et al*, 2006; Chamovitz D.A. and Segal D., 2001; Richardson S.K. and Zundel W., 2005; Wei N. and Deng X.W., 2003; Wei N. *et al*, 2008) – Fig 1.59, p.136.

The COP9 signalosome complex exhibits multi-subunit protease activities which are implicated in cytosolic regulation of cullin-RING ligase-ubiquitin E3 complex functions within the ubiquitin-targeted proteosomal pathway (Wei N. *et al*, 2008) – Figs 1.59 - 1.61, pp.136-138.

Associative Jab1 (CSN5) interactions with the Rad1 sub-unit component of the “9-1-1” DNA sliding-clamp are also known to be required for its targeted ubiquitination, mediated via E3 Ubiquitin Protein Ligases, which constitutes as key pre-requisite step for the initiation of the sequential proteolytic degradation of the heterotrimeric, toroidal Rad9-Rad1-Hus1 complex (Hirai I. *et al*, 2004; Huang J. *et al*, 2007) – Fig 1.60, p.137 and Fig 1.61, p.138.

As discussed previously (Section 1.2.4, p.84), the protein chaperone components Hsp70, Hsp90 and TPR2 which function within protein-folding complex machinery also interact and modulate Ubiquitin Protein E3 Ligases (Hatakeyama S. *et al*, 2004).

Thus potential “cross-talk” signalling between the Hsp70/Hsp90 protein complex-folding machinery and Jab1-mediated proteolytic “9-1-1” complex degradation, mediated via the differential formation of the “9-1-1”complex-TPR2 (discussed previously in Section 1.2.4, p.84) and Rad9-Rad1:Jab1-Hus1 ternary complexes, may be implicated in the selective modulation of the levels and activities of the individual isoforms of the Rad9, Hus1 and Rad17 proteins (Fig 1.3, p.9; Fig 1.4, p.10; Fig 1.6, p.12) for regulation of the functional activities of each of four potential “9-1-1” DNA sliding-clamp isoforms (Fig 1.5, p.11) and individual Rad9A and Rad9B isoforms (Fig 1.3, p.9) respectively.

This intricate “cross-talk” signalling may also be implicated in the regulation of the activities of nuclear steroidal receptors and their associated protein factors such as the Progesterone receptor and the Steroid Receptor Co-Activator (SRC1), whose respective functions are also regulated via Jab1 (CSN5)-protein interactions within the associative COP9 signalosome complex (Chauchereau A. *et al*, 2000; Wei N. *et al*, 2008) – Fig 1.59, p.136.

The ubiquitin-proteosomal system also constitutes a major mechanism for the regulation of a variety of different cytological processes, including those associated with cell cycle checkpoints and DNA repair pathways (McBride W.H. *et al*, 2003).

Furthermore, small-molecule inhibitors of specific component proteins within the ubiquitin-proteosomal system have been demonstrated to trigger activation of the G1/S, Intra-S and G2/M cell cycle checkpoints (Bendjennat M. *et al*, 2003; McBride W.H. *et al*, 2003) – discussed in detail previously in Section 1.2.2, pp.33-65.

Jab1 (CSN5)-mediated functions within the COP9 signalosome complex also modulate the respective activities of several key proteins which have been identified as critical implicators in the progression of various different types of cancerous diseases – including; AP-1, c-Jun, p27/Kip1, p53, Smad4/Smad7 (Huang J., *et al*, 2007; Shackelford T.J. *et al*, 2011; Wei N. *et al*, 2008) – Fig 1.59, p.136.

Various experimental studies have also indicated that Jab1 (CSN5) has key functional roles in the modulation of cell cycle progression, genomic stability, carcinogenesis and cell survival in response to cytological radiosensitivity (Doronkin S. *et al*, 2002; Doronkin S. *et al*, 2003; Fukumoto A. *et al*, 2005; Fukumoto A. *et al*, 2006; Huang J. *et al*, 2007; McBride W.H. *et al*, 2003; Tian L. *et al*, 2010; Tomoda K. *et al*, 2004).

Deletion of the *Jab1* gene in mouse embryonic fibroblasts and osteocarcinoma cells has been demonstrated to enhance their genomic instability as a consequence of elevated spontaneous DNA damage and homologous recombination repair defects, via p53-mediated suppressed expression of the Rad51 protein (whose key functional role in homologous recombinational repair was discussed previously in Fig 1.48, p.109), which also enhances the radiosensitivity of these cells to γ -irradiation and promotes apoptotic induction (Tian L. *et al*, 2010).

Jab1 (csn5) over-expression has also been demonstrated to suppress genotoxic and replication stress-induced Chk1 phosphorylation with consequential impairment of activated checkpoint responses and cytological propagation of genomic instability which may be implicated in the development of carcinogenesis (Tomada K. *et al*, 1999; Bech-Otschir D. *et al*, 2001; Bech-Otschir D. *et al*, 2002; Nemajerova A. *et al*, 2007).

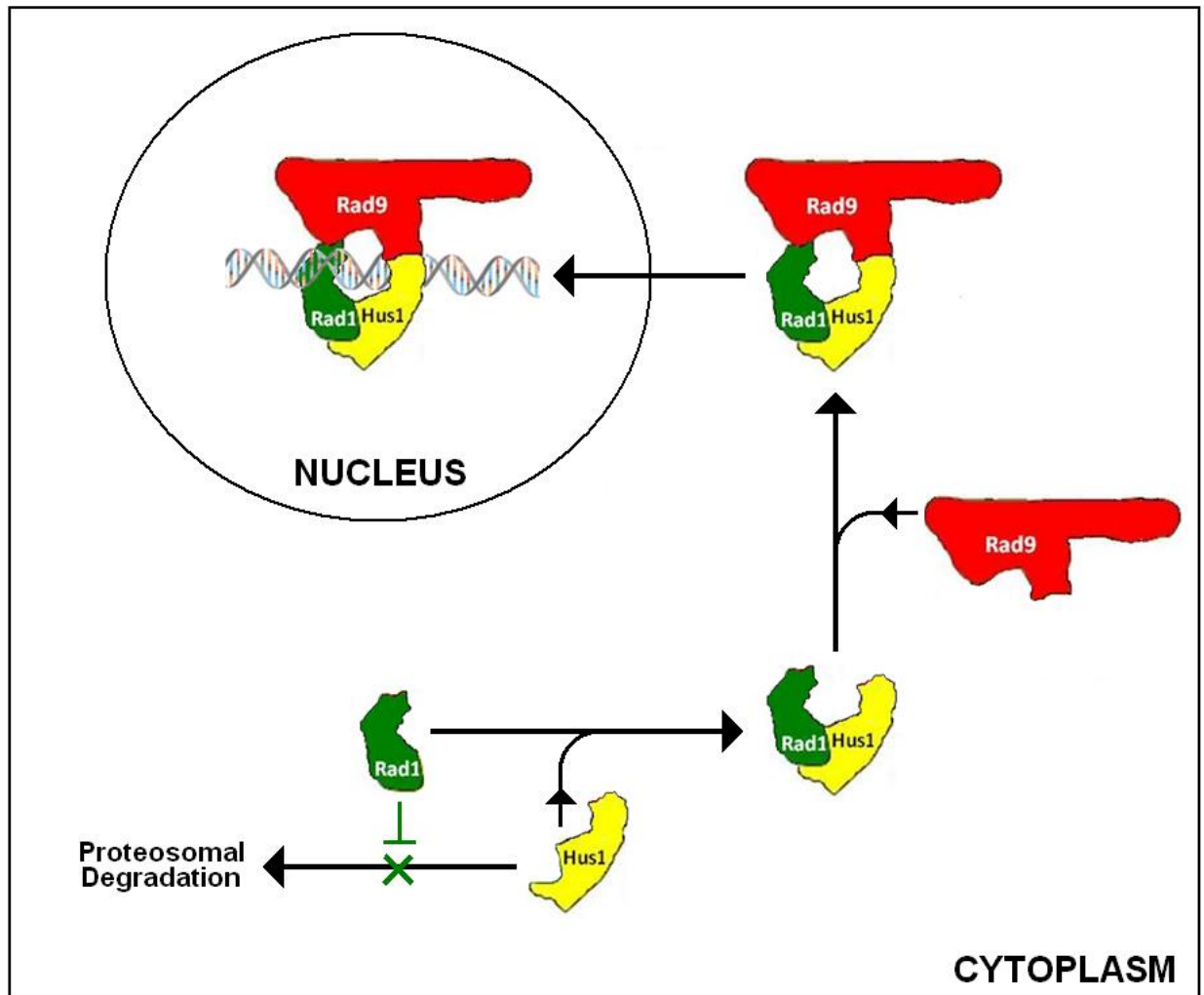
Experimental studies also indicate that the MIF1→Jab1 (CSN5)→Ubiquitin E3 Ligase (CSF) proteosomal signalling pathway may be implicated in the regulation of Chk1- and Chk2- initiated DNA damage checkpoint responses, whilst its dysfunction may have a key role in tumour cell survival and developmental progression to metastatic cytological status (Nakayama K.I. and Nakayama K., 2006; Nemajerova A. *et al*, 2007).

The heterotrimeric toroidal Rad9-Rad1-Hus1 PCNA-like DNA sliding-clamp complex is also implicated the initiation of various cell cycle checkpoint pathways via mediation of ATR/ATRIP→Chk1-activation of “down-stream” effector biochemical signalling cascades (discussed previously in detail in Section 1.2.2, pp.33-65).

This collective experimental evidence indicates the feasible existence of novel Rad9-Rad1-Hus1 sliding-clamp complex-“feed-back” mechanisms, mediated via associative Rad1-Jab1 interactions, which regulate the activity of “9-1-1” complex-initiated cell cycle checkpoint signalling (Section 1.2, pp.23-118) and independent Rad9 apoptotic modulation in response to genotoxic and/or DNA replication stresses (Section 1.3.2, pp.127-130) – Fig 1.62, p.139.

Fig 1.58: Rad1-Modulated “9-1-1” Clamp Stability & Translocation

[Taken and Adapted From: Hirai I. *et al*, 2004]



In the above model, proposed by Harai I. *et al*, 2004, the Rad1 protein functions as a chaperone stabiliser for the Hus1 protein.

Unlike Rad1, Hus1 is relatively unstable within the cytosolic environment and is highly susceptible to proteolytic degradation (Hirai I. *et al*, 2004).

Elevated Rad1 expression is a genotoxic-inductive cellular response, which promotes formation of the Rad1:Hus1 heterodimeric complex (Hirai I. *et al*, 2004)

Associative interactions of Rad1 with the Hus1 protein effectively “shield” Hus1 against proteolytic degradation and the resultant heterodimeric Rad1:Hus1 complex is sufficiently stable to enable its translocation to the nuclear environment where association with the Rad9 protein takes place for subsequent “9-1-1” clamp formation and loading of the heterotrimeric complex onto localised chromatin sites of DNA damage (Hirai I. *et al*, 2004).

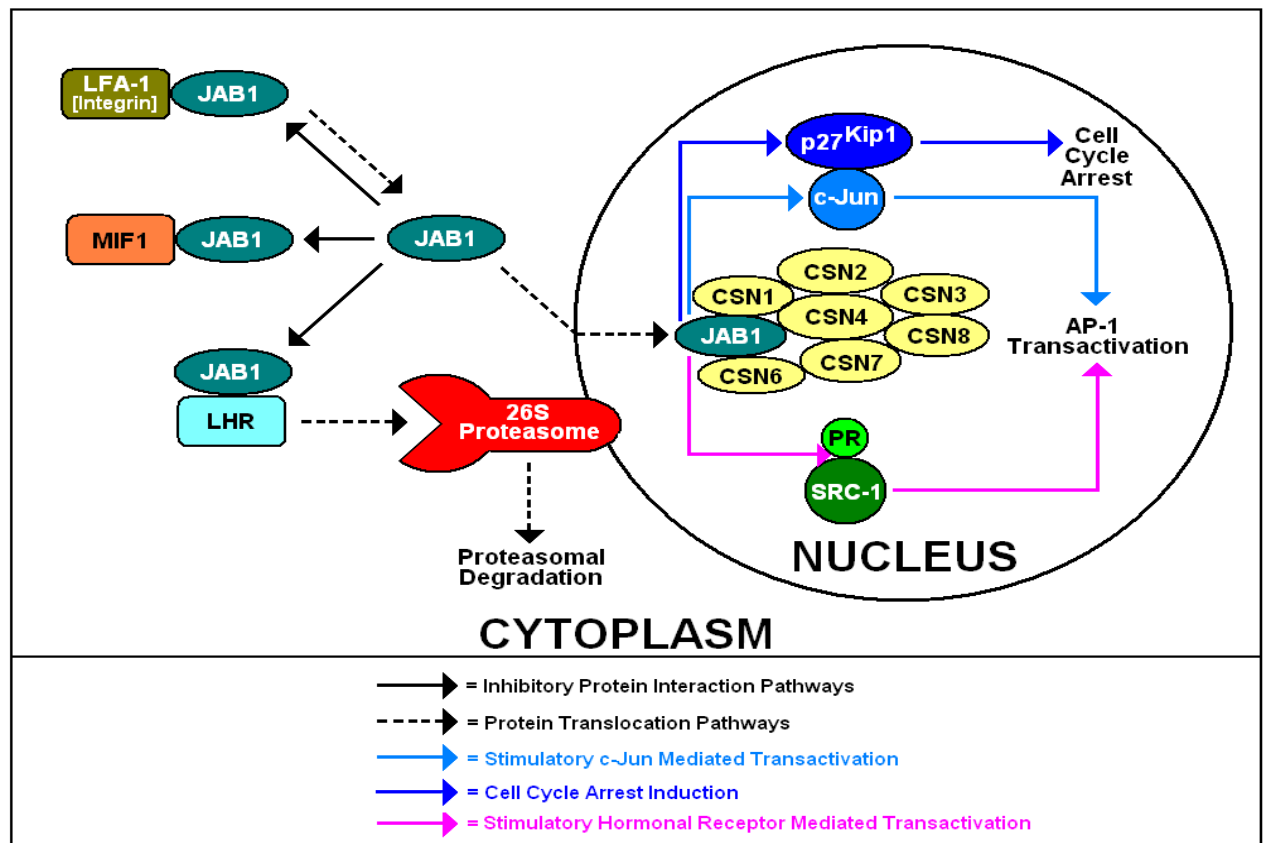
As discussed in detail later (Fig 1.60, p.137; Fig 1.61, p.138), associative interactions between the COP9 Signalosome protein component Jab1 (CSN5) and the Rad1 sub-unit within the “9-1-1” clamp promote translocation of the resultant Rad9-(Rad1-Jab1)-Hus1 ternary complex from the nucleus to the cytoplasm for sequential ubiquitination-targeted proteolytic degradation (Huang J. *et al*, 2007).

Ubiquitin-targeted proteasomal degradation of the “9-1-1” clamp via initial hydrolytic decomposition of the Rad1 sub-unit may constitute a key regulatory “rate-limiting” step implicated in the dissociation of the remnant Hus1:Rad9 heterodimeric complex via increased instability of the Hus1 sub-unit due to elimination of the protective Rad1:Hus1 associative interactions (Hirai I. *et al*, 2004; Huang J. *et al*, 2007) – Fig 1.60, p.137.

Initial proteolytic removal of the Rad1 sub-unit would thus facilitate proteasomal degradation of the remnant Hus1 and Rad9 sub-units (Hirai I. *et al*, 2004; Huang J. *et al*, 2007) – Fig 1.60, p.137.

Fig 1.59: Jab 1 Proteosomal Functions & CSN Complex Interactions

[Taken and Adapted From: Chamovitz D.A. and Segal D., 2001]



Jab1 (also known as CSN5) is a metalloproteinase protein which has distinctive functions that operate both outside of and within the COP9 signalosome (CSN) complex – which is comprised of 8 different CSN sub-units in total. (Chamovitz D.A. and Segal D., 2001; Deng X.W. *et al.*, 2000a; Deng X.W. *et al.*, 2000b; Freilich S. *et al.*, 1999; Fukumoto A. *et al.*, 2004; Kapelari B. *et al.*, 2000; Kato J.Y. *et al.*, 2006; Kwok S.F. *et al.*, 1998; Kwok S.F. *et al.*, 1999; Richardson K.S. and Zundel W., 2005; Serino G. *et al.*, 1999; Scherer S.J. *et al.*, 2000; Sugiyama Y. *et al.*, 2001; Tomoda K. *et al.*, 2002; Wei N. and Deng X.W., 2003; Wei N. *et al.*, 1998; Wei N. *et al.*, 2008).

These Jab1 functions modulate the activity of a wide variety of proteins which are implicated in regulatory cellular process, including; CDK Inhibitors (eg p27/Kip1), Cytokines (eg MIF – Macrophage Migration Inhibitory Factor), Oncoproteins (eg the c-Jun sub-unit of the AP-1 Transcription Factor Complex; eg the Steroid Receptor Co-Activator – SRC1), Integrin/Adhesion Receptors (eg LFA-1) and Hormonal Receptors (eg the G-protein coupled Lutropin/Choriogonadotropin Receptor – LHR) (Bianchi E. *et al.*, 2000; Chauchereau A. *et al.*, 2000; Claret F.X. *et al.*, 1996; Kleeman R. *et al.*, 2000; Li S. *et al.*, 2000; Richardson K.S. and Zundel W., 2005; Tomoda K. *et al.*, 1999; Wei N. *et al.*, 2008).

Dotted lines denote protein translocation trafficking and associative Jab1 (CSN5) protein interactions implicated in formation of the CSN complex, dissociative release of Jab1 from its heterodimeric complex with LFA-1 and Jab1-targeted proteolytic degradation of the LHR receptor (Bianchi E. *et al.*, 2000; Chamovitz D.A. and Segal D., 2001; Li S. *et al.*, 2000).

The Jab1 (CSN5) protein component, functioning within the nuclear CSN complex, also initiates AP-1 transactivation via associative stimulatory interactions with the oncoprotein c-Jun (which is also a sub-unit of the AP-1 transcription factor) and via associative stimulatory interactions with both the Progesterone Receptor (PR) and the Steroid Receptor Co-Activator – SRC-1 (Chauchereau A. *et al.*, 2000; Claret F.X. *et al.*, 1996; Chamovitz D.A. and Segal D., 2001).

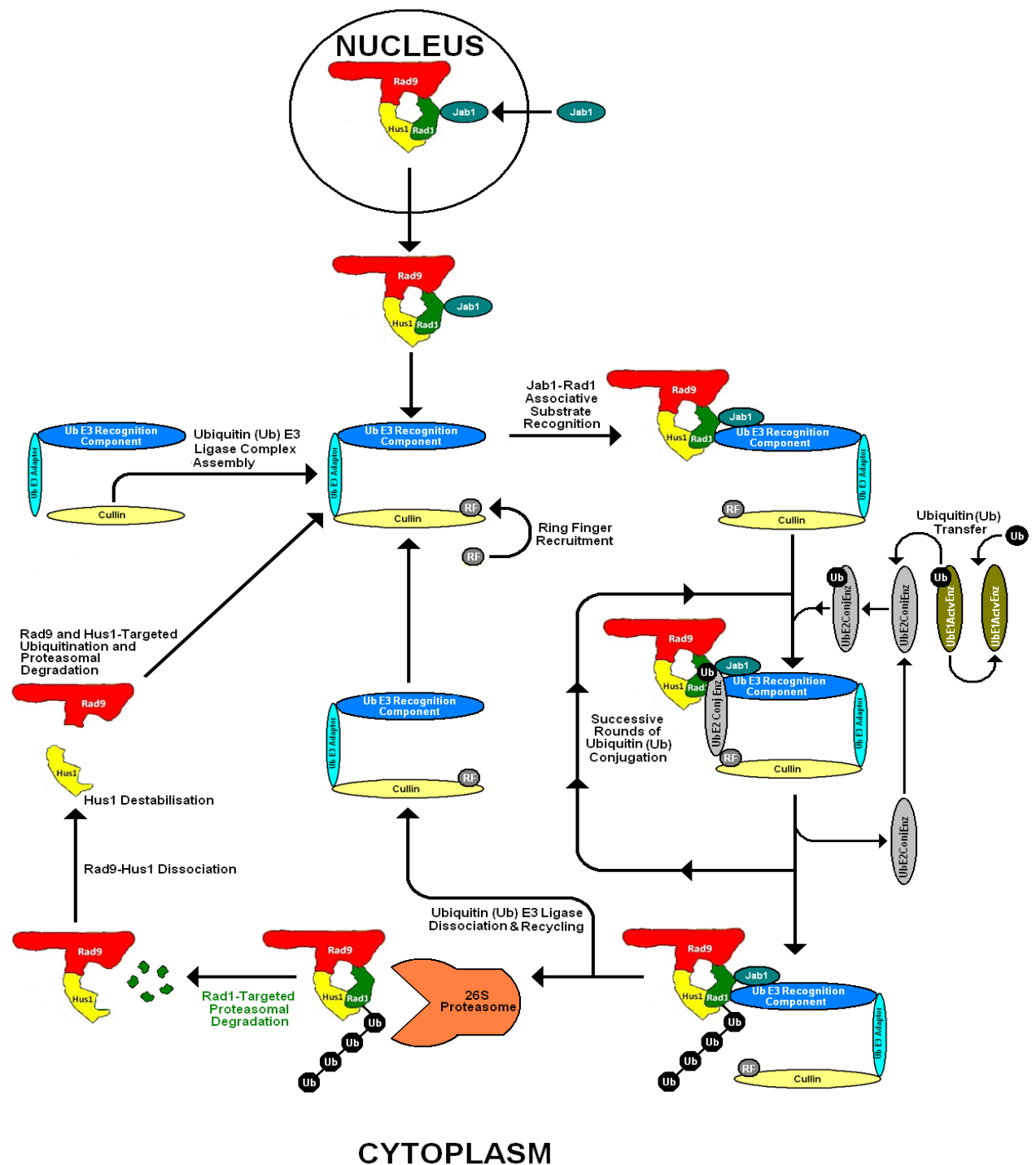
Solid black lines denote associative Jab1 (CSN5)-mediated protein interactions with either LFA-1, MIF1 or LHR which inhibit the transactivation of the AP-1 protein transcription factor (Bianchi E. *et al.*, 2000; Kleemann R. *et al.*, 2000; Li S. *et al.*, 2000; Chamovitz D.A. and Segal D., 2001).

The nuclear CSN complex suppresses the activity of the p27/Kip1 Cyclin-Dependant Kinase Inhibitor (CDKI) protein, via associative interactions with the Jab1 (CSN5) sub-unit, which promotes cell cycle progression via Jab1(CSN5)-mediated translocation and removal of p27/kip1 from the nucleus to the cytosolic environment for targeted proteolytic degradation (Chamovitz D.A. and Segal D., 2001; Fukumoto A. *et al.*, 2004; Kato J.Y. *et al.*, 2006; Tomoda K. *et al.*, 1999; Tomoda K. *et al.*, 2002; Vlach J. *et al.*, 1997).

Cytosolic sequestration of Jab1(CSN5), via associative interactions with the MIF1 protein, prevent formation of the active CSN complex with consequential nuclear accumulation of p27/Kip1 and induction of cell cycle arrest (Chamovitz D.A. and Segal D., 2001; Fukumoto A. *et al.*, 2004; Kato J.Y. *et al.*, 2005; Kleemann R. *et al.*, 2000; Tomoda K. *et al.*, 2002).

Fig 1.60: Rad1-Jab1 Associative “9-1-1” Clamp Degradation Model

[Compiled via Collated Information From: Huang J. *et al*, 2007; Richardson K.S. and Zundel W., 2005]



Associative interaction of Jab1 with the Rad1 sub-unit of the “9-1-1” clamp initiates its translocation from the nucleus to the cytoplasm and primes the complex for ubiquitin-targeted proteasomal degradation (Huang J. *et al*, 2007).

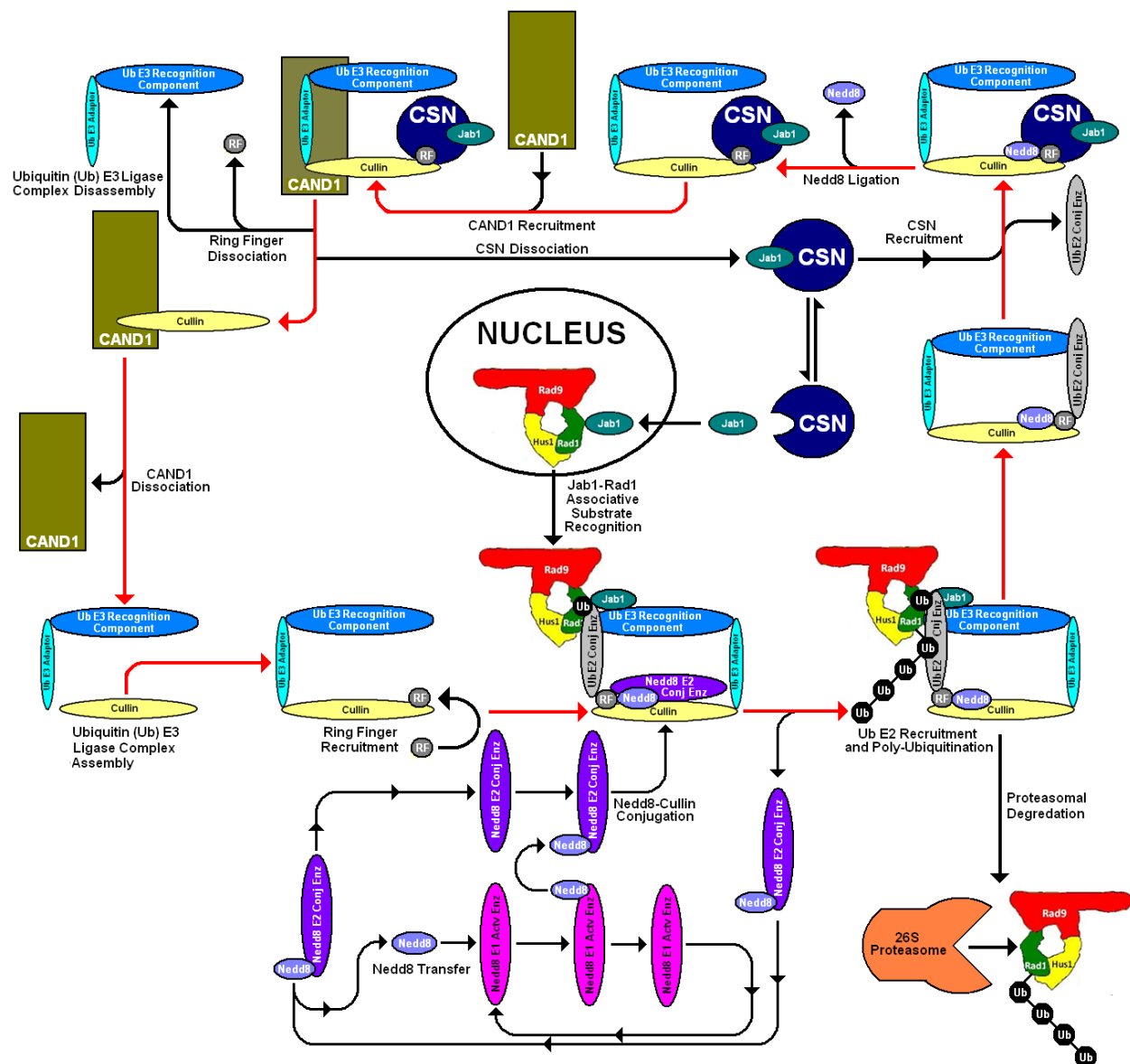
Recruitment of the Cul-E3 complex (comprised of the component assembly of the UBE3-Adaptor, UBE3-Recognition and Cullin proteins) to the “9-1-1” clamp is mediated via associative interactions between the Rad1-Jab1 sub-complex and the UBE3-Recognition component (Huang J. *et al*, 2007; Richardson K.S. and Zundel W., 2005).

Simultaneous recruitment of the Ring Finger (RF) protein component to the resultant ternary complex initiates recruitment and activation of the UBE2-Conjugating Enzyme, with subsequent transfer of ubiquitin from the UBE1 –Activating Enzyme to the UBE3-Ligase enzyme and consequential polyubiquitination of the Rad1 sub-unit (Schwecheimer C., 2004).

Jab1 and the CulE3 assembly dissociate from the resultant Rad9-Rad1(Ub)_n–Hus1 complex, prior to initial degradation of the Rad1-sub-unit by the 26S proteasomal complex, followed by subsequent polyubiquitination and degradation of the Hus1 and Rad9 sub-units respectively (Hirai I. *et al*, 2004; Huang J. *et al*, 2007; Wei N. and Deng X.W., 2003).

Fig 1.61: Jab1-Targeted “9-1-1” Clamp Proteolysis – CSN Regulation

[Compiled via Collated Information From: Huang J. *et al*, 2007; Richardson K.S. and Zundel W., 2005]



Regulation of Cullin activity and Rad1-targeted recognition of the “9-1-1” clamp is mediated via associative interactions the Jab1 (CSN5) sub-unit of the COP9 signalosome complex (CSN) (Fig 1.60, p.137).

The CSN complex also regulates Cullin assembly dissociative turn-over and recycling of the component sub-units via transient interactions with CAND1 (Glickman M.H. *et al*, 1998; Richardson K.S. and Zundel W., 2005; Schwechheimer C., 2004; Wei N. and Deng X.W., 2003).

Dissociation of the Jab1 (CSN5) sub-unit from the COP9 signalosome renders the CSN complex inactive, thereby promoting formation of the Cul-E3 assembly, whilst subsequent nuclear translocation and association of Jab1 to the nucleus with the Rad1 sub-unit of the “9-1-1” clamp initiates cytoplasmic translocation of the Rad9-Rad1-Hus1 complex to the cytoplasm for ubiquitin-targeted proteasomal degradation (Huang J. *et al*, 2007; Wei N. and Deng X.W., 2003; Schwechheimer C., 2004).

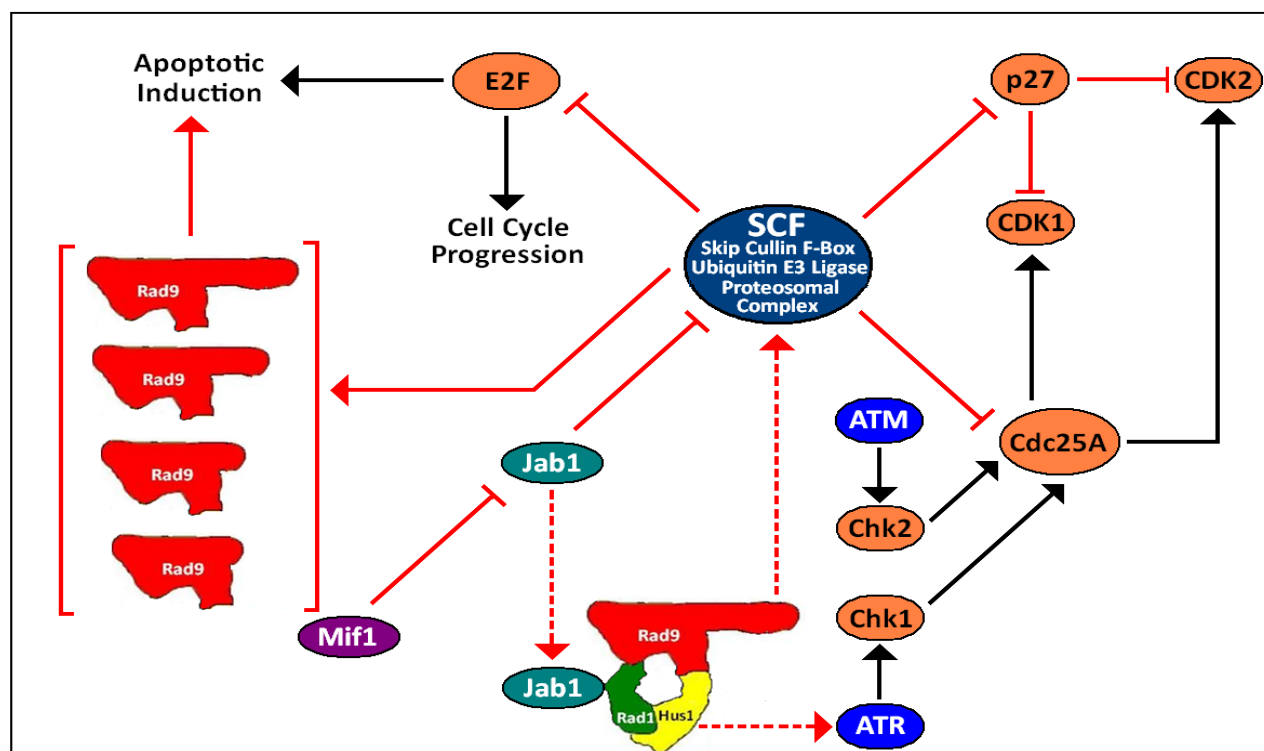
Negative regulation of Ubiquitin E3 ligase activity by the COP9 signalosome is also dependent upon the associative presence of the Jab1 (CSN5) sub-unit within the CSN complex (Richardson K.S. and Zundel W., 2005; Wei N. and Deng X.W., 2003).

Thus, Jab1 (CSN5) association with the Rad1 sub-unit of the “9-1-1” clamp suppresses formation of the active CSN complex with consequential enhancement of UbE3-Ligase activity for sequential degradation of the Rad9-Rad1-Hus1 complex.

The regulation of associative Cullin-E3 complex activities is inhibited via re-cycling of Nedd8, whilst deneddylation of Cullin within the associative “9-1-1” clamp ternary complex is an essential pre-requisite for the initiation of proteasomal degradation of the Rad1 sub-unit and subsequent successive proteasomal degradation of the Hus1 and Rad9 sub-units (Huang J. *et al*, 2007; Richardson K.S. and Zundel W., 2005; Schwechheimer C., 2004; Wei N. and Deng X.W., 2003).

Fig 1.62: Jab1-“9-1-1” Complex-Coupled Cell Cycle Regulation

[Compiled via Collated Information Taken and Adapted From: Bech-Otschir D. *et al*, 2001
 Bech-Otschir D. *et al*, 2002
 Dai Y. and Grant S., 2010
 Earnshaw W.C. *et al*, 1999
 Huang J. *et al*, 2007
 Komatsu K. *et al*, 2000
 Lee M.W. *et al*, 2003
 Nakayama K.I. and Nakayama K., 2006
 Nemaierova A. *et al*, 2007
 Nicholson D.W., 1999
 Yin Y. *et al*, 2004
 Yoshida K. *et al*, 2002



Interaction of the Macrophage Migratory Inhibitory Factor (Mif1) protein with Jab1 (CSN5) co-ordinates the secondary (distal) transducer kinase Chk1- and Chk2- mediated checkpoint signalling responses to genotoxic stress- and/or environmental stress-induced perturbation of DNA replication with SCF (Skip Cullin F-Box) Ubiquitin-targeted proteolytic degradation of key cell cycle effector proteins, such as Cdc25A phosphatase, E2F and the Cyclin-Dependent Kinase Inhibitor (CDKI) p27/Kip1, for appropriate regulation of their respective functional activities in the maintenance of cytological genomic integrity (Nemaierova A. *et al*, 2007).

Thus, the SCF multi-protein ubiquitin proteasomal complex is an integral mechanistic component for the regulated control of transitional G1/S checkpoint activities through to transitional G2/M checkpoint activities (discussed in detail previously in Section 1.2.2, pp.33-65).

Associative Jab1-Rad1 interactions target the “9-1-1” DNA sliding-clamp complex for proteolytic degradation with consequential inhibition of ATR→Chk1-initiated checkpoint signalling responses to DNA damage and/or replication stress.

CSF-mediated degradation of the “9-1-1” complex may also result in the liberation of free Rad9 which in turn may undergo phosphorylation at Y28 by c-Abl and proteolytic cleavage by Caspase 3 into truncated BH3-like domain-retained N-terminal fragments that bind and inactivate apoptotic suppressor proteins, such as Bcl-2 and Bcl-xL, with consequential induction of apoptosis (discussed previously in Section 1.3.2, pp.127-130; Fig 1.57, p.130).

The C-Tail Terminal domain of Rad9, acting independently of the “9-1-1” DNA sliding-clamp complex can also interact with the promoter of the *p21/WAF1* gene and stimulate its transcriptional activity with consequential elevated expression of the p21 protein which elicits sustained G1/S arrest (Fig 1.21, p.57) and apoptotic induction (Fig 1.57, p.130).

Red dotted lines indicate the potential interactive “feed-back” modulatory pathways which impinge upon the respective functional activities of the Jab1 and “9-1-1” DNA sliding-clamp complex.

1.5 Project Brief: Research Background, Aims and Objectives

1.5.1 *S. pombe*: A Versatile Eukaryotic Model Organism

From a historic perspective, tentative exploration into the potential versatility of the fission yeast organism *Schizosaccharomyces pombe* as an experimental homologous eukaryotic model system for the mechanistic investigation of regulatory processes implicated in cell division, growth and development, was undertaken by Murdoch Mitchison and co-workers back in the 1950's (Egel R., 2010; Mitchison J.M., 1990; Nasim A. and Hannah M.A., 1993).

In the 1970's and beyond, Sir Paul Nurse and co-workers incorporated Leupold's genetic-based studies on *S. pombe* (Leupold U., 1958) into the original experimental approaches adopted by Mitchison's research group for significant progressive development and refinement of the established eukaryotic model system prototype (Bartlett R. and Nurse P., 1990; Enoch T. *et al.*, 1992; Enoch T. *et al.*, 1993; Hayles J. and Nurse P., 1986; Kholi J. and Nurse P., 1995; Lee M. and Nurse P., 1988; Moreno S. *et al.*, 1989; Moreno S. *et al.*, 1991; Norbury C. and Nurse P., 1990; Nurse P., 1997a; Nurse P., 1997b).

Subsequent pioneering work contributed by Sir Paul Nurse, in collaboration with independent studies performed by other research teams led by Timothy R. Hunt and Leland H. Hartwell, culminated in the identification of key regulatory proteins of the cell cycle (Hartwell L., 2001; Hunt T., 2002; Nurse P., 2001; Nurse P.M., 2002a; Nurse P.M., 2002b).

Consequentially, these three scientists were jointly awarded the Nobel Prize in Physiology and Medicine for their significant contributions made to the progressive advancement of detailed knowledge of the key biochemical mechanisms implicated in the regulation of the cell cycle (http://nobelprize.org/nobel_prizes_medicine/laureates/2001).

The fission yeast *Schizosaccharomyces pombe* has since become well established universally as a robust experimental eukaryotic model system and it is also widely utilised for the elucidation and “in-depth” study of an extensive range of potential cell cycle regulatory mechanisms which may be implicated in the progressive development of carcinogenic processes (Beretta G.L. and Peregro P., 2005; Bitton D.A. *et al.*, 2011; Deshpande G.P. *et al.*, 2009; Egel R., 2010; Forsburg S.L., 1999; Forsburg S.L., 2003a; Forsburg S.L., 2005; Gómez E.B. and Forsburg S.L., 2002; Henry S.A. and Patton-Vogt J.L., 1998; Nurse P., 2009; Spradling A. *et al.*, 2006; Sugiura R., 2002; Wood V. *et al.*, 2002).

S. pombe is particularly attractive to researchers as an experimental eukaryotic model system of choice by virtue of several key advantageous features of the organism (Egel R., 2010; Nurse P., 2009) – notably;

(i) It is a unicellular fungus of comparatively simple organisation and exhibits a relatively rapid rate of growth (typically, broth culture double-time ~ 3 hours; petri-plate agar colony culture establishment ~ 3 - 4 days – at its normal physiological incubation temperature of 30°C. (Forsburg S.L. *et al.*, 2003c).

(ii) It possesses a conventional eukaryotic cell cycle and a mitotic nuclear division process, compatible to that of mammalian cells, which incorporates a wide range of conserved key functional protein homologues that are implicated in various cell cycle regulatory pathways. (Bitton D.A. *et al.*, 2011; Chen Y. and Sanchez Y., 2004; Deshpande G.P. *et al.*, 2009; Dhillon N. and Hoekstra M.F., 1994; Enoch T. *et al.*, 1992; Forsburg S.L. *et al.*, 1994a; Forsburg S.L., 1994b; Furuya K. and Carr A.M., 2003; Gómez E.B. and Forsburg S.L., 2004; Kelly T.J. *et al.*, 1993; Nurse P., 1977; Nurse P., 2009; Russell P. *et al.*, 1989; Yue M. *et al.*, 2011) – Fig 1.63,p.143; Fig 1.64, p.144.

(iii) It possesses an almost conventional meiotic cell cycle which can be readily exploited for the experimental investigation of recombinant DNA repair mechanisms and the relatively “straight-forward” selective generation of specific “gene knock-out” mutant cross-strains.

(Forsburg S.L. and Rhind P., 2006; Gutz H., 1967; Gutz H. and Doe F.J., 1973;

Hyppa R.W. and Smith G.R., 2009; Nurse P., 2009; Pankratz D.G. and Forsburg S.L., 2005;

Pryce D.W. and McFarlane R.J., 2009) – Fig 1.63, p.143.

(iv) It is relatively easily to manipulate in both classical and molecular genetic-based experimental analyses.

(Breitkreutz B.J. *et al*, 2008; Deshpande G.P. *et al*, 2009; Forsburg S.L., 1993; Forsburg S.L., 1994a; Forsburg 2003b; Forsburg 2003d; Forsburg S.L. and Nurse P., 1991; Forsburg S.L., 2001; Forsburg S.L. and Sherman D.A., 1997; Kelly T.J. *et al*, 1993; Kumar R. and Sing J., 2006; Lyne R. *et al*, 2003; Moreno S. *et al*, 1991; Moreno S. *et al*, 1989; Nurse P., 2009; Siam R. *et al*, 2004; Watson A.T. *et al*, 2008; Wood V. and Bähler J., 2002).

[http://biosci.osu.edu/~nile/nurse_lab_manual]

(v) A full range of versatile reverse genetics-based protocols has been established for the organism.

(Alfa C. *et al*, 1993; Egel R., 2010; Nurse P., 2009; Sabatinos S.A. and Forsburg S.L., 2010)

[http://biosci.osu.edu/~nile/nurse_lab_manual]

(vi) Complete library sets of *S. pombe* strains, which comprise specific genetically-defined mutants for a wide range of equivalent types of key functionally-conserved mammalian homologous proteins that are implicated in various cell cycle regulatory processes, are well established and commercially available.

(<http://pombe.bioneer.co.kr>; Nurse P., 2009; Spirek M. *et al*, 2010).

Fig 1.63: Overview of the Fission Yeast *S. pombe* Life-Cycle

[Taken and Adapted From: <http://www-rfc.usc.edu/~forsburg/cclecture.html>]

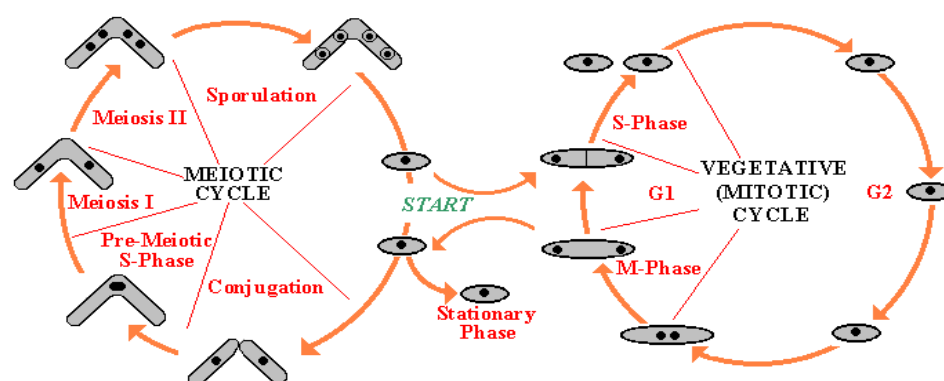


Table 1.5: *H. sapiens* and *S. pombe* Functional Protein Homologues

[Compiled via Collated Information From:

Chen Y. and Sanchez Y., 2004; Christmann M. *et al*, 2003; Ellison V. and Stillman B., 2003; Furuya K. and Carr A.M., 2003; Harrison J.C. and Haber J.E., 2006; Lieberman H.B. *et al*, 1996; Melo J. and Toczyski D., 2002; Niida H. and Nakanishi M., 2006; Nyberg K.A. *et al*, 2002; Volkmer E. and Karnitz L.M., 1999; Yue M. *et al*, 2011]

<i>H.sapiens</i>		<i>S. pombe</i>	
RAD9	"9-1-1" Sensory DNA Clamp Complex	Rad1	"9-1-1" Sensory DNA Clamp Complex
RAD1		Rad1	
HUS1		Hus1	
RAD17	RFC-Like "9-1-1" Clamp DNA Loading Complex (RSR)	Rad17	RFC-Like "9-1-1" Clamp DNA Loading Complex (RSR)
RFC2		Rfc2	
RFC3		Rfc3	
RFC4		Rfc4	
RFC5		Rfc5	
ATR		Rad3	
ATRIP		Rad26	
CLASPIN		Mrc1	
TopBP1		Rad4	
BRCA1		Crb2	
CHK1		Chk1	
CHK2		Cds1	
CDC25A, B, C		Cdc25	
WEE1		Wee1	
MYT1		Mik1	
CDK2		Cdc2	
14-3-3 σ		Rad24	

The meiotic life-cycle is particularly useful for generation of experimental *S.pombe* cross-strains, such as double knock-outs for elucidation of specific protein-protein interactions within DNA damage response pathways and investigation of recombinational DNA repair mechanisms (Top Left Figure).

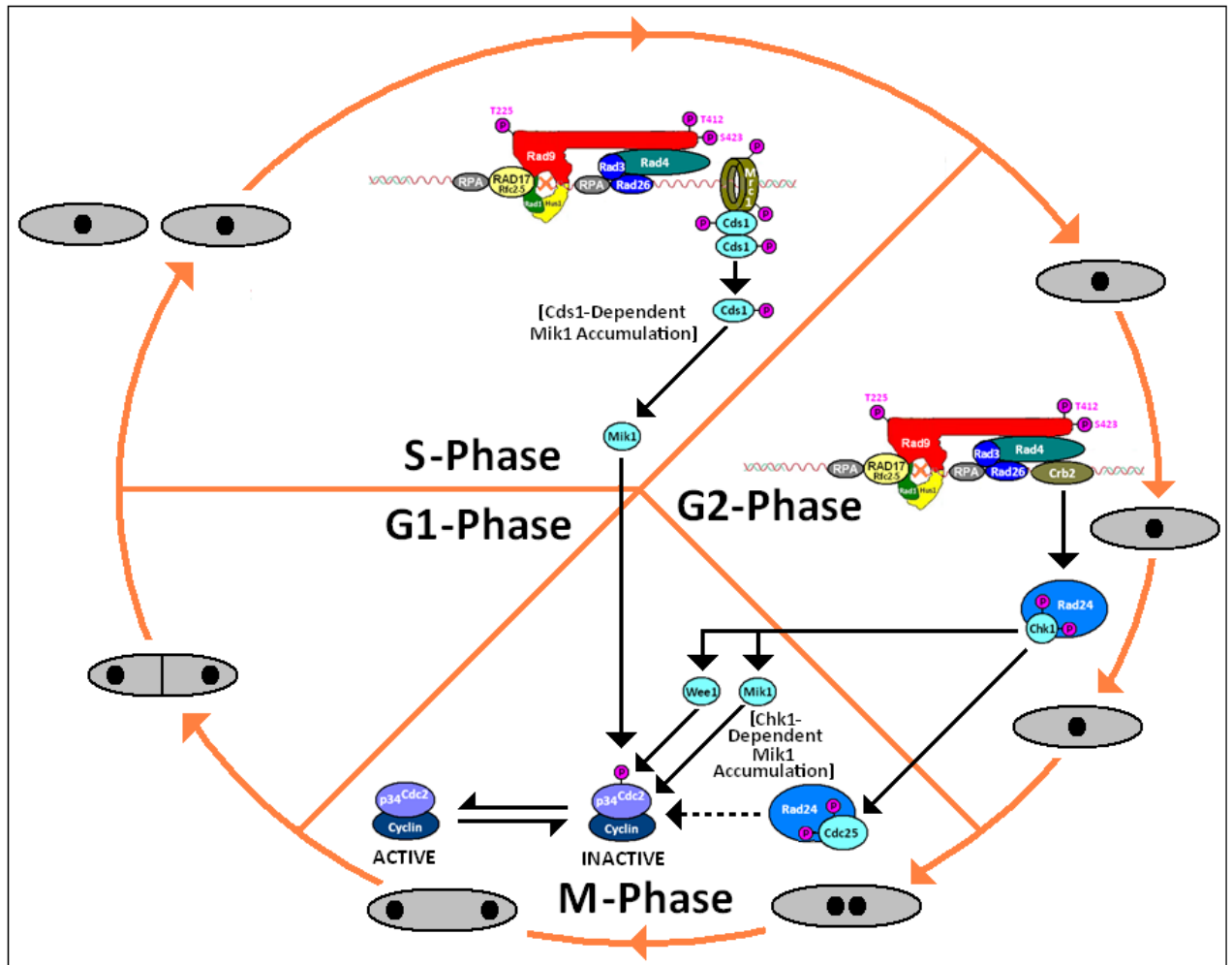
The mitotic cycle is a useful experimental eukaryotic model for elucidation of novel protein interactive signalling events in cell cycle regulatory DNA damage checkpoint pathways (Fig 1.64, p.144) which may be implicated in specific mechanisms of carcinogenesis and neoplastic transformation in Human cells respectively (Top Right Figure).

A wide range of equivalent functional proteins, implicated in DNA damage response pathways, are highly conserved between mammalian and yeast cells (selected key examples tabulated above).

Fig 1.64: Examples of Key Conserved Checkpoints in *S. pombe*

[Collative Figure Adaptation From: Furuya K. and Carr A.M., 2003

<http://www-rfc.usc.edu/~forsburg/cclecture.html>]



Conserved equivalent homologous protein functions implicated in the mammalian mitotic cell cycle checkpoint signalling responses to different types of DNA damage and/or replication stress can be conveniently studied, via appropriate experimental genetic manipulation, in the eukaryotic model organism *Schizosaccharomyces pombe* (Abraham R.T., 2001; Bitton D.A. *et al*, 2011; Deshpande G.P. *et al*, 2009; Dhillon N. and Hoekstra M.F., 1994; Enoch T. *et al*, 1992; Forsburg S.L., 2005; Furuya K. and Carr A.M., 2003; Nurse P. *et al*, 2009).

A comparative tabulated summary of conserved key equivalent protein functional homologues, implicated in mitotic checkpoint signalling responses, is provided on the previous page (Table 1.5, p.143).

The equivalent, conserved human Rad9-mediated mitotic checkpoint signalling pathways have been discussed in detail previously (Section 1.2.2, pp.33-65 – to which the reader is referred for comparative explanation of the equivalent *S. pombe* mitotic checkpoints depicted in the figure above).

1.5.2 The Initial Discovery of “spRad9-S”: A Novel spRad9 Variant

The *S. pombe* experimental eukaryotic model system was instrumental in the initial identification and functional characterisation of the human Rad9 protein in mitotic DNA damage responsive checkpoint pathways (Caspari T. *et al.*, 2000a; Caspari T., 2000b; Lieberman H.B. *et al.*, 1992; Lieberman H.B. *et al.*, 1996; Murray J.M. *et al.*, 1991; Subramani S., 1991).

The potential existence of a novel truncated variant of the spRad9 protein (termed “spRad9-S”) was discovered by Caspari T. and co-workers during the course of their investigative SDS-PAGE and Western Blot experiments, performed on precipitated protein extracts acquired from cultures of different strains of *S. pombe* cells which were genetically-engineered to express a C-terminal haemagglutinin (HA) epitope-tagged version of the spRad9 protein (spRad9-c3xHA) – Fig 1.65, p.147.

Subsequent “follow-up” experimental work revealed that the induction of “spRad9-S” expression only occurred at elevated temperatures, whilst no inducible expression of “spRad9-S” was observed in *S. pombe* strain cultures exposed to varying doses of U.V. light or ionising radiation (Caspari T. *et al.*, unpublished data) – Fig 1.65, p.147.

The research team also found that significantly lower levels of “spRad9-S” were expressed in precipitated protein extracts acquired from cell cultures of an isolated temperature-sensitive mutant *S. pombe* strain, *TCY282*, which was also genetically-engineered to express spRad9-c3xHA (Caspari T. *et al.*, unpublished data) – Fig 1.66, p.148.

The researchers also noted that the approximate molecular weight of the truncated spRad9-S variant was 40kDa (Fig 1.65, p. 147), which they postulated could be equated to a loss of the first 49 amino acids from the N-Terminus of the full-length Rad9 protein and may be correlated with a potential alternative translation AUG codon start site they identified within the *rad9* gene at Methionine 50 (Caspari T. *et al*, unpublished data).

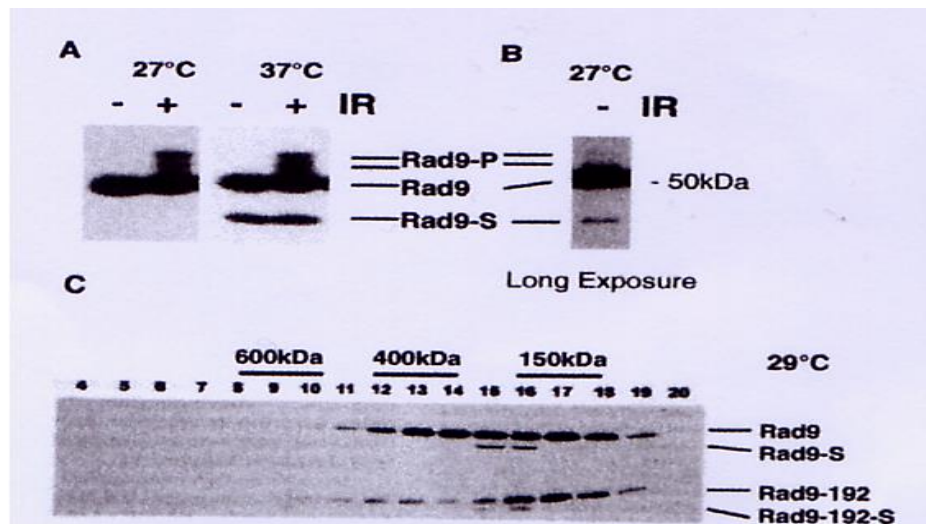
If these hypothetical deductions are correct, then the expressed “spRad9-S” protein variant may be an M50 AUG start site-encoded alternative translation product which would be unable to form a “9-1-1” clamp-like complex as a consequence of truncation of the spRad9 PCNA-like I domain via loss of the first 49 N-Terminal amino acids that form key associative interactions with the Rad1 protein (Caspari T. *et al*, unpublished data).

The researchers also observed expression of “spRad9-S” in comparative size-exclusion chromatographic analyses of protein extracts, acquired from an *S. pombe* strain expressing the wild-type Rad9-HA and a mutant *S. pombe* strain expressing the L196P site-directed PCNA-like domain mutagenised version of the Rad9-HA protein, *Rad9-192* – which cannot form associative Rad1 and Hus1 toroidal DNA sliding-clamp protein-protein interactions (Caspari T. *et al*, 2000a; Caspari T. *et al*, 2000b) – Fig 1.65, p.147.

Taken together, these tentative experimental data indicated the potential existence of a smaller truncated variant of the *S. pombe* Rad9 protein, whose regulated expression is independent from both that of the full-length Rad9 protein (Fig 1.66, p.148) and the heterotrimeric PCNA-like Rad9-Rad1-Hus1 toroidal DNA damage sensory sliding-clamp (Fig 1.65, p.147) respectively.

The data also indicate that this truncated “spRad9-S” protein variant may possess potential novel independent functions which operate outside of the canonical “9-1-1” clamp complex.

Fig 1.65: SDS-PAGE & HPLC-SEC Fractionation Analyses



A: Experimental Western blots total protein extracts acquired from *S. pombe* cells expressing the C-terminal epitope-tagged full-length spRad9-3xHA protein variant, resolved via 10% SDS-PAGE, transferred onto nitrocellulose membranes which were then probed with an Anti-HA antibody (Caspari T. [et al.](#), 2000a; Caspari T. [et al.](#), 2000b).

The experimental data are indicative of induction of “spRad9-S” in response to elevated thermal stress. Comparative studies with an administered 250Gy dose of ionising radiation (IR) are indicative that the spRad9 C-tail terminal domain is phosphorylated in response to IR-induced DNA damage and as a consequence the relative molecular mass of the protein is increased with resultant retarded migration on the SDS-PAGE gel respectively (Caspari T. [et al.](#), 2000a; Caspari T. [et al.](#), 2000b).

B: Prolonged probing of the total protein extract acquired from *S. pombe* spRad9-3xHA cells grown at 27°C facilitates detection of a relatively lower concentration of “spRad9-S” indicative of constitutive expression of “spRad9-S” (Caspari T. [et al.](#), 2000a; Caspari T. [et al.](#), 2000b).

Furthermore, a relatively low concentration of the SDS-PAGE retarded phosphorylated form of the full-length spRad9 protein was detected – indicative of endogenous constitutive phosphorylation of the full-length spRad9 protein respectively (Caspari T. [et al.](#), 2000a; Caspari T. [et al.](#), 2000b).

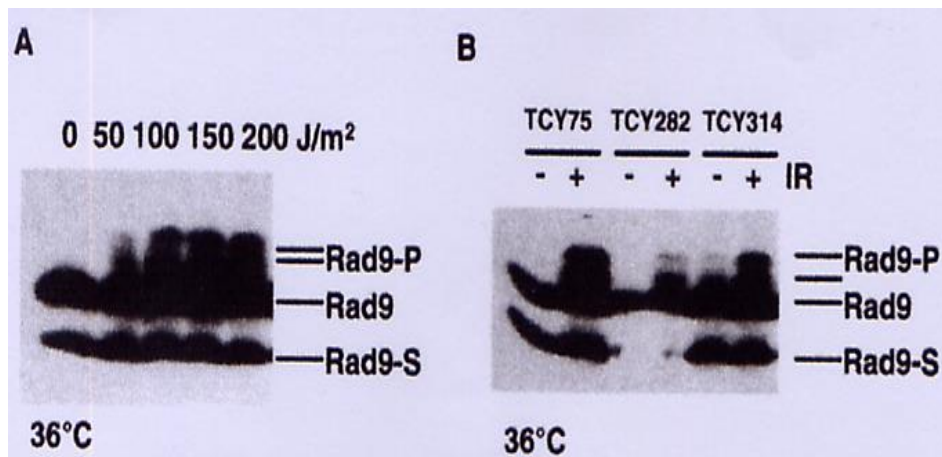
C: Size Exclusion Chromatographic data of total protein cell extracts acquired from *S. pombe* strains, incubated at 29°C, expressing C-terminal 3xHA tagged variants of full length spRad9 and the full-length spRad9-192 (L196P) mutant proteins (samples run on a Superdex 200HR 10/30 column) (Caspari T. [et al.](#), 2000a; Caspari T. [et al.](#), 2000b)

[The L→P mutation at amino acid position 196, within the full-length spRad9-192 mutant variant, is situated in a PCNA-like domain and impairs formation of the 450kDa “9-1-1” heterotrimeric toroidal associative Rad9-Rad1-Hus1 DNA “sliding-clamp” complex]

The majority of the expressed spRad-S-3xHA protein variant was eluted in fractions 15 and 16 even under conditions that prevent formation of the 9-1-1 complex, as evident in the spRad9-192 fractions above (Caspari T. [et al.](#), 2000a; Caspari T. [et al.](#), 2000b).

Thus the experimental data are indicative that expression of the novel truncated “spRad9-S” protein variant is independent of 9-1-1 complex formation respectively (Caspari T. [et al.](#), 2000a; Caspari T. [et al.](#), 2000b).

Fig 1.66: Comparative SDS-PAGE Western Blot Analyses



A: Western blot analyses of total protein extracts acquired from *S. pombe* cells expressing the full-length Rad9 C-terminal 3xHA epitope-tagged protein variant, incubated at 36°C for 90 minutes and then exposed to variable doses of U.V. radiation. (Caspari T. *et al.*, Unpublished Data).

The experimental data are indicative of an absence of a significant dose-response relationship between “spRad9-S” expression and U.V. radiation dose respectively (Caspari T. *et al.*, Unpublished Data).

Thus expression of the novel truncated “spRad9-S” protein variant is induced in response to elevated temperature/heat shock, but not in response to U.V. irradiation respectively. (Caspari T. *et al.*, Unpublished Data).

B: Comparative Western blot analyses of total protein cell extracts acquired from three *S. pombe* strains, expressing the full-length Rad9 C-terminal 3xHA epitope-tagged protein variant, incubated at 36°C for 90 minutes prior to exposure to a 450Gy dose of ionising radiation or no irradiation in the case of the experimental controls respectively (Caspari T. *et al.*, Unpublished Data).

TCY282 and TCY314 are the respective uncharacterised conditional temperature-sensitive *S. pombe* mutant strains (Caspari T. *et al.*, Unpublished Data).

TCY282 cells express normal levels of the full-length Rad9 protein, but abnormally low, suppressed levels of the novel truncated “spRad9-S” protein variant and thus indicative that the regulated expression of the novel truncated “spRad9-S” protein variant is independent of that of the full-length Rad9 protein. (Caspari T. *et al.*, Unpublished Data).

The SDS-PAGE gel-retarded phosphorylated forms of the full-length Rad9 protein are clearly detected in the absence and presence of ionising radiation, as a consequence of the increased molecular weight of the protein compared to the unphosphorylated form respectively (Caspari T. *et al.*, Unpublished Data)

The data are indicative that phosphorylation of the full-length Rad9 protein is both an endogenous constitutive process and inductive process in response to ionising radiation respectively. (Caspari T. *et al.*, Unpublished Data).

1.5.3 Ph.D. Project Experimental Aims and Objectives

The aim of this Ph.D. project was the initial biochemical characterisation of the novel “spRad9-S” truncated protein variant with specific emphasis on its mechanism of expression and potential functional/regulatory roles in DNA replication stress and/or DNA damage response pathways.

Thus, the experimental objectives of this Ph.D. project were concentrated on four defined areas of laboratory-based investigation – notably;

- (i) Elucidation of the mechanism of expression of the “spRad9-S” truncated protein variant.
- (ii) Comparative assessment of the relative sensitivity of *S. pombe* cells, engineered for the exclusive expression of the “spRad9-S” truncated variant towards different types of induced environmental stress and induced DNA damage cytological conditions.
- (iii) Genetic, proteomic and biochemical “deciphering” of potential signalling pathways mediated exclusively by the “spRad9-S” truncated protein variant in response to one or more specific types of induced environmental stress and/or induced DNA damage cytological conditions.
- (iv) Comparative analyses of the sub-cellular localisation and/or “translocational trafficking” of the “spRad9-S” truncated protein variant under normal, DNA damage and environmental stress imposed cytological conditions.

The experimental data acquired from the studies performed on the novel “spRad9-S” truncated protein variant in this Ph.D. project may provide valuable insights into potential novel independent functions of the human Rad9 protein, which act outside of the canonical Rad9-Rad1-Hus1 complex.

In stark contrast to the extensive functional characterisation of the full-length human Rad9A protein, very little information exists on the biochemical roles of the full-length human Rad9B protein paralogue and its expressed truncated isoform variants (Fig 1.3, p.9).

Intriguingly, comparative *in silico* alignment analyses of the human Rad9B isoform amino acid sequences with the hypothetical “spRad9-S” truncated protein variant sequence indicate a potential significant degree of equivalent amino acid sequence homology between “spRad9-S” and truncated Rad9B isoform 2 (Uniprot ID: Q6WBX8-2 and truncated Rad9B isoform 3 (Uniprot ID: Q6WBX8-3) respectively (Caspari T. and Janes S., unpublished data).

The experimental work undertaken in this Ph.D. project may therefore also provide useful information on the potential functions of the equivalent human Rad9B truncated isoforms, which remain unknown to date.

The initial biochemical characterization of the “spRad9-S” truncated protein variant, which constitutes the main research focus of this Ph.D. project, may culminate in the identification of potential novel Rad9-mediated checkpoint signalling functions which could be implicated in progressive stages of carcinogenesis and/or novel mechanisms of acquired tumour resistance towards particular anti-cancer clinical treatment regimens.

Chapter 2

Materials and Methods

2.1 Sourced Materials – Purchase Details

Supplier

Materials/Apparatus/Reagents

Abcam
330 Cambridge Science Park
Cambridge
CB4 0FL
U.K.

Monoclonal antibody – Cat No.:ab5467
Anti-CDK1
(*S.pombe* Cdc2 cross-reactive specificity)
Clone: Y100.4
Form: Myeloma Sp2
Host: Mouse
Isotype: IgG2b
[Ab] = 1.1mg/mL

Acros Organics
Geel
Belgium

Boric acid
Trichloroacetic acid

Alpha Laboratories Ltd
40 Parham Drive
Eastleigh
Hampshire
SO50 4NU
U.K.

1-200 μ L Gel loading pipette tips

Bassaire Ltd
Duncan Road
Park Gate
Southampton
SO31 1 ZS
U.K.

Model K4V laminar flow workstation

BDH AnalR
VWR International Ltd
Poole
Dorset
BH15 1TD
U.K.

Chloroform
Ethanol
1M HCl (aq)
Glacial acetic acid
Isopropanol
KOH pellets
MgCl₂.6H₂O
MgSO₄.7H₂O
NaH₂PO₄
Na₂H₂PO₄
Sodium dodecylsulphate
Sodium thiosulphate

Supplier

BioFX Laboratories
10715 Red Run Boulevard
Suite 114
Owings Mills
MD 21117
U.S.A

c/o Bioquote Ltd
(U.K. and Ireland Distributors
for BioFX Laboratories)
The Raylor Centre
James Street
York
YO10 3DW
U.K.

Bioline
16 The Edge Business Centre
Humber Road
London
NW2 6EW

Bio-Rad Laboratories Ltd
Bio-Rad House
Maxted Road
Hemel Hempstead
Hertfordshire
HP2 7DX
U.K.

Cleaver Scientific Ltd
Unit 4
Triton Park
Brownsover Road
Swift Valley
Rugby
Warwickshire
CV21 1SG

Cole-Palmer Instrument Company Ltd
Unit 3
River Brent Business Park
Trumpers Way
Hanwell
London
W7 2QA
U.K.

Materials/Apparatus/Reagents

Chemiluminescent sensitive HRP
Microwell and/or membrane substrate
2x 110mL kit

α -select chemically-competent *E.coli* cells
Genotype:
*F⁻ deoRendA1recA1gyrA96hsdR17(rk⁻ mk⁺)phoA
supE44thi-1Δ(lacZYA-argF)U169Φ80δlacZΔM15*

Bio-Rad Gel Doc 2000 white light and U.V.
imager system
Bio-Rad Mini-Protean® Tetra cell
Bio-Rad Protean® IEF cell

Multiple small SDS-PAGE gel western
blotting equipment

Binder incubators

Supplier

Covance
5858 Horton Street
Suite 500
Emeryville
California
94608
U.S.A.

DakoCytomation
Dako U.K. Ltd
Angel Drove
Ely
Cambridgeshire
CB7 4ET
U.K.

Dr. Adam T. Watson
Genome Damage and Stability
Centre
School of Life Sciences
University of Sussex
Falmer
Sussex
BN1 9QG
U.K.

EMD Chemicals Inc.
480 South Democrat Road
08027 Gibbstown
U.S.A.

Finnzymes OY
Keilaranta 16A
02150
Espoo
Finland

Fisher Scientific Ltd
Bishop Meadow Road
Loughborough
Leicestershire
LE11 5RG
U.K.

Fistream International Ltd
Monarch Way
Belton Park
Loughborough
Leicestershire
LE11 5XG
U.K.

Materials/Apparatus/Reagents

Monoclonal Anti-Body HA.11
Clone: 16B12
Form: Ascites
Host: Mouse
Isotype: IgG1
[Ab] = 2-3 mg/mL

Polyclonal rabbit anti-mouse
immunoglobulins/HRP

S. pombe Cre-RMCE base-strain plasmid pAW1
S. pombe Cre-RMCE donor plasmid pAW8

Calbiochem® protein G plus/protein A agarose
beads suspension (Product No. IP05)

Phusion high fidelity DNA polymerase (2U/μL)
5x Phusion polymerase GC buffer

Methanol (HPLC Grade)
Stuart heat-stir magnetic stirrer and stirrer bars

Calypso model WCA004 MH1.7/WCA300 RTA9
Coupled distilled/de-ionised purified mains water
supply treatment system

Supplier

Fuji Photofilm (Europe) GmbH
Heesenstrasse
D-40549
Dusseldorf
Germany

GE Healthcare U.K. Ltd
(Formerly Amersham Biosciences U.K. Ltd)
Amersham Place
Little Chalfont
Buckinghamshire
HP7 9NA
U.K.

Genetic Research Instrumentation Inc.
Gene House
Queenborough Lane
Rayne
Braintree
Essex
CM77 6TZ
U.K.

GeneFlow Ltd
Fradley Business Centre
Wood End Lane
Fradley
Staffordshire
WS13 8NF
U.K.

Greiner Bio-One Ltd
Stroudwater Business Park
Brunel Way
Stonehouse
Gloucestershire
GL10 3SX
U.K.

Hanna Instruments Ltd
Pages Industrial Park
Edenway
Leighton Buzzard
LU7 4AD
U.K.

Materials/Apparatus/Reagents

Fuji blue medical X-Ray film SuperRX

ÄKTA design ÄKTA-*FPLC* HPLC system
Destreak rehydration buffer solution
ECL Plus western blotting detection system kit
High molecular weight protein standard kit
(for internal standard calibration of HPLC-SEC)
Hybond-C extra nitrocellulose blotting membrane
Hyperfilm ECL
ImmobilineTMDryStrip pH3-10 11cm
IPG ampholytes buffer pH 3-10
Superdex 200HR 10/30 size exclusion HPLC
chromatographic column (for HPLC-SEC)

Dark ReaderTM CE transilluminator DR-45M
230v, 50Hz, 9W
(Clare Chemical Research Inc., Dolores CO81323)

Norgen Biotek HighRanger Plus 100 Bp DNA
marker ladder (100Bp to 10000Bp)
Mini-PAGE vertical sub-system
Maxi-PAGE vertical Sub-system
Omni-PAGE mini-blotting unit
Omni-PAGE maxi-blotting unit
Techne TC-312 PCR thermocycler

Plastic screw-cap centrifuge tubes (15mL; 50mL)
15mL capacity glass culture test tubes
1.5mL capacity plastic eppendorf microfuge tubes
1.5mL capacity screw cap plastic microfuge tubes
Petri-plates
Pipette tips
Plastic spectrophotometer cuvettes
Plastic syringes (various sizes)

pH211 microprocessor pH meter

Supplier

Hawksley Medical and Laboratory
Equipment
Marlborough Road
Lancing Business Park
Lancing
Sussex
BN15 8TN
U.K.

ID Labs Inc.
UWO Research Park
100 Collip Circle
Suite 117
London
ON
Canada
N6G 4X8

Invitrogen Ltd
3 Fountain Drive
Inchinnan Business Park
Paisley
PA4 9RF
U.K.

Jackson ImmunoResearch Europe Ltd
Unit 7
Acorn Business Centre
Oaks Drive
Newmarket
Suffolk
CB8 7SY
U.K.

Jencons Scientific Ltd
Cherrycourt Way Industrial Estate
Stanbridge Road
Leighton Buzzard
Bedfordshire
LU7 8UA
U.K.

Jet-X-Ray
Unit 7
Thurston Industrial Estate
Jerrard Street
Lewisham
London
SE13 7SH
U.K.

Materials/Apparatus/Reagents

Hawksley thoma double cell clear sight counting
chamber (haemocytometer)

IDPure™ spin column DNA Gel extraction kit
IDPure™ spin column plasmid DNA miniprep kit

PCR primer oligonucleotides

Goat affinipure anti-mouse IgG
HRP-conjugated light-chain specific
antibody – 115-035-175

Agarose gel electrophoresis equipment
Consort EV231 electrophoretic power pack
Jencons-PLS SorvallR Legend T centrifuge

MI-5 X-Ray film processor

Supplier

Keison Products
PO Box 2124
Chelmsford
Essex
CM1 3UP
U.K.

Lab M Limited
Topley House
52 Wash Lane
Bury
Lancashire
BL9 6AS
U.K.

Leica Microsystems CMS GmbH
Ernst Leitz-Str. 17-37
355 Wezlar
Germany

Melford Laboratories Ltd
Bildeston Road
Chelsworth
Ipswich
Suffolk
IP7 7LE
U.K.

Merck
VLR International Ltd
Hunter Boulevard
Magna Park
Lutterworth
Leicestershire
LE17 4XN
U.K.

Materials/Apparatus/Reagents

PTR-60 360° vertical multi-functional rotator

Agar for petri-plate media

Type F oil immersion liquid
Leitz SM-LUX fluorescent microscope
(Leitz-Wezlar)

40% Acrylamide:bisacrylamide (37.5:1 ratio)
Agarose high-strength electrophoresis grade
(molecular biology grade)
Ampicillin (sodium salt)
Disodium EDTA
5-Fluoro-orotic acid
Glycerol (DNAse, RNAse, protease free)
Glycine
KCl
Lactose
Malt extract
NaCl
Sorbitol
TEMED
Tris base (Ultra-pure)
Tryptone
Tween20
Yeast extract
Yeast nitrogen base

Isoamylalcohol

Supplier

Millipore (UK) Ltd
Units 3 and 5
The Court Yards
Hatters Lane
Watford
Hertfordshire
WD18 8YH
U.K.

National Diagnostics
Unit 4
Fleet Business Park
Itlings Lane
Hessle
Hull
HU13 9LX
U.K.

New England Biolabs (UK) Ltd
New England Biolabs Inc.
240 County Road
Ipswich
MA01938-2723

NGS Precision Cells
195 Central Avenue
Suite G
Farmingdale
NY11735

Perbio Science UK Ltd
Unit 9
Atley Way
North Nelson Industrial Estate
Cramlington
Northumberland
NE23 1WA
U.K.

PHOTOSOL Ltd
Hubert Road
Brentwood
Essex
CM14 4JE
U.K.

Materials/Apparatus/Reagents

Millipore ultra-pure water supply system

Bromophenol blue
ProtoMarkers™ pre-stained protein markers
Ultra-pure ammonium persulphate
Ultra-pure protogel
30% (w/v) Acrylamide:0.8% (w/v) bisacrylamide
(37.5:1 ratio)

SpeI restriction endonuclease (10U/μL)
10x SpeI buffer (10x NE Buffer 2)
Phusion high fidelity polymerase (2U/μL)
(Finnzymes)
5x Phusion polymerase GC buffer (Finnzymes)

701M 100μL capacity quartz microcuvette
(10mm sub-micro black masking)

UVP CL-1000 Ultra-violet cross-linker

Film processor developing reagents

Supplier

Premier International (UK) Foods Ltd
Bridge Road
Long Sutton
Spalding
Lincolnshire
PE12 9EQ
U.K.

Prior Clave
129/131 Nathan Way
Woolwich
London
SE28 0AB
U.K.

Promega Corporation
2800 Woods Hollow Road
Madison
WI 53711-5399
Madison
U.S.A.

Roche Diagnostics Ltd
Charles Avenue
Burgess Hill
West Sussex
RH15 9RY
U.K.

Santa Cruz Biotechnology Inc.
Bergheimer Str. 89-2
69115 Heidelberg
Germany

Sanyo Gallenkamp Plc
Monarch Way
Belton Park
Loughborough
Leicestershire
LE11 5XG
U.K.

Materials/Apparatus/Reagents

Marvel milk protein powder

Midas 56 Prior Clave Autoclave

Calf intestinal alkaline phosphatase (1U/ μ L)
10x "CIAP" buffer
SphI restriction endonuclease (10U/ μ L)
10x SphI buffer K
T4 DNA ligase (3U/ μ L)
10x T4 DNA ligase buffer
100 μ L (100mM) dNTPs (dATP, dGTP, dCTP, dTTP)

Complete mini protease inhibitor cocktail tablets
RNase A (100mg pure dry bovine pancreatic extract)

c-Myc antibody (9E10)
sc-40
Epitope 408-439 (h)
Isotype: Mouse IgG₁
[200 μ g/mL]

Sanyo orbisafe orbital incubators
(incubator shakers)
Sanyo SP BIO spectrophotometer
Hawk 15/05 refrigerated bench top microfuge

Supplier

Sartorius UK
Longmead Business Centre
Blenheim Road
Epsom
KT19 9QQ
U.K.

Scientific Laboratory Supplies Ltd
Wilford Industrial Estate
Ruddington Lane
Wilford
Nottingham
NG11 7EP
U.K.

Sigma-Aldrich Chemical Company Ltd
Fancy Road
Poole
Dorset
BH12 4QH
U.K.

Materials/Apparatus/Reagents

Acculab ALC-210.4 balance
Sartorius TE212 balance

DNase and RNase Free Sterile PCR Tubes
Small SDS-PAGE gel Western Blotting Tank
Apparatus (Cleaver Scientific Ltd)
Stuart Scientific Disruptor Genie
Stuart Scientific Drive Unit STR8 Platform Rocker
Stuart Scientific Gyro-Rocker SSL3
Stuart Scientific Vortex Genie-2
3MM Whatman CHR Chromatography Paper
Whatman 0.2µm Sterile Filter Units

Adenine hemi-sulphate
β-Mercaptoethanol
β-Microglobulin
CaCl₂·2H₂O
Caffeine
Calcofluor white MR2/fluorescent brightner 28
CoCl₂·6H₂O
CuSO₄·2H₂O
Cycloheximide
D-(+)-Glucose
Dimethylsulphoxide
Dithiothreitol
Ellipticine
Ethidium bromide (Fluka)
Etoposide
FICOLL400 (Fluka)
G418 antibiotic
GenElute™ plasmid miniprep kit
“General glassware” (flasks and beakers)
Glass beads (425-600µm diameter/30-40 U.S. Sieve)
HEPES
Hoechst 33258
Hoechst 33342
Hydrogen peroxide
Hydroxylamine
Hydroxyurea (Fluka)
Iodoacetamide
L-Leucine
Lithium acetate
Lyticase (200U/mg lyophilised powder preparation)
Magnetic stirrer bars
Menadione
Metal “hockey-stick” flame spreaders
Methylmethanesulphonate
MnCl₂·7H₂O
Mitomycin C
N-Ethylmaleimide (NEM)

Supplier

Sigma-Aldrich Chemical Company Ltd
Fancy Road
Poole
Dorset
BH12 4QH
U.K.

VWR International Ltd
Hunter Boulevard
Lutterworth
Leicestershire
LE17 4XN

Wolf Laboratories Ltd
Colenso House
1 Deans Lane
Pocklington
York
YO42 2PY

Yeast Genetic Resource Centre
Osaka City University
Japan

Materials/Apparatus/Reagents

NiSO₄.6H₂O
N-methyl-N'-nitrosoguanidine
Nonidet P40 (NP-40)
4-Nitroquinoline-1-oxide
Phenol (Fluka)
p-Phenylenediamine
Phenylmethanesulphonyl fluoride
Phleomycin (stabilised Cu²⁺ complex preparation)
S-(+)-camptothecin
Sodium azide
Sodium citrate
Sodium fluoride
Sodium metabisulphite
Sodium nitopruside
Sodium orthovanadate (Na₃VO₄)
t-Butylhydroperoxide
Thiabendazole
Trisodium phosphate (Na₃PO₄)
Triton X-100 (molecular biology grade)
Uracil

Glass microscope slide cover slips (18mm x 18mm)
Glass microscope slides (75mm x 25mm x 1mm)

CETI magnum B binocular light microscope

S. pombe gene-deleted and gene-mutated strains

2.2 Buffer Solutions – Composition and Function

2.2.1 Buffer Solution Details I: DNA Extraction, Purification & Analytical Sample Reagents

Buffer Solution	Composition	Functional Application(s)
Genomic DNA Extraction Buffer	2% (v/v) Triton X-100 1% (w/v) SDS 100mM NaCl 10mM Tris-HCl 1mM Disodium EDTA pH = 8.0	Crude genomic DNA extract preparations from the appropriate <i>S. pombe</i> strains for specific PCR applications
10X DNA Loading Buffer	20% (v/v) FICOLL 400 1% (w/v) SDS 100mM Disodium EDTA 0.25% (w/v) Bromophenol Blue	DNA sample pre-loading preparations for electrophoretic agarose gel analyses and/or electrophoretic agarose gel purification
50X TAE Buffer	2M Tris-HCl 1M Glacial Acetic Acid 50mM Disodium EDTA pH = 8.5	1X TAE running buffer preparation from 10X stock (20mL of 10X TAE mixed with 980mL of Ultra-Pure Millipore Water) utilised as the buffer medium for TAE-agarose gel purification of PCR products
10X TBE Buffer	0.89M Tris-HCl 0.89M Boric Acid 20mM Disodium EDTA pH = 8.3	1X TBE running buffer preparation from 10X stock (100mL of 10X TBE mixed with 900mL of Ultra-Pure Millipore Water) utilised as the buffer medium for TBE-agarose gel analyses of DNA samples

NOTE: 1% Agarose Gel Compositons

0.5g High-Strength Electrophoresis-Grade Agarose Powder

50ml of 1X TAE or 1x TBE Electrophoretic Running Buffer

5µL Ethidium Bromide Solution (final concentration = 0.5µg/mL gel)

0.5g agarose powder mixed with 50mL of the appropriate electrophoretic buffer medium in a 100mL capacity boro-silicate glass pyrex conical flask and the resultant suspension microwaved on the high power setting for ~60 seconds until completely dissolved and the result solution allowed to cool to ~40°C/"hand-warmth" prior to addition of 5µL Ethidium Bromide Solution and the resultant gel then poured immediately into casting cassette, prior to susbequent well-comb insertion and the resultant "cast assembly" stood at room temperature until set

[**Note:** The initial pH of each respective prepared buffer solution was measured with a pH211 Microprocessor pH Meter (Hanna Instruments) and adjusted when necessary to the required correct pH value via the appropriate drop-wise addition of 1M aqueous HCl or 1M aqueous KOH with constant magnetic stirring of the solution]

2.2.2. Buffer Solution Details II: TCA-Precipitated & Soluble Protein Sample Preparations

Buffer Solution	Composition	Functional Application(s)
1M Tris-HCl pH = 7.0	1M Tris-HCl pH = 7.0	Preparation of TCA-precipitated protein extract samples for 2D-PAGE Analyses
50mM Tris-HCl pH = 7.0	50mM Tris-HCl pH = 7.0	
50mM Tris-HCl 0.2% SDS pH = 7.0	50mM Tris-HCl 0.2%(w/v) SDS pH = 7.0	
1M Tris-HCl pH = 8.8	1M Tris-HCl pH = 8.8	pH adjustment of TCA-precipitated total protein extracts
Destreak™ Buffer pH = 3-10	Destreak™ Buffer 0.5% (v/v) IPG pH = 3-10	IPG strip re-hydration buffer for final preparation of protein samples for 2D-PAGE Analyses
4X SDS-PAGE Loading Buffer	240mM Tris-HCl 20% (v/v) Glycerol 16% (v/v) β-Mercaptoethanol 8% (w/v) SDS 0.01% (w/v) Bromophenol Blue pH = 6.8	Loading buffer for preparation of soluble and TCA-precipitated total protein extracts for 1D-PAGE Analyses
Buffer "HP"	50mM HEPES 150mM NaCl 5mM Disodium EDTA 10% (v/v) Glycerol 0.1% NP-40 pH = 8.0	Pre-equilibration wash buffer for preparation of total soluble protein extracts from <i>S. pombe</i> cell pellets
Buffer "HI"	10mL Buffer "HP" Containing: 50mM NaF 5mM NEM 1mM Na ₃ VO ₄ 1mM PMSF 1 Protease Inhibitor Cocktail Tablet (Roche Diagnostics) 100 µg/mL β2-Microglobulin pH = 8.0	Buffer medium for preparation of total soluble protein extracts from homogenised <i>S. pombe</i> cell pellets
Buffer "HM"	Buffer "HP" <u>WITHOUT NP-40</u> "De-gassed" under vacuum pH = 8.0	Mobile fractional elution phase buffer for HPLC-SEC of total soluble protein extracts
<p>NOTE: Prepared 1M and 50mM Tris-HCl buffer solutions stored at room-temperature until required</p> <p>Destreak™ Buffer and IPG pH = 3-10 solutions are proprietary formulations supplied by GE Healthcare stored at -20°C until required</p> <p>Prepared Destreak™ Buffer pH = 3-10 and 4X SDS-PAGE Loading buffer solutions stored at -20°C until required</p> <p>Prepared Buffer Solutions "HP" and "HM" stored at 4°C until required</p> <p>Prepared Buffer "HI" solution divided into 1mL aliquots placed into separate 1.5mL capacity plastic eppendorf microfuge tubes stored at -20°C until required</p>		

[Note: The initial pH of each respective prepared buffer solution was measured with a pH211 Microprocessor pH Meter (Hanna Instruments) and adjusted when necessary to the required correct pH value via the appropriate drop-wise addition of 1M aqueous HCl or 1M aqueous KOH with constant magnetic stirring of the solution]

2.2.3. Buffer Solution Details III: 1D-PAGE, 2D-PAGE and Western Blot Analyses

Buffer Solution	Composition	Functional Application(s)
Pre-Equilibration Buffer I	8M Urea 0.375M Tris-HCl 20% (v/v) Glycerol 2% (v/v) SDS 2% (w/v) Dithiothreitol pH = 8.8	1st Stage IPG Strip SDS-PAGE pre-equilibration of isoelectrically-focused protein samples
Pre-Equilibration Buffer II	8M Urea 0.375M Tris-HCl 20% (v/v) Glycerol 2% (v/v) SDS 2.5% (w/v) Iodacetamide pH = 8.8	2nd Stage IPG Strip SDS-PAGE pre-equilibration of isoelectrically-focused protein samples
1M Tris-HCl pH = 6.8	1M Tris-HCl pH = 6.8	Preparation of top SDS-PAGE "spacer" gel
1M Tris-HCl pH = 8.8	1M Tris-HCl pH = 8.8	Preparation of bottom SDS-PAGE "resolving" gel
10X SDS-PAGE Running Buffer	1.96M Glycine 500mM Tris-HCl 1% (v/v) SDS pH = 8.3	Prepared 1X SDS-PAGE running buffer solution (1 in 10 volumetric dilution of the 10X stock) utilised for SDS-PAGE electrophoretic medium
10X Transfer Buffer	0.25M Tris-HCl 0.19M Glycine pH = 8.3	Prepared 1X Transfer Buffer solution containing 15% (v/v) HPLC-grade Methanol utilised as the electrophoretic medium for the transfer of resolved proteins onto the blotting membrane
10X PBS	77mM Na ₂ HPO ₄ .2H ₂ O 27mM NaH ₂ PO ₄ .2H ₂ O 1.5mM NaCl pH = 7.2	Prepared 1X PBS buffer solution utilised for the preparation of 1X PBS Wash buffer and 1X PBS Block buffer solutions
1X PBS Wash Buffer	1X PBS Buffer 0.05% (v/v) Tween 20 pH = 7.2	Western blotting membrane wash buffer for removal of unbound 1 ^o and 2 ^o anti-body probes
1X PBS Block Buffer	1X PBS Wash Buffer 3% (w/v) Powdered Milk Protein pH = 7.2	Protein-rich blocking buffer for occupation of unoccupied protein binding-sites on the Western blotting membrane for prevention of non-specific anti-body binding
<p>NOTE: Prepared Pre-Equilibration Buffer Solutions I and II stored at -20°C until required Prepared 1X PBS Block Buffer stored at 4°C (3 day "shelf-life" stability) until required All other buffer solutions stored at room temperature until required</p>		

[Note: The initial pH of each respective prepared buffer solution was measured with a pH211 Microprocessor pH Meter (Hanna Instruments) and adjusted when necessary to the required correct pH value via the appropriate drop-wise addition of 1M aqueous HCl or 1M aqueous KOH with constant magnetic stirring of the solution]

2.2.4. Buffer Solution Details IV: Enzyme Storage and Reaction Media Compositions

Enzyme	Composition		Functional Application(s)
Phusion Polymerase (2U/ μ L)	Storage Buffer	Reaction Buffer	PCR Reaction Catalyses
	100mM KCl 20mM Tris-HCl 1mM Dithiothreitol 0.1mM EDTA 50% (v/v) Glycerol 200 μ g/mL BSA Additional Stabilizers pH = 7.4	5X GC Fusion Buffer Proprietary Type Formulation Containing: 7.5mM MgCl ₂ pH = 7.4	
SpeI (10U/ μ L)	50mM KCl 10mM Tris-HCl 1mM Dithiothreitol 0.1mM EDTA 50% (v/v) Glycerol 200 μ g/mL BSA Additional Stabilizers pH = 7.4	10X NE Buffer 2 50mM NaCl 10mM 100mM Tris-HCl 1mM Dithiothreitol pH = 7.9	Cre-Lox pAW8- <i>rad9</i> donor plasmid constructs and plasmid mini-prep restriction digest analyses
SphI (10U/ μ L)	100mM Na Citrate 10mM Tris-HCl 1mM Dithiothreitol 0.1mM EDTA 50% (v/v) Glycerol 0.5 μ g/mL BSA Additional Stabilizers pH = 7.4	10X Reaction Buffer K 1.5M KCl 100mM Tris-HCl 100mM MgCl ₂ pH = 7.4	Cre-Lox pAW8- <i>rad9</i> donor plasmid constructs and plasmid mini-prep restriction digest analyses
T4 DNA Ligase (3U/ μ L)	50mM KCl 10mM Tris-HCl 1mM Dithiothreitol 0.1mM EDTA 50% (v/v) Glycerol pH = 7.4	10X T4 Ligase Buffer 300mM Tris-HCl 100mM MgCl ₂ 100mM Dithiothreitol 10mM ATP pH = 7.8	Cre-Lox pAW8- <i>rad9</i> donor plasmid constructs
"CIAP" Calf-Intestinal Alkaline Phosphatase (1U/ μ L)	50mM KCl 10mM Tris-HCl 1mM MgCl ₂ 1mM Dithiothreitol 0.1mM ZnCl ₂ 50% (v/v) Glycerol pH = 8.0	10X CIAP Buffer 500mM Tris-HCl 10mM MgCl ₂ 1mM ZnCl ₂ 10mM Spermidine pH = 9.3	Preparation of de-phosphorylated <i>rad9</i> soluble protein extracts for comparative 2D-PAGE analyses
Lyticase (200U/mg)	[Lyophilised Powder]	Liquid YEA Medium 10mM Na ₂ HPO ₄ 10mM Na Citrate pH = 5.8	Preparation of "partial protoplasts" from specific strains of <i>S. pombe</i> cell cultures for Ellipticine and Etoposide acute survival assays
<p>NOTE: With the exception of Lyticase, all enzyme buffer solutions are standard proprietary formulations supplied by the company and each enzyme is supplied in solution in the respective storage buffer</p> <p>The supplied lyticase lyophilised powder and respective enzyme solutions were stored at -20°C until required</p> <p>The respective enzyme solutions were thawed on ice and vortexed briefly prior to utilisation</p> <p>The appropriate enzyme was added to its appropriate freshly-made reaction mixture, which was kept on ice, until ready for immediate incubation under the required temperature conditions</p>			

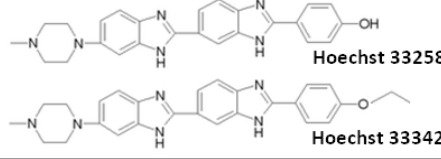
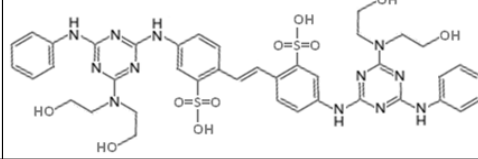
[Note: The initial pH of the prepared Lyticase Reaction Buffer solution was measured with a pH211 Microprocessor pH Meter (Hanna Instruments) and adjusted when necessary to the required correct pH value via the appropriate drop-wise addition of 1M aqueous HCl or 1M Aqueous KOH with constant magnetic stirring of the solution.

The resultant pH-corrected Lyticase Reaction Buffer was then filtered-sterilised via a sterile syringe and 0.2 μ M filter assembly prior to use]

2.2.5 Buffer Solution Details V: *S.pombe* Cre-Lox Base-Strain Transformation Reagents

Buffer Solution	Composition	Functional Application
LiAc-TE	100mM Lithium Acetate 10mM Tris-HCl 1mM Disodium EDTA pH = 7.5	pAW8- <i>rad9</i> donor plasmid construct Δ <i>rad9 S. pombe</i> "base-strain" genetic Cre-RMCE transformations
LiAc-TE-PEG	100mM Lithium Acetate 10mM Tris-HCl 1mM Disodium EDTA 40% (w/v) PEG 4000 pH = 7.5	pAW8- <i>rad9</i> donor plasmid construct Δ <i>rad9 S. pombe</i> "base-strain" genetic Cre-RMCE transformations

2.2.6 Buffer Solution Details VI: Hoechst-Calcofluor Dual Fluorescence Stain Preparation

Hoechst 33258 and Hoechst 33342		Calcofluor-White M2R/Fluorescent Brightener 28
 <p>Hoechst 33258</p> <p>Hoechst 33342</p>		
Blue-fluorescent dyes which intercalate strongly in the minor groove of DNA and are utilised to stain the nuclei of <i>S. pombe</i> cells		White-fluorescent dye which binds strongly, in a non-specific manner, to cellulose- and chitin- rich cellular components Utilised to stain <i>S. pombe</i> cell walls and septa
Solution	Composition	Functional Application
1000x Hoechst Stock Solution	1mg/mL Hoechst in 100% DMSO Stored in the dark at -20°C until required	Preparation of the 10x Hoechst stock solution which incorporates the p-Phenylenediamine (PED) reagent that functions as a fluorescence "anti-fade"
100x PED Stock	100mg/mL PED in 100% DMSO Stored in 1mL aliquots in the dark at -20°C until required	Preparation of the 10x Hoechst stock solution which incorporates the p-Phenylenediamine (PED) reagent that functions as a fluorescence "anti-fade"
10x Hoechst Stock Solution	100µL 1000x Hoechst Stock 1ml 100x PED Stock 8.9mL 50% (v/v) Glycerol (aq) Stored in 1mL aliquots in the dark at -20°C until required	Nuclear fluorescent dye component reagent for for preparation of the 1x Hoechst:Calcofluor dual staining solution
100x C-W Stock	1mg/mL Calcofluor-White (C-W) dissolved in buffer solution composition: 50mM Na Citrate 100 mM Na ₃ PO ₄ pH = 6.0 Stored in 1mL aliquots in the dark at -20°C until required	Cell wall and septa fluorescent dye component reagent for preparation of the 1x dual staining Hoechst:Calcofluor solution
1x dual staining Hoechst:Calcofluor solution	50µL 10x Hoechst Stock 5µL 100x C-W Stock 445µL 50% (v/v) Glycerol (aq) Final concentrations: Hoechst = 1µg/mL Calcofluor-White = 10µg/mL Glycerol = 44.5% (v/v) Freshly prepared prior to immediate use	Dual staining solution for differential fluorescence microscopic visualisation of septa and nuclei for proportionate counting of septated <i>S. pombe</i> cells in methanol-fixed samples acquired from lactose synchronisation time-course assay experimental strain cultures

[**Note:** The initial pH of each respective prepared buffer solution was measured with a pH211 Microprocessor pH Meter (Hanna Instruments) and adjusted when necessary to the required correct pH value via the appropriate drop-wise addition of 1M aqueous HCl or 1M aqueous KOH with constant magnetic stirring of the solution]

Hoechst 33342 proved to be better for *S. pombe* cell nuclei fluorescence staining than Hoechst 33258 due to its greater lipophilicity and capacity to permeate the cell wall and cell membrane]

2.3 Media Composition and Function

2.3.1 Liquid Media Composition and Function – Broth Culture Preparations

Medium	Composition	Functional Application(s)
Edinburgh Minimal Medium (EMM)	3% (w/v) Glucose 0.67% (w/v) Yeast Nitrogen Base 0.026% (w/v) Adenine Hemi-Sulphate 0.026% (w/v) Uracil 0.026% (w/v) Leucine pH = 5.5	Preparation of "wild-type" <i>S. pombe</i> strain 804 [<i>ura4-D18 leu1-32 ade6-M210 h⁻</i>] culture for <i>rad9</i> gene locus-targeted pAW1 Cre-Lox "base-strain" plasmid PCR-modified fragment [<i>-loxP-ura4[±]loxM3-</i>] transformation [Generation of $\Delta rad9$ Cre-Lox "base-strain"]
EMM Minus Uracil [EMM - U]	Similar composition to that of EMM <u>WITH THE NOTABLE OMISSION OF URACIL</u> from the prepared medium	Selective minimal medium for preparation of the Cre-Lox $\Delta rad9$ <i>S. pombe</i> "base-strain" [<i>rad9::loxP-ura4[±]loxM3 ura4-D18 leu1-32 ade6-M210 h⁻</i>] culture utilised in Cre-Lox donor pAW8- <i>rad9</i> plasmid construct type transformations for the generation of the experimental <i>rad9</i> -mutant <i>S. pombe</i> strains
Yeast Extract Adenine-Rich Medium (YEA)	3% (w/v) Glucose 0.5% (w/v) Yeast Extract 225µg/mL Adenine Hemi-Sulphate pH = 5.5	"General purpose" <i>S. pombe</i> cell culture liquid broth medium
YEA-Glycerol Medium (YEG)	Similar composition to that of YEA <u>WITH THE NOTABLE ADDITION OF 30% (v/v) Glycerol</u>	Viability-preservation medium for the long-term storage of <i>S. pombe</i> strains as 1mL YEG culture aliquots in 2.0mL capacity sterile/autoclaved plastic screw-lid microfuge tubes at -80°C
Luria-Base Broth Medium with Ampicillin (LB-Amp)	1% (w/v) NaCl 1% (w/v) Tryptone 0.5% (w/v) Yeast Extract 100µg/mL Ampicillin	Selective antibiotic medium for preparation of Cre-Lox pAW8- <i>rad9</i> donor plasmid ligation construct-transformed competent <i>E. coli</i> cell cultures for plasmid "mini-prep" kit extractions
SOC Medium	2% (w/v) Tryptone 0.5% (w/v) Yeast Extract 0.4% (w/v) Glucose 10mM NaCl 2.5mM KCl 10mM MgCl ₂ .6H ₂ O 10mM MgSO ₄ .7H ₂ O	Nutrient-rich medium for competent <i>E. coli</i> cell Cre-Lox pAW8- <i>rad9</i> donor plasmid ligation construct transformations

Note: Preparation of sterilised LB-Amp liquid/broth medium was accomplished via addition of 500µL of a 1mg/mL sterile stock solution of Ampicillin to 500mL of pre-autoclaved LB which had cooled to ~ 40°C.

The 1mg/mL Ampicillin stock solution comprised 0.05g Ampicillin powder dissolved in 50mL of ultra-pure millipore water, which was then passed through a sterile syringe and 0.2µM filter assembly into a fresh sterile 50mL plastic Greiner centrifuge tube.

1mL aliquots of the resultant sterile preparation of 1mg/mL Ampicillin stock solution were then pipetted into sterile 1.5mL capacity plastic eppendorf microfuge tubes which were then stored at -20°C until required.

Preparation of the EMM media was accomplished via addition of a freshly prepared, filter sterilised aqueous solution of Yeast Nitrogen Base (3.35g in 50mL millipore ultra-pure water) to 450mL of pre-autoclaved EMM medium which had cooled to ~ 40°C.

500mL of the very nutrient-rich SOC medium was prepared and aliquoted into ten 50mL capacity glass media bottles which were then autoclaved and the resultant sterile aliquots of SOC media stored at room temperature until required for use (this was necessary as an individual bottle of SOC medium became rapidly contaminated within 24-48 hours after opening and exposure to the atmosphere).

All other media were made up in 500mL aliquots with double-distilled water, autoclaved and then stored at room temperature until required for use.

2.3.2 Solid Media Composition and Function – Agar Culture Plate Preparations

Medium	Composition	Functional Application(s)
Edinburgh Minimal Medium (EMM Agar)	3% (w/v) Glucose 0.67% (w/v) Yeast Nitrogen Base 0.026% (w/v) Adenine Hemi-Sulphate 0.026% (w/v) Uracil 0.026% (w/v) Leucine 2% (w/v) Agar pH = 5.5	Comparative replica control plating medium for various <i>S. pombe</i> strain cell colony isolations
EMM Minus Uracil Agar (EMM -U Agar)	Similar composition to that of EMM <u>WITH THE NOTABLE OMISSION OF URACIL</u> from the prepared medium	Selective replica plating medium for <i>ura4⁺</i> marker gene "knock-out" <i>S. pombe</i> strain cell culture colonies
EMM Minus Leucine Agar (EMM -L Agar)	Similar composition to that of EMM <u>WITH THE NOTABLE OMISSION OF LEUCINE</u> from the prepared medium	Selective replica plating medium for <i>LEU2⁺</i> marker gene "knock-out" <i>S. pombe</i> strain cell colony isolation Selective replica plating medium for pAW8- <i>rad9</i> donor plasmid Cre-RMCE <i>S. pombe</i> Δ <i>rad9</i> "base strain" transformant cell colony isolation
Yeast Extract Adenine-Rich Medium Agar (YEA Agar)	3% (w/v) Glucose 0.5% (w/v) Yeast Extract 225 μ g/mL Adenine Hemi-Sulphate 2% (w/v) Agar pH = 5.5	"General purpose" <i>S. pombe</i> cell culture plating medium Comparative replica control plating medium for various <i>S. pombe</i> strain cell colony isolations
YEA-5FOA Agar	Similar composition to that of YEA <u>WITH THE NOTABLE ADDITION OF 0.1% (w/v) 5-Fluoroorotic Acid (5FOA)</u> in the prepared agar medium	Selective replica plating medium for pAW8- <i>rad9</i> donor plasmid Cre-RMCE <i>S. pombe</i> Δ <i>rad9</i> "base strain" transformant cell colony isolation
YEA-HU Agar	Similar composition to that of YEA <u>WITH THE NOTABLE ADDITION OF 4mM Hydroxyurea (HU)</u> in the prepared agar medium	Selective replica plating medium for HU-resistant <i>S. pombe</i> strain cell colony isolation
YEA-G418 Agar	Similar composition to that of YEA <u>WITH THE NOTABLE ADDITION OF 100μg/mL G418 Antibiotic</u> in the prepared agar medium	Selective replica plating medium for <i>kan^{GMX}</i> marker gene "knock-out" <i>S. pombe</i> strain cell colony isolation
Malt Extract Agar (ME Agar)	3% (w/v) Malt Extract 2% (w/v) Agar pH = 5.5	Induction of <i>S. pombe</i> cell mating and sporulation meiotic cycle for generation of specific gene-targeted "knock-out" "double-mutant" strains
Luria-Base Broth Medium with Ampicillin Agar (LB-Amp Agar)	1% (w/v) NaCl 1% (w/v) Tryptone 0.5% (w/v) Yeast Extract 100 μ g/mL Ampicillin 2% (w/v) Agar	Selective antibiotic medium for isolation of Cre-Lox pAW8- <i>rad9</i> donor plasmid ligation construct-transformed competent <i>E. coli</i> cell colonies

Note: Preparation of sterilised LB-Amp, YEA-5FOA, YEA-G418 and YEA-HU agar media was accomplished via addition of 500 μ L of a 1000x final concentration sterile stock solution of Ampicillin, 5-FOA, G418 or HU (in each case an aqueous solution prepared in millipore water and filtered sterilised via a sterile syringe and 0.2 μ M filter assembly) to 500mL of pre-autoclaved agar medium which had cooled to ~40°C.

Individual 1mL aliquots of the filter-sterilised 1000x stock solutions of Ampicillin, 5-FOA, G418 or HU were stored in 1.5ml capacity plastic eppendorf microfuge tubes at -20°C until required for use.

Preparation of the EMM agar media was accomplished via addition of a freshly prepared, filter sterilised aqueous solution of Yeast Nitrogen Base (3.35g in 50mL millipore ultra-pure water) to 450mL of pre-autoclaved EMM medium which had cooled to ~ 40°C.

~25mL aliquots of the prepared agar media were then poured into individual sterile plastic petri-plates, which were stood at room temperature for ~24 hours to set, then wrapped in polyethylene bags and stored in the 4°C cold-room until required for use.

2.4 *S. pombe* Genomic DNA Extraction Protocol

Total genomic DNA extracts were prepared from the required *S. pombe* strains via utilisation of the following protocol:

- (i) A sterile/autoclaved toothpick was utilised to inoculate 10mL YEA medium (Section 2.3.1, p.167) with a “tip-loaded” amount of material from each respective YEA streak-plate culture *S. pombe* strain.
[Each respective YEA medium inoculated culture was set up in a 50mL capacity Greiner plastic centrifuge tube fitted with a loose screw cap, which was then placed in a Sanyo Orbisafe type orbital incubator shaker set at 30°C, 180 r.p.m. for 24 hours]
- (ii) After the incubation time had elapsed, a 4mL aliquot of each respective culture was transferred to a fresh 15mL capacity Greiner plastic screw-cap centrifuge tube and spun down at 3,300g for 10 minutes in a Jencons-PLS SorvilleR Legend T centrifuge in the 4°C cold room.
- (iii) Each resultant supernatant was then discarded and each of the respective cell pellets was then re-suspended in 4mL millipore ultra-pure sterile/autoclaved millipore water and re-spun at 3,300g for 10 mins at 4°C (as described for stage (ii) above).
- (iv) Each resultant supernatant was then discarded and each of the respective washed cell pellets was then re-suspended in 200µL of genomic DNA extraction buffer solution (Section 2.2.1, p.162) and each resultant cell re-suspension buffer solution mixture transferred to a sterile/autoclaved screw-cap plastic 1.5mL capacity microfuge tube.
- (v) A 200µL aliquot of ice-cold Phenol/Chloroform/Isoamylalcohol solution was then added to each resultant cell pellet suspension and x8 small spatula spoonfuls of glass beads were then added to each resultant cell pellet re-suspension solvent mixture in each screw-cap microfuge tube.
- (vi) Each screw-cap microfuge tube was then placed on a Genie Disruptor for 6 minutes, in the 4°C cold room, in order to break open the cells and release the genomic DNA into solution.

- (vii) Each screw-cap microfuge was then placed in a Sanyo Hawk 15/05 refrigerated bench-top microfuge and spun at 12000 rpm, 4°C for 5 minutes, after which each resultant top aqueous layer (which contained the genomic DNA) was pipetted off, taking care not to disturb the interface and lower organic solvent layer and transferred to a sterile/autoclaved 1.5mL capacity eppendorf microfuge tube. [Whilst each resultant lower organic layer and cell debris pellet was subsequently discarded]
- (viii) 0.8x vol retained genomic DNA aqueous layer of Isopropanol (~160µL) was then added to the contents of each 1.5mL capacity plastic eppendorf tube, in order to effect precipitation of the genomic DNA from solution.
- (ix) Each plastic 1.5ml capacity eppendorf tube was then placed in the refrigerated bench-top microfuge and spun at 12000 rpm, 4°C for 30 minutes, after which each resultant supernatant was carefully pipetted off and discarded.
- (x) Each plastic 1.5mL capacity eppendorf tube was then placed in a 37°C static incubator (lid open) and allowed to stand for 20 minutes, in order to remove residual traces of isopropanol from each precipitated genomic DNA pellet.
- (xi) Each resultant precipitated genomic DNA pellet was then re-dissolved in 50µL ultra-pure, sterile/autoclaved millipore water, after which 1µL of RNase A (10mg/mL) was added to each resultant aqueous genomic DNA solution and each resultant reaction mixture incubated at 37°C for 30 minutes to degrade contaminating traces of RNA which may otherwise have adversely interfered with the PCR reactions to be performed.
- (xii) The resultant *S. pombe* strain RNA-free genomic DNA extracted preparations were then stored at -20°C until required.

2.5 Cre Recombinase-Mediated Cassette Exchange (Cre-RMCE) Protocols

The *S. pombe* Cre-RMCE transformation system methodology (devised by Watson A.T. *et al.*, 2008), was adapted for generation of the experimental engineered *rad9* mutant/variant expressing *S. pombe* strains utilised in this study (depicted summarily in Figs 2.1-2.6, pp.171-176).

Fig 2.1:PCR Protocols for the Generation of the pAW1 plasmid-Derived *loxP-ura4-LoxM3 rad9* gene locus-targeted fragment and pAW8 Donor Plasmid *SphI-rad9-SpeI* Gene Cassette Inserts

PCR Reaction Mixture Composition		
DNA Stock Solution (1 in 10 diluted) = 10µL 2mM dNTPs Stock Solution Mixture = 5µL 10µM Forward Primer Oligonucleotide Stock Solution = 2.5µL 10µM Reverse Primer Oligonucleotide Stock Solution = 2.5µL 5xGC Phusion Polymerase Buffer Solution = 10µL Sterile/Autoclaved Ultra-Pure Millipore H ₂ O = 19.5µL Phusion Polymerase Enzyme (2U/µL) = 0.5µL Total Reaction Volume = 50µL		
PCR Thermocycler Phase Reaction Parameter Programmes [x35 Denaturation-Annealing-Extension Cycles Utilised in Each Instance]		
DNA Source Utilised: pAW1 Plasmid Primer Pair: Rad9-S1 and Rad9-S2	DNA Source Utilised: <i>S.pombe</i> Strain 804 Primer Pair: Rad9-S5 and Rad9-S6	DNA Source Utilised: <i>S.pombe</i> Strain 150 Primer Pair: Rad9-S5 and Rad9-S8
Pre-Heat Hot-Lid = 105°C Hot Lid = "On" Hot Start = "Off" Pause = "Off" 98°C Pre-Cycle = 30 Seconds 98°C Denaturation = 10 Seconds 55°C Annealing = 30 Seconds 72°C Extension = 90 Seconds 72°C Post-Cycle = 10 Minutes 4°C Hold	Pre-Heat Hot-Lid = 105°C Hot Lid = "On" Hot Start = "Off" Pause = "Off" 98°C Pre-Cycle = 1 Minute 98°C Denaturation = 30 Seconds 60°C Annealing = 30 Seconds 72°C Extension = 2 Minutes 72°C Post-Cycle = 10 Minutes 4°C Hold	Pre-Heat Hot-Lid = 105°C Hot Lid = "On" Hot Start = "Off" Pause = "Off" 98°C Pre-Cycle = 1 Minute 98°C Denaturation = 30 Seconds 55°C Annealing = 30 Seconds 72°C Extension = 2.5 Minutes 72°C Post-Cycle = 10 Minutes 4°C Hold
Generated PCR Product		
Cre-RMCE pAW1 <i>rad9</i> Gene Locus Targeted Base-Strain Insertional Inactivation Exchanger Fragment: — <i>loxP-ura4⁺-loxM3</i> —	Cre-RMCE Donor Plasmid pAW8 Full-Length <i>rad9</i> Gene Cassette Insert: <i>SphI-rad9-SpeI</i>	Cre-RMCE Donor Plasmid pAW8 Full-Length <i>rad9</i> C-Terminal (HA) ₃ Epitope-Tegged Gene Cassette Insert: <i>SphI-rad9-c3xHA-SpeI</i>

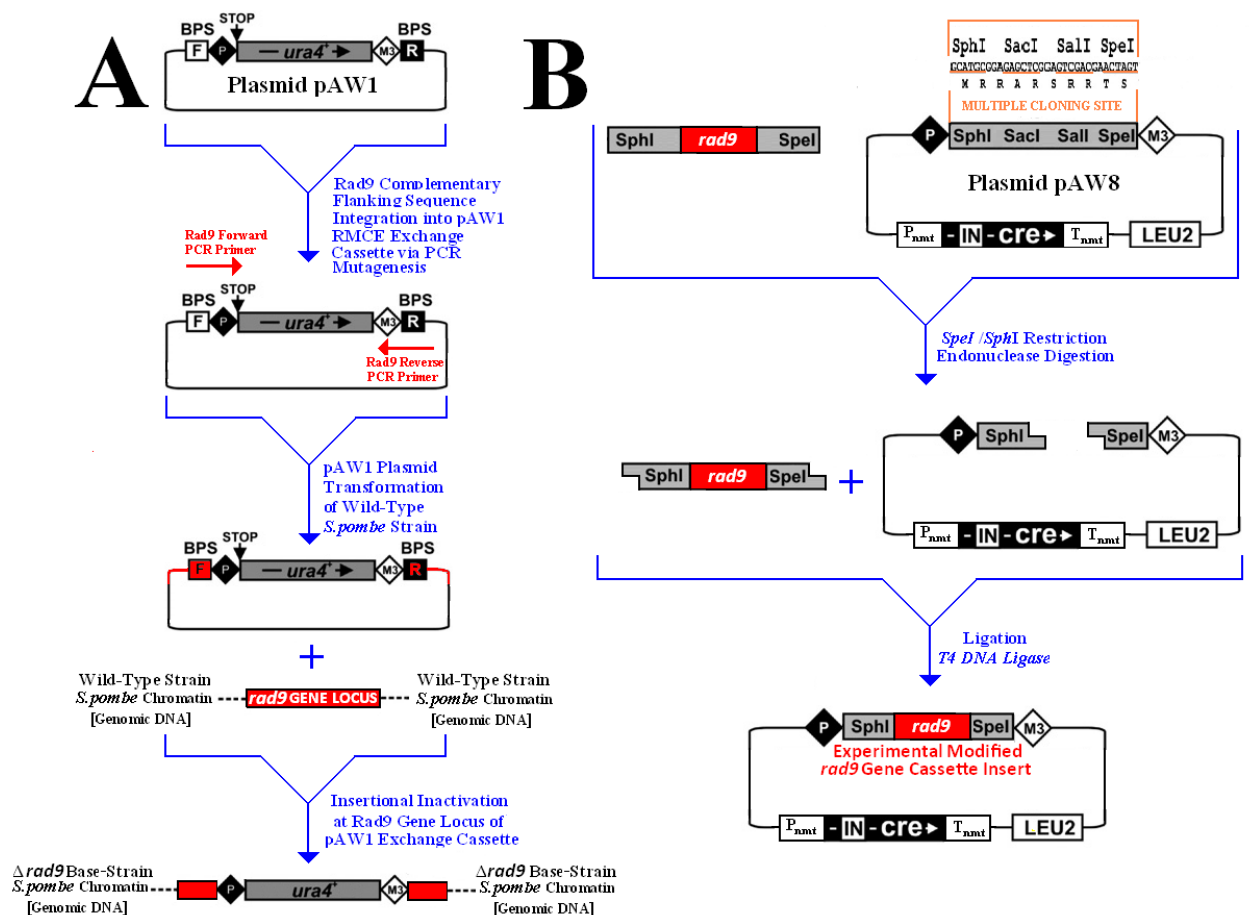
NOTE: The Phusion Polymerase enzyme possesses 3'-5' exonuclease proof-reading activity and therefore was the very last component to be added to each of the prepared PCR reaction mixtures, immediately prior to use, in order to maximise preservation of primer oligonucleotide integrity.

All PCR reactions were performed on a TECHNE TC-312 PCR Thermocycler.

Negative control PCR reactions, in which autoclaved/sterile ultra-pure millipore water was substituted in place of the genomic DNA solution, were performed in parallel for each of the respective PCR reaction mixtures utilised.

Fig 2.2: Basic Essential Components of the Cre Recombinase-Mediated Cassette Exchange System

[Taken and Adapted From: Watson A.T. *et al*, 2008]



A: Plasmid pAW1 is utilised to construct the cassette acceptor *S. pombe* transformation base-strain, in this case the plasmid is PCR-modified with wild-type *rad9* 5'-end and 3'-end primers, that include a portion of the upstream promoter for minimisation of potential gene promoter disruption.

Subsequent integration of the generated pAW1 plasmid PCR product into the *S. pombe* genomic DNA, via a standard Lithium Acetate transformation protocol, results in its targeted insertion at the *rad9* gene locus with consequential inactivation/effective deletion of the gene, thus producing the Δrad9 *S. pombe* base-strain – which expresses the *S. pombe* *Ura4+* selectable marker gene (Fig 2.3, p.173 and Fig 2.4, p.174).

B: Fusion PCR- mutagenised *rad9* gene variant cassettes were prepared via utilisation of appropriately designed primers incorporate spacer and SphI and SpeI site sequences at their respective 5' and 3' ends for integration into the pAW8 donor plasmid multiple cloning-site (Fig 2.5, p.175 and Fig 2.6, p.176).

The pAW8 donor plasmid also contains the *S. cerevisiae* *LEU2* selectable marker gene (Fig 2.3, p.173) and the *S. pombe* *CRE* recombinase gene situated downstream from the *S. pombe* *P_{nmt}* promoter and *rad50* intron1 spacer sequences and upstream from the *S. pombe* *T_{nmt}* terminator sequence respectively.

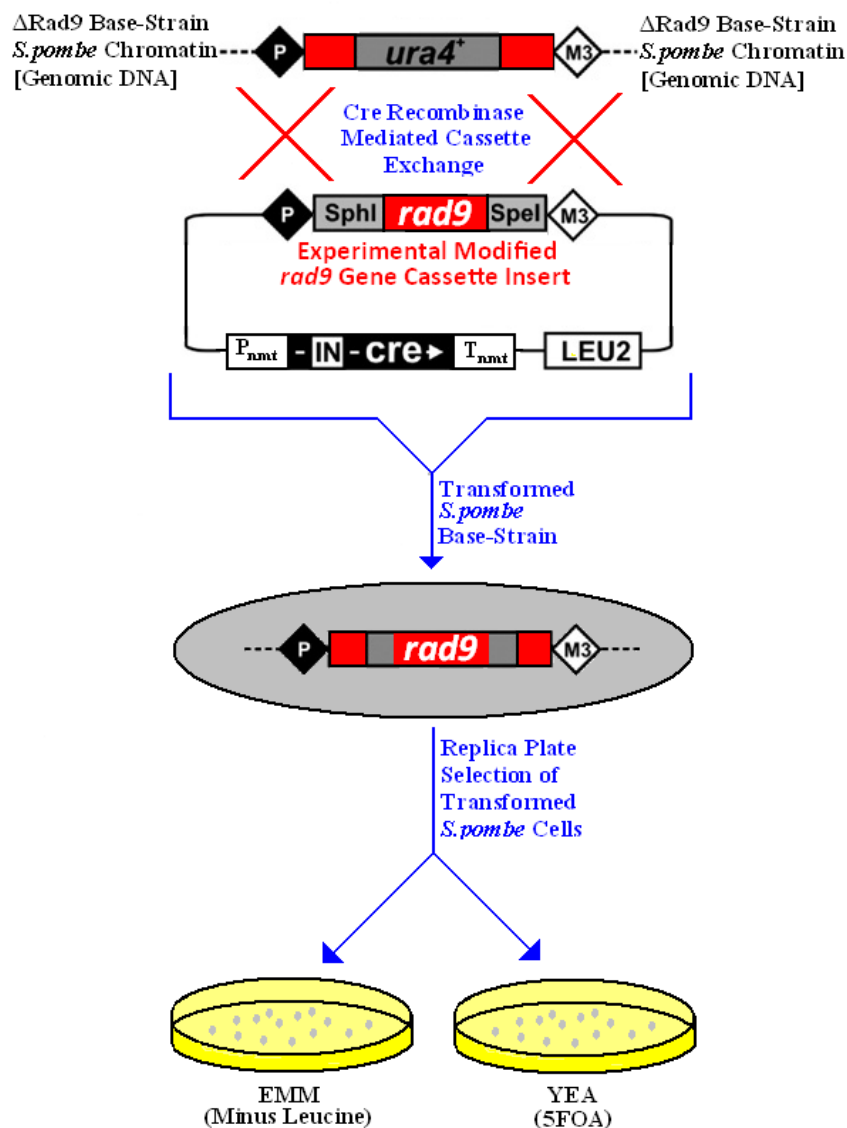
[The direction of gene transcription is indicated via the white arrow in the above figure]

Both the base-strain strain pAW1 plasmid and the donor pAW8 plasmid incorporate wild-type loxP and mutated loxM3 recombination sites, consequentially, the heterospecific nature of the designed recombination sites ensures that the cassette inserted exchange product once formed within in the base-strain is stable - ie prevents the occurrence unstable self-recombination events which would otherwise result in deleted removal/translocation of the cassette insert within the base-strain *S. pombe* genome.

The principle advantage of this Cre-RMCE system is that only one homologous integration step is required and thus the procedure is both efficient and less time-consuming in comparison with other standard molecular biology techniques.

[NOTE: pAW1 Plasmid Map – Appendix 2.11.1, pp.269-271; pAW8 Plasmid Map – Appendix 2.11.2, pp.272-275]

Fig 2.3: Mechanistic Overview of the Cre-RMCE System for Generation of Rad9/Rad9S Strains
 [Taken and Adapted From: Watson A.T. *et al*, 2008]



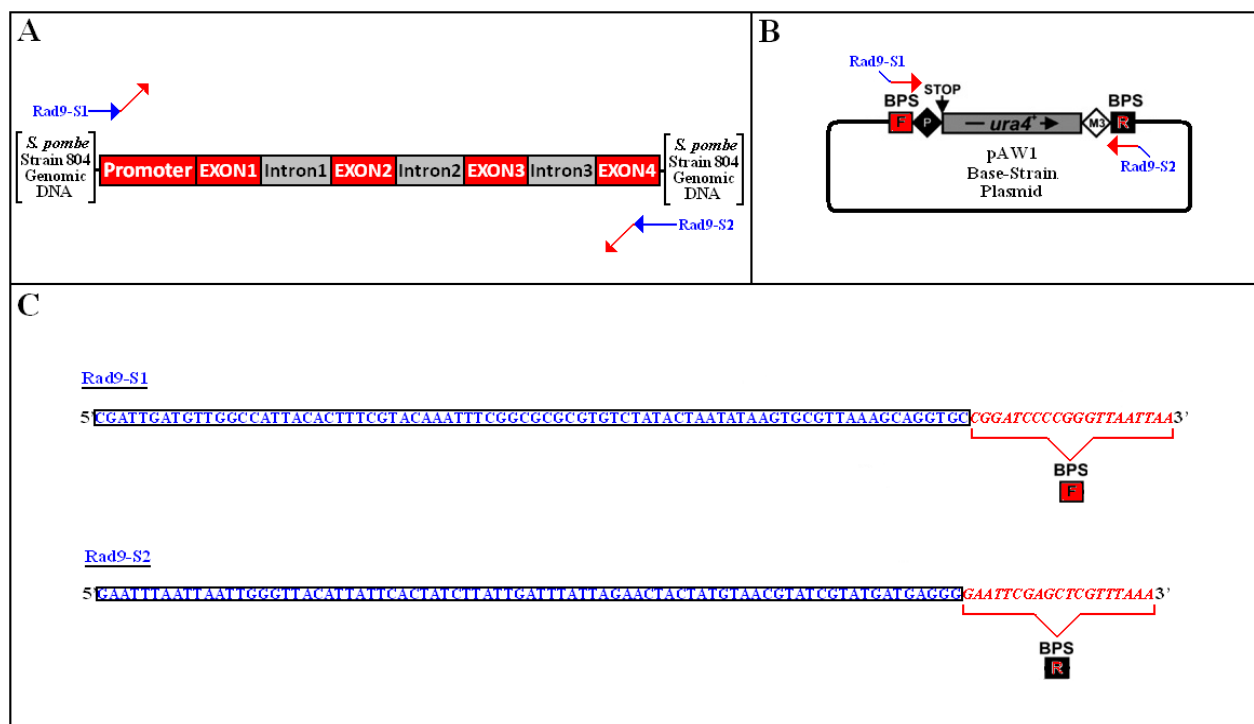
Note: Resultant transformed *S. pombe* base-strain cells grown on EMM (minus Leucine) and YEA (5-FOA) media replica plates.

Transformed cells lack the Cre-RMCE-exchanged *Ura4⁺* gene which encodes orotidine monophosphate dehydrogenase – an enzyme involved in Uracil biosynthesis and therefore cannot convert 5-FOA to the 5-Fluorouracil suicide-substrate (which inhibits the thymidylate synthetase enzyme with subsequent depletion of dTTP and abrogated DNA synthesis), thus they are able to grow on the YEA-5FOA plate.

Transformed cells also express the *S. cerevisiae LEU2* gene, incorporated via the pAW8-*Rad9* Cre-RMCE plasmid exchange – which encodes an enzyme involved in Leucine biosynthesis, namely; β -Isopropylmalate Dehydrogenase, and thus are able to grow on the EMM (minus Leucine) plate.

In contrast, the un-transformed *S. pombe* strain cells cannot grow on either plate as a consequence of expression of the *Ura4⁺* selectable marker gene and lack of the *LEU2* selectable marker gene respectively.

Fig 2.4: Base-Strain Plasmid pAW1 PCR Modification Primers: Sequences and Target Sites



Primer

Annealing Target Site

Rad9-S1

-159 to -81 bases upstream region from the *rad9* gene ATG start codon

Rad9-S2

+136 to +216 bases downstream region from the *rad9* gene TAG stop codon

A: Rad9-S1 and Rad9-S2 primer oligonucleotide-targeted *S. pombe rad9* gene sites PCR-integrated into the Cre-RMCE base-strain pAW1 plasmid

B: Rad9-S1 and Rad9-S2 primer oligonucleotide Cre-RMCE base-strain pAW1 plasmid BPS target sites utilised for PCR integration of the *S. pombe rad9* gene loci sequences

C: Rad9-S1 and Rad9-S2 PCR primer oligonucleotide base sequences

NNNNN = *rad9* gene locus targeting sequences (PCR integrated into the pAW1 plasmid)

NNNNN = Cre-RMCE base-strain pAW1 plasmid BPS complementary primer annealing sequences

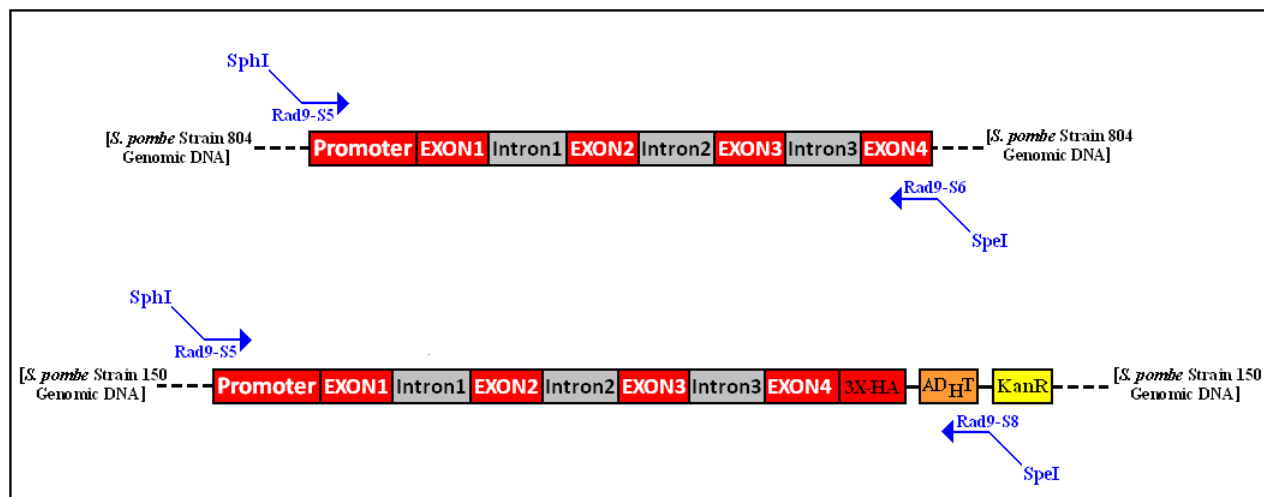
NOTE: The resultant PCR-modified pAW1 plasmid-derived *loxP-rad9-loxM3* fragment was then utilised to transform the “wild-type” *S. pombe* strain 804 to generate the $\Delta rad9$ *S. pombe* Cre-RMCE base-strain via genomic DNA *rad9* gene locus-targeted integration of the *loxP-ura4+-loxM3* cassette sequence. (Appendix 2.11.4, p.277)

[Thus, the endogenous “wild-type” *rad9* gene is deleted effectively via targeted insertional inactivation]

The Lithium Acetate Transformation protocol utilised was identical to that described in Section 2.5.3, pp.188-191, with the notable exception that an overnight culture of wild-type *S. pombe* strain 804 in EMM media (containing Adenine, Leucine and Uracil) was transformed with the PCR-modified pAW1 Plasmid fragment to generate the required $\Delta rad9$ *S. pombe* Cre-RMCE “base-strain”.

The resultant culture of transformed cells was plated out onto an EMM Minus Uracil agar petri-plate to select exclusively for Cre-Lox $\Delta rad9$ *S. pombe* Cre-RMCE “base-strain” colonies.

Fig 2.5: PCR Primers for Generation of Full-Length *rad9* Gene pAW8 Plasmid Cassette Inserts



Primer	Base-Pairing Orientation	Sequence
Rad9-S5	Forward (5' → 3')	5'-CGATAGTGGCATGCTAGAAAAACACCACATTATAGATTTACC-3' SphI
Rad9-S6	Reverse (3' ← 5')	5'-CTCGTCCAAGTACTAGTGTAACGTATCGTATGATGAGGG-3' SpeI
Rad9-S8	Reverse (3' ← 5')	5'-GCTATCACACTAGTCTAGATCTATATTACCCTGTTATCCC-3' SpeI

Primer Oligonucleotide Sequence Color Code Designation	PCR Primer Pairs and Products
NNNNN = Restriction Site-Adjacent Spacer Sequence	Rad9-S5 & Rad9-S6 = SphI- <i>rad9</i> -SpeI pAW8 Cassette Insert
NNNNN = Complementary Base-Pairing Primer Sequence Specific to Target Gene	Rad9-S5 & Rad9-S8 = SphI- <i>rad9</i> -c3xHA-SpeI pAW8 Cassette Insert

Primer

Annealing Target Site

Rad9-S5

-80 to -84 bases upstream region from the ATG start codon

Rad9-S6

+136 to +157 bases downstream region from the TAG stop codon

Rad9-S7

+198 to +219 bases downstream region from the ATG start codon

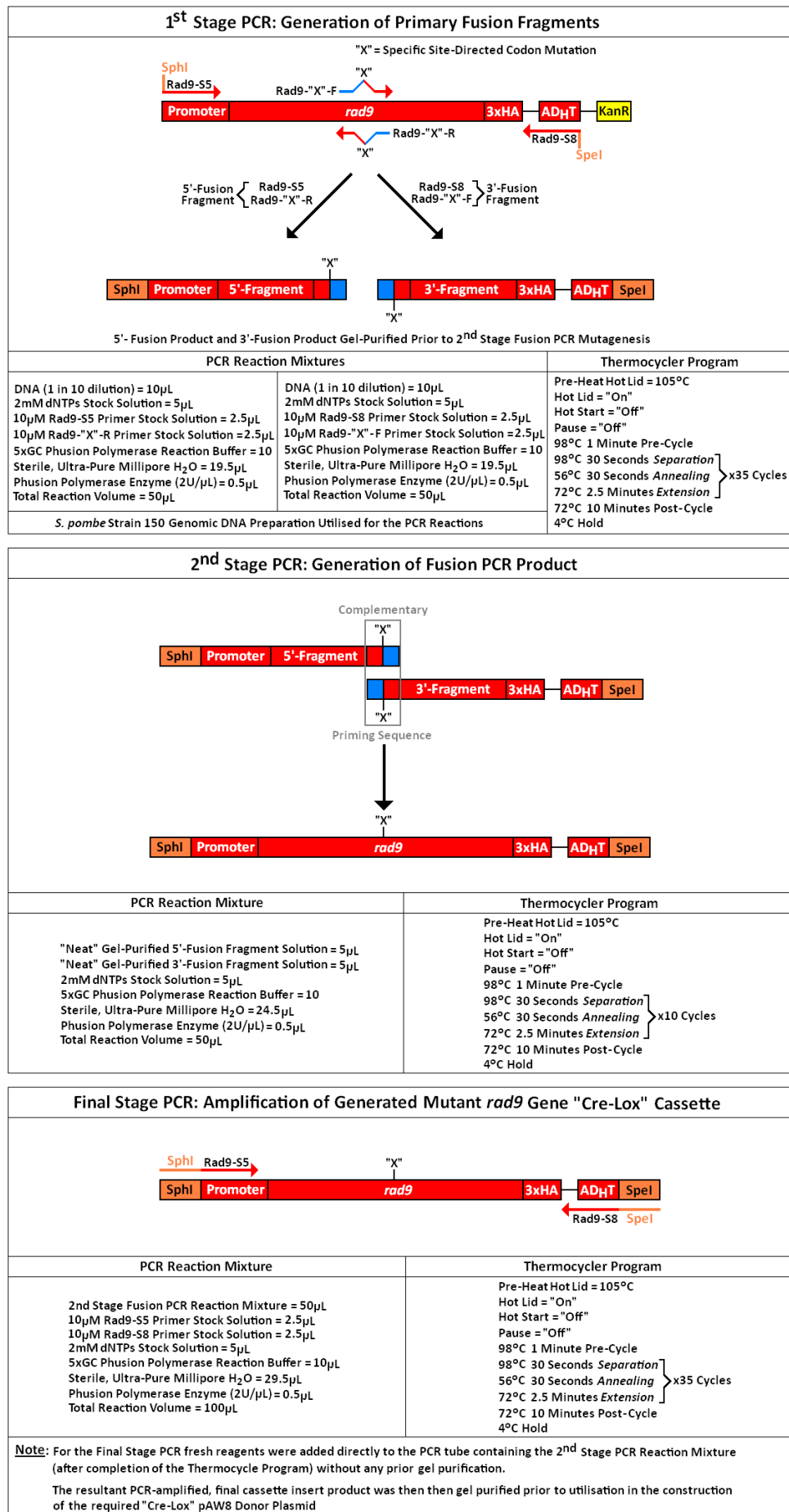
Rad9-S8

+240 to +279 bases downstream region from 3rd HA TAG stop codon

Note: *S. pombe* strain 804 genomic DNA was utilised to generate the untagged/wild-type *rad9* gene cassette insert, whilst *S. pombe* strain 150 genomic DNA was utilised to generate the C-terminal 3xHA epitope tagged full-length *rad9*-3xHA gene cassette insert respectively.

PCR primers Rad9-S5 and Rad9-S8 were also utilised in the Fusion PCR Mutagenesis Protocol (detailed in Fig 2.6, p.176) for the construction of experimental modified *rad9* gene pAW8 plasmid cassette inserts and amplification of the integrated *rad9* gene from the genomic DNA extract acquired from each of the respective “Cre-Lox”- generated *S. pombe* strain for PCR genotype assay (detailed in Section 2.6.2, p.192) and DNA sequence verification (detailed in Section 2.6.3, pp.193-195).

Fig 2.6: Fusion PCR Protocol for the Generation of pAW8 Plasmid Experimental Mutated *rad9* Gene Cassette Inserts [PCR Primer Sequences – See Appendix 2.11.3, p.269]



2.5.1 PCR Product Gel Purification Protocol

- (i) A 45µL aliquot of the appropriate PCR product was mixed with 5µL of 10x DNA Sample Loading Buffer Dye (Section 2.2.1, p.162) and the resultant 50µL sample loaded onto a 1% TAE Agarose Electrophoretic Gel (Section 2.2.1, p.162) which was then run at 120V constant setting in 1x TAE buffer for 45 minutes.
- (ii) The IDPure™ Spin Column DNA Gel Extraction Kit (ID Labs Inc.) was then utilised, in conjunction with 1% agarose electrophoretic gel purification, for isolation of the respective PCR generated pAW8 *rad9* gene cassette inserts – in accordance with the summarised kit protocol:
- (iii) The resultant resolved PCR DNA product bands on the gel were visualised via non-U.V. light-based fluorescence, for avoidance of potential U.V-induced damage and preserved DNA integrity (via utilisation of the Dark Reader™ CE Transilluminator DR-45M Imager Apparatus), excised from the gel with a clean scalpel blade, after which the resultant gel slices were weighed and placed in 1.5mL capacity plastic eppendorf microfuge tubes.
- (iv) The appropriate volume of kit binding buffer II solution (400µL/100mg of excised gel slice) was then added to each respective eppendorf tube, prior to incubation at 55°C in a hot block for ~10 minutes during which the tube contents were periodically removed and vortexed briefly every ~2 minutes until each respective gel slice had completely dissolved.
- (v) Each resultant solution was then pipetted into a supplied kit column assembly, which once loaded was stood for 2 minutes at room temperature prior to centrifugation in a Sanyo Hawk 15/05 refrigerated bench-top microfuge at 10,000rpm, 4°C for 2 minutes.
- (vi) The resultant eluents were then discarded and each column then loaded with 500µL kit wash solution, immediately after which the spin column assembly was re-spun at 10,000 rpm, 4°C for 2 minutes in a Sanyo Hawk 15/05 refrigerated bench-top microfuge and the resultant eluents discarded.

- (vii) The wash step procedure (detailed in the previous stage) was then repeated, after which each spin column assembly was re-centrifuged at 10,000rpm, 4°C for a further 2 minutes to remove any residual traces of wash solution from the columns – which would have otherwise impeded elution of the respective purified PCR products from the columns.
- (viii) The columns were then placed in fresh/clean 1.5mL capacity plastic eppendorf microfuge tubes, prior to the addition of 30µL of kit elution buffer to the centre of each column – after which each column assembly was stood at room temperature for 2 minutes prior to centrifugation at 10,000 rpm, 4°C for 2 minutes in a Sanyo Hawk 15/05 refrigerated bench-top microfuge.
- (vii) The resultant eluted/purified PCR product solutions, contained within the 1.5mL capacity plastic eppendorf microfuge tubes were then stored at -20°C until required.

2.5.2 Donor pAW8-Experimental Rad9 Cassette Insert Plasmid Construction Protocols

2.5.2.1 SphI and SpeI Restriction Enzyme Digest Protocol

The restriction digest reaction mixture, utilised for complementary multiple cloning site donor Cre-RMCE plasmid pAW8 and PCR-generated *rad9* experimental gene cassette insert SpeI and SphI restriction sequence site cleavages, comprised:

5 μ L DNA solution (Plasmid pAW8 or Cassette Insert*)

5 μ L 10x SpeI NE Buffer 2 (refer to p.165 for full details)

5 μ L 10x SphI Buffer K (refer to p.165 for full details)

0.5 μ L SpeI Restriction Enzyme (10U/ μ L)

0.5 μ L SphI Restriction Enzyme (10U/ μ L)

34 μ L Autoclaved/Sterile Ultra-Pure Millipore Water

Total Reaction Volume = 50 μ L

[*Note: Amount of DNA equivalent to 4ng]

The respective restriction digest reaction mixtures were set up in thin-walled PCR tubes which were then placed in the 37°C incubator for a time period of 24 hours.

2.5.2.2 Ligation Protocol

After the 24 hours time had elapsed, the thin-walled PCR tubes containing the restriction digest mixtures were removed from the 37°C incubator and placed in a TECHNE TC-312 PCR Thermocycler set at 65°C for 20 minutes – Programme Parameters Utilised:

Pre-Heat Hot-Lid 105°C
Hot-Lid = On
Hot Start = Off
Pause = Off
65°C Pre-Cycle = 1 Minute
65°C Post-Cycle = 19 Minutes
Hold = 25°C

Incubation of the SpeI/SphI digest reaction mixtures at 65°C for 20 minutes was an essential pre-requisite to inactivate the restriction enzymes prior to performing the ligation reactions.

[A final hold cooling temperature of 25°C was selected to ensure that the DNA remained in the double-stranded duplex configuration – since rapid cooling of the “heat-inactivated” restriction digest reaction mixtures to 4°C would have promoted the formation of DNA single-stranded molecules with consequential ligation anomalies]

The ligation reaction mixture, utilised for construction of the required Cre-RMCE pAW8 donor plasmid-gene cassette inserts; pAW8-*rad9*, pAW8-*rad9*-3xHA and pAW8-*rad9*-S-3xHA - for subsequent *S. pombe* base-strain transformations, comprised:

5µL SpeI/SphI Digested Plasmid pAW8 Reaction Mixture (~4ng)
5µL SpeI/SphI Digested PCR-Generated Cassette Gene Insert (~2ng)
2µL 10x T4 DNA Ligase Buffer
1µL T4 DNA Ligase (3U/µL)
7µL Sterile/Autoclaved Ultra-Pure Millipore Water
Total Reaction Volume = 20µL

The respective ligation reaction reaction mixtures were set up in thin-walled PCR tubes – placed in the 25°C static Binder incubator for a time period of 24 hours.

2.5.2.3 α -Competent *E. coli* Cell Transformation Protocol

A modified version of the Bioline protocol was utilised for the respective *E. coli* competent cell transformations with the Cre-RMCE donor pAW8 plasmid *rad9/rad9-S* gene cassette insert ligation constructs; pAW8-*rad9*, pAW8-*rad9*-3xHA and pAW8-*rad9-S*-3xHA.

- (i) α -select chemically-competent *E. coli* cells (commercially supplied by Bioline – see Section 2.1, p.153 for details) were removed from -80°C storage and thawed on wet ice and the resultant thawed cell suspension mixed homogeneously via light flicking of the container tube.
- (ii) 50 μ L of the homogeneous cell suspension was then mixed with the 20 μ L total volume of the respective Cre-RMCE donor pAW8 plasmid *rad9/rad9-S* gene cassette insert ligation construct reaction mixture in a 1.5mL capacity plastic eppendorf tube, which was then incubated on ice for 30 minutes.
- (iii) The 1.5mL capacity plastic eppendorf tube which contained the cooled resultant transformation reaction mixture was then placed in a 42°C hot-block for 45 seconds and then removed and placed back on wet ice for a further 2 minutes.
- (iv) 930 μ L of SOC medium (see Section 2.3.1 p.167 for full details of media composition) was then added to the tube contents (ie final total reaction volume = 1000 μ L) and the resultant transformation reaction mixture incubated at 37°C for 90 minutes – after which time the tube was then spun at 12000 rpm at 4°C for 2 minutes in a bench-top refrigerated microfuge, the supernatant removed/discarded and the resultant transformed cell pellet re-suspended in 50 μ L fresh SOC medium.
- (v) The resultant 50 μ L cell suspension was then evenly spread out onto an LB Ampicillin agar (Section 2.3.2, p.168) petri-plate – incubated for 24 hours at 37°C.

2.5.2.4 Miniprep Protocols

The IDPure™ Spin Column Plasmid DNA Miniprep Kit (ID Labs Inc.) was then utilised for extraction and purification of plasmids from selected colonies from the respective transformed α -chemically competent *E. coli* cell cultures (Section 2.5.2.3., p.181) – via the summarised Low Copy Number Kit Protocol:

- (i) A sterile/autoclaved wooden toothpick was utilised to inoculate 5mL of L.B. ampicillin broth medium (Section 2.3.1, p.167) with one transformed α -chemically competent *E. coli* cell colony, picked from the respective L.B ampicillin selection agar petri-plate, in a 50mL capacity Greiner plastic centrifuge tube (fitted with a loose screw-cap) and the resultant broth culture placed in the 37°C Sanyo orbisafe incubator (set at 180 r.p.m. shake speed) for 24 hours duration.
- (ii) 1.5mL of the resultant broth culture was then pipetted into a 1.5mL capacity plastic eppendorf microfuge tube which was then spun at 12000rpm at 4°C for 2 minutes in a Sanyo Hawk 15/05 refrigerated bench top microfuge.
- (iii) The resultant supernatant was discarded, prior to addition of further 1.5mL of culture to the tube, which contained the retained cell pellet, after which the tube was re-centrifuged at 12,000rpm, 4°C for 2 minutes and the resultant supernatant discarded.
- (iv) The resultant cell pellet was then gently re-suspended in 200 μ L of the kit solution 1 and the resultant mixture stood at room temperature for 1 minute.
- (v) 400 μ L of the kit solution II was then added and blended gently with the tube contents via successive inversion of the tube 6 times , after which the resultant mixture was stood for 1 minute at room temperature.

[Note: The mixture was NOT vortexed to prevent genomic DNA contamination of the plasmid extract]

- (vi) 700 μ L of kit solution III was then blended with the resultant tube contents, via gentle repetitive tube inversion and the resultant mixture stood at room temperature for 1 minute, prior to centrifugation in a Sanyo Hawk 15/05 refrigerated bench top microfuge at 12000rpm, 4°C for 5 minutes.
- (vii) Half of the resultant supernatant was then transferred, via pipette, to a kit column assembly – which was then placed in a Sanyo Hawk 15/05 refrigerated bench top microfuge and spun at 10,000rpm for 2 minutes at 4°C.
- (viii) The resultant eluent was discarded and the remainder of the supernatant, acquired from step (vii), was then added to the kit column assembly which was then re-spun in a Sanyo Hawk 15/05 refrigerated bench top microfuge at 10,000rpm at 4°C for 2 minutes.
- (ix) The resultant eluent was then discarded and 500 μ L of kit wash solution was then added to the column, prior to re-centrifugation of the kit column assembly at 10,000rpm, 4°C for 2 minutes in a Sanyo Hawk 15/05 refrigerated bench top microfuge.
- (x) The resultant eluent was discarded and step (ix) repeated with 500 μ L of fresh kit wash solution.
- (xi) The resultant eluent was then discarded and the kit column assembly was then re-spun at 10,000rpm, 4°C for a further 2 minutes in a Sanyo Hawk 15/05 refrigerated bench top microfuge to remove any residual traces of wash solution from the column – which would have otherwise impeded elution of the respective purified plasmid DNA from the column.
- (xii) The column was then transferred to a fresh, clean 1.5mL capacity plastic eppendorf microfuge tube and 50 μ L of the kit elution buffer was then added to the centre of the column, after which the column assembly was stood at room temperature for 2 minutes prior to centrifugation in a Sanyo Hawk 15/05 refrigerated bench top microfuge at 10,000rpm, 4°C for 2 minutes and the resultant eluted/purified plasmid DNA solution was then stored at -20°C until required.

As the research work progressed it was discovered that utilisation of the GenELute™ Plasmid Miniprep Kit (Sigma Life Sciences), in place of the IDPure™ Spin Column Plasmid DNA Miniprep Kit (ID Labs Inc.) , resulted in a significant improvement in efficient extraction yield, purification quality and stability of the constructed Cre-Lox pAW8 Cre-Lox donor plasmids isolated from selected Ampicillin-resistant colonies acquired from transformed α -chemically competent *E. coli* cell cultures (Section 2.5.2.3., p.181)

An optimised, modified protocol of the GenELute™ Plasmid Miniprep Kit (Sigma Life Sciences) was later adopted for this purpose – comprised of the following key steps:

- (i) A sterile/autoclaved wooden toothpick was utilised to inoculate 2mL of L.B. ampicillin broth medium (Section 2.3.1, p.167) with one transformed α -chemically competent *E. coli* cell colony, picked from the respective L.B ampicillin selection agar petri-plate, in a 15mL capacity Greiner plastic centrifuge tube (fitted with a loose screw-cap) and the resultant broth culture placed in the 37°C Sanyo orbisafe incubator (set at 180 r.p.m. shake speed) for 35 hours duration.
 - (ii) 1 mL of the resultant broth culture was then pipetted into a 1.5mL capacity plastic eppendorf microfuge tube which was then spun at 12000rpm at 4°C for 2 minutes in a Sanyo Hawk 15/05 refrigerated bench top microfuge.
 - (iii) The resultant supernatant was discarded , the pelleted cells were re-suspended gently re-suspended in 200 μ L of the supplied re-suspension solution and the resultant mixture incubated at room temperature for 1 minute.
 - (iv) 200 μ L of the supplied lysis solution was then added and blended gently with the tube contents via successive inversion of the tube 8 times , after which the resultant mixture was stood for 1 minute at room temperature.
- [Note: The mixture was NOT vortexed to prevent genomic DNA contamination of the plasmid extract]

- (v) 700µL of the supplied neutralization/binding solution was then blended with the resultant tube contents, via gentle repetitive tube inversion and the resultant mixture stood at room temperature for 1 minute, prior to centrifugation in a Sanyo Hawk 15/05 refrigerated bench top microfuge at 12000rpm, 4°C for 10 minutes.
- (vi) A GenElute Miniprep Binding Column-microfuge tube assembly was set up and pre-equilibrated via addition of 500 µL of the supplied column preparation solution to the column, prior to centrifugation of the assembly in the refrigerated bench-top microfuge at 12000rpm, 4°C for 1 minute.
- (vii) 750µL of cleared lysate, acquired previously from step (vi), was then loaded onto the column and the assembly incubated at room temperature for 2 minutes, prior to centrifugation at 12,000rpm, 4°C for 1 minute in a Sanyo Hawk 15/05 refrigerated bench top microfuge.
- (viii) The resultant eluent was then discarded and 750µL of kit wash solution was then added to the column, prior to re-centrifugation of the kit column assembly at 12,000rpm, 4°C for 1 minute in a Sanyo Hawk 15/05 refrigerated bench top microfuge.
- (ix) The resultant eluent was then discarded and the kit column assembly was then re-spun at 12,000rpm, 4°C for a further 1 minute in a Sanyo Hawk 15/05 refrigerated bench top microfuge to remove any residual traces of wash solution from the column – which would have otherwise impeded elution of the respective purified plasmid DNA from the column.
- (x) The column was then transferred to a fresh, clean 1.5mL capacity plastic eppendorf microfuge tube and 60µL of the kit elution buffer was then added to the centre of the column, after which the column assembly was stood at room temperature for 2 minutes prior to centrifugation in a Sanyo Hawk 15/05 refrigerated bench top microfuge at 12,000rpm, 4°C for 2 minutes and the resultant eluted/purified plasmid DNA solution was then stored at -20°C until required.

2.5.2.5 Restriction Digest Assay Verification of Donor pAW8-rad9 Plasmid Constructs

5 μ L aliquot samples of the resultant Cre-RMCE donor plasmid pAW8 mini-prepped plasmid extracts, acquired from individual colony cultures of transformed Ampicillin-resistant competent *E. coli* cells (Section 2.5.2.4, pp.182-185), were subjected to comparative SphI and SpeI restrictive digest analyses.

(i) Each restriction digest reaction comprised: 5 μ L pAW8 Plasmid DNA “mini-prep” extract (~2ng)

5 μ L 10x SpeI NE Reaction Buffer 2

5 μ L 10x SphI Reaction Buffer K

0.5 μ L SpeI Restriction Enzyme (10U/ μ L)

0.5 μ L SphI Restriction Enzyme (10U/ μ L)

34 μ L Autoclaved/Sterile Ultra-Pure Millipore Water

Total Reaction Volume = 50 μ L

Note: A negative comparative control digest was performed with 5 μ L of “empty” pAW8 Plasmid DNA (~2ng).

A comparative digest control was also performed with 5 μ L of the appropriate PCR-engineered *rad9* gene cassette insert (~2ng).

The digest reaction mixtures were set up in thin-walled PCR tubes, which were then placed in the 37°C static binder incubator for 24 hrs (this incubation time was utilised to ensure maximal restriction digestion of the DNA samples, prior to comparative ethidium gel analyses).

(ii) The following day, each 50 μ L digest reaction mixture was placed into a separate 1.5mL capacity plastic eppendorf tube containing 40 μ L isopropanol and the resultant 90 μ L total volume contents vortexed briefly (~10 seconds) prior to incubation on dry ice for 15 minutes.

(iii) Each tube contents was then spun at 12,000 r.p.m., 4°C for 20 minutes in a Sanyo Hawk 15/05 bench-top refrigerated microfuge, after which time the supernatant was removed and discarded (via utilisation of fine glass pasteur pipette-coupled vacuum aspiration, taking due caution not to disturb/dislodge the precipitated plasmid DNA pellet).

- (iv) Each tube was then placed (cap open) in the 37°C static binder incubator for 20 minutes for evaporated removal of remnant traces of isopropanol from the precipitated plasmid DNA pellet.
- (v) Each resultant dried plasmid DNA pellet was then dissolved in 18µL of sterile/autoclaved, ultra-pure millipore water, prior to the addition of 2µL of 10x DNA Sample Loading Buffer Dye and the resultant mixture vortexed briefly (~10 seconds).
- (vi) 10µL aliquots of each of the resultant prepared mini-prep pAW8 plasmid DNA samples were then loaded onto a 1% 1xTBE agarose electrophoretic gel (containing 0.5µg/mL ethidium bromide, run at 120V constant setting for 30 minutes – Section 2.2.1, p.162), after which time the gel was visualised via U.V. trans-illumination on the Bio-Rad Gel 2000 Imager System for identification and selection of plasmid mini-preps which contained the ligated PCR-engineered *rad9* gene cassette insert.
- (vii) Comparative DNA control samples of the un-digested “empty” pAW8 plasmid, appropriate PCR-engineered cassette insert and a selected pAW8-*rad9* plasmid construct mini-prep extract (identified from stage (vi) previously) were prepared via pipette-mixing of 9µL of the appropriate aqueous DNA solution with 1µL of 10x DNA Sample Loading Buffer Dye.
- (viii) These prepared un-digested samples, along with the remaining 10µL aliquots of the “empty” pAW8 plasmid digest and the corresponding selected pAW8-*rad9* plasmid construct mini-prep extract sample were then run on a 1xTBE agarose electrophoretic gel (Section 2.2.1, p.162) – as described previously in stage (vi).

NOTE: These comparative un-digested and restriction-digested sample analyses were necessary for identification of successfully-ligated pAW8-*rad9* constructs and for verification that the restriction endonucleases SpeI and SphI only cleaved within their specific base-sequence target-recognition sites (ie that the respective enzymes did not exhibit any unanticipated non-specific/“star” activity with regard to cleavage at random sites within the pAW8 plasmid and/or PCR-engineered *rad9* gene cassette inserts).

2.5.3 S.pombe Transformation Protocol

A lithium acetate-based protocol was utilised for the respective $\Delta rad9$ Cre-RMCE *S. pombe* base-strain cell transformations with the Cre-RMCE donor pAW8 plasmid mini-prepped gene cassette insert ligation constructs – comprised of the following summarised steps:

(i) A sterile/autoclaved wooden toothpick was utilised to inoculate 50mL of sterile/autoclaved EMM Minus Uracil selective medium (Section 2.3.1, p.167) with a small amount of the $\Delta rad9$ *S. pombe* Cre-RMCE base-strain YEA agar petri-plate culture, in a sterile/autoclaved 250mL capacity glass conical flask (capped loosely with aluminium foil) and the resultant broth culture placed in the 30°C Sanyo orbisafe incubator (set at 180 r.p.m. shake speed) for 24 hours duration.

(ii) The following day, a 100 μ L aliquot of the resultant broth culture was diluted with 900 μ L EMM Minus Uracil medium and the resultant 1 in 10 diluted culture sample (1mL) was then placed in a plastic microcuvette for subsequent measurement of the optical density at A₅₉₅ (O.D. 595) in a Sanyo SP BIO Spectrophotometer (against a set blank reference of 1mL EMM minus Uracil broth medium) and the optical density of the “neat” culture calculated:

$$\text{ie } A_{595} (\text{“neat” culture}) = A_{595} (1 \text{ in } 10 \text{ diluted culture}) \times 10$$

(iii) An appropriate volume of resultant broth culture was then diluted with the appropriate volume of EMM (minus Uracil) broth medium to a final A₅₉₅ optical density = 0.5 units dictated by the calculated diluent factor ratio, D.F.R.:

$$\text{ie D.F.R.} = \frac{\text{Calculated } A_{595} (\text{“neat” culture})}{0.5}$$

In accordance with the related equation: $V1 = \frac{C2 \times V2}{C1}$

Where:

V1 = Volume of measured cell culture

V2 = Volume of cell culture required

C1 = O.D.595 of cell culture measured

C2 = O.D.595 of cell culture required

- (iv) A 50mL aliquot of the adjusted $A_{595} = 0.5$ optical density units broth culture was then placed in a 50mL capacity sterile plastic Greiner screw-cap centrifuge tube and the spun at 3,300g for 5 minutes in a Jencons-PLS SorvallR Legend T Centrifuge in the 4°C cold room.
- (v) The resultant supernatant was then discarded, the cell pellet re-suspended in 50mL ultra-pure, sterile/autoclaved millipore water and the cell solution re-centrifuged at 3,300g for 10 minutes in a Jencons-PLS SorvallR Legend T Centrifuge the 4°C cold room.
- (vi) The resultant supernatant was then discarded, whilst the washed cell pellet was re-suspended in 1mL of sterile/autoclaved ultra-pure millipore water and transferred to a 1.5mL capacity eppendorf plastic microfuge tube.
- (vii) The resultant cell solution was then spun at 3000rpm at 4°C for 2 minutes in a Hawk 15/05 refrigerated bench top microfuge, the supernatant discarded and the retained cell pellet was re-suspended in 1mL of LiAc-TE buffer solution (Section 2.2.5, p.166) prior to re-centrifugation at 3000rpm at 4°C for 2 minutes.
- (viii) The supernatant was then discarded and the resultant washed cell pellet re-suspended in 250µL of LiAc-TE buffer solution (Section 2.2.5, p.166).
- (ix) Each transformation reaction mixture comprised:
- 100µL prepared Cre-RMCE *S. pombe* base-strain LiAc-TE cell suspension
 - 2µL non-denatured (ie NOT pre-heated to 95°C prior to use) salmon sperm carrier DNA (10mg/mL)
 - 10µL of the appropriate Cre-RMCE donor plasmid pAW8-*rad9* construct mini-prep solution (~4ng) – prepared previously in accordance with the protocol described in Section 2.5.2, pp.179-187
- Set up in a 1.5mL capacity plastic eppendorf microfuge tube and incubated at room temperature for 10 minutes prior to the addition of 260µL of LiAc-TE-PEG buffer solution (Section 2.2.5, p.166).
- (x) Each eppendorf tube, containing each respective transformation reaction mixture, was then placed in the 30°C static binder incubator for 1 hour.

- (xi) Each tube was then removed from the incubator, followed by the addition of 43 μ L of 42°C pre-equilibrated DMSO to each respective transformation reaction mixture, prior to placement of each tube in a 42°C hot block for 5 minutes for subsequent cell culture heat shock plasmid transformation phase.
- (xii) Each tube was then placed in a Sanyo Hawk 15/05 refrigerated bench top microfuge and the resultant heat shock transformed cell solutions spun at 3000rpm, 4°C for 2 minutes.
- (xiii) The supernatant was then discarded and each resultant cell pellet was then re-suspended in 1mL of sterile/autoclaved, ultra-pure millipore water, prior to re-centrifugation at 3000rpm, 4°C for 2 minutes in a Sanyo Hawk 15/05 refrigerated bench top microfuge.
- (xiv) The supernatant was discarded and each resultant washed transformed cell pellet was then re-suspended in 100 μ L sterile/autoclaved YEA medium (Section 2.3.1, p.167).
- (xv) 10mL aliquots of sterile/autoclaved YEA medium (Section 2.3.1, p.167), contained in 50ml capacity sterile Greiner plastic centrifuge tubes, were then inoculated with the respective 100 μ L YEA medium suspensions of transformed *S. pombe* Cre-RMCE base-strain cells, after which the tubes were loosely capped and placed in the 30°C Sanyo Orbisafe orbital incubator shaker for 24 hours.
- (xvi) The following day a 1mL aliquot of each resultant broth culture was placed in a 1.5mL capacity plastic eppendorf microfuge tube and spun at 3000rpm, 4°C for 2 mins in the Sanyo Hawk 15/05 refrigerated bench top microfuge.
- (xvii) In each case, the supernatant was subsequently discarded and the resultant pellet of transformed Cre-RMCE *S. pombe* base-strain cells was then re-suspended in 50 μ L of autoclaved/sterile YEA Medium (Section 2.3.1, p.167).

(xviii) Each resultant cell suspension was then evenly spread out onto an EMM (minus Leucine) agar selection medium petri-plate(Section 2.3.2, p.168) via utilisation of a 70% (v/v) ethanol-sterilised flame spreader and each resultant culture placed in the 30°C static binder incubator for 7 days.

(xix) The resultant colonies on each incubated EMM (Minus Leucine) agar petri plate were then replica-plated onto fresh EMM (Minus Leucine) and YEA-5FOA agar selection plates (Section 2.3.2, p.168) and the resultant cultures placed in the 30°C static binder incubator for 7 days.

[NOTE: pAW8 plasmid constructs prepared and utilised are detailed in Appendix 2.11.5, p.278

Generated “Cre-Lox” *S. pombe* strain genotypes are detailed in Appendix 2.11.7, p.280]

2.6 Initial “Cre-Lox”-Engineered *S. pombe* Strain Verification Assays

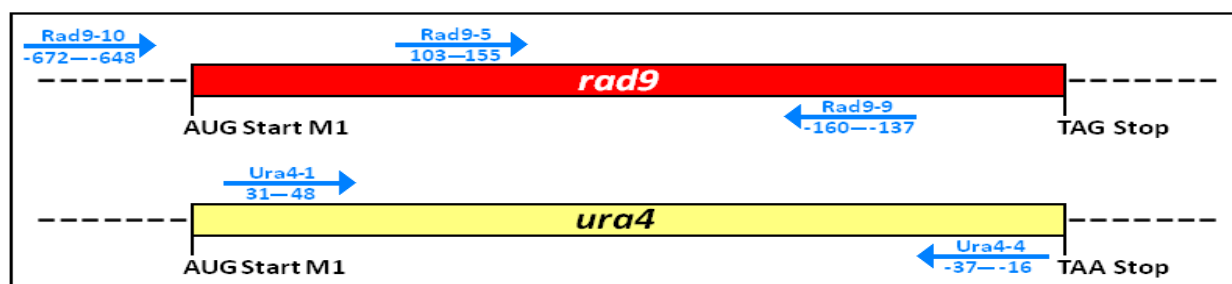
2.6.1 Selective Agar Media Phenotyping Assays

Selected colonies of the “Cre-Lox”-generated *S. pombe* strains were streaked, via utilisation of sterile/autoclaved cocktail sticks, onto YEA, EMM (Adenine, Leucine, Uracil supplemented), EMM (Minus Uracil), EMM (Minus Leucine) and YEA-5FOA agar petri-plates (Section 2.3.2, p.168), which were then placed in the 30°C static binder incubator for three days for comparative assessment of their relative growth sensitivity on the respective media utilised.

2.6.2 PCR Genotyping Assays

2.6.2.1 PCR Genotypic Verification of the $\Delta rad9$ Cre-RMCE “Base-Strain”

A genomic DNA extract of the pAW1-generated Cre-Lox “base-strain” was prepared (Section 2.4, pp.169-170) and subjected to comparative genomic PCR analyses with primer pair combinations Rad9-5, Rad9-9; Rad9-9 and Rad9-10; Ura4-1 and Ura4-4; Ura4-1 and Rad9-10; Ura4-4 and Rad9-10 respectively.



[The PCR Thermocycler Program utilised was the same as that for Rad9-S5 and Rad9-S8 primers – Fig 2.7, p.193]

2.6.2.2 PCR Genotypic Verification of pAW8-*rad9* Base-Strain Cre-RMCE Transformants

Genomic DNA extracts were prepared from the *S. pombe* strains (via the protocol described previously in Section 2.4, pp.166-167) and subjected to comparative genomic PCR analyses with primer pair combinations Rad9-S5 and Rad9-S6 (for the untagged *rad9* *S. pombe* strain) or Rad9-S5 and Rad9-S8 (for C-terminal HA epitope-tagged, engineered *rad9* *S. pombe* strains) for confirmation of the presence of the respective Cre-RMCE-integrated engineered *rad9* gene cassette – Fig 2.7, p.193]

[NOTE: All PCR primer sequences are detailed in Appendix 2.11.3, p.276]

2.6.3 DNA Sequence Verification of the “Cre-Lox” Engineered *S. pombe* Strains

(i) Genomic DNA extracts were prepared from 10mL YEA broth cell cultures of each “Cre-Lox”-engineered *S. pombe* strain (Section 2.3.1, p.167), via the protocol described previously in Section 2.4 (pp.169-170) and utilised for PCR amplification (Fig 2.7, below) of the respective modified *rad9* gene (integrated at the endogenous *rad9* gene locus situated within Chromosome 1) .

Fig 2.7: Summarised PCR Reaction Mixtures and Thermocycler Parameters

PCR Amplification of <i>rad9</i> Genes from "Cre-Lox"-Engineered <i>S. pombe</i> Strains for DNA Sequencing		
PCR Reaction Mixtures		Thermocycler Program
Un-Tagged <i>rad9</i> Gene Amplification	C-Terminal(HA) ₃ -Tag <i>rad9</i> Gene Amplification	Pre-Heat Hot Lid = 105°C Hot Lid = "On" Hot Start = "Off" Pause = "Off" 98°C 1 Minute Pre-Cycle 98°C 30 Seconds <i>Separation</i> 56°C 30 Seconds <i>Annealing</i> 72°C 2.5 Minutes <i>Extension</i> } x35 Cycles 72°C 10 Minutes Post-Cycle 4°C Hold
Genomic DNA Solution (1 in 10 Dilution)= 20µL 10µM Rad9-S5 Primer Stock Solution = 5µL 10µM Rad9-S6 Primer Stock Solution = 5µL 2mM dNTPs Stock Solution = 10µL 5xGC Phusion Polymerase Reaction Buffer = 20µL Sterile, Ultra-Pure Millipore H ₂ O = 39µL Phusion Polymerase Enzyme (2U/µL) = 1µL Total Reaction Volume = 100µL	Genomic DNA Solution (1 in 10 Dilution)= 20µL 10µM Rad9-S5 Primer Stock Solution = 5µL 10µM Rad9-S8 Primer Stock Solution = 5µL 2mM dNTPs Stock Solution = 10µL 5xGC Phusion Polymerase Reaction Buffer = 20µL Sterile, Ultra-Pure Millipore H ₂ O = 39µL Phusion Polymerase Enzyme (2U/µL) = 1µL Total Reaction Volume = 100µL	

- (ii) After completion of the thermocycler program, each PCR reaction mixture (100µL) was transferred to a 1.5mL capacity plastic eppendorf microfuge tube containing 80µL “neat” Isopropanol, after which the contents were vortexed briefly (~ 10 seconds) and the resultant mixture incubated on dry-ice for 15 mins, prior to centrifugation at 12,000 r.p.m. at 4°C for 20 minutes in a Sanyo Hawke 15/05 refrigerated microfuge.
- (iii) The resultant supernatant was removed via utilisation of fine glass Pasteur pipette evacuation (taking care not to disturb/dislodge the precipitated DNA pellet) and each tube was then placed (cap open) in the static 37°C binder incubator for 20 minutes for evaporated removal of remnant traces of isopropanol.
- (iv) 45µL of sterile/autoclaved, ultra-pure millipore water was then added to each tube, followed by the addition of 5µL of 10x DNA Loading Buffer Dye and the resultant contents mixed thoroughly via vortexing (~1 minute).

- (v) The resultant 50µL samples were then gel purified utilising a 1xTAE Agarose gel (Section 2.2.1, p.162) and the *IDPure*TM Spin Column DNA Gel Extraction Kit (ID Labs Inc.) – as described previously in Section 2.5.1 (pp.177-178).
- (vi) 2µL of each resultant purified DNA eluent solution was then transferred to a 1.5mL capacity plastic eppendorf tube containing 98µL of sterile/autoclaved, ultra-pure millipore water and the contents vortexed briefly (~10 seconds).
- (vii) The resultant DNA sample (100µL) was then placed in a Precision Cells Type 701M U.V. quartz microcuvette cell, which was then placed in a Sanyo SP BIO Spectrophotometer set at A=260nm/”DNA Measurement Mode” (“zeroed” previously against a blank reference analyte solution, placed in the identical U.V. quartz microcuvette cell, which comprised 98µL of sterile/autoclaved, ultra-pure millipore water mixed with 2µL of the elution buffer supplied in the *IDPure*TM Spin Column DNA Gel Extraction Kit).
- (viii) The corresponding concentration of the remainder of the “neat”, eluted DNA solution was then calculated via utilisation of the equation:

$$[\text{DNA}] (\mu\text{g/mL}) = \frac{\text{A}_{260} \times \text{D.F.} \times 50^*}{1000}$$

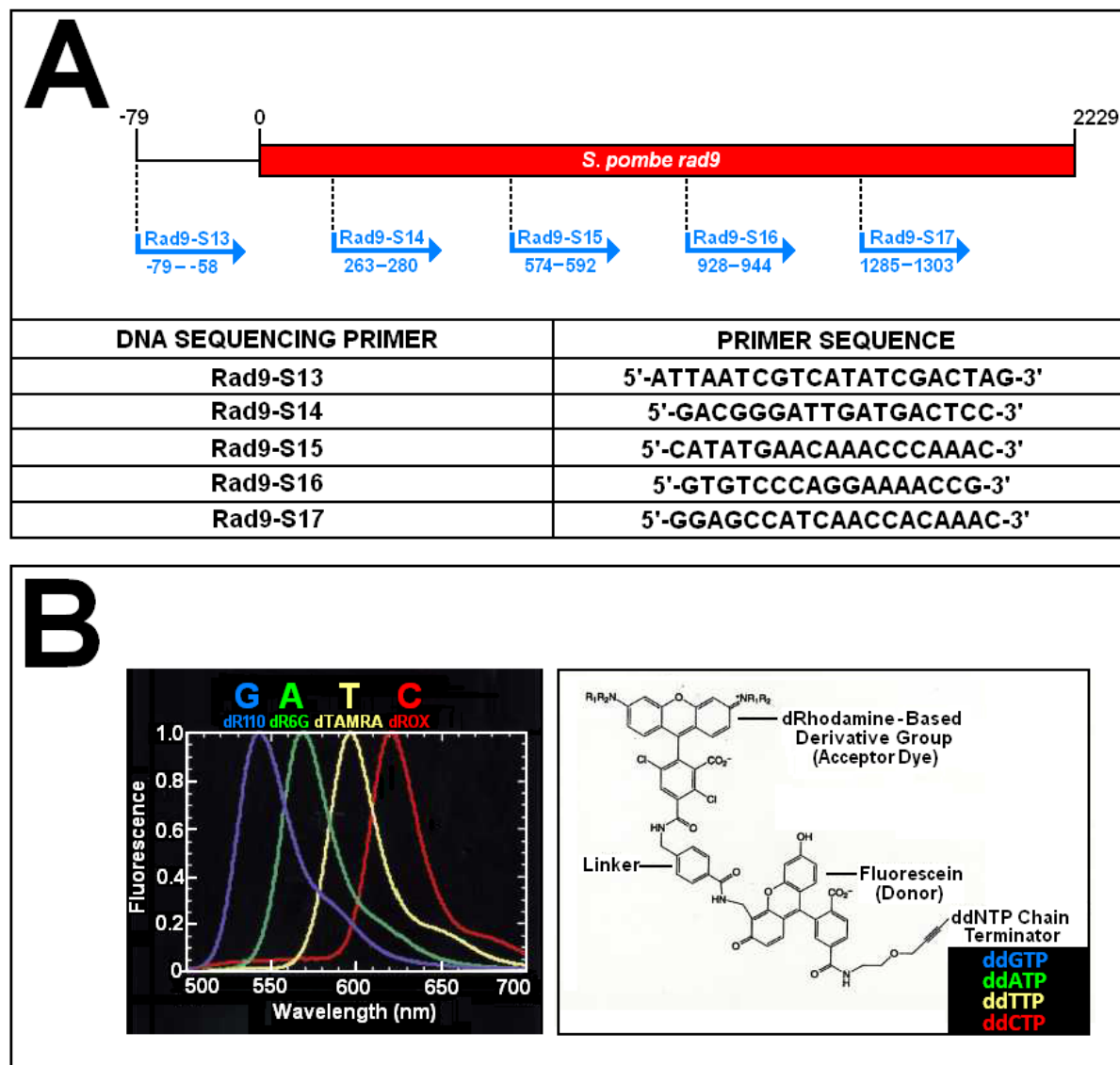
Where: A₂₆₀ = U.V. Absorbance at Wavelength, λ = 260nm

D.F. = Eluted DNA Sample Dilution Factor = 50
(ie A 1 in 50 diluted DNA Sample Prep.)

One A₂₆₀ O.D. Unit = *50µg/mL DNA

- (ix) The remainder of the “neat”, eluted DNA solution was then adjusted, via addition of the appropriate amount of sterile/autoclaved millipore water, to a final concentration of 10ng/µL and stored at -20°C until required.
- (x) A 100µL aliquot of each DNA sample (10ng/µL) and 100µL aliquots of the *rad9* gene sequencing PCR primers Rad9-S13, Rad9-S14, Rad9-S15, Rad9-S16 and Rad9-S17 (at 2pmol/µL final concentration prepared from the 10µM primer stock solutions via appropriate serial dilutions in sterile/autoclaved ultra-pure millipore water) were placed in 1.5mL capacity eppendorf tubes, marked with the appropriate sample bar-code labels (supplied by the service company) and sent to Eurofins MGW Operon for DNA sequencing (Fig 2.8, p.195).

Fig 2.8: Summarised Details of DNA Sequencing Primers and ddNTP Terminators



A: Progressive “gene-walking” site map and sequences of the PCR primers utilised for DNA sequencing of the PCR-amplified *rad9* gene samples prepared from genomic DNA extracted from cell cultures of the various “Cre-Lox”-engineered *S. pombe* strains.

[Figure ranges detailed underneath each representative primer arrow denote the relative 5’- 3’ base-pair positions spanning the complementary annealing target sequence recognised specifically by each respective primer].

B: PCR-amplified *rad9* gene samples and primers were submitted to the service company Eurofins MWG Operon (<http://www.eurofinsdna.com>) for DNA sequencing.

The samples were processed on an ABI Prism 3730xl 96 capillary electrophoresis array DNA Analyzer in conjunction with appropriate ABI Big-Dye® ddNTP fluorescent DNA chain terminators and instrument operating instructions/protocols* – as supplied by the company Applied Biosystems Life Technologies Inc. (<http://www.appliedbiosystems.com>).

[*The ratio of dNTP’s to ddNTP’s is carefully selected to ensure single-hit kinetics, in which only one ddNTP terminator is incorporated into a single DNA chain per PCR thermocycle]

Each DNA chain-incorporated ddNTP fluoresces at a distinctive wavelength for highthroughput sample scanning and efficient base detection assignment for rapid, reliable DNA sequencing.

2.6.4 Engineered *rad9* Gene Expression Verification

Comparative 1D SDS-PAGE and Western Blot Analyses were performed on TCA-precipitated total extracts acquired from 10mL YEA cell cultures of each respective “Cre-Lox”-engineered *S. pombe* strain (prepared via utilisation of the protocols described in Section 2.8.1, pp.200-202) for detected confirmation of viable protein expression of the respective “Cre-Lox”-integrated, PCR-modified *rad9* gene variants.

2.7 Preparation of *S. pombe* Genetic “Cross-Strain” Mutants

- (i) Sterile/autoclaved wooden cocktail sticks were utilised to transfer a small amount of each required *S. pombe* strain from a YEA agar plate (Section 2.3.2, p.168) culture to the same 1.5mL capacity plastic eppendorf microfuge tube which contained 50 μ L of autoclaved/sterile ultra-pure millipore water.
- (ii) The tube contents were then agitated gently via repetitive pipetting and the resultant *S. pombe* strain mixture was then pipetted as a single 50 μ L drop onto a Malt Extract Agar petri-plate (Section 2.3.2, p.168), which was then allowed to stand on the lab bench at room temperature until the drop had dried.
- (iii) The resultant Malt Extract Agar petri-plate culture was then placed in the 25°C static incubator for three days.
- (iv) After the incubation time had elapsed, a sterile/autoclaved wooden cocktail stick was utilised to transfer a small amount of the resultant cross-strain mated culture from the Malt Extract agar petri-plate to a 1.5mL capacity plastic eppendorf microfuge tube which contained 500 μ L of 30% (v/v) aqueous ethanol.
- (v) The resultant tube contents were then vortexed briefly (~30 seconds) and the resultant mixture stood on the lab bench at room temperature for 30 minutes to provide sufficient time to ensure complete cell lysis to leave only the intact mated cross-strain spores.
- (vi) 50 μ L of the resultant mixture was then pipetted onto a fresh YEA agar petri-plate and spread evenly over the plate via utilisation of a 70% ethanol-sterilised flame spreader.
- (vii) The resultant YEA agar petri-plate culture was then placed in the 30°C static incubator for three days.
- (viii) The resultant colonies were then replica-plated onto a fresh YEA agar petri-plate and the appropriate agar selection media petri-plate (detailed in Table 2.1, p.198) which were then placed in the 30°C static incubator for three days.

Table 2.1: Gene Marker-Based Replica Plate Selection of *S. pombe* “Cross-Strain” Colonies

Replica Plate Selection Medium	<i>S. pombe</i> "Cross-Strain" Genetic Hybrid Construct			
EMM Minus Leucine	<i>rad9-S-c3xHA Δhus1</i>	<i>rad9-S-c3xHA Δtop1</i>	<i>rad9-c3xHA Δrad26</i>	<i>rad9-S-c3xHA Δuvde</i>
	<i>rad9-(M50L)-c3xHA Δrad26</i>	<i>rad9-S-c3xHA Δrad26</i>		
EMM Minus Uracil	<i>rad9-S-c3xHA Δrad1</i>	<i>rad9-S-c3xHA Δrad3</i>	<i>rad9-S-c3xHA Δwis1</i>	<i>rad9-S-c3xHA Δbub1</i>
	<i>rad9-S-c3xHA Δrad17</i>	<i>rad9-S-c3xHA Δtel1</i>	<i>rad9-S-c3xHA Δsty1</i>	<i>rad9-S-c3xHA Δmad2</i>
	<i>rad9-c3xHA Δrad3</i>	<i>rad9-S-c3xHA Δcrb2</i>	<i>rad9-S-c3xHA Δcgs1</i>	<i>rad9-S-c3xHA Δrqh1</i>
	<i>rad9-(M50L)-c3xHA Δrad3</i>	<i>rad9-S-c3xHA Δchk1</i>	<i>rad9-S-c3xHA Δrad24</i>	<i>rad9-S-c3xHA Δrad16</i>
YEA 37°C	<i>rad9-S-c3xHA rad4.116</i>			
	<i>rad9-S-c3xHA cdc25.22</i>			
	<i>rad9-S-c3xHA spo12.B81</i>			
YEA-G418	<i>rad9-S-c3xHA Δmrc1</i>	<i>rad9-S-c3xHA Δclp1</i>	<i>rad9-S-c3xHA Δhhp1</i>	<i>rad9-S-c3xHA Δmus81</i>
	<i>rad9-S-c3xHA Δmph1</i>	<i>rad9-S-c3xHA Δtdp1</i>	<i>rad9-S-(Y12F)-c3xHA Δmph1</i>	<i>rad9-S-c3xHA ΔligIV</i>
YEA 30°C	<i>rad9-S-c3xHA hus1-c13xMyc</i>	} These "cross-strains" possessed no selectable marker and were verified via Western Blot Analytical Detection of the HA and Myc C-Terminal Epitope Tags	<i>rad9-S-c3xHA cds1-c13xMyc</i>	
	<i>rad9-S-c3xHA cds1-(T8A;T11A)-c13xMyc</i>			
	<i>rad9-S-c3xHA mph1-c13xMyc</i>			

[Note: The compositions of all the selection agar media utilised are detailed summarily in Section 2.3.2, p.168

Full genotypes of *S. pombe* strains utilised and double-mutant strains constructed are detailed in Appendices 2.11.6, p.279; 2.11.7, p.280 and 2.11.8, p.281]

- (ix) Sterile/autoclaved wooden cocktail sticks were then utilised to pick and streak ten individual colonies from the appropriate replica plate and onto a fresh YEA agar petri-plate (Section 2.3.2, p.168) which was then placed in the 30°C static incubator for three days.
- (x) After three days incubation had elapsed, a small amount of each resultant streak colony culture was transferred to a separate 50mL capacity plastic Greiner centrifuge screw-lid tube which contained 15mL of YEA broth medium (Section 2.3.1, p.167) .
- (xi) The resultant inoculated cultures, contained within the 10 Greiner Tubes, were then placed in the 30°C incubator and placed in the 30°C Sanyo orbisafe incubator shaker for 24 hours duration.
- (x) Total TCA-precipitated protein extract samples were then prepared from each respective culture (protocol detailed in Section 2.8.1, pp.200-202).
- (xi) The resultant total protein extracts were then subjected to SDS-PAGE/Western-Blotting analysis (protocols detailed in Section 2.8.4, pp.223-224 and Section 2.8.6, pp.231-233).
- (xii) Streak colony cultures which exhibited the appropriate selection plate phenotype and Western Blot analytical result for the respective *S. pombe* cross-strain were then transferred from the original YEA agar petri-plate and re-plated onto separate fresh YEA agar petri-plates (Section 2.3.2, p.168) which were then placed in the 30°C static incubator for three days.
- (xiii) After three days incubation time had elapsed, each correct colony culture was transferred from the YEA agar petri-plate to a 1.5mL capacity plastic screw-cap microfuge tube which contained 1mL of a solution comprised of 30%(v/v) Glycerol in YEA broth medium (Section 2.3.1, p.167).
- (ix) The tubes were then capped, the contents vortexed briefly (~30 seconds) and the resultant *S. pombe* cross-strain stock cultures stored at -80°C until required .

2.8 Protein Sample Preparation and Analysis Protocols

2.8.1 Preparation and Analysis of TCA-Precipitated Total Protein Extracts

A trichloroacetic acid (TCA)-based protocol was utilised for the preparation of precipitated total protein cellular extracts from *S. pombe* – comprised of the following summarised steps:

(i) A sterile/autoclaved wooden toothpick was utilised to inoculate 50mL of sterile/autoclaved YEA medium (see Section 2.3.1, p.167) with a small amount of the appropriate *S. pombe* strain, taken from the respective YEA agar petri-plate culture, in a sterile/autoclaved 250mL capacity glass conical flask (capped loosely with aluminium foil) and the resultant broth culture placed in the 30°C Sanyo orbisafe incubator (180 r.p.m. shaker speed) for 24 hours duration.

(ii) The following day, a 100µL aliquot of the resultant broth culture was diluted with 900µL YEA medium and the resultant 1 in 10 diluted culture sample (1mL) was then placed in a plastic microcuvette for subsequent measurement of the optical density at A₅₉₅ in a Sanyo SP BIO Spectrophotometer (against a set blank reference of 1mL YEA) and the optical density of the “neat” culture calculated:

$$\text{ie } A_{595} (\text{“neat” culture}) = A_{595} (1 \text{ in } 10 \text{ diluted culture}) \times 10$$

(iii) The equivalent volume of the resultant “neat” broth culture which corresponded to 7 equivalent A₅₉₅ optical density units was calculated, removed from the respective flask and placed in a 15mL capacity Greiner plastic screw-cap centrifuge tube:

$$\text{ie: Volume Culture Required (mL)} = \frac{7}{A_{595} \text{ "Neat Culture"}}$$

(iv) The calculated A₅₉₅ 7 optical densities equivalent volume of cell culture aliquot was then placed in a 50mL capacity plastic Greiner centrifuge screw-cap tube and spun at 3,300g for 5 minutes in a Jencons-PLS SorvallR Legend T Centrifuge in the 4°C cold room.

- (v) The supernatant was discarded, the resultant cell pellet re-suspended in 50mL of ultra-pure millipore water, after which the resultant cell was then spun at 3,300g for 10 minutes in a Jencons-PLS SorvallR Legend T Centrifuge in the 4°C cold room.
- (vi) The supernatant was discarded and the washed cell pellet re-suspended in 200µL of ultra-pure millipore water prior to transfer of the resultant cell suspension to a 1.5mL capacity plastic eppendorf microfuge tube.
- (vii) The resultant cell suspension was then spun at 12,000rpm, 4°C for 2 minutes in a Sanyo Hawk 15/05 refrigerated bench top microfuge, the supernatant discarded and the resultant cell pellet re-suspended in 200µL of ultra-pure millipore water, prior to re-centrifugation at 12,000rpm, 4°C for 2 minutes.
- (viii) The supernatant was discarded and the resultant cell pellet re-suspended in 200µL of 20% (w/v) aqueous Trichloroacetic acid solution [20% TCA(aq)], after which the resultant cell suspension was transferred to 1.5 mL capacity plastic crew-cap type microfuge tube containing 8 small spatula spoonfuls of glass beads (~150µL glass beads), prior to placement of the tube on the Genie disruptor for 6 minutes in the 4°C cold room.
- (ix) 400µL of 5% (w/v) TCA(aq) was then added to the resultant lysed cell suspension and the resultant solution transferred to a fresh 1.5mL capacity plastic eppendorf microfuge tube, which was then spun at 12,000 rpm, 4°C for 5 minutes in a Sanyo Hawk 15/05 refrigerated bench top microfuge.
- (x) The supernatant was discarded and the resultant precipitated protein pellet was then re-dissolved in 400µL of 1x SDS-PAGE protein sample loading buffer (Section 2.2.2, p.163).
- (xi) The relatively low pH/high acidity of the resultant protein solution was adjusted back to the buffer solution pH value of 6.8 via dropwise addition of 1M Tris-HCl pH8.8 solution (Section 2.2.2, p.163) until the pH indicator present in the resultant 1x SDS-PAGE protein sample loading buffer solution turned from yellow to blue.

(xii) The resultant pH-adjusted protein sample solution was then incubated in the 95°C hot block for 5 minutes and then cooled on ice for 5 minutes prior to storage at -20°C until required.

2.8.2 Preparation of Soluble Total Protein Extracts

(i) A sterile/autoclaved wooden toothpick was utilised to inoculate 100mL of sterile/autoclaved YEA medium (see Section 2.3.1, p.167) with a small amount of the appropriate *S. pombe* strain, taken from the respective YEA agar petri-plate culture, in a sterile/autoclaved 250mL capacity glass conical flask (capped loosely with aluminium foil) and the resultant broth culture placed in the 30°C Sanyo orbisafe incubator (180 r.p.m. shaker speed) for 24 hours duration.

(ii) The following day, a 100µL aliquot of the resultant broth culture was diluted with 900µL YEA medium and the resultant 1 in 10 diluted culture sample (1mL) was then placed in a plastic microcuvette for subsequent measurement of the optical density at A₅₉₅ in a Sanyo SP BIO Spectrophotometer (against a set blank reference of 1mL YEA) and the optical density of the “neat” culture calculated:

$$\text{ie } A_{595} (\text{“neat” culture}) = A_{595} (1 \text{ in } 10 \text{ diluted culture}) \times 10$$

(iii) The equivalent volume of the resultant “neat” broth culture which corresponded to 40 equivalent A₅₉₅ optical density units was calculated, removed from the respective flask and placed in a 15mL capacity Greiner plastic screw-cap centrifuge tube:

$$\text{ie: Volume Culture Required (mL)} = \frac{40}{A_{595} \text{ "Neat Culture"}}$$

(iv) The calculated A₅₉₅ 40 optical densities equivalent volume of cell culture aliquot was then placed in a 50mL capacity plastic Greiner centrifuge screw-cap tube and spun at 3,300g for 5 minutes in a Jencons-PLS SorvallR Legend T Centrifuge in the 4°C cold room.

(v) The supernatant was discarded and the resultant cell pellet re-suspended in 50mL of ultra-pure millipore water, after which the resultant cell suspension was then spun at 3,300g for 10 minutes in a Jencons-PLS SorvallR Legend T Centrifuge in the 4°C cold room.

- (vi) The supernatant was discarded and the resultant cell pellet re-suspended in 50mL of Buffer “HP” (Section 2.2.2, p.163), after which the resultant cell was then spun at 3,300g for 10 minutes in a Jencons-PLS SorvallR Legend T Centrifuge in the 4°C cold room.
- (vii) The resultant cell suspension was then spun at 12,000rpm, 4°C for 2 minutes in a Sanyo Hawk 15/05 refrigerated bench top microfuge, the supernatant discarded and the cell pellet re-suspended in 1mL of Buffer “HI” (Section 2.2.2, p.163), prior to re-centrifugation at 12,000rpm, 4°C for 5 minutes.
- (viii) The resultant cell suspension was then spun at 12,000rpm, 4°C for 2 minutes in a Sanyo Hawk 15/05 refrigerated bench top microfuge at 12000rpm, 4°C for 5 minutes, after which the supernatant was discarded and the cell pellet resuspended in 400µL of Buffer “HI” (Section 2.2.2, p.163).
- (ix) The resultant cell suspension was then transferred to a 1.5ml capacity plastic screw-cap microfuge tube, which contained 10 small spatula spoonfuls of glass beads (~200µL glass beads) and the tube was then placed on the Genie Disruptor in the 4°C cold-room for 16 minutes.
- (x) The resultant lysed cell homogenate suspension was then transferred to a 1.5ml capacity plastic eppendorf microfuge tube.
- (xi) 200µL of Buffer “HI” (Section 2.2.2, p.163) was added to the drained glass beads in the 1.5ml capacity plastic screw cap microfuge tube, the contents vortexed for 30 seconds and the resultant solution transferred to the 1.5mL capacity eppendorf microfuge tube which contained the lysed cell homogenate suspension.
- (xii) The glass bead wash step (stage xii) was repeated with a fresh 200µL aliquot of Buffer “HI” (Section 2.2.2, p.163).

(xiii) The resultant combined lysed cell homogenate solution (final total volume ~1mL) was then spun in a Sanyo Hawk 15/05 refrigerated bench top microfuge at 12000rpm, 4°C for 10 minutes.

(xiv) The supernatant (ie the soluble protein extract) was then transferred to a fresh 1.5ml capacity plastic eppendorf microfuge tube and stored at -20°C until required.

2.8.2.1 Preparation and Analysis of Cytosolic and Nuclear Fractionated Protein Samples

- (i) Both the supernatant and pellet fractions, acquired from the appropriate *S. pombe* strain culture via the total soluble protein extraction protocol described previously (Section 2.8.2, pp.203-205) were retained.
- (ii) 200 μ L of 100% (w/v) TCA(aq) was added to the total soluble protein extract (ie the cytosolic supernatant fraction) and the resultant mixture spun in a Sanyo Hawk 15/05 refrigerated bench top microfuge at 12000rpm, 4°C for 10 minutes.
- (iii) The supernatant was discarded and the precipitated protein pellet mixed with 150 μ L of 4x SDS PAGE Sample Loading Buffer (Section 2.2.2, p.163), 40 μ L of 1M Tris-HCl pH8.8 (Section 2.2.2, p.163) and 310 μ L of millipore ultra-pure water.
- (iv) The resultant, neutralised protein solution was then incubated in a 95°C hot-block for 5 minutes and then cooled on ice for 5 minutes, prior to storage of the prepared protein sample (ie the total cytosolic protein fraction) at -20°C until required.
- (v) The retained pellet fraction, acquired from the initial total soluble protein extraction (Section 2.8.2, pp.203-205) was mixed with 450 μ L of millipore ultra-pure water and 150 μ L of 4xSDS PAGE Sample Loading Buffer (Section 2.2.2, p.163).
- (vi) The resultant protein solution was then incubated in a 95°C hot-block for 5 minutes and then cooled on ice for 5 minutes, prior to storage of the prepared protein sample (ie the total nuclear protein fraction) at -20°C until required.

Phenol:chloroform:isoamylalcohol-based DNA extractions were also performed on the pellet and supernatant fractions acquired from the appropriate *S. pombe* strain cultures, via the Total Soluble Protein Extract protocol (described previously in Section 2.8.2, pp.203-205), for verification that the pellet was the nuclear fraction (ie contained DNA) and the supernatant was the cytosolic fraction (ie contained no DNA).

- (i) The insoluble retained pellet fraction in the 1.5mL capacity plastic eppendorf microfuge tube was re-suspended in 500 μ L of ultra-pure millipore water, the resultant suspension mixed with 500 μ L of Phenol:Chloroform:Isoamylalcohol and the resultant mixture vortexed (~30 seconds).
- (ii) A 500 μ L aliquot of the soluble supernatant fraction was transferred to a 1.5mL capacity plastic eppendorf microfuge tube that contained 500 μ L of Phenol:Chloroform:Isoamylalcohol and the resultant mixture vortexed briefly (~30 seconds).
- (iii) The both eppendorf tubes were then spun in a a Sanyo Hawk 15/05 refrigerated bench-top microfuge at 12000rpm, 4°C for 10 minutes.
- (iv) The upper aqueous layer (~500 μ L) from each tube was carefully transferred, via pipette, to a fresh individual 1.5mL capacity plastic eppendorf microfuge tube which contained 400 μ L of “neat” Isopropanol.
[The lower organic layer and interface contained in the original eppendorf tubes was then discarded]
- (v) The resultant contents of each tube was then vortexed (~30 seconds) prior to incubation on dry-ice for 30 minutes.
- (vi) After the incubation time had elapsed, the eppendorf tubes were spun in a a Sanyo Hawk 15/05 refrigerated bench-top microfuge at 12000rpm, 4°C for 30 minutes.

- (v) The resultant supernatants were removed via careful pipetting and discarded, after which each open-capped tube was placed in the 37°C static incubator for 20 minutes to evaporate residual traces of Isopropanol.
- (vi) A 5µL aliquot of 10x DNA Loading Buffer Dye (Section 2.2.1, p.162) and 45µL of millipore ultra-pure water was then added to each tube and the resultant mixture repeatedly vortexed (~30 second bursts) for 2 minutes.
- (vii) The resultant tube contents were then repetitively pipetted for a further minute.
- (viii) A 10µL aliquot of each prepared sample was then loaded onto a 1% (w/v) 1xTBE (0.5µg/mL ethidium bromide) agarose electrophoretic gel (0.5µg/mL ethidium bromide) run in 1xTBE buffer at 120V constant setting for 45 minutes (Section 2.2.1, p.162).
- (ix) The gel was then visualised and photographed under the U.V. transillumination setting on the Bio-Rad Gel Doc 2000 White Light and U.V. imager system.

2.8.2.2 Preparation and Analysis of Total Soluble Protein HPLC-SEC Fractionated Samples

(i) 250µL of the appropriate soluble total protein extract (Section 2.8.2, pp.203-205) was injected, via utilisation of a microlitre syringe, into the sample loop of the ÄKTAFPLC High-performance Liquid Chromatography (HPLC) System which was fitted with a Superdex 200HR 10/30 Size Exclusion Column (Amersham Pharmacia Biotech/GE Healthcare) that had been pre-equilibrated with Buffer “HM” (Section 2.2.2, p.163) and pre-calibrated with a High Molecular Weight Gel Filtration Internal Protein Standard Kit (Amersham Pharmacia Biotech/GE Healthcare).

[Instrumentation configuration and selected operating parameters for the size-exclusion chromatographic (SEC) fractionation of the loaded total soluble protein extract are summarised below]

Instrument Configuration	Operational Parameters	
Inject Valve: INV-907 Sample Loop: 500µL Capacity (10MPa) Pump: P-920 Mixer: M-925 Flow Restrictor: FR902 (0.2Pa) On-Line Filter (Pore-Size = 0.2µM) Column: Superdex 200HR 10/30 Size Exclusion (Gel Filtration) HPLC-SEC Column Combined Monitor: UPC-900 U.V. Absorption Measurement pH Measurement Conductivity Measurement Standard U.V. Flow Cell: 5mm Path Length Lamp: Fixed Wavelength (Hg; λ = 280nm) Rotary Fraction Collector: FRAC-950 (Complete Automated "Drop-Synch." Assembly) PC Operating Software: UNICORN v3.2	SELECTED PRE-PROGRAM TEMPLATE OPTIONS	
	Sample Loading Technique: "Complete Filling" Flow Rate: 0.25mL/min Fractional Elution Method: "Eluate Fractionation Combined with Peak Fractionation" Peak_Frac_Size = 1ml Peak_Start_Slope: Automatic Pre-Program Setting Peak_Stop_Slope: Automatic Pre-Program Setting Minimum_Peak_Width: Automatic Pre-Program Setting Operating Temperature: 4°C	
	PRE-EQUILIBRATION MOBILE PHASE BUFFER SOLUTION	Buffer H ("De-Gassed" Solution) Minus Protease Inhibitors Minus NP-40 Detergent
	RELATIVE PROTEIN MOLECULAR MASS PRE-CALIBRATION	High Molecular Weight Gel Filtration Internal Protein Standard Calibration Kit-Supplied by GE Healthcare (Amersham Pharmacia Biotech) <u>Internal Protein Standard Composition</u> Thyroglobulin - 669kDa Ferritin - 450kDa Catalase - 232kDa Aldolase - 100kDa

(ii) A total of 24 successive 1ml fractions were eluted into separate 15mL capacity plastic Greiner Screw-lid centrifuge tubes placed into the carousel of the FRAC-950 Rotary Fraction Collector.

(iii) Eluted fractions 8 to 16 inclusive were transferred to separate 1.5mL capacity plastic eppendorf microfuge tubes and stored at -20°C until required, whilst the remaining fractions were discarded.

(iv) 20µL of the total soluble protein extract (un-fractionated) and each of the HPLC-SEC eluate fractions were mixed with 10µL of millipore ultra-pure water and 10µL of 4xSDS PAGE Loading Buffer (Section 2.2.2, p.163) in separate 1.5mL capacity plastic crew-lid microfuge tubes, which were then incubated in a 95°C hot-block for 5 minutes.

(v) The prepared protein samples were then cooled on ice for 5 minutes and stored at -20°C until required.

(vi) 10µL of protein standard mass marker and 30µL aliquots of the prepared HPLC-SEC fractionated protein samples were loaded onto a 10% SDS-PAGE gel on the GeneFlow Mini-PAGE Vertical Sub-System (Section 2.8.4, pp.223-224).

Sample Loading Order on each of the two SDS-PAGE Gels:

Protein Standard Marker	Total (Un-Fractionated) Soluble Extract	Sample	<u>HPLC-SEC Eluate Fraction Samples</u>								
			8	9	10	11	12	13	14	15	16

(vii) After completion of electrophoresis, the resolved proteins on each gel were then transferred onto separate sheets of Hybond-C™ Nitrocellulose Blotting Membrane via utilisation of the GeneFlow Tank Sub-Electroblotter System (Section 2.8.6, pp.231-233).

(viii) After subsequent incubation in the “Blocking Buffer” (Section, p.) the Western Blot membrane was probed with the appropriate primary Anti-Body (“Anti-HA” Ab or “Anti-Myc” Ab) – described in the Western Blot Analytical Protocol (Section 2.8.6, pp.231-233).

(ix) The membrane was then washed and incubated with the secondary HRP-conjugated Polyclonal Rabbit Anti-Mouse Anti-Body and washed again prior to 30 minutes film exposure and development (described in the Western Blot Analytical Protocol – Section 2.8.6, pp.231-233).

2.8.2.3 Preparation and Analysis of Total Soluble Protein Co-IP “Pull-Down” Samples

- (i) A truncated yellow Gilson pipette tip was utilised to transfer a 150 μ L aliquot of Calbiochem® Protein G Plus/Protein A agarose bead suspension (EMD Chemicals Inc.) to a 1.5mL capacity plastic eppendorf microfuge tube.
- (ii) 1mL of Buffer “HI” (Section 2.2.2, p.163) was added to the beads in the eppendorf tube, which was then placed (cap hinge faced outwards) in a Sanyo Hawk 15/05 refrigerated bench top microfuge and spun briefly for 5 seconds at 5000 rpm, 4°C, after which the tube was re-orientated 180° in the rotot (cap hinge faced inwards) and re-spun briefly for 5 seconds at 5000 rpm, 4°C.
- (iii) The resultant supernatant was discarded, the bead pellet resuspended in another 1mL aliquot of Buffer “HI” (Section 2.2.2, p.163) and the wash step repeated (Step (ii)).
- (iv) The supernatant was discarded and the resultant washed bead pellet resuspended in 300 μ L of Buffer “HI” (Section 2.2.2, p.163).
- (v) The following “reaction mixtures” in three fresh 1.5mL capacity plastic eppendorf microfuge tubes were then set up:

	<u>Tube 1</u>	<u>Tube 2</u>	<u>Tube 3</u>
Protein G Bead Suspension	100 μ L	100 μ L	100 μ L
Soluble Total Protein Extract	150 μ L	150 μ L	150 μ L
“Neat” IgG Ab	5 μ L	None	None
“Neat” HA Ab	None	5 μ L	None
“Neat” Myc Ab	None	None	5 μ L

[Total Reaction Volume in each Tube = 255 μ L]

- (vi) The lid of each eppendorf tube was then sealed with parafilm and placed in the platform of a Keison PTR-60 360° multi-functional vertical rotator in the 4°C cold room for 24 hours total incubation time.

- (vii) Each eppendorf tube was then placed in the in a Sanyo Hawk 15/05 refrigerated bench top microfuge (cap hinge facing outwards) and spun briefly for 5 seconds at 5000 rpm, 4°C, after which the tube was re-orientated 180° in the rotor (cap hinge faced inwards) and re-spun briefly for 5 seconds at 5000 rpm, 4°C.
- (viii) The bead pellets were then resuspended in fresh 1ml of aliquots of Buffer “HI” (Section 2.2.2, p.163) and the tubes placed (cap hinge faced outwards) in a Sanyo Hawk 15/05 refrigerated bench top microfuge, spun briefly for 5 seconds at 5000 rpm, 4°C, after which the tubes was re-oreintated 180° in the rotor (cap hinge faced inwards) and re-spun briefly for 5 seconds at 5000 rpm, 4°C.
- (ix) The resultant supernatants were discarded, the bead pellets re-suspended in another 1mL aliquot of Buffer “HI” (Section 2.2.2, p.163) and the wash step repeated (Step (ix)).
- (x) The resultant supernatants were discarded, the bead pellets re-suspended in 1mL of Buffer “HI” (Section 2.2.2, p.163) and the resultant bead suspensions transferred to fresh 1.5ml capacity plastic eppendorf microfuge tubes via utilisation of truncated yellow Gilson pipette tips.
- (xi) Each eppendorf tube was then placed in the in a Sanyo Hawk 15/05 refrigerated bench top microfuge (cap hinge facing outwards) and spun briefly for 5 seconds at 5000 rpm, 4°C, after which the tube was re-orientated 180° in the rotor (cap hinge faced inwards) and re-spun briefly for 5 seconds at 5000 rpm, 4°C.
- (xii) The resultant supernatants were discarded and the bead pellets subjected to a further 4 wash cycles described previously in stages (xi) – (xii).
- (xiii) Each resultant washed bead pellet was mixed with 50µL of millipore ultra-pure water and 50µL of 4x SDS-PAGE Sample Loading Buffer (Section 2.2.2, p.163) and transferred to a 1.5ml capacity plastic screw cap microfuge tube via utilisation of a truncated yellow Gilson pipette tip.

- (xiv) The resultant bead mixtures were then incubated in the 95°C Hot-Block for 5 minutes and then cooled on ice for 5 minutes, prior to storage of the prepared “Co-IP Pull-Down” protein samples at -20°C until required.
- (xv) 10µL of the total soluble protein extract was mixed with 5µL of millipore water and 5µL of the 4x SDS-PAGE Sample Loading Buffer (Section 2.2.2, p.163) in a 1.5mL capacity plastic screw cap microfuge tube, which was then incubated in the 95°C Hot-Block for 5 minutes and then cooled on ice for 5 minutes, prior to storage of the prepared Total Input Reference protein sample at -20°C until required.
- (xvi) 10µL of the protein standard mass marker and 20µL aliquots of each protein sample were loaded onto two 10% SDS-PAGE gels on the Bio-Rad Mini-Protean® Tetra Cell System (Section 2.8.4, pp.223-224).

Sample Loading Order on each of the two SDS-PAGE Gels:

	<u>[Total Soluble Extract]</u>	<u>[Bead Samples]</u>		
Protein	Total	Input	Reference	IgG
Standard				HA
Marker				Myc

- (xvii) After completion of electrophoresis, the resolved proteins on each gel were then transferred onto separate sheets of Hybond-C™ Nitrocellulose Blotting Membrane via utilisation of the GeneFlow Tank Sub-Electroblotter System (Section 2.8.6, pp.231-233).
- (xviii) After subsequent incubation in the “Blocking Buffer” (Section 2.2.3, p.164), one of the Western Blot membranes was probed with the primary HA Antibody (1 in 3000 dilution in blocking buffer solution) and the remaining Western Blot membrane was probed with the primary Myc Antibody (1 in 500 dilution in blocking buffer solution) – as described in the protocol detailed in Section 2.8.6 (pp.231-233).
- (xix) Both membranes were then washed and incubated with the secondary HRP-conjugated Light-Chain Antibody (1 in 5000 dilution in blocking buffer) and washed again prior to 30 minutes film exposure and development (described in the protocol detailed in Section 2.8.6, pp.231-233).

2.8.3 Preparation of Total Protein Extracts for 2D-PAGE Analyses

2.8.3.1 Preparation of TCA-Precipitated Total Protein 2D-PAGE Samples

(i) A sterile/autoclaved wooden toothpick was utilised to inoculate 100mL of sterile/autoclaved YEA medium (see Section 2.3.1, p.167) with a small amount of the appropriate *S. pombe* strain, taken from the respective YEA agar petri-plate (Section 2.3.2, p.168) culture, in a sterile/autoclaved 250mL capacity glass conical flask (capped loosely with aluminium foil) and the resultant broth culture placed in the 30°C Sanyo orbisafe incubator (180 r.p.m. shaker speed) for 24 hours duration.

(ii) The following day, a 100µL aliquot of the resultant broth culture was diluted with 900µL YEA medium and the resultant 1 in 10 diluted culture sample (1mL) was then placed in a plastic microcuvette for subsequent measurement of the optical density at A₅₉₅ in a Sanyo SP BIO Spectrophotometer (against a set blank reference of 1mL YEA) and the optical density of the “neat” culture calculated:

$$\text{ie } A_{595} (\text{“neat” culture}) = A_{595} (1 \text{ in } 10 \text{ diluted culture}) \times 10$$

(iii) The equivalent volume of each resultant “neat” broth culture which corresponded to 40 equivalent A₅₉₅ optical density units was calculated, removed from the respective flask and placed in a 50mL capacity Greiner plastic screw-cap centrifuge tube:

$$\text{ie: Volume Culture Required (mL)} = \frac{40}{A_{595} \text{ "Neat Culture"}}$$

(iv) The calculated A₅₉₅ 40 optical densities equivalent volume of cell culture aliquot was then placed in a 50mL capacity plastic Greiner centrifuge screw-cap tube and spun at 3,300g for 5 minutes in a Jencons-PLS SorvallR Legend T Centrifuge in the 4°C cold room.

(v) The supernatant was discarded, the resultant cell pellet re-suspended in 50mL of ultra-pure millipore water, after which the resultant cell suspension was spun at 3,300g for 10 minutes in a Jencons-PLS SorvallR Legend T Centrifuge in the 4°C cold room.

(vi) The resultant supernatant was discarded and the pellet re-suspended in 400 μ L ice-cold 10% (v/v) TCA in Acetone, after which the resultant cell suspension was transferred to a 1.5ml capacity plastic screw-lid microfuge tube which contained add 10 small spatular spoonfuls of glass beads (~200 μ L glass beads).

Note: The 10% (v/v) TCA in Acetone solution was freshly prepared fresh, immediately prior to use, via mixing 200 μ L 20% (v/v) TCA(aq) with 200 μ L “neat” Acetone solvent.

[TCA was found to undergo a reaction with Acetone if the prepared reagent was allowed to stand at room temperature for several several hours]

(vii) The tube was then placed in the FastPrep Genie Disruptor for 16 minutes, after which time 200 μ L of 20% TCA were added and the tube contents vortexed briefly for ~10 seconds, prior to transfer of the resultant mixture to a fresh 1.ml capacity plastic eppendorf microfuge tube, which was then spun at 12000 rpm for 5 mins at 4°C in a Sanyo Hawk 15/05 refrigerated bench top microfuge.

(viii) The supernatant was discarded, the precipitated pellet re-suspended in 1mL of ice-cold Acetone and the resultant emulsion vortexed briefly for ~10 seconds, prior to incubation on dry- ice for 15 minutes, after which time the mixture was spun at 12,000 rpm for 30 minutes at 4 °C in a Sanyo Hawk 15/05 refrigerated bench top microfuge.

(ix) The supernatant was discarded and the resultant pellet re-suspended in 1mL of ice-cold wash solvent solution of composition:

20mL Isopropanol

20mL 2:1(v/v ratio) CHCl₃:CH₃OH

10mL Glycerol

[Note: This solvent was made up in a 50mL capacity Greiner Tube and stored at -20°C until required]

The resultant mixture was then placed on the Genie Disruptor in the 4°C cold room for 16 minutes (without the addition of glass beads).

- (x) The resultant emulsion was then incubated on dry-ice for 30 mins and then spun at 12,000 rpm for 30 mins at 4°C in a Sanyo Hawk 15/05 refrigerated bench top microfuge.
- (xi) The supernatant was discarded and the resultant pellet was re-suspended in 960µL of millipore water, prior to the addition of 40µL 1M Tris-HCl pH8.8 (Section 2.2.2, p.163) to neutralise the acidity of the TCA-precipitated total protein extract and the resultant mixture was then spun at 12000 rpm, 4°C for 5 minutes in a Sanyo Hawk 15/05 refrigerated bench top microfuge.
- (xii) The resultant supernatant was discarded, the neutralised protein pellet was then re-suspended in 1mL of millipore water and the resultant solution was then spun at 12,000 rpm, 4°C for 5 minutes in a Sanyo Hawk 15/05 refrigerated bench top microfuge.
- (xiii) The resultant supernatant was discarded and the wash step (stage iv) repeated.
- (xiv) The supernatant was discarded and the washed protein pellet was then re-suspended in 1mL of 1M Tris-HCl pH7.0 (Section 2.2.2, p.163), after which the resultant mixture was spun at 12,000 rpm, 4°C for 5 minutes in a Sanyo Hawk 15/05 refrigerated bench top microfuge.
- (xv) The resultant supernatant was discarded and the protein pellet re-dissolved in 1mL of millipore water, after which the resultant solution was spun at 12,000 rpm, 4°C for 5 minutes in a Sanyo Hawk 15/05 refrigerated bench top microfuge.
- (xvi) The resultant supernatant was discarded and the wash step (stage xiv) repeated.
- (xvii) The resultant supernatant was discarded and the neutralised protein pellet re-dissolved in 1mL of 50mM Tris-HCl pH7.0 (Section 2.2.2, p.163), after which the resultant solution was spun at 12,000 rpm, 4°C for 5 minutes in a Sanyo Hawk 15/05 refrigerated bench top microfuge.

(xviii) The resultant supernatant was discarded and the washed, pre-equilibrated protein pellet was then re-dissolved in 125 μ L of 0.2% SDS, 50mM Tris-HCl, pH7 (Section 2.2.2, p.163).

(xix) A GE HealthCare Destreak™ Buffer solution (proprietary formulation), which contained 0.5% (v/v) pH3-10 GE Healthcare IPG Ampholyte Buffer Solution (proprietary formulation) was prepared in accordance with the manufacturer's instructions.

(xx) 625 μ L of the prepared Destreak™ Buffer solution was then mixed with the prepared 125 μ L total protein extract (Stage xviii) and the resultant sample (750 μ L total volume) stored at -20°C until required.

[The remainder of the prepared of Destreak™ Buffer solution was also stored at -20°C until required for future 2D-PAGE sample preparations]

2.8.3.2 Preparation of Comparative Alkaline Phosphatase-Digested 2D-PAGE Samples

(i) A sterile/autoclaved wooden toothpick was utilised to inoculate 100mL of sterile/autoclaved YEA medium (see Section 2.3.1, p.167) with a small amount of the appropriate *S. pombe* strain, taken from the respective YEA agar petri-plate (Section 2.3.2, p.168) culture, in a sterile/autoclaved 250mL capacity glass conical flask (capped loosely with aluminium foil) and the resultant broth culture placed in the 30°C Sanyo orbisafe incubator shaker for 24 hours duration.

(ii) The following day, a 100µL aliquot of the resultant broth culture was diluted with 900µL YEA medium and the resultant 1 in 10 diluted culture sample (1mL) was then placed in a plastic microcuvette for subsequent measurement of the optical density at A₅₉₅ in a Sanyo SP BIO Spectrophotometer (against a set blank reference of 1mL YEA) and the optical density of the “neat” culture calculated:

$$\text{ie } A_{595} (\text{“neat” culture}) = A_{595} (1 \text{ in } 10 \text{ diluted culture}) \times 10$$

(iii) The equivalent volume of each resultant “neat” broth culture which corresponded to 50 equivalent A₅₉₅ optical density units was calculated, removed from the respective flask and placed in a 50mL capacity Greiner plastic screw-cap centrifuge tube:

$$\text{ie: Volume Culture Required (mL)} = \frac{50}{A_{595} \text{ "Neat Culture"}}$$

(iv) The calculated A₅₉₅ 50 optical densities equivalent volume of cell culture aliquot was then placed in a 50mL capacity plastic Greiner centrifuge screw-cap tube and spun at 3,300g for 5 minutes in a Jencons-PLS SorvallR Legend T Centrifuge in the 4°C cold room.

(v) The supernatant was discarded, the resultant cell pellet re-suspended in 50mL of ultra-pure millipore water, after which the resultant cell suspension was spun at 3,300g for 10 minutes in a Jencons-PLS SorvallR Legend T Centrifuge in the 4°C cold room.

- (vi) The supernatant was discarded, the resultant cell pellet re-suspended in 50mL of Buffer “HP” (Section 2.2.2, p.163) after which the resultant cell suspension was spun at 3,300g for 10 minutes in a Jencons-PLS SorvallR Legend T Centrifuge in the 4°C cold room.
- (vii) The supernatant was discarded and the resultant cell pellet re-suspended in a 1mL aliquot of Buffer “HI” (Section 2.2.2, p.163) after which the resultant cell suspension was transferred to a 1.5mL capacity plastic eppendorf microfuge tube which was then which was then spun at 12,000 r.p.m. for 5 mins at 4°C in a Sanyo Hawk 15/05 refrigerated bench top microfuge.
- (viii) The supernatant was discarded and the resultant washed cell pellet re-suspended in a 250µL aliquot of Buffer “HI” (Section 2.2.2, p.163) after which the resultant cell suspension was transferred to a 1.5mL capacity plastic screw-cap microfuge tube which contained 10 small spatula spoonfuls of glass beads (~200µL of glass beads).
- (ix) The tube was then placed in the FastPrep Genie Disruptor for 16 minutes, after which time 250µL of Buffer HI (Section 2.2.2, p.163) were added and the tube contents vortexed briefly for ~10 seconds, prior to transfer of the resultant mixture to a fresh 1.ml capacity plastic eppendorf microfuge tube, which was then spun at 12,000 rpm for 5 mins at 4°C in a Sanyo Hawk 15/05 refrigerated bench top microfuge.
- (x) The resultant lysed cell solution (~500µL total volume) was then transferred to a fresh 1.5mL capacity plastic eppendorf microfuge tube which was then spun at 12,000 rpm for 5 mins at 4°C in a Sanyo Hawk 15/05 refrigerated bench top microfuge.
- (xi) The pellet was discarded and the resultant supernatant transferred to a fresh 1.5mL capacity Eppendorf microfuge tube.
[The prepared soluble total protein extract was stored at -20°C until required]
- (xii) A truncated yellow pipette tip was utilised to transfer a 175µL aliquot of Calbiochem® Protein G Plus Protein A agarose bead suspension to a 1.5mL capacity plastic eppendorf microfuge tube.

- (xiii) 1mL of Buffer “HP” (Section 2.2.2, p.163) was then added to the beads in the eppendorf tube which was then placed (cap hinge facing outwards) in a Sanyo Hawk 15/05 refrigerated bench top microfuge, spun briefly for ~10 seconds at 5,000 r.p.m., 4°C, after which the tube was re-orientated 180° within the rotor (cap hinge facing inwards) and re-spun for ~10 seconds at 5,000 r.p.m., 4°C.
- (xiv) The resultant supernatant was discarded and the bead pellet re-suspended in 1mL of Buffer HP (Section 2.2.2, p.163) and the wash step repeated as described in the previous step (xii).
- (xv) The resultant supernatant was discarded and the entire volume of prepared total soluble protein extract (~500µL) added to the washed beads in the 1.5mL capacity plastic eppendorf microfuge tube.
- (xvi) A 15µL aliquot of “neat” HA antibody solution was then added to the bead-soluble protein mixture and the eppendorf tube sealed with parafilm prior to placement in the platform of a Keison PTR-60 360° multi-functional vertical rotator in the 4°C cold room for 24 hours total incubation time.
- (xvii) The following day, the eppendorf tube was removed from the PTR-60 rotating platform and placed (cap hinge facing outwards) in a Sanyo Hawk 15/05 refrigerated bench top microfuge, then spun briefly for ~10 seconds at 5,000 r.p.m., 4°C, after which the tube was re-orientated 180° within the rotor (cap hinge facing inwards) and re-spun for ~10 seconds at 5,000 r.p.m., 4°C.
- (xviii) 1mL of ultra-pure millipore water was then added to the beads in the eppendorf tube which was then placed (cap hinge facing outwards) in a Sanyo Hawk 15/05 refrigerated bench top microfuge, spun briefly for ~10 seconds at 5,000 r.p.m., 4°C, after which the tube was re-orientated 180° within the rotor (cap hinge facing inwards) and re-spun for ~10 seconds at 5,000 r.p.m., 4°C.

- (xix) The resultant supernatant was discarded and the bead wash step, described in the previous stage above, was then repeated a further four times with fresh 1mL aliquots of ultra-pure millipore water.
- (xx) The supernatant was discarded and the bead pellet re-suspended in 1mL of 1x Calf Intestinal Alkaline Phosphatase (CIAP) Reaction Buffer – prepared *in situ*. via the successive addition 900µL of ultra-pure millipore water, followed by 100µL of 10x CIAP Reaction Buffer (Section 2.2.4, p.165) to the eppendorf tube contents.
- (xxi) The eppendorf tube which was then placed (cap hinge facing outwards) in a Sanyo Hawk 15/05 refrigerated bench top microfuge, spun briefly for ~10 seconds at 5,000 r.p.m., 4°C, after which the tube was re-orientated 180° within the rotor (cap hinge facing inwards) and re-spun for ~10 seconds at 5,000 r.p.m., 4°C.
- (xxii) The resultant supernatant was discarded, prior to the successive addition of 350µL of ultra-pure millipore water, 50µL of 10x CIAP Reaction Buffer and 100µL (100 units) of Calf Intestinal Alkaline Phosphatase (Section 2.2.4, p.165) to the tube contents.
- (xxiii) The bead pellet was re-suspended thoroughly in the resultant reaction mixture, prior to placement of the eppendorf tube in the Sanyo 37°C incubator-shaker for 8 hours
- (xxiv) The eppendorf tube which was then placed (cap hinge facing outwards) in a Sanyo Hawk 15/05 refrigerated bench top microfuge, spun briefly for ~10 seconds at 5,000 r.p.m., 4°C, after which the tube was re-orientated 180° within the rotor (cap hinge facing inwards) and re-spun for ~10 seconds at 5,000 r.p.m., 4°C.
- (xxv) The resultant supernatant was discarded and the bead pellet subjected to five successive washes with fresh 1mL aliquots of ultra-pure millipore water (as per the method described previously – stage xviii, p.220).

- (xxvi) The resultant supernatant was discarded and a 500 μ L aliquot of an ice-cold solvent comprised of 10% TCA (w/v) in 1:1:2 (v/v) Acetone:DMSO:Glycerol, was then added to the bead pellet in the eppendorf tube, which was then sealed with parafilm, vortexed briefly (~10 seconds) and placed on the FastPrep Genie Disruptor for 16 minutes in 4°C cold-room.
- (xxvii) The resultant mixture was then transferred to a fresh 1.5ml capacity plastic eppendorf microfuge tube which contained 500 μ L of 50% (w/v) ice-cold TCA in Acetone, after which the contents were vortexed briefly (~10 seconds) and the tube incubated in dry-ice for 30 minutes.
- (xxviii) After the incubation time had elapsed, the eppendorf tube was placed in a Sanyo Hawk 15/05 refrigerated bench top microfuge and spun at 12,000 r.p.m. for 30 minutes at 4°C.
- (xxix) The supernatant was discarded and the resultant pellet was re-suspended in 900 μ L of millipore water, prior to the addition of 100 μ L 1M Tris-HCl pH8.8 (Section 2.2.2, p.163) to neutralise the acidity of the TCA-precipitated total protein extract and the resultant mixture was then spun at 12000 rpm, 4°C for 5 minutes in a Sanyo Hawk 15/05 refrigerated bench top microfuge.
- (xxx) The supernatant was discarded and the resultant protein pellet sample prepared as per the protocol described previously in Section 2.8.3.1 – stages (xii) through to (xx) inclusive (pp.216-217).
- (xxx) The prepared 2D-PAGE protein sample was then stored at -20°C until required.

- (v) The stacking polyacrylamide gel was made up in a 15mL capacity plastic Greiner centrifuge, the contents vortexed briefly (~ 10 seconds) after addition of the final reagent component (Ammonium Persulphate) and the mixture poured evenly on top of the cast resolving gel via utilisation of a 5mL capacity plastic Pasteur pipette, after which the appropriate well comb was inserted into the gel and the cast plate assembly stood at room temperature to set.
- (vi) The cast plate assembly was then placed in the appropriate gel tank system, which was then filled with 1x SDS-PAGE Running Buffer (Section 2.2.3, p.164).
- (vii) The comb was then removed and the wells flushed gently with 1x SDS-PAGE Running Buffer (Section 2.2.3, p.164), via utilisation of a 5mL capacity plastic syringe fitted with a truncated plastic Gel-Loading Gilson pipette tip, for removal of unpolymerised acrylamide:bisacrylamide from the cast well channels.
- (viii) 20µL aliquot samples of prepared protein samples and a 10µL aliquot of the ProtoMarkers™ (National Diagnostics) Protein Molecular Weight Marker Ladder Reference Standard were loaded onto the 10% SDS-PAGE gel plate assembly, immersed in the gel tank which contained 1x SDS-PAGE running buffer (Section 2.2.3, p.164)
- (ix) The resultant loaded SDS-PAGE gel assembly was then connected up to the Consort EV231 electrophoresis power pack and initially run at 90V constant setting, until the visible blue sample band had fully migrated from the upper stacking (spacer) gel into the lower resolving (separation) gel, below the stratified interface – after which time the voltage was increased to 120V constant setting and run for a total time of ~ 3 hours until the visible blue sample band had migrated to the bottom of the gel.

2.8.5 2D-PAGE Analytical Protocol

2.8.5.1 IPG Strip Rehydration: Active Protein Sample Uptake

- (i) 100 μ L of the prepared 2D-PAGE protein sample was pipetted carefully along a channel edge of the isoelectric focusing tray to form a thin, even line of liquid.
- (ii) A standard 11cm pH3-10 IPG strip (supplied by GE Healthcare) was removed from -20°C storage and allowed to defrost at room temperature for 10 minutes prior to removal of the protective plastic cover from the gel side of the strip via utilisation of fine forceps.
- (iii) The IPG strip was then placed gently, gel side down, onto the pipetted thin line of protein sample held in the channel of the isoelectric focusing tray.

[The correct polarity orientation of the IPG strip, prior to placement onto the protein sample, was verified via alignment of its “+” labelled end with the positive terminal labelled end of the isoelectric focusing tray]
- (iv) 2.5ml of electrophoresis grade mineral oil (supplied by BioRad) was then pipetted carefully over the top surface (non-gel side) of the placed IPG strip, within the channel of the isoelectric focusing tray, to prevent evaporation of the protein sample and IPG strip dehydration during the active rehydration process.
- (v) The isoelectric focusing tray was then covered with its lid and the resultant assembly placed in the BioRad Protean IEF cell, which was then set to 12 hours Active Rehydration at 50V, 20°C via selection of the appropriate pre-programmed parameter settings, in accordance with the manual instructions.

2.8.5.2 IEF-PAGE: 1st Dimension Gel Electrophoresis

- (i) After 12 hours of active rehydration had elapsed, the BioRad Protean® IEF cell was switched off and the isoelectric focusing tray removed carefully from its instrument housing.

- (ii) The IPG strip was then removed from the isoelectric focusing tray and placed on a small sheet of filter paper (non-gel side down), for 10 minutes at room temperature, to absorb any residual traces of mineral oil from the strip.

- (iii) Meanwhile, the isoelectric focusing tray assembly was carefully cleaned with a 10% (w/v) aqueous solution of Sodium Dodecylsulphonate (SDS) and then rinsed thoroughly with deionised water to ensure that no traces of SDS remained, after which the tray was dried thoroughly prior to re-use.

- (iv) Fine forceps were utilised to place a paper electrophoresis wick (supplied by BioRad) on the positive and negative termini of the sample channel within the isoelectric focusing tray, after which 10µL of millipore ultra-pure water was pipetted onto each wick.

- (v) Fine forceps were then utilised to position the IPG strip, in the correct polarity orientation, (gel side down) over the wick-covered termini of the prepared sample channel in the isoelectric focusing tray.

- (vi) 2.5ml of electrophoresis grade mineral oil (supplied by BioRad) was then pipetted carefully over the top surface (non-gel side) of the placed IPG strip, within the channel of the isoelectric focusing tray, to prevent evaporation of the protein sample and IPG strip dehydration during the isoelectric focusing process.

(vii) The isoelectric focusing tray was then covered with its lid and the resultant assembly placed in the BioRad Protean® IEF cell, in the correct polarity orientation, after which the standard “Rapid ΔV ” isoelectric focusing pre-programmed method was selected to run – in accordance with the manual instructions:

Parameter Settings: Voltage Slope: Rapid ΔV
Rehydration: No
Gel Length: 11cm
Focus Temperature: 20°C
Limit/Gel: 50 μ A
S4 500V Hold: Yes

[Note: The selected Rapid ΔV Pre-Programmed Steps S1, S2 and S3 Voltage/Time Focusing Parameters (ie the Sequential “Total Volt-Hour” Settings) are calculated automatically by the instrumentation software from the IPG Strip Length and Number of IPG Strips Entered.]

The optional S4 500V Hold Step was selected for prevention of over-focused protein samples within the IPG Strips.]

2.8.5.3 SDS-PAGE: 2nd Dimension Gel Electrophoresis

- (i) After the Rapid ΔV program had completed, the BioRad Protean® IEF cell was switched off and the isoelectric focusing tray removed carefully from its instrument housing.
- (ii) The IPG strip was then removed from the isoelectric focusing tray (via utilisation of fine forceps) and placed on a small sheet of filter paper (non-gel side down), for 10 minutes at room temperature, to absorb any residual traces of mineral oil from the strip.
- (iii) Meanwhile, the isoelectric focusing tray assembly was carefully cleaned with a 10% (w/v) aqueous solution of Sodium Dodecylsulphonate (SDS) and then rinsed thoroughly with deionised water to ensure that no traces of SDS remained, after which the tray was dried thoroughly and stored in its protective housing within BioRad Protean® IEF cell until required.
- (iv) Fine forceps were then utilised to place the IPG strip in a channel of a clean BioRad IPG Strip Equilibration Tray (gel face up), after which 3.5mL of Equilibration Buffer I (Section 2.2.3, p.164) was pipetted carefully over the gel surface of the IPG Strip and the tray placed on a orbital shaker (set to a “moderate speed” ~ 40 r.p.m.) for 10 minutes at room temperature.
- (v) After the 10 minutes incubation time had elapsed, the buffer solution was drained from the channel (via careful decantation of the tray) and discarded.
- (vi) 3.5mL of Equilibration Buffer II (Section 2.2.3, p.164) was then pipetted carefully over the gel surface of the IPG Strip and the tray placed back on the orbital shaker (set to a “moderate speed” ~ 40 r.p.m.) for 10 minutes at room temperature.

(xiii) A thin polyethylene strip was then utilised to push the IPG strip into direct contact with the surface of the resolving gel.

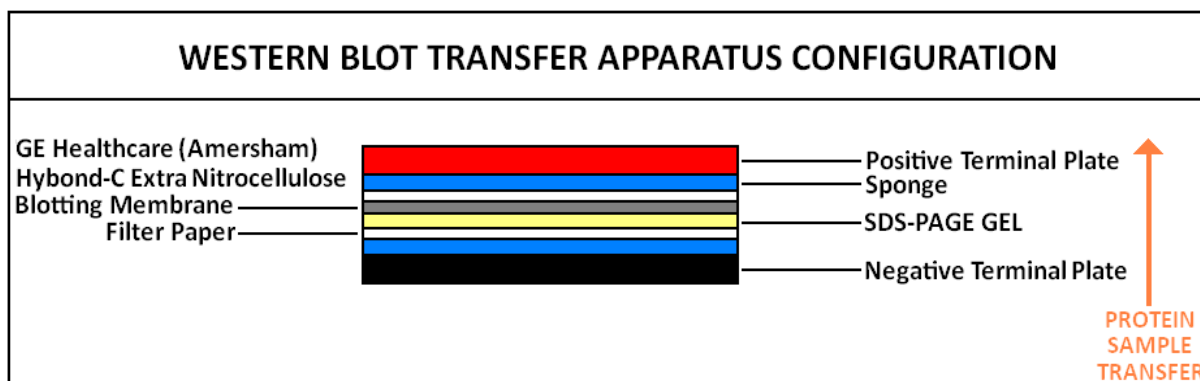
[Note: Care was taken to ensure no air bubbles were trapped between the IPG Strip and the gel surface and that the entire edge of the strip was in firm contact with the gel surface, but not pushed into the resolving gel itself]

(xiv) The resultant loaded SDS-PAGE gel assembly was then connected up to the Consort EV231 electrophoresis power pack and initially run at 240V constant setting for 60 minutes at room temperature.

(xv) The empty BioRad IPG Pre-Equilibration Tray was then washed with a 10% (w/v) aqueous solution of Sodium Dodecylsulphonate (SDS) and then rinsed thoroughly with deionised water, after which the tray was dried thoroughly and stored on the lab bench until required.

2.8.6 Western Blot Analytical Protocol

- (i) After completion of electrophoresis, the SDS-PAGE gel was carefully removed and placed in the appropriate Western Blot Transfer System assembly:



- (ii) The resultant assembly was then immersed in the appropriate tank system which contained a solution comprised of methanol (15% v/v) in 1x Transfer Buffer solution (Section 2.2.3, p.164), connected up to a Consort EV231 electrophoretic power pack and run at 50V constant setting for 3 hours.
- (iii) The resultant blotting membrane, onto which the SDS-PAGE resolved protein samples had been transferred, was then carefully removed from the blotting apparatus and immersed in a small plastic tank that contained a 100mL "Blocking Buffer" solution comprised of 3% (w/v) milk protein in 1xPBS buffer (0.05% v/v Tween20), which was then gently agitated on an orbital platform at room temperature for 30 minutes.
- (iv) The blotting membrane was then removed from the tank and placed in a plastic wallet with 5mL of the appropriate diluted solution of primary antibody probe*, which was then carefully sealed to avoid trapped air bubbles and placed on a rocker platform in the 4°C cold room for 24 hours incubation.

[*NOTE: For the primary anti-HA antibody = 1 in 1000 dilution in "Blocking Buffer"]

For the primary anti-Myc antibody = 1 in 500 dilution in "Blocking Buffer"

For the primary anti-Cdc2 antibody = 1 in 2000 dilution in "Blocking Buffer"]

- (v) The following day, the blotting membrane was removed from the plastic wallet and washed via immersion in a small plastic tank that contained 100mL of 1xPBS (0.05% Tween20) buffer solution (Section 2.2.3, p.164) – which was then agitated via placement on an orbital platform for 10 minutes at room temperature.
- (vi) The blotting membrane was then subjected to two further additional washes (as described previously above) with fresh 100mL aliquots of the 1xPBS (0.05% Tween20) solution.
- (vii) The resultant washed blotting membrane was then placed in a plastic wallet with 4mL of a 1 in 3000 diluted solution (in “Blocking Buffer” – Section 2.2.3, p.164) of the polyclonal rabbit anti-mouse derived secondary HRP-conjugated antibody probe, which was then carefully sealed to avoid trapped air bubbles and placed on an orbital platform at room temperature for one hour – after which time, the membrane was removed from the plastic wallet and subjected to a further three 10 minute washes in 1xPBS (0.05% Tween20) buffer solution (Section 2.2.3, p.164) – as described previously.
- [NOTE: In the case of Western Blot analyses of “Co-IP” samples, the HRP-conjugated Light-Chain secondary antibody was utilised as a 1 in 5000 diluted solution in “Blocking Buffer” (Section 2.2.3, p.164) instead of the polyclonal rabbit anti-mouse derived secondary HRP-conjugated antibody]
- (viii) The blotting membrane was then rinsed with 250µL of freshly prepared chemiluminescent HRP developer solution – comprised of 125µL of reagent A mixed with 125µL of reagent B, as supplied in the BioFX Chemiluminescent Sensitive HRP Microwell and/or Membrane Substrate 2x 110mL Kit (Section 2.1, p.152), prior to placement in a transparent thin plastic wallet in a film cassette.
- (ix) The film cassette was then taken to the photographic dark room, opened and a piece of Fuji Blue Medical X-Ray SuperRX film placed directly on top of the transparent thin plastic wallet which contained the blotting membrane, then the cassette was closed and the film exposed for 30 minutes, prior to subsequent development of the film on a Jet-X-Ray MI-5 X-Ray Film Processor.

NOTE: As the research work progressed it was found that a significant improved in the quality of the Western Blots was acquired with the GE Healthcare ECL Plus Western Blotting Detection Systems Kit, utilised in conjunction with GE Healthcare ECL Hyperfilm compared to those those acquired previously with the BioFX Chemiluminescent Sensitive HRP Microwell and/or Membrane Substrate 2x 110mL Kit and Fuji BlueMedical X-Ray SuperRX film.

[In this case, the GE Healthcare ECL Plus Western Blot developing solution was freshly prepared from the kit, immediately prior to use, via mixing a 1mL aliquot of the supplied Lumigen™ PS-3 Solution A (Detection Reagent) with 15µL of Solution B RPN2132V2]

2.9 Acute and Chronic Survival Assay Protocols

2.9.1 Chronic Survival Assays – “Drop-Plate” Protocol

- (i) A sterile/autoclaved wooden toothpick was utilised to inoculate 5mL of sterile/autoclaved YEA medium (Section 2.3.1, p.167) with a small amount of each appropriate *S. pombe* strain, taken from the respective YEA agar petri-plate (Section 2.3.2, p.168) culture, in a sterile/autoclaved 15ml capacity glass culture test-tube (capped loosely with a plastic top) and the resultant broth culture placed in the 30°C Sanyo orbisafe incubator (180 rpm shaker speed) for 24 hours duration.
- (ii) The following morning, the tubes were removed from the incubator and a 10µL aliquot of each broth culture placed onto the square metal grid of a Hawksley Thoma Double Cell Clear Sight Counting Chamber which was then viewed under a CETI Magnum B Binocular light microscope at 60x magnification.
- (iii) After initial visual verification had established that the cells were viable and in S-phase, the number of cells in 4 large grid squares was counted – from which the average number of cells/mL in the undiluted broth culture is calculated via the equation:

$$\text{Average cells/mL (x10}^6\text{)} = \frac{\text{Total No. of Cells Counted}}{4}$$

- (iv) An appropriate volume of cell culture was diluted with an appropriate volume of autoclaved /sterile YEA medium (Section 2.3.1, p.167) to yield 1 mL (1000µL) final broth culture concentration of 1×10^7 cells/mL*, in a sterile/autoclaved 1.5mL capacity plastic eppendorf microfuge tube.

*Via the equation: $V1 = \frac{C2 \times V2}{C1}$

Where:

V1 = Volume of measured cell culture

V2 = Volume of cell culture required

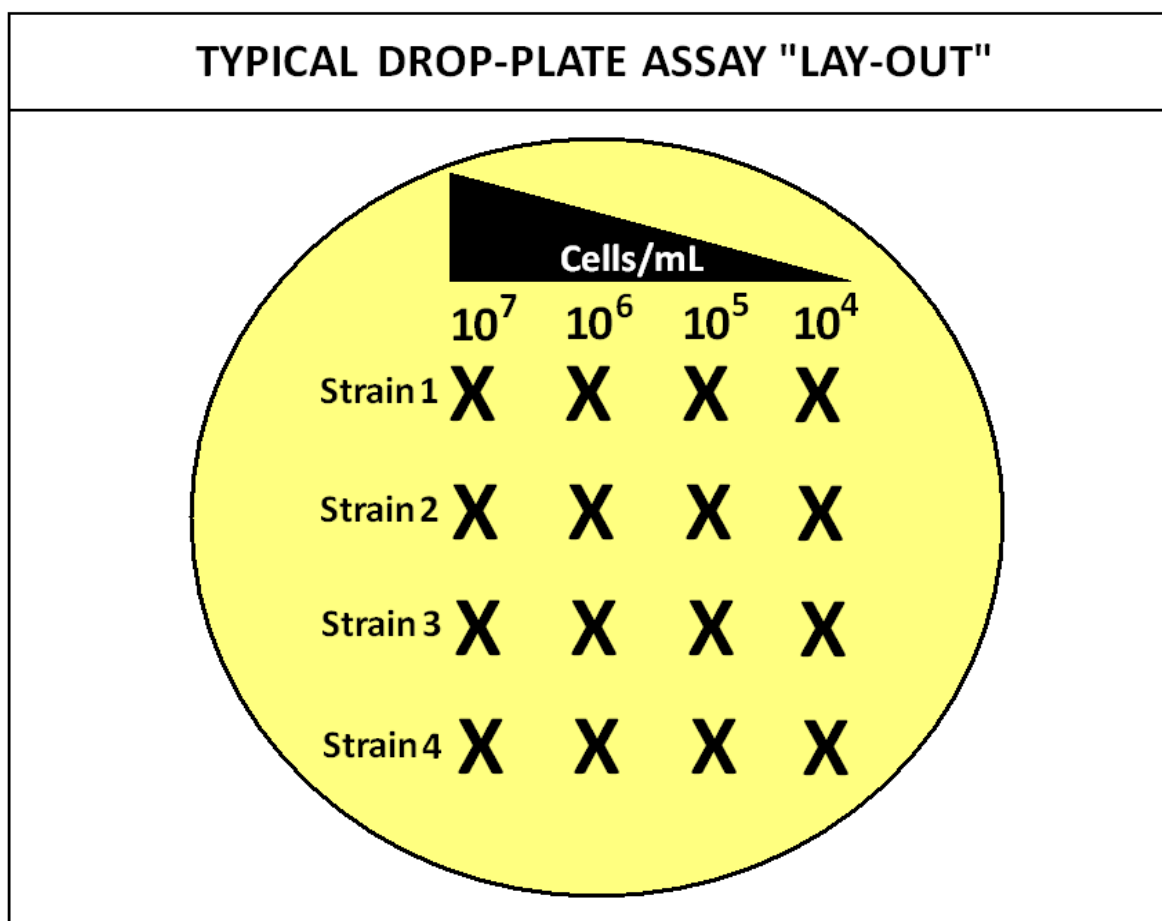
C1 = Concentration of cell culture measured

C2 = Concentration of cell culture required

(v) Successive serial dilutions (100µL of the appropriate strain culture concentration mixed with 900µL YEA medium) were prepared in sterile/autoclaved 1.5mL capacity plastic eppendorf microfuge for acquisition of 1mL total volume cultures of a final concentration of 1×10^6 cells/mL, 1×10^5 cells/mL and 1×10^4 cells/mL respectively.

(vi) 5µL drops of each appropriate strain/cell concentration culture were pipetted onto the control (YEA only) and test compound YEA-agar plates (Section 2.3.2, p.168), which were then stood at room temperature for 20 minutes to allow the drops to dry, prior to placement of the prepared “drop-plates” in the static Binder 30°C incubator for three days.

[Note: In the case of comparative heat-shock drop-plate assays the drop-plates were placed in the static Binder 37°C incubator for three days]



(vii) After three days had elapsed, the drop-plate cultures were removed from the respective incubator and photographed in a Bio-Rad Gel Doc 2000 White Light and U.V. imager system (“White-Light” mode).

2.9.2.2 Acute Survival Assays

2.9.2.2(i) Acute U.V. Survival Assay

Ultra-violet (U.V.) radiation induces Thymine dimerisation type cross-linkage adducts within DNA (eg T-T Cyclobutane dimer, T-T 6,4-photoproduct and T-T Dewar photoproduct) and other nucleobase-derived dimers such as the Thymine-Cytosine 6-4 photoproduct (Becker M.M. and Zang Z., 1989; Beukers R., 2008).

The comparative cytotoxic sensitivity of various *S. pombe* strains towards these genotoxic effects of U.V. irradiation was assayed via the following protocol:

- (i) A sterile/autoclaved wooden toothpick was utilised to inoculate 5mL of sterile/autoclaved YEA medium (Section 2.3.1, p.167) with a small amount of each appropriate *S. pombe* strain, taken from the respective YEA agar petri-plate (Section 2.3.2, p.168) culture, in a sterile/autoclaved 15ml capacity glass culture test-tube (capped loosely with a plastic) and the resultant broth culture placed in the 30°C Sanyo orbisafe incubator (180 rpm shaker speed) for 12 hours duration.
- (ii) The following morning, the tubes were removed from the incubator and a 10µL aliquot of each broth culture placed onto the square metal grid of a Hawksley Thoma Double Cell Clear Sight Counting Chamber which was then viewed under a CETI Magn B Binocular light microscope at 60x magnification.
- (iii) After initial visual verification had established that the cells were viable and in S-phase, the number of cells in 4 large grid squares was counted – from which the average number of cells/mL in the undiluted broth culture was calculated via the equation:

$$\text{Average cells/mL (x10}^6\text{)} = \frac{\text{Total No. of Cells Counted}}{4}$$

(iv) An appropriate volume of cell culture was diluted with an appropriate volume of autoclaved /sterile YEA medium (Section 2.3.1, p.167) to yield 1 mL (1000 μ L) final broth culture concentration of 1×10^7 cells/mL*, in a sterile/autoclaved 1.5mL capacity plastic eppendorf microfuge tube.

*Via the equation: $V1 = \frac{C2 \times V2}{C1}$

Where:

V1 = Volume of measured cell culture

V2 = Volume of cell culture required

C1 = Concentration of cell culture measured

C2 = Concentration of cell culture required

(v) A 10 μ L of the resultant 1×10^7 cells/mL cell culture was then mixed with 990 μ L of YEA medium (Section 2.3.1, p.167) in a fresh autoclaved/sterile 1.5mL capacity plastic eppendorf microfuge tube to yield a broth culture concentration of 1×10^5 cells/mL.

(vi) A 500 μ L aliquot of the prepared 1×10^5 cells/mL *S. pombe* strain broth culture was then mixed with 500 μ L of YEA medium (Section 2.3.1, p.167) in a fresh sterile/autoclaved 1.5mL capacity eppendorf microfuge tube and the resultant contents vortexed briefly (~10 seconds).

(vii) 10 μ L aliquots of each prepared 5×10^4 cells/mL YEA *S. pombe* strain broth culture, were then spread out onto 7 YEA agar (Section 2.3.2, p.168) petri-plates (~ 500 cells/plate), via a 70% ethanol-sterilised flame spreader and allowed to dry at room temperature for 10 minutes.

(viii) Each YEA petri-plate culture (lid removed) was then placed in the chamber of a UVP CL-1000 U.V. Cross-Linker and irradiated with a successive increased acute dose of ultra-violet light – thus each respective *S. pombe* strain culture was plated out onto 7 YEA agar petri-plates and each plate exposed to a different dose of U.V.:

UV Dose (J/M²)	0	5	10	20	30	40	50
Plate No.	1	2	3	4	5	6	7

Note: It was necessary to ensure that each YEA agar petri-plate culture was dry prior to U.V. irradiation to prevent the incidence of experimental data anomalies as a consequence of damp-quenching of the acute U.V. dose administered.

Each dry YEA agar petri-plate culture was U.V. irradiated with the petri-plate cover lid removed to prevent the incidence of experimental data anomalies as a consequence of absorbance of a fraction of the acute U.V. dose administered by the plastic cover lid – which would have otherwise effectively “shielded” the culture from the full U.V. dose exposure.

(ix) The resultant petri-plate cultures were then placed in the static 30°C Binder incubator for three days after which time the plates were removed and the number of surviving viable cell colonies counted on each plate.

The number of surviving cell colonies for each U.V. dose (J/M^2) exposure was then calculated as percentage value, relative to the total number of viable colonies counted on the plate culture which contained cells that had not been U.V.-irradiated:

$$\text{\% Cell Survival at Specific U.V. Dose - X (J/M}^2\text{)} = \frac{\text{Number of Colonies on X (J/M}^2\text{) U.V. Plate}}{\text{Number of Colonies on Non-Irradiated Plate [ie "100%" Relative Cell Survival]}}$$

These “processed data” were then plotted as a % Cell Survival (log scale) vs U.V. Dose (J/M^2) response graph for each respective *S. pombe* strain assayed.

2.9.2.2(ii) Acute Survival Assays with Different Types of Genotoxic Compounds

With the notable exception of Methylmethane Sulphonate (pp.243-247) and the Topoisomerase II Inhibitors – Ellipticine and Etoposide (pp.248-251), a standardised protocol was utilised for comparative acute survival assays of various *S. pombe* strains with different classes of genotoxic compounds (pp.239-249).

- (i) A sterile/autoclaved wooden toothpick was utilised to inoculate 5mL of sterile/autoclaved YEA medium (see Section 2.3.1, p.167) with a small amount of each appropriate *S. pombe* strain, taken from the respective YEA agar petri-plate culture, in a sterile/autoclaved 15ml capacity glass culture test-tube (capped loosely with a plastic top) and the resultant broth culture placed in the 30°C Sanyo orbisafe incubator (180 rpm shaker speed) for 12 hours duration.
- (ii) The following morning, the tubes were removed from the incubator and a 10µL aliquot of each broth culture placed onto the square metal grid of a Hawksley Thoma Double Cell Clear Sight Counting Chamber which was then viewed under a CETI Magnum B Binocular light microscope at 60x magnification.
- (iii) After initial visual verification had established that the cells were viable and in S-phase, the number of cells in 4 large grid squares was counted – from which the average number of cells/mL in the undiluted broth culture was calculated via the equation:

$$\text{Average cells/mL (x10}^6\text{)} = \frac{\text{Total No. of Cells Counted}}{4}$$

- (iv) An appropriate volume of cell culture was diluted with an appropriate volume of autoclaved /sterile YEA medium(Section 2.3.1, p.167) to yield 1 mL (1000µL) final broth culture concentration of 1×10^7 cells/mL*, in a sterile/autoclaved 1.5mL capacity plastic eppendorf microfuge tube.

*Via the equation: $V1 = \frac{C2 \times V2}{C1}$

Where:

V1 = Volume of measured cell culture

V2 = Volume of cell culture required

C1 = Concentration of cell culture measured

C2 = Concentration of cell culture required

- (v) A 10 μ L of the resultant 1×10^7 cells/mL cell culture was then mixed with 990 μ L of YEA medium (Section 2.3.1, p.167) in a fresh autoclaved/sterile 1.5mL capacity plastic eppendorf microfuge tube to yield a broth culture concentration of 1×10^5 cells/mL.
- (vi) A 200 μ L aliquot of the resultant 1×10^5 cells/mL *S. pombe* strain culture was then mixed with 800 μ L of YEA medium (Section 2.3.1, p.167) in a fresh sterile/autoclaved 1.5mL capacity plastic eppendorf microfuge tube to yield a YEA broth culture concentration of 2×10^4 cells/mL.
- (vii) A 500 μ L aliquot of the prepared 2×10^4 cells/mL *S. pombe* strain culture was then mixed with 500 μ L of a “double-strength” (2x) concentrated YEA solution of the test compound in a fresh 1.5mL capacity plastic eppendorf microfuge tube to yield the experimental culture to be assayed.
- [Thus each prepared experimental assay culture comprised 1×10^4 cells/mL with 1x final concentration strength* of the respective test compound in a total volume of 1mL YEA medium]
- *NOTE: The specific concentrations and prepared solutions of the various genotoxic agents assayed and solutions of the different genotoxic agents utilised are detailed on the following pages (pp.242-251).
- (viii) A 50 μ L aliquot was then removed from the prepared experimental assay culture and plated out onto a YEA agar (Section 2.3.2, p.168) petri-plate via utilisation of an ethanol-sterilised flame-spreader.
- (ix) The remainder of the experimental assay culture (~950 μ L) was then placed in the 30°C Sanyo Incubator Shaker for a total time of 4 hours, during which a 50 μ L aliquot of the culture was removed at regular 30 minute intervals and plated out onto a separate YEA agar (Section 2.3.2, p.168) petri-plate via utilisation of a 70% ethanol-sterilised flame-spreader.
- (x) The resultant petri-plate cultures were then placed in the static 30°C Binder incubator for three days after which time the plates were removed and the number of surviving viable cell colonies counted on each plate.

(xi) The number of surviving cell colonies at each time point was then calculated as a percentage value, relative to the total number of viable colonies counted on the initial plate culture (prepared prior to placement of the experimental assay culture in the Sanyo 30°C Incubator Shaker – which was designated the “Time = 0 minutes” culture that corresponded to the representative 100% relative cell survival).

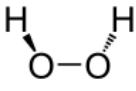
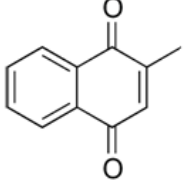
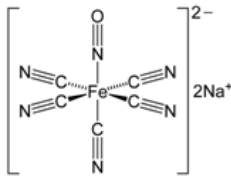
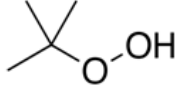
% Cell Survival

$$\begin{array}{l} \text{[At a Specific} \\ \text{Fixed-Dose} \\ \text{of Genotoxic} \\ \text{Agent]} \end{array} = \frac{\text{Number of Colonies on the Time-Point Plate}}{\text{Number of Colonies on Time, t = 0 Mins Plate}} \\ \text{[ie 100\% "Initial" Relative Cell Survival]}$$

These “processed data” were then plotted as a % Cell Survival (log scale) vs Time (Minutes) type time-course graph at the fixed-dose concentration of the specific genotoxic agent for each respective *S. pombe* strain assayed.

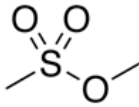
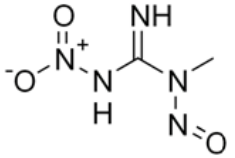
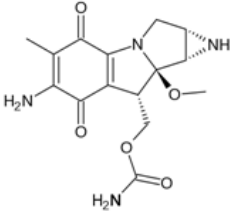
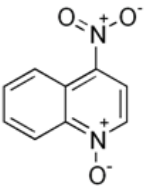
Oxidative Stress-Inductive Agents

[Compiled via Collated Information From: Hemnani T. and Parihar M.S., 1998;
Hix S. *et al*, 1995;
Marnett L.J. *et al*, 2003;
Martins E.A. and Meneghini R., 1990;
Slupphaug G. *et al*, 2003]

COMPOUND	Hydrogen Peroxide	Menadione	Sodium Nitroprusside	t-Butylhydroperoxide
ABBREVIATION	H ₂ O ₂	MDN	SNP	TBH
MOLECULAR STRUCTURE				
SUMMARISED GENOTOXIC MECHANISM OF ACTION	Generates various reactive oxygen species which react with DNA and RNA to form oxidized base adducts and initiate nucleic acid strand cleavage reactions	Generates a variety of reactive oxygen species and organic free radical species via quinone redox cycling reactions The resultant free radicals interact with DNA and RNA to form base adducts and initiate nucleic acid strand cleavage reactions	Generates a variety of reactive oxygen species and reactive nitrogen species via redox liberation of nitric oxide The resultant free radicals interact with DNA and RNA to form base adducts and initiate nucleic acid strand cleavage reactions	Generates a variety of reactive oxygen species and organic free radical species The resultant free radicals interact with DNA and RNA to form base adducts and initiate nucleic acid strand cleavage reactions
STOCK SOLUTION	Supplied undiluted liquid reagent [17.89M] stored at 4°C until required	1M solution prepared in DMSO:Ethanol (1:1) solvent, stored as 1mL aliquots at -20°C until required	1M solution prepared in "neat" DMSO (100%) solvent, stored as 1mL aliquots at -20°C until required	Supplied undiluted liquid reagent [8.86M] stored at 4°C until required
ACUTE SURVIVAL ASSAY SOLUTION [X2 FINAL CONC'N]	800µM in YEA liquid medium Freshly prepared immediately before use	800µM in YEA liquid medium Freshly prepared immediately before use	800µM in YEA liquid medium Freshly prepared immediately before use	800µM in YEA liquid medium Freshly prepared immediately before use
<p>NOTE: Acute survival assay incubation cultures comprised 1mL of YEA liquid medium containing 400µM final concentration of H₂O₂, MDN, SNP or TBH and 1x10⁴ cells/mL of the respective <i>S. pombe</i> strain In the case of MDN and SNP, a fresh 1mL stock aliquot was defrosted and utilised for each acute survival assay and the unused remainder discarded [due to the reactive instability of these compounds in solution] The remainder of the unused X2 acute survival assay solution was also discarded</p>				

DNA Alkylating and Cross-Linking Agents

[Compiled via Collated Information From: Daniel D.S. and Tainer J.A., 2000; Durante M. *et al*, 1989; Lu L.J. *et al*, 1990; Hu J. *et al*, 2008; Painter R.B., 1978; Slameová D. *et al*, 1997; Strauss B. *et al*, 1975; Tomasz M. and Palom Y., 1997; Tubbs J.L. *et al*, 2007]

COMPOUND	Methylmethane Sulphonate	N-Methyl-N'-Nitro-N-Nitrosoguanidine	Mitomycin C	4-Nitroquinoline-1-Oxide
ABBREVIATION	MMS	MNNG	Mit C	4-NQO
MOLECULAR STRUCTURE				
SUMMARISED GENOTOXIC MECHANISM OF ACTION	<p>Monoalkylating agent which predominantly methylates Guanine bases within DNA and RNA at positions N3 and N7 within the purine ring</p> <p>May also methylate other nucleobases to a lesser extent</p> <p>May also propagate formation of larger DNA and RNA adduct derivatives via <i>in situ</i> generation of reactive intermediary species</p>	<p>Monoalkylating agent which predominantly methylates Thymine at position O4 and Guanine at position O6 within DNA</p> <p>May also methylate other nucleobases to a lesser extent</p> <p>May also propagate formation of larger DNA and RNA adduct derivatives via <i>in situ</i> generation of reactive intermediary species</p>	<p>Alkylation-coupled DNA cross-linking type agent which predominantly forms 5'-CpG-3' sequence-specific Guanine inter- and intra- DNA strand cross-linkages</p> <p>May also alkylate other nucleobases to a lesser extent</p> <p>May also propagate formation of larger DNA and RNA adduct derivatives via <i>in situ</i> generation of reactive intermediary species</p>	<p>Alkylation-coupled DNA cross-linking type agent which predominantly forms deoxyguanine-aminoquinoline oxide type adducts at positions N2 & C8 of the purine ring & deoxyadenine-quinoline oxide type adduct at position N6 of the pyrimidine ring</p> <p>These adducts may undergo reaction with intra- or inter- strand proximal-situated nucleobases to form derivatised, bulky adduct species*</p> <p>*Thus 4-NQO is also referred to as a "U.V.-mimetic"</p> <p>May also alkylate other nucleobases to a lesser extent</p>
STOCK SOLUTION	Supplied 99.9% Liquid Reagent Formulation stored at 4°C until required	1 mM sol'n prepared in "neat" DMSO (100%) solvent, stored as 1mL aliquots at -20°C	1 mM sol'n prepared in "neat" DMSO (100%) solvent, stored as 1mL aliquots at -20°C until required	1 mM sol'n prepared in "neat" DMSO (100%) solvent, stored as 1mL aliquots at -20°C until required
ACUTE SURVIVAL ASSAY SOLUTION [X2 FINAL CONC'N]	Not Applicable Different acute survival assay protocol used	8µM in YEA liquid medium Freshly prepared immediately before use	8µM in YEA liquid medium Freshly prepared immediately before use	8µM in YEA liquid medium Freshly prepared immediately before use
<p>NOTE: Acute survival assay incubation cultures comprised 1mL of YEA liquid medium containing 4µM final concentration of MNNG, Mit C or 4-NQO and 1x10⁴ cells/mL of the respective <i>S. pombe</i> strain</p> <p>The remainder of the unused X2 acute survival assay solution was discarded</p>				

NOTE: The MMS Survival Assay Protocol utilised was a different procedure to that of the other mutagenic agents – described in detail on the following pages (pp.244-246).

Acute Varied Methylmethanesulphonate (MMS) Dose Survival Assay

- (i) A sterile/autoclaved wooden toothpick was utilised to inoculate 5mL of sterile/autoclaved YEA medium (Section 2.3.1, p.167) with a small amount of each appropriate *S. pombe* strain, taken from the respective YEA agar petri-plate (Section 2.3.2, p.168) culture, in a sterile/autoclaved 15ml capacity glass culture test-tube (capped loosely with a plastic) and the resultant broth culture placed in the 30°C Sanyo orbisafe incubator shaker for 12 hours duration.
- (ii) The following morning, the tubes were removed from the incubator and a 10µL aliquot of each broth culture placed onto the square metal grid of a Hawksley Thoma Double Cell Clear Sight Counting Chamber which was then viewed under a CETI Magnum B Binocular light microscope at 60x magnification.
- (iii) After initial visual verification had established that the cells were viable and in S-phase, the number of cells in 4 large grid squares was counted – from which the average number of cells/mL in the undiluted broth culture was calculated via the equation:

$$\text{Average cells/mL (x10}^6\text{)} = \frac{\text{Total No. of Cells Counted}}{4}$$

- (iv) An appropriate volume of cell culture was diluted with an appropriate volume of autoclaved /sterile YEA medium (Section 2.3.1, p.164) to yield 1 mL (1000µL) final broth culture concentration of 1×10^7 cells/mL*, in a sterile/autoclaved 1.5mL capacity plastic eppendorf microfuge tube.

*Via the equation: $V1 = \frac{C2 \times V2}{C1}$

Where:

V1 = Volume of measured cell culture

V2 = Volume of cell culture required

C1 = Concentration of cell culture measured

C2 = Concentration of cell culture required

- (v) A 10µL of the resultant 1×10^7 cells/mL cell culture was then mixed with 990µL of YEA medium (Section 2.3.1, p.164) in a fresh autoclaved/sterile 1.5mL capacity plastic eppendorf microfuge tube to yield a broth culture concentration of 1×10^5 cells/mL.

- (vi) A 400µL aliquot of the resultant 1×10^5 cells/mL *S. pombe* strain culture was then mixed with 600µL of YEA medium (Section 2.3.1, p.167) in a fresh sterile/autoclaved 1.5mL capacity plastic eppendorf microfuge tube to yield a YEA broth culture concentration of 4×10^4 cells/mL.
- (vii) Individual 250µL aliquots of each diluted *S. pombe* strain culture (4×10^4 cells/mL) were then pipetted into 6 autoclaved/sterile plastic 1.5mL capacity plastic eppendorf microfuge tubes which contained either 250µL YEA medium only (no MMS) or a 0.02% (v/v), 0.04% (v/v), 0.06% (v/v), 0.08% (v/v), 0.1% (v/v) solution of MMS in YEA.
- (viii) Thus each assay set of 6 eppendorf tubes, for each *S. pombe* strain tested, contained 2×10^4 cells/mL in 500µL of a varied concentration range of MMS in YEA medium (0% to 0.05% v/v MMS in YEA):

[MMS] (%v/v)	0	0.01%	0.02%	0.03%	0.04%	0.05%
Tube No.	1	2	3	4	5	6

- (ix) The eppendorf tubes were then placed in the 30°C Sanyo Incubator Shaker for one hour, after which time they were removed and a 500µL aliquot of a 1% (w/v) SodiumThiosulphate in YEA (“Stop”) solution added to each tube – that was then vortexed briefly (~10 seconds).

[NOTE: The Sodium Sulphate component of “Stop” solution reacts with the MMS to “neutralize” the DNA base-alkylation activity of the mutagenic agent]

- (x) A 50µL aliquot (~500 cells) from each resultant assay culture was pipetted onto a fresh, individual YEA agar plate and spread evenly over the medium surface via utilisation of a 70% ethanol-sterilised flame-spreader.
- (xi) The resultant petri-plate cultures were then placed in the static 30°C Binder incubator for three days after which time the plates were removed and the number of surviving viable cell colonies counted on each plate.

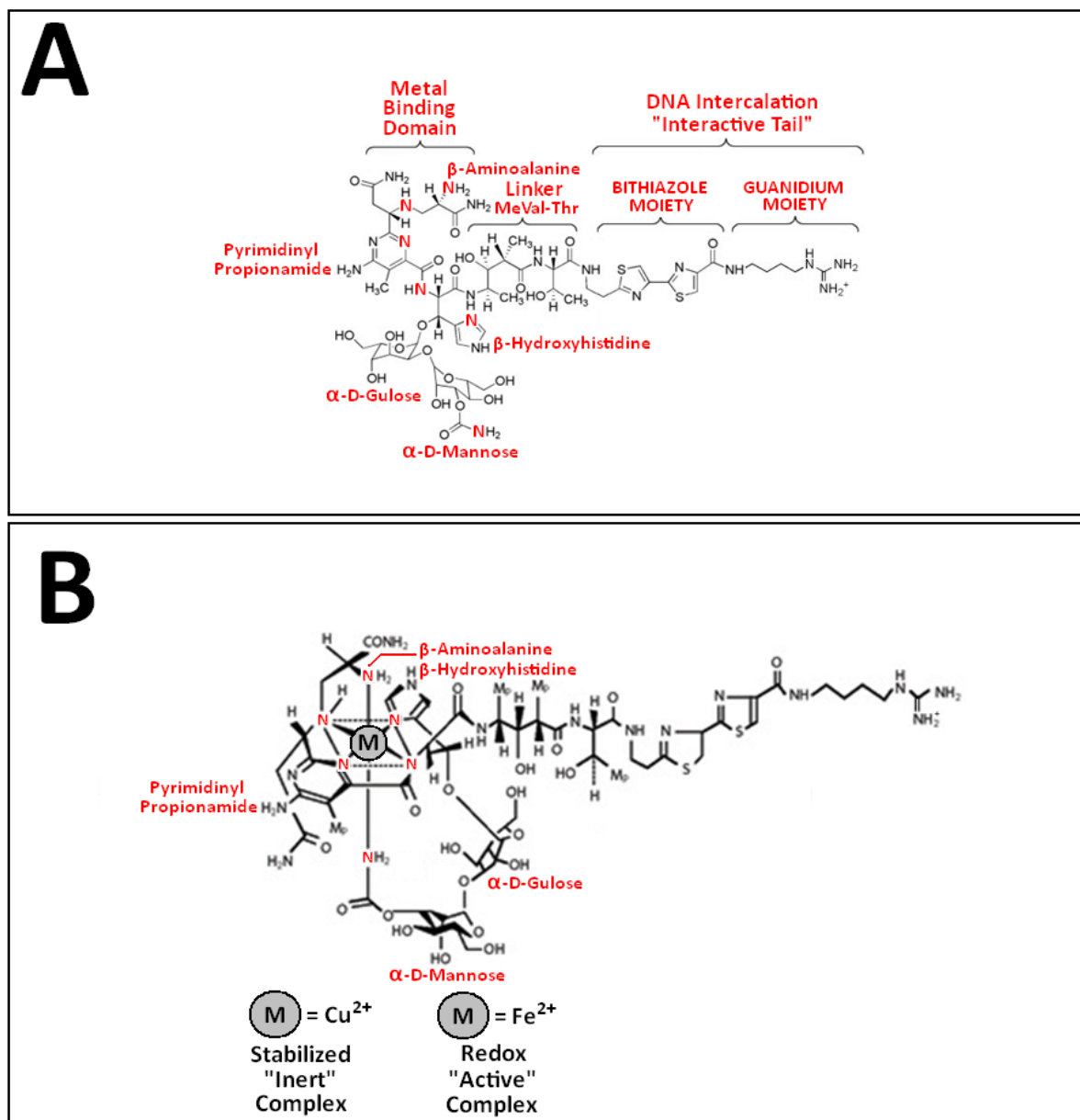
(xii) The number of surviving cell colonies for each MMS dose exposure was then calculated as a percentage value, relative to the total number of viable colonies counted on the plate culture which contained cells that had not been treated with MMS:

$$\begin{array}{l} \text{\% Cell Survival} \\ \text{at Specific MMS} \\ \text{Dose - X\%(v/v)} \end{array} = \frac{\text{Number of Colonies on X\% (v/v) MMS Plate}}{\text{Number of Colonies on 0\% (v/v) MMS Plate}} \\ \text{[ie YEA Only; "100\%" Relative Cell Survival]} \end{array}$$

These “processed data” were then plotted as a % Cell Survival (log scale) vs %(v/v) MMS dose response graph for each respective *S. pombe* strain assayed.

Phleomycin (Intercalation-Redox-Coupled DNA Cleavage Agent)

[Compiled via Collated Information From: Sleight M.J., 1976; Stern R. *et al*, 1974; Stretkowski L. *et al*, 1986; Tanaka N., 1983]



A: Phleomycin is similar to the Bleomycin anti-biotics with regard to its genotoxic biochemical mode of action. The "tail" section of the molecule intercalates within the major groove of the DNA duplex, in which the positively charged Guanidium group may form electrostatic associative interactions ("salt linkages") with the negatively charged phosphate groups of the nucleic acid polymer "backbone".

The Bithiazole group within the "intercalative tail segment" may also form associative π - π type aromatic electron base-stacking interactions with the nucleobases situated in the major groove of the duplex.

B: The metal ion-chelation domain of Phleomycin forms a redox-inert organometallic complex with Cu^{2+} ions and is supplied commercially as a stabilised preparation in this form (Sigma-Aldrich Company).

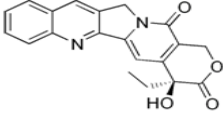
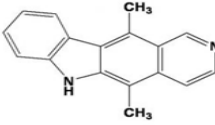
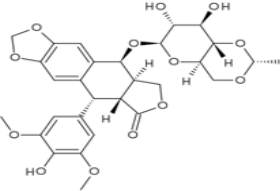
Once inside the cell, formation of the DNA-intercalated Fe^{2+} :Phleomycin complex initiates redox-cycle generation of reactive free-radical oxygen species within the major groove of the duplex which react with the phosphodiester bonds with consequential double-strand cleavage of the nucleic acid.

Stock 1mL aliquots of 1mM Phleomycin in DMSO (100%/"neat") were stored in Eppendorf tubes at -20°C until required, from which an $8\mu\text{M}$ solution of Phleomycin in YEA was prepared fresh, immediately before use.

[Thus, the acute survival assay culture comprised 1mL of YEA which contained 1×10^4 cells and $4\mu\text{M}$ of Phleomycin]

Topoisomerase Inhibitors

[Compiled via Collated Information From: Martinkova E. *et al*, 2009;
Montecucco A. and Biamonti G., 2007;
Nitiss J.L. and Wang J.C., 1996;
Pommier Y., 2006; Stiborová M. *et al*, 2004;
Stiborová M. *et al*, 2006
Zhao H. *et al*, 2012]

COMPOUND	S-(+)-Camptothecin	Ellipticine	Etoposide
ABBREVIATION	CPT	ELP	ETP
MOLECULAR STRUCTURE			
SUMMARISED GENOTOXIC MECHANISM OF ACTION	<p>Topoisomerase I Inhibitor</p> <p>Induces formation of ssDNA breaks in cell cycle S-phase due to CPT-inhibition of the enzymatic re-ligation activity</p> <p>Non-covalent complex formation between CPT, DNA & Topoisomerase I also results in stalled replication fork collision events which convert the initial ssDNA breaks into one-sided dsDNA breakages</p>	<p>Topoisomerase II Inhibitor</p> <p>Binds to Topoisomerase II and inhibits the enzyme in the absence or presence of DNA</p> <p>Interacts directly with the Topoisomerase II enzyme</p> <p>Topoisomerase II dictates the protonation status of ELP within the respective free & DNA-bound enzyme ternary complexes</p> <p>Non-covalent complex formation between Elp, DNA & Topoisomerase II elicited predominantly via the deprotonated form of ELP</p> <p>Only the protonated form of ELP binds to DNA</p> <p>Propagation of dsDNA breakage events is via ELP-mediated elevation of the forward reaction rate of enzymatic DNA cleavage, but does NOT involve inhibition of enzymatic re-ligation activity</p> <p>Oxidative metabolic action of Cytochrome P450 1A1 & 1A2 on ELP results in the formation of hydroxy-ELP derivatives 7-OH Elp and 9-OH Elp which can react with nucleic acids to form DNA & RNA base-adducts</p>	<p>Topoisomerase II Inhibitor</p> <p>Induces formation of ssDNA breaks in cell cycle S-phase due to ETP-inhibition of the enzymatic re-ligation activity</p> <p>Non-covalent complex formation between ETP, DNA & Topoisomerase II also results in stalled replication fork collision events which convert the initial ssDNA breaks into one-sided dsDNA breakages</p>
STOCK SOLUTION	10mM solution prepared in "neat" DMSO (100%) solvent, stored as 1mL aliquots at -20°C until required	10mM solution prepared in "neat" DMSO (100%) solvent, stored as 1mL aliquots at -20°C until required	10mM solution prepared in "neat" DMSO (100%) solvent, stored as 1mL aliquots at -20°C until required
ACUTE SURVIVAL ASSAY SOLUTION [X2 FINAL CONC'N]	80µM in YEA liquid medium freshly prepared prior to immediate use	80µM in YEA liquid medium freshly prepared prior to immediate use	80µM in YEA liquid medium freshly prepared prior to immediate use
<p>NOTE: Acute survival assay incubation cultures comprised 1mL of YEA liquid medium containing 40µM final concentration of CPT, ELP or ETP and 1×10^4 cells/mL of the respective <i>S. pombe</i> strain</p> <p>The remainder of the unused X2 acute survival assay solution was discarded</p>			

NOTE: ELP and ETP Survival Assays were performed on Lyticase-Treated Cell Cultures, also in comparative control with CPT – described in detail on the following pages (pp.249-251).

The Topoisomerase II inhibitors Ellipicine and Etoposide were discovered to be relatively impermeable, with regard to their inability to traverse the cell wall and membrane of *S. pombe* cells, as indicated via initial acute survival assays performed with the respective drugs with YEA broth cultures of the “Cre-Lox” *rad9*-deleted base-strain in which the cells were insensitive to even excessively high doses of the compounds.

To circumvent this experimental problem, the appropriate *S. pombe* strains were treated with lyticase in order to partially degrade the cell wall and thereby facilitate entry of the drugs into the resultant protoplast culture preparations – the treatment protocol was comprised of the following steps:

(i) A sterile/autoclaved wooden toothpick was utilised to inoculate 25mL of sterile/autoclaved YEA medium (Section 2.3.1, p.167) with a small amount of the appropriate *S. pombe* YEA agar (Section 2.3.2, p.168) petri-plate culture, in a sterile/autoclaved 100mL capacity glass conical flask (capped loosely with aluminium foil) and the resultant broth culture placed in the 30°C Sanyo orbisafe incubator (set at 180 r.p.m. shake speed) for 24 hours duration.

(ii) The following day, a 100µL aliquot of the resultant broth culture was diluted with 900µL YEA broth medium and the resultant 1 in 10 diluted culture sample (1mL) was then placed in a plastic microcuvette for measurement of the optical density at A₅₉₅ (O.D. 595) in a Sanyo SP BIO Spectrophotometer (pre-set against a blank reference of 1mL YEA broth medium) and the optical density of the “neat” culture calculated:

$$\text{ie } A_{595} (\text{“neat” culture}) = A_{595} (1 \text{ in } 10 \text{ diluted culture}) \times 10$$

(iii) An appropriate volume of resultant broth culture was then adjusted with the appropriate volume of YEA broth medium to an A₅₉₅ optical density of 0.25 units/mL, dictated by the calculated diluent factor ratio – D.F.R.

$$\text{ie D.F.R.} = \frac{\text{Calculated } A_{595} (\text{“neat” culture})}{0.5}$$

$$\text{Via the equation: } V_1 = \frac{C_2 \times V_2}{C_1}$$

Where:

V₁ = Volume of measured cell culture

V₂ = Volume of cell culture required

C₁ = O.D.595 of cell culture measured

C₂ = O.D.595 of cell culture required

[249]

- (iv) The resultant diluted culture was then returned to the 30°C Sanyo orbisafe incubator (set at 180 r.p.m. shake speed) for a further ~2.5 hours duration, until the optical density of the culture had doubled (ie $A_{595} = 0.5$).
- (v) A 40mL aliquot of the resultant culture was then transferred to a 50 mL capacity plastic Greiner centrifuge tube which was placed in a Jencons-PLS SorvallR Legend T centrifuge and spun at 3000 r.p.m. at 25°C for 5 minutes.
- (vi) The supernatant was discarded and the cell pellet re-suspended in 1mL of YEA-Lyticase reaction buffer (Section 2.4.2, p.162), prior to transfer of the resultant cell suspension to a 1.5mL capacity plastic eppendorf microfuge tube – which was then spun at 3000 r.p.m., at 25°C for 5 minutes in a Sanyo Hawk 15/05 refrigerated bench-top microfuge.
- (vii) The supernatant was discarded and cell pellet re-suspended in 1mL of YEA-Lyticase Reaction Buffer which also contained 2U/ μ L Lyticase enzyme*.
- [*Note: The prepared solution was filter-sterilised after addition of the enzyme prior to use]
- (viii) The eppendorf tube which contained the resultant cell suspension was then placed in the static 30°C Binder incubator for 20 minutes.
- (ix) After the incubation time had elapsed, the eppendorf tube which contained the cell suspension was then placed in and spun at 3000 r.p.m. at 25°C for 5 minutes in a Sanyo Hawk 15/05 refrigerated bench-top microfuge.
- (x) The supernatant was discarded, the cell pellet re-suspended in 1mL of YEA medium and the resultant cell suspension in the eppendorf tube was re-spun at 3000 at 25°C for 5 minutes in a Sanyo Hawk refrigerated bench top microfuge.
- (xi) The resultant cell pellet was washed a further four times with fresh 1mL aliquots of YEA medium as described previously in stage (x) above.

- (xii) The resultant washed cell pellet was re-suspended in a fresh 1mL aliquot of YEA medium and transferred to a 15mL capacity plastic Greiner centrifuge tube which contained 9mL of YEA medium.
- (xiii) A 10 μ L aliquot of the resultant culture preparation was placed onto the square metal grid of a Hawksley Thoma Double Cell Clear Sight Counting Chamber and viewed under a CETI Magnum B binocular light microscope at 60x magnification.
- (xiv) The total number of cells in 4 large grid squares was then counted, from which the average number of cells/mL in the culture was calculated via the equation:

$$\text{Average cells/mL (x10}^6\text{)} = \frac{\text{Total No. of Cells Counted}}{4}$$

- (xv) The cell culture was then diluted to a final concentration of 2×10^4 cells/mL via the appropriate addition of YEA medium – which was calculated via the equation:

$$V1 = \frac{C2 \times V2}{C1}$$

Where:

V1 = Volume of measured cell culture

V2 = Volume of cell culture required

C1 = Concentration of cell culture measured (cells/mL)

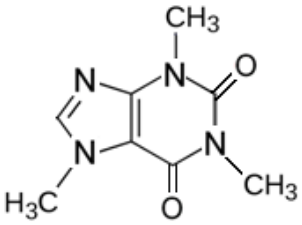
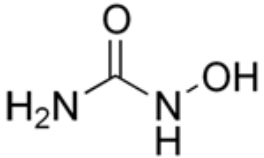
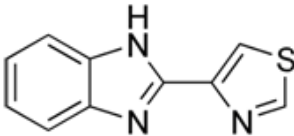
C2 = Concentration of cell culture required (cells/mL)

- (xvi) 500 μ L of the 2×10^4 cells/mL YEA cell culture was then mixed with 500 μ L of an 80 μ M solution of the appropriate drug in YEA medium (ie Etoposide, Ellipticine or Camptothecin) in a sterile/autoclaved 1.5mL capacity plastic eppendorf microfuge tube.
- (xvii) The eppendorf tube which contained the resultant experimental culture, comprised of 40 μ M of the drug and 1×10^4 cells in 1mL of YEA broth medium, was then utilised for the acute survival assay protocol described previously (Section 2.9.2.2(ii), pp.240-241).

[Note: The Lyticase Pre-Treatment Protocol was devised via collated information adapted from the methodologies described by Forsburg S.L., 2003d; Forsburg S.L. & Rhind P., 2006; Sipickzi M. *et al*, 1985]

Anti-metabolic, Anti-Mitotic and Checkpoint PI3 Kinase Inhibitor Agents

[Compiled via Collated Information From: Calvo I.A. *et al*, 2009;
Norland P. and Reichard P., 2006;
Sabisz M. and Skladanowski A., 2008;
Sakaria J.N. *et al*, 1999;
Walker G.M., 1982;
Zhou B.B. *et al*, 2000]

COMPOUND	Caffeine	Hydroxyurea	Thiabendazole
ABBREVIATION	Caff	HU	TBZ
MOLECULAR STRUCTURE			
SUMMARISED GENOTOXIC MECHANISM OF ACTION	Checkpoint Abrogator	Anti-Metabolite	Anti-Mitotic
	Inhibits PI ₃ Kinases implicated in DNA Damage Cell Cycle Checkpoint Signal Responses Blocks appropriate cell cycle arrest and/or DNA repair responses – thus DNA damage is propagated with enhanced genomic instability	Reversibly inhibits Ribonucleotide Reductase (RNR) Blocks biosynthesis of deoxyribonucleotides and thus impairs DNA replication & repair processes, thereby eliciting the G1/S cell cycle arrest	Induction of spindle instability via the depolymerisation of the microtubule sub-unit assemblies Correct segregation of chromosomes is impaired, thereby eliciting the spindle checkpoint-mediated cell cycle arrest
STOCK SOLUTION	1M solution prepared in "neat" DMSO (100%) solvent, stored as 1mL aliquots at -20°C until required	1M solution prepared in millipore ultra-pure H ₂ O, stored as 1mL aliquots at -20°C until required	10mM sol'n prepared in "neat" DMSO (100%) solvent, stored as 1mL aliquots at -20°C until required
ACUTE SURVIVAL ASSAY SOLUTION [X2 FINAL CONC'N]	20mM in YEA liquid medium Freshly prepared immediately before use	20mM in YEA liquid medium Freshly prepared immediately before use	80µM in YEA liquid medium Freshly prepared immediately before use
<p>NOTE: Acute survival assay incubation cultures comprised 1mL of YEA liquid medium containing 10mM final concentration of Caff, HU or 40µM TBZ and 1x10⁴ cells/mL of the respective <i>S. pombe</i> strain</p> <p>The remainder of the unused X2 acute survival assay solution was discarded</p>			

2.9.3 Lactose Synchronisation Assays

(i) A sterile/autoclaved wooden toothpick was utilised to inoculate 100mL of sterile/autoclaved YEA broth medium (Section 2.3.1, p.167) with a small amount of the appropriate *S. pombe* strain YEA agar (Section 2.3.2, p.168) petri-plate culture, in a sterile/autoclaved 250mL capacity glass conical flask (capped loosely with aluminium foil) and the resultant broth culture placed in the 30°C Sanyo orbisafe incubator (set at 180 r.p.m. shake speed) for 24 hours duration.

(ii) The following day, a 100µL aliquot of the resultant broth culture was diluted with 900µL YEA broth medium and the resultant 1 in 10 diluted culture sample (1mL) was then placed in a plastic microcuvette for subsequent measurement of the optical density at A₅₉₅ (O.D. 595) in a Sanyo SP BIO Spectrophotometer (against a set blank reference of 1mL YEA broth medium) and the optical density of the “neat” culture calculated:

$$\text{ie } A_{595} (\text{“neat” culture}) = A_{595} (1 \text{ in } 10 \text{ diluted culture}) \times 10$$

(iii) An appropriate volume of resultant broth culture was then adjusted with the appropriate volume of YEA broth medium to an A₅₉₅ optical density of 0.25 units/mL, dictated by the calculated diluent factor ratio – D.F.R.

$$\text{ie D.F.R.} = \frac{\text{Calculated } A_{595} (\text{“neat” culture})}{0.5}$$

$$\text{In accordance with the related equation: } V_1 = \frac{C_2 \times V_2}{C_1}$$

Where:

V1 = Volume of measured cell culture

V2 = Volume of cell culture required

C1 = O.D.595 of cell culture measured

C2 = O.D.595 of cell culture required

The resultant diluted culture was then returned to the 30°C Sanyo orbisafe incubator (set at 180 r.p.m. shake speed) for a further ~2.5 hours duration, until the optical density of the culture had doubled (ie A₅₉₅ = 0.5).

- (iv) A 50mL aliquot of the resultant culture (equivalent to 5×10^8 cells) was then transferred to a 50mL capacity plastic Greiner centrifuge tube which then spun at 3,000r.p.m at 25°C for 5 minutes in a Jencons-PLS SorvallR Legend T Centrifuge.
- (v) The supernatant was discarded and the cell pellet re-suspended in 1mL of sterile/autoclaved aqueous 7% (v/v) lactose solution, prior to transfer of the resultant solution to a sterile/autoclaved 1.5mL capacity plastic eppendorf microfuge tube – which was then spun at 3,000 r.p.m at 25°C for 5 minutes in a Sanyo Hawk 15/05 refrigerated bench top microfuge.
- (vi) The resultant superanatant was discarded and and cell pellet re-suspended in 1mL of sterile/autoclaved aqueous 7% (v/v) lactose solution.
- (vii) Aqueous lactose solutions of decreasing percentage concentration strength (% v/v) were prepared, via mixing of the appropriate volumes of sterile/autoclaved 30%(v/v) and 7% (v/v) aqueous Lactose stock solutions, which were then utilised to set up a differential Lactose density centrifugation gradient in a 15mL capacity plastic Greiner screw-cap centrifuge tube via careful successive stratification of 1.5mL aliquots of decreasing aqueous Lactose solution concentrations on top of each other:

LACTOSE DIFFERENTIAL DENSITY CENTRIFUGATION GRADIENT PREPARATION			
30% (v/v) Lactose(aq) Stock Solution (mL)	7% (v/v) Lactose(aq) Stock Solution (mL)	Final Lactose (aq) Concentration (% v/v)	
0 mL	10mL	~7% (v/v)	
1.25mL	8.75mL	~ 9% (v/v)	
2.5mL	7.5mL	~12% (v/v)	
3.75mL	6.25mL	~15% (v/v)	
5mL	5mL	~18% (v/v)	
6.25mL	3.75mL	~21% (v/v)	
7.5mL	2.5mL	~24% (v/v)	
8.75mL	1.25mL	~27% (v/v)	
10mL	0 mL	~30% (v/v)	

[Note: Successive stratification of decreasingly dense lactose solutions was accomplished via utilisation of a truncated blue Gilson tip, which was inserted just below the 1.5mL layer of the greater density lactose solution (loaded previously) to pipette the 1.5mL layer of the preceding, less dense lactose solution – detailed in Stage (vii) on the previous page.

ie A 1.5mL aliquot of the highest density solution (30% v/v lactose) was loaded first, followed by successive loading of 1.5mL aliquots of decreasingly dense lactose solution]

(viii) The resultant cell suspension [acquired from stage (vi) – on the previous page] was then pipetted carefully onto top of the freshly prepared Lactose Density Gradient contained within the 15mL capacity plastic Greiner centrifuge – which was then spun at 750r.p.m at 25°C for 8 minutes in a Jencons-PLS SorvallR Legend T Centrifuge.

(ix) A truncated blue Gilson pipette tip was utilised to transfer a 400µL aliquot of resolved G2-phase *S.pombe* cells from the upper middle section of resultant turbid white cell suspension (which appeared in the middle of the tube after density gradient centrifugation) to a fresh sterile/autoclaved 1.5mL capacity plastic eppendorf microfuge tube – which was then spun at 3,000 r.p.m. at 25°C for 5 minutes in a Sanyo Hawk 15/05 refrigerated bench top microfuge.

[Note: Caution was exercised to ensure that no *S. pombe* cells were taken from the very top of the suspension as these were in the stationary cell cycle phase]

(x) The resultant supernatant was discarded and the cell pellet re-suspended in 1mL of YEA broth medium prior to re-centrifugation in the Sanyo Hawk 15/05 refrigerated bench top microfuge at 3,000 r.p.m. at 25°C for 5 minutes.

(xi) The supernatant was discarded and the cell pellet was then re-suspended in 700µL of YEA broth medium, after which a 20µL aliquot of the resultant cell suspension was then mounted on a glass slide and cover slip assembly prior to examination at 60x magnification under a CETI Magnum B binocular light microscope for verification that exclusive isolation of small G2-phase *S.pombe* cells had been accomplished.

- (xii) The remaining cell suspension was then divided into two individual 340 μ L aliquots which were placed into separate sterile/autoclaved 1.5mL capacity plastic eppendorf microfuge tubes.
- (xiii) A 340 μ L aliquot of YEA broth medium was added to one tube (No CPT comparative control) and a 340 μ L aliquot of a 400 μ M solution of Camptothecin (CPT) in YEA broth medium was added to the other tube (comparative CPT-induced DNA damage – final CPT concentration = 200 μ M).
- (xiv) A 30 μ L aliquot (initial “zero time” sample) was then taken from each each tube and placed in separate eppendorf tubes which contained 200 μ L of “neat” (100% v/v) methanol (which instantly killed/”fixed” the cells).
- (xv) The remaining 650 μ L cell cultures, contained in the eppendorf tubes, were then placed in the 30°C Sanyo orbisafe incubator (set at 180 r.p.m. shake speed) for a total time period of 6 hours, during which 30 μ L aliquots were removed and fixed in methanol (as described in the previous stage above) at 20 minute time intervals.
- (xvi) The resultant “fixed” cell suspension aliquots, contained within the eppendorf tubes, were spun at 3,000 r.p.m. at 25°C for 5 minutes in a Sanyo Hawk 15/05 refrigerated bench top microfuge.
- (xvii) The resultant supernatants were discarded and the cell pellets re-suspended in 30 μ L of “neat” (100% v/v) methanol.
- (xviii) 5 μ L aliquots of the prepared cell suspensions were placed on glass microscope slides and allowed to dry for 5 minutes at room temperature.
- (xix) 15 μ L of prepared Hoechst 33342:Calcofluor-White staining solution (reagent composition detailed in Section 2.2.6, p.166) was then placed on top of the dried cell suspension, after which a glass microscope slide cover slip was applied.

- (xx) Each prepared slide sample was mounted on the stage of a Leiz SM-LUX fluorescence microscope and a drop of Type F lens immersion liquid (Leica Microsystems CMS GmbH) placed on top of the coverslip, prior to examination of the fixed, stained *S. pombe* cells at 1000x magnification (oil immersion – set wavelength $\lambda = 340\text{nm}$) for visualisation of the nuclei and wall septa.
- (xxi) The number of septated *S. pombe* cells was scored within a total group count of 100 cells and thus the percentage of *S. pombe* septated cells was determined for each sample.
- (xxii) The data were then plotted as a Mitotic Index Time-Course graph of % Septated Cells Vs Time (minutes).

[Note: This protocol was devised via collated information taken and adapted from the following methodology sources: Forsburg S.L. and Rhind P., 2006; Green M.D. *et al*, 2009; Luche D.D. and Forsburg S.L., 2009; Walworth N. *et al*, 2003]

2.10 In Silico Analyses – Bioinformatics Software Tools Utilised

2.10.1 Protein Physico-Biochemical Property Estimations

Estimated average masses (kDa) and/or other appropriate physico-biochemical properties of selected protein and polypeptide sequences (such as pI isoelectric point values pertinent to 2D-PAGE analyses) were determined via utilisation of the on-line software package Protein Calculator (Version 3.3).

Protein Calculator 3.3 (Scripps Institute) Server – <http://www.scripps.edu/~cdputnam/putcalc.html>

2.10.2 Protein Secondary Structural Conformation Analyses

Comparative analyses of the relative content of coil, helix and strand secondary structural motifs within selected protein and polypeptide sequences was performed via utilisation of the software package YASPIN – <http://www.ibi.vu.nl/programs/yaspin/www> (Lin K. *et al*, 2005).

2.10.3 Protein Transmembrane-Spanning Domain Analyses

Comparative identification analyses and modelling of potential transmembrane-spanning domain regions within selected protein and polypeptide sequences were performed via utilisation of the software packages Kyte-Doolittle Hydropathy Plot (Kyte J. and Doolittle R., 1982), PHOBIUS Käll L. *et al*, 2004), SPLIT 4.0 (Juretic D. *et al*, 2002), TmPred (Hofmann K. and Stoffel W., 1993) and TMRPres2D (Spyropoulos I.C. *et al*, 2004).

Kyte-Doolittle Hydropathy Plot – <http://gcat.davidson.edu/rakarnik/kyte-doolittle.htm>

PHOBIUS – <http://phobius.sbc.su.se/>

SPLIT 4.0 – <http://split.pmfst.hr/split/4/>

TmPred – http://www.ch.embnet.org/software/TMPRED_form.html

TMRPres2D – <http://bioinformatics.biol.uoa.gr/TMRpres2D/>

2.10.4 Protein Coiled-Coil Repeat Motif Analyses

Comparative identification analyses of potential coiled-coil repeat motif type domain regions within selected protein and polypeptide sequences were performed via utilisation of the software packages COILS (Lupas A. *et al.*, 1991a; Lupas A. *et al.*, 1991b), MARCOIL (Delorenzi M. and Speed T., 2002; Gruber M. *et al.*, 2006), MultiCoil (Newman J.R. *et al.*, 2000; Wolf E. *et al.*, 1997), MultiCoil2 (Trigg J. *et al.*, 2011) and REPPER (Gruber M. *et al.*, 2005).

COILS – http://www.ch.embnet.org/software/COILS_form.html

MARCOIL – <http://toolkit.tuebingen.mpg.de.marcoil>

MultiCoil – <http://groups.csail.mit.edu/cb/multicoil/cgi-bin/multicoil.cgi>

MultiCoil2 – <http://groups.csail.mit.edu/cb/multicoil2/cgi-bin/multicoil2.cgi>

REPPER – <http://toolkit.tuebingen.mpg.de/repper>

2.10.5 Comparative Protein Sequence and Functional Motif Homology Alignments

Comparative sequence homology and functional motif sequence alignments were performed via utilisation of the software packages cNLS Mapper (Kosugi S. *et al.*, 2009), COBALT Multiple Alignment (Papadopoulos J.S. and Agarwala R., 2007), ELM (Dinkel H. *et al.*, 2012; Puntervoll P. *et al.*, 2003; Perrodou E. *et al.*, 2008), PSI-BLAST and EMBOSS Pairwise Alignment in conjunction with the Jembooss Alignment Editor (Carver T.J. and Mullan L.J., 2005).

cNLS Mapper – http://nls-mapper.iab.keio.ac.jp/cgi-bin/NLS_Mapper_form.cgi

COBALT – http://www.ncbi.nlm.nih.gov/tools/cobalt/cobalt.cgi?/link_loc=BlastHomeAd

ELM – <http://elm.eu.org/>

PSI-BLAST – <http://www.ebi.ac.uk/Tools/sss/psiblast>

EMBOSS – <http://artedi.ebc.uu.se/programs/pairwise.html>

Jembooss Alignment Editor – <http://emboss.sourceforge.net/Jembooss/jae.html>

2.10.6 Kinase-Specific Protein Phosphorylation Site Target Residue Predictions

Potential phosphorylated residues within selected protein and polypeptide sequences were identified via utilisation of the on-line software packages NetPhos2.0 and NetPhos3.1b (Blom N. *et al.*, 1999; Miller M.L. and Blom N., 2009).

NetPhos Server Site – <http://www.cbs.dtu.dk/services/Netphos>.

Potential kinase-specific substrate target motifs and residues within selected protein and polypeptide sequences were identified via utilisation of the on-line software package NetPhosK Server Site – <http://www.cbs.dtu.dk/services/NetphosK> (Blom N. *et al.*, 2004; Miller M.L. and Blom N., 2009).

2.10.7 Protein Aggregate Potential Motif Sequence Predictions

Potential protein aggregation motif polypeptide sequences were identified via utilisation of the on-line software packages BETASCAN (Bryan A.W. Jr. *et al.*, 2009), TANGO (Fernández-Escamilla A.M. *et al.*, 2004a; Fernández-Escamilla A.M. *et al.*, 2004b) and ZYGGREGATOR (Routledge K.E. *et al.*, 2009; Tartaglia G.G. and Vendruscolo M., 2008; Tartaglia G.G. and Vendruscolo M., 2010)

BETASCAN Server Site – <http://groups.csail.mit.edu/cb/betascan/betascan.html>

TANGO Server Site – <http://tango.crg.es/>

ZYGGREGATOR – <http://www-venduscolo.ch.cam.ac.uk/zyggregator.php>

2.10.8 Protein Intrinsic Disorder Sequence Predictions

Many proteins possess regions of intrinsically-disordered polypeptide sequence within their respective supramolecular structures which are key functional component domains that enable them to interact with a versatile array of different ligands/substrates and/or other proteins (Dunker A.K. *et al.*, 2000; Dunker A.K. *et al.*, 2008; Follis A.V. *et al.*, 2012; Tompa P. *et al.*, 2009; Vucetic S. *et al.*, 2007; Wrabl J.O. *et al.*, 2011; Xie H. *et al.*, 2007a) – Fig 2.9, p.264.

These versatile protein interactions also orchestrate the dynamic regulation of both normal and dysfunctional cytological processes which are implicated in the suppression and promotion of pathophysiological events, including cancerous conditions (Cortese M.S. *et al.*, 2008; Hegyi H. *et al.*, 2009; Iakoncheva L.M. *et al.*, 2002; Midic U. *et al.*, 2009; Sandhu K.S., 2009; Uversky V.N. *et al.*, 2008; Uversky V.N. *et al.*, 2009; Xie H. *et al.*, 2007b).

The highly mobile/flexible C-Terminal Tail Domain of the human Rad9 protein may also possess a high degree of intrinsically-disordered structural propensity which enables it to participate in a variety of different protein-protein interactions (discussed previously in Chapter 1, pp.2-139; Fig 1.10, p.24).

The bioinformatics software programs DisCon (Fig 2.10, p.265) and metaPrDOS (Fig 2.11, p.266) were utilised for the *in silico* identification of potential intrinsically-disordered structural regions within the full-length and truncated variant forms of the *S. pombe* Rad9 protein.

These particular bioinformatics-based approaches were chosen for the prediction of intrinsically-disordered structure content (DisCon) and intrinsically-disordered structural motifs (metaPrDOS) as both programs utilise combinatorial hybrid algorithms, derived from a variety of other disorder proteomics-based software tools, for improved analytical accuracy (Ishida T. and Kinoshita K., 2007; Mizianty M.J. *et al.*, 2011; Uversky V.N. *et al.*, 2007).

Intrinsic protein disorder motifs are often identified in characteristic sequences which possess a low complexity, a higher content of Proline and charged amino acid residues and a lower relative proportion of hydrophobic and/or “large/bulky” amino acid residues (Dyson H.J. and Wright P.E. 2005; Peng K. *et al.*, 2006; Radivojac P. *et al.*, 2004; Romero P. *et al.*, 2001; Uversky V.N. *et al.*, 2000; Zhang H. *et al.*, 2009).

The aqueous intracellular environment will “thermodynamically-orientate” the configuration of the polypeptide chain(s), such that hydrophobic amino acid residues are confined to the interior of the protein supramolecular structure and are excluded from the external hydrophilic micro-environment, with consequential enhancement of ordered hydrophobic interactions/Van-der-Waal’s bonding forces (Zhang H. *et al.*, 2009).

Thus, sequence motifs which possess a high degree of ordered structure tend to contain a high proportionate number of relatively hydrophobic residues – in particular; Tryptophan, Tyrosine, Phenylalanine, Isoleucine, Leucine, Valine and Asparagine (Dunker A.K. *et al.*, 2001; Radivojac P. *et al.*, 2007; Romero P. *et al.*, 2001; Vacic V. *et al.*, 2007; Williams R.M. *et al.*, 2001).

Hydrophilic amino acid residues, within the polypeptide chain(s) of the protein, are “thermodynamically-orientated” towards the external aqueous intracellular microenvironment with consequential formation of a dynamic network of multiple hydrogen-bonding interactions with water molecules and other biomolecular species (Zhang H. *et al.*, 2009).

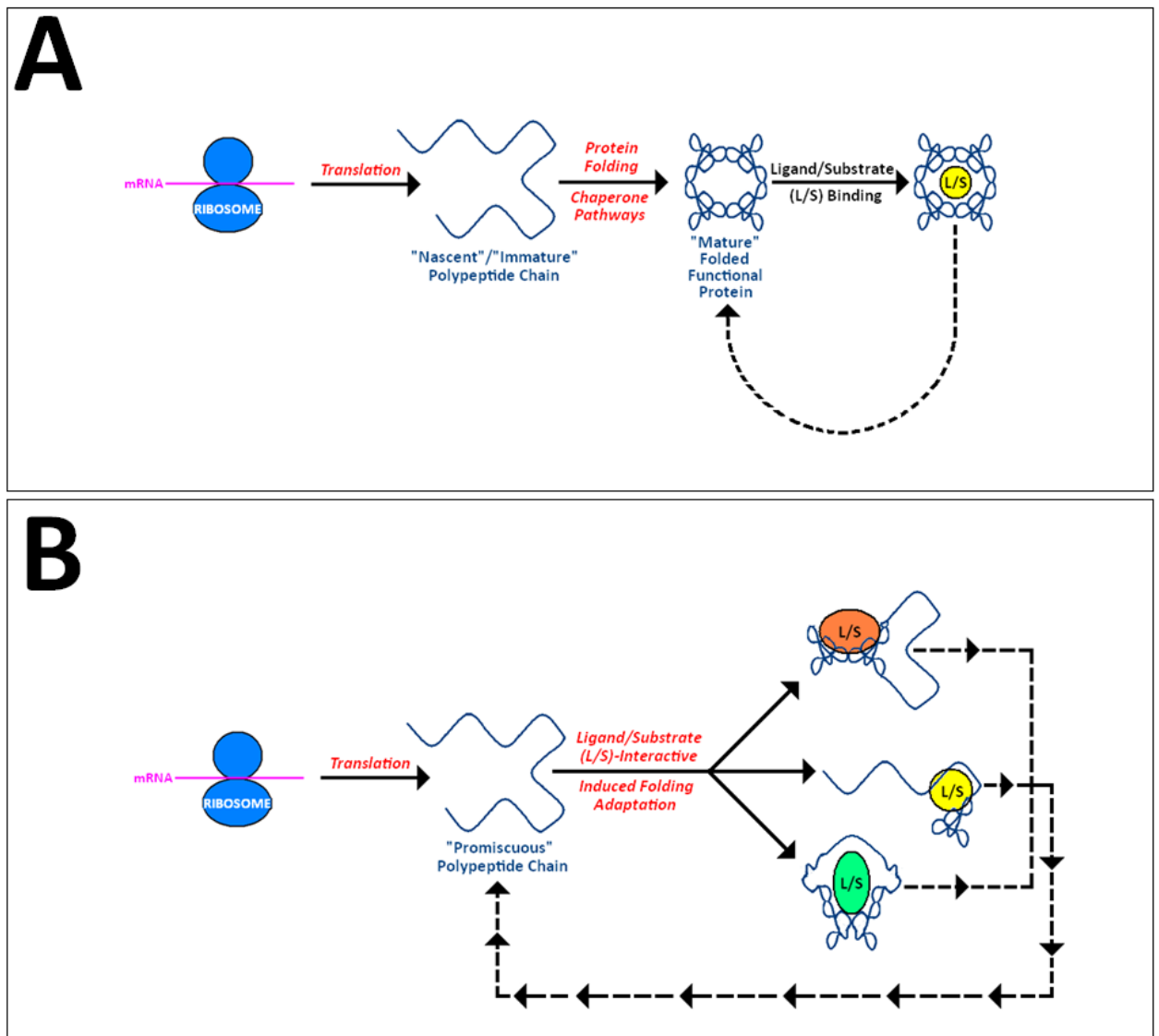
Thus, sequence motifs which possess a high degree of intrinsic structural disorder tend to contain a high proportionate number of relatively hydrophilic residues – in particular; Alanine, Arginine, Glycine, Glutamine, Serine, Glutamate, Proline and Lysine (Dunker A.K. *et al.*, 2001; Radivojac P. *et al.*, 2007; Romero P. *et al.*, 2001; Vacic V. *et al.*, 2007; Williams R.M. *et al.*, 2001).

These unstructured sequence motifs provide a relatively large accessibility surface area for multiple, dynamic solvent interactions on exposed polypeptide chain regions within the supramolecular structure of the protein and thus the majority of structurally-disordered regions tend to lack a defined secondary structure (Cheng J. *et al.*, 2005; Kim R. and Guo J.T., 2010; Le Gall T. *et al.*, 2007; Liu J. *et al.*, 2002; Mohan A. *et al.*, 2006; Radivojac P. *et al.*, 2004; Radivojac P. *et al.*, 2007; Schlessinger A. *et al.*, 2009; Uversky V.N. and Dunker A.K., 2010; Uversky V.N. *et al.*, 2000; Vucetic S. *et al.*, 2003).

The bioinformatics software programs DisCon (Fig 2.10, p.265) and metaPrDOS (Fig 2.11, p.266) scan for these characteristic biophysical traits of ordered and disordered structure sequence motifs in conjunction with secondary structure propensity and relative solvent accessibility evaluations, via a combinatorial set of algorithms, to generate the intrinsic structural disorder prediction profile for the protein (Berman H.M. *et al.*, 2000; Chang D.T. *et al.*, 2008; Dor O. and Zhou Y., 2007; Hecker J. *et al.*, 2008; Ishida T. and Kinoshita K., 2007; Jones D.T. and Wards J.J., 2003; Kumar S. and Carugo O., 2008; Mizianty M.J. *et al.*, 2011; Oldfield C.J. *et al.*, 2005; Peng K. *et al.*, 2005; Su C.T. *et al.*, 2009; Wootton J.S. and Federhen S., 1993).

Fig 2.9: Models of Conserved and Adaptable Protein Conformers

[Taken and Adapted From: Dunker A.K. and Kriwacki R.W., 2011]



A: In the “conventional conserved configuration model” the protein is maintained in a single supramolecular conformation which possesses restricted specificity for one or a very limited number of ligands/substrates (L/S) and upon dissociation of the ligand/substrate (L/S) the protein is retained in its single supramolecular configuration.

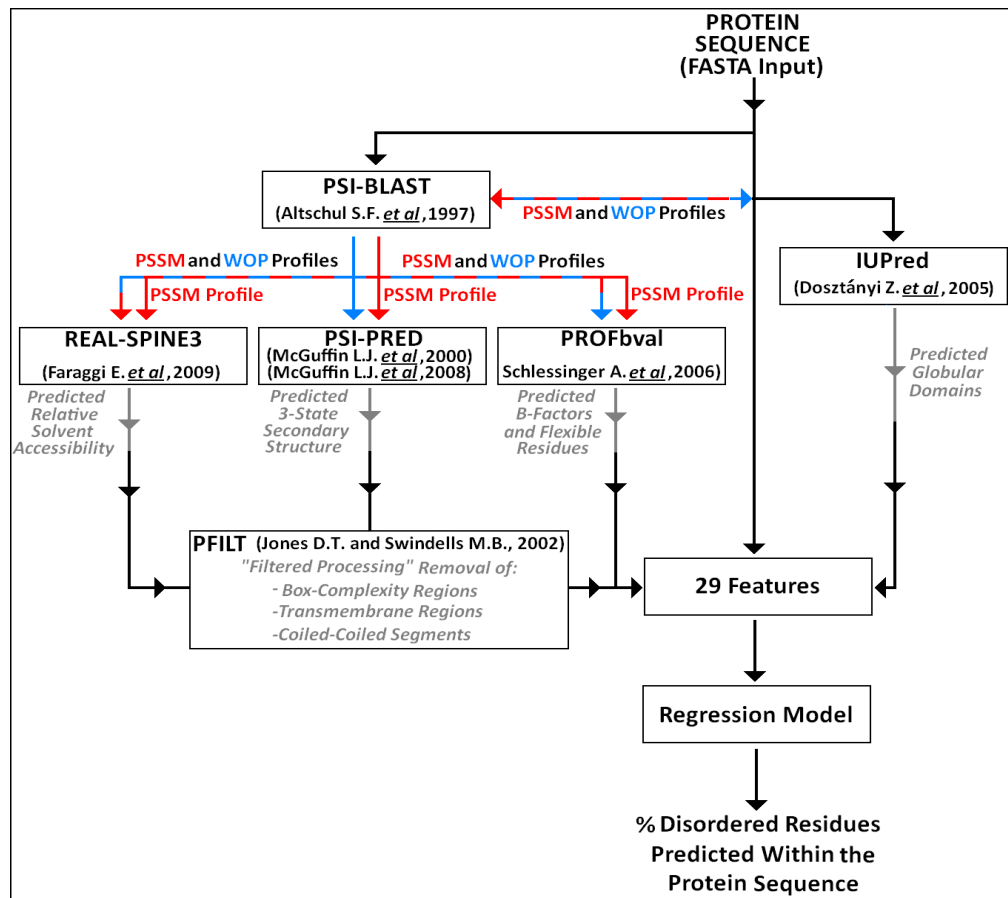
B: In recent times, classes of proteins have been discovered which have a “in-built” domains of intrinsically-disordered structure – as is the case for the Rad9 protein which has a highly flexible, structurally-disordered C-Terminal Tail Domain.

In the “unconventional intrinsic disordered structural adaptive model”, these proteins can adopt a versatile range of different binding supramolecular configurations (by virtue of their highly flexible, intrinsically-disordered domains) and thus possess “promiscuous specificity” for a wide variety of different ligands/substrates (L/S) and/or associative protein-protein interactions.

Upon dissociation of the ligand/substrate (L/S), the protein reverts to its native state of “in-built” intrinsically-disordered region-mediated supramolecular configurational flexibility/adaptability.

Fig 2.10: DisCon – Program Operational System Flow-Diagram

[Taken and Adapted From: Mizianty M.J. *et al*, 2011]



[DisCon Server – <http://biomine.ece.ualberta.ca/DisCon/>]

The DisCon bioinformatics software tool calculates the relative percentage proportionate number of amino acids residues identified as possessing significant probability of intrinsic disordered structural propensity within the total number of amino acids residue in the polypeptide chain sequence of the protein.

The software program utilises three key steps in the calculation process which determines the relative percentage of disordered amino acid residue content within the protein – notably;

1. Generation of a Position-Specific Scoring Matrix (PSSM) for the inputted amino acid sequence via the PSI-BLAST software program and Weighted Observed Percentage (WOP) profiles via the NCBI nr Data-Base – which are then processed via the PFILT software program for removal of anomalous sequence correlated to low-complexity regions, transmembrane-spanning regions and coiled-coiled segments.

Combinatorial processed data analyses of the amino acid sequence of the protein, acquired from the REAL-SPINE3, PSI-PRED and PROFbval software programs also constitute an integral for this PFILT-based “data filtering” process.

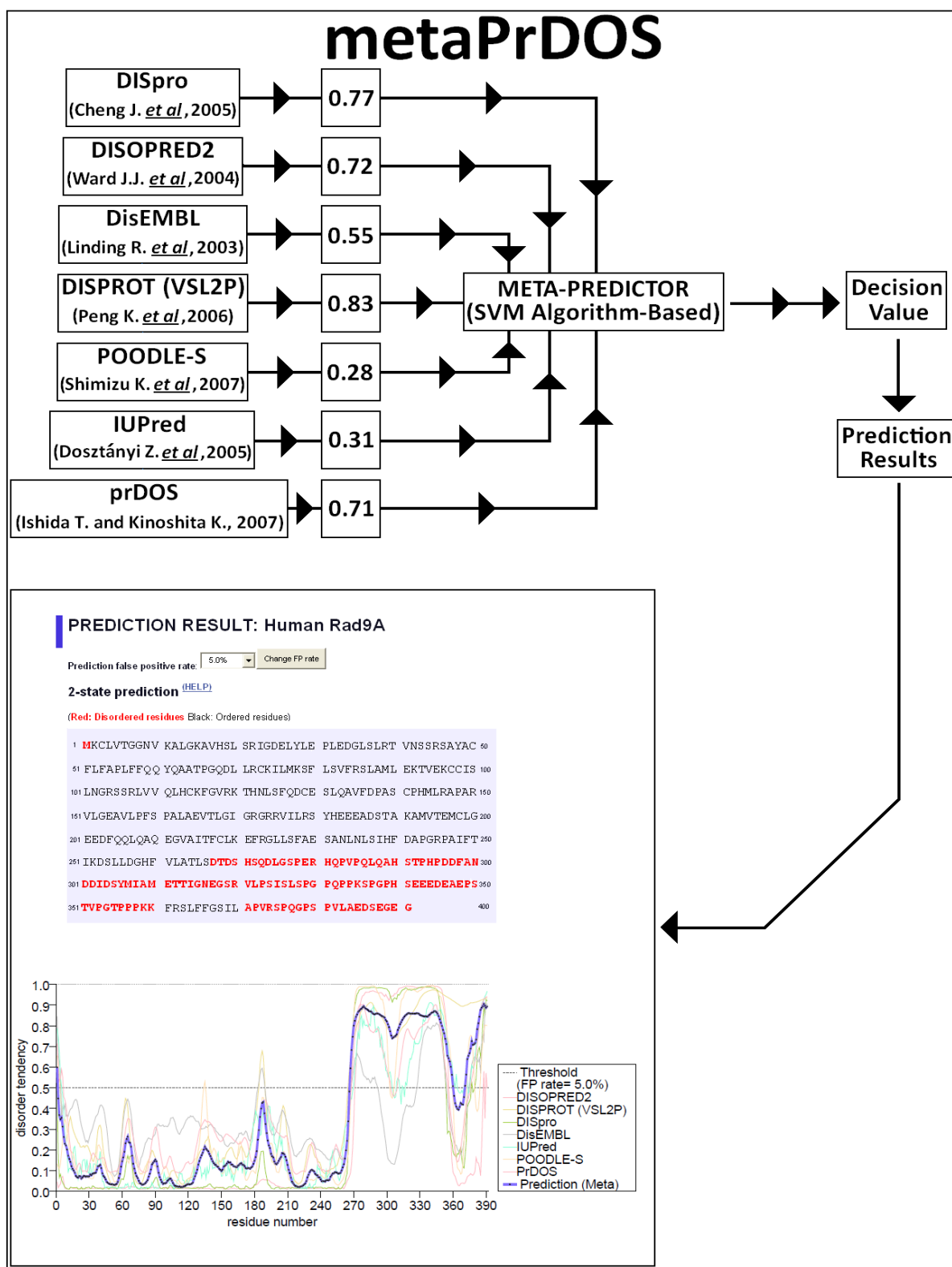
2. These derived combinatorial algorithm data predictions are then further processed, in conjunction with the IUPred (Intrinsic Unstructured Predictor) software program algorithm for the generation of a set of defined numerical-based descriptive features that quantify collectively the amino acid structural sequence information encoded in the prediction profiles generated in the initial stage (described above).

The feature selection algorithm, which incorporates components of the IUPred software program, is then utilised for the refined selection of 29 key features which are most relevant to the prediction of disorder amino acid residue content probability.

3. The selected numerical-based structural descriptors are then processed into a collective ridge regression algorithmic model system for generation of the predicted % disorder content value output.

Fig 2.11: metaPrDOS – Program Operational System Flow-Diagram

[Taken and Adapted From: Ishida T. and Kinoshita K., 2008]



[metaPrDOS – <http://prdoc.hgc.jp/cgi-bin/meta/top.cgi>]

The meta-PrDOS software program utilises a combination of algorithms derived from 7 Intrinsic Structural Disorder software program-based predictions, which are average probability-weighted and processed via the Meta-Prediction (via an SVM-based algorithm) for generation of the structural order and disorder amino acid residue profile of the inputted protein sequence – red residues above the probability value of 0.5 (ie the extrapolated Y-axis “Threshold FP rate = 5.0%” line on the graphical plot) are designated disordered.

2.10.6 RNA Secondary Structure Folding Predictions

The supramolecular secondary structure adopted by a particular RNA sequence is governed by several functional stability and thermodynamic-related constraints – notably; relative GC versus AU and GU base-pair content, the number of stem-configured base-pairs, the number of hairpin loop-configured base-pairs and the number of unpaired bases situated within interior loops and/or bulges (Nelson N. and Istrail S., 2012).

The GC base-pair contains three hydrogen bonds, whilst the AU and GC base-pair only contain two hydrogen bonds – thus more energy is required break a GC base-pair than an AU or GU base-pair and consequently, a higher GC base-pair content within a particular secondary structural RNA configuration enhances its stability (Nelson N. and Istrail S., 2012).

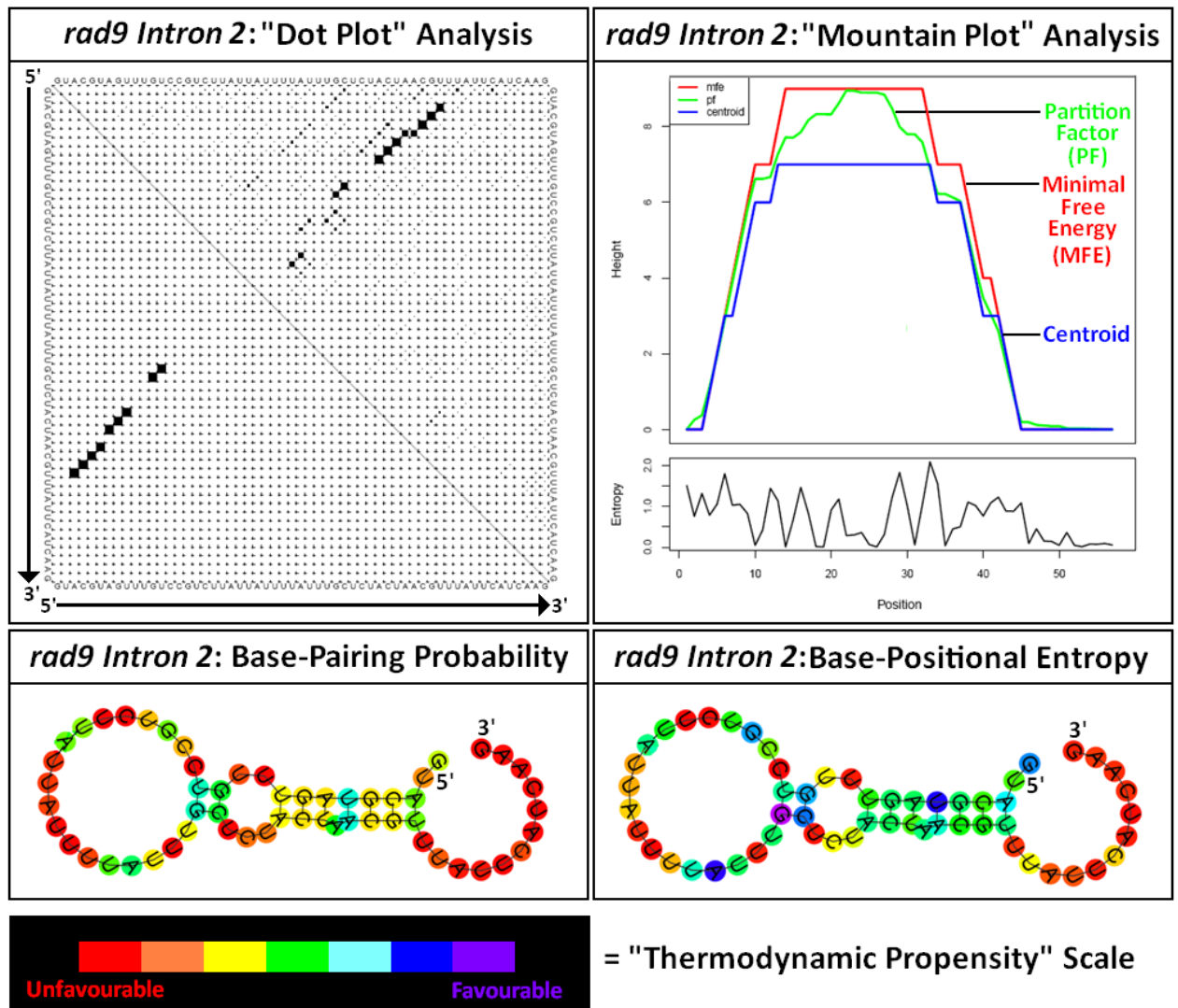
The thermodynamic stability of particular secondary structural RNA configuration is also directly related to stem-length – the longer the stem region, the more base-pairs it contains and thus the greater the energy required to denature or “melt” the stem region (Nelson N. and Istrail S., 2012).

Hairpin-loops which contain more than 10 base-pairs or less than 5 bases decrease the thermodynamic stability of the secondary structural RNA configuration as more energy is required for their formation to overcome steric constraints – thus less energy is required to denature or “melt” these loops (Nelson N. and Istrail S., 2012).

The thermodynamic stability of particular secondary structural RNA configuration is also directly related its unpaired base content – the larger the proportion of unpaired bases, the lower the number of base-pairs and the lower the stability (Nelson N. and Istrail S., 2012).

In silico bioinformatics-based predictive RNA-folded secondary structural configurational analyses of the the *S. pombe rad9* gene were performed via utilisation of the RNAfold software tool available on the Vienna RNA Secondary Structure Server site (Gruber A.R. *et al.*, 2008; Hofacker I.L., 2003) – an example of the data display is given in Fig 2.12, p.268.

Fig 2.12: Vienna RNAfold Analysis of *S. pombe rad9* Intron 2



[Vienna RNA Secondary Structure Folding Server – <http://rna.tbi.univie.ac.at/>]

The Dot-Plot analysis is a two-dimensional X-Y graphical display of the RNA sequence in which the most thermodynamically probable base-pairs are high-lighted.

The Mountain-Plot analysis is a graphical display of the Minimal Free Energy, Partition Factor and Centroid (Averaged Minimal Free Energy and Partition Factor Plots) of the positional base-pairs and their respective entropic formation propensity within the highest thermodynamically-favoured RNA secondary folded structural conformation.

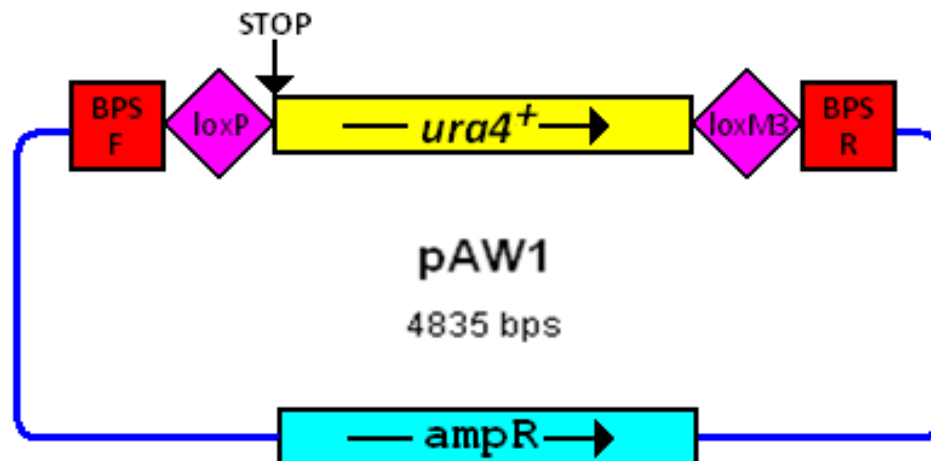
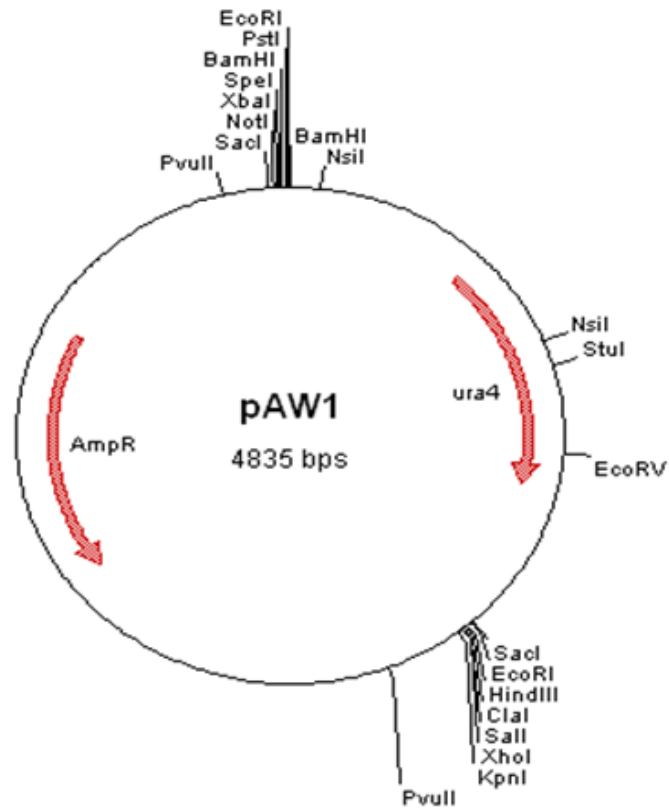
The Pairing Probability Display and Positional Entropy Display for each respective base-pair configuration within the predicted secondary RNA folded supramolecular structural conformation are colour-coded according to a "Thermodynamic Propensity" scale (as indicated above).

2.11 MATERIALS AND METHODS SUPPLEMENTARY APPENDICES

APPENDIX 2.11.1: pAW1 Cre-Lox Non-Essential Gene Replacement Plasmid Maps

Taken and Adapted From: <http://web.uni-frankfurt.de/fb15/mikro/euroscarf/data/P30537.html>

Watson A.T. *et al* (2008)



pAW1 Cre-Lox Non-Essential Gene Replacement Plasmid DNA Sequence Map

Collated Information Source: <http://web.uni-frankfurt.de/fb15/mikro/euroscarf/data/P30537.html>

```
1  cggatccccg ggtaattaa cataacttcg tatagcatac attatacga gttatagctt
61  agctacaaaat cccactggct atatgtatgc atttgtgtta aaaaagtttg tatagattat
121 ttaatctact cagcattcct tctctaaata ggaatttggt acttaatgga gaaaaaatg
181 tttcgattta cctagtgtat ttgtttgtat actcacgttt aatttcaaac atccattcta
241 tcttgtgtaa ttttggcat ggtgaaaaag ataatcagcc ttataatcct taaaaagta
301 agaaattctg taaataagcc ttaatgcct tgctttaa ataaatgggt ctttttcag
361 ataatgtttg cactttgtga atatatttta gatagttctg tgaggataa ttaagatgtt
421 ttagagactt atacaatttt gtctttataa attcttaatt gattttacca tcccagttta
481 actatgcttc gtcggcatct ctgcacatgt cgtgttttct taccgtattg tcctaccaag
541 aacctctttt ttgcttggtat cgaaattaaa gttttaaag caaagttatg gatgctagag
601 tatttcaaaag ctattcagct agagctgagg ggatgaaaaa tcccattgcc aaggaattgt
661 tggctttgat ggaagaaaag caaagcaact tgtcagtcgc ggtcgatttg acgaagaaat
721 ccgaaatcct agaattggtg gataaaattg gaccctatgt ctgtgttatc aagacacata
781 ttgacgttgt cgaggatttc gaccaggata tggtagaaaa actggtggcc ttaggtaaaa
841 agcatcgttt tcttatcctt gaggatcgca aattcgaga cattggaat accgtcaagc
901 tacaatatgc atctggtgtg tacaaaattg cttcttggc tcatatcaca aattgccata
961 cagtgccagg cgagggattt atacaaggcc tcaaagaagt tggttacct ttgggacgtg
1021 gtctcttgct tttggctgaa atgtcttcca aaggctctt ggctactggt tcctacacag
1081 agaaaacctt agaatggttt gagaagcata ccgatttttg ctttggctt atagctggtc
1141 gtogatttcc taacctcaa agcgactaca taactatgtc cctgggtatc ggcttggatg
1201 ttaaaggaga cgggctgga cagcaatata gtactcctga agaagtgatt gtaaactgcg
1261 gtagcgatat catcattgtt ggtcgtggag tctatggagc tggctgtaat cctgttgcg
1321 aagccaagag atatagagaa gctggttga aggcataca gcaaagactt tctcagcatt
1381 aaaaaagac taatgtaaaa ttttttgggt tggttattga aaaagtcgat gccttgtttg
1441 cgtttgtttt cctaggcgtt ttatgtcaga aggcathtag aattagtata caagtactct
1501 ttggtaaaat tttatgtagc gactaaaata ttaactatta tagataaaca ctttgggaat
1561 aaaaagtaat ttgctatagt aatttattaa acatgctcct acaacattac cacaatcttt
1621 tctcttggat tgacattgaa taagaaaaga gtgaattttt ttagacttgt aatgataact
1681 atgtacaaaag ccaatgaaag atgtatgtag atgaatgtaa aataccatgt agacaaacaa
1741 gataaaactt ggttataaac attggtgttg gaacagaata aattagatgt caaaaagttt
1801 cgtcaatc acaagctata acttcgtata tggattata tacgaagtta tgtttaaagc
1861 agcttgaatt catcatcaag cttatcgata ccgtcgacct cgagggggg cccgttacc
1921 agcttttgtt ccctttagtg aggttcaatt cgcgccttg cgatcattg gctatagctg
1981 tttcctgtgt gaaattgta tccgctcaca attccacaca acatacagc cgaagcata
2041 aagtgtaaag cctggggtgc ctaatgagtg agctaactca cattaattgc gttgcgctca
2101 ctgcccgtt tccagtcggg aaacctgtcg tgccagctgc attaatgaat cggccaacgc
2161 gcggggagag gcggtttgcg tattgggccc tcttccgct cctcgtcac tgactcgtg
2221 cgctcgtcgc ttcggctgcg gcgagcggta tcagctcact caaaggcgg aatacggta
2281 tccacagaat caggggataa cgcaggaaag aacatgtgag caaaaggcca gcaaaggcc
2341 aggaaccgta aaaaggcgcg gttgctggcg tttttccata ggctccgcc cctgacgag
2401 catcaaaaa atcgacgctc aagtcagagg tggcgaacc cgacaggact ataagatac
2461 caggcgttc cccctggaag ctccctcgtg cgtctcctg tccgacctt gccgttacc
2521 ggatacctgt ccgcctttct ccttcggga agcgtggcgc tttctcatag ctacgctgt
2581 aggtatctca gttcgggtgta ggtcgttcgc tcaagctgg gctgtgtgca cgaaccccc
2641 gttcagccc accgctgcgc cttatccggt aactatcgtc ttgagtccaa cccgtaaga
2701 cacgacttat cgccactggc agcagccact ggtaacagga ttagcagagc gaggtatgta
2761 ggcggtgcta cagagttctt gaagtgttg cctaactacg gctacactag aaggacagta
2821 tttggtatct gcgctctgct gaagccagtt accttcgaa aaagagttg tagctctga
2881 tcoggcaaac aaaccaccgc ttgtagcggg gtttttttg tttgcaagca gcagattacg
2941 cgcgaaaaa aaggatctca agaagatcct ttgatcttt ctacggggtc tgacgctcag
3001 tggaaacgaaa actcacgtta agggattttg gcatgagat tatcaaaaag gatcttacc
3061 tagatccttt taaattaaaa atgaagtttt aatcaatct aaagtatata tgagtaact
3121 tggcttgaca gttaccaatg cttaatcagt gaggcaccta tctcagcag ctgtctattt
3181 cgttcatcca tagttgcctg actccccgtc gtgtagataa ctacgatac ggagggctta
3241 ccatctggcc ccagtgtctc aatgataccg cgagaccac gctcaccggc tccagattta
3301 tcagcaataa accagccagc cggaggggcc gagcgcagaa gtggtcctgc aactttatcc
3361 gctccatcc agtctattaa ttgttgcggg gaagctagag taagtagttc gccagttat
3421 agtttgogca acgttgttgc cattgttaca ggcacgtgg tgtcacgctc gctgttgggt
3481 atggcttcat tcagctccgg tcccaacga tcaaggcgag ttacatgat ccccatgttg
```

```

3541 tgcaaaaaag cggtagctc cttcggctct ccgatcgttg tcagaagtaa gttggcgcga
3601 gtgttatcac tcatggttat ggcagcactg cataattctc ttactgtcat gccatccgta
3661 agatgctttt ctgtgactgg tgagtactca accaagtcat tctgagaata gtgatgcgg
3721 cgaccgagtt gctcttgccc ggcgtaata cgggataata ccgcgccaca tagcagaact
3781 ttaaaagtgc tcatcattgg aaaacgttct tcggggcgaa aactctcaag gatcttaccg
3841 ctgttgagat ccagttcgat gtaacccact cgtgcacca actgatcttc agcatctttt
3901 actttcacca gcgtttctgg gtgagcaaaa acaggaaggc aaaatgccgc aaaaaagga
3961 ataagggcga cacggaaatg ttgaatactc atactcttcc tttttcaata ttattgaagc
4021 atttatcagg gttattgtct catgagcgga tacatatttg aatgtattta gaaaaataaa
4081 caaatagggg ttccgcgcac atttccccga aaagtgccac ctgacgcgcc ctgtagcggc
4141 gcattaagcg cggcgggtgt ggtggttacg cgcagcgtga ccgctacact tgccagcgc
4201 ctagcgcgcc ctctttctgc tttcttccct tctttctcg ccacgttctc cggcttccc
4261 cgtcaagctc taaatcgggg gctcccttta gggttccgat ttagtgcttt acggcacctc
4321 gaccccaaaa aacttgatta gggtgatggg tcacgtagtg ggccatcgcc ctgatagacg
4381 gtttttctgc ctttgacggt ggagtccacg ttctttaata gtggactctt gttccaaact
4441 ggaacaacac tcaaccctat ctccgtctat tcttttgatt tataagggat tttgccgatt
4501 tgggcctatt ggttaaaaaa tgagctgatt taacaaaaat ttaacgcgaa ttttaacaaa
4561 atattaacgc ttacaatttc cattcgcctt tcaggctgcg cactgttggt gaagggcgat
4621 cggtgccggc ctcttcgcta ttacgccagc tggcgaagg gggatgtgct gcaaggggat
4681 taagttgggt aacgccaggg tttcccagc cagcagcttg taaaacgacg gccagtgagc
4741 gcgcgtaata cgactcacta tagggcgaat tggagctcca ccgcggtggc ggccgctcta
4801 gaactagtgg atccccggg ctgcaggaat tcgat

```

NNNNNNN = Forward Adaptive PCR Primer BPS Target Site [bp region: 1 – 21]

NNNNNNN = loxP [bp region: 22 – 55]

NNNNNNN = *S.pombe ura4+* gene promoter [bp region: 56 – 587]

NNNNNNN = *S. pombe ura4+* gene translation sequence [bp region: 588 – 1382]

NNNNNNN = *S.pombe ura4+* gene terminator sequence [bp region: 1383 – 1817]

NNNNNNN = loxM3 [bp region: 1818 – 1851]

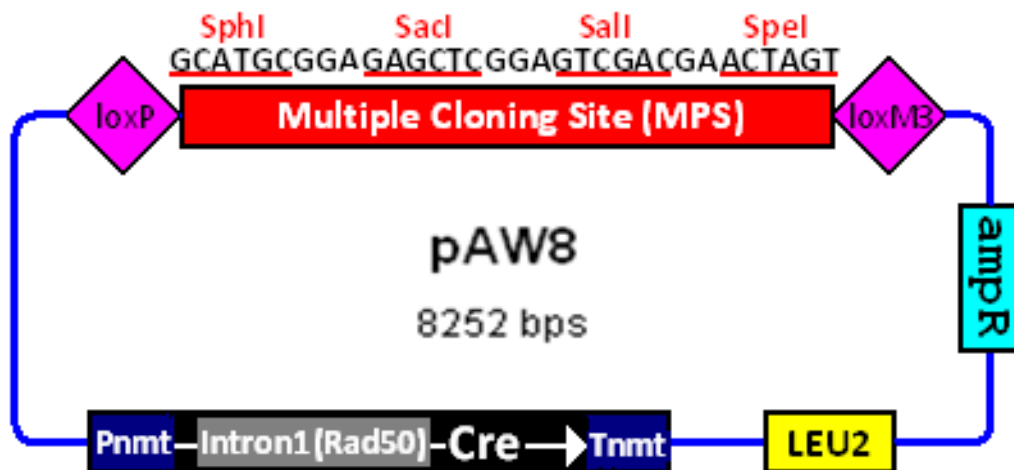
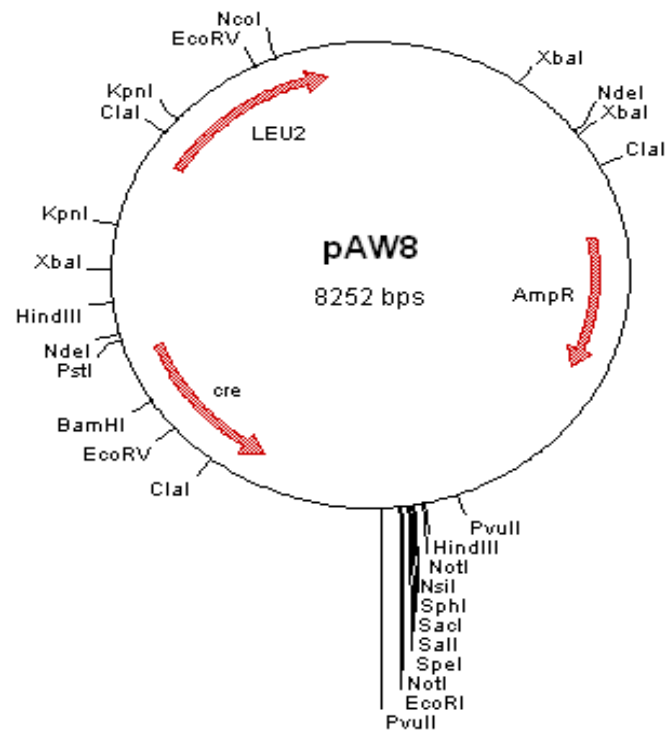
NNNNNNN = Reverse Adaptive PCR Primer BPS Target Site [bp region: 1852 – 1871]

NNNNNNN = pBluescript KS “Vector Backbone” [bp region: 1872 – 4835]
[incorporated ampR gene sequence]

APPENDIX 2.11.2: pAW8 Cre-Lox Donor Gene Exchange Plasmid Maps

Taken and Adapted From: <http://web.uni-frankfurt.de/fb15/mikro/euroscarf/data/P30545.html>

Watson A.T. *et al* (2008)



pAW8 Cre-Lox Donor Gene Exchange Plasmid DNA Sequence Map

Collated Information Source: <http://web.uni-frankfurt.de/fb15/mikro/euroscarf/data/P30545.html>

```
1 caaaaagtta ggtgtaacag aaaatcatga aactatgatt tctaatttat atattggagg
61 attttctcta aaaaaaaaaa tacaacaaat aaaaaaact caatgacctg accatttgat
121 ggagtttaag tcaatacctt cttgaacctt ttcccataat ggtgaaagtt ccctcaagaa
181 ttttactctg tcagaaacgg ccttaacgac gtagtctgatc cggacgatgg ccaaccttcc
241 aattcattaa atcgagtcct ccatcagatg atttacaagg ttttgcatag aatccctaag
301 taagagaagt tgtagtgat ttcttcaagt ttactaaaat ttacatacaa atggatgatc
361 tcttctccat tgtttctctt cttcttgcaa acgcgtttta caaagagatg acatgctatt
421 ttctgattat tttttctat agttttctat tttgtacgtc cttgggagtc cgaaatgtaa
481 aatcggggta tggtagtag cggcagcgtt cattatggta tataaaagat aaaaagtagg
541 ggcaagcgag acagaatggg atacaagggc atcgtctata attatagcta aaaattgfat
601 ttttaattgt attttttcta attttatttc tcattgtttt acttaaaatg aaatgcgaatt
661 agagaaaact tcaacgaaat gtcaaaaataa gctcagcaaa atatacaatt ttagggaaag
721 cgatcagcaa cttattctcc ggtgtagatt ctttttcttc ataaattcca acaatgtaac
781 tgccaattga tttttctcta gatgctaata aattgaaact aatgaatata ataacacagg
841 ttttgataaa ttgtaaactc ttactcaaaa aaagaatggt aaaactaatt taaccttttt
901 ataaaggctc atggcgtaa agaggatagt aaaaattcta caatttttta atttaatgct
961 acaattgtct tgcgaatata attotattaa ttttcgctaa ctgctgtttt agtactatta
1021 ctttcaatat gccttatatg caactttaat tcatgaagaa tgcaatattt ttgcaatctt
1081 tcttgactg agcgtttttt atcatttagt actcattatt taatttttca gtaaagggca
1141 ataaataaat ttgtagaaga tgcaatgtaa tctcctctat ccttttgctc atatgtttat
1201 gagtatacct agtctagaaa ggcttgatt taaaatatta ttcaataaaa attcacaatt
1261 tttacgacat gtgctacatc tcaacttaact tcttgattat aaaattgggt cgtttatact
1321 aattacttaa gtacctttaa ctaaacaana tgccatata tatattaatt tacaatgagt
1381 gtcagataag tcactatgtc cgagtggtta aggagttaga ctcgccatcg atgggatggg
1441 gcaactctcag tacaatctgc tctgatgccg catagttaag ccagccccga caccgcgcaa
1501 caccogctga cgcgcctga cgggcttgct tgctcccggc atccgcttac agacaagctg
1561 tgacogtctc cgggagctgc atgtgtcaga ggttttcacc gtcacaccg aacgcgcga
1621 gacgaaggg cctcgtgata cgcctatttt tataggtaa tgctatgata ataatggttt
1681 cttagacgct aggtggcaact tttcggggaa atgtgcgcyg aaccctattt tgtttttttt
1741 tctaaataca ttcaaatatg tatccgctca tgagacaata accctgataa atgcttcaat
1801 aatattgaaa aaggaagagt atgagtattc aacatttccg tgtcgcctt attccctttt
1861 ttgcggcatt ttgccttctt gtttttgcct acccagaaac gctggtgaaa gtaaaagatg
1921 ctgaagatca gttgggtgca cgagtgggtt acatcgaact ggatctcaac agcggtaaga
1981 tcttgagag ttttcgcccc gaagaacggt ttccaatgat gagcactttt aaagttctgc
2041 tatgtggcgc ggtattatcc cgtattgacg ccgggcaaga gcaactcggg cgcgcatac
2101 actattctca gaatgacttg gttgagtact caccagtcac agaaaagcat cttacggatg
2161 gcatgacagt aagagaatta tgcagtgtct ccataacct gagtgataac actgcccga
2221 acttacttct gacaacgacg ggaggaccga aggagctaac cgcttttttg cacaacatgg
2281 gggatcatgt aactcgcctt gatcgttggg aaccggagct gaatgaagcc ataccaaacg
2341 acgagcgtga caccacgatg cctgtagcaa tggcaacaac gttgcgcaa ctattaactg
2401 gcgaactact tactctagct tcccggcaac aattaataga ctggatggag gcggataaag
2461 ttgcaggacc acttctgcgc tcggcccttc cggctggctg gtttattgct gataaatctg
2521 gagccggatga gcgtgggtct cgcggtatca ttgcagcact gggccagat ggtaagcctc
2581 ccogtatcgt agttatctac acgacgggga gtcaggccac tatggatgaa cgaaatagac
2641 agatcgtctga gataggtgcc tcaactgata agcattggta actgtcagac caagtttact
2701 catatatact ttagattgat ttaaaaactt atttttaatt taaaaggatc taggtgaaga
2761 tcttttttga taatctcatg accaaaatcc cttaacgtga gttttcgttc cactgagcgt
2821 cagacccggt agaaaagatc aaaggatctt cttgagatcc ttttttctg cgcgtaactt
2881 gctgcttgca acaaaaaaaa ccaccgctac cagcggtggt ttgtttgccg gatcaagagc
2941 taccaactct ttttccgaag gtaactggct tcagcagagc gcagatacca aatactgttc
3001 ttctagtgtg gccgtagtta ggccaccact tcaagaacte tgtagcaccg cctacatacc
3061 togtctctgt aatcctgtta ccagtggctg ctgccagtgg cgataagtcg tgtcttaccg
3121 ggttggactc aagacgatag ttaccggata aggcgcagcg gtcgggctga acggggggtt
3181 cgtgcacaca gccagcttg gagcgaacga cctacaccga actgagatac ctacagcgtg
3241 agctatgaga aagcgcacg cttcccgaag ggagaaaggc ggacaggtat ccggtaaagc
3301 gcagggctgg aacaggagag cgcacgaggg agcttccagg gggaaacgcc tggtatcttt
3361 atagtctctg cgggtttctc cacctctgac ttgagcgtcg atttttgtga tgcctcgtcg
3421 gggggcggag cctatggaaa aacgccagca acgcggcctt tttacggttc ctggcctttt
3481 gctggccttt tgctcacatg ttctttctct cgttatcccc tgattctgtg gataaccgta
```

3541	ttacogcett	tgagtgagct	gataccgctc	gccgcagccg	aacgaccgag	cgcagcgagt
3601	cagtgagcga	ggaagcggaa	gagcgcccaa	tacgcaaacc	gcctctcccc	gcgcggtggc
3661	cgattcatta	atgcagctgg	cacgacaggt	ttcccgactg	gaaagcgggc	agtgagcgca
3721	acgcaattaa	tgtgagttag	ctcactcatt	aggcacccca	ggctttacac	tttatgcttc
3781	cggtctgfat	gttgtgtgga	attgtgagcg	gataacaatt	tcacacagga	aacagctatg
3841	accatgatta	cgccaagctt	gcatggcggc	cgcataactt	cgtatagcat	acattatagc
3901	aagttatgca	tgccggagagc	tccggagtcca	cgaactagta	taacttcgta	tatgggtatta
3961	tatacgaagt	tatgcccggc	cgcgaattca	ctggcccgtc	ttttacaacg	tcgtgactgg
4021	gaaaaccctg	gcgttaccca	acttaatcgc	cttgccagcac	atcccccttt	cgccagctgg
4081	cgtaatagcg	aagaggcccg	caccgatcgc	ccttcccac	agttgcgcag	cctgaatggc
4141	gaatggcgcc	tgatgcccga	ttttctcctt	acgcatctgt	gcggtatttc	acaccgcata
4201	ccatcgtccg	gatcaatgaa	gtagatgagt	ttactacctg	tatatacttt	tttttttgtc
4261	aaagtcactt	ttatggcatt	tccatggtga	aggattagcc	acagcactaa	attttcagcg
4321	tatgattgct	tttaaatatt	taattttcat	cgttttttaa	ttaatattca	aaacgattta
4381	atgccttcta	catctgaagt	caagctcata	gactcgggtt	gggtagctaa	aactacatct
4441	aacacgaagg	ggtatagcct	tcttaaaagta	tactcatgta	taaacgtttt	gggttcataat
4501	ttttgggcca	cgtggtttat	aaaaattcct	aactacacca	ctcggtatcc	cgcaccgctc
4561	taogtttcta	cgatttcgag	ctaataattga	gtaaagtgat	tagcaaaaaa	aataaaagta
4621	ctogttgtcg	gagatcaaga	atttttctat	tatctcatct	aaaccacttt	ctaaaagcga
4681	aaaacaaaat	cgtaatatgc	agcttgaatg	ggcttccata	gtttgaaaga	aaacccttag
4741	cagtaactggc	aagggagaca	ttccttttac	ctggcctaate	gccatcttcc	agcaggcgca
4801	ccattgcccc	tgtttcaacta	tccaggttac	ggataatagtt	catgacaata	tttacattgg
4861	tccagccacc	agcttgcatg	atctccggta	ttgaaactcc	agcgcggggc	atatctcgcg
4921	cggtctccgac	acgggcactg	tgtccagacc	aggccaggta	tctctgacca	gagtcacctt
4981	tagcgcgcta	aatcaatcga	tgagttgctt	caaaaaatccc	ttccagggcg	cgagttgata
5041	gctggctggg	ggcagatggc	gcccgaacac	cattttttct	gaccgggcaa	aacaggtagt
5101	tattoggatc	atcagctaca	ccagagacgg	aaatccatcg	ctcgcagcag	ttagttacc
5161	ccaggctaag	tgctttctct	acacctgcgg	tgctaaccag	cgttttcggt	ctgccaatat
5221	ggattaacat	tctcccaccg	tcagtaactg	agatatcttt	aacctgatc	ctggcaattt
5281	cggtctatacg	taacagggtg	ttataagcaa	tccccagaaa	tgccagatta	cgtatactct
5341	ggcagcgatc	gctattttcc	atgagtgaac	gaacctggtc	gaaatcagtg	cgttcgaacg
5401	ctagagcctg	ttttgcacgt	tcaccggcat	caacgttttc	ttttcggatc	cgccgcataa
5461	ccagtgaaac	agcattgctg	tcacttggtc	gtggcagccc	ggaccgacga	tgaagcatgt
5521	ttagctggcc	caaatggtgc	tggatagttt	ttactgccag	accgcgcgcc	tgaagatata
5581	gaagataatc	gogaacatct	tcaggttctg	cgggaaacca	tttccgggta	ttcaacttgc
5641	accatgcgc	ccacgaccgg	caaacggaca	gaagcatttt	ccaggtatgc	tcagaaaacg
5701	cctggcgatc	cctgaacatg	tccatcaggt	tcttgccaac	ctcatcactc	gttgcatcga
5761	ccggtaactt	ttagattaac	atttgtttaa	atatgaaatt	aggcaatgta	acatactgca
5821	ggcaaatttt	ggtgtacggt	aagtaaattg	gacatatgat	ttaacaaagc	gactataagt
5881	cagaaagtga	gaatgagatt	gaaataatta	attcaactta	ttcaattgat	gatatgccag
5941	gattcctctt	cctttatctt	caatgtttcg	attaacaggt	ccattatccg	gttttttagtt
6001	tcgctgcaca	ttgccgaatg	acaatcggat	tcctttaagc	tttgcttttg	ccctgttttc
6061	tctcccagc	aatcgttggg	tgactgaacc	atccagtagc	cgagagttac	gtttttcctg
6121	atttaataaa	tatccataatc	tattgtctc	gtggtgtttt	acagaaacta	accgaaatta
6181	ctattttgca	tcattccaacc	ataaagagac	aacaataatt	ctagaaaaca	tataacaagt
6241	gtttttttct	atttacgtct	catacgcaaa	gtccacttta	ccatgttttg	gaaacttgta
6301	cccaaccatt	catttttoga	ttttgtaatg	aggctctttt	cttctaacaa	tcattgaggt
6361	cattatcatg	tgtcctcacc	tattgtttaa	attgaggett	gcgctattcc	caaaattgtg
6421	ggtattattt	tcataataca	gtatctgcaa	tttcggttca	actccggaag	ctcggtagcc
6481	aaactgtggga	atactcaggt	atcgtaaagt	gcaagagttc	gaatctctta	gcaaccatta
6541	ttttttttct	ctcaacataa	cgagaacaca	caggggcgct	atcgcacaga	atcaaattcg
6601	atgactggaa	attttttggt	aatttcagag	gtcgcctgac	gcataacct	ttttcaactg
6661	aaaaattggg	agaaaaagga	aaggtgagag	cgccggaacc	ggcttttcat	atagaataga
6721	gaagcgttca	tgactaaatg	cttgcacac	aatacttgaa	gttgacaata	ttatttaagg
6781	acctattggt	ttttccaata	ggtggttagc	aatcgtctta	ctttctaact	tttcttacct
6841	tttacatttc	agcaatatat	atatatatat	atatatatat	ttcaaggata	taccattgta
6901	atgtctgccc	ctaagaagat	cgctgttttg	ccaggtgacc	acgttggtca	agaaatcaca
6961	gccaagcca	ttaaggttct	taaagctatt	tctgatgttc	gttccaatgt	caagttcgat
7021	ttcgaaaatc	attttaattg	tggtgctgct	atcogatgcta	caggtgttcc	acttccagat
7081	gagggcgtgg	aagcctccaa	gaaggctgat	gccgttttgt	taggtgctgt	gggtggctct
7141	aaatggggta	cggtagtgt	tagacctgaa	caaggtttac	taaaaatccg	taaagaactt
7201	caattgtacg	ccaacttaag	accatgtaac	tttgcatccg	actctctttt	agacttatct
7261	ccaatcaagc	cacaatttgc	taaaggtaact	gacttcggtg	ttgttagaga	attagtgga
7321	ggtatttact	ttggtaagag	aaaggaagac	gatgggtgatg	gtgtcgcctg	ggatagtgaa

7381 caatacaccg ttccagaagt gcaaagaatc acaagaatgg ccgctttcat ggcctacaa
 7441 catgagccac cattgcctat ttggtccttg gataaagcta atgttttggc ctcttcaaga
 7501 ttatggagaa aaactgtgga ggaaaccatc aagaacgaat ttcctacatt gaaagttcaa
 7561 catcaattga ttgattctgc cgccatgatc ctagttaaga acccaaccca cctaaatggt
 7621 attataatca ccagcaacat gtttggtgat atcatctccg atgaagcctc cgttatccca
 7681 ggctccttgg gtttggtgcc atctgcgtcc ttggcctctt tgccagacaa gaacaccgca
 7741 tttggtttgt acgaaccatg ccatggttcc gctccagatt tgccaaagaa taaggtaaac
 7801 cctatogcca ctatcttgtc tgctgcaatg atgttgaaat tgtcattgaa cttgcctgaa
 7861 gaaggtaaag ccattgaaga tgcagttaaa aaggttttgg atgcaggtat cagaactggt
 7921 gatttaggtg gttccaacag taccaccgaa gtcggtgatg ctgtcgccga agaagttaag
 7981 aaaatccttg cttaaaaga ttctcttttt ttgtgatatt tgtacataaa ctttataaat
 8041 gaaattcata atagaaacga cacgaaatta caaaatggaa tatgttcata gggtagacga
 8101 aactatatac gcaatctaca tacatztatc aagaaggaga aaaaggagga tgtaaaggaa
 8161 tacaggtaag caaattgata ctaatggctc aacgtgataa ggaaaaagaa ttgcacttta
 8221 acattaatat tgacaaggag gagggcatca ca

NNNNNNN = *S.pombe* ars1 Replication Origin [bp region: 231 – 1424]

NNNNNNN = pUC19 “Vector Backbone” [bp region: 1425 – 3860]
 [Incorporated ampR gene sequence]

NNNNNNN = loxP [bp region: 3874 – 3907]

NNNNNNN = Multiple Cloning Site {SphI-SacI-SalI-SpeI} [bp region: 3908 – 3939]

NNNNNNN = loxM3 [bp region: 3940 – 3972]

NNNNNNN = nmt1 Terminator [bp region: 4213 – 4769]

NNNNNNN = Cre bacteriophage P1 recombinase [bp regions: 4775 – 5767; 5817 – 5855]

NNNNNNN = *S.pombe rad50* Intron 1 [bp region: 5768 – 5816]

NNNNNNN = nmt41 Promoter [bp region: 5856 – 6462]

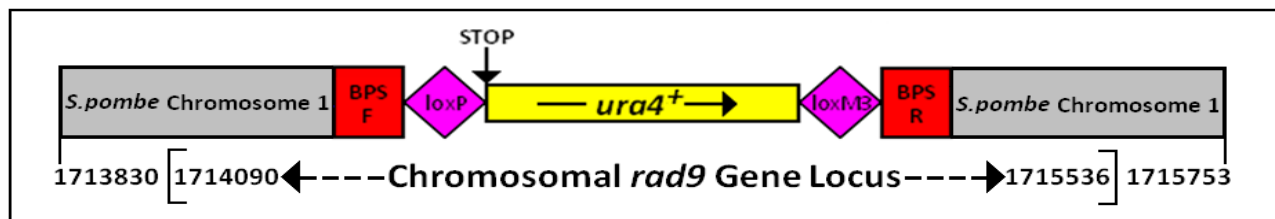
NNNNNNN = *S. cerevisiae LEU2* [bp region: 6481 – 7995]

NNNNNNN = *S. cerevisiae LEU2* Terminator [bp region: 7996 – 8252]

APPENDIX 2.11.3: PCR Primers – Sequence and Function

PRIMER	BASE SEQUENCE	ORIENTATION	FUNCTION
Rad9-S1	5'-CGATTGATGTTGGCCATTACACTTTCGTACAAATTCGGCGCGCGTGTCTA TACTAATATAAGTGCCTTAAAGCAGGTGCCGGATCCCGGGTTAATTAA-3'	5' → Forward → 3'	pAW1 Plasmid <i>rad9</i> gene locus-specific targeting
Rad9-S2	5'-GAATTTAATTAATGGGTTACATTATCACTATCTTATTGATTTATTAGAAC TACTATGTAACGTATCGTATGATGAGGGGAATTCGAGCTCGTTTAAAC-3'	3' ← Reverse ← 5'	-- <i>rad9::loxP-ura4⁺loxM3</i> -- Integration
Rad9-5	5'-CTTCTAGGTCAGGATTTAGCGCTGTGACTTTAAAAAAGGC-3'	5' → Forward → 3'	Cre-Lox "Base-Strain" <i>Δrad9</i> PCR Genotyping Verification of <i>rad9</i> Locus Integration
Rad9-9	5'-GCATCGTTTGTGGTTGATGGCTCC-3'	3' ← Reverse ← 5'	
Rad9-10	5'-GCTTGTGCGTGTGGATAAGCTTC-3'	5' → Forward → 3'	
Ura4-1	5'-GCTAGAGCTGAGGGGATG-3'	5' → Forward → 3'	<i>Δrad9</i> "Base-Strain" PCR Genotyping <i>ura4⁺</i> gene detection
Ura4-4	5'-GCTGGTTGGAAGGCATATCAGC-3'	3' ← Reverse ← 5'	
Rad9-S5	5'-CGATAGTGGCATGCTAGAAAACACCACATTATAGATTACC-3'	5' → Forward → 3'	Fusion PCR Construction of <i>sph-rad9-spel Rad9-S5 & Rad9-S6</i> <i>sph-rad9-c3xHA-spel Rad9-S5 & Rad9-S8</i>
Rad9-S6	5'-CTCGTCCAAC TAGTAACTGATCGTATGATGAGGG-3'	3' ← Reverse ← 5'	
Rad9-S8	5'-GCTATCACACTAGTCAGATCTATATTACCTGTTATCCC-3'	3' ← Reverse ← 5'	Rad9-S5 & Rad9-S8 Fusion PCR Fragments Rad9-S5 & Rad9-S8 <i>rad9</i> Amplifications
Rad9-S9	5'-GAAGAATTTAAACATGTAATCTCTATCTGATTTTTGTTAATTTCCAGTTG-3'	3' ← Reverse ← 5'	Fusion PCR Construction of <i>sph-ND1intron1-rad9-c3xHA-spel</i>
Rad9-S10	5'-CAACTGGGAAATTAACAAAATCAGATAGAGATTACATGTTTAAATTCCTC-3'	5' → Forward → 3'	Cre-Lox pAW8 Plasmid Ligation Insert
Rad9-M50L-F	5'-AGGTCAGGATTTAGCCTGGTGACTTTAAAAAAGGC-3'	5' → (F)orward → 3'	Fusion PCR Construction of <i>sph-rad9-(M50L)-c3xHA-spel</i>
Rad9-M50L-R	5'-GCCTTTTTTAAAGTCAACAGGCTAAATCTGACCT-3'	3' ← (R)everse ← 5'	Cre-Lox pAW8 Plasmid Ligation Insert
Rad9-S11	5'-GCCTTTTTTAAAGTCAACATTTTATATACCAGTACGTGAATTG-3'	3' ← Reverse ← 5'	Fusion PCR Construction of <i>sph-ND49-rad9-c3xHA-spel</i>
Rad9-S12	5'-CAATTCACGTA CTGGTATATAAAATGGTGACTTTAAAAAAGGC-3'	5' → Forward → 3'	Cre-Lox pAW8 Plasmid Ligation Insert
Rad9-M74-F	5'-CAATTCACGTA CTGGTATATAAAATGACTCTACAATACG-3'	5' → (F)orward → 3'	Fusion PCR Construction of <i>sph-ND73-rad9-c3xHA-spel</i>
Rad9-M74-R	5'-CGTATTGTAGGATCATT TATATACCAGTACGTGAATTG-3'	3' ← (R)everse ← 5'	Cre-Lox pAW8 Plasmid Ligation Insert
Rad9-M312-F	5'-CAATTCACGTA CTGGTATATAAAATGGGAAATAGATGGCAGC-3'	5' → (F)orward → 3'	Fusion PCR Construction of <i>sph-ND311-rad9-c3xHA-spel</i>
Rad9-M312-R	5'-GCTGCCATCTATTTCCATTTTATATACCAGTACGTGAATTG-3'	3' ← (R)everse ← 5'	Cre-Lox pAW8 Plasmid Ligation Insert
Rad9-M358-F	5'-CAATTCACGTA CTGGTATATAAAATGTTAATCTGCGCTTGACCG-3'	5' → (F)orward → 3'	Fusion PCR Construction of <i>sph-ND357-rad9-c3xHA-spel</i>
Rad9-M358-R	5'-CGGTCAGCGCAGAAATTAACATTTTATATACCAGTACGTGAATTG-3'	3' ← (R)everse ← 5'	Cre-Lox pAW8 Plasmid Ligation Insert
Rad9-T3A-F	5'-CAATTCACGTA CTGGTATATAAAATGGTGGCTTTAAAAAAGGC-3'	5' → (F)orward → 3'	Fusion PCR Construction of <i>sph-ND49-rad9-(T52A)-c3xHA-spel</i>
Rad9-T3A-R	5'-GCCTTTTTTAAAGCCACCATTTTATATACCAGTACGTGAATTG-3'	3' ← (R)everse ← 5'	Cre-Lox pAW8 Plasmid Ligation Insert
Rad9-Y61F-F	5'-GACAAGTTCATTTTCAGCCGGATCCGTC-3'	5' → (F)orward → 3'	Fusion PCR Construction of <i>sph-ND49-rad9-(Y61F)-c3xHA-spel</i>
Rad9-Y61F-R	5'-GGACGGAATCCGGCTGAAAAATGAACTTGTC-3'	3' ← (R)everse ← 5'	<i>sph-ND49-rad9-(T52A;Y61F)-c3xHA-spel</i> Cre-Lox pAW8 Plasmid Ligation Inserts
Rad9-Y111F-F	5'-AGCAAGAACGGTTTTGGCAGTGAATCTGCAAG-3'	5' → (F)orward → 3'	Fusion PCR Construction of <i>sph-ND49-rad9-(Y111F)-c3xHA-spel</i>
Rad9-Y111F-R	5'-CTTGCAAGTCACTGCCAAAACCGTTCTTGCT-3'	3' ← (R)everse ← 5'	Cre-Lox pAW8 Plasmid Ligation Insert
Rad9-L196P-F	5'-GGTCAGAGAACGGAAGAGCCTACAATCAACCACTTCAAG-3'	5' → (F)orward → 3'	Fusion PCR Construction of <i>sph-rad9-(L196P)-c3xHA-spel</i>
Rad9-L196P-R	5'-CTTGAAGTGGTTGAATTGTGGACTCTCCGTTCTGACC-3'	3' ← (R)everse ← 5'	<i>sph-rad9-M50L-(L196P)-c3xHA-spel</i> <i>sph-ND49-rad9-(L196P)-c3xHA-spel</i> Cre-Lox pAW8 Plasmid Ligation Inserts
Rad9-T225A-F	5'-GAAGCAACCTGCCAAACAACCTGTTCCATTGATGG-3'	5' → (F)orward → 3'	Fusion PCR Construction of <i>sph-rad9-c3xHA-spel</i> <i>sph-rad9-M50L-c3xHA-spel</i> <i>sph-ND49-rad9-c3xHA-spel</i>
Rad9-T225A-R	5'-CCATCAATGGAAACAGTTGTTGGCAGGTTGCTC-3'	3' ← (R)everse ← 5'	
Rad9-T225E-F	5'-GAAGCAACCTGAAACAAACAACCTGTTCCATTGATGG-3'	5' → (F)orward → 3'	T225A T225E T412A T412E S423A S423E
Rad9-T225E-R	5'-CCATCAATGGAAACAGTTGTTGTTCAAGTTGCTC-3'	3' ← (R)everse ← 5'	
Rad9-T412E-F	5'-GCCGAATTTGGACCAGAGCAAGCTGAACAA-3'	5' → (F)orward → 3'	T412A;S423A T225A;T412A;S423A
Rad9-T412E-R	5'-TTGTTCACTGCTCTGGTCCAAATTCGGC-3'	3' ← (R)everse ← 5'	
Rad9-S423E-F	5'-AGTTATCATGGCATTTCGAACAGGAAGAC-3'	5' → (F)orward → 3'	<i>rad9</i> gene Point Mutant Cre-Lox pAW8 Donor Plasmid Ligation Inserts
Rad9-S423E-R	5'-GTCTTCCTGTTGAAAATGCCATGATAACT-3'	3' ← (R)everse ← 5'	
Rad9-S13	5'-ATTAATCGTCATATCGACTAG-3'	5' → → → 3'	DNA Sequence Verification of "Cre-Lox Engineered" "Wild-Type" and modified <i>rad9</i> gene <i>S. pombe</i> Strains
Rad9-S14	5'-GACGGGATTGATGACTCC-3'	5' → → → 3'	
Rad9-S15	5'-CATATGAACAAACCAAAC-3'	5' → → → 3'	Progressive PCR 5' → → 3' <i>rad9</i> "gene-walking"
Rad9-S16	5'-GTGTCCAGGAAACCG-3'	5' → → → 3'	
Rad9-S17	5'-GGAGCCATCAACCAAAAC-3'	5' → → → 3'	Fluorescent-Tag ddNTP Terminator Sequencing

APPENDIX 2.11.4: pAW1 Plasmid PCR Fragment-Integrated *rad9* Gene Locus Map



```

CGATTGATGT TGGCCATTAC ACTTTCGTAC AAATTTTCGGC GCGCGTGTCT ATACTAATAT
AAGTGCGTTA AAGCAGGTGC CGGATCCCCG GGTAAATTAA CGGATCCCCG GGTAAATTAA
cataacttcg tatagcatac attatagcaa gttatagcct agctacaaat cccactggct
atatgtatgc atttgtgta aaaaagtttg tatagattat ttaatctact cagcattcct
tctctaaata ggaatttggt acttaatgga gaaaaaaatg tttcgattta cctagtgtat
ttgtttgat actcacgttt aatttcaaac atccattcta tcttgtgtaa tttttggcat
ggtgaaaaag ataatcagcc ttataatcct tacaaaagta agaaattctg taataagcc
ttaatgcct tgctttaaat taaaatggtt ctttttcag ataatgtttg cactttgtga
atatatttta gatagttctg tgaggtataa ttaagatggt ttagagactt atacaatttt
gtctttataa attcttaatt gattttacca tcccagttta actatgcttc gtcggcatct
ctgcacatgt cgtgttttct taccgtattg toctaccaag aacctctttt ttgcttggat
cgaaattaaa ggtttaaaag caaagttag gatgctagag tatttcaaag ctattcagct
agagctgagg ggatgaaaa tcccattgcc aaggaattgt tggctttgat ggaagaaaag
caaagcaact tgtcagtcgc ggtcagtttg acgaagaaat ccgaaatctt agaattggta
gataaaattg gaccctatgt ctgtgttate aagacacata ttgacgttg cgaggatttc
gaccaggata tggtagaaa actggtggcc ttaggtaaaa agcatcgttt tcttatcttt
gaggatcgca aattcgcaga cattggaat accgtcaagc tacaatatgc atctgggtgtg
tacaaaattg cttcttgggc tcatatcaca aattgccata cagtgccagg cgagggtatt
atacaaggcc tcaaagaagt tggtttacct ttgggacgtg gtctcttgc tttggctgaa
atgtctcca aaggctcttt ggctactggt toctacacag agaaaacctt agaatggttt
gagaagcata ccgatttttg ctttggcttt atagctggtc gtcgatttcc taaccttcaa
agcgactaca taaactatgtc coctggtatc ggcttggatg ttaaaggaga cgggctggga
cagcaatata gtactcctga agaagtgatt gtaaactgcg gtagegatat catcattgtt
ggtcgtggag tctatggagc tggtcgtaat cctgttgcg aagccaagag atatagagaa
gctggttga aggcatatca gcaaagactt tctcagcatt aaaaaagac taatgtaaaa
tttttttgg tggttattga aaaagtcgat gccttgtttg cgtttgtttt cctaggcgtt
ttatgtcaga aggcatttag aattagata caagtactct ttggtaaaat tttatgtagc
gactaaaata ttaactatta tagataaaca ccttgggaat aaaaagtaat ttgctatagt
aatttattaa acatgctcct acaacattac cacaatcttt tctcttggat tgacattgaa
taagaaaaga gtgaattttt ttagacttgt aatgataact atgtacaaag ccaatgaaag
atgtatgtag atgaatgtaa aataccatgt agacaaaca gataaaactt gttataaac
attggtgttg gaacagaata aattagatgt caaaaagttt cgtcaatata acaagctata
acttctgata tggtattata tacgaagtta tgtttaaacg agctcgaatt CCCTCATCAT
ACGATACGTT ACATAGTAGT TCTAATAAAT CAATAAGATA GTGAATAATG TAACCCAATT
AATTAAATTC

```

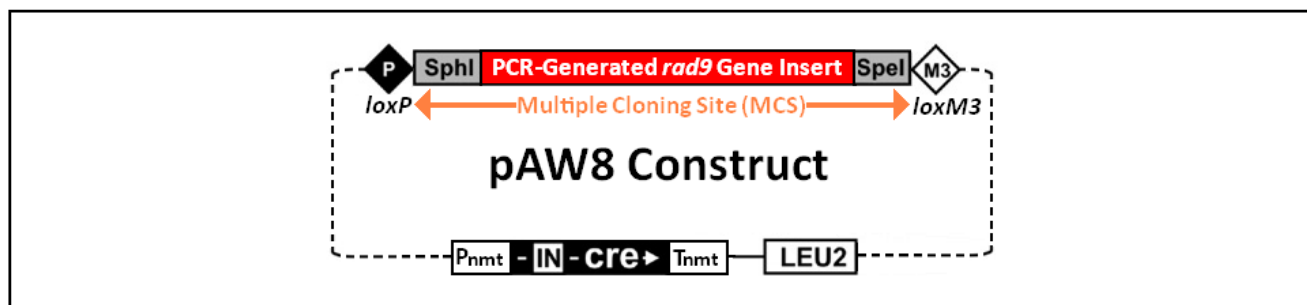
NNNNNNNN = Flanking *S. pombe* Chromosome 1 Base Sequences

NNNNNNNN = pAW1 Plasmid Flanking (F)orward and (R)everse BPS Base Sequences

NNNNNNNN = pAW1 Plasmid Flanking LoxP and LoxM3 Base Sequences

NNNNNNNN = pAW1 Plasmid *Ura4+* Gene Base Sequence

APPENDIX 2.11.5: pAW8 Cre-Lox Donor *rad9* Gene Exchange Plasmid Constructs



pAW8 Donor Plasmid Construct (Base-Strain Transformation)	MCS-Ligated Restriction-Site SphI- SpeI- Sequence-Complementary <i>rad9</i> Insert
pAW8- <i>rad9</i> ("untagged")	----loxP-sphI- <i>rad9</i> -speI-loxM3----
pAW8- <i>rad9</i> -c3xHA	----loxP-sphI- <i>rad9</i> -c3xHA-speI-loxM3----
pAW8- Δ Intron1-c3xHA	----loxP-sphI- <i>rad9</i> - Δ Intron1-c3xHA-speI-loxM3----
pAW8- <i>rad9</i> -M50L-c3xHA	----loxP-sphI- <i>rad9</i> -M50L-c3xHA-speI-loxM3----
pAW8- <i>rad9</i> -S-c3xHA	----loxP-sphI-N Δ 49- <i>rad9</i> -c3xHA-speI-loxM3----
pAW8- <i>rad9</i> -M74-c3xHA	----loxP-sphI-N Δ 73- <i>rad9</i> -c3xHA-speI-loxM3----
pAW8- <i>rad9</i> -M312-c3xHA	----loxP-sphI-N Δ 311- <i>rad9</i> -c3xHA-speI-loxM3----
pAW8- <i>rad9</i> -M358-c3xHA	----loxP-sphI-N Δ 357- <i>rad9</i> -c3xHA-speI-loxM3----
pAW8- <i>rad9</i> -(L196P)-c3xHA	----loxP-sphI- <i>rad9</i> -(L196P)-c3xHA-speI-loxM3----
pAW8- <i>rad9</i> -M50L-(L196P)-c3xHA	----loxP-sphI-(M50L;L196P)-c3xHA-speI-loxM3----
pAW8- <i>rad9</i> -S-(L147P)-c3xHA	----loxP-sphI-N Δ 49- <i>rad9</i> -(L196P)-c3xHA-speI-loxM3----
pAW8- <i>rad9</i> -(T225A)-c3xHA	----loxP-sphI- <i>rad9</i> -(T225A)-c3xHA-speI-loxM3----
pAW8- <i>rad9</i> -(T225A;T412A;S423A)-c3xHA	----loxP-sphI- <i>rad9</i> -(T225A;T412A;S423A)-c3xHA-speI-loxM3----
pAW8- <i>rad9</i> -M50L-(T255A)-c3xHA	----loxP-sphI-(M50L;T255A)-c3xHA-speI-loxM3----
pAW8- <i>rad9</i> -M50L-(T412A)-c3xHA	----loxP-sphI-(M50L;T412A)-c3xHA-speI-loxM3----
pAW8- <i>rad9</i> -M50L-(S423A)-c3xHA	----loxP-sphI-(M50L;S423A)-c3xHA-speI-loxM3----
pAW8- <i>rad9</i> -M50L-(T412A;S423A)-c3xHA	----loxP-sphI- <i>rad9</i> -(M50L;T412A;S423A)-c3xHA-speI-loxM3----
pAW8- <i>rad9</i> -M50L-(T225A;T412A;S423A)-c3xHA	----loxP-sphI- <i>rad9</i> -(M50L;T225A;T412A;S423A)-c3xHA-speI-loxM3----
pAW8- <i>rad9</i> -S-(T3A)-c3xHA	----loxP-sphI-N Δ 49- <i>rad9</i> -(T52A)-c3xHA-speI-loxM3----
pAW8- <i>rad9</i> -S-(Y12F)-c3xHA	----loxP-sphI-N Δ 49- <i>rad9</i> -(Y61F)-c3xHA-speI-loxM3----
pAW8- <i>rad9</i> -S-(T3A;Y12F)-c3xHA	----loxP-sphI-N Δ 49- <i>rad9</i> -(T52A;Y61F)-c3xHA-speI-loxM3----
pAW8- <i>rad9</i> -S-(Y62F)-c3xHA	----loxP-sphI-N Δ 49- <i>rad9</i> -(Y111F)-c3xHA-speI-loxM3----
pAW8- <i>rad9</i> -S-(T176A)-c3xHA	----loxP-sphI-N Δ 49- <i>rad9</i> -(T225A)-c3xHA-speI-loxM3----
pAW8- <i>rad9</i> -S-(T176E)-c3xHA	----loxP-sphI-N Δ 49- <i>rad9</i> -(T225E)-c3xHA-speI-loxM3----
pAW8- <i>rad9</i> -S-(T363A)-c3xHA	----loxP-sphI-N Δ 49- <i>rad9</i> -(T412A)-c3xHA-speI-loxM3----
pAW8- <i>rad9</i> -S-(T363E)-c3xHA	----loxP-sphI-N Δ 49- <i>rad9</i> -(T412E)-c3xHA-speI-loxM3----
pAW8- <i>rad9</i> -S-(S374A)-c3xHA	----loxP-sphI-N Δ 49- <i>rad9</i> -(S423A)-c3xHA-speI-loxM3----
pAW8- <i>rad9</i> -S-(S374E)-c3xHA	----loxP-sphI-N Δ 49- <i>rad9</i> -(S423E)-c3xHA-speI-loxM3----
pAW8- <i>rad9</i> -S-(T363A;S374A)-c3xHA	----loxP-sphI-N Δ 49- <i>rad9</i> -(T412A;S423A)-c3xHA-speI-loxM3----
pAW8- <i>rad9</i> -S-(T176A;T363A;S374A)-c3xHA	----loxP-sphI-N Δ 49- <i>rad9</i> -(T225A;T412A;S423A)-c3xHA-speI-loxM3----

APPENDIX 2.11.6: Pre-Constructed (Pre-Supplied) *S. pombe* Strains Utilised in this Study

<i>S. pombe</i> Strain	Genotype
"Wild-Type"	<i>ura4-D18 leu1-32 ade6-M210 h⁻</i>
"Wild-Type"	<i>ura4-D18 leu1-32 ade6-M210 h⁺</i>
<i>rad9-c3xHA</i>	<i>rad9-c3xHA kanMX6 ura4-D18 leu1-32 ade6-M210 h⁻</i>
Δ <i>rad9</i>	<i>rad9::ura4⁺ura4-D18 leu1-32 ade6-M210 h⁻</i>
Δ <i>rad1</i>	<i>rad1::ura4⁺ura4-D18 leu1-32 ade6-M210 h⁻</i>
Δ <i>hus1</i>	<i>hus1::LEU2 ura4-D18 leu1-32 ade6-M210 h⁻</i>
<i>hus1-c13xMyc</i>	<i>hus1-c13xMyc ura4-D18 leu1-32 ade6-704 h⁻</i>
Δ <i>rad17</i>	<i>rad17::ura4⁺ura4-D18 leu1-32 ade6-M210 h⁻</i>
Δ <i>rad3</i>	<i>rad3::ura4⁺ura4-D18 leu1-32 ade6-M210 h⁻</i>
Δ <i>rad26</i>	<i>rad26::LEU2 ura4-D18 leu1-32 ade6-M210 h⁺</i>
Δ <i>tel1</i>	<i>tel1::ura4⁺ura4-D18 leu1-32 ade6-M210 h⁻</i>
<i>rad9-(T412A)-c3xHA</i>	<i>rad9-(T412A)-c3xHA.kanMX6 ura4-D18 leu1-32 ade6-M210 h⁻</i>
<i>rad9-(S423A)-c3xHA</i>	<i>rad9-(S423A)-c3xHA.kanMX6 ura4-D18 leu1-32 ade6-M210 h⁻</i>
<i>rad9-(T412A;S423A)-c3xHA</i>	<i>rad9-(T412A;S423A)-c3xHA.kanMX6 ura4-D18 leu1-32 ade6-M210 h⁻</i>
<i>rad4.116</i>	<i>rad4.116 ura4-D18 leu1-32 ade6-M210 h⁻</i>
Δ <i>crb2</i>	<i>crb2::ura4⁺ura4-D18 leu1-32 ade6-M210 h⁻</i>
Δ <i>mrc1</i>	<i>mrc1::kanMX6 ura4-D18 leu1-32 ade6-M210 h⁻</i>
Δ <i>chk1</i>	<i>chk1::ura4⁺ura4-D18 leu1-32 ade6-M210 h⁻</i>
Δ <i>cds1</i>	<i>cds1::ura4⁺ura4-D18 leu1-32 ade6-M210 h⁻</i>
<i>cds1-(T8A;T11A)-c13xMyc</i>	<i>cds1(T8A;T11A)-c13xMyc ura4-D18 leu1-32 ade6-M210 h⁻</i>
<i>cds1-c13xMyc</i>	<i>cds1-c13xMyc ura4-D18 leu1-32 ade6-M210 h⁻</i>
Δ <i>hhp1</i>	<i>hhp1::kanMX6 ura4-D18 leu1-32 lys1-31 ade6-M216 h90</i>
Δ <i>wis1</i>	<i>wis1::ura4⁺ rad9-c3xHA ura4-D18 leu1-32 ade6-M210 h⁻</i>
Δ <i>sty1</i>	<i>sty1::ura4⁺ rad9-c3xHA ura4-D18 leu1-32 ade6-M210 h⁻</i>
Δ <i>hsk1</i>	<i>hsk1-89::ura4⁺ura4-D18 leu1-32 ade6-M210 h⁻</i>
<i>cdc25.22</i>	<i>cdc25.22 ura4-D18 leu1-32 ade6-M210 h⁻</i>
Δ <i>rad24</i>	<i>rad24::ura4⁺ura4-D18 leu1-32 ade6-M210 h⁻</i>
Δ <i>bub1</i>	<i>bub1::ura4⁺ura4-D18 leu1-32 ade6-M210 h⁻</i>
Δ <i>mad2</i>	<i>mad2::ura4⁺ura4-D18 leu1-32 ade6-M210 h⁻</i>
Δ <i>mph1</i>	<i>mph1::kanMX6 ura4-D18 leu1-32 ade6-M210 h⁻</i>
<i>mph1-c13xMyc</i>	<i>mph1-c13xMyc ura4-D18 leu1-32 ade6-M210 h⁻</i>
<i>spo12.B81</i>	<i>spo12.B81 ura4-D18 leu1-32 ade6-M210 h90</i>
Δ <i>clp1</i>	<i>clp1::kanMX6 ura4-D18 leu1-32 ade6-M210 h90</i>
Δ <i>top1</i>	<i>top1::LEU2 ura4-D18 leu1-32 ade6-M210 h⁺</i>
Δ <i>rqh1</i>	<i>rqh1::ura4⁺ura4-D18 leu1-32 ade6-M210 h⁺</i>
Δ <i>mus81</i>	<i>mus81::kanMX6 ura4-D18 leu1-32 ade6-M210 h⁺</i>
Δ <i>rad16</i>	<i>rad16::ura4⁺ura4-D18 leu1-32 ade6-M210 h⁺</i>
Δ <i>tdp1</i>	<i>tdp1::kanMX6 ura4-D18 leu1-32 ade6-M210 h⁻</i>
Δ <i>uvde</i>	<i>uvde::LEU2 ura4-D18 leu1-32 ade6-M210 h⁺</i>
Δ <i>ligIV</i>	<i>ligIV::kanMX6 ura4-D18 his3-D1 leu1-32 ade6-M210 h⁺</i>

APPENDIX 2.11.7: Constructed Full-Length, Truncated and Point-Mutated *rad9* Strains

<i>S. pombe</i> Strain	Genotype
$\Delta rad9$ ("base-strain")	<i>rad9::loxP-ura4⁺-loxM3 ura4-D18 leu1-32 ade6-M210 h⁻</i>
<i>rad9</i> ("untagged")	<i>rad9::loxP-rad9-loxM3 ura4-D18 leu1-32 ade6-M210 h⁻</i>
<i>rad9-c3xHA</i>	<i>rad9::loxP-rad9-c3xHA-loxM3 ura4-D18 leu1-32 ade6-M210 h⁻</i>
<i>rad9-c3xHA</i>	<i>rad9::loxP-rad9-c3xHA-loxM3 ura4-D18 leu1-32 ade6-M210 h⁺</i>
Δ Intron1-c3xHA	<i>rad9::loxP-rad9-ΔIntron1-c3xHA-loxM3 ura4-D18 leu1-32 ade6-M210 h⁻</i>
<i>rad9-M50A-c3xHA</i>	<i>rad9::loxP-rad9-M50A-c3xHA-loxM3 ura4-D18 leu1-32 ade6-M210 h⁻</i>
<i>rad9-M50L-c3xHA</i>	<i>rad9::loxP-rad9-M50L-c3xHA-loxM3 ura4-D18 leu1-32 ade6-M210 h⁻</i>
<i>rad9-M50L-c3xHA</i>	<i>rad9::loxP-rad9-M50L-c3xHA-loxM3 ura4-D18 leu1-32 ade6-M210 h⁺</i>
<i>rad9-S-c3xHA</i>	<i>rad9::loxP-NΔ49-rad9-c3xHA-loxM3 ura4-D18 leu1-32 ade6-M210 h⁻</i>
<i>rad9-S-c3xHA</i>	<i>rad9::loxP-NΔ49-rad9-c3xHA-loxM3 ura4-D18 leu1-32 ade6-M210 h⁺</i>
<i>rad9-M74-c3xHA</i>	<i>rad9::loxP-NΔ73-rad9-c3xHA-loxM3 ura4-D18 leu1-32 ade6-M210 h⁻</i>
<i>rad9-M312-c3xHA</i>	<i>rad9::loxP-NΔ311-rad9-c3xHA-loxM3 ura4-D18 leu1-32 ade6-M210 h⁻</i>
<i>rad9-M358-c3xHA</i>	<i>rad9::loxP-NΔ357-rad9-c3xHA-loxM3 ura4-D18 leu1-32 ade6-M210 h⁻</i>
<i>rad9-(L196P)-c3xHA</i>	<i>rad9::loxP-rad9-(L196P)-c3xHA-loxM3 ura4-D18 leu1-32 ade6-M210 h⁻</i>
<i>rad9-M50L-(L196P)-c3xHA</i>	<i>rad9::loxP-rad9-(M50L;L196P)-c3xHA-loxM3 ura4-D18 leu1-32 ade6-M210 h⁻</i>
<i>rad9-S-(L147P)-c3xHA</i>	<i>rad9::loxP-NΔ49-rad9-(L196P)-c3xHA-loxM3 ura4-D18 leu1-32 ade6-M210 h⁻</i>
<i>rad9-(T225A)-c3xHA</i>	<i>rad9::loxP-rad9-(T225A)-c3xHA-loxM3 ura4-D18 leu1-32 ade6-M210 h⁻</i>
<i>rad9-(T225A;T412A;S423A)-c3xHA</i>	<i>rad9::loxP-rad9-(T225A;T412A;S423A)-c3xHA-loxM3 ura4-D18 leu1-32 ade6-M210 h⁻</i>
<i>rad9-M50L-(T255A)-c3xHA</i>	<i>rad9::loxP-rad9-(M50L;T255A)-c3xHA-loxM3 ura4-D18 leu1-32 ade6-M210 h⁻</i>
<i>rad9-M50L-(T412A)-c3xHA</i>	<i>rad9::loxP-rad9-(M50L;T412A)-c3xHA-loxM3 ura4-D18 leu1-32 ade6-M210 h⁻</i>
<i>rad9-M50L-(S423A)-c3xHA</i>	<i>rad9::loxP-rad9-(M50L;S423A)-c3xHA-loxM3 ura4-D18 leu1-32 ade6-M210 h⁻</i>
<i>rad9-M50L-(T412A;S423A)-c3xHA</i>	<i>rad9::loxP-rad9-(M50L;T412A;S423A)-c3xHA-loxM3 ura4-D18 leu1-32 ade6-M210 h⁻</i>
<i>rad9-M50L-(T225A;T412A;S423A)-c3xHA</i>	<i>rad9::loxP-rad9-(M50L;T225A;T412A;S423A)-c3xHA-loxM3 ura4-D18 leu1-32 ade6-M210 h⁻</i>
<i>rad9-S-(T3A)-c3xHA</i>	<i>rad9::loxP-NΔ49-rad9-(T52A)-c3xHA-loxM3 ura4-D18 leu1-32 ade6-M210 h⁻</i>
<i>rad9-S-(Y12F)-c3xHA</i>	<i>rad9::loxP-NΔ49-rad9-(Y61F)-c3xHA-loxM3 ura4-D18 leu1-32 ade6-M210 h⁻</i>
<i>rad9-S-(T3A;Y12F)-c3xHA</i>	<i>rad9::loxP-NΔ49-rad9-(T52A;Y61F)-c3xHA-loxM3 ura4-D18 leu1-32 ade6-M210 h⁻</i>
<i>rad9-S-(Y62F)-c3xHA</i>	<i>rad9::loxP-NΔ49-rad9-(Y111F)-c3xHA-loxM3 ura4-D18 leu1-32 ade6-M210 h⁻</i>
<i>rad9-S-(T176A)-c3xHA</i>	<i>rad9::loxP-NΔ49-rad9-(T225A)-c3xHA-loxM3 ura4-D18 leu1-32 ade6-M210 h⁻</i>
<i>rad9-S-(T176E)-c3xHA</i>	<i>rad9::loxP-NΔ49-rad9-(T225E)-c3xHA-loxM3 ura4-D18 leu1-32 ade6-M210 h⁻</i>
<i>rad9-S-(T363A)-c3xHA</i>	<i>rad9::loxP-NΔ49-rad9-(T412A)-c3xHA-loxM3 ura4-D18 leu1-32 ade6-M210 h⁻</i>
<i>rad9-S-(T363E)-c3xHA</i>	<i>rad9::loxP-NΔ49-rad9-(T412E)-c3xHA-loxM3 ura4-D18 leu1-32 ade6-M210 h⁻</i>
<i>rad9-S-(S374A)-c3xHA</i>	<i>rad9::loxP-NΔ49-rad9-(S423A)-c3xHA-loxM3 ura4-D18 leu1-32 ade6-M210 h⁻</i>
<i>rad9-S-(S374E)-c3xHA</i>	<i>rad9::loxP-NΔ49-rad9-(S423E)-c3xHA-loxM3 ura4-D18 leu1-32 ade6-M210 h⁻</i>
<i>rad9-S-(T363A;S374A)-c3xHA</i>	<i>rad9::loxP-NΔ49-rad9-(T412A;S423A)-c3xHA-loxM3 ura4-D18 leu1-32 ade6-M210 h⁻</i>
<i>rad9-S-(T176A;T363A;S374A)-c3xHA</i>	<i>rad9::loxP-NΔ49-rad9-(T225A;T412A;S423A)-c3xHA-loxM3 ura4-D18 leu1-32 ade6-M210 h⁻</i>

APPENDIX 2.11.8: Cre-Lox Double-Mutant *S. pombe* Strains Constructed for this Study

<i>S. pombe</i> Strain	Genotype
<i>rad9-c3xHA Δrad1</i>	<i>rad1::ura4⁺rad9::loxP-rad9-c3xHA-loxM3 ura4-D18 leu1-32 ade6-M210 h⁻</i>
<i>rad9-c3xHA Δhus1</i>	<i>hus1::LEU2 rad9::loxP-rad9-c3xHA-loxM3 ura4-D18 leu1-32 ade6-M210 h⁻</i>
<i>rad9-c3xHA Δrad17</i>	<i>rad17::ura4⁺rad9::loxP-rad9-c3xHA-loxM3 ura4-D18 leu1-32 ade6-M210 h⁻</i>
<i>rad9-M50L-c3xHA Δrad1</i>	<i>rad1::ura4⁺rad9::loxP-rad9-M50L-c3xHA-loxM3 ura4-D18 leu1-32 ade6-M210 h⁻</i>
<i>rad9-M50L-c3xHA Δhus1</i>	<i>hus1::LEU2 rad9::loxP-rad9-M50L-c3xHA-loxM3 ura4-D18 leu1-32 ade6-M210 h⁻</i>
<i>rad9-M50L-c3xHA Δrad17</i>	<i>rad17::ura4⁺rad9::loxP-rad9-M50L-c3xHA-loxM3 ura4-D18 leu1-32 ade6-M210 h⁻</i>
<i>rad9-S-c3xHA Δrad1</i>	<i>rad1::ura4⁺rad9::loxP-NΔ49-rad9-c3xHA-loxM3 ura4-D18 leu1-32 ade6-M210 h⁻</i>
<i>rad9-S-c3xHA Δhus1</i>	<i>hus1::LEU2 rad9::loxP-NΔ49-rad9-c3xHA-loxM3 ura4-D18 leu1-32 ade6-M210 h⁻</i>
<i>rad9-S-c3xHA hus1-c13xMyc</i>	<i>hus1-c13xMyc rad9::loxP-NΔ49-rad9-c3xHA-loxM3 ura4-D18 leu1-32 ade6-M210 h⁻</i>
<i>rad9-S-c3xHA Δrad17</i>	<i>rad17::ura4⁺rad9::loxP-NΔ49-rad9-c3xHA-loxM3 ura4-D18 leu1-32 ade6-M210 h⁻</i>
<i>rad9-c3xHA Δrad3</i>	<i>rad3::ura4⁺rad9::loxP-rad9-c3xHA-loxM3 ura4-D18 leu1-32 ade6-M210 h⁻</i>
<i>rad9-c3xHA Δrad26</i>	<i>rad26::LEU2 rad9::loxP-rad9-c3xHA-loxM3 ura4-D18 leu1-32 ade6-M210 h⁻</i>
<i>rad9-M50L-c3xHA Δrad3</i>	<i>rad3::ura4⁺rad9::loxP-rad9-M50L-c3xHA-loxM3 ura4-D18 leu1-32 ade6-M210 h⁻</i>
<i>rad9-M50L-c3xHA Δrad26</i>	<i>rad26::LEU2 rad9::loxP-rad9-M50L-c3xHA-loxM3 ura4-D18 leu1-32 ade6-M210 h⁻</i>
<i>rad9-S-c3xHA Δrad3</i>	<i>rad3::ura4⁺rad9::loxP-NΔ49-rad9-c3xHA-loxM3 ura4-D18 leu1-32 ade6-M210 h⁻</i>
<i>rad9-S-c3xHA Δrad26</i>	<i>rad26::LEU2 rad9::loxP-NΔ49-rad9-c3xHA-loxM3 ura4-D18 leu1-32 ade6-M210 h⁻</i>
<i>rad9-S-c3xHA Δtel1</i>	<i>tel1::ura4⁺rad9::loxP-NΔ49-rad9-c3xHA-loxM3 ura4-D18 leu1-32 ade6-M210 h⁻</i>
<i>rad9-S-c3xHA rad4.116</i>	<i>rad4.116 rad9::loxP-NΔ49-rad9-c3xHA-loxM3 ura4-D18 leu1-32 ade6-M210 h⁻</i>
<i>rad9-S-c3xHA Δcrb2</i>	<i>crb2::ura4⁺rad9::loxP-NΔ49-rad9-c3xHA-loxM3 ura4-D18 leu1-32 ade6-M210 h⁻</i>
<i>rad9-S-c3xHA Δmrc1</i>	<i>mrc1::kanMX6 rad9::loxP-NΔ49-rad9-c3xHA-loxM3 ura4-D18 leu1-32 ade6-M210 h⁻</i>
<i>rad9-S-c3xHA Δchk1</i>	<i>chk1::ura4⁺rad9::loxP-NΔ49-rad9-c3xHA-loxM3 ura4-D18 leu1-32 ade6-M210 h⁻</i>
<i>rad9-S-c3xHA Δcds1</i>	<i>cds1::ura4⁺rad9::loxP-NΔ49-rad9-c3xHA-loxM3 ura4-D18 leu1-32 ade6-M210 h⁻</i>
<i>rad9-S-c3xHA cds1-(T8A;T11A)-c13xMyc</i>	<i>cds1(T8A;T11A)-c13xMyc rad9::loxP-NΔ49-rad9-c3xHA-loxM3 ura4-D18 leu1-32 ade6-M210 h⁻</i>
<i>rad9-S-c3xHA cds1-c13xMyc</i>	<i>cds1-c13xMyc rad9::loxP-NΔ49-rad9-c3xHA-loxM3 ura4-D18 leu1-32 ade6-M210 h⁻</i>
<i>rad9-S-c3xHA Δhhp1</i>	<i>hhp1::kanMX6 rad9::loxP-NΔ49-rad9-c3xHA-loxM3 ura4-D18 leu1-32 lys1-31 ade6-M210 h⁻</i>
<i>rad9-S-c3xHA Δwis1</i>	<i>wis1::ura4⁺rad9::loxP-NΔ49-rad9-c3xHA-loxM3 ura4-D18 leu1-32 ade6-M210 h⁻</i>
<i>rad9-S-c3xHA Δsty1</i>	<i>sty1::ura4⁺rad9::loxP-NΔ49-rad9-c3xHA-loxM3 ura4-D18 leu1-32 ade6-M210 h⁻</i>
<i>rad9-S-c3xHA cdc25.22</i>	<i>cdc25.22 rad9::loxP-NΔ49-rad9-c3xHA-loxM3 ura4-D18 leu1-32 ade6-M210 h⁻</i>
<i>rad9-S-c3xHA Δrad24</i>	<i>rad24::ura4⁺rad9::loxP-NΔ49-rad9-c3xHA-loxM3 ura4-D18 leu1-32 ade6-M210 h⁻</i>
<i>rad9-S-c3xHA Δbub1</i>	<i>bub1::ura4⁺rad9::loxP-NΔ49-rad9-c3xHA-loxM3 ura4-D18 leu1-32 ade6-M210 h⁻</i>
<i>rad9-S-c3xHA Δmad2</i>	<i>mad2::ura4⁺rad9::loxP-NΔ49-rad9-c3xHA-loxM3 ura4-D18 leu1-32 ade6-M210 h⁻</i>
<i>rad9-S-c3xHA Δmph1</i>	<i>mph1::kanMX6 rad9::loxP-NΔ49-rad9-c3xHA-loxM3 ura4-D18 leu1-32 ade6-M210 h⁻</i>
<i>rad9-S-(Y12F)-c3xHA Δmph1</i>	<i>mph1::kanMX6 rad9::loxP-NΔ49-rad9-(Y61F)-c3xHA-loxM3 ura4-D18 leu1-32 ade6-M210 h⁻</i>
<i>rad9-S-c3xHA mph1-c13xMyc</i>	<i>mph1-c13xMyc rad9::loxP-NΔ49-rad9-c3xHA-loxM3 ura4-D18 leu1-32 ade6-M210 h⁻</i>
<i>rad9-S-c3xHA spo12.B81</i>	<i>spo12.B81 rad9::loxP-NΔ49-rad9-c3xHA-loxM3 ura4-D18 leu1-32 ade6-M210 h⁻</i>
<i>rad9-S-c3xHA Δclp1</i>	<i>clp1::kanMX6 rad9::loxP-NΔ49-rad9-c3xHA-loxM3 ura4-D18 leu1-32 ade6-M210 h⁻</i>
<i>rad9-S-c3xHA Δtop1</i>	<i>top1::LEU2 rad9::loxP-NΔ49-rad9-c3xHA-loxM3 ura4-D18 leu1-32 ade6-M210 h⁻</i>
<i>rad9-S-c3xHA Δrqh1</i>	<i>rqh1::ura4⁺rad9::loxP-NΔ49-rad9-c3xHA-loxM3 ura4-D18 leu1-32 ade6-M210 h⁻</i>
<i>rad9-S-c3xHA Δmus81</i>	<i>mus81::kanMX6 rad9::loxP-NΔ49-rad9-c3xHA-loxM3 ura4-D18 leu1-32 ade6-M210 h⁻</i>
<i>rad9-S-c3xHA Δrad16</i>	<i>rad16::ura4⁺rad9::loxP-NΔ49-rad9-c3xHA-loxM3 ura4-D18 leu1-32 ade6-M210 h⁻</i>
<i>rad9-S-c3xHA Δtdp1</i>	<i>tdp1::kanMX6 rad9::loxP-NΔ49-rad9-c3xHA-loxM3 ura4-D18 leu1-32 ade6-M210 h⁻</i>
<i>rad9-S-c3xHA Δuvde</i>	<i>uvde::LEU2 rad9::loxP-NΔ49-rad9-c3xHA-loxM3 ura4-D18 leu1-32 ade6-M210 h⁻</i>
<i>rad9-S-c3xHA ΔligIV</i>	<i>ligIV::kanMX6 rad9::loxP-NΔ49-rad9-c3xHA-loxM3 ura4-D18 leu1-32 ade6-M210 h⁻</i>

Chapter 3

Construction of Initial Experimental *S.pombe* Strains: Genotypic and Phenotypic Verification

3.1 Introduction

Comparative western blot analyses of TCA-precipitated total protein samples, prepared from YEA broth cultures of cells of an *S. pombe* strain which expressed an HA epitope-tagged C-terminal variant of the Rad9 protein, indicated the existence of a novel constitutive and heat shock-inducible truncated variant of lower molecular mass (~40kDa) than that of the full-length protein (~50kDa) – Fig 3.1, p.286.

There are several plausible hypothetical mechanisms which may account for the expression of this short protein variant (termed “Rad9-S”) – notably;

(i) The Expressed *S. pombe* Rad-S Variant is a De-Phosphorylated Version of the Rad9 Protein

A significant shift in molecular weight from ~60kDa to ~45kDa has been observed in SDS-PAGE analyses of *in vitro* de-phosphorylation within the C-terminal domain of human Rad9 (hRad9), in which the constitutively-phosphorylated form migrates with the corresponding 60kDa higher molecular weight marker band position on the gel (St. Onge R.P. *et al.*, 2001).

In contrast with this observation, initial experimental work has indicated the molecular weight of the un-phosphorylated *S. pombe* Rad9 protein does not correlate with an equivalent molecular weight reduction to that of the characteristic 40kDa of the novel Rad9-S protein variant (Fig 3.1, p.286).

Therefore it is unlikely that the Rad9-S variant is a de-phosphorylated form of the full length *S. pombe* Rad9 protein.

(ii) Rad9-S is a Post-Translational Modified Limited-Proteolytic Cleavage Product of Rad9

It is feasible that Rad9-S may actually be the resultant product of limited proteolytic post-translational modification of the full length Rad9 protein in *S. pombe* cells.

This hypothesis would be consistent with the fact that caspase-3-mediated cleavage of the hRad9 protein during apoptotic processes triggered via DNA damage events has been observed to occur in both *in vitro* and *in vivo* types of experimental study (Lee M.W. *et al.*, 2003) – as discussed in detail previously in Chapter 1 (Section 1.3.2, pp.127-130).

(iii) The Expressed Rad-S Protein is an Alternative Gene-Spliced Translational Product

Rad9-S expression in *S. pombe* cells may originate from alternative mRNA splicing of the full-length Rad9 gene, involving retention of intron 1, with a consequential translational shift to a downstream AUG initiation site at M50 respectively – discussed in detail in Chapter 4.

This hypothesis is currently considered to be the most favourable explanation for the mechanism of Rad9-S expression as it is also validated via previous experimental studies which have isolated and identified up to three tissue-specific different mRNA molecular variants of hRad9 (Hopkins K.M. *et al.*, 2003).

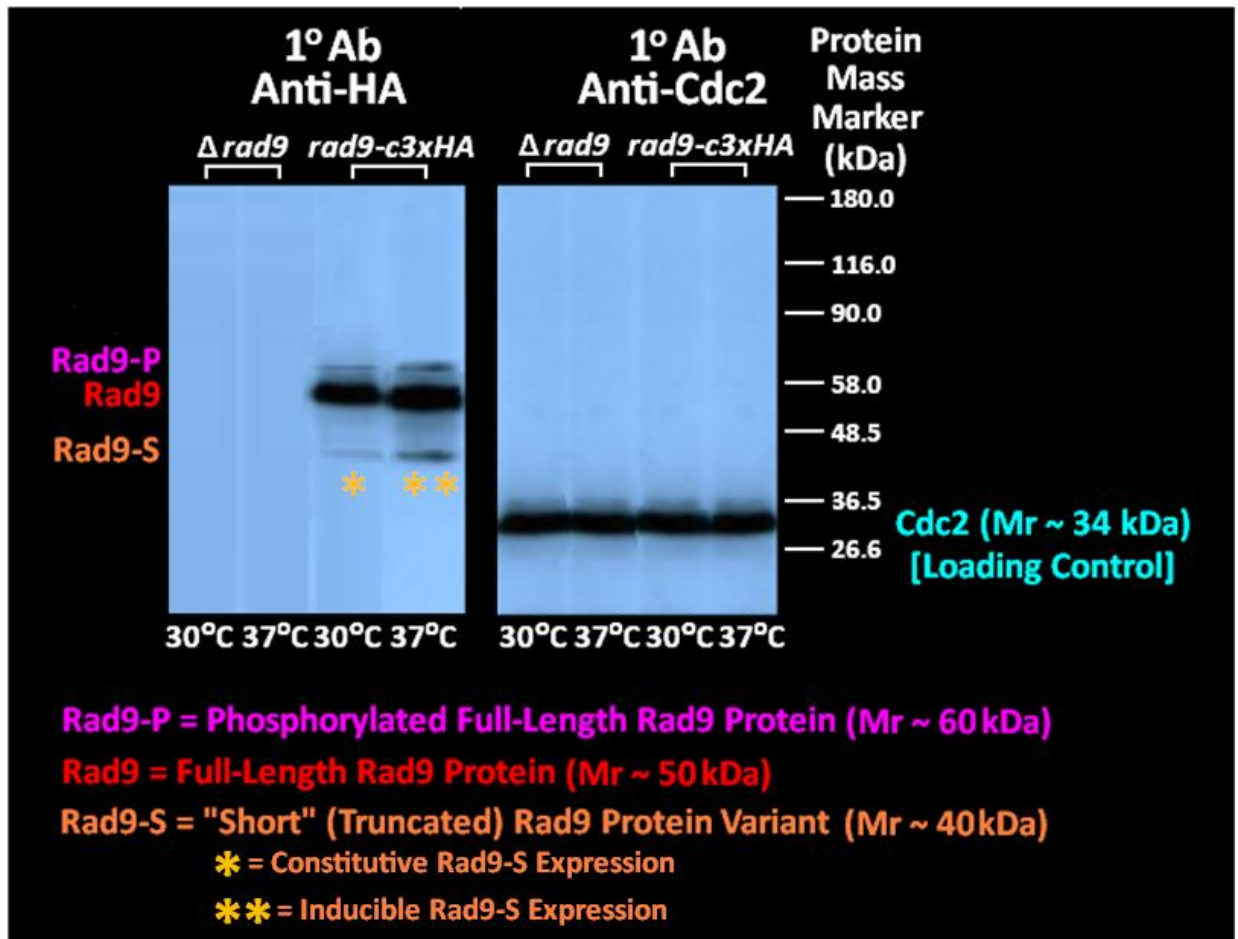
Other experimental work, which supports this particular hypothesis, indicates the existence of a paralogue sequence variant of hRad9 - designated as hRad9B, in certain tissue types (Dufault V.M. *et al.*, 2003).

Progressive experimental studies into potential alternative expression of the *hRad9B* gene have thus far identified 4 smaller isoform variants of the Rad9B protein (discussed previously in Chapter 1, Section 1.1, pp.2-22; Fig 1.3, p.9).

The full-length human hRad9A and hRad9B paralogue (Isoform 5) proteins also exhibit characteristically very different expression profiles in a variety of normal and cancerous tissue types (discussed previously in Chapter 1, Section 1.1, pp.2-22; Fig 1.3, p.9).

Whether or not expression of alternative mRNA splice-variants of *hRAD9A* and *hRAD9B* genes in human cells is correlated with characteristic expression profiles for different levels of specific isoform sub-type sets of the hRad9A and hRad9B proteins, which are unique to particular normal and cancerous human cell tissue types, remains to be determined.

Fig 3.1: Constitutive and Heat-Inducible “Rad9-S” Expression



Experimental confirmation of the original observations made by Caspari T. and co-workers (discussed previously in Chapter 1, Section 1.5.2, pp.145-148).

rad9-deleted ($\Delta rad9 = rad9::ura4^+$) and “wild-type” *S. pombe* cells (*rad9-c3xHA*) were cultured in YEA medium at 30°C to a density of 1×10^7 cells/mL.

[The full genotypes of the utilised *S. pombe* strains are detailed in Appendix 2.11.6 , p.279].

Aliquots (5×10^8 cells) were then withdrawn from the respective cultures and re-incubated in YEA medium at either 30°C or 37°C for a further 30 minutes.

1.4×10^7 cells, acquired from each respective re-incubated culture, were utilised for the preparation of TCA-precipitated total protein extracts.

20µL aliquots of the prepared protein samples were resolved on 10% SDS-PAGE gels which were then utilised in comparative Western blot analyses probed with either the anti-HA or anti-Cdc2 primary antibody.

[Protein sample preparation, SDS-PAGE resolution and Western blot methodologies are detailed in Section 2.8.1, pp.200-202; Section 2.8.4, pp.223-224 and Section 2.8.6, pp.231-233]

Protein samples isolated from the *rad9*-deleted *S. pombe* cell cultures served as comparative negative non-specific/cross-reactivity controls in the anti-HA Western blot for verification that the detected protein bands in the *rad9-c3xHA* samples were exclusive to the specific expression of Rad9 protein isoforms.

The comparative anti-Cdc2 Western blot served as a qualitative control for verification that equivalent amounts of total protein for each sample had been loaded.

3.2 Creation of Experimental *S. pombe* Strains

The *S. pombe rad9* gene is comprised of four protein-encoding exons separated by three interstitial non-coding introns and also contains 4 methionine AUG codons (at positions M74, M311, M312 and M358), in addition to the M1 and M50 AUG codon sites (Fig 3.2, pp.289-290).

Thus the *S. pombe rad9* gene possesses the potential to express up to 4 progressively smaller novel spRad9 isoforms, in addition to the full-length spRad9 protein and the postulated spRad9-S truncated variant (Fig 3.2, pp.289-290).

It was proposed that if these potential alternative AUG codon start-site translational products of the *S. pombe rad9* gene are expressed as stable protein products then they may also exhibit novel functions, outside of the canonical Rad9-Rad1-Hus1 heterotrimeric DNA sliding-clamp complex, towards different types of induced DNA replication stress and DNA damage.

The Cre-Lox system (devised by Watson A.T. *et al*, 2008) was adapted for the generation of an initial set of novel *S. pombe* strains, whose respective cells were engineered for the exclusive expression of specific experimental Rad9 protein variants (Fig 3.2, pp.289-290).

This Cre-Recombinase-Mediated Cassette Exchange (Cre-RMCE) adaptation was a binary system which required the preparation of two essential components (Fig 3.3, p.291) – notably;

- (i) The *rad9* gene-deleted *S. pombe* base-strain (Section 3.2.1, pp.292-297), whose cells contained the LoxP-*ura4*⁺-LoxM3 exchange cassette integrated at the endogenous *rad9* gene locus within chromosome 1 (Fig 3.3, p.291).

(ii) A set of pAW8 donor plasmid constructs (Section 3.2.2, pp.298-307) which contained the *LoxP-modified rad9 allele-LoxM3* exchange cassettes (Fig 3.3, p.291), that encoded the experimental Rad9 protein variants (Fig 3.2, pp.289-290).

Transformation of the $\Delta rad9$ base-strain with the pAW8 donor plasmid constructs resulted in the Cre-RMCE-integration of the PCR-modified *rad9* alleles at the endogenous *rad9* gene locus situated within chromosome 1 (Fig 3.3, p.291) for consequential generation of the desired initial set of novel experimental *S. pombe* strains whose cells expressed specific Rad9 protein variants (Fig 3.2, pp.289-290).

Fig 3.2: Experimental *S. pombe rad9* Gene Constructs

<i>S. pombe</i> Strain	Engineered Genotype	Expression Phenotype
Full-Length Rad9	<i>rad9</i>	Full-Length Rad9 Truncated Variants?
Full-Length Rad9 C-Terminal HA Tagged	<i>rad9-c3xHA</i>	Full-Length Rad9 Truncated Variants?
Full-Length Rad9 C-Terminal HA Tagged Intron 1 Deletion Mutant	<i>rad9-(ΔIntron1)-c3xHA</i>	Full-Length Rad9-c3xHA "Rad9-S"-c3xHA Absence? Other Truncated Rad9-c3xHA's?
Full-Length Rad9 M50A Point Mutant C-Terminal HA Tagged	<i>rad9-(M50A)-c3HA</i>	Full-Length Rad9-(M50A)-c3xHA "Rad9-S"-c3xHA Absence? Other Truncated Rad9-c3xHA's?
Full-Length Rad9 M50L Point Mutant C-Terminal HA Tagged	<i>rad9-(M50L)-c3HA</i>	Full-Length Rad9-(M50L)-c3xHA "Rad9-S"-c3xHA Absence? Other Truncated Rad9-c3xHA's?
Modified N-Terminal M1-S49 Residue Deletion Mutant C-Terminal HA Tagged	<i>NΔ49-rad9-c3xHA</i>	Full-Length Rad9-c3xHA Absence NΔ49-Rad9-c3xHA? ("Rad9-S"-c3xHA) Other Truncated Rad9-c3xHA's?
Modified N-Terminal M1-L73 Residue Deletion Mutant C-Terminal HA Tagged	<i>NΔ73-rad9-c3xHA</i>	Full-Length Rad9-c3xHA Absence "Rad9-S"-c3xHA Absence NΔ73-Rad9-c3xHA? ("Rad9-M74-c3xHA") Other Truncated Rad9-c3xHA's?
Modified N-Terminal M1-M311 Residue Deletion Mutant C-Terminal HA Tagged	<i>NΔ311-rad9-c3xHA</i>	Full-Length Rad9-c3xHA Absence "Rad9-S"-c3xHA Absence "Rad9-M74-c3xHA" Absence NΔ311-Rad9-c3xHA? ("Rad9-M312-c3xHA") Other Truncated Rad9-c3xHA's?
Modified N-Terminal M1-R357 Residue Deletion Mutant C-Terminal HA Tagged	<i>NΔ357-rad9-c3xHA</i>	Full-Length Rad9-c3xHA Absence "Rad9-S"-c3xHA Absence "Rad9-M74-c3xHA" Absence "Rad9-M312-c3xHA" Absence NΔ357-Rad9-c3xHA? ("Rad9-M358-c3xHA") Other Truncated Rad9-c3xHA's?

The structure of the *S. pombe rad9* gene is indicated, together with the relative positions of the introns, exons and potential alternative translational AUG codon start sites at M50, M74, M311, M312 and M358.

The residue-spanning regions and the total number of amino acids (in brackets) encoded by each respective exon are also indicated.

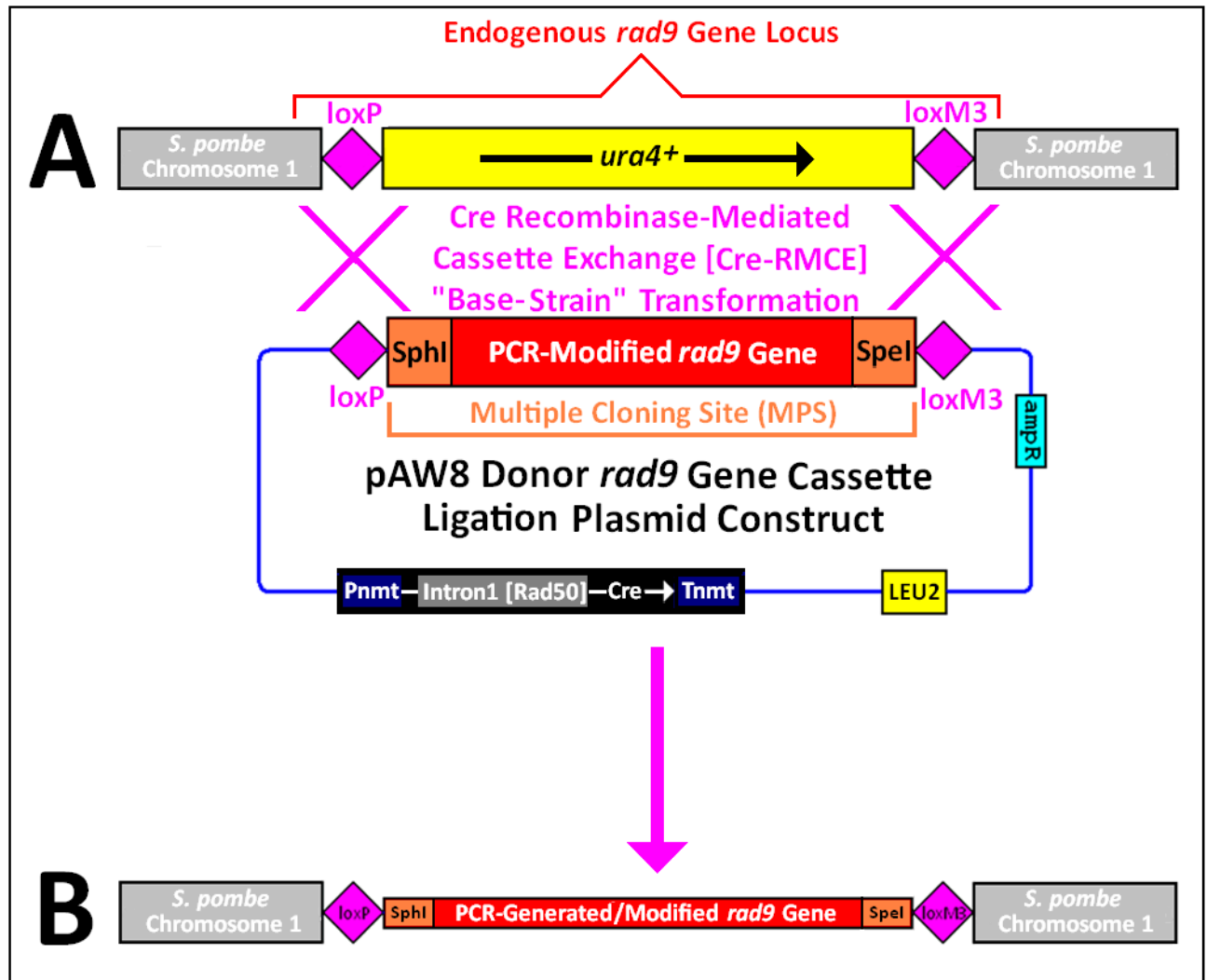
Details of the “cre-lox”–engineered *rad9* allele *S. pombe* strain genotypes and their respective hypothetical Rad9 protein expression phenotypes are provided and summarily tabulated.

Cre-lox construction of the *rad9-M50A-c3xHA S. pombe* strain was later undertaken by Dr. Thomas Caspari for utilisation in comparative experiments with the *rad9-M50L-c3xHA S. pombe* strain, constructed by the author, to ascertain whether or not the Rad9-S protein variant is an alternative translation product at the Methionine 50 AUG codon initiation site.

[In this context, the *rad9-M50A-c3xHA* strain served as an experimental control to accommodate the documented phenomenon that the *S. pombe* organism can utilise the CUG codon (encoding leucine) as an alternative translation start codon substitute for the normal AUG methionine codon under certain conditions]

NOTE: Other truncated Rad9 protein variants derived from limited-proteolytic processing of the full-length Rad9 protein and/or the potential alternative translation site-type truncated Rad9 protein isoforms may also exist.

Fig 3.3: Overview of the Adapted Cre-RMCE System



The *rad9*-deleted base-strain (*Δrad9*) contains the loxP-*ura4⁺*-loxM3 cassette integrated at the endogenous *rad9* gene locus situated within chromosome 1 (Fig A).

The pAW8 donor plasmid construct contains the PCR-modified *rad9* allele, which is cloned within the loxP- and loxM3- flanked MPS via complementary SphI and SpeI restriction site digestion and ligation (Fig A).

The pAW8 donor plasmid construct also contains the *S. pombe* CRE gene, which encodes the recombinase enzyme that catalyses the “cre-lox” cassette exchange transformation reaction, is situated downstream from the *S. pombe* Pnmt promoter and *rad50*-intron1 spacer sequences and upstream from the *S. pombe* Tnmt terminator sequence – the direction of gene transcription is indicated via the white arrow (Fig A).

Transformation of the base-strain with the appropriate pAW8 donor plasmid construct (Fig A) results in Cre-Recombinase-Mediated-Cassette-Exchange (Cre-RMCE) of the PCR-modified *rad9* allele at the endogenous *rad9* gene locus situated within chromosome 1 and consequential generation of the experimental *S. pombe* strain whose cells exclusively express the modified Rad9 protein variant (Fig B).

The heterospecific nature of the wild-type loxP and mutated loxM3 recombination sites ensures that the inserted exchange product, once formed within the transformed base-strain, is stable and prevents the occurrence of unstable self-recombination events which would otherwise result in deleted removal and/or translocation of the PCR-engineered *rad9* allele cassette insert within the transformed base-strain.

The *ura4⁺* gene encodes an enzyme involved in uracil biosynthesis (orotidine monophosphate dehydrogenase) which converts 5-Fluoro-orotic acid (5-FOA) to 5-Fluorouracil – which is a suicide substrate that inhibits the enzyme thymidylate synthetase, thereby blocking DNA replication as a consequence of impaired dTTP synthesis that results in cell death.

Thus, only transformed base-strain cells are able to grow on YEA agar containing 5-FOA, due to the fact they lack the *ura4⁺* gene – which serves as a positive selection marker for the exclusion of colonies which arise from untransformed base-strain cells.

3.2.1 Construction and Genotypic Verification of the “Cre-Lox” Δ rad9 Base-Strain

The loxP-*ura4*⁺-loxM3 exchange cassette fragment was generated via endogenous *rad9* gene locus BPS site-directed PCR-modification of the pAW1 non-essential gene replacement plasmid and utilised to transform the *S. pombe* strain 804 (genotype: *ura4-D18 leu1-32 ade6-M210 h*⁻) – via the methodologies described in detail in Section 2.5, pp.171-191.

The orientation of the resultant *rad9* gene locus-integrated exchange cassette fragment (incorporated within chromosome 1 of the transformed *S. pombe* strain 804) was such that the loxP sequence was situated 181 nucleotides upstream of the *rad9* gene start codon at position 1714271, whilst the loxM3 sequence was situated 136 nucleotides downstream of the *rad9* gene stop codon at position 1715762 respectively (Fig 3.4, pp.296-297).

The genotype of the constructed base-strain (designated strain no.1339) was verified via comparative PCR analyses performed with selective pairs of *rad9*- and *ura4*- targeting primer probes on genomic DNA extracts acquired from the “wild-type” strain 804 and the *rad9::ura4*⁺-deleted strain 917 (Fig 3.4, p.296) – whose respective genotypes are;

804 genotype = *ura4-D18 leu1-32 ade6-M210 h*⁻

917 genotype = *rad9::ura4*⁺ *ura4-D18 leu1-32 ade6-M210 h*⁻

1339 (“base-strain”) genotype = *rad9::loxP-ura4*⁺-*loxM3 ura4-D18 leu1-32 ade6-M210 h*⁻

Comparative PCR genotyping analyses performed with the primer probe pair Ura4-1 and Ura4-4 resulted in the generation of detectable products from crude genomic DNA extracts of all three strains which indicated that they all contained the *ura4* gene (Fig 3.4, pp.296-297).

Detection of a significantly weaker PCR product band, acquired from the *S. pombe* strain 804 genomic DNA extract, was attributed to sub-optimal annealing of the Ura4-1 and Ura4-4 primer probe pair to the altered base-sequence of the *ura4-D18* gene – which is a site-directed mutagenised modification of the “wild-type” *ura4*⁺ gene that encodes a catalytically-inactive orotidine monophosphate dehydrogenase enzyme (Fig 3.4, pp.296-297).

Comparative PCR genotyping analyses performed with the primer probe pair Rad9-5 and Rad9-9 resulted in the detection of a very strong product band acquired from the *S. pombe* strain 804 genomic DNA extract, that was not detected in the genomic DNA extracts isolated from the *rad9*-deleted *S. pombe* strains 917 and 1339 (Fig 3.4, pp.296-297) – which verified the presence of the *rad9* gene in the “wild-type” *S. pombe* strain 804 and confirmed the absence of the *rad9* gene within the *S. pombe* strains 917 and 1339.

Detection of a strong PCR product band via primer probe pair Rad9-9 and Rad9-10 analysis of crude genomic DNA extract acquired from the “wild-type” *S. pombe* strain 804 confirmed the presence of the *rad9* gene (Fig 3.4, pp.296-297).

PCR primer probe pair Rad9-9 and Rad9-10 analysis of the crude genomic DNA extract acquired from the *S. pombe* strain 917 yielded two thinner bands of higher base-pair content than the *rad9* gene which was attributed to sub-optimal primer annealing to segments of residual complementary *rad9* base sequence that were present as a consequence of the method utilised to construct this strain – in which the *ura4*⁺ gene had been inserted directly within the endogenous *rad9* gene locus to prevent its functional expression (Fig 3.4, pp.296-297).

Lack of a detectable product band in the case of the PCR primer probe pair Rad9-9 and Rad9-10 analysis of the crude genomic DNA extract acquired from the constructed cre-lox base-strain 1339, was attributed to the successful integration of the loxP-ura4⁺-loxM3 at the endogenous *rad9* gene locus and consequential deletion of the complementary *rad9* base sequences for primer annealing (Fig 3.4, pp.296-297).

PCR primer probe pair Ura4-1 and Rad9-10 and Ura4-4 and Rad9-10 analyses of the crude genomic DNA extract acquired from the “wild-type” *S. pombe* strain 804 failed to yield any product bands, which was attributed to the fact that the respective *rad9* and mutated *ura4-D18* genes are isolated from each other (ie not situated in adjacent proximity) within the genotype of this strain and the mutated *ura4-D18* gene contains an altered base-sequence which prevents optimal complementary annealing of the Ura4-1 and Ura4-4 primers (Fig 3.4, pp.296-297).

PCR primer probe pair Ura4-1 and Rad9-10 analysis of the crude genomic DNA extracts acquired from the *rad9*-deleted *S. pombe* strains 917 and 1339 yielded single band products, which was attributed to the presence of complementary *ura4*⁺ gene primer-annealing base-sequences within the genetic constructs of these strains (Fig 3.4, pp.296-297).

PCR primer probe pair Ura4-4 and Rad9-10 analysis of the crude genomic DNA acquired from the *rad9*-deleted *S. pombe* strains 917 and 1339 yielded a single band product in the case of *S. pombe* 917, whilst no product was detected in the case of *S. pombe* strain 1339 (Fig 3.4, pp.296-297).

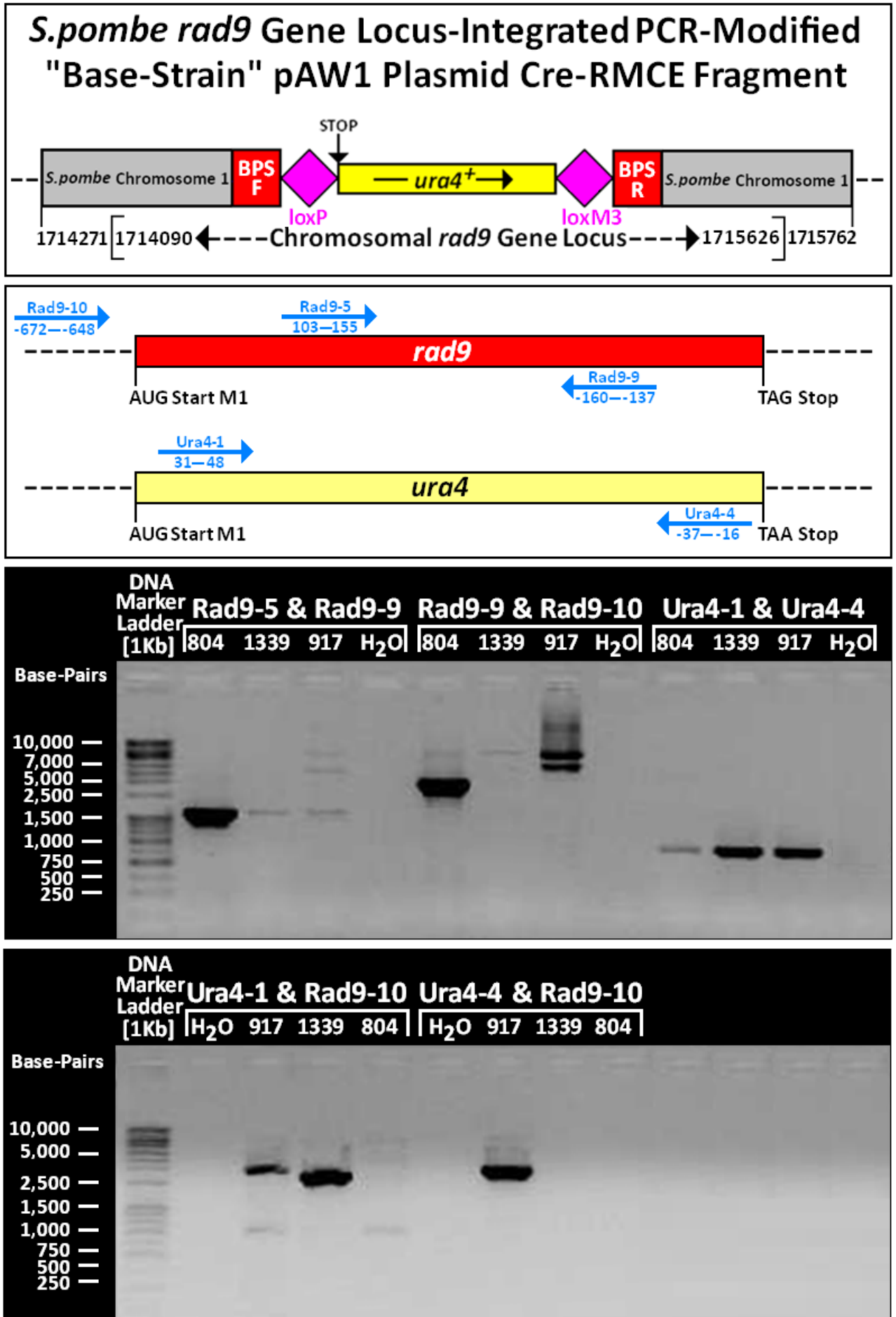
In the case of the *S. pombe* strain 917 genomic construct, the *ura4*⁺ gene is inserted directly within the endogenous *rad9* gene locus to prevent its functional expression which enables complementary Rad9-10 and Ura4-4 primer annealing and consequential formation of a PCR product (Fig 3.4, pp. 296-297).

But in the case of the cre-lox *S. pombe* base-strain 1339 genomic construct, the *ura4⁺* gene is situated with a cre-lox exchange cassette flanked by complementary *rad9* gene BPS, loxP and loxM3 which is inserted at the endogenous *rad9* gene locus on chromosome 1 (Fig 3.4, pp.296-297).

Consequently, no PCR product is formed with the primer probe pair Rad9-10 and Ura4-4 due to the deletion of the Rad9-10 primer-targeted complementary annealing base-sequence in the cre-lox base-strain construct (Fig 3.4, pp.296-297).

Taken together, these comparative PCR genotyping data confirmed that the genetic construction of the *rad9*-deleted “cre-lox” base-strain (strain no. 1339) was correct and contained the exchange cassette (loxP-*ura4⁺*-loxM3) integrated at the endogenous *rad9* gene locus situated within chromosome 1 (Fig 3.4, pp.296-297).

Fig 3.4: *Δrad9* “Cre-Lox Base-Strain” Genotype Verification



A summarised structural map of the *loxP-ura4⁺-loxM3* integrated at the endogenous *S. pombe rad9* gene locus within chromosome 1 is illustrated in the top figure.

[NOTE: Refer to appendix 2.11.4, p.270 for DNA sequence details of the *rad9* gene locus-integrated *loxP-ura4⁺-loxM3* pAW1 fragment]

The base sequence-complementary annealing sites of the *rad9* and *ura4⁺* gene-targeting primers are illustrated in the middle figure:

Rad9-5 binds within the *rad9* gene at 103 base-pairs downstream from the translational AUG start-codon of the first methionine.

Rad9-9 binds with the *rad9* gene -137 base-pairs upstream from the TAG stop codon.

Rad9-10 binds -648 base-pairs upstream from the translational AUG start-codon of the first methionine encoded by the *rad9* gene.

Ura4-1 binds within the *ura4⁺* gene 31 bases downstream from the translational AUG start-codon of the first methionine.

Ura4-4 binds within the *ura4⁺* gene 16 bases upstream from the TAA stop codon.

[NOTE: Refer to appendix 2.11.3, p.269 for details of the PCR primer sequences]

The acquired genotypic data for each PCR primer probe pair combination is provided in the bottom two figures.

H₂O = Ultra-pure millipore water (negative PCR control)

804 = Genomic DNA extract from the “wild-type”
S. pombe strain – genotype: *ura4-D18 leu1-32 ade6-M210 h⁻*

917 = Genomic DNA extract from *rad9::ura4⁺* gene-deleted
S. pombe strain – genotype: *rad9::ura4⁺ ura4-D18 leu1-32 ade6-M210 h⁻*

1339 = Genomic DNA extract from constructed *rad9::loxP-ura4⁺-loxM3* *S. pombe* “Cre-Lox”
“Base-Strain” – genotype: *rad9::loxP-ura4⁺-loxM3 ura4-D18 leu1-32 ade6-M210 h⁻*

Crude genomic DNA extracts, prepared from overnight 30°C YEA broth cultures of the respective *S. pombe* strains, were utilised as PCR templates in comparative genotyping assays with the primer probe pairs indicated.

Comparative 1.0% TBE agarose gel (0.5µg/ml ethidium bromide) gel analysis was performed on 10 µL loaded samples (each sample comprised a 5µL aliquot of the crude PCR product combined with 5µL of 2x DNA loading dye buffer – detailed in Section 2.2.1, p.162)

[Total genomic DNA extract preparation, PCR and agarose gel analysis methodologies are detailed in Section 2.2.1, p.162, Section 2.4, pp.169-170; Section 2.6.2, p.192]

3.2.2 Construction and Restriction Digest Verification of the pAW8

Donor Plasmid Set

The full-length untagged *rad9* allele cassette insert was constructed via a single PCR reaction with a 5'-flanking forward primer which contained the SphI restriction site (Rad9-S5) and a 3'-flanking reverse primer which contained the SpeI restriction site (Rad9-S6), utilising genomic DNA isolated from the "wild-type" *S. pombe* strain 804 (genotype: *ura4-D18 leu1-32 ade6-M210 h⁻*) – Fig 3.5, p.300.

The full-length C-terminal HA-tagged *rad9* allele cassette was constructed via a single PCR reaction with a 5'-flanking forward primer which contained the SphI restriction site (Rad9-S5) and a 3'-flanking reverse primer which contained the SpeI restriction site (Rad9-S8), utilising genomic DNA isolated from the "wild-type" *S. pombe* strain 150 (genotype: *rad9-c3xHA kan^{MX6} ura4-D18 leu1-32 ade6-M210 h⁻*) – Fig 3.6, p.301.

Mutated C-terminal HA-tagged *rad9* alleles were constructed via a fusion PCR protocol (described in detail in Section 2.5, p.176; Fig 2.6, p.176) utilising genomic DNA isolated from *S. pombe* strain 150 with two PCR primer sets (Figs 3.7-3.12, pp.302-307).

- (i) A 5'-flanking forward primer which contained the SphI restriction site (Rad9-S5) with the mutant reverse primer.
- (ii) A 3'-flanking reverse primer which contained the SpeI restriction site (Rad9-S8) with the mutant forward primer.

The two mutant primers also contained complementary overlapping annealing sequences which accommodated the desired modification to enable fusion of the initial products in a subsequent PCR reaction.

The resultant final fusion PCR product was then amplified, utilising the 5'-flanking forward primer (Rad9-S5) and 3'-flanking reverse primer (Rad9-S8).

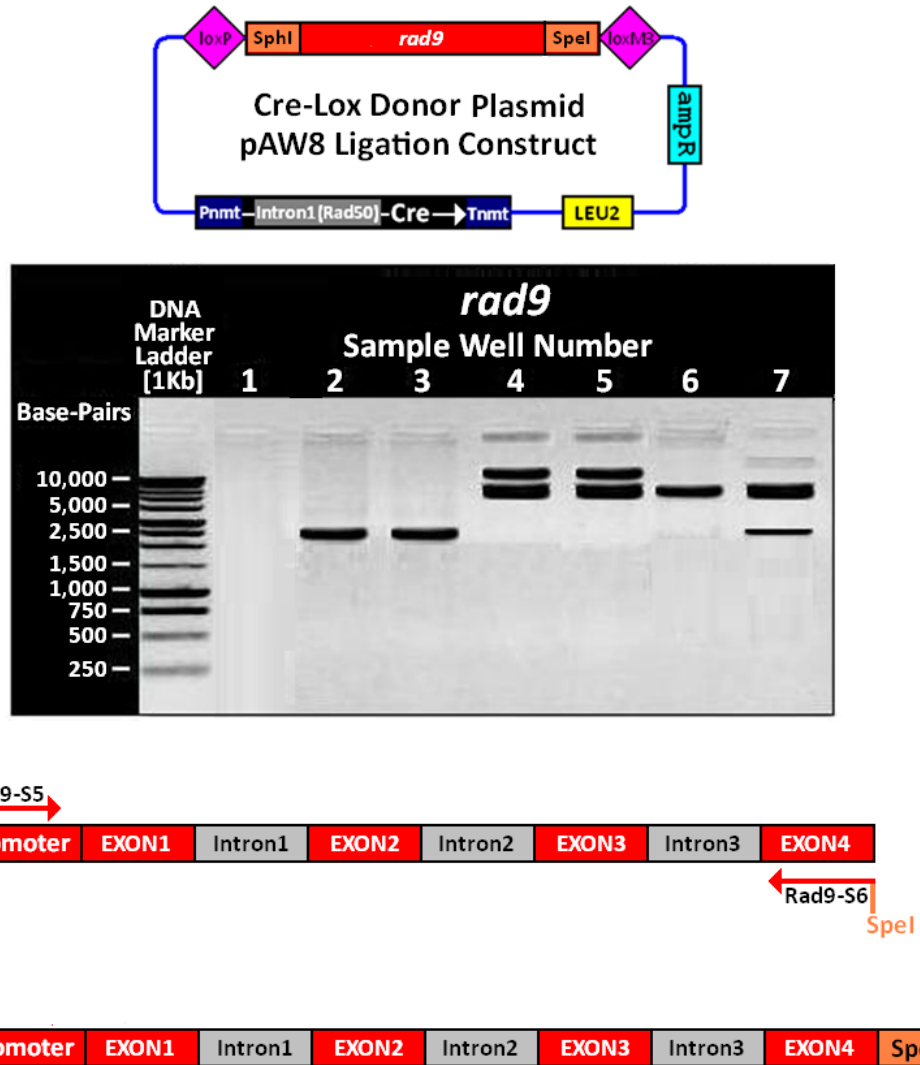
The promoter sequence of 181 nucleotides between loxP and the appropriate translational start codon (ATG1, ATG50, ATG74, ATG312 or ATG358) was restored in these PCR-generated *rad9* allele cassette inserts.

The prepared *rad9* allele cassette inserts were then cloned into the cre-lox pAW8 donor plasmid, via complementary SphI and SpeI restriction site digestion and ligation reactions (described in detail in Section 2.5.2, pp.179-187).

Comparative undigested and SphI/SpeI-digested PCR product, “empty” pAW8 plasmid and ligated pAW8 plasmid construct samples were then prepared and analysed on 1% (w/v) TBE-agarose gels (which contained 0.5µg/ml ethidium bromide) – as per the methodologies described in detail in Section 2.5.2.5, pp.186-187.

The resultant data verified that construction of the required cre-lox pAW8 plasmid set had been accomplished and that the SphI and SpeI restriction enzymes utilised did not cleave at any internal sites within the *rad9* alleles of the PCR-generated pAW8 donor plasmid cassette inserts (Figs 3.5-3.12, pp.300-307).

Fig 3.5: pAW8-rad9 Plasmid Construction

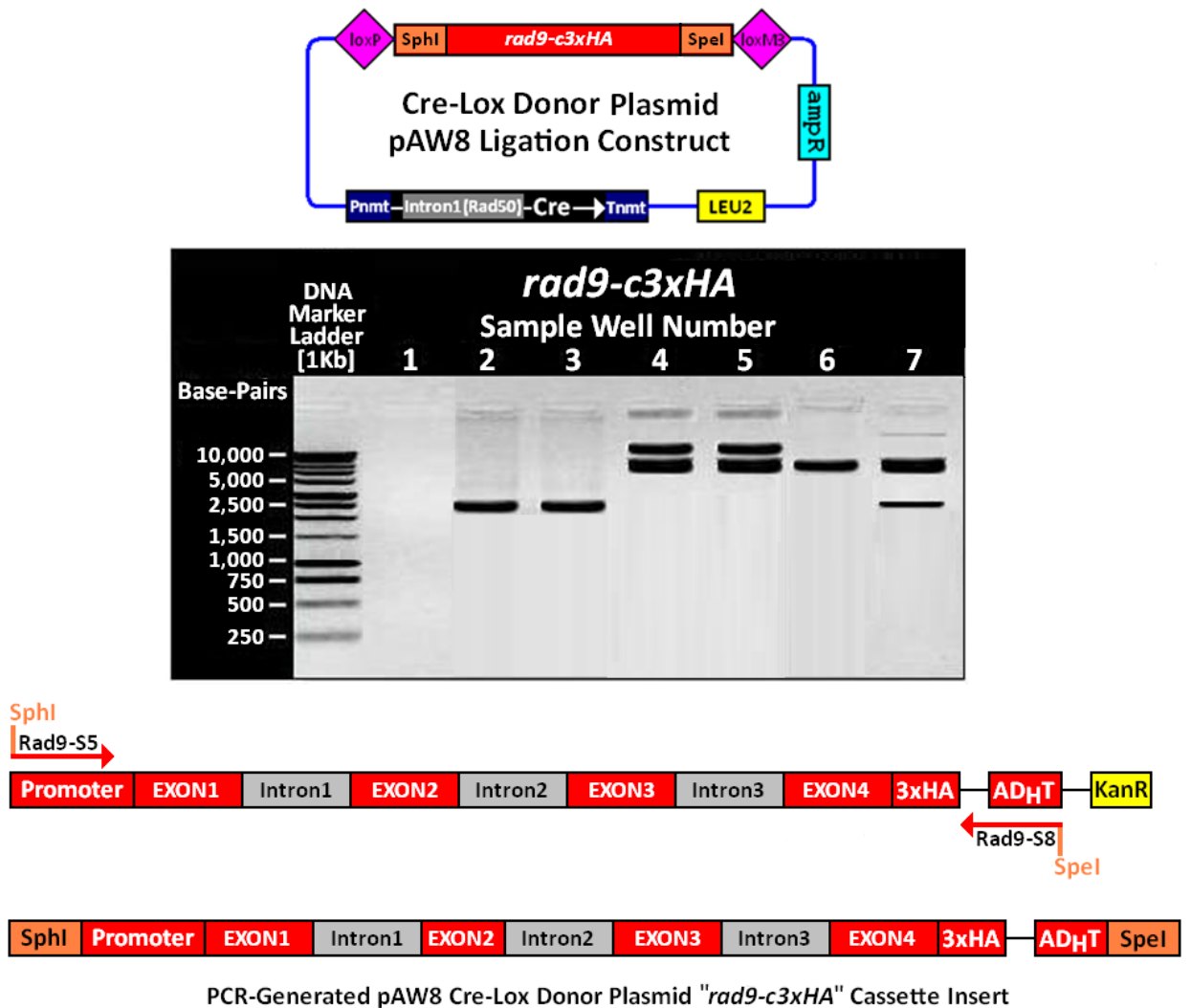


PCR-Generated pAW8 Cre-Lox Donor Plasmid "rad9" Cassette Insert

- 1 = Millipore water with PCR primers Rad9-S5 and Rad9-S6 (negative contamination PCR control)
- 2 = "Wild-type" *rad9* (*S. pombe* strain 804) genomic DNA with Rad9-S5 and Rad9-S6 PCR primers
- 3 = Resultant Rad9-S5 and Rad9-S6 PCR primer product cleaved with SpeI and SphI restriction enzymes
- 4 = "Empty" pAW8 "cre-lox" donor plasmid DNA (uncleaved)
- 5 = Ligated pAW8-*rad9* donor plasmid DNA construct (uncleaved)
- 6 = "Empty" pAW8 "cre-lox" donor plasmid DNA (SpeI and SphI restriction enzyme digested)
- 7 = Ligated pAW8-*rad9* donor plasmid DNA construct (SpeI and SphI restriction enzyme digested)

Comparative 1.0% TBE agarose gel (0.5µg/ml ethidium bromide) gel analysis was performed with 20µL loaded sample aliquots.

Fig 3.6: pAW8-*rad9-c3xHA* Plasmid Construction

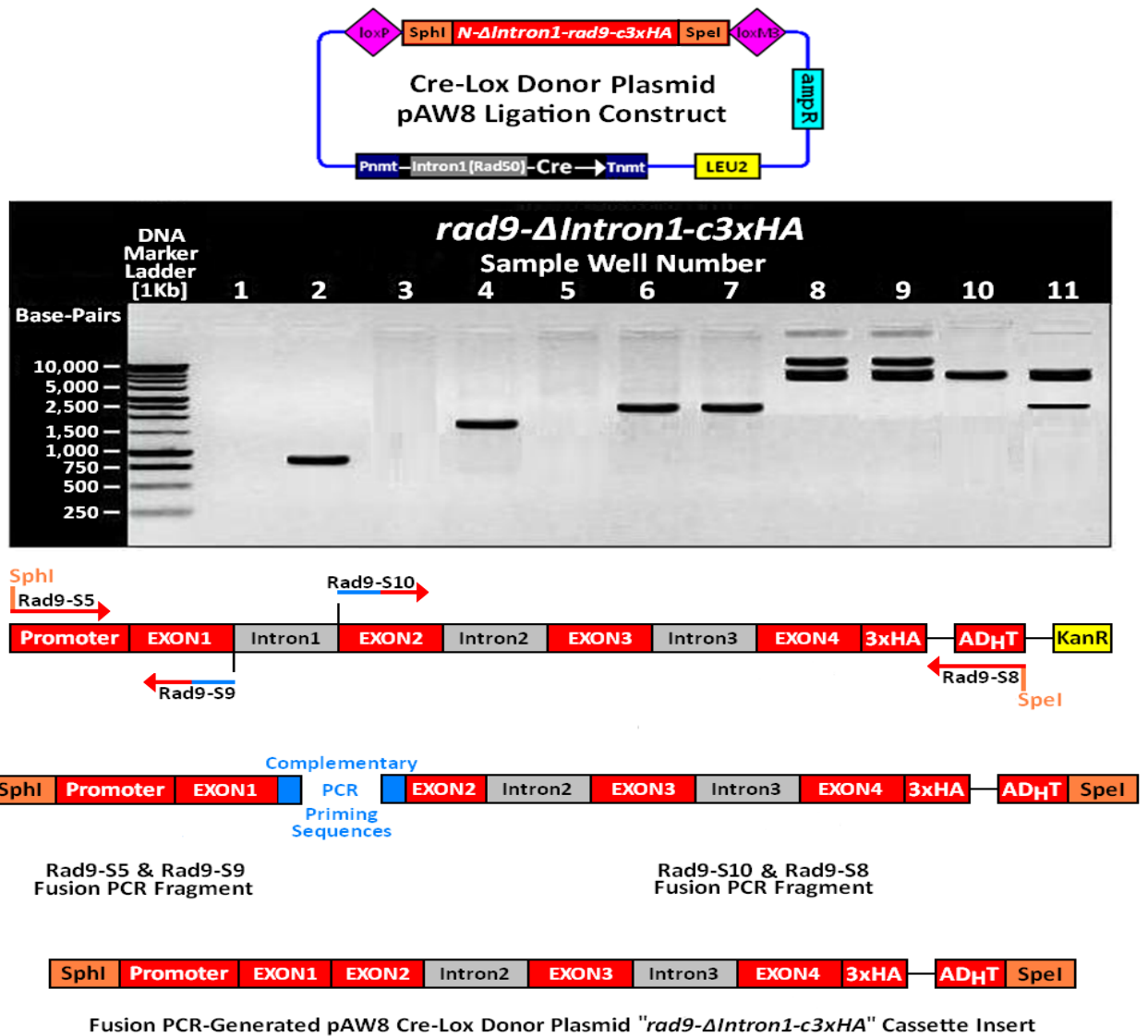


PCR-Generated pAW8 Cre-Lox Donor Plasmid "*rad9-c3xHA*" Cassette Insert

- 1 = Millipore water with PCR primers Rad9-S5 and Rad9-S8 (negative contamination PCR control)
- 2 = *rad9-c3xHA* (*S. pombe* strain 150) genomic DNA with Rad9-S5 and Rad9-S8 PCR primers
- 3 = Resultant Rad9-S5 and Rad9-S8 PCR primer product cleaved with *SpeI* and *SphI* restriction enzymes
- 4 = "Empty" pAW8 "cre-lox" donor plasmid DNA (uncleaved)
- 5 = Ligated pAW8-*rad9-c3xHA* donor plasmid DNA construct (uncleaved)
- 6 = "Empty" pAW8 "cre-lox" donor plasmid DNA (*SpeI* and *SphI* restriction enzyme digested)
- 7 = Ligated pAW8-*rad9-c3xHA* donor plasmid DNA construct (*SpeI* and *SphI* restriction enzyme digested)

Comparative 1.0% TBE agarose gel (0.5µg/ml ethidium bromide) gel analysis was performed with 20µL loaded sample aliquots.

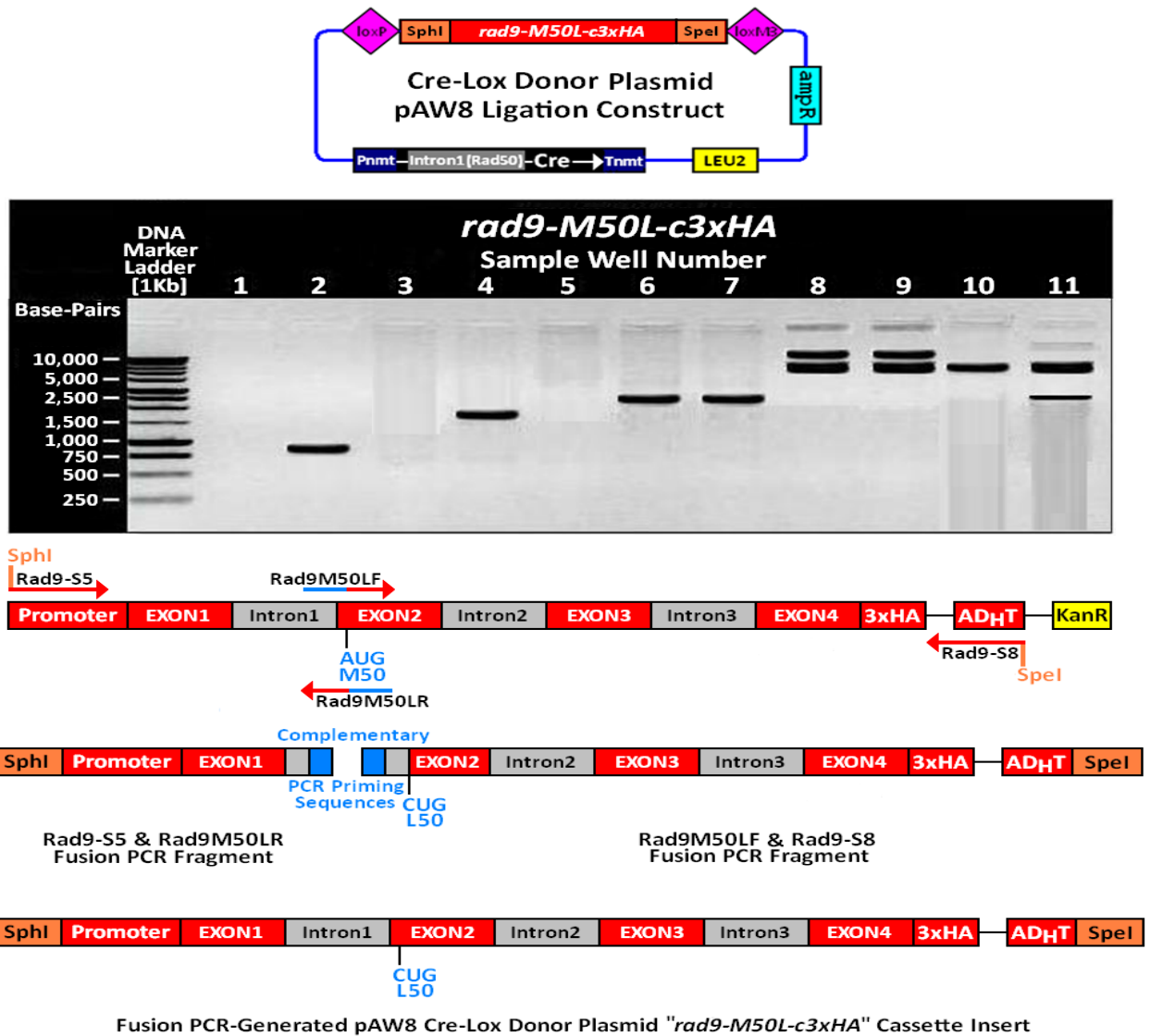
Fig 3.7: pAW8-*rad9-ΔIntron1-c3xHA* Plasmid Construction



- 1 = Millipore water with PCR primers Rad9-S5 and Rad9-S9 (negative contamination PCR control)
- 2 = *rad9-c3xHA* (*S. pombe* strain 150) genomic DNA with Rad9-S5 and Rad9-S9 PCR primer product
- 3 = Millipore water with PCR Primers Rad9-S8 and Rad9-S10 (negative contamination PCR control)
- 4 = *rad9-c3xHA* (*S. pombe* strain 150) genomic DNA with Rad9-S8 and Rad9-S10 PCR primer product
- 5 = Millipore water and PCR master-mix only (negative fusion PCR control)
- 6 = PCR product from Rad9-S5–Rad9-S9 and Rad9-S8–Rad9-S10 PCR fragments (unligated)
- 7 = PCR product from Rad9-S5–Rad9-S9 and Rad9-S8–Rad9-S10 PCR fragments (SpeI and SphI digest)
- 8 = “Empty” pAW8 “cre-lox” donor plasmid DNA (unligated)
- 9 = Ligated pAW8-*rad9-ΔIntron1-c3xHA* donor plasmid DNA construct (unligated)
- 10 = “Empty” pAW8 “cre-lox” donor plasmid DNA (SpeI and SphI digest)
- 11 = Ligated pAW8-*rad9-ΔIntron1-c3xHA* donor plasmid DNA construct (SpeI and SphI digest)

Comparative 1.0% TBE agarose gel (0.5μg/ml ethidium bromide) gel analysis was performed with 20μL loaded sample aliquots.

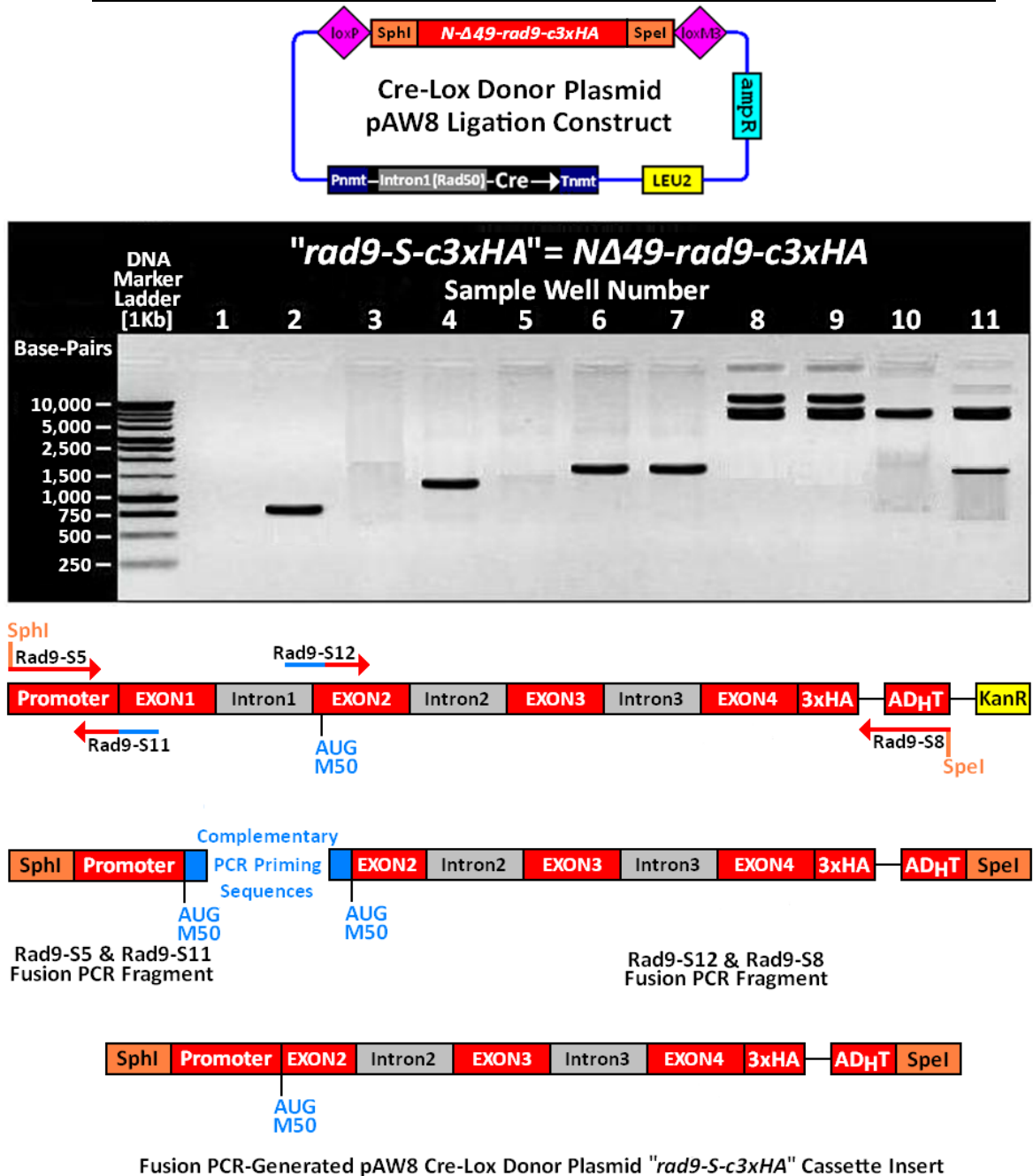
Fig 3.8: pAW8-*rad9-M50L-c3xHA* Plasmid Construction



- 1 = Millipore water with PCR primers Rad9-S5 and Rad9-M50LR (negative contamination PCR control)
- 2 = *rad9-c3xHA* (*S. pombe* strain 150) genomic DNA with Rad9-S5 and Rad9-M50LR PCR primer product
- 3 = Millipore water with PCR primers Rad9-S8 and Rad9-M50LF (negative contamination PCR control)
- 4 = *rad9-c3xHA* (*S. pombe* strain 150) genomic DNA with Rad9-S8 and Rad9-M50LF PCR primer product
- 5 = Millipore water and PCR master-mix only (negative fusion PCR control)
- 6 = PCR product from Rad9-S5–Rad9-M50LR and Rad9-S8–Rad9-M50LF PCR fragments (uncleaved)
- 7 = PCR product from Rad9-S5–Rad9-M50LR & Rad9-S8–Rad9-M50LF PCR fragments (SpeI/SphI digest)
- 8 = “Empty” pAW8 “Cre-Lox” donor plasmid DNA (uncleaved)
- 9 = Ligated pAW8-*rad9-M50Lc3xHA* donor plasmid DNA construct (uncleaved)
- 10 = “Empty” pAW8 “Cre-Lox” donor plasmid DNA (SpeI and SphI digest)
- 11 = Ligated pAW8-*rad9-M50L-c3xHA* donor plasmid DNA construct (SpeI and SphI digest)

Comparative 1.0% TBE agarose gel (0.5µg/ml ethidium bromide) gel analysis was performed with 20µL loaded sample aliquots.

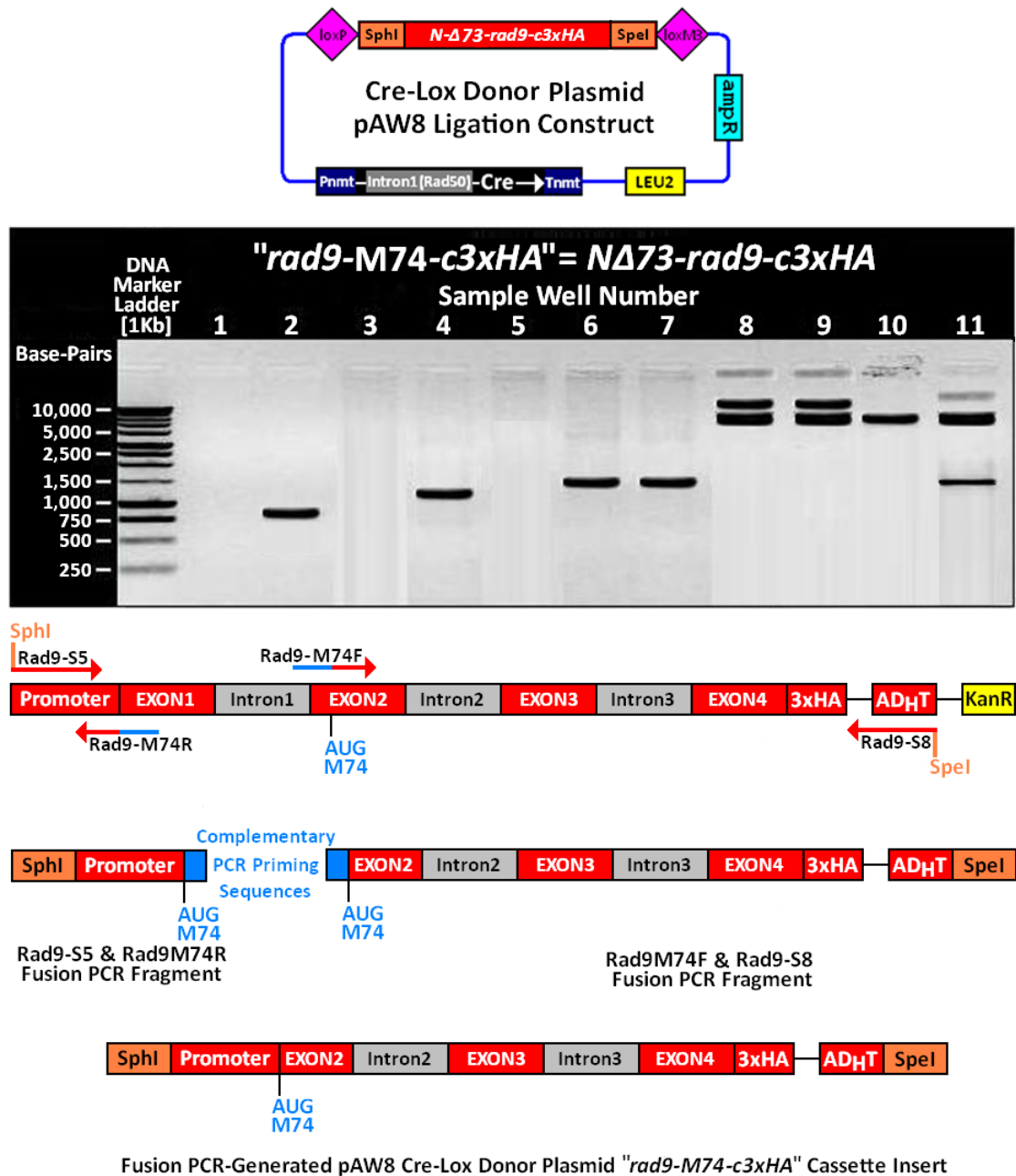
Fig 3.9: pAW8-*NΔ49-rad9-c3xHA* Plasmid Construction



- 1 = Millipore water with PCR primers Rad9-S5 and Rad9-S12 (negative contamination PCR control)
- 2 = *rad9-c3xHA* (*S. pombe* strain 150) genomic DNA with Rad9-S5 and Rad9-S12 PCR primer product
- 3 = Millipore water with PCR primers Rad9-S8 and Rad9-S11 (negative contamination PCR control)
- 4 = *rad9-c3xHA* (*S. pombe* strain 150) genomic DNA with Rad9-S8 and Rad9-S11 PCR primer product
- 5 = Millipore water and PCR master-mix only (negative fusion PCR control)
- 6 = PCR product from Rad9-S5–Rad9-S12 and Rad9-S8–Rad9-S11 PCR fragments (uncleaved)
- 7 = PCR product from Rad9-S5–Rad9-S12 & Rad9-S8–Rad9-S11 PCR fragments (SpeI/SphI digest)
- 8 = “Empty” pAW8 “cre-lox” donor plasmid DNA (uncleaved)
- 9 = Ligated pAW8-*NΔ49-rad9-c3xHA* donor plasmid DNA construct (uncleaved)
- 10 = “Empty” pAW8 “cre-lox” donor plasmid DNA (SpeI and SphI digest)
- 11 = Ligated pAW8- *NΔ49-rad9-c3xHA* donor plasmid DNA construct (SpeI and SphI digest)

Comparative 1.0% TBE agarose gel (0.5μg/ml ethidium bromide) gel analysis was performed with 20μL loaded sample aliquots.

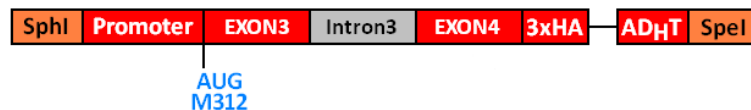
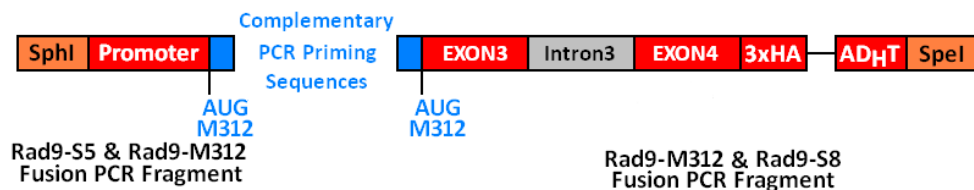
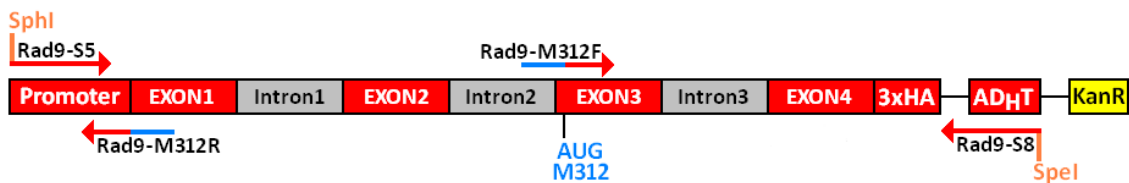
Fig 3.10: pAW8-*NΔ73-rad9-c3xHA* Plasmid Construction



- 1 = Millipore water with PCR primers Rad9-S5 and Rad9-M74R (negative contamination PCR control)
- 2 = *rad9-c3xHA* (*S. pombe* strain 150) genomic DNA with Rad9-S5 and Rad9-M74R PCR primer product
- 3 = Millipore water with PCR primers Rad9-S8 and Rad9-M74F (negative contamination PCR control)
- 4 = *rad9-c3xHA* (*S. pombe* strain 150) genomic DNA with Rad9-S8 and Rad9-M74F PCR primer product
- 5 = Millipore water and PCR master-mix only (negative fusion PCR control)
- 6 = PCR product from Rad9-S5–Rad9-M74R and Rad9-S8–Rad9-M74F PCR fragments (uncleaved)
- 7 = PCR product from Rad9-S5–Rad9-M74R & Rad9-S8–Rad9-M74F PCR fragments (*SpeI/SphI* digest)
- 8 = "Empty" pAW8 "cre-lox" donor plasmid DNA (uncleaved)
- 9 = Ligated pAW8-*NΔ73-rad9-c3xHA* donor plasmid DNA construct (uncleaved)
- 10 = "Empty" pAW8 "Cre-Lox" donor plasmid DNA (*SpeI* and *SphI* digest)
- 11 = Ligated pAW8- *NΔ73-rad9-c3xHA* donor plasmid DNA construct (*SpeI* and *SphI* digest)

Comparative 1.0% TBE agarose gel (0.5μg/ml ethidium bromide) gel analysis was performed with 20μL loaded sample aliquots.

Fig 3.11: pAW8-*NΔ311-rad9-c3xHA* Plasmid Construction

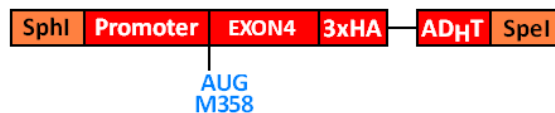
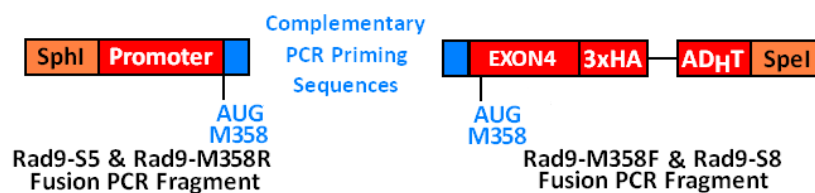
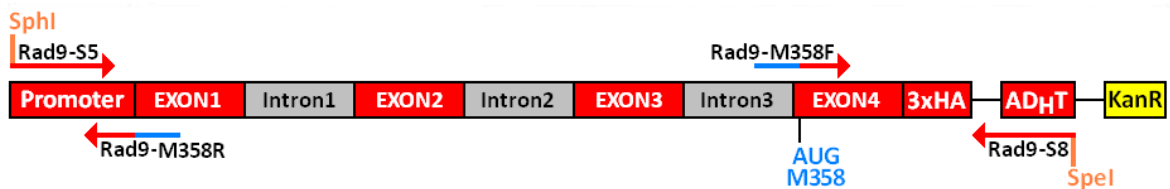
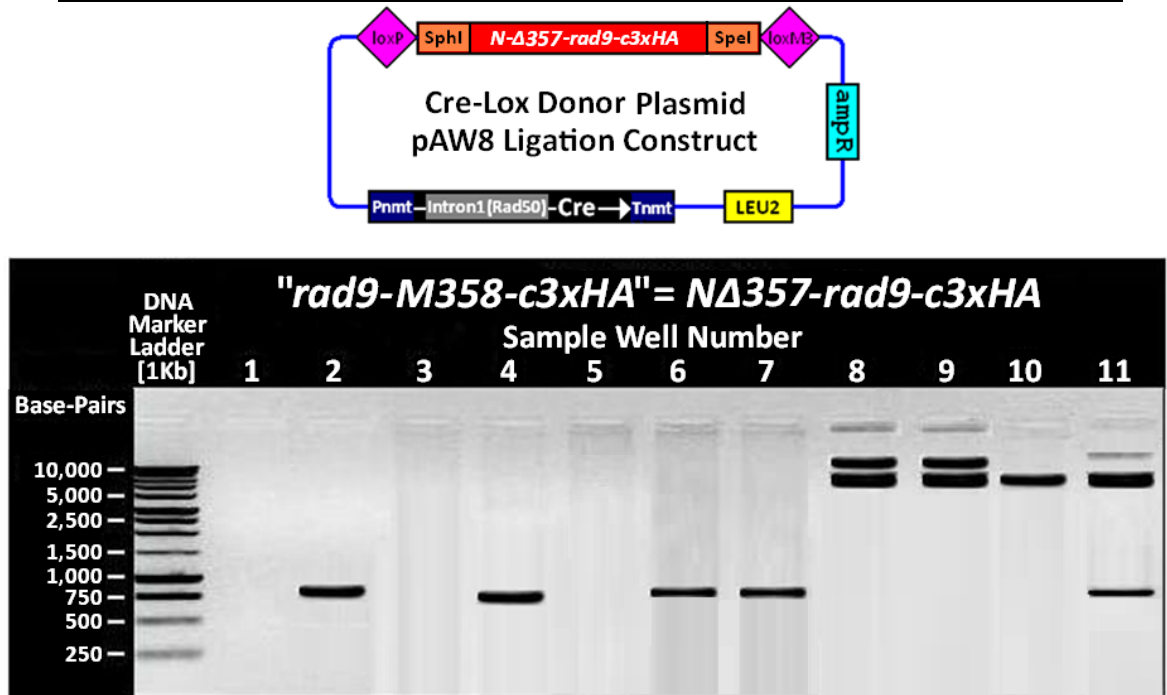


Fusion PCR-Generated pAW8 Cre-Lox Donor Plasmid "*rad9-M312-c3xHA*" Cassette Insert

- 1 = Millipore water with PCR Primers Rad9-S5 and Rad9-M312R (negative contamination PCR control)
- 2 = *rad9-c3xHA* (*S. pombe* strain 150) genomic DNA with Rad9-S5 and Rad9-M312R PCR primer product
- 3 = Millipore water with PCR primers Rad9-S8 and Rad9-M312F (negative contamination PCR control)
- 4 = *rad9-c3xHA* (*S. pombe* strain 150) genomic DNA with Rad9-S8 and Rad9-M312F PCR primer product
- 5 = Millipore water and PCR master-mix only (negative fusion PCR control)
- 6 = PCR product from Rad9-S5–Rad9-M312R and Rad9-S8–Rad9-M312F PCR fragments (uncleaved)
- 7 = PCR product from Rad9-S5–Rad9-M312R & Rad9-S8–Rad9-M312F PCR fragments (SpeI/SphI digest)
- 8 = “Empty” pAW8 “cre-lox” Donor Plasmid DNA (uncleaved)
- 9 = Ligated pAW8-*NΔ311-rad9-c3xHA* donor plasmid DNA construct (uncleaved)
- 10 = “Empty” pAW8 “cre-lox” donor plasmid DNA (SpeI and SphI digest)
- 11 = Ligated pAW8- *NΔ311-rad9-c3xHA* donor plasmid DNA construct (SpeI and SphI digest)

Comparative 1.0% TBE agarose gel (0.5μg/ml ethidium bromide) gel analysis was performed with 20μL loaded sample aliquots.

Fig 3.12: pAW8-*NΔ357-rad9-c3xHA* Plasmid Construction



Fusion PCR-Generated pAW8 Cre-Lox Donor Plasmid "*rad9-M358-c3xHA*" Cassette Insert

- 1 = Millipore water with PCR primers Rad9-S5 and Rad9-M358R (negative contamination PCR control)
- 2 = *rad9-c3xHA* (*S. pombe* strain 150) genomic DNA with Rad9-S5 and Rad9-M358R PCR primer product
- 3 = Millipore water with PCR primers Rad9-S8 and Rad9-M358F (negative contamination PCR control)
- 4 = *rad9-c3xHA* (*S. pombe* strain 150) genomic DNA with Rad9-S8 and Rad9-M358F PCR primer product
- 5 = Millipore water and PCR master-mix only (negative fusion PCR control)
- 6 = PCR product from Rad9-S5–Rad9-M358R and Rad9-S8–Rad9-M358F PCR fragments (uncleaved)
- 7 = PCR product from Rad9-S5–Rad9-M358R & Rad9-S8–Rad9-M358F PCR fragments (SpeI/SphI digest)
- 8 = “Empty” pAW8 “cre-lox” donor plasmid DNA (uncleaved)
- 9 = Ligated pAW8-*NΔ357-rad9-c3xHA* donor plasmid DNA construct (uncleaved)
- 10 = “Empty” pAW8 “cre-lox” donor plasmid DNA (SpeI and SphI digest)
- 11 = Ligated pAW8- *NΔ357-rad9-c3xHA* donor plasmid DNA construct (SpeI and SphI digest)

Comparative 1.0% TBE agarose gel (0.5μg/ml ethidium bromide) gel analysis was performed with 20μL loaded sample aliquots.

3.3 Genotypic and Phenotypic Analyses of the Constructed Strains

The genotype of the “cre-lox” *rad9*-deleted *S. pombe* “base-strain” ($\Delta rad9$), constructed from the wild-type *S. pombe* strain 804 (whose genotype is defined as: *ura4-D18 leu1-32 ade6-M210 h⁻*), is *rad9::loxP-ura4⁺-loxM3 ura4-D18 leu1-32 ade6-M210 h⁻* such that it expresses the “wild-type” *ura4⁺* gene which encodes the normal functional form of an enzyme that is involved in uracil biosynthesis (orotidine monophosphate dehydrogenase) and compensates for the presence of the mutant *ura4-D18* gene which encodes a catalytically-inactive version of this enzyme.

Cells of this “cre-lox”- constructed ($\Delta rad9$) “base-strain” are therefore able to grow on Edingburgh minimal agar medium which does not contain uracil (“EMM minus U”), but die on yeast adenine rich agar medium containing 5-Fluoro-orotic acid (“YEA – 5-FOA”) due to the fact that the expressed functionally-active orotidine monophosphate dehydrogenase enzyme catalyses the conversion of 5-FOA to the “suicide substrate” 5-Fluorouracil (5-FU) which blocks the biosynthesis of 2'-deoxyribothymidine-5'-triphosphate (dTTP), via the inhibition of the enzyme thymidylate synthetase, with consequential depletion of the cellular dTTP pool and inhibition of DNA replication (Fig 3.13, p. 311).

The “generalised genotype” of the “cre-lox” – transformed *S. pombe* base-strain ($\Delta rad9$) cells may be defined as: *rad9::loxP-“rad9X”-loxM3 ura4-D18 leu1-32 ade6-M210 h⁻* (where “*rad9X*” represents a specific PCR-modified/mutant *rad9* allele which is incorporated into the base-strain via Cre-recombinase cassette-mediated exchange of the *ura4⁺* gene that of the modified/mutant *rad9* gene via transformation with the appropriate pAW8 “cre-lox” donor plasmid construct – described previously in Fig 3.3, p.291).

Cells of these $\Delta rad9$ “base-strain” – transformed *S. pombe* strains are therefore unable to grow on the “EMM minus U” agar medium, but retain growth viability on the “YEA – 5FOA” agar medium due to the fact that they only contain the mutant *ura4-D18* gene (Fig 3.13, p.311).

The selection plate phenotype data (Fig 3.13, p.311) and PCR genotype assay (Fig 3.14, p.312), indicated conclusively that the intended “cre-lox”-construction of the required initial set of experimental *S. pombe* strains had been accomplished.

DNA sequencing was also employed to confirm that the “cre-lox” – engineered *S. pombe* strains contained the correct specifically PCR-modified/mutated *rad9* alleles (as per the methodology described previously in Section 2.6.3, pp.193-195).

Comparative Western blot analyses detected equivalent levels of expression of the respective engineered Rad9 protein in the case of the *S. pombe* strains *rad9-c3xHA*, *rad9-(Δ Intron1)-c3xHA*, *rad9-(M50A)-c3xHA*, *rad9-(M50L)-c3xHA* and *N Δ 49-rad9-c3xHA* (“*rad9-S*”-*c3xHA*), but a significant lower level of protein expression in the case of the *S. pombe* strain *N Δ 73-rad9-c3xHA* (Fig 3.15, p.313) – which may be due to suppressed expression and/or enhanced cytological instability of this particular engineered N Δ 73-Rad9 truncated Rad9 protein variant.

Whilst the experimental *S. pombe* strains “cre-lox”-engineered for the exclusive expression of the Rad9 protein truncated variants N- Δ 310-Rad9-c3xHA and N- Δ 357-Rad9-c3xHA contained the correct integrated fusion PCR-modified *rad9*, as verified via PCR genotyping (Fig 3.14, p.312) and DNA sequencing, no expressed protein was detected in the Western blot assay (Fig 3.15, p.313).

This may be due to the fact that expression of these two truncated protein variants is at a very low level within the respective “cre-lox”- engineered *S. pombe* cells which is beyond the detection threshold limit of the Western blot assay.

Alternatively, these particular engineered truncated protein variants may be highly unstable and/or non-functional expression products which are “primed” for rapid proteasomal pathway degradation via specific amino acid residue target-site ubiquitination- and/or sumoylation- type post-translational modifications.

Fig 3.13: Plate Selection of Cre-RMCE-Generated *S.pombe* Strains

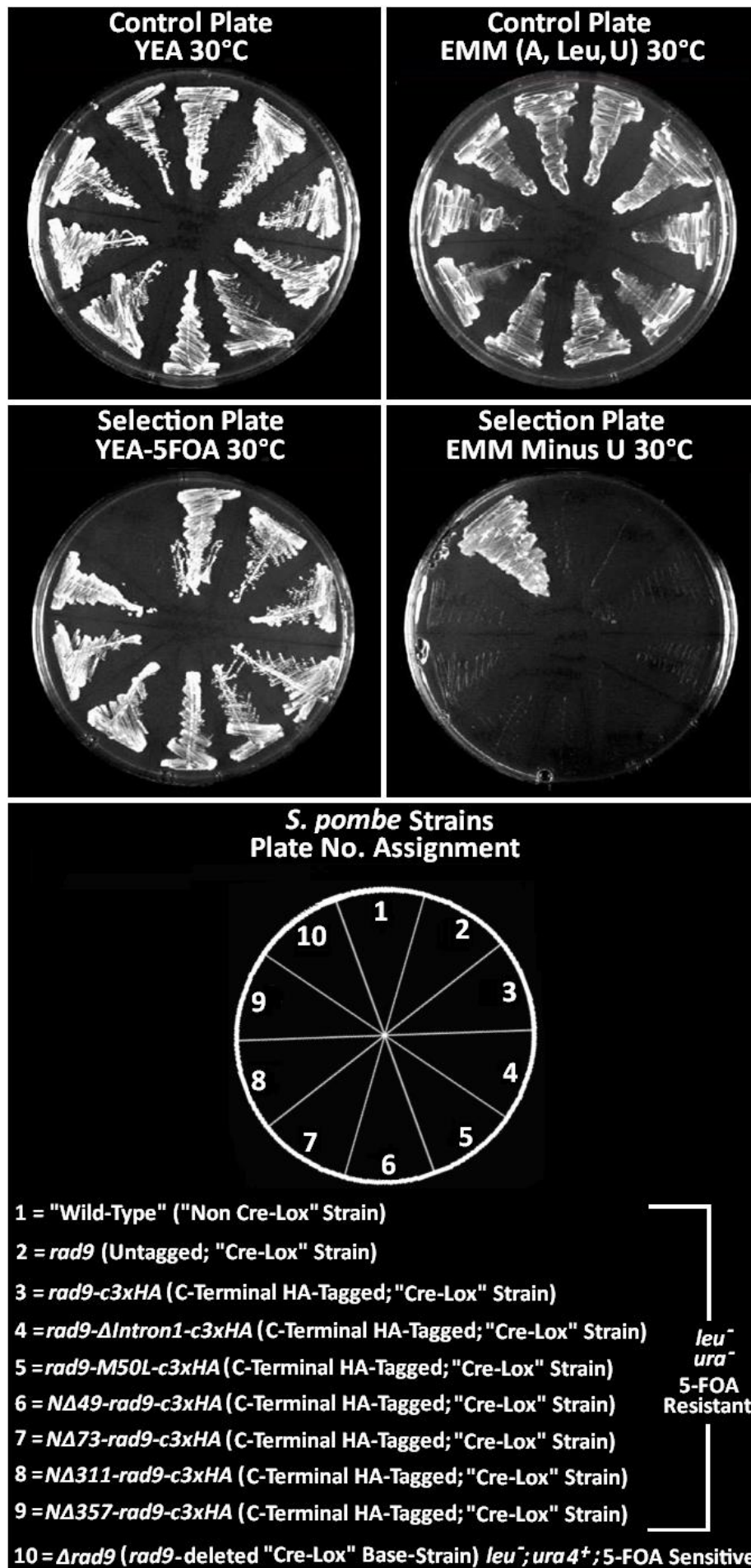
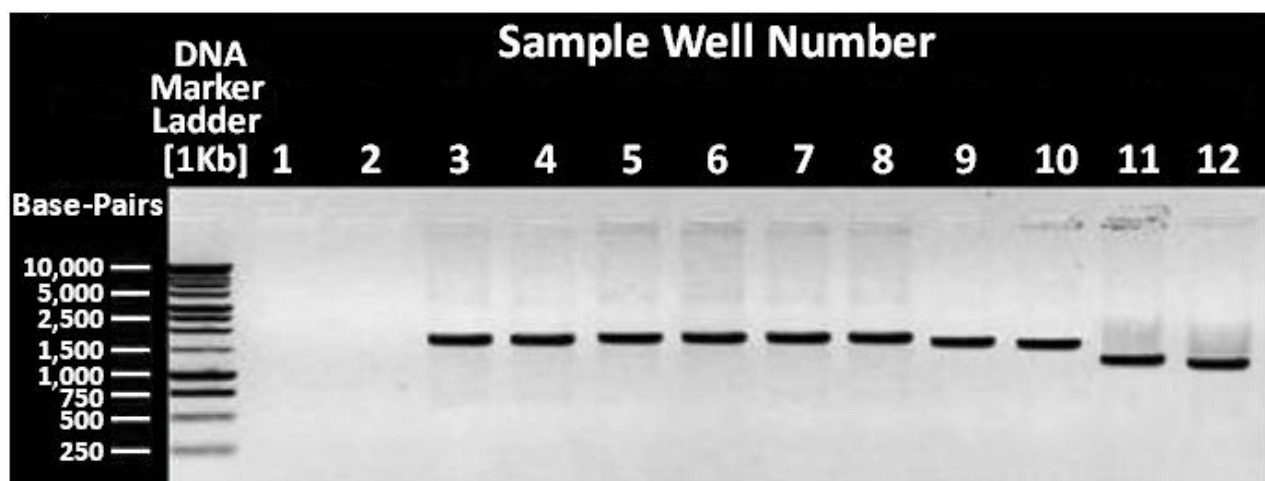


Fig 3.14: Comparative *rad9*-Specific PCR Genotype Analysis



1 = Millipore Water (Negative Contamination PCR Control)

2 = $\Delta rad9$ (*S. pombe* Cre-Lox Base-Strain)

3 = “Wild-Type” Strain 804 *rad9* (~2.2 kBp)

4 = *rad9* (~2.2kBp)

5 = *rad9-c3xHA* (~2.3 kBp)

6 = *rad9- Δ Intron1-c3xHA* (~2.3 kBp)

7 = *rad9-M50A-c3xHA* (~2.3 kBp)

8 = *rad9-M50L-c3xHA* (~2.3 kBp)

9 = *N Δ 49-rad9-c3xHA* (~2.1 kBp)

10 = *N Δ 73-rad9-c3xHA* (~2.09 kBp)

11 = *N Δ 311-rad9-c3xHA* (~1.3kBp)

12 = *N Δ 357-rad9-c3xHA* (~1.2 kBp)

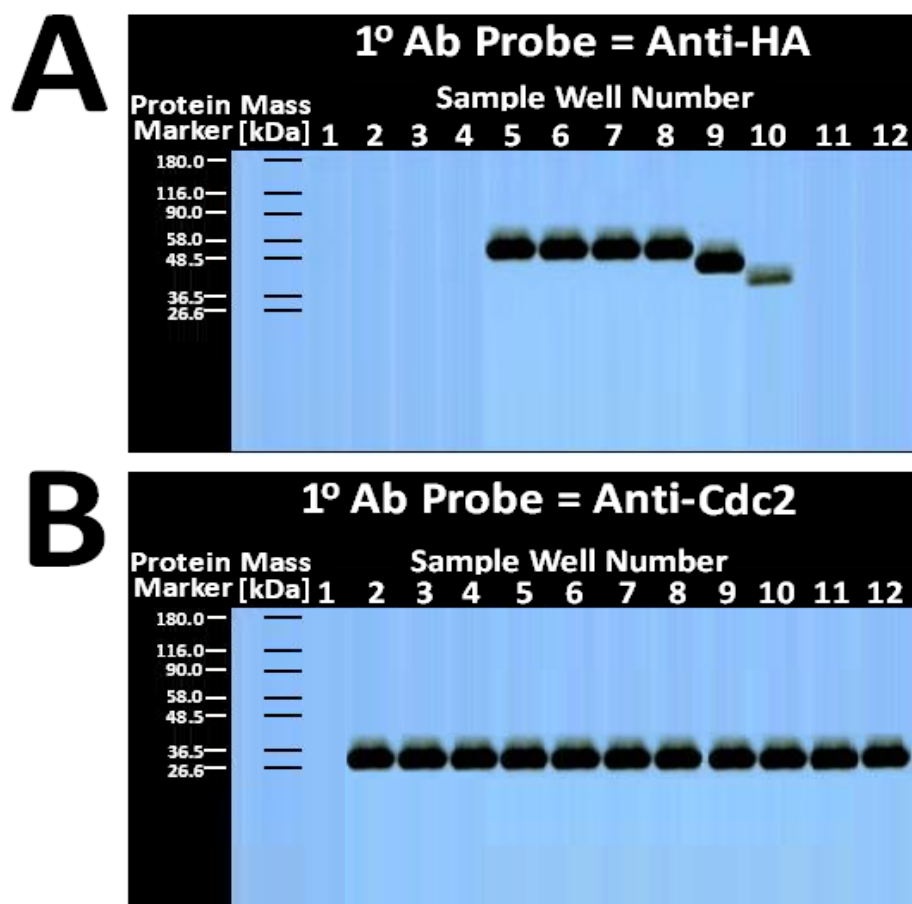
Crude genomic DNA extracts, prepared from overnight 30°C YEA broth cultures of the respective *S. pombe* strains, were utilised as PCR templates for comparative genotyping analyses .

Comparative 1.0% TBE agarose gel (0.5 μ g/ml ethidium bromide) gel analysis was performed on 10 μ L loaded samples (each sample comprised a 5 μ L aliquot of the crude PCR product combined with 5 μ L of 2x DNA loading dye buffer – composition detailed in Section 2.2.1, p.162).

[Total genomic DNA extract preparation, PCR and agarose gel analysis methodologies are detailed in Section 2.2.1, p.162, Section 2.4, pp.169-170; Section 2.6.2.2, p.192]

The expected approximate sizes (kilobase-pairs – kBp) of the respective amplified *rad9* gene PCR products are indicated in brackets.

Fig 3.15: *rad9*-Specific Gene Expression Profile Analysis



1 = Millipore Water (Negative protein detection control)

2 = $\Delta rad9$ (*S. pombe* Cre-Lox base-strain; Negative Rad9 protein detection control)

3 = "Wild-Type" Strain 804 - Expressed Rad9 Protein Mr ~ 50kDa

4 = *rad9* - Expressed Rad9 protein Mr ~ 50kDa

5 = *rad9-c3xHA* - Expressed Rad9 protein Mr ~ 50kDa

6 = *rad9- Δ Intron1-c3xHA* - Expressed Rad9 protein Mr ~ 50kDa

7 = *rad9-M50A-c3xHA* - Expressed Rad9 protein Mr ~ 50kDa

8 = *rad9-M50L-c3xHA* - Expressed Rad9 protein Mr ~ 50kDa

9 = *N Δ 49-rad9-c3xHA* - Expressed Rad9 protein Mr ~ 42kDa

10 = *N Δ 73-rad9-c3xHA* - Expressed Rad9 protein Mr ~ 39kDa

11 = *N Δ 311-rad9-c3xHA* - Expressed Rad9 protein Mr ~ 13kDa

12 = *N Δ 357-rad9-c3xHA* - Expressed Rad9 protein Mr ~ 8kDa

A: Western Blot membrane probed with the anti-HA primary anti-body.

B: Western Blot membrane probed with the anti-Cdc2 primary anti-body.

[Positive protein detection and equivalent protein loading control – Cdc2 Mr ~ 34kDa]

20 μ L sample aliquots of TCA-precipitated total protein extracts (prepared from overnight 30°C YEA broth cultures of each strain) were loaded onto 10% SDS-PAGE gels, run at 120V for 5 hours at room temperature, prior to Western blot analysis.

[Protein sample preparation, SDS-PAGE resolution and Western blot methodologies are detailed in Section 2.8.1, pp.200-202; Section 2.8.4, pp.223-224 and Section 2.8.6, pp.231-233]

The expected molecular mass of each protein was estimated via utilisation of the on-line Scripps Institute software tool Protein Calculator v3.3 (<http://www.scripps.edu/~cdputnam/putcalc.html>).

3.4 In Silico Protein Stability Assessment of the Engineered *S. pombe* Rad9 Protein Variants

Comparative Western blot analyses performed on TCA total protein extracts, acquired from overnight 30°C YEA cell cultures of *S. pombe* strains “Cre-Lox”-engineered for the exclusive expression of the hypothetical truncated variants NΔ310-Rad9-c3xHA and NΔ357-Rad9-c3xHA, failed to detect any translational products (Fig 3.15, p.313).

One plausible explanation for this experimental observation is that these specific truncated Rad9 protein variants are unstable translational products, which retain negligible functional viability and are therefore highly susceptible to proteolytic pathway-targeted degradation.

Protein folding, anti-/pro- aggregation propensity and intrinsic order/disorder relationships are key interactive supra-molecular structural parameters which impinge upon the relative stability, half-life and functional viability of an expressed protein within its localised cytological microenvironment(s) (Banavar J.R. *et al.*, 2007; Chakrobortee S. *et al.*, 2012; Fawzi N.L. *et al.*, 2008a; Fawzi N.L. *et al.*, 2008b; Hoang T.X. *et al.*, 2006; Kulkarni P. *et al.*, 2011; Liu J. *et al.*, 2006; Mohan A. *et al.*, 2009; Morimoto R.I. *et al.*, 2012; Nair S.S. *et al.*, 2011; Sanchez-Ruiz J.M., 2010; Tompa P. and Kovacs D., 2010; Trovato A. *et al.*, 2006; Wang Y. *et al.*, 2009; Xie H. *et al.*, 2007b; Zhang Y. and Calderwood S.K., 2011).

Therefore, comparative *in silico* analyses of the relative proportions of localised intrinsic structural order/disorder regions (Section 3.4.1, pp.315-319), anti-/pro- aggregative functional motifs (Section 3.4.2, pp.320-330) and secondary structural helix, strand and coil motifs (Section 3.4.3, pp.331-353) were performed on the amino acid sequences of the engineered experimental full-length and truncated variant isoforms of the *S. pombe* Rad9 protein (Fig 3.2, p.289) for hypothetical prediction of their respective cytological stabilities and identification of the key common protein structure-stability relationships implicated (Section 3.4.4, pp.354-357).

3.4.1 Intrinsic Structural Disorder Analyses

Comparative metaPrDOS (Ishida K. and Kinoshita K., 2007) analyses of the full-length “wild-type” Rad9 protein with the full-length Rad9-M50A (“M50A”) and Rad9-M50L (“M50L”) mutants indicated that all three polypeptide sequences possessed identical localised regions of intrinsic structural order and a highly significant level of intrinsic structural disorder propensity confined almost exclusively to the C-terminal tail domain (Fig 3.16, p.317).

These *in silico* data observations are consistent with the highly flexible mobile nature of the Rad9 C-terminal tail domain which is postulated to be an essential physico-biochemical functional property that enables it to associatively interact with and modulate the activity of a variety of different proteins implicated in regulatory cell cycle checkpoint-signalling responses (Broustas C.G. and Lieberman H.B., 2012).

Comparative metaPrDOS analyses of the truncated N Δ 49-Rad9 and N Δ 73-Rad9 polypeptide sequences yielded equivalent localised region-specific intrinsic structural order/disorder profiles to that of the “wild-type”, “M50A”- and “M50L”- point-mutant full-length Rad9 polypeptide sequences (Fig 3.17, p.318).

The conserved intrinsically-disordered structure of the highly flexible C-tail terminal domain, within the truncated protein variants N Δ 49-Rad9 (“Rad9-S”) and N Δ 73-Rad9 (“M74”) – Fig 3.17, p.318, may also be implicated in specific protein-protein interactions which function in checkpoint signalling responses to replicative stress and/or DNA damage.

Whilst comparative metaPrDOS analyses of the Sty1 kinase phosphorylation target-like motif ¹¹⁰GYGSES¹¹⁵ indicated that it was a 100% structurally-ordered in the case of the “wild-type” and point mutant M50A and M50L full-length Rad9 polypeptide sequences (Fig 3.16, p.317), this was not the case with the truncated protein variants N Δ 49-Rad9 (“Rad9-S”) and N Δ 73-Rad9 (“M74”) – Fig 3.17, p.318

Intriguingly, comparative metaPrDOS analyses of this equivalent “**GYGSES**” motif within the truncated protein variants NΔ49-Rad9 (⁶¹**GYGSES**⁶⁶) and NΔ73-Rad9 (³⁷**GYGSES**⁴²) indicated that it was ~90% structurally-ordered and ~10% structurally-disordered as a consequence of the first “position-equivalent” glycine residue (⁶¹**G** – “Rad9-S”; ³⁷**G** – “M74”) which was identified as a high-probability intrinsically-disordered residue (Fig 3.17, p.318).

This particular glycine residue is adjacent to a potential tyrosine phosphorylation site, which may be targeted by the Sty1 kinase (predicted via comparative polypeptide sequence analyses with the on-line software tools NetPhos 2.0 and NetPhosK – discussed later in detail in Chapter 6).

Taken together, these *in silico* data analyses may be indicative of novel replication- and/or environmental stress- type checkpoint-responsive signalling pathway functions of the truncated protein variants NΔ49-Rad9 (“Rad9-S”) and NΔ73-Rad9 (“M74”) which are distinct from those of the full-length Rad9 protein (discussed later in detail in Chapter 6).

In contrast with the full-length Rad9, “Rad9-S” and “M74” truncated Rad9 protein variants (Fig 3.16, p.317 and Fig 3.17, p.318), metaPrDOS analyses of the hypothetical polypeptide sequences for the truncated Rad9 variants; NΔ310-Rad9 (“M311”), N-Δ311Rad9 (“M312”) and NΔ357-Rad9 (“M358”), indicated that these three proteins possessed a very high degree of intrinsically-disordered propensity with very limited/negligible ordered structure (Fig 3.18, p.319).

These *in silico* data are also consistent with the highly flexible nature of the “structurally-adaptive” C-terminal tail domain (Broustas C.G. and Lieberman H.B., 2012), progressively smaller fragments of which comprise the entire polypeptide sequences of the truncated Rad9 protein variants NΔ310-Rad9 (“M311”), NΔ311-Rad9 (“M312”) and NΔ357-Rad9 (“M358”) – Fig 3.18, p.319.

Fig 3.16 metaPrDOS Analyses of Rad9, M50A and M50L Mutants

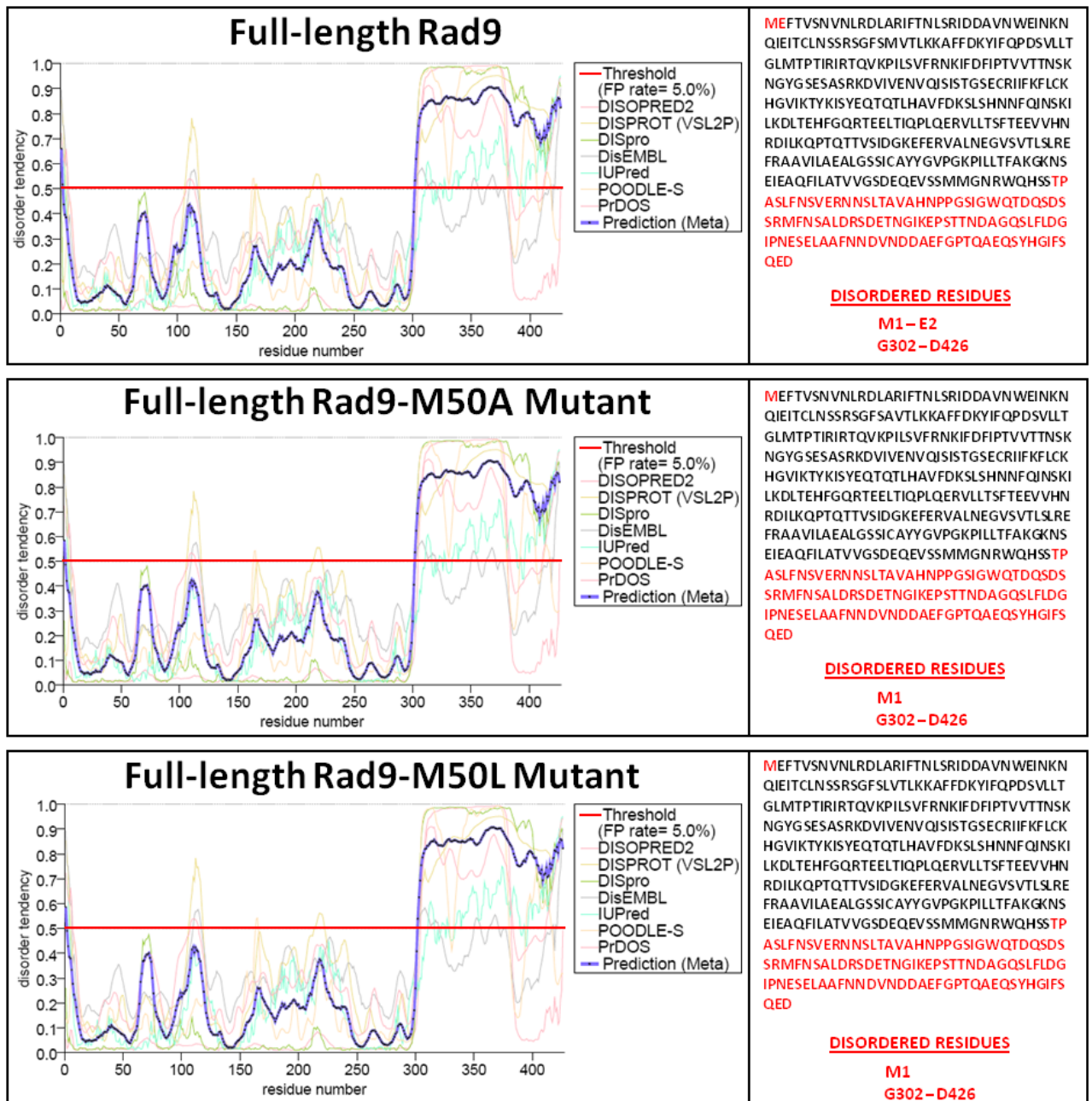


Fig 3.17 metaPrDOS Analyses of Rad9, "Rad9-S" & "M74" Variants

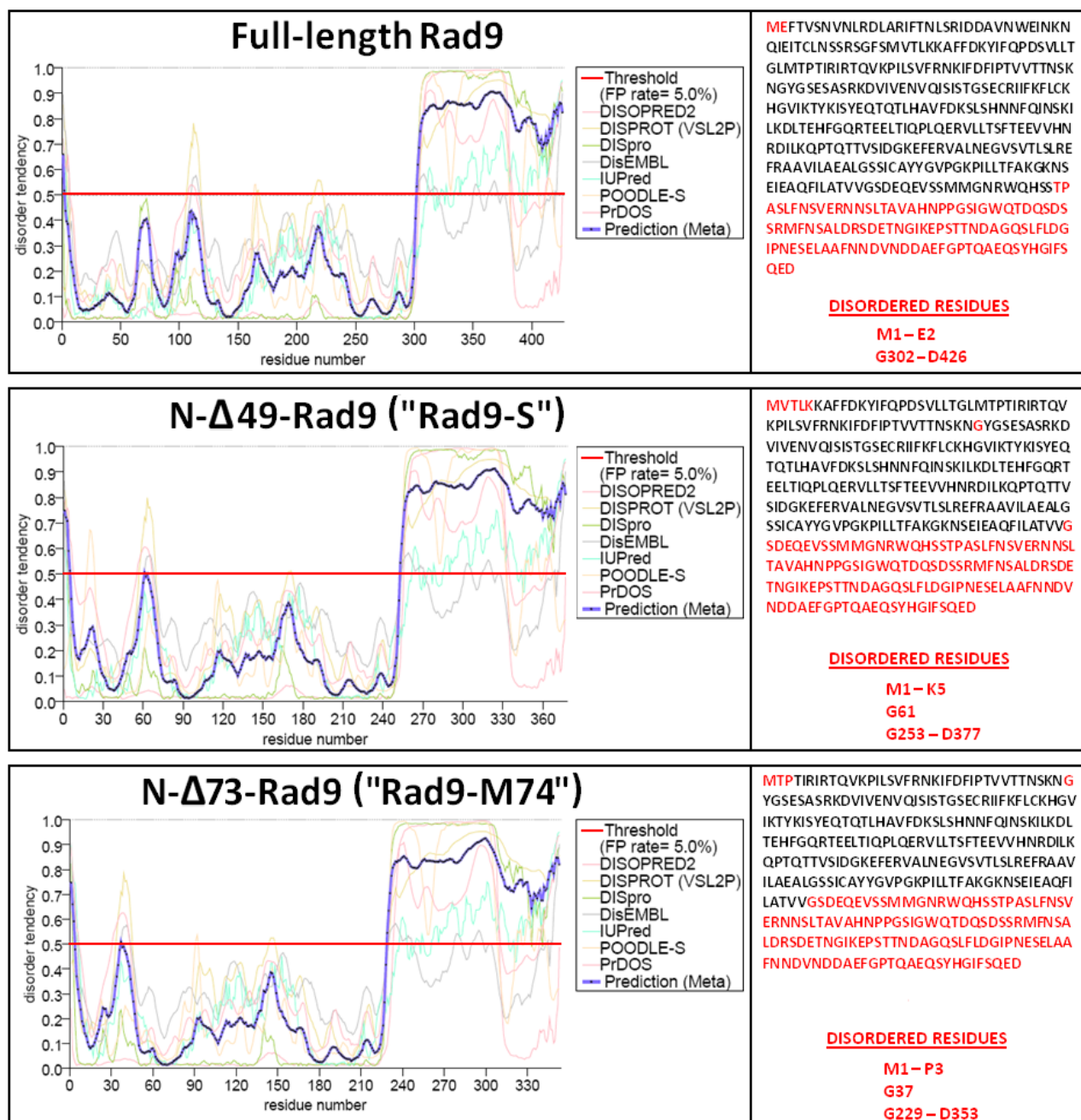
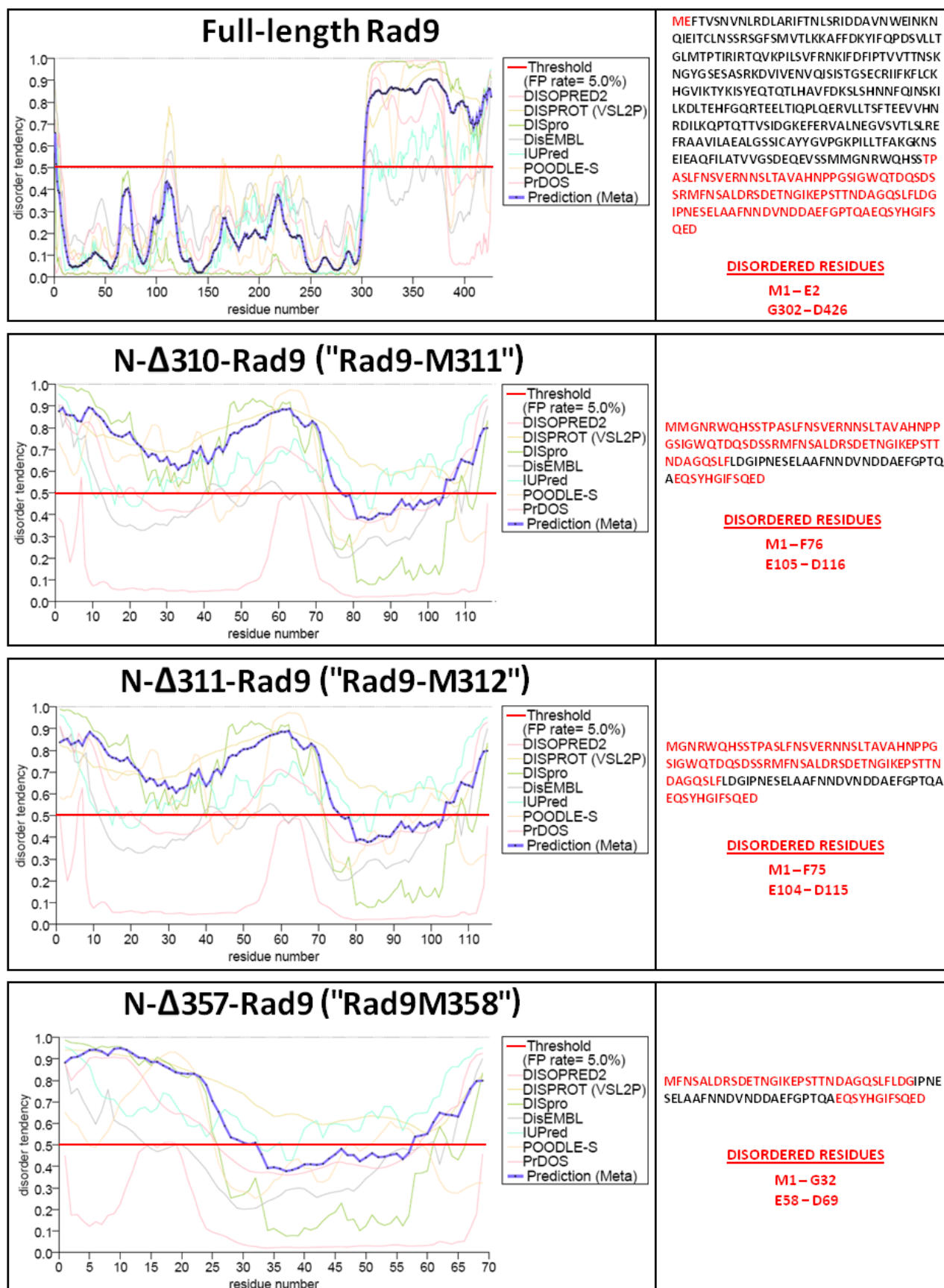


Fig 3.18: metaPrDOS Analyses of Rad9, “M311”, “M312” & “M358”



3.4.2 Anti- and Pro- Aggregation Functional Motif Analyses

Amphiphilic motifs of general sequence: (X)(n)Z, Z(X)(n) ($n \geq 2$) or (XZ)(n) ($n \geq 2$), in which X is representative of a hydrophobic amino acid residue and Z is representative of a charged or polar amino acid residue, are implicated in the formation of supramolecular aggregation-type structures within proteins that include fibres, tubes, ribbons or rolled sheets – which may also infer an enhanced level of resistance to proteolytic degradation and therefore prolong the cytological “half-life” of a particular protein (Kulkarni P. *et al.*, 2011; Moore C.L. *et al.*, 2000; Moore C.L. *et al.*, 2011; Zhang Y. and Calderwood S.K., 2011).

A higher degree of hydrophobicity within these amphiphilic motifs enhances their relative intrinsic structural order propensity and promotes aggregate formation, whilst a higher degree of hydrophilicity within these amphiphilic motifs enhances their relative intrinsic structural disorder with consequential suppression of aggregate formation (Banavar J.R. *et al.*, 2007; Chakrabortee S. *et al.*, 2012; Hoang T.X. *et al.*, 2006; Kulkarni P. *et al.*, 2011; Moore C.L. *et al.*, 2011; Morimoto R.I. *et al.*, 2012; Trovato A. *et al.*, 2006; Zhang Y. and Calderwood S.K., 2011).

Several *in silico*-based analytical approaches were utilised to ascertain the relative content of potential anti-aggregative, pro-aggregative and protease-resistant type motifs contained within the respective amino acid sequences of the engineered *S. pombe* Rad9 proteins in order to acquire some predictive hypothetical insights into their comparative cytological stabilities – these were:

- (i) Multiple sequence alignments between the full-length *S. pombe* Rad9 protein and the anti-aggregative sequence motifs KLVFF, KLVF, VLFKF (Castelletto V. *et al.*, 2011a; Castelletto V. *et al.*, 2011b) and FAEDVG (Kalkarni P. *et al.*, 2011) – Fig 3.19, p.328.

(ii) Multiple sequence alignments between the full-length *S. pombe* Rad9 protein and the pro-aggregative/protease resistance sequence motif QIVYK (Moore C.L. *et al*, 2011) and the pro-aggregative sequence motif PQLATLADEVSAASLAKQGL situated within the PHF43 (paired helical filament) of the Tau protein C-terminal domain (Esposito G. *et al*, 2000)

Fig 3.19, p.328.

(iii) Identification of potential pro-aggregative motifs within the full-length *S. pombe* Rad9 protein via analysis of its amino acid sequence with the on-line bioinformatics software programs BETASCAN (Bryan A.W. Jr. *et al*, 2009), TANGO (Fernández-Escamilla A.M. *et al*, 2004a; Fernández-Escamilla A.M. *et al*, 2004b) – Fig 3.19, p.328.

(iv) Identification of potential pro-aggregative regions with the full-length *S. pombe* Rad9 protein via analysis of its amino acid sequence with the on-line bioinformatics software program ZYGGREGATOR (Routledge K.E. *et al*, 2009; Tartaglia G.G. and Vendruscolo M., 2008; Tartaglia G.G. and Vendruscolo M., 2010) – Fig 3.20, pp.329-330.

These combined analyses identified 10 potential motifs which may be implicated in the relative functional stability of the engineered *S. pombe* Rad9 protein variants (Table 3.1, p.327).

The engineered full-length *S. pombe* Rad9 proteins Rad9-c3xHA, Rad9-(M50A)-c3xHA, Rad9-(M50L)-c3xHA and the truncated N Δ 49-Rad9-c3xHA protein variant (“Rad9-S”) contained a total of 7 aggregation-inductive motifs, 4 aggregation-suppressive motifs and 5 protease-resistant motifs (Table 3.1, p.327; Fig 3.19, p.328).

The engineered truncated “M74” *S. pombe* Rad9 protein variant, N Δ 73-Rad9-c3xHA, contained a total of 7 aggregation-inductive motifs, 5 protease-resistance motifs, but only 2 aggregation-suppressive motifs (Table 3.1, p.327; Fig 3.19, p.328).

This reduction in the number of aggregation-suppressive motifs within the engineered truncated NΔ73-Rad9-c3xHA *S. pombe* Rad9 protein variant, compared with that of the engineered full-length *S. pombe* Rad9 proteins Rad9-c3xHA, Rad9-(M50A)-c3xHA, Rad9-(M50L)-c3xHA and the truncated NΔ49-Rad9-c3xHA protein variant (“Rad9-S”), may be implicated in its relatively low level of expression – which was approximately half the level of that observed for the other full-length Rad9 and “Rad9-S” proteins detected in the Western blot assay (Fig 3.15, p.313).

The hypothetical amino acid sequences for the alternative translational AUG codon initiation start site-derived truncated *S. pombe* Rad9 variants NΔ310-Rad9, NΔ311-Rad9 and NΔ357-Rad9 contained none of these potential motifs (Table 3.1, p.327; Fig 3.19, p.328).

Analysis of the full-length *S. pombe* Rad9 amino acid sequence with the on-line software program ZYGGREGATOR (Routledge K.E. *et al.*, 2009; Tartaglia G.G. and Vendruscolo M., 2008; Tartaglia G.G. and Vendruscolo M., 2010) also indicated very narrow marginal regions of moderate to high aggregative propensity score, which were negatively countered by interspaced regions of low aggregative propensity score within the AUG codon initiation start site-derived truncated *S. pombe* Rad9 variants NΔ310-Rad9, NΔ311-Rad9 and NΔ357-Rad9 (Fig 3.20, pp.329-330).

Taken together, these *in silico* analyses indicated a significant the lack of potential pro-, anti- and protease-resistant motifs within the AUG codon initiation start site-derived *S. pombe* Rad9 variants NΔ310-Rad9, NΔ311-Rad9 and NΔ357-Rad9 which may render these truncated isoforms highly unstable and functionally non-viable – this could also account for the lack of detected expression of the engineered *S. pombe* truncated protein variants NΔ311-Rad9-c3xHA and NΔ357-Rad9-c3xHA observed in the Western blot assay (Fig 3.15, p.313).

Phosphorylated amino acid residues situated adjacent to or within pro-aggregative amphiphilic sequences may also increase their hydrophilicity due to the proximal presence of the polar, ionised phosphate groups, with consequential suppression of critical non-polar/hydrophobic interactions that are required for the functional aggregative propensity of these motif types (discussed previously in detail on p.320).

Kinase phosphorylation residue target site probability predictions were therefore performed on the identified 10 potential anti-aggregative, pro-aggregative and protease-resistance sequence motifs which may be implicated in the relative functional stability of the engineered *S. pombe* Rad9 protein variants (Table 3.1, p.327; Fig 3.19, p.328) via utilisation of the on-line NetPhos software tools (Blom N. *et al.*, 1999; Blom N. *et al.*, 2004; Miller M.L. and Blom N., 2009).

Only four, out of the total of 10, of these motifs contained potential kinase target-site residues with high phosphorylation probability scores (predicted via *in silico* sequence analyses with the on-line NetPhos 2.0 and 3.1b programs) – notably; ⁶⁰KYIF⁶³

¹¹⁰GYGSESASRKD¹²⁰,

²⁰⁰PLQERVLLTSFTEEVVHNRDILKQ²²³

²²⁴PTQTTVSIDGKEFERVALENGVSVTLRLRE²⁵³

With the exception of the anti-aggregative ⁶⁰KYIF⁶³, the remaining 3 of these motifs were pro-aggregative and protease-resistance (Table 3.1, p.327).

The engineered full-length *S. pombe* Rad9 protein variants Rad9-c3xHA, Rad9-M50A-c3xHA, Rad9-M50L-c3xHA and the truncated *S. pombe* Rad9 variants NΔ49-Rad9-c3xHA (“Rad9-S”) and NΔ73-Rad9-c3xHA (“M74”) all contained these three pro-aggregative motifs (Fig 3.19, p.328), which may infer an enhanced degree of stability within these respective proteins.

In silico analysis of the tyrosine and three serine residues contained within the identified pro-aggregative and protease-resistant ¹¹⁰GYGSESASRKD¹²⁰ motif, via utilisation of the on-line software programs Netphos2.0 and Netphos3.1b (Blom N. *et al.*, 1999; Miller M.L. and Blom N., 2009), were all identified as high-probability phosphorylation residues – Table 3.1, p.327.

Intriguingly, the tyrosine residue (at position 111) within this sequence was also identified as a potential Wis1 kinase target site, predicted by the software program NetPhosK (Table 3.1, p.326), whilst the adjacent glycine residue (at position 110) was identified (by the software program MetaPrDOS) as an exclusively intrinsic structurally-disordered residue within the engineered *S. pombe* Rad9 truncated variants NΔ49Rad9-c3xHA (“Rad9-S-c3xHA”) and NΔ73Rad9-c3xHA (Fig 3.17, p.318; Table 3.1, p.327).

Analysis of the full-length *S. pombe* Rad9 amino acid sequence, with the on-line software program ZYGREGATOR (Routledge K.E. *et al.*, 2009; Tartaglia G.G. and Vendruscolo M., 2008; Tartaglia G.G. and Vendruscolo M., 2010), also indicated that the identified pro-aggregative and protease-resistant ¹¹⁰GYGSESASRKD¹²⁰ motif sequence was also situated within a region (spanning residues ~¹¹⁵S through to ¹⁴⁰F) of moderate to high aggregative propensity with relatively little negative “counter-acting” regions of low aggregative propensity (Fig 3.20, pp.329-330).

Taken together, these *in silico* analyses may be indicative that the relative stability of the engineered full-length *S. pombe* Rad9 variants Rad9-c3xHA, Rad9-M50A-c3xHA, Rad9-M50L-c3xHA and truncated *S. pombe* Rad9 isoforms NΔ49Rad9-c3xHA (“Rad9-S-c3xHA”) and NΔ73Rad9-c3xHA, is potentially regulated via Wis1 kinase-mediated phosphorylated-modulation of the relative aggregation propensity of the ¹¹⁰GYGSESASRKD¹²⁰ motif.

Netphos 2.0 and 3.1b software analyses of the pro-aggregative and protease-resistant ²⁰⁰PLQERVLLTSFTEEVVHNRDILKQ²²³ motif indicated that only the serine residue at position 209 possessed high phosphorylation-site probability status and this particular sequence was also situated directly adjacent to the ²²⁴PTQTTVSIDGKEFERVALENGVSVTSLRE²⁵³ pro-aggregative and protease-resistant motif which contained the Rad3 kinase target phosphorylation site at threonine 225 (Kai M. *et al.*, 2007) – Table 3.1, p.327.

Netphos 2.0 and 3.1b software analyses of the identified pro-aggregative and protease-resistant ²²⁴PTQTTVSIDGKEFERVALENGVSVTSLRE²⁵³ motif indicated that the serine residues at positions 230 and 250 also possessed high phosphorylation-site probability status, whilst the threonine residues at positions 227 and 228 were assigned borderline/moderate threshold phosphorylation-site probability values (Table 3.1, p.327).

Taken together, these *in silico* analyses may be indicative that the relative stability of the engineered full-length *S. pombe* Rad9 variants Rad9-c3xHA, Rad9-M50A-c3xHA, Rad9-M50L-c3xHA and truncated *S. pombe* Rad9 isoforms NΔ49Rad9-c3xHA (“Rad9-S-c3xHA”) and NΔ73Rad9-c3xHA, is also potentially regulated via Rad3 and/or other protein kinase-mediated phosphorylated-modulation of the relative aggregation propensity of these two motifs.

In *S. pombe*, Rad3 kinase-mediated phosphorylation of Rad9 is implicated in various checkpoint responses to DNA damage, whilst Wis1 kinase-mediated phosphorylated-activation of Sty1 kinase is implicated in a variety of checkpoint responses to U.V.-induced DNA damage and environmental cytological stresses that may adversely impinge on DNA replication, DNA repair and/or other co-ordinated biochemical processes which work collectively to maintain the preservation of genomic integrity (Alao J.P. and Sunnerhagen P., 2008; Furuya K. and Carr A.M., 2003; Furuya K. *et al.*, 2010; Nurse P. *et al.*, 2009; Paek A.L. and Weinert T., 2010).

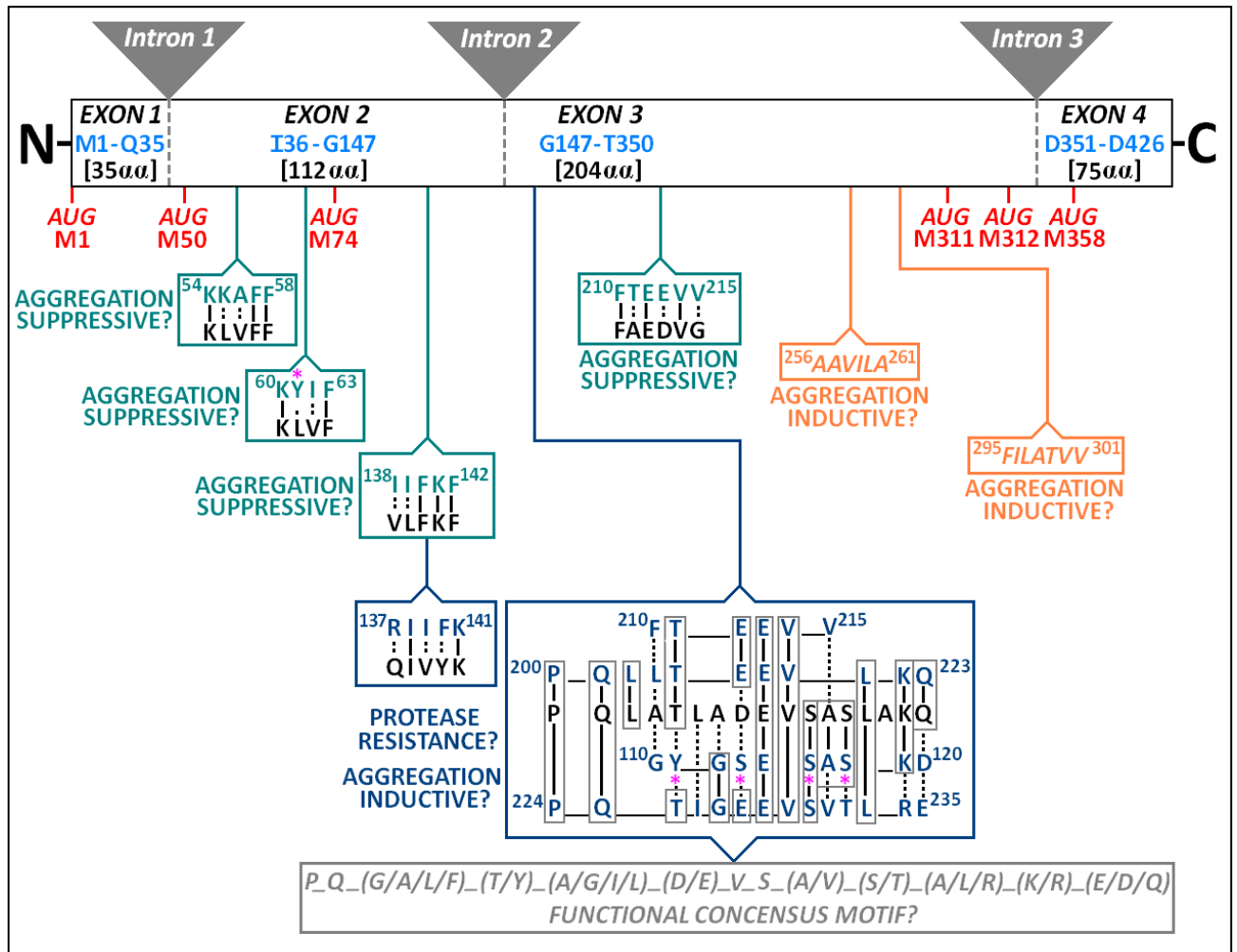
Taken these phenomena into consideration, it is possible that cell cycle checkpoints may also be implicated in the regulation of the cytological stability, levels and functional activities of a variety of *S. pombe* Rad9 isoforms via signal pathway activation of specific kinases which mediate the phosphorylated-modulation of the aggregation propensity of the three Rad9 pro-aggregative and protease resistant type motifs; “GYGSESASRKD”, “PLQERVLLTSFTEEVVHNRDILKQ” and “PTQTTVSIDGKEFERVSVTLSLRE” (Table 3.1, p.327; Fig 3.19, p.328).

Table 3.1: Identified SpRad9 Protein Stability Modulation Motifs

IDENTIFIED POTENTIAL MODULATORY PROTEIN STABILITY MOTIF SEQUENCE AND SITE LOCATION	MODULATORY PROTEIN STABILITY FUNCTION(S)	metaPrDOS PREDICTED INTRINSIC ORDER/DISORDER % PROPENSITY	PHOSPHORYLATION SITE POTENTIAL(S) [NetPhos Probability Score > 0.5 = Significant]
54KKAFF ⁵⁸	ANTI-AGGREGATIVE	100% ORDERED	ABSENT
60K ⁶¹ YIF ⁶³	ANTI-AGGREGATIVE	100% ORDERED	⁶¹ Y = 0.894 SIGNIFICANT*
110GYGSESASRKD ¹²⁰	PRO-AGGREGATIVE PROTEASE RESISTANCE	Rad9 ("M1") Rad9-M50A ("M50A") Rad9-M50L ("M50L") 100% ORDERED NΔ49-Rad9 ("M50") NΔ73-Rad9 ("M74") ~90% Ordered ~10% Disordered G ¹¹⁰ YGSESASRK	¹¹¹ Y = 0.878 SIGNIFICANT* ¹¹³ S = 0.981 SIGNIFICANT* ¹¹⁵ S = 0.974 SIGNIFICANT* ¹¹⁷ S = 0.997 SIGNIFICANT*
139RIIFK ¹⁴¹	ANTI-AGGREGATIVE	100% ORDERED	ABSENT
138IIFKF ¹⁴²	PRO-AGGREGATIVE PROTEASE RESISTANCE	100% ORDERED	ABSENT
200PLQERVLLTSFTEEVVHNRDILKQ ²²³	PRO-AGGREGATIVE PROTEASE RESISTANCE	100% ORDERED	²⁰⁸ T = 0.137 Non-Significant ²⁰⁹ S = 0.977 SIGNIFICANT* ²¹¹ T = 0.100 Non-Significant
210FTEEVV ²¹⁵	ANTI-AGGREGATIVE PRO-AGGREGATIVE PROTEASE RESISTANCE	100% ORDERED	²¹¹ T = 0.100 Non-Significant
224PTQTTVSIDGKEFERVALENGVSVTSLRE ²⁵³	PRO-AGGREGATIVE PROTEASE RESISTANCE	100% ORDERED	²²⁵ T = Rad3 Kinase Target ²²⁷ T = 0.486 ²²⁸ T = 0.540 } SIGNIFICANT? ²³⁰ S = 0.878 SIGNIFICANT* ²⁴⁶ S = 0.121 Non-Significant ²⁴⁸ T = 0.017 Non-Significant ²⁵⁰ S = 0.982 SIGNIFICANT*
256AAVILA ²⁶¹	PRO-AGGREGATIVE	100% ORDERED	ABSENT
295FILATVV ³⁰¹	PRO-AGGREGATIVE	100% ORDERED	²⁹⁹ T = 0.049 Non-Significant

* = High-probability phosphorylation sites identified by the NetPhos on-line bioinformatics tools (Blom N. *et al.*, 1999; Blom N. *et al.*, 2004; Miller M.L. and Blom N., 2009)

Fig 3.19: Site Map of SpRad9 Protein Stability Modulation Motifs



Structural map of the *S. pombe rad9* gene indicating the relative positions of the introns, exon-encoded amino acid-spanning regions, potential alternative AUG codon translational start sites and identified potential pro-aggregative, anti-aggregative and protease-resistance type functional motif sites:

XXXXXX = Potential KLVFF-, VLFKF- and FAEDVG- equivalent peptide aggregation suppressive motifs identified via comparative pair-wise sequence alignments performed with the on-line bioinformatics software tools EMBOSS and JEMBOSS.

XXXXXX = *H. sapiens* microtubule-associated Tau protein C terminus equivalent pro-aggregative and protease resistance motif.

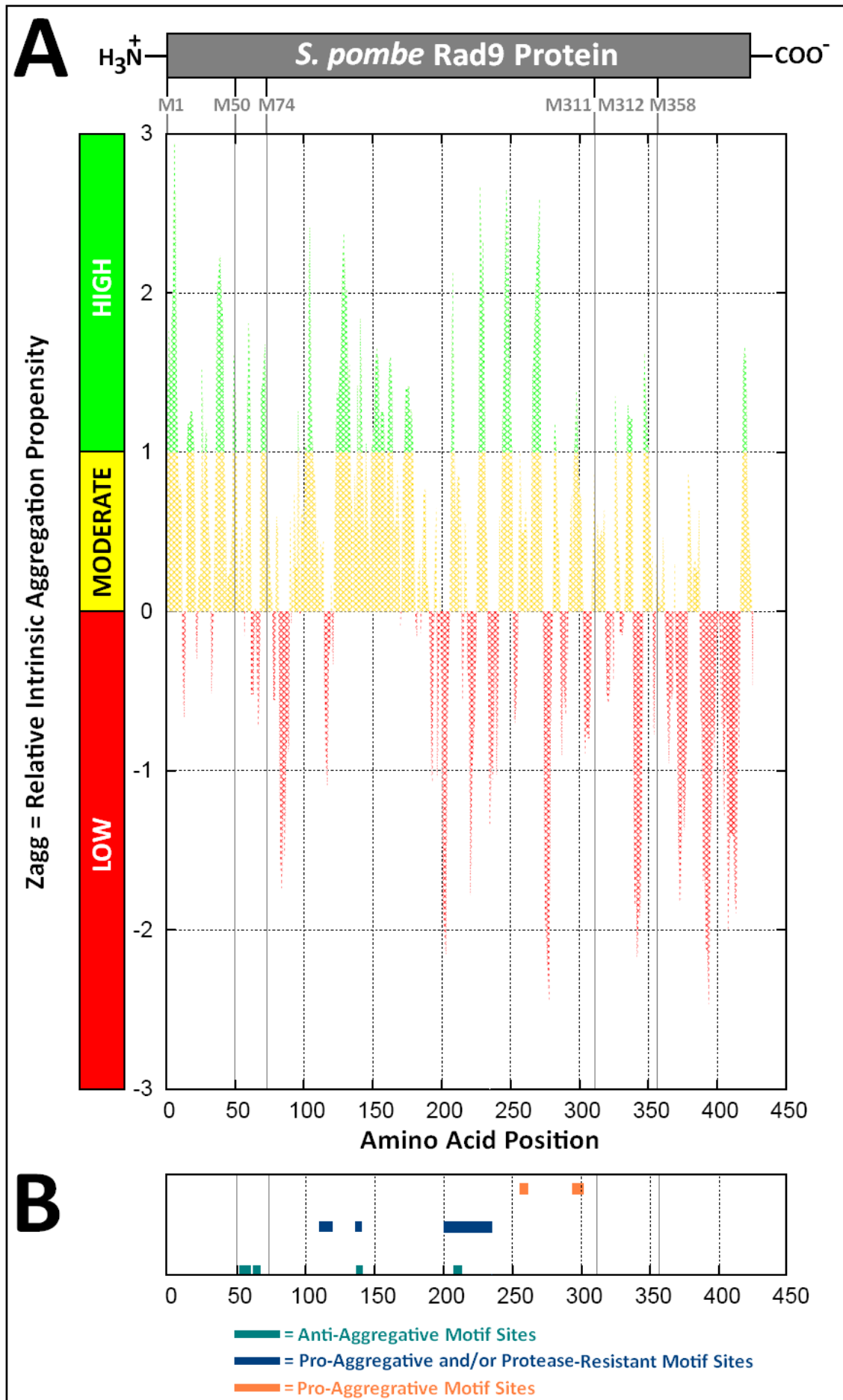
XXXXXX = Potential *H. sapiens* microtubule-associated Tau protein C terminus functional motif-equivalent protein aggregation/protease resistant motifs identified via comparative pair-wise sequence analyses performed with the on-line bioinformatics tools EMBOSS and JEMBOSS

XXXXXX = Potential protein aggregation-associated protease resistance functional motif identified via multiple sequence alignment analyses performed with the on-line bioinformatics software tools EMBOSS, JEMBOSS and PSI-BLAST

XXXXXX = Potential peptide aggregation inductive motifs identified via sequence analyses performed with the on-line bioinformatics software tools BETASCAN and TANGO.

* = High-probability phosphorylation sites (identified by the NetPhos on-line bioinformatics tool)

Fig 3.20: Comparative Map of SpRad9 Stability Modulation Motifs



A: ZYGGREGATOR software-generated mapping of identified regions of high, moderate and low probability aggregation propensity.

The relative positions of the potential alternative AUG methionine translational start codon sites of the engineered *S. pombe* Rad9 full-length and truncated protein isoforms are also indicated.

B: Residue-spanning regional map of the anti-, pro- and protease-resistant motif sites within the *S. pombe* Rad9 protein identified via multiple sequence alignment analyses (described previously on p.321) and utilisation of the aggregation sequence motif-predictive on-line software programs BETASCAN and TANGO.

[Details of these identified motif sequences are provided in Table 3.1, p.327 and Fig 3.19, p.328]

3.4.3 Secondary Supra-Molecular Structural Motif Analyses

The relative stability of a particular protein is also dependent upon the arrangement and content of secondary structural motifs (ie helices, strands and coils) within its supramolecular architecture (Banavar J.R. *et al*, 2007; Hoang T.X. *et al*, 2006; Kulkarni P. *et al*, 2011).

Several *in silico*-based analytical approaches were utilised to ascertain the relative proportions and types of helix-, strand- and coil- based secondary structural motif “sub-architecture” contained within the respective amino acid sequences of the engineered *S. pombe* Rad9 proteins in order to acquire some predictive hypothetical insights into their comparative cytological stabilities – these were:

- (i) *In silico* prediction and modelling of potential transmembrane spanning domains via amino acid sequence analyses of the full-length *S. pombe* Rad9 protein with the on-line software tools Kyte-Doolittle Hydrophathy Plotter (Kyte J. and Doolittle R., 1982) , PHOBIUS (Käll L. *et al*, 2004), SPLIT 4.0 (Juretic D. *et al*, 2002), TMpred (Hofmann K. and Stoffel W., 1993) and TMPres2D (Spyropoulos I.C. *et al*, 2004) – Sub-section 3.4.3.1, pp.332-339.
- (ii) *In silico* prediction of potential secondary structure repeat motifs and/or associated coiled-coiled domains via comparative amino sequence analyses of the full-length *S. pombe* Rad9 protein with the on-line software tools COILS (Lupas A. *et al* 1991), MULTI-COIL (Newman J.R. *et al*, 2000; Wolf E. *et al*, 1997; Trigg J. *et al*, 2011), MARCOIL (Delorenzi M. and Speed T., 2002; Gruber M. *et al*, 2006) and REPPER (Gruber M. *et al*, 2005) – Sub-section 3.4.3.2, pp.340-350.
- (iii) *In silico* predictive assessment of the relative proportional content of helix-, strand- and coil- secondary structural motif regions within the engineered full-length and truncated *S. pombe* Rad9 variants via comparative amino sequence analyses of the full-length *S. pombe* Rad9 protein with the on-line software tool YASPIN (Lin K. *et al*, 2005) – Sub-section 3.4.3.3, pp.351-353.

3.4.3.1 Transmembrane-Spanning Domain Analyses

In silico analysis of the full-length *S. pombe* Rad9 amino acid sequence with the on-line software program TMPred resulted in the identification of a high-probability potential transmembrane domain region comprised of 20 amino acids, spanning residues ²⁵⁴F – ²⁷⁴V inclusive (Fig 3.22A, pp.335-336).

Intriguingly, this predicted transmembrane-spanning domain region also contained the AAVILA pro-aggregative sequence, identified via previous analyses of the full-length *S. pombe* Rad9 amino acid sequence with the software tools BETASCAN and TANGO (Section 3.4.2, pp.320-330; Fig 3.19, p.328), which was also flanked by the hydrophilic, charged ionic residues arginine (²⁵⁵R = positive electrostatic potential) and glutamate (²⁶²E = negative electrostatic potential) – Fig 3.22A, pp.335-336.

The pro-aggregative AAVILA motif could be implicated in the enhancement of the relative stability of the full-length *S. pombe* Rad9 protein and/or its truncated isoforms, via promotion of hydrophobic interactions which increase intrinsic structural order within the protein supramolecular architecture and suppress proteolytic degradation.

In this hypothetical context, the hydrophilic ²⁵⁵R and ²⁶²E flanking residues (Fig 3.22A, pp.335-336) may serve to reduce the aggregative propensity of the AAVILA motif to suppress catastrophic irreversible denaturation of the supramolecular architecture of the full-length *S. pombe* Rad9 protein and/or its truncated isoforms which would otherwise result in their rapid proteolytic degradation.

Comparative transmembrane-spanning domain helix and strand models of this potential domain were constructed via utilisation of the software program TMPres2D (Fig 3.22B and Fig 3.22C, pp.335-336), in concurrence with the data acquired from analysis of the ²⁵⁴F – ²⁷⁴V sequence with the software program YASPIN – which indicated a high probability of helix (~50% relative proportion), strand (~45% relative proportion) and coil (~5% relative proportion) secondary structural motifs within this domain (Fig 3.22D, pp.335-336).

Although comparative predictive transmembrane-spanning domain analyses performed on the full-length *S. pombe* Rad9 amino acid sequence with the software programs PHOBIUS, Kyte-Doolittle Hydropathy Plotter and SPLIT 4.0 indicated that it was highly improbable that the TMPred-identified ²⁵⁴F – ²⁷⁴V domain was a conventional transmembrane-spanning domain (Fig 3.23, pp.337-338).

However, the PHOBIUS data plot did indicate a highly significant non-cytoplasmic motif posterior label probability prediction for the ²⁵⁴F – ²⁷⁴V amino acid sequence (Fig 3.23A, pp.337-338).

This identified non-cytoplasmic motif ²⁵⁴F – ²⁷⁴V amino acid sequence was contained within the engineered full-length *S. pombe* Rad9 protein variants; Rad9-c3xHA, Rad9-(M50A)-c3xHA and Rad9-(M50L)-c3xHA and the engineered truncated *S. pombe* Rad9 proteins; NΔ49-Rad9-c3xHA (“Rad9-S”) and NΔ73-Rad9-c3xHA (“Rad9-M74”) – Fig 3.2, p.289; Fig 3.23A, pp.337-338.

Comparative multiple alignment analyses of the identified non-cytoplasmic motif ²⁵⁴F – ²⁷⁴V within the *S. pombe* Rad9 protein with other *Schizosaccharomyces* yeast Rad9 proteins, in conjunction with the *H. sapiens* RadA and Rad9B proteins, indicated that homologous variants of this motif were conserved and also contained potential “HFD-like” ATR^{Rad3} checkpoint kinase-activation motifs (Fig 3.24, p.339).

Taken together, these *in silico* data are indicative that this non-cytoplasmic motif sequence may be implication in the co-ordinated nuclear translocation of the Rad9 protein and Rad9-mediated activation of the the ATR^{Rad3} kinase within various cell cycle checkpoint pathways.

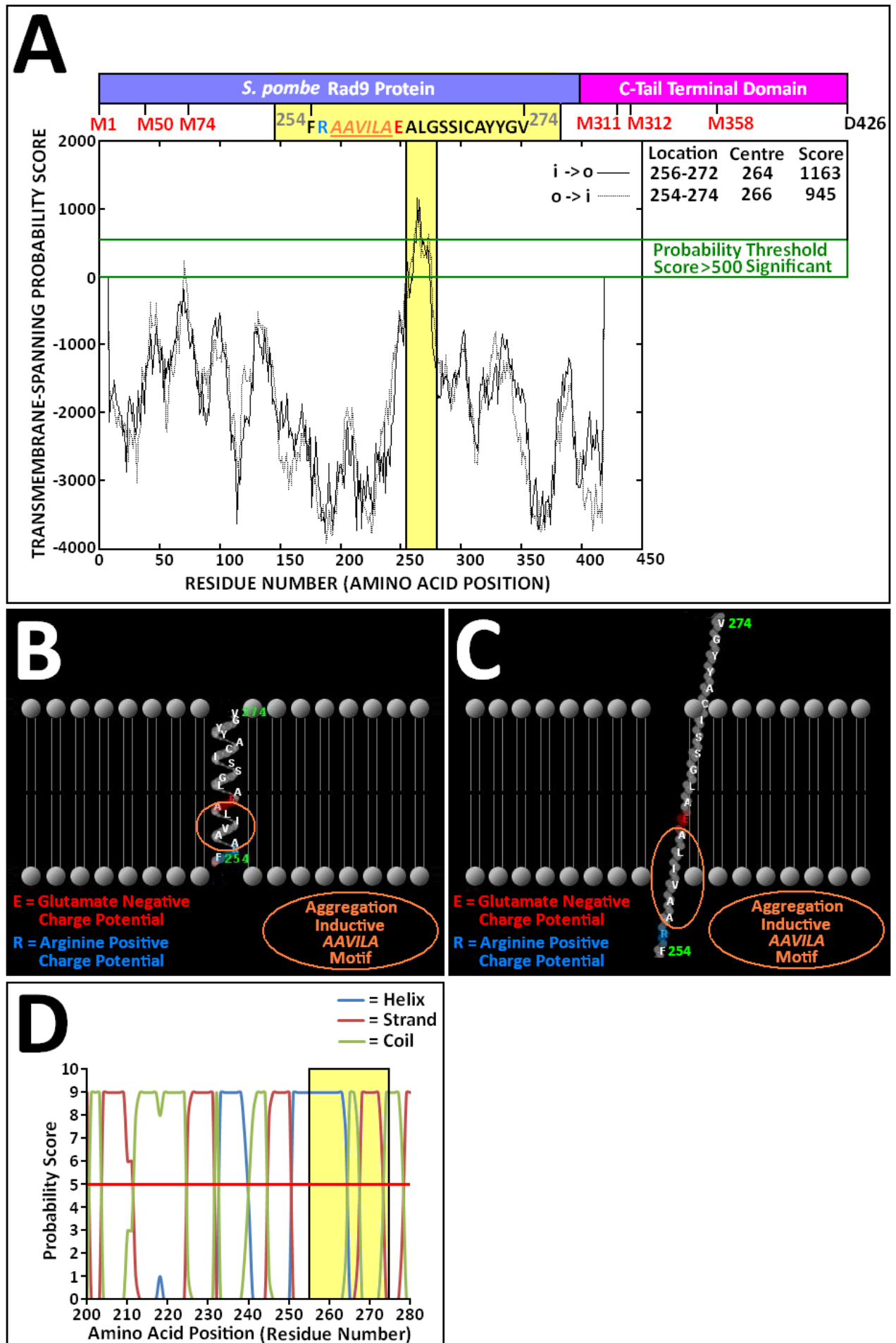
One plausible hypothetical function of this non-cytoplasmic motif could be the facilitated transportation of the full-length *S. pombe* Rad9 protein and its truncated isoforms through the nuclear membrane to chromatin lesion sites, via transient formation of an unconventionally-configured transmembrane-spanning (TM) domain (Fig 3.22A and Fig 3.22B, pp.335-336) which may be initiated and/or stabilised via the pro-aggregative AAVILA motif, during checkpoint responses to genotoxic damage and/or other cytological stresses that adversely impinge upon DNA replication and/or other biochemical processes which are implicated in the maintenance of genomic integrity.

COIL, MULTICOIL and MARCOIL analyses of the *S. pombe* Rad9 protein (Fig 3.26, pp.347-348) predicted zero coiled-coil structural repeat probability within the protein, which may be indicative that the potential non-cytoplasmic ²⁵⁴F – ²⁷⁴V type motif may adopt a strand-configured TM domain (Fig 3.22C, p.335-336).

The absence of this non-cytoplasmic motif, in the case of the hypothetical amino acid sequences of the alternative translation-generated truncated *S. pombe* Rad9 isoform products NΔ310-Rad9, NΔ311-Rad9 and NΔ357-Rad9 (Fig 3.22, pp.335-336 and Fig 3.23A, pp.337-338), may render these proteins functionally non-viable and susceptible to ubiquitination- and/or sumoylation-targeted proteolytic degradation as a consequence of their impaired capacity to penetrate the nuclear membrane and prolonged cytoplasmic retention.

This hypothetical postulate may also account for the lack of detected expression of the engineered *S. pombe* truncated variants NΔ311-Rad9-c3xHA and NΔ357-Rad9-c3xHA in the comparative Western blot assay (Fig 3.15, p.313). **[334]**

Fig 3.22: Transmembrane-Spanning Domain Modelling of SpRad9



A: Analysis of the full-length *S. pombe* Rad9 protein amino acid sequence with the on-line TMpred software tool.

The X-axis defines the amino acid residue position and the Y-axis defines the transmembrane-spanning probability score on the data plot: probability score values of over 500 are significant, the higher these score values the more significant the predicted probability.

The relative positions of the potential alternative AUG methionine translational start codon sites of the engineered *S. pombe* Rad9 full-length and truncated protein isoforms (Fig 3.2, p.289) and the C-terminal tail domain region are indicated.

The identified potential transmembrane-spanning ²⁵⁴F – ²⁷⁴V sequence is highlighted in yellow and also contains the pro-aggregative AAVILA motif (identified previously via analyses with the on-line software tools BETASCAN and TANGO – Section 3.4.2, pp.320-330; Fig 3.19, p.328).

B: Transmembrane-spanning helical model of the identified ²⁵⁴F – ²⁷⁴V sequence, generated via utilisation of the on-line TMPres2D software program.

The charged residues ²⁵⁵R (positive electrostatic potential, indicated in blue) and ²⁶²E (negative electrostatic potential, indicated in red) which flank the the pro-aggregative AAVILA motif (circled in orange) are indicated.

C: Transmembrane-spanning strand model of the identified ²⁵⁴F – ²⁷⁴V sequence, generated via utilisation of the on-line TMPres2D software program.

The charged residues ²⁵⁵R (positive electrostatic potential, indicated in blue) and ²⁶²E (negative electrostatic potential, indicated in red) which flank the the pro-aggregative AAVILA motif (circled in orange) are indicated.

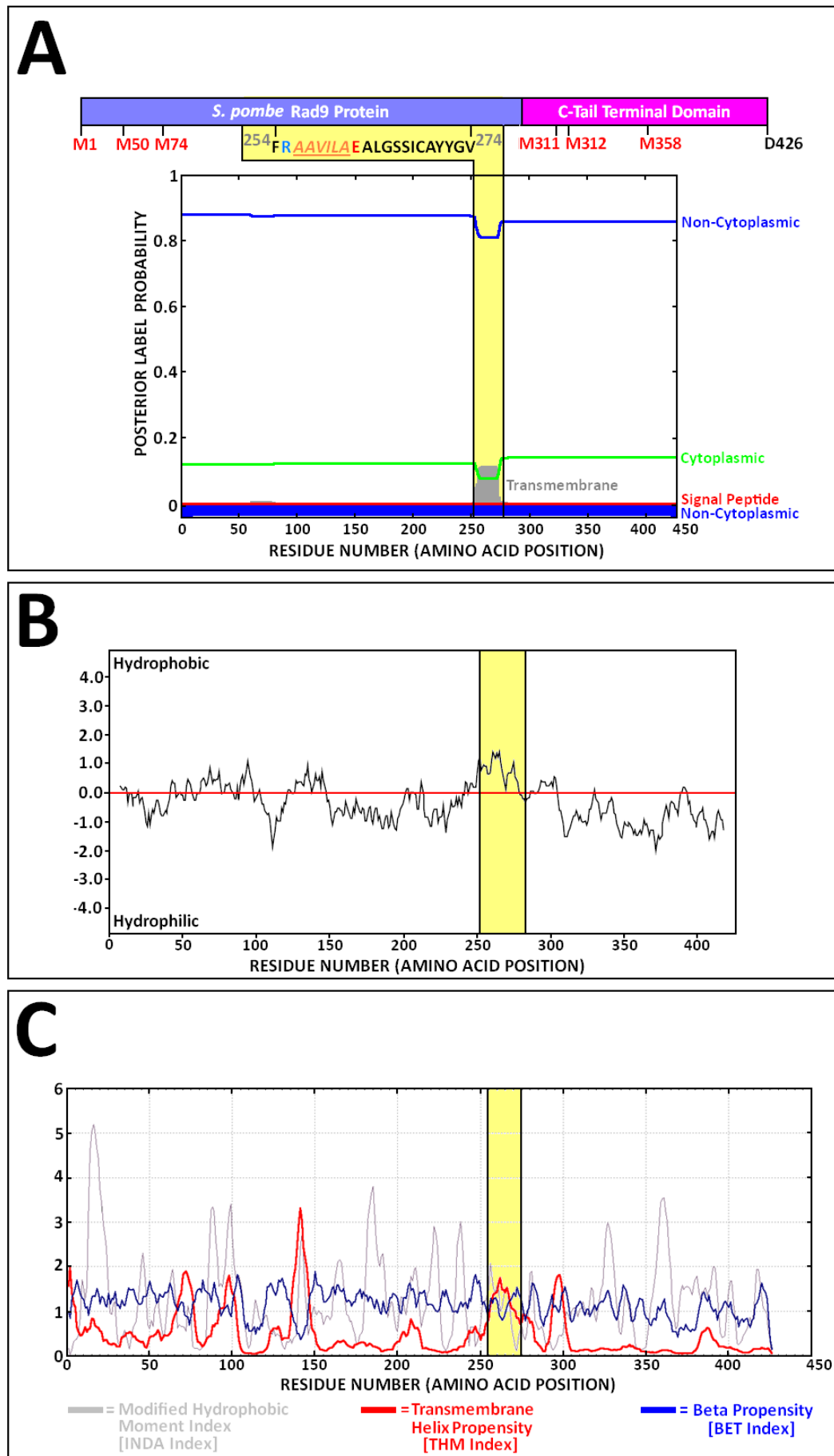
D: Analysis of the relative proportions and localised distribution of helix, strand and coil secondary structural motifs within the identified ²⁵⁴F – ²⁷⁴V sequence (highlighted in yellow).

The “wild-type” full-length *S. pombe* Rad9 amino acid region spanning residues ²⁰⁰P through to ²⁸⁰L was analysed with the on-line software tool YASPIN and the acquired data converted into a graphical format via utilisation of the Microsoft Excel software program.

The X-axis defines the amino acid residue position and the Y-axis defines the predicted helix, strand and coil propensity probability score on the data plot.

The horizontal red line on the data plot denotes the propensity prediction threshold [probability scores above 5 are significant and correlate with plotted values above the threshold line]

Fig 3.23: Hydropathy Profile Analyses of the *S. pombe* Rad9 Protein



A: Analysis of the full-length *S. pombe* Rad9 protein amino acid sequence with the on-line PHOBIUS software tool.

The X-axis defines the amino acid residue position and the Y-axis defines the Posterior label probability score on the data plot: the higher the score the more significant the predicted probability.

The relative positions of the potential alternative AUG methionine translational start codon sites of the engineered *S. pombe* Rad9 full-length and truncated protein isoforms and the C-terminal tail domain region are indicated (Fig 3.2, p.289).

The TMpred-identified potential transmembrane-spanning ²⁵⁴F – ²⁷⁴V sequence (Fig 3.22A, p.335), containing the pro-aggregative AAVILA motif (identified previously via analyses with the on-line software tools BETASCAN and TANGO – Section 3.4.2, pp.320-330; Fig 3.19, p.328) is highlighted in yellow.

B: Analysis of the full-length *S. pombe* Rad9 protein amino acid sequence with the on-line Kyte-Doolittle Hydropathy Plotter software tool.

The X-axis defines the amino acid residue position and the Y-axis defines the relative hydrophility/hydrophobicity score on the data plot: the more negative the score, the more more hydrophobic the residue, the more positive the score the more hydrophilic the residue.

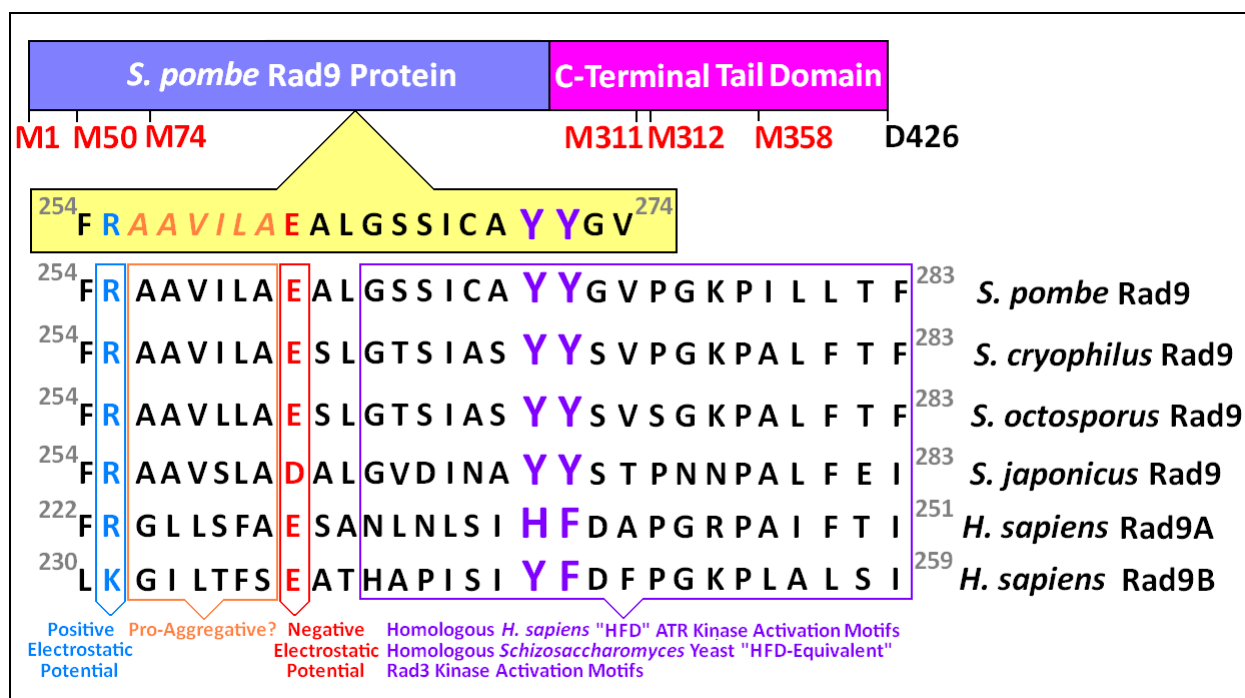
The relative regional position of the TMpred-identified potential transmembrane-spanning ²⁵⁴F – ²⁷⁴V sequence (Fig 3.22A, p.335) is highlighted in yellow.

C: Analysis of the full-length *S. pombe* Rad9 protein amino acid sequence with the on-line SPLIT 4.0 software tool.

The X-axis defines the amino acid residue position and the Y-axis defines the relative propensity index score for the appropriate parameter (modified hydrophobic moment, transmembrane helix, beta propensity) on the data plot: the higher the score, the more significant the predicted propensity.

The relative regional position of the TMpred-identified potential transmembrane-spanning ²⁵⁴F – ²⁷⁴V sequence (Fig 3.22A, p.335) is highlighted in yellow.

Fig 3.24: *In Silico* Identification of a Conserved 29 Residue-Spanning Potential Non-Cytoplasmic ATR^{Rad3} Kinase Activation Motif



The relative positions of the potential alternative AUG methionine translational start codon sites of the engineered *S. pombe* Rad9 full-length and truncated protein isoforms (Fig 3.2, p.289) and the C-terminal tail domain region are indicated.

The TMpred- and PHOBIUS-identified potential transmembrane-spanning/non-cytoplasmic ²⁵⁴F – ²⁷⁴V sequence, containing the pro-aggregative AAVILA motif flanked by the hydrophilic arginine = R and glutamate = E residues (identified previously via analyses with the on-line software tools BETASCAN and TANGO – Section 3.4.2, pp.320-330; Fig 3.19, p.328), is highlighted in yellow.

In silico comparative multiple-alignment analyses of the identified transmembrane-spanning/non-cytoplasmic *S. pombe* Rad9 ²⁵⁴F – ²⁷⁴V sequence, with those of the homologous functionally-equivalent proteins *H. sapiens* Rad9A, full-length Rad9B (isoform 5) and other *Schizosaccharomyces* yeast strains indicated, were performed with the on-line bioinformatics software tools COBALT, EMBOSS, JEMBOSS and PSI-BLAST.

Conserved (R/K)-(A/G)-(A/L/I)-(V/L)-(I/L/S/T)-(L/F)-(A/S)-(D/E) potential pro-aggregative motif-incorporated transmembrane-spanning/non-cytoplasmic domain sequences are highlighted in the blue, orange and red boxes.

Conserved equivalent *Schizosaccharomyces* yeast Rad3 kinase-activation motifs and the conserved equivalent ATR kinase-activation motif within the full-length and truncated isoforms of *H. sapiens* Rad9B paralogue, that bear significant homologous resemblance to the *H. sapiens* Rad9A “HFD”-type ATR activation motif are highlighted in the purple box – in which the key aromatic-type residue pairs (HF, YF and YY) that interact with specific allosteric binding-sites within the ATR^{Rad3} kinase enzyme are indicated (determined via information acquired from the research published by Burgers V.M. and Navadgi-Patil P.M., 2009).

3.4.3.2 Secondary Structural Repeat Motif Domain Analyses

In silico analysis of the full-length *S. pombe* Rad9 amino acid sequence with the on-line software program REPPER identified two potential repeat secondary structural type motifs within the protein of relatively low periodicity which spanned regional domains located between the residues ²⁷V – E¹⁵⁷ and ¹⁵²Y – K²⁸⁷ respectively (Fig 3.25B, pp.345-346).

The presence of these two domain sequences within in the engineered full-length *S. pombe* Rad9 protein variants and truncated *S. pombe* Rad9 protein variants NΔ49-Rad9-c3xHA (“Rad9-S”) and NΔ73-Rad9-c3xHA (“Rad9-M74”) may contribute to the functional stability of these proteins.

In this context, the distinctive absence of these two domain sequences within the engineered truncated *S. pombe* Rad9 variants NΔ311-Rad9-c3xHA and NΔ357-Rad9-c3xHA may render these proteins highly unstable and could account for their lack of detected expression in the Western blot assay (Fig 3.15, p.313).

This hypothetical postulation is also supported by additional comparative *in silico* analyses of the identified ²⁷V – E¹⁵⁷ and ¹⁵²Y – K²⁸⁷ domain sequences (discussed in the following latter part of this section).

The identified ²⁷V – E¹⁵⁷ domain sequence contained the anti-aggregative motifs ⁵⁴KKAFF⁵⁸, ⁶⁰KYIF⁶³, ¹³⁹RIIFK¹⁴¹, along with the pro-aggregative/protease resistant motifs ¹¹⁰GYGSESASRKD¹²⁰ and ¹³⁸IIFKF¹⁴² (discussed previously in Section 3.4.2, pp.320-330) – Fig 3.27B, pp.349-350.

Whilst the identified $^{152}\text{Y} - \text{K}^{287}$ domain sequence contained the multi-functional anti-aggregative/pro-aggregative/protease resistant motif $^{210}\text{FTEEVV}^{215}$, along with the pro-aggregative/protease-resistance sequences $^{200}\text{PLQERVLLTSFTEEVVHNRDILKQ}^{223}$, $^{224}\text{PTQTTVSIDGKEFERVALENGVSVTLSLRE}^{253}$ and $^{256}\text{AAVILA}^{261}$ (discussed previously in Section 3.4.2, pp.320-330) – Fig 3.27B, pp.349-350.

The distinctive lower proportion of anti-aggregative motifs in the identified $^{152}\text{Y} - \text{K}^{287}$ domain sequence may account for its assigned high significance probability score, as a consequence of increased structural order propensity, compared with that of the identified $^{27}\text{V} - \text{E}^{157}$ domain sequence – which contained two anti-aggregative motifs and was assigned a relatively moderate probability score (Fig 3.25B, pp.345-346).

Comparative phosphorylation site prediction analyses performed on both the $^{27}\text{V} - \text{E}^{157}$ and $^{152}\text{Y} - \text{K}^{287}$ domain sequences, with the on-line bioinformatics software tools NetPhos2.0, NetPhos3.1b and NetPhosK (Blom N. *et al.*, 1999; Blom N. *et al.*, 2004; Miller M.L. and Blom N., 2009), indicated that both these secondary structural motifs contained number of potential kinase target sites which were assigned significant probability scores (Fig 3.27, pp.349-350).

These *in silico* analyses also indicated that the $^{27}\text{V} - \text{E}^{157}$ sequence contained more potential phosphorylated residues than the $^{152}\text{Y} - \text{K}^{287}$ sequence (Fig 3.27, pp.349-350), which could be implicated in the kinase-modulated hydrophilicity enhancement and suppressed aggregative propensity of the pro-aggregative/protease resistant motifs (discussed previously in Section 3.4.2, pp.320-330) contained within these domains.

In this hypothetical context, the higher proportion of potential phosphorylated residues within the $^{27}\text{V} - \text{E}^{157}$ sequence (Fig 3.27, pp.349-350), in conjunction with its two anti-aggregative motifs may enhance the intrinsic disordered structural instability of this domain which could also account for its lower assigned probability score compared with that of the $^{152}\text{Y} - \text{K}^{287}$ domain sequence (Fig 3.25B, pp.345-346).

The very low probability score of the $^{290}\text{I} - \text{D}^{426}$ domain, identified via analysis of the “wild-type” full-length *S. pombe* Rad9 protein with the on-line bioinformatics program REPPER (Fig 3.25B, pp.345-346), may also be a consequence of the fact that it contains only one pro-aggregative motif ($^{295}\text{FILATVV}^{301}$) and 11 potential phosphorylated serine residues (Fig 3.27, pp.349-350) – which could be implicated in the kinase-modulated enhancement and suppressed aggregative propensity of the $^{295}\text{FILATVV}^{301}$ motif which would also significantly increase extent of the intrinsic structural disorder within the $^{290}\text{I} - \text{D}^{426}$ domain.

This hypothetical postulate is also consistent with the fact that the identified $^{290}\text{I} - \text{D}^{426}$ sequence is situated within the C-terminal tail domain of the *S. pombe* Rad9 protein – which possesses highly mobile, “structurally-adaptive” properties that enable it interact with a variety of different proteins implicated in cell cycle checkpoint responses and DNA repair pathways (Broustas C.G. and Lieberman H.B., 2012).

The predicted high instability of the potential $^{290}\text{I} - \text{D}^{426}$ secondary structural repeat motif, which would be the only domain of this type contained within the supramolecular architecture of the engineered truncated *S. pombe* Rad9 variants NΔ311-Rad9-c3xHA and NΔ357-Rad9-c3xHA, may render these proteins particularly susceptible to proteolytic degradation and thus also account for the lack of their detected expression in the comparative Western blot assay (Fig 3.15, p.313).

The pro-aggregative/protease resistant $^{110}\text{GYGSESASRKD}^{120}$, contained within the $^{27}\text{V} - \text{E}^{157}$ domain sequence (Fig 3.27, p.349-350), also possessed several unique features, notably; a Wis1 kinase phosphorylation target residue ^{111}Y (situated within a Sty1 kinase-like Wis1 target recognition motif sequence) and the intrinsic structural variability of the ^{110}G residue, which was ordered in the case of the engineered full-length *S. pombe* Rad9 protein variants and disordered in the case of the engineered truncated *S. pombe* Rad9 protein variants N Δ 49-Rad9-c3xHA (“Rad9-S”) and N Δ 73-Rad9-c3xHA (“Rad9-M74”) – discussed previously in Section 3.4.1, pp.315-319.

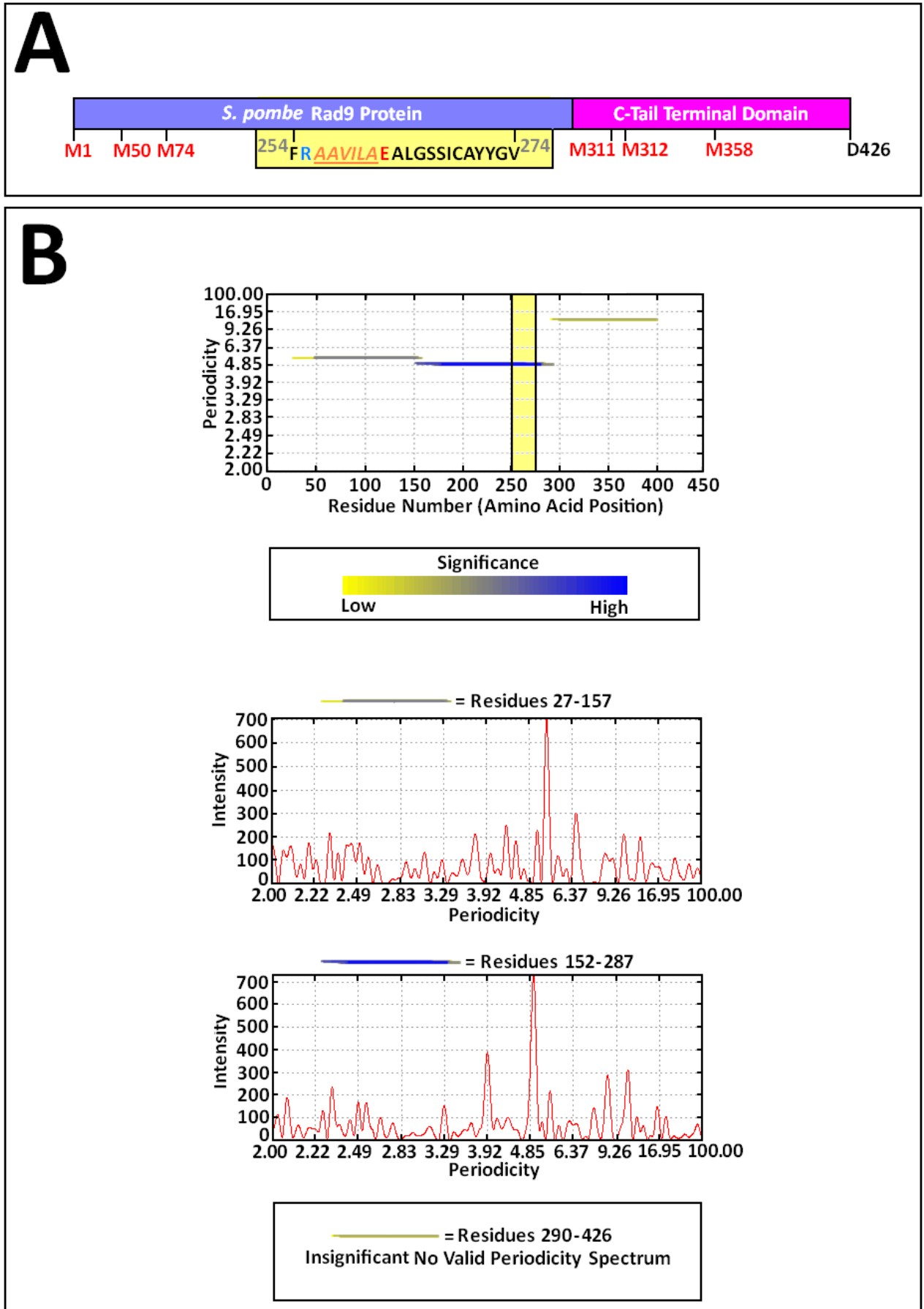
The $^{152}\text{Y} - \text{K}^{287}$ domain sequence also contained the transmembrane-spanning/non-cytoplasmic ATR^{Rad3} kinase-activation motif (Fig 3.25, p.345-346 and Fig 3.27, p.349-350), identified via the on-line bioinformatics programs TMpred and PHOBIUS, in conjunction with multiple alignment analyses with the *H. sapiens* “HFD” ATR-activation motif sequence (discussed previously in Sub-section 3.4.3.1, pp.332-339).

Confinement of the potential Wis1 kinase-targeted Sty1 kinase-like $^{110}\text{GYGSESASRKD}^{120}$ motif to the $^{27}\text{V} - \text{E}^{157}$ region and the potential “HFD”-like ATR^{Rad3} kinase-activation motif to the $^{152}\text{Y} - \text{K}^{287}$ region may also be indicative of separate, differential functions of these domains within the full-length *S. pombe* Rad9 protein and/or its truncated isoforms (Fig 3.27, pp.349-350).

Comparative analyses of the full-length *S. pombe* Rad9 amino acid sequence with the on-line software programs COILS, MULTICOIL and MARCOIL indicated a very low/insignificant probability of the existence of coiled-coil repeat type secondary structural motifs within the protein (Fig 3.26, pp.347-348).

Taken together, these *in silico* data may be indicative that the intrinsic secondary structural configurations of the $^{27}\text{V} - \text{E}^{157}$ and $^{152}\text{Y} - \text{K}^{287}$ domains, are regulated via specific kinase-mediated post-translational phosphorylation events which alter the transient supramolecular structure-function relationships of the full-length *S. pombe* Rad9 protein and/or its truncated isoforms (ie N Δ 49-Rad9-c3xHA and N Δ 73-Rad9-c3xHA) to enable them to act as key component initiators of differential cell cycle checkpoint signalling pathway responses to genotoxic and/or other environmental type cytological stresses which adversely impinge upon various biochemical processes implicated in the propagation of genomic integrity – such as DNA replication and DNA repair (Alao J.P. and Sunnerhagen P., 2008; Furuya K. and Carr A.M., 2003; Furuya K. *et al.*, 2010; Nurse P. *et al.*, 2009; Paek A.L. and Weinert T., 2010).

Fig 3.25: Secondary Structure Repeat Motif Analysis of SpRad9



A: The relative positions of the potential alternative AUG methionine translational start codon sites of the engineered *S. pombe* Rad9 full-length and truncated protein isoforms (Fig 3.2, p.289) and the C-terminal tail domain region are indicated.

The TMpred- and PHOBIUS-identified potential transmembrane-spanning/non-cytoplasmic ²⁵⁴F – ²⁷⁴V sequence, containing the pro-aggregative AAVILA motif flanked by the hydrophilic arginine = **R** and glutamate = **E** residues (identified previously via analyses with the on-line software tools BETASCAN and TANGO – Section 3.4.2, pp.320-330; Fig 3.19, p.328), is highlighted in yellow.

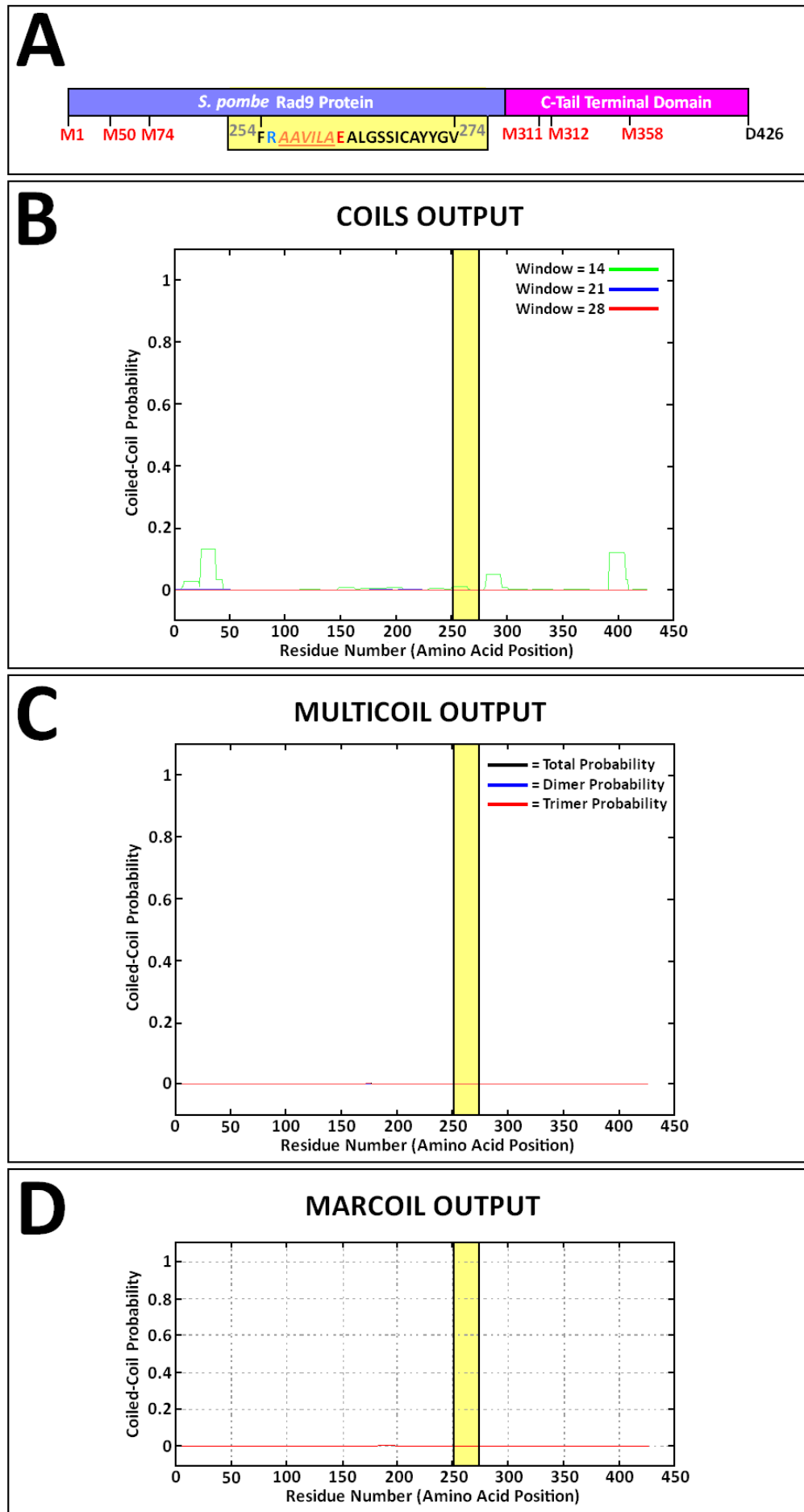
B: Analysis of the full-length *S. pombe* Rad9 protein amino acid sequence with the on-line bioinformatics software tool REPPER.

The X-axis defines the amino acid residue position and the Y-axis defines the relative periodicity score on the top data plot – in which regional locations of potential repeat and/or coiled-coil motifs are presented as lines that are colour-coded according to their determined relative probability weightings via the significance scale indicated underneath.

The relative regional position of the TMpred- and PHOBIUS- identified potential transmembrane-spanning /non-cytoplasmic motif sequence ²⁵⁴F – ²⁷⁴V motif sequence (Fig 3.22A, p.335) is highlighted in yellow.

The two graphs, situated below the colour-coded significance scale, are data plots of the relative intensity (Y-axis) vs periodicity score (X-axis) for the two amino acid residue-spanning regions identified as potential repeat and/or coiled-coil secondary structural motifs.

Fig 3.26: Coiled-Coil Motif Analyses of the *S. pombe* Rad9 Protein



A: The relative positions of the potential alternative AUG methionine translational start codon sites of the engineered *S. pombe* Rad9 full-length and truncated protein isoforms (Fig 3.2, p.289) and the C-terminal tail domain region are indicated.

The TMpred- and PHOBIUS-identified potential transmembrane-spanning/non-cytoplasmic ²⁵⁴F – ²⁷⁴V sequence, containing the pro-aggregative AAVILA motif flanked by the hydrophilic arginine = **R** and glutamate = **E** residues (identified previously via analyses with the on-line software tools BETASCAN and TANGO – Section 3.4.2, pp.320-330; Fig 3.19, p.328), is highlighted in yellow.

B: Analysis of the full-length *S. pombe* Rad9 protein amino acid sequence with the on-line bioinformatics software tool COILS.

The X-axis defines the amino acid residue position and the Y-axis defines the relative coiled-coiled probability score on the data plot – probability scores of above 0.5 are significant.

The standard program window settings (14, 21, 28) utilised to dictate the algorithm analytical stringency are indicated – the higher the window setting value the higher the analytical stringency.

The relative regional position of the TMpred- and PHOBIUS- identified potential transmembrane-spanning ²⁵⁴F – ²⁷⁴V/non-cytoplasmic motif sequence (Fig 3.22A, p.335) is highlighted in yellow.

C: Analysis of the full-length *S. pombe* Rad9 protein amino acid sequence with the on-line bioinformatics software tool MULTICOIL.

The X-axis defines the amino acid residue position and the Y-axis defines the relative coiled-coiled probability score on the data plot – probability scores of above 0.5 are significant.

Probability score plots for dimeric repeat motifs, trimeric repeat motifs and the sum total of dimeric and trimeric repeat motifs are indicated.

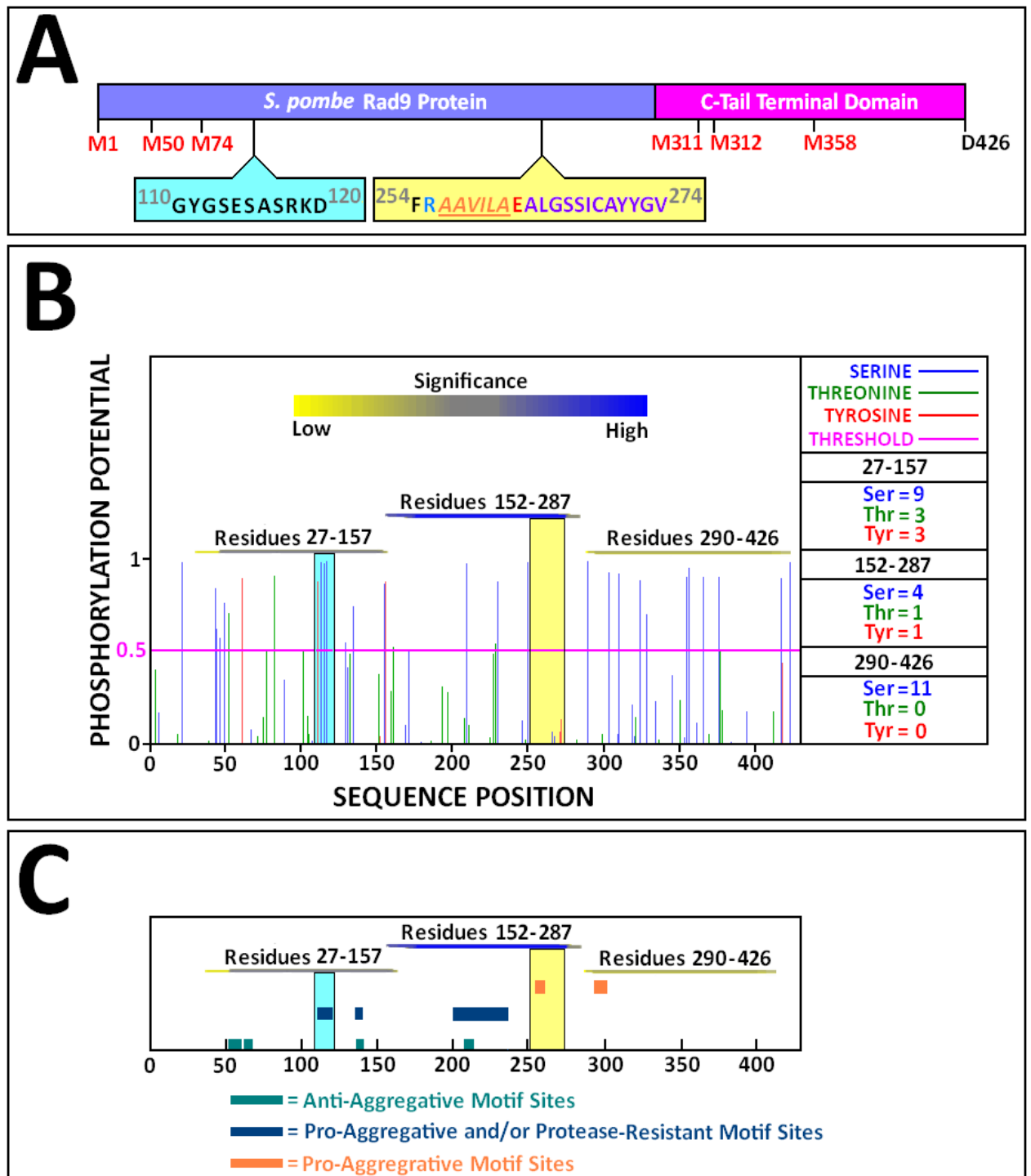
The relative regional position of the TMpred- and PHOBIUS- identified potential transmembrane-spanning ²⁵⁴F – ²⁷⁴V/non-cytoplasmic motif sequence (Fig 3.22A, p.335) is highlighted in yellow.

D: Analysis of the full-length *S. pombe* Rad9 protein amino acid sequence with the on-line bioinformatics software tool MARCOIL.

The X-axis defines the amino acid residue position and the Y-axis defines the relative coiled-coiled probability score on the data plot – probability scores of above 0.5 are significant.

The relative regional position of the TMpred- and PHOBIUS- identified potential transmembrane-spanning ²⁵⁴F – ²⁷⁴V/non-cytoplasmic motif sequence (Fig 3.22A, p.335) is highlighted in yellow.

Fig 3.27: Kinase Site and Aggregative Modulatory Motif Analyses of the REPPER-Identified Coiled-Coil Repeat Domain Sequences within the *S. pombe* Rad9 Protein



A: The relative positions of the potential alternative AUG methionine translational start codon sites of the engineered *S. pombe* Rad9 full-length and truncated protein isoforms (Fig 3.2, p.289) and the C-terminal tail domain region are indicated.

The pro-aggregative protease resistant motif ¹¹⁰G – ¹²⁰D motif, which also contains the potential Wis1 kinase target site at ¹¹¹Y and potential phosphorylated residues ¹¹³S, ¹¹⁵S and ¹¹⁷S (discussed previously in Section 3.4.2, pp.320-330), is highlighted in light blue.

The TMpred- and PHOBIUS-identified potential transmembrane-spanning/non-cytoplasmic ²⁵⁴F – ²⁷⁴V sequence, containing the pro-aggregative AAVILA motif (indicated in orange) flanked by the hydrophilic arginine = **R** and glutamate = **E** residues (identified previously via analyses with the on-line software tools BETASCAN and TANGO – Section 3.4.2, pp.320-330; Fig 3.19, p.328), is highlighted in yellow.

The transmembrane-spanning/non-cytoplasmic ²⁵⁴F – ²⁷⁴V sequence (highlighted in yellow) also contains a putative ATR^{Rad3} kinase-activation “HFD-like” motif (Fig 3.24, p.339), indicated in purple.

B: Analysis of the full-length *S. pombe* Rad9 protein amino acid sequence with the on-line bioinformatics software tool NetPhos2.0.

The X-axis defines the amino acid residue position and the Y-axis defines the relative phosphorylation probability score on the data plot.

The horizontal pink line on the data plot denotes the probability threshold – scores of above 0.5 are significant.

Correlated positions of potential coiled-coil repeat domains and their colour-coded probability significance scale (identified via analysis of the full-length *S. pombe* Rad9 protein amino acid sequence with the on-line bioinformatics software tool REPPER – Fig 3.25, p.) are superimposed on the data plot.

The right margin of the data plot indicates the number of high probability-predicted serine, threonine and tyrosine residues within each potential coiled-coil repeat domain.

The relative positions of the pro-aggregative protease resistant motif ¹¹⁰G – ¹²⁰D motif (highlighted in light blue) and the transmembrane-spanning/non-cytoplasmic ATR^{Rad3} kinase-activation motif (highlighted in yellow) are also indicated.

C: Residue-spanning regional map of the anti-, pro- and protease-resistant motif sites within the *S. pombe* Rad9 protein identified via multiple sequence alignment analyses (described previously on p.321) and utilisation of the aggregation sequence motif-predictive on-line software programs BETASCAN and TANGO.

[Details of these identified motif sequences are provided in Table 3.1, p.327 and Fig 3.19, p.328]

The relative positions of the pro-aggregative protease resistant motif ¹¹⁰G – ¹²⁰D motif (highlighted in light blue) and the transmembrane-spanning/non-cytoplasmic ATR^{Rad3} kinase-activation motif (highlighted in yellow) are indicated.

3.4.3.3 Helix, Strand and Coil Secondary Structural Motif Analyses

In silico analysis of the full-length “wild-type” *S. pombe* Rad9 amino acid sequence with the on-line software program YASPIN indicated that all the engineered *S. pombe* full-length Rad9 variants and the truncated Rad9 variants NΔ49-Rad9-c3xHA (“Rad9-S”) and NΔ73-Rad9-c3xHA (Fig 3.2, p.289) contained significant regions of helix, strand and coil secondary structural motifs within their respective protein supramolecular architectures (Fig 3.28, p.353).

The acquired data also indicated that the protein supramolecular architectures of the engineered *S. pombe* truncated Rad9 variants NΔ311-Rad9-c3xHA and NΔ357-Rad9-c3xHA were comprised almost extensively of significant regions of coil secondary structural motif, interspaced with very low proportions of significant regions of helix secondary structural motif, with a distinctive absence of significant regions of strand secondary structural motif (Fig 3.28, p.353).

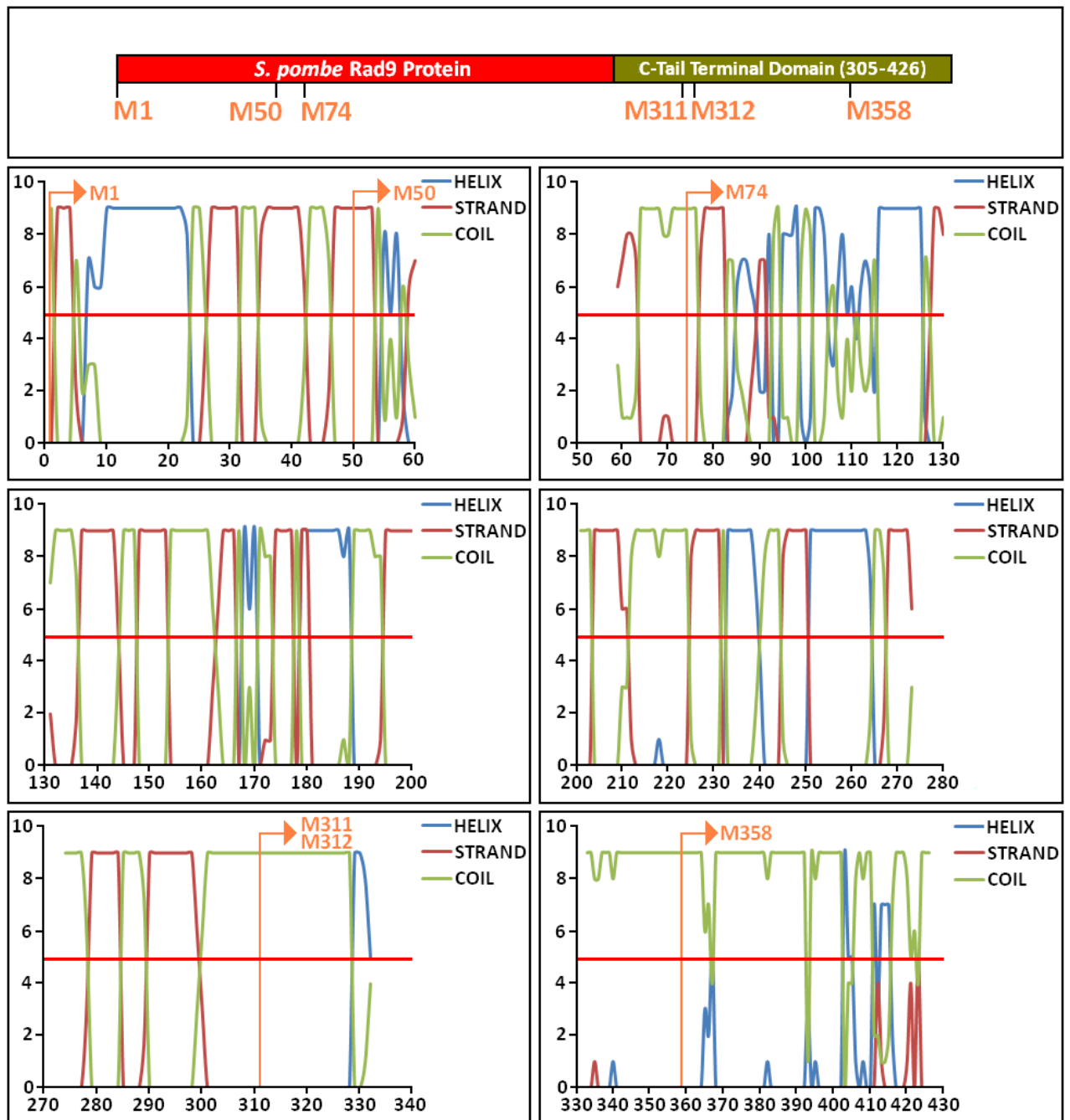
In silico analysis of the full-length “wild-type” *S. pombe* Rad9 amino acid sequence with the on-line software programs COILS, MARCOIL, MULTICOIL and REPPER also indicated zero coiled-coil structural repeat propensity within the C-terminal tail domain of the protein (discussed previously in Section 3.4.3.2, pp.340-350).

Taken together, these *in silico* data are indicative that the supramolecular structural architecture of the engineered *S. pombe* truncated Rad9 variants NΔ311-Rad9-c3xHA and NΔ357-Rad9-c3xHA is of a predominantly random coil nature, which would also account for their almost exclusive intrinsic structural disorder propensity (discussed previously in Section 3.4.1, pp.315-319).

These postulated *in silico* data correlations are also consistent with the highly flexible nature of the “structurally-adaptive” Rad9 C-terminal tail domain (Broustas C.G. and Lieberman H.B., 2012), progressively smaller fragments of which comprise the entire polypeptide sequences of the engineered truncated Rad9 protein variants NΔ311-Rad9-c3xHA and NΔ357-Rad9-c3xHA.

The distinctive absence of extensively distributed helix and strand secondary structural motifs within the sequences of the engineered *S. pombe* Rad9 truncated variants N Δ 311-Rad9-c3xHA and N Δ 357-Rad9-c3xHA (Fig 3.28, p.353) may render these proteins highly unstable and prone to rapid proteolytic degradation, which could also account for the lack of their detected expression in the comparative Western blot assay (Fig 3.15, p.313).

Fig 3.28: Secondary Structural Motif Profile Analysis of spRad9



The relative positions of the potential alternative AUG methionine translational start codon sites of the engineered *S. pombe* Rad9 full-length and truncated protein isoforms (Fig 3.2, p.289) and the C-terminal tail domain region are indicated in the top figure.

Analysis of the relative proportions and localised distribution of helix, strand and coil secondary structural motifs within the “wild-type” full-length *S. pombe* Rad9 amino acid sequence was performed with the on-line software tool YASPIN and the acquired data converted into a graphical format via utilisation of the Microsoft Excel software program.

The X-axis defines the amino acid residue position and the Y-axis defines the predicted helix, strand and coil propensity probability score on the data plots, whilst the orange right-angled arrows indicate the relative positions of the N-terminal methionine start residues of the engineered full-length and truncated *S. pombe* Rad9 protein variants.

The horizontal red line on the data plots denotes the propensity prediction threshold, probability scores above 5 are significant and correlate with plotted values above the threshold line.

3.4.4 Correlated *In Silico* Data Analyses: A Comparative Review of the Critical Structure-Stability Relationships Identified Within the Engineered Full-length and Truncated *S. pombe* Rad9 Isoformic Variants

The degree of intrinsic structural order decreases proportionately with the progressive deletion of increasing longer polypeptide regions relative to the N-terminus within the engineered *S. pombe* Rad9 variants (Fig 3.29A and Fig 3.29B, pp.356-357) – which may be defined in the hierarchy of most structurally ordered as;

Rad9 > Rad9 NΔ49-Rad9 > NΔ73-Rad9 >>> NΔ310-Rad9 = NΔ311-Rad9 >>>> NΔ357-Rad9.

The engineered full-length *S. pombe* Rad9 variants and truncated isoforms NΔ49-Rad9 and NΔ73-Rad9 all contain helix-, strand- and coil- of secondary structural motifs – which may be defined in the hierarchy of most abundant as: coil >strand > helix (Fig 3.29A and Fig 3.29D, pp.356-357).

In contrast, the amino acid sequences of the truncated Rad9 variants NΔ310-Rad9, NΔ311-Rad9 and NΔ357-Rad9 are progressively smaller fragments of the C-terminal tail domain whose secondary structural motif composition approximates to ~95% random coil and ~5% helix (Fig 3.29D, pp.356-357).

These *in silico* data observations are consistent with the highly mobile, intrinsically disordered structural nature of the Rad9 C-terminal tail domain which enables it to engage with a variety of different proteins implicated in cell cycle checkpoint signalling responses and DNA repair pathways (Broustas C.G. and Lieberman H.B., 2012).

The engineered full-length *S. pombe* Rad9 variants and truncated isoforms NΔ49-Rad9 and NΔ73-Rad9 all contain aggregation modulatory and protease resistant motifs (Fig 3.29C, pp.356-357) – which may be defined in the hierarchy of most abundant as:

Aggregation inductive > protease resistant > aggregation suppressive

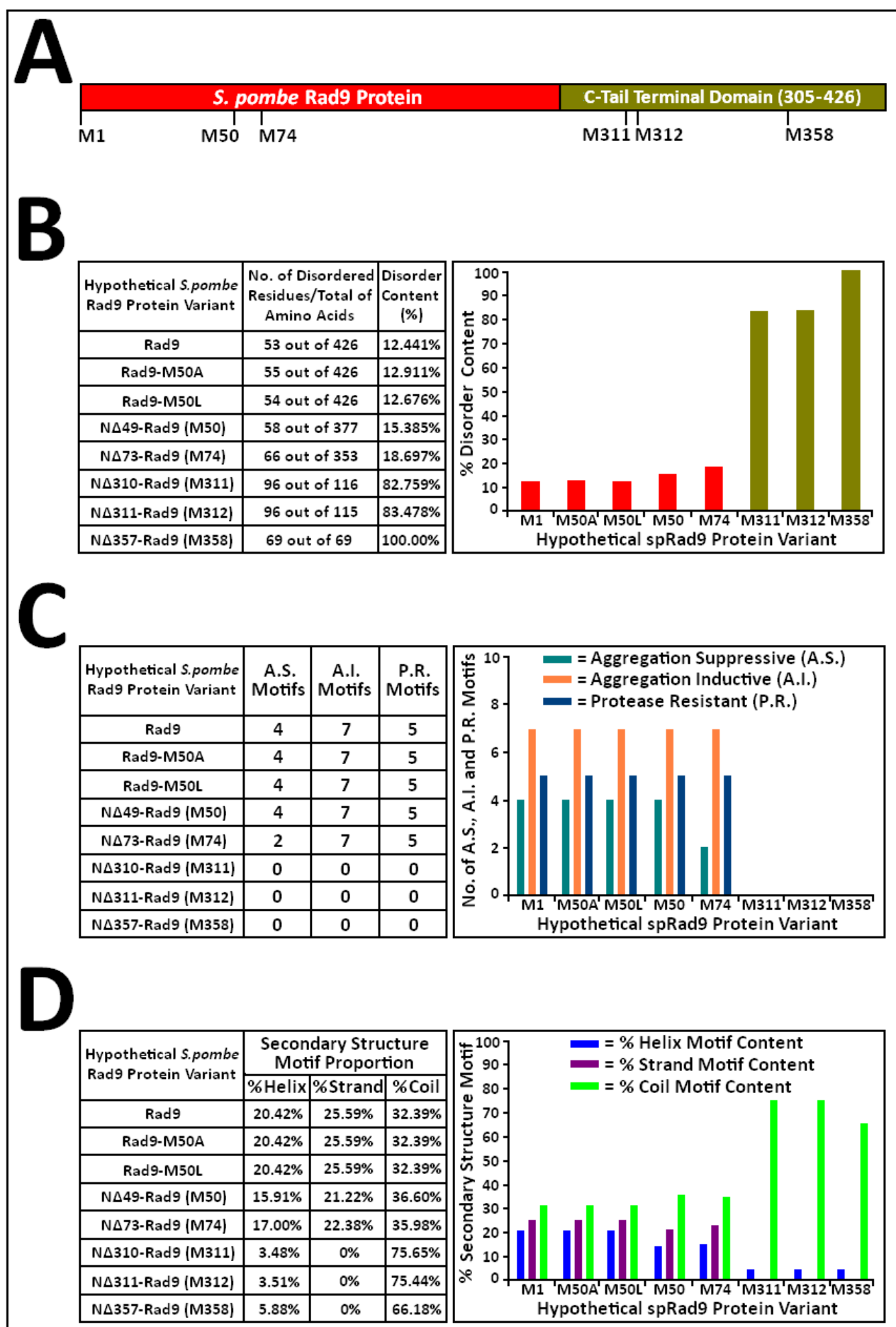
Intriguingly, the relative proportion of aggregation suppressive motifs within the engineered truncated *S. pombe* Rad9 variant NΔ73-Rad9-c3xHA is 50% less than that of the engineered *S. pombe* full-length Rad9 variants (Rad9-c3xHA, Rad9-(M50A)-c3xHA and Rad9-(M50L)-c3xHA) and the truncated NΔ49-Rad9-c3xHA variant (Fig 3.29C, pp.356-357) – which may be correlated with the observed ~50% equivalent reduction in the relative level of expression of the NΔ73-Rad9-c3xHA protein in the comparative Western blot assay (Fig 3.15, p.313).

In this context, the suppressed level of NΔ73-Rad9-c3xHA protein expression may be a consequence of its lower anti-aggregative motif content which could enhance its aggregation and denaturing propensity, such that it is more prone to sumoylation- and/or ubiquitination- mediated proteolytic targeting and thus reduce its cytological half-life.

In contrast, the amino acid sequences of the truncated Rad9 variants NΔ310-Rad9, NΔ311-Rad9 and NΔ357-Rad9 all lack aggregation modulatory and protease resistance motifs (Fig 3.29, pp.356-357).

The lack of substantial intrinsic structural order, protein aggregation modulatory motifs, protease resistant motifs and functional secondary structural domains within the engineered C-terminal tail domain-derived truncated *S. pombe* Rad9 variants, NΔ311-Rad9-c3xHA and NΔ357-Rad9-C3xHA, may render these proteins highly unstable within the cell and particularly susceptible to rapid proteolytic degradation, which would account for the absence of their detected expression in the Western blot assay (Fig 3.15, p.313).

Fig 3.29: Stability Profiling of the *S. pombe* Rad9 Protein Isoforms



A: Basic map of the *S. pombe* Rad9 protein indicating the relative positions of the alternative translational start-site AUG-encoded methionine residues, which are the equivalent N-termini of the engineered Rad9 isoforms.

The C-terminal tail domain region is also indicated.

B: Comparative analysis of the relative intrinsic structural disorder content within the engineered full-length and truncated *S. pombe* Rad9 protein variants performed via analysis of their respective amino acid sequences with the on-line software tool DisCon (Mizianty M.L. *et al*, 2011).

C: Comparative analysis of the relative potential pro-aggregative, anti-aggregative and protease resistant motif content within the engineered full-length and truncated *S. pombe* Rad9 protein variants (discussed previously in Section 3.4.2, pp.320-330).

D: Comparative analysis of the relative percentage of potential secondary structural helix, strand and coil motif content within the engineered full-length and truncated *S. pombe* Rad9 protein variants determined via utilisation of the on-line bioinformatics tool YASPIN (Lin K. *et al*, 2004) – discussed previously in Section 3.4.3.3, pp.351-353.

Chapter 4

**Supportive Experimental Evidence for
the Expression of Novel Truncated Type
Variants of the *S. pombe* Rad9 Protein**

4.1 Introduction

Early experimental investigations into *S. pombe rad9* gene expression revealed that it was comprised of 4 exons and three introns which were spliced into two alternative transcriptional products – notably; one mRNA sequence in which all the introns were excised and another mRNA sequence in which intron 1 was retained (Murray J.M. *et al.*, 1991).

Retention of intron 1 within the *S. pombe rad9* mRNA transcript would result in the premature termination of the translational product acquired from the first AUG initiation start-codon corresponding to the first methionine residue (M1) of the *S. pombe* Rad9 protein (Fig 4.1, p.361)

The next accessible translation-viable “down-stream” AUG initiation start-codon, within this intron 1-retained *rad9* mRNA transcript would correspond to the 50th methionine amino acid residue (M50) within the *S. pombe* Rad9 protein with consequential expression of a truncated Rad9 protein variant (“Rad9-S”) which lacks the first 49 amino acids situated in the N-terminus of the full-length *S. pombe* Rad9 protein (Fig 4.1, p.361).

Since internal ribosome entry sites (IRES) are typically situated upstream of the first AUG translational start codon (Spriggs K.A. *et al.*, 2005; King H.A. *et al.*, 2010), it is also unlikely that a functional IRES sequence exists within the transcribed mRNA region spanning the AUG1 and AUG50 codons.

Correlated with these phenomena, the mechanism of expression of the “Rad9-S” truncated protein variant in *S. pombe* cells may originate from alternative mRNA splicing of the full-length Rad9 gene, involving retention of intron 1, with a consequential translational shift to a downstream AUG initiation site at M50 respectively (Fig 4.1, p.361).

Certain types of RNA hairpin motifs possess the capability to recruit ribosomes independently of IRES sequences and the formation of these secondary loop structures may also be temperature dependent, in which their respective supramolecular topologies are modulated via conjunctive interactions with RNA annealers, RNA helicases and/or RNA chaperones (Choi S.I. *et al.*, 2009; Dunker A.K. and Uversky V.N., 2010; Herschlag D., 2005; Liu J. *et al.*, 2006; Rajowitsch L. *et al.*, 2007; Russell R. *et al.*, 2008; Tompa P. and Csermely P., 2004; Zu T. *et al.*, 2011).

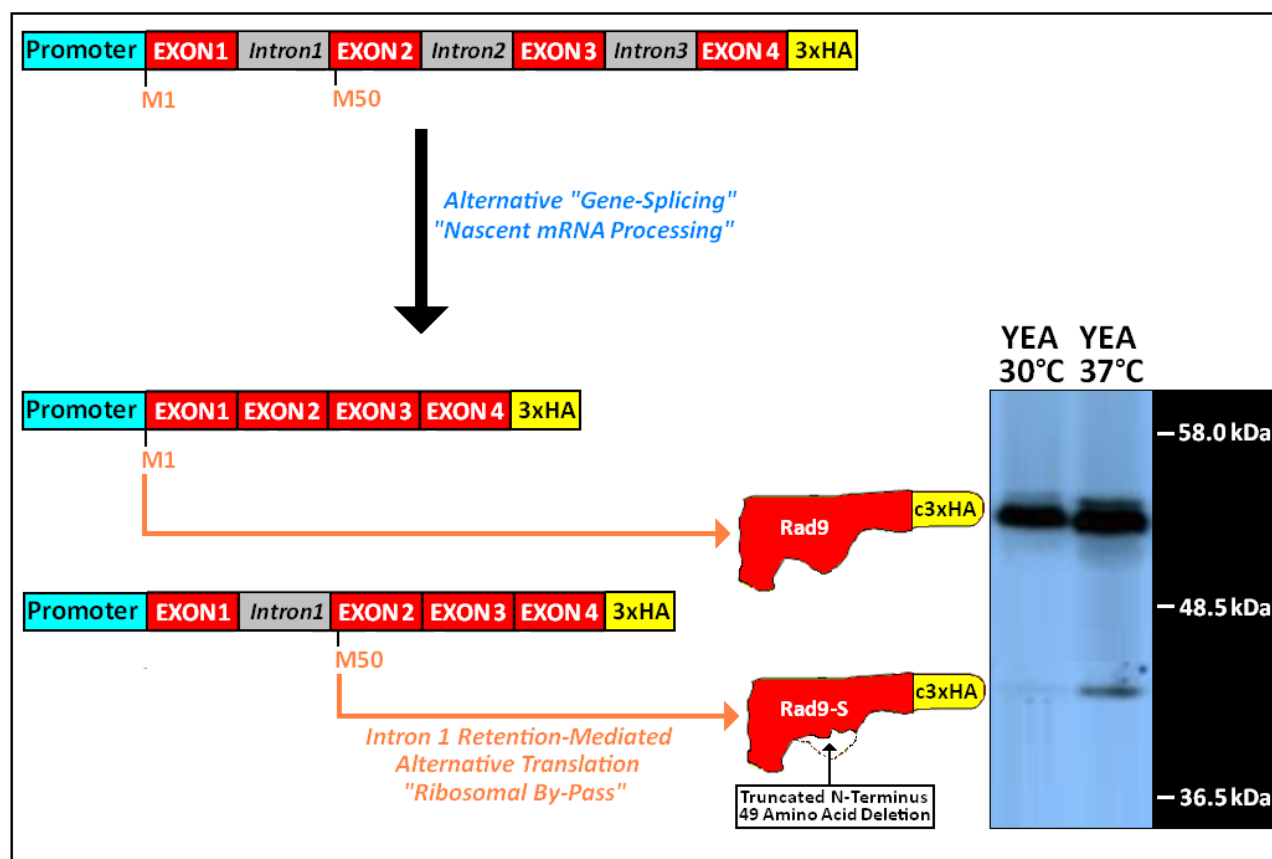
Comparative sequence analysis of the three introns contained within the *S. pombe rad9* gene indicated that intron 1 possesses an unconventional degenerative 5' splice-site consensus sequence and contained a unique, potential stem-loop aptamer-like consensus sequence (Fig 4.2, p.362).

On the basis of these phenomena and *in silico* observations, it was postulated that under certain conditions of environmental stress (eg heat shock) and/or genotoxic stress, intron 1 may adopt a unique stem-loop type of secondary structural configuration which prevents its excision during splice-processing of the *S. pombe rad9* gene (Fig 4.3, p.363; Fig 4.4, p.364).

In this hypothetical context, it was also postulated that the retained intron 1 sequence within the transcribed mRNA of the *S. pombe rad9* gene may also function as a novel RNA stem-loop aptamer-based “riboswitch” that may induce supramolecular configurational changes within the mRNA molecule (Fig 4.3, p.363; Fig 4.4, p.364).

It was proposed that these intron 1-mediated supramolecular configurational changes within the transcribed *S. pombe rad9* mRNA may block access of the ribosomal-based translational machinery at the first AUG start codon (methionine 1), but facilitate its access to the alternative AUG start codon at Methionine 50 – with consequential induction of elevated translational expression of the truncated “Rad9-S” protein variant (Fig 4.3, p.363; Fig 4.4, p.364).

Fig 4.1: Postulated Intron 1 Retention Model of “Rad9-S” Expression



Retention of intron 1 within the *S. pombe rad9* mRNA transcript could result in premature translational termination of full-length Rad9 protein expression (via ribosomal recruitment to the first AUG methionine codon initiation site) and re-initiation of translation via ribosomal recruitment at the next downstream AUG codon initiation site (situated at methionine 50).

The right-hand side of the figure indicates the protein bands, detected in the Western blot assay (described below), that correspond to expression of the full-length Rad9 protein (Mr ~ 50kDa) and the truncated “Rad9-S” variant (Mr ~ 40kDa).

“Wild-type” *S. pombe* cells (*rad9-c3xHA*) were cultured in YEA medium at 30°C to a density of 1×10^7 cells/mL.

[The full genotypes of the utilised *S. pombe* strains are detailed in Appendix 2.11.6 , p.279].

Aliquots (5×10^8 cells) were then withdrawn from the respective cultures and re-incubated in YEA medium at either 30°C or 37°C for a further 30 minutes.

1.4×10^7 cells, acquired from each respective re-incubated culture, were utilised for the preparation of TCA-precipitated total protein extracts.

20µL aliquots of the prepared protein samples were resolved on a 10% SDS-PAGE gel which was then utilised in a Western blot analysis probed with the anti-HA primary antibody.

[Protein sample preparation, SDS-PAGE resolution and Western blot methodologies are detailed in Section 2.8.1, pp.200-202; Section 2.8.4, pp.223-224 and Section 2.8.6, pp.231-233]

Fig 4.2: Internal Intron Sequences within the *S. pombe* Rad9 Gene

The *Schizosaccharomyces pombe rad9* Gene Sequence (DNA Sense Strand)

5'ACCAGTTTCAATTCTGTTTGTCAAAAATTGCTATCGTTATTCGTTTCAGCATTTCGTCTACATCAAT
 TCACGTA CTGGTATATAAAATGGAATTCACTGTTTCAAATGTTAATCTTCGGGACCTCGCAAGGAT
 CTTTACAAATCTTTCTAGAATCGATGATGCTGTCAACTGGGAAATTAACAAAAATCAGGTGTGTG
 GAACTTTTTTCAAACCTTACTAAACATTGAAAATAATTGGTAAAGATAGAGATTACATGTTTAAATT
 CTTCTAGGTCAGGATTTAGCATGTGACTTTAAAAAAGGCATTTTTTTGACAAGTACATTTTTTCAGC
 CGGATTCCGTCCTGTTGACGGGATTGATGACTCCTACAATACGTATTCGTACGCAAGTCAAGCCCA
 TACTATCTGTGTTAGAAAACAAAATCTTTGATTTTCATCCCGACTGTCGTCACTACCAATAGCAAGA
 ACGGTTATGGCAGTGAATCTGCAAGCAGAAAAGATGTGATTGTCGAGAATGTTCAAATCTCAATCT
 CTA CTGGTAGCGAGTG TAGGATTATATTTAAATTCTTATGCAAGCACGTTACTGTAGTTTGTCCGTC
 TTATTATTTTATTTGCTCTAATAACGTTTATTCATCAAGGAGTGATTA AAAACATATAAAAATATCATA
 TGAACAAACCCAAACTTTACACGCTGTTTTTGATAAATCTCTTAGTCAACAATAATTTTCAAATAAAC
 TCAAAAATCTAAAAGATTTGACTGAACATTTTGGTCAGAGAACGGAAGAGCTTACAATTCAACCA
 CTTCAAGAACGTGTTTTACTTACAAGTTTACAGAAGAGGTCGTACATAATAGAGATATTTTGAAG
 CAACCTACCCAAACAACCTGTTTCCATTGATGGTAAAGAATTTGAACGCGTCGCACTTAATGAGGGA
 GTCTCTGTTACCCTTTCTCTACGTGAATTTCTGTGCTGCCGTCAATTTAGCAGAGGCATTGGGAAGC
 TCGATTTGTGCATATTACGGTGTCCAGGAAAACCGATACTTTTAACTTTTGCAAAGGGGAAAAAT
 TCCGAAATTGAAGCGCAGTTCATTCTTGCAACTGTAGTTGGATCAGATGAACAAGAGGTGTCATCT
 ATGATGGGAAAATAGATGGCAGCACAGTTCAACACCAGCTTCTCTGTTCAATTCAGTAGAGCGCAAC
 AACTCATTGACTGCTGTAGCACATAATCCCCTGGATCTATTGGATGGCAAACCTGATGTATGTAAAT
 TCGGCTTTAGTAACTAACAATAATTTATTAACATTAACTTTATAGCAAAGTGACTCATCCAGAAT
 GTTAAATCTGCGCTTGACCGAAGCGACGAAACTAATGGCATTAAAGGAGCCATCAACCACAAACG
 ATGCTGGTCAATCATTGTTCTTAGATGGTATTCCAAATGAATCCGAGCTTGCTGCTTTTAATAATG
 ATGTGAACGATGATGCCGAATTTGGACCAACGCAAGCTGAACAAAGTTATCATGGCATTCTCTC
 AGGAAGACTAGGAAAATCCTTCTTTGCTATGGTGTGTAATAATTAAGAACATTTACAGGTGCTTGTG
 ACAACCTCATAAAAACACAGCACTCATATTATATAATGTACAATATTTATCAATAATTTAGTTTTTTT
 TAAC3'

 = Exon 1 5' Un-Translated Region

 = Exon 4 3' Un-Translated Region

NNNNNNN = Exons 1 – 4 Translated Regions

 = Introns 1 – 3

NNNNNNN = Consensus Splice Signal Sequences within Introns 1 – 3: GTANGT = 5' Donor Site*

CTAAN = Branch Point

AG = 3' Acceptor Site

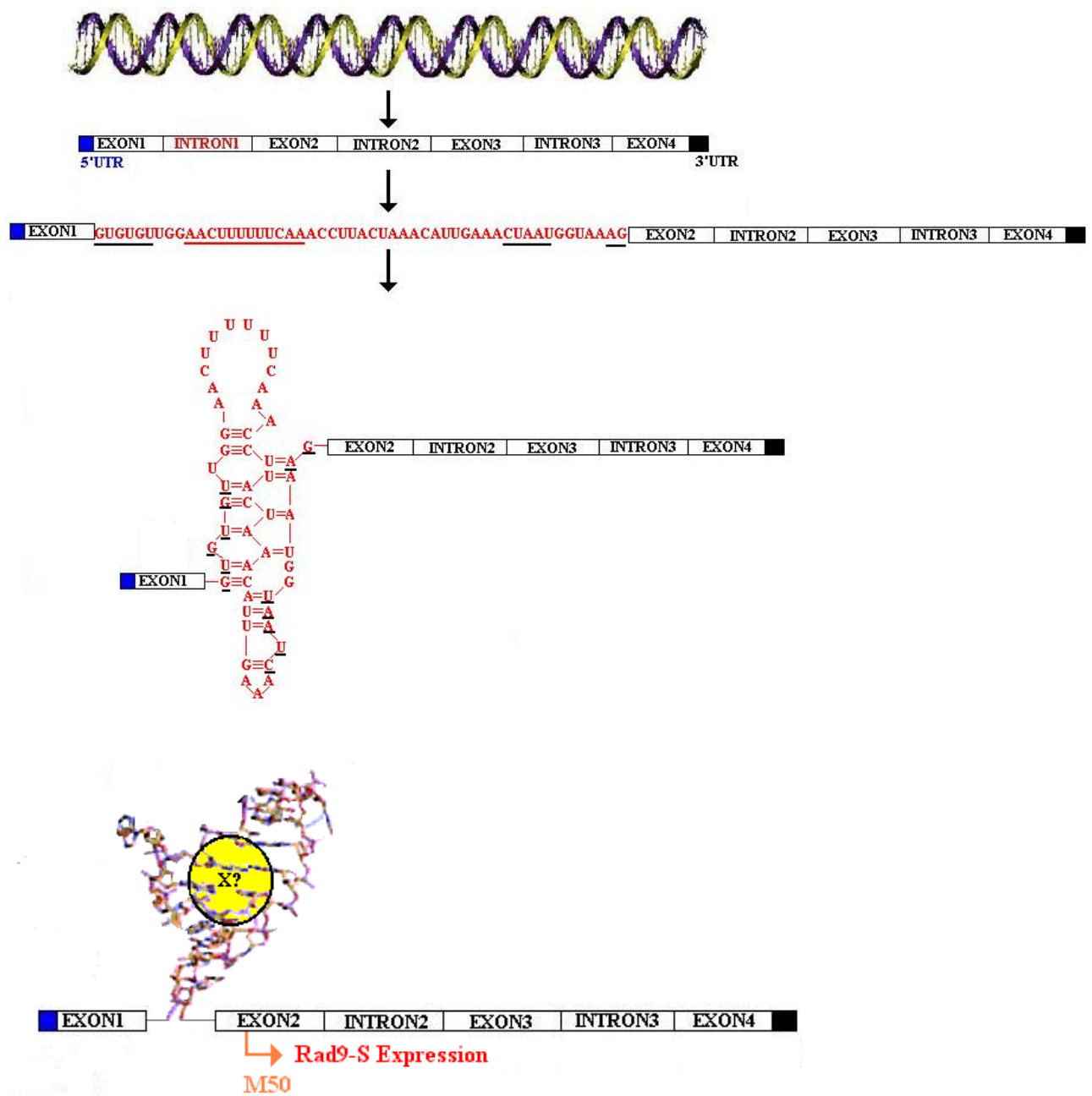
[*NOTE: Intron 1 Contains the Degenerative 5' Donor Site Sequence GTGTGT as Opposed to the Conventional 5' Donor Site Consensus Sequence GTANGT]

ATG = Full-Length Rad9 Translation Met Start Codon Site

ATG = Rad9-S Alternative Splice Translation Met Start Codon Site

Note: Intron 1 also contains a potential AACTTTTTCAA stem-loop consensus sequence which may function as a component of an RNA aptamer/Riboswitch-linked regulatory mechanism, that upon folding, may adopt secondary RNA structure(s) which effectively block the 5'-donor, branch and the 3'-acceptor splice sites from snRNP-processed cleavage via sterically-shielded extensive base-pair formation respectively.

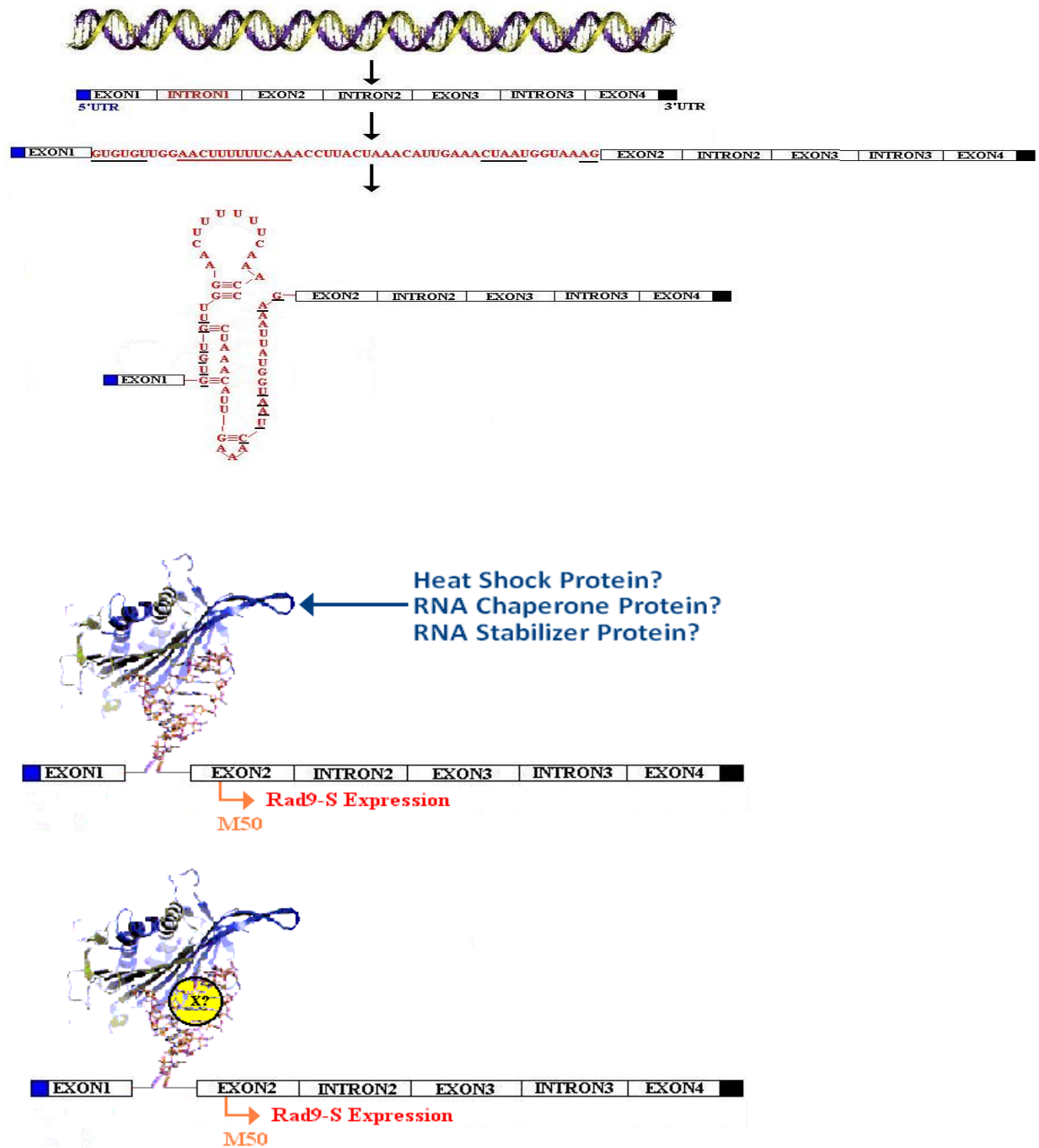
Fig 4.3: Intron 1 RNA Aptamer-Mediated Rad9-S Expression Model



An unusual palindromic stem-loop like sequence identified within Intron 1, absent in Introns 2 and 3 of the *S. pombe rad9* gene, may act as a stem-operator loop and/or RNA aptamer/Riboswitch binding-site for specific ligand(s) – “X?” depicted above, in which ligand-binding induces a supramolecular conformational change in the secondary intron 1 RNA structure with consequential thermodynamically/entropically stabilised alternative hydrogen-bond associations which sterically-shield the 5'-donor, branch and 3'-acceptor splice sites from the snRNP proteins with consequential intron 1 retention in the processed mature mRNA and expression of the truncated Rad9-S protein variant via the alternative AUG codon start site at position M50 respectively.

Alternatively, the 5'-untranslated region and Exon 1 sequences may participate in associative supramolecular secondary structure interactions with ligand(s) – “X?”, thereby acting as a RNA-aptamer/riboswitch trigger which promotes formation of the intron 1 step-loop secondary supramolecular figuration that prevents its excision via snRNPs during mRNA splicing and processing, resulting in favoured expression of the truncated Rad9-S protein via the alternative AUG start codon site at position M50 respectively.

Fig 4.4: Intron 1 Aptamer Model of Heat-Shock Rad9-S Induction



Elevated levels of the truncated Rad9-S protein variant in response to heat stress induction may be a consequence of increased flexibility modifications to the supramolecular structure of the postulated intron 1 RNA stem operator loop, mediated via thermal dissociation of the lower energy A=T base-pairs, thereby facilitating ribosomal access to the alternative translational AUG codon initiation site at position M50 with subsequent enhancement Rad9-S Expression.

The 5'-donor, branch and 3'-acceptor splice sites within the intron 1 mRNA sequence are still sterically-shielded from the snRNP spliceosomal complexes due to retention of its stem operator loop configuration via the higher energy GC base-pairs and /or associative interactions with other ligand(s) – “X?” or proteins (eg heat shock proteins, RNA chaperone proteins and/or RNA stabilizer proteins).

4.2 Induced Expression of Rad9-S is a Specific Cytological Response to Hyperthermic Stress

In order to ascertain whether or not the induction of the truncated “Rad9-S” protein variant was an exclusive heat shock response, as opposed to alternative types of genotoxic and/or micro-environment stresses, Western Blot analyses were performed on TCA-precipitated total protein extracts acquired from YEA broth cell cultures of the “cre-lox”– constructed *S. pombe* strain *rad9-c3xHA* exposed to a variety induced adverse cytological conditions.

These induced stresses were cold shock, heat shock, pH shock (acidic shock vs alkaline shock), osmotic stress (1M sorbitol, LiAc-TE-PEG, polyethyleneglycol – PEG), glucose starvation (lactose substituted for glucose in the YEA medium), oxidative stress (in the presence of hydrogen peroxide, menadione, sodium nitroprusside and tert-butylhydroperoxide), mutagenic stress (hydroxylamine, ethidium Bromide, sodium metabisulphite), metal ion toxicity (Li^+ , Na^+ , K^+ , Mg^{2+} , Ca^{2+} , Mn^{2+} , Co^{2+} , Ni^{2+} , Cu^{2+}), PI3-kinase inhibition (caffeine), ribonucleotide biosynthesis inhibition (hydroxyurea), mitotic inhibition (thiabendazole), DNA cleavage/cross-linking/adduct-forming agent exposure (methylmethane sulphonate, mitomycin C, 4-methyl-N'-nitro-N-nitrosoguanidine, 4-nitroquinoline-1-oxide, phleomycin, U.V. irradiation) and topoisomerase inhibition (camptothecin, ellipticine, etoposide) – Fig 4.5, pp.368-370.

Increasing % (v/v) concentrations of dimethylsulphoxide (DMSO) and ethanol (EtOH), which were utilised for preparation of the stock solutions of the oxidative stress inducers, caffeine and various genotoxic agents, were also tested and served as negative experimental controls for confirmation that exposure of “cre-lox”– constructed *S. pombe* strain *rad9-c3xHA* cultures to these solvents did not induce expression of the truncated “Rad9-S” protein variant within the cells (Figs 4.5H and 4.5I, pp.368-370).

Whilst the acquired Western blot data indicated that genotoxic-, hypothermic-, redox-, glucose depletion-, acidic- and alkaline- induced stresses did not induce expression of the truncated “Rad9-S” protein variant (Fig 4.5, pp.368-370), the possibility that one or more of these conditions may be implicated in the suppression of “Rad9-S” expression cannot be ruled out.

Hypo-osmotic, hyper-osmotic and high concentrations of specific metal ions within the cytological nuclear micro-environment can alter the topological configuration of DNA and/or the chromatin supramolecular structure with consequential suppression or induction of the expression of specific genes, in which the modulation of specific DNA-protein interactions may be implicated and in some instances contribute to the development of carcinogenesis (Desoize B., 2003; Durham T.R. and Snow E.T., 2006; McClellan J.A. *et al*, 1990; Ni Bhriain N. *et al*, 1989; Ordóñez E. *et al*, 2008; Zambelli B. *et al*, 2012).

In order to ascertain whether or not hypo-osmotic, hyper-osmotic and/or high concentrations of specific metal ions of the *S. pombe rad9* gene may also be implicated in the modulated expression of the truncated “Rad9-S” protein, individual YEA broth cultures of the “cre-lox”– constructed *S. pombe* strain *rad9-c3xHA* cells were exposed to either 1M sorbitol, LiAc-TE-PEG, polyethyleneglycol – PEG, Li⁺, Na⁺, K⁺, Mg²⁺, Ca²⁺, Mn²⁺, Co²⁺, Ni²⁺ or Cu²⁺ (Fig 4.5, pp.368-370).

Subsequent Western blot analysis of the TCA total protein extracts acquired from these experimental *S. pombe rad9-c3xHA* cell cultures treated failed to detect the presence of “Rad9-S” (Fig 4.5, pp.368-370), which was indicative that hypo-osmotic, hyper-osmotic and high concentrations of metal ions are not implicated in the mechanism of induction of “Rad9-S” truncated protein variant expression.

However, these data could be indicative that hypo-osmotic, hyper-osmotic and/or high concentrations of specific metal ions may be implicated in the suppression of “Rad9-S” truncated protein variant expression (Fig 4.5, pp.368-370).

Post-transcriptional 5'-methylcytosine DNA modifications are also known to be implicated in epigenetic-based mechanisms which may regulate the expression of various genes and/or result in their “silenced” suppression (Jones P.A. *et al*, 2012).

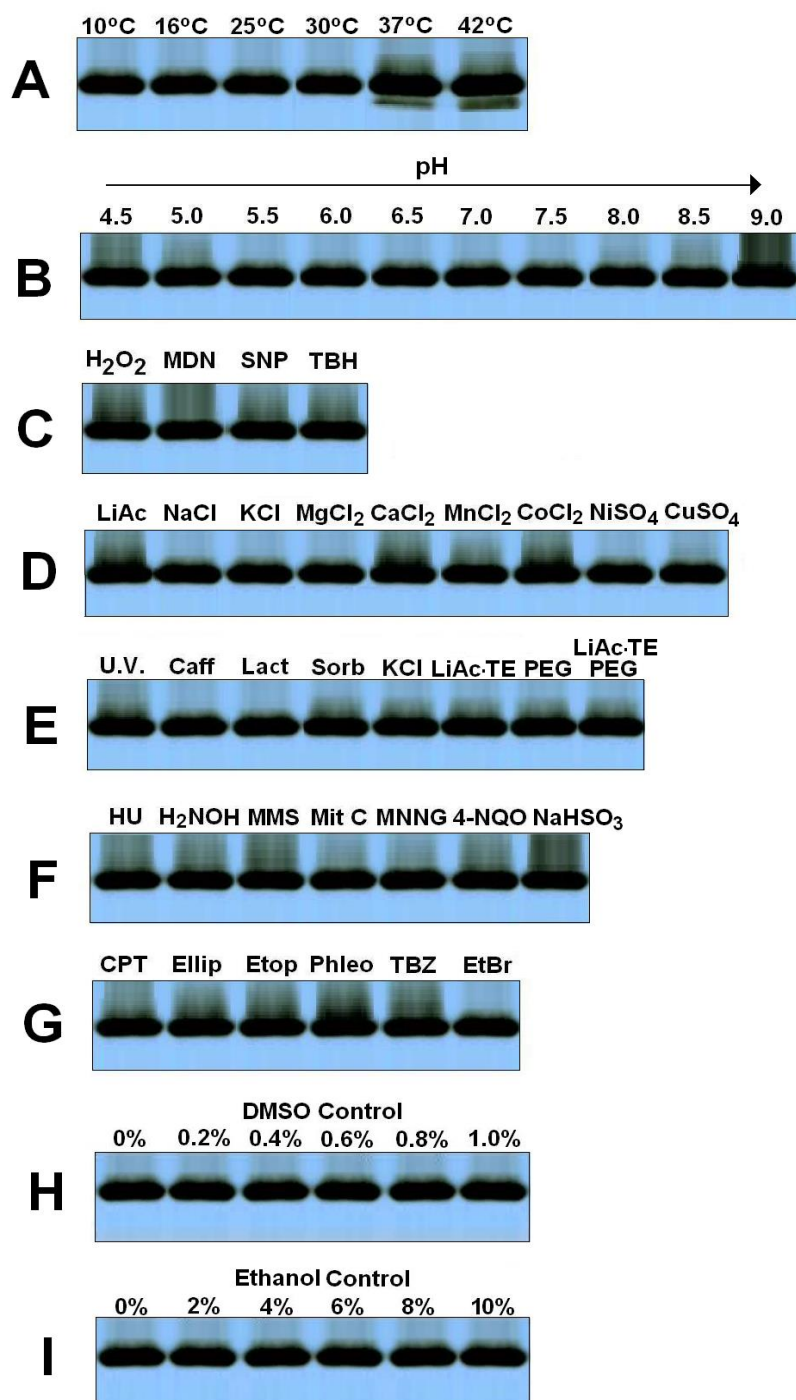
Intriguingly, hypermethylation at CpG islands within introns 1 and 2 of the human *RAD9A* gene has been detected within breast and prostate tumours, that may be implicated in the regulation of expressed Rad9A protein levels within these neoplastic cell types which may also be a key biochemical factor that “governs” their metastatic capacity (Chan V. *et al*, 2008; Cheng C.K. *et al*, 2005; Zhu A. *et al*, 2008).

In order to ascertain whether or not DNA methylation of the *S. pombe rad9* gene may also be implicated in the modulated expression of the truncated “Rad9-S” protein, a YEA broth culture of the “cre-lox”– constructed *S. pombe* strain *rad9-c3xHA* cells was exposed to the mutagenic agent sodium metabisulphite, which initiates the sulphation-mediated deamination-type reactive conversion of cytosine to uracil and 5'-methylcytosine to thymine within DNA (Clark S.J. *et al*, 1994).

Subsequent Western blot analysis of the TCA total protein extract acquired from the *S. pombe* strain *rad9-c3xHA* cell culture treated with sodium metabisulphite failed to detect the presence of “Rad9-S” (Fig 4.5F, pp.368-370) – which may indicate that DNA methylation of the *S. pombe rad9* gene is not implicated in epigenetically-silenced “Rad9-S” expression.

Taken together, the acquired experimental data confirmed that the mechanism of inductive expression of the truncated “Rad9-S” variant is an exclusive heat shock type response (Fig 4.5, pp.368-370).

Fig 4.5: Experimental Induction of *S. pombe* “Rad9-S” Expression



Individual 50mL YEA broth medium cell cultures of the “Cre-Lox” – constructed *S. pombe* strain *rad9-c3xHA* were incubated at 30°C over a 12 hour time period, then diluted to an optical density $A_{595} = 0.25$ with the appropriate volume of YEA medium and the resultant diluted cultures re-incubated at 30°C for a further time period of ~2.5 hours until they had attained an optical density value of $A_{595} = 0.5$ – after which time the resultant cultures of actively cycling cells were re-incubated at 30°C for a further 30 minutes under imposed experimental conditions of specific types of environmental stress or induced DNA damage exposure (a comprehensive explanation of Figs A – I is provided on the following pages, pp.369-370).

TCA-precipitated total protein extract samples were then prepared from the appropriate *calculated volumetric aliquot of each culture (*equivalent to 10 A_{595} optical density units) of which 20 μ L aliquots were resolved on 10% SDS-PAGE gels which were then utilised in comparative Western blot analyses probed with the anti-HA primary antibody (Figs A – I above).

[Protein sample preparation, SDS-PAGE resolution and Western blot methodologies are detailed in Section 2.8.1, pp.200-202; Section 2.8.4, pp.223-224 and Section 2.8.6, pp.231-233]

Experimental Induction of “Rad9-S” – Figure Legend (Fig 4.5)

A: Exposure of each YEA broth culture to the defined temperature for 30 minutes.

B: Exposure of each YEA broth culture to the defined pH for 30 minutes
[in this case the cell culture was spun down at 3000rpm at 25°C for 5 minutes, the supernatant discarded and the cell pellet re-suspended in the identical volume of YEA medium adjusted to the specific pH value*, prior to incubation at 30°C for 30 minutes]

[* **Note**: Each aliquot of pH-adjusted YEA medium was filter-sterilised, via utilisation of a sterile syringe and 0.2µm filter assembly prior to cell pellet re-suspension]

C: Exposure of each YEA broth culture to the oxidative stress-inducing agent for 30 minutes
[in this case the cell culture was spun down at 3000rpm at 25°C for 5 minutes, the supernatant discarded and the cell pellet re-suspended in the identical volume of YEA medium which contained 400µM of either:
Hydrogen Peroxide (H₂O₂)
Menadione (MDN)
t-Butylhydroperoxide (TBH)
Sodium Nitroprusside (SNP)]

The resultant cultures were then incubated at 30°C for 30 minutes

D: Exposure of each YEA broth culture to the respective metal ion species for 30 minutes
[in this case the cell culture was spun down at 3000rpm at 25°C for 5 minutes, the supernatant discarded and the cell pellet re-suspended in the identical volume of YEA medium which contained 400mM of the appropriate metal ion salt]

The resultant cultures were then incubated at 30°C for 30 minutes

E: Exposure of each YEA broth culture to the respective environmental condition for 30 minutes
[In the case of U.V. exposure, the cell culture was spun down at 3000rpm at 25°C for 5 minutes, the supernatant discarded and bottom of the centrifuge tube (containing the cell pellet) excised with a scalpel blade and exposed to 50 J/M² U.V. irradiation prior to re-suspension of the treated cell pellet in the identical volume of YEA medium]

[In the case of the other imposed environmental conditions, the cell culture was spun down at 3000rpm at 25°C for 5 minutes, the supernatant discarded and the cell pellet re-suspended in the identical volume of YEA medium which comprised either:

10mM Caffeine in YEA (Caff)
3% (w/v) Lactose in YEA (Lact)
1M Sorbitol in YEA (Sorb)
1M KCl in YEA (KCl)

LiAcTE Buffer (made up in YEA medium instead of water) – detailed in Ch.2, Section 2.2.5, p.166

40% (w/v) Polyethylene Glycol 4000 in YEA (PEG)

LiAc-TE-PEG Buffer (made up in YEA instead of water) – detailed in Ch.2, Section 2.2.5, p.166

The resultant cultures were then incubated at 30°C for 30 minutes

Experimental Induction of “Rad9-S” – Figure Legend (Fig 4.5)

[Continued]

F: Exposure of each YEA broth culture to the respective genotoxic agent for 30 minutes
[in this case the cell culture was spun down at 3000rpm at 25°C for 5 minutes, the supernatant discarded and the cell pellet re-suspended in the identical volume of YEA medium which contained either:
10mM Hydroxyurea (HU)
4µM Hydroxylamine (H₂NOH)
0.05%(v/v) Methylmethanesulphonate (MMS)
4µM Mitomycin C (Mit C)
4µM 4-Methyl-N'-Nitro-N-Nitrosoguanidine (MNNG)
4µM 4-Nitroquinoline-1-Oxide (4-NQO)
4µM Sodium Metabisulphite (NaHSO₃)

The resultant cultures were then incubated at 30°C for 30 minutes.

G: Exposure of each YEA broth culture to the respective genotoxic agent for 30 minutes
[in this case the cell culture was spun down at 3000rpm at 25°C for 5 minutes, the supernatant discarded and the cell pellet re-suspended in the identical volume of YEA medium which contained either:
40µM S-(+)-Camptothecin (CPT)
4µM Phleomycin (Phleo)
40µM Thiabendazole (TBZ)
4µM Ethidium Bromide (EtBr)

[in the case of Ellipticine (Ellip) and Etoposide (Etop) the cell pellet was re-suspended in 1mL of Lyticase-YEA and incubated at 30°C for 20 minutes – as described in Section 2.9.2.2 (ii), protocol stages (vi) and (vii), p. 250, after which time the treated cells were pelleted and washed in 4x 1mL fresh aliquots of YEA – as described in the Section 2.9.2.2 (ii), protocol stage (xi), p.250.

The resultant cell pellet was then re-suspended in an initial identical volume of YEA (ie the total volume of YEA in the diluted *S. pombe* strain culture which had an adjusted optical density value of $A_{595} = 0.5$ and also contained 40µM of Ellipticine or Etoposide]

The resultant cultures were then incubated at 30°C for 30 minutes.

H: Exposure of each YEA broth culture to the respective concentration of Dimethylsulphoxide solvent (DMSO) for 30 minutes
[in this case the cell culture was spun down at 3000rpm at 25°C for 5 minutes, the supernatant discarded and the cell pellet re-suspended in the identical volume of YEA medium which contained the appropriate % (v/v) of DMSO solvent prior to re-incubation at 30°C for 30 minutes]

I: Exposure of each YEA broth culture to the respective concentration of % (v/v) Ethanol (EtoH) for 30 minutes at 30°C
[in this case the cell culture was spun down at 3000rpm at 25°C for 5 minutes, the supernatant discarded and the cell pellet re-suspended in the identical volume of YEA medium which contained the appropriate % (v/v) of DMSO solvent prior to re-incubation at 30°C for 30 minutes]

4.3 The Truncated “Rad9-S” Protein Variant is an Alternative Translational Product that Originates from the Internal AUG Initiation Codon Situated at Methionine 50 and Whose Expression is Independent of Intron 1 Retention Within the Transcribed *S. pombe rad9* mRNA

In order to verify whether or not the truncated “Rad9-S” protein variant was indeed an alternative translation product, originating from ribosomal scanning at the internal AUG codon start-site at methionine 50 within a transcribed intron 1-retained *rad9* mRNA, comparative Western blot analyses were performed on TCA-precipitated total protein extracts acquired from YEA broth cell cultures of the “Cre-Lox”-constructed *S. pombe* strains *rad9-c3xHA*, *rad9-(Δ Intron1)-c3xHA*, *rad9-M50A-c3xHA*, *rad9-M50L-c3xHA*, *N Δ 49-rad9-c3xHA* and *N Δ 73-rad9-c3xHA* exposed to heat shock in the absence or presence of a translational inhibitor type anti-biotic – cycloheximide (Fig 4.6, p.373).

The presence of detected “Rad9-S” expression in TCA-precipitated total protein extracts acquired from the experimental culture of the *rad9- Δ Intron1-c3xHA* strain, under heat-shock conditions (37°C) in the absence of cycloheximide, indicates that retention of intron 1 within the transcribed *rad9* mRNA sequence is not implicated in the mechanism of alternative translated expression of the “Rad9-S” protein (Fig 4.6, p.373).

In silico RNA secondary structural folding analyses of intron 1, performed via utilisation of the bioinformatics Vienna RNA-Fold software tool, also indicated that it would be unlikely to adopt the postulated aptamer configuration (Fig 4.3, p.363; Fig 4.4, p.364) in the alternative-translation mechanism of expression of the truncated “Rad9-S” protein variant (Fig 4.7, p.374).

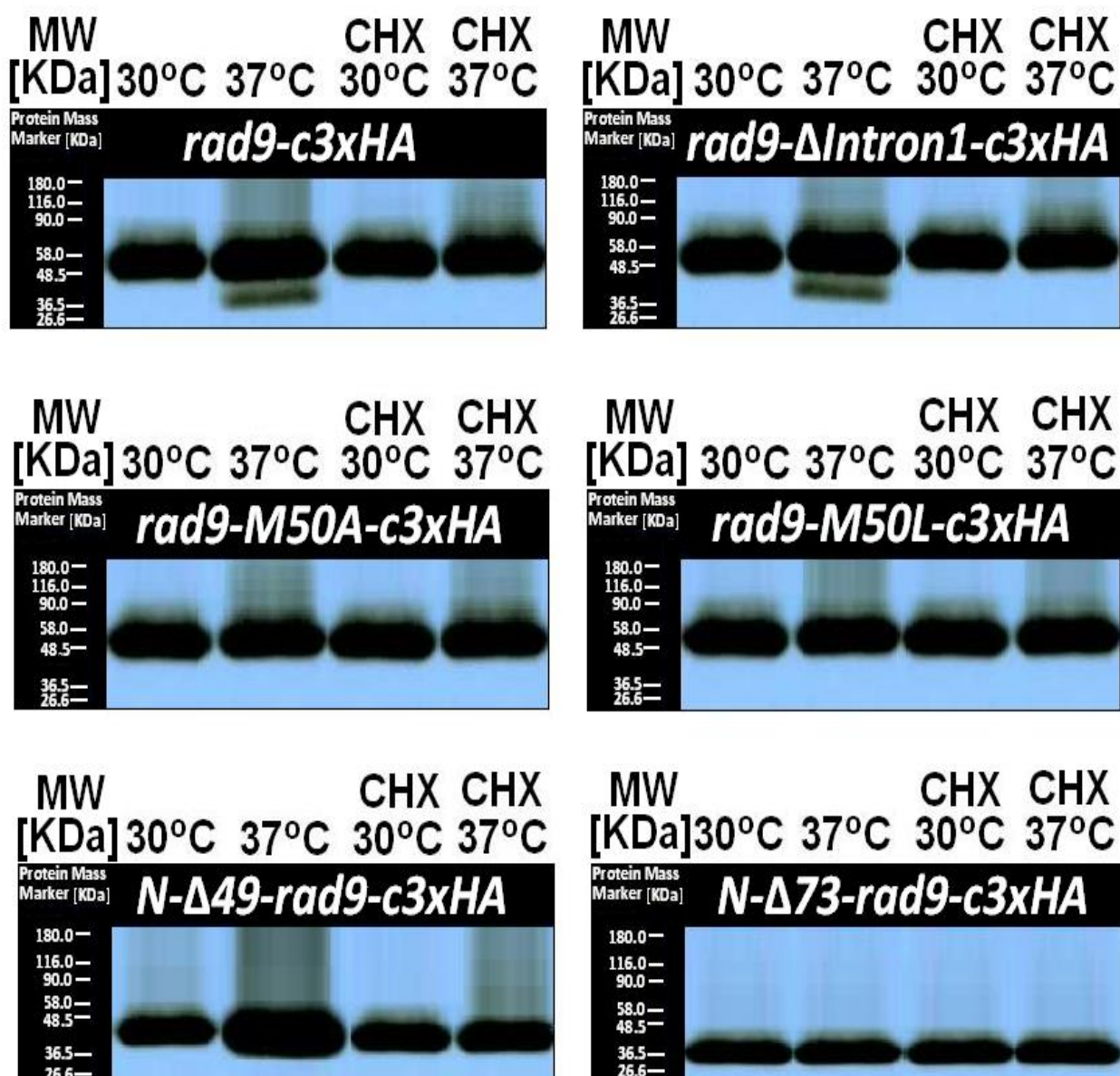
The absence of detected “Rad9-S” expression in TCA-precipitated total protein extracts acquired from the experimental cell cultures of the *rad9-c3xHA* and *rad9-ΔIntron1-c3xHA S. pombe* strains, incubated under heat-shock conditions (37°C) in the presence of cycloheximide, indicate that the truncated “Rad9-S” protein variant is an alternative translational product (Fig 4.6, p.373).

The absence of detected “Rad9-S” expression in TCA-precipitated total protein extracts acquired from the experimental cell cultures of the *rad9-M50A-c3xHA* and *rad9-M50L-c3xHA S. pombe* strains, incubated under heat-shock conditions (37°C) in the absence of cycloheximide, also indicate that the “Rad9-S” protein is most likely to be an alternative translational product which is expressed via the AUG start codon at Methionine 50 (ie NΔ49-Rad9-c3xHA) – Fig 4.6, p.373.

Eukaryotic alternative N-terminal translated protein expression can also be initiated at non-AUG codon start sites, such as leucine CUG codons, contained within microsatellite expansions of the transcribed mRNA (Kochetov A.V., 2008a; Kochetov A.V. *et al*, 2008b; Zu T. *et al*, 2011).

The absence of “Rad9-S” in TCA-precipitated total protein extracts acquired from the experimental cell cultures of the *rad9-M50A-c3xHA* and *rad9-M50L-c3xHA S. pombe* strains, incubated under heat-shock conditions (37°C) in the absence and presence of cycloheximide, also indicates that the CUG codon at leucine 50 is not utilised as a non-AUG type of alternative translational initiation start codon for expression of the truncated “Rad9-S” protein variant (Fig 4.6, p.373).

Fig 4.6: Heat-Specific Induction of *S. pombe* “Rad9-S” Expression

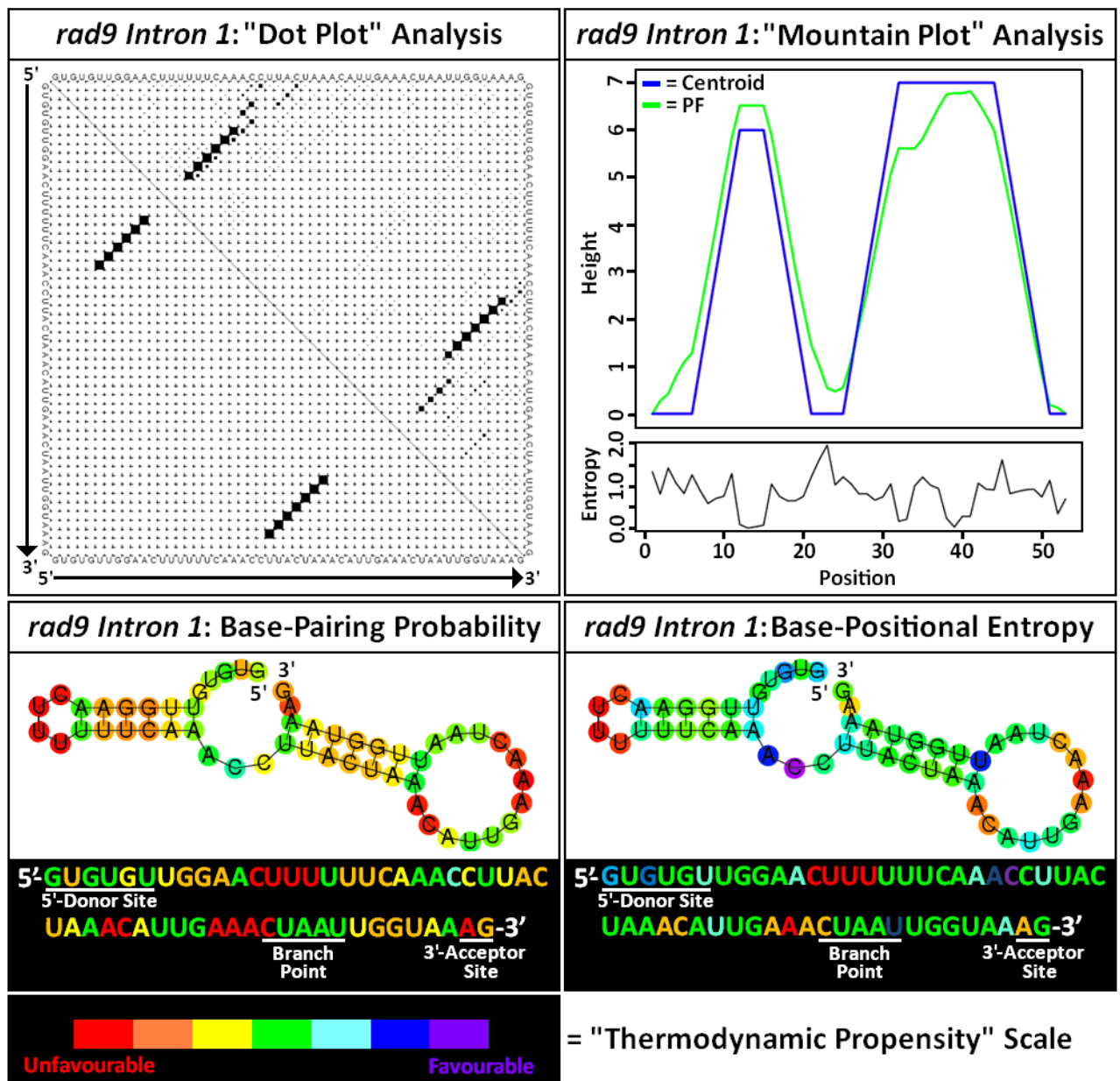


Individual 50mL YEA broth medium cell cultures of the appropriate “Cre-Lox” – constructed *S. pombe* strain were grown to overnight (30°C for ~12 hour time period), then diluted to an optical density $A_{595} = 0.25$ with the appropriate volume of YEA medium and the resultant diluted cultures re-incubated at 30°C for a further time period of ~2.5 hours until they had attained an optical density value of $A_{595} = 0.5$ – after which time the cultures of actively cycling cells were re-incubated either at 30°C or 37°C for a further 30 minutes in the absence or presence of 100μg/mL cycloheximide (CHX) – a translational inhibitor type antibiotic.

TCA-precipitated total protein extract samples were then prepared from the appropriate *calculated volumetric aliquot of each culture (*equivalent to 10 A_{595} optical density units) of which 20μL aliquots were resolved on 10% SDS-PAGE gels which were then utilised in comparative Western blot analyses probed with either anti-HA primary antibody.

[Protein sample preparation, SDS-PAGE resolution and Western blot methodologies are detailed in Section 2.8.1, pp.200-202; Section 2.8.4, pp.223-224 and Section 2.8.6, pp.231-233]

Fig 4.7: Vienna RNAfold Analysis of the Intron 1 mRNA Sequence of the *S. pombe rad9* Gene



4.4 In Silico RNA Folding Analyses of the Untranslated Regions Within the *S. pombe rad9* Gene Reveal that the 3'-UTR May be Implicated in Hyperthermally-Induced Expression of the Truncated “Rad9-S” Protein Variant

Internal ribosome entry sites (IRES), typically situated upstream of the first AUG translational start codon within the 5'-untranslated region (5'-UTR), may regulate translational initiation of alternative downstream AUG start codon sites within the transcribed RNA (Araujo P.R. *et al.*, 2012; Bazykin G.A. and Kochetov K.A., 2011; King H.A. *et al.*, 2010; Kochetov A.V. *et al.*, 2005; Kochetov A.V., 2008a; Kochetov A.V. *et al.*, 2008b; Spriggs K.A. *et al.*, 2005; Vazquez-Pianzola P. and Suter B., 2012; Zu T. *et al.*, 2011).

Functional 5'-UTR and 3'-UTR regions within transcribed yeast mRNA molecules have also been correlated with high levels of gene expression (Kochetov A.V. *et al.*, 2002).

In silico prediction and modelling analyses of the optimal thermodynamically-adopted secondary structural configurations of the 5'-UTR and 3'-UTR domains contained within the *S. pombe rad9* mRNA were performed, via utilisation of the on-line bioinformatics software program Vienna RNAfold, in order to ascertain whether or not these sequences had the potential capacity to regulate expression of the truncated “Rad9-S” protein variant (Fig 4.8, p.377; Fig 4.9, p.378).

The acquired *in silico* data indicated that whilst the 5'-UTR RNA sequence was unlikely to adopt an energetically-favorable functional loop secondary structural configuration that would be capable of regulating translational initiation within the transcribed *S. pombe rad9* gene (Fig 4.8, p.377), the 3'-UTR sequence was predicted to fold into a thermodynamically-favorable secondary structural configuration comprised of several stem-loop sub-domains (Fig 4.9, p.378).

The complexity of the supramolecular architecture of the predicted optimal 3'-UTR secondary RNA structure (Fig 4.9, p.378) may be indicative that this sequence possesses the latent adaptive capacity to switch between different stem-loop configurations whose energetically-favored formation is temperature-dependent.

It is therefore hypothetically conceivable that the 3'-UTR sequence may function as a temperature-responsive translational regulatory element, within the *S. pombe rad9* gene, which may also be implicated in the hyperthermic induction of "Rad9-S" expression.

Fig 4.8: Vienna RNAfold Analysis of the 5'-UTR Sequence of the *S. pombe rad9* Gene

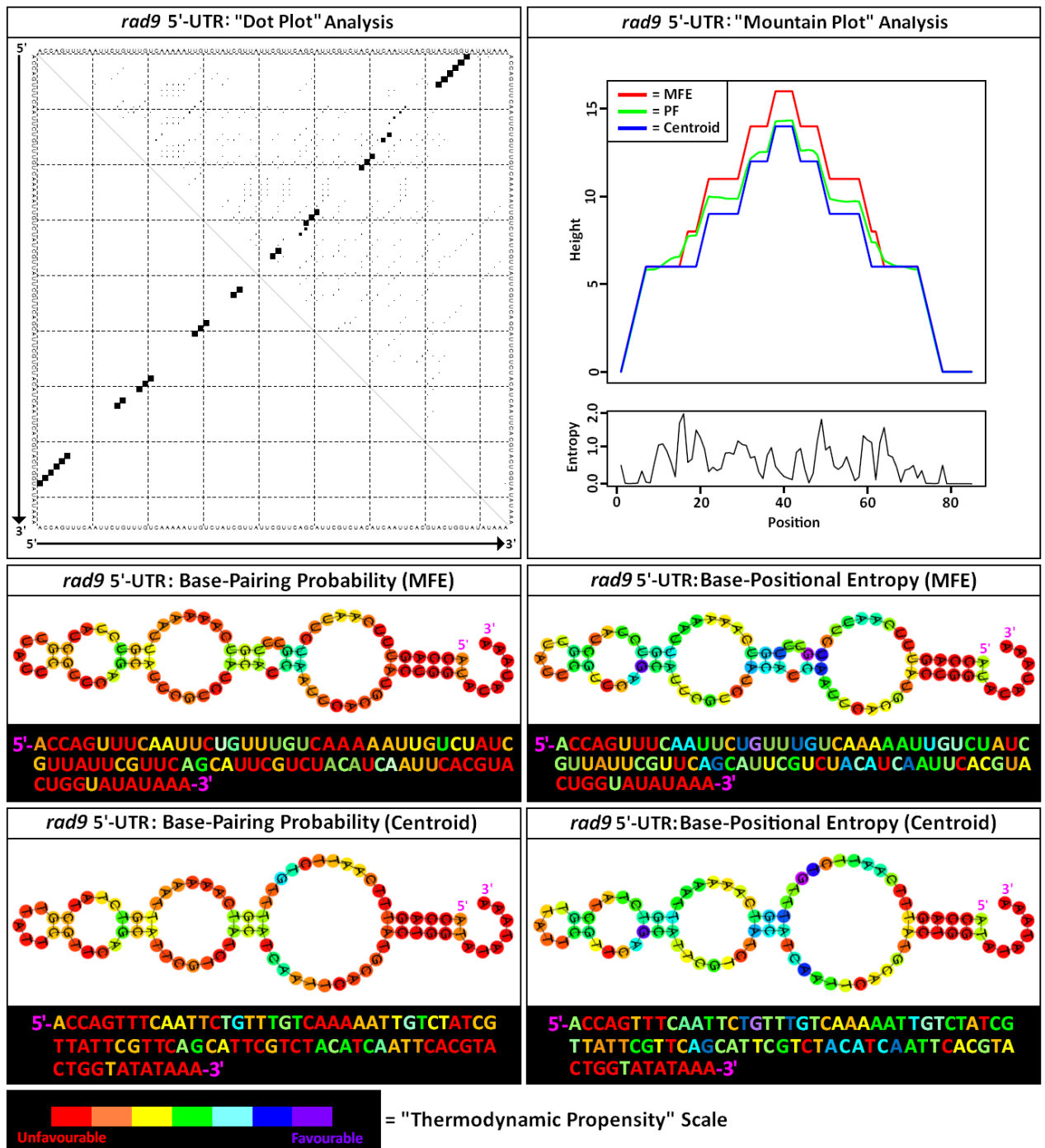
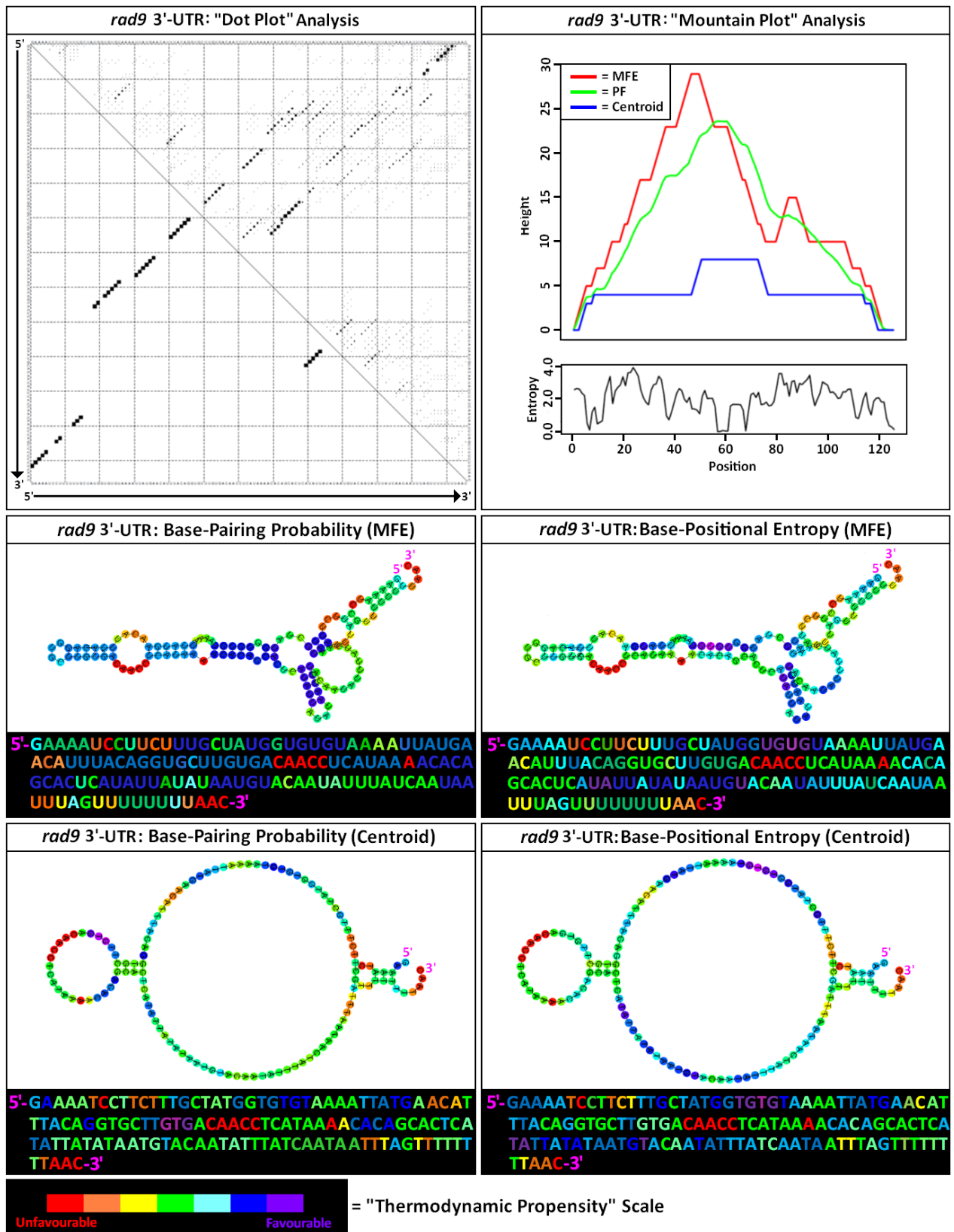


Fig 4.9: Vienna RNAfold Analysis of the 3'-UTR Sequence of the *S. pombe rad9* Gene



4.5 The Amino Acid Encoded mRNA M1-S49 Spanning Region of the *S. pombe rad9* Gene May Be Implicated in the Hypothermic Suppression of Truncated “Rad9-S” Protein Variant Expression

Comparative Western blot assays performed on TCA-precipitated total protein extracts acquired from YEA cell cultures of the “cre-lox” – constructed *S. pombe* strains $\Delta rad9$, *rad9-c3xHA* and *N149-rad9-c3xHA* (“*rad9-S*”-*c3xHA*) incubated at 16°C (hypothermic stress), 30°C (nominal temperature) or 37°C (hyperthermic stress) indicated that expression of the truncated “Rad9-S” protein variant is suppressed at lower temperatures (Fig 4.10, p.384).

The acquired Western blot assay data also indicated that phosphorylation of the “Rad9-S” truncated protein variant is suppressed under cytological conditions of hyperthermic stress (Fig 4.10, p.384).

Taken together, these experimental observations may be indicative that protein phosphatase-mediated post-translational modifications of the truncated “Rad9-S” protein variant are implicated in the mediation of novel cell cycle checkpoint responses to specific heat-shock type cytological stresses that may impair a variety of biochemical mechanisms which collectively maintain genomic integrity.

The hypothermically-suppressed expression and post-translational dephosphorylation of the truncated “Rad9-S” protein variant, under the imposed lower temperature conditions of 16°C and 30°C (Fig 4.10, p.384), may also be indicative of novel mechanisms which regulate its relative levels and functional activities within the cell.

These Western blot assay data also revealed both a significant enhancement of lower temperature basal level expression and reduction of hyperthermically-induced expression of the truncated “Rad9-S” protein variant within the TCA-precipitated total protein extracts acquired from the experimental YEA cultures of the *ND49-rad9-c3xHA S. pombe* strain, whose cells were “cre-lox” – engineered for the exclusive expression of “Rad9-S” (Fig 4.10, p.384).

These experimental observations may be indicative of a responsive elemental domain, contained within the M1 – M50 segment of the transcribed *S. pombe rad9* mRNA, which inhibits the direct recruitment of ribosomes to the downstream AUG50 codon initiation site and thereby suppresses alternative translational expression of the truncated “Rad9-S” protein variant under hypothermic (16°C) and lower nominal (30°C) temperature conditions within the cell.

In order to test this hypothesis, comparative *in silico* RNA optimal secondary structure prediction analyses were performed on the amino acid encoded M1 – S49 base sequence region contained within the *S. pombe rad9* mRNA transcript via utilisation of the on-line bioinformatics software tool Vienna RNAfold (Figs 4.11- 4.14, pp.385-390).

The acquired *in silico* data indicated that the T18 – C40 codon region, contained within the encoded M1 – S49 segment of the transcribed *S. pombe rad9* mRNA, was predicted to fold into a thermodynamically-favorable secondary structural configuration comprised of several stem-loop sub-domains (Fig 4.11, pp.385-386 and Fig 4.12, pp.387-388).

Dispersed responsive elements, organised within functional regions of yeast mRNA molecules, are known to modulate the translational activity of the transcribed genes and thus regulate the expressed cellular levels of their encoded proteins (Kochetov A.V. *et al*, 2002).

The nucleotide composition, dinucleotide, base-paired and unpaired base content of the linear sequences and/or secondary structures of these dispersed responsive elements, contained within the transcribed yeast mRNA molecules, also determines their functional capacity with regard to the degree of translational expression they induce or suppress in the respective genes (Kochetov *et al.*, 2002).

In silico composition profiling of the loop, unpaired and paired bases, contained within the optimal T18 – C40 secondary RNA structure (Fig 4.13, p.389), predicted by the Vienna RNAfold software tool, indicated that its supramolecular fold architecture consisted of 5 loops, in which the hierarchical order of abundance of unpaired and paired bases was defined as:

unpaired bases > stem-loop bases > A:U base-pairs > G:C base-pairs > G:U base-pairs

These *in silico* analyses also estimated the denaturing “melting temperature” (T_m) of the predicted optimal T18 – C40 secondary RNA structure to be around 30°C, which correlated with the relatively low proportional content of G:C base-pairs (that contain three hydrogen bonds and require more energy for their thermal dissociation compared with A:U or G:U base-pairs which only contain two hydrogen bonds and therefore require less energy for their thermal dissociation) – Fig 4.13, p.389.

Thus, the relatively low T_m and multi-loop supramolecular architectural complexity of the predicted optimal T18 – C40 secondary RNA structure may be indicative that this sequence acts as a hypothermic responsive element that possesses the latent adaptive capacity to switch between different configurations whose energetically-favored formation is temperature-dependent.

Comparative *in silico* modelling of the optimal thermodynamically-favoured supramolecular configurations of the isolated T18 – C40 encoded mRNA sequence and the T18 – C40 region incorporated within the M1 – S49 encoded mRNA sequence, predicted by the on-line Vienna RNAfold bioinformatics software tool, yielded two distinctive RNA secondary structures which contained different stem-loop arrangements (Fig 4.14, p.390).

These acquired *in silico* data were indicative that the sequences flanking the potential T18 – C40 hypothermic responsive *cis*-element, situated within the encoded M1 – S49 segment of the transcribed *S. pombe rad9* mRNA, may be implicated in the modulation of its secondary supramolecular architecture (Fig 4.14, p.390).

Taken together, these acquired Western blot data and comparative *in silico* RNA secondary structure analyses indicate a hypothetical mechanism for hypothermically-suppressed truncated “Rad9-S” protein variant expression, which is mediated via dispersed responsive elements situated within the encoded M1 – S49 segment of the transcribed *S. pombe rad9* mRNA (Fig 4.15, p.391).

Low temperature conditions (below 30°C) may promote formation of the predicted T18 – C40 multi stem loop-configured secondary RNA structure whose supramolecular configuration sterically hinders ribosomal access to the downstream AUG50 translational initiation codon and thus prevents expression of the truncated “Rad9-S” protein variant, whilst ribosomal access to the AUG1 start codon remains unaffected and enables translation of the first N-terminal 17 amino acids of the full-length *S. pombe* Rad9 protein to proceed (Fig 4.15A, p.391).

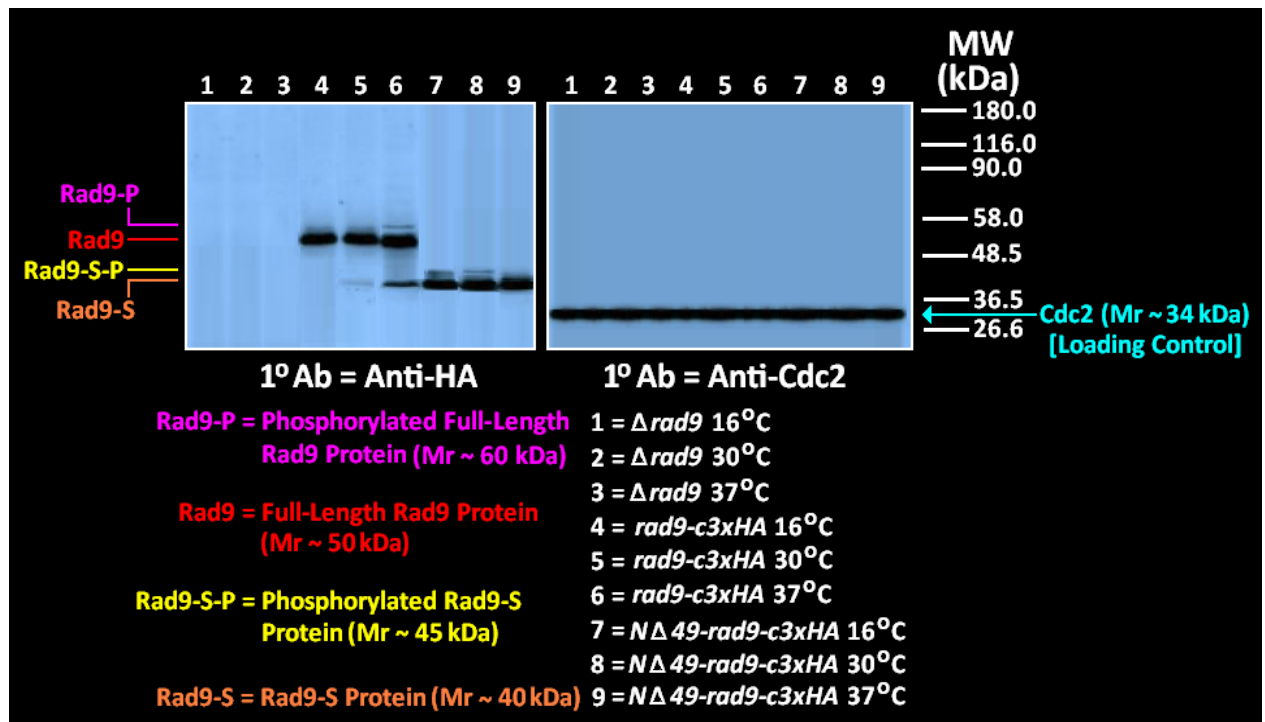
Subsequent ribosomal progression to the T18 RNA codon may then initiate a translational pause and induce transient supramolecular configurational changes within the transcribed *S. pombe rad9* mRNA that result in the specific recognition recruitment of an RNA chaperone/helicase complex to the T18 – C40 multi stem loop-configured secondary RNA structure (Fig4.15B, p.391)

The recruited RNA chaperone/helicase complex may then catalyze the unfolding of the T18 – C40 multi stem loop-configured secondary RNA structure, which in turn promotes its dissociation from the transcribed *S. pombe rad9* mRNA and re-initiates progressive ribosomal translation of the encoded T18 – C40 amino acid sequence (Fig 4.15C, p.391).

Subsequent ribosomal translation of the encoded C40 – M50 amino acid sequence may then induce transient supramolecular changes within the transcribed *S. pombe rad9* mRNA that trigger the re-formation of the T18 – C40 multi stem loop-configured secondary RNA structure which blocks leaky ribosomal scanning of the AUG50 translational initiation codon and thus prevents expression of the truncated “Rad9-S” protein variant, whilst progressive ribosomal translation results in the exclusive expression of the full-length *S.pombe* Rad9 protein (Fig 4.15D, p.391).

Thus sequential induction of exclusive full-length Rad9 protein expression is permitted under hypothermic cytological conditions that suppress the expression of the truncated “Rad9-S” protein variant (Fig 4.15, p.391).

Fig 4.10: Hypothermic Suppression of Rad9-S Expression



Individual 50mL YEA broth medium cell cultures of the appropriate “Cre-Lox” – constructed *S. pombe* strain were grown to overnight (30°C for ~12 hour time period), then diluted to an optical density A595 = 0.25 with the appropriate volume of YEA medium and the resultant diluted cultures re-incubated at 30°C for a further time period of ~2.5 hours until they had attained an optical density value of A595 = 0.5 – after which time the cultures of actively cycling cells were re-incubated either at 16°C, 30°C or 37°C for a further 30 minutes.

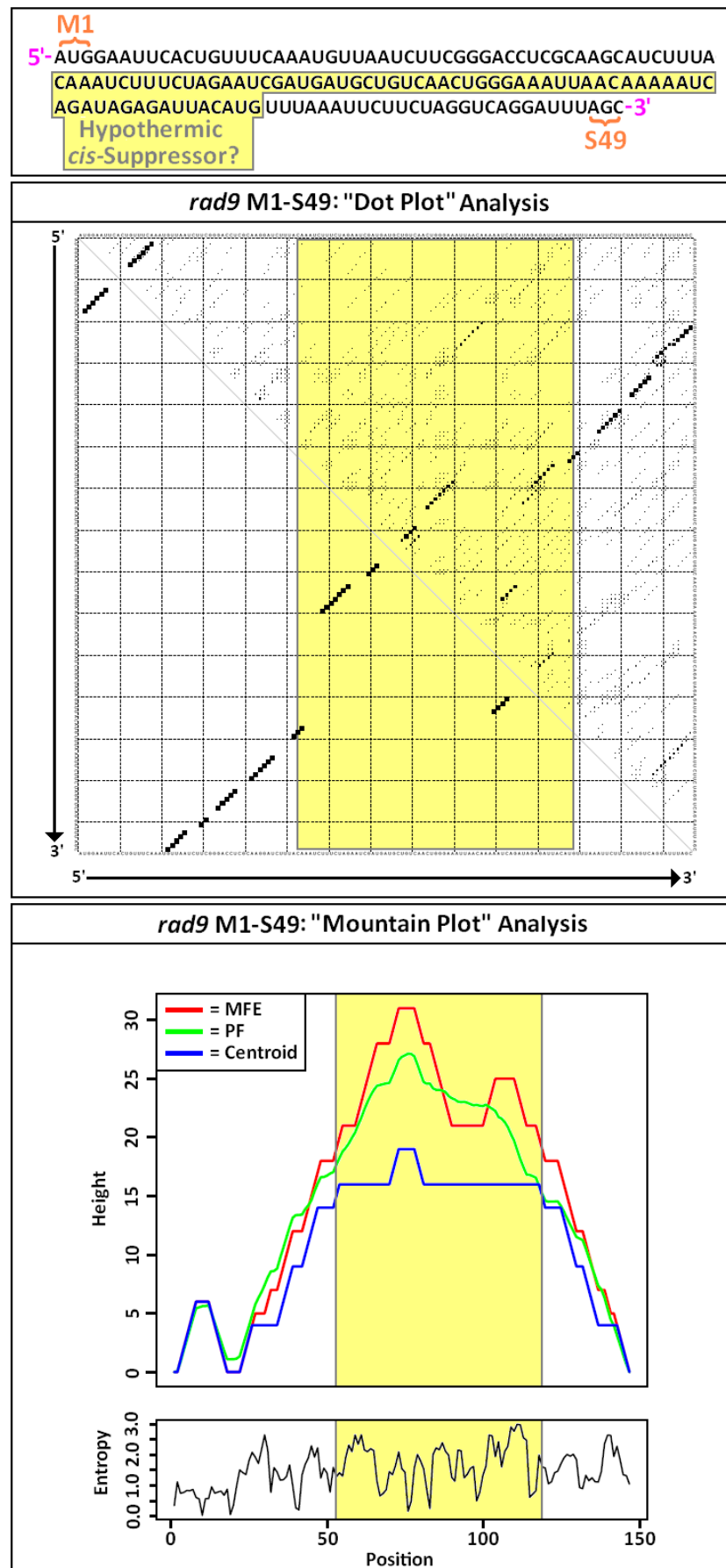
TCA-precipitated total protein extract samples were then prepared from the appropriate *calculated volumetric aliquot of each culture (*equivalent to 10 A595 optical density units) of which 20µL aliquots were resolved on 10% SDS-PAGE gels which were then utilised in comparative Western blot analyses probed with either the anti-HA primary antibody or the anti-Cdc2 primary anti-body.

[Protein sample preparation, SDS-PAGE resolution and Western blot methodologies are detailed in Section 2.8.1, pp.200-202; Section 2.8.4, pp.223-224 and Section 2.8.6, pp.231-233]

Protein samples prepared from the *rad9*-deleted *S. pombe* strain cell cultures served as comparative negative non-specific/cross-reactivity controls in the anti-HA Western blot for verification that the detected bands in the protein extracts prepared from the cell cultures of the *rad9-c3xHA* and *NΔ49-rad9-c3xHA* *S. pombe* strains were exclusive to the specific expression of Rad9 protein isoforms.

The comparative anti-Cdc2 Western blot served as a qualitative control for verification that equivalent amounts of total protein for each sample had been loaded.

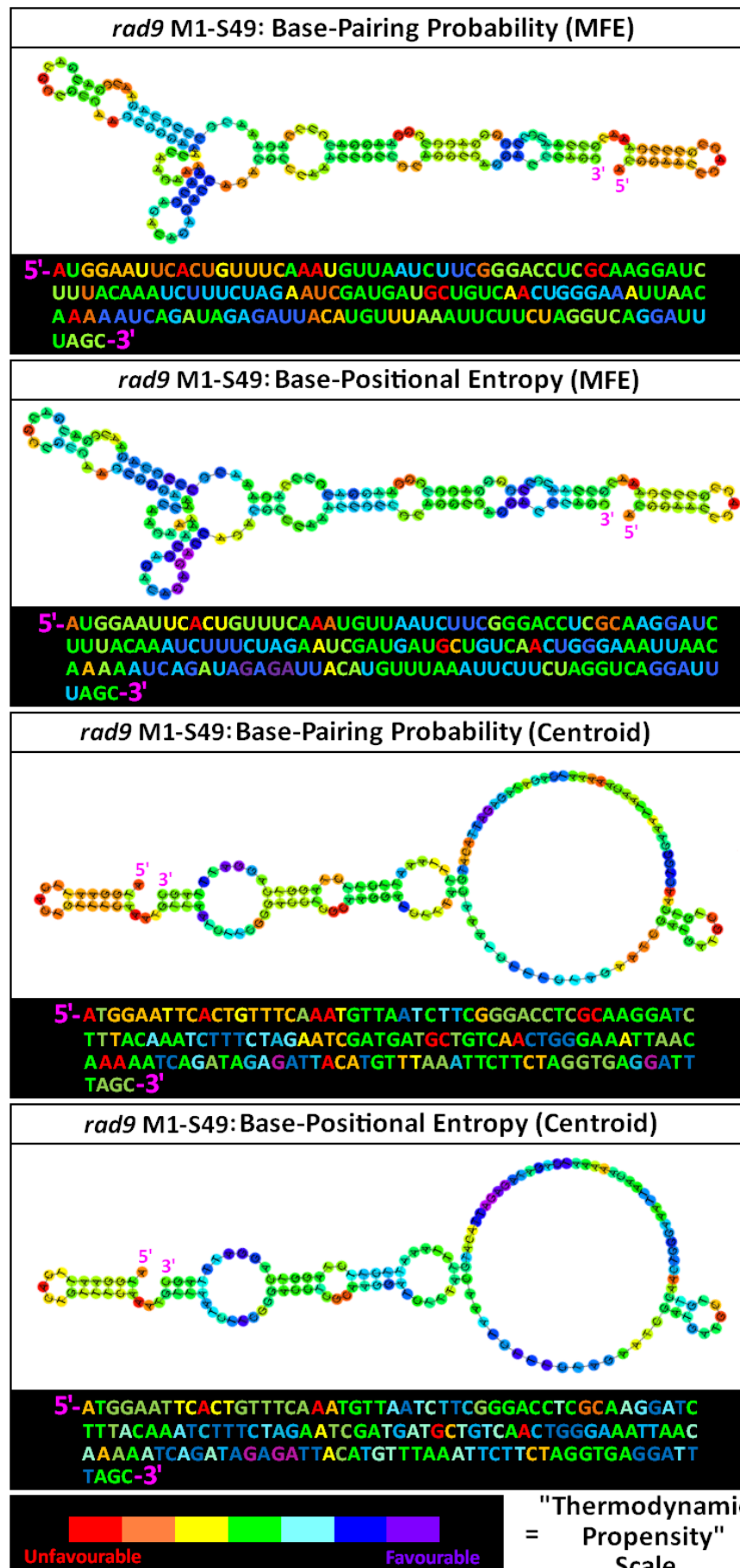
Fig 4.11: Vienna RNAfold Analysis (“Raw Data” Output) of the Encoded M1 – S49 Sequence Within the Transcribed *S. pombe rad9* mRNA



Vienna RNAfold Analysis (“Raw Data” Output) of the Encoded M1 – S49 Sequence Within the Transcribed *S. pombe rad9* mRNA – Figure Legend (Fig 4.11)

The potential hypothermic responsive *cis*-elemental T18 – C40 sequence, identified within the transcribed M1 – S49 *S. pombe rad9* mRNA, is highlighted in yellow (top figure) and its relative base-positional location within the dot (middle figure) and mountain (bottom figure) “raw data” plots is also highlighted in yellow.

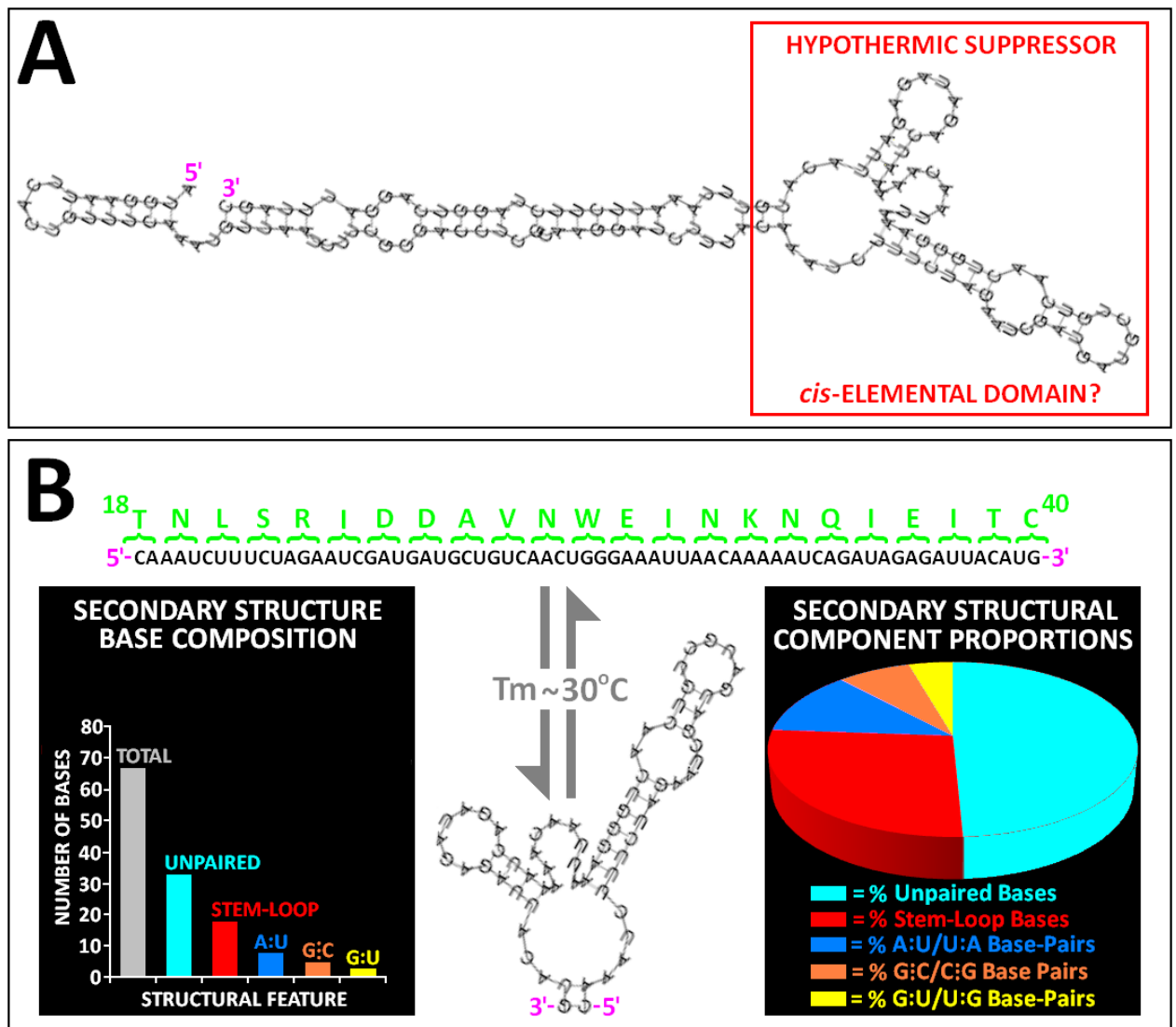
Fig 4.12: Vienna RNAfold Analysis (“Processed Data” Output) of the Encoded M1 – S49 Sequence Within the Transcribed *S. pombe rad9* mRNA



Vienna RNAfold Analysis (“Processed Data” Output) of the Encoded M1 – S49 Sequence Within the Transcribed *S. pombe rad9* mRNA – Figure Legend (Fig 4.12)

Comparative minimal free energy (MFE) and centroid base-pairing probability and base-positional entropy “processed data” analysis plots of the predicted optimal secondary structure of the M1 – S49 encoded sequence within the transcribed *S. pombe rad9* mRNA are indicated.

Fig 4.13: Structural Component Analysis of the Encoded M1 – S49 Sequence Within the Transcribed *S. pombe rad9* mRNA



A: *In silico* optimal secondary structural configuration of the M1 – S49 encoded mRNA region of the transcribed *S. pombe rad9* gene predicted with the on-line bioinformatics software tool Vienna RNAfold.

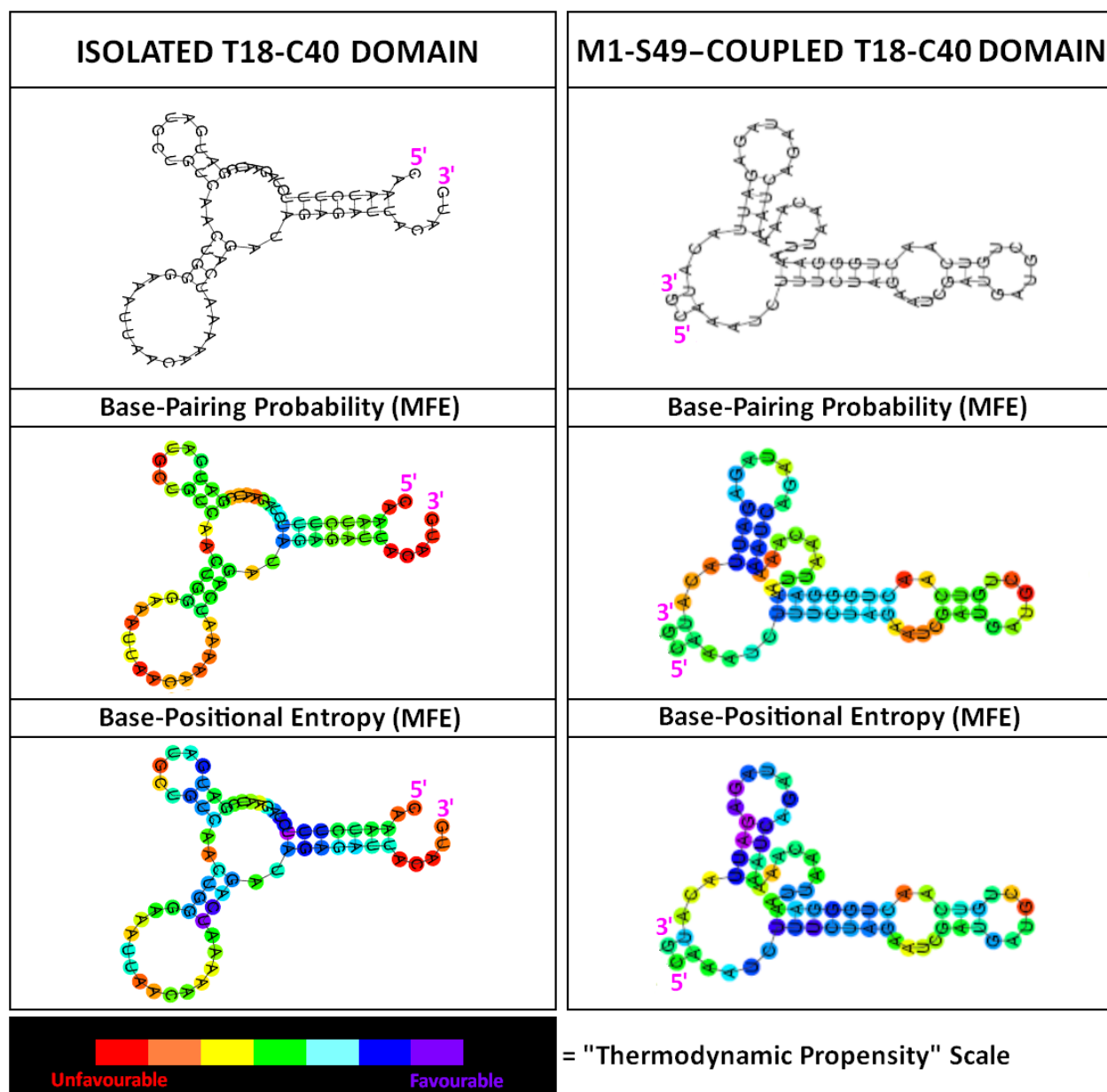
The multi-looped configuration of the potential hypothermic responsive suppressor *cis*-element, comprised of the T18 – C40 codon mRNA sequence, is highlighted in the red box.

B: *In silico* supramolecular architecture composition analysis of the optimal secondary structural configuration of the identified potential hypothermic responsive suppressor *cis*-element (predicted with the on-line bioinformatics software tool Vienna RNAfold).

The transcribed *rad9* mRNA base sequence (black) and corresponding codon-translated amino acid sequence (green) is indicated.

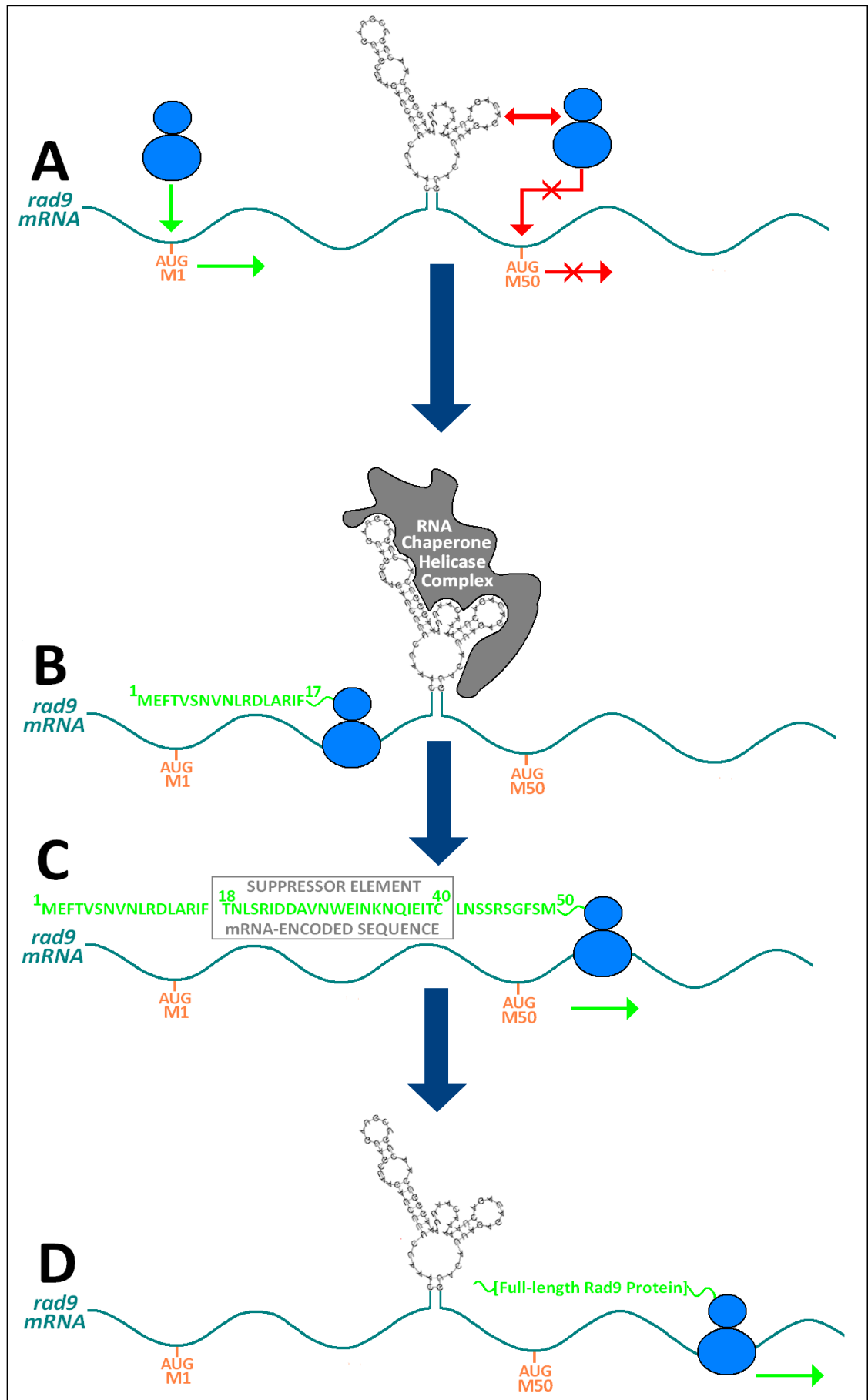
The estimated melting temperature ($T_m \sim 30^\circ\text{C}$) of the secondary RNA structure is also indicated.

Fig 4.14: Comparative Secondary RNA Structural Conformer Analyses of the Isolated and M1–S49-Incorporated T18–C40 Encoded Sequences Within the Transcribed *S. pombe rad9* mRNA



Comparative minimal free energy (MFE) base-pairing probability and base-positional entropy “processed data” analysis plots of the optimal secondary structures of the isolated (left) and M1–S49-incorporated (right) potential hypothermic responsive *cis*-elemental suppressor T18 – C40 encoded *S. pombe rad9* mRNA base sequence, were generated via *in silico* predictive modelling with the on-line bioinformatics software tool Vienna RNAfold.

Fig 4.15: Hypothermic Inhibition Model of “Rad9-S” Suppression



[A detailed explanation of this hypothetical model is provide in the text on pp.382-383]

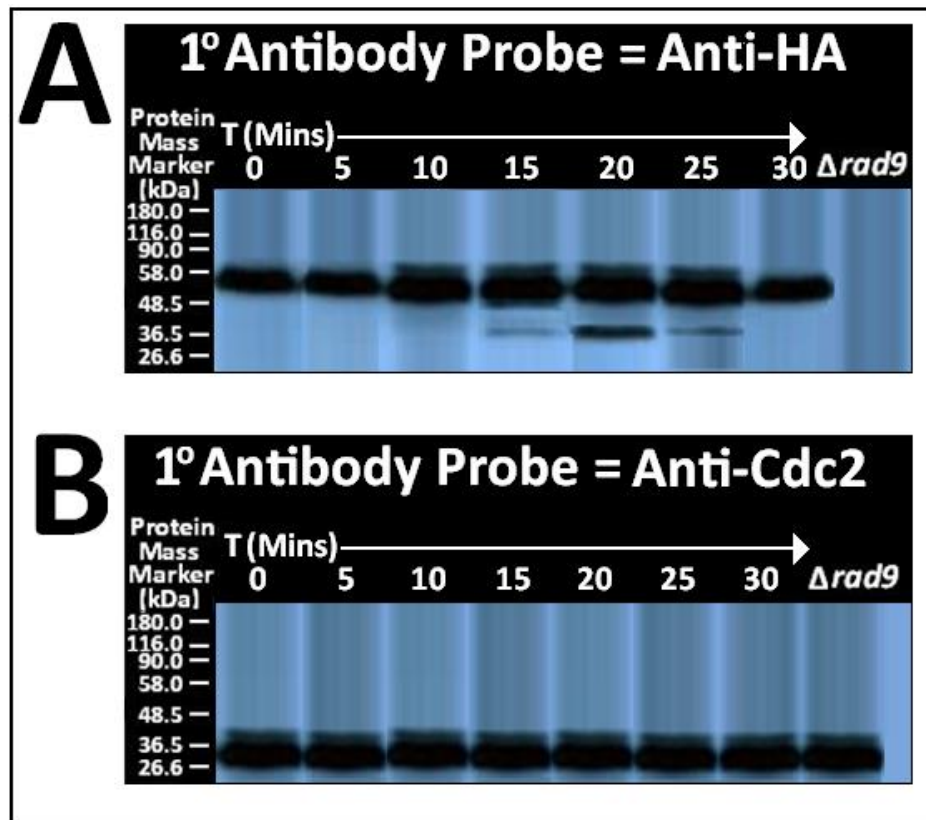
4.6 Heat-Induction of Rad9-S is Restricted to Actively Cycling Cells

In order to ascertain whether heat-induced expression of the truncated “Rad9-S” protein variant was co-ordinated temporally with specific phases of the cell cycle, a comparative Western blot analysis was performed on TCA-precipitated total protein extracts acquired from aliquots taken over regular 5 minute time intervals from a YEA broth cell culture of the “Cre-Lox”– constructed *S. pombe* strain *rad9-c3xHA* incubated under heat stress conditions (37°C) – Fig 4.16, p.393.

The acquired data indicated that maximal heat-induced expression of the truncated “Rad9-S” protein variant is restricted to a 20 minute time period within actively cycling *S. pombe* cells (Fig 4.16, p.393), which could be temporally co-ordinated with the typical ~20 minute duration of replicative DNA processes in the S phase of the *S. pombe* cell cycle (Carlson C.R. *et al*, 1999; Lygeros J. *et al*, 2008; Nasmyth K. *et al*, 1979).

Thus, these experimental observations may indicate that the truncated “Rad9-S” protein variant is implicated in a novel checkpoint pathway responses to hyperthermally-induced DNA damage and or replication fork arrest.

Fig 4.16: Temporal Assay of Heat-Induced Rad9-S Expression



A 100mL YEA broth medium cell culture of the “cre-lox” – constructed *S. pombe* strain *rad9-c3xHA* was grown overnight (30°C for ~12 hour time period), then diluted to an optical density $A_{595} = 0.25$ with the appropriate volume of YEA medium and the resultant diluted culture re-incubated at 30°C for a further time period of ~2.5 hours until it had attained an optical density value of $A_{595} = 0.5$ – after which time the culture of actively cycling cells was re-incubated at 37°C for a further 30 minutes.

TCA-precipitated total protein extract samples were then prepared from the appropriate *calculated volumetric aliquots of each culture (*equivalent to 10 A_{595} optical density units) at 5 minute time intervals over the total incubation time of 30 minutes.

A 100mL YEA broth medium cell culture of the “cre-lox” – constructed *S. pombe* strain $\Delta rad9$ was also grown overnight (30°C for ~12 hour time period), then diluted to an optical density $A_{595} = 0.25$ with the appropriate volume of YEA medium and the resultant diluted culture re-incubated at 30°C for a further time period of ~2.5 hours until it had attained an optical density value of $A_{595} = 0.5$ – after which time the culture of actively cycling cells was re-incubated at 37°C for a further 30 minutes, prior to preparation of a TCA-precipitated total protein extract sample from the appropriate *calculated volumetric aliquot of the culture (*equivalent to 10 A_{595} optical density units).

20 μ L aliquots of these prepared protein samples were resolved on 10% SDS-PAGE gels which were then utilised in comparative Western blot analyses probed with either the anti-HA primary antibody (Fig A) or the anti-Cdc2 primary anti-body (Fig B).

The protein sample prepared from the *rad9*-deleted ($\Delta rad9$) *S. pombe* strain cell culture served as comparative negative non-specific/cross-reactivity control in the anti-HA Western blot for verification that the detected bands in the protein extracts prepared from the cell cultures of the *rad9-c3xHA* were the expressed full-length Rad9 (Mr ~ 50 kDa) and N Δ 49-Rad9-c3xHA/“Rad9-S” (Mr ~ 40kDa) proteins.

[Protein sample preparation, SDS-PAGE resolution and Western blot methodologies are detailed in Section 2.8.1, pp.200-202; Section 2.8.4, pp.223-224 and Section 2.8.6, pp.231-233]

The comparative anti-Cdc2 Western blot served as a qualitative control for verification that equivalent amounts of total protein for each sample had been loaded (Fig B).

4.7 Impaired Formation and DNA Clamp-Loading of the “9-1-1” Complex Does Not Induce Expression of the “Rad9-S” Truncated Protein Variant

It was postulated that inductive expression of the truncated “Rad9-S” protein variant may be implicated in an auxiliary type of compensatory mechanism for mediation of alternative DNA damage checkpoint signalling responses and preservation of genomic integrity under adverse cytological conditions in which the normal formation and/or functional activities of the canonical full-length Rad9-Rad1-Hus1 complex have been perturbed.

In order to test this hypothesis, Western blot analyses were performed on TCA-precipitated total protein extracts acquired from YEA broth cultures of the “Cre-Lox”– constructed *S. pombe* strains *rad9-c3xHA*, *rad9-M50L-c3xHA* and *NΔ49-rad9-c3xHA* – in which the cells also contained deletions of either the *rad1*, *hus1* or *rad17* genes respectively (Fig 4.17, p.396).

The data indicate that perturbation of the canonical Rad9-Rad1-Hus1 complex, via deletion of the *rad1* or *hus1* genes, is not implicated in the induction mechanism of expression of the truncated NΔ49-Rad9-c3xHA (“Rad9-S”) protein variant.

Likewise, perturbation of DNA-loading of the “9-1-1” clamp (via deletion of the *rad17* gene) is also not implicated in the induction mechanism of expression of the truncated NΔ49-Rad9-c3xHA (“Rad9-S”) protein variant.

Intriguingly, the data also indicate that *rad1* gene deletion-perturbation of formation of the Rad9-Rad1-Hus1 complex within an excluded “Rad9-S” expression genetic background (*rad9-M50L-c3xHA*) results in the induction of a smaller truncated isoform, termed “Rad9-VS” (“Very Short”) – which may be a consequence of translation at the next alternative AUG codon start, downstream of Methionine 50 at Methionine 74, within the *rad9* gene (Fig 4.17, p.396).

Since the postulated “Rad9-VS” truncated isoform would still retain the C-terminal tail protein-interactive domain and a conserved component of intrinsic stability/order (discussed previously in Chapter 3, pp.295-296 and Fig 3.15, p.293), *S. pombe* cells “cre-lox”-engineered for the exclusive expression of only the full-length Rad9 protein may utilise a “leaky ribosomal scanning” type compensatory mechanism for the expression of the NΔ73-Rad9 protein variant – which may retain some unknown DNA damage response signal functions.

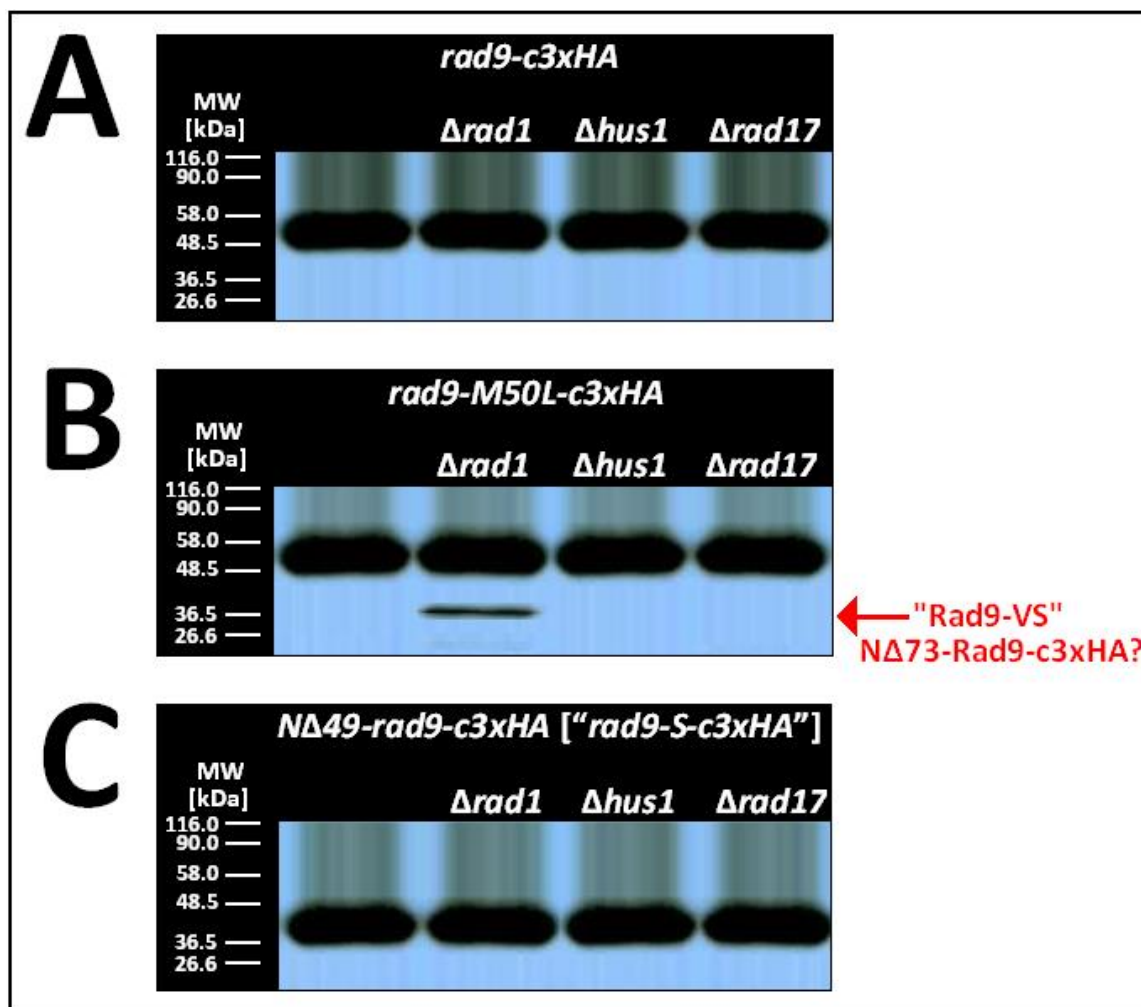
No “Rad9-VS” expression was detected in comparative Western blot analyses of TCA-precipitated total protein extracts acquired from YEA cell cultures of the *rad9-c3xHA Δrad1* and *NΔ49-rad9-c3xHA Δrad1 S. pombe* strains (Fig 4.17, p.396).

This may be due to the fact that both the *rad9-c3xHA Δrad1* and *NΔ49-rad9-c3xHA Δrad1 S. pombe* strains retain the capability to express the truncated “Rad9-S” protein variant, which may also perform critical roles in the regulation of “9-1-1” complex-independent functional activities of the full-length Rad9 protein.

Taken together, these experimental observations may indicate that induced expression of the postulated NΔ73-Rad9 protein variant (“Rad9-VS”) within the cells of the *rad1* gene-deleted *rad9-M50L-c3xHA* strain may enable them to regulate “9-1-1” complex-independent functions of the full-length Rad9 protein via an alternative compensatory mechanism in the absence of “Rad9-S” (NΔ49-Rad9) expression.

However, the lack of detected “Rad9-S” or “Rad9-VS” isoforms in the Western blot analysis of the protein sample prepared from *rad9-c3xHA Δrad1 S. pombe* strain culture may be indicative of independent functions of the full-length Rad9 protein, that act outside of the “9-1-1” complex and suppress the expression of the truncated “Rad9-S” and/or “Rad9-VS” protein variants (Fig 4.17, p.396).

Fig 4.17: Perturbed “9-1-1” Complex-Induced Expression of a Novel Truncated *S. pombe* Rad9 Variant – “Rad9-VS”



50mL YEA broth medium cell cultures of the appropriate *S. pombe* strains were grown overnight (30°C for ~12 hour time period), then diluted to an optical density $A_{595} = 0.25$ with the appropriate volume of YEA medium and the resultant diluted cultures re-incubated at 30°C for a further time period of ~2.5 hours until it had attained an optical density value of $A_{595} = 0.5$.

TCA-precipitated total protein extract samples were then prepared from the appropriate *calculated volumetric aliquots of each culture (*equivalent to 10 A_{595} optical density units).

20 μ L aliquots of these prepared protein samples were resolved on 10% SDS-PAGE gels which were then utilised in comparative Western blot analyses probed with either the anti-HA primary antibody (Fig A) or the anti-Cdc2 primary anti-body (Fig B).

[Protein sample preparation, SDS-PAGE resolution and Western blot methodologies are detailed in Section 2.8.1, pp.200-202; Section 2.8.4, pp.223-224 and Section 2.8.6, pp.231-233]

A: Comparative Western blot assay of SDS-PAGE-resolved protein samples prepared from the YEA cell cultures of the *rad9-c3xHA*, *rad9-c3xHA* $\Delta rad1$, *rad9-c3xHA* $\Delta hus1$ and *rad9-c3xHA* $\Delta rad17$ *S. pombe* strains.

B: Comparative Western blot assay of SDS-PAGE-resolved protein samples prepared from the YEA cell cultures of the *rad9-(M50L)-c3xHA*, *rad9-(M50L)-c3xHA* $\Delta rad1$, *rad9-(M50L)-c3xHA* $\Delta hus1$ and *rad9-(M50L)-c3xHA* $\Delta rad17$ *S. pombe* strains.

C: Comparative Western blot assay of SDS-PAGE-resolved protein samples prepared from the YEA cell cultures of the *NΔ49-rad9-c3xHA*, *NΔ49-rad9-c3xHA* $\Delta rad1$, *NΔ49-rad9-c3xHA* $\Delta hus1$ and *NΔ49-rad9-c3xHA* $\Delta rad17$ *S. pombe* strains.

4.8: Comparative 2D PAGE-Coupled Western Blot Analyses Reveal the Expression of Additional Novel Truncated Rad9 Isoforms Within *S. pombe*

2D PAGE-coupled Western blot analyses were utilised for the enhanced resolution and detection of other potential *S. pombe* Rad9 isoforms which may be expressed at lower cellular levels beyond the effective detection capacity of conventional 1D SDS-PAGE-coupled Western blot assays.

Comparative 2D PAGE-coupled Western blot analyses performed on TCA-precipitated total protein extracts acquired from YEA cell cultures of the *S. pombe* strain *rad9-c3xHA*, incubated under nominal temperature (30°C) or heat shock (37°C) conditions, indicated the expression of two smaller truncated variants – termed “Rad9 Very Small” (“Rad9-VS”) and “Rad9 Tiny” (“Rad9-T”), in addition to the full-length Rad9 protein and “Rad9 Short” (“Rad9-S”) truncated protein variant (Fig 4.18, p.399).

The data also indicated that post-translational dephosphorylation of these four *S. pombe* Rad9 isoforms occurred under conditions of hyperthermally-induced cytological stress, which was evident from changes in their respective profile patterns in which some of the resolved phosphoisoform species expressed at the nominal 30°C incubation temperature were absent or were shifted more towards the cathode terminal (Fig 4.18, p.399).

Taken together, these experimental observations were indicative that specific checkpoint phosphatases may be implicated in the post-translational modification of the *S. pombe* Rad9 isoforms in response to hyperthermally-induced cytological stresses which may also adversely impinge upon a variety of biochemical processes that orchestrate the maintenance of genomic integrity.

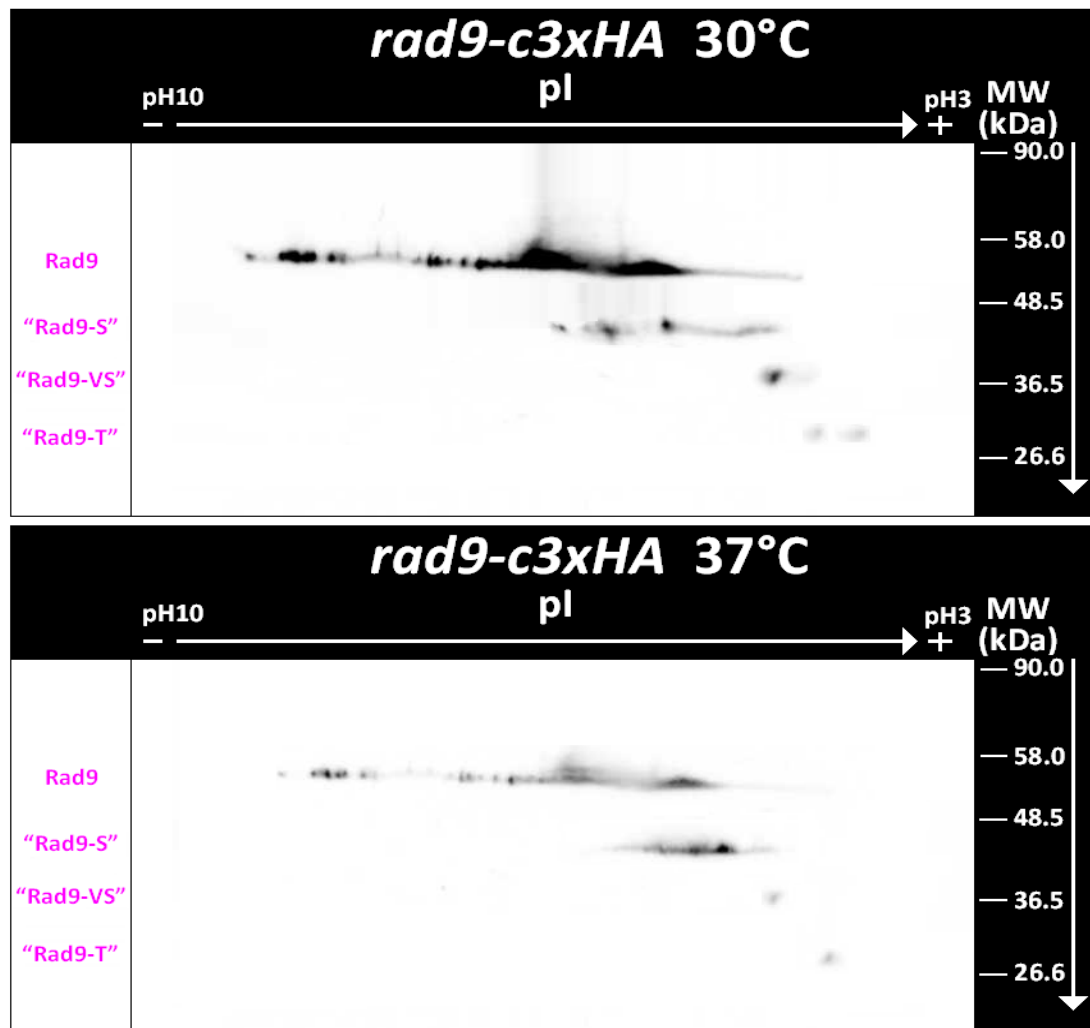
Comparative 2D PAGE-coupled Western blot analyses performed on TCA-precipitated total protein extracts acquired from YEA cell cultures of experimental “cre-lox” – constructed *S. pombe* strains, which either expressed phosphorylation site-mutagenised variants of the “Rad9-S” protein or the unmutagenised “Rad9-S” protein within kinase-specific deletion type genetic backgrounds, indicated that specific phosphoisoforms of the “Rad9-S” protein may be implicated in the regulation of the levels of expressed “Rad9-VS” and “Rad9-T” isoforms (Fig 4.19, p.400; Fig 4.20, p.401).

These data observations are indicative that specific kinase-mediated post-translational phosphorylation modifications of the larger “Rad9-S” truncated protein variant may be implicated in the regulation of the levels of expression and functional activities of the two smaller truncated “Rad9-VS” and “Rad9-T” isoforms in checkpoint responses to different genotoxic and/or environmental types of cytological stresses.

Comparative 2D PAGE-coupled Western blot analyses performed on TCA-precipitated total protein extracts acquired from YEA cell cultures of experimental “cre-lox” – constructed *S. pombe* strains, which either expressed phosphorylation site-mutagenised variants of the “Rad9-S” protein or the unmutagenised “Rad9-S” protein within a variety of checkpoint gene-specific deletion type genetic backgrounds, revealed that this truncated protein variant may exist in a variety of hypophosphorylated, hyperphosphorylated and unphosphorylated isoforms which may have distinctive differential functions in the cytological maintenance of genomic integrity (Fig 4.20, p.401).

Taken together, these experimental observations are indicative that the larger truncated “Rad9-S” protein variant, possibly in conjunction with the two successively smaller truncated “Rad9-VS” and “Rad9-T” isoforms, are functionally implicated in cell cycle checkpoint signalling pathways.

Fig 4.18: 2D-PAGE Analytical Detection of spRad9 Isoforms

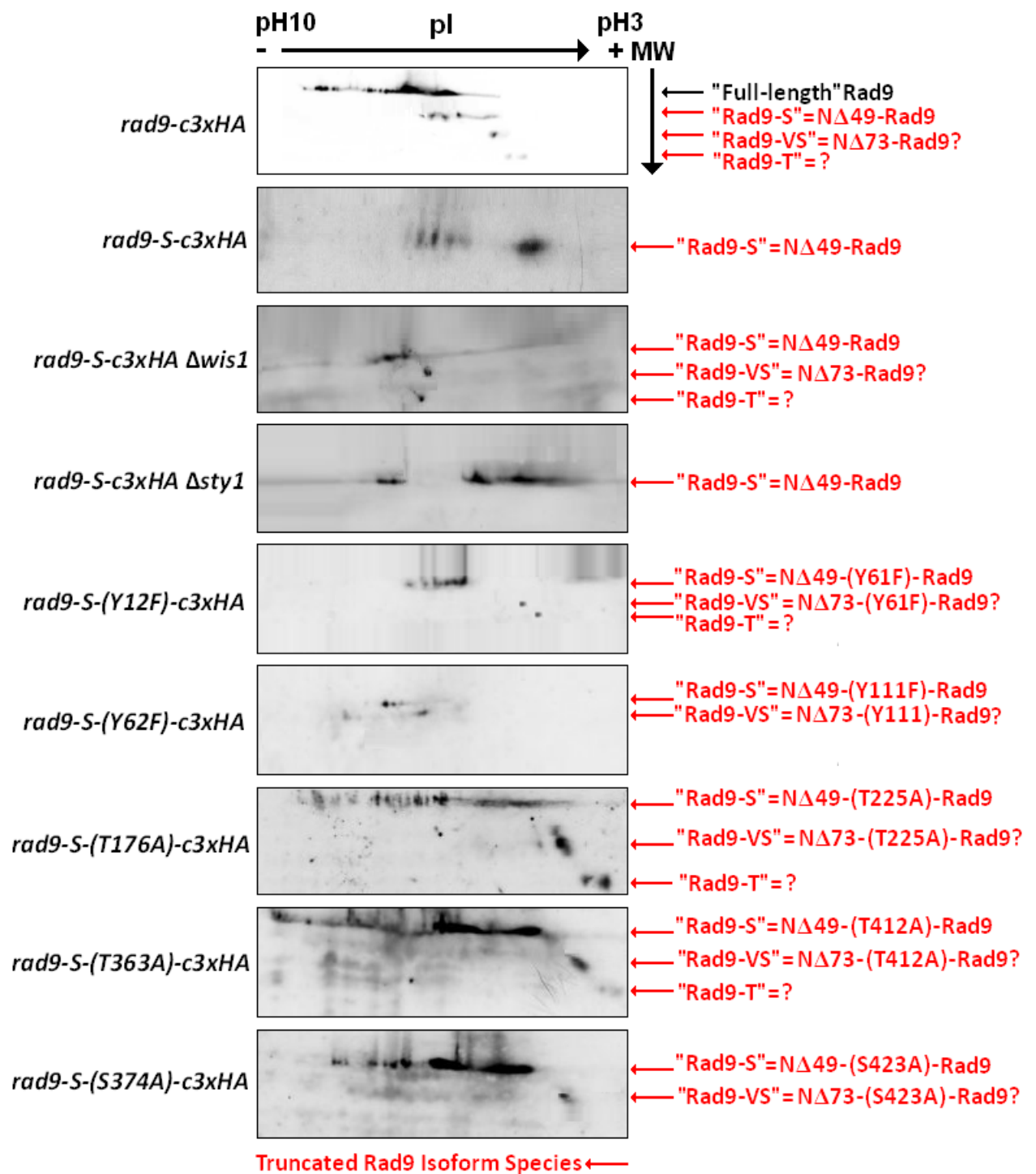


Individual 100mL YEA broth medium cell cultures of “Cre-Lox” – constructed *rad9-c3xHA S. pombe* strain were grown overnight (30°C for ~12 hour time period), then diluted to an optical density $A_{595} = 0.25$ with the appropriate volume of YEA medium and the resultant diluted cultures re-incubated at 30°C for a further time period of ~2.5 hours until they had attained an optical density value of $A_{595} = 0.5$ – after which time the cultures were re-incubated either at 30°C or 37°C (induced “heat shock” stress) for a further 30 minutes.

TCA-precipitated total protein extract samples were then prepared from the appropriate *calculated volumetric aliquot of each culture of actively cycling cells (*equivalent to 40 A_{595} optical density units) and utilised in comparative 2D-PAGE–coupled Western Blot analyses – probed with the primary “anti-HA” antibody.

[Protein sample preparation, 2D-PAGE resolution and Western blot methodologies are detailed in Section 2.8.3.1, pp.214-217; Section 2.8.5.2, pp.226-224; Section 2.8.5.3, pp.228-230; Section 2.8.6, pp.231-233]

Fig 4.19: Kinase-Site Modulation of Rad9 Isoform Expression

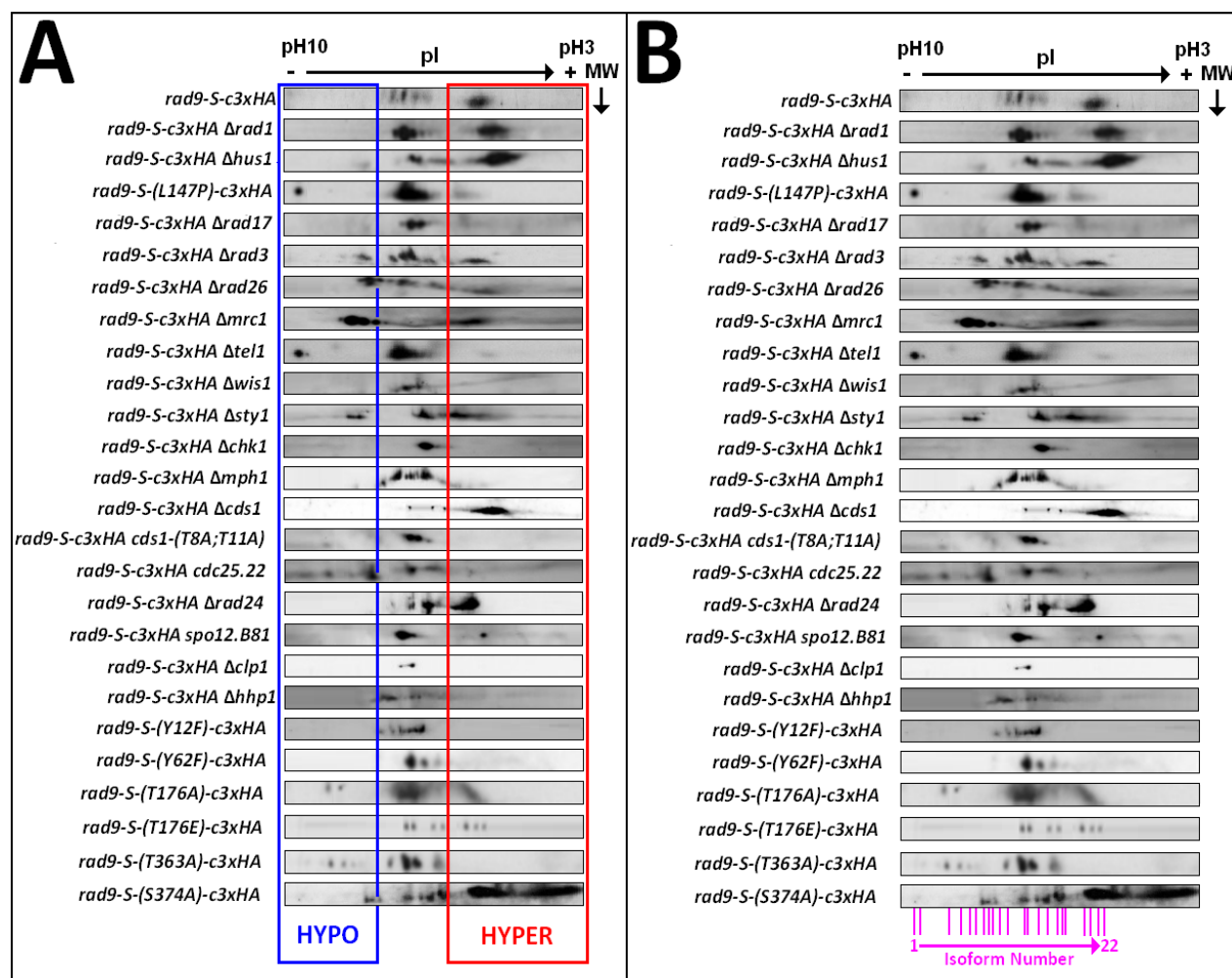


Individual 100mL YEA broth medium cell cultures of the appropriate *S. pombe* strain were grown overnight (30°C for ~12 hour time period), then diluted to an optical density $A_{595} = 0.25$ with the appropriate volume of YEA medium and the resultant diluted cultures re-incubated at 30°C for a further time period of ~2.5 hours until they had attained an optical density value of $A_{595} = 0.5$, after which time they were incubated for a further 30 minutes at 30°C.

TCA-precipitated total protein extract samples were then prepared from the appropriate *calculated volumetric aliquot of each culture of actively cycling cells (*equivalent to 40 A_{595} optical density units) and utilised in comparative 2D-PAGE-coupled Western Blot analyses – probed with the primary “anti-HA” antibody.

[Protein sample preparation, 2D-PAGE resolution and Western blot methodologies are detailed in Section 2.8.3.1, pp.214-217; Section 2.8.5.2, pp.226-224; Section 2.8.5.3, pp.228-230; Section 2.8.6, pp.231-233]

Fig 4.20: 2D-PAGE Alignment Analyses of Rad9-S Phosphoisoforms



Comparative 2D-PAGE-coupled Western Blot alignment analyses of TCA-precipitated total protein extracts acquired from specific gene “knock-out” and kinase site-directed mutagenised *NA49-rad9-c3xHA* type *S. pombe* strains.

Individual 100mL YEA broth medium cell cultures of the appropriate *S. pombe* strain were grown overnight (30°C for ~12 hour time period), then diluted to an optical density $A_{595} = 0.25$ with the appropriate volume of YEA medium and the resultant diluted cultures re-incubated at 30°C for a further time period of ~2.5 hours until they had attained an optical density value of $A_{595} = 0.5$, after which time they were incubated for a further 30 minutes at 30°C.

TCA-precipitated total protein extract samples were then prepared from the appropriate *calculated volumetric aliquot of each culture of actively cycling cells (*equivalent to 40 A_{595} optical density units) and utilised in comparative 2D-PAGE-coupled Western Blot analyses – probed with the primary “anti-HA” antibody.

[Protein sample preparation, 2D-PAGE resolution and Western blot methodologies are detailed in Section 2.8.3.1, pp.214-217; Section 2.8.5.2, pp.226-224; Section 2.8.5.3, pp.228-230; Section 2.8.6, pp.231-233]

A: Aligned 2D PAGE-coupled Western blot analyses with the hypophosphorylated (HYPO) and hyperphosphorylation (HYPER) isoforms indicated.

B: Aligned 2D-PAGE-coupled Western blot analyses indicating the identified 22 phosphoisoforms.

4.9: *In Silico* Elucidation of Hypothetically Feasible Mechanisms of Expression of the Truncated “Rad9-VS” and “Rad9-T” Isoforms

The estimated molecular mass of the engineered N Δ 73-Rad9-c3xHA truncated variant (~39 kDa) was equivalent to that of the “Rad9-VS” isoform detected in the 2D PAGE-coupled Western blot assays (Fig 4.18, p.399).

Comparative *in silico* and Western blot analyses, discussed in detail previously in Chapter 3 (Section 3.3, pp.308-313; Section 3.4, pp.314-357) also indicate that the engineered N Δ 73-Rad9-c3xHA truncated protein variant is most likely to be a functional protein product that originates from downstream ribosomal scanning of the AUG initiation codon translation site at methionine 74.

Taken together, these experimental observations indicate that amino acid sequence of the expressed “Rad9-VS” truncated variant is identical to that of the engineered N Δ 73-Rad9-c3xHA truncated variant.

The molecular mass of the truncated “Rad9-T” isoform (~34 kDa), detected in the 2D PAGE-coupled Western blot assays, did not correlated closely with those of the engineered truncated protein variants N Δ 311-Rad9-c3xHA (~13 kDa) and N Δ 357-Rad9-c3xHA (~8 kDa)

Comparative *in silico* and Western blot analyses, discussed in detail previously in Chapter 3 (Section 3.3, pp.308-313; Section 3.4, pp.314-357) also indicated that the engineered N Δ 311-Rad9-c3xHA and N Δ 357-Rad9-c3xHA truncated variants are likely to be non-functional, highly unstable proteins which are rapidly targeted for proteolytic degradation.

Taken together, these experimental observations indicate the truncated “Rad9-T” variant is not an expressed protein product that originates from downstream ribosomal scanning of the AUG initiation methionine codon translation sites at M311, M312 or M358.

Several hypothetical mechanisms may account for the expression of the truncated “Rad9-T” isoform detected in comparative 2D PAGE-coupled Western blot assays (Fig 4.18, p.399; Fig 4.19, p.400).

Differential *S. pombe rad9* gene splicing, with or without retention of one or more of the three introns, may result in the generation of *rad9* mRNA transcripts that contain alternative AUG translational initiation codon sites, at different positions to those of the “wild-type” *rad9* mRNA transcript, which may encode alternative Rad9 protein isoforms such as “Rad9-T”.

Alternatively, expression of the truncated “Rad9-T” variant may be a consequence of limited proteolytic processing of the full-length *S. pombe* Rad9 protein and/or the truncated N Δ 49-Rad9 (“Rad9-S”) variant and/or the truncated N Δ 73-Rad9 (“Rad9-VS”) variant.

Several comparative *in silico*-based analytical approaches were utilised in order to ascertain which of these postulated mechanisms was most likely to be implicated in the expression of the truncated “Rad9-T” isoform – notably;

(i) *In silico* prediction and modelling of thermodynamically-optimised secondary structures for the three introns contained within the *S. pombe rad9* gene via analyses of their respective RNA base-sequences with the on-line bioinformatics software tool Vienna RNAfold.

(Section 4.8.1, pp.404-406).

(ii) Multiple sequence alignments between the full-length *S. pombe* Rad9 protein, *S. pombe* metacaspase cleavage target motifs and *H. sapiens* Rad9A caspase 3 cleavage target motifs, performed via utilisation of the on-line bioinformatics software tools EMBOSS, JEMBOSS and PSI-BLAST – Section 4.8.2, pp.407-417).

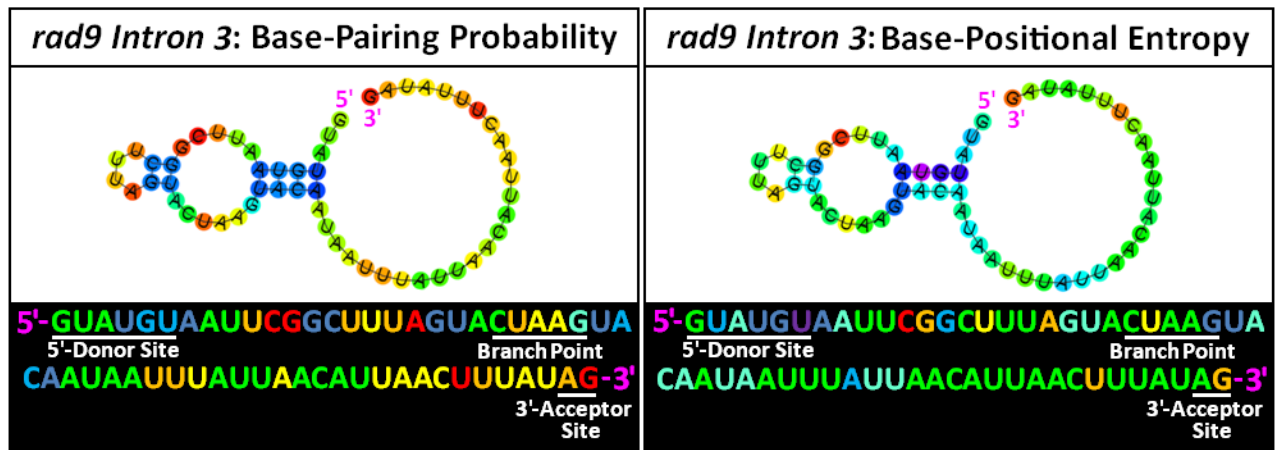
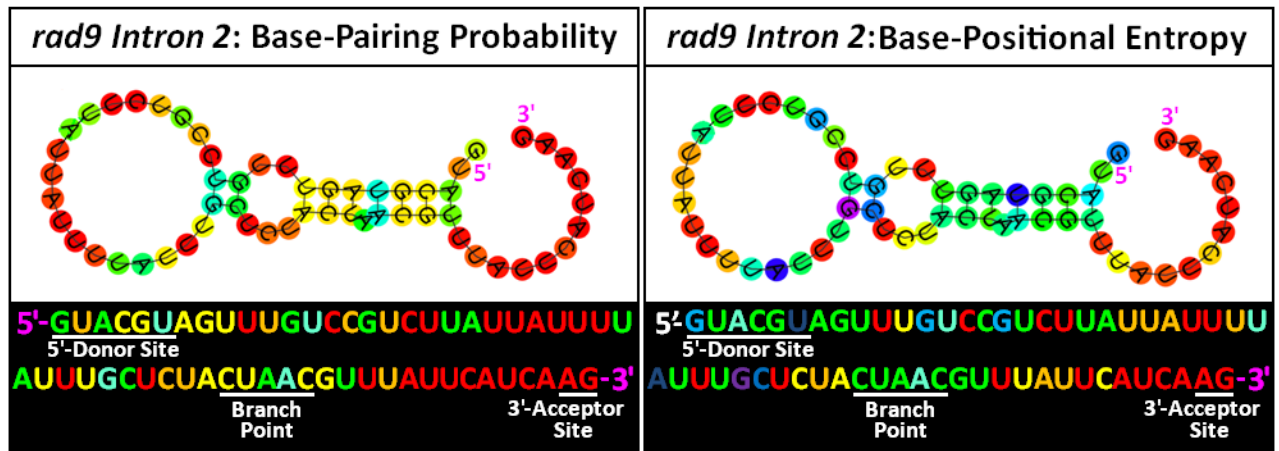
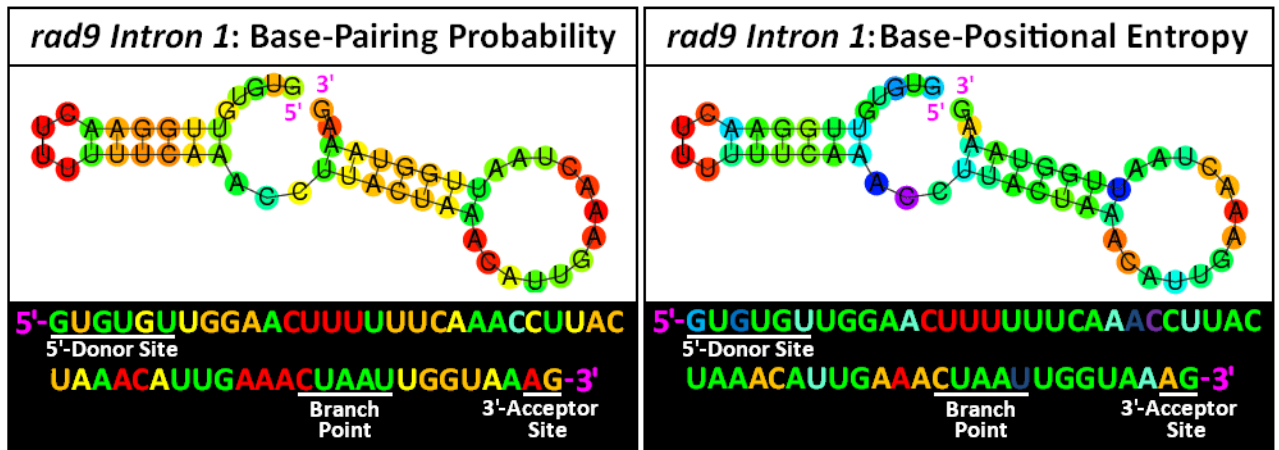
4.9.1 Intron-Retained *S. pombe rad9* mRNA Transcripts are Unlikely to be Implicated in the Expression of the “Rad9-T” Truncated Isoform

The fact that two isoformic *rad9* mRNA transcripts have been identified within *S. pombe* (Murray J.M. *et al.*, 1991) prompted comparative *in silico* RNA secondary structure prediction analyses of the three introns within the *S. pombe rad9* gene, which were performed via utilisation of the bioinformatics software tool Vienna RNAfold, in order to ascertain whether or not their retention within *rad9* mRNA transcripts was likely to be implicated in the expression of the truncated “Rad9-T” protein variant.

The acquired *in silico* data indicated that all three introns of the *S. pombe rad9* gene are most likely to adopt typical intronic-excision type conformations, which would be removed via spliceosomal processing of the nascent *S. pombe rad9* mRNA transcript (Fig 4.21, p.405; Fig 4.22, p.406).

Thus, these data indicate that retention of introns 1, 2 and/or 3 within the transcribed *S. pombe rad9* mRNA is unlikely to be implicated in potential riboswitch/aptamer type functions that modulate the translational expression of the “Rad9-T” isoform detected in comparative 2D PAGE-coupled Western blot assays (Fig 4.18, p.399; Fig 4.19, p.400).

Fig 4.22: *rad9* Intronic RNA Folding Analyses – “Processed Data”



= "Thermodynamic Propensity" Scale

4.9.2 A Limited-Proteolytic Cleavage Mechanism May be Implicated in the Expression of the Truncated “Rad9-T” Isoform

The COP9 signalosome (CSN) is implicated in the 26S proteasomal pathway-directed degradation of the human Rad9-Rad1-Hus1 complex – which is initiated via associative interactions between the Rad1 sub-unit of the “9-1-1” DNA “sliding-clamp” and the Jab1 (CSN5) sub-unit of the CSN complex (Huang J. *et al.*, 2007).

Various experimental studies in the fission yeast *S. pombe* have also demonstrated that a homologous functional equivalent COP9 signalosome complex is implicated in the proteasomal pathway-targeted degradation of proteins, for regulation of their respective concentration levels and activities within the cell (Liu C. *et al.*, 2003; Mundt K.E. *et al.*, 1999; Mundt K.E. *et al.*, 2002; Zhou C. *et al.*, 2001; Zhou L. and Watts F.Z., 2005).

A feasible hypothetical postulation is that Dbp1, via associative interactions with DET1, histones and histone deacetylases (Benvenuto G. *et al.*, 2002; Martinez E. *et al.*, 2001; Schroeder D.F. *et al.*, 2002), may serve as a protein mediator type recruitment platform for the co-ordinated assembly of the CSN complex, Rad9 and the Cullin-Rbx-E2 to specific DNA damage lesion sites within the chromatin supramolecular architecture and facilitate later interactions of the Rad9 protein with specific sub-units of the COP9 signalosome complex (CSN) – Fig 4.23, p.413.

In this respect, COP9-initiated polyubiquination-mediated “proteolytic processing” of the *S. pombe* Rad9 protein (Fig 4.23, p.412) may be implicated in the formation of truncated variant type isoforms with potential novel functions, such as the truncated “Rad9-T” isoform which was detected in comparative 2D PAGE-coupled Western blot assays (Fig 4.18, p.399; Fig 4.19, p.400).

Taken together in the context of the hypothetical “working model”, illustrated in Fig 4.23 (p.413), CSN proteolytic degradation of the DNA-associated *S. pombe* full-length Rad9 protein and/or the truncated “Rad9-S” and/or “Rad9-VS” isoforms, may also serve as a regulatory control mechanism for termination of Rad9-initiated checkpoint signalling responses once DNA damage lesion sites within the chromatin have been detected and repaired to enable phasic re-engagement of the arrested cell cycle.

Several caspase 3 target cleavage motif sites have also been identified within the human Rad9A protein (Lee M.W. *et al*, 2003).

In *S. pombe*, under conditions of oxidative stress-induced post-mitotic arrest in Edinburgh Minimal Medium (EMM), elevated levels of diacylglycerol have been demonstrated to initiate a caspase-dependent apoptotic-like pathway in which metacaspase enzyme Pca1, the BH3-domain protein Rad9 and diacylglycerol-binding proteins Pck1 and Bzz1 are implicated (Low C.P. *et al*, 2008) – summarily depicted in Fig 4.24 (p.414).

In YEA medium, associative Rad9-metacaspase interactions may result in “limited proteolytic processing” of the full-length *S. pombe* Rad9 protein and/or truncated “Rad9-S” and “Rad9-VS” variants with consequential formation of shorter truncated variant type isoforms (such as the “Rad9-T” isoform) with potential novel functions, in addition to regulation of the concentration levels and activities of the respective full-length, “Rad9-S” and/or “Rad9-VS” isoforms (Fig 4.24, p.414).

This hypothetical “working model” is also supported by bioinformatics-based data acquired from comparative *in silico* caspase and metacaspase optimal proteolytic target substrate motif sequence alignments performed on the *S. pombe* Rad9 protein (Fig 4.25, p.415)

These comparative *in silico* analyses identified a distinctive metacaspase proteolytic target site within the regional sequence ¹¹⁰GYGSESASRKV¹²⁰ of the *S. pombe* Rad9 protein, which upon cleavage was predicted to yield a detectable C-terminal tail HA epitope-tagged polypeptide fragment with an estimated molecular weight of ~34 kDa (Fig 4.25, p.415) that was equivalent to the molecular weight of the “Rad9-T” isoform detected in the 2D PAGE-coupled Western blot assays (Fig 4.18, p.399; Fig 4.19, p.400).

Comparative multiple sequence alignment analyses of this potential metacaspase cleavage target motif also indicated that equivalent homologues were conserved within the Rad9 proteins of different *Schizosaccharomyces* clades (Fig 4.26B, p.416).

In silico analysis of this ¹¹⁰GYGSESASRKV¹²⁰ motif with the on-line bioinformatics NetPhos tools indicated that the tyrosine and serine residues were high-probability phosphorylation sites and that the tyrosine residue was situated within a potential Wis1 kinase-target Sty1 kinase-like substrate motif type phosphorylation site (Fig 4.25, p.415).

Intriguingly, *in silico* sequence alignment analyses of the *S. pombe* Rad9 protein with the 5 isoforms of the *H. sapiens* Rad9B paralogue identified two sequences, situated within and flanking the ¹¹⁰GYGSESASRKV¹²⁰ metacaspase cleavage target motif, which were equivalent homologues of the alternative GSFSIF and VVCRKEFNGSDAKYFCII C-terminal sequences of the human Rad9B full-length and truncated protein isoforms (Fig 4.26A, p.416).

In silico comparative modelling analysis also indicated that this potential ¹¹⁰GYGSESASRKV¹²⁰ metacaspase cleavage target motif was also situated within the Rad9:Rad1 interactive domain of the heterotrimeric Rad9-Rad1-Hus1 DNA sliding-clamp complex (Fig 4.26C, p.416).

Taken together, these *in silico* indicate that cell cycle checkpoint signalling responses to specific types of genotoxic and environmental cytological stresses may be implicated in the regulation of functional activities of the heterotrimeric Rad9-Rad1-Hus1 DNA sliding-clamp complex, via kinase-mediated phosphorylation and/or phosphatase-mediated dephosphorylation post-translational modifications of the ¹¹⁰GYGSESASRKV¹²⁰ proteolytic motif which alter its supramolecular configuration and render it susceptible or resistant to metacaspase cleavage.

In this hypothetical context, metacaspase-mediated proteolytic cleavage of the ¹¹⁰GYGSESASRKV¹²⁰ target motif (which is situated within the Rad9:Rad1 interface of the heterotrimeric heterotrimeric Rad9-Rad1-Hus1 DNA sliding-clamp – Fig 4.26C, p.416) may promote dissociation of the “9-1-1” complex and generate two truncated Rad9 isoforms; Rad9-CΔ118-426 and “Rad9-T” (NΔ117-Rad9), that may be functionally-implicated in novel cell cycle checkpoint signalling responses to specific types of genotoxic and/or environmental cytological stresses.

Loss of the protein-interactive C-terminal domain in the truncated Rad9-CΔ118-426 protein variant may be compensated via its ¹¹²GSESAS¹¹⁷ motif, which has equivalent homology to the C-terminus GSFSIF sequence of the human Rad9B isoforms 1, 2 and 3 (Fig 4.26A, p.416) and contains three serine residues, which may undergo kinase-mediated phosphorylation and/or phosphatase-mediated dephosphorylation type post-translational modifications that enable the motif to engage with and modulate the functional activities of a variety of proteins implicated in cell cycle checkpoint signalling and/or DNA repair pathways.

NΔ117-Rad9 (“Rad9-T”) truncated variant would contain the ¹¹⁸RKDVIVENVQISISIGSECRII¹³⁹ motif, which has equivalent homology to the C-terminus VVCRKEFNGSDAKYFCII sequence of the human Rad9B isoforms 4 and 5 (Fig 4.26A, p.416), which may likewise undergo kinase-mediated phosphorylation and/or phosphatase-mediated dephosphorylation type post-translational modifications at the Ser129 and Ser134 residues that enable the motif to engage with and modulate the functional activities of a variety of proteins implicated in cell cycle checkpoint signalling and/or DNA repair pathways.

The NΔ117-Rad9 (“Rad9-T”) truncated variant would also contain the C-terminal tail domain, which enables the Rad9 protein to interact with and modulate the functional activities of a variety of proteins that are implicated in the mediation of DNA damage checkpoint signalling responses and DNA repair pathways (Broustas C.G. and Lieberman H.B., 2012).

Taken together, these *in silico* data observations indicate that these two truncated *S. pombe* Rad9-CΔ118-426 and NΔ117-Rad9 (“Rad9-T”) variants may elicit different checkpoint responses to specific types of genotoxic and environmental cytological stresses and whose respective functions may be equivalent to those of the human Rad9B isoforms.

In this respect, *S. pombe* may also prove to be a useful eukaryotic model system for future investigative studies of unknown cell cycle checkpoint and DNA repair functions which may be specific to particular human Rad9B isoforms.

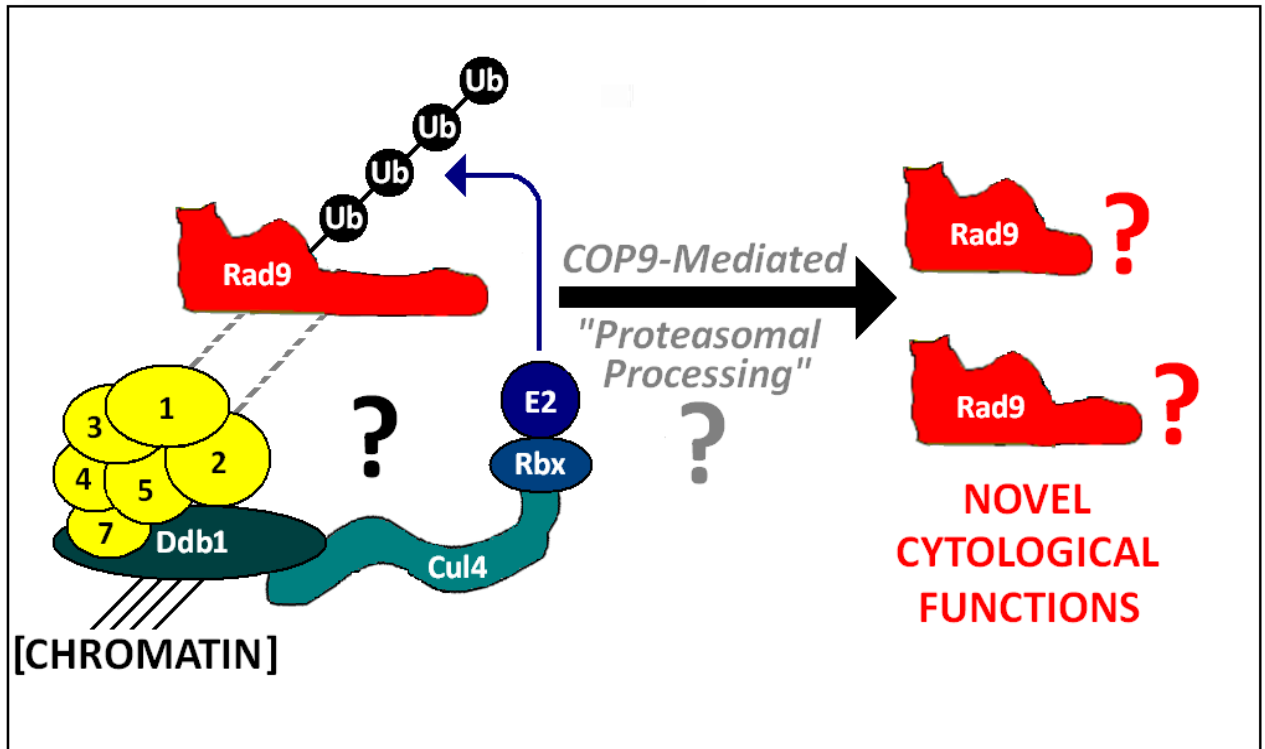
TCA-precipitated total protein samples prepared from “cre-lox”-constructed *rad9-c3xHA* strain cultures, which were utilised in comparative 2D PAGE-coupled Western blot analyses, only enabled the detection of the C-terminal HA epitope-tagged Rad9 protein isoforms Rad9-c3xHA, NΔ49-Rad9-c3xHA (“Rad9-S”), NΔ73-Rad9-c3xHA (“Rad9-VS”) and NΔ117-Rad9-c3xHA (“Rad9-T”) – Fig 4.27, p.417.

Thus the potential expression of novel C-terminal truncated *S. pombe* Rad9 protein isoforms, which could be derived from metacaspase or other limited-proteolytic processes, may remain undetected in these comparative 2D PAGE-coupled Western blot assays due to removal of a portion of the protein which contains the HA epitope-tagged C-terminus – as would be the case for the postulated truncated Rad9-C Δ 118-426, N Δ 49-Rad9-C Δ 118-426 and N Δ 73-Rad9-C Δ 118-426 variants which may result from metacaspase cleavage of the alternative translationally expressed full-length Rad9, Rad9-S and Rad9-VS isoforms (Fig 4.27, p.417).

Therefore the possible existence of additional C-terminal truncated *S. pombe* Rad9 isoforms cannot be excluded as these would also remain undetected.

Fig 4.23: COP9-Directed Rad9 Partial Proteasomal Processing Model

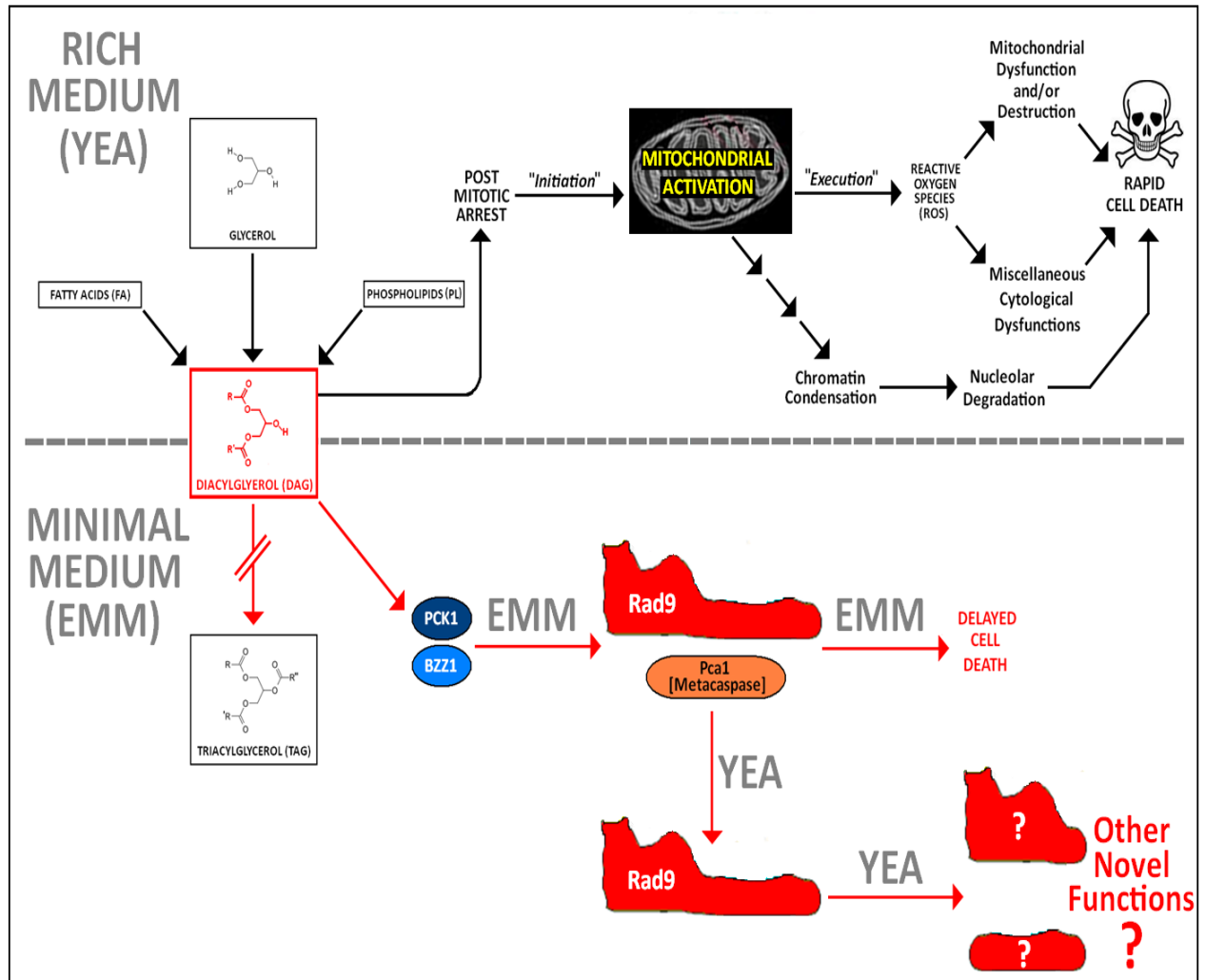
[Compiled via Collated Information Adapted From: Liu C. *et al.*, 2003; Mundt K.E. *et al.*, 1999; Mundt K.E. *et al.*, 2002; Zhou C. *et al.*, 2001; Zhou L. and Watts F.Z., 2005]



A detailed explanation of this hypothetical model is provided in the text (pp.407-408)

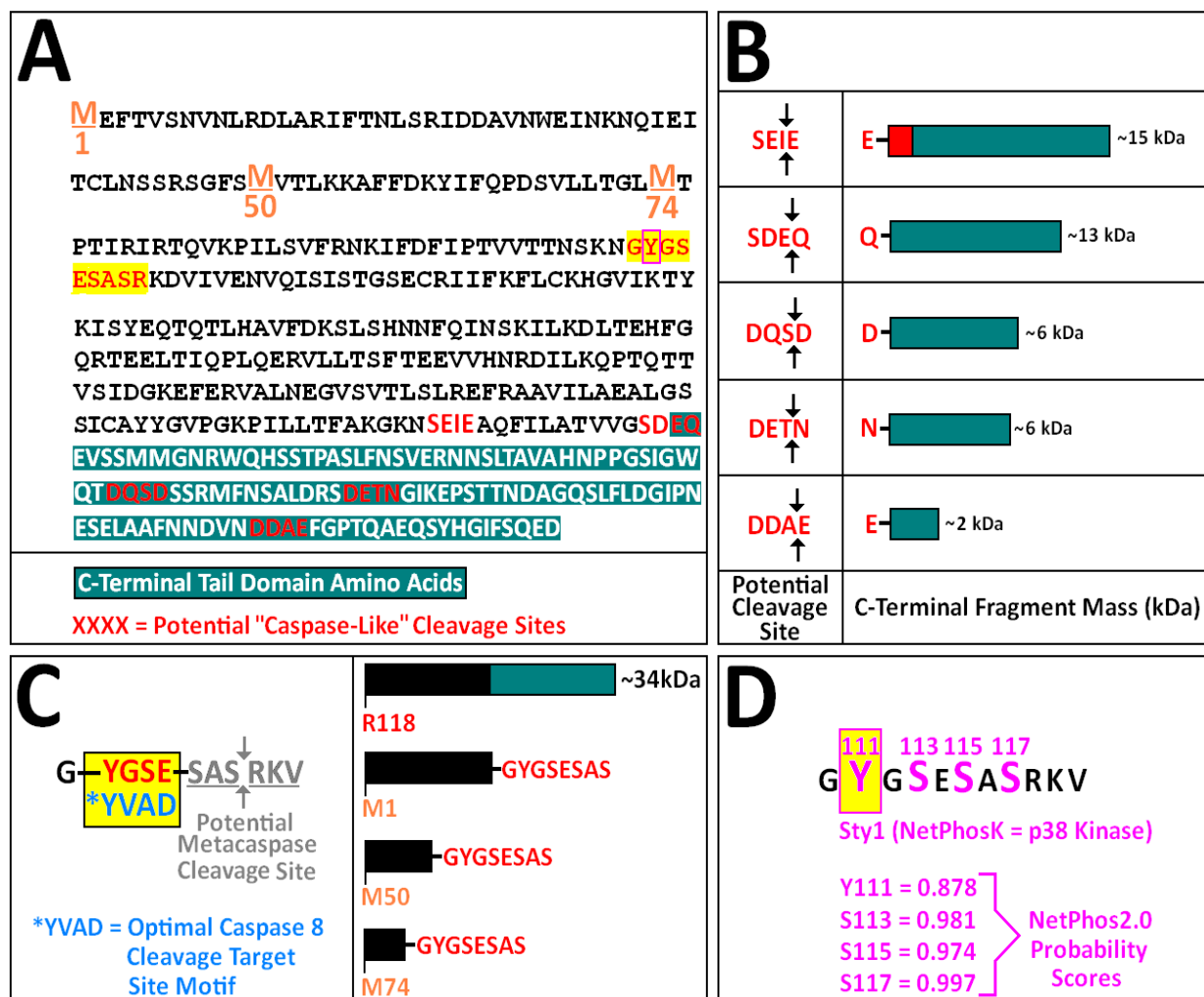
Fig 4.24: Rad9-Targeted Metacaspase Cleavage Processing Model

[Compiled via Collated Information Adapted From: Lim H.W. *et al.*, 2007; Low C.P. *et al.*, 2008; Low C.P. and Yang H., 2008; Rodriguez-Menocal L. and D'Urso G., 2004



A detailed explanation of this hypothetical model is provided in the text (p.408)

Fig 4.25: *In Silico* Identification of Potential Caspase Cleavage Sites Within the *S. pombe* Rad9 Protein



A: *In Silico* Identification of Potential Caspase-Like Cleavage Target Sites within the *S. pombe* Rad9 Protein
M1, **M50**, **M74** = Postulated Alternative Translation AUG Start-Codon Sites

XXXX = Identified Potential Caspase Cleavage Target Motifs

XXXXX = Potential Identified Metacaspase-Like Cleavage Target Motif

[Potential caspase cleavage target sites were identified via *in silico* multiple sequence alignment analyses with optimal caspase cleavage motifs – which were derived via compiled information collated from Agard N.J. and Wells J.A., 2009; Garcia-Calvo M. *et al.*, 1998; Geley S. *et al.*, 1997; Pereira N.A. and Song Z., 2008; Stenicke H.R. *et al.*, 2000; Thornberry N.A. *et al.*, 1997; Tiatsiaki L. *et al.*, 2011.

B: *Relative molecular masses of the hypothetical C-terminal HA epitope-tagged polypeptide fragments produced via hypothetical caspase-like proteolytic cleavage of the *S. pombe* Rad9 protein situated in close proximity to or within the C-Terminal Domain

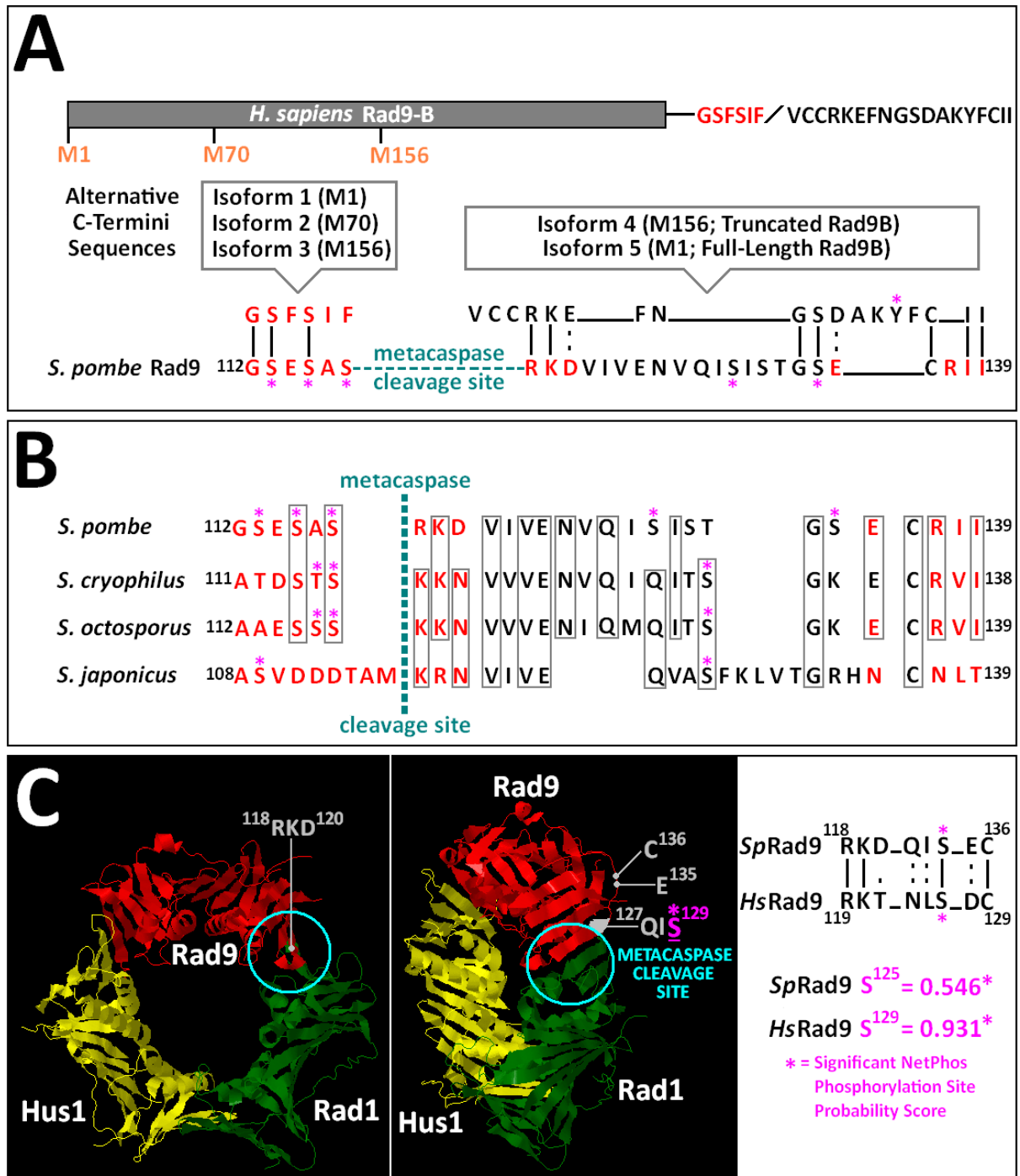
[*The kDa values were determined via utilisation of the “on-line” software tool Protein Calculator v3.3]

C: The identified potential metacaspase-like target site within the *S. pombe* Rad9 protein would result in the generation of a C-Terminal HA-Tagged fragment of approximate mass ~34kDa, upon proteolytic cleavage – this determined molecular mass also correlates closely with the molecular weight range of the “Rad9-T” truncated protein variant that was detected on Western blot of the 2D PAGE-resolved total protein extract samples (Fig 4.18, p.399).

This potential metacaspase-like cleavage site is situated within a distinctive Sty1 kinase target motif and is distinctive from the other identified caspase-like sites.

D: The distinctive “YVAD-like” potential metacaspase-like cleavage site is also situated within close proximity to adjacent tyrosine and serine residues which are identified as high-probability phosphorylation kinase-target sites.

Fig 4.26: Comparative *In Silico* Alignment Analyses of the Potential Metacaspase Target Motif Sequence Identified Within the *S. pombe* Rad9 Protein

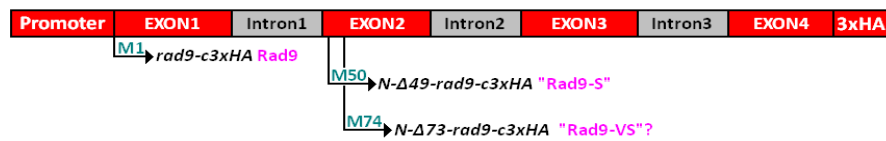
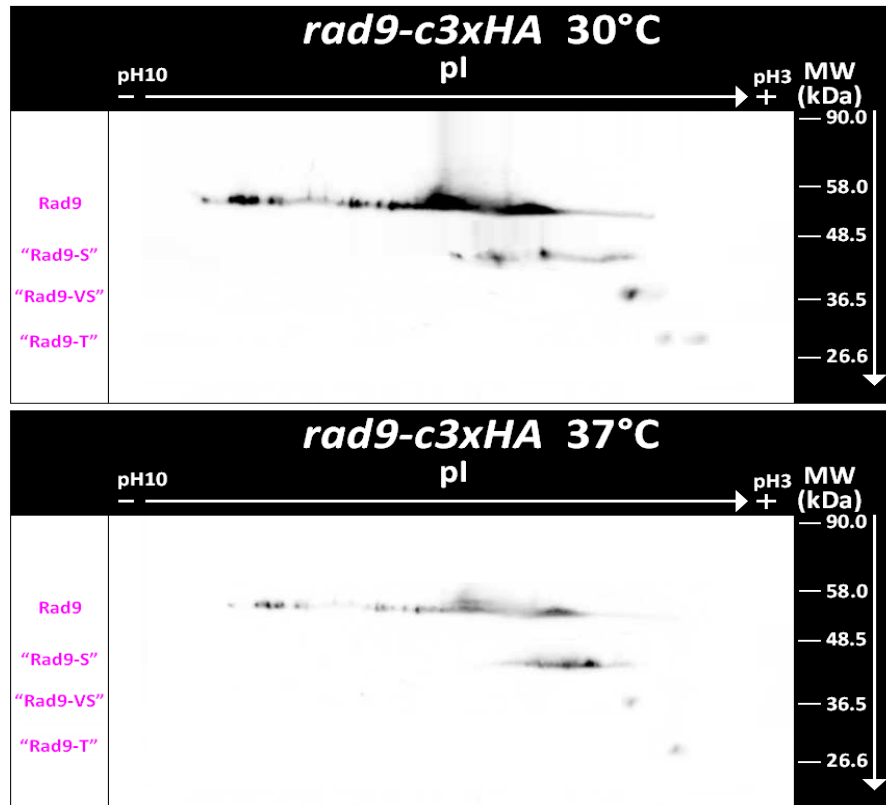


A: *In silico* alignments of the two alternative C-terminal sequences of the *H. sapiens* Rad9B isoforms with the amino acid sequence of the *S. pombe* Rad9 protein, performed with the on-line bioinformatics software tools EMBOSS, JEMBOSS and PSI-BLAST

B: *In silico* multiple alignment analyses of *Schizosaccharomyces* Rad9 proteins with the potential metacaspase target motif sequence identified within the *S. pombe* Rad9 protein, performed with the on-line software programs EMBOSS, JEMBOSS and PSI-BLAST

C: *In silico* comparative modelling analysis of the potential *S. pombe* Rad9 metacaspase target motif sequence within the resolved structure of the human Rad9-Rad1-Hus1 DNA sliding-clamp complex (PDB file: 3G65) were performed with the RasMol software program, structural images were generated by the PolyView3D program.

Fig 4.27: Possible Identity of 2D-PAGE-Detected spRad9 Isoforms



POTENTIAL ALTERNATIVE TRANSLATION PRODUCTS



POTENTIAL METACASPASE CLEAVAGE-GENERATED FRAGMENTS



4.10 In Silico Protein Stability Assessment of the Hypothetically Predicted Amino Acid Sequences of the Detected *S. pombe* Rad9 Isoforms – “Rad9-S”, “Rad-VS” and “Rad9-T” and Undetected Metacaspase-Mediated Limited-Proteolytic Rad9 Cleavage Products

Protein folding, anti-/pro- aggregation propensity and intrinsic order/disorder relationships are key interactive supra-molecular structural parameters which impinge upon the relative stability, half-life and functional viability of an expressed protein within its localised cytological microenvironment(s) (Banavar J.R. *et al.*, 2007; Chakrobortee S. *et al.*, 2012; Fawzi N.L. *et al.*, 2008a; Fawzi N.L. *et al.*, 2008b; Hoang T.X. *et al.*, 2006; Kulkarni P. *et al.*, 2011; Morimoto R.I. *et al.*, 2012; Nair S.S. *et al.*, 2011; Trovato A. *et al.*, 2006; Zhang Y. and Calderwood S.K., 2011).

Therefore, comparative *in silico* analyses of the relative proportions of localised intrinsic structural order/disorder regions (Section 4.10.1, pp.419-421), anti-/pro- aggregative functional motifs (Section 4.10.2, pp.422-426) and secondary structural helix, strand and coil motifs (Section 4.10.3, pp.427-429) were performed on the amino acid sequences of the postulated full-length and truncated variant isoforms of the *S. pombe* Rad9 protein (Fig 4.27, p.417) for hypothetical prediction of their respective cytological stabilities and identification of the key common protein structure-stability relationships implicated (Section 4.10.4, pp.430-434).

4.10.1 *In Silico* Predictive Intrinsic Structural Disorder Analyses

Comparative *in silico* intrinsic structural disorder analyses, performed with the on-line bioinformatics software tools metaPrDOS (Fig 4.28, p.420; Fig 4.29, p.421) and DisCon (Fig 4.33, pp.433-434), indicated that the full-length Rad9 and truncated protein isoforms “Rad9-S” (NΔ49-Rad9), “Rad9-VS” (NΔ73-Rad9) and “Rad9-T” (NΔ117-Rad9) all retained the intact highly mobile/flexible protein-interactive C-terminal tail domain – in which the relative hierarchy of intrinsic structural disorder propensity (highest → lowest) may be defined as:

$$\text{“Rad9-T”} > \text{“Rad 9-VS”} > \text{“Rad9-S”} > \text{Rad9}$$

Comparative *in silico* intrinsic structural disorder analyses, performed with the on-line bioinformatics software tools metaPrDOS (Fig 4.28, p.420; Fig 4.29, p.421) and DisCon (Fig 4.33, pp.433-434), indicated that the metacaspase-generated C-terminal truncated protein isoforms Rad9-cΔ118-426, NΔ49-Rad9-cΔ118-426 and NΔ73-Rad9-cΔ118-426 (Fig 4.27, p.417), all highly lacked the highly mobile/flexible protein-interactive C-terminal tail domain and contained a distinctive region of very low structural disorder probability (Fig 4.28, p.420; Fig 4.29, p.421) in which the relative hierarchy of intrinsic structural disorder propensity (highest → lowest) may be defined as:

$$\text{N}\Delta\text{73-Rad9-c}\Delta\text{118-426} > \text{N}\Delta\text{49-Rad9-c}\Delta\text{118-426} > \text{Rad9-c}\Delta\text{118-426}$$

These acquired *in silico* data also revealed that the hypothetical metacaspase-generated “Rad9-T” isoform (NΔ117-Rad9) had the highest structural disorder propensity and that of the limited proteolytic process-generated cΔ118-426 truncated variants was higher than that of their uncleaved sources, with the exception of the full-length Rad9 protein (ie Rad9 \simeq Rad9-cΔ118-426;

NΔ49-Rad9-cΔ118-426 > NΔ49-Rad9; NΔ73-Rad9-cΔ118-426 > NΔ73-Rad9) – Fig 4.33, pp.433-434.

These structural order hierarchies correlate with the relationship of increased intrinsic disorder as a function of decreased N-terminal amino acids which constitute the major intrinsically-ordered structural component of the respective full-length and truncated Rad9 protein isoforms.

Fig 4.28: metaPrDOS Analyses of Detected spRad9 Isoforms

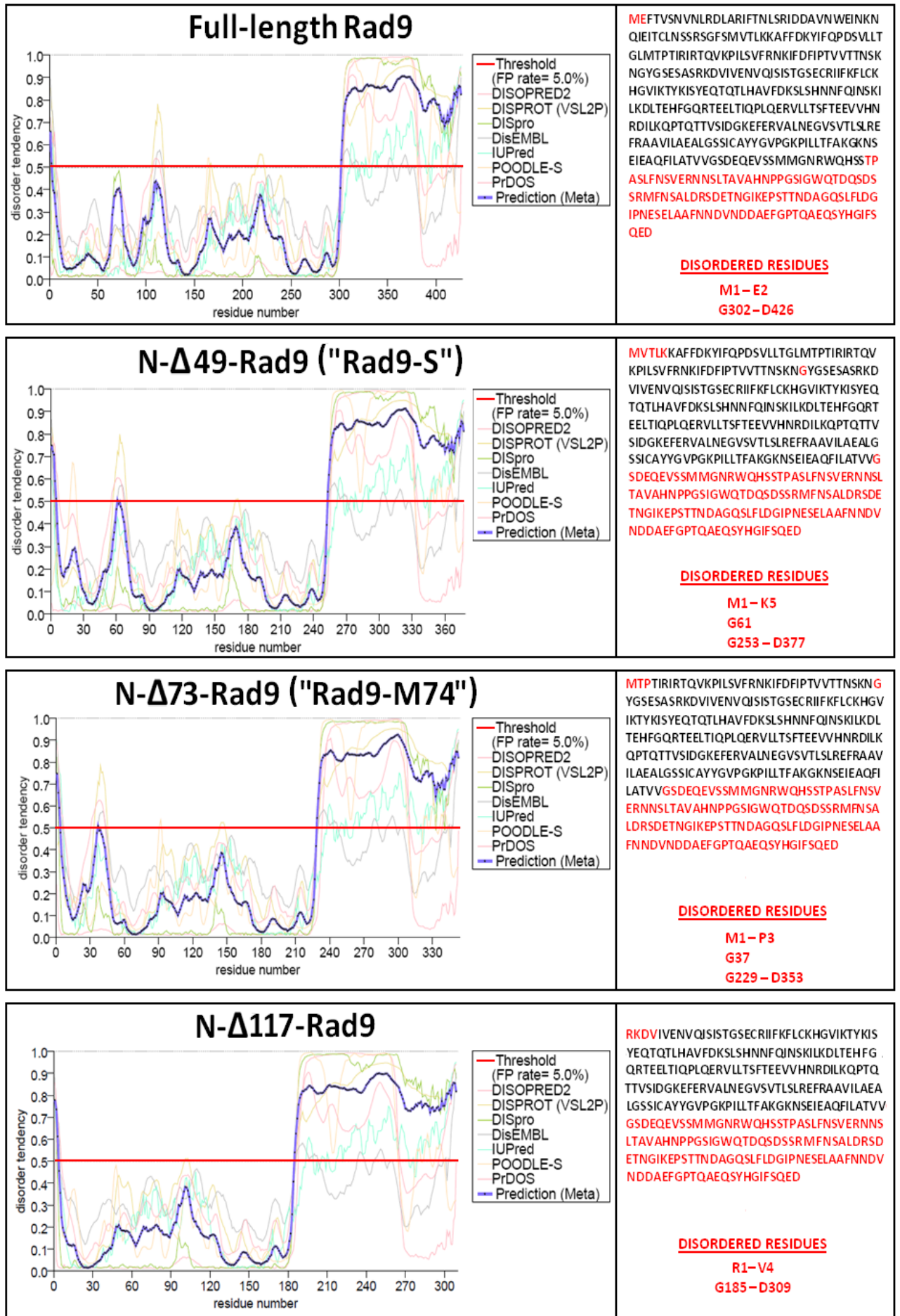
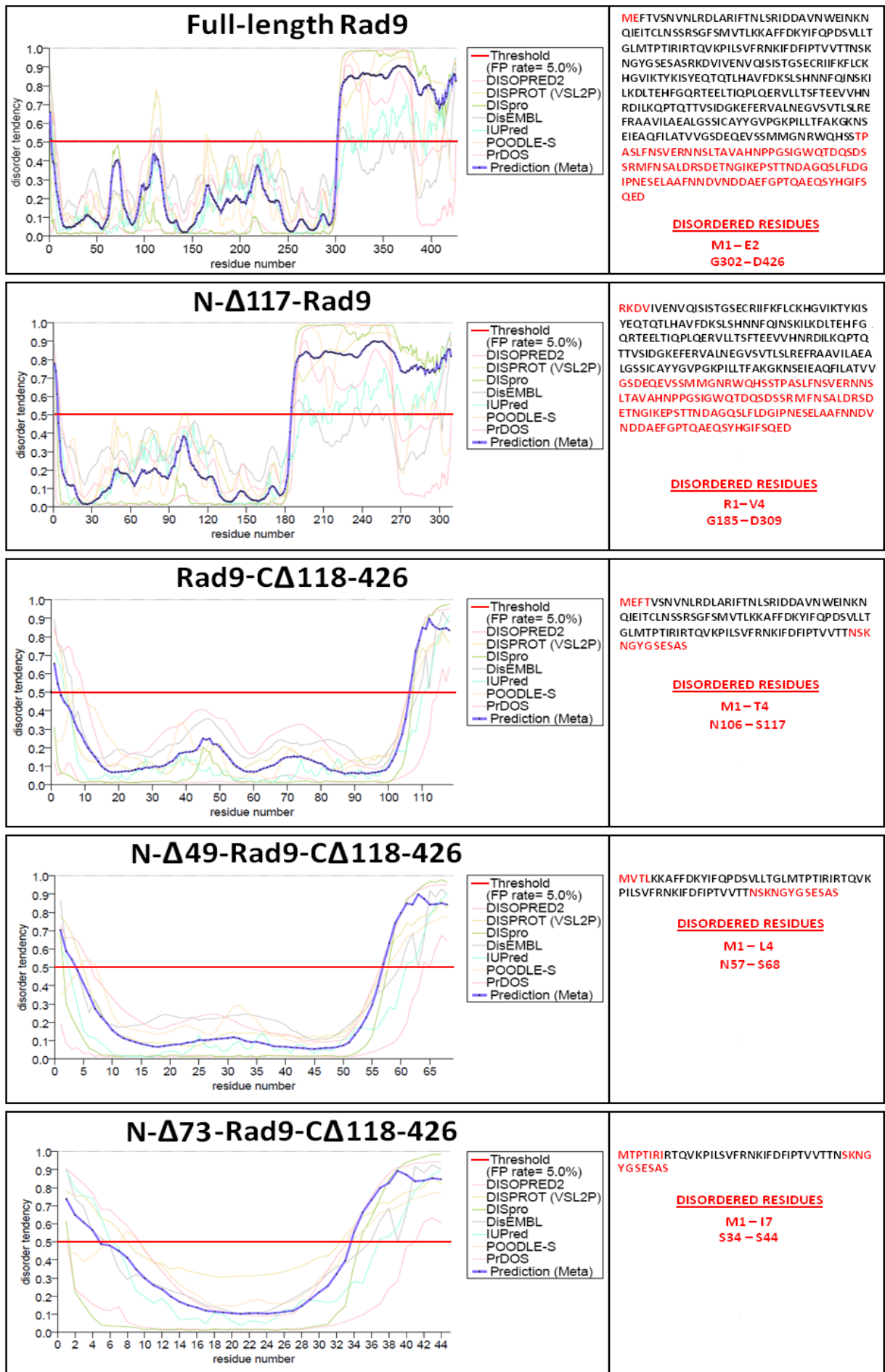


Fig 4.29: metaPrDOS Analyses of spRad9 Cleavage Products



4.10.2 In Silico Predictive Aggregation and Protease Susceptibility

Comparative *in silico* analyses of the relative abundance of anti-aggregative, pro-aggregative and protease-resistance sites (identified via the applied bioinformatics strategies discussed in detail previously in Chapter 3, Section 3.4.2, pp.320-330) were performed on the full-length and predicted truncated isoform amino acid sequences of the *S. pombe* Rad9 protein (Fig 4.30, p.424; Fig 4.31, pp.425-426; Fig 4.33, pp.433-434).

The acquired data indicated that the relative proportion of anti-/pro- aggregative and protease resistant motifs within the full-length Rad9 protein and its postulated truncated isoforms “Rad9-S” (NΔ49-Rad9), “Rad9-VS” (NΔ73-Rad9) and “Rad9-T” (NΔ117-Rad9), summarised graphically in Fig 4.33, pp. , was in a hierachical order (most abundant → least abundant) – which may be defined as:

Aggregation Inductive Motifs > Protease Resistant Motifs > Aggregation Suppressive Motifs

In contrast, these data also revealed that the relative proportion of anti-/pro- aggregative and protease resistant motifs within the hypothetical predicted amino acid sequences of the truncated isoforms Rad9-cΔ118-426 and NΔ49-Rad9-cΔ118-426, summarised graphically in Fig 4.33, pp.433-434, was in a hierachical order (most abundant → least abundant) – which may be defined as:

Aggregation Suppressive Motifs > Protease Resistant Motifs = Aggregation Inductive Motifs

In the case of the postulated NΔ73-Rad9-cΔ118-426 variant, the data indicated that the hypothetical amino acid sequence of this protein did not contain any aggregation suppressive motifs, but did contain protease resistance and aggregation inductive motifs in identical proportions to those found within the Rad9-cΔ118-426 and NΔ49-Rad9-cΔ118-426 truncated isoforms (Fig 4.33, pp.433-434).

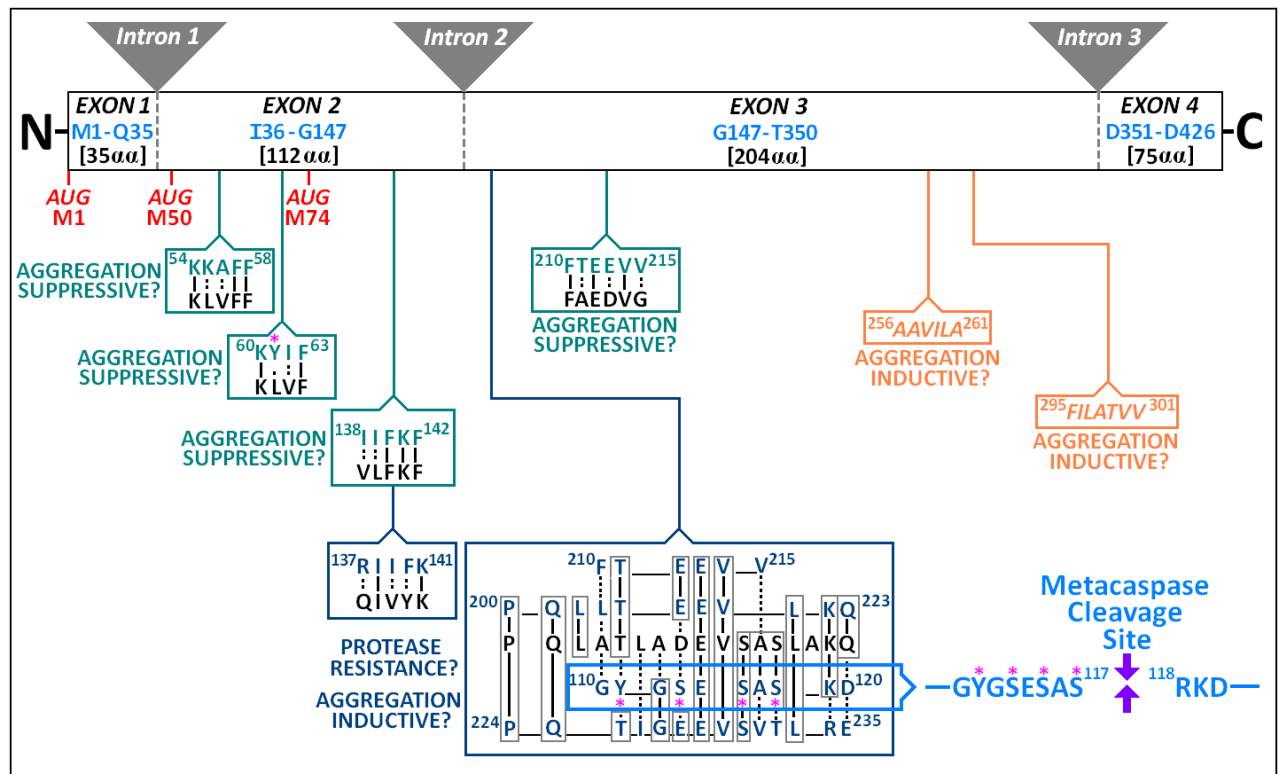
The acquired *in silico* data also indicated that the full-length Rad9 protein and truncated protein variant “Rad9-S” (NΔ49-Rad9) contained equivalent proportions of anti-aggregative, pro-aggregative and protease resistant motifs, whilst the truncated isoforms “Rad9-VS” (NΔ73-Rad9) and “Rad9-T” (NΔ117-Rad9) contained equivalent proportions of pro-aggregative and protease resistant motifs, but only half the number of anti-aggregative motifs to that of full-length Rad9 and “Rad9-S” proteins (Fig 4.33, pp.433-434).

Comparative *in silico* analyses of the relative abundance of anti-/pro- aggregative and protease resistant motifs within the hypothetical amino acid sequences of the postulated truncated isoforms “Rad9-VS”, “Rad9-T”, Rad9-cΔ118-426 and NΔ49-Rad9-cΔ118-426 indicated that they contained an equivalent proportion of anti-aggregative motifs which correlated to 50% less than that found in the full-length Rad9 and truncated “Rad9-S” protein variant (Fig 4.33, pp.433-434).

These data also revealed that the hypothetical amino acid sequences of the Rad9-cΔ118-426, NΔ49-Rad9-cΔ118-426 and NΔ73-Rad9-cΔ118-426 truncated protein variants contained identical proportions of pro-aggregative and protease resistance motifs, in which the relative abundance of pro-aggregative motifs was ~14% and protease resistant motifs was ~20% of those found within the Rad9, “Rad9-S”, “Rad9-VS” and “Rad9-T” isoforms (Fig 4.33, pp.433-434).

The data also indicated a distinctive absence of anti-aggregative motifs in the case of the truncated NΔ73-Rad9-cΔ118-426 isoform (Fig 4.33, pp.433-434).

Fig 4.30: Site Map of SpRad9 Isoform Stability Modulation Motifs



Structural map of the *S. pombe rad9* gene indicating the relative positions of the introns, exon-encoded amino acid-spanning regions, potential alternative AUG codon translational start sites (full-length Rad9 = M1, “Rad9-S” = M50 and “Rad9-VS” = M74), the metacaspase cleavage site (which generates the “Rad9-T” = N Δ 117-Rad9 isoform and the truncated protein variants Rad9-c Δ 118-426, N Δ 49-Rad9-c Δ 118-426 and N Δ 73-Rad9-c Δ 118-426) and identified potential pro-aggregative, anti-aggregative and protease-resistance type functional motif sites:

XXXXXX = Potential KLVFF-, VLFKF- and FAEDVG- equivalent peptide aggregation suppressive motifs identified via comparative pair-wise sequence alignments performed with the on-line bioinformatics software tools EMBOSS and JEMBOSS.

XXXXXX = *H. sapiens* microtubule-associated Tau protein C terminus equivalent pro-aggregative and protease resistance motif.

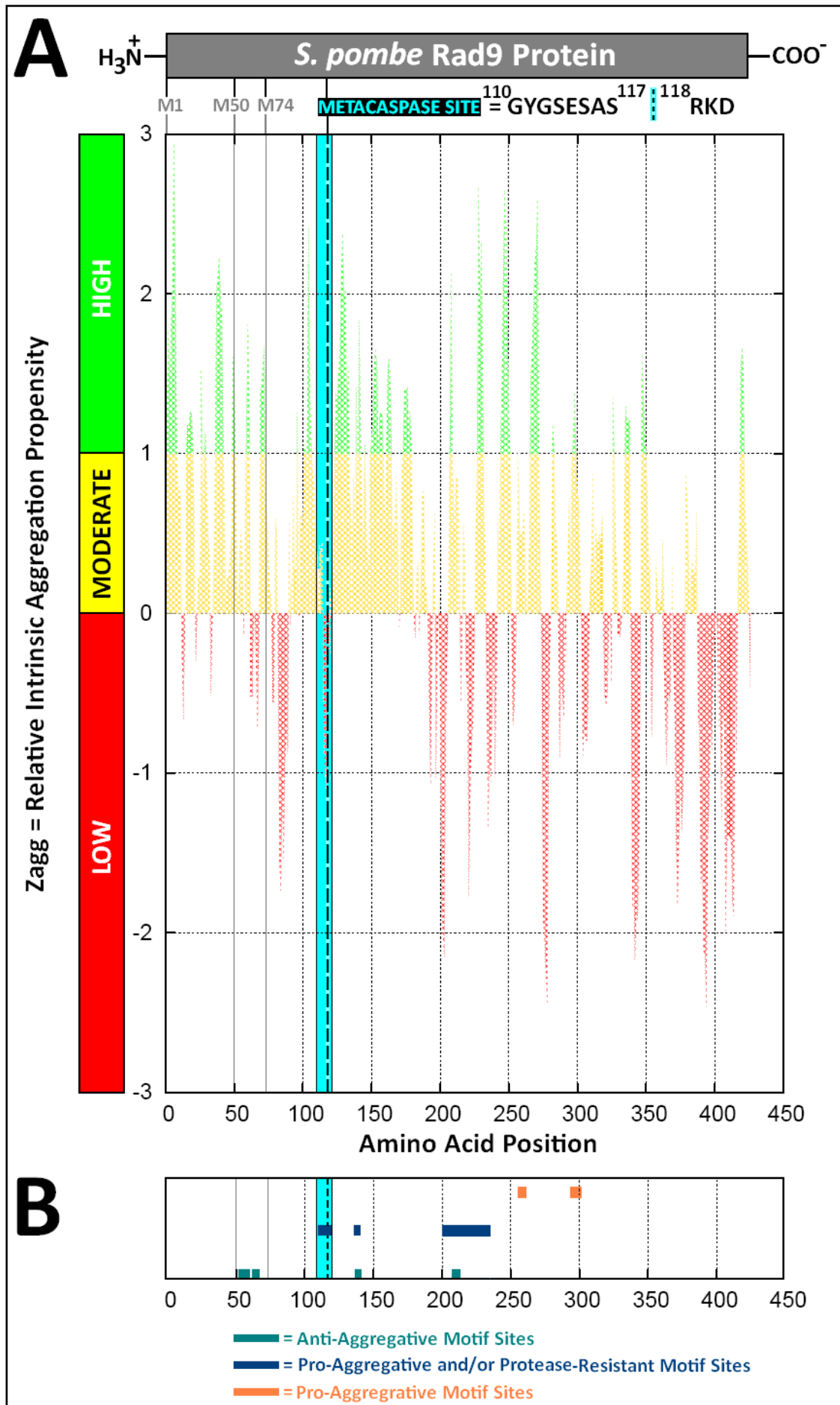
XXXXXX = Potential *H. sapiens* microtubule-associated Tau protein C terminus functional motif-equivalent protein aggregation/protease resistant motifs identified via comparative pair-wise sequence analyses performed with the on-line bioinformatics tools EMBOSS and JEMBOSS

XXXXXX = Potential protein aggregation-associated protease resistance functional motif identified via multiple sequence alignment analyses performed with the on-line bioinformatics software tools EMBOSS, JEMBOSS and PSI-BLAST

XXXXXX = Potential peptide aggregation inductive motifs identified via sequence analyses performed with the on-line bioinformatics software tools BETASCAN and TANGO.

* = High-probability phosphorylation sites (identified by the NetPhos on-line bioinformatics tool)

Fig 4.31: Zyggregator Analysis of the Postulated Rad9 Isoforms



A: ZYGGREGATOR software-generated mapping of identified regions of high, moderate and low probability aggregation propensity.

The relative positions of the potential alternative AUG methionine translational start codon sites of the *S. pombe* Rad9 isoforms (full-length Rad9 = M1, “Rad9-S” = M50 and “Rad9-VS” = M74) and the metacaspase cleavage site (which generates the “Rad9-T” = NΔ117-Rad9 isoform and the truncated protein variants Rad9-cΔ118-426, NΔ49-Rad9-cΔ118-426 and NΔ73-Rad9-cΔ118-426) are also indicated.

B: Residue-spanning regional map of the anti-, pro- and protease-resistant motif sites within the *S. pombe* Rad9 protein identified via multiple sequence alignment analyses (discussed previously in Section 3.4.2, pp.320-330) and utilisation of the aggregation sequence motif-predictive on-line software programs BETASCAN and TANGO.

[Details of these identified motif sequences are also provided in Table 3.1, p.327 and Fig 4.30, p.424]

4.10.3 In Silico Predictive Coil, Helix and Strand Secondary Structural Sub-Type Motif Content

In silico analysis of the full-length “wild-type” *S. pombe* Rad9 amino acid sequence with the on-line software program YASPIN indicated that *S. pombe* full-length Rad9 and all of its truncated variants contained significant regions of helix, strand and coil secondary structural motifs within their respective protein supramolecular architectures (Fig 4.32, p.429).

The acquired data indicated that the relative proportion of component secondary structural sub-motifs within the full-length Rad9 protein and its postulated truncated isoforms “Rad9-S” (NΔ49-Rad9) and “Rad9-VS” (NΔ73-Rad9), summarised graphically in Fig 4.33, pp.433-434, was in a hierachical order (most abundant → least abundant) – which may be defined as:

Coil > Non-Defined > Strand > Helix

In the case of the postulated NΔ117-Rad9-cΔ118-426 9 (“Rad9-T”) variant, the data indicated that the hypothetical amino acid sequence did not contain any structurally undefined regions and retained the hierachical order (most abundant → least abundant) of Coil > Strand > Helix, similar to that defined for the full-length Rad9 protein and truncated “Rad9-S” and “Rad9-VS” isoforms (Fig 4.33, pp.433-434).

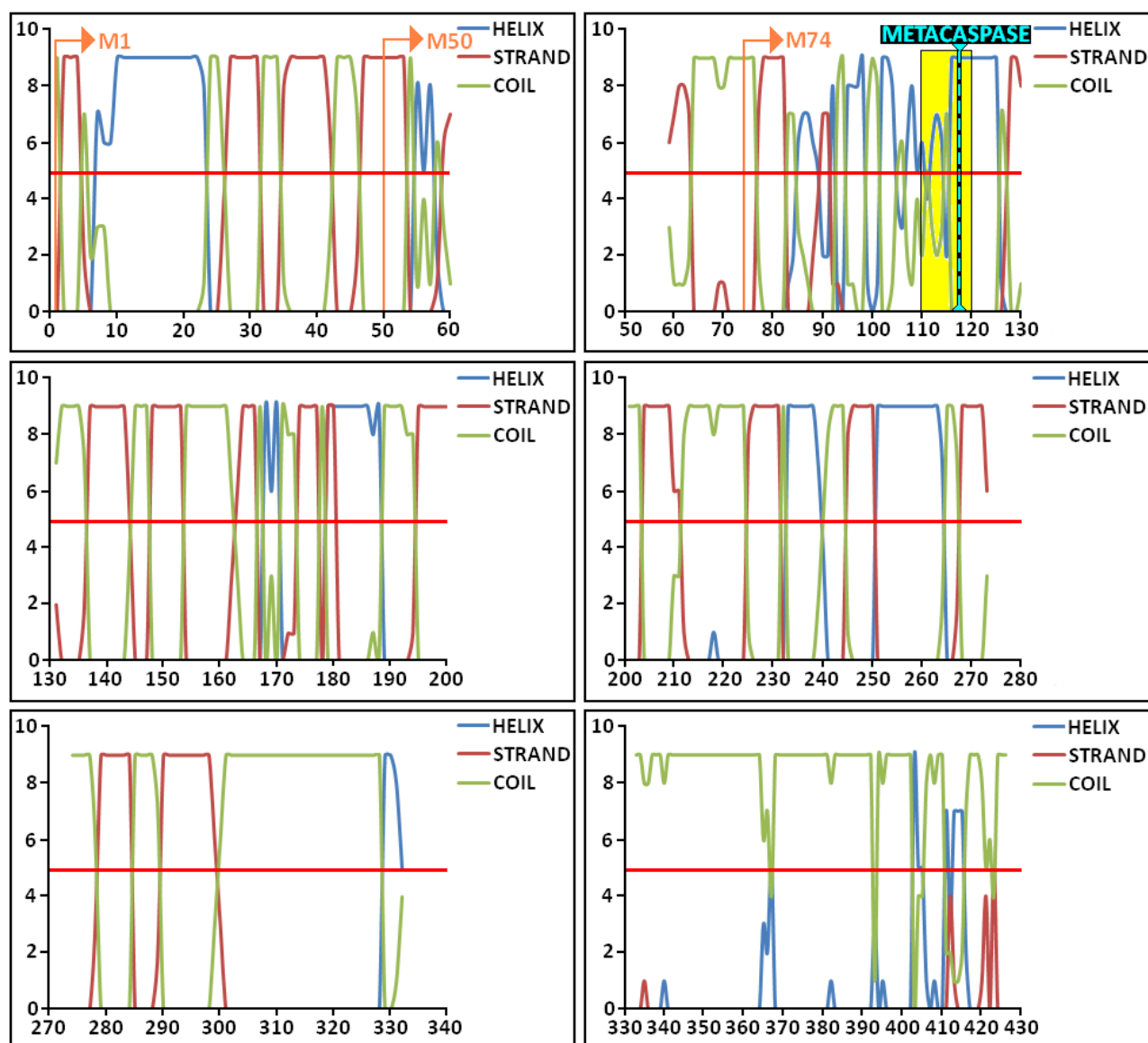
In contrast, these data also revealed that the relative proportion of component secondary structural sub-motifs within the hypothetical predicted amino acid sequences of the truncated isoforms Rad9-cΔ118-426, NΔ49-Rad9-cΔ118-426 and NΔ73-Rad9-cΔ118-426 summarised graphically in Fig 4.33, pp.433-434, was in a hierachical order (most abundant → least abundant) – which may be defined as: Helix > Coil > Strand.

The data also indicated that these truncated isoforms did not contain any non-defined structural regions.

These data also indicated that the full-length Rad9 protein and truncated isoforms “Rad9-S” (N Δ 49-Rad9), “Rad9-VS” (N Δ 73-Rad9) and “Rad9-T” (N Δ 73-Rad9) consisted of a predominant random coil secondary supramolecular structural sub-architecture (Fig 4.33, pp.433-434), which may be correlated with the conserved region high structural disorder propensity attributed to the retained highly mobile/flexible protein-interactive C-terminal tail domain that was identified via comparative metaPrDOS analytical plots of the hypothetical amino acid sequences of the respective proteins (Fig 4.28, p. 420).

In contrast, the data also revealed that the truncated isoforms Rad9-c Δ 118-426, N Δ 49-Rad9-c Δ 118-426 and N Δ 73-Rad9-c Δ 118-426 were comprised of a predominant helix secondary supramolecular structural sub-architecture (Fig 4.33, pp.433-434), which may be correlated with the conserved relative large region of very low structural disorder propensity that was identified in comparative metaPrDOS analytical plots of the hypothetical amino acid sequences of the respective proteins (Fig 4.29, p.421).

Fig 4.32: YASPIN Analysis of the Postulated Rad9 Isoforms



Analysis of the relative proportions and localised distribution of helix, strand and coil secondary structural motifs within the “wild-type” full-length *S. pombe* Rad9 amino acid sequence was performed with the on-line software tool YASPIN and the acquired data converted into a graphical format via utilisation of the Microsoft Excel software program.

The X-axis defines the amino acid residue position and the Y-axis defines the predicted helix, strand and coil propensity probability score on the data plots, whilst the orange right-angled arrows indicate the relative positions of the N-terminal methionine start residues of the *S. pombe* Rad9 protein isoforms (full-length Rad9 = M1, “Rad9-S” = M50 and “Rad9-VS” = M74) and the metacaspase cleavage site (which generates the “Rad9-T” = N Δ 117-Rad9 isoform and the truncated protein variants Rad9-c Δ 118-426, N Δ 49-Rad9-c Δ 118-426 and N Δ 73-Rad9-c Δ 118-426) is denoted via the black and light blue dotted line.

The horizontal red line on the data plots denotes the propensity prediction threshold, probability scores above 5 are significant and correlate with plotted values above the threshold line.

4.10.4 Correlated *In Silico* Data Analyses: A Comparative Review of the Critical Structure-Stability and Potential Functional Viability Relationships Identified Within the Full-length Rad9 Protein and Truncated *S. pombe* Rad9 Isoforms

Taking all of the *in silico* analytical data into consideration (Fig 4.33, pp.433-434), the most probable hierarchy of relative functional stability (most stable → least stable) of the full-length Rad9 protein and the postulated Rad9 truncated isoforms may be defined summarily as:

Rad9 ≈ "Rad9-S" > "Rad9-VS" ≈ "Rad9-T" > Rad9-cΔ118-426 ≈ NΔ49-Rad9-cΔ118-426 > NΔ73-Rad9-cΔ118-426

All these Rad9 isoforms contain conserved protease resistance motifs and definitive regions of conserved secondary structural supramolecular sub-architecture, which is indicative that they could possess functional activities that may be implicated in novel checkpoint signalling responses to specific genotoxic and/or environmental types of cytological stresses which adversely impinge on biochemical processes implicated in the maintenance and propagation of genomic integrity.

The postulated metacaspase cleavage site (¹¹¹**GYGSESASRKD**¹²⁰) contained within the full-length Rad9 protein and truncated "Rad9-S" and "Rad9-VS" variants is situated within a Sty1 kinase-like substrate motif, in which tyrosine 111 is a potential phosphorylation target of the Wis1 kinase and may thus be indicative that MAP kinase checkpoint signalling pathways are implicated in the modulation of limit proteolytic processing-mediated expression and/or functional activities of the truncated NΔ117-Rad9, Rad9-cΔ118-426, NΔ49-Rad9-cΔ118-426 and NΔ73-Rad9-cΔ118-426 isoforms.

This metacaspase target motif is also situated at the associative Rad9:Rad1 interfacial junction (Fig 4.26, p.416), which upon limited proteolytic cleavage may result in the dissociation of the heterotrimeric toroidal Rad9-Rad1-Hus1 DNA “sliding-clamp” complex and/or the potential alternative “Rad9-S”:Hus1:Rad1 and “Rad9-VS”:Hus1-Rad1 DNA “sliding-clamp” complexes (identified via predictive *in silico* comparative modelling analyses – discussed in detail in Chapter 5, Section 5.2, p.442, Fig 5.1, p.446)

In silico comparative multiple sequence alignment analyses also indicated that the *S. pombe* full-length Rad9 protein contains two distinctive sequences flanking the metacaspase cleavage motif which bear significant homologous resemblance to the two alternative C-termini of the full-length human Rad9B paralogue and its isoforms (Fig 4.26, p.416).

In this context, metacaspase-mediated limited proteolytic processing of the full-length *S. pombe* Rad9 protein and truncated “Rad9-S” and “Rad9-VS” variants would result in generation of the truncated “Rad9-T” variant (N Δ 117-Rad9) whose N-terminus would contain the **RKDVIVENQISISTGSECRII** sequence which is homologous to the C-terminal **VCCRKEFNNGSDAKYFCII** sequence of the human Rad9B full-length isoform 5 and truncated isoform 4 (in addition to the *S. pombe* C-terminal tail domain sequence), along with the simultaneous generation of the truncated Rad9-c Δ 118-426, N Δ 49-Rad9-c Δ 118-426 and N Δ 73-Rad9-c Δ 118-426 whose C-termini contain the **GYGSESAS** sequence which is homologous to the C-terminal **GSFSIF** sequence of the human Rad9B isoforms 1, 2 and 3 (Fig 4.26, p.416).

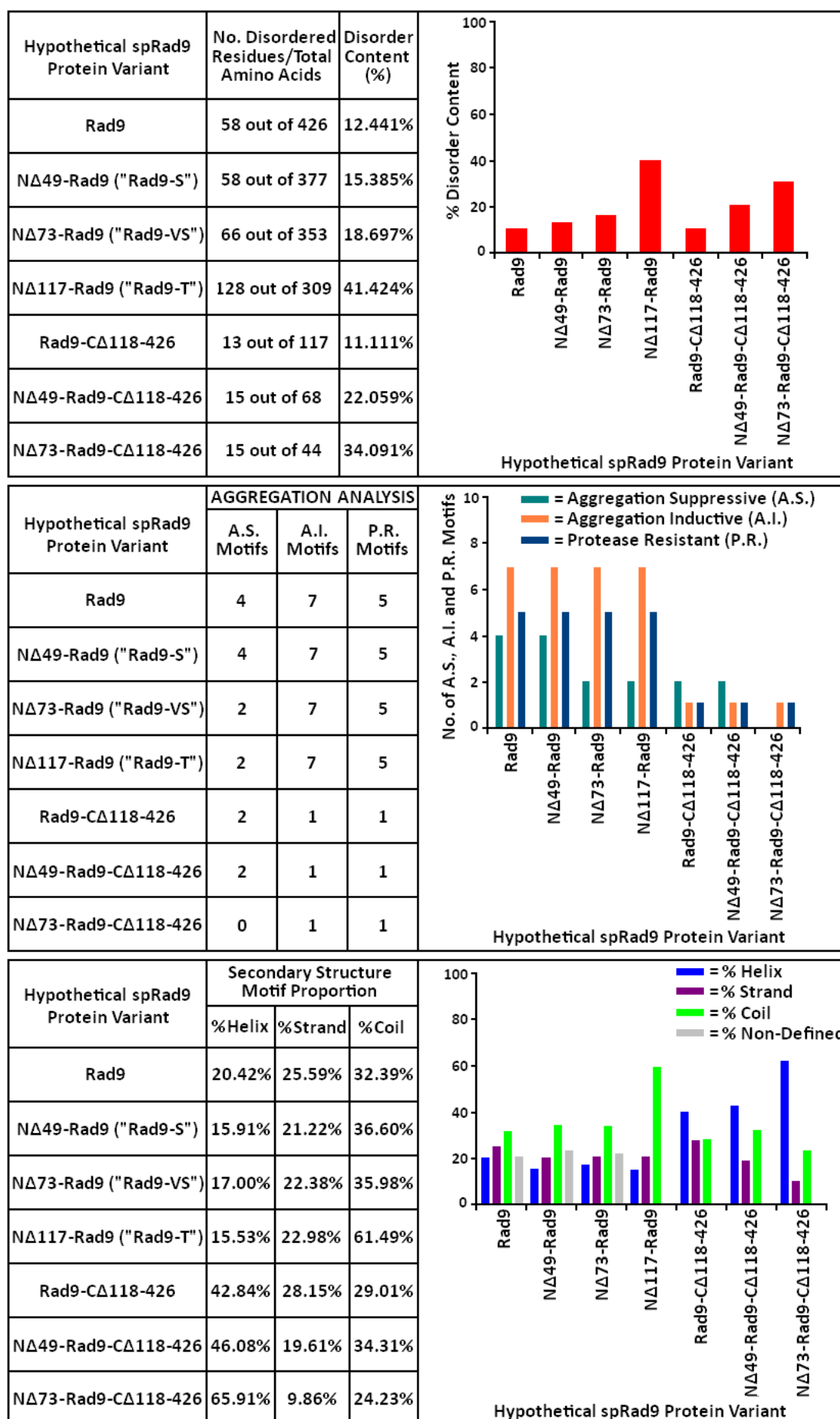
The presence of two potential protein-interactive sequences within the “Rad9-T” isoform (ie the Rad9B isoform 4 and 5 C-terminal homologous sequence situated within the “Rad9-T” N-terminus and the *S. pombe* C-terminal tail domain sequence) is also consistent and may correlate directly with the acquired comparative *in silico* DisCon data analyses which indicated that this protein variant possessed the highest degree of intrinsic structural disorder propensity (Fig 4.33, pp.433-434).

Whilst the presence of the C-terminal human RadB isoform 1, 2 and 3 homologous sequence within the truncated *S. pombe* isoforms Rad9-c Δ 118-426, N Δ 49-Rad9-c Δ 118-426 and N Δ 73-Rad9-c Δ 118-426 may correlate with the conserved minor region of high probability intrinsic structural disorder propensity at the C-terminal end of their respective hypothetical amino acid sequences observed on the *in silico* metaPrDOS analytical data plots (Fig 4.29, p.421).

Taking together, these *in silico* data analyses indicate that these distinctive isoforms of the full-length *S. pombe* Rad9 protein may have differential functions which could be implicated in the modulation of novel checkpoint responses to genotoxic and/or environmental cytological stresses which impair the propagation of genomic integrity and such functions may be equivalent to those of the human RadB paralogue and its isoforms which are largely unknown.

In this hypothetical context, these truncated structural isoforms could also be implicated in auto-regulatory mechanisms of specific cytological levels and/or functional activities of the full-length Rad9 protein and the identified Rad9 truncated isoforms within the *S. pombe* eukaryotic model organism which may be equivalent to those of the human Rad9B paralogue and its isoforms.

Fig 4.33: Stability Profiling of the Truncated SpRad9 Isoforms



Top Figure: Comparative analysis of the relative intrinsic structural disorder content within the full-length and truncated *S. pombe* Rad9 protein isoforms performed via analysis of their respective amino acid sequences with the on-line software tool DisCon (Mizianty M.L. *et al*, 2011).

Middle Figure: Comparative analysis of the relative potential pro-aggregative, anti-aggregative and protease resistant motif content within the full-length and truncated *S. pombe* Rad9 protein isoforms – discussed previously in Section 4.10.2, pp.422-426.

Bottom Figure: Comparative analysis of the relative percentage of potential secondary structural helix, strand and coil motif content within the full-length and truncated *S. pombe* Rad9 protein isoforms determined via utilisation of the on-line bioinformatics tool YASPIN (Lin K. *et al*, 2004) – discussed previously in Section 4.10.3, pp.427-429.

4.11 A Complex Signalling Network May Regulate the Levels of Expression and Functional Activities of the *S. pombe* Rad9 Isoforms in Selective Checkpoint Responses to Specific Types of Genotoxic and Environmental Cytological Stresses

The experimental observation that specific phosphoisoforms of the “Rad9-S” truncated protein variant may be implicated in the modulated expression of the “Rad9-VS” and “Rad9-T” isoforms (Section 4.8, pp.397-401), taken together with the restrictive temporal expression of “Rad9-S” in actively cycling cells in S-phase (Section 4.6, pp.392-393), may be indicative of co-ordinated functional roles of “Rad9-VS”, “Rad9-T” and possibly other proteolytic cleavage-derived Rad9 isoforms in the “feedback” regulation of “Rad9-S”-mediated DNA damage checkpoint signalling activities (Fig 4.34, p.439).

The mechanism of expression of the full-length Rad9, “Rad9-S” and “Rad9-VS” truncated protein variants may comprise alternative translation at the alternative AUG start-codon sites at the respective methionine 1 (M1), methionine 50 (M50) and methionine 74 (M74) situated within the mRNA of the transcribed *S. pombe rad9* gene, in which leaky ribosomal scanning is implicated (Janes S. *et al*, 2012, *Journal of Cell Science*, recently accepted manuscript publication “in press” – see Appendix 8.1) – Fig 4.34, p.439.

Hypothermic stress and nominal temperature ($\leq 30^{\circ}\text{C}$) conditions may induce supramolecular configurational changes within the secondary structure of a responsive *cis*-element contained within the encoded M1 – M50 segment of the transcribed *S. pombe rad9* mRNA (Section 4.5, pp.-) which sterically hinders leaky ribosomal scanning with consequential suppressed expression of the truncated “Rad9-S” variant and/or the truncated “Rad9-VS” protein variant.

In this hypothetical context, hyperthermic stress conditions (>30°C) would “melt” the secondary structure of the hypothermic stress responsive RNA *cis*-element (Section 4.5, pp.379-391), situated within the encoded M1 – M50 domain, enhancing the relaxation and topological flexibility of the transcribed *S. pombe rad9* mRNA and thereby increasing the frequency of leaky ribosome scanning with consequential induced expression of elevated levels of the truncated “Rad9-S” variant and/or the truncated “Rad9-VS” protein variant.

Associative *rad9* mRNA interactions with heat-shock proteins, RNA chaperones and/or RNA stabilisers may also be implicated in the regulated expression of the full-length Rad9, “Rad9-S” and “Rad9-VS” protein isoforms (Fig 4.34, p.439).

Different phosphoisoforms of the *S. pombe* full-length Rad9, “Rad9-S”, “Rad9-VS”, “Rad9-T” and/or other proteolytically-derived truncated *rad9* variants could also act as RNA stabilisers and/or RNA chaperones which modulate the supramolecular structure of the transcribed *rad9* mRNA to direct the ribosomal machinery to specific AUG translational start-codon sites in a “feedback” mechanism which serves to regulate the expressed levels and functional activities of specific Rad9 variants (Fig 4.34, p.439).

Expression of the “Rad9-T” truncated protein variant may involve a limited proteolytic cleavage mechanism in which metacaspase-mediated and/or COP9 signalosome-mediated limited proteolytic processing may be implicated (Fig 4.34, p.439).

Kinase-mediated phosphorylation of several key residues, identified in the conserved potential metacaspase site within the full-length Rad9, “Rad9-S” and “Rad9-VS” protein isoforms, may inhibit proteolytic-cleavage formation of the detected “Rad9-T” truncated protein variant and the undetected Rad9-C Δ 118-426, N Δ 49-Rad9-C Δ 118-426 and N Δ 473-Rad9-C Δ 118-426 truncated isoforms (Section 4.9, pp.402-417) – Fig 4.34, p.439.

Whilst phosphatase-mediated dephosphorylation of several key residues, identified in the conserved potential metacaspase site within the full-length Rad9, “Rad9-S” and “Rad9-VS” protein isoforms, may promote proteolytic-cleavage formation of the detected “Rad9-T” truncated protein variant and the undetected Rad9-C Δ 118-426, N Δ 49-Rad9-C Δ 118-426 and N Δ 473-Rad9-C Δ 118-426 truncated isoforms (Section 4.9, pp.402-417) – Fig 4.34, p.439.

The C-terminal tail domain, which enables the Rad9 protein to interact with and modulate the functional activities of a variety of proteins that are implicated in the mediation of DNA damage checkpoint signalling responses and DNA repair pathways (Broustas C.G. and Lieberman H.B., 2012), is conserved within the the full-length Rad9, “Rad9-S” ,“Rad9-VS” and “Rad9-T” protein isoforms, but is absent in the Rad9-C Δ 118-426, N Δ 49-Rad9-C Δ 118-426 and N Δ 473-Rad9-C Δ 118-426 truncated isoforms.

These Rad9-C Δ 118-426, N Δ 49-Rad9-C Δ 118-426 and N Δ 473-Rad9-C Δ 118-426 truncated isoforms may be implicated in the competitive suppressive regulation of the functional activities of the full-length Rad9, “Rad9-S” ,“Rad9-VS” and “Rad9-T” protein isoforms in various protein complexes, via formation of equivalent complexes which are lack the capability to initiate functional Rad9 protein C-terminal tail domain checkpoint signalling responses.

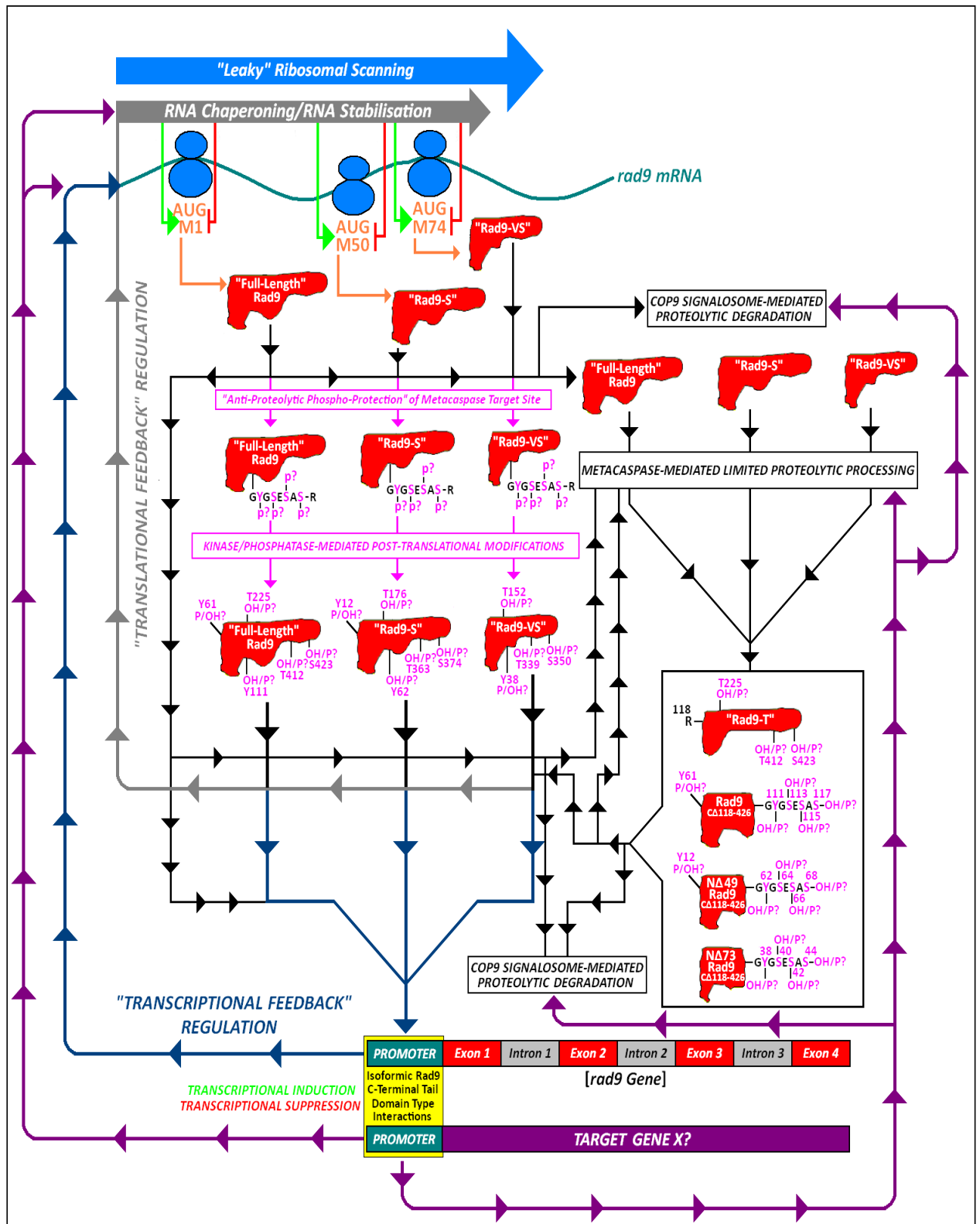
Specific checkpoint kinase-mediated post-translational phosphorylation modifications within the C-terminal tail domain of the human Rad9A protein enable it to interact with the promoter consensus DNA-binding sequence of the *WAF1* gene and induce expression of the p21 protein, independently of the Rad9A-Rad1-Hus1 heterotrimeric DNA sliding clamp complex, thereby modulating apoptotic signalling pathways (Yin Y. *et al*, 2004).

On the basis of this observed phenomenon, it is hypothetically conceivable that different phosphoisoforms of the *S. pombe* full-length Rad9 protein and truncated “Rad9-S”, “Rad9-VS” and “Rad9-T” variants could participate in C-terminal tail domain interactions with the promoter region of the *S. pombe rad9* gene, in which they act as active transcriptional inducers and/or suppressors in a “feedback” mechanism which also serve to regulate the expressed levels and functional activities of specific *S. pombe* Rad9 isoforms.

In addition, these potential *S. pombe* Rad9 phospho-isoforms could also function as transcriptional inducers and/or suppressors of other target genes, via associative C-terminal tail domain-gene promoter type interactions, which may encode checkpoint proteins (including kinases and phosphatases), gene transcriptional and translational modification proteins (including RNA chaperones, RNA stabilisers, and RNA helicases), COP9 signalosome components and/or metacaspases – which could also be implicated in the “feed-back” regulation of expressed levels and functional activities of specific *S. pombe* Rad9 isoforms (Fig 4.34, p.439).

It is also conceivable that a complex network of different regulatory cross-talk pathways between cell cycle checkpoints may exist, which are mediated via phosphatase and kinase interactions with the full-length Rad9 protein and the truncated “Rad9-S”, “Rad9-VS”, “Rad9-T” variants and possibly other Rad9 isoforms, for the co-ordinated selection and initiation of appropriate cytological responses to specific types of genotoxic and environmental stresses.

Fig 4.34: Rad9 Isoformic-Modulated “Feed-Back” Expression Model



A detailed explanation of this hypothetical model is provided in the text (pp.435-438).

Chapter 5

Functional Viability Assessment of the Engineered *S. pombe* Rad9 Proteins

5.1 Introduction

The human Rad9A protein is known to possess several independent functions that operate outside of the canonical Rad9-Rad1-Hus1 (“9-1-1”) complex and are implicated in the modulation of nucleotide biosynthesis and apoptotic signalling pathways (Broustas C.G. and Lieberman H.B., 2012).

Four truncated isoforms of the full-length human Rad9B paralogue have been identified (discussed previously in Chapter 1) whose respective functions are unknown.

Comparative *in silico* analyses and 2D PAGE-coupled Western blot assays also indicated that three novel truncated Rad9 isoforms were expressed within *S. pombe* cells, which may be equivalent functional homologues of the truncated human Rad9B isoforms (discussed previously in Chapter 4).

Several experimental approaches were therefore undertaken in order to determine whether or not the full-length *S. pombe* Rad9 protein and/or any of its truncated isoforms had any novel, “9-1-1” complex-independent functional capabilities, notably;

- (i) *In silico* assessment of the functional viability of the “cre-lox”-engineered full-length and truncated *S. pombe* Rad9 protein variants via comparative modelling and structural motif analyses of their respective amino acid sequences (Section 5.2, pp.442-454).
- (ii) Comparative *in vivo* assessment of the relative cytotoxic sensitivities of *S. pombe* strains, whose cells were “cre-lox”-engineered for the exclusive expression of specific full-length and truncated Rad9 protein variants (discussed previously in Chapter 3), to different types of induced genotoxic and environmental cytological stresses (Section 5.3, pp.455- 470).

5.2 Comparative *In Silico* Functional Viability Analyses of the Engineered Full-Length and Truncated *S. pombe* Rad9 Protein Variants

Whilst the expressed truncated “Rad9-S” protein (N Δ 49-Rad9) and “Rad9-VS” variants (N Δ 74-Rad9) would lack the first 49 N-terminal amino acids and 74 N-terminal amino acids respectively, *in silico* comparative modelling analyses indicated that they may still retain the capability to form alternative “Rad9-S-“Rad1-Hus1 and “Rad9-VS”-Rad1-Hus1 heterotrimeric DNA sliding-clamp complexes, as a consequence of conserved interfacial Hus1 and Rad1 associative domains within their respective structures (Fig 5.1, p.446).

In silico comparative modelling analyses combined with multiple sequence alignment analyses of the full-length *H.sapiens* Rad9B protein, the full-length *S. pombe* Rad9 protein and the potential exonuclease domain within the human Rad9A protein (identified by Bessho T. and Sancar A., 2000) indicated that the *S. pombe* full-length Rad9 protein and the truncated “Rad9-S” variant may also contain a functionally homologous exonuclease motif (Fig 5.1, p.446)

These *in silico* comparative modelling data also revealed that the truncated “Rad9-VS” variant would not contain the identified exonuclease domain and therefore may not be implicated in the functional mediation and/or regulation of DNA repair pathway activities, in contrast with the full-length Rad9 protein and the truncated “Rad9-S” variant (Fig 5.1, p.446)

Comparative *in silico* eukaryotic linear motif sequence analyses of the *S. pombe* full-length Rad9 protein and truncated “Rad9-S” and “Rad9-VS” protein variants, performed with the on-line bioinformatics software tool ELM, indicated that they all contained a variety of cytosol-, endoplasmic reticulum- golgi apparatus-, nucleus- and plasma membrane- associated types of functional protein motifs (Fig 5.2, p.447; Table 5.1, pp.448-450; Fig 5.3, p.451).

These *in silico* data analyses also revealed that the full-length *S. pombe* Rad9 protein and the truncated “Rad9-S” and “Rad9-VS” protein variants contained equivalent proportions of the identified endoplasmic reticulum- and golgi apparatus- associated types of functional protein motifs (Fig 5.3, p.451).

The truncated *S. pombe* “Rad9-S” and “Rad9-VS” protein variants also contained equivalent proportions of the identified cytosol-, nucleus- and plasma membrane- associated types of functional protein motifs, which were found in higher proportions within the full-length *S. pombe* Rad9 protein (Fig 5.3, p.451).

In silico analysis of the full-length *S. pombe* Rad9 sequence with the on-line NetPhos bioinformatics software tools revealed that the full-length Rad9 protein and truncated “Rad9-S” and “Rad9-VS” isoforms all contained distinctive serine, threonine and tyrosine residues which were assigned phosphorylation high-probability scores (Fig 5.4, p.452; Table 5.2, p.453; Table 5.3, p.453; Fig 5.5, p.454).

These *in silico* data analyses also indicated these proteins may undergo transient post-translational phosphorylation and dephosphorylation modifications, mediated by specific checkpoint kinase and phosphatases, which alter their functional activities (Fig 5.4, p.452; Table 5.2, p.453; Table 5.3, p.453; Fig 5.5, p.454).

Taken together, these *in silico* data indicated that the full-length *S. pombe* Rad9 protein and the truncated “Rad9-S” and “Rad9-VS” may elicit different types of functional checkpoint responses to genotoxic and/or environmental cytological stresses.

In silico comparative modelling indicated that the amino acid sequences of the truncated NΔ311-Rad9, NΔ312-Rad9 and NΔ357-Rad9 protein variants were progressively smaller fragments of the C-terminal tail domain (Fig 5.1, p.446).

Comparative *in silico* eukaryotic linear motif sequence analyses of the truncated NΔ311-Rad9, NΔ312-Rad9 and NΔ357-Rad9 proteins, performed with the on-line bioinformatics software tool ELM, indicated that they contained only very low equivalent proportions of cytosol-type associated functional protein motifs and relatively low proportions of nucleus-type associated functional protein motifs which were approximately 4 fold more abundant than the identified cytosol-type associated functional protein motifs (Fig 5.2, p.447; Table 5.1, pp.448-450; Fig 5.3, p.451).

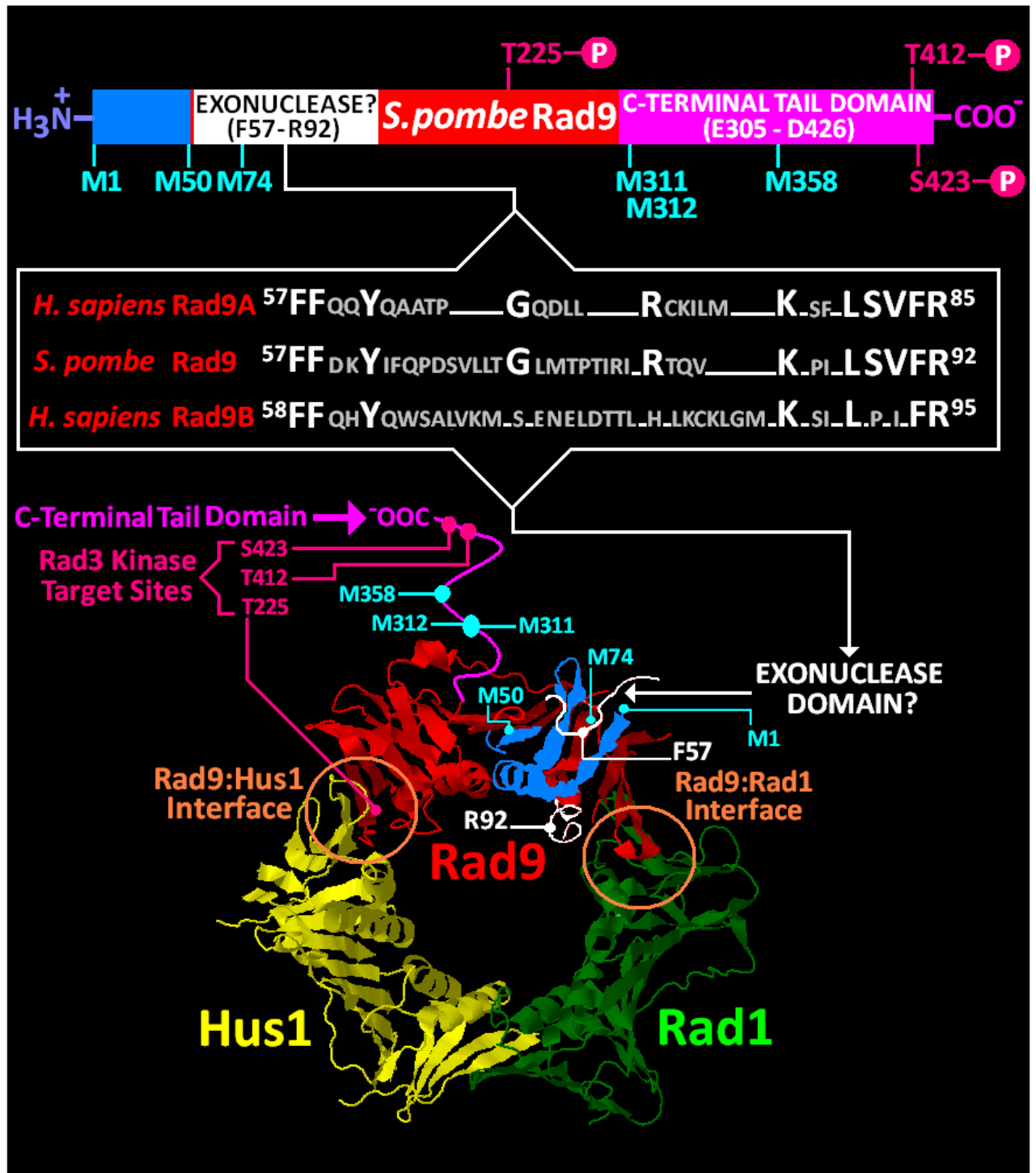
In silico analysis of the full-length *S. pombe* Rad9 sequence with the on-line NetPhos bioinformatics software tools revealed that these truncated NΔ311-Rad9, NΔ312-Rad9 and NΔ357-Rad9 proteins all contained significantly less numbers of distinctive serine and threonine residues which were assigned phosphorylation high-probability scores and a notable absence of phosphorylated tyrosine residues (Fig 5.4, p.452; Table 5.2, pp.453; Table 5.3, p.453; Fig 5.5, p.454).

The NΔ311-Rad9, NΔ312-Rad9 and NΔ357-Rad9 truncated protein variants may still retain some capacity to elicit checkpoint responses to environmental and genotoxic cytological stresses due to the adaptive structural nature of their respective C-terminal tail domain segments which may undergo transient kinase- and /or phosphatase- mediated post-translational phosphorylation and dephosphorylation modifications which enable them to engage with and modulate the functional activities of proteins implicated in the maintenance of genomic integrity.

However, the feasibility of this speculative hypothesis is highly improbable as a consequence of the experimental data acquired from comparative *in silico* assessment analyses of the relative stability of the N Δ 311-Rad9, N Δ 312-Rad9 and N Δ 357-Rad9 truncated protein variants that indicated a predominant intrinsic structural disorder propensity and a significant lack of protease resistant type motifs within their supramolecular architectures which would render them functionally non-viable and highly susceptible to ubiquitination- and/or sumoylation- post-translation modification-targeted proteasomal degradation (discussed previously in Chapter 3, Section 3.4, pp.314-357).

This may also account for the absence of detected expression of the N Δ 311-Rad9-c3xHA and N Δ 357-Rad9-C3xHA truncated isoforms in comparative Western blot analyses of TCA-precipitated total protein samples prepared from the cell cultures of the appropriate *S. pombe* strains which were cre-lox – engineered for the exclusively expression of these proteins (discussed previously in Chapter 3, Section 3.3, pp.308-313; Fig 3.15, p.313).

Fig 5.1: Comparative Modelling of Engineered Rad9 Isoforms

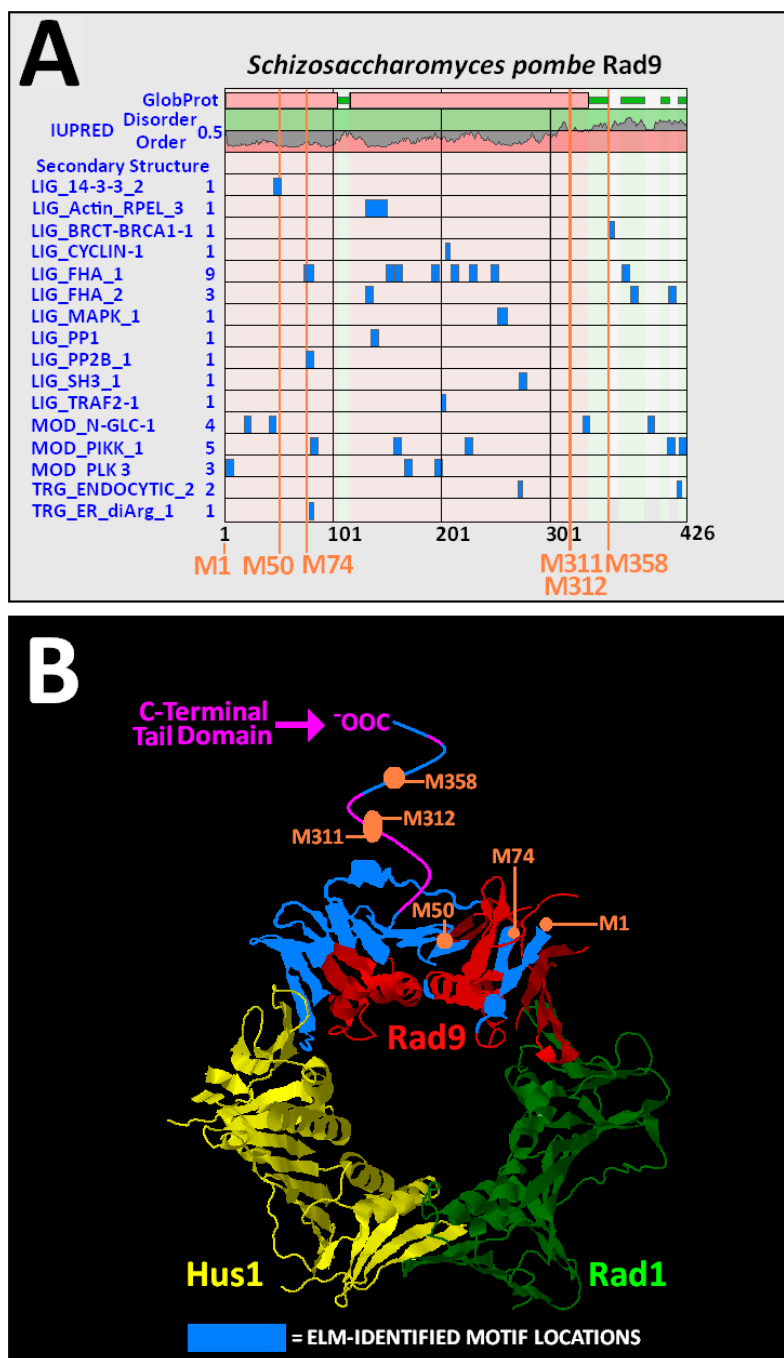


In silico comparative modelling of the engineered full-length and truncated *S. pombe* Rad9 protein variants within the X-ray crystallographic resolved structure of the human Rad9-Rad1-Hus complex (PDB file: 3G65) was accomplished via utilisation of the on-line bioinformatics software tool RasMol and the molecular graphics were generated via utilisation of the on-line PolyView3D software tool.

The relative positions of N-terminal methionine residues at the start of each respective protein sequence are indicated in light blue and the M1–M50 region is highlighted in blue.

The approximate location of the highly mobile C-terminal tail is indicated in purple and the potential exonuclease domain in *S. pombe* Rad9 is indicated in white, determined via comparative sequence alignment analyses of the human RadA exonuclease domain with the full-length human Rad9B paralogue (Isoform 5) and *S. pombe* Rad9 protein, performed with the on-line bioinformatics software tools EMBOSS, JEMBOSS and PSI-BLAST.

Fig 5.2: Eukaryotic Linear Motif (ELM) Analysis of *S. pombe* Rad9



A: *In silico* prediction of potential functional protein motifs within the full-length *S. pombe* Rad9 protein and truncated Rad9 isoforms via amino acid sequence analysis with the on-line bioinformatics software tool ELM (the secondary structure motifs are listed on the left of the data plot and their functional characteristics are summarised in Table 5.1, pp.448-450)

The top of the data plot indicates the regions of intrinsic structural order and disorder, identified by the integrated programs GlobProt and IUPRED.

The relative amino acid position (residue number) is provided at the bottom of the data blot and the N-terminal methionines that correspond to the translation start sites of the *S. pombe* full-length Rad9 protein and truncated variants are indicated in orange.

B: *In silico* comparative modelling of the ELM-identified functional motif sites and relative positions of the N-terminal methionines that correspond to the translation start sites of the *S. pombe* full-length Rad9 protein and truncated variants within the X-ray crystallographic structure of the human Rad9-Rad1-Hus1 heterotrimeric DNA sliding clamp complex (PDB file: 3G65) was performed via utilisation of the on-line bioinformatics tool RasMol and the structural graphic generated via utilisation of the on-line software tool PolyView3D.

Table 5.1(i): ELM-Identified Functional Sequences in *S. pombe* Rad9

Elm Name	Instances (Matched Sequence)	Elm Description	Cellular Location
LIG_14-3-3_2	⁴⁵ RSGFSM ⁵¹	Longer mode 2 interacting phospho-motif for 14-3-3 proteins Key conservation RxxxS#p	Nucleus Cytosol Mitochondrion Intracellular Side of Plasma Membrane
LIG_Actin_RPEL_3	¹³⁰ ISTGSECRIIFKLCKHGV ¹⁴⁹	RPEL motif, binds to the hydrophobic cleft created by subdomains 1 and 3 of G-actin	Cytosol
LIG_BRCT_BRCA1_1	³⁵⁵ SSRMF ³⁵⁹	Phosphopeptide motif which interacts with the BRCT domain of BRCA1 with low affinity [Potential interaction with <i>S. pombe</i> Crb2?]	Nucleus BRCA1-BARD1 Complex
LIG_CYCLIN_1	²⁰⁴ RVLL ²⁰⁷	Substrate recognition site that interacts with cyclin for enhanced phosphorylation by cyclin/Cdk complexes	Nucleus Cytosol
LIG_FHA_1	⁷³ TMTPTIR ⁷⁹ ⁷⁵ TPTIRIR ⁸¹ ¹⁴⁹ IKTYKIS ¹⁵⁵ ¹⁵⁷ EQTQTLH ¹⁶³ ¹⁹¹ QRTEELT ¹⁹⁷ ²⁰⁹ SFTEEVV ²¹⁵ ²²⁶ QTTVSID ²³² ²⁴⁶ SVTSLR ²⁵² ³⁶⁷ DETNGIK ³⁷³	Phosphothreonine motif binding a subset of FHA domains that have a preferential specificity for a large aliphatic amino acid residue at the pT+3 position	Nucleus
LIG_FHA_2	¹³⁰ ISTGSEC ¹³⁶ ³⁷⁵ PSTTND ³⁸¹ ⁴¹⁰ GPTQAEA ⁴¹⁶	Phosphothreonine motif binding a subset of FHA domains that have a preferential specificity for an acidic amino acid residue at the pT+3 position	Nucleus Replication Fork

Table 5.1(ii): ELM-Identified Functional Sequences in *S. pombe* Rad9**(continued)**

Elm Name	Instances (Matched Sequence)	Elm Description	Cellular Location
LIG_MAPK_1	252 _{REFRAAVIL} 260	MAPK-interacting motif: (R/K)xxxx#x# where # = hydrophobic residue	Nucleus Cytosol
LIG_PP1	135 _{ECRIIFK} 141	Protein phosphatase 1 catalytic subunit (PP1c)-interacting motif: [RK]{0,1}[VI][^P][FW] where [^P] = Phosphorylated Residue {0,1} = No Residue or One Residue	Phosphatase Type 1 Complex Cytosol
LIG_PP2B_1	75 _{TPTIRIR} 81	Calcineurin substrate docking site leads to phosphatase-mediated dephosphorylation of phosphorylated Ser and Thr sites	Nucleus Cytosol Extrinsic to Endoplasmic Reticulum Membrane Extrinsic to Internal Side of Plasma Membrane Intrinsic to Internal Side of Plasma Membrane Calcineurin Complex
LIG_SH3_1	272 _{YVGP GKP} 278	Class I SH3 type domain-binding motif	Plasma Membrane Focal Adhesion
LIG_TRAF2_1	200 _{PLQE} 203	Major TRAF2-binding consensus motif	Cytosol

Table 5.1(iii): ELM-Identified Functional Sequences in *S. pombe***Rad9 (continued)**

Elm Name	Instances (Matched Sequence)	Elm Description	Cellular Location
MOD_N_GLC_1	18 _{TNLSRI} ²³ 41 _{LNSSRS} ⁴⁶ 331 _{RNNSLT} ³³⁶ 391 _{PNESEL} ³⁹⁶	Generic motif for N-glycosylation	Extracellular Golgi Apparatus Endoplasmic Reticulum
MOD_PIKK_1	79 _{RIRTQVK} ⁸⁵ 156 _{YEQTQL} ¹⁶² 222 _{KQPTQT} ²²⁸ 409 _{FGPTQAE} ⁴¹⁵ 420 _{GIFSQED} ⁴²⁶	PIKK phosphorylation (S/T)Q target motif [<i>S. pombe</i> Rad3 and/or Tel1 kinase targets]	Nucleus
MOD_PLK	1 _{MEFTVSN} ⁷ 166 _{FDKSLSH} ¹⁷² 194 _{EELTIQP} ²⁰⁰	Polo-like kinase target sites	Nucleus Cytosol
TRG_ENDOCYTIC_2	271 _{YYGV} ²⁷⁴ 418 _{YHGI} ⁴²¹	Tyrosine-based sorting signal motif involved in mu subunit interactions with the adaptor protein complex	Cytosol Plasma membrane Clathrin coated endocytic vesicle
TRG_ER_diARG_1	78 _{IRIR} ⁸¹	Di-Arg endoplasmic reticulum retention #(R/R)# or #(RXR)# motifs where X = single residue insertion # = hydrophobic residue	Rough Endoplasmic Reticulum Endoplasmic Reticulum Endoplasmic Reticulum Membrane ER-Golgi Transport Vesicle Membrane Golgi-ER Transport Vesicle Membrane Integral Protein Cisterna Cytosol

Fig 5.3: Comparative Analyses of the Relative Abundance of Localised Functional Protein Motif Types Within the Full-Length and Truncated *S. pombe* Rad9 Protein Variants

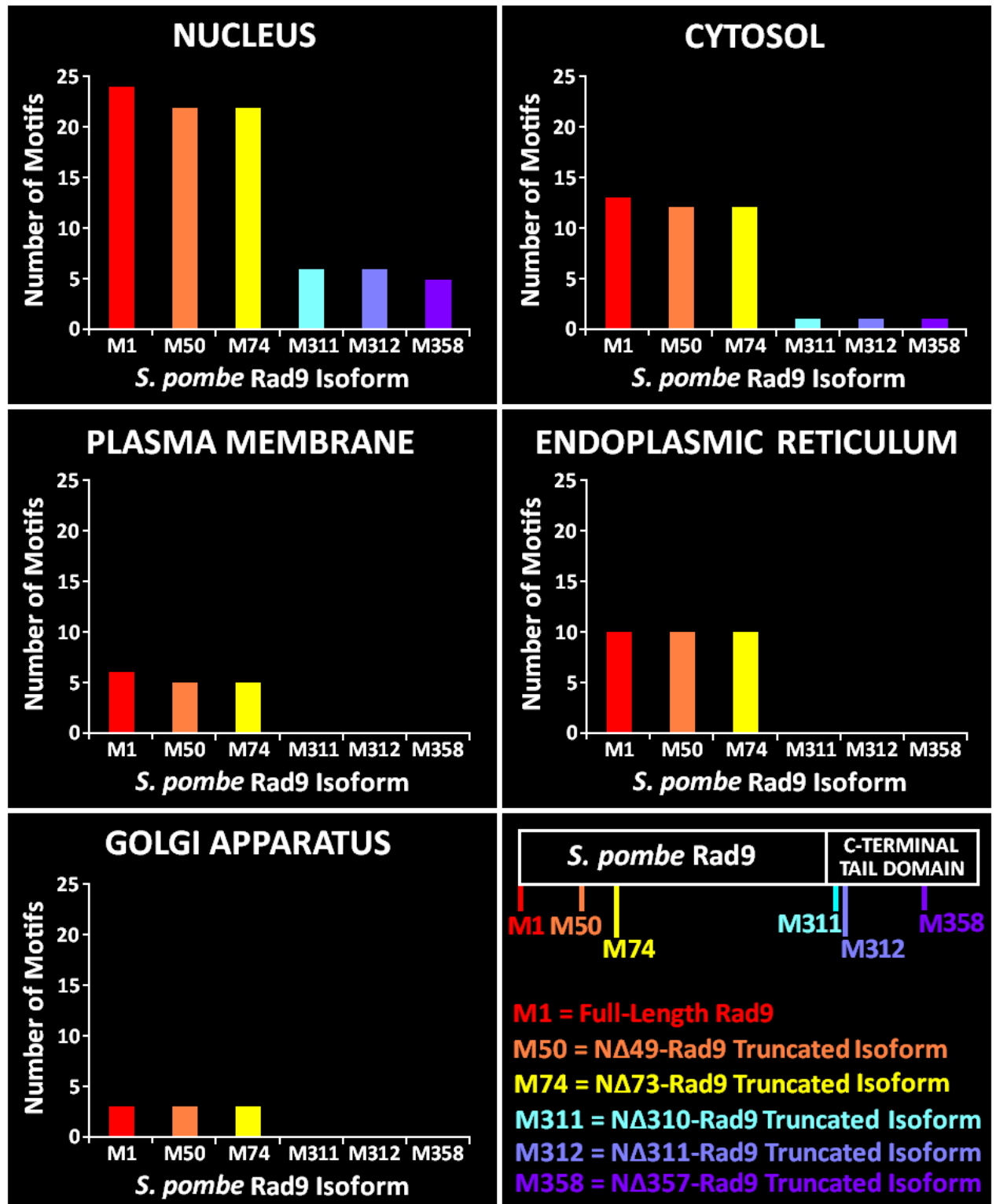
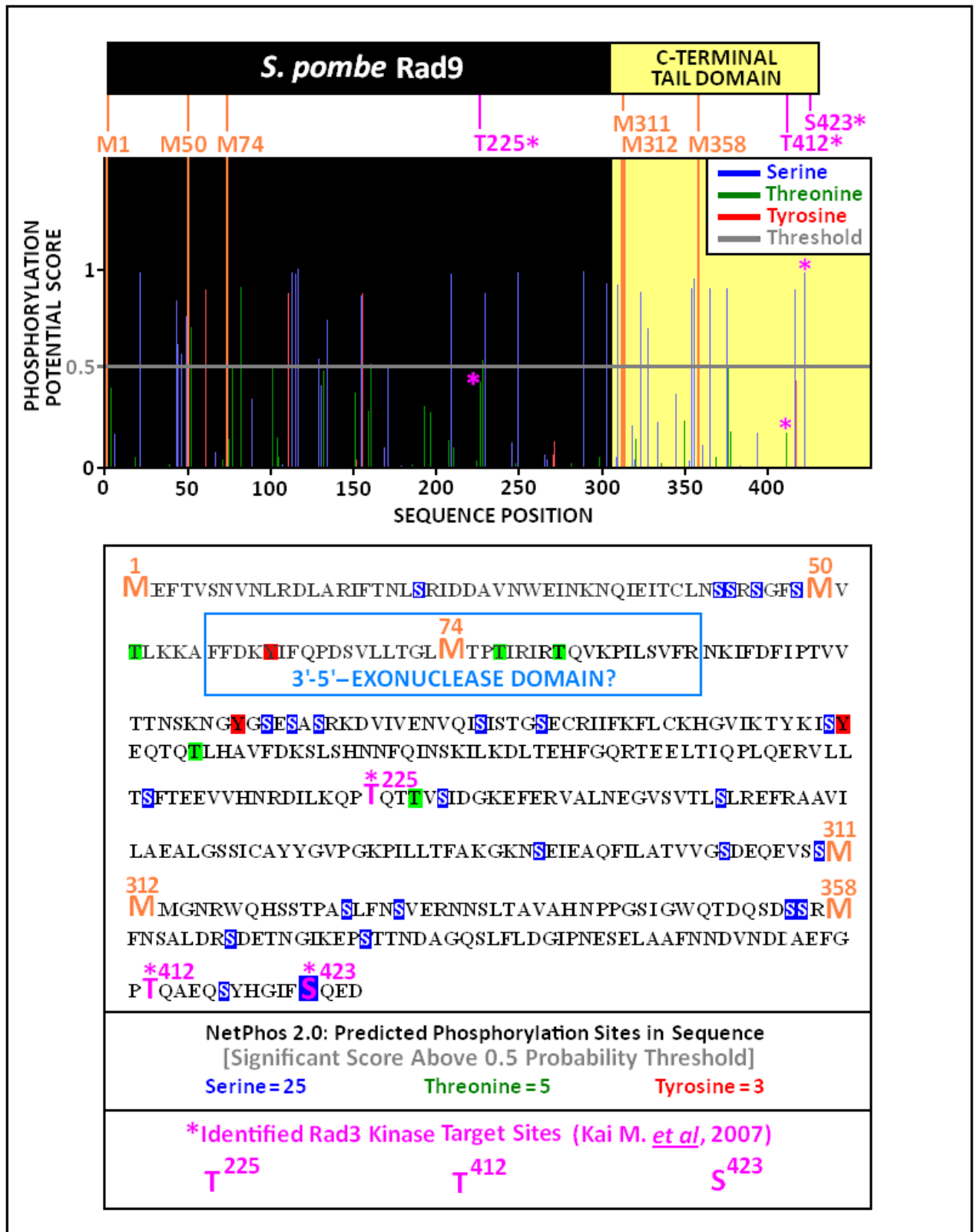


Fig 5.4: Phosphorylation Site Analysis of the *S. pombe* Rad9 Protein



The relative positions of the N-terminal methionines which correspond to the translational start sites of the amino acid sequences of the engineered *S. pombe* full length Rad9 and truncated Rad9 isoforms are indicated (X-axis on the NetPhos data plot).

Phosphorylation site probability scores (Y-axis on the NetPhos data plot) above the threshold value of 0.5 (represented by grey line on the NetPhos data plot) are significant.

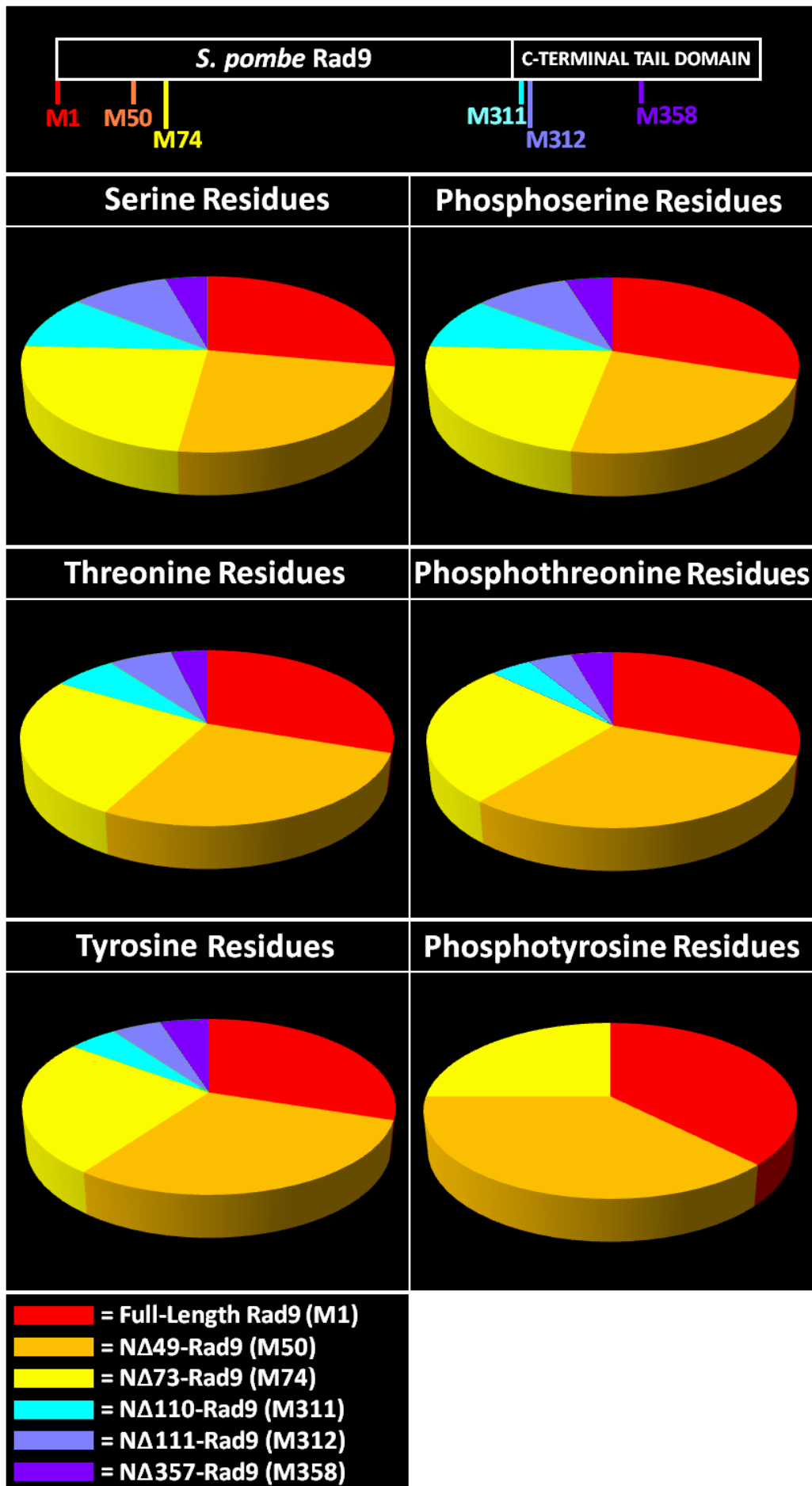
Table 5.2: Potential Number of Kinase Target Sites in Rad9 Variants

Rad9 Isoform	Number of Ser, Thr, Tyr Residues	Number of Ser Residues	Number of Thr Residues	Number of Tyr Residues
Full-Length Rad9 (M1)	84	45	33	6
NΔ49-Rad9 (M50)	75	39	30	6
NΔ73-Rad9 (M74)	72	39	28	5
NΔ310-Rad9 (M311)	24	16	7	1
NΔ311-Rad9 (M312)	24	16	7	1
NΔ357-Rad9 (M358)	12	7	4	1

Table 5.3: Predicted Number of Kinase Target Sites in Rad9 Variants

Rad9 Isoform	Number of Ser, Thr, Tyr Residues	Number of Ser Residues	Number of Thr Residues	Number of Tyr Residues
Full-Length Rad9 (M1)	35	25	7	3
NΔ49-Rad9 (M50)	30	20	7	3
NΔ73-Rad9 (M74)	28	20	6	2
NΔ310-Rad9 (M311)	9	8	1	0
NΔ311-Rad9 (M312)	9	8	1	0
NΔ357-Rad9 (M358)	5	4	1	0

Fig 5.5: Relative Numbers of Potential Kinase Sites in Rad9 Variants



5.3 Exclusive Expression of the Engineered Truncated Rad9 Variants Enhances Cellular Sensitivity to Various Types of Induced Genotoxic and Environmental Stresses

Comparative *in silico* data analyses of the full-length and truncated *S. pombe* Rad9 isoforms provided some hypothetical insights into their functional viabilities (Section 5.2, pp.442-454).

The “cre-lox” – engineered full-length *S. pombe* Rad9 protein variants were predicted to function in a similar manner to that of that of the wild-type *S. pombe* Rad9 protein and would elicit appropriate checkpoint point responses to genotoxic and environmental cytological stresses via Rad3 kinase-mediated activation of “9-1-1” complex DNA sliding-clamp type signalling events (Fig 5.6A and Fig 5.6B, p.460) and perhaps elicit other independent functional responses to these stresses (Fig 5.6B, p.460).

The “cre-lox” – engineered N Δ 49-Rad9-c3xHA (“Rad9-S”) and N Δ 73-Rad9-c3xHA (“Rad9-VS”) truncated protein variants were predicted to form “closed-ring” or “open-ring” alternative heterotrimeric “9-1-1” DNA sliding-clamp complexes, or form heterodimeric DNA sliding-clamp complexes with Hus1, which may participate in Rad3 kinase-activated checkpoint responses to genotoxic and environmental cytological stresses (Fig 5.6A, Fig 5.6C and Fig 5.6D, p.460).

Since the smaller ring configurations of these alternative complexes may cause them to become sterically stalled at bulky DNA lesion sites, it was predicted therefore these proteins may also elicit independent functional responses to these stresses (Fig 5.6C and Fig 5.6D, p.460).

The “cre-lox”-engineered NΔ311-Rad9-c3xHA and NΔ358-Rad9-c3xHA truncated protein variants were predicted to be either functionally non-viable and unable to elicit checkpoint responses to genotoxic and environmental cytological stresses or may retain some partial C-terminal domain functions which enable them to engage with some proteins and elicit sub-optimal checkpoint signalling responses (Fig 5.6E, p.460)

In order to ascertain the validity of these functional predictions, comparative acute survival assays were performed with YEA cultures of the cre-lox–engineered *S. pombe* strains *rad9*, *rad9-c3xHA*, *rad9-(Δintron 1)-c3xHA*, *rad9-(M50L)-c3xHA*, *NΔ49-rad9-c3xHA*, *NΔ73-rad9-c3xHA*, *NΔ311-rad9-c3xHA* and *NΔ311-rad9-c3xHA* exposed to a variety of induced different types of genotoxic and environmental cytological stresses (pp.461-470)

A “wild-type” *S. pombe* strain and the *rad9*-deleted “cre-lox” base-strain ($\Delta rad9$) were also utilised as comparative positive and negative controls for these acute survival assays (pp.461-470).

These induced stresses were cold shock (16°C), heat shock (37°C), osmotic stress (1M sorbitol), oxidative stress (hydrogen peroxide, menadione, sodium nitroprusside and tert-butylhydroperoxide), PI3-kinase inhibition (caffeine), ribonucleotide biosynthesis inhibition (hydroxyurea), mitotic inhibition (thiabendazole), DNA cleavage/cross-linking/adduct-forming agent exposure (methylmethane sulphonate, mitomycin C, 4-methyl-N'-nitro-N-nitrosoguanidine, 4-nitroquinoline-1-oxide, phleomycin, U.V. irradiation) and topoisomerase inhibition (camptothecin, ellipticine, etoposide) – Figs 5.7-5.12, pp.461-468.

Acute exposure to ethanol (1% v/v), DMSO (1% v/v) and ethanol:DMSO (1% v/v) had no adverse effect on the growth and cell survival of all the *S. pombe* strains tested and served as experimental controls for confirmation that their presence in the YEA broth cultures elicited no cytotoxic effects in addition to the test agents utilised in the acute survival assays (Fig 5.7, p.461).

The control acute survival assays were necessary as these solvents were utilised to prepare some of the test compound stock solutions.

S. pombe strains whose cells were “cre-lox”–engineered for expression of full-length Rad9 protein variants (ie *rad9*, *rad9-c3xHA*, *rad9- Δ intron1-c3xHA*, *rad9-(M50A)-c3xHA* and *rad9-(M50L)-c3xHA*) were resistant to all the genotoxic and environmental stress conditions tested (Figs 5.7-5.12, pp.461-468).

Acute exposure to cold-shock (16°C), heat-shock (37°C), osmotic shock (1M sorbitol), PI3 kinase inhibition (10mM caffeine) and mitotic inhibition (40µM thiabendazole) also had no adverse effect on the growth and cell survival of any of the *S. pombe* strains tested (Fig 5.8, p.462 and Fig 5.12, p.468).

Acute exposure to hydrogen peroxide, menadione, sodium nitroprusside and tert-butylhydroperoxide, hydroxyurea, methylmethane sulphonate, mitomycin C, 4-methyl-N'-nitro-N-nitrosoguanidine, 4-nitroquinoline-1-oxide, phleomycin, U.V. irradiation, camptothecin, ellipticine, and etoposide adversely affected the growth and cell survival of *S. pombe* strains whose cells were cre-lox engineered for the exclusive expression of truncated Rad9 protein variants (ie *N149-rad9-c3xHA*, *N173-rad9-c3xHA*, *N1311-rad9-c3xHA* and *N1357-rad9-c3xHA*) – Fig 5.9, p.463; Fig 5.10(i), p.464; Fig 5.10(ii), p.465, Fig 5.11(ii), p.467; Fig 5.12, p.468.

The acquired experimental data indicated a general trend of increasing sensitivity to these genotoxic agents correlated with decreasing length of the truncated Rad9 protein variant exclusively expressed within the cells of the “cre-lox” – engineered *S. pombe* strain (Fig 5.13, pp.469-470) – which may be defined in the order of decreasing cell survival as;

NΔ49-rad9-c3xHA > *NΔ73-rad9-c3xHA* > *NΔ311-rad9-c3xHA* > *NΔ357-rad9-c3xHA* > $\Delta rad9$

The *NΔ311-rad9-c3xHA* and *NΔ357-rad9-c3xHA* *S. pombe* strains were also less sensitive to the genotoxic effects of the test compounds camptothecin, hydrogen peroxide, hydroxyurea and 4-nitroquinoline-1-oxide than the *rad9*-deleted base strain ($\Delta rad9$), but equally sensitive to the genotoxic effects of menadione, tert-butylhydroperoxide, ellipticine, etoposide, 4-methyl-N'-nitro-N-nitrosoguanidine, 4-nitroquinoline-1-oxide, methylmethane sulphonate, mitomycin C, phleomycin and U.V. irradiation (Fig 5.13, pp.469-470).

These experimental observations may be indicative of retention of some potential “9-1-1” complex-independent Rad9 C-terminal tail domain functional activities within the *NΔ311-rad9-c3xHA* and *NΔ357-rad9-c3xHA* *S. pombe* strains, which may elicit partial checkpoint responses to specific types of genotoxic stress induced by camptothecin, hydrogen peroxide, hydroxyurea and 4-nitroquinoline-1-oxide.

Initial acute survival assays performed with the test compounds ellipticine and etoposide failed to kill the *S. pombe* $\Delta rad9$ base-strain (negative control) as a consequence of the fact that they were unable to penetrate the cells (Fig 5.11(i), p.466).

Lyticase pre-treatment of the *S. pombe* strains, prior to performing acute cell survival assays with ellipticine and etoposide, enabled these genotoxic compounds to penetrate the cells as a consequence of their weakened cell walls and resulted in rapid killing of the *S. pombe* $\Delta rad9$ base-strain culture (negative control) – Fig 5.11(ii), p.467.

The *NΔ49-rad9-c3xHA*, *NΔ73-rad9-c3xHA*, *NΔ311-rad9-c3xHA*, *NΔ357-rad9-c3xHA* and Δ *rad9* *S. pombe* strains also exhibited an equivalent level of sensitivity to the genotoxic effects of acute exposure to ellipticine and etoposide (Fig 5.11(ii), p.467; Fig 5.13, pp.469-470).

The *NΔ49-rad9-c3xHA*, and *NΔ73-rad9-c3xHA* *S. pombe* strains were also equally sensitive, but more resilient to the genotoxic effects of acute exposure to U.V. irradiation than the *S. pombe* strains *NΔ311-rad9-c3xHA*, *NΔ357-rad9-c3xHA* and Δ *rad9* (Fig 5.13, pp.469-470).

S. pombe cells which were “cre-lox”-engineered for the exclusive expression of the truncated protein variant “Rad9-S” (*NΔ49-rad9-c3xHA*) also exhibited a distinctive partial resistance (~30% cell survival) and were significantly less sensitive to the genotoxic effects of acute exposure to camptothecin compared with the cells of the other *S. pombe* strains which were “cre-lox”-engineered for the exclusive expression of the *NΔ73-rad9-c3xHA*, *NΔ311-rad9-c3xHA* and *NΔ357-rad9-c3xHA* truncated Rad9 protein variants (Fig 5.13, pp.469-470).

These experimental data observations indicate that the truncated “Rad9-S” protein variant may be functionally-implicated in novel checkpoint signalling pathway responses (discussed in Chapter 6) and/or DNA repair pathways which are specific to camptothecin-induced DNA damage (discussed in Chapter 7).

Fig 5.6: Predictive Genotoxic Responsive Models for Rad9 Isoforms

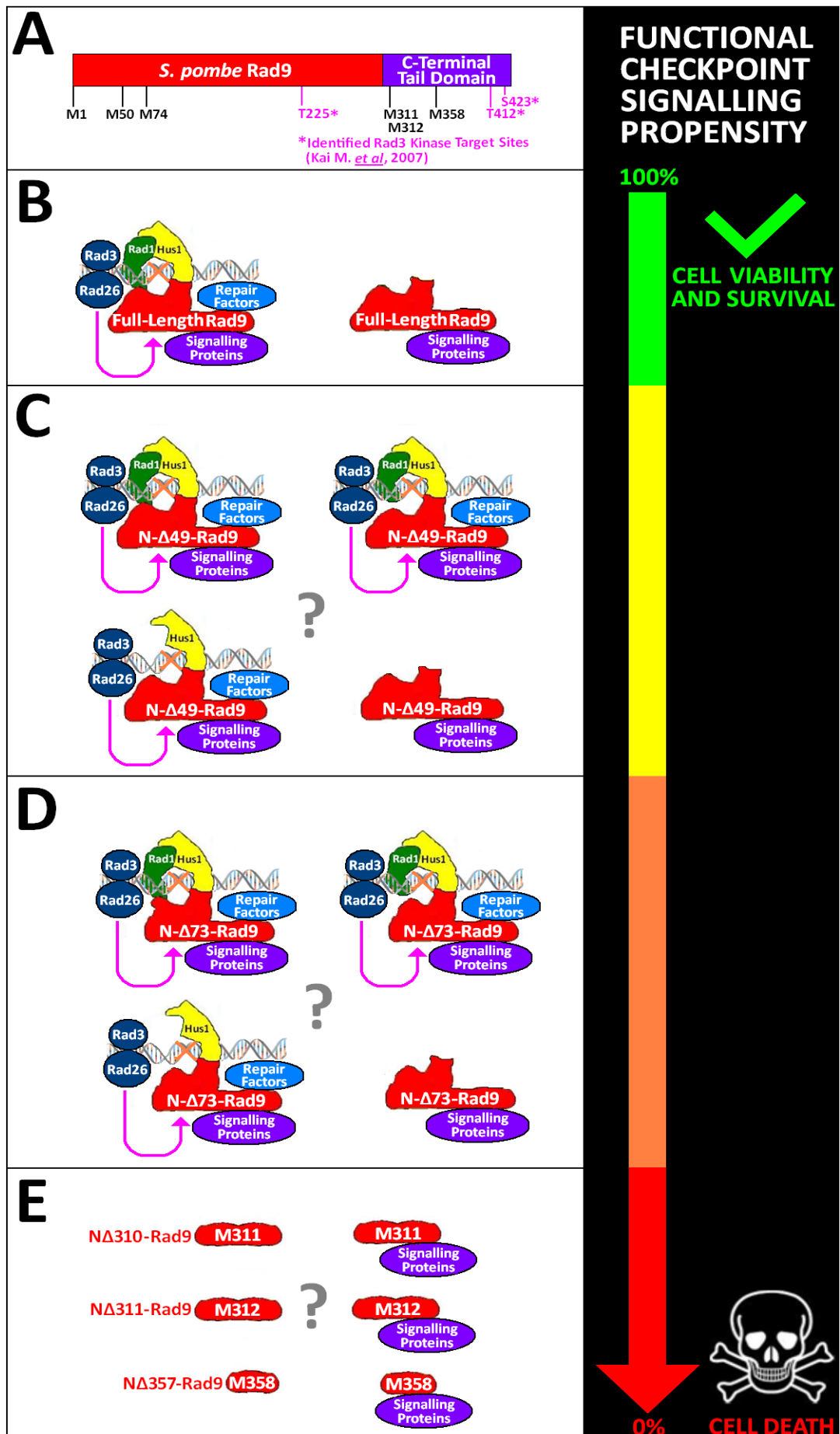
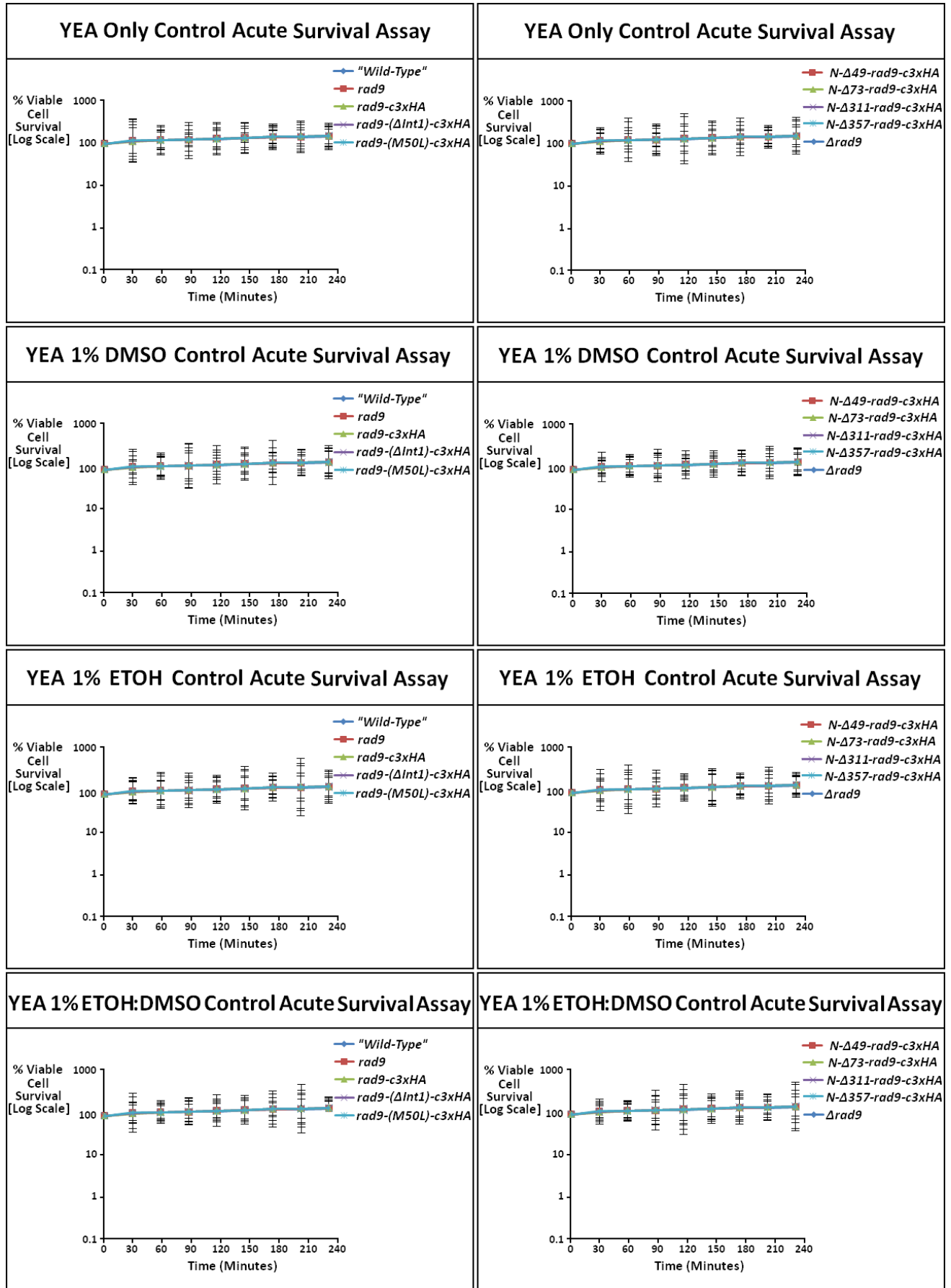
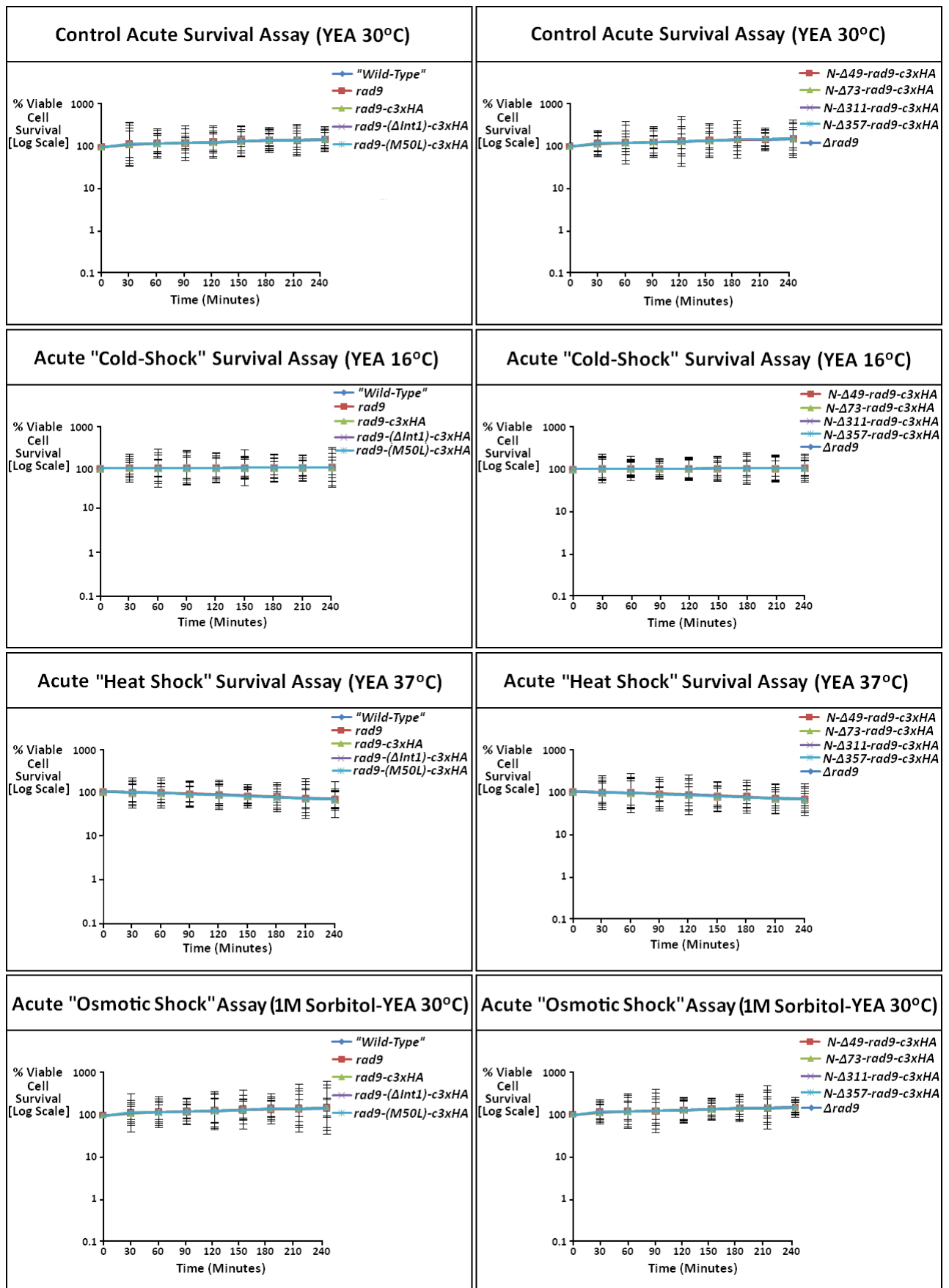


Fig 5.7: Comparative “Solvent Control” Acute Survival Assays



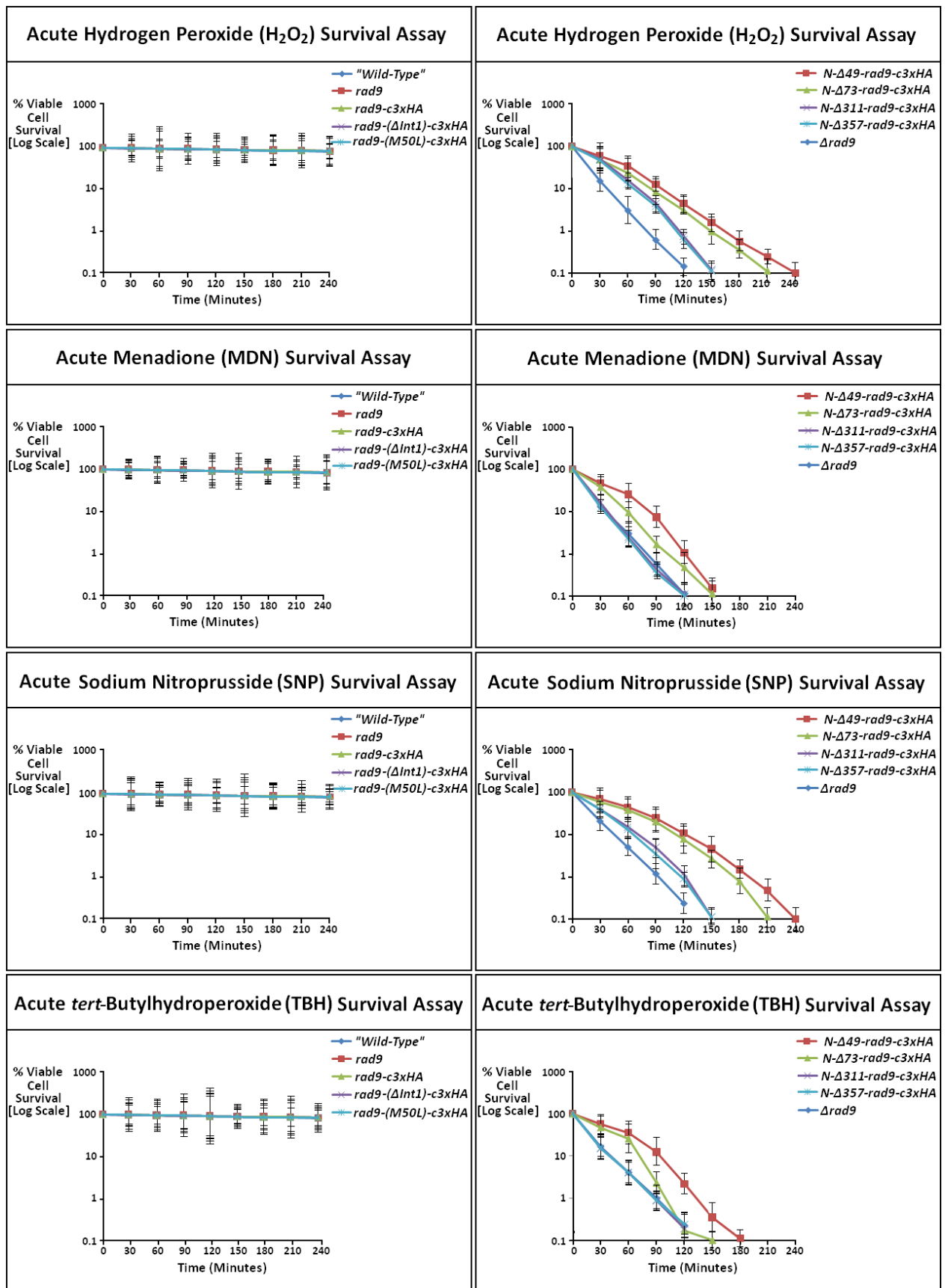
[Acute cell survival assays were performed as per the methodology described in Chapter 2, Section 2.9.2.2(ii), pp.239-241]

Fig 5.8: Comparative Heat and Osmotic Stress Acute Survival Assays



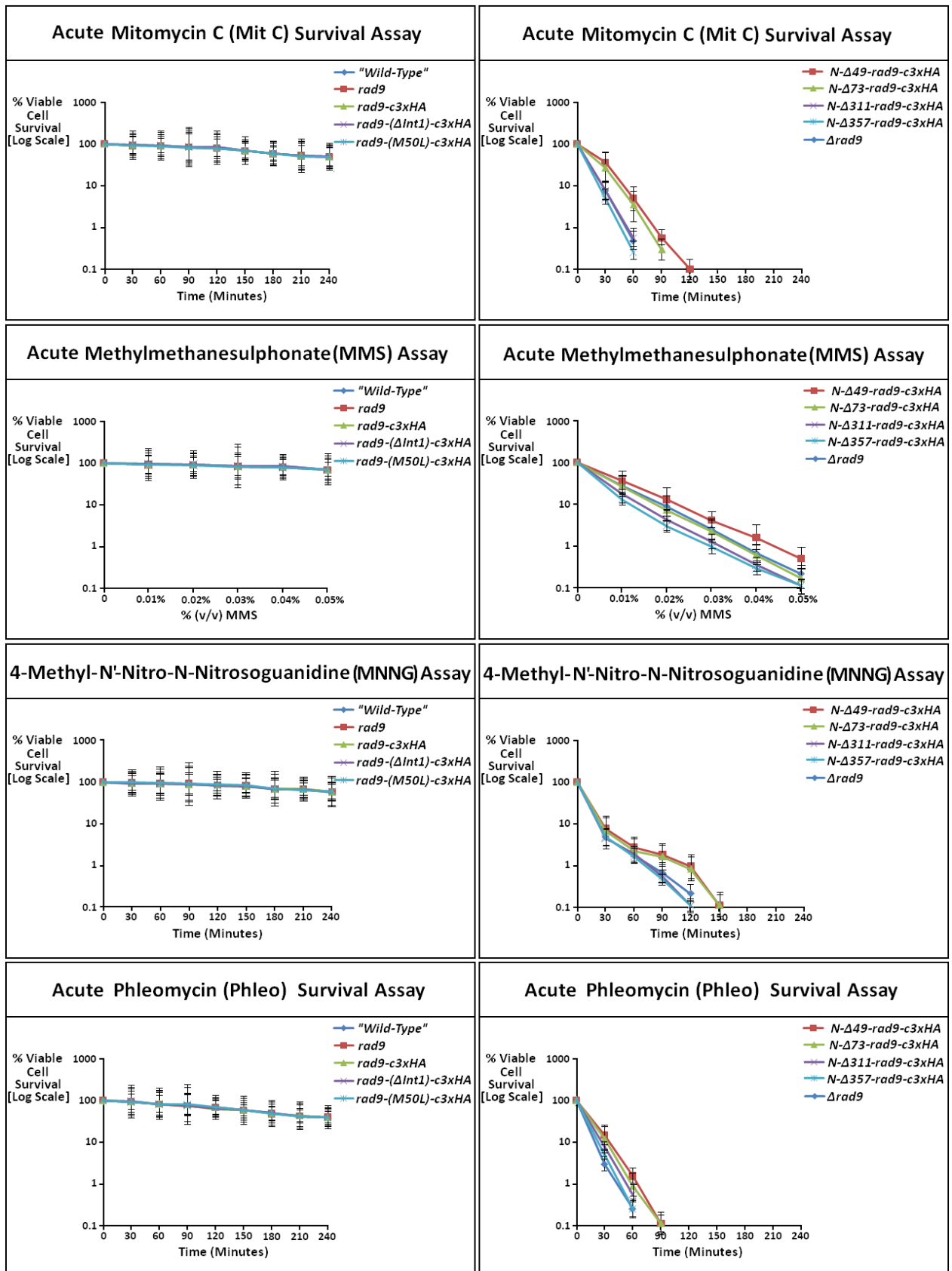
[Acute cell survival assays were performed as per the methodology described in Chapter 2, Section 2.9.2.2(ii), pp.239-241]

Fig 5.9: Comparative Acute Oxidative Stress Survival Assays



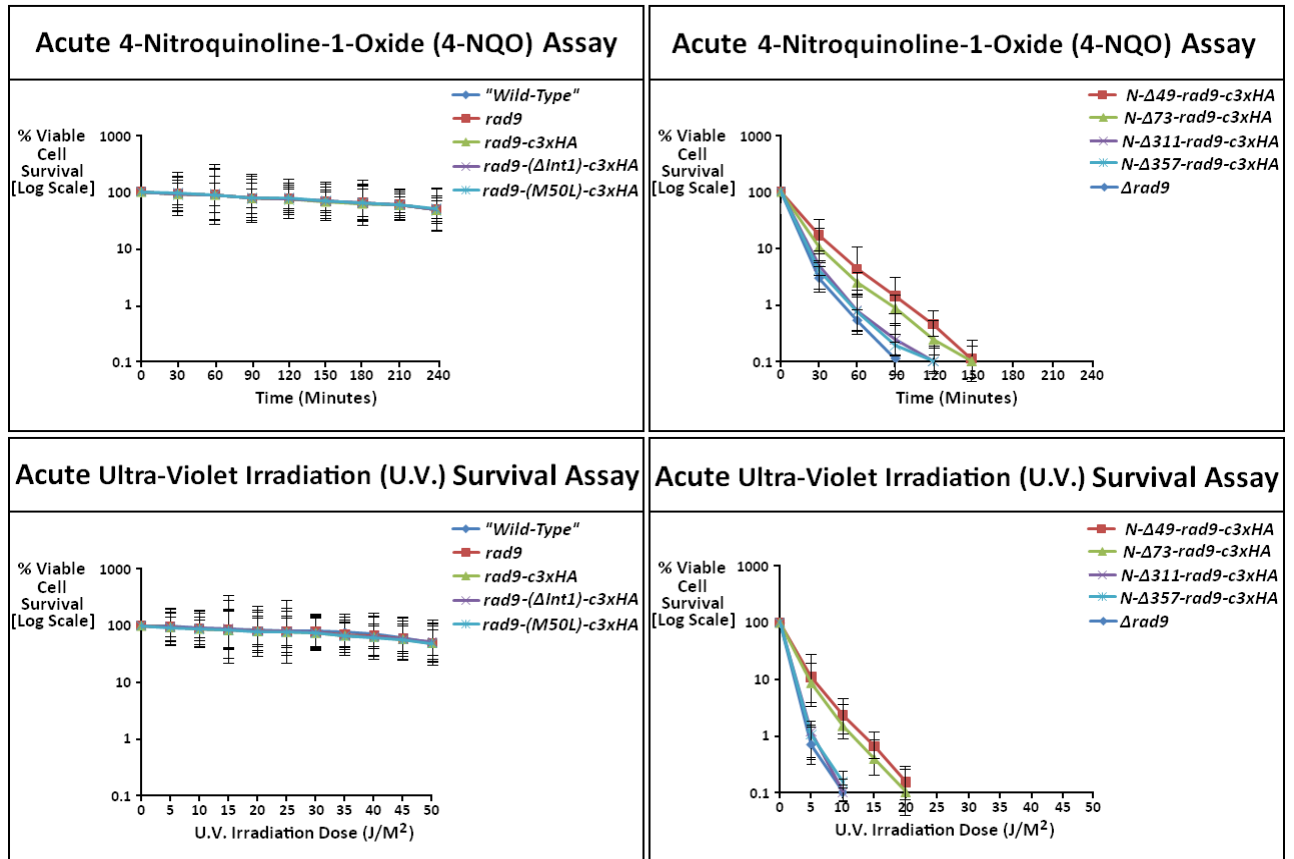
[Acute cell survival assays were performed as per the methodology described in Chapter 2, Section 2.9.2.2(ii), pp.239-242]

Fig 5.10(i): Acute Survival Assays with Adduct-Forming/Cross-Linking Agents



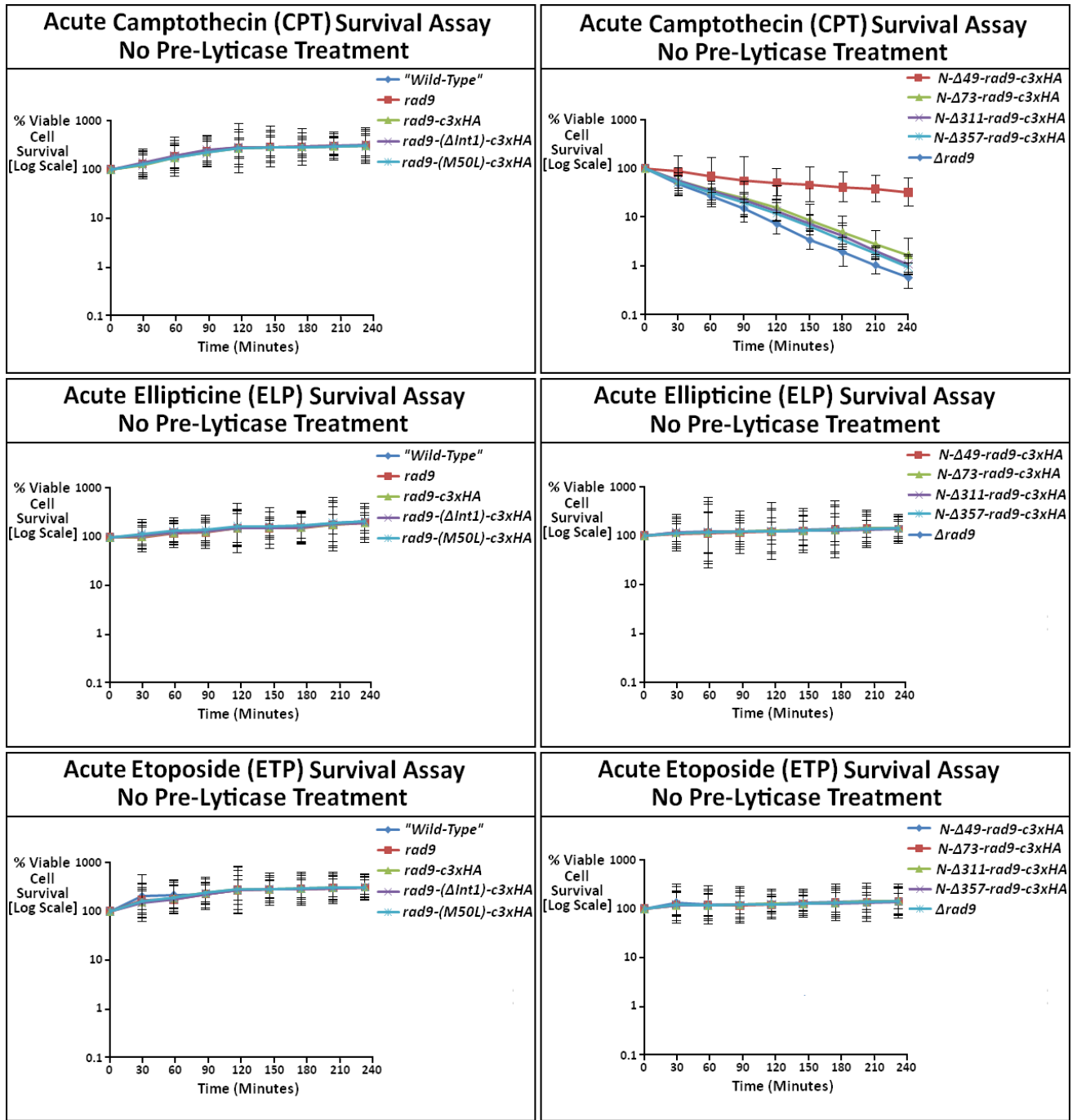
[Acute cell survival assays were performed as per the methodologies described in Chapter 2, Section 2.9.2.2(ii), pp.239-247]

Fig 5.10(ii): Acute Survival Assays with Adduct-Forming/Cross-Linking Agents



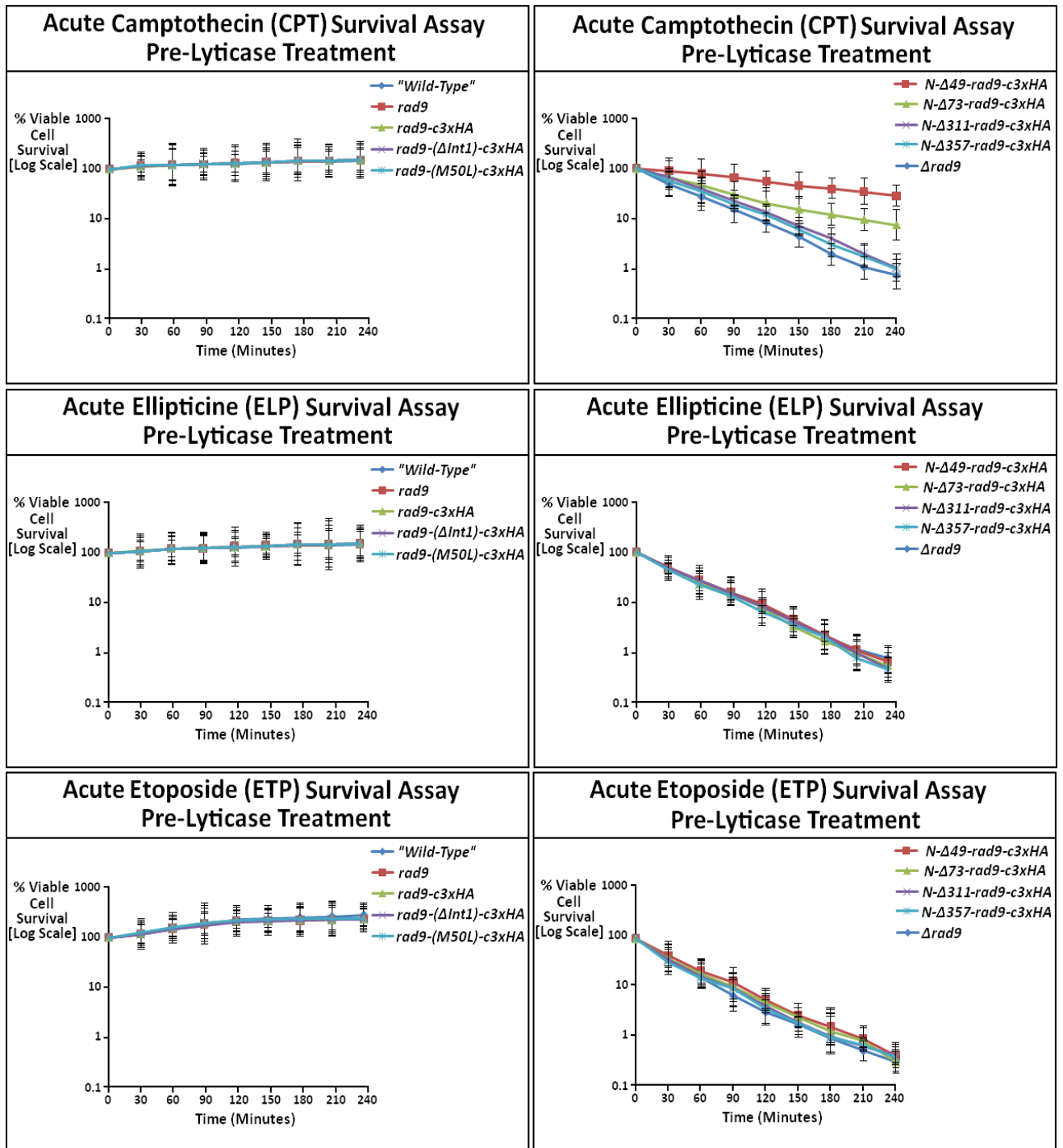
[Acute cell survival assays were performed as per the methodology described in Chapter 2, Section 2.9.2.2(i), pp.236-238; Section 2.9.2.2(ii), pp.239-241 and p.243]

Fig 5.11(i): Acute Survival Assays with Topoisomerase Inhibitors



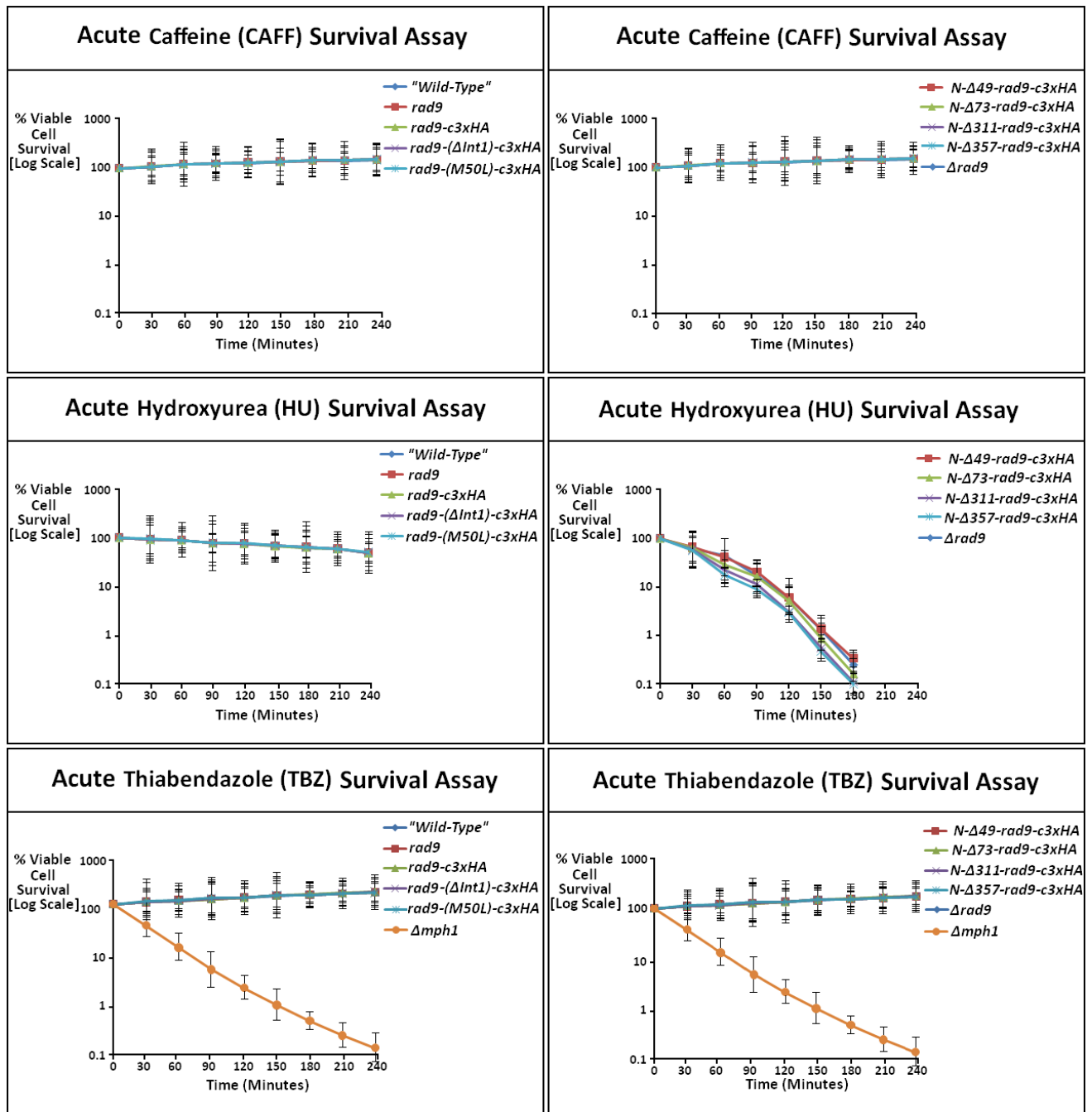
[Acute cell survival assays were performed as per the methodologies described in Chapter 2, Section 2.9.2.2(ii), pp.239-241 and p.248]

Fig 5.11(ii): Acute Survival Assays with Topoisomerase Inhibitors



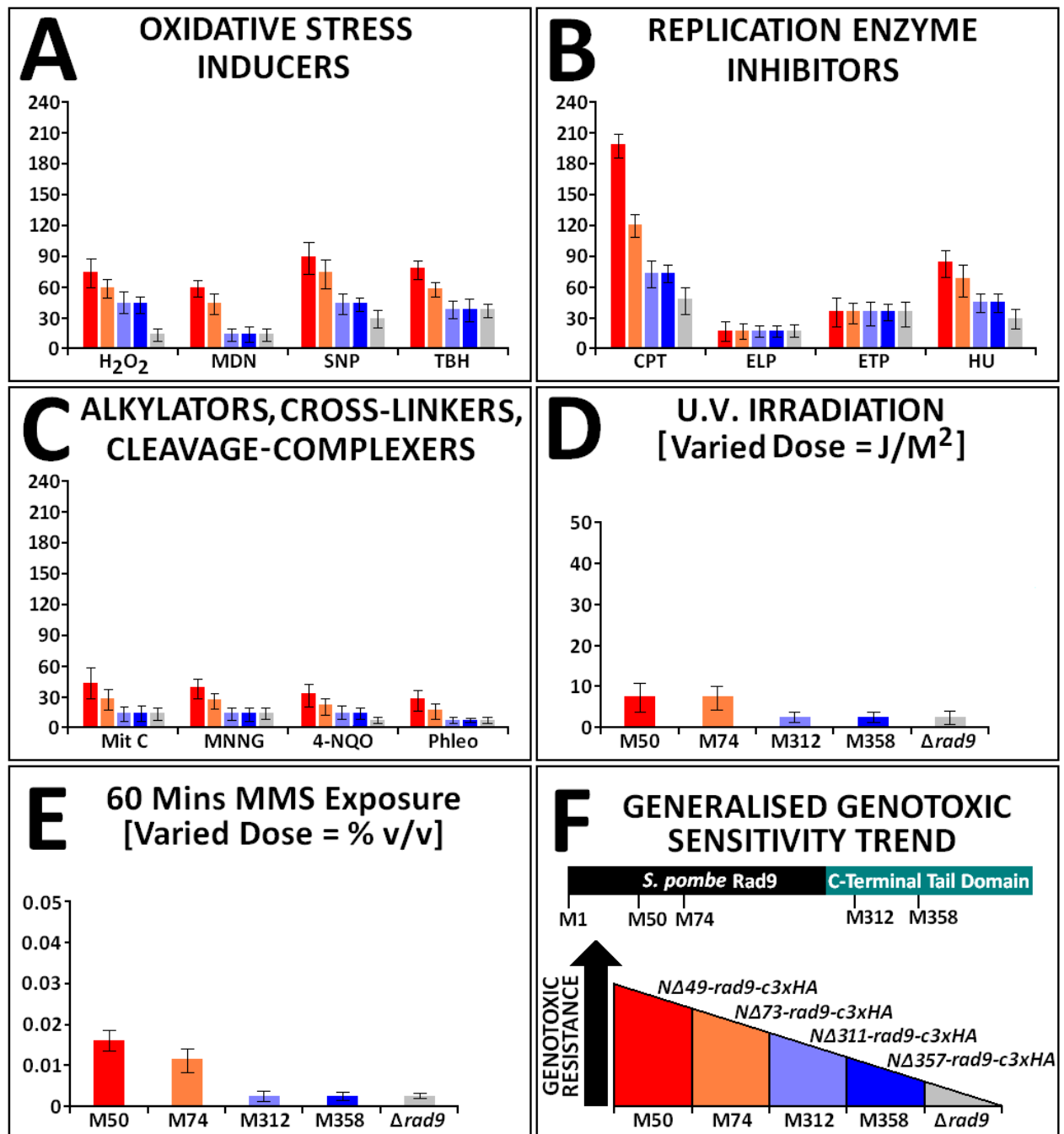
[Acute cell survival assays were performed as per the methodologies described in Chapter 2, Section 2.9.2.2(ii), pp.239-241 and pp.249-251]

Fig 5.12: Acute Survival Assays with Caffeine, HU and TBZ



[Acute cell survival assays were performed as per the methodology described in Chapter 2, Section 2.9.2.2(ii), pp.239-241 and p.252]

Fig 5.13: Comparative Analyses of the Relative Degree of Enhanced Sensitivity of *S. pombe* Strains, Engineered for the Exclusive Expression of Specific Truncated Rad9 Variants, to Different Types of Induced Genotoxic Stresses



[Descriptive details are provided in the figure legend – p.470]

Figure Legend – Fig 5.13

Figs A – C are comparative histogram plots of the relative cytotoxicity sensitivity of *S. pombe* strains, whose cells were “cre-lox” – engineered for the exclusive expression of the indicated truncated Rad9 variants and the Rad9 deleted ($\Delta rad9$) base-strain, to different types of acute genotoxic-induced stresses.

S. pombe strains and genotoxic agents are indicated on the X-axis of the data plots, the average time (in minutes) equivalent to 50% cell survival is indicated on the Y-axis of the data plots and was determined from the acute survival survival assays performed on these strains with the indicated genotoxic agents.

Oxidative Stress Inducers

H₂O₂ = Hydrogen peroxide (400 μ M)

MDN = Menadione (400 μ M)

SNP = Sodium nitroprusside (400 μ M)

TBH = t-Butylhydroperoxide (400 μ M)

DNA Replication Enzyme Inhibitors

CPT = Camptothecin (40 μ M)

ELP = Ellipticine (40 μ M)

ETP = Etoposide (40 μ M)

HU = Hydroxyurea (10mM)

DNA Alkylator, Cross-Linking, Cleavage Agents

Mit C = Mitomycin C (4 μ M)

MNNG = 4-Methyl-N'-Nitro-N-Nitrosoguanidine

4-NQO = 4-Nitroquinoline-1-Oxide(4 μ M)

Phleo = Phleomycin (4 μ M)

Fig D is the comparative histogram plot of the relative cytotoxicity sensitivity of *S. pombe* strains, whose cells were “cre-lox” – engineered for the exclusive expression of the indicated truncated Rad9 variants and the Rad9 deleted ($\Delta rad9$) base-strain, to acute exposure to U.V. irradiation.

S. pombe strains are indicated on the X-axis of the data plots, the average U.V. dose (J/M²) equivalent to 50% cell survival is indicated on the Y-axis of the data plots and was determined from the acute U.V. survival assays performed on these strains.

Fig E is the comparative histogram plot of the relative cytotoxicity sensitivity of *S. pombe* strains, whose cells were “cre-lox” – engineered for the exclusive expression of the indicated truncated Rad9 variants and the Rad9 deleted ($\Delta rad9$) base-strain, to acute methylmethanesulphonate (MMS) exposure.

S. pombe strains are indicated on the X-axis of the data plots, the average MMS dose (% v/v) equivalent to 50% cell survival is indicated on the Y-axis of the data plots and was determined from the acute MMS survival assays performed on these strains.

Fig F is a graphical summary of the general cytotoxic sensitivity trend of the “cre-lox”-engineered *S. pombe* strains to induced genotoxic stress.

5.4 Distinctive Phosphoisoform Profiles of the “Rad9-S” Truncated Protein Variant are Generated in Cellular Responses to Specific Types of Induced Genotoxic Stresses

Comparative 2D-PAGE-coupled Western blot analyses of TCA-precipitated total protein extracts acquired from YEA broth cell cultures of the *S. pombe* strain *NA49-rad9-c3xHA* (“Rad9-S”), incubated in the presence of the genotoxic agents; camptothecin, ellipticine, etoposide, hydrogen peroxide and phleomycin, hydroxyurea and methylmethane sulphonate revealed that the “Rad9-S” truncated protein exhibited differential phosphoisoform profiles for different types of induced DNA damage (Fig 5.14, p.473).

Comparative 2D-PAGE-coupled Western blot analyses of TCA-precipitated total protein extracts acquired from YEA broth cell cultures of the *S. pombe* strain *NA49-rad9-c3xHA* (“Rad9-S”), in the presence of the DNA double-strand break (DSB) inducing genotoxic agents; camptothecin, ellipticine, etoposide, hydrogen peroxide and phleomycin, also revealed that the “Rad9-S” truncated protein exhibited differential phosphoisoform profiles for different types of induced DSBs (Fig 5.15A, p.474).

Ellipticine induces DSBs via inhibition of topoisomerase II, but unlike etoposide, it does not trap the enzyme on the DNA, whilst hydrogen peroxide induces free-radical DSB cleavage reactions – in both instances the respective compounds do not form bulky/sterically-hindered complexes with the DNA.

In contrast, the topoisomerase inhibitors camptothecin and etoposide trap the respective topoisomerase I (CPT) and topoisomerase II (Etp) enzymes on the DNA in bulky, sterically-hindered complex at the replication fork.

The DSB-inducing agent phleomycin forms a redox-reactive Fe^{2+} -organometallic type intercalating bulky, sterically-hindered complex with the DNA prior to duplex cleavage.

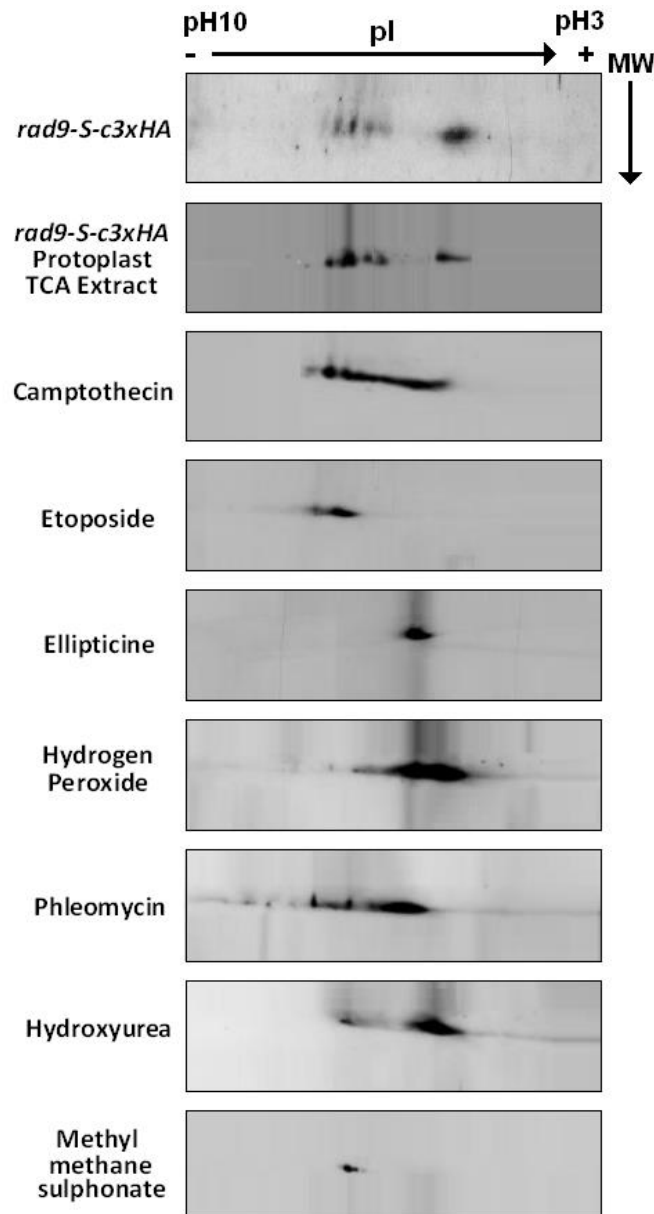
The notable absence of hypophosphorylated “Rad9-S” protein isoforms towards the negative (pH10) terminus within the hydrogen peroxide and ellipticine 2D-PAGE expression profiles, which are present in the case of the camptothecin, etoposide and phleomycin 2D PAGE-coupled Western blot expression profiles may be indicative of a functional region within the truncated “Rad9-S” protein variant which is implicated in the detection of adverse genotoxin-induced alterations of DNA topological and/or chromatin supramolecular structural configurations (Fig 5.15A and Fig 5.15C, p.474).

With the exception of etoposide, the 2D PAGE-coupled Western blot expression profiles obtained for the other DSB-inducing DNA damaging agents contain hyperphosphorylated “Rad9-S” isoforms towards the positive (pH3) terminus which may be indicative of functional phosphorylated C-terminal tail domain-mediated DNA damage signalling responsive regions within the truncated “Rad9-S” protein variant (Fig 5.15A and Fig 5.15C, p.474).

Comparative acute survival assays performed on YEA broth cell cultures of the *NA49-rad9-c3xHA S. pombe* strain with the different DSB-inducing DNA damaging agents indicate that the partial resistance of “Rad9-S” cells (~30% retained cell viability/cell survival) is an exclusive response to the topoisomerase I inhibitor camptothecin (Fig 5.15B, p.474).

Taken together, these experimental data indicate that the truncated “Rad9-S” protein variant may associate with Hus1 and Rad1 to form an alternative heterotrimeric “Rad9-S”-Hus1-Rad1 DNA sliding-clamp complex which detects camptothecin-topoisomerase 1-DNA complex lesions and mediates appropriate signalling responses via C-terminal tail engagement with checkpoint proteins (eg kinases and phosphatases) and/or DNA repair factors (Fig 5.15C, p.474).

Fig 5.14: 2D-PAGE Data – Genotoxic Type “Rad9-S” Modifications



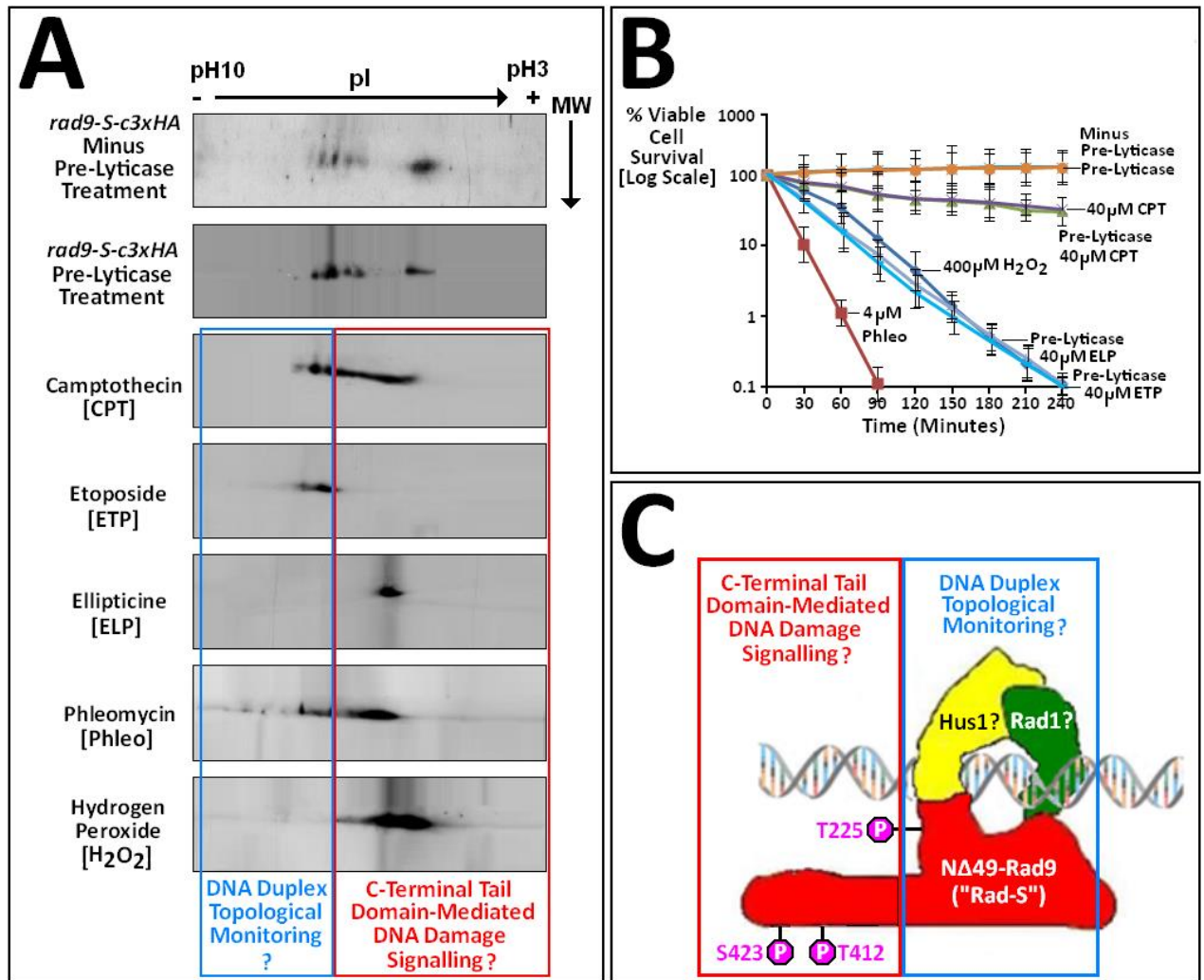
Individual 100mL YEA broth medium cell cultures of the “Cre-Lox” – constructed *NA49-rad9-c3xHA* (“Rad9-S”) *S. pombe* strain were grown overnight (30°C for ~12 hour time period), then diluted to an optical density $A_{595} = 0.25$ with the appropriate volume of YEA medium and the resultant diluted cultures re-incubated at 30°C for a further time period of ~2.5 hours until they had attained an optical density value of $A_{595} = 0.5$, after which time they were incubated for a further 30 minutes at 30°C in the absence or presence of the appropriate genotoxic agent.

[In the case of ellipticine and etoposide cell cultures, the cells were pelleted after overnight incubation and pre-treated with lyticase, as per the protocol described in Ch.2, Section 2.9.2.2(ii), pp.248-251, prior to re-suspension in 100mL fresh YEA which contained 40µM of ellipticine or Etoposide]

TCA-precipitated total protein extract samples were then prepared from the appropriate *calculated volumetric aliquot of each culture (*equivalent to 40 A_{595} optical density units) and utilised in comparative 2D-PAGE–coupled Western Blot analyses – probed with the primary “anti-HA” antibody.

[Protein sample preparation, 2D PAGE and Western blot methodologies are described in Chapter 2, Section 2.8.3.1, pp.214-217; Section 2.8.5.1, pp.225-230 and Section 2.8.6., pp.231-233]

Fig 5.15: Rad9-S Responses to Different Types of Induced DSBs



A: Individual 100mL YEA broth medium cell cultures of the “Cre-Lox” – constructed *NΔ49-rad9- c3xHA* (“Rad9-S”) *S. pombe* strain were grown overnight (30°C for ~12 hour time period), then diluted to an optical density $A_{595} = 0.25$ with the appropriate volume of YEA medium and the resultant diluted cultures re-incubated at 30°C for a further time period of ~2.5 hours until they had attained an optical density value of $A_{595} = 0.5$, after which time they were incubated for a further 30 minutes at 30°C in the absence or presence of the appropriate genotoxic agent.

[In the case of Ellipticine and Etoposide cell cultures, the cells were pelleted after overnight incubation and pre-treated with lyticase, as per the protocol described in Ch.2, Section 2.9.2.2(ii), pp.246-248, prior to re-suspension in 100mL fresh YEA which contained 40µM of ELP or Etp]

TCA-precipitated total protein extract samples were then prepared from the appropriate *calculated volumetric aliquot of each culture (*equivalent to 40 A_{595} optical density units) and utilised in comparative 2D-PAGE–coupled Western Blot analyses – probed with the primary “anti-HA” Antibody. [Performed as per the methodologies described in Chapter 2, Section 2.8.3.1, pp.214-217; Section 2.8.5.1, pp.225-230 and Section 2.8.6., pp.231-233]

B: Comparative acute cell survival assays performed with the genotoxic compounds camptothecin (CPT), ellipticine (ELP), etoposide (ETP), hydrogen peroxide (H₂O₂) and phleomycin (Phleo) on the *S. pombe* strain *NΔ49-rad9- c3xHA* (“Rad9-S”).

[Acute cell survival assays were performed as per the methodologies described in Chapter 2, Section 2.9.2.2(ii), pp.239-242 and pp.247-251]

C: Functional compartmentalisation model of co-ordinated DNA damage detection and checkpoint signal initiation within the truncated “Rad9-S” sub-unit of an alternative “Rad9-S”:Hus1:Rad1 DNA sliding-clamp complex.

5.5 The Identification of the M50 – M74 Domain as a Potential Key Functional Component of Protective “Rad9-S”-Mediated Cellular Responses Against Camptothecin-Induced DNA Damage

Comparative acute cell survival assays revealed that the *N173-rad9-c3xHA*, *N1311-rad9-c3xHA* and *N1357-rad9-c3xHA S. pombe* strains exhibited an equivalent genotoxic sensitivity to camptothecin-induced DNA damage, which was significantly higher than that of the *rad9-c3xHA* and *N149-rad9-c3xHA S. pombe* strains (Fig 5.16A, p.479) - which may indicate that the *S. pombe* Rad9 protein contains a novel functional domain spanning residues M50 and M74 (Fig 5.16C, p.479).

Comparative multiple sequence alignments of Rad9 proteins expressed in various yeasts, in conjunction with the full-length human Rad9A protein and full-length Rad9B paralogue and its four truncated isoforms (via utilisation of on-line bioinformatics software tools COBAL, EMBOSS, JEMBOSS and PSI-BLAST) identified this “M50 – M74” sequence as a functional eukaryotic linear motif, in which two key positionally-equivalent conserved phenylalanine residues and two key positionally-equivalent Lysine residues were conserved amongst the Rad9 sequences of a variety of different yeast species (Fig 5.16D, p.479) – which may be critical for functional DNA-binding interactions of the Rad9 protein (Fig 5.16C, p.479).

In Silico potential kinase phosphorylation-site prediction analyses, performed via utilisation of the bioinformatics software tool Netphos2.0, also indicated high phosphorylation probability scores for the T52 and Y61 residues situated within the identified novel M50-M74 domain (Fig 5.16C, p.479)

Comparative acute cell survival assays performed with YEA broth cultures of the indicated “cre-lox”-engineered *S. pombe* strains in the presence of 40µM Camptothecin revealed that the *NΔ49-rad9-(T52A)-c3xHA* a similar degree of partial resistance to CPT-induced DNA damage, in contrast to the *NΔ49-rad9-(Y61F)-c3xHA* and *NΔ49-rad9-(T52A;Y61F)-c3xHA* cells which exhibited enhanced resistance to the genotoxic effects of camptothecin (Fig 5.16B, p.479).

The un-phosphorylated form of the Tyrosine 61 residue, situated within the M50-M74 domain, may facilitate stronger associative binding of the Rad9 and/or “Rad9-S” proteins to DNA via intercalative Π - Π electron-stacking aromatic ring type interactions of Y61 with the duplex nucleobases.

These DNA via intercalative Π - Π electron-stacking aromatic ring type interactions may be perturbed when Y61 is phosphorylated as a consequence of the hydrophilic, negatively-charged ionic properties of the phosphate group which would be repelled by the negatively-charged duplex sugar-phosphate backbone and would also be incompatible with the hydrophobic nature of the DNA bases and result in modification of the Π -electron distribution within the aromatic Tyr phenolic ring that would perturb the Π - Π aromatic electron-stacking interactions with the duplex nucleobases (Fig 5.16C, p.479).

In silico comparative molecular modelling and multiple alignment analyses also indicated that this identified DNA-binding M50 – M74 domain motif was situated in adjacent sequence overlap with the putative 3’-5’ exonuclease domain motif and that this dual motif configuration within the *S. pombe* Rad9 protein exhibited significant homology to equivalent sequences identified within the *H. sapiens* Rad9A and Rad9B proteins (Fig 5.17, p.480).

Taken together, these experimental data observations indicate that the truncated Rad9-S protein variant may have functional roles in the repair of camptothecin-induced DNA damage.

Comparative 2D PAGE-coupled Western blot analyses of the untreated and alkaline phosphatase treated soluble supernatant extracts (cytosolic protein localisation) indicated only minor subtle changes in the phosphoisoform profiles of the truncated Rad9-S protein variant in response to camptothecin-induced DNA damage (Fig 5.18A, p.481).

Comparative 2D PAGE-coupled Western blot analyses of the untreated and alkaline phosphatase treated soluble supernatant extracts (cytosolic protein localisation) indicated only minor subtle changes in the phosphoisoform profiles of the truncated Rad9-S protein variant in response to camptothecin-induced DNA damage (Fig 5.18A, p.481).

Comparative 2D PAGE-coupled Western blot analyses of the total soluble protein extract pellet (nuclear protein localisation) fractions revealed that the hyperphosphorylated form of the truncated “Rad9-S” protein variant is retained in the nucleus in both the absence and presence of camptothecin-induced damage (Fig 5.18B, p.481) – which may indicate that “Rad9-S” has constitutive “house-keeping” and inducible DNA damage responsive checkpoint signalling functions which are implicated in the maintenance of genomic integrity.

These comparative 2D PAGE-coupled Western blot analyses also indicate subtle hypophosphorylation modifications of the truncated “Rad9-S” protein variant in response to camptothecin-induced DNA damage (Fig 5.18B, p.481)

Hyperphosphorylation of “Rad9-S” in the absence of camptothecin-induced DNA damage may include the phosphotyrosine residue at position 61 within the identified M50 – M74 DNA binding domain and thus serve to prevent the truncated protein variant from binding to the DNA.

The 2D-PAGE data also indicate that expression of the “Rad9-VS” variant is suppressed in response to camptothecin-mediated DNA damage, but induced in the absence of camptothecin-mediated DNA damage and retained exclusively in the nucleus (Fig 5.18A and Fig 5.18B, p.481).

These experimental observations indicate that the truncated “Rad9-VS” protein variant may have a regulatory role in the suppression of inappropriate “Rad9-S” – mediated checkpoint signalling functions in the absence of camptothecin-induced DNA damage within the nucleus.

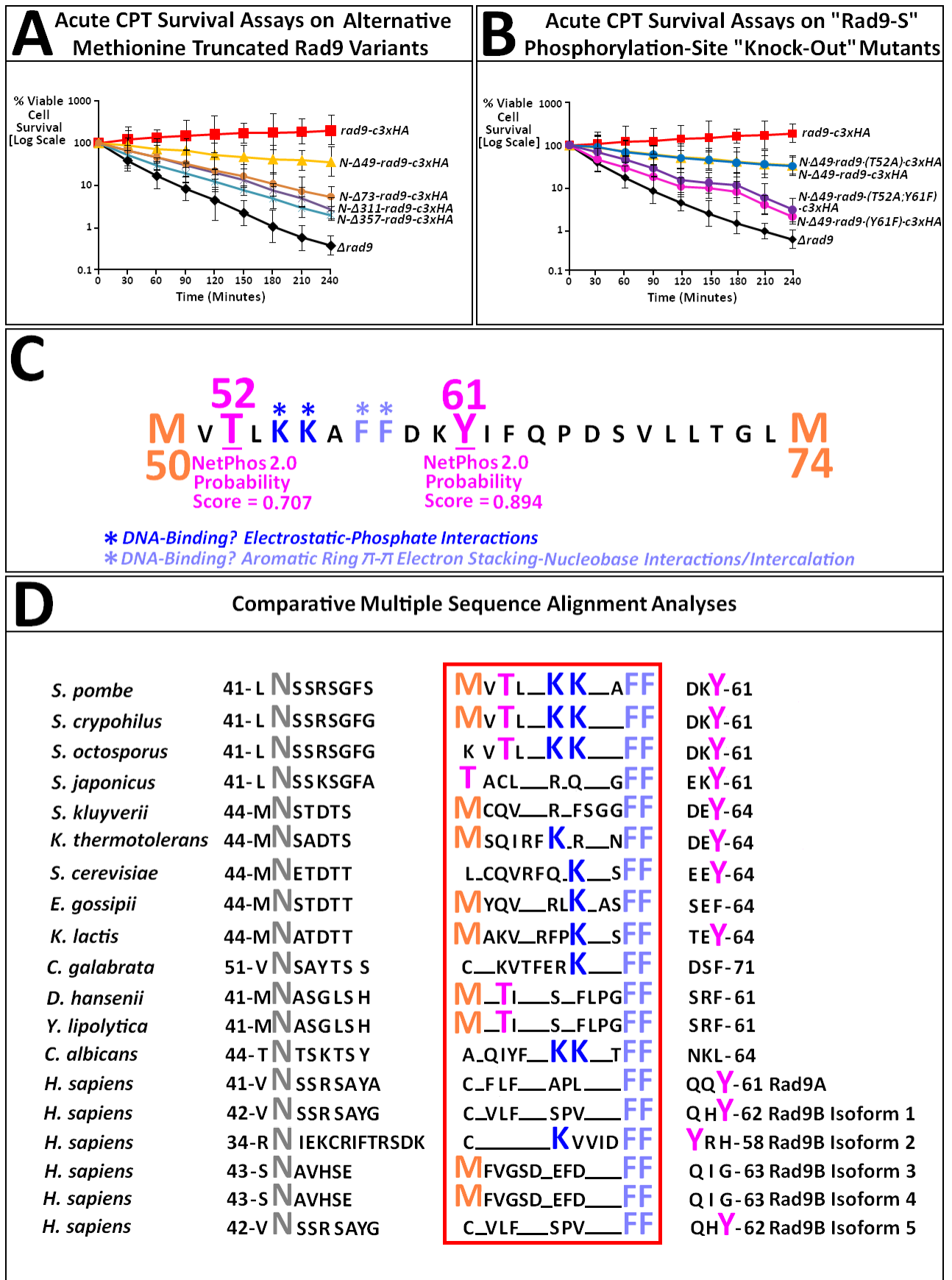
In this hypothetical context, the truncated “Rad9-VS” protein variant may engage with protein phosphatases to competitively block dephosphorylation of the truncated “Rad9-S” protein variant to prevent it binding to DNA and eliciting inappropriate checkpoint signalling and/or DNA repair mechanisms in the absence of camptothecin-induced genotoxicity.

Camptothecin-induced genotoxic stress may trigger checkpoint signalling responses which suppress expression of the “Rad9-VS” truncated protein variant, enabling the truncated “Rad9-S” protein variant to engage with phosphatases which dephosphorylate the tyrosine 61 residue within the M50 – M74 domain, thus facilitating Rad9-S:DNA binding interactions which initiate appropriate checkpoint signalling and/or DNA repair pathways.

In this respect, Rad9-S –initiated checkpoint signalling responses to camptothecin-induced DNA damage may also be implicated in regulatory “feed-back” mechanisms of co-ordinated suppressed and induced expression of the truncated “Rad9-VS” protein.

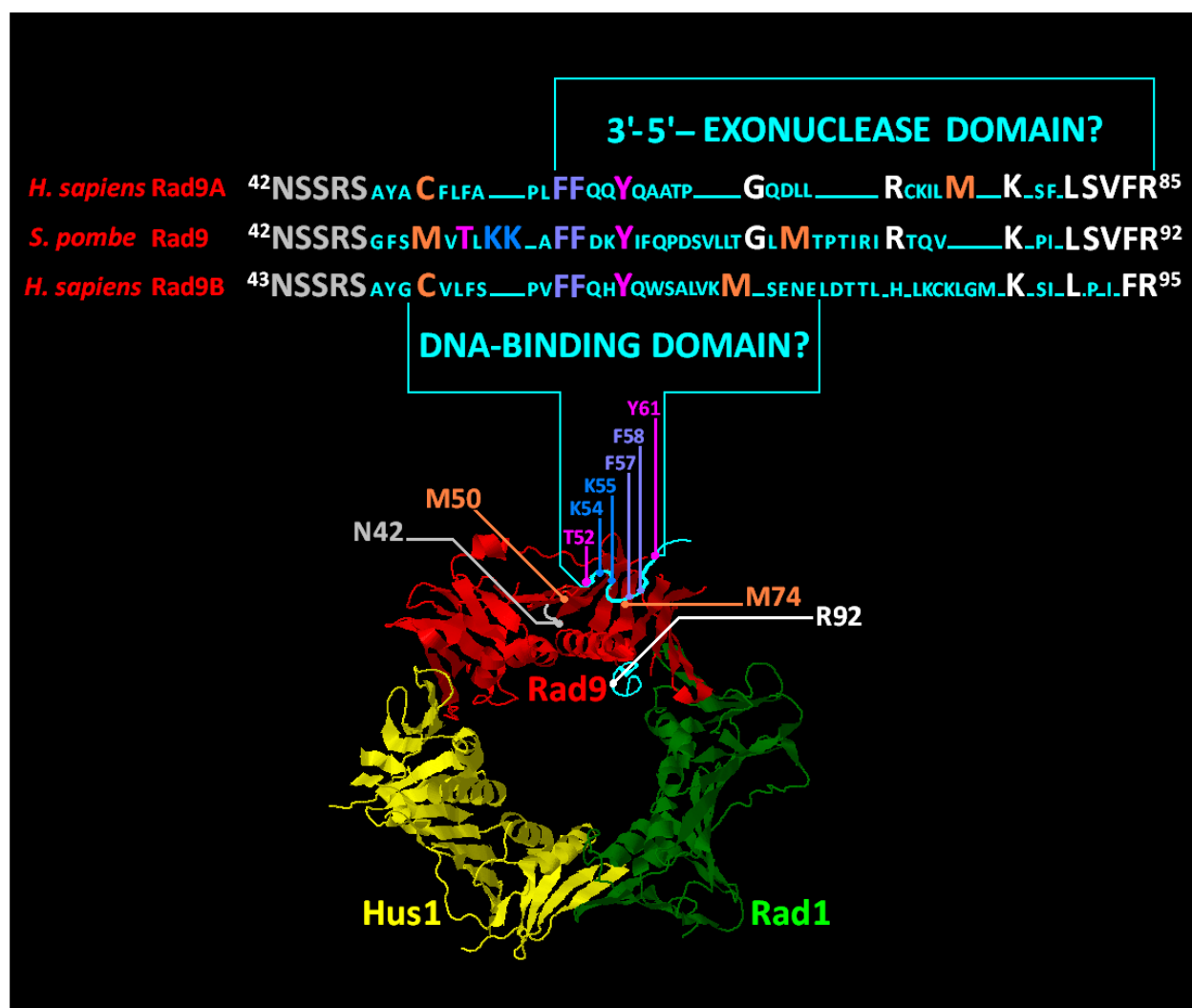
These “feed-back” mechanisms may function as regulatory switches to prevent catastrophic uncontrolled and/or prolonged “Rad9-S” –initiated checkpoint signalling and/or DNA repair pathway activities which may compromise genomic integrity.

Fig 5.16: Identification of a Novel Functional Domain in Rad9



[An explanatory discussion of the experimental data is provided in the text – pp.475-476]

Fig 5.17: Comparative Modelling of the M50 – M74 Functional Domain Within the Full-Length *S. pombe* Rad9 Protein

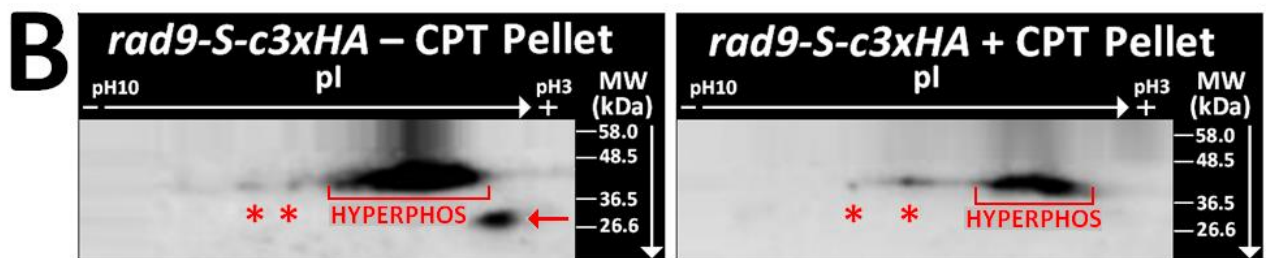
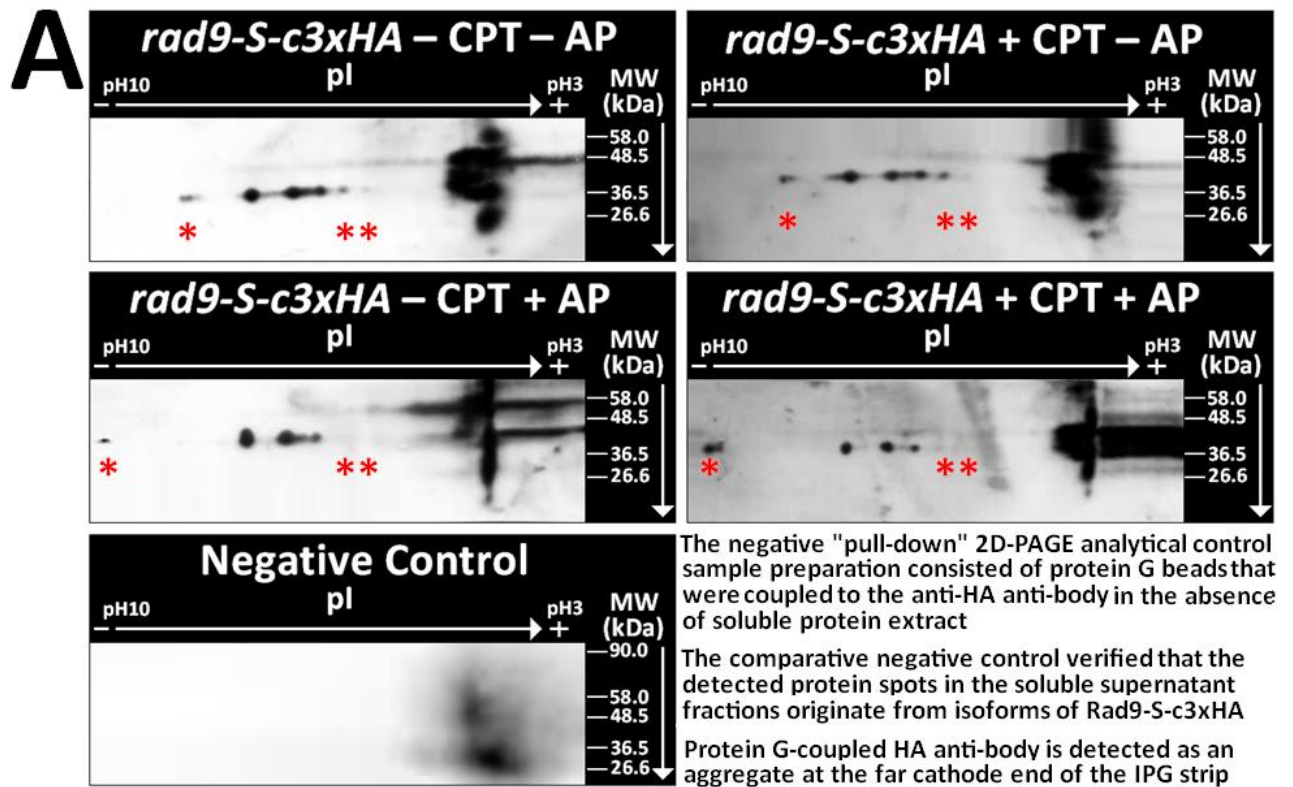


In silico comparative modelling of the M50 –M74 functional domain in the full-length *S. pombe* Rad9 protein within the X-ray crystallographic resolved structure of the human Rad9-Rad1-Hus1 complex (PDB file: 3G65) was accomplished via utilisation of the on-line bioinformatics software tool RasMol and the molecular graphics were generated via utilisation of the on-line PolyView3D software tool.

The relative positions of the M50 and M74 methionine residues which span the identified DNA binding domain motif and the adjacent overlapping 3'-5' exonuclease motif are indicated.

The conserved, homologous-equivalent “overlap-configured” DNA binding and 3'-5' exonuclease functional motif sequences contained within the *H. sapiens* Rad9A, Rad9B and *S. pombe* Rad9 proteins were identified via comparative multiple alignment analyses with the on-line bioinformatics software tools COBALT, EMBOSS, JEMBOSS and PSI-BLAST.

Fig 5.18: 2D-PAGE Data – Localisation of Rad9-S Phosphoisoforms



Individual 100mL YEA broth medium cell cultures of the “Cre-Lox” – constructed *ND49-rad9-c3xHA* (“Rad9-S”) *S. pombe* strain were grown overnight (30°C for ~12 hour time period), then diluted to an optical density $A_{595} = 0.25$ with the appropriate volume of YEA medium and the resultant diluted cultures re-incubated at 30°C for a further time period of ~2.5 hours until they had attained an optical density value of $A_{595} = 0.5$, after which time they were incubated for a further 30 minutes at 30°C in the absence or presence of 40µM camptothecin.

Soluble total protein extract samples were then prepared from the appropriate *calculated volumetric aliquot of each culture (*equivalent to 40 A_{595} optical density units) and utilised for preparation of untreated and treated alkaline phosphatase-digested 2D-PAGE analyses – as per the methodology described in Chapter 2, Section 2.8.3.2, pp.218-222.

TCA-precipitated total protein extracts were also prepared from the nuclear fraction pellets (treated as per stage ix onwards in the protocol described in Chapter 2, Section 2.8.3.1, pp.215-217), acquired from the initial preparation of the soluble total protein extract supernatant samples, for comparative 2D-PAGE analyses.

A: Comparative 2D PAGE-coupled Western blot analyses of the un-treated and alkaline phosphatase-treated soluble protein supernatant extracts (cytosolic protein localisation).

B: Comparative 2D PAGE-coupled Western blot analyses of the total soluble protein extract pellet fractions (nuclear protein localisation).

* Subtle shifts within the phosphoisoform profiles of the Rad9-S protein

Detected expression of the truncated “Rad9-VS” isoform ←

HYPERPHOS = Hyperphosphorylation

Chapter 6

**Genetic and Biochemical “Deciphering” of
Differential “Rad9-S”-Initiated Checkpoint
Responses to Camptothecin-Induced DNA
Damage and Hyperthermic Stress**

Introduction

Camptothecin is a topoisomerase I inhibitor type compound, isolated from bark extracts from Chinese “Tree of Joy” *Camptotheca accuminata*, which was discovered to possess potent cytotoxic activity against tumour cells (Fig 6.1, p.484).

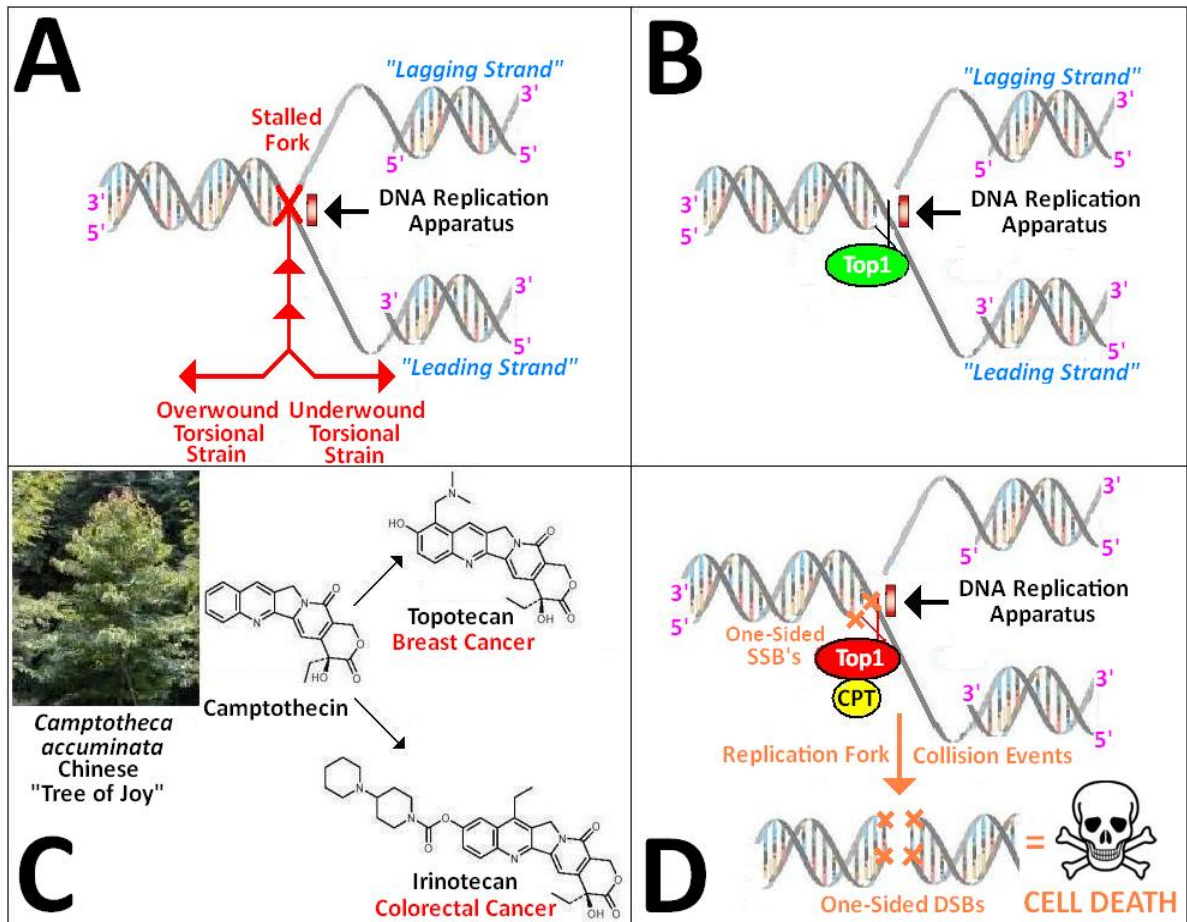
The cytotoxicity of camptothecin (CPT) is mediated via the formation of a “DNA-CPT-TopI” type complex, which traps the topoisomerase I enzyme on the DNA and inhibits its catalytic re-ligation activity with consequential induction of one-sided single-stranded DNA breaks at the stalled DNA replication fork during the S-phase of the first round of the cell cycle in which the drug is encountered (Fig 6.1, p.484).

Subsequent DNA replication fork collisions with the “DNA-CPT-TopI” ternary complex-stalled replication fork, during successive rounds of the cell cycle, results in the conversion of the one-sided single-stranded DNA breaks into one-sided double-stranded DNA breakages with consequential abrogation of viable functional genomic integrity and resultant cell death (Fig 6.1, p.484).

The first round of the cell cycle proceeds through the initial camptothecin-induced ssDNA breaks in S-Phase, which are propagated into the second round of the cell cycle at S-phase with consequential formation of one-sided double-stranded breaks which trigger a cytological G2/M phasic cell cycle arrest DNA damage signal response in both mammalian and yeast cells – including those of *H.sapiens* (discussed in detail previously in Chapter 1, Section 1.2.2, p.57) and *S. pombe* (discussed summarily in Section 6.2, pp.489-490; Fig 6.4, p.492).

Fig 6.1: Summarised Cytotoxic Mode of Action of Camptothecin

[Compiled via Collated Information Adapted From: Chhatriwala H. *et al*, 2006; Nakagawa H. *et al*, 2006; He X. *et al*, 2007]



A: Unwinding of the DNA duplex during replication in cell cycle S-phase results in negative and positive Supercoiled duplex torsional strain, which if unrectified would result in “supramolecular tangling/knotting” of the DNA which would stall the replication fork and inhibit mitotic progression.

B: Topoisomerase I alleviates torsional supercoiled duplex strain during DNA replication in the cell cycle S-phase via cleavage of the phosphodiester backbone and passage of one strand through the site of the cleaved strand, mediated via formation of a covalent phospho-tyrosine linkage, followed by subsequent re-ligation of the cleaved DNA strand site (He X. *et al*, 2007) .

C: S-(+)-camptothecin, initially isolated from the tree bark of *Camptotheca accuminata*, was discovered to be a potent topoisomerase I Inhibitor type compound which was cytotoxically-active against tumour cells.

Synthetic derivatised analogues of camptothecin, designed for improved pharmacokinetics and anti-neoplastic pharmacological efficacy with reduced toxicological side-effects are currently in development – examples of two such drugs, recently approved for clinical use are topotecan and irinotecan.

D: Camptothecin (CPT) forms a stable, cleavable covalent topoisomerase I-CPT-DNA-trapped transition-state intermediary complex via associative interaction between topoisomerase I and DNA within the enzymatic active site and specifically inhibits the re-ligation reaction, with resultant collision of replication forks during the cell cycle S-phase and consequential conversion of the initial stabilised topoisomerase I-induced single-stranded DNA breaks into one-sided double-stranded DNA breaks respectively (Nakagawa H. *et al*, 2006).

6.1 The *top1* Gene is Not Suppressed Within Engineered *S. pombe* Cells that Exclusively Express the Truncated Rad9-S Protein Variant

The observed partial resistance of *S. pombe* cells “Cre-Lox”– engineered for the exclusive expression of the truncated “Rad9-S” protein variant (NΔ49-rad9-c3xHA) to acute camptothecin-induced DNA damage (discussed previously in Chapter 5, Section 5.3, pp.455-470; Section 5.4, pp.471-474) could be indicative of a true novel signalling response pathway which functions outside of the canonical Rad9-Rad1-Hus1 complex or a manifested “experimental artefact” as a consequence of “inadvertently-engineered” suppressed expression and activity of the topoisomerase I enzyme within the *NΔ49-rad9-c3xHA S. pombe* strain.

Therefore the *NΔ49-rad9-c3xHA S.pombe* strain was cross-mated with a $\Delta top1$ (*top1*-deleted) *S. pombe* strain to generate the *NΔ49-rad9-c3xHA Δtop1* double-mutant *S. pombe* strain which was then utilised in comparative acute camptothecin cell survival assays (Fig 6.3, p.488).

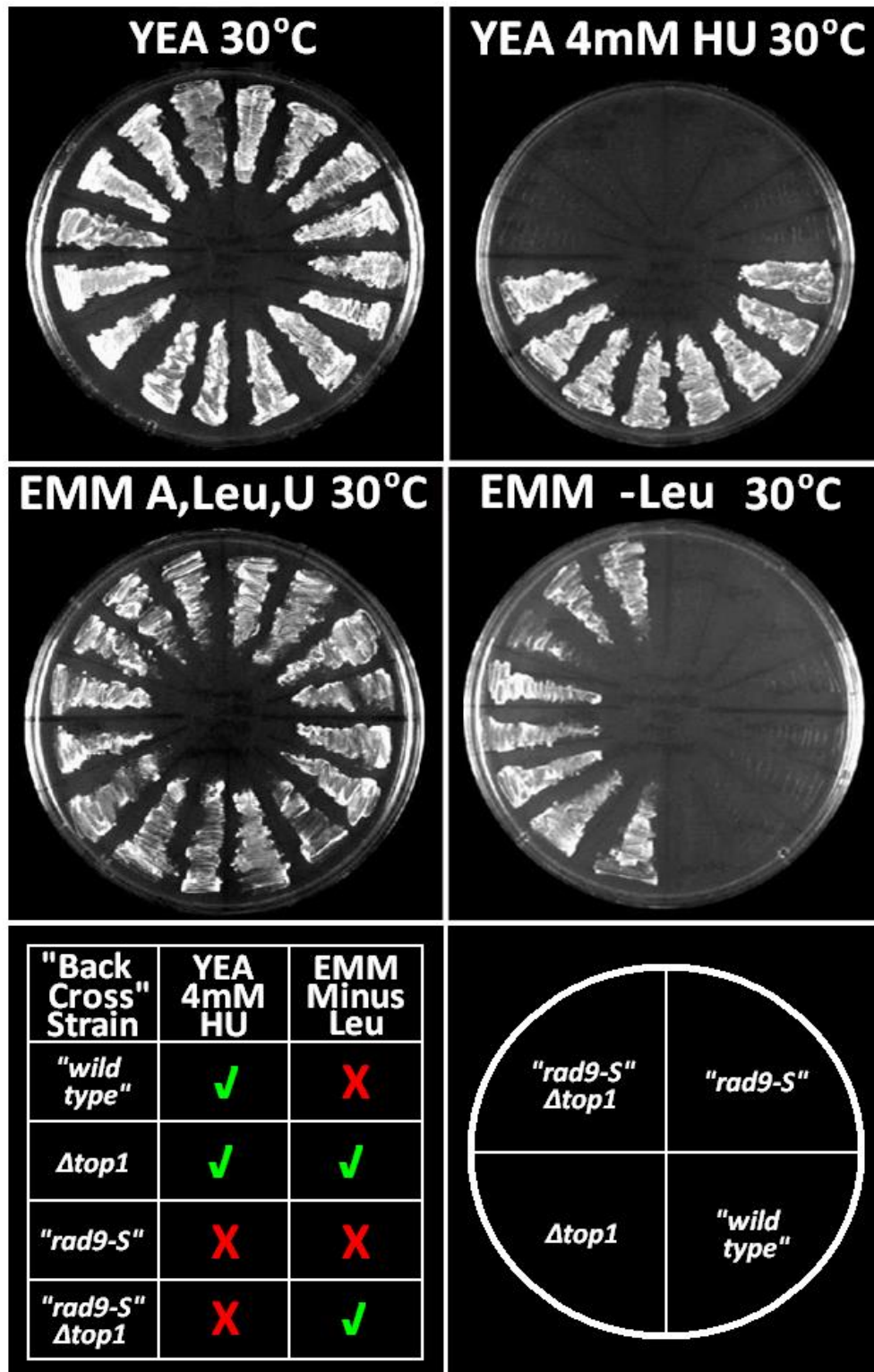
The *NΔ49-rad9-c3xHA Δtop1* double-mutant *S. pombe* strain was also “back-cross”-mated with a “wild-type” *S. pombe* strain and the resultant colonies replica-plated onto YEA-HU and EMM minus leucine plates for the selection of the resolved “wild-type”, *NΔ49-rad9-c3xHA*, $\Delta top1$ and *NΔ49-rad9-c3xHA Δtop1 S. pombe* strains (Fig 6.2, p.487) – which were then also utilised in comparative acute camptothecin cell survival assays (Fig 6.3, p.488).

The acquired comparative acute camptothecin cell survival assay data indicated that the initial generated *NΔ49-rad9-c3xHA Δtop1* double-mutant *S. pombe* strain and the “back-crossed”-resolved *NΔ49-rad9-c3xHA Δtop1* double-mutant *S. pombe* strain exhibited a significantly higher cytotoxic resistance to CPT-induced DNA damage than that of the initial generated and “back-cross”-resolved $\Delta top1$ and “wild-type” *S. pombe* strain) – Fig 6.3, p.488

Whilst the initial generated *N149-rad9-c3xHA S. pombe* strain and *N149-rad9-c3xHA S. pombe* strain which was “back-cross”-resolved from the *N149-rad9-c3xHA Δtop1* double-mutant *S. pombe* strain both exhibited a similar partial resistance to acute CPT-induced genotoxic exposure (retained cell viability ~30%) – Fig 6.3, p.488.

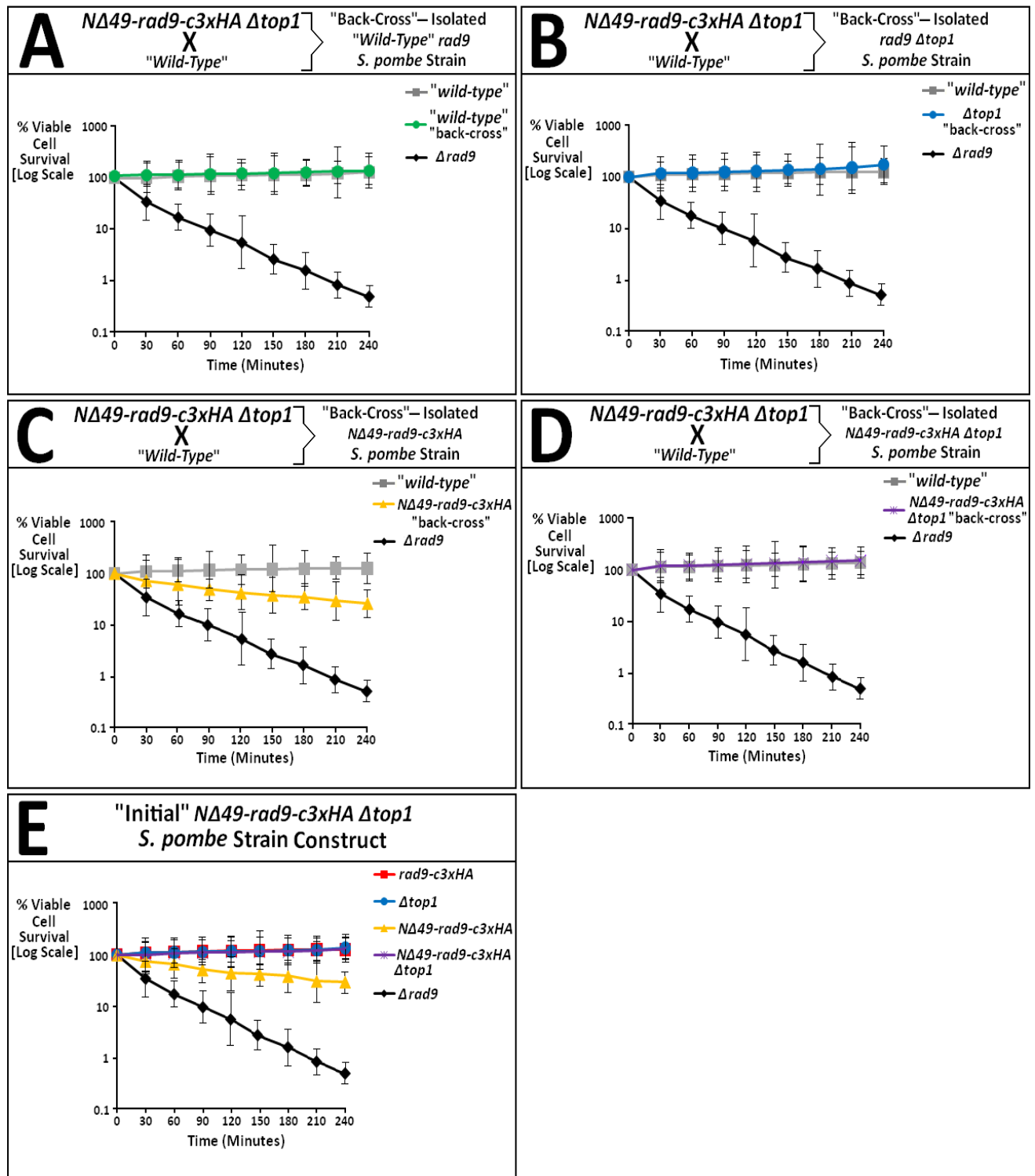
Taken collectively, these acute survival assay data revealed that the observed partial resistance of *N149-rad9-c3xHA* (“Rad9-S”) *S. pombe* cells to camptothecin-induced DNA damage is unlikely to be a consequence of “inadvertently-engineered” *top1* gene suppression and thus indicated the potential existence of a novel “rad9-S”-mediated DNA damage response signalling pathway which functioned independently of the Rad9-Rad1-Hus1 heterotrimeric toroidal DNA sliding-clamp complex.

Fig 6.2: *rad9-S Δtop1* x “Wild-Type” Back-Crossed Strain Isolation



The *NΔ49-rad9-c3xHA Δtop1 S. pombe* strain was “cross-mated” into a “wild-type” *S. pombe* strain and the resultant colonies replica-plated onto YEA agar plates which contained 4mM hydroxyurea and EMM agar plates in which leucine was omitted from the minimal medium for selection of the “back-crossed”-resolved “wild-type”, *Δtop1*, *NΔ49-rad9-c3xHA* (“*rad9-S-c3xHA*”) and *NΔ49-rad9-c3xHA Δtop1 S. pombe* strains.

Fig 6.3: Comparative *rad9-S Δtop1* Acute CPT Survival Assays



Four colonies of each “back-crossed”-resolved strain were then selected and utilised in comparative acute cell survival assays with camptothecin.

[Acute cell survival assays were performed as per the methodology described in Chapter 2, Section 2.9.2.2(ii), pp.239-241]

6.2 Component G2-M Cell Cycle Checkpoint Pathway Inputs

The full-length Rad9 protein interacts with the proteins Rad1 and Hus1 to form the associative heterotrimeric toroidal PCNA-like DNA sliding-clamp “9-1-1” complex which functions as both an initial DNA damage sensor and recruitment platform for a variety of other interactive proteins involved in DNA damage/repair response pathways – in which the C-terminal domain of the Rad9 protrudes out from the “9-1-1” complex, contains ATM and ATR kinase target motifs and participates in a variety of kinase/phosphatase-mediated transitional protein-protein allosteric regulatory interactions which alter the activity of particular proteins respectively.

[The “9-1-1” complex is loaded onto RPA protein-coated single-stranded sites of DNA damage via the loading complex comprised of the proteins Rad17 and the RFC sub-units Rfc2, Rfc3, Rfc4 and Rfc5 respectively]

A. priori two critical determinant checkpoint response pathways are initially triggered, dependent upon the nature and severity of the DNA damage encountered in conjunction with the transitional stage of the cell cycle when DNA damage occurs, with resultant downstream activation of complex signalling cascades – comprised of various interactive proteins in the form of damage sensors, mediators, primary transducers, secondary transducers and effectors which cumulatively result in paused cell cycle delay and/or DNA damage repair or programmed cell death (apoptosis) .

The ATR pathway is activated in response to camptothecin-induced disruption of DNA replication fork progression in the cell cycle S-phase - in which ATR co-functional associative recruitment with ATRIP results in subsequent formation of the ATR/ATRIP complex leads to activation of Chk2 which phosphorylates and thereby inactivates cyclin Cdc25 phosphatases with consequential downstream inactivation of Cdk/Cyclin complexes with induction of cell cycle arrest and/or DNA repair.

The overall biochemical functional objective of the ATR pathway is the “safe-guarded” prevention of catastrophic mitotic cytological events, as a consequence of inaccurate and/or incomplete DNA replication during the cell cycle S phase, via induction of high fidelity homologous recombination DNA repair pathways.

[Equivalent functional homologue proteins in the experimental *S.pombe* eukaryotic model system are Rad3/Rad26, Cds1, Cdc25 and Cdc2/cyclinB – Fig 6.4, p.492]

The ATM pathway may also be activated in response to camptothecin-induced double-stranded DNA breaks in the cell cycle S phase – with consequential activation of Chk2-triggered proteasome-mediated degradation of Cdc25A accompanied by resultant downstream perturbation of active cyclin/Cdk2 complexes and thus inhibited DNA synthesis respectively.

[Equivalent functional homologue proteins in the experimental *S. pombe* eukaryotic model system are Tel1, Cds1, Cdc25 and Cdc2/cyclin respectively]

Since the “Cre-Lox”–engineered truncated “Rad9-S” protein variant (N Δ 49-Rad9-c3xHA) retains the Rad1- and Hus1- interacting domains (Chapter 5, Section 5.2, pp.442-454; Fig 5.1, p.446), it was speculated that formation of an alternative “Rad9-S”:Hus1:Rad1 type heterotrimeric complex may function in a similar manner to that of the canonical Rad9-Rad1-Hus1 heterotrimeric complex with regard to mediation of a G2/M type phasic cell cycle checkpoint signal arrest response to camptothecin-induced DNA damage (Fig 6.4, p.492).

In order to test this hypothetical postulation, the *N149-rad9-c3xHA S. pombe* strain was cross-mated with various single deleted/inactivated G2/M-associated checkpoint type gene deleted/inactivated type *S. pombe* strains $\Delta rad1$, $\Delta hus1$, $\Delta rad17$, $\Delta rad3$, $\Delta rad26$, $\Delta tel1$ *rad4.116* (temperature sensitive gene inactive mutant), $\Delta crb2$, $\Delta mrc1$, $\Delta chk1$, $\Delta cds1$, *cds1-(T8A;T11A)* (autophosphorylation site-inactivated Cds1 kinase mutant), *cdc25.22* (temperature sensitive gene inactive mutant) and $\Delta rad24$ (Fig 6.4, p.492).

These generated *N149-rad9-c3xHA* “checkpoint gene knock-out double-mutant” strains were then utilised in comparative acute camptothecin cell survival assays in order to determine which G2/M checkpoint-associated proteins were likely to be implicated in the observed “Rad9-S” partial resistance signal response to camptothecin-induced DNA damage.

The acquired experimental data and summarised inferences are discussed within Sections 6.2.1-6.2.6, pp.493-555.

Fig 6.4: Overview of the *S. pombe* G2/M Checkpoint Pathway

[Compiled via Collated Information From: Christmann M. *et al*, 2003;

Collura A. *et al*, 2005

Ellison V. and Stillman B., 2003;

Furuya K. and Carr A.M., 2003;

Harrison J.C. and Haber J.E., 2006;

Lieberman H.B. *et al*, 1996;

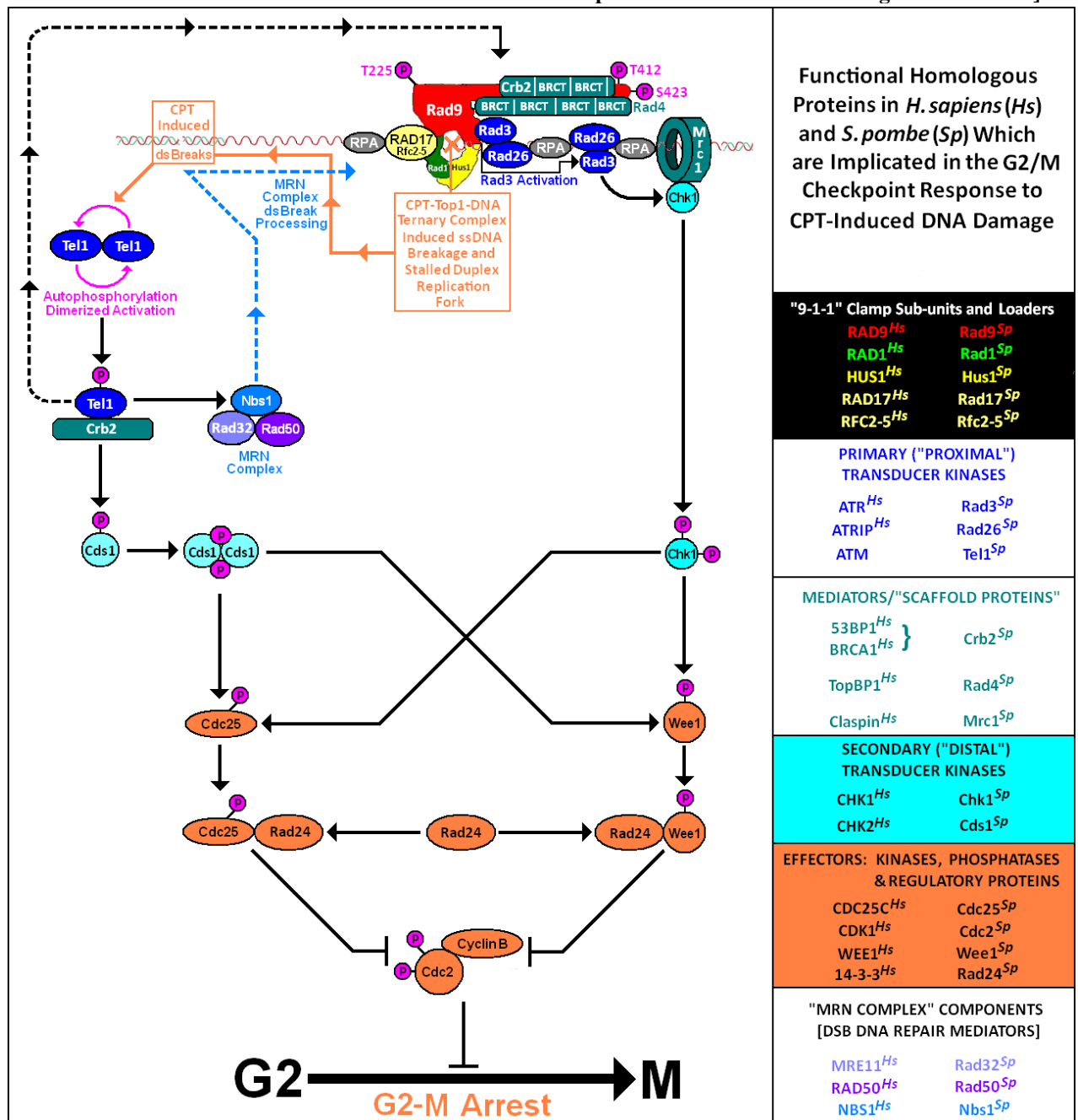
Melo J. and Toczyski D., 2002;

Niida H. and Nakanishi M., 2006;

Nyberg K.A. *et al*, 2002;

Volkmer E. and Karnitz L., 1998

<http://www-rfc.usc.edu/~forsburg/cclecture.html>]



Homologous proteins, which perform equivalent functions within the *S. pombe* G2/M checkpoint pathway, are indicated (the mammalian G2/M checkpoint was discussed in detail previously in Chapter 1, Section 1.2.2, p.59).

6.2.1 Hus1 is a Critical Clamp Protein Sub-Unit Component of the “Rad9-S”–Mediated Checkpoint Response to Camptothecin-Induced DNA Damage, in Which Rad1 and Rad17 are Not Implicated

In silico comparative model mapping of the full-length *S. pombe* Rad9 protein onto the X-ray crystallographically-resolved human Rad9-Rad1-Hus1 heterotrimeric DNA sliding-clamp complex structure (Doré A.S. *et al.*, 2009; PDB file I.D.: 3G65) indicated that the “cre-lox”–engineered “Rad9-S” truncated protein variant (NΔ49-Rad9-c3xHA) may retain the capability to associate with the Rad1 and Hus1 sub-units to form an alternative, functional “Rad9-S”:Rad1:Hus1 heterotrimeric complex (discussed in detail previously in Chapter 5, Section 5.5, pp.471-481).

On the basis of these *in silico* data predictions, it was postulated that the alternative heterotrimeric Rad9-S:Rad1:Hus1 toroidal complex may be loaded onto localised sites of DNA damage within the chromatin, via the Rad17:Rfc2-5 clamp-loader complex and initiate checkpoint arrest and/or DNA repair responses to camptothecin-top1-DNA complex- induced stalled replication forks and double-stranded breaks (Fig 6.1, p.484).

In order to test this hypothesis, comparative acute cell survival assays were performed with YEA broth cultures of the “double-mutant” *S. pombe* strains *NΔ49-rad9-c3xHA Δrad1*, *NΔ49-rad9-c3xHA Δhus1* and *NΔ49-rad9-c3xHA Δrad17* which were incubated at 30°C in the presence of 40μM camptothecin (CPT) – Fig 6.5, p.505.

The acquired experimental data revealed that deletion of *rad1* within an exclusively expressed “Rad9-S” genetic background had no effect on the cytotoxic sensitivity of the cells to CPT-induced genotoxicity – indicative that the Rad1 protein was not implicated in the “Rad9-S” mediated checkpoint signalling response to CPT-induced DNA damage (Fig 6.5A, p.505).

The *NΔ49-rad9-c3xHA Δrad17* “double-mutant” *S. pombe* strain exhibited hypersensitivity to camptothecin and was more sensitive to CPT-induced genotoxicity than either the “Rad9-S” (*NΔ49-rad9-c3xHA*) or the *Δrad17* single mutant *S. pombe* strains (Fig 6.5C, p.505) which was indicative that the truncated “Rad9-S” protein variant and the Rad17 clamp-loader complex subunit protein probably function in separate parallel checkpoint signalling pathways.

Whilst deletion of *hus1* within an exclusively expressed “Rad9-S” genetic background enhanced the cytotoxic sensitivity of the cells to CPT-induced genotoxicity (Fig 6.5B, p.505) – indicative that the Hus1 protein was implicated in the “Rad9-S” mediated checkpoint signalling response to CPT-induced DNA damage.

Comparative Western blot analyses performed on TCA-precipitated total protein extracts acquired from 30°C YEA broth cell cultures of the *S. pombe* strains *hus1-c13xMyc*, *rad9-c3xHA hus1-c13xMyc* and *rad9-(M50L)-c3xHA hus1-c13xMyc*, probed with the anti-Myc primary antibody, confirmed previous experimental observations that the *S. pombe* Hus1 protein exists in 4 main isoforms – termed “Hus1-A”, “Hus1-B”, “Hus1-C” and “Hus1-D” (Fig 6.6A, pp.506-507), as reported by Caspari T. *et al.*, 2000b.

These could originate from alternative translational expression of the *hus1* gene, which contains 5 potential AUG initiation-site methionine codons (Fig 6.6B, pp.506-507), possibly with post-translational phosphorylation, sumoylation and/or ubiquitylation type isoformic modifications.

Comparative Western blot analyses of TCA-precipitated total protein extracts prepared from 30°C YEA broth cell cultures of the *S. pombe* strains *NΔ49-rad9-c3xHA hus1-c13xMyc* and *NΔ73-rad9-c3xHA hus1-c13xMyc* double-mutant *S. pombe* strains, probed with the anti-Myc primary antibody, revealed a notable absence of expressed “Hus1-C” isoform in the case of the *NΔ73-rad9-c3xHA hus1-c13xMyc* protein sample (Fig 6.6A, p.506-507).

Two additional Hus1 protein bands were also detected in the prepared total protein extracts from the *NΔ49-rad9-c3xHA hus1-c13xMyc* and *NΔ73-rad9-c3xHA hus1-c13xMyc* double-mutant *S. pombe* strains, which may be indicative of discrete non-phosphorylated and limited-phosphorylation isoforms of the “Hus1-C” protein isoform – in which case the “Hus1-C” isoform band detected in the all analysed protein samples, with the notable exception of *NΔ73-rad9-c3xHA hus1-c13xMyc*, could be a hyperphosphorylated post-translational modification variant of the “Hus1-C” isoform (Fig 6.6A, pp.506-507).

Consistent with this hypothesis, comparative *in silico* sequence alignment analyses (performed with the on-line software tools EMBOSS and JEMBOSS) also identified a potential tyrosine kinase target motif (identified via comparative analyses performed with the on-line NetPhos software tools) of significant homology in both the “Rad9-S” and “Hus1-C” protein isoforms (Fig 6.6C, pp.506-507).

An alternative possibility is that these smaller bands are proteolytic degradation products of the “Hus1-C” isoform – which may be relatively unstable in its free, un-complexed form (which is stabilised in complex-association with the full-length Rad9 protein and/or “Rad9-S” truncated protein variant) – Fig 6.6A, pp.506-507.

In this hypothetical context, *S. pombe* cells which were “cre-lox”-engineered for the exclusive expression of the *NΔ73-Rad9-c3xHA* (“M74”/“Rad9-VS”) truncated protein variant may have suppressed levels of the “Hus1-C” isoform as a consequence of the fact that “Rad9-VS” lacks the M50-M74 DNA-binding domain which prevents assembly of a “Rad9-VS”：“Hus1-C”-DNA complex and thus results in the predominant expression of the free, unbound form of the “Hus1-C” protein isoform which may be relatively unstable and rapidly targeted for sumoylation- and/or ubiquitylation- post-translational modification-mediated proteasomal degradation.

Comparative Western Blot analyses of HPLC-SEC fractionated samples of soluble total protein extracts acquired from 30°C YEA broth cell cultures of the *S. pombe* strains *rad9- c3xHA hus1-c13xMyc* and *N-Δ49-rad9-c3xHA (“rad9-S-c3xHA) hus1-c13xMyc*, which utilised either the anti-HA or anti-Myc primary anti-body probes indicated distinctively different protein complex fractionation profiles (Fig 6.7A, p.508).

Detected full-length Rad9-c3xHA protein bands in fractions 11-13 correlated with the mass of the canonical Rad9-Rad1-Hus1 heterotrimeric complex, whilst no NΔ49-Rad9-c3xHA protein bands were detected in these eluted fractions – indicative that the “Rad9-S” truncated protein variant was unlikely to form an alternative “Rad9-S”:Rad1-Hus1 complex (Fig 6.7A, p.508).

Both the “Rad9-S” truncated protein variant and the “Hus1-C” protein isoform were detected in fraction 8, whilst neither the full-length Rad9 protein or Hus1 protein isoforms were present in this fraction – indicative that “Rad9-S” and the “Hus1-C” isoform may form part of a distinctive high molecular weight complex (~700 kDa) – Fig 6.7A, p.508.

Both the “Rad9-S” truncated protein variant and “Hus1-C” isoform were also detected in both anti-HA and anti-Myc anti-body probe-primed comparative co-immunoprecipitation “pull-down” analyses performed with a total soluble protein extract acquired from the 30°C YEA broth cell culture of the *S. pombe N-Δ49-rad9-c3xHA hus1-c13xMyc* strain, which may be indicative of an associative interaction between both proteins (Fig 6.7B, p.508).

In silico analytical predictions also revealed that the “Rad9-S” truncated protein variant would contain the M50 – M74 DNA binding domain identified in this work (discussed previously in Chapter 5, Section 5.5, pp.471-481), whilst the *S. pombe* Hus1 sub-unit may contain a nucleobase-binding pocket functionally homologous to that identified within the human Hus1 sub-unit (Doré *et al.*, 2009) – Fig 6.8, p.509.

Both human Rad9 and Hus1, but not Rad1, proteins also contain PIP (PCNA-interacting protein) box motif binding sites (Doré A.S. *et al*, 2009), which may be implicated in the associative “9-1-1” complex-mediated recruitment of various repair factors and checkpoint proteins that possess these motifs to localised DNA damage lesion sites within the chromatin (Fig 6.8, 509).

Taken together, these experimental data indicated that the truncated “Rad9-S” protein variant may associate with the “Hus1-C” isoform to form a novel “open-ring”/“C-clamp” type heterodimeric “Rad9-S”：“Hus1-C” complex, that acts outside of the canonical full-length Rad9-Rad1-Hus1 heterotrimeric DNA sliding clamp.

This “Rad9-S”：“Hus1-C” heterodimeric clamp may be able to detect and bind directly to localised sites of DNA damage within chromatin, independently of the Rad17:Rfc2-5 clamp-loader complex, after which the complex may engage with specific checkpoint signalling proteins and possibly DNA repair factors in response to camptothecin-induced genotoxicity.

In silico comparative modelling of the postulated *S. pombe* heterodimeric “Rad9-S”：“Hus1-C” “open-ring/C-clamp” complex, identified potential homologous functionally-equivalent PIP-box binding motifs in both of the respective sub-units and a potential homologous functionally-equivalent nucleobase-binding pocket within the “Hus1-C” sub-unit (Fig 6.8, p.509).

These *in silico* data analyses also indicated that the leucine residue at residue position 196 may be critical for stabilisation of the “Rad9-S”：“Hus1-C” interface and also identified three tyrosine residues (via analyses with the NetPhos software tools) whose transient post-translational phosphorylation and/or dephosphorylation may be implicated in the regulation of the functional activities of the heterodimeric complex – notably; ⁶¹Y and ¹¹¹Y within the Rad9 sub-unit and ⁶²Y within the Hus1 sub-unit (Fig 6.8, p.509).

Comparative acute cell survival assays were performed on YEA broth cultures of the experimental *S. pombe* strains which were “Cre-Lox”–engineered for the expression of L196P site-directed mutagenised variants of the full-length Rad9 proteins Rad9-(L196P)-c3xHA and Rad9-M50L-(L196P)-c3xHA and the truncated “Rad9-S” protein variant NΔ49-Rad9-(L196P)-c3xHA incubated at 30°C in the presence of 40μM camptothecin(CPT) or 10mM hydroxyurea (HU).

Site-directed mutagenic substitution of leucine for proline (a cyclic imino acid which acts as a steric supramolecular structural “helix-breaker” within the *S. pombe* Rad9 protein) results in the functional perturbation of Rad9:Hus1-type associative interactions at the N-C interface (Fig 6.8, p.509)

The acute hydroxyurea (HU) survival assay data indicated that all three “L196P” mutant strains exhibited enhanced cytotoxic sensitivity to HU-induced inhibition of deoxyribonucleotide synthesis (Fig 6.9B, p.510).

The acute camptothecin survival assay data revealed that the full-length Rad9 “L196P” and “M50L;L196P” mutant strains exhibited enhanced cytotoxic sensitivity to CPT-induced DNA damage, whilst the truncated “Rad9-S-L147P” mutant strain exhibited enhanced resistance to CPT-induced genotoxicity – indicative that the postulated “Rad9-S”：“Hus1-C” “open-ring/C-clamp” complex may function as a negative regulator of a particular DNA damage checkpoint response to CPT-induced perturbation of DNA replication (Fig 6.9A, p.510).

Comparative 2D PAGE-coupled Western blot analyses of TCA-precipitated total protein extracts acquired from 30°C YEA broth cell cultures of the NΔ49-rad9-c3xHA, *S. pombe* strains revealed that the *tell*-deleted phosphoisoform profile is identical to that of the L196P site-directed mutagenized phosphoisoform profile, whilst the identical *hus1*-deleted and hydroxyurea-treatment phosphoisoform profiles are hyper-phosphorylation-shifted nearer to the anode (Fig 6.9D, p.510).

Both the *tell1*-deleted and *L196P* site-mutagenised strains were also camptothecin-resistant – indicative that both the Tel1 kinase and the free form of the truncated “Rad9-S” protein variant may be implicated in a separate Hus1-independent signalling pathway (Fig 6.9A and Fig 6.9C, p.510).

Comparative acute cell survival assays performed with YEA broth cultures of the indicated “cre-lox”-engineered *S. pombe* strains in the presence of 40µM camptothecin revealed that the *NΔ49-rad9-(T52A)-c3xHA* a similar degree of partial resistance to CPT-induced DNA damage, in contrast to the *NΔ49-rad9-(Y61F)-c3xHA* and *NΔ49-rad9-(T52A;Y61F)-c3xHA* cells which exhibited enhanced resistance to the genotoxic effects of camptothecin (Fig 6.10B, p.511).

Comparative 2D PAGE-coupled Western blot analyses of TCA total protein extracts, prepared from 30°C YEA broth cultures of the *S. pombe* strains *NΔ49-rad9(Y61F)-c3xHA* and *NΔ49-rad9(Y111F)-c3xHA* also indicated distinctive hypophosphorylation shift patterns within the “rad9-S” phosphoisoformic profile – thus providing biochemical evidence that these tyrosines are phosphorylated within this truncated protein variant (Fig 6.10D, p.511).

The un-phosphorylated form of the Tyrosine 61 residue, situated within the M50-M74 domain, may facilitate stronger associative binding of the Rad9 and/or “Rad9-S” proteins to DNA via intercalative Π - Π electron-stacking aromatic ring type interactions of Y61 with the duplex nucleobases (discussed in detail previously in Chapter 5, Section 5.5, pp.471-481).

Comparative acute cell survival assays revealed that the *NΔ49-rad9(Y111F)-c3xHA S. pombe* strain exhibited significantly higher cytotoxic sensitivity to CPT-induced DNA damage than the *NΔ49-rad9-c3xHA* strain – indicative that phosphorylation of the Y111 residue is critical to the functional activity of the “Rad9-S” protein (Fig 6.10C, p.511).

Kinase-mediated phosphorylation of the Y111 residue, which is situated in close proximity to the M50-M74 DNA-binding domain (Fig 6.6A and Fig 6.6B, p.506; Fig 6.8, p.509), may induce supramolecular configurational changes within the “Rad9-S” protein which facilitate and/or stabilise associative engagement of the M50-M74 domain with the duplex.

In silico predictive phosphorylation propensity analyses of the *S. pombe* Rad9^{61Y} and ^{111Y} and Hus1^{62Y}, performed via utilisation of the NetPhos2.0 and NetPhosK bioinformatics software tools, indicated that these three residues had significant phosphorylation probability scores and may be substrate targets of the Mph1 kinase (Fig 6.11A, p.512).

Comparative HPLC-SEC fractionation-coupled Western blot analyses, performed on total soluble protein extract samples, acquired from 30°C YEA broth cell cultures of the *S. pombe* strains *rad9-S-c3xHA mph1-c13xmyc* and *rad9-S-c3xHA hus1-c13xmyc*, detected the presence of “Rad9-S”, “Hus1-C” and Mph1 proteins in fraction 9 (Fig 6.11B, p.512).

Taken together, these experimental data indicate that specific transient differential Mph1 kinase-mediated post-translational phosphorylation modifications of the “Rad9-S” and “Hus1-C” subunits may be implicated in the regulation of the functional activities of the heterodimeric “Rad9-S”：“Hus1-C” “open-ring/C-clamp” complex.

Comparative Western blot assays performed with total soluble extract protein supernatant (cytosolic) and pellet (nuclear) fractions, acquired from YEA broth cultures incubated at 30°C in the absence or presence of 40µM camptothecin for 30 minutes or incubated at 37°C for 30 minutes, indicated that translocation of the “Rad9-S” protein variant from the cytosol to the nucleus occurred under conditions of induced heat shock (37°C) or CPT-induced DNA damage (Fig 6.12, p.513) .

Intriguingly, these data indicated that under hyperthermic conditions the unphosphorylated form of the truncated “Rad9-S” protein variant was translocated to the nucleus, in contrast with the nuclear translocation of the phosphorylated form of “Rad9-S” under conditions of camptothecin-induced DNA damage (Fig 6.12, p.513) and thus constituted supportive experimental evidence for differential checkpoint signalling pathways that may be mediated by the protein in response to specific types of genotoxic and/or environmental stresses which may impinge adversely on various biochemical processes implicated in the cytological maintenance of genomic integrity.

The experimental data also revealed that perturbation of the “Rad9-S”：“Hus1-C” interactions, via site-directed L147P or Y62F mutagenesis within the truncated Rad9-S protein variant, deletion of *hus1* within an exclusively expressed “*rad9-S*”-*c3xHA* genetic background or a functional loss of the M50-M74 DNA-binding domain (in the case of the truncated protein variant N Δ 73-Rad9-*c3xHA* = “Rad9-VS”) inhibited translocation of the protein into the nucleus (Fig 6.12, p.513).

Surprisingly, deletion of *rad17* within an exclusively expressed “*rad9-S*”-*c3xHA* genetic background was also found to inhibit translocation of the protein into the nucleus (Fig 6.12, p.513), which was unexpected in the context of the comparative acute survival assay data which indicated that *rad17* and *rad9-S* most likely function in separate parallel pathways in response to camptothecin-induced DNA damage (discussed previously on p.494).

Furthermore, comparative 2D PAGE-coupled Western blot analyses indicated that deletion of *rad17* within an exclusively expressed “*rad9-S*”-*c3xHA* genetic background resulted in the loss of several “*rad9-S*”-*c3xHA* phosphoisoforms, which may be indicative that Rad17 stabilises associative kinase interactions with the heterodimeric “Rad9-S”：“Hus1-C” open ring/C-clamp complex. (Fig 6.11D, p.512)

These contradictory experimental observations may be explained by the fact that three of the Rad17:(Rfc2-5) clamp-loader complex sub-units (Rfc2, Rfc3 and Rfc4) associate with the Hus1 sub-unit (Fig 6.14B, p.515) such that whilst the Rad17 protein may not be implicated in the “Rad9-S”-mediated checkpoint signalling response to camptothecin-induced DNA damage, it may be required to stabilise the Hus1 protein and/or its isoforms to enable the cytosolic formation and translocation of the heterodimeric “Rad9-S”-“Hus1-C” “open-ring/C-clamp” to the nucleus.

Comparative 2D-PAGE analyses of un-treated and alkaline phosphatase-treated soluble protein supernatant extracts (cytosolic protein localisation) indicate only very subtle changes in the phosphoisoform patterns of the truncated “Rad9-S” protein variant in response to CPT-induced DNA damage (Fig 6.13A, p.514).

Comparative 2D PAGE-coupled Western blot analyses of the total soluble protein extract pellet fractions (nuclear protein localisation) indicate that the hyperphosphorylated form of the truncated “Rad9-S” is exclusively retained in the nucleus in both the absence and present of CPT-induced DNA damage (Fig 6.13B, p.514).

The 2D PAGE-coupled Western blot data also indicate that expression of the “Rad9-VS” variant is suppressed in response to CPT-induced DNA damage but induced in the absence of CPT-induced DNA damage and retained exclusively in the nucleus – which may indicate that the truncated “Rad9-VS” protein variant has a regulatory role with regard to suppression of inappropriate “Rad9-S” signalling/functional responses in the absence of CPT-induced DNA damage within the nucleus (discussed previously in detail in Chapter 5, Section 5.5, pp.471-481).

Taking all the experimental data into consideration, a hypothetical model was formulated for the functional roles of the heterodimeric “Rad9-S”：“Hus1-C” “open-ring/C-clamp” complex which may be implicated in novel checkpoint and/or DNA repair pathway responses to camptothecin-induced DNA damage (Fig 6.14A, p.515).

In response to camptothecin-induced genotoxicity, Mph1 and/or other kinase-mediated phosphorylated post-translational modification of the truncated “Rad9-S” protein variant at tyrosine 62 and the “Hus1-C” isoform at tyrosine 62 may induce transient configurational changes within the supramolecular architecture of the two protein sub-units that thermodynamically promote the associative formation of the heterodimeric “Rad9-S”：“Hus1-C” complex (Fig 6.14A, p.515).

The Rad17:(Rfc2-5) complex may have functional roles in both the stabilisation of the “Hus1-C” isoform and/or the heterodimeric “Rad9-S”：“Hus1-C” “open-ring/C-clamp” complex and its translocation to the nucleus (Fig 6.14B, p.515).

The “Rad9-S” M50-M74 DNA-binding and “Hus1-C” nucleobase-binding domains within the heterodimeric “Rad9-S”：“Hus1-C” “open-ring/C-clamp” complex may mediate its duplex association and recognition of the CPT-Top1-DNA ternary complex-stalled replication forks and/or CPT-induced DSBs within the chromatin supramolecular architecture (Fig 6.14A, p.515).

Subsequent phasic cell cycle arrest and repair of the CPT-induced DNA damage lesions is initiated via “Rad9-S”：“Hus1-C” complex-mediated recruitment and/or functional activity modulation of the appropriate proteins that are implicated in the mediation of checkpoint signalling and DNA repair pathways (Fig 6.14A, p.515).

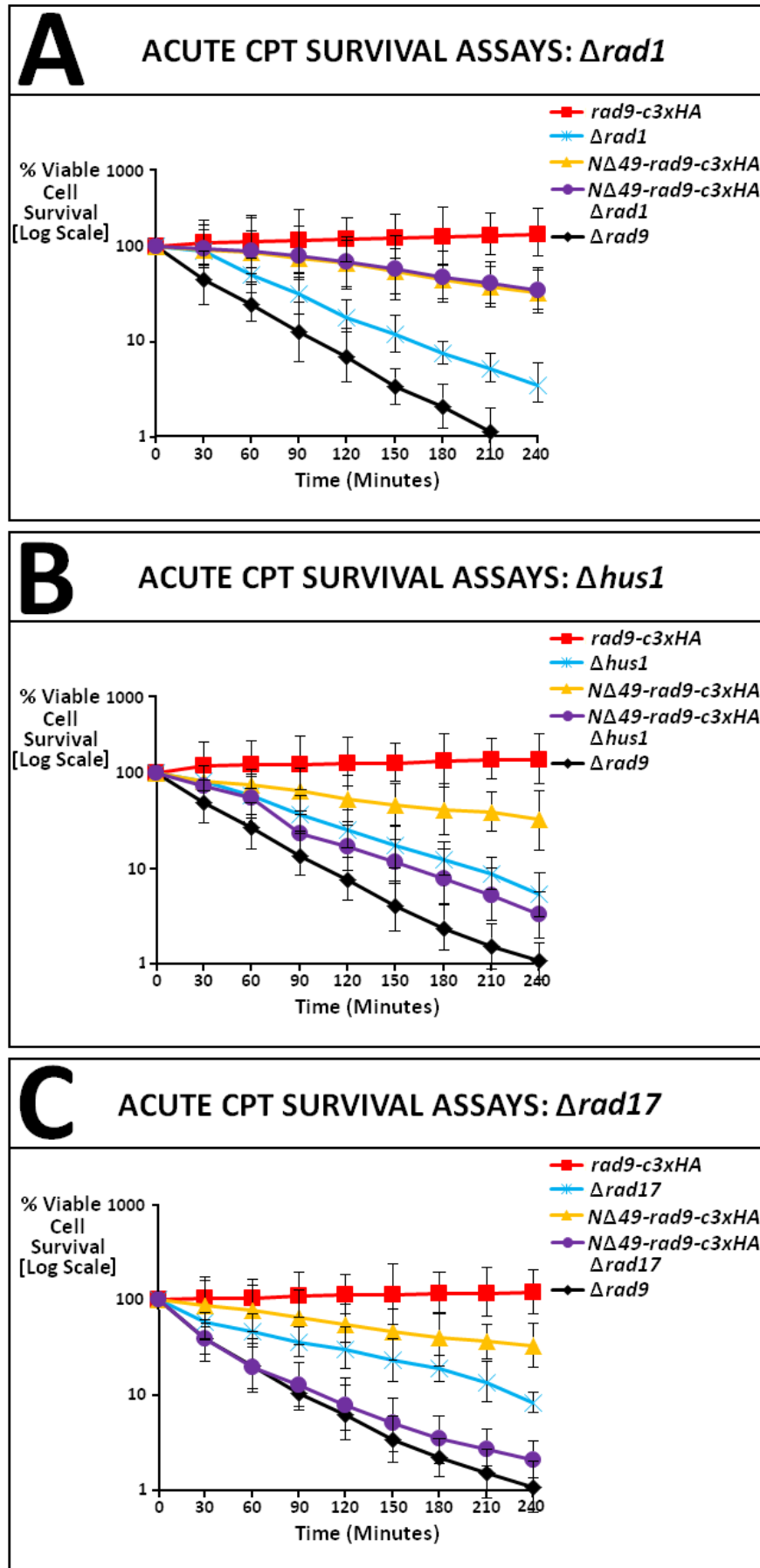
During these processes, Mph1 and/or other other kinase-mediated phosphorylated post-translational modification at tyrosine 12 within the “Rad9-S” sub-unit may induce transient configurational changes within the supramolecular architecture of the heterodimeric Rad9-S :Hus1-C complex which facilitate the access of the repairsome machinery to the CPT-induced DNA damage lesion site to enable rectification of DSBs, stalled replication fork recovery in coordination with secondary checkpoint signalling processes which terminate cell cycle arrest and re-initiate DNA replication (Fig 6.14A, p.515).

These secondary checkpoint signalling processes may also initiate phosphatase-targeted post-translational dephosphorylated modification of phosphotyrosine 62 within the “Rad9-S” sub-unit and phosphotyrosine 62 within the “Hus1-C” sub-unit which induces transient configurational alterations within the supramolecular architecture of the “Rad9-S”：“Hus1-C” heterodimeric complex which promote its dissociation after DNA repair has been accomplished (Fig 6.14A, p.515).

Checkpoint phosphatase post-translational dephosphorylated modification-mediated chromatin dissociation of the heterodimeric “Rad9-S”：“Hus1-C” “open-ring/C-clamp complex” also enables unhindered re-initiation of DNA replication after repairsome-instigated CPT-induced stalled replication fork recovery and rectification of CPT-induced DSBs has been accomplished (Fig 6.14A, p.515).

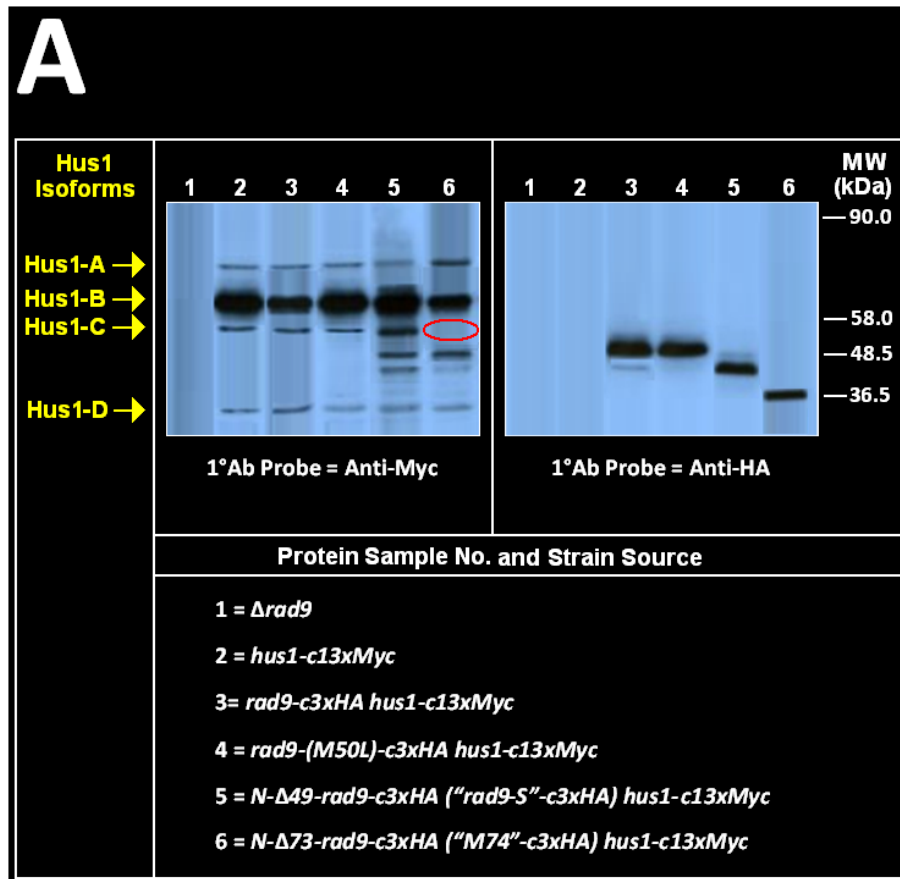
The truncated protein isoform NΔ73-Rad9 (“Rad9-VS”) may regulate these heterodimeric “Rad9-S”：“Hus1-C” complex co-ordinated cell cycle checkpoint arrest, DNA repair, replication fork recovery and re-initiation of DNA repair processes via competing with the “Rad9-S” and “Hus1-C” sub-units for associative interactions with the checkpoint kinases and phosphatases which modify key tyrosine residues within these two proteins to modulate the specific functional activities of the “Rad9-S”：“Hus1-C” “open-ring/C-clamp” (Fig 6.14A, p.515).

Fig 6.5: CPT Survival Assays – Clamp & Clamp-Loader Sub Units



[Acute cell survival assays were performed as per the methodology described in Chapter 2, Section 2.9.2.2(ii), pp.239-241]

Fig 6.6: Comparative Rad9 and Hus1 Isoformic Protein Analyses



B

Intron1

MRFKTRISNLYTLTR|LVQALDKIGRFCWLRLMPE

Intron2 Intron3 62

TVNFBVIVPDFR **M**TQVWS|VLEV|ETIFED **Y**VVQS

46 "Hus1-C"?

NADNVINLEVPIDNFYKALRSAANASDSTVRLSKK

NNQPLLSLSTTWSGRAFGSNIVTHNIPVRVLSQS

YVSVIKEPTAPEPDCHIFLPQLNFLRHVVVDKYKSL

DRII **M**SAN**M**SGELQLSVNIPSARVSTKWKGLN

PELDPSQVEDISRHPSQTRAPEEFVH**M**RLDSKDL

Intron4

VN**M**LKISSVAKRVIA|CFCEGHALVLYVYITDPED

EHTAVLTYTYISTYVD

C

N-Terminus Sequence Alignment

"Hus1-C" IFED **Y**VVQSN 62*0.579

"Rad9-S" FFDK **Y**IFQDP 12*0.894

Figure Legend – Fig 6.6

A: Individual 50mL YEA broth medium cell cultures of the “cre-lox” – constructed *S. pombe* strain *rad9-c3xHA* were incubated at 30°C over a 12 hour time period, then diluted to an optical density $A_{595} = 0.25$ with the appropriate volume of YEA medium and the resultant diluted cultures re-incubated at 30°C for a further time period of ~2.5 hours until they had attained an optical density value of $A_{595} = 0.5$ – after which time the resultant cultures of actively cycling cells were re-incubated at 30°C for a further 30 minutes.

TCA-precipitated total protein extract samples were then prepared from the appropriate *calculated volumetric aliquot of each culture (*equivalent to 10 A_{595} optical density units) of which 20 μ L aliquots were resolved on 10% SDS-PAGE gels which were then utilised in comparative Western blot analyses probed with either the anti-HA primary antibody or the anti-Myc primary antibody.

The red circle indicates the absence of the “Hus1-C” protein isoform, which was not detected in the TCA-precipitated total protein extract acquired from the 30°C YEA culture of the *NA73-rad9-c3xHA S. pombe* strain.

[Protein sample preparation, SDS-PAGE resolution and Western blot methodologies are detailed in Section 2.8.1, pp.200-202; Section 2.8.4, pp.223-224 and Section 2.8.6, pp.231-233]

B: The *S. pombe* Hus1 protein sequence contains 6 potential alternative methionine AUG codon-start translation sites, in addition to the primary AUG codon start-site at methionine 1 (the relative positions of the four introns of the *hus1* gene are indicated via the grey vertical bars).

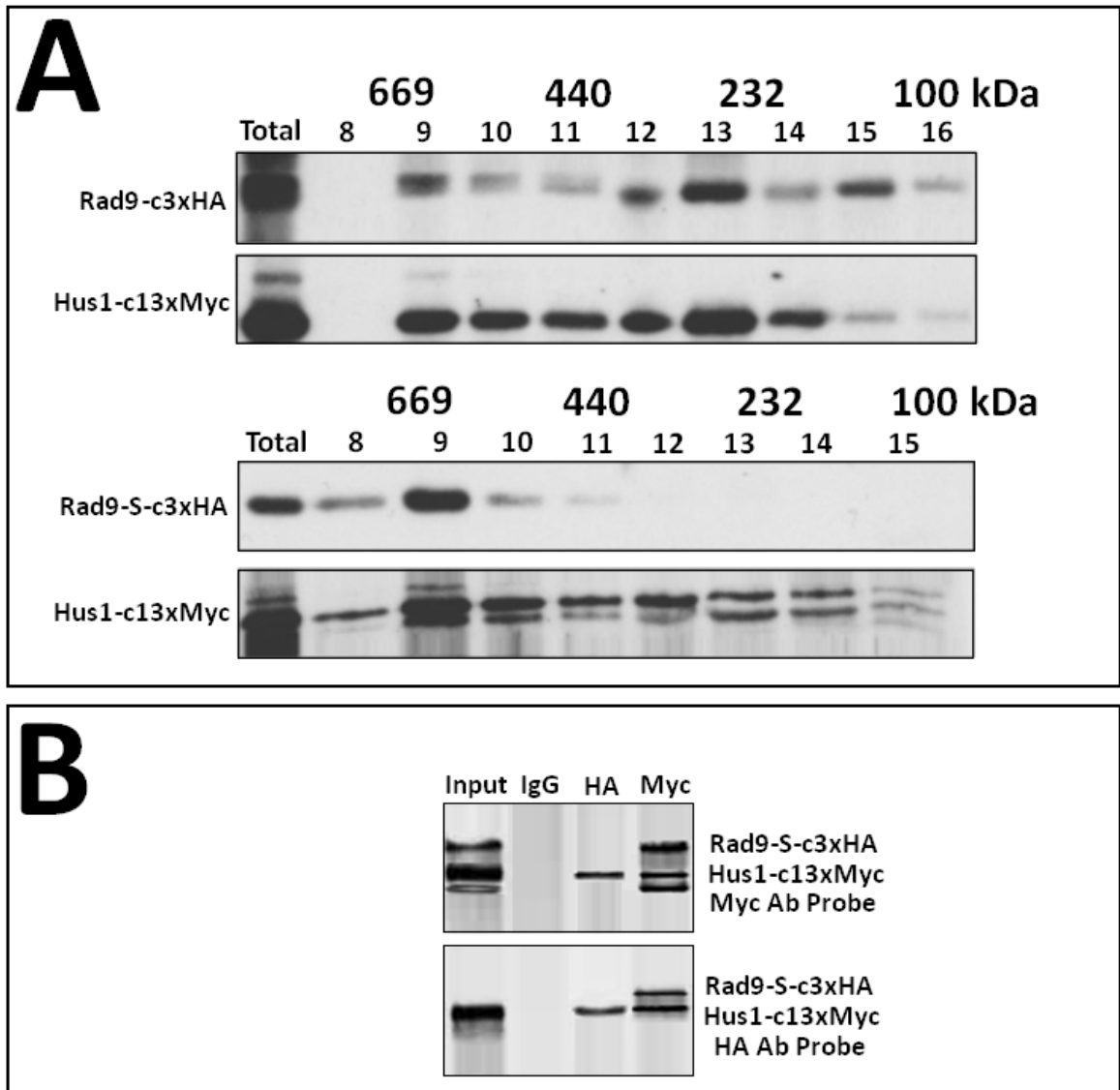
The “Hus1-C” protein isoform is postulated to be an alternative translational product generated via initiated ribosomal scanning at the AUG codon-start site at methionine 46.

C: *In silico* comparative sequence alignment analyses of the *S. pombe* “Rad9-S” and Hus1 proteins, performed via utilisation of the on-line BLAST-PSI, EMBOSS and JEMBOSS bioinformatics software tools

Conserved positional equivalent tyrosines at Y12 within “Rad9-S” truncated protein variant (Y61 in the full-length Rad9 protein) and Y62 within the “Hus1-C” isoform.

In silico predictive phosphorylation propensity analyses of these two tyrosines was performed via utilisation of the on-line software tool Netphos2.0 (probability scores are indicated – values above the 0.5 threshold are significant)

Fig 6.7: Comparative Analyses of “Rad9-S”:Hus1 Interactions



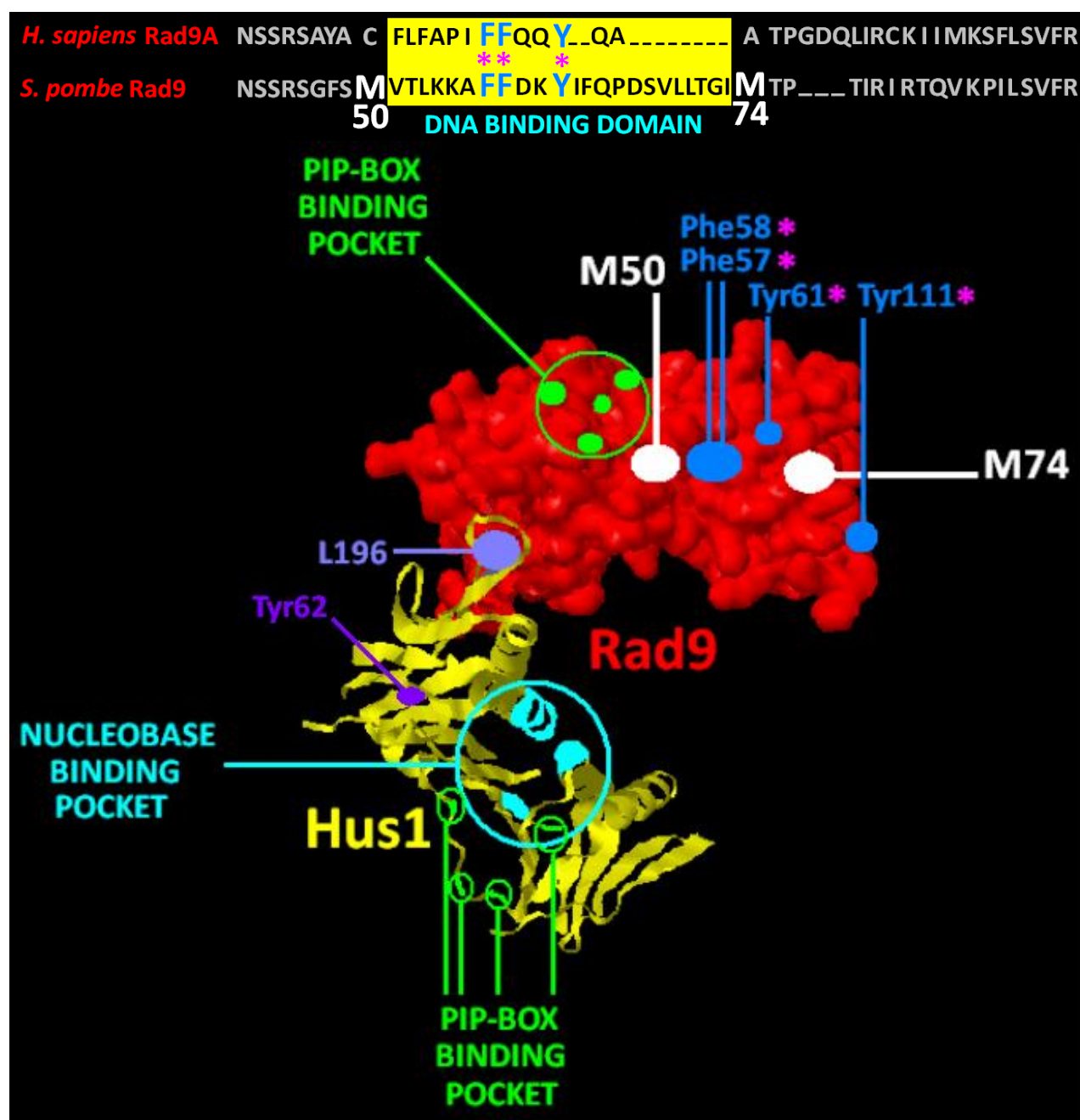
A: Comparative Western blot analyses of HPLC-SEC fractionated samples of soluble total protein extracts acquired from 30°C YEA broth cell cultures of the *S. pombe* strains *rad9-c3xHA hus1-c13xMyc* and *N-Δ49-rad9-c3xHA* (“*rad9-S-c3xHA*”) *hus1-c13xMyc*, probed with the anti-HA and anti-Myc primary anti-bodies.

Note: These data sets were acquired by Ms. Amber Maltby, working under the practical supervision of the author

[Protein sample preparation, HPLC-SEC, SDS-PAGE and Western blot methodologies described in detail previously in Chapter 2, Section 2.8.2, pp.203-205; Section 2.8.2.2, pp.209-210; Section 2.8.4, pp. 223-224 and Section 2.8.6, pp.231-233]

B: Anti-HA and anti-Myc anti-body probe-primed comparative co-immunoprecipitation “pull-down” analyses performed with a total soluble protein extract acquired from a 30°C YEA broth cell culture of the *S. pombe* *N-Δ49-rad9-c3xHA hus1-c13xMyc* strain. [Protein sample preparation, “Pull-Down” Co-IPs, SDS-PAGE and Western blot Methodologies described in detail previously in Chapter 2, Section 2.8.2, pp.203-205; Section 2.8.2.3, pp.211-213; Section 2.8.4, pp. 223-224 and Section 2.8.6, pp.231-233]

Fig 6.8: Functional Domain Map of the “Rad9-S”：“Hus1-C” Complex



In silico comparative sequence alignment analyses of the identified functional M50-M74 domain, situated in the *S. pombe* Rad9 protein, with the Human Rad9A protein, in conjunction with comparative modelling of the X-ray crystallographic-resolved Human Rad9A-Rad1-Hus1 complex – PDB I.D.:3G65 (Doré A.S. *et al.*, 2009) with the heterodimeric “Rad9-S”：“Hus1-C” clamp.

Comparative sequence alignment analyses were performed with the on-line bioinformatics software tools EMBOSS, JEMBOSS and PSI-BLAST.

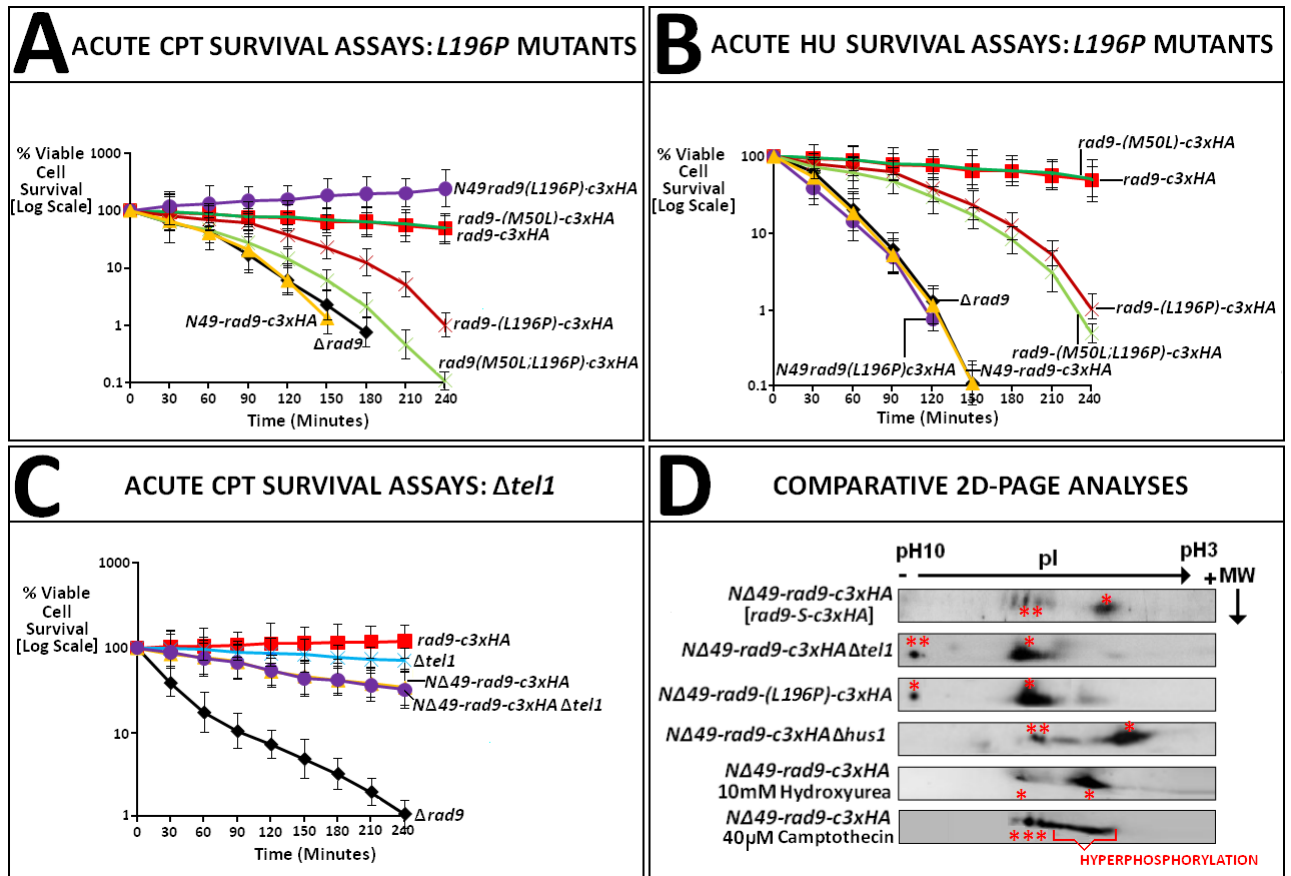
Comparative modelling analyses was performed with the on-line bioinformatics software tool RasMol.

The structural graphic was produced via utilisation of the on-line software tool PolyView3D.

The critical L196 residue within the Rad9:Hus1 N/C associative interface, the residues which are critical to the DNA-binding function of the Rad9 M50 – M74 domain and the critical residues within Hus1 nucleobase binding pocket are indicated.

Potential PIP-box motif-binding site residues and key tyrosine residues identified as potential kinase substrate targets (via sequence analyses with the on-line NetPhos software tools) are also indicated.

Fig 6.9: CPT, HU and 2D-PAGE Assays – “Hus1-Binding” Mutants



A: Comparative acute cell survival assays were performed on YEA broth cultures of the experimental *S. pombe* strains which were “cre-lox”–engineered for the expression of L196P site-directed mutagenised variants of the full-length Rad9 proteins Rad9-(L196P)-c3xHA and Rad9-M50L-(L196P)-c3xHA and the truncated “Rad9-S” protein variant NΔ49-Rad9-(L196P)-c3xHA incubated at 30°C in the presence of 40μM camptothecin (CPT) for a total time period of 4 hours.

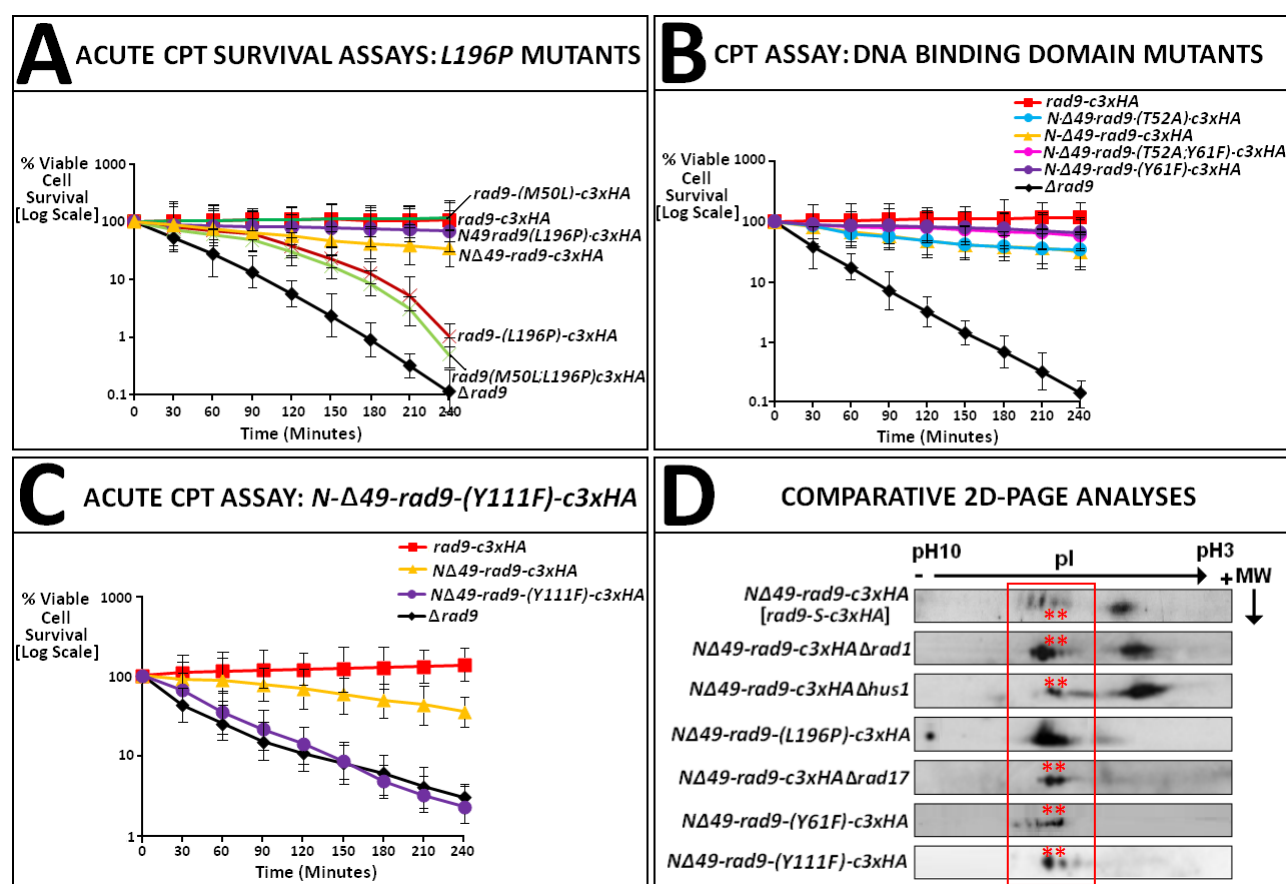
B: Comparative acute cell survival assays were performed on YEA broth cultures of the experimental *S. pombe* strains which were “cre-lox”–engineered for the expression of L196P site-directed mutagenised variants of the full-length Rad9 proteins Rad9-(L196P)-c3xHA and Rad9-M50L-(L196P)-c3xHA and the truncated “Rad9-S” protein variant NΔ49-Rad9-(L196P)-c3xHA incubated at 30°C in the presence of 10mM hydroxyurea (HU) for a total time period of 4 hours.

C: Comparative acute cell survival assays were performed on YEA broth cultures of the indicated *S. pombe* *tel1*-deletion strains, incubated at 30°C in the presence of 40μM camptothecin (CPT) for a total time period of 4 hours.

[Acute cell survival assays were performed as per the methodology described in Chapter 2, Section 2.9.2.2(ii), pp.239-241]

D: Comparative 2D PAGE-coupled Western blot analyses of TCA-precipitated total protein extracts acquired from 30°C YEA broth cell cultures of the indicated *S. pombe* strains (key hyper- and hypo- phosphorylation events are indicated by red asterisks). [Methodologies as described previously in detail in Chapter 2, Section 2.8.3.1, pp.214-217; Section 2.8.5, pp.225-230 and Section 2.8.6, pp.231-233]

Fig 6.10: CPT and 2D-PAGE Assays – “Hus1-Binding” Mutants and “DNA-Binding Phosphorylation Site Knock-Out” Mutants



A: Comparative acute cell survival assays were performed on YEA broth cultures of the experimental *S. pombe* strains which were “cre-lox”–engineered for the expression of L196P site-directed mutagenised variants of the full-length Rad9 proteins Rad9-(L196P)-c3xHA and Rad9-M50L-(L196P)-c3xHA and the truncated “Rad9-S” protein variant NΔ49-Rad9-(L196P)-c3xHA incubated at 30°C in the presence of 40μM camptothecin (CPT).

B: Comparative acute cell survival assays were performed on YEA broth cultures of the indicated *S. pombe* kinase site mutant strains (T52A, Y61F and T52A;Y61F) incubated at 30°C in the presence of 40μM camptothecin (CPT) for a total time period of 4 hours.

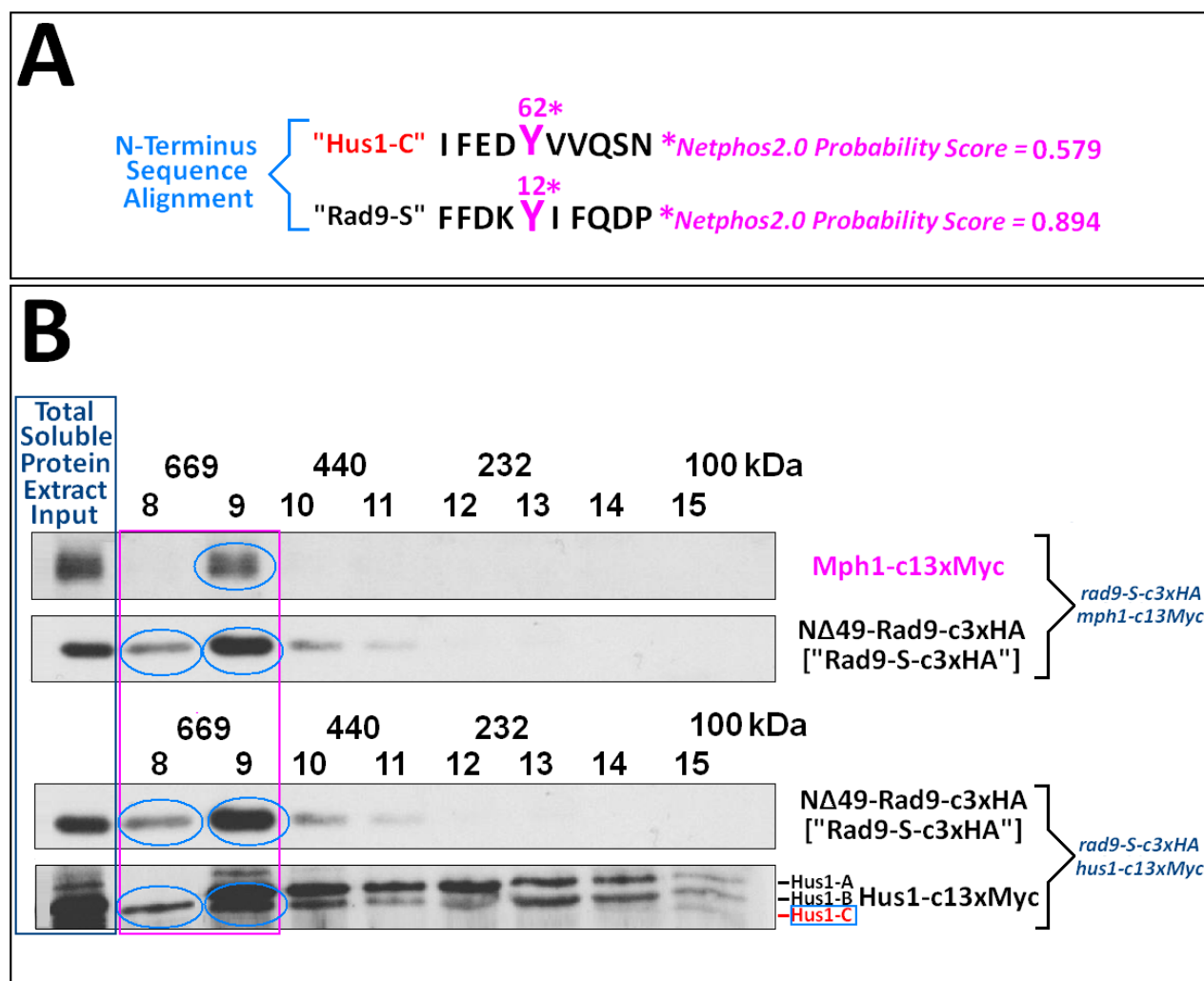
C: Comparative acute cell survival assays were performed on YEA broth cultures of the indicated *S. pombe* kinase site mutant strains (T52A, Y61F and T52A;Y61F) incubated at 30°C in the presence of 40μM camptothecin (CPT) for a total time period of 4 hours.

[Acute cell survival assays were performed as per the methodology described in Chapter 2, Section 2.9.2.2(ii), pp.239-241]

D: Comparative 2D PAGE-coupled Western blot analyses of TCA-precipitated total protein extracts acquired from YEA broth cell cultures of the indicated *S. pombe* strains (conserved “neutral” isoformic species are indicated via the red asterisks within the red box).

[Methodologies as described previously in detail in Chapter 2, Section 2.8.3.1, pp.214-217; Section 2.8.5, pp.225-230 and Section 2.8.6, pp.231-233]

Fig 6.11: Evidence for Novel “Rad9-S”, Hus1-C & Mph1 Interactions



A: *In silico* comparative sequence alignment analyses of the *S. pombe* “Rad9-S” and Hus1 proteins, performed via utilisation of the on-line bioinformatics software tools EMBOSS, JEMBOSS and PSI-BLAST.

Conserved positional equivalent tyrosines at Y12 within “Rad9-S” truncated protein variant (Y61 in the full-length Rad9 protein) and Y62 within the Hus1-C isoform.

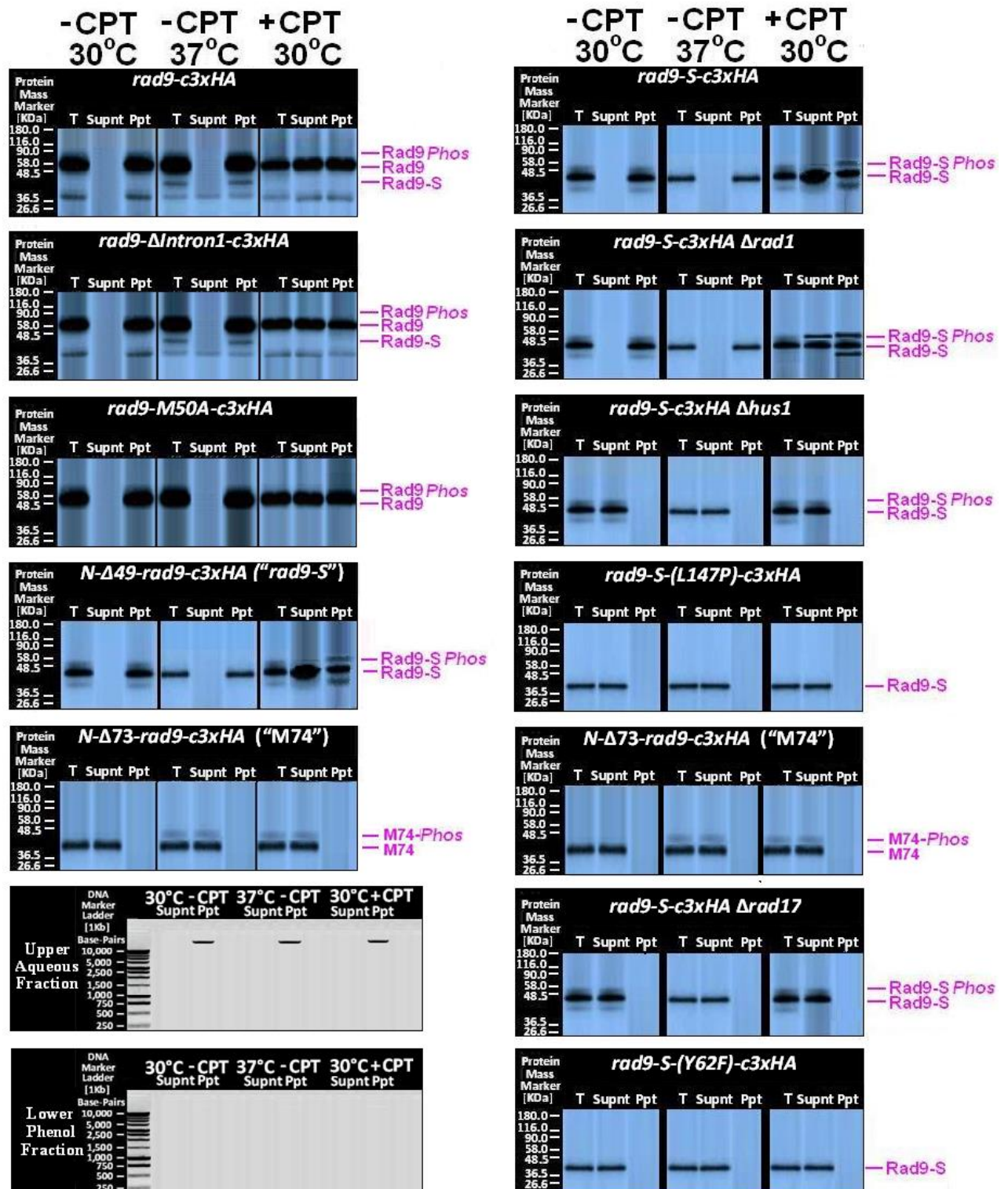
In silico predictive phosphorylation propensity analyses of these two tyrosines was performed via utilisation of the on-line software tool Netphos2.0 (probability scores are indicated – values above the 0.5 threshold are significant).

B: Comparative Western Blot analyses of HPLC-SEC fractionated samples of soluble total protein extracts acquired from 30°C YEA broth cell cultures of the *S. pombe* strains *N-Δ49-rad9-c3xHA* (“*rad9-S-c3xHA*”) *hus1-c13xMyc* and *N-Δ49-rad9-c3xHA mph1-c13xMyc* probed with the anti-HA and anti-Myc primary anti-bodies.

Note: The *rad9-S-c3xHA hus1-c13xMyc* data set was acquired by Ms. Amber Maltby, working under the practical supervision of the author

[Protein sample preparation, HPLC-SEC, SDS-PAGE and Western blot methodologies described in detail previously in Chapter 2, Section 2.8.2, pp.203-205; Section 2.8.2.2, pp.209-210; Section 2.8.4, pp. 223-224 and Section 2.8.6, pp.231-233]

Fig 6.12: Rad9-S Mutant - Comparative Cellular Localisation Assays

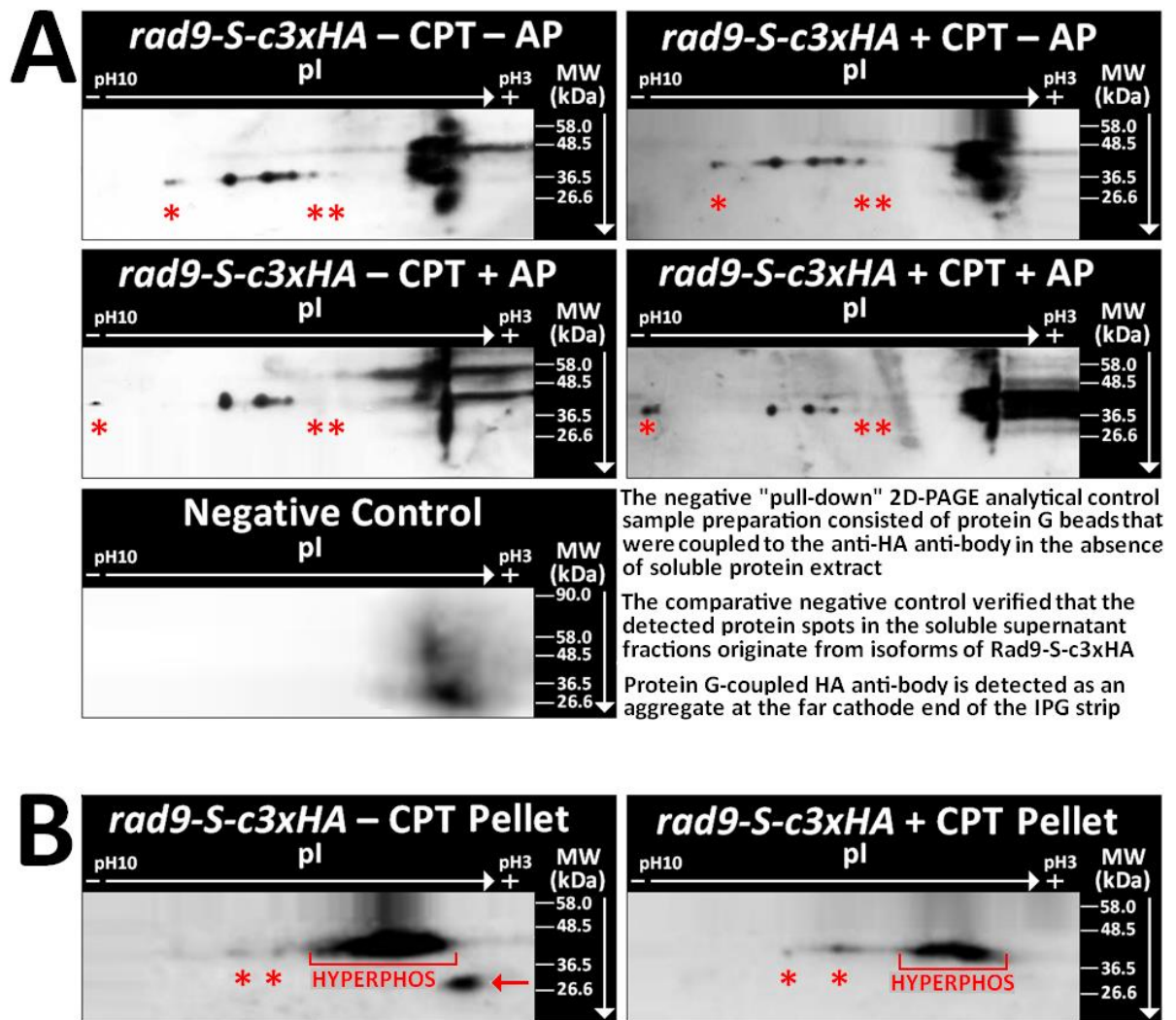


Comparative Western blot assays performed with total soluble extract protein supernatant “supnt” (cytosolic) and “Ppt” pellet (nuclear) fractions acquired from YEA broth cultures incubated at 30°C in the absence or presence of 40μM Camptothecin for 30 minutes or incubated at 37°C for 30 minutes, indicated that translocation of the “Rad9-S” protein variant from the cytosol to the nucleus occurred under conditions of induced heat shock (37°C) or CPT-induced DNA damage .

Precipitated genomic DNA extractions were also performed with the supernatant and pellet fractions and the resultant samples run on 1% 1xTBE agarose gels which contained 0.5μg/mL ethidium bromide) – the data indicate the DNA is only present in the pellet fractions, thus confirming that these are the nucleus-associated protein fractions.

[Methodologies as described in detail previously in Chapter 2 Section 2.8.2, pp.203-305; Section 2.8.2.1, pp.206-208, Section 2.8.4, pp.223-224 and Section 2.8.6, pp.231-233]

Fig 6.13: Differential Phosphoisoformic Localisation of “Rad9-S”



Individual 100mL YEA broth medium cell cultures of the “Cre-Lox” – constructed *NA49-rad9-c3xHA* (“Rad9-S”) *S. pombe* strain were grown overnight (30°C for ~12 hour time period), then diluted to an optical density $A_{595} = 0.25$ with the appropriate volume of YEA medium and the resultant diluted cultures re-incubated at 30°C for a further time period of ~2.5 hours until they had attained an optical density value of $A_{595} = 0.5$, after which time they were incubated for a further 30 minutes at 30°C in the absence or presence of 40 μ M camptothecin.

Soluble total protein extract samples were then prepared from the appropriate *calculated volumetric aliquot of each culture (*equivalent to 40 A_{595} optical density units) and utilised for preparation of untreated and treated alkaline phosphatase-digested 2D-PAGE analyses – as per the methodology described in Chapter 2, Section 2.8.3.2, pp.218-222.

TCA-precipitated total protein extracts were also prepared from the nuclear fraction pellets (treated as per stage ix onwards in the protocol described in Chapter 2, Section 2.8.3.1, pp.215-217), acquired from the initial preparation of the soluble total protein extract supernatant samples, for comparative 2D PAGE-coupled Western blot analyses (methodologies as described in detail previously in Chapter 2, Section 2.8.5, pp.225-230 and Section 2.8.6, pp.231-233)..

A: Comparative 2D PAGE-coupled Western blot analyses of the un-treated and alkaline phosphatase-treated soluble protein supernatant extracts (cytosolic protein localisation).

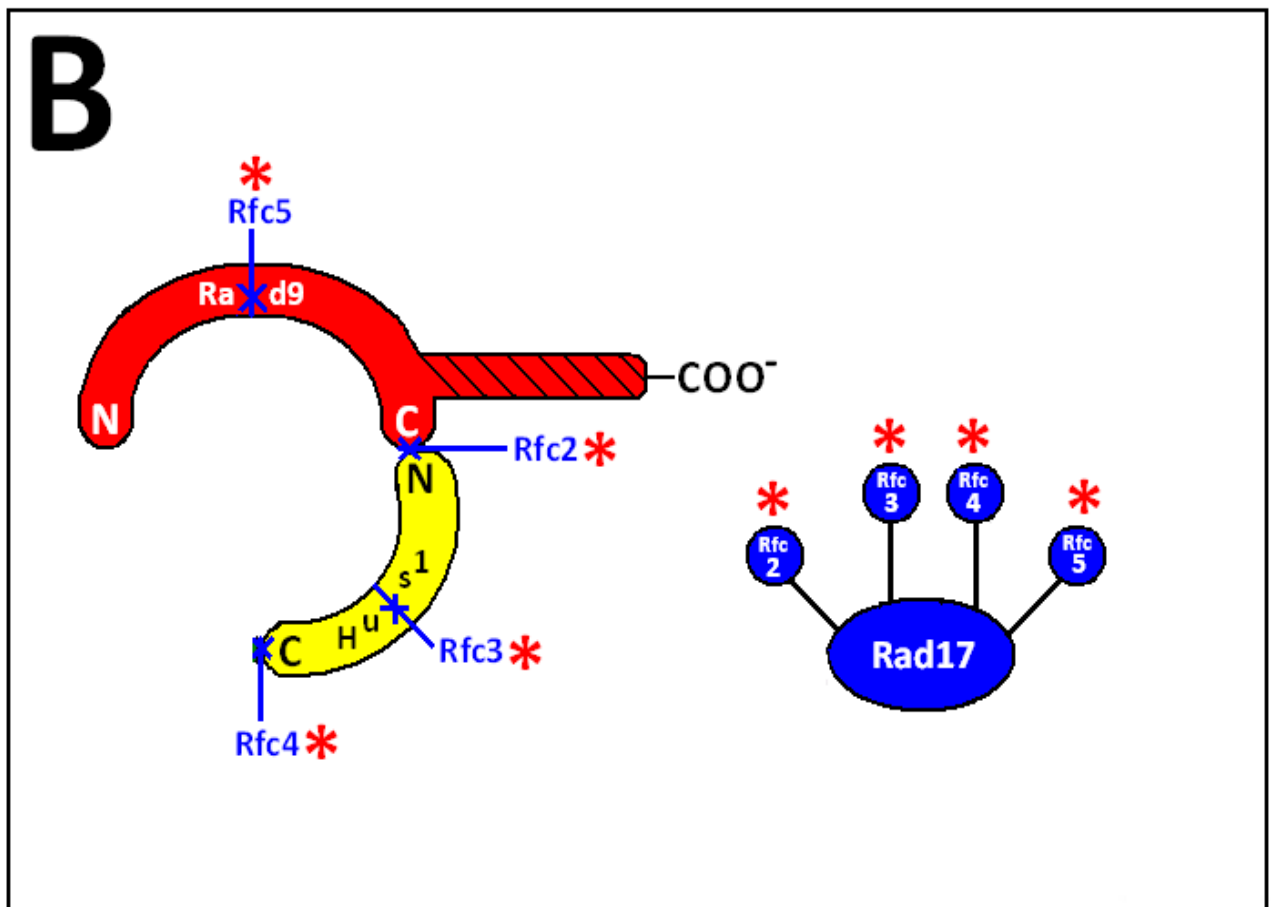
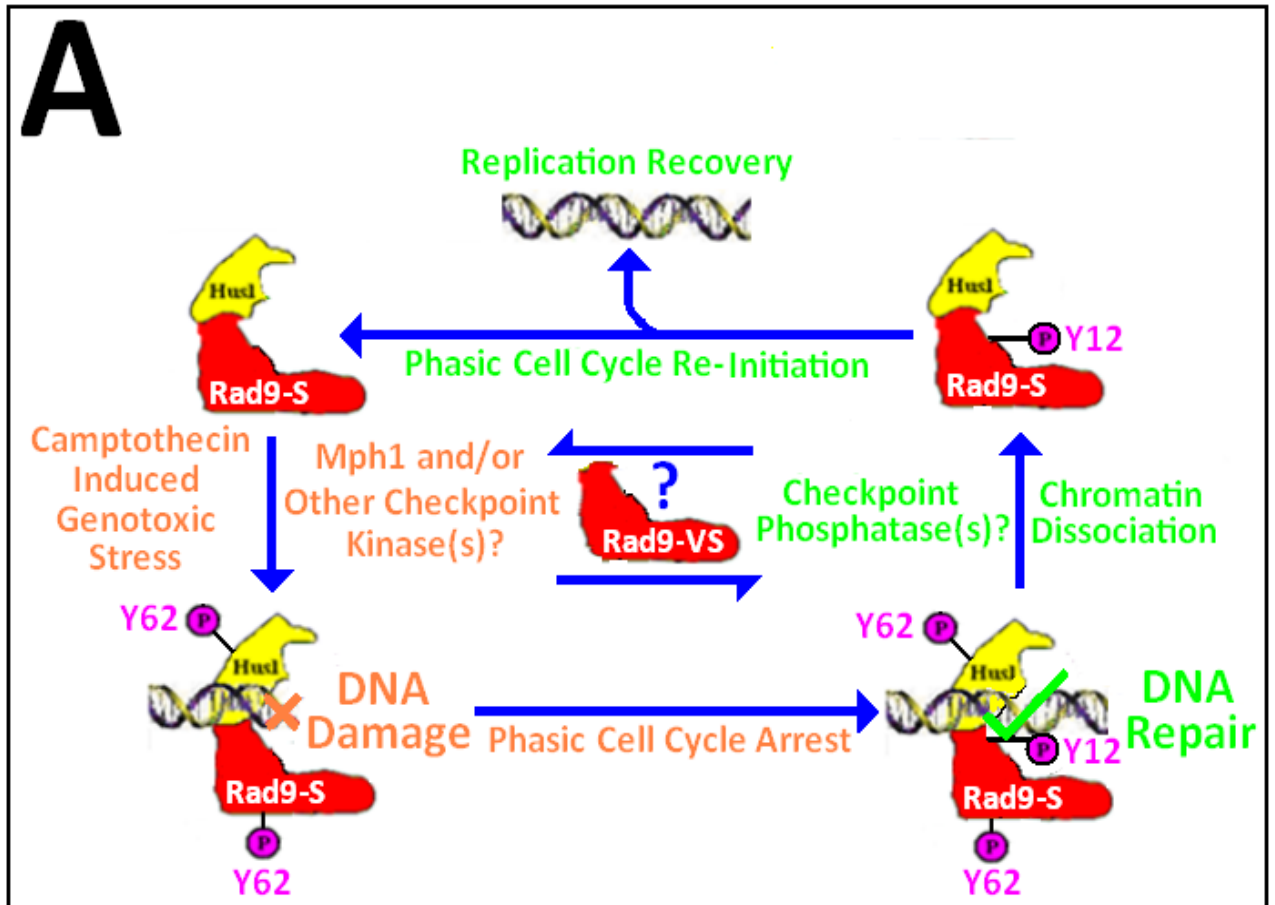
B: Comparative 2D PAGE-coupled Western blot analyses of the total soluble protein extract pellet fractions (nuclear protein localisation).

* Subtle shifts within the phosphoisoform profiles of the Rad9-S protein

Detected expression of the truncated “Rad9-VS” isoform ←

HYPERPHOS = Hyperphosphorylation

Fig 6.14: Functional Model for the Rad9-S:Hus1 Heterodimer



[An explanatory discussion of the hypothetical model concepts is provided in the text – pp.503-504]

6.2.2 The Rad3:Rad26 Heterodimeric DNA-Associated Complex is a Critical Functional Component of the “Rad9-S”-Initiated Checkpoint Response to Camptothecin-Induced Genotoxicity

In order to ascertain whether the primary (proximal) checkpoint kinases Rad3 and Tel1 could be functionally implicated in the “Rad9-S”-initiated checkpoint signalling response to camptothecin-induced DNA damage, comparative acute cell survival assays performed with YEA broth cultures of the *S. pombe* strains *N149-rad9-c3xHA Δrad3*, *N149-rad9-c3xHA Δrad26* and *N149-rad9-c3xHA Δtell*, incubated at 30°C in the presence of 40μM camptothecin (CPT) – Fig 6.15, p.523.

The experimental data revealed that the primary (proximal) transducer cell cycle checkpoint kinase Rad3, in association with its interactive protein partner Rad26, is an essential component of both the full-length Rad9 protein- and truncated “Rad9-S” protein variant- mediated signalling responses to CPT-induced DNA damage (Fig 6.15A and Fig 6.15B, p.523).

Comparative 2D-PAGE-coupled Western blot analyses of TCA-precipitated total protein extracts, acquired from YEA broth cell cultures of the appropriate *S. pombe* strains revealed that deletion of the *rad3* and *rad26* genes produced similar hypo-phosphorylated shift profiles for the truncated “Rad9-S” protein variant – indicative that the Rad3 kinase, in association with its component protein partner Rad26, may interact with and phosphorylate “Rad9-S” (Fig 6.15D, p.523).

In contrast, the acute CPT cell survival assay data indicated that the primary (proximal) transducer checkpoint kinase Tel1 is a non-essential component of either the full-length Rad9 protein- and truncated “Rad9-S” protein variant- mediated signalling responses to CPT-induced DNA damage (Fig 6.15C, p.523).

Comparative 2D-PAGE-coupled Western Blot analyses of TCA-precipitated total protein extracts, acquired from YEA broth cell cultures of the *S. pombe* strains *NΔ49-rad9-c3xHA* and *NΔ49-rad9-c3xHA Δtell* revealed that deletion of *tell* produces a hypo-phosphorylated shift profile which is distinctive from those of the *rad3* and *rad26* gene deletions – indicative that the Tel1 kinase may also interact with and phosphorylate “Rad9-S” (Fig 6.15D, p.523).

Taken together, these experimental data indicate that Rad26-associated Rad3 kinase-mediated phosphorylation of the truncated “Rad9-S” protein variant is a component of the signal pathway response to CPT-induced DNA damage, in which Tel1 kinase-mediated phosphorylation of “Rad9-S” is not implicated.

However, Tel1 kinase-mediated phosphorylation of “Rad9-S” may be implicated in other cell cycle regulatory functions of the truncated protein variant – which remain to be elucidated.

Previous experimental studies with *S. pombe* have indicated that Rad3 kinase-mediated phosphorylation of the residues threonine 225, threonine 412 and serine 423 within the full-length Rad9 protein, in which phosphorylation of threonine 225 is a critical priming pre-requisite for the heterotrimeric Rad9-Rad1-Hus1” PCNA-like DNA sliding-clamp complex-orchestrated template-switching in DNA repair pathways, are essential post-translational modifications which enable the Rad9 C-terminal domain (that protrudes outside of the “9-1-1” complex) to interact with and/or modulate the activity of a variety of proteins in order to initiate the G2 checkpoint arrest in response to camptothecin-induced genotoxic stress (Furuya K. *et al*, 2004; Furuya K. *et al*, 2010; Jansen J.G. *et al*, 2007; Kai M. *et al*, 2007).

In this context, it was postulated that phosphorylation of the equivalent residues (ie threonine 176, threonine 363 and serine 374) within the truncated “Rad9-S” protein variant may also be an essential post-translational modification pre-requisite for the heterodimeric “Rad9-S”：“Hus1-C” “open-ring/C-clamp”-initiated functional checkpoint signalling response to camptothecin-induced DNA damage and stalled replication forks.

In order to test this hypothesis, comparative acute cell survival assays were performed with YEA broth cultures of the *S. pombe* phosphorylation “knock-out” type site-directed mutagenised strains *NA49-rad9-(T225A)-c3xHA*, *NA49-rad9-(T412A)-c3xHA* and *NA49-rad9-(S423A)-c3xHA* and the *S. pombe* phosphomimetic type site-directed mutagenised strains *NA49-rad9-(T225E)-c3xHA*, *NA49-rad9-(T412E)-c3xHA* and *NA49-rad9-(S423E)-c3xHA* incubated at 30°C in the presence of 40µM camptothecin (CPT) – Fig 6.16, p.524 and Fig 6.17, pp.525-526.

The experimental data indicate that these positional equivalent Rad3 kinase-targeted phosphorylation sites (at T176, T363 and S374) are a critical post-translational modification pre-requisite for the truncated “Rad9-S” protein variant-mediated checkpoint pathway signal response to CPT-induced DNA damage – as a consequence of the fact that the alanine point mutations enhanced the sensitivity of the cells to camptothecin, whilst no significant reduction in camptothecin resistance was observed in the glutamate mutants (Fig 6.17, pp.525-526)

The acute survival assay data also indicated that the *NA49-rad9-(T176A)-c3xHA* (Fig 6.16B, p.524) mutant was significantly more sensitive to camptothecin-induced genotoxicity than that of the the *NA49-rad9-(T363A)-c3xHA* (Fig C) and *NA49-rad9-(S374A)-c3xHA* (Fig D) mutants (Fig 6.16, p.524) – which may be indicative that Rad3 kinase-mediated phosphorylation of ¹⁷⁶T within the truncated “Rad9-S” protein variant may be a critical functional pre-requisite which induces conformational changes within its supramolecular structure to enable subsequent Rad3 kinase-mediated phosphorylation of the C-terminal tail domain at ³⁶³T and ³⁷⁴S (Fig 6.16, p.524)

These genetic data interpretations were also supported by biochemical evidence acquired from comparative 2D-PAGE-coupled Western Blot analyses of TCA-precipitated total protein extracts, prepared from 30°C YEA broth cell cultures of Rad3 kinase site-directed mutagenised “*rad9-S-c3xHA*”-type *S. pombe* strains produced distinctive hypophosphorylation-shifted isoform profiles for the “Rad9-S” protein for each respective site-directed phosphorylation “knock-out” alanine mutagenised Rad3 kinase-targeted amino acid residue and distinctive hyperphosphorylation-shifted isoform profiles for the “Rad9-S” protein for each respective phosphomimetic type site-directed glutamate mutagenised Rad3 kinase-targeted amino acid residue (Fig 6.17E, pp.525-526).

Taking all the experimental data into consideration, a hypothetical model was formulated for the sequential Rad3 kinase-mediated post-translational phosphorylated-activation of the heterodimeric “Rad9-S”：“Hus1-C” “open-ring/C-clamp” complex which may be implicated in the initiation of novel checkpoint and/or DNA repair pathway responses to camptothecin-induced DNA damage (Fig 6.18, p.527).

In response to detected camptothecin-induced DNA damage lesion sites, initial Rad26-associated Rad3 kinase-mediated phosphorylation of “Rad9-S” at T176 induces supramolecular configurational changes within the truncated protein variant which enable Rad26/Rad3 kinase-mediated phosphorylation of the T363 and S374 residues – which are situated within its C-terminal tail domain (Fig 6.18, p.527).

Subsequent Rad26/Rad3 kinase-mediated phosphorylation of the T363 and S374 residues induces further supramolecular configurational changes within the C-terminal tail domain of the “Rad9-S” truncated protein variant, that protrudes out from the heterodimeric “Rad9-S”：“Hus1-C” “open-ring/C-clamp” complex bound to the duplex, which may then enable it to engage with and/or modulate the functional activity of specific checkpoint-signalling and DNA repair proteins in response to camptothecin-induced genotoxic events (Fig 6.18, p.527).

Surprisingly, these data also revealed that the Rad3 kinase-mediated phosphorylation of the positional equivalent ^{225}T , ^{412}T and ^{423}S residues are non-essential for the checkpoint signalling response pathway to CPT-induced DNA damage in the case of the full-length *S. pombe* Rad9 protein – as a consequence of the fact that the alanine site-directed point mutations did not enhance the sensitivity of the cells to camptothecin (Fig 6.16, p.524).

Comparative Western blot analyses of TCA-precipitated total protein extracts acquired from YEA broth cell cultures of the full-length Rad9 and truncated “Rad9-S” phosphorylation site “knock-out” mutant *S. pombe* strains, incubated at 30°C in the absence or presence of 40µM camptothecin (CPT), indicate that both the full-length Rad9 protein and “Rad9-S” truncated protein variant are phosphorylated by the primary (proximal) transducer Rad3 checkpoint kinase at the equivalent positional residues T225, T412 and S423 in response to CPT-induced DNA damage (Fig 6.19, pp.528-529).

Intriguingly, the data also reveal that deletion of the *rad3* gene within an exclusive full-length *rad9* expression type genetic background (ie *rad9-M50L-c3xHA Δrad3*) resulted in the generation of another protein isoform that was independent of the CPT-induced DNA damage response, which may be indicative of alternative kinase-mediated post-translational phosphorylated modifications of the full-length Rad9 protein which are suppressed in the presence of the truncated “Rad9-S” protein variant (Fig 6.19, pp.528-529).

These experimental data may also indicate that the truncated “Rad9-VS” protein variant engages with and modulates the activity of Tel1 and/or other alternative checkpoint kinases which give rise to the postulated alternative post-translational phosphorylated modifications of the full-length Rad9 protein that alter its functional properties which could initiate other specific checkpoint and DNA repair pathway responses to different types of genotoxic and/or environmental stresses that impinge adversely on a variety of different biochemical processes implicated in the cytological propagation of genomic integrity (Fig 6.19, pp.528-529).

Comparative mitotic checkpoint time-course assays were performed on cell cycle G2 phase-isolated cells of a “wild-type” *S. Pombe* strain, in parallel with those of the “cre-lox”-constructed *rad9*-deleted ($\Delta rad9$), full-length *rad9* (*rad9-c3xHA* and *rad9-(M50L)-c3xHA*) and truncated *rad9* variant (*N149-rad9-c3xHA* and *N173-rad9-c3xHA*) *S. pombe* strains, released into YEA broth medium that contained 200 μ M camptothecin (CPT), incubated at 30°C over a total time period of 400 minutes, in order to ascertain whether or not alternative checkpoint signalling pathway responses could be elicited by the “cre-lox”-engineered full-length and truncated *S. pombe* Rad9 protein variants (Fig 6.20, pp.530-531).

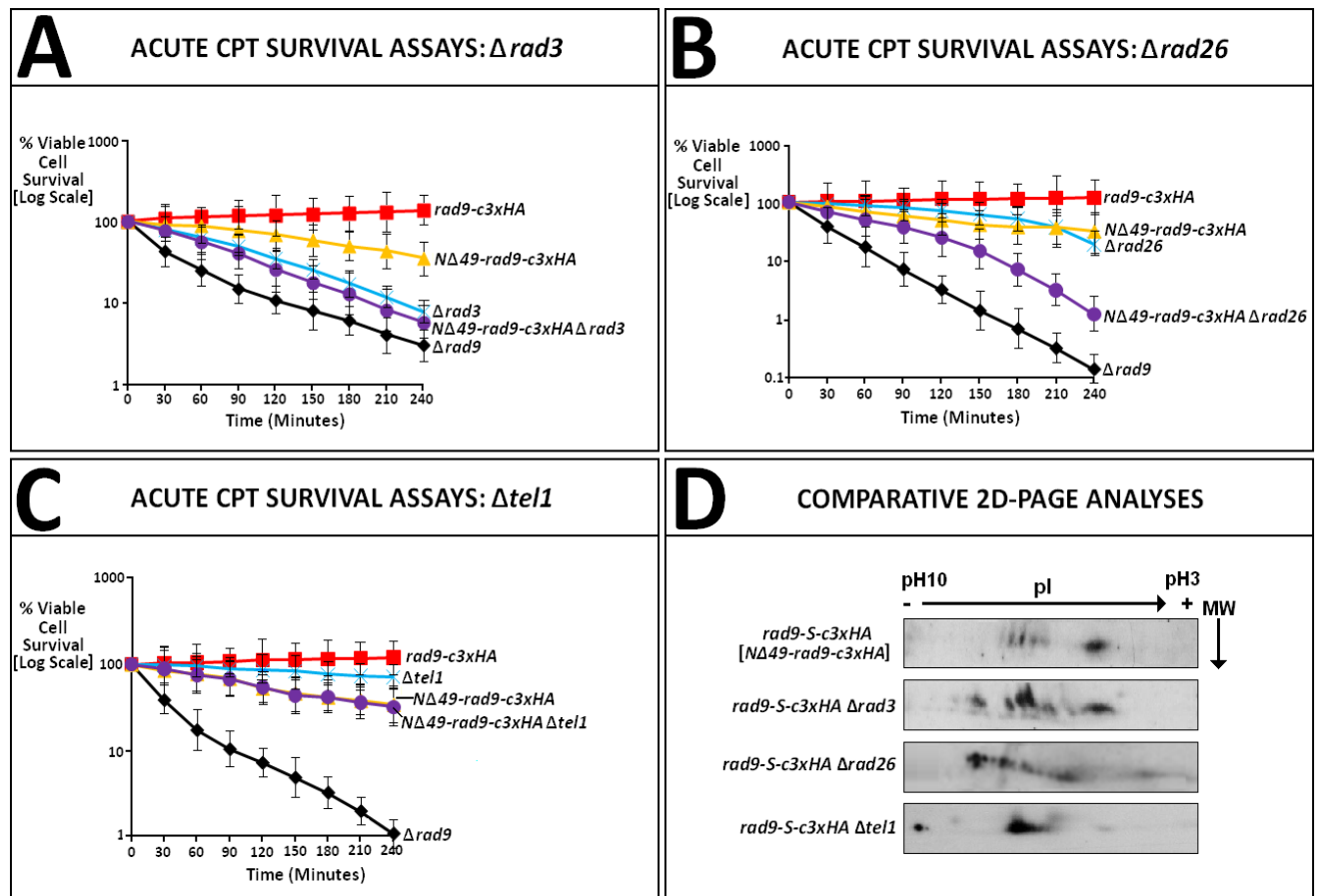
The experimental data indicated that the “wild-type” and full-length Rad9 protein-expressing strains initiated a G2/M checkpoint response to CPT-induced DNA damage which elicited entry into mitosis during the second round of the cell cycle, whilst *rad9*-deleted cells and the *N173-rad-c3xHA* strains were defective in DNA damage signalling and therefore did not elicit a G2/M arrest response, as anticipated (Fig 6.20, pp.530-531).

Intriguingly, the data also revealed *rad9-M50L-c3xHA* cells (which cannot express the truncated “Rad9-S” protein variant) elicited a distinctively different delayed cell cycle arrest which may be a consequence of an alternative switching pathway elicited via alternative kinase-mediated phosphorylation events in the full-length Rad9 protein which are suppressed in the presence of the truncated” Rad9-S”protein variant – discussed previously on p.501 (Fig 6.20, pp.530-531).

In the case of the “cre-lox”-engineered *S. pombe* cells that exclusively expressed the NΔ49-Rad9-c3HA (“Rad9-S”), the experimental data revealed that induction of a G2/M-type cell cycle arrest in response to camptothecin-induced DNA damage did not occur – which may be indicative of a checkpoint suppressor function of the protein (Fig 6.20, pp.530-531).

Taken together, these respective experimental observations indicate that the full-length Rad9 protein and truncated “Rad9-S” protein variant channel differential signalling responses to camptothecin-induced DNA damage within distinctive cell cycle checkpoint pathways.

Fig 6.15: Acute CPT Survival Assays – Proximal Transducer Kinases



Figs A, B and C: Comparative acute cell survival assays performed with YEA broth cultures of the indicated *S. pombe* strains, incubated at 30°C in the presence of 40 μ M camptothecin (CPT) – Figs A, B and C.

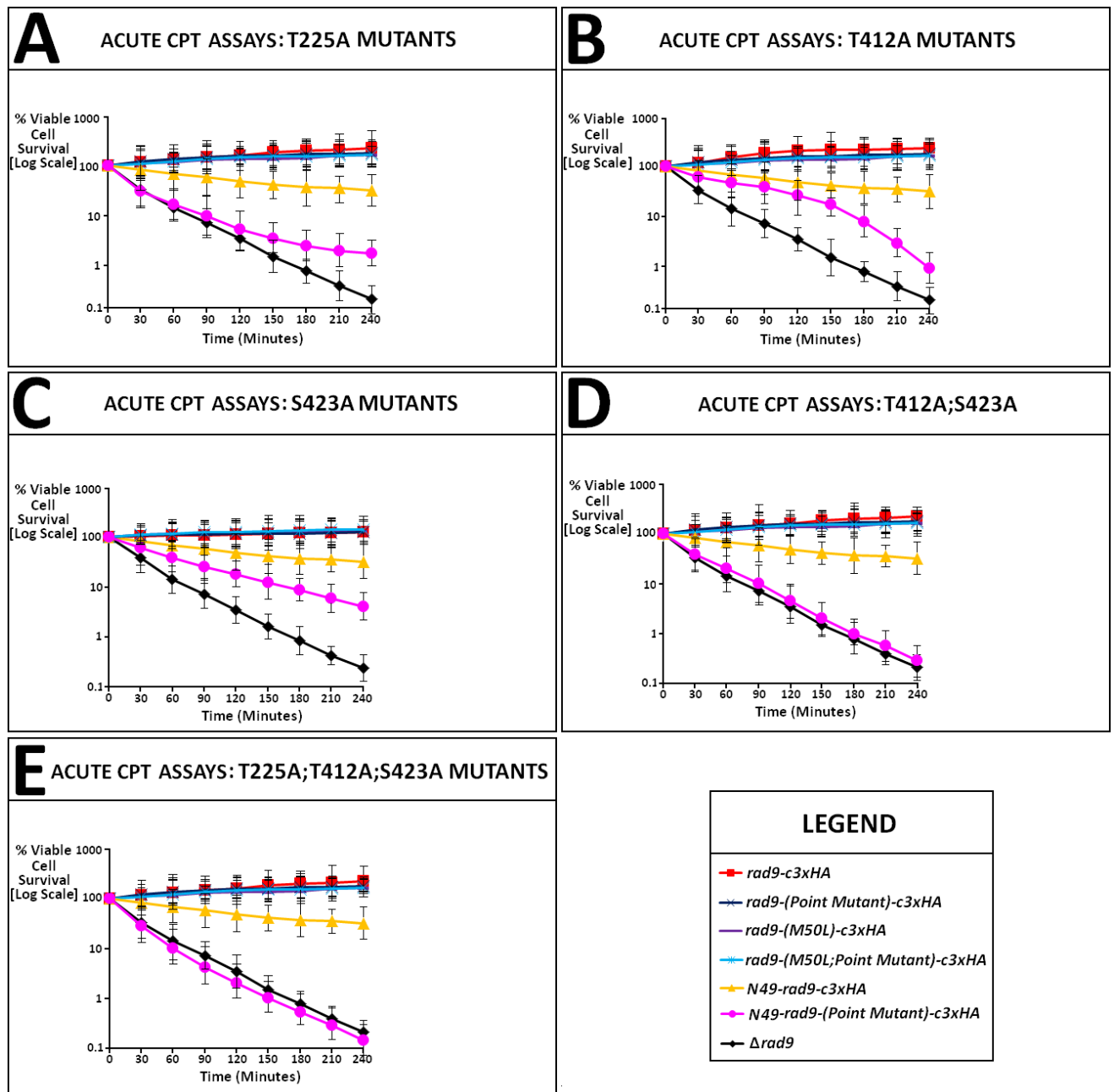
[Acute cell survival assays were performed as per the methodology described in Chapter 2, Section 2.9.2.2(ii), pp.239-241]

Fig D: Individual 100mL YEA broth medium cell cultures of the indicated *S. pombe* strains were grown overnight (30°C for ~12 hour time period), then diluted to an optical density $A_{595} = 0.25$ with the appropriate volume of YEA medium and the resultant diluted cultures re-incubated at 30°C for a further time period of ~2.5 hours until they had attained an optical density value of $A_{595} = 0.5$.

TCA-precipitated total protein extract samples were then prepared from the appropriate *calculated volumetric aliquot of each culture (*equivalent to 40 A_{595} optical density units) and utilised in comparative 2D PAGE–coupled Western blot analyses – probed with the primary “anti-HA” antibody.

[Performed as per the methodologies described in Chapter 2, Section 2.8.3.1, pp.214-217; Section 2.8.5.1, pp.225-230 and Section 2.8.6., pp.231-233]

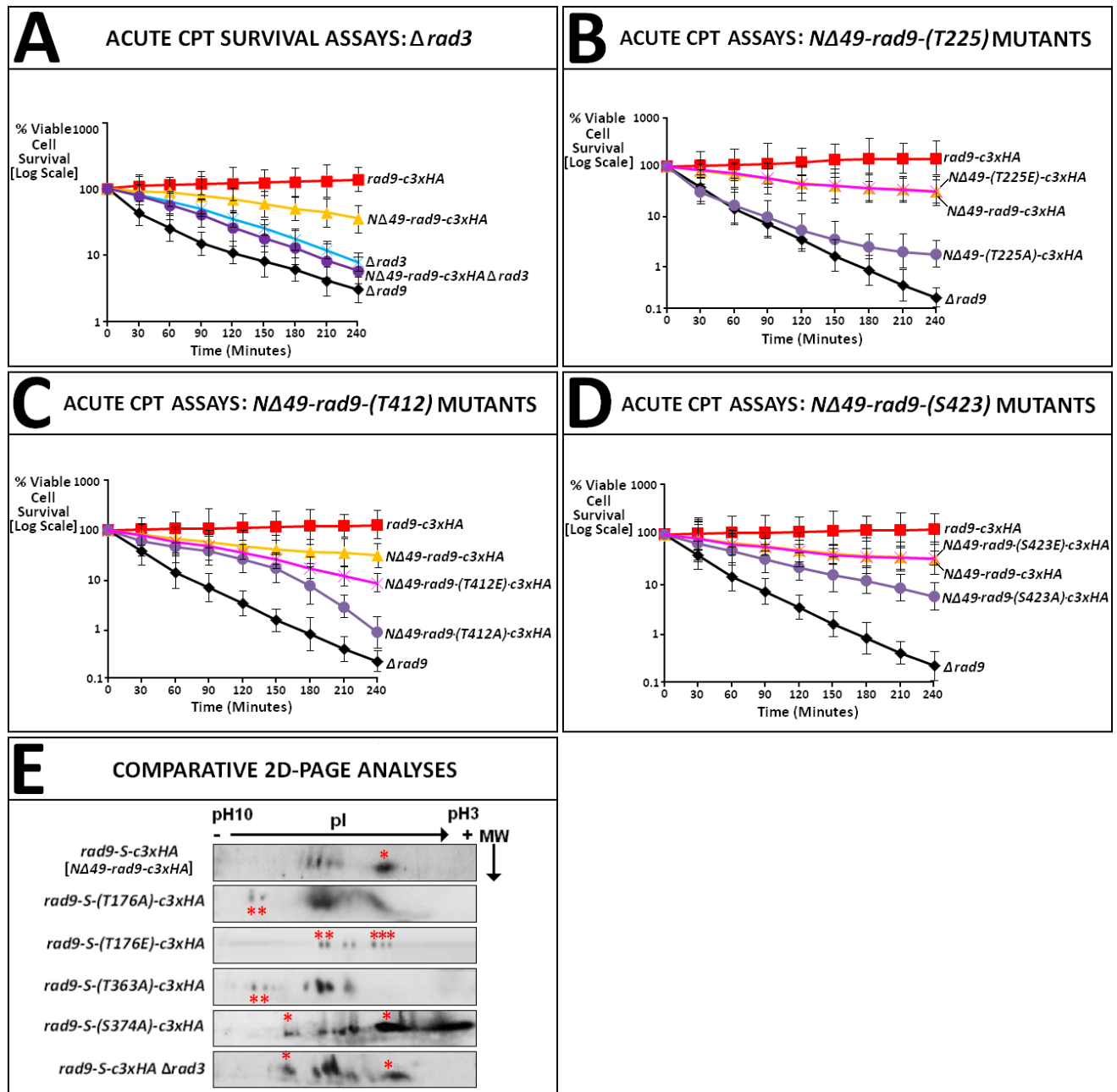
Fig 6.16: CPT Assays – Rad3 Kinase Ala “Knock-Out” Point Mutants



Comparative acute cell survival assays performed with YEA broth cultures of the indicated *S. pombe* strains, incubated at 30°C in the presence of 40μM camptothecin (CPT)

[Acute cell survival assays were performed as per the methodology described in Chapter 2, Section 2.9.2.2(ii), pp.239-241]

Fig 6.17: CPT Assays – Ala and Glu Rad3 Kinase-Site Point Mutants



[See Figure Legend, p.526, for a full description of the experimental data]

Figure Legend: Fig 6.17

Figs A, B, C and D: Comparative acute cell survival assays performed with YEA broth cultures of the indicated *S. pombe* strains, incubated at 30°C in the presence of 40µM camptothecin (CPT) – Figs A, B and C.

[Acute cell survival assays were performed as per the methodology described in Chapter 2, Section 2.9.2.2(ii), pp.239-241]

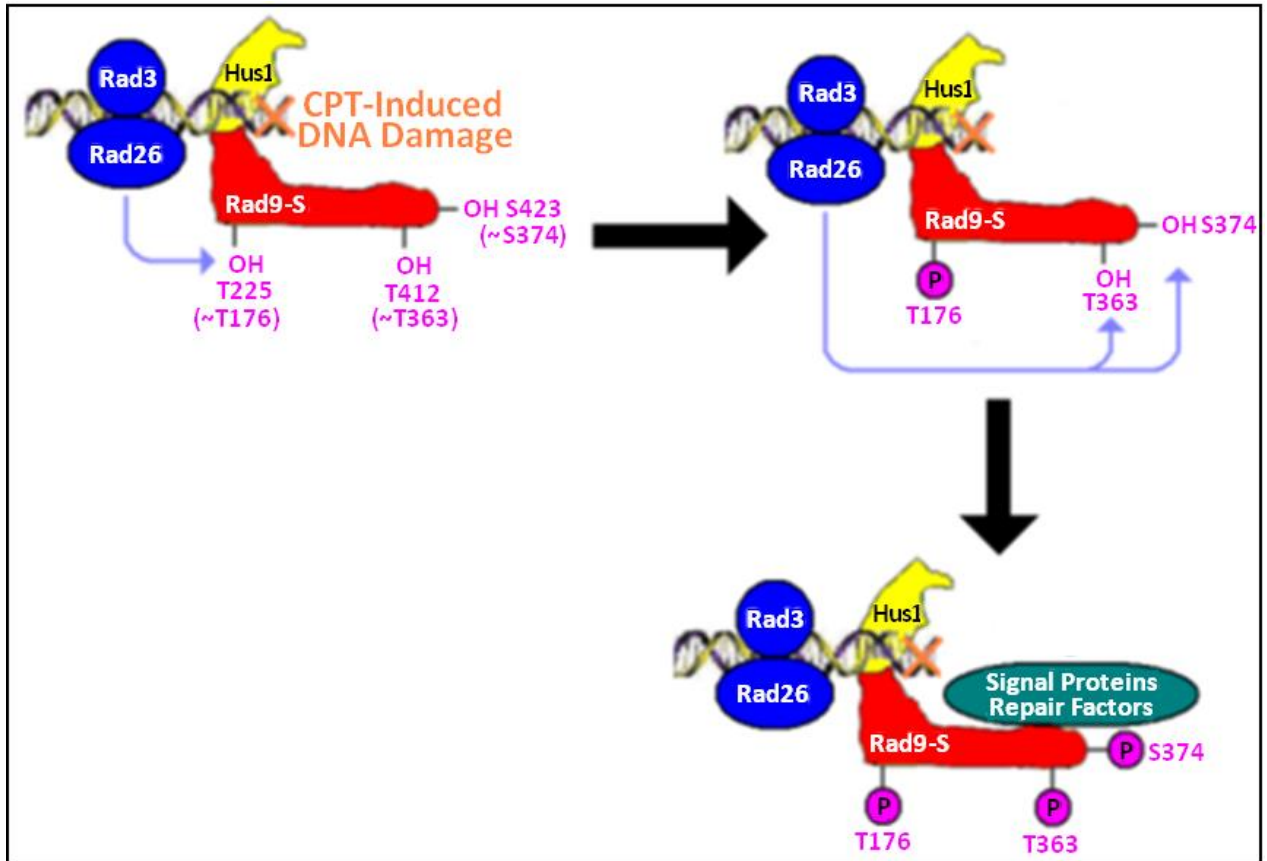
Fig E: Individual 100mL YEA broth medium cell cultures of the indicated *S. pombe* strains were grown overnight (30°C for ~12 hour time period), then diluted to an optical density $A_{595} = 0.25$ with the appropriate volume of YEA medium and the resultant diluted cultures re-incubated at 30°C for a further time period of ~2.5 hours until they had attained an optical density value of $A_{595} = 0.5$.

TCA-precipitated total protein extract samples were then prepared from the appropriate *calculated volumetric aliquot of each culture (*equivalent to 40 A_{595} optical density units) and utilised in comparative 2D PAGE–coupled Western blot analyses – probed with the primary “anti-HA” antibody.

[Performed as per the methodologies described in Chapter 2, Section 2.8.3.1, pp.214-217; Section 2.8.5.1, pp.225-230 and Section 2.8.6., pp.231-233]

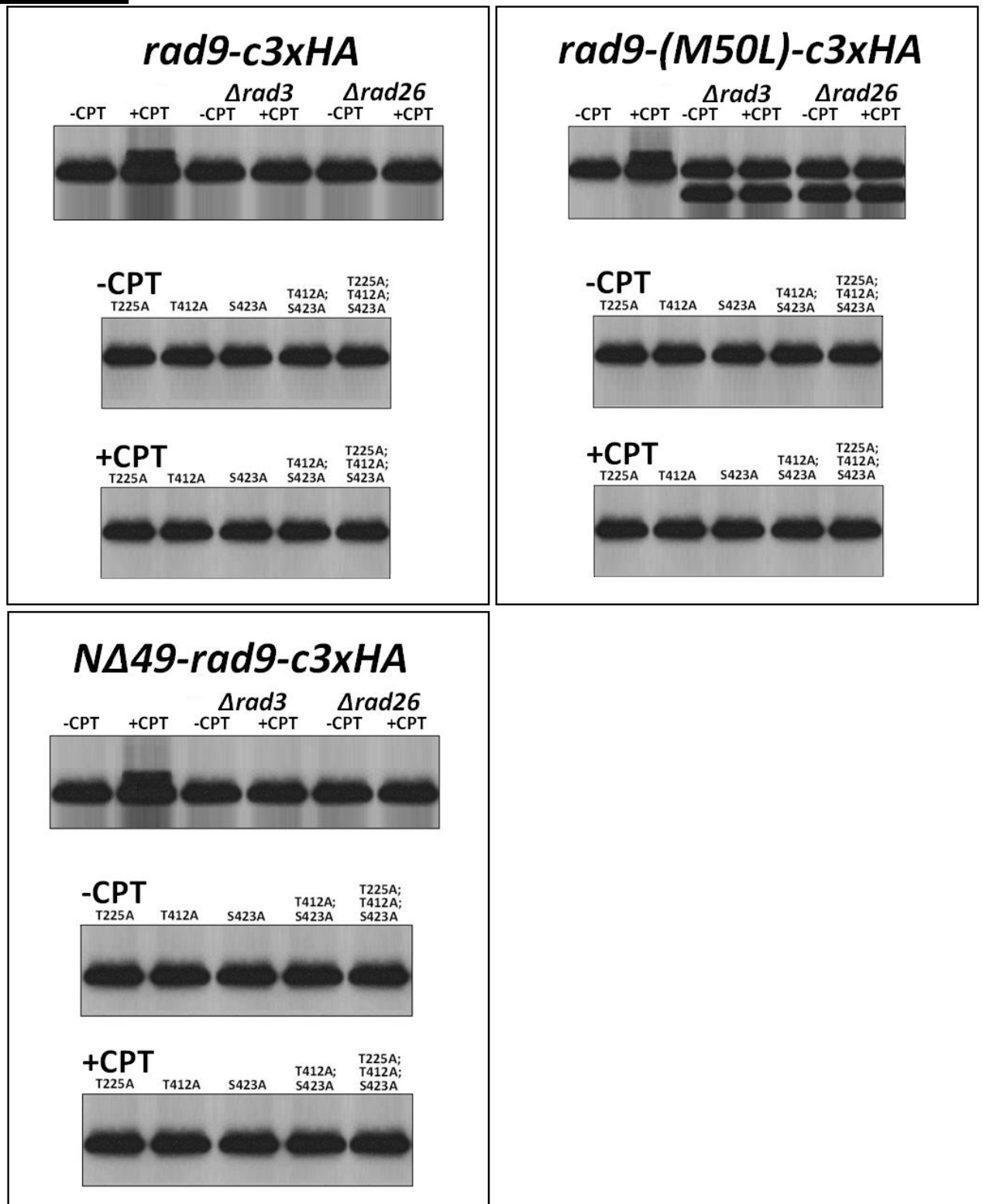
Note: The *rad9-S-(T176E)-c3xHA* 2D PAGE-coupled Western Blot phosphorylation profile was acquired by the trainee MSc. project student Ms. Anna Isermann, under the supervision of the author.

Fig 6.18: Rad3 Kinase-Initiated T176 Target-Site “Priming” Model



Rad3 kinase-mediated sequential phosphorylation of the equivalent residues (T176, T363 and S374) within the “Rad9-S” sub-unit of the heterodimeric “Rad9-S”:“Hus1-C” “opening/C-clamp” complex, bound at camptothecin-induced DNA damage lesion sites within chromatin, enables the C-terminal tail domain to engage and/or modulated the functional activities of specific proteins implicated in the appropriate initiation of particular checkpoint and DNA repair pathways (discussed in detail in the text on p.518).

Fig 6.19: Comparative Western Blot Analyses of Full-Length Rad9 and Truncated “Rad9-S” Isoform Expression in the Absence and Presence of CPT-Induced DNA Damage with *rad3* and *rad26* Gene Deletions



[See Figure Legend, p.529, for a full description of the experimental data]

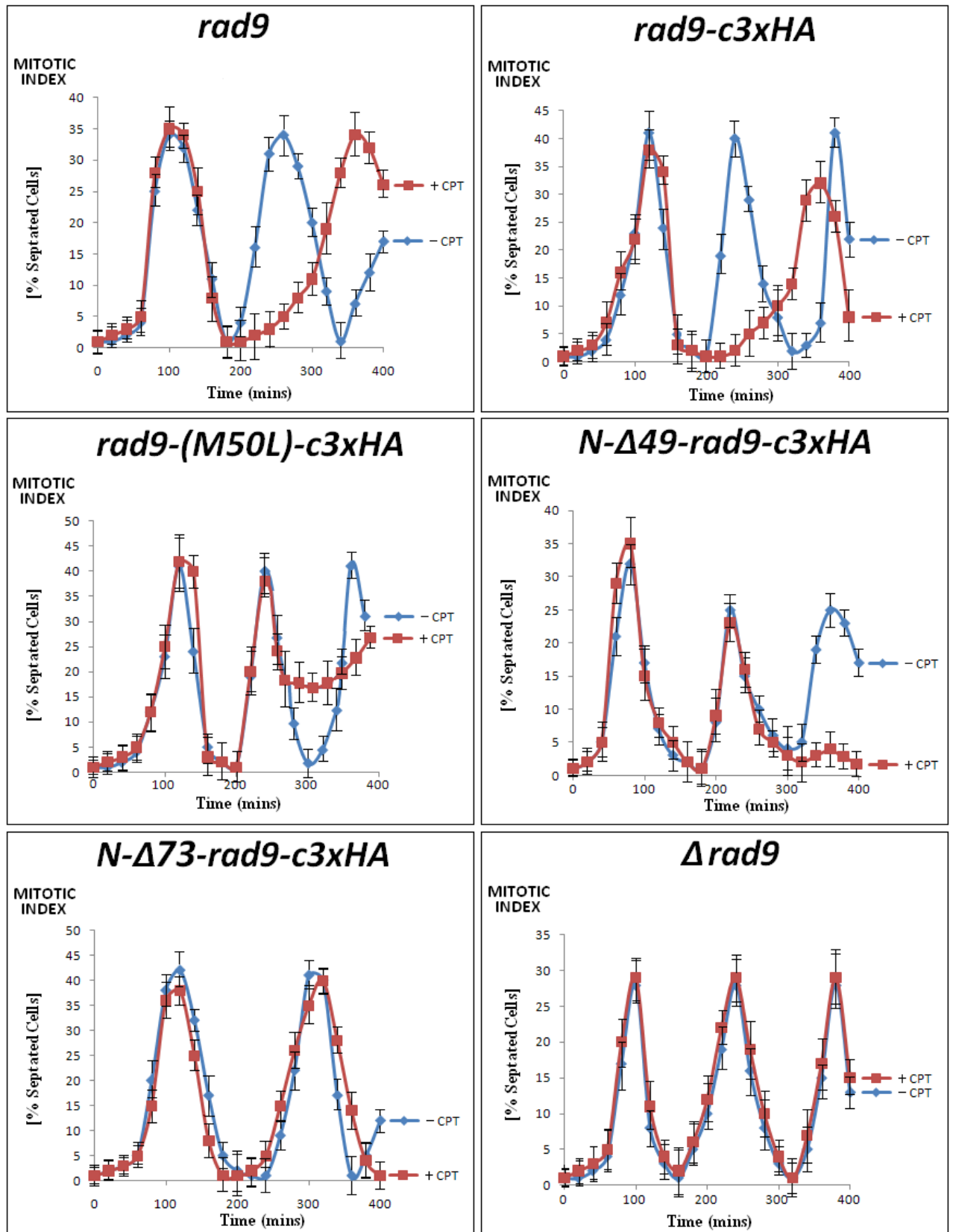
Figure Legend – Fig 6.19

Individual 50mL YEA broth medium cell cultures of the indicated *S. pombe* strains were incubated at 30°C over a 12 hour time period, then diluted to an optical density $A_{595} = 0.25$ with the appropriate volume of YEA medium and the resultant diluted cultures re-incubated at 30°C for a further time period of ~2.5 hours until they had attained an optical density value of $A_{595} = 0.5$ – after which time the resultant cultures of actively cycling cells were re-incubated at 30°C for a further 30 minutes in YEA in the absence (-CPT) and presence (+CPT) of 40 μ M camptothecin.

TCA-precipitated total protein extract samples were then prepared from the appropriate *calculated volumetric aliquot of each culture (*equivalent to 10 A_{595} optical density units) of which 20 μ L aliquots were resolved on 10% SDS-PAGE gels which were then utilised in comparative Western blot analyses probed with the anti-HA primary antibody.

[Protein sample preparation, SDS-PAGE resolution and Western blot methodologies are detailed in Section 2.8.1, pp.200-202; Section 2.8.4, pp.223-224 and Section 2.8.6, pp.231-233]

Fig 6.20: Comparative Lactose Synchronisation Assays



[See Figure Legend, p.531, for a full description of the experimental data]

Figure Legend – Fig 6.20

Individual 100mL YEA broth medium cell cultures of the indicated *S. pombe* strains were incubated at 30°C over a 12 hour time period, then diluted to an optical density $A_{595} = 0.25$ with the appropriate volume of YEA medium and the resultant diluted cultures re-incubated at 30°C for a further time period of ~2.5 hours until they had attained an optical density value of $A_{595} = 0.5$

5×10^8 actively cycling cells were taken from each resultant culture and were synchronised in G2, via the utilisation of lactose density gradient centrifugation, after which time mitotic checkpoint time-course assays were performed on the G2-isolated cells released into 50mL of YEA broth medium that contained 200µM camptothecin (CPT), incubated at 30°C over a total time period of 400 minutes.

[The assay methodology is described in detail in Chapter 2, Section 2.9.3, pp.253-257]

The *S. pombe* cell cycle G1 phase is relatively short such that the septation index (mitotic index on the Y-axis) correlates with the cell cycle S-phase (Collura A. *et al*, 2005).

6.2.3 Mrc1 is a Critical Mediator Component of the “Rad9-S” – Initiated Checkpoint Response to Camptothecin-Induced DNA Damage in Which Neither Crb2 or Rad4 are Implicated

In mammalian cells, the mediator ring-protein Claspin is functionally implicated in the initiation of the ATR→Chk1 checkpoint pathway which elicits a G2/M phasic cell cycle arrest in response to camptothecin-induced genotoxicity (Liu S. *et al.*, 2012) – discussed previously in Chapter 1, Section 1.2.2, pp.33-65.

Other mediator/scaffold proteins which are implicated in the activation of this checkpoint pathway are BRCA1 and TopBP1 (discussed previously in Chapter 1, Section 1.2.2, pp.33-65).

Recent experimental studies have also indicated that the conserved functionality of the C-terminus domain of Claspin interacts with the Rad9 protein to promote rapid activation of the secondary (distal) checkpoint kinase Chk1 (Liu S. *et al.*, 2012).

In *S. pombe*, the functionally-equivalent homolog of Claspin is Mrc1, which initiates the Rad3^{Sp} (ATR^{Hs})→Chk1^{Sp} (Chk1^{Hs}) pathway that elicits a G2/M phasic cell cycle arrest in response to camptothecin-induced DNA damage and stalled replication forks (discussed in detail previously on pp.489-490).

The other functionally-equivalent *S. pombe* mediator/scaffold protein homologs which are implicated in the activation of the Rad3→Chk1 pathway are Crb2^{Sp} (functional homologue equivalent of 53BP1^{Hs} and BRCA1^{Hs}) and Rad4^{Sp} (functional homologue equivalent of TopBP1^{Hs}) – depicted summarily and discussed in detail in Fig 6.21, pp.535-537.

Functionally-equivalent conserved C-terminal domain interactions between Mrc1 and Rad9 may also elicit rapid activation of the Chk1 kinase in *S. pombe* cells (Nitani N. *et al.*, 2006; Shikata M. *et al.*, 2007; Yasuhira S. *et al.*, 2009; Yin L. *et al.*, 2008; Zhao H. *et al.*, 2003).

In order to ascertain whether scaffold/mediator proteins could be functionally implicated in the “Rad9-S”-initiated checkpoint signalling response to camptothecin-induced DNA damage, comparative acute survival assays were performed on 30°C YEA broth cultures of the double-mutant *S. pombe* strains *NΔ49-rad9-c3xHA Δcrb2*, *NΔ49-rad9-c3xHA Δmrc1* and *NΔ49-rad9-c3xHA rad4.116* in the presence of 40μM camptothecin for a total incubation time of 4 hours (Fig 6.22A, p.538).

The acquired experimental data revealed that functional perturbation of the *rad4* gene (*rad4.116*) and deletion of the *crb2* gene within an exclusively expressed “*rad9-S*” genetic background, had negligible effect of the sensitivity of the cells to CPT-induced DNA damage (Fig 6.22A and Fig 6.22C, p.538) – indicative that the respective proteins are non-essential to the “Rad9-S” truncated protein variant-mediated checkpoint signalling response to CPT-induced genotoxicity.

In contrast, deletion of *mrc1* within an exclusively expressed “*rad9-S*” genetic background, resulted in the significant enhancement of the sensitivity of the cells to CPT-induced genotoxicity – indicative that the adapter protein is a key functional component within the “Rad9-S” truncated protein variant-mediated checkpoint signalling response to CPT-induced DNA damage (Fig 6.22B, p.538).

Comparative 2D PAGE-coupled Western Blot analyses, performed on TCA-precipitated total protein extracts acquired from YEA broth cultures of the *NΔ49-rad9-c3xHA* and *NΔ49-rad9-c3xHA Δmrc1* *S. pombe* strains revealed that deletion of *mrc1* results in a hypo-phosphorylated shift phosphoisoform profile for the “Rad9-S” truncated protein variant – indicative that Mrc1 may be functionally implicated in “Rad9-S”-mediated checkpoint signalling responses to genotoxic and/or environmental stresses which impinge adversely on various biochemical processes involved in the cytological preservation of genomic integrity (Fig 6.22D, p.538).

Experimental data acquired in this Ph.D. project also indicated that both the Tel1 and Rad3 primary (proximal) transducer checkpoint kinases may be implicated in the differential phosphorylation of the truncated “Rad9-S” protein variant (discussed in detail previously in Section 6.2.2, pp.516-531).

Differential phosphorylation of Mrc1 by Tel1 and Rad3 kinases has also been observed in previous experimental studies (Zhao H. *et al.*, 2003).

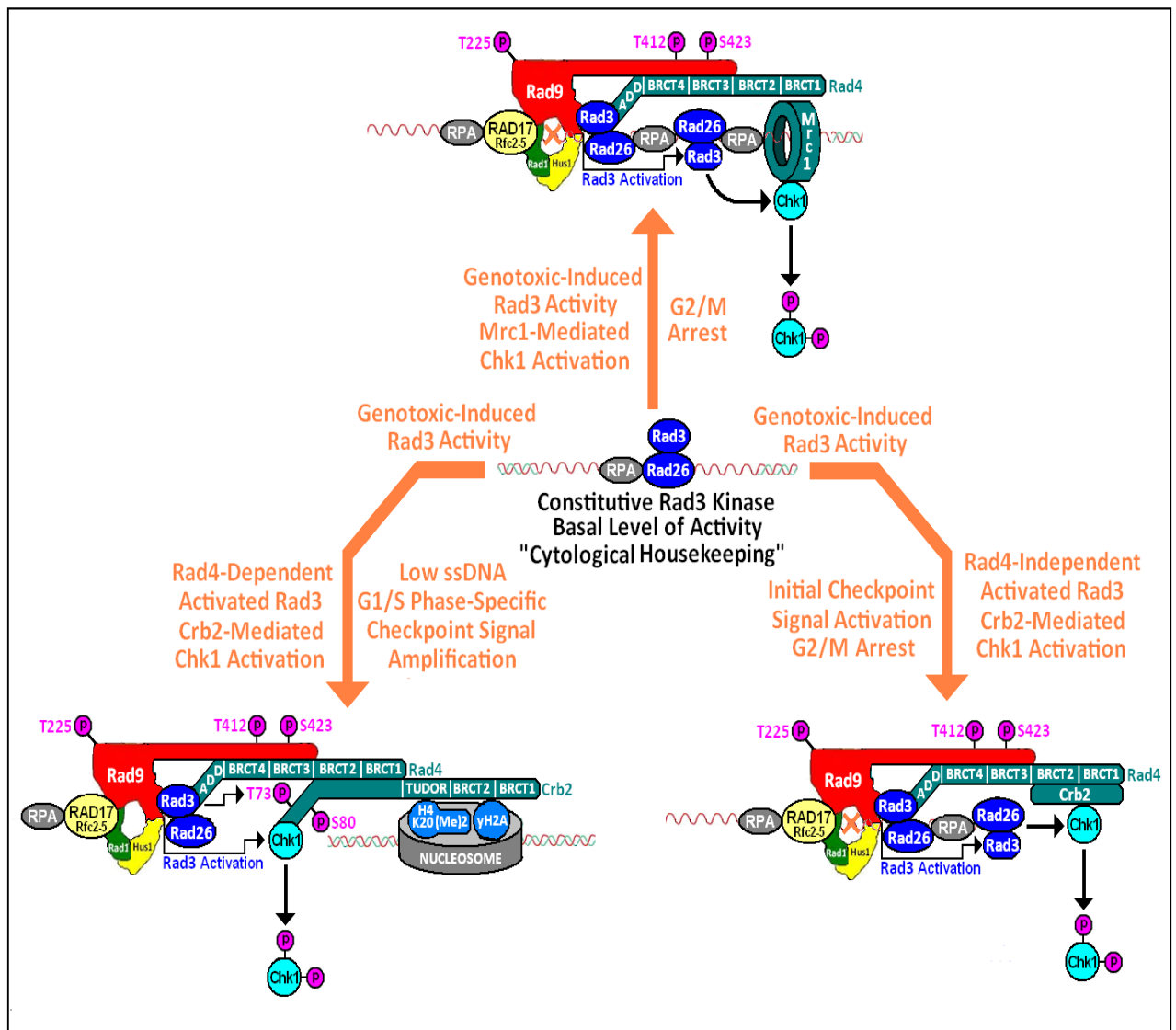
Taking all the experimental observations into consideration, a hypothetical model was formulated for the Rad3 and Tel1 kinase-mediated post-translational differential phosphorylated modulation of functional Mrc1-“Rad-S” activities within the heterodimeric “Rad9-S”：“Hus1-C” “open-ring/C-clamp” complex which may be influential in the selective initiation of specific checkpoint signalling and/or DNA repair pathway responses to particular types of genotoxic and/or environmental stresses which impinge adversely on biochemical processes implicated in the cytological propagation of genomic integrity (Section 6.2.4, pp.539-546; Fig 6.25, p.545-546).

Comparative lactose synchronisation assay experimental data, acquired in this Ph.D. project, also revealed that *S. pombe* cells which were “cre-lox”–engineered for the exclusive expression of the truncated NΔ49-Rad9-c3xHA variant did not elicit a G2/M phasic cell cycle arrest in response to camptothecin-induced genotoxicity (discussed previously in detail in Section 6.2.2, pp.521-522; Fig 6.20, pp.530-531).

Taking this experimental observation into consideration with the hypothetical model, the “Rad9-S” sub-unit, together with Mrc1, Rad3 and/or Tel1 interactions may be functionally implicated in a heterodimeric “Rad9-S”：“Hus1-C” “open-ring/C-clamp” complex-mediated checkpoint signalling pathway which suppresses Chk1 activation in response to camptothecin-induced DNA damage (discussed in detail later in Section 6.2.4, pp.539-546; Fig 6.25, pp.545-546).

Fig 6.21: Functional Roles of the *S. pombe* Scaffold/Mediator Proteins Crb2, Mrc1 and Rad4 in Chk1 Activation-Mediated Checkpoint Signalling Responses to DNA Damage

[Compiled Via Collated Information Adapted From: Alcasabas A.A. *et al*, 2001;
 Lin S.J. *et al*, 2012;
 Nitani N. *et al*, 2006;
 Qu M. *et al*, 2012;
 Shikata M. *et al*, 2007;
 Yasuhira S. *et al*, 2009;
 Yin L. *et al*, 2008;
 Zhao H. *et al*, 2003]



[See Figure Legend, pp.536-537, for a full description of the mechanistic pathways illustrated summarily above]

Figure Legend – Fig 6.21

In the absence of DNA damage, constitutive activation of *SpRad3*^{HsATR} maintains a basal level of the active primary (proximal) transducer kinase which may be required for the initiation of a variety of signalling pathways that modulate the appropriate selection and functions of specific biochemical “house-keeping” processes implicated in propagation of cytological and/or genomic integrity (Lin S.J. *et al.*, 2012; Nitani N. *et al.*, 2006; Smits V.A. *et al.*, 2010; Qu M. *et al.*, 2012; Yin L. *et al.*, 2008).

DNA damage-induced activation of Rad3 proceeds via differential checkpoint pathways which are coupled to the activation of Chk1-initiated checkpoint signalling responses to genotoxic stress mediated via “Rad9 C-terminal tail domain:Rad4” (Rad9-c:Rad4) interactions within the heterotrimeric, toroidal Rad9-Rad1-Hus1 PCNA-like DNA sliding-clamp complex that is loaded onto chromatin at DNA lesion sites via the Rad17:(Rfc2-5) clamp-loader complex (Lin S.J. *et al.*, 2012; Qu M. *et al.*, 2012).

The Rad4 mediator protein sub-unit of the ternary Rad9-c:Rad4-Rad1-Hus1 complex also contains a homologous functionally-equivalent ATR activation domain (AAD) which interacts with an allosteric site within the Rad3 primary (proximal) transducer kinase and induces supramolecular conformational changes within the enzyme which enhance its catalytic activity under specific conditions of genotoxic-induced cytologic stress (Lin S.J. *et al.*, 2012; Qu M. *et al.*, 2012).

Initial Rad4 AAD domain-independent activation of Rad3 proceeds via a primary ssDNA pathway in which the Rad9 sub-unit of the Rad9-Rad1-Hus1 (“9-1-1”) complex contains an “HFD-like” motif that also interacts with an allosteric site within the Rad3 primary (proximal) transducer kinase and induces supramolecular conformational changes within the enzyme which enhance its catalytic activity (Lin S.J. *et al.*, 2012; Navadgi-Patil V.M. and Burgers P.M., 2009; Qu M. *et al.*, 2012).

Subsequent Rad3-mediated sequential post-translational phosphorylation-type modifications of the Rad9 sub-unit within the “9-1-1” complex (at residues T225, T412 and S423), induces supramolecular conformational changes with the Rad9 C-terminal tail domain which enable it to associate with either the Crb2 or Mrc1 scaffold/mediator proteins – dependent upon the type of DNA lesion encountered (Lin S.J. *et al.*, 2012; Qu M. *et al.*, 2012).

“9-1-1” complex-mediated recruitment of Crb2 occurs at detected double-stranded breakage (DSB) sites, whilst detected stalled replication forks and/or branched DNA structural anomalies result in “9-1-1” complex-mediated recruitment of Mrc1 (Lin S.J. *et al.*, 2012; Qu M. *et al.*, 2012).

“9-1-1” complex-orchestrated recruitment of Crb2 or Mrc1 to specific DNA lesion sites, brings the respective scaffold/mediator protein into close proximity to the primary (proximal) transducer kinase Rad3 (Lin S.J. *et al.*, 2012; Qu M. *et al.*, 2012).

Subsequent Rad3-mediated post-translational phosphorylation-type modifications of Crb2 (at T73 and T80), or Mrc1 (at S604 and S645), induces supramolecular configurational changes within the respective scaffold/mediator protein which enable it to engage with the secondary (distal) transducer checkpoint kinase Chk1 (Lin S.J. *et al.*, 2012; Qu M. *et al.*, 2012).

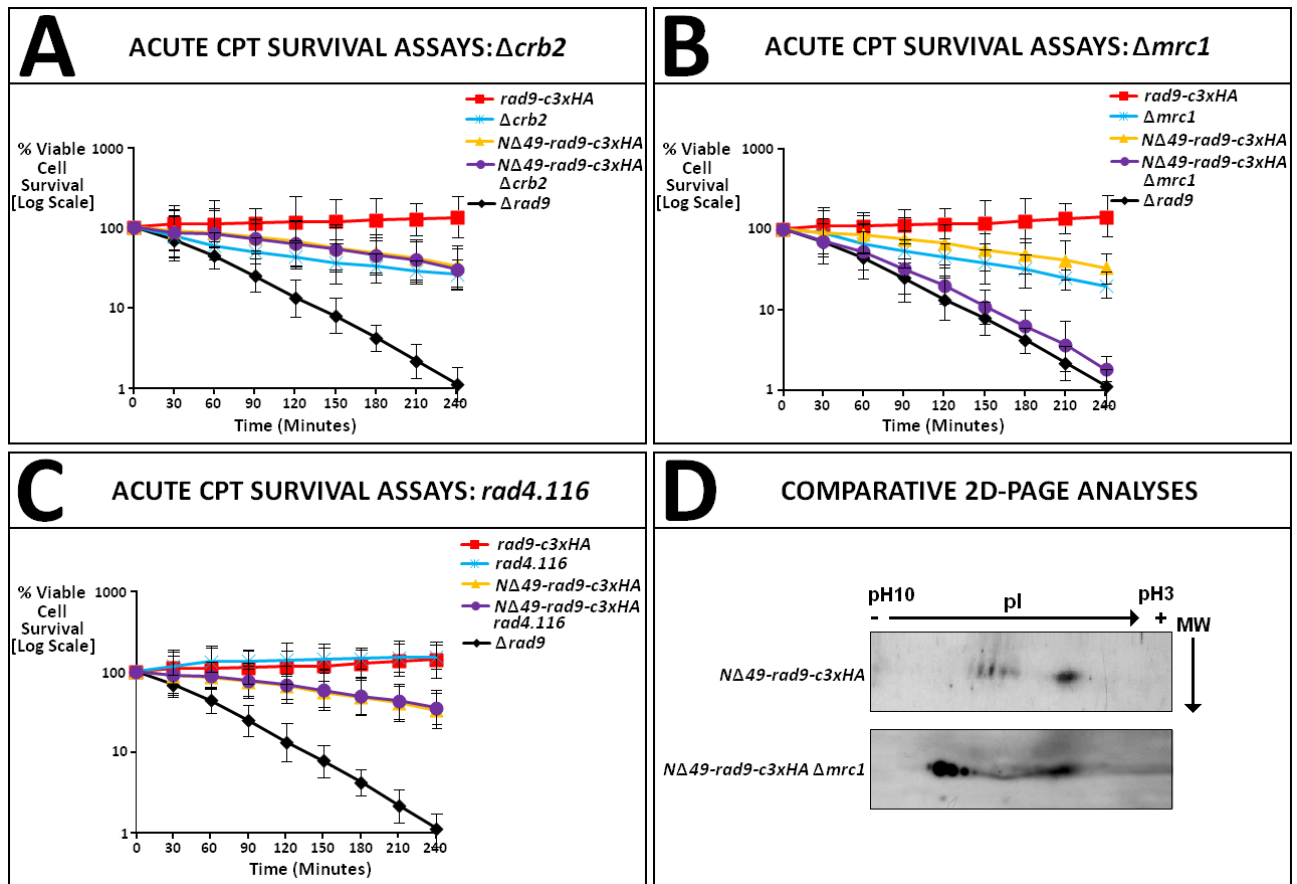
Subsequent Rad3-mediated post-translational phosphorylation-type modifications of Chk1 induce supramolecular conformational changes within the secondary (distal) checkpoint kinase which result in its catalytic activation and promote its thermodynamic dissociation from the respective scaffold/mediator protein (Lin S.J. *et al*, 2012; Qu M. *et al*, 2012).

The liberated, functionally-active Chk1 kinase then initiates “down-stream” biochemical signalling cascades which trigger a G(2)/M phasic cell cycle arrest in response to DNA damage (Lin S.J. *et al*, 2012; Qu M. *et al*, 2012).

Rad4 AAD domain-dependent activation of Rad3 proceeds via an alternative pathway which is G1/S cell cycle phase-specific and enables amplification of the Rad3→Chk1 checkpoint signal response to genotoxic stress under cytological conditions in which low levels of ssDNA, within the chromatin supramolecular architecture, may hinder “9-1-1” complex recruitment to DNA damage lesion sites (Lin S.J. *et al*, 2012; Qu M. *et al*, 2012).

This secondary pathway involves the exclusive recruitment of the Crb2 scaffold/mediator protein to DSB sites via Rad9-c:(Rad4:Crb2)-Rad1-Hus1 ternary complex formation and Crb2:nucleosomal interactions in which the tudor domain of Crb2 is in direct association with the H4 nucleosomal sub-unit (via a specific dimethylated lysine 20 residue within H4) and the BRCT domains of Crb2 are in direct association with the phosphorylated γ H2A nucleosomal sub-unit (Lin S.J. *et al*, 2012; Qu M. *et al*, 2012).

Fig 6.22: Acute CPT Survival Assays – Scaffold Proteins/Mediators



Figs A, B and C: Comparative acute cell survival assays performed with YEA broth cultures of the indicated *S. pombe* strains, incubated at 30°C in the presence of 40 μ M camptothecin (CPT) – Figs A, B and C.

[Acute cell survival assays were performed as per the methodology described in Chapter 2, Section 2.9.2.2(ii), pp.239-241]

Fig D: Individual 100mL YEA broth medium cell cultures of the indicated *S. pombe* strains were grown overnight (30°C for ~12 hour time period), then diluted to an optical density $A_{595} = 0.25$ with the appropriate volume of YEA medium and the resultant diluted cultures re-incubated at 30°C for a further time period of ~2.5 hours until they had attained an optical density value of $A_{595} = 0.5$.

TCA-precipitated total protein extract samples were then prepared from the appropriate *calculated volumetric aliquot of each culture (*equivalent to 40 A_{595} optical density units) and utilised in comparative 2D PAGE–coupled Western blot analyses – probed with the primary “anti-HA” antibody.

[Performed as per the methodologies described in Chapter 2, Section 2.8.3.1, pp.214-217; Section 2.8.5.1, pp.225-230 and Section 2.8.6., pp.231-233]

6.2.4 Cds1 is a Critical Secondary (Distal) Transducer/Effector Kinase Component of the “Rad9-S”–Mediated Checkpoint Response to Camptothecin-Induced DNA Damage, in Which the Suppression of Chk1 Functional Activity May Be Implicated

Comparative lactose synchronisation assay experimental data, acquired in this Ph.D. project, also revealed that *S. pombe* cells which were “cre-lox”–engineered for the exclusive expression of the truncated NΔ49-Rad9-c3xHA variant did not elicit a G2/M phasic cell cycle arrest in response to camptothecin-induced genotoxicity – which may be indicative that “Rad9-S” elicits a novel checkpoint pathway which suppresses the functional activation of the Chk1 secondary (distal) transducer kinase in response to CPT-induced DNA damage (discussed previously in detail in Section 6.2.3, pp.514-516).

It was therefore postulated that the truncated “Rad9-S” protein variant, acting within the heterodimeric “Rad9-S”：“Hus1-C” “open-ring/C-clamp” complex, may initiate an alternative checkpoint signal via activation of the Cds1 secondary (distal) transducer kinase in response to CPT-induced genotoxicity.

In order to test these hypotheses, comparative acute cell survival assays were performed on 30°C YEA broth cultures of the *S. pombe* double-mutant strains *NΔ49-rad9-c3xHA Δcds1* and *NΔ49-rad9-c3xHA Δchk1* and the side-directed mutagenized inactive Cds1 kinase double-mutant strain *NΔ49-rad9-c3xHA cds1-(T8A;T11A)* – Fig 6.23, p.543.

The acquired experimental data revealed that deletion of *cds1* within an exclusively expressed “*rad9-S*” genetic background, resulted in the significant enhancement of the sensitivity of the cells to CPT-induced DNA damage (Fig 6.23B, p.543), whilst perturbed autophosphorylated activation of Cds1 – ie site-directed mutagenized expression of *cds1-(T8A;T11A)* within an exclusively expressed “*rad9-S*” genetic background had negligible effect on the sensitivity of the cells to CPT-induced DNA damage (Fig 6.23C, p.543).

Taken together, these acute survival assay data indicated that although Cds1 kinase activity may be a key signalling component of the “Rad9-S”-mediated checkpoint pathway response to camptothecin genotoxicity, the activation of the Cds1 kinase protein is unlikely to proceed via the conventional autophosphorylation mechanism by which the individual monomeric Cds1 sub-units within a homodimeric (Cds1)₂ complex activate each other’s catalytic sites (Nitani N. *et al*, 2006; Xu X.J. *et al*, 2006; Xu X.J. and Kelly T.J., 2009).

In contrast, the acute survival assay data also revealed that deletion of *chk1* within an exclusively expressed “*rad9-S*” genetic background had negligible effect on the sensitivity of the cells to CPT-induced damage – indicative that functional Chk1 activity is not implicated in the truncated “Rad9-S” protein variant-mediated checkpoint signalling pathway response to CPT-induced DNA damage (Fig 6.23A, p.543).

Comparative 2D PAGE-coupled Western blot analyses of TCA-precipitated total protein extracts acquired from YEA broth cultures of the appropriate *S. pombe* strains revealed that deletion of *chk1* and perturbed Cds1 autophosphorylated-activation (ie the “*rad9-S*” *cds1-T8A;T11A* double-mutant) yield similar “static” phosphoisoform profiles, whilst deletion of *rad3*, *mrc1* and *cds1* yield hypo-phosphorylation profiles – indicative that Rad3, Mrc1 and Cds1 may be implicated in “Rad9-S”-mediated checkpoint signalling responses, in which Cds1 activation proceeds via an alternative mechanism (Fig 6.23D, p.543).

Comparative 2D-PAGE-coupled Western Blot analyses were also performed on TCA-precipitated total extracts acquired from YEA broth cultures of the *N149-rad9-c3xHA cds1-c13xMyc* strain incubated at 30°C in the absence and presence of 40µM camptothecin (CPT) for 30 minutes – which utilised the anti-HA and anti-Myc primary anti-body probes (Fig 6.24, p.544).

The acquired data indicated a hypo-phosphorylation shift within the phosphoisoform profile of “Rad9-S” in the absence and presence of CPT which may be due to perturbation of the C-terminal domain Cds1-Rad-S interactions as a consequence of steric hindrance influences exerted via the C-terminal HA- and Myc- epitope tags on the two respective proteins (Fig 6.24, p.544).

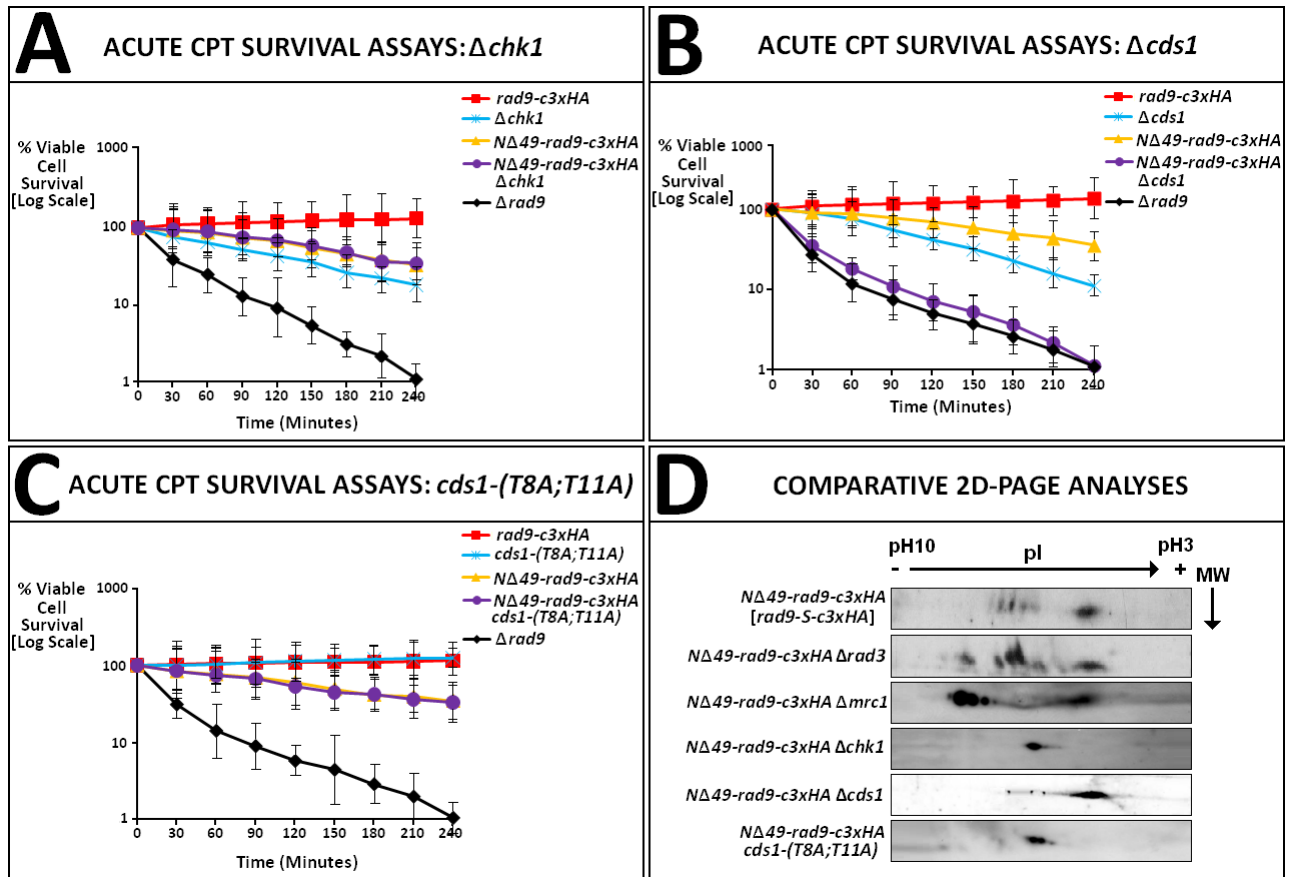
The acquired experimental data also indicate that three isoforms of Cds1 are expressed, in which the “Cds1” phosphoisoform profile undergoes a hyperphosphorylation shift in the presence of CPT, whilst two spots are absent in the phosphoisoform profile of “Cds1-VS” in the presence of CPT (Fig 6.24, p.544).

The notable exception the phosphoisoform profile of the “Cds1-S” protein, which remained unaltered in the presence of CPT and may be implicated in the regulation of the functional activities of the “Cds1” and “Cds1-VS” isoforms (Fig 6.24, p.544).

Taken together, these experimental observations indicate that the truncated “Rad9-S” protein variant may suppress the functional activity of Chk1 and initiate an alternative checkpoint signalling pathway, via a novel mechanism of Cds1 activation, in response to camptothecin-induced DNA damage (Fig 6.25, pp.545-546).

In this hypothetical context, the “Cds1”, “Cds1-S” and “Cds1-VS” isoforms may also interact with the two alternative truncated Rad9 isoforms identified in this Ph.D research project (discussed previously in detail in Chapter 4) – notably; “Rad9-VS” (NΔ73-Rad9), “Rad9-T” (NΔ117-Rad9) as part of a mechanism which could be implicated in the differential regulation of the full-length Rad9-mediated and truncated Rad9-S protein variant-mediated cell cycle checkpoint signalling pathway responses to CPT-induced damage (Fig 6.25, pp.545-546).

Fig 6.23: Acute CPT Survival Assays – Distal Transducer Kinases



Figs A, B and C: Comparative acute cell survival assays performed with YEA broth cultures of the indicated *S. pombe* strains, incubated at 30°C in the presence of 40µM camptothecin (CPT) – Figs A, B and C.

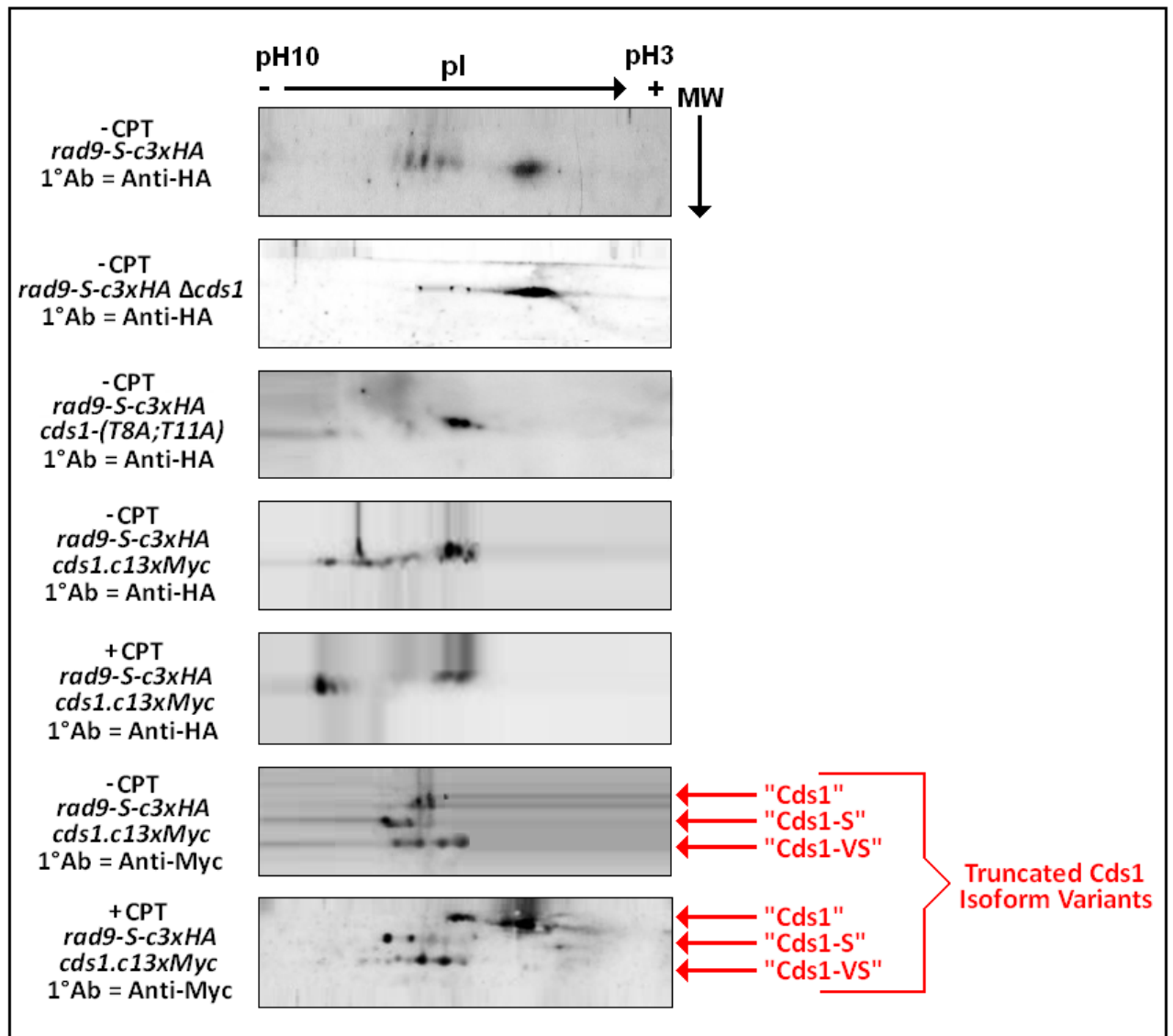
[Acute cell survival assays were performed as per the methodology described in Chapter 2, Section 2.9.2.2(ii), pp.239-241]

Fig D: Individual 100mL YEA broth medium cell cultures of the indicated *S. pombe* strains were grown overnight (30°C for ~12 hour time period), then diluted to an optical density $A_{595} = 0.25$ with the appropriate volume of YEA medium and the resultant diluted cultures re-incubated at 30°C for a further time period of ~2.5 hours until they had attained an optical density value of $A_{595} = 0.5$.

TCA-precipitated total protein extract samples were then prepared from the appropriate *calculated volumetric aliquot of each culture (*equivalent to 40 A_{595} optical density units) and utilised in comparative 2D PAGE–coupled Western blot analyses – probed with the primary “anti-HA” antibody.

[Performed as per the methodologies described in Chapter 2, Section 2.8.3.1, pp.214-217; Section 2.8.5.1, pp.225-230 and Section 2.8.6., pp.231-233]

Fig 6.24: 2D-PAGE Analyses of Potential Rad9-S – Cds1 Interactions



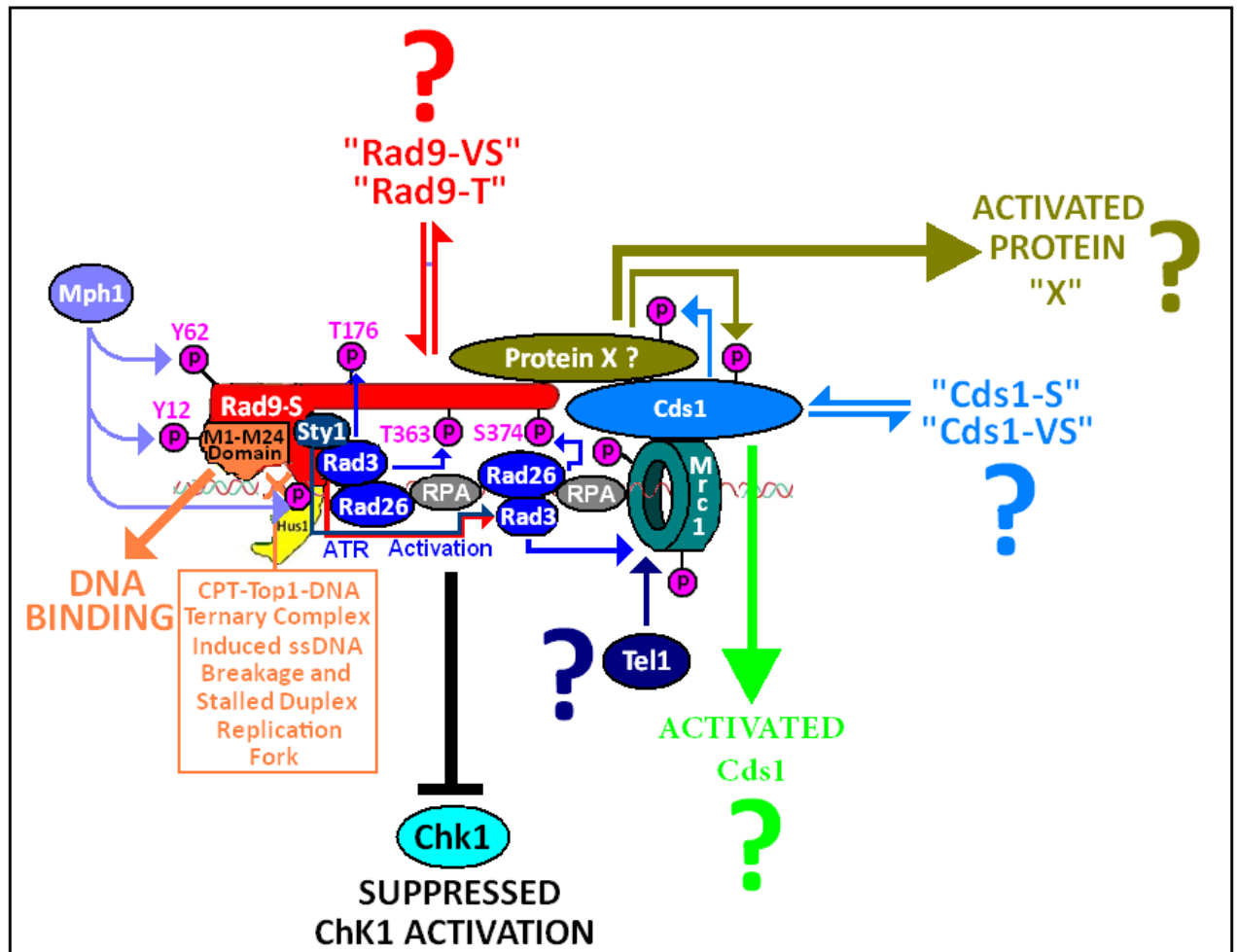
Individual 100mL YEA broth medium cell cultures of the indicated *S. pombe* strains were grown overnight (30°C for ~12 hour time period), then diluted to an optical density $A_{595} = 0.25$ with the appropriate volume of YEA medium and the resultant diluted cultures re-incubated at 30°C for a further time period of ~2.5 hours until they had attained an optical density value of $A_{595} = 0.5$.

The resultant *S. pombe* strain cultures of actively cycling cells were then incubated in YEA medium at 30°C in the absence (-CPT) or presence (+CPT) of 40μM camptothecin for a further 30 minutes.

TCA-precipitated total protein extract samples were then prepared from the appropriate *calculated volumetric aliquot of each culture (*equivalent to 40 A_{595} optical density units) and utilised in comparative 2D PAGE–coupled Western blot analyses – probed with the primary “anti-HA” antibody.

[Performed as per the methodologies described in Chapter 2, Section 2.8.3.1, pp.214-217; Section 2.8.5.1, pp.225-230 and Section 2.8.6., pp.231-233]

Fig 6.25: Hypothetical Model of Rad3- and Tel1- Differential Phosphorylation-Mediated Modulation of Functional Mrc1-“Rad9-S” Interactive Activities Which May Influence Specific Checkpoint Pathway Selective Activation Initiated Via the Heterodimeric “Rad9-S”：“Hus1-C” “Open-Ring/C-clamp” Complex



Mph1 and/or other checkpoint kinase-mediated phosphorylation of Y12 and Y62 within the “Rad9-S” protein and Y62 within the “Hus1-C” protein initiates complex formation and chromatin-association of the heterodimeric “Rad9-S”：“Hus1-C” “open-ring/C-clamp” in response to camptothecin (CPT)-induced genotoxicity.

In response to detected CPT-induced DNA damage lesion sites, initial Rad26-associated Rad3 kinase-mediated phosphorylation of “Rad9-S” at T176 induces supramolecular configurational changes within the truncated protein variant which enable Rad26/Rad3 kinase-mediated phosphorylation of the T363 and S374 residues – which are situated within its C-terminal tail domain.

Subsequent Rad26/Rad3 kinase-mediated phosphorylation of the T363 and S374 residues induces supramolecular configurational changes within the C-terminal tail domain of the “Rad9-S” truncated protein variant which may then enable it to engage with another checkpoint protein kinase “X”

Rad26/Rad3 kinase-mediated phosphorylation of Mrc1, at residues, enables the mediator protein to recruit the monomeric form of Cds1 kinase.

Mrc1-mediated recruitment Cds1 monomer, orientates the catalytic C-terminal domain of the protein in to close proximity with the “Rad9-S”-bound protein kinase “X” at the C-terminal domain to enable interactions between the Cds1 and protein “X” which may activate the Cds1 kinase via phosphorylation of T254, Y322 and S353 within the catalytic C-terminal domain of the Cds1 kinase.

Subsequent Cds1 kinase-mediated phosphorylation of residues within the the catalytic C-terminal domain of the protein kinase “X” may modulate its activity in other checkpoint signalling pathways.

The identified isoforms “Rad9-VS”, “Rad9 T”, “Cds1-S” and “Cds1-VS” may act as competitive-binding type inducers or suppressors within a regulatory mechanism which modulates the functional activities of the “Rad9-S” – Mrc1-co-ordinated Cds1-protein kinase “X” activated signalling responses.

Differential phosphorylation of Mrc1 by Tel1 and Rad3 kinases may be implicated in “switching-modulation” of the functional activities of the “Rad9-S”-Mrc1 co-ordinated activation of Cds1 and protein kinase “X” which could be associated with specific Hus1-dependent and Hus1-independent “Rad9-S”-mediated signalling pathways in response to camptothecin-induced DNA damage and/or environmental stresses that impinge adversely upon DNA replication, such as heat shock.

6.2.5 Hhp1 is a Critical Effector Kinase Component Which May be Implicated in the Temporal Cell Cycle Phasic Co-Ordination and Functional Activity Regulation of the “Rad9-S”-Initiated Checkpoint Response to Camptothecin-Induced Genotoxicity

Comparative temporal protein expression analyses revealed that camptothecin-induced DNA damage results in the phosphorylation of both the full-length Rad9 protein and truncated “Rad9-S” protein variant between 60-90 minutes exposure to camptothecin and that CPT-mediated topoisomerase I inhibition does not induce expression of the truncated “Rad9-S” protein variant (Fig 6.26A, pp.549-550).

These experimental data also indicated that prolonged exposure to camptothecin induces expression of the “Rad9-VS” isoform with consequential suppressed phosphorylation and/or induced phosphatase-targeted dephosphorylation of “Rad9-S” within a 5 – 6 hour elapsed time period – which may constitute a functional role of the truncated “Rad9-VS” isoform in the regulation of “Rad9-S”-mediated checkpoint signalling activities (Fig 6.26A, pp.549-550).

Previous experimental studies have demonstrated that casein kinase I (of which Hhp1 is the *S. pombe* functional homolog) is implicated in the regulation of the circadian clock (Agostino P.V. *et al.*, 2008) and Hhp1 is also implicated in DNA repair pathways (Dhillon N. and Hoekstra M.F., 1994).

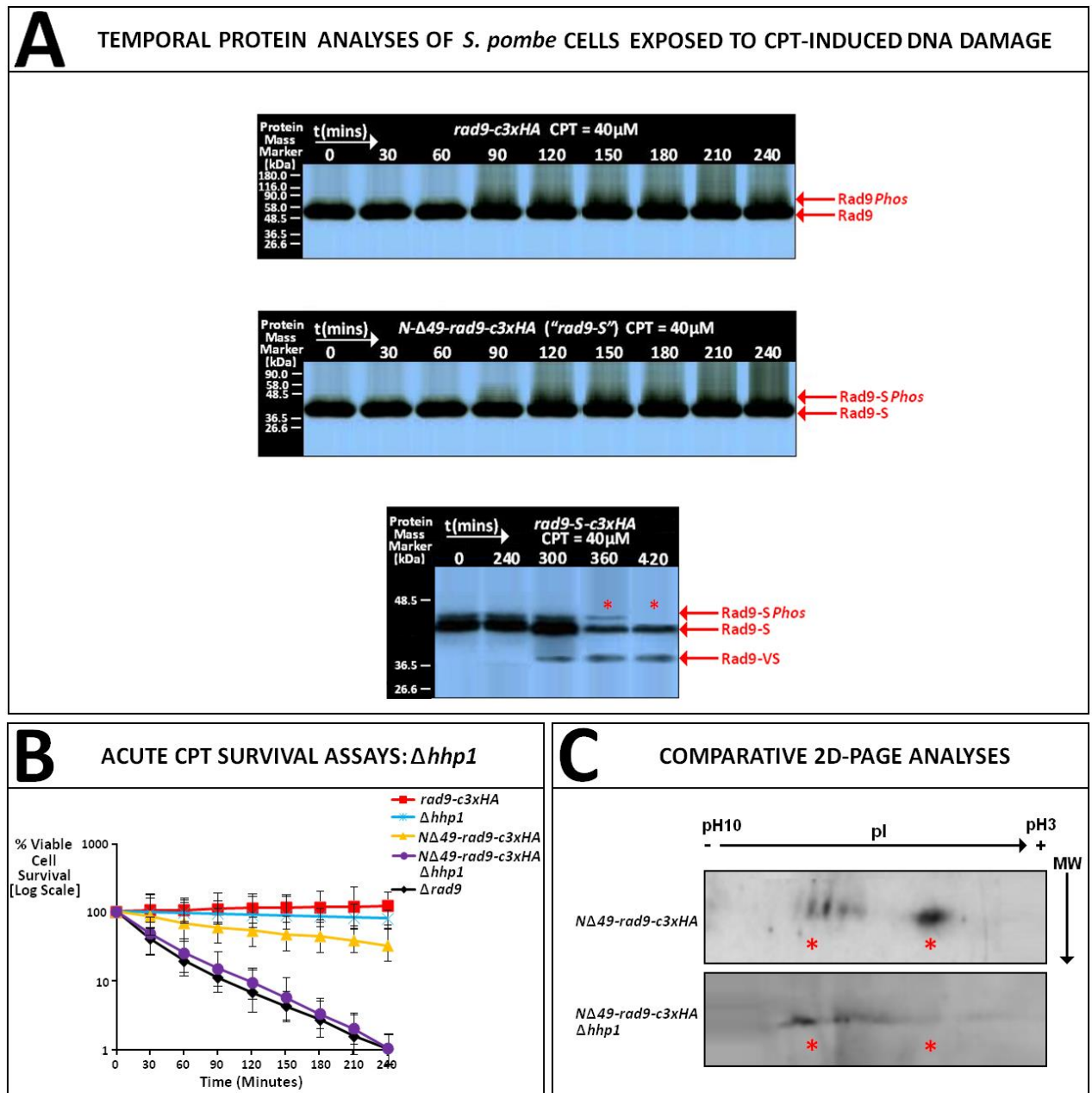
In order to ascertain whether or not Hhp1 kinase may be implicated in the temporal regulation of the functional activities of the truncated “Rad9-S” protein variant associated with the phasic cell cycle co-ordination of camptothecin-induced checkpoint signalling arrest and subsequent DNA repair, comparative acute CPT survival assays were performed with the double-mutant *S. pombe* strain *NA49-rad9-c3xHA Δhhp1* (Fig 6.25B, pp.549-550).

The acquired experimental data indicated that deletion of the *hhp1* gene (which encodes a Casein Kinase 1 type homolog) within an exclusively expressed “*rad9-S*” genetic background, increased of the sensitivity of the cells to camptothecin-induced DNA damage (Fig 6.26B, pp.549-550) – indicative that the protein is an essential component of the “Rad9-S” truncated protein variant-initiated checkpoint signalling pathway implicated in a “9-1-1” complex-independent response to CPT-induced DNA damage.

Comparative 2D-PAGE-coupled Western blot analyses also revealed that deletion of *hhp1* within an exclusively expressed “*rad9-S*” genetic background results in a hypo-phosphorylation shift within the phosphoisoform profile of the “Rad9-S” truncated protein variant (Fig 6.26C, pp.549-550) – indicative that Hhp1 kinase-mediated phosphorylation of “Rad9-S” may be implicated in the functional activity of its initiated checkpoint response to camptothecin-induced genotoxicity.

Taken together, these experimental data may indicate that the functional activity of “Rad9-S” in the checkpoint signalling response to CPT-induced DNA damage is temporally regulated and/or may be sequentially cell cycle phase co-ordinated with DNA repair and reinitiation of DNA replication, via a mechanism in which the truncated “Rad-VS” isoform and Hhp1 Kinase may be implicated.

Fig 6.26: Evidence for Potential Roles of the Truncated “Rad9-VS” Isoform and Hhp1 Kinase in the Temporal Regulation of Functional “Rad9-S” Activities



[See Figure Legend, p.550, for a full description of the experimental data]

Figure Legend – Fig 6.26

A: 150mL YEA broth medium cell cultures of the “Cre-Lox” – constructed *rad9-c3xHA* and *NΔ49-rad9-c3xHA S. pombe* strains were grown overnight to (30°C for ~12 hour time period), then diluted to an optical density $A_{595} = 0.5$ with the appropriate volume of YEA medium and the resultant diluted cultures re-incubated at 30°C in the presence of 40μM camptothecin (CPT) for a total time period of 4 hours.

TCA-precipitated total protein extract samples were then prepared from the appropriate *calculated volumetric aliquots of the respective cultures (*equivalent to 10 A_{595} optical density units) which were taken regular 30 minute time intervals.

20μL aliquots of the prepared samples were resolved on a 10% SDS-PAGE gels which were then subjected to Western blot analyses – probed with the primary “anti-HA” antibody.

[Protein sample preparation, SDS-PAGE resolution and Western blot methodologies are detailed in Section 2.8.1, pp.200-202; Section 2.8.4, pp.223-224 and Section 2.8.6, pp.231-233]

B: Comparative acute cell survival assays performed on YEA broth cultures of the indicated *S. pombe* strains, incubated at 30°C in the presence of 40μM camptothecin for a total time period of 4 hours.

[Acute cell survival assays were performed as per the methodology described in Chapter 2, Section 2.9.2.2(ii), pp.239-241]

C: Individual 100mL YEA broth medium cell cultures of the indicated *S. pombe* strains were grown overnight (30°C for ~12 hour time period), then diluted to an optical density of $A_{595} = 0.25$ with the appropriate volume of YEA medium and the resultant diluted cultures re-incubated at 30°C for a further time period of ~2.5 hours until they had attained an optical density value of $A_{595} = 0.5$.

TCA-precipitated total protein extract samples were then prepared from the appropriate *calculated volumetric aliquot of each culture (*equivalent to 40 A_{595} optical density units) and utilised in comparative 2D PAGE–coupled Western blot analyses – probed with the primary “anti-HA” antibody.

[Performed as per the methodologies described in Chapter 2, Section 2.8.3.1, pp.214-217; Section 2.8.5.1, pp.225-230 and Section 2.8.6., pp.231-233]

6.2.6 Cdc25 and Rad24 May Modulate the Phosphoisoform-Specific Functional Activities of the Truncated “Rad9-S” Protein

The Cdc25 phosphatase protein mediates the post-translational dephosphorylated modification-initiated activation of the Cdc2 checkpoint kinase, whilst the Rad24 protein targets the Cds1-phosphorylated Cdc25 phosphatase for cytosolic sequestration and proteasomal degradation thereby regulating the functional activity of the Cdc2 protein kinase (Lopez-Gerona A. *et al.*, 1999; Zeng Y. *et al.*, 1998).

In order to ascertain whether Cdc25 and Rad24 could be implicated in the regulation of Cdc2 kinase-mediated post-translational phosphorylated-modulation of the truncated “Rad9-S” protein variant-initiated checkpoint response to camptothecin-induced DNA damage, in which Cds1 is implicated (discussed previously in Section 6.2.4, pp.539-546), comparative acute cell survival assays were performed on YEA broth cultures of the *S. pombe* strains NΔ49-rad9-c3xHA *cdc25.22* (a functionally-impaired phosphatase mutant) and NΔ49-rad9-c3xHA Δ*rad24* (*rad24* deletion mutant) – Fig 6.27A and Fig 6.27B, pp.554-555.

The acquired experimental data revealed that functional perturbation of the *cdc25* gene (ie the *cdc25.22* mutant) and deletion of the *rad24* gene within an exclusively expressed “*rad9-S*” genetic background, had negligible effect on the sensitivity of the cells to CPT-induced DNA damage (Fig 6.27A and Fig 6.27B, pp.554-555).

Comparative 2D-PAGE-coupled Western blot analyses indicate that perturbation of the functional activity of the Cdc25 phosphatase (ie the *cdc25.22* mutant) within an exclusively expressed “*rad9-S*” genetic background results in a hypo-phosphorylation shift within the phosphoisoform profile of the “Rad9-S” truncated protein variant (Fig 6.27C, pp.554-555) – which may be indicative that Cdc25 phosphatase-initiated Cdc2-kinase-mediated phosphorylation of “Rad9-S” is implicated in the checkpoint signalling response to CPT-induced genotoxicity

Comparative 2D-PAGE-coupled Western blot analyses indicate that deletion of *rad24* within an exclusively expressed “*rad9-S*” genetic background results in a hyper-phosphorylation shift within the phosphoisoform profile of the “Rad9-S” truncated protein variant (Fig 6.27C, pp.554-555) – which may due to enhanced Cdc25 phosphatase-activation of the Cdc2 kinase and subsequent enhanced Cdc2 kinase-mediated phosphorylation of “Rad9-S” as a consequence of perturbed Rad24-mediated sequestration and proteolytic targeted degradation of the Cdc25 phosphatase.

Comparative 2D-PAGE-coupled Western blot analyses indicate that deletion of *rad24* within an exclusively expressed “*rad9-S*” genetic background results in a hyper-phosphorylation shift within the phosphoisoform profile of the “Rad9-S” truncated protein variant (Fig 6.27D, pp.554-555) – which may due to enhanced Cdc25 phosphatase-activation of the Cdc2 kinase and subsequent enhanced Cdc2 kinase-mediated phosphorylation of “Rad9-S” as a consequence of perturbed Rad24-mediated sequestration and proteolytic targeted degradation of the Cdc25 phosphatase.

Comparative 2D-PAGE-coupled Western blot analyses indicate that deletion of *hhp1* within an exclusively expressed “*rad9-S*” genetic background results in a hypo-phosphorylation shift within the phosphoisoform profile of the “Rad9-S” truncated protein variant, similar in pattern to the “Rad9-S” phosphoisoform profile of the *NA49-rad9-c3xHA cdc25.22* double mutant (Fig 6.27C, pp.554-555).

Comparative acute survival assays indicated that deletion of *hhp1*, within an exclusively expressed “*rad9-S*” genetic background enhanced the sensitivity of the *S. pombe* cells to camptothecin-induced DNA damage (discussed in detail previously in Section 6.2.5., pp.547-550).

Cds1 kinase phosphorylates and inactivates Wee1 kinase, whilst Cds1 kinase-mediated phosphorylation of Cdc25 primes this phosphatase for associative Rad24-mediated cytosolic sequestration and proteasomal degradation (Blasina A. *et al*, 1999; Furnani B. *et al*, 1999).

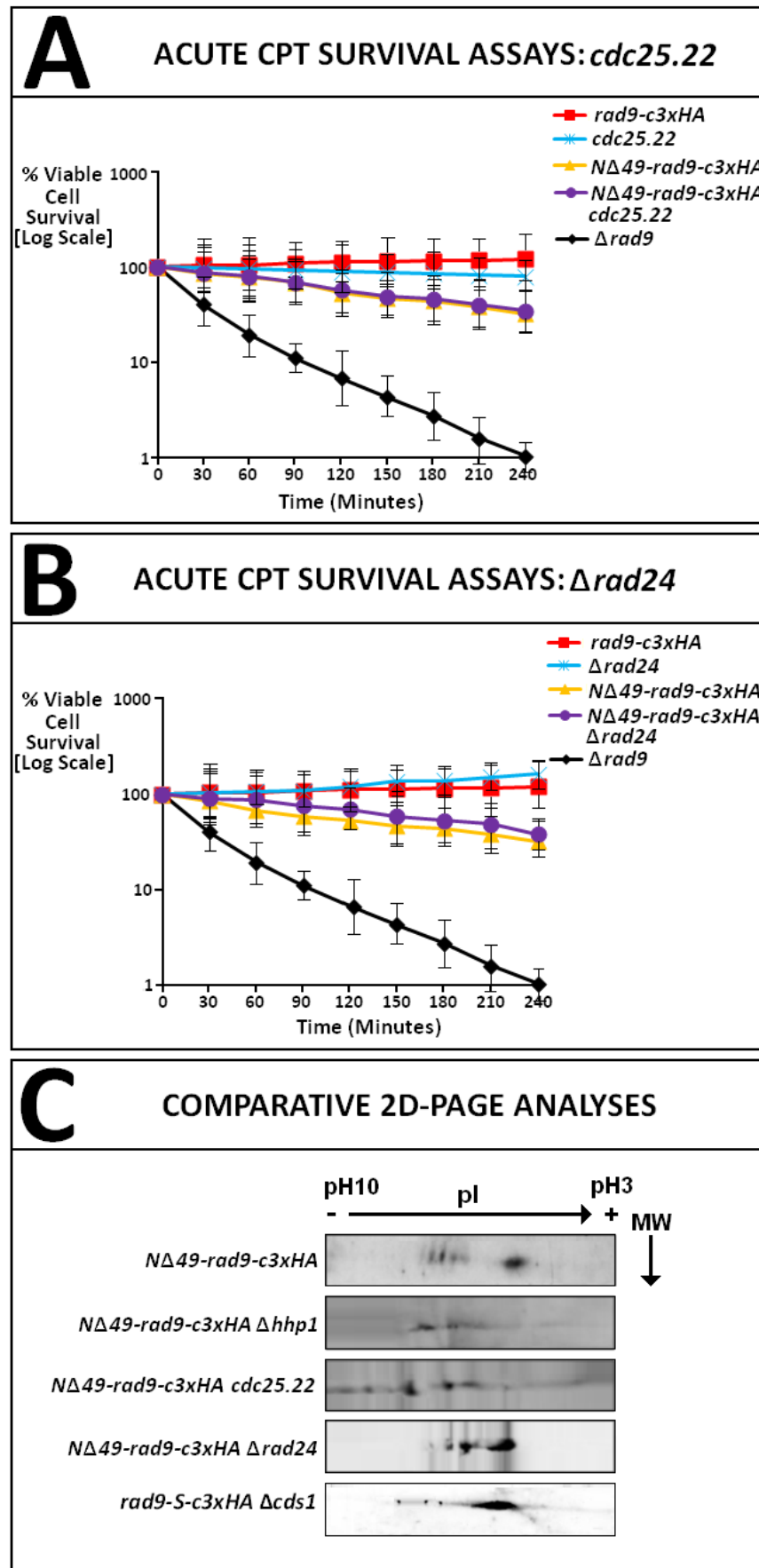
Comparative acute survival assays indicated that deletion of *cds1* within an exclusively expressed “*rad9-S*” genetic background enhanced the sensitivity of the *S.pombe* cells to camptothecin-induced DNA damage (discussed in detail previously in Section 6.2.4, pp.539-546).

Comparative 2D-PAGE-coupled Western blot analyses indicate that deletion of *cds1* within an exclusively expressed “*rad9-S*” genetic background results in a hypo-phosphorylation shift within the phosphoisoform profile of the “Rad9-S” truncated protein variant, similar in pattern to the “Rad9-S” phosphoisoform profile of the *NΔ49-rad9-c3xHA cdc25.22* double-mutant – with the notable exception of a short hyperphosphorylated tail towards the anode (Fig 6.27C, pp.554-555).

Taken together, these experimental observations indicate that the functional activity of “Rad9-S” in the checkpoint signalling response to CPT-induced DNA damage may be the initiation of a Cds1 kinase-mediated checkpoint response, which may be temporally regulated and co-ordinated with DNA repair pathways via an Hhp1 kinase-mediated signalling mechanism and involving Cdc2 kinase-mediated post-translational phosphorylated modulation of the truncated “Rad9-S” protein variant functional activities.

In this hypothetical context, the “Cds1-S” and “Cds1-VS” isoforms (discussed previously in Section 6.2.4, pp.539-546) may also interact with the two alternative truncated Rad9 isoforms identified in this Ph.D research project (discussed previously in detail in Chapter 4) – notably; “Rad9-VS” (NΔ73-Rad9) and “Rad9-T” (NΔ117-Rad9), as part of a mechanism which could be implicated in the regulation of the truncated Rad9-S protein variant-mediated cell cycle checkpoint signalling pathway responses to CPT-induced damage.

Fig 6.27: Comparative Acute CPT Survival Assays and 2D PAGE-Coupled Western Blot Analyses – Effectors and Regulators



[See Figure Legend, p.555, for a full description of the experimental data]

Figure Legend – Fig 6.27

Fig A and Fig B: Comparative acute cell survival assays performed on YEA broth cultures of the indicated *S. pombe* strains, incubated at 30°C in the presence of 40µM camptothecin for a total time period of 4 hours.

[Acute cell survival assays were performed as per the methodology described in Chapter 2, Section 2.9.2.2(ii), pp.239-241]

Fig C: Individual 100mL YEA broth medium cell cultures of the indicated *S. pombe* strains were grown overnight (30°C for ~12 hour time period), then diluted to an optical density of $A_{595} = 0.25$ with the appropriate volume of YEA medium and the resultant diluted cultures re-incubated at 30°C for a further time period of ~2.5 hours until they had attained an optical density value of $A_{595} = 0.5$.

TCA-precipitated total protein extract samples were then prepared from the appropriate *calculated volumetric aliquot of each culture (*equivalent to 40 A_{595} optical density units) and utilised in comparative 2D PAGE–coupled Western blot analyses – probed with the primary “anti-HA” antibody.

[Performed as per the methodologies described in Chapter 2, Section 2.8.3.1, pp.214-217; Section 2.8.5.1, pp.225-230 and Section 2.8.6., pp.231-233]

6.3 Component MAP Kinase Cell Cycle Checkpoint Pathway Inputs

In silico comparative sequence alignments of the *S. pombe* Sty1 kinase and Rad9 proteins, via utilisation of the JemBOSS and PSI-BLAST bioinformatics software tools, indicated that the Rad9 protein contained a Wis1-like kinase target site motif ¹¹⁰**GYGSESASR¹¹⁸**, with similar homology to the site found in Sty1 – in which **Y¹¹¹** (equivalent to to **Y⁶²** within the truncated “Rad9-S” protein variant) may be phosphorylated by the Wis1 kinase (Fig 6.29D, p.564)

In order to determine whether the MAP Kinase pathway was implicated in the “Rad9-S”-mediated signalling response to camptothecin-induced DNA damage the *NΔ49-rad9-c3xHA S. pombe* strain was cross-mated with the MAP kinase checkpoint-associated type gene deleted type *S. pombe* strains *Δwis* and *Δsty1* which were then utilised in comparative acute assays with camptothecin (Fig 6.29, p.564).

The data identified that the Sty1 kinase, but not Wis kinase, was a putative component of the “Rad9-S”-mediated checkpoint signalling pathway response to camptothecin-induced DNA damage and therefore indicated that Wis1 kinase-mediated phosphorylation of Y62 within the “Rad9-S” truncated protein variant was not implicated (Fig 6.29, p.564).

Comparative acute and chronic (drop-plate) heat-shock and camptothecin survival assays were also performed with the *S. pombe* strains *Δrad9*, *rad9-c3xHA*, *rad9-(M50L)-c3xHA* and *NΔ49-rad9-c3xHA* (“Rad9-S”) in the absence and presence of 1M sorbitol (induced osmotic shock) – Fig 6.31, p.566 and Fig 6.32, p.567.

In *S. pombe* cells, osmotic shock has also been demonstrated to initiate a MAP kinase-mediated cell cycle stress checkpoint signalling response that triggers activation of the Atf1 transcription factor protein (Fig 6.28, p.563) which then targets the promoter of the *gpd1* gene and induces expression of the glycerol-3-phosphate dehydrogenase enzyme (Degols G. *et al*, 1996).

Consequential induction of elevated glycerol-3-dehydrogenase enzymatic activity results in increased levels of intracellular glycerol to counter-act the extracellular osmotic stress environment (Degols G. *et al*, 1996).

The data acquired from heat shock (at 37°C) and camptothecin (40µM CPT) acute and chronic cell survival assays performed under osmotic stress conditions (1M Sorbitol), with *S. pombe* cells “Cre-Lox”- engineered for the exclusive expression of the truncated “Rad9-S” protein variant, indicated enhanced sensitivity of the cells to CPT-induced DNA damage, but enhanced resistance of the cells to thermal stress (Fig 6.31, p.566, Fig 6.32, p.567).

Osmotic stress-induced elevation of intracellular glycerol levels may increase levels of diacylglycerol with consequential activation of the metacaspase pathway, in which the Rad9 protein has been implicated in *S. pombe* cells (Low C.P. *et al*, 2008) – discussed previously in Chapter 4.

Comparative *in Silico* analyses, which involved bioinformatics-based caspase/metacaspase substrate target motif sequence alignments, identified a putative target cleavage site within the regional sequence ¹¹⁰**GY¹¹¹** **GSESASR¹¹⁸** of the *S. pombe* Rad9 protein (discussed previously in Chapter 4) – that also contains the identified Wis1-like kinase target site motif with similar homology to the site found in Sty1 (Fig 6.29D, p.564).

Although the acquired acute camptothecin survival assay data indicate that Wis1 kinase-mediated phosphorylation of Rad9-S at Y62 (the equivalent **Y¹¹¹** site in the full-length Rad9 protein) within this motif is not implicated in the “Rad9-S”-mediated signalling response to CPT-induced DNA damage (Fig 6.29A, p.564), this tyrosine residue may be a putative phosphorylation target for the mitotic spindle checkpoint kinase Mph1 (discussed later in Section 6.4, pp.568-583).

Recent experimental studies have indicated that kinase-mediated phosphorylation of adjacent amino acid residues flanking caspase-type target site sequences induces supramolecular configurational changes within their structural motifs which protects them against proteolytic cleavage by the respective caspase enzymes in various cell cycle checkpoint signalling networks that are implicated in the regulatory control of apoptotic pathways (Filhol O. *et al*, 2011; Turowec J.P. *et al*, 2011).

Two putative interactive-motifs have been identified within the *S. cerevisiae* Ddc1 protein (Rad9^{Sp}, Rad9^{Hs}) – which associate with the Mec1 kinase (Rad3^{Sp}, ATR^{Hs}) and induce supramolecular configurational changes within the protein that enhance its catalytic activity (Navadgi-Patil V.M. and Burgers P.M., 2009).

In silico comparative sequence alignments of the *S. pombe* Sty1 kinase, Wis1 kinase, Rad9 and “Rad9-S” proteins with these two Mec1 interactive motifs, via utilisation of the JemBOSS and PSI-BLAST bioinformatics software tools, identified equivalent putative equivalent motifs, with two conserved tyrosine residues, which may interact with and enhance the activity of the Rad3 kinase (Fig 6.29F, p.564).

In the case of the Sty1 kinase, these two conserved tyrosine residues were also situated within its Wis1-like kinase target site motif (Fig 6.29F, p.564).

Taken together, these experimental observations indicate that the truncated the “Rad9-S” protein variant may be implicated in the modulation of two distinctive pathways with regard to differential signalling responses to heat shock and camptothecin-induced DNA damage respectively.

Hyperosmotic conditions have been demonstrated experimentally to alter the topology of DNA from the A or B conformers, to the more slender Z conformer (Lee J. *et al*, 2010) and can also induce superhelical torsional configurations within the duplex (Aoki K. and Murayama K., 2012; Choi J. and Majima T., 2011; Dickerson R.E. *et al*, 1982; Drew H. *et al*, 1980; Hansen P.L. *et al*, 2001; Lee D.J. *et al*, 2010; McClellan J.A. *et al*, 1990; Bi Bhriain N. *et al*, 1989; Podgomik R. *et al*, 1995; Tan Z.J. and Chen S.J., 2006; Yarmola E.G. *et al*, 1985; Zakrzewska K. *et al*, 1980).

Recent “follow-up” research work by Caspari T. and co-workers has indicated that a novel heat-shock checkpoint response pathway may be mediated via an alternative heterotrimeric, toroidal “Rad9-S”:Rad1:Hus1 DNA sliding-clamp complex (Janes S. *et al*, 2012, *Journal of Cell Science*, publication “in press” – see Appendix 6.1, pp.626-663).

The “Rad9-S” sub-unit lacks the first 49 amino acids which could enforce tighter steric constraints of the alternative “Rad9-S”:Rad1:Hus1 DNA sliding-clamp complex around the DNA, thus hyperosmotic stress-induced conversion of the duplex topology to the more slender Z-conformer may increase the mobility of this heterotrimeric complex and facilitate initiation of the checkpoint signalling response to hyperthermic stress with consequential enhanced cytological resistance to heat shock.

In contrast, hyperosmotic stress-induced conversion of the duplex topology to the more slender Z-conformer may abrogate associative “Rad9-S”:“Hus1-C” “open-ring/C-clamp” complex-DNA interactions with consequential enhanced cytological sensitivity to camptothecin-induced genotoxic stress.

Osmotic stress may also modulate chromatin supramolecular architecture, via local and/or global alteration of DNA supercoiling topological configuration (McClellan J.A. *et al*, 1990; Ni Bhriain N. *et al*, 1989), which may hinder and/or facilitate access of transcriptional and translational ribosomal complexes to specific gene loci and thus influence their expression and cytological levels of the respective encoded proteins.

In this context, hyperosmotic stress-induced potentiation of the cytotoxic sensitivity of the $\Delta rad9$ and $N\Delta49-rad9-c3xHA$ *S. pombe* strains to camptothecin (CPT)-induced DNA damage may be a consequence of elevated topoisomerase I expression and/or abrogated expression of one or more genes which encode critical checkpoint proteins that orchestrate the G(2)/M phasic cell cycle arrest response to CPT-induced genotoxicity (Fig 6.31, p.566; Fig 6.32, p.567).

Whilst hyperosmotic stress-induced resilience of the $\Delta rad9$, $rad9-c3xHA$, $rad9-(M50L)-c3xHA$ and $N\Delta49-rad9-c3xHA$ *S. pombe* strains to hyperthermic stress may be a consequence of elevated expression of one or more genes which encode critical MAP kinase checkpoint proteins (Fig 6.31, p.566; Fig 6.32, p.567).

Experimental studies have also demonstrated that the specific geometric conformational topology of duplex supercoiling can have profound influence on the catalytic DNA cleavage activity of human topoisomerase I (Gentry A.C. *et al*, 2011)

Taking this phenomenon into consideration, another plausible hypothesis is that hyperosmotic stress-induced alteration of the chromatin supramolecular architecture may also affect the geometry of supercoiled topology in the DNA which may elevate the catalytic DNA cleavage activity of topoisomerase I with consequential potentiation of camptothecin-induced cytotoxicity.

A Sty1 kinase differential activity-based switching mechanism, that is based upon its ability to interact with and induce the activity of the Rad3 kinase in conjunction with “Rad9-S”, may also be implicated in the specific selection of the “Rad9-S” truncated protein-mediated signalling responses to thermal stress or camptothecin-induced damage.

Osmotic shock induction of the MAP kinase cell cycle stress pathway may trigger elevation of intracellular glycerol levels (that initiate the metacaspase pathway) and also initiate Wis 1 kinase-mediated phosphorylation of Sty1 kinase which induces supramolecular conformational changes within the protein that render it unable to interact with and activate the Rad3 kinase.

The observed osmotic stress-enhanced camptothecin (CPT) sensitivity of *S. pombe* cells, which were “cre-lox”-engineered for the exclusive expression of the truncated “Rad9-S” protein variant, may be due to Wis 1 kinase-suppression of co-operative Sty1 kinase-mediated Rad3 kinase activation, which would suppress Rad3 kinase-mediated phosphorylation of the “Rad9-S” truncated protein variant with consequential suppression of the “Rad9-S”-mediated checkpoint signalling response to CPT-induced DNA damage.

Whilst the observed osmotic stress-enhanced heat shock resistance of *S. pombe* cells, which were “Cre-Lox”-engineered for the exclusive expression of the truncated “Rad9-S” protein variant, may be an independent function of the metacaspase cleavage-generated “Rad9-T” protein variant – whose functional activities are regulated by the postulated metacaspase cleavage-generated N Δ 49-Rad9-C Δ 118-426 and N Δ 73-Rad9-C Δ 118-426 proteins (discussed previously in Chapter 4).

The truncated “Rad9-T” isoform may be functional and elicit appropriate checkpoint signal responses to heat-induced damage to DNA and/or other cytological components via associative protein-interactions within its C-Terminal domain, under conditions of elevated thermal stress which would result in heat-denatured inactivation of the “Rad9-S” protein.

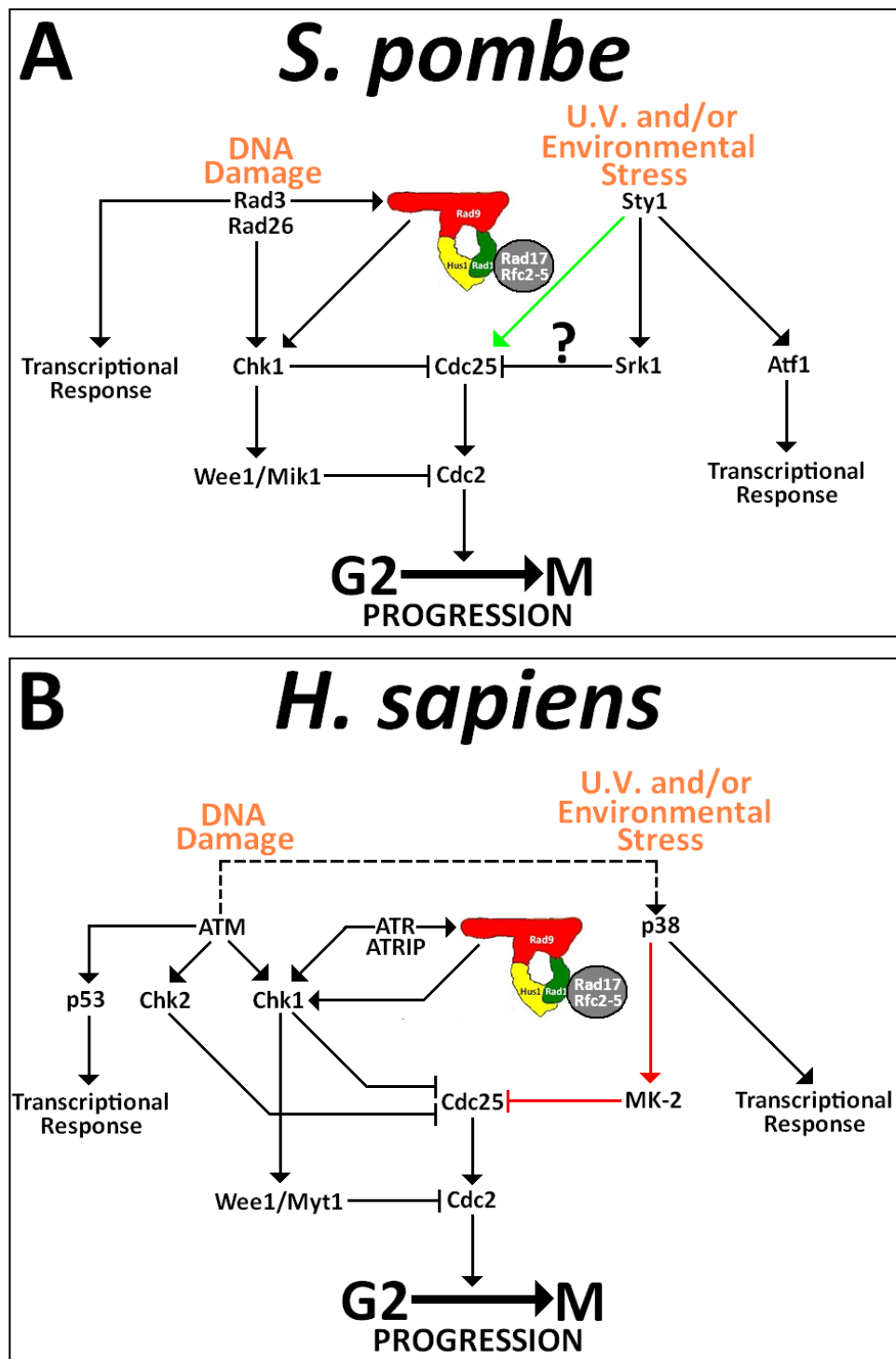
Comparative 2D PAGE-coupled Western blot analyses also revealed that deletion of *wis1*, but not *sty1* or *rad3*, within an exclusively expressed “*rad9-S*” genetic background induces the expression of the “Rad9-VS” and “Rad9-T” isoforms, whilst site-directed mutagenesis of tyrosine 62 to phenylalanine within the “Rad9-S” truncated protein only induces expression of the “Rad9-VS” isoform (Fig 6.30, p.565).

Acute camptothecin cell survival assay data also indicated that Wis1 was not required for the “Rad9-S”-mediated response to CPT-induced DNA damage (Fig 6.29A, p.564).

Taken together, these data indicate that Wis1 may also be implicated in regulatory control of “Rad9-T” isoform expression via suppression of the metacaspase pathway under normal “stress-free” cytological conditions, whilst expression of the “Rad9-VS” isoform may be regulated via phosphorylation of Y62 and that “Rad9-VS” may possibly be implicated in the regulation of both “Rad9-S” and “Rad9-T” functional activities.

Fig 6.28: Overview of DNA Damage & Cell Cycle Stress Responses

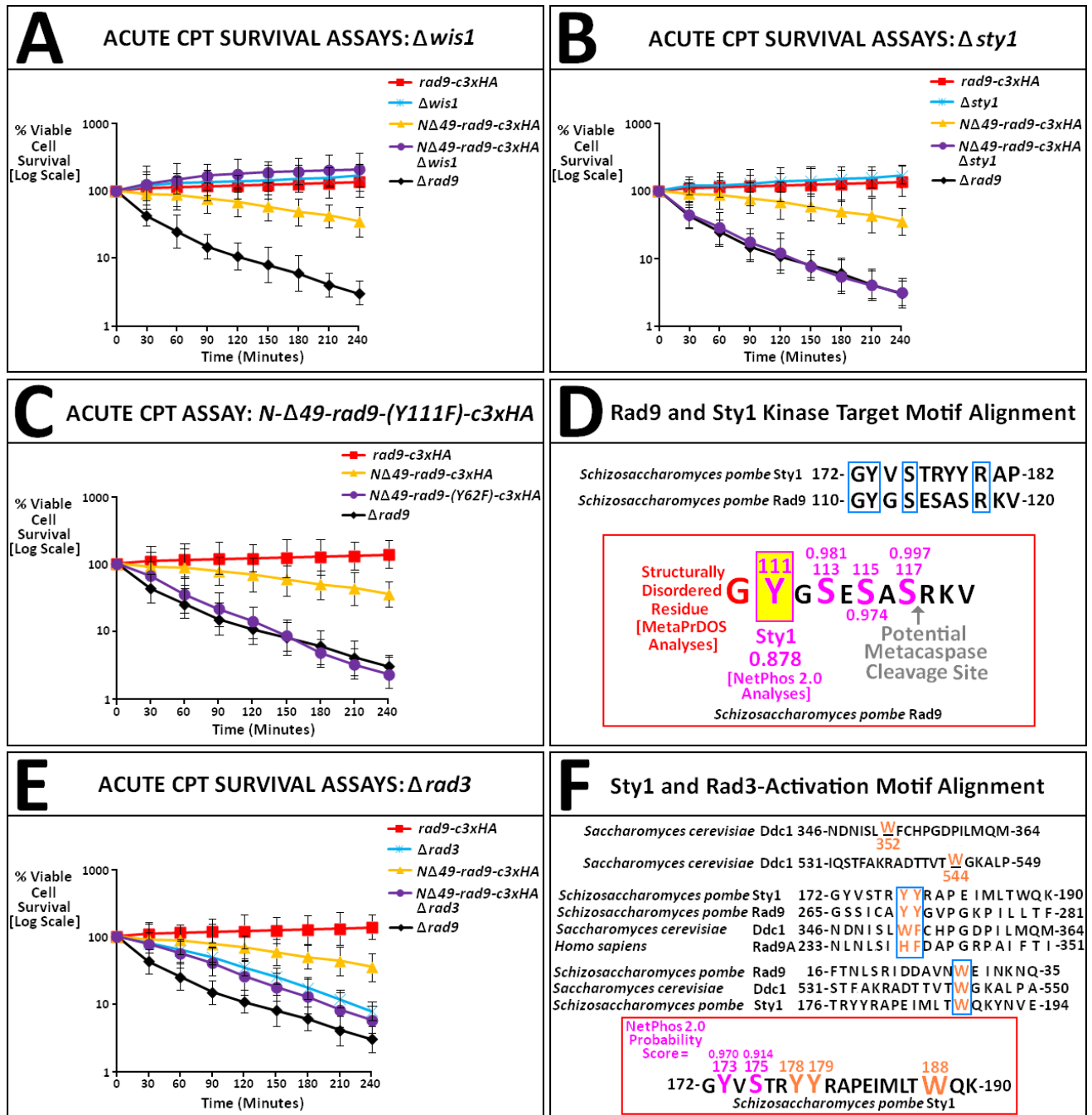
[Taken and Adapted From: Alao J.P. and Sunnerhagen P., 2008]



Summarised equivalent functional protein homologs of the DNA damage response and MAP kinase stress-induced checkpoint pathways in DNA in *S. pombe* cells (Fig A) and those of mammalian cells (B) are indicated, the respective pathways in mammalian cells were discussed previously in Chapter 1, Section 1.2.2, p.60. (to which the reader is referred).

Note: In *S. pombe* cells activation of the Sty1 kinase accelerates the cell cycle, whilst in mammalian cells activation of the equivalent functional protein homolog p38 MAP kinase induces a mitotic delay (discussed in detail previously in Chapter 1, Section 1.2.2, p.60).

Fig 6.29: Acute CPT Survival Assays – Mitogen-Activated Kinases



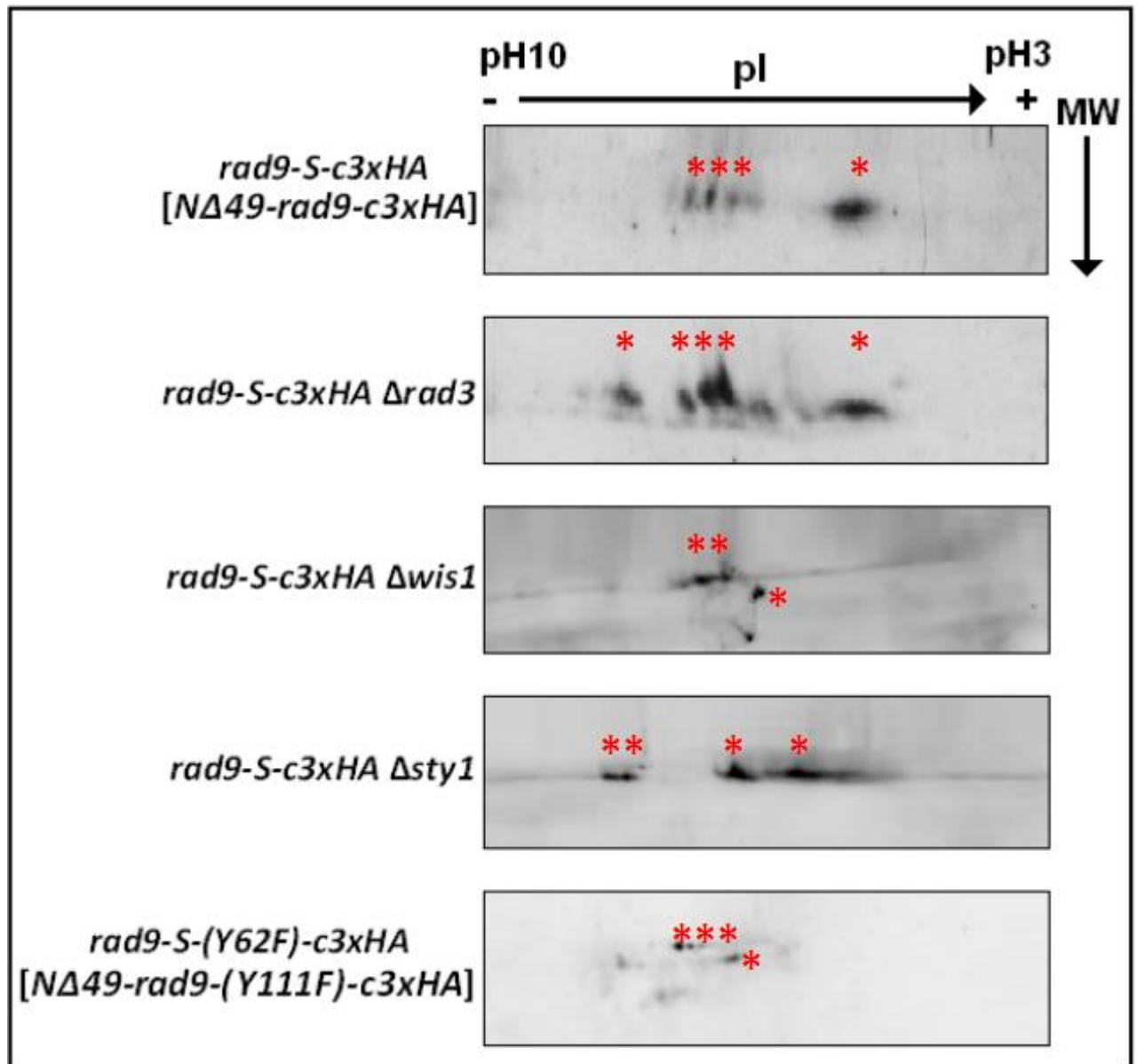
Comparative acute Camptothecin (CPT) cell survival assays performed with YEA broth cultures of the *S. pombe* strains (indicated above), incubated at 30°C in the presence of 40μM camptothecin indicate that Wis 1 is not implicated in the “Rad9-S”-mediated signal pathway response to CPT-induced DNA damage (Fig A).

In contrast, the acute CPT survival assay data indicate that the Rad3 and Sty1 Kinases and phosphorylation of the positional equivalent Y111 residual site within the truncated “Rad9-S” protein variant are all implicated in the CPT-induced DNA damage response signalling pathway (Fig B, Fig C and Fig E).

Comparative *In silico* functional homologous *S. cerevisiae* Mec1 kinase activation-type (ATR^{Hs}, Rad3^{Sp}) sequence motif alignments (Navadgi-Patil V.M. and Burgers P.M., 2009), performed via utilisation of the PSI-BLAST, EMBOSS Pair-WiseAlignment and JemBOSS bioinformatics software tools, indicate the conservation of key equivalent Tyrosine residues in both the *S. pombe* Rad9 and Sty1 proteins (Fig F) which are also situated within *S. pombe* Wis1 kinase-equivalent phosphorylation substrate target motif sequences in both the *S. pombe* Sty1 and Rad9 proteins (Fig D and Fig F).

The identified key aromatic tyrosine residues situated within the potential homologous equivalent Rad3 kinase-activation functional motifs were found to be absent in comparative sequence alignments with the *S. pombe* Wis 1 MAP kinase.

Fig 6.30: 2D-PAGE Analyses of Potential MAP Kinase Interactions



Comparative 2D-PAGE-coupled Western blot analyses performed on TCA-precipitated total protein extracts acquired from 30°C YEA broth cell cultures of the indicated *S. pombe* strains revealed that deletion of *wis1*, but not *sty1* or *rad3*, within an exclusively expressed “*rad9-S*” genetic background induces the expression of the “Rad9-VS” and “Rad9-T” isoforms, whilst site-directed mutagenesis of tyrosine 62 to phenylalanine within the “Rad9-S” truncated protein only induces expression of the “Rad9-VS” isoform.

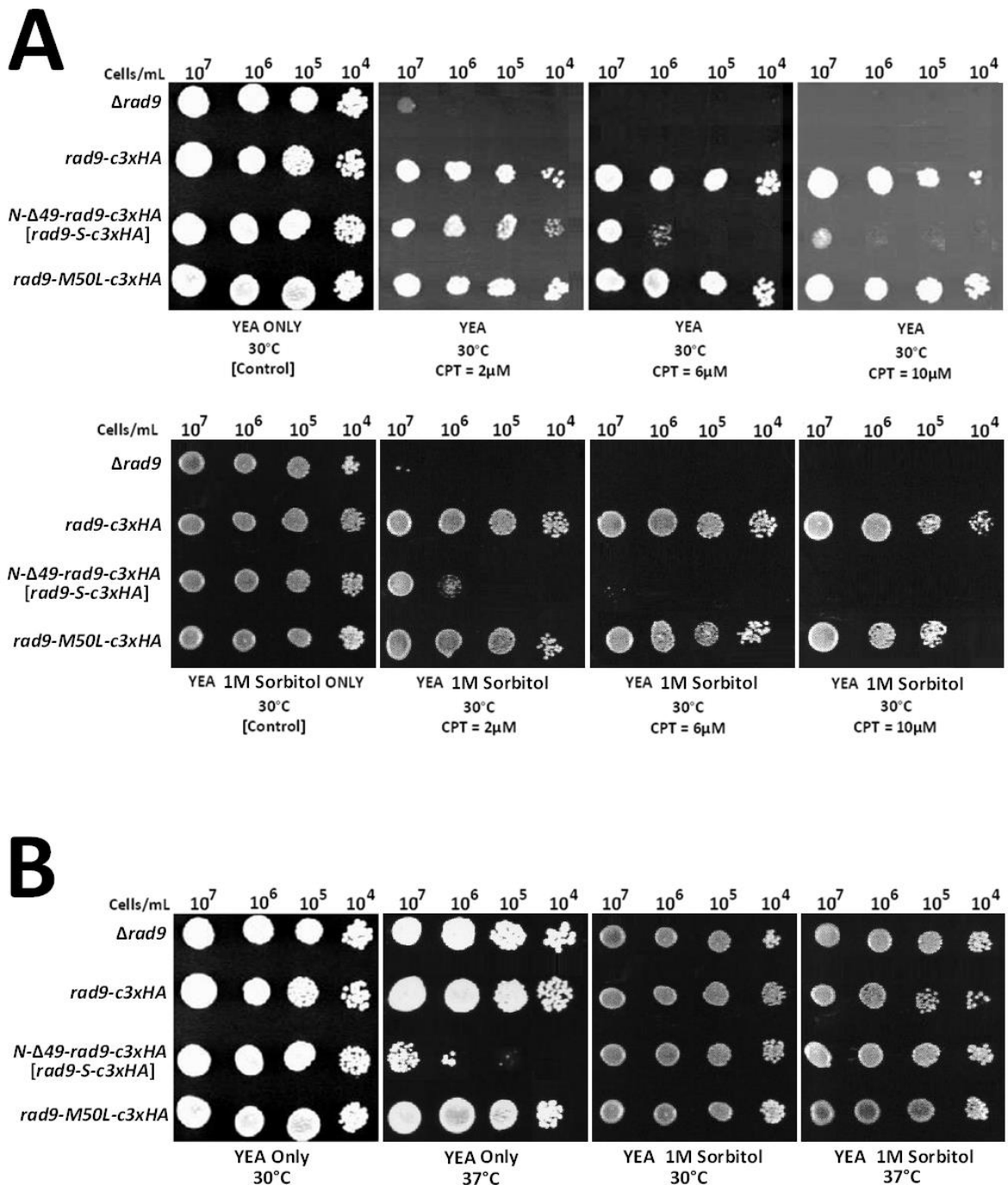
The *Δwis1* gene deletion yields a distinctively different “Rad9-S” phosphoisoform profile to that of the *Δsty1* and *Δrad3* gene deletions.

Phosphoisoform profiles of the “Rad9-S” protein for the *Δwis1* gene deletion site-directed mutagenized Y62 residue are similar, with the notable exception of the “Rad9-T” isoform – which is only expressed in the *Δwis1* gene deletion profile.

[Key similarities and differences in the phosphoisoform profiles are indicated with red asterices]

Fig 6.31: Osmotic Stress Responses I: Drop-Plate (Chronic) Assays

[**Note:** These data sets were acquired by Ms. Susan Davies, working under the practical supervision of the author]

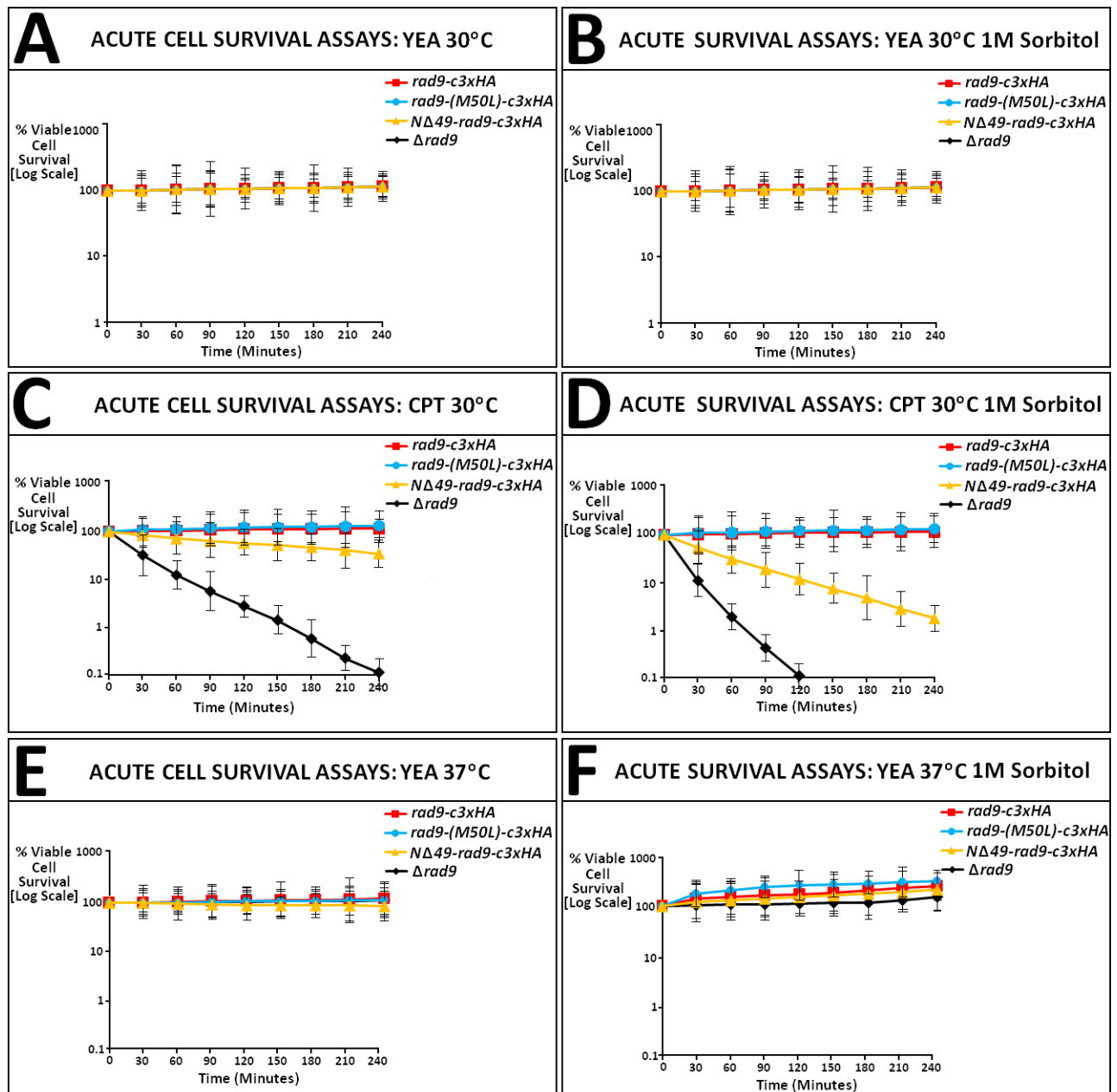


A: The comparative Camptothecin (CPT) dose-response drop-plate assay data indicate that chronic exposure of the *Δrad9* (*rad9* gene-deleted) and *NΔ49-rad9-c3xHA S. pombe* strains to CPT-induced DNA damage in the presence of 1M Sorbitol (induced osmotic shock conditions) significantly enhances their cytotoxic sensitivity to the genotoxic drug.

B: In stark contrast, comparative heat-shock drop-plate assay data indicate that chronic exposure of the *NΔ49-rad9-c3xHA S. pombe* strain to heat shock in the presence of 1M sorbitol (induced osmotic shock) significantly enhances its resistance to thermal stress.

Taken collectively, these experimental data are indicative that the truncated “Rad9-S” protein variant may be implicated in the mediation two different types of cell cycle regulatory signalling pathways.

Fig 6.32: Osmotic Stress Responses II: Acute Cell Survival Assays



Comparative acute camptothecin (CPT) cell survival assays performed with YEA broth cultures of the *S. pombe* strains (indicated above), incubated at 30°C in the absence and presence of 40μM CPT (Figs A and C) in the absence and presence of 1M Sorbitol (induced osmotic shock) – Figs B and D, are also indicative that osmotic shock causes enhances the sensitivity of *rad9* gene-deleted and *NΔrad9-c3xHA* cells to CPT-induced damage.

Comparative cell survival assays performed with YEA broth cultures of the *S. pombe* strains (indicated above), incubated at 37°C in the absence and presence of 1M Sorbitol (induced osmotic shock) – Figs E and F, are also indicative that osmotic shock causes enhances the resistance all the *S. pombe* strains to elevated thermal stress.

Thus, these experimental data correlate with the drop-plate assay data (Fig 6.31, p.566) – indicative that the truncated “Rad9-S” protein variant may be implicated in the mediation two different types of cell cycle regulatory signalling pathways whose selection is independent of chronic or acute exposure to CPT-induced damage or elevated thermal stress.

6.4 Component Spindle Checkpoint Inputs

Comparative acute cell survival assay data indicated that the phosphorylation of Y62 within the truncated “Rad9-S” protein variant, which is functionally-implicated in its camptothecin-induced DNA damage signalling response, was not mediated via Wis1 kinase interactions (Section 6.3, pp.556-567; Fig 629., p.564).

It was therefore postulated that the Y62 residue may be a phosphorylation target for the monopolar spindle checkpoint kinase Mph1.

In order to determine whether the mitotic spindle checkpoint (discussed in detail previously in Chapter 1, Section 1.2.2, pp.63-65) was implicated in the “Rad9-S” truncated protein variant-mediated signalling response to camptothecin-induced DNA damage, the *NΔ49-rad9-c3xHA S. pombe* strain was cross-mated with mitotic checkpoint-associated type gene deleted *S. pombe* strains Δ *bub1*, Δ *mad2* and Δ *mph1* which were then utilised in comparative acute assays (Fig 6.33, p.575).

Deletion of *bub1* and *mad2* within an exclusively expressed “*rad9-S*” genetic background did not enhance the sensitivity of the cells to Camptothecin (CPT) and thus indicated that the Bub1 and Mad2 proteins were not implicated in the “Rad9-S”-mediated signalling response to CPT-induced DNA damage (Fig 6.33A and Fig 6.33B, p.575).

Whilst deletion of *mph1* within an exclusively expressed “*rad9-S*” genetic background increased the sensitivity of the cells to Camptothecin (CPT) and thus indicated that this monopolar spindle checkpoint kinase was implicated in the “Rad9-S” mediated response to CPT-induced DNA damage (Fig 6.33E, p.575).

Comparative acute survival assays performed with YEA broth cultures of the *S. pombe* strains *NΔ49-rad9-c3xHA*, *NΔ49-rad9-c3xHA Δmph1*, *NΔ49-(Y111F)-rad9-c3xHA* and *NΔ49-(Y111F)-rad9-c3xHA Δmph1*, incubated at 30°C in the presence of 40μM Camptothecin, revealed that the *NΔ49-(Y111F)-rad9-c3xHA Δmph1* cells were more resistant than either the *NΔ49-(Y111F)-rad9-c3xHA* or *NΔ49-rad9-c3xHA Δmph1* cells to CPT-induced DNA damage (Fig 6.33F, p.575).

Thus, these acute CPT survival assay data revealed an epistatic response of the “cre-lox”-constructed “double-mutant” *NΔ49-(Y111F)-rad9-c3xHA Δmph1 S. pombe* cells – indicative that Mph1 kinase-mediated phosphorylation of the “Rad9-S” Y62 residue was implicated in the CPT-induced DNA damage signalling response elicited by the truncated protein variant (Fig 6.33F, p.575).

Comparative *in silico* predictive phosphorylation target-site analyses of the *S. pombe* full-length Rad9 protein and truncated “Rad9-S” protein variant sequences, via utilisation of the bioinformatics software packages NetPhos2.0 and NetPhosK, identified Tyrosine 61 (equivalent to tyrosine 12 in the truncated “Rad9-S” polypeptide amino acid sequence) as a very high probability kinase target site – possibly for the dual Tyr/Thr/Ser Monopolar Spindle Checkpoint Kinase – Mph1 (Fig 6.37, p.580).

Comparative acute survival assays performed with YEA broth cultures of the *S. pombe* strains *NΔ49-rad9-c3xHA*, *NΔ49-rad9-c3xHA Δmph1* and *NΔ49-(Y61F)-rad9-c3xHA*, incubated at 30°C in the presence of 40μM camptothecin, revealed that the *NΔ49-(Y61F)-rad9-c3xHA* cells were more resistant than either the *NΔ49-rad9-c3xHA* or *NΔ49-rad9-c3xHA Δmph1* cells to CPT-induced DNA damage (Fig 6.36C and Fig 6.36E, p.579).

These data may indicate that Mph1-mediated phosphorylation of Y61 within the “Rad9-S” protein (Y12) may constitute part of mechanism which negatively regulates “Rad9-S”-mediated checkpoint signalling responses to CPT-induced DNA damage.

This particular tyrosine residue (Y61 in full-length Rad9 and Y12 in “Rad9-S”) is also situated within the M50-M74 DNA-binding functional domain – which constitutes ~50% of the identified sequence of a potential “nuclease-binding/nuclease-active” motif (Fig 6.37, p.580).

Mph1 kinase-mediated phosphorylation of Y12 within the identified DNA-binding domain of the “Rad9-S” protein would perturb aromatic ring duplex-intercalative type Π - Π electron-stacking interactions between the unphosphorylated tyrosine ring and nucleobases as a consequence of phosphate group-induced alteration of ring electron configurations, whilst increased hydrophilicity of the phosphorylated tyrosine residue which would perturb Van der Waal’s-type associative interactions with the hydrophobic DNA bases and negative charge repulsion between the phosphate groups on phosphorylated Y12 and the deoxyribose-phosphate “backbone” of the duplex would also block access of the tyrosine residue the “nucleobase-core” of the duplex .

Taken together, these experimental observations may indicate that Mph1-phosphorylation of this tyrosine residue is a critical pre-requisite post-translational modification of the truncated “Rad9-S” protein variant which is implicated in the mechanism of functional activation of the “nuclease-like” M50-M74 domain (discussed in detail later in Chapter 7).

In this context, Mph1-mediated phosphorylation of tyrosine 12 may be also be a pre-requisite for initiation of “Rad9-S” mediated suppression of specific checkpoint-initiated DNA repair activities, which may otherwise adversely interfere with the postulated M50-M74 nuclease-like domain-mediated functional DNA repair activities (discussed in detail later in Chapter 7).

Comparative protein analyses of TCA-precipitated- and soluble- total protein extracts, acquired from 30°C YEA broth cell cultures of the *NΔ49-rad9-c3xHA*, *NΔ49-rad9-c3xHA Δmph1* and *NΔ49-rad9-c3xHA mph1-c13xMyc S.pombe* strains, incubated in the absence and presence of 40μM camptothecin (CPT) for 30 minutes, provided additional biochemical evidence that Mph1 kinase-mediated phosphorylation of “Rad9-S” was implicated in the CPT-induced DNA damage signalling response elicited by the truncated protein variant (Fig 6.34, p.576; Fig 6.35, pp.577-578).

Comparative acute survival assays performed with YEA broth cultures of the *S. pombe* strains *NΔ49-rad9-c3xHA*, *NΔ49-rad9-c3xHA Δmph1*, *NΔ49-(Y111F)-rad9-c3xHA* and *NΔ49-(Y111F)-rad9-c3xHA Δmph1*, incubated at 30°C in the presence of 40μM Thiabendazole (TBZ), revealed that all the cell types were resistant to TBZ-induced microtubule perturbation (Fig 6.33G, p.575) – indicative that functional Mph1 kinase interactions within the “Rad9-S”-mediated signalling response to CPT-induced DNA damage were distinctively independent from those of the mitotic spindle checkpoint.

Comparative acute cell survival assays performed on YEA broth cultures of the indicated *S. pombe* strains revealed that deletion of *cds1* within an exclusively expressed “*rad9-S*” genetic background, resulted in the significant enhancement of the sensitivity of the cells to CPT-induced DNA damage (Fig 6.38C, p.581), whilst perturbed autophosphorylated activation of Cds1 – ie site-directed mutagenized expression of *Cds1-(T8A;T11A)* within an exclusively expressed “*rad9-S*” genetic background had negligible effect on the sensitivity of the cells to CPT-induced DNA damage (Fig 6.38E, p.581)

These survival assay data indicated that although Cds1 kinase activity may be a key signalling component of the “Rad9-S”-mediated checkpoint pathway response to camptothecin genotoxicity, the activation of the Cds1 kinase protein is unlikely to proceed via the conventional autophosphorylation mechanism.

Acute survival assay data also indicated that the Rad3 kinase and adaptor/mediator protein Mrc1 were also implicated in the “Rad9-S”-mediated signalling response to camptothecin-induced DNA damage – as a consequence of the fact that deletion of *rad3* and *mrc1* within an exclusively expressed “Rad9-S” genetic background enhanced the sensitivity of the cells to CPT genotoxicity (Fig 6.38A and Fig 6.38B, p.581).

Previous experimental studies have demonstrated that Rad3 kinase-mediated phosphorylation of Mrc1 induces supramolecular conformational changes within the adaptor protein which enable it to associatively-activate the Cds1 kinase, via an alternative mechanism to that of the conventional dimerisation-mediated autophosphorylated initiation of the catalytically-functional Cds1 kinase (Zhao H. *et al*, 2003).

In Silico comparative sequence alignments of the C-Terminal catalytic active sites of the *S. pombe* Cds1 and Mph1 kinases with the equivalent functional *H. sapiens* homolog Mps1 (Kang J. *et al*, 2007), performed via utilisation of the PSI-BLAST, EMBOSS PairWise Alignment and JemBOSS bioinformatics software tools, identified several key conserved features within the two proteins (Fig 6.38G, p.581) – notably;

- (i) A conserved Mg^{2+} -ATP-binding “DFG” motif, situated at D459 within the *S. pombe* Mph1 kinase and at D244 within the *S. pombe* Cds1 kinase.
- (ii) Three conserved equivalent potential phosphorylation sites situated at T254, Y322 and S353 within the *S. pombe* Cds1 kinase, correlated to T471, Y546 and T593 within the *S. pombe* Mph1 kinase.

In Silico predictive phosphorylation analyses of these residues, via utilisation of the NetPhos2.0 bioinformatics software tool, yielded high probability scores for all the identified residues – with the notable exception of T471, although this residue may still have a critical role in the autophosphorylated-activation of the Mph1 kinase]

Acute survival assay data also indicated that both Cds1 kinase and Mph1 kinase were implicated in the “Rad9-S”-mediated signalling response to Camptothecin-induced DNA damage – as a consequence of the fact that deletion of *cds1* and *mph1* within an exclusively expressed “Rad9-S” genetic background enhanced the sensitivity of the cells to CPT genotoxicity (Fig 6.38C, p.581 and Fig 6.38E, p.581).

Whilst comparative 2D PAGE-coupled Western Blot analyses of TCA-precipitated total protein extracts, acquired from 30°C YEA broth cell cultures of the *S. pombe* strains *NΔ49-rad9-c3xHA* (“*rad9-S*”-*c3xHA*), *NΔ49-rad9-c3xHA Δcds1* and *NΔ49-rad9-c3xHA Δmph1* yielded similar profiles for the “Rad9-S” protein, with three conserved phosphoisoforms (Fig 6.38H, p.581).

Comparative 2D PAGE-coupled Western Blot analyses of TCA-precipitated total protein extracts, acquired from 30°C YEA broth cell cultures of the *S. pombe* strains *NΔ49-rad9-c3xHA* (“*rad9-S*”-*c3xHA*), *NΔ49-rad9-c3xHA cds1-c13xMyc* and *NΔ49-rad9-c3xHA mph1-c13xMyc*, incubated in the absence or presence of 40μM camptothecin for 30 minutes, probed with the anti-HA and anti-Myc primary anti-bodies, yielded a series of profiles for the “Rad9-S” protein which also exhibited these three conserved phosphoisoforms (Fig 6.39, p.582).

Acute survival assay data also revealed that the *NΔ49-rad9-c3xHA mph1-c13xMyc S. pombe* strain was very sensitive to camptothecin-induced DNA damage, in contrast to the *S. pombe* strains *NΔ49-rad9-c3xHA* and *mph1-c13xMyc* (Fig 6.38F, p.581) – indicative of HA and Myc epitope tag-mediated perturbed functional interactions between C-Termini of the “Rad9-S” and Mph1 kinase proteins.

Taken together, these experimental data observations indicate that “Rad9-S”-mediated recruitment of Mph1, in conjunction with Mrc1-mediated recruitment of Cds1, may comprise a co-operative functional complex in which the C-Termini of the Mph1 and Cds1 kinases are orientated for associative reciprocal phosphorylated-activation of their respective catalytic domains (Fig 6.40, p.583).

Consequential kinase-mutual phosphorylation of these proteins may also promote dissociation of activated Cds1 kinase from Mrc1 and activated Mph1 kinase from the C-Terminal Tail domain of “Rad9-S” to enable the respective kinases to elicit “downstream” cell cycle checkpoint signalling responses to camptothecin-induced DNA damage and/or other replication stresses such as elevated thermal shock (Fig 6.40, p.583).

Fig 6.33: Acute CPT & TBZ Assays – Bub1, Mad2 & Mph1 Mutants

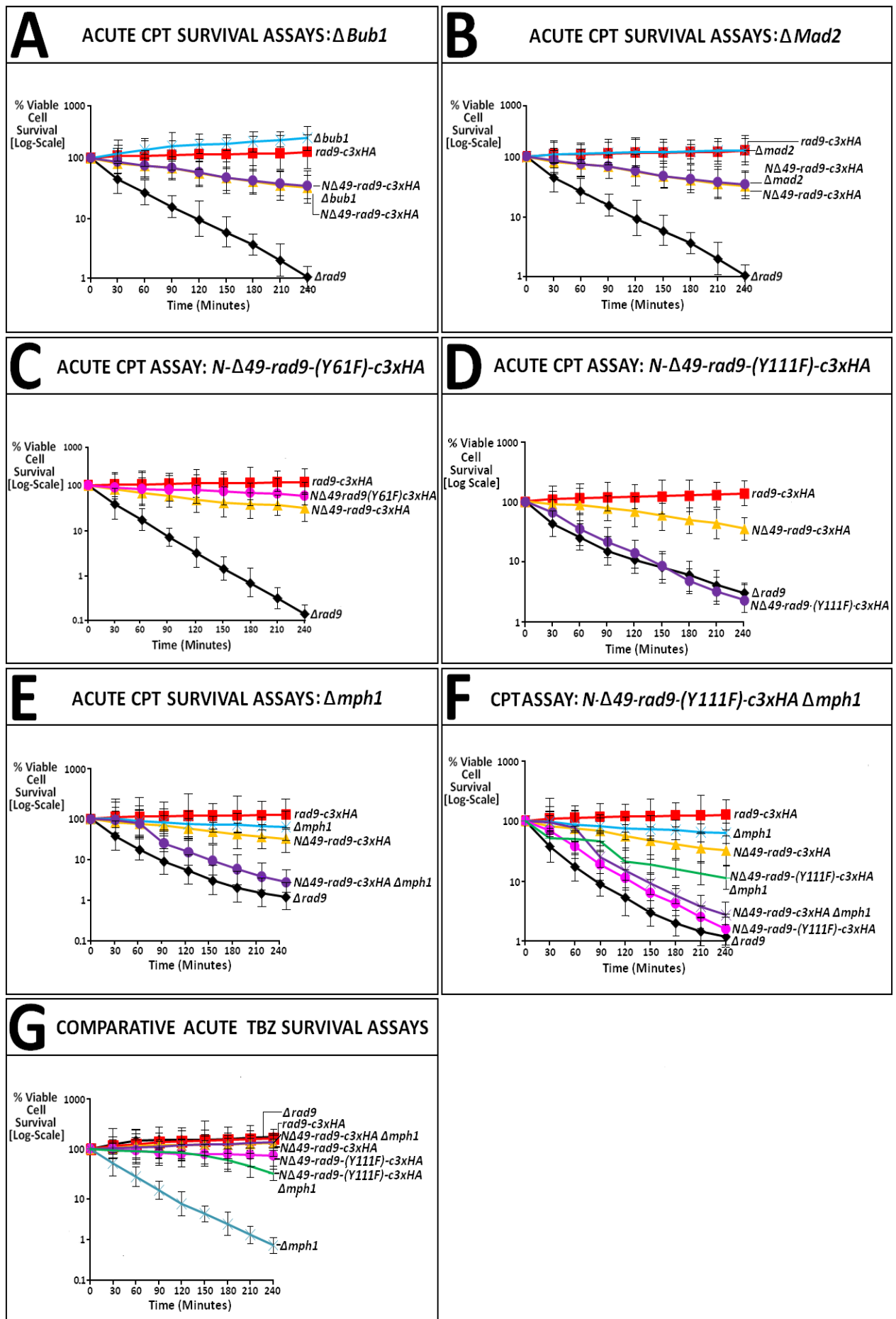
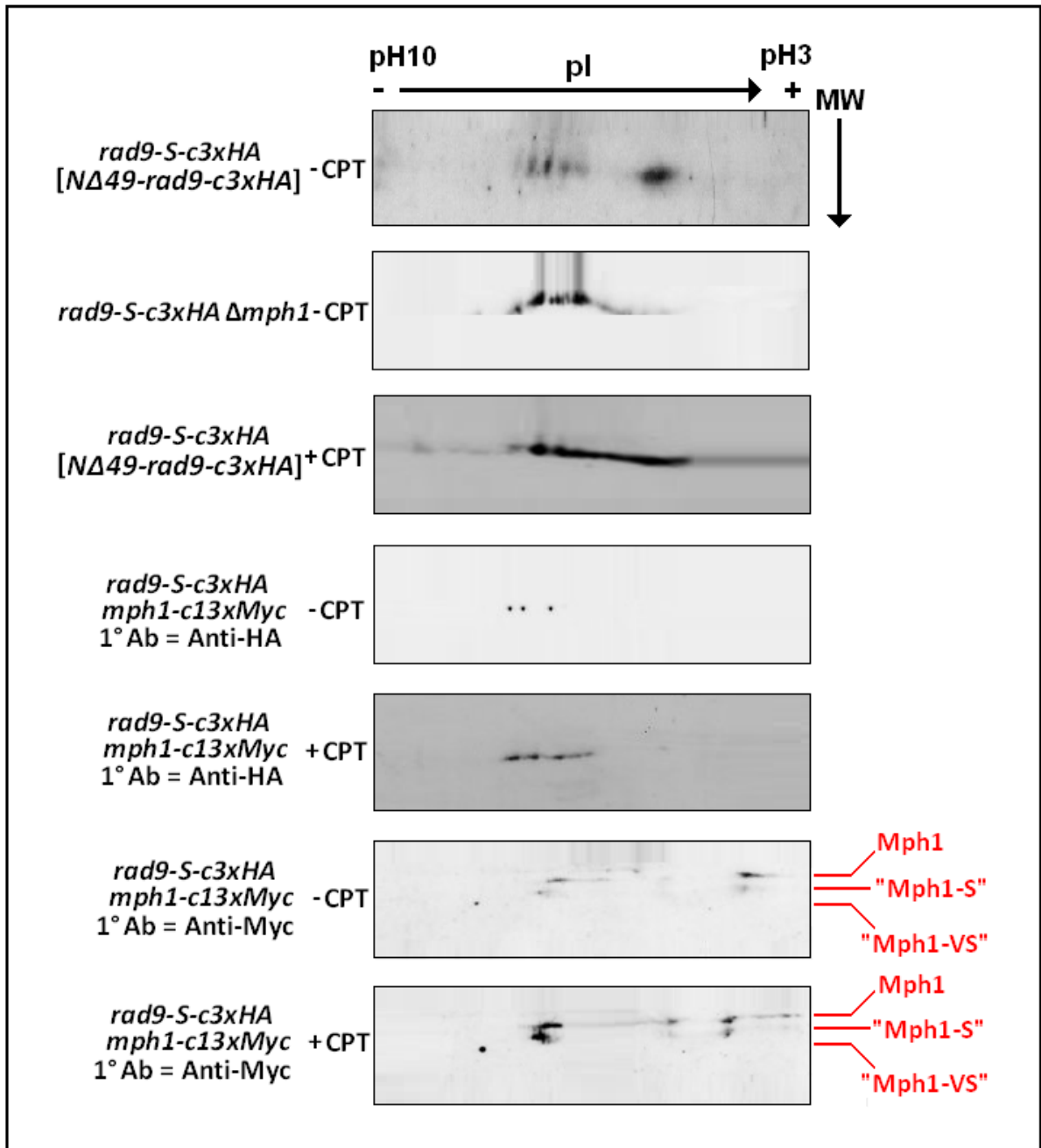


Fig 6.34: 2D-PAGE Analysis of “Rad9-S”:Mph1 Interactions



Comparative 2D-PAGE-coupled Western Blot analyses of TCA-precipitated total protein extracts acquired from YEA broth cell cultures of the indicated *S. pombe* strains, incubated at 30°C in the absence and presence of 40μM Camptothecin (CPT) for 30 minutes.

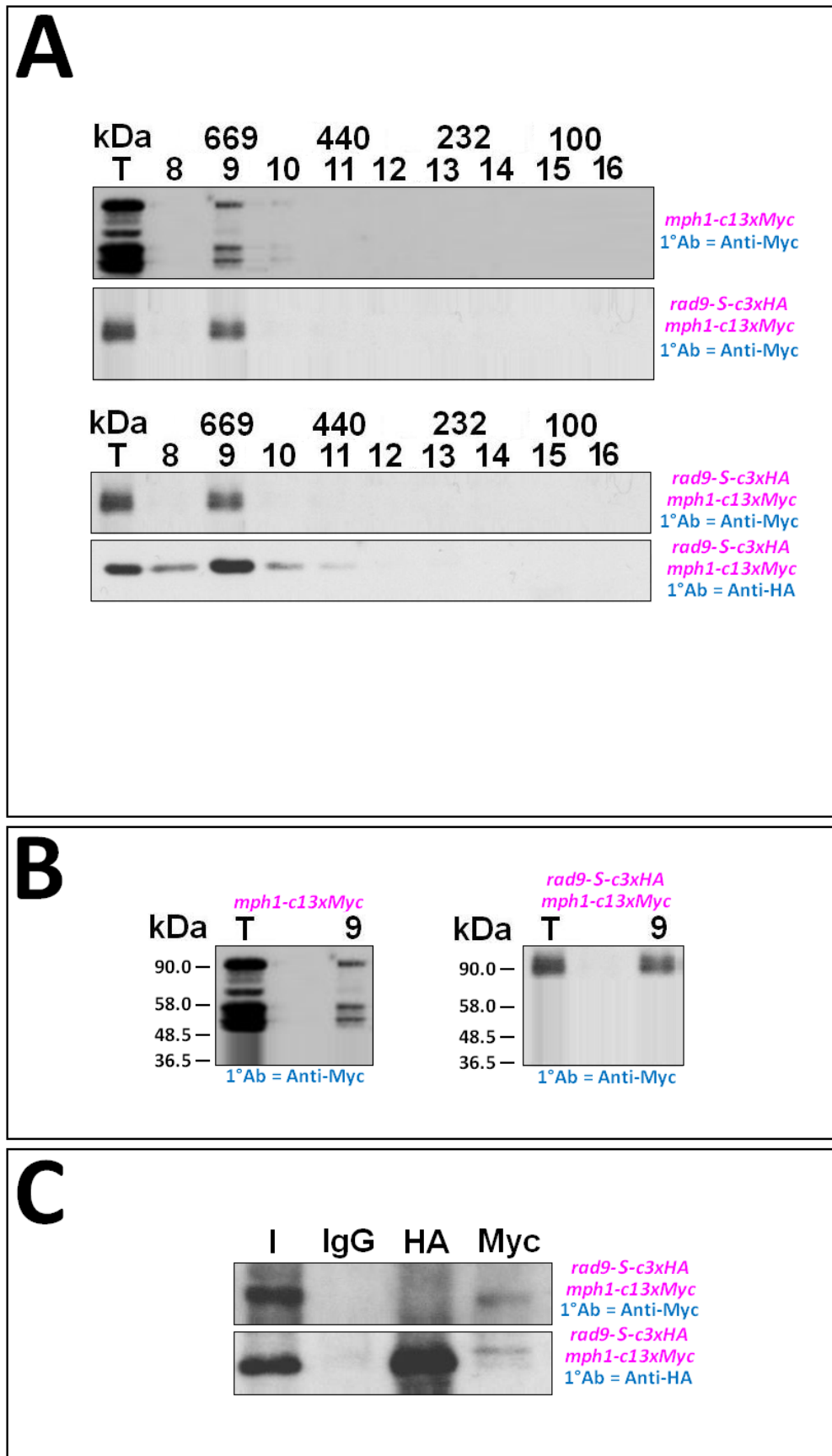
Deletion of *mph1* (*rad9-S-c3xHA Δmph1*) results in loss of a phosphoisoform, compared with the “control” phosphoform profile (*rad9-S-c3xHA*) – indicative that Mph1 kinase is implicated in the “Rad9-S”-mediated signalling responses to DNA damage.

Comparison of the 2D-PAGE-resolved phosphoisoform profiles of the *rad9-S-c3xHA mph1-C13xMyc* *S. pombe* strain (probed with the primary anti-HA and anti-Myc anti-bodies) indicate similar hypophosphorylation shifts of the “native”/“control” phosphoisoform profile *rad9-S-c3xHA*, in the absence or presence of CPT – which may be indicative of HA- and Myc- epitope tag-mediated perturbation of associative C-terminal domain interactions between “Rad9-S” and Mph1.

These 2D-PAGE data indicate the expression of three isoforms of Mph1 – termed Mph1, “Mph1-S” and “Mph1-VS”.

The 2D data also reveal a discrete hyperphosphorylation shift in the phosphoisoform profile of the Mph1 isoform upon treatment of the cells with camptothecin – indicative that the Mph1 isoform is phosphorylated in response to CPT-induced DNA damage.

Fig 6.35: HPLC-SEC and Co-Immunoprecipitation Analyses



[See Figure Legend, p.578, for a full description of the experimental data]

Figure Legend – Fig 6.33

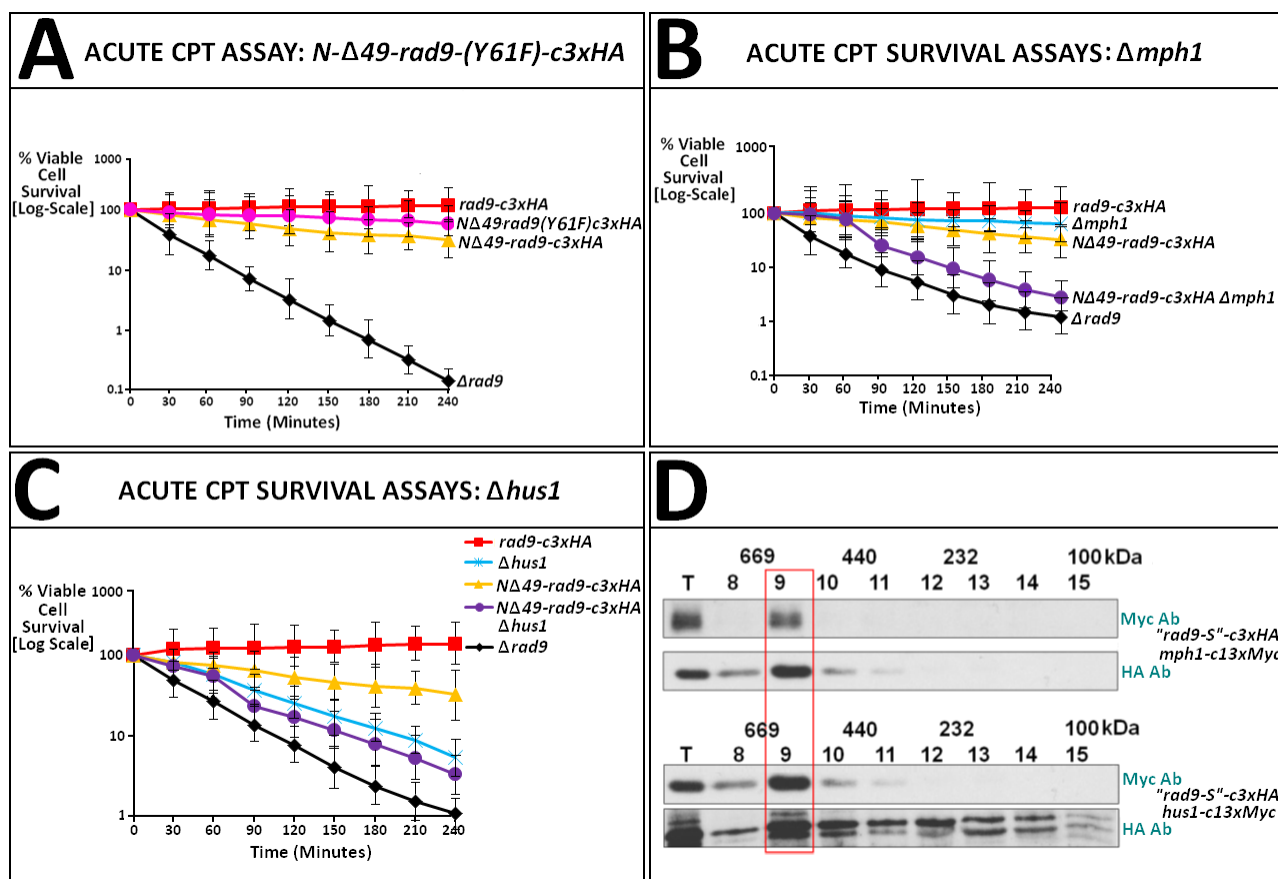
A: Comparative Western Blot analyses of HPLC-SEC fractionated samples of soluble total protein extracts acquired from YEA broth cell cultures of the *S. pombe* strain *mph1-c13xMyc* and *N-Δ49-rad9-c3xHA* (“*rad9-S-c3xHA*”) *mph1-c13xMyc*, which utilised either the anti-HA or anti-Myc primary anti-body probes reveal that Mph1 co-fractionates with the truncated “Rad9-S” protein variant in fractions 8 and 9 – indicative that Mph1 may be a functional interactive component of the large “Rad9-S”-associative complex (~700kDa) indicated in Fraction 9.

B: Both the “Rad9-S” truncated protein variant and Mph1 were detected in the anti-HA anti-body probe-primed comparative co-immunoprecipitation “pull-down” (Co-IP) analysis performed with a total soluble protein extract acquired from a YEA broth cell culture of the *S. pombe* *N-Δ49-rad9-c3xHA mph1-c13xMyc* strain – indicative of an associative interaction between both proteins.

The lack of detection of the “Rad9-S” protein in the anti-Myc anti-body probe-primed comparative Co-IP assay may be a consequence of multiple convergent associative protein interactions at the “Rad9-S” C-Terminal Tail domain which sterically hinder anti-HA anti-body interactions with the C-terminal HA epitope tag and thus “mask” detection of the truncated “Rad9-S” protein variant.

C: Comparative 1D SDS-PAGE-coupled Western Blot analyses HPLC-SEC fraction 9 samples acquired from total soluble extracts of the the *mph1-c13xMyc* and *N-Δ49-rad9-c3xHA mph1-c13xMyc* *S. pombe* strains indicate an exclusive association between “Rad9-S” and the Mph1 isoform (but not the “Mph1-S” or “Mph1-VS” isoforms).

Fig 6.36: Collated Genetic and Biochemical Evidence for “Rad9-S”-Mph1-Hus1 Interactions

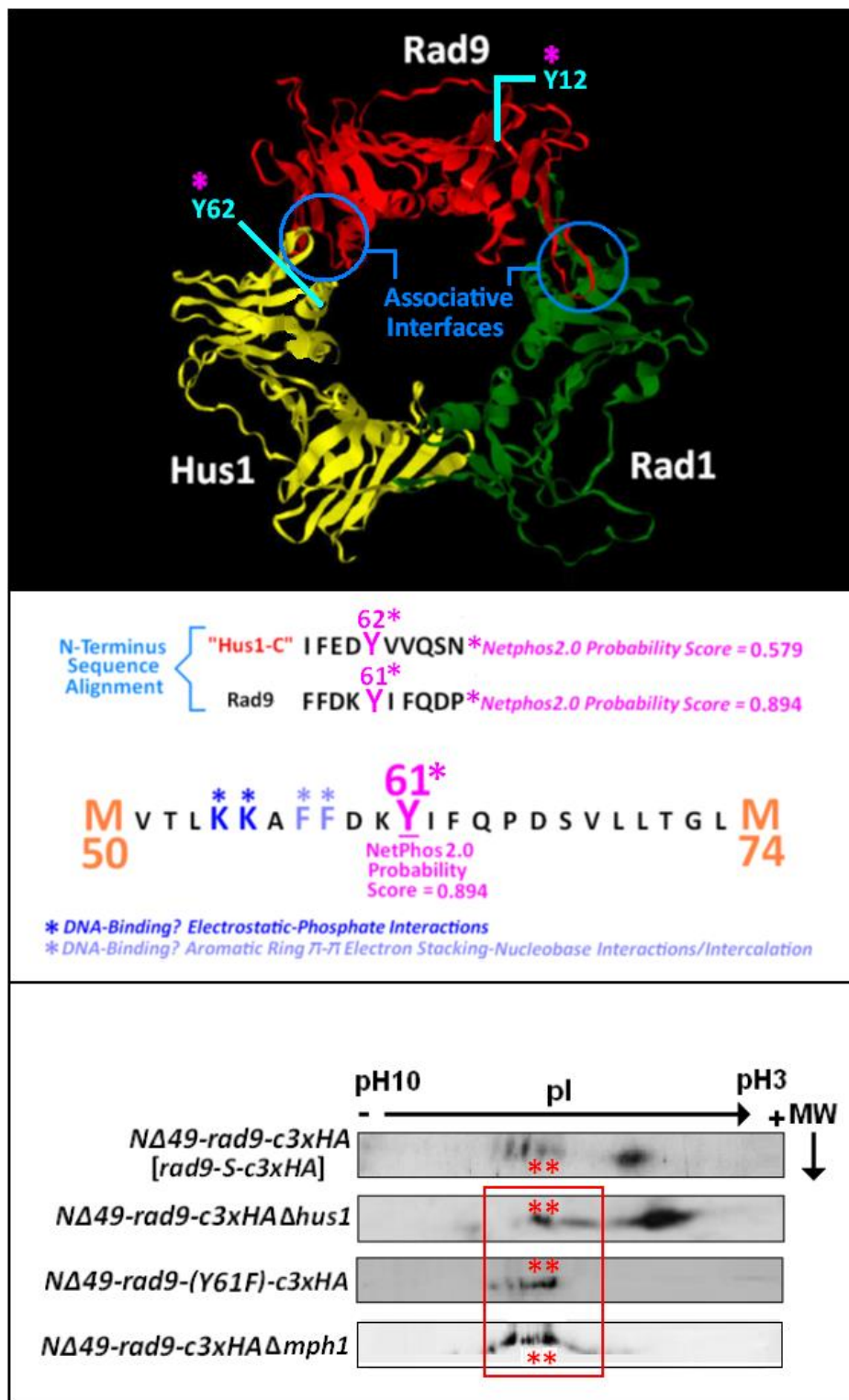


Comparative acute Camptothecin cell survivals indicate that deletion of *hus1* or *mph1* within an exclusively expressed “*rad9-S*” genetic background enhances the sensitivity of the cells to CPT-induced DNA (Fig B and Fig C), whereas cells “*cre-lox*” –engineered for the exclusive expression of the Rad9-S-(Y12F)-*c3xHA* site-directed mutagenized protein variant (*N* Δ 49-*rad9*-(Y61F)-*c3xHA*) exhibit enhanced resistance to CPT-induced genotoxicity.

The data indicate that both Hus1 and Mph1 are implicated in the “Rad9-S”-mediated signalling pathway response to CPT-induced DNA damage, whilst the unphosphorylated Y12 residue within “Rad9-S” may be implicated in associative DNA nucleobase-binding interactions which are perturbed via Mph1-mediated phosphorylation of Y12.

Comparative HPLC-SEC analyses reveal that both Mph1 and Hus1 co-fractionate with “Rad9-S” within a complex of ~600kDa mass – indicative that both Mph1 and Hus1 are implicated in the “Rad9-S”-mediated signalling pathway responses to DNA damage and replication stress (Fig D).

Fig 6.37 Collated *In Silico* and Biochemical Evidence for “Rad9-S”-Mph1-Hus1 Interactions



In silico comparative alignment of the amino sequence flanking the potential Mph1 kinase-phosphorylated Y61 residue, situated within the identified M50 – M74 DNA binding domain of the *S. pombe* Rad9 protein, with the *S. pombe* Hus1 amino acid sequence indicates that Y62 within Hus1 may also be a phosphorylation target for Mph1 kinase.

Comparative 2D PAGE-coupled Western blot data indicate conserved phosphoisoforms within the four aligned profiles (indicated by the red box and asterisks) – which may be indicative that Mph1 phosphorylates both “Rad9-S” (at Y12) and Hus1 (at Y62).

Fig 6.38: Data Evidence for “Rad9-S”-Mph1-Cds1 Interactions

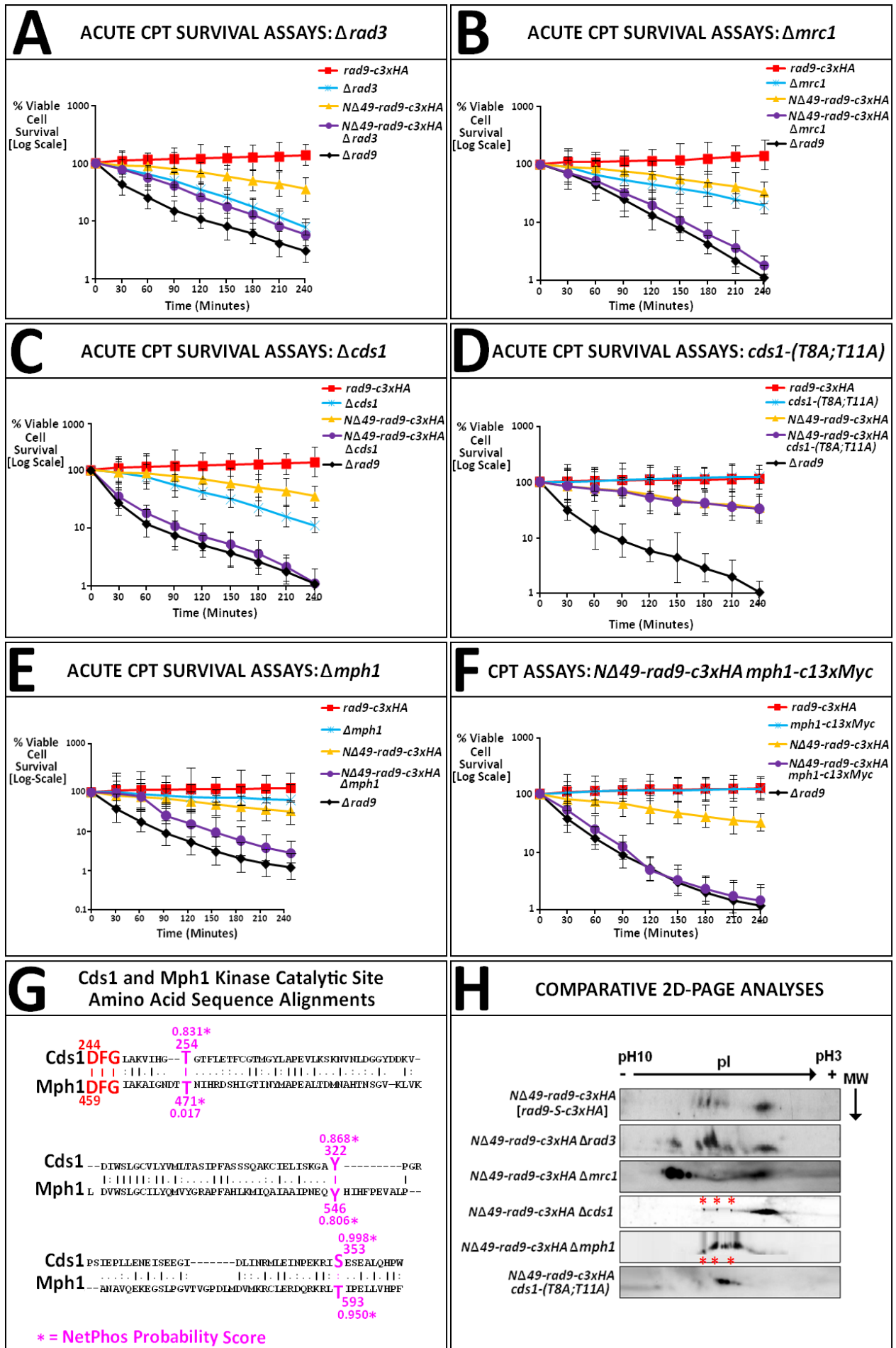
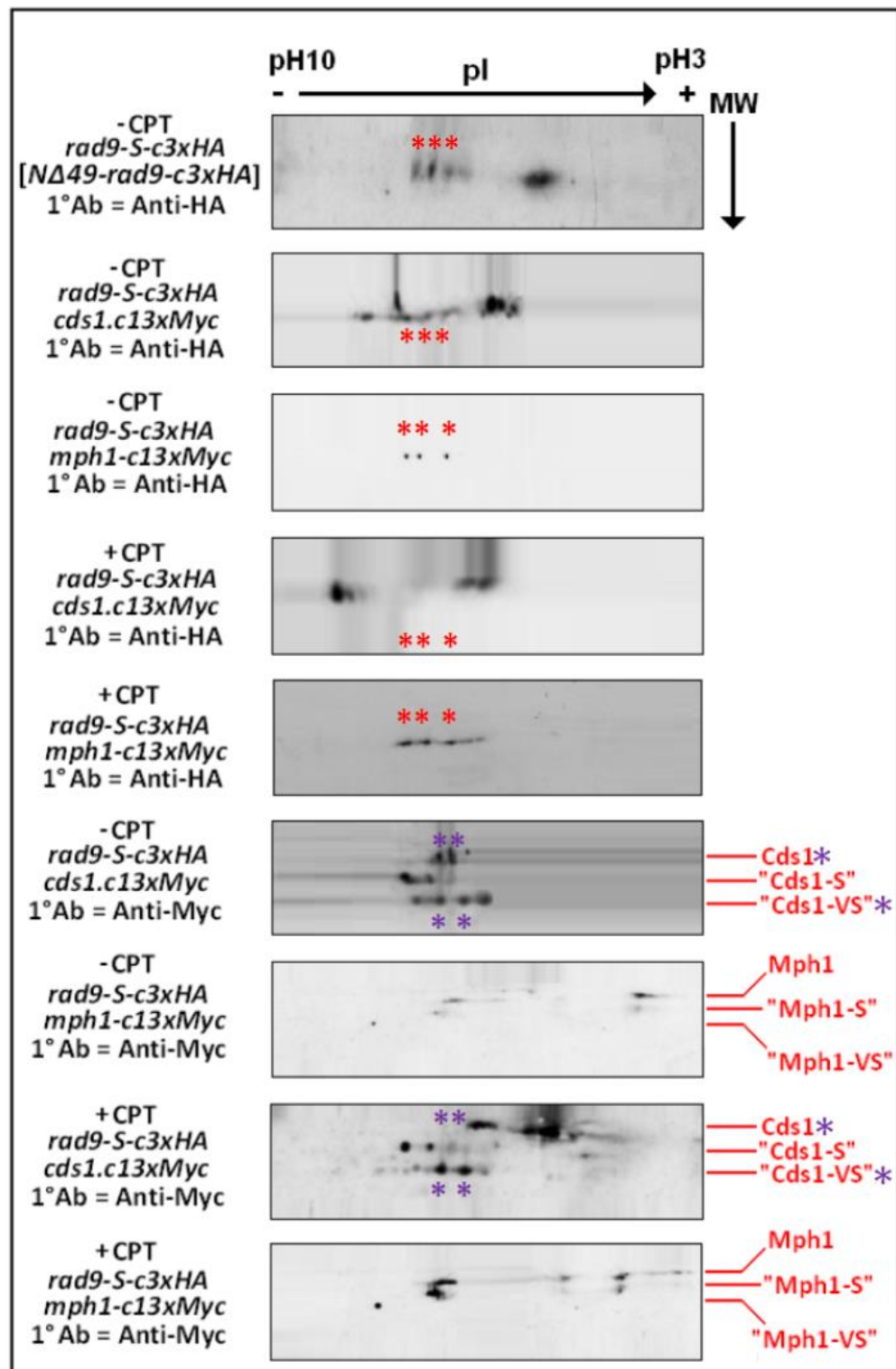


Fig 6.39: 2D-PAGE-Resolved Cds1 & Mph1 Phosphoisoform Profiles

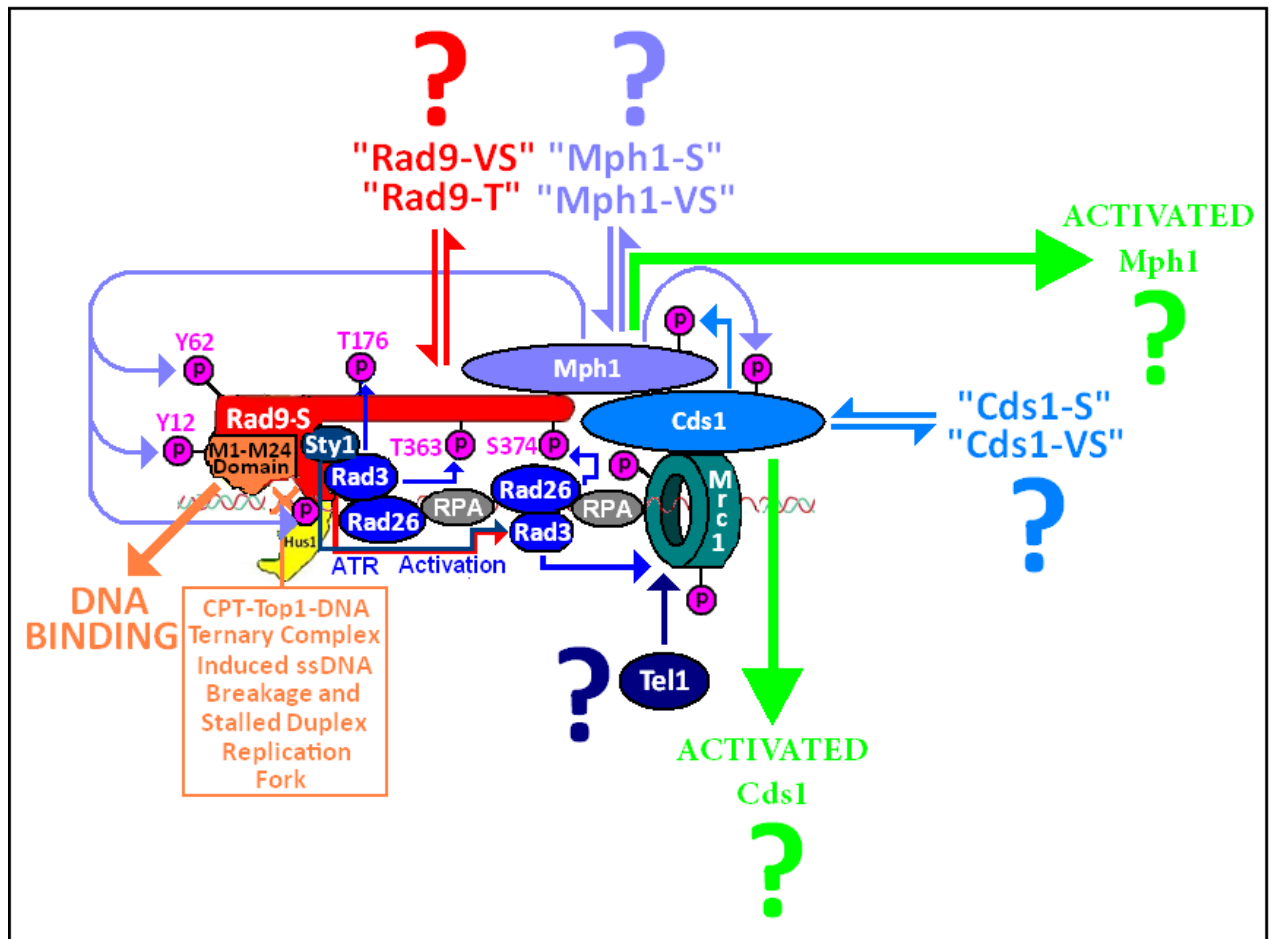


Comparative 2D-PAGE-coupled Western Blot analyses were performed on TCA-precipitated total protein extracts acquired from YEA broth cell cultures of the indicated *S. pombe* strains, incubated at 30°C in the absence and presence of 40µM Camptothecin (CPT) for 30 minutes.

Comparison of the resultant data reveal distinctive similarities within the acquired phosphoisoform profiles of the truncated “Rad-S” protein variant in the *rad9-S-c3xHA cds1-c13xMyc* and *rad9-S-c3xHA mph1-c13xmyc* *S. pombe* strains (indicated via red and purple asterisks).

Taken together, these data may be indicative of co-ordinated synergistic interactions between the Cds1 and Mph1 kinases within the “Rad9-S”-mediated signalling pathway response to CPT-induced DNA damage.

Fig 6.40: Mph1–Cds1 Complementary Kinase-Site Activation Model



In response to detected CPT-induced DNA damage lesion sites, initial Rad26-associated Rad3 kinase-mediated phosphorylation of “Rad9-S” at T176 induces supramolecular configurational changes within the truncated protein variant which enable Rad26/Rad3 kinase-mediated phosphorylation of the T363 and S374 residues – which are situated within its C-Terminal Tail Domain.

Subsequent Rad26/Rad3 kinase-mediated phosphorylation of the T363 and S374 residues induces supramolecular configurational changes within the C-Terminal Tail Domain of the “Rad9-S” truncated protein variant which may then enable it to engage with the monopolar spindle checkpoint kinase Mph1.

Rad26/Rad3 kinase-mediated phosphorylation of Mrc1, at residues, enables the mediator protein to recruit the monomeric form of Cds1 kinase.

Mrc1-mediated recruitment Cds1 monomer, orientates the catalytic C-terminal domain of the protein in to close proximity with the “Rad9-S”-bound Mph1 C-Tail terminal domain to enable mutual phosphorylation interactions between the two kinases.

Cds1 kinase-mediated phosphorylation of residues T471, Y546 and T593 within the the catalytic C-terminal domain of Mph1 kinase and reciprocal Mph1 kinase-mediated phosphorylation of T254, Y322 and S353 within the catalytic C-terminal domain of the Cds1 kinase (Fig 6.30, p.399), results in mutual activation of both kinases which may then be released and initiate various cell cycle checkpoint signalling responses to Camptothecin-induced DNA damage.

The identified isoforms “Rad9-VS”, “Rad9 T”, “Mph1-S”, “Mph1-VS”, “Cds1-S” and “Cds1-VS” may act as competitive-binding type inducers or suppressors within a regulatory mechanism which modulates the functional activities of the “Rad9-S” – Mrc1-co-ordinated Cds1-Mph1 activated signalling responses.

Differential phosphorylation of Mrc1 by Tel1 and Rad3 kinases has been observed in other experimental studies (Zhao H. *et al*, 2003) and may also be implicated in “switching-modulation” of the functional activities of the “Rad9-S”-Mrc1 co-ordinated activation of Cds1 and Mph1 kinases which could be associated with specific Hus1-dependent and Hus1-independent “Rad9-S”-mediated signalling pathways in response to camptothecin-induced DNA damage and environmental stresses that impinge adversely upon DNA replication, such as heat shock.

6.5 Component FEAR Network Pathway Inputs

Experimental studies have demonstrated that the Cds1 kinase may be implicated in the nucleolar release of the Clp1 kinase within the FEAR (Cdc-Fourteen Early Anaphase Release) pathway (Diaz-Cuervo H. and Bueno A., 2008), whilst hypertonic osmotic stress has been implicated in activation of a Cdc14-mediated Mitotic Exit Network (MEN) pathway in *S.cerevisiae* (Reiser V. *et al.*, 2006).

Heat shock (at 37°C) and camptothecin (40µM CPT) acute and chronic cell survival assays performed under osmotic stress conditions (1M Sorbitol), with *S. pombe* cells “cre-lox”-engineered for the exclusive expression of the truncated “Rad9-S” protein variant in this study (Fig 6.31, p.566; Fig 6.32, p.567), also indicated enhanced sensitivity of the cells to CPT-induced DNA damage, but enhanced resistance of the cells to thermal stress (discussed previously in Section 6.3, pp.556-567).

On the basis of these observed phenomena, it was postulated that “Rad9-S” truncated protein variant-mediated signalling responses to camptothecin-induced DNA damage and elevated thermal stress may converge at the “Rad9-S”-Hus1-C-Mph1-Cds1 functional ternary complex for the modulated release of the nucleolin homologue Gar2 and/or the Cdc14 phosphatase homologue Clp1 from the nucleolus – under the control of the Spo12 protein, which is a negative regulator that suppresses nucleolar translocation of Clp1 to the nucleus (Samuel J.M. *et al.*, 2000).

In human cells, one mechanism of resistance to camptothecin-induced DNA damage is nucleolin-mediated translocation and sequestration of the topoisomerase I (Top1) enzyme to the nucleolus where its retention prevents the formation of the DNA-CPT-Top1 complexes at duplex replication forks (Edwards T.K. *et al.*, 2000; Mi Y. *et al.*, 2003).

“Rad9-S”-Hus1-C-Mph1-Cds1 functional ternary complex-activated Cds1-mediated translocational liberation of Gar2 from the nucleolus to the nucleus and subsequent formation of the Gar2-Top1 complex may likewise result in nucleolar sequestration of topoisomerase I to prevent formation of the DNA-CPT-Top1 complexes at DNA replication forks, with consequent suppression of camptothecin-induced DNA damage.

“Rad9-S”-Hus1-C-Mph1-Cds1 functional ternary complex-activated Cds1-mediated translocational liberation of Gar2 from the nucleolus to the nucleus may also result in the subsequent formation of the Gar2-RPA complex with transient inhibition of DNA replication in response to both elevated thermal stress and CPT-induced DNA damage.

Whilst “Rad9-S”-Hus1-C-Mph1-Cds1 functional ternary complex-activated Mph1 kinase-mediated post-translational phosphorylated modification of the chromosomal passenger complex within the mitotic spindle checkpoint may be implicated in the nucleolar release of the Clp1 phosphatase into the nucleus.

In order to test this hypotheses, the *N149-rad9-c3xHA S. pombe* strain was cross-mated with various single deleted/inactivated G2/M-associated checkpoint type gene deleted/inactivated type *S. pombe* strains $\Delta clp1$ and *spo12.B81*.

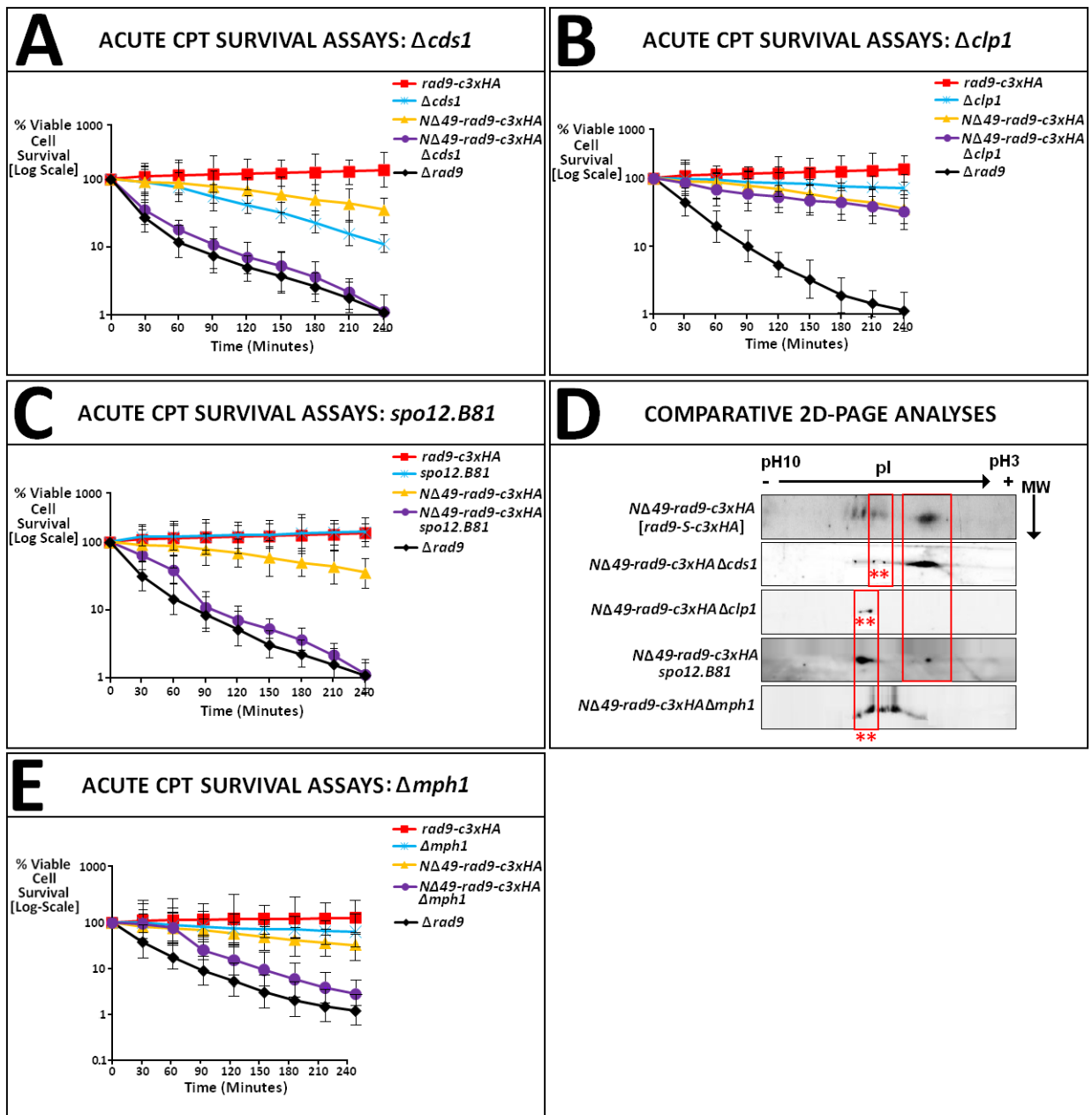
The generated *N149-rad9-c3xHA* “gene knock-out” mutant strains were then utilised in comparative acute camptothecin (CPT) cell survival assays in order to determine whether Clp1 and/or Spo12 were implicated in the “Rad9-S”-mediated checkpoint signalling response to CPT-induced DNA damage (Fig 6.41, p.587).

The survival assay data indicated that deletion of *clp1* within an exclusively expressed “*rad9-S*” genetic background did not enhance the cytotoxic sensitivity of the cells to Camptothecin-induced DNA damage (Fig 6.41B, p.587), whilst perturbation of Spo12 (ie *spo12.B81* mutagenised inactive variant) within an exclusively expressed “*rad9-S*” genetic background potentiated the sensitivity of the cells to camptothecin-induced genotoxicity (Fig 6.41C, p.587).

2D PAGE-coupled Western blot analyses performed on TCA-precipitated total protein extracts acquired from 30°C YEA broth cell cultures of the *S. pombe* $\Delta cds1$, $\Delta clp1$ and *spo12.B81* “*rad9-S*”-*c3xHA* cross-strains and “*rad9-S*”-*c3xHA* strain revealed a distinctive set of correlated hypophosphorylation shifts within the four respective phosphoisoform profiles (Fig 6.41D, p.587).

Taken together, the data indicate potential collaborative Cds1, Clp1 and Spo12 component functions, within the “Rad9-S” truncated protein variant-mediated response to CPT-induced damage, which may operate in novel roles that are independent of the FEAR network pathway.

Fig 6.41: Acute CPT Survival Assays – FEAR Network Mutants



A: Comparative acute survival assays, performed on 30°C YEA broth cultures of the indicated *S. pombe* strains in the presence of 40 μ M Camptothecin, revealed that deletion of *cds1* within an exclusively expressed “*rad9-S-c3xHA*” genetic background enhanced the sensitivity of the cells to CPT-induced DNA damage.

B: Comparative acute survival assays, performed on 30°C YEA broth cultures of the indicated *S. pombe* strains in the presence of 40 μ M Camptothecin, revealed that deletion of *clp1* within an exclusively expressed “*rad9-S-c3xHA*” genetic background did not enhance the sensitivity of the cells to CPT-induced DNA damage.

C: Comparative acute survival assays, performed on 30°C YEA broth cultures of the indicated *S. pombe* strains in the presence of 40 μ M Camptothecin, revealed that perturbed functional activity of the Spo12 protein (via utilisation of the *spo12.B81* mutant) within an exclusively expressed “*rad9-S-c3xHA*” genetic background also enhanced the sensitivity of the cells to CPT-induced DNA damage.

D: Comparative 2D PAGE-coupled Western Blot analyses performed on TCA-precipitated total extracts acquired from 30°C YEA broth cultures of the indicated *S. pombe* strains revealed conserved phosphoisomeric shifts within the aligned profiles of the “Rad9-S” truncated protein variant for the *cds1*-, *clp1*-, *mph1*- deleted and *spo12.B81*-mutated *S. pombe* strains (indicated via the asterisks within in the red boxes).

E: Comparative acute survival assays, performed on 30°C YEA broth cultures of the indicated *S. pombe* strains in the presence of 40 μ M Camptothecin, revealed that deletion of *mph1* within an exclusively expressed “*rad9-S-c3xHA*” genetic background enhanced the sensitivity of the cells to CPT-induced DNA damage.

6.6 Differential Checkpoint Responses to Camptothecin-Induced DNA Damage and Hyperthermic Stress are Initiated by “Rad9-S”

Taken together, the experimental data indicate the potential existence of two novel DNA damage checkpoint response pathways to camptothecin-induced/topoisomerase I-inhibitory types of DNA damage and heat shock, possibly in conjunction with other types of induced cytological stress (such as osmotic shock), which function exclusively outside of the canonical Rad9-Rad1-Hus1 complex – discussed summarily in Fig 6.42, pp.592-593 and Fig 6.43, pp.594-595.

The hyper-phosphorylated form of the Rad9-S truncated protein may function as a dominant repressor of Chk1 activation in response to camptothecin-induced DNA damage.

Whilst the unphosphorylated form of Rad9-S may elicit an extended G2/M phasic cell cycle arrest in response to heat shock (Janes S. *et al*, 2012, *Journal of Cell Science*, “in press” – see Appendix 6.1, pp.626-663).

Thermal stress may have indirect effects on the rectification of chromosomal catenanes via thermal-induced suppression of the functional activity of DNA Topoisomerase II within the G2-decatenation checkpoint pathway in which human Rad9 is also functionally implicated together with the WRN protein (discussed previously in Chapter 1., Section 1.2.2 , p.60).

Thermal stress could act as a “camptothecin-mimetic” via induction of “denaturation-trapped” topoisomerase-DNA complexes which inhibit DNA replication and result in stalled fork collision events with in consequential formation of one-sided double-stranded DNA breaks.

Heat-induced denaturation of the Rad9-Rad1-Hus1 complex could prevent it from disengaging from the DNA and/or may also result in the dysfunctional activation of Chk-initiated cell cycle checkpoint signalling activities.

In this context, expression of the “9-1-1” clamp-independent truncated “Rad9-S” protein variant, which acts as a dominant suppressor of Chk1, would effectively “counter-act” these potentially catastrophic dysfunctional Chk1 activities.

The postulated DNA repair and Cds1-initiated G2/M arrest functional activities of the truncated “Rad9-S” protein variant may therefore serve as an auxiliary mechanism for the temporary maintenance of cytological genomic integrity until properly functioning Rad9-Rad1-Hus1 complex-initiated Chk1 signalling has been restored.

Thermally-induced pleiotropic effects instigate alterations in chromatin supramolecular architecture, in conjunction with structural damage at centrosomal sites and may also be implicated in associative heat shock factor Hsp90-Wee1 type modulation of functional cell cycle checkpoint activities (Aligue R. *et al*, 1994; Goes F.S. and Martin J., 2001; Laszlo A. and Fleischer I, 2009; Munoz M.J. *et al*, 1999; Munoz M.J. and Jimenez J., 1999).

Associative human Rad9A-TPR2 interactions are also implicated in the modulation of the functional activities of the heat shock factor Hsp90/Hsp70-mediated protein chaperone pathway (discussed previously in Chapter 1, Section 1.2.4, pp.73-83) – which may also impinge on these Hsp90-Wee1 interactions.

Formation of the ATM-associative 53BP1-MDC1-H2AX and/or 53BP1-MDC1-BRCA1 type complexes, which are also implicated in the MRN complex-mediated processing repair of DNA double-stranded breaks within the G1/S, Intra-S and G2/M checkpoints (discussed previously in Chapter 1, Section 1.2.2, pp.54-57 and Chapter 1, Section 1.2.5, p.106) is also suppressed under cytological conditions of elevated thermal stress (Seno J.D. and Dynlacht J.R., 2004; Hunt C.R. *et al*, 2007; Köhl N.M. and Rensing L., 2000).

Thermal stress is also known to enhance the cytotoxic sensitivity of human tumour cells to radiotherapy-induced double-stranded DNA breaks via an as yet undefined pathway that involves switching of the ATM kinase from its normal DNA damage signalling function to a heat shock response, in conjunction with nuclear export of the Mre1-Rad50-Nbs1 (“MRN”) complex and consequential abrogation of MRN-mediated recruitment of ATM to damaged chromosomes (Seno J.D. and Dynlacht J.R., 2004; Hunt C.R. *et al*, 2007; Kühl N.M. and Rensing L., 2000).

Whether or not an equivalent type of type switch operates in *S. pombe* cells to modulate the functional activity of Rad3 or Tel1 in a similar manner is unknown, but these kinases may be required for the initiation of a G2 type checkpoint arrest to enable time for the appropriate repair of heat-induced damage to proteins and other cytological structures.

Tel1 and Rad3 kinases have been demonstrated to be implicated in the differential regulation of the functional activities of the Mrc1 adaptor/mediator protein (Zhao H. *et al*, 2003).

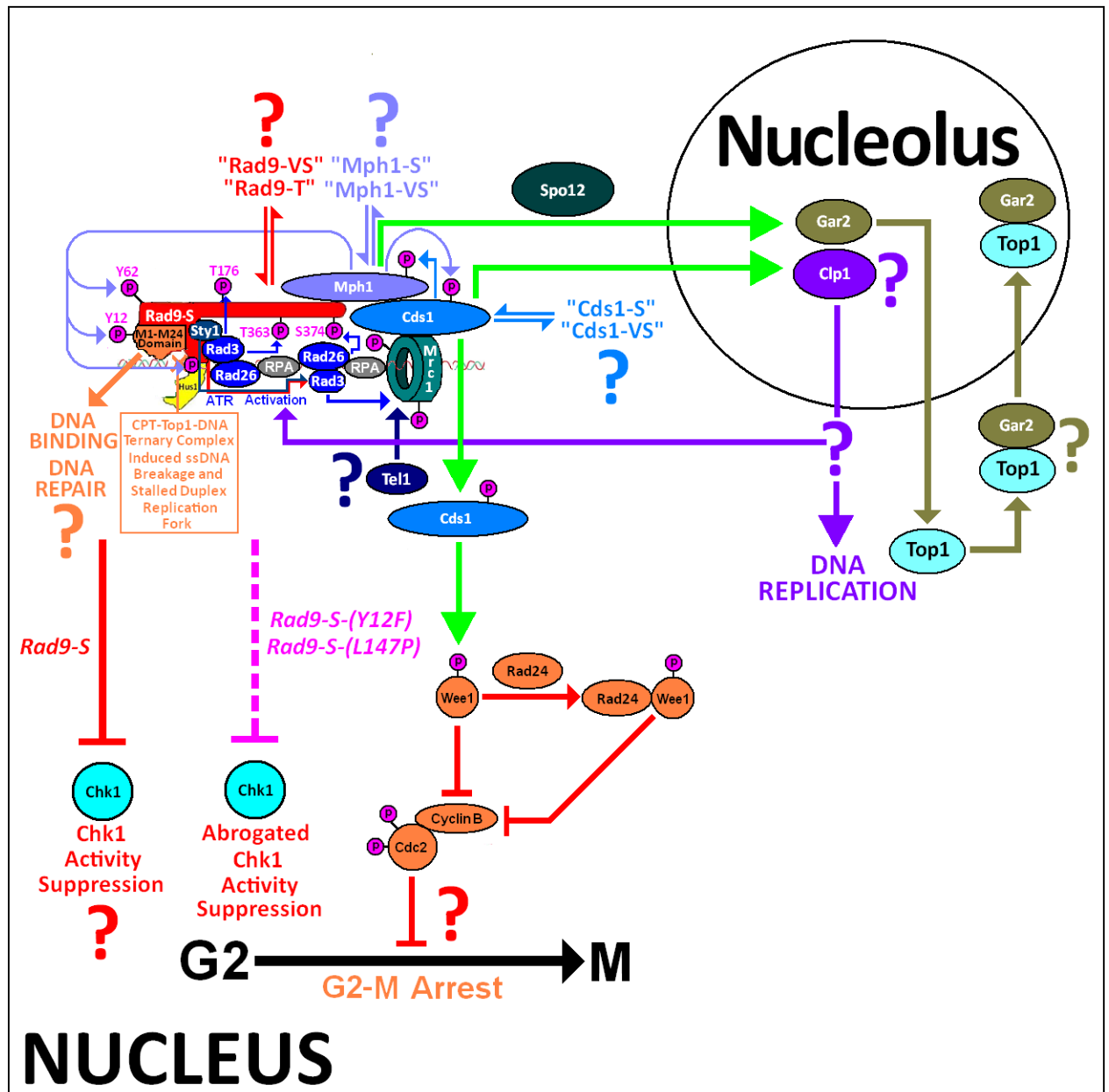
Both Rad3 and Mrc1 have been identified as key functional components of the “Rad9-S” truncated protein variant-mediated signalling pathway response to camptothecin-induced DNA damage in this research work (Fig 6.42, pp.592-593).

Whilst Tel1 kinase phosphorylation of Mrc1 may be implicated in the selective switching of the truncated Rad9-S protein variant-initiated signalling pathways for mediation of the heat-shock checkpoint response (Fig 6.43, p.594-595).

Experimental data acquired in this Ph.D. project indicated that differential activation of the Rad3 kinase, via Sty1-independent and Sty1-co-operative type “Rad9-S” interactions, may also mediate selective switching of the checkpoint pathways implicated in “Rad9-S” signalling response to camptothecin-induced damage (Fig 6.42, pp.592-593) and elevated thermal stress (Fig 6.43, pp.594-595) – Section 6.3, pp.556-567.

These pathways may form part of a complex intricate network of full-length Rad9- and truncated Rad9 protein- mediated signalling responses to different types of genotoxic and cytological stresses, whose respective activities may be regulated via epigenetic and proteomic interactions with the truncated Rad9 variants (“Rad9-VS” and “Rad9-T” – discussed previously in Chapter 4) and their respective phosphoisoforms (Fig 6.44, p.596-597).

Fig 6.42: Model for the “Rad9-S” Signal Response to Camptothecin



The truncated “Rad9-S” protein variant forms an associative complex with the Hus1-C isoform, in which the resultant “Rad9-S”:Hus1-C “open-ring” heterodimeric complex may act as a “sliding-clamp” DNA sensor for CPT-induced DNA damage and/or Top1-CPT-DNA ternary complex lesions at stalled replication forks.

Upon detection of the DNA lesion, “Rad9-S” in conjunction with Sty1, may participate in the synergistic activation of the Rad3 kinase, mediated via associative interactions with their respective Rad3-interactive motifs.

“Rad9-S” is then phosphorylated by the Rad3 kinase, in association with its functional counter-part Rad26, at T176 which induces supramolecular conformational changes within the truncated protein variant that enable Rad3/Rad26-mediated phosphorylation of its C-Terminal Tail Domain at the T363 and S374 residues.

Rad3/Rad26-mediated phosphorylation of T363 and S374 induces supramolecular configurational changes within the “Rad9-S” C-Terminal Tail Domain which enable it to associate with the C-Terminus of the Mph1 spindle-checkpoint kinase.

Rad3/Rad26-mediated phosphorylation of Mrc1, induces supramolecular configurational changes within the adaptor protein which enables it to associatively interact with the Cds1 kinase in close proximity to the C-Terminal catalytic domain of the “Rad9-S” C-Tail Domain-bound Mph1 kinase.

Tel1 kinase-mediated phosphorylation of Mrc1 may be implicated in the selective activation of the heat shock checkpoint pathway response (Fig 6.43, pp.594-595).

Direct interactive C-terminal catalytic site phosphorylation events between the Mph1 and Cds1 kinases result in their mutual activation, after which Cds1 could elicit a G2/M arrest, whilst Mph1 kinase-mediated phosphorylation of Rad9-S induces supramolecular configurational changes within the truncated protein variant which enable it to act as a dominant suppressor of Chk1 to prevent Chk1-initiated Intra-S phase checkpoint-activated inhibition of the homologous recombinational repair of CPT-induced DSB's.

Other detected isoforms of the Rad9, Mph1 and Cds1 proteins may be implicated in transient competitive inhibition and/or activation type regulation of the functional activities within the postulated mechanistic signalling pathway mediated by the truncated “Rad9-S” protein variant.

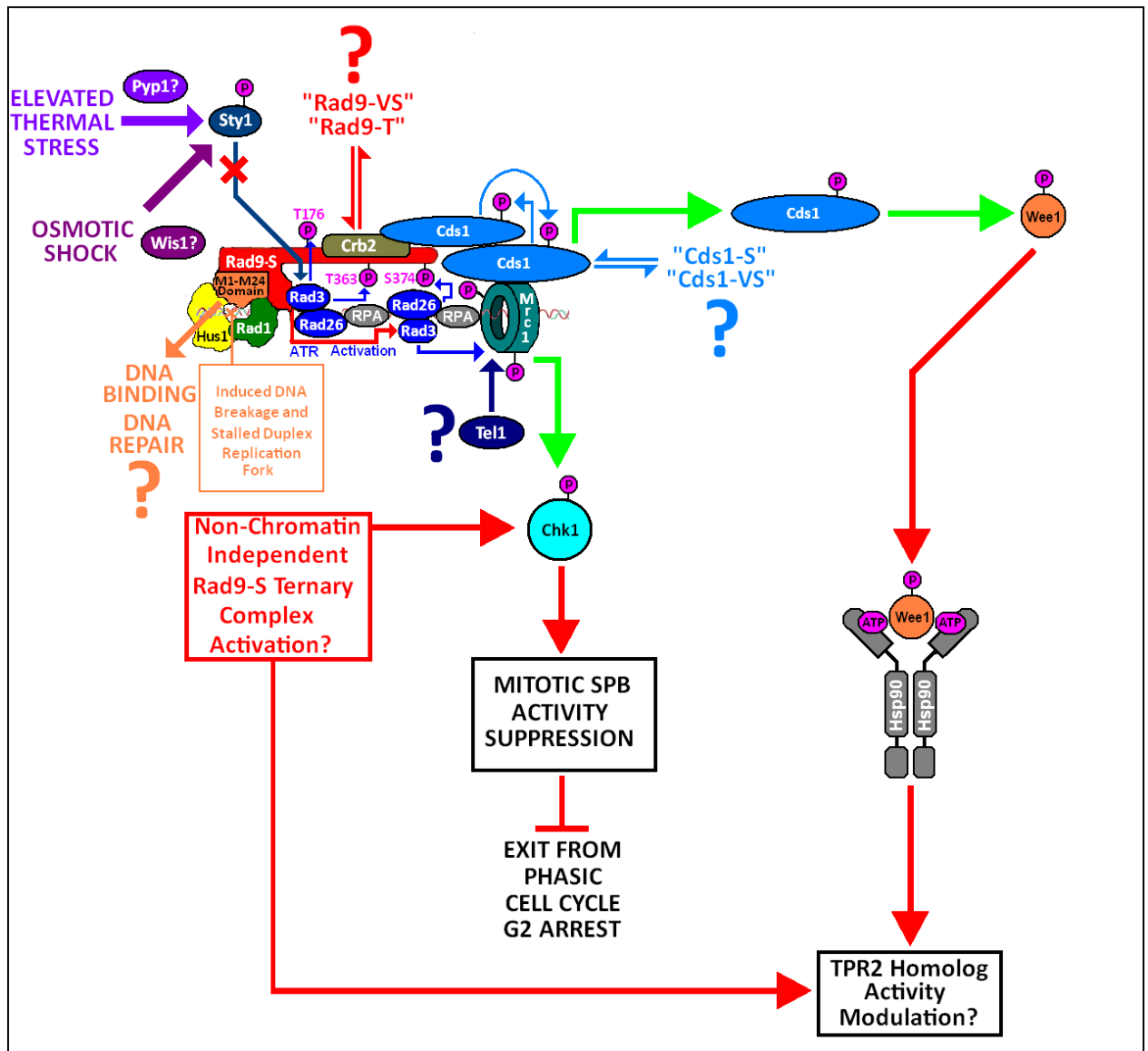
Rad9-S interactions with the Spo12 protein, in conjunction with the activated Mph1 and Cds1 kinases may also be implicated in the regulated nucleolar release of the Clp1 phosphatase and/or Gar2 for co-ordinated transient inhibition of DNA replication to allow repair of the CPT-induced DSB's and subsequent re-initiation of DNA replication after DNA repair has been effected.

Topoisomerase 1 (Top 1) may also associate with Gar2 with resultant translocation of the Top1:Gar2 heterodimer complex from the nucleus to the nucleolus.

Sequestration of Top1 in the nucleolus, via Gar2-targeted translocation, would prevent camptothecin (CPT) association with Top1 in the nucleus and suppress the formation of the trapped CPT-Top1-DNA complexes, thereby serving as a protective mechanism of resistance against CPT-induced DNA damage.

The Rad9-S-(Y12F) and Rad9-S-(L147P) mutants may restore a Chk1-mediated G2/M checkpoint response to CPT-induced DNA damage as a consequence of perturbed “Rad9-S”-mediated Chk1 suppression.

Fig 6.43: Model for the “Rad-S” Signal Response to Thermal Stress



Environmental stresses, trigger activation of the MAP kinase checkpoint pathway with consequential phosphorylation of Sty1 (mediated via Wis1 kinase in the case of osmotic stress and Pyp1 kinase in the case of heat shock) which induces supramolecular conformational changes within the protein that prevent it from interacting and activating the Rad3 primary (proximal) transducer checkpoint kinase in synergistic concert with the “Rad9-S” truncated protein variant.

In the absence of Sty1-associative Rad3 kinase activation, the truncated “Rad9-S” protein variant adopts a different supramolecular configuration which enables it to engage with the Rad26-associated Rad3 kinase – which phosphorylates “Rad9-S” at the T176, T363 and S374 residues.

Rad26/Rad3-kinase-mediated phosphorylation of the T363 and S374 residues induces supramolecular configurational changes within the C-Terminal Tail domain of “Rad9-S” which enable it to associate and engage with the adaptor/mediator protein Crb2.

Formation of the resultant “Rad9-S”-Hus1-Rad1:Crb2 complex, induces co-operative supramolecular configurational changes within the proteins which enable the associative recruitment of the Cds1 kinase.

Normally, Rad26/Rad3-mediated phosphorylation of Mrc1 induces supramolecular configurational changes within the adaptor protein which enable it to recruit the secondary (distal) transducer checkpoint kinase Chk1 which is then activated via phosphorylation by Rad26/Rad3 kinase which may then elicit a G2/M arrest (discussed previously in Chapter 1, Section 1.2.2, p.55) – but this signal response may be suppressed in response to thermal stress via Tel1-mediated phosphorylation of the Mrc1 adaptor protein.

In this case, chromatin-independent “Rad9-S”:Hus1:Rad1:Rad3:Crb2 complex-mediated activation of Chk1 may initiate a novel checkpoint response which suppresses the functional mitotic activity of the spindle polar body (SPB) and initiates a G2 phasic cell cycle arrest in response to elevated thermal stress (Janes S. *et al*, 2012, *Journal of Cell Science*, “in press” – see Appendix 6.1, pp.626-663).

The identified M50-M74 DNA-binding/Nuclease-Interactive motif within the truncated “Rad9-S” protein variant may also be implicated in the repair of thermally-induced DNA damage.

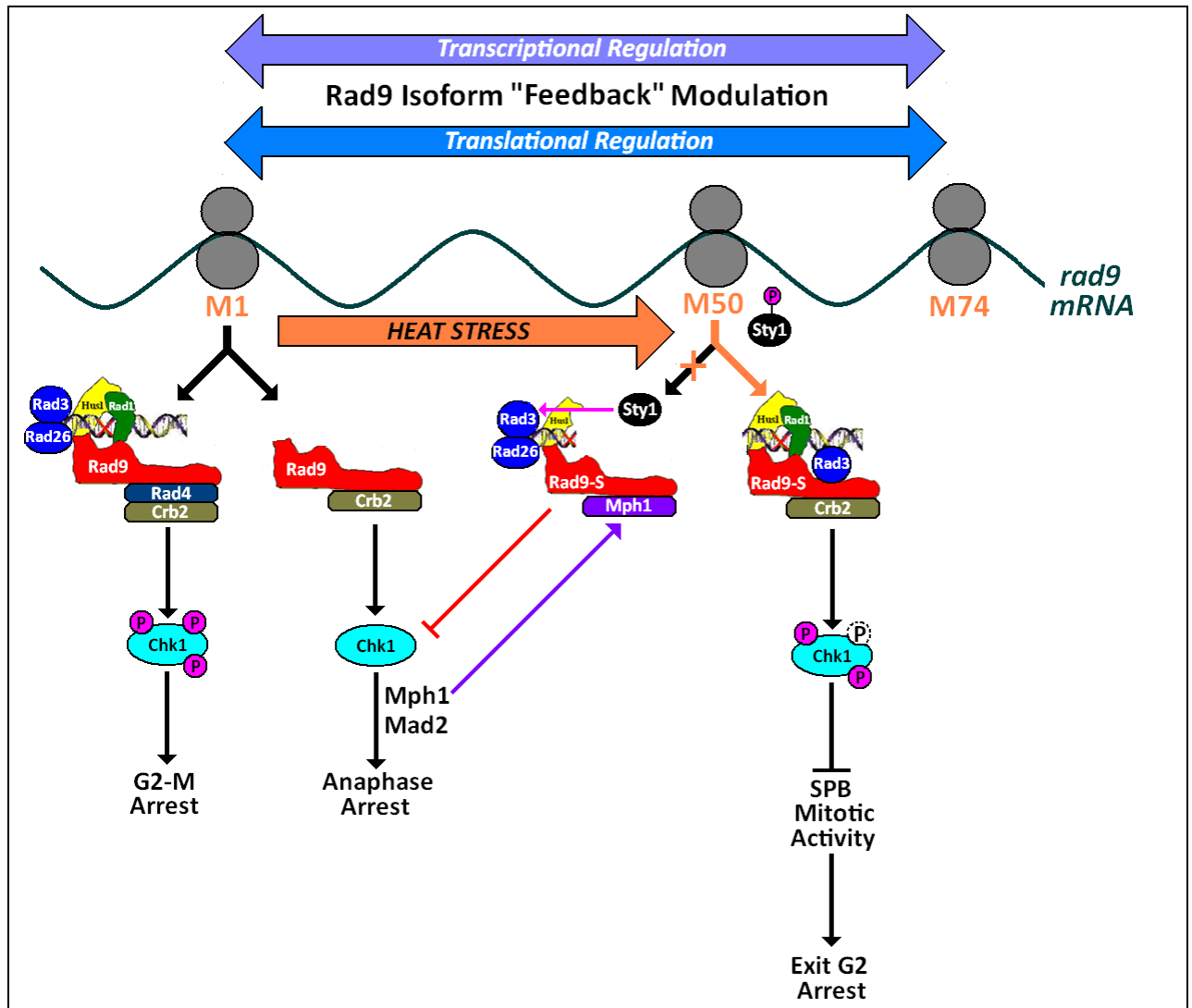
In response to heat shock, Tel1-mediated phosphorylation of Mrc1 induces supramolecular configurational changes within the adaptor protein which enables it to associatively interact with the Cds1 kinase in close proximity to the C-Terminal catalytic domain of the “Rad9-S” C-Tail Domain-bound Cds1 kinase – which triggers autophosphorylation-mediated activation of the Cds1 kinase.

Cds1 kinase-mediated phosphorylation of the Wee1 kinase, induces supramolecular conformational changes within Wee1 which enable it interact with the Hsp90 chaperone protein which may then serve as a novel checkpoint signalling response which initiates homologous TPR2-type functions that modulate the activity the Hsp70/Hsp90 chaperone protein folding pathway (discussed previously in Chapter 1, Section 1.2.4, pp.73-83) to enable resolution of partially denatured proteins as a consequence of elevated thermal stress or osmotic stress, thereby preventing the occurrence of dysfunctional cytological processes due to incorrectly configured proteins.

Human Rad9A has also been demonstrated to interact with and modulate the activity of the TPR2 protein (discussed previously in Chapter 1, Section 1.2.4, pp.73-83) and it is therefore conceivable that the truncated “Rad9-S” protein may also be implicated in the modulation of TPR2 activity in response to elevated thermal stress – which may impinge upon the associative Wee1-Hsp90 signalling interactions as part of a regulatory “feedback” mechanism for the co-ordination of a G2 phasic cycle cycle arrest with DNA repair processes and/or supramolecular conformational rectification of partially denatured/misfolded proteins.

Other detected isoforms of the Rad9 and Cds1 proteins may be implicated in transient competitive inhibition and/or activation type regulation of the functional activities within the postulated mechanistic signalling pathway mediated by the truncated “Rad9-S” protein variant.

Fig 6.44: Epigenetic and Proteomic Differential Pathway Model



Rad3 kinase-mediated phosphorylation of the C-Terminal Tail Domain within the full-length Rad9 protein, in conjunction with associative interactions with the Rad4 and Crb2 adaptor proteins, results in phosphorylated activation of Chk1 which elicits a G2/M arrest in response to Camptothecin-induced DNA damage.

The full-length Rad9 protein may also target Chk1 outside of the "9-1-1" clamp, independently of Rad3 kinase-targeted Chk1 activation, in which an alternative Mad2-mediated anaphase cell cycle arrest is initiated.

"Rad9-S" initiates differential checkpoint responses to camptothecin genotoxic stress and hyperthermic stress which are mediated via formation of either the "Rad9-S":Hus1 heterodimeric complex or an alternative "Rad9-S":Hus1:Rad1 heterotrimeric complex.

In response to camptothecin-induced DNA damage, Sty1 and "Rad9-S" co-operatively interact with the Rad3 kinase and induce its catalytic activity for subsequent Rad3 kinase-mediated phosphorylation of "Rad9-S" – which induces supramolecular conformational changes within the C-Terminal Tail domain of the protein that enable associative interactions with the Mph1 kinase with consequential suppression of the Chk1-mediated Mad2-dependent anaphase arrest.

The mechanism of expression of the full-length Rad9, Rad9-S and Rad9-VS truncated protein variants may comprise alternative translation at the alternative AUG start-codon sites at the respective Methionine 1 (M1), Methionine 50 (M50) and Methionine 74 (M74) situated within the mRNA of the transcribed *S. pombe rad9* gene, in which leaky ribosomal scanning is implicated.

Heat shock may increase the frequency of leaky ribosome scanning, via alterations of the secondary topological configuration of the *rad9* mRNA, in which *rad9* mRNA-protein associative interactions with heat-shock proteins, RNA chaperones and/or RNA stabilisers may also be implicated – with consequential elevated expression of the Rad9-S protein.

Heat shock also initiates the MAP kinase pathway, with resultant phosphorylation of Sty1 – which induces supramolecular configurational changes within the kinase which prevent it from engaging with and co-operatively activating Rad3 kinase, with Rad9-S.

Thus, thermal stress initiates formation of the “Rad-S”:Hus1:Rad1:Crb2:Rad3 ternary complex which targets Chk1 for suppression of the functional mitotic activity of the Spindle Polar Body (SPB) with consequential initiation of a G2 arrest to provide time for the repair of DNA, resolution of partially denatured proteins and other cytological structures (Janes S. *et al*, 2012, *Journal of Cell Science*, “in press” – see Appendix 6.1, pp.626-663).

A variety of potential Rad9 phospho-isoforms may be implicated in various interactive “activity-modulatory feedback” mechanisms, in which they function as transcriptional and/or translational regulators of the expression of the full-length Rad9, N Δ 49-Rad9 (“Rad9-S”) and N Δ 73-Rad9 (“Rad-VS”) proteins (discussed previously in Chapter 4) – which in turn may impinge upon the functional activities of the respective DNA damage/replication stress-induced checkpoint pathways.

6.7 Caffeine Significantly Potentiates the Sensitivity of *S. pombe* Cells “Cre-Lox” Engineered for the Exclusive Expression of the Truncated “Rad9-S” Variant to Camptothecin-Induced DNA Damage and Hyperthermic Stress: Potential Indications of Equivalent Novel Human Rad9B Functional Checkpoint Signalling Responses

Caffeine is a xanthine-based analogous adenine mimetic which interacts competitively with different classes of adenosine receptor proteins to induce localised conformational changes within their respective supramolecular architectures which alter their specific functional activities that are coupled to the initiation and/or regulation of particular biochemical processes (Daly J.W. *et al.*, 1991; Daly J.W., 2007; Franco R., 2008; Gao Z.G. and Jacobson K.A., 2011; Loegering D. *et al.*, 2004; Nabetani A. *et al.*, 2004).

These “caffeine-adenosine receptor” interactions may result in the suppression of DNA damage checkpoint signalling pathways (via inhibition of transducer kinases such as ATM and ATR), impairment of nucleic acid metabolism and/or DNA repair pathways (via inhibition of DNA-PK, nucleases, ligases and polymerases), abrogation of innate and adaptive immune responses (via inhibition of cAMP phosphodiesterases), suppression of tumour multiple drug resistance (via inhibition of membrane-bound ATPase-driven drug transporter proteins) and inhibition of tumour metastatic progression via destabilisation of HIF1 α , VEGF and IL-8 expression (Ding R. *et al.*, 2012; Gao Z.G. and Jacobson K.A., 2011; Pantelias G.E. and Terzoudi G.I., 2011; Sabisz M. and Skladanowski A., 2008; Sarkaria J.N. *et al.*, 1999; You L.P. *et al.*, 2011; Zhou B.B. *et al.*, 2000).

These pharmacodynamic properties of caffeine have been exploited clinically as a complementary adjuvant therapy which may potentiate the cytotoxic efficacy of particular polychemotherapeutic, radiotherapeutic and gene therapeutic regimens that are employed in the palliative management and treatment of aggressive, late-stage metastatic cancerous pathophysiological conditions (Asaad N.A. *et al.*, 2000; Franco R. *et al.*, 2008; Jones R.L. and Constantinidou A., 2012; Kawano Y. *et al.*, 2012; Niknafs B. *et al.*, 2011; Saito Y. *et al.*, 2003).

Somewhat paradoxically, caffeine may also attenuate the cytotoxic efficacy of DNA-intercalating classes of anti-cancer chemotherapeutics (such as berberine, camptothecin, chelerythrine, doxorubicin, ellipticine, sanguinarine and topotecan), via associative π - π non-covalent types of “caffeine-drug” interactions which compete with and suppress the formation of the respective drug-DNA complexes (Hill G.M. *et al.*, 2011; Evstigneev M.P. *et al.*, 2011).

Human Rad9 is implicated in the initiation, selection and regulation of appropriate cell cycle checkpoint and/or DNA repair pathways in response to particular genotoxic and environmental cytological stresses, as well as alteration of immune responses via Rad9-mediated modulation of immunoglobulin class switching type V, D., J gene recombination events (Broustas C.G. and Lieberman H.B., 2012), all of which may also be perturbed via the inhibitory effects of caffeine on the specific adenosine receptor proteins that are implicated in the mediation of these biochemical processes (discussed on the previous page).

A variety of experimental studies have also demonstrated that caffeine suppresses DNA damage checkpoint signalling pathways in the eukaryotic model organism *S. pombe* via inhibition of the functional activities of transducer kinases such as Rad3, Tel1, Wis1 and Sty1 (Benzo K. *et al.*, 1997; Calvo I.A. *et al.*, 2009; Osman F. and McCready S., 1998).

Experimental data acquired in this Ph.D. project indicated that differential activation of the Rad3 kinase, via Sty1-independent and Sty1-co-operative type “Rad9-S” (N Δ 49-Rad9), may be implicated in a selective switching mechanism between two distinctive novel checkpoint pathways (discussed previously in Section 6.3, pp.556-567) in response to camptothecin-induced genotoxic stress (Fig 6.42, pp.592-593) or hyperthermally-induced environmental stress (Fig 6.43, pp.594-595) – which might also be suppressed via caffeine-mediated inhibition of the transducer kinases.

In order to determine the effects of caffeine on these two novel “Rad9-S”-mediated checkpoint signalling pathways, comparative acute survival assays were performed on YEA broth cell cultures of the “cre-lox”-constructed $\Delta rad9$, $rad9-c3xHA$, $rad9-(M50L)-c3xHA$ and $N\Delta49-rad9-c3xHA$ *S. pombe* strains incubated at 30°C in the absence and presence of 10mM caffeine and/or 40µM camptothecin (Fig 6.45, p.618), or at 37°C in the absence and presence of 10mM caffeine (Fig 6.46, p.619).

The acquired acute cell survival assay data revealed that caffeine enhanced the sensitivity of all the *S. pombe* strains tested to camptothecin-induced genotoxic stress and hyperthermally-induced cytological stress (Fig 6.45, p.618 and Fig 6.46, p.619).

The observed caffeine-potentiated cytotoxic sensitivity to camptothecin-induced DNA damage also indicated that potential associative JI-JI “caffeine-camptothecin” interactions did not attenuate the genotoxic mechanism of action of this topoisomerase I inhibitor (discussed previously on p.599) in the case of the experimental *S. pombe* strains utilised in these acute survival assays (Fig 6.45, p.618).

Taken together, these two experimental data sets indicated that the caffeine-potentiated cytotoxic sensitivity of the *S. pombe* strains to camptothecin-induced DNA damage and hyperthermally-induced cytological stress is a consequence of inhibited transducer checkpoint kinases (Fig 6.45, p.618; Fig 6.46, p.619; Fig 6.48, p.623).

Intriguingly, all the camptothecin acute cell survival assay data plots exhibited a partial lag phase of ~60 minutes duration that was initiated after ~90 minutes elapsed incubation time and terminated after ~150 minutes incubation time (Fig 6.45, p.618), whilst no similar partial lag phase was observed in the heat shock acute cell survival assay data (Fig 6.46, p.619).

A plausible hypothetical explanation for these observed experimental phenomena may be that caffeine and/or the “caffeine-camptothecin” complex interact with the nuclease-docking/DNA binding site within the “Rad9” and “Rad9-S” sub-units and/or nucleobase binding site within the Hus1 and/or “Hus1-C” sub-units of the respective full-length heterotrimeric Rad9-Rad1-Hus1 “closed-ring” complex and the “Rad9-S”-Hus1-C “open-ring/C-clamp” which perturb detection and/or DNA repair of the camptothecin-induced ssDNA and dsDNA breaks, whilst initiating a checkpoint signalling response that is terminated prematurely by the inhibitory action of caffeine on transducer and effector kinases (Fig 6.48, p.623) – which could be responsible for the partial ~60 minute lag-phase manifested in the acute camptothecin survival assay data (Fig 6.45, p.618).

In this hypothetical context, lack of an observable partial lag phase in the acute heat shock survival assay data (Fig 6.46, p.619) may be a consequence of hyperthermally-induced disruption of associative non-covalent bond formation which are critical for the potential interactions of caffeine with the Rad9 and “Rad9-S” nuclease-docking/DNA binding site and Hus1 and/or “Hus1-C” nucleobase binding site (discussed in detail previously in Section 6.2.1, pp.493-515).

Comparative 2D PAGE-coupled Western blot analyses of TCA-precipitated total protein extracts, acquired from 30°C YEA broth cell cultures of the *S. pombe* strains *NΔ49-rad9-c3xHA* (“*rad9-S*”-*c3xHA*), *NΔ49-rad9-c3xHA Δrad3* and *NΔ49-rad9-c3xHA Δsty1*, incubated in the absence of camptothecin or caffeine for 30 minutes and YEA broth cell cultures of the *S. pombe* strain *NΔ49-rad9-c3xHA* incubated at 30°C in the absence or presence of 40μM camptothecin in the absence or presence of 10mM caffeine, or at 37°C in the absence and presence of 10mM caffeine, probed with the anti-HA anti-body, were performed for biochemical verification that caffeine was implicated in the inhibition of checkpoint transducer kinases (Fig 6.47, pp.620-622).

The acquired data revealed a series of correlated phosphoisoformic profiles for the “Rad9-S” truncated variant that were specific to camptothecin-induced DNA damage and hyperthermic stress-induced checkpoint pathway signalling responses in which caffeine initiated distinctive hypophosphoisoformic shifts as a consequence of caffeine-mediated inhibition of the transducer kinases (Fig 6.47, pp.620-622).

Commonly conserved phosphoisoformic traits within all the analysed 2D-PAGE protein samples (Fig 6.47A and Fig 6.47B, pp.620-622) and conserved phosphoisoformic traits specific to the camptothecin 2D-PAGE profile data set (Fig 6.47A, pp.620-622) and hypothermic stress 2D-PAGE profile data set (Fig 6.47B, pp.620-622) were also found to correlate with distinctive phosphoisoforms in the 2D-PAGE profiles acquired from protein analyses of the 30°C and 37°C caffeine-treated *S. pombe* *NΔ49-rad9-c3xHA* YEA broth cultures, *NΔ49-rad9-c3xHA Δrad3* and *NΔ49-rad9-c3xHA Δsty1* 30°C YEA broth cultures incubated in the absence of caffeine and camptothecin (Fig 6.47A and Fig 6.47B, pp.620-622).

Taken together, these 2D-PAGE-coupled Western blot assay data (Fig 6.47, pp.620-622) provide additional biochemical evidence for the postulated Sty1-independent and Sty1-co-operative type “Rad9-S” (*NΔ49-Rad9*), selective Rad3-activated switching mechanism between two distinctive novel checkpoint pathways (discussed previously in Section 6.3, pp.556-567) in response to camptothecin-induced genotoxic stress (Fig 6.42, pp.592-593) or hyperthermally-induced environmental stress (Fig 6.43, pp.594-595) – which are suppressed via caffeine-mediated inhibition of the respective transducer kinases (Fig 6.48, p.623).

In addition to abrogation of checkpoint transducer kinase functional activities, caffeine may also be implicated in the inhibition of other adenosine receptor-coupled biochemical processes which may potentiate the cytotoxic sensitivity of *S. pombe* cells to camptothecin-induced DNA damage and hyperthermally-induced cytological stresses (Fig 6.48, p.623).

Caffeine-mediated impairment of DNA repair pathways may occur as a consequence of its ability to interact with and inhibit the catalytic functional activities of specific adenosine receptors which are implicated, notably; kinases (eg DNA-PK), nucleases, ligases, polymerases and key enzymatic components of nucleotide biosynthesis (Gentner N.E. and Werner N.M., 1975; Kaufmann W.K. *et al.*, 2003; Tempel K. and Zellinger C.,1997) – Fig 6.48, p.623.

In the case of both the full-length Rad9 and truncated “Rad9-S” *S. pombe* proteins, caffeine and/or the caffeine-camptothecin complex may also associate with the novel M50-M74 nuclease interactive/DNA-binding domain within these respective proteins (identified via experimental work performed in this Ph.D. project – discussed in detail previously in Chapter 5, Section 5.5, pp.475-481).

These interactions may perturb the functional activities of the M50-74 domain within the Rad9 and “Rad9-S” proteins and/or block duplex access to the nucleobase binding pocket located within the Hus1 and “Hus1-C” proteins with consequential abrogation of the detection and/or repair of camptothecin- and/or hyperthermically- induced DNA damage lesion sites within the chromatin supramolecular architecture, which would otherwise be mediated via the respective Rad9-Rad1-Hus1, “Rad9-S”:Rad1:Hus1/”Hus1-C” and/or “Rad9-S”:“Hus1-C” clamp complexes.

In the case of the truncated “Rad9-S” variant, caffeine-mediated inhibition of Mph1 kinase, Rad16 nuclease and DNA ligase IV enzymes (all of which were identified as critical components of a novel DNA repair mechanism via experimental work performed in this Ph.D. project – discussed in detail in Chapter 7) could also render *S. pombe* cells “cre-lox”–engineered for the exclusive expression of the NΔ49-Rad9-c3xHA protein highly sensitive to the cytotoxic effects of camptothecin- and hyperthermically- induced DNA damage – Fig 6.48, p.623.

Caffeine-mediated inhibition of proton pump proteins, such as H⁺-ATPases and/or vacuolar ATPases (V-ATPases) found in both mammalian and *S. pombe* cells (Iwaki T. *et al*, 2004; Supino R. *et al*, 2009), may also be implicated in the potentiation of the cytotoxic effects of hyperthermally-induced and/or camptothecin induced DNA damage – Fig 6.48, p.623.

V-ATPases are also overexpressed in some tumour cell types, in which their elevated activities have been postulated to increase the pH level of intracellular microenvironments to protect the abnormally actively cycling cells from the deleterious effects of excessive proton production as a consequence of hypoxia-related hyperglycolytic metabolism, whilst promoting angiogenesis (via induced expression of genes that encode various angiogenesis factors – such as VEGF) which contributes to metastatic progression (Supino R. *et al*, 2009).

In the case of the eukaryotic model organism *S. pombe*, caffeine-mediated inhibition of V-ATPases may increase cell wall and plasma membrane permeability and thereby facilitate the intracellular accumulation of camptothecin, in addition to enhancement of cellular sensitivity to the genotoxic effects of the drug (Chardwiriyaapreecha S. *et al*, 2009; Codlin S. *et al*, 2008; Dawson K. et al, 2008) – Fig 6.48, p.623.

The molecular structure of camptothecin (CPT) is comprised of 5 fused rings (designated A, B, C, D and E), in which the A, B, C and D rings constitute the indolizinoquinone functional group which enables the drug to intercalate with DNA and the lactone E ring which engages with the topoisomerase I enzyme and elicits the formation of DNA breakages within the resultant topoisomerase I-CPT-DNA ternary complex formed at the stalled duplex replication fork (Fan Y. et al, 1998; Giovanella B.C. *et al*, 2000; Kerrigan J.E. and Pilch D.S., 2001; Kohn K.W. and Pommier Y., 2000; Redinbo M.R. *et al*, 1998) – Fig 6.48, p.623.

Conversion of camptothecin to the inactive carboxylate species, via lactone E ring hydrolysis, predominates under conditions of high pH, whilst low pH environments favour the formation of the active lactone form of the drug (Beretta G.L. and Zunino F., 2007; Ivanova B. and Spitteller M., 2012; Liu L.F. *et al*, 2000) – Fig 6.48, p.623.

At the normal physiological pH value of pH7.4 the intracellular concentrations of carboxylate (inactive form) and lactone (active form) species of camptothecin are equivalent (Ivanova B. and Spitteller M., 2012; Liu L.F. *et al*, 2000).

Caffeine-mediated inhibition of V-ATPases could result in a significant fall in intracellular pH which would favour predominant formation of the protonated, cytotoxically-active lactone form of camptothecin, in which the positively charged nitrogen atoms within the B and C rings may also enhance the DNA-binding affinity of the drug via additional electrostatic interactions with the negatively charged phosphate groups of the duplex sugar-phosphate backbone.

In *S. pombe*, Hal4 kinase is an essential regulator of major potassium ion transporters (such as Trk1 and Trk2) in which experimental studies have also demonstrated that abrogated Hal4 functional activities result in membrane hyperpolarisation-mediated intracellular transport of various cationic species and may as a pleiotropic determinant of cellular hypersensitivity to the cytotoxic effects of a range of different types of chemotherapeutic agents which act as environmental stress- or genotoxic- inducers (Thornton G. *et al*, 2005).

Previous experimental studies have also revealed that Hal4 kinase may be implicated in the activation of the *S. pombe* Bfr1 protein, which is a functionally equivalent homologue of the mammalian ATPase-binding cassette P-glycoprotein class of multiple drug transporters (ABC-MDRs), in which Bfr1 also mediates the induced expression of the Bfr2 ABC-MDR protein homologue (Arioka M. *et al*, 1998; Thornton G. *et al*, 2005; Turi G. and Rose J.K., 1995).

It is therefore hypothetically conceivable that caffeine-mediated inhibition of Hal4 kinase, in conjunction with abrogated V-ATPase functional activities, may result in the cytological accumulation of high levels of the active, protonated form of camptothecin (CPT) with consequential potentiation of CPT-induced DNA damage which renders *S. pombe* cells hypersensitive to the cytotoxic effects of the drug (Fig 6.48, p.623).

In *S. pombe*, Hal4 kinase-mediated activation of Brf1 may also impinge upon Brf1-mediated activation of the transcriptional factor Pap1 which is then translocated from the cytoplasm to the nucleus via the Ran nucleotide GDP/GTP exchange factor: Hba1 GTPase complex where Pap1 then binds to its target promoters of the *brf1/hba2*, *caf5* and *pmd1* genes with consequential elevation of expressed cytological levels and associated up-regulated functional activities of the Hba2, Caf5 and Pmd1 proteins (Arioka M. *et al.*, 1998; Calvo I.A. *et al.*, 2009; Thornton G. *et al.*, 2005; Toone M.W. *et al.*, 1998; Turi G. and Rose J.K., 1995) – Fig 6.48, p.623.

Specific caffeine- and oxidative stress- induced cytological stress checkpoint signalling responses are also initiated via Sty1 kinase-mediated activation of the Pap1 transcription factor, which in turn up-regulates the activities of the Brf1/Hba2, Caf5 and Pmd1 proteins that are exported to the plasma membrane where they function as ATPase-driven pumps for the intracellular removal of caffeine, in which Hba2 is the major caffeine transporter (Arioka M. *et al.*, 1998; Calvo I.A. *et al.*, 2009; Thornton G. *et al.*, 2005; Toda T. *et al.*, 1991; Toone M.W. *et al.*, 1998; Turi G. and Rose J.K., 1995) – Fig 6.48, p.623.

Experimental data acquired in this Ph.D project also indicated that Sty1-coupled “Rad9-S”-mediated Rad3 activation may constitute a critical initiation component of a novel checkpoint response to camptothecin-induced DNA damage (discussed previously in Section 6.3, pp.556-567 and in Fig 6.42, pp.592-593) which may impinge upon and modulate the functional activity of this Sty1 → Pap1 pathway.

Both the Brf1/Hba2 and Pmd1 proteins also act functionally-equivalent homologues of mammalian classes of P-glycoprotein ABC-MDR transporters, which may be implicated in the attenuation of the cytotoxicity of genotoxic- and stress- inducing agents (such as anti-cancer chemotherapeutics) via expediting their intracellular removal (Arioka M. *et al*, 1998; Calvo I.A. *et al*, 2009; Thornton G. *et al*, 2005; Toda T. *et al*, 1991; Toone M.W. *et al*, 1998; Turi G. and Rose J.K., 1995) – Fig 6.48, p.623.

The functional activity of the Pap1 transcription factor is regulated via the nuclear exportin protein Crm1, which translocates Pap1 from the nucleus to the cytoplasm (Calvo I.A. *et al*, 2009; Kumada K. *et al*, 1996; Toda T. *et al*, 1992; Toone W.M. *et al*, 1998) – Fig 6.48, p.623.

Specific caffeine-adenosine receptor interactions may be implicated in the direct inhibition of the Brf1/Hba2, Pmd1 and Brf2 ATPase-driven protein transporters and abrogation of Pap1 transcriptional activities via inhibition of the Sty1 transducer kinase and the Ran nucleotide GDP/GTP exchange factor: Hba1 GTPase complex nuclear transporter which would result in the cytosolic retention of Pap1 (Fig 6.48, p.623).

The net effect of these inhibitory caffeine-adenosine receptor interactions would be the elevated cytological accumulation of intracellular caffeine and the active lactone form of camptothecin, in conjunction with the consequential enhanced caffeine-mediated suppression of DNA repair pathways and cell cycle checkpoint signalling responses (discussed previously – pp.600-606) which would potentiate the cytotoxic sensitivity of the *S. pombe* cells to hyperthermally-induced stress and camptothecin-induced DNA damage (Fig 6.48, p.623).

Functionally-equivalent homologous components of these *S. pombe* caffeine-inhibited adenosine receptor proteins are also expressed in mammalian cells (Table 6.1, p.624).

Recent experimental studies have also indicated that ATR and JNK kinase-mediated post-translational modifications of the human Rad9B C-terminal tail domain may enable it to interact with other signalling proteins which are implicated in novel G1/S cell cycle checkpoint pathways in response to nucleolar stress (Pérez-Castro A.J. and Freire R. *et al*, 2012).

Both the ATR and JNK kinases are mammalian equivalent functional homologues of the *S. pombe* Rad3 and Pap1 kinases which may be implicated in caffeine-modulated checkpoint responsive pathways (Fig 6.48, p.623; Table 6.1, p.624) – discussed previously on pp.606-607.

In silico multiple sequence alignment analyses of the *S. pombe* Rad9 protein with the human Rad9B paralogue and its truncated isoforms indicated significant conserved homology between the *S. pombe* “Rad9-S” variant, *H. sapiens* Rad9B isoform 2 (Uniprot ID: Q6WBX8-2) and *H. sapiens* Rad9B isoform 3 (Uniprot ID: Q6WBX8-3).

Whilst comparative *in silico* multiple sequence analyses of the *S. pombe* full-length Rad9 protein and its novel truncated variants “Rad9-S”, “Rad9-VS” and “Rad9-T” with the full-length *H. sapiens* Rad9B protein and its truncated variants indicated significant conserved homology within the two alternative C-termini of the Rad9B isoforms.

These bioinformatics-based analyses also revealed that the *S. pombe* full-length Rad9 and truncated “Rad9-S” proteins contained two conserved sequences of significant homology to the two alternative human Rad9B C-termini (discussed previously in Chapter 4, Section 4.9.2, pp.407-417).

The *S. pombe* “Rad9-VS” C-terminus exhibited a significant degree of homology with the “GSFSIF” C-terminal sequence of the human Rad9B isoforms 1, 2 and 3, whilst the N-terminus of the *S. pombe* “Rad9-T” exhibited a significant degree of homology with the “VCCRKEFNGSDAKYFCII” C-terminal sequence of the human Rad9B isoforms 4 and 5.

These *in silico* data indicate the intriguing possibility that the identified *S. pombe* truncated Rad9 isoforms; “Rad9-S”, “Rad9-VS” and “Rad9-T” may possess novel functions equivalent to those of the *H. sapiens* full-length Rad9B paralogue and its respective isoforms.

Whether or not hyperthermically-induced expression of the Rad9B paralogue and/or its isoforms occurs in human cells remains to be elucidated.

However taking into consideration the experimental data acquired in this Ph.D. project, which indicate two distinctive novel checkpoint pathways mediated by the truncated “Rad9-S” protein variant in response to camptothecin-induced DNA damage or heat shock that are suppressed by caffeine (discussed in detail previously in Section 6.6, pp.588-597), it is hypothetically conceivable that homologous equivalent functional pathways are elicited by the human Rad9B paralogue and/or its isoforms (Fig 6.49, p.625).

The heat shock transcription factor, HSF1, is implicated in tumour metastatic progression and regulation of the relative expression, cytological levels and functional activities of Hsp27, Hsp70, Hsp90 and the hypoxia inducible factor, HIF1 α (Calderwood S.K., 2000; Calderwood S.K. and Gong J., 2011; Ciocca D.R. and Calderwood S.K., 2005; Gabai V.L. *et al.*, 2012; Meng L. *et al.*, 2010; Meng L. *et al.*, 2011) – Fig 6.49, p.625.

Elevated cytosolic levels of Hsp27 and Hsp70 chaperone proteins are implicated in the suppression of malignant neoplastic transformation-induced apoptotic pathways, whilst Hsp90 mediates a range of dysfunctional proto-oncogenic activities via the induced transcription, translation and subsequent cytological accumulation of oncogenes and mutated oncoproteins (oncogene), with consequential promotion of metastatic evolution (Calderwood S.K., 2000) – Fig 6.49, p.625.

A variety of experimental studies have indicated that thermal stress responsive heat shock proteins, including Hsp27, Hsp70, Hsp72 and Hsp90, are implicated in the development of acquired multiple drug resistance in breast tumour cells (Burke A.R. *et al*, 2012; Calderwood S.K. *et al*, 2010; Calderwood S.K. and Gong J., 2011; Ciocca D.R. and Calderwood S.K., 2005; Gabai V.L. *et al*, 2009; McDowell C.L. *et al*, 2009; Meng L. *et al*, 2011; Rylander M. *et al*, 2010; Vargas-Roig L.M. *et al*, 1998).

Human Rad9A-TPR2 interactions (Xiang S.L. *et al*, 2001) may also modulate specific functional activities of the Hsp90/Hsp70-mediated chaperone protein-folding pathway which is implicated in the suppression of proteotoxic-induced carcinogenesis events (discussed in detail previously in Chapter 1, Section 1.2.4, pp.75-85).

Human Rad9B-TPR2 interactions, may likewise be implicated in the functional activity modulation of the Hsp90/Hsp70-mediated chaperone protein-folding pathway for suppression of proteotoxic-induced impairment of cytological mechanisms which maintain genomic integrity/stability and act as a preventative “safe-guard” against the development of carcinogenesis (Neznanov N. *et al*, 2011; Sherman M.Y. *et al*, 2011; Xiang S-L. *et al*, 2001) – Fig 6.49, p.625.

The Hsp90 protein may also modulate Wee1 kinase functions that trigger “down-stream” effector signalling-mediated pathways which are implicated in the initiation of G2/M cell cycle checkpoint arrest responses to genotoxic stress “feedback-regulation” of Hsp90 functional activities within the Hsp90/Hsp70-mediated protein chaperone pathway (Aligue R. *et al*, 1994; Mollapour M. *et al*, 2010; Tse A.N. *et al*, 2009) – Fig 6.49, p.625.

Post-translational phosphorylation-mediated activation of the Wee1 kinase is also mediated via the secondary (distal) checkpoint kinase, CHK2, which may be elicited via novel human Rad9-B-initiated differential checkpoint signalling pathways in response to hypoxically- and hyperthermally-induced cytological stresses (via the Rad9-B:Rad1:Hus1/Hus1B heterotrimeric clamp complex) or specific types of DNA damage (via the Rad9-B:Hus1/Hus1B heterodimeric complex) – Fig 6.49, p.625.

These distinctive checkpoint pathways may be homologous functional equivalents of the two novel “Rad9-S”-mediated differential checkpoint responsive pathways which are initiated via hyperthermic stress and camptothecin-induced DNA damage and involve the heterotrimeric “Rad9-S”:Rad1:“Hus1-C” clamp complex and the heterodimeric “Rad9-S”:“Hus1-C” clamp complex (discussed in detail previously in Section 6.6, pp.588-597) – Fig 6.49, p.625.

In this hypothetical context, Rad9B:Rad1:Hus1/Hus1B-associative p38-MAPK, ATR/ATRIP, 53BP1, BRCA1, Claspin ternary complex interactions may regulate the levels and activities of specific hypophosphorylated isoforms of the secondary (distal) transducer kinase CHK1 (Ikegami Y. *et al*, 2008; Lu Y.P. *et al*, 2011; Kim A.J. *et al*, 2011; Petermann E. *et al*, 2008; Rybaczek D. *et al*, 2011; Shiromizu T. *et al*, 2006), which elicit a prolonged G2 arrest (via inhibition of spindle polar body functions that promote mitotic exit) and suppress catastrophic premature chromosomal condensation in response to hyperthermally-induced cytological stress (Fig 6.49, p.625).

Whilst the Rad9B:Hus1/Hus1B-associative ATR/ATRIP, p38-MAPK, Mph1, CHK2, Claspin ternary complex interactions may suppress phosphorylated-activation of the secondary (distal) CHK1 transducer kinase and initiate mutual activation of Mph1 and CHK2 kinases which may elicit “down-stream” effects such as Cdc14-activation of DNA replication and nucleolin-mediated complex-sequestration regulation of DNA damage responsive proteins (discussed previously in Section 6.5, pp.584-587 and Section 6.6, pp.588-597) in response to genotoxically-induced DNA damage events (Fig 6.49, p.625).

“Phosphorylated conservation” of the Serine 317 residue may be a critical pre-requisite for the nuclear translocation of Chk1 in the case of the Rad9B:Rad1:Hus/Hus1-B-mediated checkpoint signalling responses to oxidative and hyperthermic stresses, which is suppressed in the case of the Rad9B:Hus1/Hus1-B-mediated checkpoint responses to genotoxic stresses and/or DNA damage events (Fig 6.49, p.625).

Co-ordinated DNA replication, chromosomal condensation and anaphase entry cytological events are also orchestrated via both the Chk1 and Wee1 kinases (Fasulo B. *et al*, 2012), in which ATM and ATR primary (proximal) transducer checkpoint kinase-mediated post-translational phosphorylation-modification of Chk1 at Ser317 initiates a mitotic arrest that prevents catastrophic premature chromosomal condensation in response to dysfunctional S-phase events induced by genotoxic and/or environmental stresses (Rybaczek D. and Kowalewicz-Kulbat M., 2011).

It is therefore hypothetically conceivable that Rad9B:Rad1:Hus/Hus1-B-mediated checkpoint signalling responses may also be implicated in the modulation of ATM and ATR primary (proximal) transducer checkpoint kinase-mediated post-translational phosphorylation-modification of Chk1 at Ser317 which serves as biochemical trigger for the initiation of a prolonged G2 arrest (ie blocked G2 exit into anaphase) which prevents premature chromosomal condensation-mediated propagation of detrimental genetic mutations under genotoxic and/or environmental types of cytological stress conditions – Fig 6.49, p.625.

Rad9B:Hus1/Hus1B-associative ATR/ATRIP, p38-MAPK, Mph1, CHK2, Claspin ternary complex interactions may also be implicated in the checkpoint – co-ordinated initiation of DNA repair processes via Mph1-mediated post-translational phosphorylated activation of a potential nuclease-interactive/DNA-binding site domain (discussed in detail previously in Chapter 5, Section 5.5, pp.475-481) within the Rad9B protein (discussed in detail in Chapter 7) – Fig 6.49, p.625.

The secondary (proximal) transducer kinase, CHK2, may also participate in biochemical “cross-talk” regulation of the respective differential checkpoint pathway responses – Fig 6.49, p.625.

Experimental studies performed in this Ph.D. research work also indicated that both the truncated “Rad-S” protein variant and Hhp1 kinase may be implicated in the temporal regulation of a novel camptothecin-induced DNA damage checkpoint signalling (discussed previously in detail in Chapter 6, Section 6.2.5, pp.547-550), whilst induction of “Rad9-S” expression was an exclusive heat shock response which was limited to rapidly cycling cells within a ~20 minute period of hyperthermic exposure which coincided with the approximate duration of the G1/S phase of the *S. pombe* cell cycle (discussed previously in detail in Chapter 4, Section 4.6, pp.392-393).

These observed phenomena may also correlate with experimental studies which have revealed that the human Rad9B paralogue initiates a novel checkpoint signalling response to nucleolar stress responses, via C-terminal tail domain interactions with both ATR and JNK kinases, which elicits a G1/S phasic cell cycle arrest (Pérez-Castro A.J., and Freire R., 2012).

In mammalian cells, Casein kinase 2 is implicated in the modulation of circadian checkpoints (Allada R. and Meissner R.A, 2005; Lee C.C., 2005; Olsen B.B. *et al*, 2012; Smith E.M. *et al*, 2008; Yagita K. *et al*, 2009).

Casein kinase 2 also regulates the human RadA C-terminal tail domain interactions with the TopBP1 mediator/scaffold protein via phosphorylation of human Rad9A at Ser341 and Ser387 – which is also phosphorylated by ATM (Takeishi Y. *et al*, 2010).

These phosphorylation types of post-translational modifications of the human Rad9A protein enable the Rad9A:Rad1:Hus1 complex to engage with TopBP1 and other proteins to elicit differential cell cycle checkpoint responses to environmental and genotoxic stresses which adversely impinge upon the cytological propagation of genomic integrity (discussed previously in detail in Chapter 1, Section 1.2.2, pp.33-65).

In human tumour cell lines, topoisomerase I hyperphosphorylation-related cytotoxic sensitivity to camptothecin-based anti-neoplastic chemotherapeutic agents is also modulated via casein kinase 2 (Bandyopadhyay K. and Gjerset R.A. 2011).

Taken together, it is hypothetically conceivable that casein kinase 2- and ATM- mediated post-translational phosphorylated modifications of the human Rad9B protein may be implicated in the temporal regulation of its mediated differential checkpoint signalling responses to oxidative, hyperthermic and genotoxic types of cytological stresses (Fig 6.49, p.625).

These Rad9B post-translational modifications may also induce specific localised conformational changes within its supramolecular structure which enable it to engage with other proteins which are implicated in the initiation and/or signal propagation of the differential checkpoint pathways (Fig 6.49, p.625).

Casein kinase 2-mediated phosphorylated-modulation of the functional activities of the Hsp90 protein impinge upon the regulation the Hsp70/Hsp90 chaperone pathway and may also dictate the relative sensitivity of tumour cells to anti-neoplastic chemotherapeutic drug-induced proteotoxicity (Mollapour M. *et al*, 2011) – Fig 6.49, p.625.

These differentially-orchestrated pathway interactions may also adversely impinge upon and negate the pharmacological efficacy of proteotoxic stress-targeted chemotherapeutic agents, such as Hsp90 inhibitors, which are utilised to combat the development of acquired tumour multiple drug resistance to genotoxic-inducing classes of anti-neoplastic drugs (Neznanov N. *et al*, 2011; Sherman M.Y. *et al*, 2011a ; Sherman M.Y. *et al*, 2011b).

HIF1 α may also be implicated in the initiation of the p38-MAPK-mediated checkpoint pathways which in turn initiate induced expression of V-ATPases and activation of the bZip transcriptional protein kinase c-Jun, in response to oxidative and possibly hyperthermic cytological stresses.

These HIF1 α -initiated biochemical pathways could attenuate the pharmacological efficacy of various anti-cancer chemotherapeutic agents via deleterious V-ATPase-mediated intracellular compartmentalised pH alteration of their respective pharmacodynamic and pharmacokinetic properties (as may be the case for camptothecin – discussed previously on pp.604-607) and c-Jun-induced expression of different types of ATPase cassette-binding multiple drug transporters (ABC-MDRs), including the P-glycoprotein superfamily, MRP1 = Mitoxantrone-Resistant Protein 1 and BCRP = Breast Cancer Resistant Protein (Rajendra R. *et al*, 2003; Schellens J.H.M. *et al*, 2000) – Fig 6.49, p.625.

HIF1 α -modulation of specific V-ATPase functional activities may protect abnormally actively cycling neoplastic cells from the deleterious effects of hypoxia-related hyperglycolytic metabolism and confer genotoxic-resistance to radiotherapy treatments (ie tumour radioresistance), as a consequence of removal and suppression of harmful intracellular accumulative levels of protons which are generated via ionising radiation-induced hydrolytic free radical reactions and elevated glycolysis (Supino R. *et al*, 2009).

Anti- and pro- apoptotic signalling pathways within mitochondria (Zeng C.W. *et al*, 2012) may also be subject to biochemical modulation via combinatorial alterations of the relative sub-compartmental levels of protons (ie pH microenvironments) within these organelles, which in turn may be “governed” via the functional activities of specific HIF1 α -regulated V-ATPases that maybe implicated in the activation or inhibition of mortalin- and/or TRAP1- initiated apoptotic suppression (Calderwood S.K., 2010), with consequential promotion of metastatic tumour evolution and resistance to the cytotoxic effects of hyperthermally-potentiated anti-neoplastic polychemotherapeutic and radiotherapeutic treatment efficacies – Fig 6.49, p.625.

HIF1 α -enhanced V-ATPase functional activities may also promote angiogenesis, via induced expression of genes that encode various angiogenesis factors – such as VEGF, which could be a key biochemical factor in the promotion of tumour metastatic progression (Supino R. *et al*, 2009) – Fig 6.49, p.625.

These pathways may adversely impinge upon and attenuate the pharmacological efficacy of camptothecin analogues, Hsp90 inhibitors and mTOR inhibitors which are utilised to suppress HIF1 α -mediated biochemical mechanisms of hypoxic resistance of solid tumours to radiotherapeutic and polychemotherapeutic regimens employed in the clinical treatment and palliative manage of aggressive, malignant neoplastic pathophysiological conditions (Gabai V.L. *et al*, 2008; Gabai V.L. *et al*, 2009; Gabai V.L. *et al*, 2012; Li L. *et al*, 2011; Meng L. *et al*, 2010; Wilczynski J. *et al*, 2011).

Both the ATM primary (proximal) transducer kinase ATM casein kinase 2 (CK2) are implicated in the post-translational phosphorylated-mediated modulation of cAMP response element co-activators, such as the bZip protein CREB (Shanware T.P. *et al*, 2007).

ATM and p38-MAPK-mediated checkpoint pathways are also implicated in the activation of the bZip transcriptional protein kinase c-Jun, in response to oxidative and possibly hyperthermic cytological stresses, which are inhibited by caffeine (Ravi D. *et al*, 2008) – Fig 6.49, p.625.

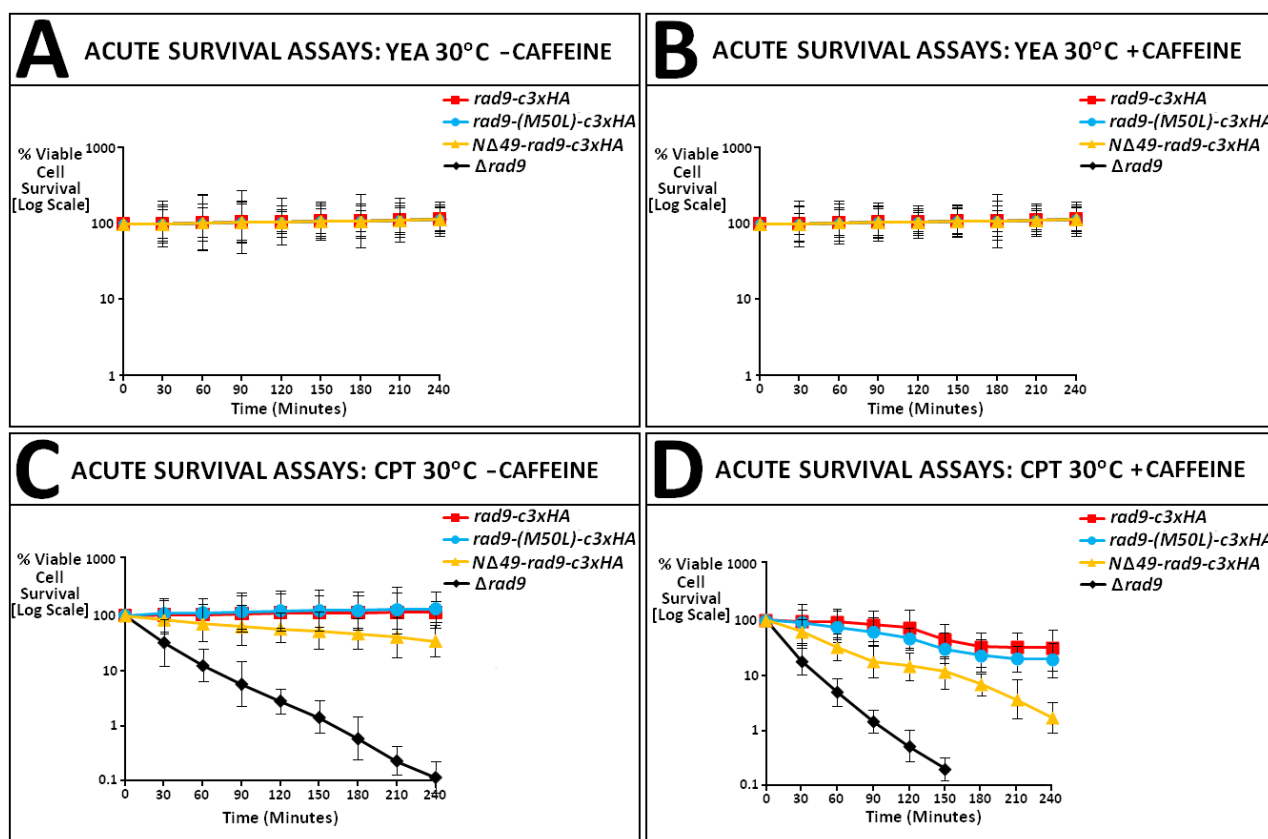
The interaction of CKIP1 with the ATM, CK2 α and c-Jun kinases may modulate their respective functional activities (Nie J. *et al*, 2012; Zhang L. *et al*, 2006), which may impinge upon the differential ATM- and ATR- mediated signalling pathways that elicit specific alterations of post-translational phosphorylation profiles of the secondary (distal) transducer checkpoint kinase Chk1 in response to hypoxically-induced cytological stresses (Kulkarni A. and Das K-C., 2008) – Fig 6.49, p.625.

Both caffeine and hyperthermia may be utilised advantageously as potentiate adjuvants in the clinical treatment and palliative management of a variety of aggressive, malignant neoplastic pathophysiological conditions in order to enhance the efficacy of the wide range of employed polychemotherapeutic and radiotherapeutic regimens (Asaad N.A. *et al*, 2000; Belka C. *et al*, 2006; Burke A.R. *et al*, 2012; de Anta J.M. *et al*, 2006; Farray D. *et al*, 2006; Franco R. *et al*, 2008; Overgaard K. and Overgaard J., 1974; Horsman M.R. and Overgaard J., 2007; Le Page S. *et al*, 2006; Maskaleris T. *et al*, 1998; Miwa S. *et al*, 2010; Mohamed F. *et al*, 2003; Ng C.E. *et al*, 1996; Niknafs B. *et al*, 2011; Nozoe T. *et al*, 2007; Palazzi M. *et al*, 2010; Pantazis P. *et al*, 1999; Sinn B. *et al*, 2010; Wang T.J. *et al*, 2010; Zagar T.M. *et al*, 2010).

The clinical administration of these combinatorial adjuvant caffeine and/or hyperthermic chemotherapeutic and/or radiotherapeutic treatments to the cancer patient may also be conducted under rigorous, specific chronological dosing schedules in order to maximise their respective efficacies (Ahowesso C. *et al*, 2011; Ballesta A. *et al*, 2011; Garufi C. *et al*, 2011; Giacchetti S. *et al*, 2002; Giacchetti S. *et al*, 2012; Innominato P.F. *et al*, 2012; Lévi F. *et al*, 2011; Lévi F. and Okyar A., 2011; Kirichenko A.V. and Rich T.A., 1999; Kobayashi A. *et al*, 2002; Rich T.A. *et al*, 2000; Rich T.A. *et al*, 2002; Savvidis C. and Koutsilieris M., 2012; Sukhina E.N. *et al*, 2012).

The postulated novel checkpoint response pathway signalling pathway models, deduced hypothetically with regard to the potential formation and activities of the novel *S. pombe* “Rad9-S” equivalent functional human Rad9B:Rad1:Hus1/Hus1-B and Rad9B:Hus1/Hus1-B DNA clamp complex homologues (discussed in detail previously on pp.607-616), could also be implicated in novel cytotoxic attenuation mechanisms of metastatic tumour resistance to these anti-neoplastic clinical treatment regimens (Fig 6.49, p.625).

Fig 6.45: Acute Cell Survival Assays – Caffeine & Camptothecin

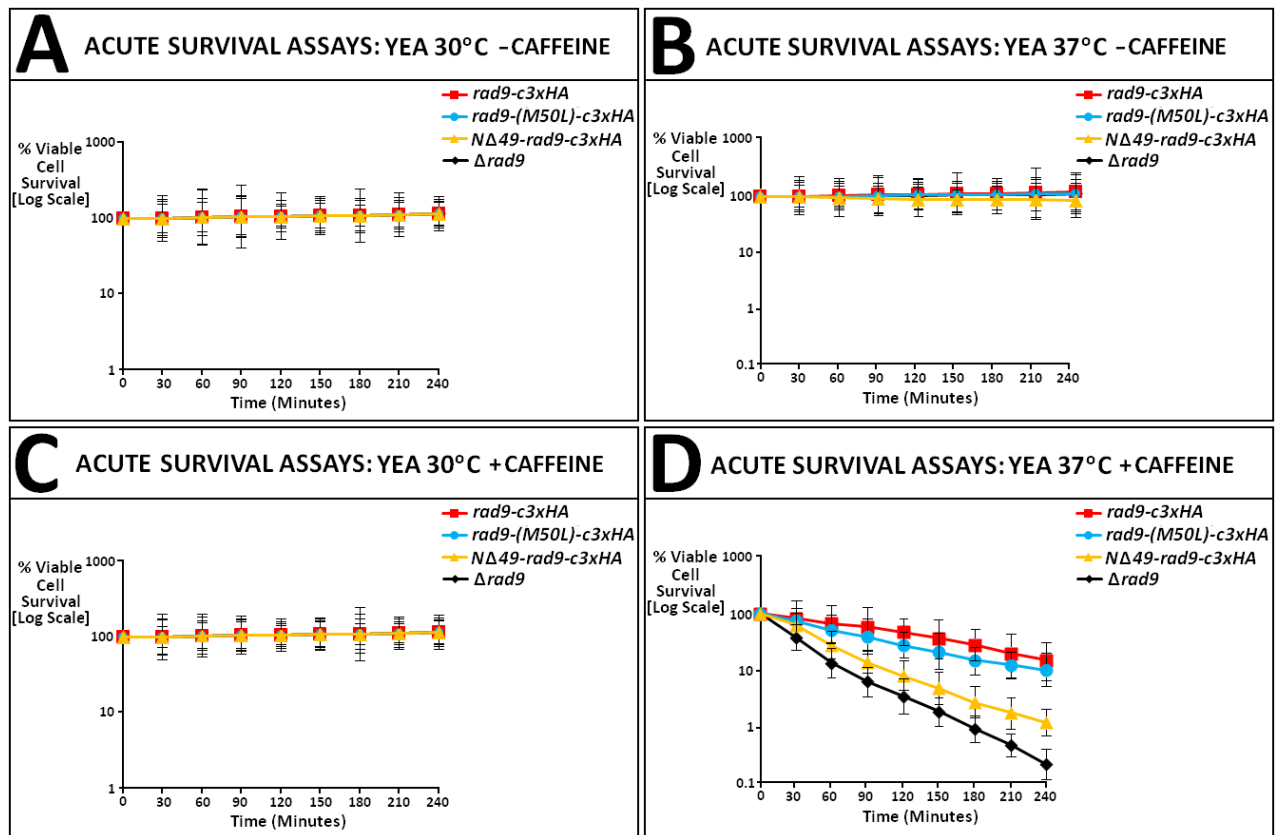


Individual 25mL YEA broth medium cell cultures of the indicated *S. pombe* strains were incubated at 30°C over a 12 hour time period, then diluted to an optical density $A_{595} = 0.25$ with the appropriate volume of YEA medium and the resultant diluted cultures re-incubated at 30°C for a further time period of ~2.5 hours until they had attained an optical density value of $A_{595} = 0.5$ – after which time the resultant cultures of actively cycling cells were re-incubated at 30°C for a further 60 minutes in YEA in the absence of caffeine or in the presence of 10mM caffeine.

Comparative acute cell survival assays were then performed on the resultant YEA broth cultures of the indicated *S. pombe* strains over a total time period of 4 hours, in the absence or presence of 40 μ M camptothecin (CPT), as per the methodology described in Chapter 2, Section 2.9.2.2(ii), pp.239-241.

- A:** Comparative control acute cell survival assays performed with the indicated *S. pombe* strain cultures, which had no caffeine treatment, in the absence of camptothecin.
- B:** Comparative acute cell survival assays performed with the indicated *S. pombe* strain cultures incubated in 10mM caffeine, in the absence of camptothecin.
- C:** Comparative control acute cell survival assays performed with the indicated *S. pombe* strain cultures, which had no caffeine treatment, in the presence of 40 μ M camptothecin.
- D:** Comparative acute cell survival assays performed with the indicated *S. pombe* strain cultures incubated in 10mM caffeine, in the presence of 40 μ M camptothecin.

Fig 6.46: Acute Cell Survival Assays – Caffeine and Heat Shock



Individual 25mL YEA broth medium cell cultures of the indicated *S. pombe* strains were incubated at 30°C over a 12 hour time period, then diluted to an optical density $A_{595} = 0.25$ with the appropriate volume of YEA medium and the resultant diluted cultures re-incubated at 30°C for a further time period of ~2.5 hours until they had attained an optical density value of $A_{595} = 0.5$ – after which time the resultant cultures of actively cycling cells were re-incubated at 30°C for a further 60 minutes in YEA in the absence of caffeine or in the presence of 10mM caffeine.

Comparative acute cell survival assays were then performed on the resultant YEA broth cultures of the indicated *S. pombe* strains over a total time period of 4 hours at either 30°C or 37°C, as per the methodology described in Chapter 2, Section 2.9.2.2(ii), pp.239-241.

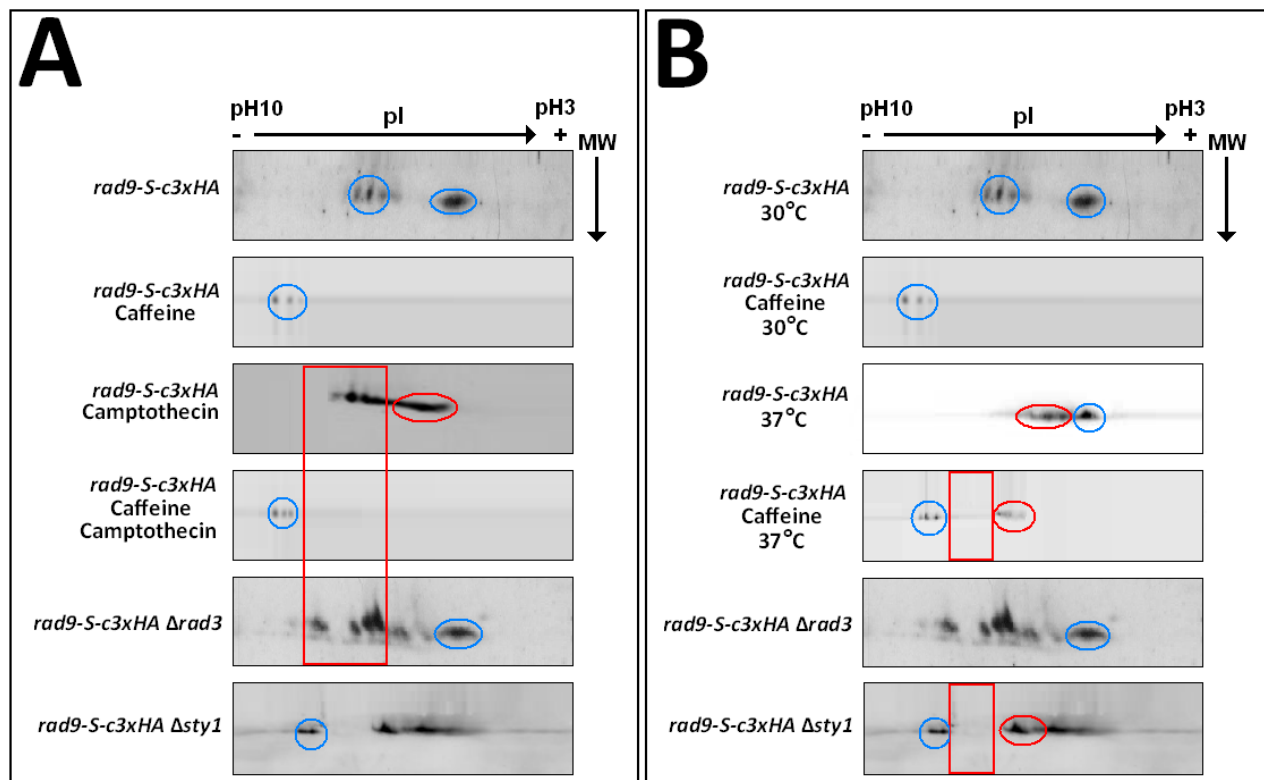
A: Comparative control acute cell survival assays performed with the indicated *S. pombe* strain cultures, which had no caffeine treatment, incubated at 30°C.

B: Comparative control acute cell survival assays performed with the indicated *S. pombe* strain cultures, which had no caffeine treatment, incubated at 37°C.

C: Comparative acute cell survival assays performed with the indicated *S. pombe* strain cultures, incubated in the presence of 10mM caffeine at 30°C.

D: Comparative acute cell survival assays performed with the indicated *S. pombe* strain cultures, incubated in the presence of 10mM caffeine at 37°C.

Fig 6.47: Comparative 2D PAGE – Coupled Western Blot Analyses of Differential Phosphoisoform Modulation of the Truncated “Rad9-S” Protein Variant Implicated in Cytological Checkpoint Signalling Responses to Camptothecin-Induced Genotoxicity and Hyperthermic Stress



A: Comparative “caffeine versus camptothecin” combinatorial analyses
 (A detailed description of these data analyses is provided in the figure legend on p.621)

B: Comparative “caffeine versus heat shock” combinatorial analyses
 (A detailed description of these data analyses is provided in the figure legend on p.622)

NOTE: Blue circles denote conserved phosphoisoforms which are common to both data sets.

Red boxes and circles denote conserved phosphoisoform differences and similarities which are distinctive to each respective data set.

A: Comparative “Caffeine Versus Camptothecin” Combinatorial Analyses

rad9-S-c3xHA, *rad9-S-c3xHA Δrad3* and *rad9-S-c3xHA Δsty1*

Individual 100mL YEA broth medium cell cultures of the “Cre-Lox” – constructed *S. pombe* strains *NA49-rad9-c3xHA* (“Rad9-S”), *NA49-rad9-c3xHA Δrad3* and *NA49-rad9-c3xHA Δsty1*, were grown overnight (30°C for ~12 hour time period), then diluted to an optical density of $A_{595} = 0.25$ with the appropriate volume of YEA medium and the resultant diluted cultures re-incubated at 30°C for a further time period of ~2.5 hours until they had attained an optical density value of $A_{595} = 0.5$.

The resultant YEA broth cultures of actively cycling cells, were then incubated at 30°C for a further 30 minutes in the absence of 10mM caffeine and 40μM camptothecin.

rad9-S-c3xHA + Caffeine and *rad9-S-c3xHA* + Camptothecin Analyses

Individual 100mL YEA broth medium cell cultures of the “Cre-Lox” – constructed *S. pombe* strain *NA49-rad9-c3xHA* (“Rad9-S”) were grown overnight (30°C for ~12 hour time period), then diluted to an optical density of $A_{595} = 0.25$ with the appropriate volume of YEA medium and the resultant diluted cultures re-incubated at 30°C for a further time period of ~2.5 hours until they had attained an optical density value of $A_{595} = 0.5$.

The resultant YEA broth cultures of actively cycling cells, were then incubated at 30°C for a further 30 minutes in the presence of either 10mM caffeine or 40μM camptothecin.

rad9-S-c3xHA + Caffeine and Camptothecin

An individual 100mL YEA broth medium cell culture of the “Cre-Lox” – constructed *S. pombe* strain *NA49-rad9-c3xHA* (“Rad9-S”) was grown overnight (30°C for ~12 hour time period), then diluted to an optical density of $A_{595} = 0.25$ with the appropriate volume of YEA medium and the resultant diluted culture re-incubated at 30°C for a further time period of ~2.5 hours until it had attained an optical density value of $A_{595} = 0.5$.

The resultant YEA broth culture of actively cycling cells was then incubated with 10mM caffeine and 40μM camptothecin for a further 30 minutes at 30°C.

TCA-precipitated total protein extract samples were then prepared from the appropriate *calculated volumetric aliquot of each culture (*equivalent to 40 A_{595} optical density units) and utilised in comparative 2D-PAGE–coupled Western Blot analyses – probed with the primary “anti-HA” antibody.

[Protein sample preparation, 2D PAGE and Western blot methodologies are described in Chapter 2, Section 2.8.3.1, pp.214-217; Section 2.8.5.1, pp.225-230 and Section 2.8.6., pp.231-233]

B: Comparative “Caffeine Versus Heat Shock” Combinatorial Analyses

rad9-S-c3xHA*, *rad9-S-c3xHA Δrad3* and *rad9-S-c3xHA Δsty1

Individual 100mL YEA broth medium cell cultures of the “Cre-Lox” – constructed *S. pombe* strains *NA49-rad9-c3xHA* (“Rad9-S”), *NA49-rad9-c3xHA Δrad3* and *NA49-rad9-c3xHA Δsty1*, were grown overnight (30°C for ~12 hour time period), then diluted to an optical density of $A_{595} = 0.25$ with the appropriate volume of YEA medium and the resultant diluted cultures re-incubated at 30°C for a further time period of ~2.5 hours until they had attained an optical density value of $A_{595} = 0.5$.

The resultant YEA broth cultures of actively cycling cells, were then incubated at 30°C for a further 30 minutes in the absence of 10mM caffeine.

***rad9-S-c3xHA* + Caffeine and *rad9-S-c3xHA* + Heat Shock Analyses**

Individual 100mL YEA broth medium cell cultures of the “Cre-Lox” – constructed *S. pombe* strain *NA49-rad9-c3xHA* (“Rad9-S”) were grown overnight (30°C for ~12 hour time period), then diluted to an optical density of $A_{595} = 0.25$ with the appropriate volume of YEA medium and the resultant diluted cultures re-incubated at 30°C for a further time period of ~2.5 hours until they had attained an optical density value of $A_{595} = 0.5$.

The resultant YEA broth cultures of actively cycling cells, were then incubated at 30°C for a further 30 minutes in the presence of 10mM caffeine or at 37°C in the absence of caffeine.

***rad9-S-c3xHA* + Caffeine and Heat Shock**

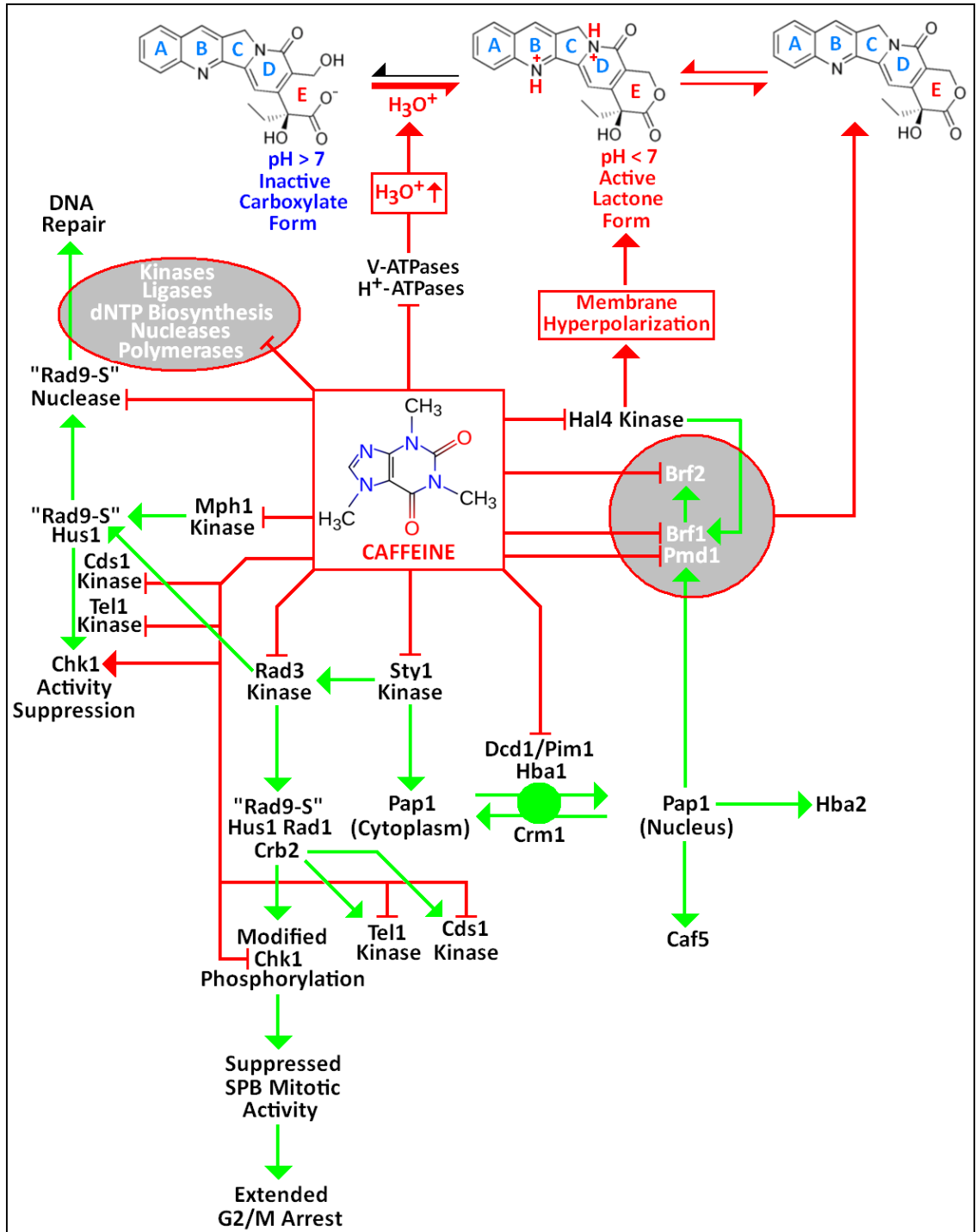
An individual 100mL YEA broth medium cell culture of the “Cre-Lox” – constructed *S. pombe* strain *NA49-rad9-c3xHA* (“Rad9-S”) was grown overnight (30°C for ~12 hour time period), then diluted to an optical density of $A_{595} = 0.25$ with the appropriate volume of YEA medium and the resultant diluted culture re-incubated at 30°C for a further time period of ~2.5 hours until it had attained an optical density value of $A_{595} = 0.5$.

The resultant YEA broth culture of actively cycling cells was then incubated with 10mM caffeine and for a further 30 minutes at 37°C.

TCA-precipitated total protein extract samples were then prepared from the appropriate *calculated volumetric aliquot of each culture (*equivalent to 40 A_{595} optical density units) and utilised in comparative 2D-PAGE–coupled Western Blot analyses – probed with the primary “anti-HA” antibody.

[Protein sample preparation, 2D PAGE and Western blot methodologies are described in Chapter 2, Section 2.8.3.1, pp.214-217; Section 2.8.5.1, pp.225-230 and Section 2.8.6., pp.231-233]

Fig 6.48: Potential Biochemical Targets Implicated in Caffeine-Mediated Potentiation of the Cytotoxic Effects of Hyperthermic Stress and Camptothecin-Induced DNA Damage in *S. pombe* Cells “Cre-Lox”–Engineered for the Exclusive Expression of the “Rad9-S” Truncated Protein Variant



→ = Functional Pathways → and —| = Potential Caffeine-Targeted Adenosine Receptor-Mediated Pathway Functions

A detailed explanation of this hypothetical model is provided in the text (pp.600-607).

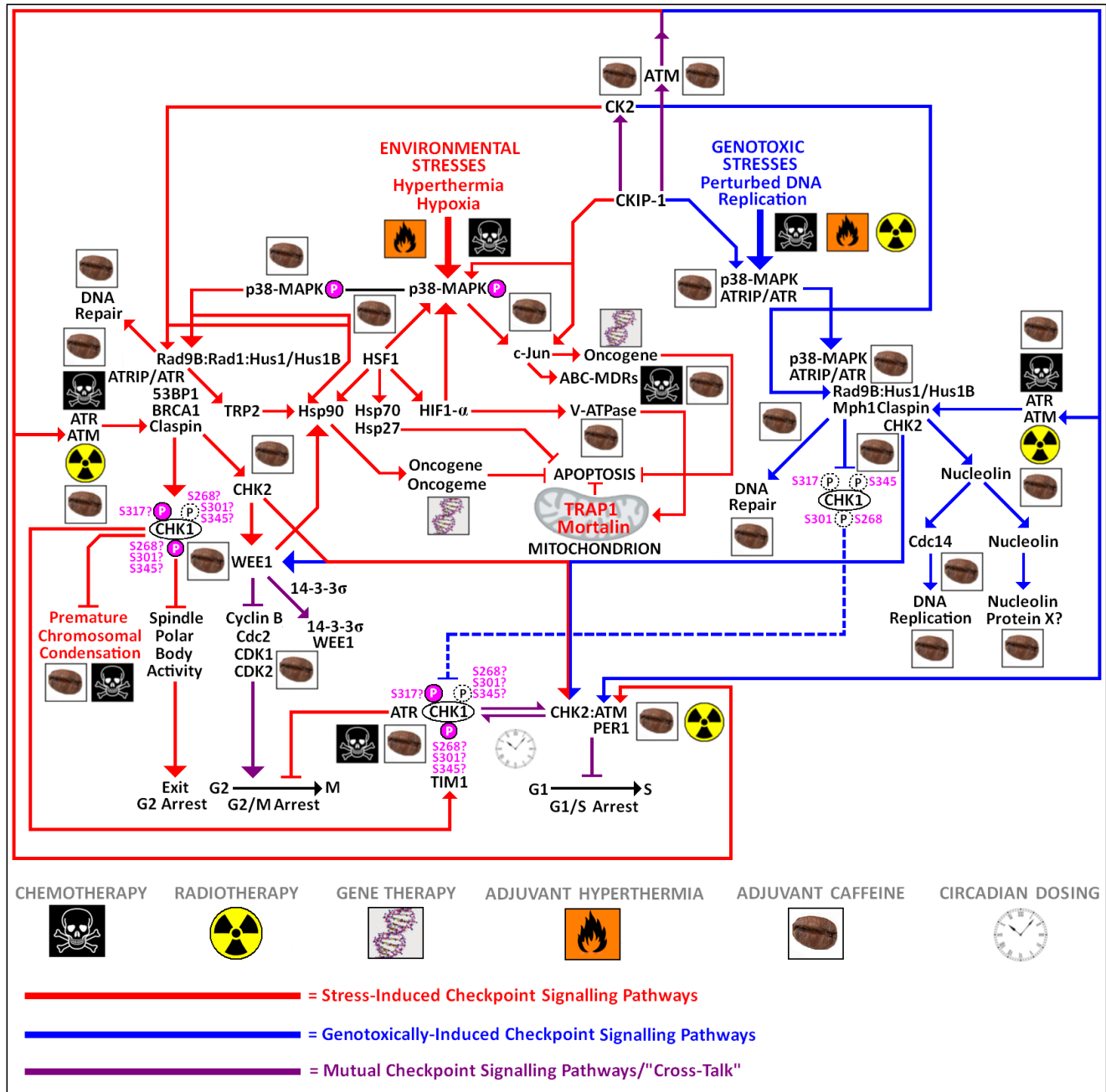
Table 6.1: Comparative Summary of Functionally-Equivalent Homologous Protein Targets in *S. pombe* and *H. sapiens* Implicated in Caffeine-Induced Potentiation of the Cytotoxic Effects of Hyperthermic Stress and Camptothecin-Induced DNA Damage

[Compiled via Collated Information From:

Arioka M. *et al*, 1998; Calvo I.A. *et al*, 2009; Castillo E.A. *et al*, 2003; Hirose E. *et al*, 2006; Kumada K. *et al*, 1996; Kudo N. *et al*, 1997; Nishi K. *et al* 1996a; Nishi K. *et al*, 1996b; Toda T. *et al*, 1991; Toda T. *et al*, 1992; Toone W.M. *et al*, 1998]

<i>S. pombe</i>	<i>H. sapiens</i>	HOMOLOGOUS BIOCHEMICAL FUNCTION
Rad3	ATR	Primary (Proximal) Transducer Checkpoint Kinase
Sty1	p38-MAPK	Mitogen-Activated Protein Transducer Kinase Stress Response Checkpoint Pathway Initiation
Pap1	c-Jun	bZip DNA-Binding Transcriptional Regulator
Crm1	CRM1	Nuclear Protein Export Factor (Exportin)
Dcd1/Pim1	RCC	Ran Nucleotide GDP/GTP Exchange Factor
Hba1	RCC	Functional Modulatory Component of Ran
Hba2/Brf1	ABC-MDR Transporters	<u>A</u> TPase- <u>B</u> inding <u>C</u> assette <u>M</u> ultiple <u>D</u> rug Resistance Transporter Proteins Active Export of Cytotoxic Agents from the Intracellular Environment
Brf2		
Pmd1		

Fig 6.49: Hypothetical Human Rad9B-Mediated Checkpoint Pathway Signalling Models Which May be Implicated in the Development of Metastatic Tumour Resistance to the Combinatorial Adjuvant Hyperthermic- and Caffeine- Potentiated Anti-Neoplastic Cytotoxic Efficacy of Polychemotherapeutic and Radiotherapeutic Treatments



A detailed explanation of these hypothetical models is provided in the text (pp.607-618).

Appendix 6.1

**Journal of Cell Science Publication
(Editor and Referee Panel Accepted – *In Press*)**

**“Heat Induction of a Novel Rad9 Variant From
a Cryptic Translation Initiation Site Reduces
Mitotic Commitment”**

**Simon Janes, Ulrike Schmidt, Nadja Ney, Susanna Concilio,
Mohamed Zekri and Thomas Caspari**

[Electronic Publication Ahead of Print 13th July 2012]

Heat induction of a novel Rad9 variant from a cryptic translation initiation site reduces mitotic commitment

**Simon Janes, Ulrike Schmidt, Karim Ashour Garrido, Nadja Ney, Susanna Concilio,
Mohamed Zekri, and Thomas Caspari***

Address:

Bangor University

Genome Biology Group

College of Natural Sciences

School of Biological Sciences

Brambell Building

Deiniol Road

Bangor LL57 2UW

Wales, United Kingdom

E-mail: t.caspari@bangor.ac.uk

Web page: <http://genome-biology.bangor.ac.uk/>

Phone: +44-(0)1248382526

Fax: +44-(0)1248371644

***Author of Correspondence:** Thomas Caspari

Word Count: 7855

Running Title: A novel Rad9 variant blocks mitosis

Key Words: DNA damage checkpoint, hyperthermia, cell cycle, translation

Summary

Exposure of human cells to heat switches DNA damage signaling from genotoxic to temperature stress. This change reduces mitotic commitment at the expense of DNA break repair. The thermal alterations behind this switch remain elusive despite the successful use of heat to sensitize cancer cells to DNA breaks. Rad9 is a highly conserved subunit of the Rad9-Rad1-Hus1 (9-1-1) checkpoint-clamp that is loaded by Rad17 onto damaged chromatin. At the DNA, Rad9 activates the checkpoint kinases Rad3^{ATR} and Chk1 to arrest cells in G2. Using *Schizosaccharomyces pombe* as a model eukaryote, we discovered a new variant of Rad9, Rad9-M50, expression of which is specifically induced by heat. High temperatures promote alternative translation from a cryptic initiation codon at methionine-50. This process is restricted to cycling cells and independent of the temperature-sensing MAP kinase pathway. While full-length Rad9 delays mitosis in the presence of DNA lesions, Rad9-M50 functions in a remodeled checkpoint pathway to reduce mitotic commitment at elevated temperatures. This remodeled pathway still relies on Rad1 and Hus1, but acts independently of Rad17. Heat-induction of Rad9-M50 ensures that Chk1 kinase remains in a hypo-phosphorylated state. Elevated temperatures specifically reverse the DNA damage-induced modification of Chk1 in a manner dependent on Rad9-M50. Taken together, heat reprograms the DNA damage checkpoint at the level of Chk1 by inducing a Rad9 variant that can act outside of the canonical 9-1-1 complex.

Introduction

Temperature has the enigmatic ability to inactivate DNA break repair in human cells (Pandita et al., 2009). The Mre11-Rad50-Nbs1 (MRN) complex recruits the DNA damage sensor ATM^{Tel1} kinase to broken chromosomes (Falck et al., 2005), where the kinase phosphorylates the histone variant γ -H2AX within megabase regions surrounding the lesion (Rogakou et al., 1998). This chromatin modification attracts additional repair factors like the scaffold protein 53BP1^{Ctb2} (Ward et al., 2003) which form a large checkpoint complex to inactivate the cell cycle regulator Cdc2^{CDK1} (Gould and Nurse, 1989) (O'Connell et al., 1997) (Smith et al., 2010). A small rise in temperature from ~37°C to ~40°C blocks this signaling process by inducing the rapid relocalization of the MRN complex from the nucleus to the cytoplasm (Seno and Dynlacht, 2004) and by delaying the recruitment of 53BP1 to chromatin (Laszlo and Fleischer, 2009).

Unexpectedly, ATM kinase remains active under heat stress conditions still modifying histone γ -H2AX despite the absence of detectable DNA breaks (Hunt et al., 2007). Although the biological details of ATM activation are unknown, the underlying mechanism may be equivalent to its stimulation by oxidative stress. An increase in reactive oxygen activates ATM directly in the absence of the MRN complex by inducing the formation of a disulfide-crosslinked dimer (Guo et al., 2010). The cellular targets of ATM at high temperatures remain to be identified, but they may be linked with apoptosis (Furusawa et al., 2011) or a prolonged G2-M arrest (Zölzer and Streffer, 2001).

While ATM signals unprocessed DNA double-strand breaks, the related kinase ATR^{Rad3} binds via its partner protein ATRIP^{Rad26} directly to the ssDNA Binding Protein (RPA) after the ends of the break have been converted to ssDNA tails (Zou and Elledge, 2003) (Sartori et al., 2007) (Zierhut and Diffley, 2008). This end processing is crucial for dsDNA break repair by homologous recombination in G2 (Caspari et al., 2002) (Ferreira and Cooper, 2004) (Huertas et al., 2008). The resulting junctions between ssDNA and dsDNA are independently recognized as a damage signal by

the Rad17 complex that loads the Rad9-Rad1-Hus1 ring (9-1-1) next to ATR-ATRIP (Bermudez et al., 2003). The 9-1-1 ring resembles the replicative clamp PCNA (Caspari et al., 2000) (Xu et al., 2009) (Doré et al., 2009), but in contrast to PCNA, contains an extended and highly flexible domain which is provided by the tail of the Rad9 subunit. This tail domain, which is phosphorylated during the unperturbed cell cycle and in response to DNA damage (Caspari *et al.*, 2000b) (St Onge et al., 2001) (Roos-Mattjus et al., 2003), co-activates ATR^{Rad3} jointly with the scaffold protein Rad4^{TopBP1} that is preloaded onto chromatin at the start of S phase (Furuya et al., 2004) (Delacroix *et al.*, 2007) (Navadgi-Patil and Burgers, 2009) (Zegerman and Diffley, 2007). Assembly of the ATR^{Rad3} complex in S phase and G2 signals to Cdc2 via the checkpoint kinase 1 (Chk1), whereas ATM^{Tell} utilizes checkpoint kinase 2 (Chk2^{Cds1}) independently of the cell cycle stage (Smith et al., 2010).

We report here a novel requirement of the DNA damage checkpoint kinases Rad3^{ATR}, Tell^{ATM}, Cds1^{Chk2} and Chk1 for the maintenance of a heat-induced G2 arrest. Our experiments reveal striking differences between genotoxic and temperature stress. While detection of DNA lesions requires the recruitment of Rad9 to the chromatin, the 9-1-1 loader Rad17 is obsolete for heat signaling. Consistent with the conclusion that the normal 9-1-1 complex is not involved, cells induce a N-terminally truncated Rad9 variant (Rad9-M50) at elevated temperatures by utilizing a cryptic start site in the *rad9* mRNA (AUG-50). Thus, the ability of Rad3^{ATR} to delay mitosis at high temperatures requires a different Rad9 protein than its checkpoint function in response to DNA damage. Induction of Rad9-M50 ensures that Chk1 remains in a hypo-phosphorylated state by facilitating the removal of its DNA-damage induced modification under heat stress conditions.

Results

Heat induction of a novel Rad9 variant

Rad9-M50 was discovered whilst conducting experiments at elevated temperatures with the well characterized *rad9-HA* strain. This strain expresses a Rad9 protein with a C-terminal hemagglutinin (HA) tag from its endogenous locus on chromosome 1 (Caspari et al., 2000) (Harris *et al.*, 2003) (Furuya et al., 2004). Exposure of *rad9-HA* cells to 40°C for 20 min resulted in the appearance of a smaller band (Fig. 1A). Induction of this variant was independent of the growth medium and occurred to a similar extent between 37°C and 40°C. Its expression was effectively blocked by the ribosome inhibitor cycloheximide (Fig. 1B) strongly indicating that active translation is important. Expression of the isoform was independent of the HA tag and occurred also when Rad9 was C-terminally fused to GFP (Fig. S1A).

Given that the Wis1-Sty1 MAP kinase pathway detects environmental stress (Shiozaki and Russell, 1995) (Shiozaki et al., 1998) (Millar et al., 1995), we investigated Rad9-M50 expression in the presence of high osmotic and oxidative conditions. As shown in Figure 1C, induction was specific to temperature stress at 40°C and not observed when *rad9-HA* cells were exposed to 0.6M KCl, 1M sorbitol or 0.3mM H₂O₂ for 30 min at 30°C. Neither mutation of the MAP kinase kinase Wis1 nor loss of the MAP kinase Sty1 reduced Rad9-M50 expression (Fig. S1B, C). We also excluded an involvement of the nutrient sensing Tor1 pathway (Petersen and Nurse, 2007) and of the Srk1 kinase acting down-stream of the Wis1-Sty1 pathway (Lopez-Girona et al., 1999) (Fig. S1 D).

A cryptic translation initiation site is required for heat induction

Because inhibition of translation blocked synthesis of this variant (Fig. 1B), we decided to mutate all internal methionine codons to alanine to test whether they act as a start site at high temperatures (Fig. 1D). Mutant alleles were generated by fusion PCR and integrated at the *rad9*

chromosomal locus using the Cre-*lox* cassette exchange technique (Watson et al., 2008). This technique allows for the targeted integration of *rad9* genes at its chromosomal locus which was replaced by a marker gene (*ura4+*) flanked by the recognition sites (*loxP*, *loxM*) of the Cre recombinase. Transformation of this strain with a plasmid that encodes Cre and contains a *rad9-HA* allele flanked by the same *lox* sequences results in the exchange of *rad9* with the chromosomal marker. The integrated *rad9-HA* alleles were amplified from genomic DNA and sequenced to confirm the mutation.

Intriguingly, only replacement of methionine 50 (M50A) abolished expression of the variant, thereafter referred to as Rad9-M50 (Fig. 1E). Since AUG-50 is down-stream of the first intron (Fig. 1D) and because this intron is retained in some *rad9* cDNA clones (Murray *et al.*, 1991), we deleted this sequence in-frame. Usage of AUG-50 was however not influenced by this intron (Fig. S1D).

Ribosomes could either reach AUG-50 by moving past the first AUG codon in a process known as leaky ribosome scanning (Kochetov, 2008) or they could enter the transcript downstream of the first initiation site. Leaky ribosome scanning is used, for example, to synthesize a mitochondrial and cytoplasmic variant of the *S.cerevisiae* glutaredoxin-2 enzyme. Translation from the first AUG produces the mitochondrial variant, while initiation at AUG-35 deletes the leader peptide allowing the protein to remain in the cytoplasm (Porrás et al., 2006). Internal ribosome entry sites (IRES) are normally located up-stream of the first AUG (King et al., 2010) making it less likely that such a sequence exists between AUG-1 and AUG-50. However, RNA hairpin structures can recruit ribosomes independently of IRES (Zu et al., 2011) and such secondary structures may form in a temperature-dependent manner.

Rad9-M50 is post-translationally modified

To test whether Rad9-M50 is post-translationally modified, we exposed *rad9-HA* cells to 30°C or 40°C for 1 hour and subjected soluble protein extracts to isoelectric focusing on an immobilized

pH gradient (non-linear, pH3-10) prior to electrophoresis on a 10% SDS page. While the phosphoisoforms of full-length Rad9 do not separate under these conditions, two distinct isoforms of Rad9-M50 were present at 40°C (Fig. 1F). Although this indicates that the variant is phosphorylated, we failed to detect a change in cells devoid of Rad3 kinase, the 9-1-1 subunit Hus1, the 9-1-1 loader Rad17 or the MAP kinase Sty1 (Fig. S1E, F).

The sequence between AUG-1 and AUG-50 suppresses usage of the cryptic initiation site

To investigate whether expression of Rad9-M50 is dependent on the full-length protein, we mutated the first methionine to alanine (*rad9-M1A-HA*) (Fig. 2A). As expected, this *rad9-M1A-HA* strain lacked Rad9 rendering cells highly DNA damage sensitive and checkpoint deficient (Fig. 2C, Fig. 3C, D, E). Loss of Rad9 had no influence on expression of Rad9-M50 which was fully induced at 40°C (Fig. 2B). Removal of Rad9, whilst allowing cells to express Rad9-M50, had an unexpected effect on HU sensitivity. As shown in Fig. 2C, *rad9-M1A* cells lose viability faster than *rad9* deletion cells (Δ *rad9*). This implies that the truncated protein, which is expressed at low levels at 30°C in *rad9-M1A* cells (Fig. 2B), may substitute for Rad9 thereby acting in a dominant negative manner. This genotoxic function of Rad9-M50 was not abolished upon deletion of *rad1* (Fig. 2B) suggesting that it does not depend on the formation of a 9-1-1 like complex.

Since the RNA sequence between methionine-1 and serine-49 may be involved in the regulation of AUG-50, we deleted this sequence from the genomic *rad9* gene using the *Cre-lox* technique (Fig. 2A). Interestingly, the basal levels of Rad9-M50 increased sharply in this *rad9-Δ1-49-HA* strain at 30°C thereby reducing the degree of induction at 40°C (Fig. 2B). This suggests a role of the mRNA segment between M1 and S49 in the suppression of AUG-50 usage at low temperatures.

We also mutated AUG-1 and AUG-50 simultaneously to alanine to test whether ribosomes could utilize any of the remaining AUG codons (Fig. 2A). This *rad9-M1A+M50A-HA* strain neither expressed Rad9 nor Rad9-M50, but weakly induced a smaller variant at 40°C which was also

detectable in the absence of AUG-50 (Fig. 2B, D). These observations imply that heat relaxes the usage of internal initiation sites in the *rad9* transcript allowing ribosomes to initiate down-stream of AUG-1. This conclusion was confirmed by the absence of any inducible band in cells expressing a *rad9* gene in which M50 and M74 were both replaced by an alanine residue (*rad9-M50A+M74A-HA*) or in which all remaining methionine codons were mutated to alanine (*rad9-M50A+M74A+M311A+M312A+M357A*) (Fig. 2D).

Rad9-M50 acts outside of the canonical 9-1-1 complex

Alignment of the N-terminal sequences of Rad9^{Sp}, Rad9A^{Hs} and Rad9B^{Hs} shows that M50 is replaced by a cysteine in both human proteins (Fig. 3A). Interestingly, the Ensembl database (release 64 - Sep 2011) curates a yet uncharacterized splice variant of Rad9B (ENSP00000387329; Rad9B-001; 345aa) that lacks the first 72aa starting at methionine 73. Further work is however required to establish whether this splice variant is a functional paralog of Rad9-M50. We also analyzed Rad9 proteins from other yeast species across the *Ascomycota* group and found that M50 is the only internal start site that is conserved across diverse clades (Fig. S1G). For example, Rad9 from *Kluyveromyces thermotolerans* shares only 19.9% identity with *S.pombe* Rad9 but has a methionine residue at position 51 (Fig. S1G).

To test whether Rad9-M50 can replace the full-length protein in the 9-1-1 ring, we took advantage of the *rad9 Δ 1-49-HA* strain that lacks Rad9 but expresses high levels of the variant at 30°C (Fig. 2B). As shown in Figure 3B, loss of the N-terminal domain would delete an internal segment of Rad9 without affecting the contact interfaces with Hus1 and Rad1. Hence, the truncated protein may still be able to associate with both proteins. If such a complex were to exist, it does not respond to DNA damage since *rad9 Δ 1-49-HA* cells are highly DNA damage sensitive (Fig. 3C) and lack a cell cycle arrest when DNA replication was challenged with the Ribonucleotide Reductase (RNR) inhibitor hydroxyurea (HU) (Fig. 3E). To measure the checkpoint arrest, wild type (*rad9-*

HA) and *rad9 Δ 1-49-HA* cells were both enriched in early G2 by isolating small G2 cells from a lactose gradient (Forsburg and Rhind, 2006), and released into rich medium with and without 12mM HU at 30°C. While wild type cells delayed cell cycle progression (Fig. 3D), *rad9 Δ 1-49-HA* cells were as deficient as cells devoid of the full-length protein (*rad9-M1A-HA*) (Fig. 3E).

We employed size fractionation chromatography to test whether *rad9 Δ 1-49-HA* cells, which only express Rad9-M50, form the 9-1-1 complex. As reported previously (Caspari et al., 2000), the complex was present in fractions 12 to 14 (Superdex-200 column) when protein extracts from *rad9-HA* wild type cells (30°C) were used. Rad9 was however absent from these fractions when extracts from *rad9- Δ 1-49-HA* cells (30°C) were analyzed. The variant eluted instead in fractions 8 to 11 that contain protein complexes larger than 400kDa (Fig. 3F). To find out whether the same changes apply to the endogenous variant, we fractionated an extract from *rad9-HA* cells after having heat shocked the cells at 40°C for 30 min. The induced variant possessed a very similar elution profile as Rad9-M50 in *rad9- Δ 1-49-HA* cells, although fractions 12 and 13 contained some of the variant (Fig. 3G). Deletion of the 9-1-1 subunit Rad1 caused the expected loss of Rad9 from fractions 12 to 14 and induced a shift of the full-length protein to the high molecular weight fractions 8 to 11 (Fig. 3H). This confirms that fractions 12 to 14 contain the 9-1-1 complex and it suggests that Rad9 and Rad9-M50 present in fractions 8 to 11 form alternative protein complexes. While detection of Rad9-M50 in the high molecular weight fractions was not affected by loss of Rad1, the small amount detected in fractions 12 and 13 was lost (Fig. 3H). Taken together, some Rad9-M50 may assemble with Rad1 in a 9-1-1 like complex (frac. 12 & 13), but the majority of the protein appears to be in alternative protein complexes (frac. 8-11).

Consistent with the inability of Rad9-M50 to substitute for Rad9, Chk1 phosphorylation, which is dependent on the 9-1-1 ring (Capasso et al., 2002), was abolished when *rad9 Δ 1-49-HA* cells were treated with the topoisomerase I inhibitor camptothecin (CPT) (Fig. 3I).

Induction of Rad9-M50 delays mitosis at elevated temperatures

The first insight into the biological roles of Rad9-M50 came from the observation that its induction level dropped with an increase in cell number. To systematically analyze this observation, we grew a *rad9-HA* wild type culture in rich medium at 30°C from logarithmic into stationary phase and exposed cells at 4 different stages to 40°C for 30 min (Fig. 4A, B). Intriguingly, induction of Rad9-M50 declined whilst cells exited the logarithmic growth phase (Fig. 4B; time points 1, 2 & 3). Once cells entered stationary phase, expression of the full-length protein started to decline as well (Fig. 4B; time point 4). Since this suggests that only cycling cells express Rad9-M50, we resorted to defined minimal medium to compare cycling with non-cycling cells. While phenylalanine as a nitrogen source still permits slow progression through the cell cycle, the absence of nitrogen arrests cells in G1 (Fantès and Nurse, 1977). In agreement with the earlier observation, only slowly cycling cells, but not arrested cells, induced Rad9-M50 (Fig. 4C).

Intrigued by the disappearance of Rad9 in stationary cells, we extended this analysis to Rad1, Hus1, Rad3, Rad17 and Chk1. Interestingly, only the 9-1-1 subunits showed a significant drop in expression once cells entered stationary phase (Fig. S2). The amount of Chk1 and Rad17 declined to a much smaller extent, and the level of Rad3 kinase remained constant (Fig. S2). The situation for Hus1 was even more intriguing. As previously reported (Caspari et al., 2000), *S.pombe* cells constitutively express three Hus1 isoforms with yet unknown functions in addition to the full-length protein. While variant B remained largely unchanged, the other three isoforms (A, C & D) disappeared in stationary phase (Fig. S2C). The loss of the 9-1-1 complex in non-cycling cells may explain why so far no mutation in this complex has been linked with a disorder in post-mitotic cells (O'Driscoll and Jeggo, 2003).

Since it was previously reported that asynchronous *S.pombe* cultures arrest cell cycle progression at elevated temperatures (Nurse, 1975) (Petersen and Hagan, 2005), we wanted to know whether induction of Rad9-M50 blocks the cell cycle at 40°C. To this end, we synchronized wild type cells

(*rad9-HA*), cells unable to express Rad9-M50 (*rad9-M50A-HA*), and cells devoid of full-length Rad9, but able to induce Rad9-M50 (*rad9-M1A-HA*), in G2 using lactose gradients. Small G2 cells were released into rich medium at either 30°C or 40°C, and samples were withdrawn over a period of 300 min (Fig. 4D-F). At 30°C, wild type cells progressed through two cell cycle rounds as indicated by the two peaks of septation that coincide with G1/S phase (Mitchison and Nurse, 1985). At 40°C, wild type cells remained in G2 for up to 200 min before re-entering the cell cycle (Fig. 4D). In contrast, cells devoid of Rad9-M50 (*rad9-M50A-HA*), but still expressing Rad9, terminated this heat-induced arrest ~40 min prematurely (Fig. 4E). On the contrary, cells lacking Rad9, but expressing Rad9-M50 (*rad9-M1A-HA*), showed a wild-type like arrest (Fig. 4F). We repeated this experiment with back-crossed strains and obtained the same results (Fig. 4H).

Since wild type cells suppress expression of Rad9-M50 at 30°C (Fig. 1A), we tested whether its untimely induction at 30°C would enforce a G2 arrest. To do this, we took advantage of the novel *urg1* (uracil regulated gene 1) expression system (Watson et al., 2011). Expression of *urg1* is rapidly induced upon addition of uracil to cells grown in minimal medium. Using the *Cre-lox* cassette exchange technique, we integrated a *rad9-M50-EGFP* fusion gene down-stream of the *urg1* promotor on chromosome 1 in *rad9⁺* and *rad9* deleted cells (Fig. S3A). Addition of uracil induced expression of Rad9-M50-EGFP within 15 min at 30°C (Fig. S3B) closely resembling its rapid induction by heat stress (Fig. 1A). Interestingly, its up-regulation in G2 synchronized cells had no effect on cell cycle progression at 30°C, but extended the heat-induced G2 arrest by ~40 min at 40°C (Fig. 4I, J). This cell cycle effect was independent of the presence of the endogenous *rad9* gene (Fig. S3C, D). Over-expression of Rad1 had no effect on the G2 arrest at 40°C showing that this is a specific function of Rad9-M50 (Fig. S3E, F). These experiments confirm a role of Rad9-M50 in cell cycle regulation and they also show that Rad9-M50 requires heat shock conditions to be active.

Rad9-M50 acts independently of the 9-1-1 loader Rad17

Very little is currently known about the role of DNA damage checkpoint proteins in the response to heat stress (Pandita et al., 2009). To find out whether Rad9-M50 acts in the context of the checkpoint or independently of it, we measured the G2 arrest at 40°C of strains either deleted for a checkpoint gene or carrying a kinase-dead (KD) allele of checkpoint kinases. Each experiment was repeated at least three times with two independently isolated mutants to cater for any inter-experimental variations (Fig. 5). This analysis revealed three different phenotypes: (i) cells deficient in Tel1^{ATM} or Rad3^{ATR} kinase entered mitosis on average 60 min earlier than wild type cells (Fig. 5B, C), (ii) cells deleted for *rad9*, *hus1*, *rad1*, *cds1*^{Chk2}, *chk1* or *crb2*^{53BP1} entered mitosis ~40 min earlier (Fig. 5A, G, H, J, L, N), and (iii) cells without the 9-1-1 loader Rad17 displayed a normal G2 arrest (Fig. 5I). On balance, these results reveal a novel requirement of the DNA damage checkpoint for the maintenance of a heat-induced G2 arrest. But in contrast to genotoxic stress, the checkpoint genes are not required for its induction. This is not the only striking difference between genotoxic and thermal stress. While Rad17 is essential to load the 9-1-1 ring onto damaged chromatin, the loader is dispensable under heat stress conditions (Fig. 5I). To confirm this important observation, we repeated this experiment with cells devoid of *rad17* and cells lacking both Rad17 and Rad9-M50 (*Δrad17 rad9-M50A*). While *Δrad17* cells showed a wild type-like arrest, cells devoid of Rad17 and Rad9-M50 displayed a shorter arrest (Fig. 5P). Although this shows that Rad9-M50 acts independently of Rad17, we were surprised to find that deletion of *rad1* or *hus1* shortened the G2 arrest to a similar extent as loss of Rad9-M50. This could be explained by an alternative complex containing these proteins which is not dependent on Rad17. The requirement of Cds1 kinase for this G2 arrest was also unexpected (Fig. 5L), because this kinase acts normally in S phase in response to DNA replication stress (Lindsay et al, 1998). Premature entry into mitosis did not correlate with a temperature sensitivity of the checkpoint mutants (Fig. S2D). The only exception were cells deleted for *crb2* which are temperature sensitive. The latter observation points towards an additional

function of this protein outside of the normal checkpoint response.

Rad9-M50 acts jointly with Rad3, Crb2 and Chk1

While human ATM^{Tell} performs a dominant DNA damage checkpoint role, *S.pombe* Tell is much less important as long as Rad3 is active (Furuya et al, 2004). To probe their relationship in response to heat stress, we combined the *tell* deletion with a kinase-dead allele of *rad3*. In contrast to the single mutants, the Δ *tell rad3-KD* double mutant never arrested completely slowly entering mitosis at 40°C (Fig. 5F). This shows that both kinases contribute more equally to a heat-induced arrest than to a G2 delay triggered by genotoxic stress.

Given that the 9-1-1 ring activates Rad3-to-Chk1 signaling (Furuya et al., 2004) (Navadgi-Patil and Burgers, 2009), we combined the *rad9-M50A* mutation with gene deletions in *chk1*, *cds1* and *crb2*, and with a kinase-dead allele of *rad3*. While loss of the variant had no additive effect in the absence of Rad3, Crb2 or Chk1, its ablation shortened the arrest in a *cds1* mutant to a similar extent as observed in *rad3* and *tell* mutants (Fig. 5D, K, M, O) (Lindsay et al., 1998). As summarized in Figure 5Q, these findings imply that Rad9-M50 acts in the same heat response pathway as Rad3, Crb2 and Chk1, but in parallel to Cds1.

Rad9-M50 promotes de-phosphorylation of Chk1 under heat-stress conditions

Given that Chk1 is phosphorylated at S345 by Rad3 kinase whilst bound to damaged chromatin (Capasso et al., 2002)(Kosoy and O'Connell, 2008), we analysed the modification status of Chk1 in response to genotoxic and heat stress utilizing normal SDS page and isoelectric focusing. We used two different types of genotoxic stress, the chronic modification of Chk1 in cells with hyper-active Cdc2 kinase (Capasso et al., 2002) and the induced modification upon inhibition of topoisomerase 1 (camptothecin (CPT)) (Walworth et al., 1993).

To this end, we grew Chk1-HA and Chk1-HA *cdc2.1w* cells at 30°C, and shifted samples to 40°C

for 1 hour. The *Cdc2.1w* kinase harbours a point mutation (G146D) that renders the cell cycle regulator hyper-active (Booher and Beach, 1986). As reported previously, this aberrant increase in *Cdc2* activity triggered the constitutive phosphorylation of *Chk1* at 30°C resulting in a slower migrating band (Fig. 6A). Unexpectedly, exposure to 40°C suppressed this band shift suggesting that heat reverses *Chk1* modifications triggered by genotoxic stress. Heat itself failed to produce a band shift in *Chk1* wild type cells (Figure 6A). The same extracts were then subjected to isoelectric focusing using a non-linear pH gradient from 3 to 10. This assay revealed 4 isoforms of *Chk1* at 30°C in the absence of DNA damage. This implies that *Chk1* can be multiply phosphorylated, and that some of these phosphorylation events occur in undamaged cells (Fig. 6B, panel 1). While isoforms 2, 3 and 4 remained unchanged at 40°C, the abundance of isoform 1 declined (Fig. 6B, panel 2). Consistent with the band shift in a *cdc2.1w* background at 30 °C, we observed significant changes to *Chk1*. The abundance of isoform 4 strongly increased at the expense of isoform 3, and a novel, more alkaline isoform was present (Fig. 6B, panel 3). These changes were reversed at 40°C as indicated by the presence of only two isoforms (No 2 & 3) (Fig. 6B, panel 4). These findings imply that isoform 4 and the more alkaline isoform correspond to the conformational changes induced by phosphorylation of *Chk1* at S345 (Kosoy and O'Connell, 2008).

To test whether heat also suppresses *Chk1* phosphorylation induced by acute DNA damage, we grew *chk1-HA* cells at 30°C in presence of 40µM CPT for 3 hours before splitting the culture. One sample was shifted to 40°C for 1 hour while the other remained at the lower temperature (Fig. 6C). Although CPT was present throughout the experiment, heat efficiently suppressed the modification of *Chk1* resulting in the disappearance of the slower migrating band (Fig. 6D).

Given that heat also induces Rad9-M50, we compared the kinetics of its up-regulation with the suppression of *Chk1* phosphorylation upon a temperature shift to 40°C. To this end, *chk1-HA* and *rad9-HA* cells were pre-incubated for 3 hours at 30°C in the presence of 40µM CPT, and samples were withdrawn 0, 10, 20 and 30 min after a shift to 40°C . As shown in Figure 6E, the slower

migrating Chk1 band started to decline after 20min, at the same time as Rad9-M50 appeared. Interestingly, this decline was specific to Chk1 and not observed for the slower migrating Rad9 bands (Fig. 6E, lower panel). Isoelectric focusing of Chk1 extracts taken at 0 min and 30 min after the shift revealed that CPT triggered a strong increase in isoform 4 (Fig. 6F; 0 min) that was reversed by heat stress (Fig. 6F; 30 min). Interestingly, the more alkaline isoform, present in *cdc2.1w* cells at 30°C, was absent after CPT treatment suggesting that chronic and acute genotoxic stress affect Chk1 in different ways.

To test whether Rad9-M50 is linked with Chk1 de-phosphorylation, we combined the *chk1-HA* gene with the *rad9-M50A-HA* allele in the same strain (*chk1-HA rad9-M50A-HA*). These cells are able to phosphorylate Chk1 in the presence of CPT, because they express Rad9, but they should be unable to reverse this modification since Rad9-M50 is absent. Isoelectric focusing of protein extracts obtained from *chk1-HA rad9-M50A-HA* cells, which were pre-incubated for 3 hours at 30°C in the presence of 40µM CPT before a shift to 40°C for 30 min, showed the expected increase in isoform 4 at 0 min (Fig. 6G, panel 1), but in contrast to wild type cells, the intensity of isoform 4 did not decline at 40°C. On the contrary, the damage-induced modifications became more abundant as indicated by a significant increase in the alkaline isoform (Fig. 6G panel 2).

We concluded from these data that Rad9-M50 signaling modulates the DNA damage response at elevated temperatures by promoting the removal of modifications from Chk1 kinase that were induced by genotoxic stress (Fig. 6H).

Discussion

In summary, our data entertain a model such that heat-induction of Rad9-M50 from a cryptic translation initiation site results in the assembly of an alternative Rad9-Rad1-Hus1 complex that activates Rad3 in a chromosomal context which is inaccessible to Rad17. Activation of Rad3 ensures that Chk1 kinase remains in a hypo-phosphorylated state thereby preventing premature mitosis under heat stress conditions.

These findings are consistent with a recent report showing that ATR^{Rad3}-to-Chk1 signaling is activated when human cells are exposed to elevated temperatures (Furusawa et al., 2011). Which heat alterations stimulate ATR is unknown and its signaling output is the phosphorylation of Chk1 at S345 and not its dephosphorylation. Why *S.pombe* cells remove this modification at elevated temperatures is currently unclear, but it may allow them to modulate Chk1 activity to maintain a heat-induced G2 arrest (Fig. 5). Chk1 kinase has a basal activity level which increases ~5-10 fold upon phosphorylation of S345 in its C-terminal domain (Capasso et al., 2002) (Kosoy and O'Connell, 2008). The details of its activation remain to be resolved, but it is generally believed that modification of S345 by ATR^{Rad3} releases the C-terminal domain from the N-terminal catalytic domain thereby stimulating kinase activity (Tapia-Alveal et al., 2009). DNA damage-induced phosphorylation at S345 is removed by Dis2 phosphatase in *S.pombe* (den Elzen and O'Connell, 2004) and by protein phosphatase 2A (PP2A) in human cells (Leung-Pineda et al., 2006). Our data show that Chk1 dephosphorylation is limited to the DNA damage-induced modifications (Fig. 6). This selectivity could be achieved by different phosphatases, by different adapter proteins for the same phosphatase or by conformational changes within the kinase shielding some phosphate groups. The precise mechanism remains to be uncovered, but our data show a strong correlation between Chk1 dephosphorylation and the induction of Rad9-M50. The requirement of Rad3, Rad1, Hus1 and Crb2 for the heat-induced G2 arrest suggests that Rad9-M50 targets Chk1 indirectly.

Our conclusion that Rad9-M50 reprograms Rad3 to maintain Chk1 in a hypo-modified state is in

line with the observation that ATR^{Rad3} kinase stimulates PPA2 to dephosphorylate Chk1 in human cells (Leung-Pineda et al., 2006). Taken together, Rad3 may target a protein phosphatase like PPA2 or Dis2 to remove the damage-induced modifications from Chk1 at elevated temperatures.

How heat activates ATM^{Tell} and ATR^{Rad3} remains a mystery. Given that S phase is the most temperature-sensitive cell cycle stage (VanderWaal et al., 2001), heat could cause chromosomal alterations during DNA replication. Human cells arrest S phase at elevated temperatures upon the release of nucleolin from the nucleolus (Wang et al., 2001). A role of Rad9-M50 in S phase would be consistent with its induction in cycling cells (Fig. 4). Perhaps heat causes a DNA alteration which is not accessible to the normal 9-1-1 complex. This would explain the need for an alternative variant. Both, human Rad17 and the 9-1-1 complex are stimulated by ssDNA Binding Protein (RPA) (Zou et al., 2003), but RPA is the target of nucleolin upon its release from the nucleolus at high temperatures (Wang et al., 2001). Hence, binding of nucleolin to RPA may interfere with the loading of the 9-1-1 ring at elevated temperatures. Alternatively, hyperthermia could directly affect the activity of enzymes like topoisomerases which are involved in DNA replication (Bromberg and Osheroff, 2001).

On the other hand, there is evidence that heat damages DNA directly. For example, 8-oxoguanine accumulates in DNA at elevated temperatures in the presence of reactive oxygen (Bruskov et al., 2002) and heat-labile repair intermediates caused by DNA methylation are converted into DNA breaks (Lundin et al., 2005). Whether any of these changes lead to the heat-activation of ATR^{Rad3} and ATM^{Tell} kinase remains to be discovered.

Intriguingly, human cells also respond to cellular stress by synthesizing N-terminally truncated proteins and many of them regulate mitotic commitment. Genotoxic stress activates a cryptic *cdc25B* promoter in a Chk1-dependent manner to produce a shorter variant of this phosphatase allowing cells to exit the G2 arrest (Jullien et al., 2011). Stress caused by the accumulation of unfolded protein in the endoplasmic reticulum triggers binding of MDM2 to the *p53* mRNA

thereby inducing a p53 variant (p53/47) that lacks the first 39aa and arrests cells in G2 (Bourougaa et al., 2010). Finally, heat stress induces a shorter variant of the transcription factor Oct4, Oct4B1, which regulates cell cycle progression in stem cells (Farashahi et al., 2011). Although the induction mechanisms are different, the processes are limited to dividing cells and the variants are involved in cell cycle regulation.

Further work is however necessary to explore whether human cells use a similar Rad9 variant to activate ATR kinase under heat stress conditions.

Materials and Methods

S.pombe strains and Cre-Lox system

A complete strain list is available under Supplementary Materials.

As described by Watson and colleagues (Watson et al., 2008), the *loxP* sequence was integrated 181nt upstream of the *rad9* start codon at position 1,714,271 and the *loxM* sequence was placed 136nt down-stream of the stop codon at position 1,715,672 on chromosome 1. All *rad9* mutant strains described in this report are variants of this 'base' strain (*h- ade6-M216 rad9::loxP-ura4+-loxM leu1-32 ura4-D18*). The mutated *rad9* alleles were constructed using a fusion PCR protocol. To this end, genomic DNA was isolated from the *rad9-HA* wild type strain and used as a PCR template with two primer sets. The 5'-flanking forward primer containing two tandem *SphI* sites together with the mutant reverse primer, and the 3'-flanking reverse primer containing two tandem *SpeI* sites together with the forward mutant primer. The two mutant primers (35-45bp) have complementary sequences accommodating the desired mutation. This overlap sequence was used to fuse the two fragments in a subsequent PCR. All PCR steps were conducted with Phusion DNA Polymerase from New England Biolabs. The resulting *SphI-rad9-HA-SpeI* fragments were cloned between the *loxM* and *loxP* repeats in the plasmid pAW8 which also contains the *cre* recombinase gene. The promoter sequence of 181nt between *loxP* and ATG-1 (or ATG-50 in *rad9-Δ1-49-HA*) was restored in these constructs. Integrated *rad9* alleles were amplified from the corresponding strains and sequenced.

The *wrg1::rad9-M50-EGFP* and the *wrg1::rad1-HA* strains were both constructed as described by Watson and colleagues (Watson et al., 2011). ATG-50 is the first start codon in the *wrg1::rad9-M50-EGFP* construct down-stream of the *wrg1* promoter and ATG-1 is the first start codon in the *wrg1::rad1-HA* construct. Both ORFs ends with the last codon before the stop codon to allow for translation into the linker and the tag sequences.

Isoelectric Focusing

Protein extracts for the 2D protein electrophoresis were prepared from 5×10^8 cells as described by Schmidt and colleagues (Schmidt et al., 2007). Between 10 μ g and 15 μ g protein was loaded onto Immobiline™ DryStrip gels pH3-10NL 7cm (GE Healthcare) in Destreak™ rehydration solution with 0.5% of the corresponding IPG buffer. Strips were rehydrated for 12 hours at 50V on a Biorad PROTEAN IEF cell and focused using the rapid ΔV (for Rad9-HA) or linear ΔV (for Chk1-HA) preset method (10,000Vh). Before applying strips onto a 10% SDS page, they were sequentially incubated in a IPG tray on a orbital rocking platform for 10 min in 2.0ml of equilibration buffer I (6M urea 0.375M Tris-HCl (pH8.8), 2% SDS, 20% glycerol, 2% (w/v) DTT) and 2.0ml equilibration buffer II (6M urea, 0.375M Tris-HCl (pH8.8), 2% SDS, 20% Glycerol, 2.5% (w/v) Iodoacetamide).

G2 synchronisation

Lactose gradients were performed as described in (Forsburg and Rhind, 2006) with the following changes. Cells were grown at 30°C in rich medium to a low cell number 10^6 - 10^7 cells/ml, and 5×10^8 cells were harvested from these cultures. Lactose gradients were centrifuged at 750rpm for 7min in a Sorvall RT Legend bench top centrifuge and small G2 cells were taken from the top of the cell cloud. G2 cells were washed in rich medium and split into two equal 1ml samples. One sample was incubated at 30°C, whereas the second sample was re-suspended in pre-warmed rich medium and incubated at 40°C. 40 μ l aliquots were withdrawn in 20 min intervals and added to 200 μ l methanol. Cells were pelleted and stained with 30 μ l of a hoechst (1:1000)-calcofluor (1:100) solution (stocks: calcofluor 1mg/ml in 50mM sodium citrate, 100mM sodium phosphate pH 6.0; hoechst 10mg/ml in water) prior to scoring under a fluorescence microscope.

The *wrg1* expression strains were grown in minimal medium minus uracil at 30°C, harvested and loaded onto a lactose gradient prepared with the same minimal medium. Small G2 cells were split

into four samples in minimal medium. Two samples were incubated at 30°C and two samples at 40°C. Uracil was added to a final concentration of 0.25mg/ml to only one sample at either temperature.

Protein extracts and size fractionation

Preparation of both, total and soluble protein extracts, and performance of size fractionation are described in (Caspari et al., 2000). The anti-HA antibody (HA.11, clone 16B12, Covance Ltd) was used to detect Rad9-HA, the anti-HA antibody (ab9110, ABCAM) was used to detect Chk1-HA.

Acknowledgments

We would like to thank Cancer Research Wales for the financial support of Simon Janes, the European Leonardo DaVinci exchange program for the support of Ulrike Schmidt and Nadja Ney, and the Lybian Embassy for the support of Mohamed Zekri. Susanna Concilio and Karim Ashour Garrido were a self-funded exchange students. We are grateful to Mrs Muneera Hamdi Alghannami for her assistance constructing the Rad9 quintuple mutant and to Mr H.M. Syfuddin for his assistance constructing the Rad9M1A-CFP strain. We would like to thank the Yeast Genetic Resource Center (YGRC) based at Osaka City University and Osaka University for strains. We would like to acknowledge Adam Watson for his advice on the *Cre-Lox* and *urg1* systems. We also thank Dr Nancy Walworth, Dr Claudia Barros and Dr Nia Whitely for helpful comments on the manuscript. This manuscript is dedicated to the late Per Christensen.

Conflict of interest

The authors declare that they have no conflict of interest.

Figure Legends

Figure 1. Heat induction of Rad9-M50.

(A) Wild type (*rad9-HA*) cells were grown in rich medium at 30°C to a cell number below 10^7 cells/ml. Aliquots (5×10^8 cells) were withdrawn and incubated in rich medium at 40°C for the indicated times. Total protein extracts were separated on a 10% SDS page and decorated with an anti-HA antibody (Rad9: full-length; M50: Rad9-M50). (B) *rad9-HA* cells were shifted to 40°C for 30 min in the absence or presence of 100 µg/ml cycloheximide (CHX). (C) *rad9-HA* cells were incubated for 30 min at 30°C, 40°C, 30°C + 0.6M KCl, 30°C + 1M sorbitol, 30°C + 0.3mM H₂O₂ and 40°C + 1M sorbitol (P: phosphorylated form of full-length Rad9). (D) Organization of the *rad9* gene on chromosome 1 (I: intron; M: methionine; the number of amino acids per exon are indicated). (E) *rad9-HA* mutant strains with alanine substitutions at the indicated methionine codons were incubated for 30 min at 30°C or 40°C. (F) Isoelectric focusing of Rad9-HA isolated from cells grown at 30°C and shifted for 1 hour to 40°C (pH 3-10NL, 7cm). The arrows highlight the two isoforms of Rad9-M50.

Figure 2. Analysis of *rad9-HA* mutant strains.

(A) Schematic representation of the different mutations in *rad9-HA*. (B) The indicated strains were incubated for 30 min at 30°C or 40°C, and total protein extracts were separated on a 10% SDS page prior to staining with an anti-HA antibody (Rad9: full-length; M50: Rad9-M50; Δ chk1: *rad9-HA* Δ chk1). (C) The indicated strains were incubated at 30°C in rich medium containing 12mM HU and cell survival was analyzed in 1 hour intervals for 6 hours ([□]: *rad9-HA* [WT]; [○]: Δ rad9; [Δ]: *rad9-M1A-HA*; [◇]: Δ rad1; [▲]: Δ rad1 *rad9-M1A-HA*). (D) Heat induction at 40°C for 30 min of the indicated *rad9* strains carrying indicated methionine-to-alanine substitutions (Q: *rad9-M50A+M74A+M311A+M312A+M357A*)

Figure 3. Rad9-M50 cannot substitute for full-length Rad9 in the 9-1-1 ring.

(A) Sequence alignment of Rad9^{Sp}, Rad9A^{Hs} and Rad9B^{Hs}. The alternative start sites M50 (yeast) and M73 (human) are indicated. (B) Crystal structure of the human 9-1-1 complex (PDB ID: 3G65) (Doré et al., 2009). M1 and M50 are indicated by arrows. The image was generated using Polyview 3D. (C) Serial dilutions (10^7 -to- 10^4 cells/ml) of the indicated strains were dropped (5 μ l) onto rich medium plates without a drug, with HU (4mM) or CPT (10 μ M). Plates were incubated for 3 days at either 30°C (no, HU, CPT) or 37°C ($\Delta wis1$: deletion of the MAPK kinase Wis1). (D, E) The indicated strains were synchronized in G2 and released into rich medium without HU or with 12mM HU ([□]: *rad9-HA* [WT]; [■]: *rad9-HA* [WT] +HU; [○]: *rad9-M1A-HA*; [●]: *rad9-M1A-HA* +HU; [▼]: *rad9- Δ 1-49-HA* +HU). (F) Soluble protein extracts were prepared from *rad9-HA* (Rad9) and *rad9- Δ 1-49-HA* (M50) cells grown at 30°C and separated on a Superdex-200 column. The 9-1-1 ring elutes in fractions 12-14. (G) Size fractionation of an extract from *rad9-HA* cells incubated for 30 min at 40°C. (H) Size fractionation of an extract from *rad9-HA Δ rad1* cells incubated for 30 min at 40°C. (I) Anti-HA decorated Western blot of total extracts isolated from *chk1-HA* [Chk1] and *chk1-HA rad9- Δ 1-49-HA* cells [Chk1+M50] grown in the absence or presence of 40 μ M CPT for 1 hour at 30°C.

Figure 4. Rad9-M50 is required for an extended G2/M arrest at elevated temperatures.

(A + B) Four aliquots (1-4) (5×10^8 cells) were withdrawn whilst a culture of *rad9-HA* cells was growing in rich medium at 30°C from 1.8×10^7 cells/ml (1) to 1.5×10^8 cells/ml (B). Aliquots were incubated at 30°C or 40°C for 30 min prior to the preparation of total cell extracts. (C) *rad9-HA* cells were grown at 30°C in minimal with phenylalanine (+N) as nitrogen source or in the same medium without nitrogen (-N). Aliquots were incubated at 30°C or 40°C for 30 min. (D) *rad9-HA* (□; wild type) cells were synchronized in G2 and released into rich medium at 30°C (open symbols) or 40°C (closed symbols). (E) G2 synchronized *rad9-M50A-HA* (◇) cells. (F) G2

synchronized *rad9-M1A-HA* (○) cells. (G) Aliquots from the same cell cultures were harvested and incubated for 1 hours at 30°C or 40°C prior to the preparation of total cell extracts. (H) Repeat experiment with G2 synchronized *rad9-HA* (□; wild type), *rad9-M50A-HA* (◇), $\Delta rad9::loxP-ura4^+$ -*loxM* (Δ) and *rad9-M1A-HA* (○) strains after back-cross. (I) *urg1::rad9-M50-EGFP rad9+* cells were incubated in the absence or presence of uracil (0.25mg/ml) for 20min at 30°C and 40°C in EMM minimal medium. Total protein extracts were probed with an anti-GFP (Roche Applied Science) (Rad9-M50) and an anti-Cdc2 antibody (Abcam). (J) G2 synchronized *urg1::rad9-M50-EGFP rad9+* cells were released in minimal medium with or without uracil (0.25mg/ml) at 30°C and 40°C (+M50 indicates addition of uracil).

Figure 5: Heat-induced G2 arrest in DNA damage checkpoint mutants.

Cells of the indicated genotypes were grown at 30°C in rich medium, synchronized in G2 by lactose gradient centrifugation and released into medium at 40°C to measure the delay time. The average results for wild type and the *rad9* deletion strain are shown without error bars in all panels to allow for comparison (n = number of experiments). (A) wild type 804 [□] (n=4); $\Delta rad9::ura4^+$ and $\Delta rad9::kanMX4$ [Δ] (n=4); (B) *rad3-D2249E-KD* and $\Delta rad3::ura4^+$ [●] (n=3); (C) $\Delta tell::ura4^+$ [●] (n=3); (D) *rad3-KD rad9-M50A-HA* [●] (n=3); (E) *rad9-M50A-HA* [●] (n=3); (F) $\Delta tell::ura4^+$ *rad3-D2249E-KD* [●] (n=3); (G) $\Delta rad1::ura4^+$ [●] (n=5); (H) $\Delta hus1::leu2^+$ and $\Delta hus1::loxP-ura4^+$ -*loxM* [●] (n=7); (I) $\Delta rad17::ura4^+$ [●] (n=4); (J) $\Delta chk1::kanMX4$ and *chk1-D155E-KD* [●] (n=4); (K) $\Delta chk1::kanMX4 rad9-M50A-HA$ [●] (n=4); (L) $\Delta cds1::ura4^+$ and *cds1-D312E-KD* kinase dead [●] (n=3); (M) $\Delta cds1::ura4^+$ *rad9-M50A-HA* [●] (n=3); (N) $\Delta crb2::ura4^+$ and $\Delta crb2::kanMX4$ [●] (n=4); (O) $\Delta crb2::ura4^+$ *rad9-M50A-HA* [●] (n=3); (P) $\Delta rad17::ura4^+$ *rad9-M50A-HA* [●] (n=1); (Q) Summary of the genetic interactions.

Figure 6: Rad9-M50 is required for the heat suppression of Chk1 phosphorylation.

(A) Chk1-HA and Chk1-HA *cdc2.1w* (G146D) strains were grown at 30°C and shifted for 1 hour to 40°C (Chk1-P = phosphorylated Chk1, * = cross-reacting band). (B) The same extracts were subjected to isoelectric focusing (pH3-10NL, 7cm) (1,2,3,4 = four different isoforms of Chk1-HA). (C) Experimental design to analyse whether heat suppresses Chk1 phosphorylation induced by CPT. (D) SDS page of extracts prepared from cells pre-incubated for 3 hours at 30°C in the presence of 40µM CPT prior to a shift to 30°C or 40°C for 1 hour. (E) Chk1-HA and Rad9-HA strains were pre-incubated for 3 hours at 30°C in the presence of 40µM CPT prior to a shift to 40°C. Samples were withdrawn at the indicated time points after the shift. (F) Chk1-HA extracts from this experiment (0 min & 30 min) were subjected to isoelectric focusing. (G) Isoelectric focusing of extracts prepared from Chk1-HA Rad9-M50A-HA cells that were pre-incubated for 3 hours at 30°C in the presence of 40µM CPT prior to a shift to 40°C for 30 min. (H) Model showing that heat specifically suppresses the DNA damage-induced modification of Chk1 in a manner dependent on Rad9-M50.

Reference List

- Bentley, N. J., Holtzman, D. A., Flaggs, G., Keegan, K. S., DeMaggio, A., Ford, J. C., Hoekstra, M., and Carr, A M (1996). The Schizosaccharomyces pombe rad3 checkpoint gene. *EMBO J*, **15**, 6641–6651.
- Bermudez, V. P., Lindsey-Boltz, L. A., Cesare, A. J., Maniwa, Y., Griffith, J. D., Hurwitz, J., and Sancar, A. (2003). Loading of the human 9-1-1 checkpoint complex onto DNA by the checkpoint clamp loader hRad17-replication factor C complex in vitro. *Proc. Natl. Acad. Sci. U.S.A.*, **100**, 1633–1638.
- Booher, R. and Beach, D. (1986). Site-specific mutagenesis of cdc2+, a cell cycle control gene of the fission yeast Schizosaccharomyces pombe. *Mol. Cell. Biol.*, **6**, 3523–3530.
- Bourougaa, K., Naski, N., Boularan, C., Mlynarczyk, C., Candeias, M. M., Marullo, S., and Fåhraeus, R. (2010). Endoplasmic reticulum stress induces G2 cell-cycle arrest via mRNA translation of the p53 isoform p53/47. *Mol. Cell*, **38**, 78–88.
- Bromberg, K. D. and Osheroff, N. (2001). DNA cleavage and religation by human topoisomerase II alpha at high temperature. *Biochemistry*, **40**, 8410–8418.
- Bruskov, V. I., Malakhova, L. V., Masalimov, Z. K., and Chernikov, A. V. (2002). Heat-induced formation of reactive oxygen species and 8-oxoguanine, a biomarker of damage to DNA. *Nucleic Acids Res.*, **30**, 1354–1363.
- Capasso, H., Palermo, C., Wan, S., Rao, H., John, U. P., O’Connell, Matthew J, and Walworth, N. C. (2002). Phosphorylation activates Chk1 and is required for checkpoint-mediated cell cycle arrest. *J. Cell. Sci.*, **115**, 4555–4564.
- Caspari, T, Dahlen, M., Kanter-Smoler, G., Lindsay, H. D., Hofmann, K., Papadimitriou, K., Sunnerhagen, P., and Carr, A M (2000). Characterization of Schizosaccharomyces pombe Hus1: a PCNA-related protein that associates with Rad1 and Rad9. *Mol. Cell. Biol*, **20**, 1254–1262.
- Caspari, T, Davies, C., and Carr, A M (2000). Analysis of the fission yeast checkpoint Rad proteins. *Cold Spring Harb. Symp. Quant. Biol*, **65**, 451–456.
- Caspari, Thomas, Murray, Johanne M, and Carr, Antony M (2002). Cdc2-cyclin B kinase activity links Crb2 and Rqh1-topoisomerase III. *Genes Dev*, **16**, 1195–1208.
- Doré, A. S., Kilkenny, M. L., Rzechorzek, N. J., and Pearl, L. H. (2009). Crystal structure of the rad9-rad1-hus1 DNA damage checkpoint complex--implications for clamp loading and regulation. *Mol. Cell*, **34**, 735–745.
- den Elzen, N. R. and O’Connell, Matthew J (2004). Recovery from DNA damage checkpoint arrest by PP1-mediated inhibition of Chk1. *EMBO J*, **23**, 908–918.
- Falck, J., Coates, J., and Jackson, S. P. (2005). Conserved modes of recruitment of ATM, ATR and DNA-PKcs to sites of DNA damage. *Nature*, **434**, 605–611.

- Fantes, P. and Nurse, P** (1977). Control of cell size at division in fission yeast by a growth-modulated size control over nuclear division. *Exp. Cell Res.*, **107**, 377–386.
- Farashahi Yazd, E., Rafiee, M. R., Soleimani, M., Tavallaei, M., Salmani, M. K., and Mowla, S. J.** (2011). OCT4B1, a novel spliced variant of OCT4, generates a stable truncated protein with a potential role in stress response. *Cancer Lett.*, **309**, 170–175.
- Ferreira, M. G. and Cooper, J. P.** (2004). Two modes of DNA double-strand break repair are reciprocally regulated through the fission yeast cell cycle. *Genes Dev.*, **18**, 2249–2254.
- Forsburg, S. L. and Rhind, N.** (2006). Basic methods for fission yeast. *Yeast*, **23**, 173–183.
- Furusawa, Y., Iizumi, T., Fujiwara, Y., Zhao, Q.-L., Tabuchi, Y., Nomura, T., and Kondo, T.** (2011). Inhibition of checkpoint kinase 1 abrogates G2/M checkpoint activation and promotes apoptosis under heat stress. *Apoptosis: An International Journal on Programmed Cell Death*.
- Furuya, K., Poitelea, M., Guo, L., Caspari, Thomas, and Carr, Antony M** (2004). Chk1 activation requires Rad9 S/TQ-site phosphorylation to promote association with C-terminal BRCT domains of Rad4TOPBP1. *Genes Dev.*, **18**, 1154–1164.
- Gould, K. L. and Nurse, P** (1989). Tyrosine phosphorylation of the fission yeast *cdc2+* protein kinase regulates entry into mitosis. *Nature*, **342**, 39–45.
- Guo, Z., Kozlov, S., Lavin, M. F., Person, M. D., and Paull, T. T.** (2010). ATM activation by oxidative stress. *Science*, **330**, 517–521.
- Huertas, P., Cortés-Ledesma, F., Sartori, A. A., Aguilera, A., and Jackson, S. P.** (2008). CDK targets Sae2 to control DNA-end resection and homologous recombination. *Nature*, **455**, 689–692.
- Hunt, C. R., Pandita, R. K., Laszlo, A., Higashikubo, R., Agarwal, M., Kitamura, T., Gupta, A., Rief, N., Horikoshi, N., Baskaran, R., u. a.** (2007). Hyperthermia activates a subset of ataxia-telangiectasia mutated effectors independent of DNA strand breaks and heat shock protein 70 status. *Cancer Res*, **67**, 3010–3017.
- Jullien, D., Bugler, B., Dozier, C., Cazales, M., and Ducommun, B.** (2011). Identification of N-terminally truncated stable nuclear isoforms of CDC25B that are specifically involved in G2/M checkpoint recovery. *Cancer Res.*, **71**, 1968–1977.
- King, H. A., Cobbold, L. C., and Willis, A. E.** (2010). The role of IRES trans-acting factors in regulating translation initiation. *Biochem. Soc. Trans.*, **38**, 1581–1586.
- Kochetov, A. V.** (2008). Alternative translation start sites and hidden coding potential of eukaryotic mRNAs. *Bioessays*, **30**, 683–691.
- Kosoy, A. and O'Connell, Matthew J** (2008). Regulation of Chk1 by its C-terminal domain. *Mol. Biol. Cell*, **19**, 4546–4553.
- Laszlo, A. and Fleischer, I.** (2009). Heat-induced perturbations of DNA damage signaling pathways are modulated by molecular chaperones. *Cancer Res*, **69**, 2042–2049.

- Leung-Pineda, V., Ryan, C. E., and Piwnica-Worms, H.** (2006). Phosphorylation of Chk1 by ATR is antagonized by a Chk1-regulated protein phosphatase 2A circuit. *Mol. Cell. Biol.*, **26**, 7529–7538.
- Lindsay, H. D., Griffiths, D. J., Edwards, R. J., Christensen, P. U., Murray, J M, Osman, F., Walworth, N., and Carr, A M** (1998). S-phase-specific activation of Cds1 kinase defines a subpathway of the checkpoint response in *Schizosaccharomyces pombe*. *Genes Dev.*, **12**, 382–395.
- Lopez-Girona, A., Furnari, B., Mondesert, O., and Russell, P.** (1999). Nuclear localization of Cdc25 is regulated by DNA damage and a 14-3-3 protein. *Nature*, **397**, 172–175.
- Lundin, C., North, M., Erixon, K., Walters, K., Jenssen, D., Goldman, A. S. H., and Helleday, T.** (2005). Methyl methanesulfonate (MMS) produces heat-labile DNA damage but no detectable in vivo DNA double-strand breaks. *Nucleic Acids Res.*, **33**, 3799–3811.
- Millar, J. B., Buck, V., and Wilkinson, M. G.** (1995). Pyp1 and Pyp2 PTPases dephosphorylate an osmosensing MAP kinase controlling cell size at division in fission yeast. *Genes Dev.*, **9**, 2117–2130.
- Mitchison, J. M. and Nurse, P** (1985). Growth in cell length in the fission yeast *Schizosaccharomyces pombe*. *J. Cell. Sci.*, **75**, 357–376.
- Navadgi-Patil, V. M. and Burgers, P. M.** (2009). The unstructured C-terminal tail of the 9-1-1 clamp subunit Ddc1 activates Mec1/ATR via two distinct mechanisms. *Mol. Cell*, **36**, 743–753.
- Nurse, P** (1975). Genetic control of cell size at cell division in yeast. *Nature*, **256**, 547–551.
- O’Connell, M J, Raleigh, J. M., Verkade, H. M., and Nurse, P** (1997). Chk1 is a wee1 kinase in the G2 DNA damage checkpoint inhibiting cdc2 by Y15 phosphorylation. *EMBO J.*, **16**, 545–554.
- O’Driscoll, M. and Jeggo, P. A.** (2003). Clinical impact of ATR checkpoint signalling failure in humans. *Cell Cycle*, **2**, 194–195.
- Pandita, T. K., Pandita, S., and Bhaumik, S. R.** (2009). Molecular parameters of hyperthermia for radiosensitization. *Crit. Rev. Eukaryot. Gene Expr.*, **19**, 235–251.
- Petersen, J. and Hagan, I. M.** (2005). Polo kinase links the stress pathway to cell cycle control and tip growth in fission yeast. *Nature*, **435**, 507–512.
- Petersen, J. and Nurse, Paul** (2007). TOR signalling regulates mitotic commitment through the stress MAP kinase pathway and the Polo and Cdc2 kinases. *Nat. Cell Biol.*, **9**, 1263–1272.
- Porras, P., Padilla, C. A., Krayl, M., Voos, W., and Bárcena, J. A.** (2006). One single in-frame AUG codon is responsible for a diversity of subcellular localizations of glutaredoxin 2 in *Saccharomyces cerevisiae*. *J. Biol. Chem.*, **281**, 16551–16562.
- Rogakou, E. P., Pilch, D. R., Orr, A. H., Ivanova, V. S., and Bonner, W. M.** (1998). DNA double-stranded breaks induce histone H2AX phosphorylation on serine 139. *J. Biol. Chem.*, **273**, 5858–5868.

- Roos-Mattjus, P., Hopkins, K. M., Oestreich, A. J., Vroman, B. T., Johnson, K. L., Naylor, S., Lieberman, H. B., and Karnitz, L. M. (2003). Phosphorylation of human Rad9 is required for genotoxin-activated checkpoint signaling. *J. Biol. Chem.*, **278**, 24428–24437.
- Sartori, A. A., Lukas, C., Coates, J., Mistrik, M., Fu, S., Bartek, J., Baer, R., Lukas, J., and Jackson, S. P. (2007). Human CtIP promotes DNA end resection. *Nature*, **450**, 509–514.
- Schmidt, M. W., Houseman, A., Ivanov, A. R., and Wolf, D. A. (2007). Comparative proteomic and transcriptomic profiling of the fission yeast *Schizosaccharomyces pombe*. *Mol. Syst. Biol.*, **3**, 79.
- Seno, J. D. and Dynlacht, J. R. (2004). Intracellular redistribution and modification of proteins of the Mre11/Rad50/Nbs1 DNA repair complex following irradiation and heat-shock. *J. Cell. Physiol.*, **199**, 157–170.
- Shiozaki, K. and Russell, P. (1995). Cell-cycle control linked to extracellular environment by MAP kinase pathway in fission yeast. *Nature*, **378**, 739–743.
- Shiozaki, K., Shiozaki, M., and Russell, P. (1998). Heat stress activates fission yeast Spc1/Sty1 MAPK by a MEKK-independent mechanism. *Mol. Biol. Cell.*, **9**, 1339–1349.
- Smith, J., Tho, L. M., Xu, N., and Gillespie, D. A. (2010). The ATM-Chk2 and ATR-Chk1 pathways in DNA damage signaling and cancer. *Adv. Cancer Res.*, **108**, 73–112.
- St Onge, R. P., Besley, B. D., Park, M., Casselman, R., and Davey, S. (2001). DNA damage-dependent and -independent phosphorylation of the hRad9 checkpoint protein. *J. Biol. Chem.*, **276**, 41898–41905.
- Tapia-Alveal, C., Calonge, T. M., and O'Connell, Matthew J (2009). Regulation of chk1. *Cell Div.*, **4**, 8.
- VanderWaal, R. P., Griffith, C. L., Wright, W. D., Borrelli, M. J., and Roti, J. L. (2001). Delaying S-phase progression rescues cells from heat-induced S-phase hypertoxicity. *J. Cell. Physiol.*, **187**, 236–243.
- Walworth, N., Davey, S., and Beach, D. (1993). Fission yeast chk1 protein kinase links the rad checkpoint pathway to cdc2. *Nature*, **363**, 368–371.
- Wang, Y., Guan, J., Wang, H., Wang, Y., Leeper, D., and Iliakis, G. (2001). Regulation of dna replication after heat shock by replication protein a-nucleolin interactions. *J. Biol. Chem.*, **276**, 20579–20588.
- Ward, I. M., Minn, K., Jorda, K. G., and Chen, J. (2003). Accumulation of checkpoint protein 53BP1 at DNA breaks involves its binding to phosphorylated histone H2AX. *J. Biol. Chem.*, **278**, 19579–19582.
- Watson, A. T., Garcia, V., Bone, N., Carr, Antony M, and Armstrong, J. (2008). Gene tagging and gene replacement using recombinase-mediated cassette exchange in *Schizosaccharomyces pombe*. *Gene*, **407**, 63–74.
- Watson, A. T., Werler, P., and Carr, Antony M (2011). Regulation of gene expression at the fission yeast *Schizosaccharomyces pombe* *urg1* locus. *Gene*, **484**, 75–85.

- Xu, M., Bai, L., Gong, Y., Xie, W., Hang, H., and Jiang, T.** (2009). Structure and functional implications of the human rad9-hus1-rad1 cell cycle checkpoint complex. *J. Biol. Chem.*, **284**, 20457–20461.
- Zegerman, P. and Diffley, J. F. X.** (2007). Phosphorylation of Sld2 and Sld3 by cyclin-dependent kinases promotes DNA replication in budding yeast. *Nature*, **445**, 281–285.
- Zierhut, C. and Diffley, J. F. X.** (2008). Break dosage, cell cycle stage and DNA replication influence DNA double strand break response. *EMBO J.*, **27**, 1875–1885.
- Zölzer, F. and Streffer, C.** (2001). G2-phase delays after irradiation and/or heat treatment as assessed by two-parameter flow cytometry. *Radiat. Res.*, **155**, 50–56.
- Zou, L. and Elledge, S. J.** (2003). Sensing DNA damage through ATRIP recognition of RPA-ssDNA complexes. *Science*, **300**, 1542–1548.
- Zou, L., Liu, D., and Elledge, S. J.** (2003). Replication protein A-mediated recruitment and activation of Rad17 complexes. *Proc. Natl. Acad. Sci. U.S.A.*, **100**, 13827–13832.
- Zu, T., Gibbens, B., Doty, N. S., Gomes-Pereira, M., Huguet, A., Stone, M. D., Margolis, J., Peterson, M., Markowski, T. W., Ingram, M. A. C., et al** (2011). Non-ATG-initiated translation directed by microsatellite expansions. *Proc. Natl. Acad. Sci. U.S.A.*, **108**, 260–265.

Figure 1: Heat Induction of Rad9-M50

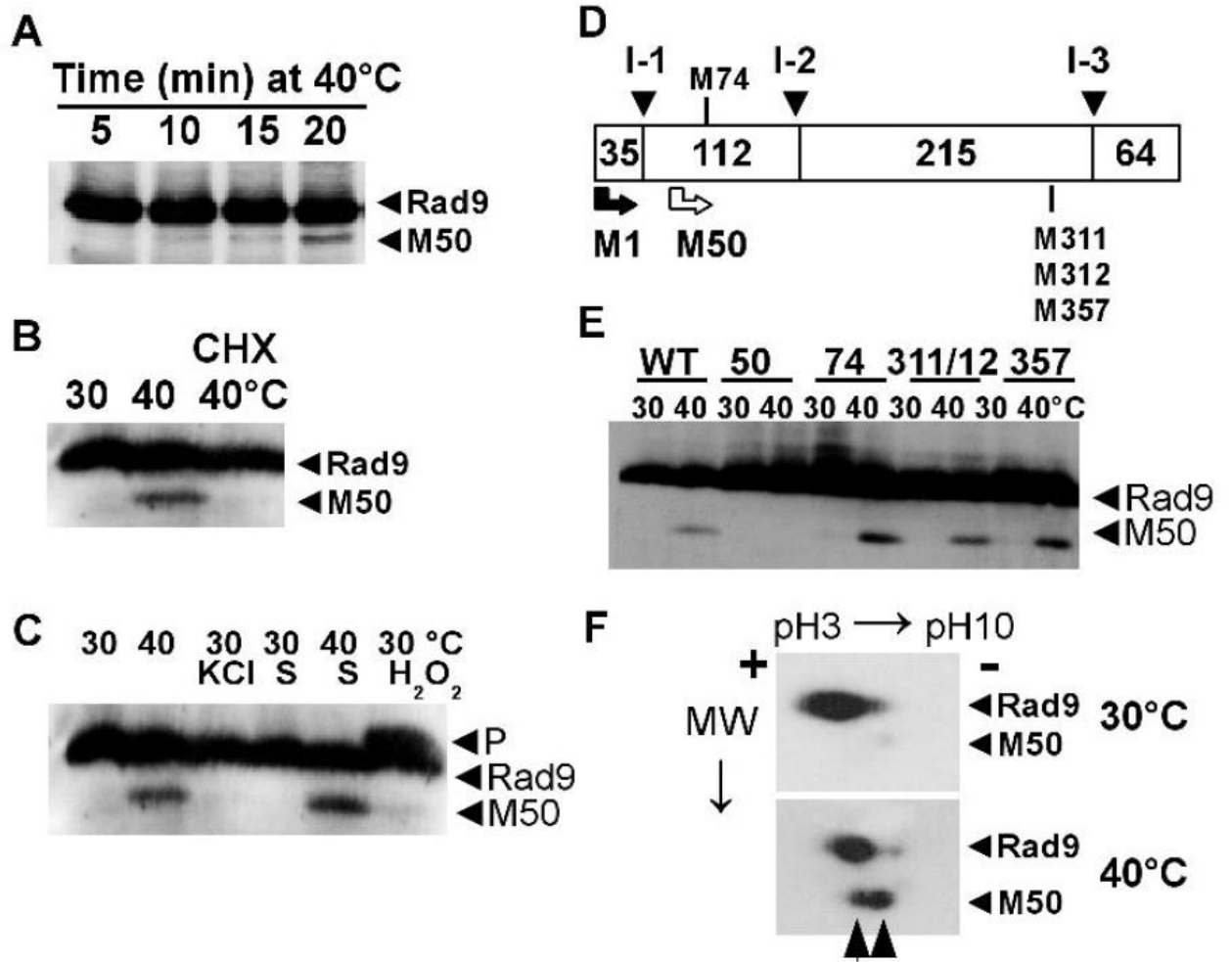


Figure 2: Analysis of *rad9-HA* Mutant Strains

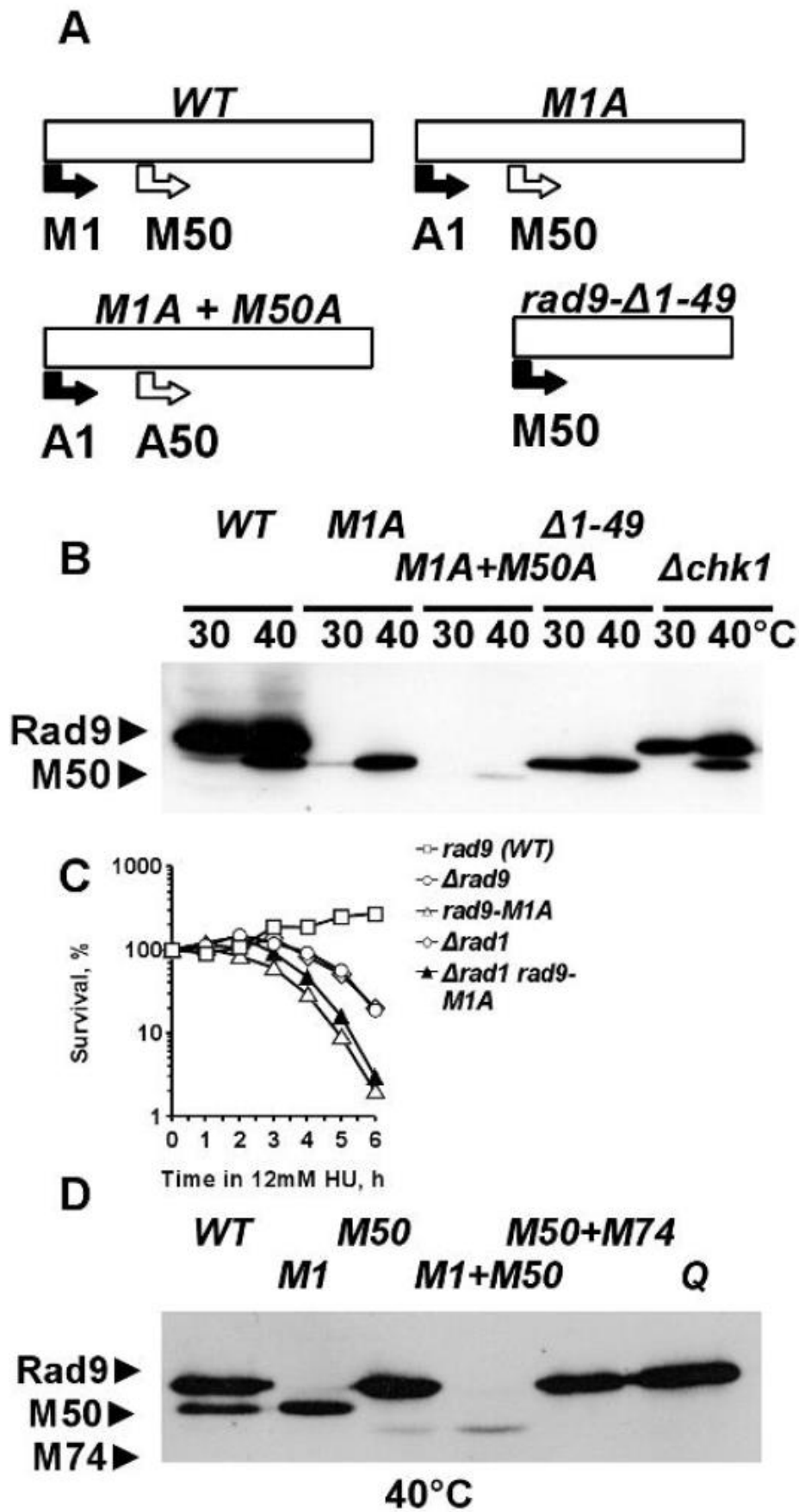


Figure 3: Rad9-M50 Cannot Substitute for Full-Length Rad9 in the 9-1-1 Ring

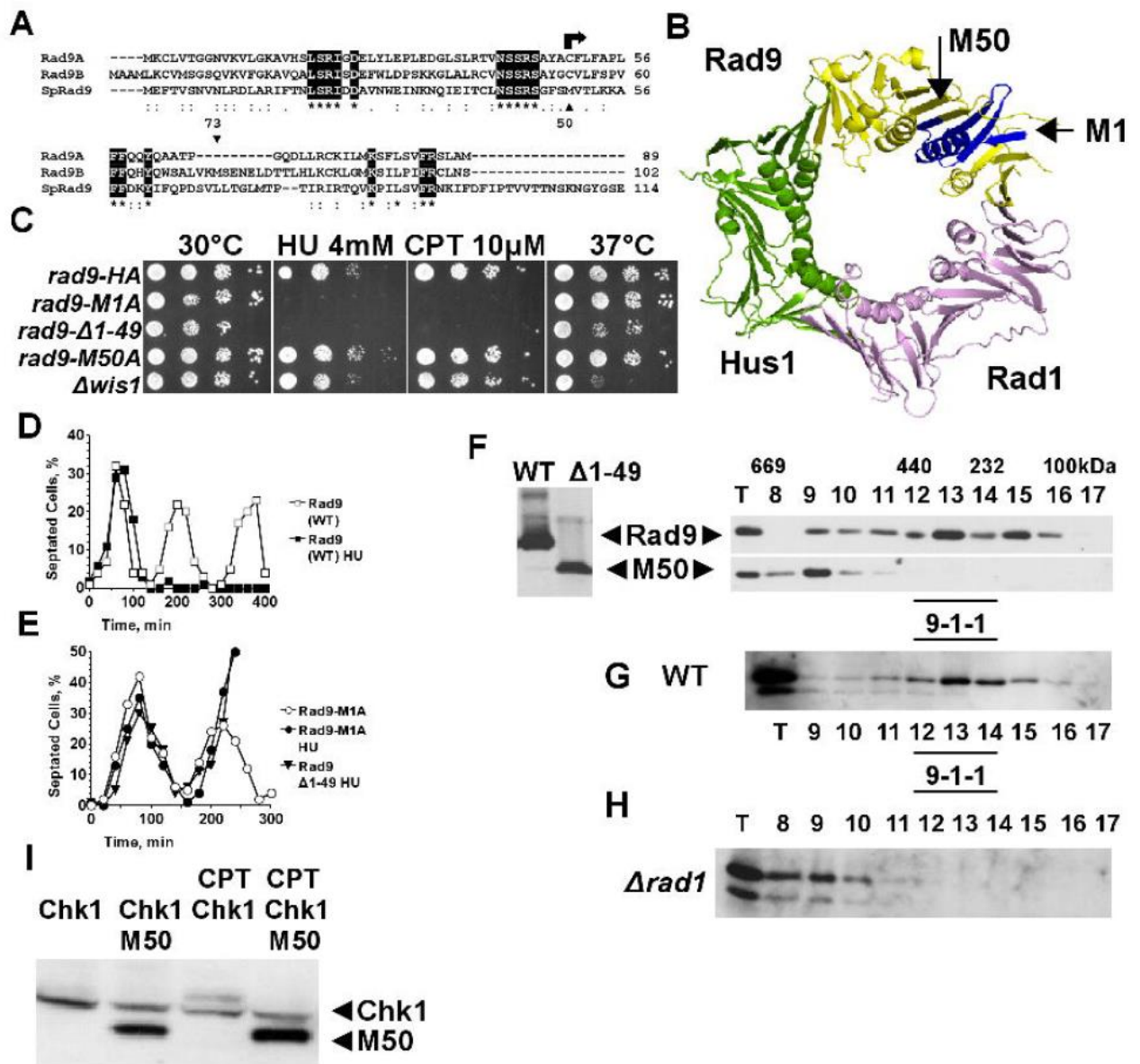


Figure 4: Rad9-M50 is Required for an Extended G2/M Arrest at Elevated Temperatures

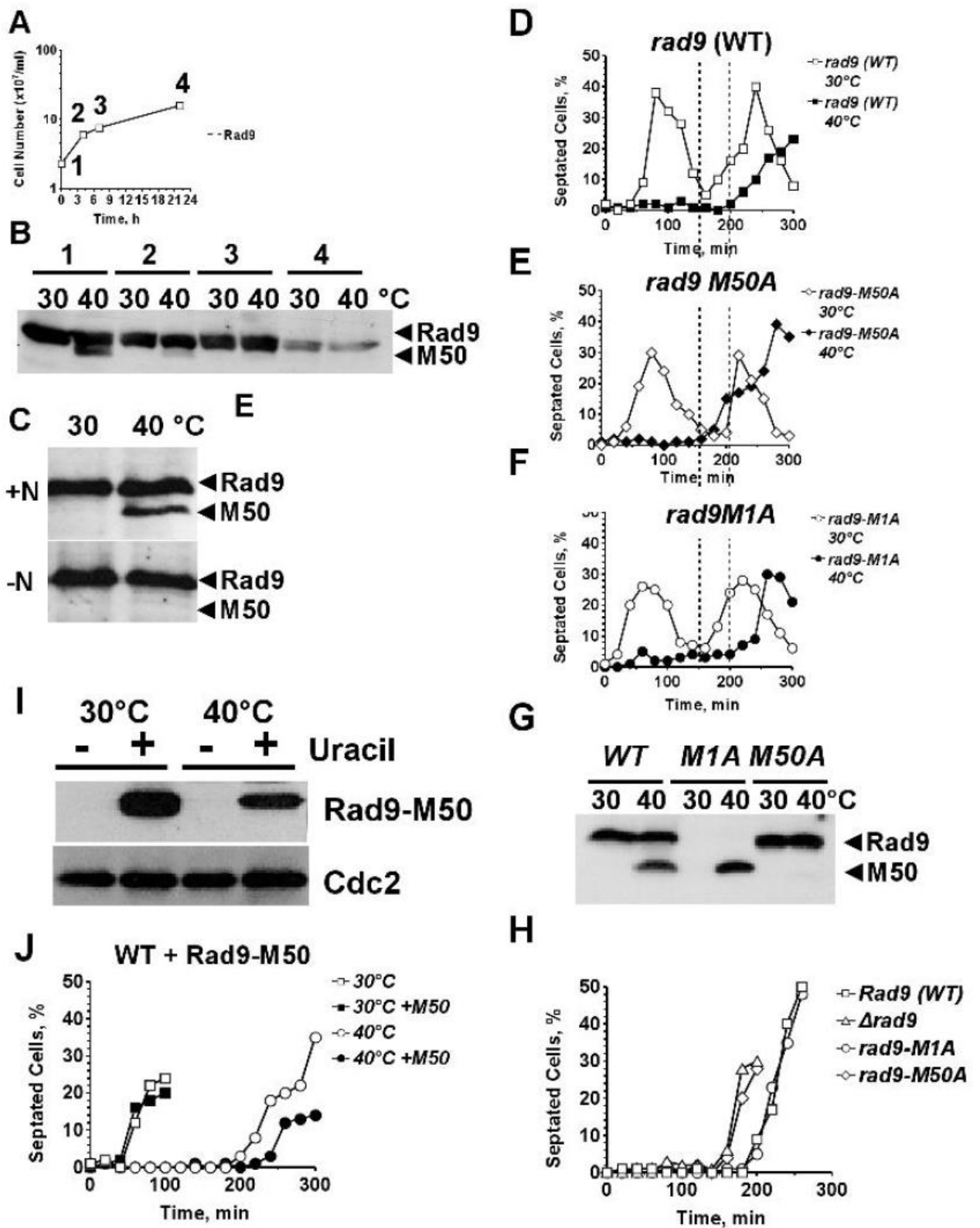


Figure 5: Heat-Induced G2 Arrest in DNA Damage Checkpoint Mutants

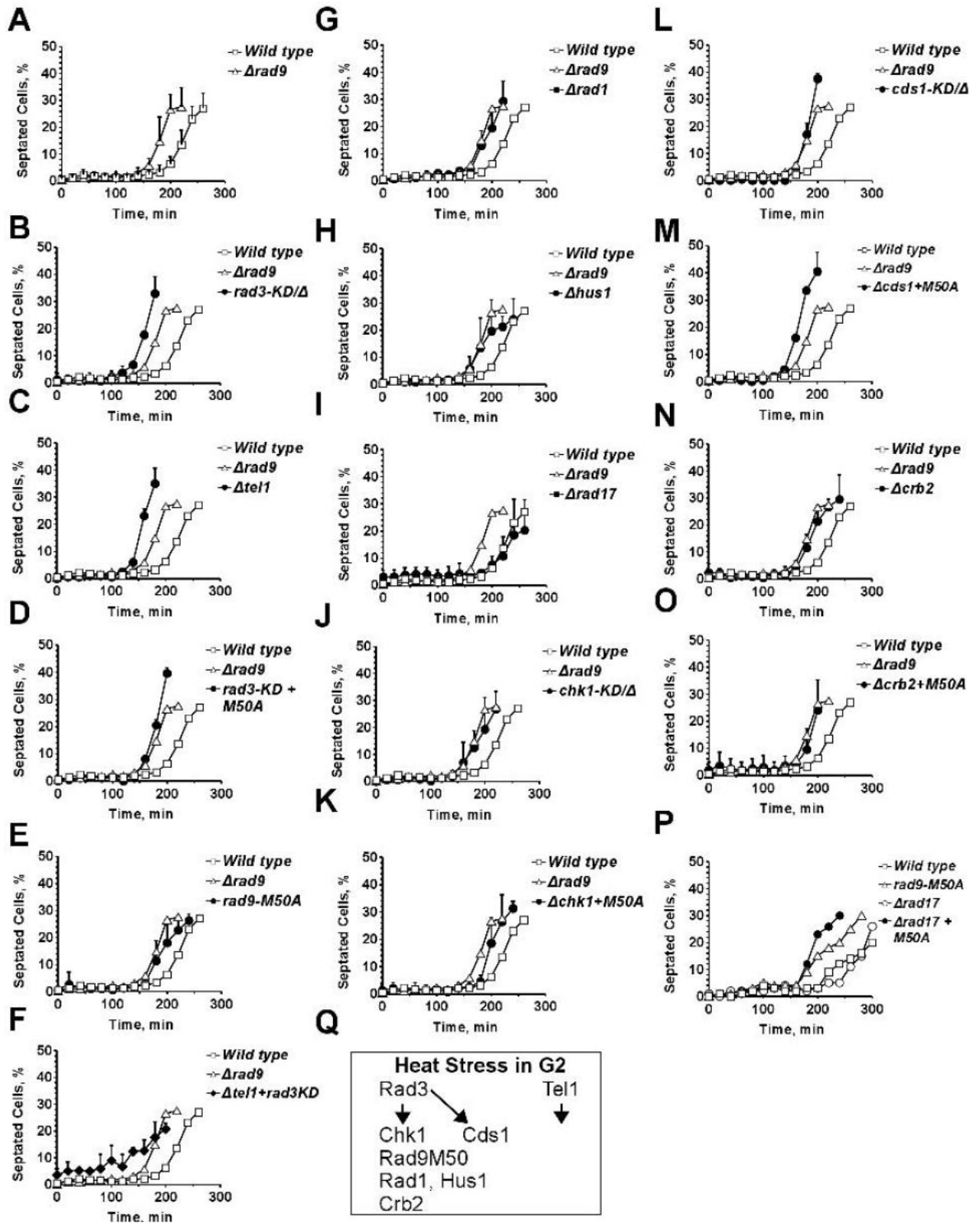
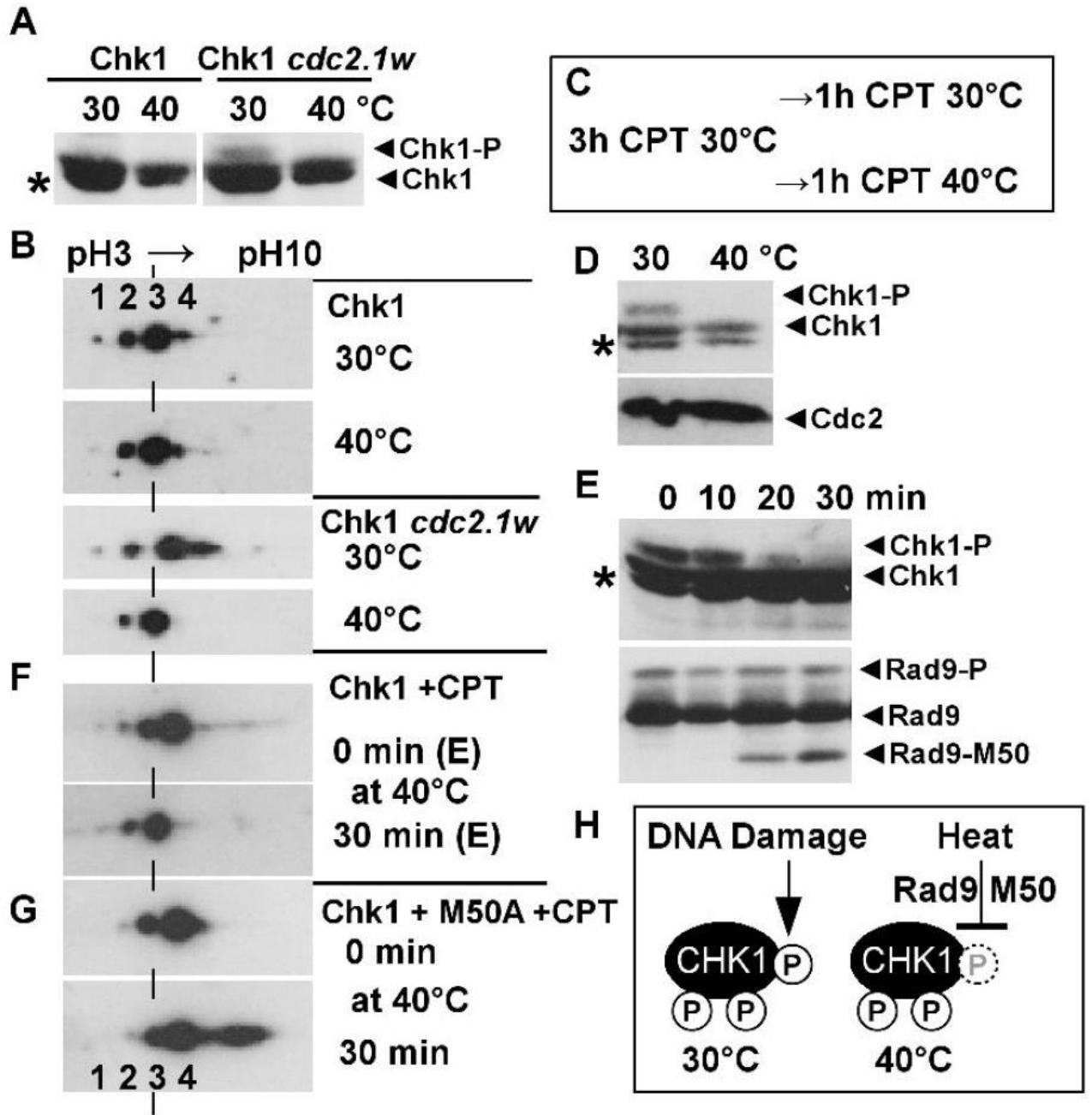


Figure 6: Rad9-M50 is Required for Heat Suppression of Chk1 Phosphorylation



Chapter 7

Experimental Evidence for Functional Roles of “Rad9-S” in DNA Repair

7.1 Introduction

Purified recombinant human Rad9A protein (hRad9A) exhibited 3'→5' exonuclease activity in which the postulated nuclease active site was mapped to a region between amino acid residues 51 and 91 situated within the N-terminus of the protein respectively (Bessho T. and Sancar A., 2000) – Fig 7.1A, p.668.

However, comparative *in silico* bioinformatics-based sequence analyses of the postulated nuclease active site region revealed no significant sequence homology between exonuclease I and the hRad9A protein (Bessho T. and Sancar A., 2000).

Thus, the *in vitro* nuclease activity observed in the purified recombinant hRad9A protein could be attributed to co-purification of an exonuclease enzyme in an associative complex with hRad9A and thus the mapped nuclease motif within the N-terminus region of the protein may instead function as an interactive docking site for nuclease enzymes (Bessho T. and Sancar A., 2000).

Initial *in silico* bioinformatics comparative alignment-based analyses of the human Rad9A protein sequence with the *S. pombe* Rad9 sequence indicated that this postulated nuclease-binding/nuclease-active domain may also be functional in the N-terminus of both the *S.pombe* full-length Rad9 protein and truncated “Rad9-S” (N-Δ49-Rad9) protein variant (Fig 7.1B, p.668).

Approximately 50% of this nuclease-binding/nuclease-active motif sequence is situated within the potential M50 – M74 functional domain (identified and discussed previously in Chapter 5, Section 5.5, pp.475-481) – Fig 7.1C, p.668.

This potential M50 – M74 functional domain also contains a key tyrosine residue which may be the phosphorylation target for the dual Monopolar Spindle Checkpoint Kinase – Mph1 (discussed previously in Chapter 6) – Fig 7.1C, p.668.

Comparative acute survival assays performed with YEA broth medium cell cultures of the “Cre-Lox”-engineered *S. pombe* strains $\Delta rad9$ (*rad9*-deleted “base-strain”), *rad9-c3xHA*, “*rad9-S*” (*N149-rad9-c3xHA*) and “*rad9-M74*” (*N173-rad9-c3xHA*), in the presence of 40 μ M S-(+)-camptothecin (CPT), indicated that the “*rad9-M74*” strain was significantly more sensitive to CPT-induced DNA damage than the “*rad9-S*” strain (Fig 7.1D, p.668).

Taken together (Fig 7.1, p.668), these experimental data may indicate a novel role for the identified potential M50 – M74 functional domain, within the *S. pombe* Rad9 protein, in which it may interact with nucleases and modulate their respective activities in the repair of double-stranded DNA breaks (DSBs) – including those induced by the CPT topoisomerase I inhibitor.

The potential “nuclease-like” motif, identified within both the full-length *S. pombe* Rad9 protein and *S. pombe* truncated “Rad9-S” protein variant (Fig 7.1B, p.668), could also possess its own nuclease catalytic activity and may thus have a functional role in DSB repair pathways.

Comparative acute survival assays performed with YEA broth medium cell cultures of the “Cre-Lox”-engineered *S. pombe* strains $\Delta rad9$ (*rad9*-deleted “base-strain”), *rad9-c3xHA*, “*rad9-S*” (*N149-rad9-c3xHA*) and “*rad9-S-(Y12F)*” (*N149-rad9-(Y61F)-c3xHA*), in the presence 40 μ M S-(+)-camptothecin (CPT), indicated that the “*rad9-S-(Y12F)*” mutant strain was significantly more sensitive to CPT-induced damage than the “*rad9-S*” strain (Fig 7.2C, p.669).

Comparative *in silico* predictive phosphorylation target-site analyses of the *S. pombe* full-length Rad9 protein and truncated “Rad9-S” protein variant sequences, via utilisation of the bioinformatics software packages NetPhos2.0 and NetPhosK, identified tyrosine 61 (equivalent to Tyrosine 12 in the truncated “Rad9-S” polypeptide amino acid sequence) as a very high probability kinase target site – possibly for the dual Tyr/Thr/Ser Monopolar Spindle Checkpoint Kinase – Mph1 (Fig 7.1C, p.668 and Fig 7.2, p.669).

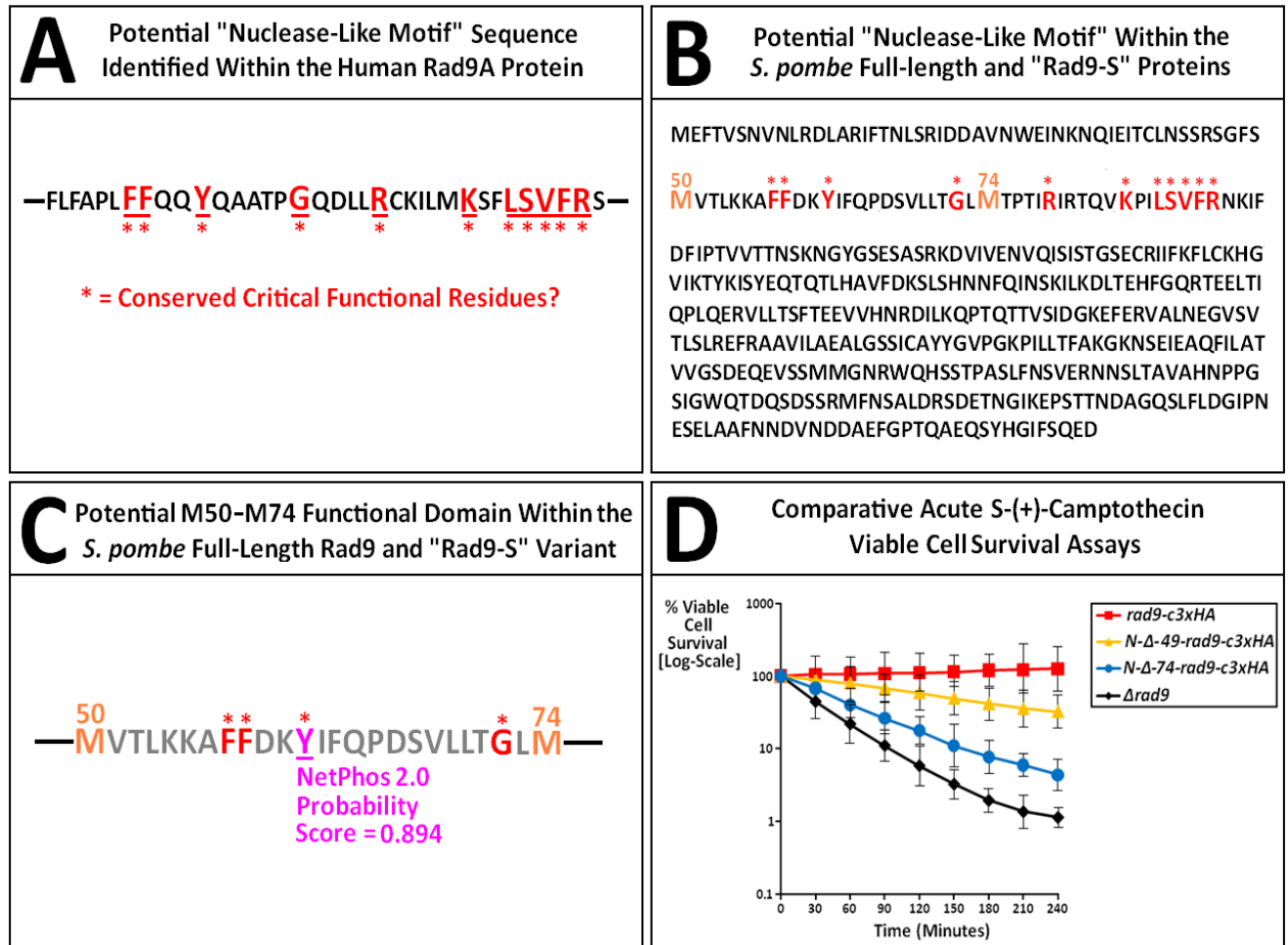
This particular tyrosine residue (Y61 in full-length Rad9 and Y12 in “Rad9-S”) is also situated within the M50-M74 functional domain – which constitutes ~50% of the identified sequence of the potential “nuclease-binding/nuclease-active” motif (Fig 7.2A and Fig 7.2B, p.669).

Comparative acute survival assays performed with YEA broth medium cell cultures of the “Cre-Lox”-engineered *S. pombe* strains $\Delta rad9$ (*rad9*-deleted “base-strain”), *rad9-c3xHA*, “*rad9-S*” (*NΔ49-rad9-c3xHA*) and “*rad9-S Δmph1*” (*NΔ49-rad9-c3xHA Δmph1*), in the presence 40μM S-(+)-camptothecin (CPT), also indicated that the “*rad9-S Δmph1*” double-mutant strain was significantly more sensitive to CPT-induced damage than the “*rad9-S*” strain (discussed previously in Chapter 6, Section 6.4, pp.568-583).

Taken together (Fig 7.2, p.669), these experimental data may indicate that Mph1-phosphorylation of this tyrosine residue is a critical pre-requisite post-translational modification of the truncated “Rad9-S” protein variant which is implicated in the mechanism of functional activation of the “nuclease-like” domain.

Thus, *S. pombe* cells “cre-lox”-engineered for the exclusive expression of the site-directed mutagenic “Rad9-S-(Y12F)” (*NΔ49-Rad9-(Y61F)-c3xHA*) truncated protein variant are very sensitive to CPT-induced cytotoxicity due to inhibited Mph1-mediated phosphorylated-activation of the “nuclease-binding/nuclease-active” domain and impairment of its functional roles in the repair of CPT-induced DNA double-stranded breaks with consequential cell death (Fig 7.2C, p.669)

Fig 7.1: Data Evidence for a Nuclease-Like Domain in *S. pombe* Rad9



A: The potential nuclease-like motif sequence identified within the Human Rad9A protein may possess catalytic nuclease activity and/or interact with various nucleases – highly conserved amino residues (*X) may be critical to the function of this potential domain (Bessho T. and Sancar A., 2000).

B: *In silico* comparative sequence alignment analyses of the nuclease-like motif with the *S. pombe* Rad9 indicate that both the full-length and “Rad9-S” (NΔ49-Rad9) proteins may contain a similar catalytic nuclease/nuclease-interactive motif with the identical, highly conserved amino acid residues (*X) which may be critical to the function of this potential domain.

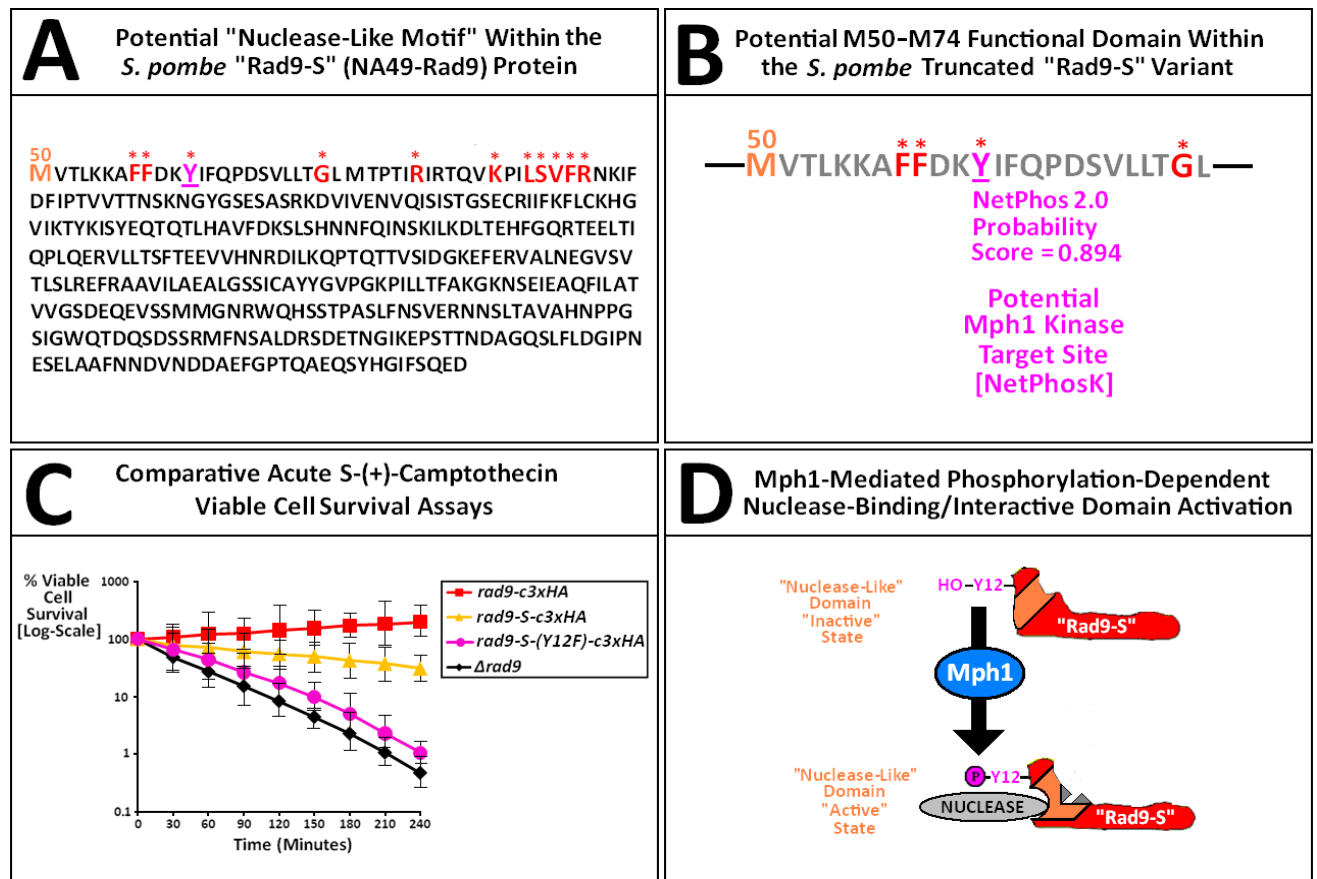
In the case of the “Rad9-M74” (NΔ73-Rad9) truncated protein variant, approximately 50% of the potential catalytic nuclease/nuclease-interactive motif sequence is missing, along with the absence of ~50% of the highly conserved amino acid residues (*X).

C: The potential M50 – M74 functional domain, identified within the *S. pombe* Rad9 protein in this study (discussed in detail previously in Chapter 5, Section 5.5, pp.475-481 and Chapter 6, Section 6.4, pp.568-583) contains three of the conserved potential nuclease-like motif amino acid residues (*X).

This M50 – M74 domain also contains an identified key Tyrosine residue (at position Y61 in the full-length Rad9 protein, which corresponds to position Y12 in the “Rad9-S” truncated protein variant) which has a high phosphorylation potential probability score and may be a novel target for the dual Monopolar Spindle Checkpoint Kinase, Mph1 (discussed previously in Chapter 6, Section 6.4, pp.568-583).

D: Comparative acute cell survival assays, performed with 40μM S-(+)-camptothecin (CPT), indicate that the “Rad9-M74” truncated protein variant is significantly more sensitive to CPT-induced DNA damage than either the full-length Rad9 protein or the Rad9-S truncated protein variant.

Fig 7.2: Mph1-Activation of the “Rad9-S” “Nuclease-Like” Domain



A: The potential nuclease-like motif sequence identified within the *S. pombe* “Rad9-S” truncated protein variant – highly conserved amino residues (*X) may be critical to the function of this potential domain.

B: The potential M50 – M74 functional domain, identified within the *S. pombe* Rad9 protein in this study (discussed in detail previously in Chapter 5, Section 5.5, pp.475-481 and Chapter 6, Section 6.4, pp.568-583) contains three of the conserved potential nuclease-like motif amino acid residues (*X) – which correspond to the equivalent positional residues M1 – M24 in the “Rad9-S” truncated protein variant.

This novel functional domain also contains an identified key Tyrosine residue (at position Y61 in the full-length Rad9 protein, which corresponds to position Y12 in the “Rad9-S” truncated protein variant) which has a high phosphorylation potential probability score and may be a novel target for the dual Monopolar Spindle Checkpoint Kinase, Mph1 – NetPhosK software prediction (discussed previously in Chapter 6, Section 6.4, pp.568-583).

C: Comparative acute cell survival assays, performed with 40µM S-(+)-Camptothecin (Methodology described in Chapter 2, Section 2.9.2.2(ii), pp.239-241, p.248) indicate that the “Rad9-S-(Y12F)” mutant truncated protein variant is significantly more sensitive to CPT-induced DNA damage than either the full-length Rad9 protein or the “Rad9-S” truncated protein variant.

D: Postulated hypothetical “working model” for Mph1-mediated activation of the identified potential “nuclease-like” functional domain within the *S. pombe* truncated “Rad9-S” protein variant.

Mph1-mediated phosphorylation of residue Y12 within the “Rad9-S” truncated protein variant induces supramolecular configurational changes within its “nuclease-like” functional domain which may expose a potential binding site for associative interactions with nuclease enzymes implicated in double-stranded DNA (DSB) break repair pathways and/or expose a catalytic nuclease active site for 3'-5'-exonuclease DNA degradation in proximity to DSB lesion site as part of a co-ordinated DSB repair pathway in response to CPT-induced DNA damage.

7.2 Rad16 Endonuclease and DNA Ligase IV are Critical Components that are Functionally-Implicated in the DNA Repair Mechanism Mediated by the Heterodimeric “Rad9-S”：“Hus1-C” Complex in Response to Camptothecin-Induced Genotoxicity

The topoisomerase I inhibitor S-(+)-camptothecin (CPT) forms a stable, cleavable covalent topoisomerase I-CPT-DNA-trapped transition-state intermediary complex via associative interactions between the topoisomerase I protein and the DNA substrate bound within the enzymatic active site and specifically inhibits the re-ligation reaction with consequential formation of single-stranded DNA breaks at the stalled replication fork during S-phase in the “first/initial” cell cycle (Fig 7.3, p.674).

Propagated collision of these complex-stalled replication forks, during successive rounds of cell cycle S-phase, results in the conversion of these initial stabilised Topoisomerase I-induced single-stranded DNA breaks into one-sided double-stranded DNA breaks (DSBs) respectively (Nakagawa H. *et al*, 2006) – Fig 7.3, p.674.

The endonucleases Mus81-Eme1, Rad16-Swi10 and Mre11 (which functions within the “MRN”; Mre11-Rad50-Nbs1 complex – whose role in the repair of DSBs was discussed previously in Chapter 1, Section 1.2.5, p.106) are implicated in the rectification of CPT-induced DNA damage and act in parallel DNA repair pathway mechanisms (Deng C.C. *et al*, 2005; Liu C.Y. *et al*, 2002; Hartsuiker E. *et al*, 2009) – Fig 7.3, p.674.

Whilst the enzyme tyrosyl-DNA-phosphodiesterase I (Tdp1) mediates the removal of the “CPT-trapped” topoisomerase I-DNA complex type lesion at the stalled replication fork via catalyzed hydrolysis of the covalent phosphodiester bond between the 3’-end of the DNA and a key tyrosine residue situated within the active-site of the topoisomerase I enzyme (Deng C.C. *et al*, 2005; Liu C.Y. *et al*, 2002; Hartsuiker E. *et al*, 2009) – Fig 7.3, p.674.

The enzyme DNA ligase IV is also required for covalent annealing of the rectified DNA fragments, generated as a consequence of the “nuclease-processed” DSB termini, which is the critical final step in the respective repair mechanism (discussed previously in Chapter 1, Section 1.2.5, p.109).

The experimental *S. pombe* double-mutant strains; *rad9-S Δlig IV*, *rad9-S Δmus81*, *rad9-S Δrad16*, *rad9-S Δtdp1* (where *rad9-S* = *NA49-rad9-c3xHA*), were constructed and utilised in comparative acute viable cell survival assays with 40µM S-(+)-camptothecin with the “cre-lox”-constructed *S. pombe* strains *Δrad9* (“Cre-Lox” *rad9*-deleted base-strain), *rad9-c3xHA* and *NA49-rad9-c3xHA* in order to ascertain whether any of these enzymes were implicated in a novel “Rad9-S”-mediated mechanistic repair response to CPT-induced DNA damage – Fig 7.4 , p.675.

The acquired experimental data revealed that deletion of *rad16* or *ligIV* within an exclusively expressed “*rad9-S*” genetic background enhanced the sensitivity of the cells to camptothecin-induced DNA damage, which indicated that both these enzymes may be functionally implicated in a novel DNA repair pathway instigated by the heterodimeric “Rad9-S”：“Hus1-C” “open-ring/C-clamp” complex response to CPT-induced genotoxicity (Fig 7.4, p.675).

In contrast, these acute survival assay data also revealed that deletion of *Δmus81* and *Δtdp1* within an exclusively expressed “*rad9-S*” genetic background, did not enhance the sensitivity of the cells to camptothecin-induced DNA damages, which indicated that these enzymes were not functionally implicated in the DNA repair mechanism elicited by the heterodimeric “Rad9-S”：“Hus1-C” “open-ring/C-clamp” complex response to CPT-induced genotoxicity (Fig 7.4, p.675).

The mechanistic processes of DSB repair also involve the transient formation of DNA topological structures, such as D-loops (in the case of Homologous Recombination pathways) and/or the deletion and insertion of DNA fragments of variable base-pair length (in the case of NHEJ, MMEJ and SSA pathways) – discussed previously in Chapter 1, Section 1.2.5, p.109.

The U.V. Damage Endonuclease (UVDE) is a versatile enzyme implicated in DNA repair which recognises and excises specific types of DNA lesions – notably; abasic sites, mis-matched base-pairs, short single-stranded loops and various U.V.–induced base-dimerised DNA adducts, including Cis-Syn, Trans-Syn-I, 6,4-Photoproducts and Dewar Types of inter-strand and intra-strand Thymidyl-dimeric cross-linked adduct species (Davey S. *et al.*, 1998; Knauer B. and Doetsch P.W., 2000; Kunz C. and Fleck O., 2001; Ribar B. *et al.*, 2004).

Thus, the possibility was considered that novel UVDE–“Rad9-S” interactions may also be implicated in various DSB repair pathways, with respect to the removal of D-Loops in homologous recombination-mediated re-initiation of DNA replication in CPT-stalled replication forks.

The experimental *S. pombe* double-mutant strain; *rad9-S Δuvde* was constructed and utilised in comparative acute viable cell survival assays with 40μM S-(+)-camptothecin with the “cre-lox”-constructed *S. pombe* strains *Δrad9* (“Cre-Lox” *rad9*-deleted base-strain), *rad9-c3xHA* and *N149-rad9-c3xHA* in order to ascertain whether this enzyme was functional component of a novel “Rad9-S”-mediated mechanistic repair response to CPT-induced DNA damage – Fig 7.4 , p.675.

The acquired experimental data revealed that deletion of *uvde* within an exclusively expressed “*rad9-S*” genetic background did not enhance the sensitivity of the cells to camptothecin-induced DNA damage, which indicated that the UVDE enzyme was not functionally implicated in a novel DNA repair pathway instigated by the heterodimeric “Rad9-S”：“Hus1-C” “open-ring/C-clamp” complex response to CPT-induced genotoxicity (Fig 7.4, p.675).

In *H. sapiens* (Hs), the ATM primary (proximal) transducer checkpoint kinase is the principle initiator of DNA damage signal responses that are implicated in the downstream activation of “MRN” complex-mediated DSB repair pathways (discussed previously in Ch.1, Section 1.2.2, pp.33-65) – in which ATM is also activated in checkpoint responses to transcription- and/or camptothecin- induced DSB formation (Sordet O. *et al.*, 2009).

The equivalent ATM functional protein homolog in *S. pombe* (Sp) is the primary (proximal) transducer checkpoint kinase Tel1, whilst component functional homologs of the “MRN” complex are Rad32^{Sp} (Mre11^{Hs}), Rad50^{Sp} (Rad50^{Hs}) and Nbs1^{Sp} (Nbs1^{Hs}) respectively.

Comparative acute survival assays performed with YEA broth cell cultures of the *S. pombe* strains $\Delta rad9$, *rad9-c3xHA*, *rad9-S* and *rad9-S $\Delta tel1$* , in the presence of 40 μ M CPT, indicated that both the *rad9-S* and *rad9-S $\Delta tel1$* strains exhibited a similar degree of cytotoxic sensitivity to CPT such that Tel1 is unlikely to be implicated in the “Rad9-S”-mediated signal pathway response to CPT-induced DNA damage (discussed previously in Chapter 6, Section 6.2.3, pp.516-531).

On the basis of this experimental observation, in conjunction with the time constraints of the Ph.D. project and prioritised laboratory work, experimental construction and investigation of the relative CPT cytotoxic sensitivity of *S. pombe rad9-S* double-mutants with perturbed MRN complex activities – such as *rad9-S rad32D65N* (catalytically-inactive Rad32 endonuclease mutant), *rad9-S $\Delta rad50$* , *rad9-S rad50S* (functionally-inactive Rad50 mutant) and *rad9-S $\Delta nbs1$* was not undertaken (although this experimental work may yield potentially useful data in future research).

Fig 7.3: Key Proteins Implicated in the Repair of CPT-Induced DSBs

[Figure Constructed via Collated Information From: Hartsuiker E. *et al*, 2009

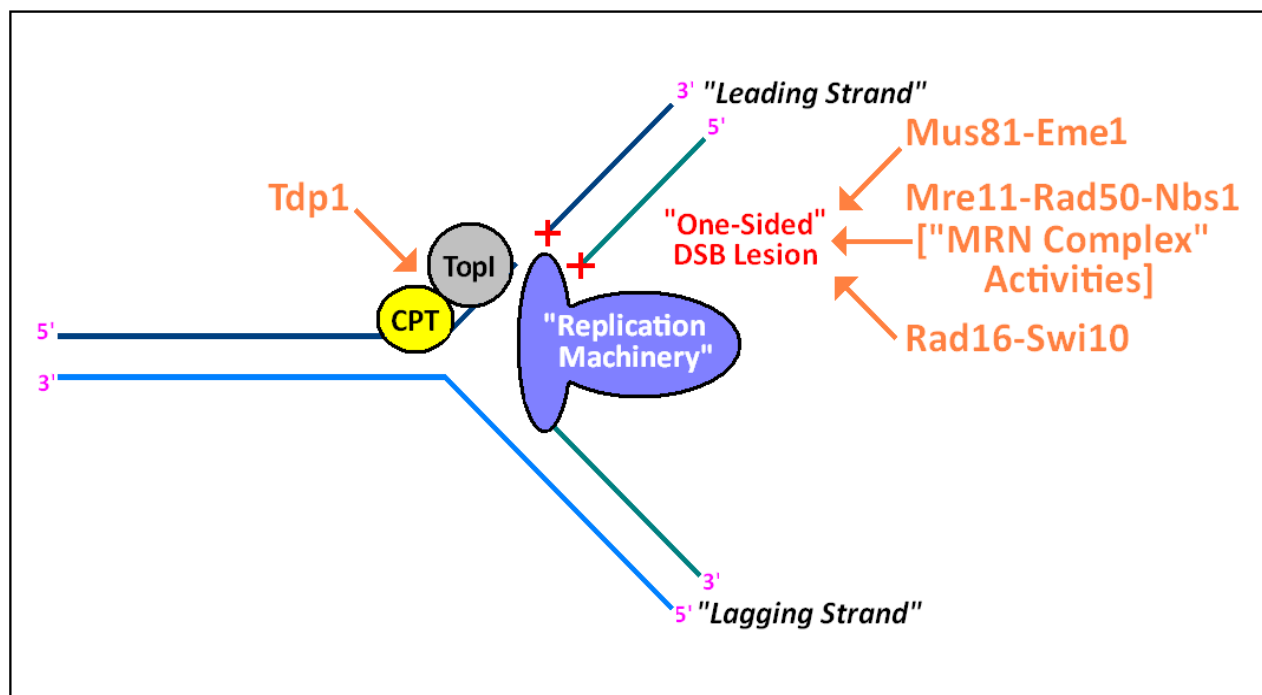
He X. *et al*, 2007

Nakagawa H. *et al*, 2006

Perego P. *et al*, 2012

Pommier Y., 2006

Regairaz M. *et al*, 2011



Unwinding of the DNA duplex during replication in S-phase results in negative and positive supercoiled torsional strain which is alleviated by the enzyme Topoisomerase I.

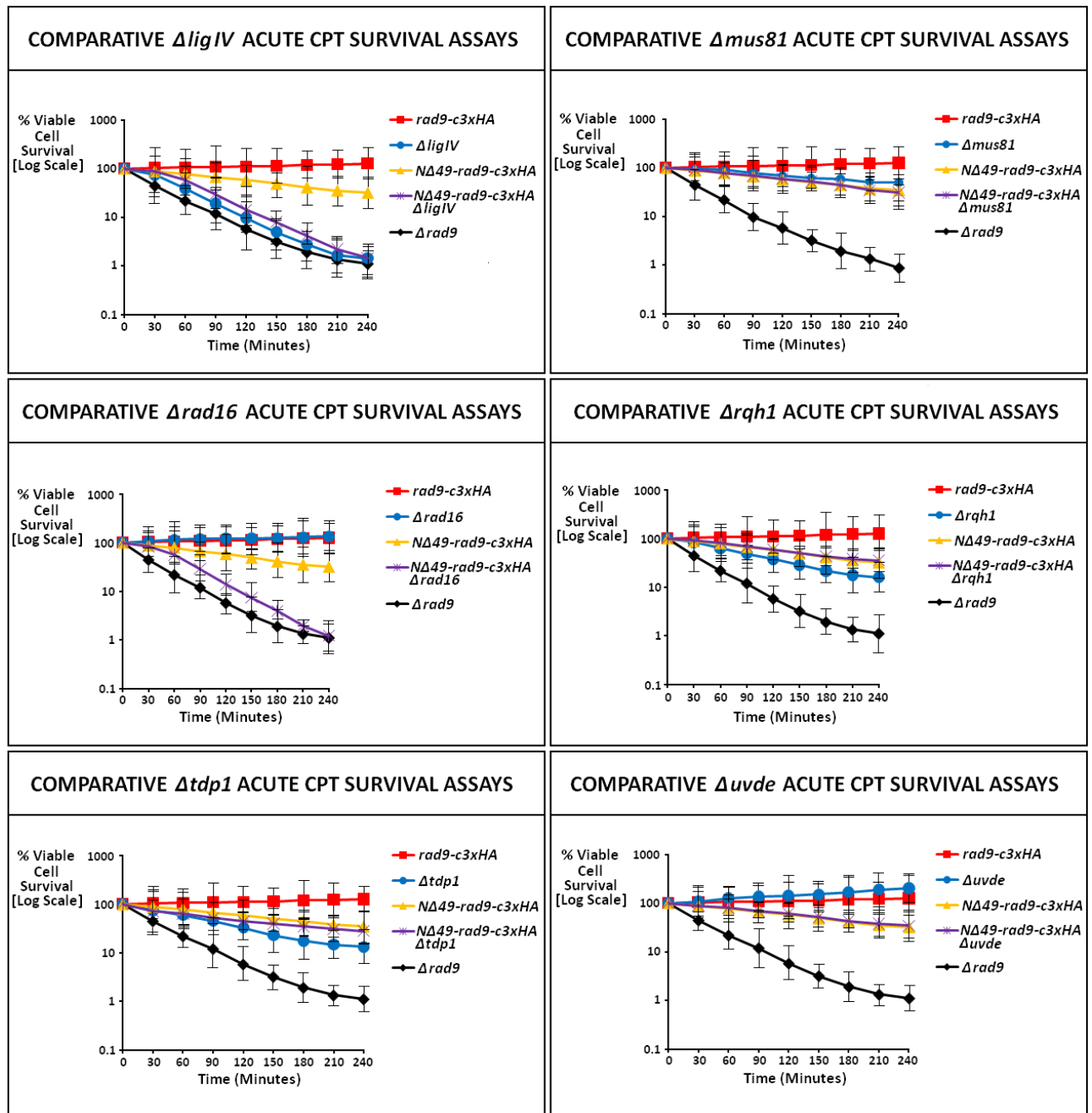
Topoisomerase I catalyses the hydrolysis of phosphodiester backbone, via formation of a transient covalent phospho-tyrosine linkage between the 3'-terminus of the DNA strand and a critical Tyrosine residue within its active site, prior to passage of the opposing strand through the gap site of the cleaved strand and subsequent re-ligation of the the cleavage site which is also performed by this enzyme (He X. *et al*, 2007)

S-(+)-Camptothecin (CPT) binds to this transient covalent protein-DNA intermediate to form a stable, cleavable covalent Topoisomerase I-CPT-DNA-trapped transition-state intermediary complex via associative interaction between Topoisomerase I and DNA within the enzymatic active site and specifically inhibits the re-ligation reaction, with resultant collision of replication forks during the cell cycle S-phase and consequential conversion of the initial stabilised Topoisomerase I-induced single-stranded DNA breaks into one-sided double-stranded DNA breaks (DSBs) respectively (Nakagawa H. *et al*, 2006).

Cleavage removal of the resultant Topoisomerase I-CPT-DNA-trapped transition state intermediate is effected via the enzyme Tyrosyl-DNA-Phosphodiesterase (Tdp1), which catalyzes the hydrolysis of the phospho-Tyrosine linkage between the 3'-terminus of the DNA strand and a critical Tyrosine residue within the active site of Topoisomerase I, with consequential liberation of the enzyme from the stalled replication fork (Deng C.C. *et al*, 2005; Hartsuiker E. *et al*, 2009; Liu C.Y. *et al*, 2002; Perego P. *et al*, 2012).

The endonuclease enzymes Mre11 – whose activities are co-ordinated within the Mre11-Rad50-Nbs1 ("MRN") complex), Mus81-Eme1 and Rad16-Swi10, are all implicated in the rectification of CPT-Induced DSBs and function in parallel DNA repair pathways (Deng C.C. *et al*, 2005; Hartsuiker E. *et al*, 2009; Liu C.Y. *et al*, 2002; Regairaz M. *et al*, 2011).

Fig 7.4 Acute CPT Survival Assays – Nuclease and Ligase IV Mutants



[Acute cell survival assays were performed as per the methodology described in Chapter 2, Section 2.9.2.2(ii), pp.239-241]

7.3 Rqh1 Helicase is Not Functionally-Implicated in the DNA Repair Mechanism Mediated by the Heterodimeric “Rad9-S”：“Hus1-C” Complex in Response to Camptothecin-Induced Genotoxicity

In *H. sapiens* the DNA helicase BLM is implicated in the cell-cycle phase-dependent suppression or promotion of Homologous Recombinational Repair (HR) of double-stranded DNA breaks (DSBs) – discussed in detail in Fig 7.5, p.678.

BLM also has associated functional roles in both the regression and recombination-mediated replication re-initiation of stalled DNA replication forks (Sun W. *et al*, 2008) – discussed in detail in Fig 7.6, p.679.

The equivalent functional protein homolog of BLM, implicated in the repair of DSBs in *S.pombe*, is the DNA helicase Rqh1 (Fig 7.5, p.678 and Fig 7.6, p.679).

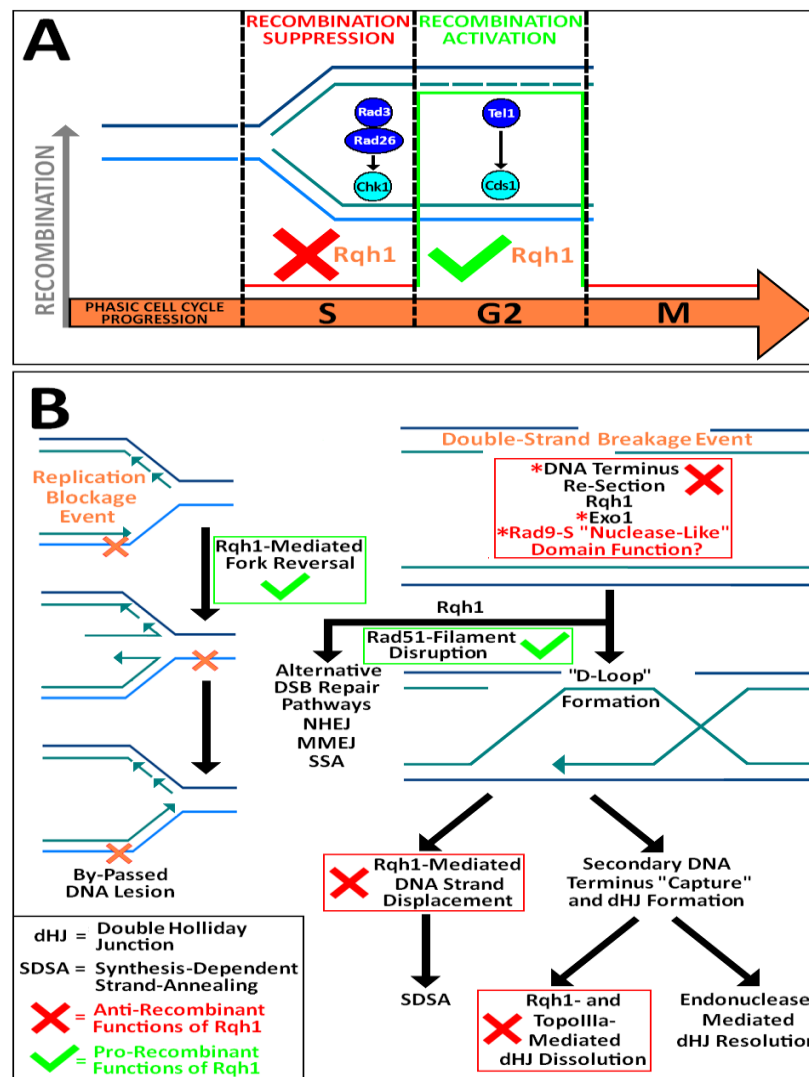
The experimental *S. pombe* double-mutant strain; *rad9-S Δrqh1* was constructed and utilised in comparative acute viable cell survival assays with 40µM S-(+)-camptothecin with the “cre-lox”-constructed *S. pombe* strains *Δrad9* (“Cre-Lox” *rad9*-deleted base-strain), *rad9-c3xHA* and *N149-rad9-c3xHA* in order to ascertain whether this enzyme was a functional component of a novel “Rad9-S”-mediated mechanistic repair response to CPT-induced DNA damage – Fig 7.7 , p.680.

The acquired experimental data revealed that deletion of *rqh1* within an exclusively expressed “*rad9-S*” genetic background did not enhance the sensitivity of the cells to camptothecin-induced DNA damage, which indicated that this helicase was not functionally implicated in in a novel DNA repair pathway instigated by the heterodimeric “Rad9-S”：“Hus1-C” “open-ring/C-clamp” complex response to CPT-induced genotoxicity (Fig 7.7, p.680).

Whilst the acute survival assay data indicated that Rqh1 was unlikely to be required for the potential “Rad9-S”-mediated repair response to camptothecin-induced DNA damage, the possibility that other helicase such as Srs2^{Sp} (RQHL5^{Hs}) and/or Fbh1^{Sp} (Laursen L.V. *et al.*, 2003a; Laursen L.V. *et al.*, 2003b; Osman F. *et al.*, 2005) may be implicated cannot be ruled out – which may warrant further investigation in future experimental work.

Fig 7.5: Pro- and Anti- Recombinant Functions of the Rqh1 Helicase

[Compiled via Collated Information From: Aylon Y. *et al*, 2004; Barlow J.H. *et al*, 2008; Finn K. *et al*, 2012; Goldwasser F. *et al*, 1996; Ira G. and Hastings P.J., 2012; Karran P., 2000; McGowan C.H. *et al*, 2003; Maki K. *et al*, 2011; Meister P. *et al*, 2005; Michel B. *et al*, 2007]



A: The ATR→Chk1-initiated Intra-S Phase Checkpoint Pathway (discussed previously in Chapter 1, Section 1.2.2, p.58) elicits stalled DNA replication fork stabilization with consequential suppression of recombination during DNA replication (in *S. pombe* this is the homologous equivalent Rad3→Chk1 pathway – discussed previously in Chapter 1, Section 1.2.2, p.59 and Chapter 6, Section 6.2, pp.489-492).

B: DNA helicases such as BLM in *H. Sapiens* (equivalent functional homolog Rqh1 in *S. pombe*) possess the capability to either suppress or induce DNA recombination events dependent upon the particular phase of the cell cycle (Fig A).

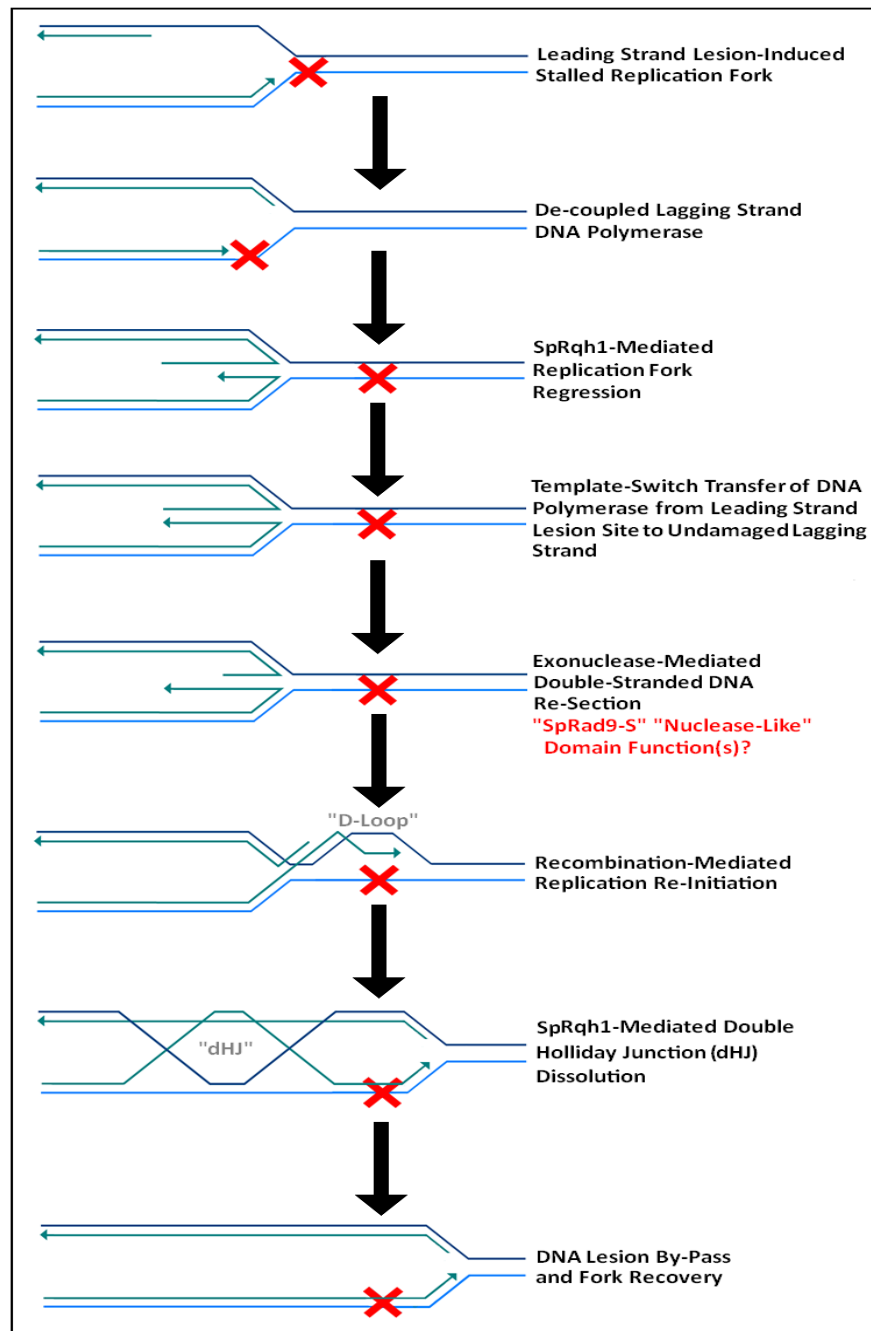
These types of DNA helicases inhibit homologous recombination at stalled replication forks via perturbation of Rad51 filaments and induction of alternative DNA repair pathways in which initial fork regression may be implicated.

In the case of double-stranded DNA breaks (DSBs), these types of helicases may suppress homologous recombination, via structural perturbation of Rad51 filaments and/or "D-Loop" formation, with consequential induction of alternative DSB repair pathways in the S-phase of the cell cycle.

Whilst in the G2 cell cycle phase, these types of DNA helicases may engage the homologous recombination repair pathway via promotional re-section of the DNA ends of the DSB lesion (in conjunction with Exonuclease I), prior to resolution of the double Holliday junctions (dHJ's) via co-ordinated, associative interactions with Topoisomerase III α (TopoIII α).

Fig 7.6: Regression-Coupled Recombination-Initiated Fork Recovery

[Taken and Adapted From: Ira G. and Hastings P.J., 2012; Sun W. *et al*, 2008]



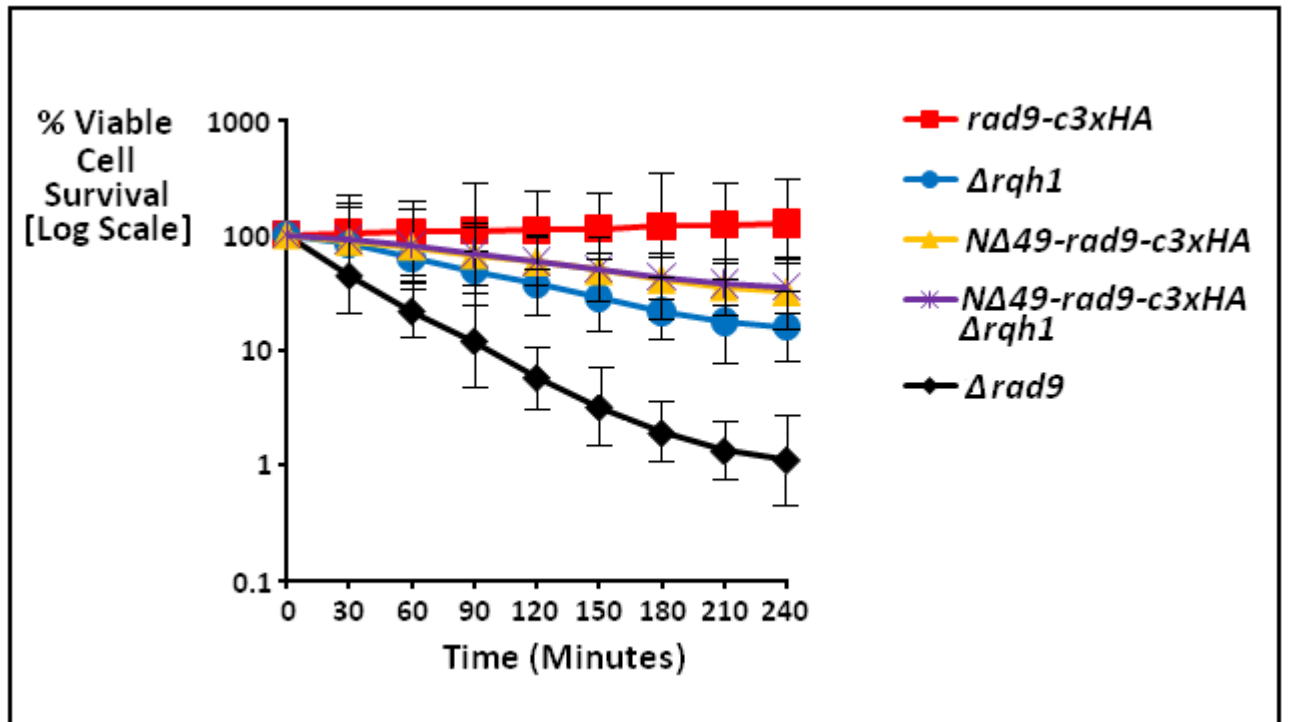
Formation of a CPT-trapped DNA-Topoisomerase I ternary complex type lesion on the leading strand template (Fig 7.3, p.674) during DNA replication inhibits fork progression with consequential uncoupling of DNA polymerases.

Regression of the resultant stalled replication fork, mediated via DNA helicases such as BLM in *H. Sapiens* (equivalent functional homolog Rqh1 in *S. pombe*), facilitates transitional template-switching transference from the damaged leading strand section to the "positional-equivalent" undamaged lagging strand to enable DNA lesion by-pass extension of the leading strand.

The resultant "reversed replication fork" is then reset via exonuclease I-mediated double-stranded DNA end re-section.

Rad51-mediated strand invasion of the extended template DNA, ahead of the by-passed DNA lesion, results in the formation of transient D-Loop and dHJ structures, which are dissolved via DNA helicases such as BLM in *H. Sapiens* (equivalent functional homolog Rqh1 in *S. pombe*), prior to fork recovery and initiated replication re-start.

Fig 7.7: Acute CPT Survival Assays *rqh1*-Deletion Mutants



[Acute cell survival assays were performed as per the methodology described in Chapter 2, Section 2.9.2.2(ii), pp.239-241]

7.4 The Heterodimeric “Rad9-S”：“Hus1-C” Complex May Elicit a Novel DNA Repair Pathway for the Rectification of Double-Stranded Breaks Induced by Camptothecin

The potential 3'-5' exonuclease catalytic activity of the “nuclease-like” motif domain, identified within the full-length Rad9 protein and “Rad9-S” truncated protein variant, remains to be confirmed experimentally in future research work.

If this identified Rad9 “nuclease-like” motif domain does indeed possess 3'-5' exonuclease catalytic activity, it may have functional interactive roles within the dsDNA end re-section phase of regression-coupled recombinant repair-mediated DNA replication re-initiation (Fig 7.5, p.678).

Taken together, these experimental data may indicate the existence of a novel DNA repair pathway in which the associative activities of Rad16 (and possibly other endonucleases), in conjunction with DNA ligase IV, exonuclease 1 and/or the potential 3'-5' exonuclease catalytic activity of the “nuclease-like” motif domain (situated within the “Rad9-S” truncated protein variant) engage in a co-ordinated recombination-mediated replication fork recovery/re-start mechanism which involves “template-switching”/TLS by-pass of the CPT-topoisomerase I-DNA complex type lesion, prior to repair of the CPT-induced one-sided double-stranded breaks (DSBs).

Recent experimental research indicates that the human ubiquitin ligase Rad18, which is implicated in the ubiquitination of PCNA in “template-switching”/TLS DNA repair mechanisms (discussed previously in Chapter 1, Section 1.2.5, pp.112-116), also interacts with ubiquitylated chromatin proteins and is implicated in the targeted localisation of the human Rad9A protein to DSB lesion sites, mediated via associative “Rad9 – Rad18 RING/Zinc-Finger” type interactions (Inagaki A. *et al.*, 2011).

Inagaki A. and co-workers (2011), also postulated that localisation of Rad18 to DSB lesion sites within the chromatin supramolecular structure proceeds via its associative interaction with ubiquitylated histone H2A sub-units, which facilitates Rad18-directed recruitment of human Rad9A to the DNA damage site.

Taken together, these experimental observations provide evidence for a potential direct functional role of human Rad9A in DSB repair, which acts outside of the canonical “9-1-1” complex, in a novel pathway that is independent of the downstream activation of the secondary (distal) transducer checkpoint kinases Chk1 and Chk2 respectively (Inagaki A. *et al*, 2011).

As discussed previously (Chapter 6, Section , pp.), deletion of the *chk1* gene in *S. pombe* cells engineered to exclusively express the “Rad9-S” truncated protein variant did not increase their cytotoxic sensitivity towards CPT-induced DNA damage in acute survival assays.

The “Rad9-S”- mediated response to CPT-induced DNA damage may comprise a co-ordinated pathway in which suppression of secondary (distal) transducer Chk1 kinase-initiated cell cycle checkpoint responses results in the alternative activation of a mitotic spindle checkpoint arrest (discussed previously in Chapter 6, Section 6.2.4, pp.539-546), prior to template-switching by-pass of the CPT-trapped topoisomerase I-DNA lesion complex and repair of the CPT-induced one-sided double-stranded DNA breaks (discussed summarily in the postulated hypothetical pathway models depicted in Fig 7.8, p.687 and Fig 7.9, pp.688-689).

It is possible that Rad18 and ubiquitylated H2A histone sub-units may also be implicated in the associative recruitment of “Rad9-S” to CPT-induced double-stranded break sites within the chromatin supramolecular structure, via a similar mechanism to that proposed recently by Inagaki A. *et al*, 2011.

Hsk1^{Sp} kinase (Cdc7^{Hs}) –mediated phosphorylation of Rad9^{Sp} has been postulated to be a critical pre-requisite for dissociation of the canonical Rad9-Rad1-Hus1 complex from chromatin, after initial DNA damage detection and subsequent initiation of the appropriate cell cycle checkpoint signal response, for the unhindered access of the DNA repair machinery to the lesion site (Furuya K. *et al*, 2010; Paek A.L. and Weinert T., 2010) – discussed previously in Chapter 1, Section 1.2.5, p.118.

The Hsk1^{Sp} kinase, in conjunction with Cdc45, also has regulatory functions in the modulation of DNA replication stress-induced responses (discussed previously in Chapter 1, Section 1.2.2, pp.33-65) – notably; the efficient initiation of DNA replication and activation of the Cds1^{Sp} (Chk2^{Hs}) secondary (distal) transducer checkpoint kinase (Matsumoto S. *et al*, 2010; Vaziri C., 2010).

Comparative acute survival assays performed with *rad9-S (N149-rad9-c3xHA)* and *rad9-S Δcds1 S. pombe* strains indicated that deletion of the *cds1* gene within an exclusively expressed *rad9-S* genetic background significantly increased the sensitivity of the cells to CPT-induced DNA damage (discussed previously in Chapter 6, Section 6.2.4, pp.539-546).

Numerous experimental attempts to construct the *rad9-S Δhsk1 S. pombe* strain, for utilisation in comparative acute CPT survival assays, resulted in the generation of non-viable/dead cells.

Taken together, these experimental observations may be indicative that Hsk1 kinase-mediated phosphorylation of the “Rad9-S” protein is a critical functional requirement which enables the postulated Rad9-S–Hus1 heterodimeric complex to disengage from DNA, in order to provide unhindered access of the DNA repair machinery to the DSB lesion site(s) and/or modulate the Rad9-S–initiated mitotic spindle checkpoint pathway to enable re-initiation of DNA replication and cell cycle progression after DNA repair has been accomplished.

Alternatively, deletion of the *hsk1* gene within an exclusively expressed *N149-rad9-c3xHA* (“*rad9-S*”) genetic background may result in the generation of non-viable cells as a consequence of a dysfunctional “Rad9-S”-initiated mitotic spindle checkpoint pathway due to suppressed Cds1 activation.

Topoisomerase I is also implicated in the modulation of gene expression, in which the enzyme may mediate global and local alterations within the topological supercoiling configuration of the DNA that induce specific rearrangements within the chromatin supramolecular architecture (Durand-Dubief M. *et al*, 2010; Sun M. *et al*, 2000).

These topoisomerase I-mediated chromatin supramolecular structural reorganisation events involve co-operative interactions with the ATP-dependent chromatin modeller Hrp1^{Sp} (Chd1^{Hs}) which elicits dissociation of localised nucleosomal sub-assemblies from the DNA without the loss of histones, in conjunction with alterations to the DNA linking number topology (Durand-Dubief M. *et al*, 2010; Sun M. *et al*, 2000).

Recent studies have also indicated that topoisomerase I inhibitor-induced formation of Top1-Drug-DNA ternary complexes occurs preferentially in genes which encode splicing factors (Solier S. *et al*, 2010).

Taken these observed experimental phenomena into consideration, it is hypothetically conceivable that hyperthermic- and/or CPT- induced formation of trapped Top1-DNA ternary complexes and consequential generation of DSBs may result in rearrangements within the chromatin supramolecular architecture which may constitute a novel mechanism for the modulation of the expression, cytological levels and functional activities of the truncated “Rad9-S” and “Rad9-VS” protein isoforms that in turn may regulate the differential “Rad9-S”-mediated DNA damage checkpoint-coupled DNA repair responses to camptothecin-induced genotoxic and/or hyperthermally-induced replication stresses (discussed previously in detail in Chapter 6, Section 6.6, pp.588-597).

Thus, the possibility exists that the ATP-dependent chromatin modeller Hrp1^{Sp} may be implicated in novel “Rad9-S”-mediated mechanisms that regulate topoisomerase I-mediated chromatin supramolecular structural rearrangements which modulate the expression of specific genes – which may warrant further investigation in future experimental work.

Very recent experimental studies have also revealed that the heterotrimeric human Rad9A-Rad1-Hus1 toroidal DNA sliding-clamp complex is implicated in the functional recognition of palindromic-repeat homopurine-homopyrimidine DNA sequences which adopt non-canonical secondary duplex structures (such as hairpin loops, triplexes and G-quadruplexes) that induce polar-orientated replication fork stalling (Liu G. *et al*, 2012).

These experimental studies also revealed that the human Rad9A-Rad1-Hus1 toroidal DNA sliding-clamp complex, in conjunction with replication protein A (RPA) and the primary (proximal) transducer kinase ATR, elicits the Chk1-mediated G2/M arrest in response to these duplex topological conformer-induced stalled replication fork events (Liu G. *et al*, 2012).

This Chk1-mediated G2/M checkpoint arrest was suppressed via DNA repair nuclease-mediated excision of these palindromic-repeat homopurine-homopyrimidine DNA sequences (Liu G. *et al*, 2012).

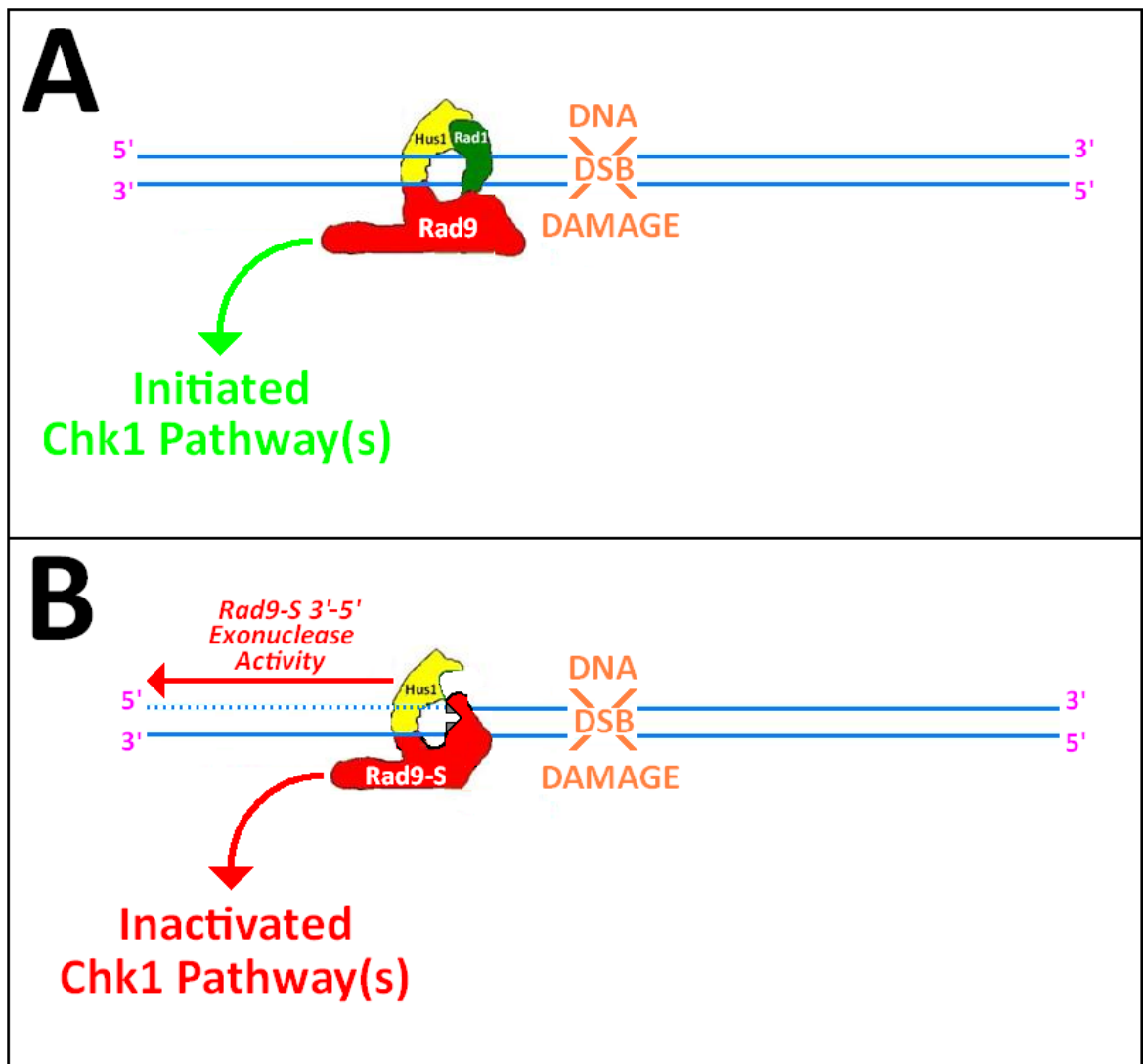
These types of palindromic-repeat homopurine-homopyrimidine DNA sequences were also found to invoke constitutive phosphorylation-mediated activation Chk1 that effected by-pass of the G2/M arrest response and enable continued cellular growth with consequential cytological cumulative propagation of genomic mutations which are responsible for the progressive development of tumour metastatic checkpoint adaptation (Liu G. *et al*, 2012).

Whether or not the human Rad9B paralogue and/or its truncated isoforms are implicated in similar DNA repair-coupled checkpoint responses to palindromic-repeat homopurine-homopyrimidine duplex conformer-induced DNA replication fork stalling events is unknown.

However, the postulated hypothetical models of “Rad9-S”-initiated checkpoint signalling and DNA repair responses to camptothecin-induced DNA damage (Fig 7.8, p. 687 and Fig 7.9, pp.688-689) may be indicative of homologously-equivalent functional processes which are mediated by the human Rad9B paralogue and/or its truncated isoforms.

Further “in-depth” experimental investigation of these phenomena, in conjunction with the data acquired in this Ph.D. project, may provide useful insights for the future development of novel topoisomerase I inhibitor classes of anti-cancer chemotherapeutics (such as sequence-specific base-pair mimetics) with enhanced pharmacodynamic properties (Drawl M. *et al*, 2011; Pourquier P. and Langsiaux P., 2011; Vekhoff P. *et al*, 2012) and whose respective anti-neoplastic cytotoxic efficacies are not attenuated via potential Rad9B-initiated metastatic tumour multi-drug resistance mechanisms.

Fig 7.8: Model of Rad9-S “Nuclease-Mediated” Chk1 Suppression



A: Full-length Rad9^{Sp} (Rad9^{Hs}) associates with the Hus1^{Sp} (Hus1^{Hs}) and Rad1^{Sp} (Rad1^{Hs}) proteins to form the heterotrimeric PCNA-like toroidal “9-1-1” sliding-clamp complex which detects the CPT-induced DNA damage lesion site and initiates the Chk1^{Sp} (Chk1^{Hs})-mediated G2/M checkpoint cycle cell arrest response (discussed in further detail in Fig 7.9, pp.688-689).

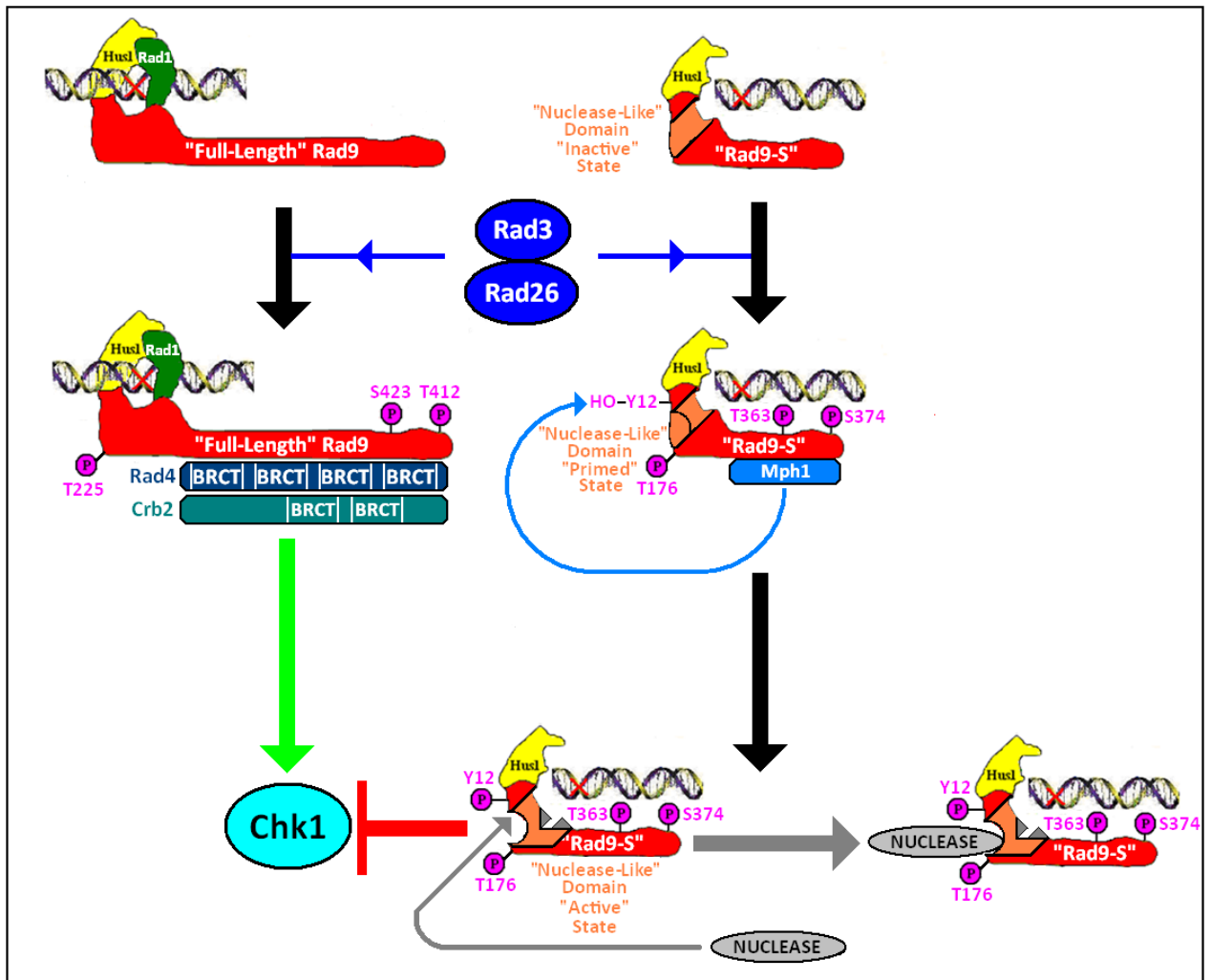
B: The truncated Rad9^{Sp} protein variant “Rad9-S^{Sp}” lacks the first 49 N-Terminal amino acids, which constitute the the major component of the PCNA-Like Domain I region that is implicated in associative interactions with the Rad1^{Sp} protein.

In this case “Rad9-S^{Sp}” forms an associative heterdimeric “partial open-ring” complex with Hus1^{Sp} (Hus1^{Hs}) which interacts with the DNA at the CPT-induced DSB lesion site.

The “nuclease-like” domain, situated within the “Rad9-S^{Sp}” sub-unit of the resultant ternary DNA complex (ie “Rad9-S^{Sp}”:Hus1^{Sp}:DNA complex) may possess 3'-5' exonuclease activity which degrades the terminal end of the CPT induced DSB lesion in a novel mechanism of DSB repair (discussed in detail in Fig 7.9, pp.688-689).

The “Rad9-S^{Sp}” truncated protein variant may also be implicated in suppression of the functional activities of the secondary (distal) transducer checkpoint kinase Chk1^{Sp} (Chk1^{Hs}) in a novel response to CPT-induced DNA damage which involves an “Rad9-S^{Sp}”-initiated mitotic spindle checkpoint arrest to enable sufficient time for completion of a novel “Rad9-S^{Sp}”-co-ordinated mechanism of CPT-induced DSB lesion repair (discussed in detail in Fig 7.9, pp.688-689).

Fig 7.9: “Rad9-S” Co-Ordinated Chk1 Suppression & DNA Repair



Full-length Rad9^{Sp} (Rad9^{Hs}) associates with the Hus1^{Sp} (Hus1^{Hs}) and Rad1^{Sp} (Rad1^{Hs}) proteins to form the heterotrimeric PCNA-like toroidal “9-1-1” sliding-clamp complex which detects the CPT-induced DNA damage lesion site.

Primary (proximal) transducer checkpoint Rad3^{Sp} (ATR^{Hs}) kinase-mediated phosphorylation of the full-length Rad9^{Sp} sub-unit (at residues T225, T412 and S423), within the 9-1-1 complex, induces supramolecular configurational changes within the protein which enable its C-Terminal Tail domain to interact associatively with the BRCT domains of the Rad4^{Sp} (TopBP1^{Hs}) mediator protein.

“9-1-1” complex-mediated recruitment of the Rad4^{Sp} (TopBP1^{Hs}) protein to the detected CPT-induced DNA damage lesion site enables recruitment of the Crb2^{Sp} (BRCA1^{Hs}) protein via associative BRCT domain interactions with the SpRad9 sub-unit C-Terminal-bound Rad4 protein for activation of the secondary (distal) transducer checkpoint kinase Chk1 which elicits a G2/M cell cycle arrest signal response – discussed previously in Chapter 1, Section 1.2.2, p.57.

The SpRad9 truncated protein variant, “Rad9-S^{Sp}”, associates with Hus1^{Sp} to form a heterodimeric “partial open-ring” DNA-binding complex at the CPT-induced DNA damage lesion site, prior to phosphorylation of the “Rad9-S^{Sp}” sub-unit by the Rad3 kinase (at the equivalent residue positions T176, T363 and S374) to induce supramolecular configurational changes within the protein that enable its C-Tail Terminal Domain to interact associatively

with the Monopolar Spindle Checkpoint Effector Kinase Mph1^{Sp} (Mps1^{Hs}/TTK^{Hs}), in which the resultant ternary complex “primes” the “Rad9-S^{Sp}” “nuclease-like” domain for Mph1^{Sp} kinase phosphorylation-mediated activation.

Subsequent Mph1^{Sp} kinase-mediated phosphorylation of “Rad9-S^{Sp}” (at residue Y12) induces further supramolecular configuration changes within the protein to expose its “nuclease-like” domain for facilitated interaction with nucleases, such as Rad16^{Sp} which are implicated in the repair of CPT-induced DSBs.

Mph1^{Sp} kinase mediated phosphorylation of “Rad-S^{Sp}” (at residue Y12) may also induce localised supramolecular changes within the “nuclease-like” domain of the protein that are required for initiation of its potential catalytic 3’-5’-exonuclease activity – which may be implicated in the associative repair of CPT-induced DSBs with endonucleases such as Rad16.

The resultant phosphorylated form of the “Rad9-S” protein (ie phosphorylated at residues Y12, T176, T363, and S374) may also maintain the protein in a supramolecular configuration state which inhibits the functional activities of the secondary (distal) transducer checkpoint kinase SpChk1 and initiation of Mitotic Spindle Checkpoint type cell cycle arrest (discussed in detail previously in Chapter 6) to enable time for “Rad9-S”-mediated repair of the CPT-induced DSB lesion in a novel mechanism that may involve the associative co-ordination of functional interactions of the potential “Rad9-S^{Sp}” catalytic 3’-5’ exonuclease activity, Rad16^{Sp} and other endonucleases, DNA Lig IV^{Sp}, in conjunction with other protein factors – which remains to be elucidated.

Chapter 8

Evaluative Discussion

8.1 Critical Appraisal of the Acquired Experimental Data

The investigation of potential novel Rad9 isoforms and functions in this research work was accomplished via utilisation of “cre-lox”-generated experimental *S. pombe* strains whose cells were engineered for the excluded expression of the full-length Rad9 protein such that they were “pre-programmed” for “forced reliance” upon the adaptive cytological employment of the truncated Rad9 variants; “Rad9-S”, Rad9-VS” and “Rad9-T”.

The relative levels and associated functions of these truncated Rad9 variants under cytological conditions of genotoxic and/or environmental stresses, in the presence of unhindered expression of the full-length Rad9 protein and full-length Rad9-Rad1-Hus1 complex formation, may therefore differ significantly from those identified in this Ph.D. project.

Nevertheless, the acquired experimental data may be indicative of several adaptive compensatory truncated Rad9 isoform-mediated “auxiliary” checkpoint responses to genotoxically- and thermally- induced cytological stresses in which expression of the full-length Rad9 protein and/or formation of the full-length Rad9-Rad1-Hus1 complex is perturbed – notably;

- (i) A novel checkpoint pathway whose signalling functions are coupled and co-ordinated with the specific functions of a novel DNA repair mechanism, via an “open-ring/C-clamp”-type “Rad9-S”-Hus1 heterodimeric complex.

- (ii) A novel checkpoint signalling pathway in response to hyperthermally-induced cytological stresses, mediated via an alternative “Rad9-S”-Rad1-Hus1 heterotrimeric complex which may adopt distinctive functional “closed-ring clamp” and/or “open-ring/split-washer clamp” type supramolecular configurations.

(iii) “Rad9-S” phosphoisoformic-modulated expression of the novel truncated Rad9 protein variants; “Rad9-VS” and “Rad9-T” – whose functions are unknown, but which may be implicated in the regulation of various checkpoint protein activities, including those of full-length Rad9 and “Rad9-S”.

Future comparative experimental studies into the specific functional properties of the “Rad9-S”, “Rad9-VS” and “Rad9-T” truncated protein variants, under conditions of induced and suppressed full-length Rad9 protein activities in the absence and presence of particular types of genotoxic and environmental cytological stresses, may provide valuable insights into the roles of the full-length human Rad9B paralogue and its isoforms in the suppression, induction, promotion and progression of carcinogenesis.

8.2 Future Implications in the Clinical Management of Cancer

The clinical management of cancerous diseases necessitates the employment of a range of systemic-based treatments that often encompass both radiotherapeutic and chemotherapeutic combinatorial treatment regimens as a consequence of the heterogeneous nature of the tumours whose respective composite cells exhibit differential cytotoxic sensitivities towards ionising radiation and specific classes/types of anti-neoplastic drugs (Larsen I.K. and Kastrup J.S., 2002; Pecorino L. *et al*, 2008).

The majority of polychemotherapeutic regimens are anti-proliferative and consist of combinatorial classes of anti-neoplastic agents whose respective efficacious cytotoxic mechanisms of action are focused upon the induction of various genotoxic lesions or perturbation of replicative processes such that they are somewhat limited, pharmacologically, to the destruction of actively cycling cells (Larsen I.K. and Kastrup J.S., 2002; Pecorino L. *et al*, 2008).

Quiescent tumour cells in the dormant G₀ phase of the cell cycle may evade the induced cytotoxic effects of radiotherapeutic and chemotherapeutic treatments as a consequence of the transient cessation of DNA replication and thus retain their proliferative viability (Larsen I.K. and Kastrup J.S., 2002; Pecorino L. *et al*, 2008; Sherman M.Y. *et al*, 2011; Weinberg R.A., 2006;).

Regular clinical monitoring of cancer patients, typically over a 5 year remission period following apparently successful treatments, is therefore required for the early detection and appropriate management of relapse incidences in which the proliferative re-emergence of the dormant tumour cells results in the re-establishment of the neoplastic pathophysiological condition (Larsen I.K. and Kastrup J.S., 2002; Pecorino L. *et al*, 2008; Sherman M.Y. *et al*, 2001; Weinberg R.A., 2006).

The checkpoint protein, Rad9A, is also known to be implicated in the co-ordinated modulation of cell cycle checkpoint signalling pathways, DNA repair pathways and the maintenance of cytological senescence (Broustas C.G. and Lieberman H.B., 2012; Deshpande A.M. *et al*, 2011).

The major cell cycle checkpoint functions of human Rad9A are the initiation and/or modulation of intra-S and G2/M arrest, which are mediated via TopBP1-dependent ATR activation interactions and are also dependent upon the activities of Chk1, Chk2, p53, p21 and H2AX (Broustas C.G. and Lieberman H.B., 2012; Pérez-Castro A.J. and Freire R., 2012).

Whilst recent experimental studies have indicated that the cell cycle checkpoint functions of the human Rad9B paralogue are the initiation and/or modulation of G1/S arrest in response to nucleolar stress, that are mediated via “downstream” ATR and JNK signal transduction pathways which do not involve TopBP1-dependent ATR activation interactions and are not dependent upon the activities of of Chk1, Chk2, p53, p21 and H2AX (Pérez-Castro A.J. and Freire R., 2012).

Pharmacological modulation of these specific differential functions of the Rad9A and Rad9B checkpoint proteins may thus prove to be a useful future clinical approach to be implemented to enhance the cytotoxic sensitivity of tumour cells to particular radiotherapeutic and chemotherapeutic treatment regimens.

Intriguingly, the experimental data acquired in this Ph.D. project indicated that the expression of the novel *S. pombe* truncated “Rad9-S” protein variant was an exclusive heat shock response which was restricted to actively cycling cells within a 20 minute time interval of hyperthermic exposure.

Furthermore, these data indicated that this novel *S. pombe* “Rad9-S” truncated protein variant exhibited significant sequence homology to the *H. sapiens* Rad9B paralogue isoforms 2 and 3.

Whether or not expression of the *H. sapiens* Rad9B paralogue and/or its isoforms is also induced by hyperthermic stress is at present unknown, however taken together, these experimental data may be indicative of novel functions of the human Rad9B protein and/or its isoforms.

Anti-cancer drug-induced hypersensitivity reactions are relatively rare phenomena, with the notable exception of specific classes and types of chemotherapeutic agents which may elicit adverse side effects, such as severe nausea, fever, elevated body temperature (pyrexia), flushing, pruritis, rashes, cardiac arrhythmias, blood pressure fluctuations, back pain, bronchospasm and dyspnea, as a consequence of non-immune cytotoxic-mediated release of histamine and cytokines (Ruhlmann C.H. and Hersteddt J., 2011; Shepherd G.M., 2003).

Anti-neoplastic chemotherapeutic-induced hypersensitivity is a particularly common problem encountered with the clinical administration of the DNA alkylating agent procarbazine, the platinum complex-based DNA cross-linking agents cisplatin and carboplatin, the epipodophyllotoxin-derived topoisomerase II inhibitors etoposide and teniposide, the taxane-type mitotic inhibitor paclitaxel and asparaginase inhibitors (Ruhlmann C.H. and Hersteddt J., 2011; Shepherd G.M., 2003).

Cytotoxically-induced afebrile neutropenia, in conjunction with other immunosuppressant complications associated with the administration of anti-cancer chemotherapeutics, may also promote the proliferation of opportunistic bacterial infections with consequential pathophysiological manifestation of elevated body temperature (pyrexia) and fever (Gafer-Gvili A. *et al*, 2012).

These immunosuppressive-type toxicological side-effects may also be implicated in observed clinical cases of interstitial pneumonia-induced pyrexia in the treatment of aggressive cancerous conditions with camptothecin-based chemotherapeutics (Farray D. *et al*, 2006; Kuga Y. *et al*, 2011; Verschraegen C.F. *et al*, 2000; Yokota M. *et al*, 2010).

If hyperthermic-induced expression of human Rad9B and/or its isoforms does take place, then it is also hypothetically conceivable that chemotherapeutic-induced pyrexia could result in the expression of elevated levels of Rad9B and/or its isoforms within tumour cells which may be implicated in novel checkpoint and/or DNA repair responses which attenuate the cytotoxic efficacy of the administered anti-cancer drugs.

Current clinical management of anthracycline- and taxane- refractory metastatic breast cancer (ATRMBC) involves the administration of camptothecin-based topoisomerase I inhibitors and geldanamycin-based Hsp90 inhibitors (Dean-Columb W. and Esteva F.J., 2008).

The exclusive elevated expression of Rad9, but neither Hus1 or Rad1, is also a distinctive genotypic trait of aggressive ATRMBC-type tumour cells (Chan V. *et al.*, 2008; Cheng C.K. *et al.*, 2005).

The elucidated *S. pombe* “Rad9-S”-mediated signalling pathway responses to camptothecin-induced genotoxicity and thermal stress, in conjunction with identified potential roles of the truncated “Rad9-S” protein variant in the co-ordinated repair of camptothecin-induced DNA damage, may be implicated in the development and metastatic progression of refractory breast tumour cells which have acquired broad-spectrum multiple drug resistance.

Taken together, in the context of the experimental data acquired in this Ph.D. project, heat shock induction of the human Rad9B protein and/or its isoforms may be implicated in novel biochemical mechanisms of acquired tumour resistance to polychemotherapeutic and radiotherapeutic regimens that could also impinge adversely upon the clinical application of hyperthermic adjuvant strategies which potentiate the cytotoxic efficacies of these treatments (discussed in detail previously in Chapter 6, Section 6.7, pp.598-625).

Progressive research into the initial “pilot data” acquired from this Ph.D. project may provide vital information for the future treatment of chronic breast cancer patients administered camptothecin-derivatised agents to combat the metastatic spread of refractory tumours which have developed multiple drug resistance to the “conventional arsenal” of chemotherapeutic drugs utilised in standard clinical practice – such as taxols and anthracyclics.

REFERENCES

Journal & Bibliographical Citations

Internet-Based Electronic Resources

REFERENCES – Journal and Bibliographical Citations

Aboussekhra A., Biggerstaff M., Shivji M.K., Vilpo J.A., Moncollin V., Podust V.N., Protic M., Hubscher U., Egly J.M., Wood R.D. (1995), “Mammalian DNA Nucleotide Excision Repair Reconstituted with Purified Protein Components”, *Cell*, **80(6)**:859-868

Abraham R.T. (2001), “Cell Cycle Checkpoint Signalling Through the ATM and ATR Kinases”, *Genes and Development*, **15(17)**:2177-2196

Acharya S., Wilson T., Gradia S., Kane M.F., Guerrette S., Marsischky G.T., Kolodner R., Fishel R. (1996), “hMSH2 Forms Specific Mismatch-Binding Complexes with hMSH3 and hMSH6”, *Proceedings of the National Academy of Sciences U.S.A.*, **93(24)**:13629-13634

Acquaviva C. and Pines J. (2006), “The Anaphase-Promoting Complex/Cyclosome: APC/C”, *Journal of Cell Science*, **119(Pt.12)**:2401-2404

Adelman J.L., Chodera J.D., Kuo I.F., Miller T.F. 3rd, Barsky D. (2010), “The Mechanical Properties of PCNA: Implications for Loading and Function of a DNA Sliding Clamp”, *Biophysical Journal*, **98(12)**:3062-3069

Adkins M.W. and Tyler J.K. (2004), “The Histone Chaperone Asf1p Mediates Global Chromatin Disassembly *in Vivo*”, *Journal of Biological Chemistry*, **279(50)**:52069-52074

Adler A.J., Scheller A., Robins D.M. (1993), “The Stringency and Magnitude of Androgen-Specific Gene Activation are Combinatorial Functions of Receptor and Non-Receptor Binding Site Sequences”, *Molecular and Cellular Biology*, **13(10)**:6326-6335

Adler A.S., Lin M., Horlings M., Nuyten D.S., van der Vijver M.J., Chang H.Y. (2006), “Genetic Regulators of Large-Scale Transcriptional Signatures in Cancer”, *Nature Genetics*, **38(4)**:421-430

Agard N.J. and Wells J.A. (2009), “Methods for the Proteomic Identification of Protease Substrates”, *Current Opinion in Chemical Biology*, **13(5-6)**:503-509

Agostino P.V., Plano S.A., Golombek D.A. (2008), “Circadian and Pharmacological Regulation of Casein Kinase I in the Hamster Suprachiasmatic Nucleus”, *Journal of Genetics*, **87(5)**:467-471

Ahowesso C., Li X.M., Zampera S., Peteri-Brunbäck B., Dulong S., Beau J., Hossard V., Filipinski E., Delaunay F., Claustrat B., Lévi F. (2011), “Sex and Dosing-Time Dependencies in Irinotecan-Induced Circadian Disruption”, *Chronobiology International*, **28(5)**:458-470

Alani E., Sokolsky T., Studamire B., Miret J., Lahue R. (1997), “Genetic and Biochemical Analysis of Msh2p-Msh6p: Role of ATP Hydrolysis and Msh2p-Msh6p Subunit Interactions in Mismatch Base Pair Recognition”, *Mol. Cell. Biol.*, **17(5)**:2436-2447

Alao J.P. and Sunnerhagen P. (2008), “Rad3 and Sty1 Function in *Schizosaccharomyces pombe*: An Integrated Response to DNA Damage and Environmental Stress?”, *Molecular Microbiology*, **68(2)**:246-254

Alcasabas A.A., Osborn A.J., Bachant J., Hu F., Werler P.J., Bousset K., Furuya K., Diffley J.F., Carr A.M., Elledge S.J. (2001), “Mrc1 Transduces Signals of DNA Replication Stress to Activate Rad53”, *Nature Cell Biology*, **3(11)**:958-965

- Alderton G.K., Joenje H., Varon R., Borglum A.D., Jeggo P.A., O'Driscoll M. (2004), "Seckel Syndrome Exhibits Cellular Features Demonstrating Defects in the ATR-Signalling Pathway", *Human Molecular Genetics*, **13(24)**:3127-3138
- Alfa C., Fantes P., Hyams J., McLeod M., Warbrick E. (1993), "Experiments with Fission Yeast: A Laboratory Course Manual", 1st Edition, Cold Spring Harbour Laboratory Press
- Aligue R., Akhavan-Niak H., Russell P. (1994), "A Role for Hsp90 in Cell Cycle Control: Wee1 Tyrosine Kinase Activity Requires Interaction with Hsp90", *The EMBO Journal*, **13(24)**:6099-6106
- Allada R. and Meissner R.A. (2005), "Casein Kinase 2, Circadian Clocks and the Flight From Mutagenic Light", *Molecular and Cellular Biochemistry*, **274(1-2)**:141-149
- Altschul S.F., Madden T.L., Schäffer A.A., Zhang J., Zhang Z., Miller W., Lipman D.J. (1997), "Gapped BLAST and PSI-BLAST: A New Generation of Protein Database Search Programs", *Nucleic Acids Research*, **25(17)**:3389-3402
- Ammazzalorso F., Pirzio L.M., Bignami N., Franchitto A., Pichierri P. (2010), "ATR and ATM Differentially Regulate WRN to Prevent DSBs at Stalled Replication Forks and Promote Replication Fork Recovery", *The EMBO Journal*, **29(18)**:3156-3169
- An L., Wang Y., Liu Y., Yang X., Liu C., Hu Z., He W., Song W., Hang H. (2010), "Rad9 is Required for B Cell Proliferation and Immunoglobulin Class Switch Recombination", *Journal of Biological Chemistry*, **285(46)**:35267-35273
- Angeletti P.C. and Engler J.A. (1998), "Adenovirus Pre-Terminal Protein Binds to the CAD Enzyme at Active Sites of Viral DNA Replication on the Nuclear Matrix", *Journal of Virology*, **72(4)**:2896-2904
- Antoch M.P. and Kondratov R.V. (2010), "Circadian Proteins and Genotoxic Stress Response", *Circulation Research*, **106(1)**:68-78
- Antoch M.P., Kondratov R.V., Takahashi J.S. (2005), "Circadian Clock Genes as Modulators of Sensitivity to Genotoxic Stress", *Cell Cycle*, **4(7)**:901-907
- Aoki K. and Murayama K. (2012), "Nucleic Acid-Metal Ion Interactions in the Solid State", *Metal Ions Life Sciences*, **10**:43-102
- Araujo P.R., Yoon K., Ko D., Smith A.D., Qiao M., Suresh U., Burns S.C., Penalva L.O. (2012), "Before It Gets Started: Regulating Translation at the 5'-UTR", *Computational and Functional Genomics*, **electronic publication ahead of print, 2012:475731 (28th May 2012)**
- Araujo S.J., Tirode F., Coin F., Pospiech H., Syvaioja J.E., Stucki M., Hubscher U., Egly J.M., Wood R.D. (2000), "Nucleotide Excision Repair of DNA with Recombinant Human Proteins: Definition of the Minimal Set of Factors, Active Forms of TFIIH and Modulation by CAK", *Genes and Development*, **14(3)**:349-359
- Arioka M., Kouhashi M., Yoda K., Takasuki A., Yamasuki M., Kitamoto K. (1998), "Multidrug Resistance Phenotype Conferred by Overexpressing *brf2*⁺/*pad1*⁺/*sks*⁺ or *pap1*⁺ Genes and Mediated by *brf1*⁺ Gene Product, a Structural and Functional Homologue of P-Glycoprotein in *Schizosaccharomyces pombe*", *Bioscience, Biotechnology and Biochemistry*, **62(2)**:1437-1444

- Asaad N.A., Zeng Z-C., Guan J., Thacker J., Iliakis G. (2000), "Homologous Recombination as a Potential Target for Caffeine Radiosensitization in Mammalian Cells: Reduced Caffeine Radiosensitization in *XRCC2* and *XRCC3* Mutants", *Oncogene*, **19(50)**:5788-5800
- Ashby J., Brady A., Elcombe C.R., Elliott B.M., Ishmael J., Odum J., Tugwood J.D., Kettle S., Purchase I.F. (1994), "Mechanistically-Based Human Hazard Assessment of Peroxisome Proliferator-Induced Hepatocarcinogenesis", *Human and Experimental Toxicology*, **13 (Suppl. 2)**:S1-S117
- Aylon Y., Liefshitz B., Kupiec M. (2004), "The CDK Regulates Repair of Double-Strand Breaks by Homologous Recombination During the Cell Cycle", *The EMBO Journal*, **23(24)**:4868-4875
- Bai H., Madabushi A., Guan X., Lu A.L. (2010), "Interaction Between Human Mismatch Repair Proteins and Checkpoint Sensor Rad9-Rad1-Hus1", *DNA Repair (Amst.)*, **9(5)**:478-487
- Bakkenist C.J. and Kastan M.B. (2003), "DNA Damage Activates ATM Through Intermolecular Autophosphorylation and Dimer Association", *Nature*, **421(6922)**:499-506
- Balajee A.S., May A., Dianov G.L., Friedberg F.C., Bohr V.A. (1997), "Reduced RNA Polymerase II Transcription in Intact and Permeabilized Cockayne Syndrome Group B Cells", *Proceedings of the National Academy of Sciences U.S.A.*, **94(9)**:4306-4311
- Balakrishnan L., Brandt P.D., Lindsey-Boltz L.A., Sancar A., Bambara R.A. (2009), "Long Patch Base Excision Repair Proceeds via Coordinated Stimulation of the Multienzyme DNA Repair Complex", *Journal of Biological Chemistry*, **284(22)**:15158-15172
- Ballesta A., Dulong S., Abbara C., Cohen B., Okyar A., Clairambault J., Lévi F. (2011), "A Combined Experimental and Mathematical Approach for Molecular-Based Optimization of Irinotecan Circadian Delivery", *PLoS Computational Biology*, **7(9)**:e1002143
- Banavar J.R., Hoang T.X., Maddocks J.H., Maritan A., Poletto C., Stasiak A., Trovato A. (2007), "Structural Motifs of Biomolecules", *Proceedings of the National Academy of Sciences U.S.A.*, **104(44)**:17283-17286
- Bandyopadhyay K. and Gjerset R.A. (2011), "Protein Kinase CK2 is a Central Regulator of Topoisomerase I Hyperphosphorylation and Camptothecin Sensitivity in Cancer Cell Lines", *Biochemistry*, **50(5)**:704-714
- Banin S., Moyal L., Shieh S., Taya Y., Anderson C.W., Chessa L., Smorodinsky N.I., Prives C., Reiss Y., Shiloh Y., Ziv Y. (1998), "Enhanced Phosphorylation of p53 by ATM in Response to DNA Damage", *Science*, **281(5383)**:1674-1677
- Bao S., Tibbetts R.S., Brumbaugh K.M., Fang Y., Richardson D.A., Ali A., Chen S.M., Abraham R.T., Wang X.F. (2001), "ATR/ATM-Mediated Phosphorylation of Human Rad17 is Required for Genotoxic Stress Responses", *Nature*, **411(6840)**:969-974
- Barlow J.H., Lisby M., Rothstein R. (2008), "Differential Regulation of the Cellular Response to DNA Double-Strand Breaks in G1", *Molecular Cell*, **30(1)**:73-85
- Barnes D.E. and Lindahl T. (2004), "Repair and Genetic Consequences of Endogenous DNA Base Damage in Mammalian Cells", *Annual Reviews in Genetics*, **38**:445-476

- Bartek J., Bartkova J., Lukas J. (2007a), “DNA Damage Signalling Guards Against Oncogenes and Tumour Progression”, *Oncogene*, **26(56)**:7773-7779
- Bartek J., Falck J., Lukas J. (2001), “Chk2 Kinase – A Busy Messenger”, *Nature Reviews Molecular Cell Biology*, **2(12)**:877-886
- Bartek J., Lukas J., Bartkova J. (1999), “Perspective: Defects in Cell Cycle Control and Cancer”, *Journal of Pathology*, **187(1)**:95-99
- Bartek J., Lukas J., Bartkova J. (2007b), “DNA Damage Response as an Anti-Cancer Barrier-Damage Threshold and the Concept of Haploinsufficiency”, *Cell Cycle*, **6(19)**:2344-2347
- Bartek J. and Lukas J. (2001a), “Mammalian G1- and S- Phase Checkpoints in Response to DNA Damage”, *Current Opinion in Cell Biology*, **13(6)**:738-747
- Bartek J. and Lukas J. (2001b), “Pathways Governing G1/S Transition and Their Response to DNA Damage”, *FEBS Letters*, **490(3)**:117-122
- Bartkova J., Horejsi Z., Koed K., Krämer T., Tort F., Zieger K., Guldberg P., Selsted M., Nesland J.M., Lukas C., Orntoft T., Lucas J., Bartek J. (2005), “DNA Damage Response as Candidate Anti-Cancer Barrier in Early Tumourigenesis”, *Nature*, **434(7035)**:864-870
- Bartkova J., Rezaei N., Liontos M., Karakaidos P., Kletsas D., Issaeva N., Vassiliou L.V., Kolettas E., Niforou K., Zoumpourlis V.C., Takaoka M., Nakagawa H., Tort F., Fugger K., Johansson F., Selsted M., Andersen C.L., Dyrskjot L., Orntoft T., Lukas J., Kittas C., Helleday T., Halazonetis T.D., Bartek J., Gorgoulis V.G. (2006), “Oncogene-Induced Senescence is Part of the Tumourigenesis Barrier Imposed by DNA Damage Checkpoints”, *Nature*, **444(7119)**:633-637
- Bartlett R. and Nurse P. (1990), “Yeast as a Model System for Understanding the Control of DNA Replication in Eukaryotes”, *Bioessays*, **12(10)**:457-463
- Baumann P. and West S.C. (1997), “The Human Rad51 Protein: Polarity of Strand Transfer and Stimulation by hRP-A”, *The EMBO Journal*, **16(17)**:5198-5206
- Bazykin G.A. and Kochetov K.A. (2011), “Alternative Translation Start Sites are Conserved in Eukaryotic Genomes”, *Nucleic Acids Research*, **39(2)**:567-577
- Beato M. (1989), “Gene Regulation by Steroid Hormones”, *Cell*, **56(3)**:335-344
- Beato M., Herrlich P., Schutz G. (1995), “Steroid Hormone Receptors: Many Actors in Search of a Plot”, *Cell*, **83(6)**:851-857
- Bech-Otschir D., Kraft R., Huang X., Henklein P., Kapelari P., Pollmann C., Dubiel W. (2001), “COP9 Signalosome Phosphorylation Targets p53 to Degradation by the Ubiquitin System”, *The EMBO Journal*, **20(7)**:1630-1639
- Bech-Otschir D., Seeger M., Dubiel W. (2002), “The COP9 Signalosome; At the Interface Between Signal Transduction and Ubiquitin-Mediated Proteolysis”, *Journal of Cell Science*, **115(Pt.3)**:467-473
- Beck B.D., Park S.J., Lee Y.J., Roman Y., Hromas R.A., Lee S.H. (2008), “Human PSO4 is a Metnase (SETMAR) Binding Partner that Regulates Metnase Function in DNA Repair”, *Journal of Biological Chemistry*, **283(14)**:9023-9030

- Beck S. and Olek A. (2003), "The Epigenome: Molecular Hide and Seek", 1st Edition, Wiley-VCH
- Becker M.M. and Wang Z. (1989), "Origin of Ultra-Violet Damage in DNA", *Journal of Molecular Biology*, **210(3)**:429-438
- Beere H.M., Wolf B.B., Cain K., Mosser D.D., Mahboubi A., Kuwana T., Taylor P., Morimoto R.I., Cohen G.M., Green D.R. (2000), "Heat Shock Protein 70 Inhibits Apoptosis by Preventing Recruitment of Procaspase-9 to the Apaf-1 Apoptosome", *Nature Cell Biology*, **2(8)**:469-475
- Behari J. and Paulraj R. (2007), "Biomarkers of Induced Electromagnetic Field and Cancer", *Indian Journal of Experimental Biology*, **45(1)**:77-85
- Bendjennat M., Boulaire J., Jascur T., Brickner H., Barbier V., Sarasin A., Fotedar A., Fotedar R. (2003), "U.V. Irradiation Triggers Ubiquitin-Dependent Degradation of p21(WAF1) to Promote DNA Repair", *Cell*, **114(5)**:599-610
- Benko Z., Miklos I., Carr A.M., Sipiczki M. (1999), "Caffeine-Resistance in *S. pombe*: Mutations in Three Novel Caf Genes Increase Caffeine Tolerance and Affect Radiation Sensitivity, Fertility and Cell Cycle", *Current Genetics*, **31(6)**:481-487
- Bennett N.C., Gardiner R.A., Hooper D.J., Johnson D.W., Gobe G.C. (2010), "Molecular Cell Biology of Androgen Signalling", *International Journal of Biochemistry and Cell Signalling*, **42(6)**:813-827
- Benson F.E., Stasiak A., West S.C. (1994), "Purification and Characterization of the Human Rad51 Protein, an Analogue of *E. coli* RecA", *The EMBO Journal*, **13(23)**:5764-5771
- Benvenuto G., Formiggini F., Laflamme P., Malakhov M., Bowler C. (2002), "The Photomorphogenesis Regulator DET1 Binds the Amino-Terminal Tail of Histone H2B in a Nucleosome Context", *Current Biology*, **12(17)**:1529-1534
- Berardini M., Mazurek A., Fishel R. (2000), "The Effect of O⁶-Methylguanine DNA Adducts on the Adenosine Nucleotide Switch Functions of hMSH2-hMSH6 and hMSH2-hMSH3", *Journal of Biological Chemistry*, **275(36)**:27851-27857
- Beretta G.L. and Perego P. (2005), "Genetic Manipulation of Yeast to Identify Genes in Regulation of Chemosensitivity", *Methods in Molecular Medicine*, **111**:241-255
- Beretta G.L. and Zunino F. (2007), "Relevance of Extracellular and Intracellular Interactions of Camptothecins as Determinants of Anti-Tumour Activity", *Biochemical Pharmacology*, **74(10)**:1437-1444
- Berman H.M., Westbrook J., Feng Z., Gilliland G., Bhat T.N., Weissig H., Shindyalov I.N., Bourne P.E. (2000), "The Protein Data Bank", *Nucleic Acids Research*, **28(1)**:235-242
- Bermudez V.P., Lindsey-Boltz L.A., Cesare A.J., Maniwa Y., Griffith J.D., Hurwitz J., Sancar A. (2003), "Loading of the Human 9-1-1 Checkpoint Complex onto DNA by the Checkpoint Clamp Loader hRad17-Replication Factor C Complex *in Vitro*", *Proceedings of the National Academy of Sciences U.S.A.*, **100(4)**:1633-1638
- Bessho T. and Sancar A. (2000), "Human DNA Damage Checkpoint Protein hRAD9 is a 3' to 5' Exonuclease", *Journal of Biological Chemistry*, **275(11)**:7451-7454

- Beukers R., Eker A.P.M., Lohman P.H.M. (2008), "50 Years Thymine Dimer", *DNA Repair*, **7(3)**:530-543
- Bianchi E., Denti S., Granata A., Bossi G., Geginat J., Villa A., Rogge L., Pardi R. (2000), "Integrin LFA-1 Interacts with the Transcriptional Co-Activator JAB1 to Modulate AP-1 Activity", *Nature*, **404(6778)**:617-621
- Binz S.K. and Wold M.S. (2008), "Regulatory Functions of the N-Terminal Domain of the 70-kDa Subunit of Replication Protein A (RPA)", *Journal of Biological Chemistry*, **283(31)**:21559-21570
- Bitton D.A., Wood V., Scutt P.J., Grallert A., Yates T., Smith D.L., Hagan I.M., Miller C.J. (2011), "Augmented Annotation of the *Schizosaccharomyces pombe* Genome Reveals Additional Genes Required for Growth and Viability", *Genetics*, **187(4)**:1207-1217
- Blackwell L.J., Bjornson K.P., Allen D.J., Modrich P. (2001), "Distinct MutS DNA Binding Modes that are Differentially Modulated by ATP Binding and Hydrolysis", *Journal of Biological Chemistry*, **276(36)**:34339-34347
- Blackwell L.J., Bjornson K.P., Modrich P. (1998a), "DNA-Dependent Activation of the hMutS α ATPase", *Journal of Biological Chemistry*, **273(48)**:32049-32054
- Blackwell L.J., Martik D., Bjornson K.P., Bjornson E.S., Modrich P. (1998b), "Nucleotide-Promoted Release of hMutS α from Heteroduplex DNA is Consistent with an ATP-Dependent Translocation Mechanism", *Journal of Biological Chemistry*, **273(48)**:32055-32062
- Blanco F.J. and Montoya G. (2011), "Transient DNA/RNA-Protein Interactions", *FEBS Journal*, **278(10)**:1643-1650
- Blank M. and Goodman R. (1999), "Electromagnetic Fields May Act Directly on DNA", *Journal of Cellular Biochemistry*, **75(3)**:369-374
- Blatch G.L. and Lässle M. (1999), "The Tetratricopeptide Repeat: A Structural Motif Mediating Protein-Protein Interactions", *Bioessays*, **21(11)**:932-939
- Bledsoe R.K., Montana V.G., Stanley T.B., Delves C.J., Apolito C.J., McKee D.D., Consler T.G., Parks D.J., Stewart E.L., Willson T.M., Lambert M.H., Moore J.T., Pearce K.H., Xu H.E. (2002), "Crystal Structure of the Glucocorticoid Receptor Ligand Binding Domain Reveals a Novel Mode of Receptor Dimerization and Co-Activation Recognition", *Cell*, **110(1)**:93-105
- Block L.J., de Ruiter P.E., Brinkmann A.O. (1998), "Forskolin-Induced Dephosphorylation of the Androgen Receptor Impairs Ligand Binding", *Biochemistry*, **37(11)**:3850-3857
- Blom N., Gammeltoft S., Brunak S. (1999), "Sequence and Structure-Based Prediction of Eukaryotic Protein Phosphorylation Sites", *Journal of Molecular Biology*, **294(5)**:1351-1362
- Blom N., Sicheritz-Ponten T., Gupta R., Gammeltoft S., Brunak S. (2004), "Prediction of Post-Translational Glycosylation and Phosphorylation of Proteins From the Amino Acid Sequence", *Proteomics*, **4(6)**:1633-1649
- Bloom L.B. (2009), "Loading Clamps for DNA Replication and Repair", *DNA Repair (Amst.)*, **8(5)**:570-578

- Bohr V.A., Smith C.A., Okumoto D.S., Hanawalt P.C. (1985), "DNA Repair in an Active Gene: Removal of Pyridine Dimers from the DHFR Gene of CHO Cells is Much More Efficient than in the Genome Overall", *Cell*, **40(2)**:359-369
- Bolsterli U.A. (2007), "Mechanistic Toxicology: The Molecular Basis of How Chemicals Disrupt Biological Targets", 2nd Edition, Informa Healthcare
- Bolton E.C., So A.Y., Chaivorapol C., Haqq C.M., Li H., Yamamoto K.R. (2007), "Cell- and Gene- Specific Regulation of Primary Target Genes by the Androgen Receptor", *Genes and Development*, **21(16)**:2005-2017
- Bork P., Hofmann K., Bucher P., Neuwald A.F., Altschul S.F., Koonin E.V. (1997), "A Superfamily of Conserved Domains in DNA Damage-Responsive Cell Cycle Checkpoint Proteins", *FASEB Journal*, **11(1)**:68-76
- Boucher D., Testard T., Averbek D. (2006), "Low Levels of Clustered Oxidative DNA Damage Induced at Low and High LET Irradiation in Mammalian Cells", *Radiation and Environmental Biophysics*, **45(4)**:267-276
- Bowman G.D., Goedken E.R., Kazmirski S.L., O'Donnell M., Kuriyan J. (2005), "DNA Polymerase Clamp Loaders and DNA Recognition", *FEBS Letters*, **579(4)**:863-867
- Boye E., Skjølberg H.C., Grallert B. (2009), "Checkpoint Regulation of DNA Replication", *Methods in Molecular Biology*, **521**:55-70
- Brady D.M. and Hardwick K.G. (2000), "Complex Formation Between Mad1p, Bub1p and Bub3p is Crucial for Spindle Checkpoint Function", *Current Biology*, **10(11)**:675-678
- Branzie D. and Foiani M. (2008), "Regulation of DNA Repair Throughout the Cell Cycle", *Nature Reviews Molecular Cell Biology*, **9(4)**:297-308
- Breitkreutz B.J., Stark C., Reguly T., Boucher L., Breitkrautz A., Livstone M., Oughtred R., Lackner D.H., Bähler J., Wood V., Dolinski K., Tyers M. (2008), "The BioGRID Interaction Database: 2008 Update", *Nucleic Acids Research*, **36 (Database Issue)**:D637-D640
- Brinkmann A.O., Blok L.J., de Ruiter P.E., Doesburg P., Steketee K., Berrevoets C.A., Trapman J. (1999), "Mechanisms of Androgen Receptor Activation and Function", *Journal of Steroid Biochemistry and Molecular Biology*, **69(1-6)**:307-313
- Brinkmann A.O., Faber P.W., van Rooij H.C., Kuiper G.G., Ris C., Klaassen P., van der Korput J.A., Voorhorst M.M., van Laar J.H., Mulder E., Trapman J. (1989), "The Human Androgen Receptor: Domain Structure, Genomic Organization and Regulation of Expression", *Journal of Steroid Biochemistry*, **34(1-6)**:307-310
- Broustas C.G. and Lieberman H.B. (2012), "Contributions of Rad9 to Tumorigenesis", *Journal of Cellular Biochemistry*, **113(3)**:742-751
- Brown A.L., Lee C.H., Schwarz J.K., Mitiku N., Piwnicka-Worms H., Chung J.H. (1999), "A Human Cds1-Related Kinase that Functions Downstream of ATM Protein in the Cellular Response to DNA Damage", *Proceedings of the National Academy of Sciences U.S.A.*, **96(7)**:3745-3750
- Brown K.D., Rathi A., Kamath R., Beardsley D.I., Zhan Q., Mannino J.L., Baskaran R. (2003), "The Mismatch Repair System is Required for S-Phase Checkpoint Activation", *Nature Genetics*, **33(1)**:80-84

- Bryan A.W. Jr., Memke M., Cowen L.J., Lindquist S.L., Berger B. (2009), "BETASCAN: Probable β -Amyloids Identified by Pairwise Probabilistic Analysis", *PLoS Computational Biology*, **5(3)**:e1000333
- Bryant P.E. (2004), "Repair and Chromosomal Damage", *Radiotherapy and Oncology*, **72(3)**:251-265
- Brychzy A., Rein T., Winklehofer K.F., Hartl F.U., Young J.C., Obermann W.M. (2003), "Cofactor Tpr2 Combines Two TPR Domains and a J Domain to Regulate the Hsp70/Hsp90 Chaperone System", *The EMBO Journal*, **22(14)**:3613-3623
- Bulavin D.V., Amundson S.A., Fornace A.J. (2002), "p38 and Chk1 Kinases: Different Conductors for the G(2)/M Checkpoint Symphony", *Current Opinion in Genetics and Development*, **12(1)**:92-97
- Bulavin D.V., Higashimoto Y., Popoff I.J., Gaarde W.A., Basrur V., Potapova O., Appella E., Fornace A.J. Jr (2001), "Initiation of a G2/M Checkpoint After Ultraviolet Radiation Requires p38 Kinase", *Nature*, **411(6833)**:102-107
- Bulavin D.V., Phillips C., Nannenga B., Timofeev O., Donehower L.A., Anderson C.W., Appella E., Fornace A.J. Jr. (2004), "Inactivation of the Wip1 Phosphatase Inhibits Mammary Tumorigenesis Through p38 MAPK-Mediated Activation of the p16(Ink4a)-p19(Arf) Pathway", *Nature Genetics*, **36(4)**:343-350
- Bulavin D.V., Saito S., Hollander M.C., Sakaguchi K., Anderson C.W., Appella E., Fornace A.J. Jr. (1999), "Phosphorylation of Human p53 by p38 Kinase Co-ordinates N-Terminal Phosphorylation and Apoptosis in Response to U.V. Radiation", *The EMBO Journal*, **18(23)**:6845-6854
- Burke A.R., Singh R.N., Carroll D.L., Wood J.C., D'Agostino R.B. Jr., Ajayan P.M., Torti F.M., Torti S.V. (2012), "The Resistance of Breast Cancer Stem Cells to Conventional Hyperthermia and Their Sensitivity to Nanoparticle-Mediated Photothermal Therapy", *Biomaterials*, **33(10)**:2961-2970
- Burma S., Chen B.P., Murphy M., Kurimasa A., Chen D.J. (2001), "ATM Phosphorylates Histone H2AX in Response to DNA Double-Strand Breaks", *Journal of Biological Chemistry*, **276(45)**:42462-42467
- Burns J.L., Guzder S.N., Sung P., Prakash S., Prakash L. (1996), "An Affinity of Human Replication Protein A for Ultraviolet-Damaged DNA", *Journal of Biological Chemistry*, **271(20)**:11607-11610
- Burtelow M.A., Kaufmann S.H., Karnitz L.M. (2000), "Retention of the Human Rad9 Checkpoint Complex in Extraction-Resistant Nuclear Complexes After DNA Damage", *Journal of Biological Chemistry*, **275(34)**:26343-26348
- Burtelow M.A., Roos-Mattjus P.M.K., Rauen M., Babendure J.R., Karnitz L.M. (2001), "Reconstitution and Molecular Analysis of the hRad9-hHus1-hRad1 (9-1-1) DNA Damage Responsive Checkpoint Complex", *Journal of Biological Chemistry*, **276(28)**:25903-25909
- Bylund G.O., Majka J., Burgers P.M. (2006), "Overpopulation and Purification of RFC-Related Clamp Loaders and PCNA-Related Clamps from *Saccharomyces cerevisiae*", *Methods in Enzymology*, **409**:1-11

- Byun T.S., Pacek M., Yee M.C., Walter J.C., Cimprich K.A. (2005), "Functional Uncoupling of MCM Helicase and DNA Polymerase Activities Activates the ATR-Dependent Checkpoint", *Genes and Development*, **19(9)**:1040-1052
- Cai R.L., Yan-Neale Y., Cueto M.A., Xu H., Cohen D. (2000), "HDAC1, a Histone Deacetylase, Forms a Complex with Hus1 and Rad9, Two G2/M Checkpoint Rad Proteins", *Journal of Biological Chemistry*, **275(36)**:27909-27916
- Cai Z., Greene M.I., Berezov A. (2008), "Modulation of Biomolecular Interactions with Complex-Binding Small Molecules", *Methods*, **46(1)**:39-46
- Caldecott K.W. (2008), "Single-Strand Break Repair and Human Genetic Disease", *Nature Reviews Genetics*, **9(8)**:619-631
- Calderwood S.K. (2010), "Heat Shock Proteins in Breast Cancer Progression – A Suitable Case for Treatment?", *International Journal of Hyperthermia*, **26(7)**:681-685
- Calderwood S.K. and Gong J. (2011), "Molecular Chaperones in Mammary Cancer Growth and Breast Tumour Therapy", *Journal of Cellular Biochemistry*, **113(4)**:1096-1103
- Calvo I.A., Gabrielli N., Iglesias-Baena I., García-Santamarina S., Hoe K.L., Kim D.U., Sansó M., Zuin A., Pérez P., Ayté J., Hidalgo E. (2009), "Genome-Wide Screen of Genes Required for Caffeine Tolerance in Fission Yeast", *PLoS One*, **4(8)**:e6619
- Canfield C., Rains J., De Benedetti A. (2009), "TLK1B Promotes Repair of DSB's via Its Interaction with Rad9 and Asf1", *BMC Molecular Biology*, **10**:110
- Canman C.E., Lim D.S., Cimprich K.A., Taya Y., Tamai K., Sakaguchi K., Appella E., Kastan M.B., Siliciano J.D. (1998), "Activation of the ATM Kinase by Ionizing Radiation and Phosphorylation of p53", *Science*, **281(5383)**:1677-1679
- Canton D.A. and Scott J.D. (2010), "Chk-ing In and Chk-ing Out: Kinase Compartmentalization Comes to Checkpoint Control", *Molecular Cell*, **40(1)**:1-2
- Carlson C.R., Grallert B., Stokke T., Boye E. (1999), "Regulation of the Start of DNA Replication in *Schizosaccharomyces pombe*", *Journal of Cell Science*, **112(Pt.6)**:939-946
- Carmeliet P. and Jain R.K. (2000), "Angiogenesis in Cancer and Other Diseases", *Nature*, **407(6801)**:249-257
- Carneiro T., Khair L., Reis C.C., Borges V., Moser B.A., Nakamura T.M., Ferreira M.G. (2010), "Telomeres Avoid End Detection by Severing the Checkpoint Signal Transduction Pathway", *Nature*, **467(7312)**:228-232
- Carney J.P., Maser R.S., Olivares H., Davis E.M., Le Beau M., Yates J.R. 3rd, Hays L., Morgan W.F., Petrini J.H. (1998), "The hMre11/hRad50 Protein Complex and Nijmegen Breakage Syndrome: Linkage of Double-Strand Break Repair to the Cellular DNA Damage Response", *Cell*, **93(3)**:477-486
- Carrey E.A., Campbell D.G., Hardie D.G. (1985), "Phosphorylation and Activation of Hamster Carbamyl Phosphate Synthetase II by Camp-Dependent Protein Kinase: A Novel Mechanism for Regulation of Pyrimidine Nucleotide Biosynthesis", *EMBO Journal*, **4(13B)**:3735-3742

- Carrey E.A. and Hardie D.G. (1988), "Mapping of Catalytic Domains and Phosphorylation Sites in the Multi-Functional Pyrimidine-Biosynthetic Protein CAD", *European Journal of Biochemistry*, **171(3)**:583-588
- Carrey E.A., Dietz C., Glubb D.M., Loffler M., Lucocq J.M., Watson P.F. (2002), "Detection and Location of the Enzymes of De Novo Pyrimidine Biosynthesis in Mammalian Spermatozoa", *Reproduction*, **123(6)**:757-768
- Carrigan P.E., Sikkink L.A., Smith D.F., Ramirez-Alvarado M. (2006), "Domain-Domain Interactions Within Hop, the Hsp70/Hsp90 Organizing Protein, are Required for Protein Stability and Structure", *Protein Science*, **15(3)**:522-532
- Carver T.J. and Mullan L.J. (2005), "JAE: Jemboss Alignment Editor", *Applied Bioinformatics*, **4(2)**:151-154
- Casanovas O., Miró F., Estanyol J.M., Itarte E., Agell N., Bachs O. (2000), "Osmotic Stress Regulates the Stability of Cyclin D1 in a p38SAPK2-Dependent Manner", *Journal of Biological Chemistry*, **275(45)**:35091-35097
- Caspari T., Davies C., Carr A.M. (2000a), "Analysis of the Fission Yeast Checkpoint Rad Proteins", *Cold Spring Harbour Symposium on Quantitative Biology*, **65**:451-456
- Caspari T., Dhaleen M., Kanter-Smoler G., Lindsay H.D., Hofmann K., Papadimitriou K., Sunnerhagen P., Carr A.M. (2000b), "Characterization of *Schizosaccharomyces pombe* Hus1: A PCNA-Related Protein that Associates with Rad1 and Rad9", *Molecular and Cellular Biology*, **74(4)**:1254-1262
- Castelletto V., Cheng G., Hamley I.W. (2011a), "Amyloid Peptides Incorporating a Core Sequence From the Amyloid Beta Peptide and Gamma Amino Acids: Relating Bioactivity to Self-Assembly", *Chemical Communications (Cambridge)*, **47(46)**:12470-12472
- Castelletto V., Hamley I.W., Cenker C., Olsson U., Adamcik J., Mezzenga R., Miravet J.F., Escuder B., Rodríguez-Llansola F. (2011b), "Influence of End-Capping on the Self-Assembly of Model Amyloid Peptide Fragments", *Journal of Physical Chemistry B*, **115(9)**:2107-2116
- Castillo E.A., Vivancos A.P., Jones N., Ayté J., Hidalgo E. (2003), "*Schizosaccharomyces pombe* cells Lacking the Ran-Binding Protein Hba1 Show a Multidrug Resistance Phenotype Due to Constitutive Nuclear Accumulation of Pap1", *Journal of Biological Chemistry*, **278(42)**:40565-40572
- Centenera M.M., Harris J.M., Tilley W.D., Butler L.M. (2008), "The Contribution of Different Androgen Receptor Domains to Receptor Dimerization and Signaling", *Molecular Endocrinology*, **22(11)**:2373-2382
- Chamovitz D.A. and Segal D. (2001), "JAB1/CSN5 and the COP9 Signalosome: A Complex Situation", *EMBO Reports*, **21(21)**:96-101
- Chan G.K. and Yen T.J. (2003), "The Mitotic Checkpoint: A Signaling Pathway that Allows a Single Unattached Kinetochores to Inhibit Mitotic Exit", *Progress in Cell Cycle Research*, **5**:431-439
- Chan S.W. and Dedon P.C. (2010), "The Biological and Metabolic Fates of Endogenous DNA Damage Products", *Journal of Nucleic Acids*, **929047**:1-13

- Chan T.A., Hermeking H., Lengauer C., Kinzler K.W., Vogelstein B. (1999), "14-3-3Sigma is Required to Prevent Mitotic Catastrophe After DNA Damage", *Nature*, **401(6753)**:616-620
- Chan V., Khoo U.S., Wong M.S., Lau K., Suen D., Li G., Kwong A., Chan T.K. (2008), "Localisation of hRad9 in Breast Cancer", *BMC Cancer*, **8**:196
- Chang C., Norris J.D., Gron H., Paige L.A., Hamilton P.T., Kenan D.J., Fowlkes D., McDonnell D.P. (1999), "Dissection of the LXXLL Nuclear Receptor Coactivator Interaction Motif Using Combinatorial Peptide Libraries: Discovery of Peptide Antagonists", *Molecular Cell Biology*, **19(12)**:8226-8239
- Chang C., Saltzman A., Yeh S., Young W., Keller E., Lee H.J., Wang C., Mizokami A. (1995), "Androgen Receptor: An Overview", *Critical Reviews in Eukaryotic Gene Expression*, **5(2)**:97-125
- Chang C.S., Kokontis J., Liao S.T. (1988a), "Molecular Cloning of Human and Rat Complementary DNA Encoding Androgen Receptors", *Science*, **240(4850)**:324-326
- Chang C.S., Kokontis J., Liao S.T. (1988b), "Structural Analysis of Complementary DNA and Amino Acid Sequences of Human and Rat Androgen Receptors", *Proceedings of the National Academy of Sciences U.S.A.*, **85(19)**:7211-7215
- Chang C-Y. and McDonnell D.P. (2005), "Androgen Receptor-Cofactor Interactions as Targets for New Drug Discovery", *Trends in Pharmacological Sciences*, **26(5)**:225-228
- Chang D.J. and Cimprich K.A. (2009), "DNA Damage Tolerance: When Its OK to Make Mistakes", *Nature Chemical Biology*, **5(2)**:82-90
- Chang D.T., Huang H.Y., Syu Y.T., Wu C.P. (2008), "Real Value Prediction of Protein Solvent Accessibility Using Enhanced PSSM Features", *BMC Bioinformatics*, **9 (Supplement 12)**:S12
- Chang D.Y. and Lu A.L. (2005), "Interaction of Checkpoint Proteins Hus1/Rad1/Rad9 with DNA Base Excision Repair Enzyme MutY Homolog in Fission Yeast *Schizosaccharomyces pombe*", *Journal of Biological Chemistry*, **280(1)**:408-417
- Chang D-Y., Shi G., Durand-Bubrief M., Ekwall K., Lu A.L. (2011), "The Role of MutY Homolog (Myh1) in Controlling the Histone Deacetylase Hst4 in the Fission Yeast *Schizosaccharomyces pombe*", *Journal of Molecular Biology*, **405(3)**:653-665
- Chakrabortee S., Tripathi R., Watson M., Schierle G.S., Kurniawan D.P., Kaminski C.F., Wise M.J., Tunnacliffe A. (2012), "Intrinsically Disordered Proteins as Molecular Shields", *Molecular Biosystems*, **8(1)**:210-219
- Chardwiriyaapreecha S., Hondo K., Inada H., Chahomchuen T., Sekito T., Kakinuma Y. (2009), "A Simple and Specific Procedure to Permealize the Plasma Membrane of *Schizosaccharomyces pombe*", *Bioscience, Biotechnology and Biochemistry*, **73(9)**:2090-2095
- Chaturvedi P., Eng W.K., Zhu Y., Mattern M.R., Mishra R., Hurle M.R., Zhang X., Annan R.S., Lu Q., Faucette L.F., Scott G.F., Li X., Carr S.A., Johnson R.K., Winkler J.D., Zhou B.B. (1999), "Mammalian Chk2 is a Downstream Effector of the ATM-Dependent DNA Damage Checkpoint Pathway", *Oncogene*, **18(28)**:4047-4054

- Chauchereau A., Georgiakaki M., Perrin-Wolff M., Milgrom E., Loosfelt H. (2000), "JAB1 Interacts with Both the Progesterone Receptor and SRC-1", *Journal of Biological Chemistry*, **275(12)**:8540-8548
- Chehab N.H., Malikzay A., Stavridi E.S., Halazonetis T.D. (1999), "Phosphorylation of Ser-20 Mediates Stabilization of Human p53 in Response to DNA Damage", *Proceedings of the National Academy of Sciences U.S.A.*, **96(24)**:13777-13782
- Chen B.J., Carroll P., Samson L. (1994), "The *Escherichia coli* AlkB Protein Protects Human Cells Against Alkylation-Induced Toxicity", *Journal of Bacteriology*, **176(20)**:6255-6261
- Chen M-J., Lin Y-T., Lieberman H.B., Chen G., Lee E.Y. (2001), "ATM-Dependent Phosphorylation of Human Rad9 is Required for Ionization Radiation-Induced Checkpoint Activation", *Journal of Biological Chemistry*, **276(19)**:16580-16586
- Chen T. (2008), "Nuclear Receptor Drug Discovery", *Current Opinion in Chemical Biology*, **12(4)**:418-426
- Chen Y. and Sanchez Y. (2004), "ChK1 in the DNA Damage Response: Conserved Roles from Yeast to Mammals", *DNA Repair (Amst.)*, **3(8-9)**:1025-1032
- Chen Z. and McKnight S.L. (2007), "A Conserved DNA Damage Response Pathway Responsible for Coupling the Cell Division Cycle to the Circadian and Metabolic Cycles", *Cell Cycle*, **6(23)**:2906-2912
- Cheng C.K., Chow L.W., Loo W.T., Chan T.K., Chan V. (2005), "The Cell Cycle Checkpoint Gene Rad9 is a Novel Oncogene Activated by 11q13 Amplification and DNA Methylation in Breast Cancer", *Cancer Research*, **65(19)**:8646-8654
- Cheng J., Sweredoski M., Baldi P. (2005), "Accurate Prediction of Protein Disordered Regions by Mining Protein Structure Data", *Data Mining Knowledge Discourses*, **11**:213-222
- Chhatiwala H., Jafri N., Salgia R. (2006), "A Review of Topoisomerase Inhibition in Lung Cancer", *Cancer Biology and Therapy*, **5(12)**:1600-1607
- Chiarugi V., Magnelli L., Ruggiero M. (1994), "Apoptosis, Senescence, Immortalisation and Cancer", *Pharmacological Research*, **30(4)**:301-315
- Child E.S. and Mann D.J. (2006), "The Intricacies of p21 Phosphorylated Protein-Protein Interactions, Subcellular Localisation and Stability", *Cell Cycle*, **5(12)**:1313-1319
- Chin C.F. and Yeong F.M. (2010), "Safeguarding Entry Into Mitosis: The Antephase Checkpoint", *Molecular and Cellular Biology*, **30(1)**:22-32
- Chini C.C. and Chen J. (2003), "Human Claspin is Required for Replication Checkpoint Control", *Journal of Biological Chemistry*, **278(32)**:30057-30062
- Choi J. and Majima T. (2011), "Conformational Changes of Non-B DNA", *Chemical Society Reviews*, **40(12)**:5893-5909
- Choi S.I., Ryu K., Seong B.L. (2009), "RNA-Mediated Chaperone Type for *de Novo* Protein Folding", *RNA Biology*, **6(1)**:21-24

- Christmann M. and Kaina B. (2000), "Nuclear Translocation of Mismatch Repair Proteins MSH2 and MSH6 as a Response of Cells to Alkylating Agents", *Journal of Biological Chemistry*, **275(46)**:36256-36262
- Christmann M., Tomicic M.T., Roos W.P., Kaina B. (2003), "Mechanisms of Human DNA Repair: An Update", *Toxicology*, **193(1-2)**:3-34
- Chu L-H. and Chen B-S. (2008), "Construction of a Cancer-Perturbed Protein-Protein Interaction Network for Discovery of Apoptosis Drug Targets", *BMC Systems Biology*, **2(56)**:1-17
- Chung I., Leonhardt H. Rippe K. (2011), "De Novo Assembly of a PML Nuclear Subcompartment Occurs Through Multiple Pathways and Induces Telomere Elongation", *Journal of Cell Science*, **124 (Pt. 21)**:3603-3618
- Cimprich K.A. and Cortez D. (2008), "ATR: An Essential Regulator of Genome Integrity", *Nature Reviews Molecular Cell Biology*, **9(8)**:616-627
- Cimprich K.A., Shin T.B., Keith C.T., Schrieber S.L. (1996), "cDNA Cloning and Gene Mapping of a Candidate Human Cell Cycle Checkpoint Protein", *Proceedings of the National Academy of Sciences U.S.A.*, **93(7)**:2850-2855
- Ciocca D.R. and Calderwood S.K. (2005), "Heat Shock Proteins in Cancer: Diagnostic, Predictive and Treatment Implications", *Cell Stress and Chaperones*, **10(2)**:86-103
- Ciombella R., Montrone G., Stoppacciaro A., Giglio S., Volinia S., Graziano P., Huebner K., Vecchione A. (2010), "Fhit Loss in Lung Preneoplasia: Relation to DNA Damage Response Checkpoint Activation", *Cancer Letters*, **291(2)**:230-236
- Claessens F., Verrijdt G., Schoenmakers E., Haelens A., Peeters B., Verhoeven G., Rombauts W. (2001), "Selective DNA Binding by the Androgen Receptor as a Mechanism for Hormone-Specific Gene Regulation", *Journal of Steroid Biochemistry and Molecular Biology*, **76(1-5)**:23-30
- Claret F.X., Hibi M., Dhut S., Toda T., Karin M. (1996), "A New Group of Conserved Coactivators that Increase the Specificity of AP-1 Transcription Factors", *Nature*, **383(6599)**:453-457
- Clark S.J., Harrison J., Paul C.L., Frommer M. (1994), "High Sensitivity Mapping of Methylated Cytosines", *Nucleic Acids Research*, **22(15)**:2990-2997
- Clerici M., Paciotti V., Baldo V., Romano M., Lucchini G., Longhese M.P. (2001), "Hyperactivation of the Yeast DNA Damage Checkpoint by TEL1 and DDC2 Overexpression", *The EMBO Journal*, **20(22)**:6485-6498
- Cleutjens C.B., Steketeer K., van Eekelen C.C., van der Korput J.A., Brinkmann A.O., Trapman J. (1997), "Both Androgen Receptor and Glucocorticoid Receptor are Able to Induce Prostate-Specific Antigen Expression, but Differ in Their Growth-Stimulating Properties of LNCaP Cells", *Endocrinology*, **138(12)**:5293-5300
- Codlin S., Hains R.L., Burden J.J., Mole S.E. (2008), "Btn1 Affects Cytokinesis and Cell Wall Deposition by Independent Mechanisms, One of Which is Linked to Dysregulation of Vacuolar pH", *Journal of Cell Science*, **121(Pt.17)**:2860-2870

- Coleman P.F., Suttle D.P., Stark G.R. (1977), "Purification From Hamster Cells of the Multifunctional Protein that Initiates De Novo Synthesis of Pyrimidine Nucleotides", *Journal of Biological Chemistry*, **252(18)**:6379-6385
- Collis S.J. and Boulton S.J. (2007), "Emerging Links Between the Biological Clock and the DNA Damage Response", *Chromosoma*, **116(4)**:331-339
- Collura A., Auffret Van Der Kemp P., Boiteux S. (2012), "Abasic Sites Linked to dUTP Incorporation in DNA are a Major Cause of Spontaneous Mutations in Absence of Base Excision Repair and Rad17-Mec3-Ddc1 (9-1-1) DNA Damage Checkpoint Clamp in *Saccharomyces cerevisiae*", *DNA Repair (Amst.)*, **11(3)**:294-303
- Collura A., Blaisonneau J., Baldacci G., Francesconi S. (2005), "The Fission Yeast Crb2/Chk1 Pathway Coordinates the DNA Damage and Spindle Checkpoint in Response to Replication Stress Induced by Topoisomerase I Inhibitor", *Molecular and Cellular Biology*, **25(17)**:7889-7899
- Cooper W.G. (1993), "Roles of Evolution, Quantum mechanics and Point Mutations in Origins of Cancer", *Cancer Biochemistry and Biophysics*, **13(3)**:147-170
- Cooper W.G. (1996), "Hypothesis on a Casual Link Between EMF and an Evolutionary Class of Cancer and Spontaneous Abortion", *Cancer Biochemistry and Biophysics*, **15(3)**:151-170
- Cortajarena A.L., Yi F., Regan L. (2008), "Designed TPR Molecules as Novel Anti-Cancer Agents", *ACS Chemical Biology*, **3(3)**:161-166
- Cortese M.S., Uversky V.N., Dunker A.K. (2008), "Intrinsic Disorder in Scaffold Proteins: Getting More from Less", *Progress in Biophysical and Molecular Biology*, **98(1)**:85-106
- Cortez D., Guntuku S., Qin J., Elledge S.J. (2001), "ATR and ATRIP: Partners in Checkpoint Signaling", *Science*, **294(5547)**:1713-1716
- Cortez D., Wang Y., Qin J., Elledge S.J. (1999), "Requirement of ATM-Dependent Phosphorylation of BRCA1 in the DNA Damage Response to Double-Strand Breaks", *Science*, **286(5442)**:1162-1166
- Cotta-Ramusino C., McDonald E.R. 3rd, Hurov K., Sowa M.E., Harper J.W., Elledge S.J. (2011), "A DNA Damage Response Screen Identifies RHINO, a 9-1-1 and TopBP1 Interacting Protein Required for ATR Signaling", *Science*, **332(6035)**:1313-1317
- Crespan E., Czabany T., Maga G., Hübscher U. (2012), "Microhomology-Mediated DNA Strand Annealing and Elongation by Human DNA Polymerases λ and β on Normal and Replicative DNA Sequences", *Nucleic Acids Research*, **40(12)**:5577-5590
- Crumpton M.J. and Collins A.R. (2004), "Are Environmental Electromagnetic Fields Genotoxic?", *DNA Repair (Amst.)*, **3(10)**:1385-1387
- D'Adda di Fagagna F., Teo S.H., Jackson S.P. (2004), "Functional Links Between Telomeres and Proteins of the DNA Damage Response", *Genes and Development*, **18(15)**:1781-1799
- Dahlman-Wright K., Wright A., Gustafsson J.A., Carlstedt-Duke J. (1991), "Interaction of the Glucocorticoid Receptor DNA-Binding Domain with DNA as a Dimer is Mediated by a Short Segment of Five Amino Acids", *Journal of Biological Chemistry*, **266(5)**:3107-3112

- Dai Y. and Grant S. (2010), "New Insights into Checkpoint Kinase I in the DNA Damage Response Signaling Network", *Clinical Cancer Research*, **16(2)**:376-383
- Dalal S.N., Schweitzer C.M., Gan J., De Caprio J.A. (1999), "Cytoplasmic Localization of Human Cdc25C During Interphase Requires an Intact 14-3-3 Binding Site", *Molecular and Cellular Biology*, **19(6)**:4465-4479
- Daly J.W. (2007), "Caffeine Analogs: Biomedical Impact", *Cellular and Molecular Life Sciences*, **64(16)**:2153-2169
- Daly J.W., Hide I., Miller C.E., Shamim M. (1991), "Caffeine Analogues: Structure-Activity Relationships of Adenosine Receptors", *Pharmacology*, **42(6)**:309-321
- D'Amours D. and Jackson S.P. (2001), "The Mre11 Complex: At the Cross Roads of DNA Repair and Checkpoint Signalling", *Nature Reviews Cell Biology*, **3(5)**:317-327
- d'Andrea L.D. and Regan L. (2003), "TPR Proteins: The Versatile Helix", *Trends in Biochemical Sciences*, **28(12)**:655-662
- Daniels D.S. and Tainer J.A. (2000), "Conserved Structural Motifs Governing the Stoichiometric Repair of Alkylated DNA by O(6)-Alkylguanine-DNA Alkyltransferase", *Mutation Research*, **460(3-4)**:151-163
- Darimont B.D., Wagner R.L., Apriletti J.W., Stallcup M.R., Kushner P.J., Baxter J.D., Fletterick R.J., Yamamoto K.R. (1998), "Structure and Specificity of Nuclear Receptor-Coactivator Interactions", *Genes and Development*, **12(21)**:3343-3356
- Dasika G.K., Lin S.C., Zhao S., Sung P., Tomkinson A., Lee E.Y. (1999), "DNA Damage-Induced Cell Cycle Checkpoints and DNA Strand Break Repair in Development and Tumorigenesis", *Oncogene*, **18(55)**:7883-7899
- Davey S., Han C.S., Ramer S.A., Klassen J.C., Jacobson A., Eisenberger A., Hopkins K.M., Lieberman H.B., Freyer G.A. (1998), "Fission Yeast Rad12+ Regulates Cell Cycle Checkpoint Control and is Homologous to the Bloom's Syndrome Disease Gene", *Molecular and Cellular Biology*, **18(5)**:2721-2728
- Dauids L.M. and Kleemann B. (2011), "Combating Melanoma: The Use of Photodynamic Therapy as a Novel, Adjuvant Therapeutic Tool", *Cancer Treatment Reviews*, **37(6)**:465-475
- Dawson K., Toone W.M., Jones N., Wilkinson C.R. (2008), "Loss of Regulators of Vacuolar ATPase Function and Ceramide Synthesis Results in Multiple Drug Sensitivity in *Schizosaccharomyces pombe*", *Eukaryotic Cell*, **7(6)**:926-937
- de Anta J.M., Pérez-Castro A.J., Freire R., Mayol X. (2006), "The DNA Damage Checkpoint is Activated During Residual Tumour Cell Survival to Methotrexate Treatment as an Initial Step of Acquired Drug Resistance", *Anticancer Drugs*, **17(10)**:1171-1177
- Dean-Columb W. and Esteva F.J. (2008), "Emerging Agents in the Treatment of Anthracycline- and Taxane- Refractory Metastatic Breast Cancer", *Seminars in Oncology*, **35(2 Supplement 2)**:S31-S38
- De Benedetti A. (2009), "Tousled Kinase TLK1B Counteracts the Effect of Asf1 in Inhibition of Histone H3-H4 Tetramer Formation", *BMC Research Notes*, **2**:128

- De Benedetti A. (2010), "Tousled Kinase TLK1B Mediates Chromatin Assembly in Conjunction with Asf1 Regardless of its Kinase Activity", *BMC Research Notes*, **3**:68
- Decottignies A. (2007), "Microhomology-Mediated End-Joining in Fission Yeast is Repressed by Pku70 and Relies on Genes Involved in Homologous Recombination", *Genetics*, **176**(3):1403-1415
- Degols G., Shiozaki K., Russell P. (1996), "Activation and Regulation of the Spc1 Stress-Activated Protein Kinase in *Schizosaccharomyces pombe*", *Molecular and Cellular Biology*, **16**(6):287002877
- De Haro L.P., Wray J., Williamson E.A., Durant S.T., Corwin L., Gentry A.C., Osheroff N., Lee S.H., Hromas R., Nickoloff J.A. (2010), "Metnase Promotes Restart and Repair of Stalled and Collapsed Replication Forks", *Nucleic Acids Research*, **38**(17):5681-5691
- Delacroix S., Wagner J.M., Kobayashi M., Yamamoto K., Karnitz L.M. (2007), "The Rad9-Hus1-Rad1 (9-1-1) Clamp Activates Checkpoint Signaling via TopBP1", *Genes and Development*, **21**(12):1472-1477
- de la Torre J., Gil-Moreno A., Garcia A., Rojo F., Xercavins J., Salido E., Freire R. (2008), "Expression of DNA Damage Checkpoint Protein Hus1 in Epithelial Ovarian Tumours Correlates with Prognostic Markers", *International Journal of Gynecological Pathology*, **27**(1):24-32
- Delorenzi M. and Speed T. (2002), "An HMM Model for Coiled-Coil Domains and a Comparison with PSSM-Based Predictions", *Bioinformatics*, **18**(4):617-625
- den Elzen N., Kosoy A., Christopoulos H., O'Connell M.J. (2004), "Resisting Arrest: Recovery From Checkpoint Arrest Through Dephosphorylation of Chk1 by PP1", *Cell Cycle*, **3**(5):529-533
- Denny W.A. (2004), "Tumour-Activated Prodrugs: A New Approach to Cancer Therapy", *Cancer Investigation*, **22**(4):604-619
- Deng C.C., Brown J.A., You D., Brown J.M. (2005), "Multiple Endonucleases Function to Repair Covalent Topoisomerase I Complexes in *Saccharomyces cerevisiae*", *Genetics*, **170**(2):591-600
- Deng X.W., Dubiel W., Wei N., Hofmann K., Mundt K., Colicelli K., Kato J., Naumann M., Segal D., Seeger M. (2000a), "Unified Nomenclature for the COP9 Signalosome and Its Sub-Units: An Essential Regulator of Development", *Trends in Genetics*, **16**(5):202-203
- Deng X.W., Dubiel W., Wei N., Hofmann K., Mundt K. (2000b), "Unified Nomenclature for the COP9 Signalosome and Its Sub-Units: An Essential Regulator of Development", *Trends in Genetics*, **16**(7):289
- Denoyelle C., Abou-Rjaily G., Bezrookove V., Verhaegen M., Johnson T.M., Fullen D.R., Pointer J.N., Gruber S.B., Su L.D., Nikiforov M.A., Kaufman R.J., Bastian B.C., Soengas M.S. (2006), "Anti-Oncogenic Role of the Endoplasmic Reticulum Differentially Activated by Mutations in the MAPK Pathway", *Nature Cell Biology*, **8**(10):1053-1063
- De Palmer M. and Hanahan D. (2012), "The Biology of Personalized Cancer Medicine: Facing Individual Complexities Underlying Hallmark Capabilities", *Molecular Oncology*, **6**(2):111-127
- Deshpande A.M., Ivanova G., Raykov V., Xue Y., Maringele L. (2011), "Polymerase Epsilon is Required to Maintain Replicative Senescence", *Molecular and Cellular Biology*, **31**(8):1637-1645

- Deshpande G.P., Hayles J., Hoe K.L., Kim D.U., Park H.O., Hartsuiker E. (2009), "Screening a Genome-Wide *S. pombe* Deletion Library Identifies Novel Genes and Pathways Involved in Genome Stability Maintenance", *DNA Repair (Amst.)*, **8(5)**:672-679
- Desoize B. (2003), "Metal Ions and Metal Compounds in Carcinogenesis", *In Vivo*, **17(6)**:529-539
- Dhillon N. and Hoekstra M.F. (1994), "Characterization of Two Protein Kinases From *Schizosaccharomyces pombe* Involved in the Regulation of DNA Repair", *The EMBO Journal*, **13(12)**:2777-2788
- Dianov G.L. (2011), "Base Excision Repair Targets for Cancer Therapy", *American Journal of Cancer Research*, **1(7)**:845-851
- Dianov G.L., Price A., Lindahl T. (1992), "Generation of Single-Nucleotide Repair Patches Following Excision of Uracil Residues from DNA", *Molecular and Cellular Biology*, **12(4)**:1605-1612
- Diaz-Cuervo H. and Bueno A. (2008), "Cds1 Controls the Release of Cdc14-Like Phosphatase Flp1 From the Nucleolus to Drive Full Activation of the Checkpoint Response to Replication Stress in Fission Yeast", *Molecular Biology of the Cell*, **19(6)**:2488-2499
- Dickerson R.E., Drew H.R., Conner B.N., Wing R.M., Fratini A.V., Kopka M.L. (1982), "The Anatomy of A-, B- and Z- DNA", *Science*, **216(4545)**:475-485
- Dillon L.W., Burrow A.A., Wang Y.H. (2010), "DNA Instability at Chromosomal Fragile Sites in Cancer", *Current Genomics*, **11(5)**:326-337
- Ding R., Shi J., Pabon K., Scotto K.W. (2012), "Xanthines Down-Regulate the Drug Transporter ABCG2 and Reverse Multiple Drug Resistance", *Molecular Pharmacology*, **81(3)**:328-337
- Dinkel H., Michael S., Weatheritt R.J., Davey N.E., Van Roey K., Altenberg B., Toedt G., Uyar B., Seiler M., Budd A., Jödicke L., Dammert M.A., Schroeter C., Hammer M., Schmidt T., Jehl P., McGuigan C., Dymecka M., Chica C., Luck K., Via A., Chatr-Aryamontri A., Haslam N., Grebnev G., Edwards R.J., Steinmetz M.O., Meiselbach H., Diella F., Gibson T.J. (2012), "ELM: The Database of Eukaryotic Linear Motifs", *Nucleic Acids Research*, **40 (Database Issue)**:D242-D251
- Dion V., Kalck V., Horigome C., Towbin B.D., Gasser S.M. (2012), "Increased Mobility of Double-Strand Breaks Requires Mec1, Rad9 and the Homologous Recombination Machinery", *Nature Cell Biology*, **14(5)**:502-509
- Ditchfield C., Johnson V.L., Tighe A., Ellston R., Haworth C., Johnson T., Mortlock A., Keen N., Taylor S.S. (2003), "Aurora B Couples Chromosome Alignment with Anaphase by Targeting BubR1, Mad2 and Cenp-E to Kinetochores", *Journal of Cell Biology*, **161(2)**:267-280
- Doré A.S., Kilkenny M.L., Rzechorzek N.J., Pearl L.H. (2009), "Crystal Structure of the Rad9-Rad1-Hus1 Complex: Implications for Clamp Loading and Regulation", *Molecular Cell*, **34(6)**:735-745
- Doronkin S., Djagaeva I., Beckendorf S.K. (2002), "CSN5/Jab1 Mutations Affect Axis Formation in the *Drosophila* Oocyte by Activating a Meiotic Checkpoint", *Development*, **129(21)**:5053-5064
- Doronkin S., Djagaeva I., Beckendorf S.K. (2003), "The COP9 Signalosome Promotes Degradation of Cyclin E During Early *Drosophila* Oogenesis", *Developmental Cell*, **4(5)**:699-710

- Dor O. and Zhou Y. (2007), “Real-SPINE: An Integrated System of Neural Networks for Real Value Prediction of Protein Structural Properties”, *Proteins*, **68(1)**:76-81
- Dosztányi Z., Csizmok V., Tompa P., Simon I. (2005), “IUPred: Web Server for the Prediction of Intrinsically Unstructured Regions of Proteins Based on Estimated Energy Content”, **21(16)**:3433-3434
- Drwal M., Agama K., Wakelin L.P., Pommier Y., Griffith R. (2011), “Exploring DNA Topoisomerase I Ligand Space in Search of Novel Anticancer Agents”, *PLoS One*, **6(9)**:e25150
- Drew H., Takano T., Tanaka S., Itakura K., Dickerson R.E. (1980), “High-Salt d(CpGpCpG), a Left-Handed Double Helix”, *Nature*, **286(5773)**:567-573
- Dufault V.M., Oestrich A.J., Vroman B.T., Karnitz L.M. (2003), “Identification and Characterization of RAD9B, a Paralog of the RAD9 Checkpoint Gene”, *Genomics*, **82(6)**:644-651
- Duffield G.E., Best J.D., Meurers B.H., Bittner A., Loros J.J., Dunlap J.C. (2002), “Circadian Programs of Transcriptional Activation, Signaling and Protein Turnover Revealed by Microarray Analysis of Mammalian Cells”, *Current Biology*, **12(7)**:551-557
- Dukina A.S. and Lindsley C.W. (2007), “Small Molecule Protein-Protein Inhibitors for the p53-MDM2 Interaction”, *Current Topics in Medicinal Chemistry*, **7(10)**:952-960
- Dunaway S., Liu H.Y., Walworth N.C. (2005), “Interaction of 14-3-3 Protein with Chk1 Affects Localization and Checkpoint Function”, *Journal of Cell Science*, **118(Pt.1)**:39-50
- Dunker A.K. and Kriwacki R.W. (2011), “The Orderly Chaos of Proteins”, *Scientific American*, **(April) 304(4)**:68-73
- Dunker A.K., Obradovic Z., Romero P., Garner E.C., Brown C.J. (2000), “Intrinsic Protein Disorder in Complete Genomes”, *Genome Informatics: Workshop on Genome Information*, **11**:161-171
- Dunker A.K., Lawson J.D., Brown C.J., Williams R.M., Romero P., Oh J.S., Oldfield C.J., Campen A.M. Ratcliff C.M., Hipps K.W., Ausio J., Nissen M.S., Reeves R., Kang C., Kissinger C.R., Bailey R.W., Griswold M.D., Chiu W., Garner E.C., Obradovic Z. (2001), “Intrinsically Disordered Protein”, *Journal of Molecular Graphics and Modelling*, **19(1)**:26-59
- Dunker A.K., Oldfield C.J., Meng J., Romero P., Yang J.Y., Chen J.W., Vacic V., Obradovic Z., Uversky V.N. (2008), “The Unfoldomics Decade: An Update on Intrinsically Disordered Proteins”, *BMC Genomics*, **9 (Supplement 2)**:S1
- Dunker A.K. and Uversky V.N. (2010), “Drugs for ‘Protein Clouds’: Targeting Intrinsically-Disordered Transcription Factors”, *Current Opinion in Pharmacology*, **10(6)**:782-788
- Durand-Dubief M., Persson J., Norman U., Hartsuiker E., Ekwall K. (2010), “Topoisomerase I Regulates Open Chromatin and Controls Gene Expression *In Vivo*”, *The EMBO Journal*, **29(13)**:2126-2134
- Durante M., Geri C., Bonatti S., Parenti R. (1989), “Non-Random Alkylation of DNA Sequences Induced *In Vivo* by Chemical Mutagens”, *Carcinogenesis*, **10(8)**:1357-1361
- Durham T.R. and Snow E.T. (2006), “Metal Ions and Carcinogenesis”, *EXS*, **(96)**:97-130

- Dyson H.J. and Wright P.E. (2005), "Intrinsically Unstructured Proteins and Their Functions", *Nature Reviews Molecular Cell Biology*, **6(3)**:197-208
- Earnshaw W.C., Martins L.M., Kaufmann S.H. (1999), "Mammalian Caspases: Structure, Activation, Substrates and Function During Apoptosis", *Annual Review of Biochemistry*, **68**:383-424
- Egel R. (2010), "The Molecular Biology of *Schizosaccharomyces pombe*: Genetics, Genomics and Beyond", 2nd Edition, Springer
- Eggleter A.L., Inman R.B., Cox M.M. (2002), "The Rad51-Dependent Pairing of Long DNA Substrates is Stabilised by Replication Protein A", *Journal of Biological Chemistry*, **277(42)**:39280-39288
- Eichinger C.S. and Jentsch S. (2011), "9-1-1: PCNA's Specialized Cousin", *Trends in Biochemical Sciences*, **36(11)**:563-568
- el-Deiry W.S., Tokino T., Velculescu V.E., Levy D.B., Parsons R., Trent J.M., Lin D., Mercer W.E., Kinzler K.W., Vogelstein B. (1993), "WAF1: A Potential Mediator of p53 Suppression", *Cell*, **75(4)**:817-825
- Ellison V. and Stillman B. (2003), "Biochemical Characterization of DNA Damage Checkpoint Complexes: Clamp Loader and Clamp Complexes with Specificity for 5'-Recessed DNA", *PLoS Biology*, **1(2)**:231-243
- Emre D., Terracol R., Poncet A., Rahmani Z., Karess R.E. (2011), "A Mitotic Role for Mad1 Beyond the Spindle Checkpoint", *Journal of Cell Science*, **124(Pt.10)**:1664-1671
- Enders G.H. (2008), "Expanded Roles for Chk1 in Genome Maintenance", *Journal of Biological Chemistry*, **283(26)**:17749-17752
- Enoch T., Carr A.M., Nurse P. (1992), "Fission Yeast Genes Involved in Coupling Mitosis to Completion of DNA Replication", *Genes and Development*, **6(11)**:2035-2046
- Enoch T., Carr A.M., Nurse P. (1993), "Checkpoint Check", *Nature*, **361(6407)**:26
- Esposito G., Viglino P., Novak M., Cattaneo A. (2000), "The Solution Structure of the C-Terminal Segment of Tau Protein", *Journal of Peptide Science*, **6(11)**:550-559
- Essers M.A. and Trumpp A. (2010), "Targeting Leukemic Stem Cells by Breaking Their Dormancy", *Molecular Oncology*, **4(5)**:443-450
- Eustace B.K. and Jay D.G. (2004), "Extracellular Roles for the Molecular Chaperone Hsp90", *Cell Cycle*, **3(9)**:1098-1100
- Evans D.R. and Guy H.I. (2004), "Mammalian Pyrimidine Biosynthesis: Fresh Insights into an Ancient Pathway", *Journal of Biological Chemistry*, **279(32)**:33035-33038
- Evans E., Moggs J.G., Hwang J.R., Egly J.M., Wood R.D. (1997), "Mechanism of Open Complex and DNA Incision Formation by Human Nucleotide Excision Repair Factors", *The EMBO Journal*, **16(21)**:6559-6573

- Evstigneev M.P., Mosounov A.A., Evstigneev V.P., Parkes H.G., Davies D.B. (2011), "Quantification of the Interceptor Action of Caffeine on the *In Vitro* Biological Effect of the Anti-Tumour Agent Topotecan", *European Biophysics Journal*, **40(8)**:969-980
- Falck J., Lukas C., Protopopova M., Lukas J., Selivanova G., Bartek J. (2001a), "Functional Impact of Concomitant Versus Alternative Defects in the Chk2-p53 Tumour Suppressor Pathway", *Oncogene*, **20(39)**:5503-5510
- Falck J., Mailand N., Syljuasen R.G., Bartek J., Lukas J. (2001b), "The ATM-Chk2-Cdc25A Checkpoint Pathway Guards Against Radioresistant DNA Synthesis", *Nature*, **410(6830)**:842-847
- Falck J., Petrini J.H., Williams B.R., Lukas J., Bartek J. (2002), "The DNA Damage-Dependent Intra-S Phase Checkpoint is Regulated by Parallel Pathways", *Nature Genetics*, **30(3)**:290-294
- Falone S., Grossi M.R., Cinque B., D'Angelo B., Tettamani E., Cimini A., Di Ilio C., Amicarelli F. (2007), "Fifty Hertz Extremely Low-Frequency Electromagnetic Field Causes Changes in Redox and Differentiation Status in Neuroblastoma Cells", *International Journal of Biochemistry and Cell Biology*, **39(11)**:2093-2106
- Fan Y., Borowski A.D., Weiss R.H. (2003), "An Anti-Sense Oligonucleotide to p21 (Waf1/Cip1) Causes Apoptosis in Human Breast Cancer Cells", *Molecular Cancer Therapeutics*, **2(8)**:773-782
- Fan Y., Weinstein J.N., Kohn K.W., Shii L.M., Pommier Y. (1998), "Molecular Modelling Studies of the DNA Topoisomerase I Ternary Cleavable Complex with Camptothecin", *Journal of Medicinal Chemistry*, **41(13)**:2216-2226
- Fang Y.Z., Yang S., Wu G.Y. (2002), "Free Radicals, Antioxidants and Nutrition", *Nutrition*, **18(10)**:872-879
- Faraggi E., Xue B., Zhou Y. (2009), "Improving the Prediction Accuracy of Residue Solvent Accessibility and Real-Value Backbone Torsion Angles of Proteins by Fast Guided Learning Through a Two-Layer Neural Network", *Proteins*, **74(4)**:847-856
- Farray D., Ahuwalia M.S., Snyder J., Barnett G.H., Cohen B.H., Such J.H., Peereboom D.M. (2006), "Pre-Irradiation 9-Amino [20S] Camptothecin (9-AC) in Patients with Newly Diagnosed Glioblastoma Multiforme", *Investigational New Drugs*, **24(3)**:177-180
- Farver O. (2000), "CH.13 Metals in Medicine: Inorganic Medicinal Chemistry", in Kronsgaard-Larsen P., Lilijefors T., Madsen U. (2002), "Textbook of Drug Design and Drug Discovery", 3rd Edition, Taylor and Francis, **CH13**:364-409
- Fasulo B., Koyama C., Yu K.R., Homola E.M., Hsieh T.S., Campbell S.D., Sullivan W. (2012), "Chk1 and Wee1 Kinases Coordinate DNA Replication, Chromosome Condensation and Anaphase Entry", *Molecular Biology of the Cell*, **Electronic Publication Ahead of Print**
- Faust D., Dolado I., Cuadrado A., Oesch F., Weiss C., Nebreda A.R., Dietrich C. (2005), "p38alpha MAPK is Required for Contact Inhibition", *Oncogene*, **24(53)**:7941-7945
- Fava L.L., Kaulich M., Nigg E.A., Santamaria A. (2011), "Probing the *In Vivo* Function of Mad1:C-Mad2 in the Spindle Assembly Checkpoint", *The EMBO Journal*, **30(16)**:3322-3336

- Fawzi N.L., Phillips A.H., Ruscio J.Z., Doucleff M., Wemmer D.E., Head-Gordon T. (2008a), "Structure and Dynamics of the Abeta(21-30) Peptide From the Interplay of NMR Experiments and Molecular Simulations", *Journal of the American Chemical Society*, **130(19)**:6145-6158
[Erratum in: *Journal of the American Chemical Society*, 2011 133(30):11816]
- Fawzi N.L., Yap E.H., Okabe Y., Kohlstedt K.L., Brown S.P., Head-Gordon T. (2008b), "Contrasting Disease and Non-Disease Protein Aggregation by Molecular Simulation", *Accounts of Chemical Research*, **41(8)**:1037-1047
- Felts S.J., Karnitz L.M., Toft D.O. (2007), "Functioning of the Hsp90 Machine in Chaperoning Checkpoint Kinase I (Chk1) and the Progesterone Receptor (PR)", *Cell Stress and Chaperones*, **12(4)**:353-363
- Feng W., Ribeiro R.C., Wagner R.L., Nguyen H., Apriletti J.W., Fletterick R.J., Baxter J.D., Kushner P.J., West B.L. (1998), "Hormone-Dependent Coactivator Binding to a Hydrophobic Cleft on Nuclear Receptors", *Science*, **280(5370)**:1747-1749
- Ferguson L.R. and Denny W.A. (2007), "Genotoxicity of Non-Covalent Interactions: DNA Intercalators", *Mutation Research*, **623(1-2)**:14-23
- Fernández-Escamilla A.M., Cheung M.S., Vega M.C., Wilmanns M., Onuchic J.N., Serrano L. (2004a), "Solvation in Protein Folding Analysis: Combination of Theoretical and Experimental Approaches", *Proceedings of the National Academy of Sciences U.S.A.*, **101(9)**:2834-2839
- Fernández-Escamilla A.M., Rousseau F., Schymkowitz J., Serrano L. (2004b), "Prediction of Sequence-Dependent and Mutational Effects on the Aggregation of Peptides and Proteins", *Nature Biotechnology*, **22(10)**:1302-1306
- Feyzi E., Sundheim O., Westbye M.P., Aas P.A., Vagbo C.B., Otterlei M., Slupphaug G. (2007), "RNA Base Damage and Repair", *Current Pharmaceutical Biotechnology*, **8(6)**:326-331
- Filhol O. and Cochet C. (2011), "Protein Kinases Curb Cell Death", *Science Signaling*, **4(172)**:pe26
- Fink A.L. (1999), "Chaperone-Mediated Protein Folding", *Physiological Reviews*, **79(2)**:425-449
- Finn K. , Lowndes N.F., Grenon M. (2012), "Eukaryotic DNA Damage Checkpoint Activation in Response to Double-Strand Breaks", *Cellular and Molecular Life Sciences*, **69(9)**:1447-1473
- Fishel R. (1998), "Mismatch Repair, Molecular Switches and Signal Transduction", *Genes and Development*, **12(14)**:2096-2101
- Fishel R., Lescoe M.K., Rao M.R., Copeland N.G., Jenkins N.A., Garber J., Kane M., Kolodner R. (1993), "The Human Mutator Gene Homolog MSH2 and its Association with Hereditary Nonpolyposis Colon Cancer", *Cell*, **75(5)**:1027-1038
- Fnu S., Williamson E.A., De Haro L.P., Brenneman M., Wray J., Shaheen M., Radhakrishnan K., Lee S.H., Nickoloff J.A., Hromas R. (2011), "Methylation of Histone H3 Lysine 36 Enhances DNA Repair by Non-Homologous End-Joining", *Proceedings of the National Academy of Sciences U.S.A.*, **108(2)**:540-545
- Follis A.V., Galea C.A., Kriwacki R.W. (2012), "Intrinsic Protein Flexibility in Regulation of Cell Proliferation: Advantages for Signaling and Opportunities for Novel Therapeutics", *Advances in Experimental Medicine and Biology*, **725**:27-49

- Foray N., Marot D., Gabriel A., Randrianarison V., Carr A.M., Perricaudet M., Ashworth A., Jeggo P. (2003), "A Subset of ATM- and ATR- Dependent Phosphorylation Events Requires the BRCA1 Protein", *The EMBO Journal*, **22(11)**:2860-2871
- Forsburg S.L. and Nurse P. (1991), "Cell Cycle Regulation in the Yeasts *Saccharomyces cerevisiae* and *Schizosaccharomyces pombe*", *Annual Review of Cell Biology*, **7**:227-256
- Forsburg S.L. (1993), "Comparison of *Schizosaccharomyces pombe* Expression Systems", *Nucleic Acids Research*, **21(12)**:2955-2956
- Forsburg S.L. (1994a), "Cell Cycle: In and Out of the Cell Cycle", *Current Biology*, **4(9)**:828-830
- Forsburg S.L. (1994b), "Codon Usage Table for *Schizosaccharomyces pombe*", *Yeast*, **10(8)**:1045-1047
- Forsburg S.L. and Sherman D.A., (1997), "General Purpose Tagging Vectors for Fission Yeast", *Gene*, **191(2)**:191-195
- Forsburg S.L. (1999), "The Best Yeast?", *Genetics*, **152(3)**:839-851
- Forsburg S.L. (2001), "The Art and Design of Genetic Screens:Yeast", *Nature Reviews Genetics*, **2(9)**:659-668
- Forsburg S.L. (2003a), "Overview of *Schizosaccharomyces pombe*", *Current Protocols in Molecular Biology*, **Ch.13**: Unit13:14
- Forsburg S.L. (2003b), "Growth and Manipulation of *S. pombe*", *Current Protocols in Molecular Biology*, **Ch.13**: Unit13:15
- Forsburg S.L. (2003c), "*S. pombe* Strain Maintenance and Media", *Current Protocols in Molecular Biology*, **Ch.13**: Unit13:16
- Forsburg S.L. (2003d), "Introduction of DNA into *S. pombe* Cells", *Current Protocols in Molecular Biology*, **Ch.13**: Unit13:17
- Forsburg S.L. (2005), "The Yeasts *Saccharomyces cerevisiae* and *Schizosaccharomyces pombe*: Models for Cell Biology Research", *Gravitational and Space Biology Bulletin*, **18(2)**:3-9
- Forsburg S.L. and Rhind P. (2006), "Basic Methods for Fission Yeast", *Yeast*, **23(3)**:173-183
- Fousteri M. and Mullenders L.H.F. (2008), "Transcription-Coupled Nucleotide Excision Repair in Mammalian Cells: Molecular Mechanisms and Biological Effects", *Cell Research*, **18(1)**:73-84
- Francia S., Weiss R.S., d'Adda di Fagagna F. (2007), "Need Telomere Maintenance? Call 9-1-1)", *Cell Division*, **2**:3
- Francia S., Weiss R.S., Hande M.P., Freire R., d'Adda di Fagagna F. (2006), "Telomere and Telomerase Modulation by the Mammalian Rad9/Rad1/Hus1 DNA-Damage-Checkpoint Complex", *Current Biology*, **16(15)**:1551-1558
- Franco R. (2008), "Coffee and Cancer", *Medicina Clinica*, **131(16)**:633-635

- Freedman L.P., Luisi B.F., Korszun Z.R., Basavappa R., Sigler P.B., Yamamoto K.R. (1988), "The Function and Structure of the Metal Coordination Sites Within the Glucocorticoid Receptor DNA Binding Domain", *Nature*, **334(6182)**:543-546
- Freilich S., Oron E., Kapp Y., Nevo-Caspi Y., Orgad S., Segal D., Chamovitz D.A. (1999), "The COP9 Signalosome is Essential for Development of *Drosophila melanogaster*", *Current Biology*, **9(20)**:1187-1190
- Friedberg E.C. (2005), "Suffering in Silence: The Tolerance of DNA Damage", *Nature Reviews Molecular Cell Biology*, **6(12)**:943-953
- Fujikawa K., Kamiya H., Yakushiji H., Fujii Y., Nakabeppu Y., Kasai H. (1999), "The Oxidized Forms of dATP are Substrates for the Human MutT Homologue, the hMTH1 Protein", *Journal of Biological Chemistry*, **274(26)**:18201-18205
- Fujinaka Y., Matsuoka K., Limori M., Tuul M., Sakasai R., Yoshinaga K., Saeki H., Morita M., Kakeji Y., Gillespie D.A., Yamamoto K., Takata M., Kitao H., Maehara Y. (2012), "ATR-Chk1 Signaling Pathway and Homologous Recombinational Repair Protect Cells from 5-Fluorouracil Cytotoxicity", *DNA Repair (Amst.)*, **11(3)**:247-258
- Fukumoto A., Ikeda N., Sho M., Tomoda K., Kanehiro H., Hisanaga M., Tsurui Y., Tsutsumi M., Kato J.Y., Nakajima Y. (2004), "Prognostic Significance of Localized p27Kip1 and Potential Role of Jab1/CSN5 in Pancreatic Cancer", *Oncology Reports*, **11(2)**:277-284
- Fukumoto A., Tomoda K., Kubota M., Kato J.Y., Yoneda-Kato N. (2005), "Small Jab1-Containing Sub-Complex is Regulated in an Anchorage- and Cell Cycle-Dependent Manner, Which is Abrogated by Ras Transformation", *FEBS Letters*, **579(5)**:1047-1054
- Fukumoto A., Tomoda K., Yoneda-Kato N., Nakajima Y., Kato J.Y. (2006), "Depletion of Jab1 Inhibits Proliferation of Pancreatic Cell Lines", *FEBS Letters*, **580(25)**:5836-5844
- Fuller B.G. and Stukenberg P.T. (2009), "Cell Division: Righting the Check", *Current Biology*, **19(14)**:R550-R553
- Funder J.W. (1993), "Mineralocorticoids, Glucocorticoids, Receptors and Response Elements", *Science*, **259(5098)**:1132-1133
- Fung H. and Weinstock D.M. (2011), "Repair at Single Targeted DNA Double-Strand Breaks in Pluripotent and Differentiated Human Cells", *PLoS One*, **6(5)**:e20514
- Furuya K. and Carr A.M. (2003), "DNA Checkpoints in Fission Yeast", *Journal of Cell Science*, **116(Pt.19)**:3847-3848
- Furuya K., Miyabe I., Tsutsui Y., Paderi F., Kakusho N., Masai H., Niki H., Carr A.M. (2010), "DDK Phosphorylates Checkpoint Clamp Component Rad9 and Promotes Its Release from Damaged Chromatin", *Molecular Cell*, **40(4)**:606-618
- Furuya K., Poitelea M., Guo L., Caspari T., Carr A.M. (2004), "Chk1 Activation Requires Rad9 S/TQ-Site Phosphorylation to Promote C-Terminal Association with BRCT Domains of Rad4TOPBP1", *Genes and Development*, **18(10)**:1154-1164
- Gao Z.G. and Jacobson K.A. (2011), "Emerging Adenosine Receptor Agonists: An Update", *Expert Opinion on Emerging Drugs*, **16(4)**:597-602

- Gabai V.L., Meng L., Kim G., Mills T.A., Benjamin I.J., Sherman M.Y. (2012), "Heat Shock Transcription Factor Hsf1 is Involved in Tumour Progression via Regulation of Hypoxia-Inducible Factor 1 and RNA-Binding Protein HuR", *Molecular and Cellular Biology*, **32(5)**:929-940
- Gabai V.L., O'Callaghan-Sunol C., Meng L., Sherman M.Y., Yaglom J. (2008), "Triggering Senescence Programs Suppresses Chk1 Kinases and Sensitises Cells to Genotoxic Stress", *Cancer Research*, **68(6)**:1834-1842
- Gabai V.L., Yaglom J.A., Volloch V., Merlin A.B., Force T., Koutroumanis M., Massie B., Mosser D.D., Sherman M.Y. (2000), "Hsp72-Mediated Suppression of c-Jun N-Terminal Kinase is Implicated in Development of Tolerance to Caspase-Independent Cell Death", *Molecular and Cellular Biology*, **20(18)**:6826-6836
- Gabai V.L., Yaglom J.A., Waldman T., Sherman M.Y. (2009), "Heat Shock Protein Hsp72 Controls Oncogene-Induced Senescence Pathways in Cancer Cells", *Molecular and Cellular Biology*, **29(2)**:559-569
- Gafter-Gvili A., Fraser A., Paul M., Vidal L., Lawrie T.A., van der Wetering M.D., Kremer L.C., Leibovici L. (2012), "Antibiotic Prophylaxis for Bacterial Infections in Afebrile Neutropenia Patients Following Chemotherapy", *Cochrane Database of Systematic Reviews*, **1**:CD004386
- Gaiser A.M., Kretschmar A., Richter K. (2010), "Cdc37-Hsp90 Complexes are Responsive to Nucleotide-Induced Conformational Changes and Binding of Further Cofactors", *Journal of Biological Chemistry*, **285(52)**:40921-40932
- Garcia-Calvo M., Peterson E.P., Leiting B., Ruel R., Nicholson D.W., Thornberry N.A. (1998), "Inhibition of Human Caspases by Peptide-Based and Macromolecular Inhibitors", *Journal of Biological Chemistry*, **273(49)**:32608-32613
- Garrett M.D. and Workman P. (1999), "Discovering Novel Chemotherapeutic Drugs for the Third Millennium", *European Journal of Cancer*, **45(14)**:2010-2030
- Garufi C., Dogliotti L., D'Attino R.M., Tampellini M., Aschelter A.M., Pugliese P., Perrone M., Nistico C., Comis S., Terzoli E. (2001), "Irinotecan and Chronomodulated Infusion of 5-Fluorouracil and Folinic Acid in the Treatment of Patients with Advanced Colorectal Carcinoma: A Phase I Study", *Cancer*, **91(4)**:712-720
- Garvik B., Carson M., Hartwell L. (1995), "Single-Stranded DNA Arising at Telomeres in Cdc13 Mutants May Constitute a Specific Signal for the RAD9 Checkpoint", *Molecular and Cellular Biology*, **15(11)**:6128-6138
- Gauger M.A. and Sancar A. (2005), "Cryptochrome, Circadian Cycle, Cell Cycle Checkpoints and Cancer", *Cancer Research*, **65(15)**:6828-6834
- Geley S., Hartmann B.L., Hattmannstorfer R., Löffler M., Ausserlechner M.J., Bernhard D., Sgonc R., Strasser-Wozak E.M., Ebner M., Auer B., Kofler R. (1997), "p53-Induced Apoptosis in Human T-ALL Cell Line CCRF-CEM", *Oncogene*, **15(20)**:2429-2437
- Gembka A., Toueille M., Smirnova E., Poltz R., Ferrari E., Villani G. Hübscher U. (2007), "The Checkpoint Clamp, Rad9-Rad1-Hus1 Complex, Preferentially Stimulates the Activity of Apurinic/Apyrimidinic Endonuclease I and DNA Polymerase Beta in Long-Patch Base Excision Repair", *Nucleic Acids Research*, **35(8)**:2596-2608

- Genschel J., Bazemore L.R., Modrich P. (2002), "Human Exonuclease I is Required for 5' and 3' Mismatch Repair", *Journal of Biological Chemistry*, **277(15)**:13302-13311
- Genschel J., Littenman S.J., Drummond J.T., Modrich P. (1998), "Isolation of MutSbeta from Human Cells and Comparison of the Mismatch Repair Specificities of MutSbeta and MutSalpha", *Journal of Biological Chemistry*, **273(31)**:19895-19901
- Gentner N.E. and Werner N.M. (1975), "Repair in *Schizosaccharomyces pombe* as Measured by Recovery from Caffeine Enhancement of Radiation-Induced Lethality", *Molecular and General Genetics*, **142(3)**:171-183
- Gentry A.C., Juul S., Veigaard C., Knudsen B.R., Osheroff N. (2011), "The Geometry of Supercoils Modulates the Cleavage Activity of Human Topoisomerase I", *Nucleic Acids Research*, **39(3)**:1014-1022
- George C.M., Lyndaker A.M., Alani E. (2011), "The DNA Damage Checkpoint Allows Recombination Between Divergent DNA Sequences in Budding Yeast", *DNA Repair (Amst.)*, **10(11)**:1086-1094
- Georgescu R.E., Kim S.S., Yurieva O., Kuriyan J., Kong X-P., O'Donnell M. (2008), "Structure of a Sliding Clamp on DNA", *Cell*, **132(1)**:43-54
- Germann M.W., Johnson C.N., Spring A.M. (2010), "Recognition of Damaged DNA: Structure and Dynamic Markers", *Medicinal Research Reviews*, doi **10.1002/med20226**
- Giacchetti S. (2002), "Chronotherapy of Colorectal Cancer", *Chronobiology International*, **19(1)**:207-219
- Giacchetti S., Dugué P.A., Innominato P.F., Bjarnason G.A., Focan C., Garufi C., Tumolo S., Coudert B., Lacobellu S., Smaaland R., Tampellini M., Adam R., Moreau T., Lévi F. (2012), "Sex Moderates Circadian Chemotherapy Effects on Survival of Patients with Metastatic Colorectal Cancer: A Meta-Analysis", *Annals of Oncology*, **Electronic Publication Ahead of Print (27th June 2012)**
- Gilljam K.M., Feyzi E., Aas P.A., Sousa M.M.L., Müller R., Vågbo C.B., Catterall T.C., Liabakk N.B., Slupphaug G., Drablos F., Krokan H.E., Otterlei M. (2009), "Identification of a Novel, Widespread Functionally Important PCNA-Binding Motif", *Journal of Cell Biology*, **186(5)**:645-654
- Gioeli D., Ficarro S.B., Kwiek J.J., Aaronson D., Hancock M., Catling A.D., White F.M., Christian R.E., Settlage R.E., Shabanowitz J., Hunt D.F., Weber M.J. (2002), "Androgen Receptor Phosphorylation: Regulation and Identification of the Phosphorylation Sites", *Journal of Biological Chemistry*, **277(32)**:29304-29314
- Giovanella B.C., Harris N., Mendoza J., Cao Z., Liehr J., Stehlin J.S. (2000), "Dependence of Anti-Cancer Activity of Camptothecins on Maintaining Their Lactone Function", *Annals of the New York Academy of Sciences*, **922**:27-35
- Glanzer J.G., Liu S., Oakley G.G. (2011), "Small Molecule Inhibitor of the RPA70 N-Terminal Protein Interaction Domain Discovered Using *In Silico* and *In Vitro* Methods", *Bioorganic and Medicinal Chemistry*, **19(8)**:2589-2595
- Glass C.K. and Rosenfeld M.G. (2000), "The Co-Regulator Exchange in Transcriptional Functions of Nuclear Receptors", *Genes and Development*, **14(2)**:121-141

- Glickman M.H., Rubin D.M., Coux O., Wefes I., Pfeifer G., Cjeka Z., Baumeister W., Fried V.A., Finley D. (1998), "A Sub-Complex of the Proteasome Regulatory Particle Required for Ubiquitin-Conjugate Degradation and Related to the COP9-Signalosome and eIF3", *Cell*, **94(5)**:615-623
- Goebel M. and Yanagida M. (1991), "The TPR Snap Helix: A Novel Protein Motif from Mitosis to Transcription", *Trends in Biochemical Sciences*, **16(5)**:173-177
- Goes F.S. and Martin J. (2001), "Hsp90 Chaperone Complexes are Required for the Activity and Stability of Yeast Protein Kinases Mik1, Wee1 and Swe1", *European Journal of Biochemistry/FEBS*, **268(8)**:2281-2289
- Goetz M.P., Toft D.O., Ames M.M., Erlichman C. (2003), "The Hsp90 Chaperone Complex as a Novel Target for Cancer Therapy", *Annals of Oncology*, **14(8)**:1169-1176
- Goldwasser F., Shimizu T., Jackman J., Hoki Y., O'Connor P.M., Kohn K.W., Pommier Y. (1998), "Correlations Between S and G2 Arrest and the Cytotoxicity of Camptothecin in Human Colon Carcinoma Cells", *Cancer Research*, **56(19)**:4430-4437
- Goloudino A., Yamaguchi H., Chervyakova D.B., Appella E., Fornace A.J. Jr., Bulavin D.V. (2003), "Regulation of Human CDC25A Stability by Serine 75 Phosphorylation is Not Sufficient to Activate a S Phase Checkpoint", *Cell Cycle*, **2(5)**:473-478
- Gómez E.B. and Forsburg S.L. (2002), "Fission Yeast Enters a Joyful New Era", *Genome Biology*, **3(6)**:REPORTS4017
- Gómez E.B. and Forsburg S.L. (2004), "Analysis of the Fission Yeast *Schizosaccharomyces pombe* Cell Cycle", *Methods in Molecular Biology*, **241**:93-111
- Gorgoulis V.G., Vassiliou L.V., Karakaidos P., Zacharatos P., Kotsinas A., Ligolou T., Venere M., Dittullo R.A. Jr., Kastriakis N.G., Levy B., Kleitas D., Yoneta A., Herlyn M., Kittas C., Halazonetis T.D. (2005), "Activation of the DNA Damage Checkpoint and Genomic Instability in Human Precancerous Lesions", *Nature*, **434(7035)**:907-913
- Gotter A.L. (2003), "Tipin, a Novel Timeless-Interacting Protein, is Developmentally Co-Expressed with Timeless and Disrupts its Self-Association", *Journal of Molecular Biology*, **331(1)**:167-176
- Gotter A.L., Suppa C., Emanuel B.S. (2007), "Mammalian TIMELESS and Tipin are Evolutionary Conserved Replication Fork-Associated Factors", *Journal of Molecular Biology*, **366(1)**:36-52
- Govindan S.V. and Goldenberg D.M. (2010), "New Antibody Conjugates in Cancer Therapy", *Scientific World Journal*, **10**:2070-2089
- Gowers D.M. and Halford S.E. (2003), "Protein Motion from Non-Specific DNA by Three-Dimensional Routes Aided by Supercoiling", *EMBO Journal*, **22(6)**:1410-1418
- Gowers D.M., Wilson G.G., Halford S.E. (2005), "Measurement of the Contributions of 1D and 3D Pathways to the Translocation of a Protein Along DNA", *Proceedings of the National Academy of Sciences U.S.A.*, **102(44)**:15883-15888
- Gradia S., Achyara S., Fishel R. (1997), "The Human Mismatch Recognition Complex hMSH2-hMSH6 Functions as a Novel Molecular Switch", *Cell*, **91(7)**:995-1005

Gradia S., Acharya S., Fishel R. (2000), "The Role of Mismatched Nucleotides in Activating the hMSH2-hMSH6 Molecular Switch", *Journal of Biological Chemistry*, **275(6)**:3922-3930

Gradia S., Subramanian D., Wilson T., Acharya S., Makhov A., Griffith J., Fishel R. (1999), "hMSH2-hMSH6 Forms a Hydrolysis-Independent Sliding Clamp on Mismatched DNA", *Mol. Cell*, **3(2)**:255-261

Graves L.M., Guy H.I., Kozlowski P., Huang M., Lazarowski E., Pope R.M., Collins M.A., Dahlstrand E.N., Earp H.S., III, Evans D.R. (2000), "Regulation of Carbamoyl Phosphate Synthetase by MAP Kinase", *Nature*, **403(6767)**:328-332

Gray M.D., Mann M., Nitiss J.L., Hendershot L.M. (2005), "Activation of the Unfolded Protein Response is Necessary and Sufficient for Reducing Topoisomerase II α Protein Levels and Decreasing Sensitivity to Topoisomerase-Targeted Drugs", *Molecular Pharmacology*, **68(6)**:1699-1707

Green M.D., Sabatinos S.A., Forsburg S.L. (2009), "Microscopy Techniques to Examine DNA Replication in Fission Yeast", *Methods in Molecular Biology*, **521**:463-482

Greer Card D.A., Sierant M.L., Davey S. (2010), "Rad9A is Required for G2 Decatenation Checkpoint and to Prevent Endoreduplication in Response to Topoisomerase II Inhibition", *Journal of Biological Chemistry*, **285(20)**:15653-15661

Grenert J.P., Johnson B.D., Toft D.O. (1999), "The Importance of ATP Binding and Hydrolysis by Hsp90 in Formation and Function of Protein Heterocomplexes", *Journal of Biological Chemistry*, **273(6)**:3679-3686

Griffith J.D., Lindsey-Boltz L.A., Sancar A. (2002), "Structures of the Human Rad17-Replication Factor C and Checkpoint 9-1-1 Complexes Visualized by Glycerol Spray/Low Voltage Microscopy", *Journal of Biological Chemistry*, **277(18)**:15233-15236

Grimison B., Liu J., Lewellyn A.L., Maller J.L. (2006), "Metaphase Arrest by Cyclin E-Cdk2 Requires the Spindel-Checkpoint Kinase Mps1", *Current Biology*, **16(19)**:1968-1973

Groth A., Lukas J., Nigg E., Sillje H., Wernstedt C., Bartek J., Hansen K. (2003), "Human Tousled-Like Kinases are Targeted by an ATM- and Chk1- Dependent DNA Damage Checkpoint", *EMBO Journal*, **22(7)**:1676-1687

Gruber A.R., Lorenz R., Bernhart S.H., Neuböck I.L., Hofacker I.L. (2008), "The Vienna RNA Websuite", *Nucleic Acids Research*, **36 (Web Server Issue)**:W70-W74

Gruber M., Söding J., Lupas A.N. (2005), "REPPER: Repeats and Their Periodicities in Fibrous Proteins", *Nucleic Acids Research*, **33 (Web Server Issue)**:W239-243

Gruber M., Söding J., Lupas A.N. (2006), "Comparative Analysis of Coiled-Coiled Prediction Methods", *Journal of Structural Biology*, **155(2)**:140-145

Guan X., Bai H., Shi G., Theriot C.A., Hazra T.K., Mitra S., Lu A.L. (2007a), "The Human Checkpoint Sensor Rad9-Rad1-Hus1 Interacts with and Stimulates NEIL1 Glycosylase", *Nucleic Acids Research*, **35(8)**:2463-2472

- Guan X., Madabushi A., Chang D-Y., Fitzgerald M.E., Shi G., Drohat A.C., Lu A.L. (2007b), "The Human Checkpoint Sensor Rad9-Rad1-Hus1 Interacts with and Stimulates DNA Repair Enzyme TDG Glycosylase", *Nucleic Acids Research*, **35(18)**:6207-6218
- Guo Z., Chavez V., Singh P., Finger L.D., Hang H., Hegde M.L., Shen B. (2008), "Comprehensive Mapping of the C-Terminus of Flap Endonuclease I Reveals Distinct Interaction Sites for Five Proteins that Represent Different DNA Replication and Repair Pathways", *Journal of Molecular Biology*, **377(3)**:679-690
- Gupta R.C., Golub E.I., Wold M.S., Radding C.M. (1998), "Polarity of DNA Strand Exchange Promoted by Recombination Proteins of the RecA Family", *Proceedings of the National Academy of Sciences U.S.A.*, **95(17)**:9843-9848
- Gutz H. (1967) "Twin Meiosis and Other Ambivalences in the Life Cycle of *Schizosaccharomyces pombe*", *Science*, **158(802)**:796-798
- Gutz H. and Doe F.J. (1973), "Two Different Mating Types in *Schizosaccharomyces pombe*", *Genetics*, **74(4)**:563-569
- Habraken Y., Sung P., Prakash L., Prakash S., (1994), "A Conserved 5' to 3' Exonuclease Activity in the Yeast and Human Nucleotide Excision Repair Proteins RAD2 and XPG", *Journal of Biological Chemistry*, **269(50)**:31342-31345
- Haelens A., Verrijdt G., Callewaert L., Peeters B., Rombauts W., Claessens F. (2001), "Androgen-Receptor-Specific DNA Binding to an Element in the First Exon of the Human Secretory Component Gene", *Biochemical Journal*, **353(Pt.3)**:611-620
- Hager S.E. and Jones M.E. (1967), "Initial Steps in Pyrimidine Biosynthesis in Ehrlich Ascites Carcinoma *in Vitro*", *Journal of Biological Chemistry*, **242(24)**:5667-5673
- Hakem R. (2008), "DNA Damage Repair; The Good, the Bad and the Ugly", *EMBO Journal*, **27(4)**:589-605
- Hall D.B., Holmlin R.E., Barton J.K. (1996), "Oxidative DNA Damage Through Long-Range Electron Transfer", *Nature* **382(6593)**:731-735
- Halford S.E. (2009), "An End to 40 Years of Mistakes in DNA-Protein Association Kinetics?", *Biochemical Society Transactions*, **37(Pt 2)**:343-348
- Halford S.E. and Marko J.F. (2004), "How Do Site-Specific DNA-Binding Proteins Find Their Targets?", *Nucleic Acids Research*, **32(10)**:3040-3052
- Ham J., Thomson A., Needham M., Webb P., Parker M. (1988), "Characterization of Response Elements for Androgens, Glucocorticoids and Progestins in Mouse Mammary Tumour Virus", *Nucleic Acids Research*, **16(12)**:5263-5276
- Han J. and Sun P. (2007), "The Pathways to Tumor Suppression via Route p38", *Trends in Biochemical Sciences*, **32(8)**:364-371
- Hanahan D. and Weinberg R.A. (2000), "The Hall Marks of Cancer", *Cell*, **100(1)**:57-70
- Hanahan D. and Weinberg R.A. (2011), "Hall Marks of Cancer: The Next Generation", *Cell*, **144(5)**:646-674

- Hanawalt P.C. (2002), "Subpathways of Nucleotide Excision Repair and Their Regulation", *Oncogene*, **21(58)**:8949-8956
- Hang H., Zhang R.C., Dubrack Jr., Wang C., Lieberman H.B. (2002), "Identification and Characterisation of Human Cell Cycle Checkpoint Gene *HUS1*", *Genomics*, **79(4)**:487-492
- Hansen P.L., Podgornik R., Parsegian V.A. (2001), "Osmotic Properties of DNA: Critical Evaluation of Counterion Condensation Theory", *Physiological Reviews of Effect of Static Non-Linear Soft Matter Physics*, **64(2 Part 1)**:021907
- Harrison J.C. and Haber J.E. (2006), "Surviving the Breakup: The DNA Damage Checkpoint", *Annual Reviews in Genetics*, **40**:209-235
- Harst A., Lin H., Obermann W.M. (2005), "Aha1 Competes with Hop, p50 and p23 for Binding to the Molecular Chaperone Hsp90 and Contributes to Kinase and Hormone Receptor Activation", *The Biochemical Journal*, **387(Pt.3)**:789-796
- Hartsuiker E., Neale M.J., Carr A.M. (2009), "Distinct Requirements for the Rad32(Mre11) Nuclease and Ctp1(CtIP) in the Removal of Covalently Bound Topoisomerase I and II from DNA", *Molecular Cell*, **33(1)**:117-123
- Hartwell L. (2001), "Interview: Leland Hartwell, Ph.D. Nobel Prize for Medicine Winner", *Medscape General Medicine*, **3(4)**:3
- Hatakeyama S., Matsumoto M., Yada M., Nakayama K.I. (2004), "Interaction of U-Box Type Ubiquitin Protein Ligases (E3s) with Molecular Chaperones", *Genes to Cells*, **9(6)**:533-548
- Hayashi K., Kuniyasu H., One N., Shigeishi H., Kuraoka K., Nakayama H., Yasui W. (2002), "Induction of hRad9 is Required for G2/M Checkpoint Signal Transduction in Gastric Cancer Cells", *Pathobiology*, **70(1)**:40-46
- Hayles J. and Nurse P. (1986), "Cell Cycle Regulation in Yeast", *Journal of Cell Science*, **(Supplement 4)**:155-170
- He B., Bowen N.T., Minges J.T., Wilson E.M. (2001), "Androgen-Induced NH₂- and C00-Terminal Interaction Inhibits p160 Co-Activator Recruitment by Activation Function 2", *Journal of Biological Chemistry*, **276(45)**:42293-42301
- He B., Gampe Jr R.T., Kole A.J., Hnat A.T., Stanley T.B., An G., Stewart E.L., Kalman R.I., Minges J.T., Wilson E.M. (2004), "Structural Basis for Androgen Receptor Interdomain and Co-Activator Interactions Suggest a Transition in Nuclear Receptor Activation Function Dominance", *Molecular Cell*, **16(3)**:425-438
- He B., Kempainen J.A., Voegel J.J., Gronemeyer H., Wilson E.M. (1999), "Activation Function 2 in the Human Androgen Receptor Ligand Binding Domain Mediates Interdomain Communication with the NH₂-Terminal Domain", *Journal of Biological Chemistry*, **274(52)**:37219-37225
- He B., Kempainen J.A., Wilson E.M. (2000), "FXXLF and WXXLF Sequences Mediate the NH₂-Terminal Interaction with the Ligand Binding Domain of the Androgen Receptor", *Journal of Biological Chemistry*, **275(30)**:22986-22994
- He B., Minges J.T., Lee L.W., Wilson E.M. (2002), "The FXXLF Motif Regulates Androgen Receptor-Specific Interactions with Coregulators", *Journal of Biological Chemistry*, **277(12)**:10226-10235

- He B. and Wilson E.M. (2002), "The NH₂-Terminal and Carboxyl-Terminal Interaction in the Human Androgen Receptor", *Molecular Genetics and Metabolism*, **75(4)**:293-298
- He B. and Wilson E.M. (2003), "Electrostatic Modulation in Steroid Receptor Recruitment of LXXLL and FXXLF Motifs", *Molecular and Cellular Biology*, **23(6)**:2135-2150
- He W., Ma X., Yang X., Zhao Y., Chu J., Hang H. (2011), "A Role for the Arginine Methylation of Rad9 in Checkpoint Control and Cellular Sensitivity to DNA Damage", *Nucleic Acids Research*, **39(11)**:4719-4727
- He W., Zhao Y., Zhang C., An L., Hu Z., Liu Y., Han L., Bi L., Xie Z., Xue P., Yang F., Hang H. (2008), "Rad9 Plays an Important Role in DNA Mismatch Repair Through Physical Interaction with MLH1", *Nucleic Acids Research*, **36(20)**:6046-6417
- He X., van Waardenburg R.C., Babaoglu K., Price A.C., Nitiss K.C., Nitiss J.L., Bjornsti M.A., White S.W. (2007), "Mutation of a Conserved Active Site Residue Converts Tyrosyl-DNA Phosphodiesterase I into a DNA Topoisomerase I-Dependent Poison", *Journal of Molecular Biology*, **372(4)**:1070-1081
- He Z., Henriksen L.A., Wold M.S., Ingles C.J. (1995), "RPA Involvement in the Damage-Recognition and Incision Steps of Nucleotide Excision Repair", *Nature*, **374(6522)**:566-569
- Hecker J., Yang J.Y., Chen J. (2008), "Protein Disorder Prediction at Multiple Levels of Sensitivity and Specificity", *BMC Genomics*, **9 (Supplement 1)**:S9
- Heery D.M., Kalkhoven E., Hoare S., Parker M.G. (1997), "A Signature Motif in Transcriptional Coactivators Mediates Binding to Nuclear Receptors", *Nature*, **387(6634)**:733-736
- Hegyí H., Buday L., Tompa P. (2009), "Intrinsic Structural Disorder Confers Cellular Viability on Oncogenic Fusion Proteins", *PLoS Computational Biology*, **5(10)**:e1000552
- Heinlein C.A. and Chang C. (2002), "Androgen Receptor (AR) Coregulators: An Overview", *Endocrinology Reviews*, **23(2)**:175-200
- Helt C.E., Wang W., Keng P.C., Bambara R.A. (2005), "Evidence that DNA Damage Detection Machinery Participates in DNA Repair", *Cell Cycle*, **4(4)**:529-532
- Hemnani T. and Parihar M.S. (1998), "Reactive Oxygen Species and Oxidative DNA Damage", *Indian Journal of Physiology and Pharmacology*, **42(4)**:440-452
- Henry S.A. and Patton-Vogt J.L. (1998), "Genetic Regulation of Phospholipid Metabolism: Yeast as a Model Eukaryote", *Progress in Nucleic Acids Research Molecular Biology*, **61**:133-179
- Hermeking H., Lengauer C., Polyak K., He T.C., Zhang L., Thiagalingam S., Kinzler K.W., Vogelstein B. (1997), "14-3-3 Sigma is a p53-Regulated Inhibitor of G2/M Progression", *Molecular Cell*, **1(1)**:3-11
- Herschlag D. (1995), "RNA Chaperones and the RNA Folding Problem", *Journal of Biological Chemistry*, **270(36)**:20871-20874
- Hewitt L., Tighe A., Santaguida S., White A.M., Jones C.D., Musacchio A., Green S., Taylor S.S. (2010), "Sustained Mps1 Activity is Required in Mitosis to Recruit O-Mad2 to the Mad1-C-Mad2 Core Complex", *Journal of Cell Biology*, **190(1)**:25-34

- Hey T., Lipps G., Sugasawa K., Iwai S., Hanaoka F., Krauss G. (2002), "The XPC HR23B Complex Displays High Affinity and Specificity for Damaged DNA in a True Equilibrium Fluorescence Assay", *Biochemistry*, **41(21)**:6583-6587
- Hill G.M., Moriarity D.M., Setzer W.N. (2011), "Attenuation of Cytotoxic Natural Product DNA Intercalating Agents by Caffeine", *Scientia Pharmaceutica*, **79(4)**:729-747
- Hill M.A. (1999), "Radiation Damage to DNA: The Importance of Track Structure", *Radiation Measurements*, **31(1-6)**:15-23
- Hirai I., Sasaki T., Wang H.G. (2004), "Human hRad1 but not hRad9 Protects hHus1 from Ubiquitin-Proteasomal Degradation", *Oncogene*, **23(30)**:5124-5130
- Hirai I. and Wang H-G. (2002), "A Role of the C-Terminal Region of Human Rad9 (hRad9) in Nuclear Transport of the hRad9 Checkpoint Complex", *Journal of Biological Chemistry*, **277(28)**:25722-25727
- Hirao A., Kong Y.Y., Matsuoka S., Wakeham A., Ruland J., Yoshida H., Liu D., Elledge S.J., Mak T.W. (2000), "DNA Damage-Induced Activation of p53 by the Checkpoint Kinase Chk2", *Science*, **287(5459)**:1824-1827
- Hirose E., Mukai M., Shimada A., Nishitani H., Shibeta Y., Nishimoto T. (2006), "Loss of RanGEF/Pim1 Activity Abolishes the Orchestration of Ran-Mediated Mitotic Cellular Events in *S. pombe*", *Genes to Cells*, **11(1)**:29-46
- Hix S., Morais Mda S., Augusto O. (1995), "DNA Methylation by *tert*-Butylhydroperoxide-Iron(II)", *Free Radical Biology and Medicine*, **19(3)**:293-301
- Hoang T.X., Marsella L., Trovato A., Seno F., Banavar J.R., Maritan A. (2006), "Common Attributes of Native-State Structures of Proteins, Disordered Proteins and Amyloid", *Proceedings of the National Academy of Sciences U.S.A.*, **103(18)**:6883-6888
- Hofaker I.L. (2003), "Vienna RNA Secondary Structure Server", *Nucleic Acids Research*, **31(13)**:3429-3431
- Hofmann K. and Stoffel W. (1993), "TMBase: A Database of Membrane-Spanning Protein Segments", *Biological Chemistry Hopper Seyler*, **374**:166
- Hong C.I., Zámboorszky J., Csikász-Nagy A. (2009), "Minimum Criteria for DNA Damage-Induced Phase Advances in Circadian Rhythms", *PLoS Computational Biology*, **5(5)**:e1000384
- Hopkins K.M., Wang X., Berlin A., Hang H., Thaker H.M., Lieberman H.B. (2003), "Expression of Mammalian Paralogues of *HRAD9* and *Mrad9* Checkpoint Control Genes in Normal and Cancerous Testicular Tissue", *Cancer Research*, **63(17)**:5291-5298
- Horsman M.R. and Overgaard J. (2007), "Hyperthermia: A Potent Enhancer of Radiotherapy", *Clinical Oncology*, **19**:418-426
- Horton A.A. and Fairhurst S. (1987), "Lipid Peroxidation and Mechanisms of Toxicity", *R.C. Critical Reviews in Toxicology*, **18(1)**:27-29
- Houtgraaf J.H., Versmissen J., van der Giessen W.J. (2006), "A Concise Review of DNA Damage Checkpoints and Repair in Mammalian Cells", *Cardiovascular Revascularization Medicine: Including Molecular Interventions*, **7(3)**:165-172

Howell B.J., McEwen B.F., Canman J.C., Hoffman D.B., Farrar E.M., Rieder C.L., Salmon E.D. (2001), "Cytoplasmic Dynein/Dynactin Drives Kinetochore Protein Transport to the Spindle Poles and has a Role in Mitotic Spindle Checkpoint Inactivation", *Journal of Cell Biology*, **155(7)**:1159-1172

Hromas R., Wray J., Lee S.H., Martinez L., Farrington J., Corwin L.K., Ramsey H., Nickoloff J.A., Williamson E.A. (2008), "The Human SET and Transposase Domain Protein Metnase Interacts with DNA Ligase IV and Enhances the Efficiency and Accuracy of Non-Homologous End-Joining", *DNA Repair (Amst.)*, **7(12)**:1927-1937

Hsu C.L., Chen Y.L., Ting H.J., Lin W.J., Yang Z., Zhang Y., Wang L., Wu C.T., Cahng H.C., Yeh S., Pimplikar S.W., Chang C. (2005), "Androgen Receptor (AR) NH₂- and COOH- Terminal Interactions Present in the Differential Influences on AR-Mediated Transactivation and Cell Growth", *Molecular Endocrinology*, **19(2)**:350-361

Hsu C.L., Chen Y.L., Yeh S., Ting H.J., Hu Y.C., Lin H., Wang X., Chang C. (2003), "The Use of Phage Display Techniques for the Isolation of Androgen Receptor Interacting Peptides with (F/W)XXL(F/W) and FXXLY New Signature Motifs", *Journal of Biological Chemistry*, **278(26)**:23691-23698

Hu J.C., Booth M.J., Tripuraneni G., Davies D., Zaidi S.A., Tamburo de Bella M., Slade M.J., Marley S.B., Gordon M.Y., Coffin R.S., Coombes R.C., Kamalati T. (2006), "A Novel HSV-1 Virus, JS1/34.5-/47-, Purges Contaminating Breast Cancer Cells from Bone Marrow", *Clinical Cancer Research*, **12(22)**:6853-6862

Huang C., Ma W.Y., Maxiner A., Sun Y., Dong Z. (1999), "p38 Kinase Mediates U.V-Induced Phosphorylation of p53 Protein at Ser389", *Journal of Biological Chemistry*, **274(18)**:12229-12235

Huang J., Yuan H., Lu C., Liu X., Cao X., Wan M. (2007), "Jab1 Mediates Protein Degradation of the Rad9-Rad1-Hus1 Complex", *Journal of Molecular Biology*, **371(2)**:514-527

Huang M., Dorsey J.F., Epling-Burnette P.K., Nimmanapalli R., Landowski T.H., Mora L.B., Niu G., Sinibaldi D., Bai F., Kraker A., Yu H., Moscinski L., Wei S., Djeu J., Dalton W.S., Bhalla K., Longhran T.P., Wu J., Jove R. (2002a), "Inhibition of Bcr-Abl Kinase Activity by PD180970 Blocks Constitutive Activity of Stat5 and Growth of CML Cells", *Oncogene*, **21(57)**:8804-8816

Huang M., Kozlowski P., Collins M., Wang Y., Haystead T.A., Graves L.M. (2002b), "Caspase-Dependent Cleavage of Carbamoyl Phosphate Synthetase II During Apoptosis", *Molecular Pharmacology*, **61(3)**:569-577

Huang M. and Graves L.M. (2003), "De Novo Synthesis of Pyrimidine Nucleotides: Emerging Interfaces with Signal Transduction Pathways", *Cellular and Molecular Life Sciences*, **60(2)**:321-336

Huang Y., Yao Y., Xu H.Z., Wang Z.G., Lu L., Dai W. (2009), "Defects in Chromosome Congression and Mitotic Progression in KIF18A-Deficient Cells are Partly Mediated Through Impaired Functions of CENP-E", *Cell Cycle*, **8(16)**:2643-2649

Hui L., Bakiri L., Stepniak E., Wagner E.F. (2007), "p38alpha: A suppressor of Cell Proliferation and Tumourigenesis", *Cell Cycle*, **6(20)**:2429-2433

- Humpal S.E., Robinson D.A., Krebs J.E. (2009), "Marks to Stop the Clock: Histone Modifications and Checkpoint Regulation in the DNA Damage Response", *Biochemistry and Cell Biology*, **87(1)**:243-253
- Hunt C.R., Pandita R.K., Laszlo A., Higashikubo R., Agarwal M., Kitamura T., Gupta A., Rief N., Horikoshi N., Baskaran R., Lee J.H., Löbrich M., Paull T.T., Roti Roti J.L., Pandita T.K. (2007), "Hyperthermia Activates a Subset of Ataxia-Telangiectasia Mutated Effectors Independent of DNA Strand Breaks and Heat Shock Protein 70 Status", *Cancer Research*, **67(7)**:3010-3017
- Hunt T. (2002), "Nobel Lecture: Protein Synthesis, Proteolysis and Cell Cycle Transitions", *Bioscience Reports*, **22(5-6)**:465-486
- Huo Y.G., Bai L., Xu M., Jiang T. (2010), "Crystal Structure of the N-Terminal Region of Human Topoisomerase II β Binding Protein 1", *Biochemical and Biophysical Research Communications*, **401(3)**:401-405
- Hur E., Pfaff S.J., Payne E.S., Gron H., Buehrer B.M., Fletterick R.J. (2004), "Recognition and Accomodation at the Androgen Receptor Coactivator Binding Interface", *PLoS Biology*, **2(9)**:E274
- Hwang B.J., Toering S., Francke U., Chi G. (1998), "p48 Activates a U.V.-Damaged-DNA Binding Factor and is Defective in Xeroderma Pigmentosum Group E Cells that Lack Binding Affinity", *Molecular and Cellular Biology*, **18(7)**:4391-4399
- Hyppa R.W. and Smith G.R. (2009), "Using *Schizosaccharomyces pombe* Meiosis to Analyse DNA Recombination Intermediates", *Methods In Molecular Biology*, **557**:235-252
- Iakoucheva L.M., Brown C.J., Lawson J.D., Obradovic Z., Dunker A.K. (2002), "Intrinsic Disorder in Cell-Signaling and Cancer-Associated Proteins", *Journal of Molecular Biology*, **232(3)**:573-584
- Ikegami Y., Goto H., Kiyono T., Enomoto M., Kasahara K., Tomono Y., Tozawa K., Morita A., Kohri K., Inagaki M. (2008), "Chk1 Phosphorylation at Ser286 and Ser301 Occurs with Both Stalled DNA Replication and Damage Checkpoint Simulation", *Biochemical and Biophysical Research Communications*, **377(4)**:1227-1231
- Inagaki A., Sleddens-Linkels E., van Cappellen W.A., Hibbert R.G., Sixma T.K., Hoeijmakers J.H., Grootegeod J.A., Baarends W.M. (2011), "Human RAD18 Interacts with Ubiquitylated Chromatin Components and Facilitates RAD9 Recruitment to DNA Double Strand Breaks", *PLoS One*, **6(8)**:e23155
- Innominato P.F., Giacchetti S., Bjarnason G.A., Focan C., Garufi C., Coudert B., Lacobelli S., Tampellini M., Durando X., Mormont M.C., Waterhouse J., Lévi F.A. (2012), "Prediction of Overall Survival Through Circadian Rest-Activity Monitoring During Chemotherapy for Metastatic Colorectal Cancer", *International Journal of Cancer*, **Electronic Publication Ahead of Print (5th April 2012)**
- Ira G. and Hastings P.J. (2012), "DNA Breakage Drives Nuclear Search", *Nature Cell Biology*, **14(5)**:448-450
- Ishida T. and Kinoshita K. (2007), "PrDOS: Prediction of Disordered Protein Regions from Amino Acid Sequence", *Nucleic Acids Research*, (Web Server Issue), **35**:W460-W464

- Ishii H., Mimori K., Inoue H., Inageta T., Ishikawa K., Semba S., Druck T., Trapasso F., Tani K., Vecchione A., Croce C.M., Mori M., Huebner K. (2006), "Fhit Modulates the DNA Damage Checkpoint Response", *Cancer Research*, **66(23)**:11287-11292
- Ishikawa K., Ishii H., Ichimura K. (2008), "Modulation of DNA Damage Checkpoint: Patenting and Possible Application for Cancer Medicine", *Recent Patents from DNA and Gene Sequences*, **2(1)**:34-39
- Ishikawa K., Ishii H., Saito T., Ichimura K. (2006), "Multiple Functions of Rad9 for Preserving Genomic Integrity", *Current Genomics*, **7(8)**:477-480
- Ito K., Hirao A., Arai F., Takubo K., Matsuoka S., Miyamoto K., Ohmura M., Naka K., Hosokawa K., Ikeda Y., Suda T. (2006), "Reactive Oxygen Species Act Through p38 MAPK to Limit the Lifespan of Haematopoietic Stem Cells", *Nature Medicine*, **12(4)**:446-451
- Ivanova B. and Spiteller M. (2012), "Structure and Properties of Camptothecin Derivatives, Their Protonated Forms and Model Interaction with the Topoisomerase I-DNA Complex", *Biopolymers*, **97(2)**:134-144
- Ivanov I., Chapados B.R., McCammon J.A., Tainer J.A. (2006), "Proliferating Cell Nuclear Antigen Loaded Onto Double-Stranded DNA: Dynamics, Minor Groove Interactions and Functional Implications", *Nucleic Acids Research*, **34(20)**:6023-6033
- Iwaki K., Goa T., Tanaka N., Takegawa K. (2004), "Characterization of *Schizosaccharomyces pombe* Mutants Defective in Vacuolar Acidification and Protein Sorting", *Molecular Genetics and Genomics*, **271(2)**:197-207
- Janes S.R.C. (1999), "A Comparative Study of *In Vivo* Urethane-Induced and Spontaneous Type Mutations via DNA Sequence Analyses of Mutant Plaques Derived from the MutaTM Mouse Transgenic Assay System", MSc. in Toxicology Thesis, School of Biosciences, University of Birmingham in Collaboration with Astra-Zeneca, Toxicogenomics Laboratory D24, Safety of Medicines Site., Alderley Park, Macclesfield, Cheshire (Unpublished Work).
- Janes S.R.C. (2006), "Probing Chemical and Biological SAR Characteristics of a Novel Series of Potential Anti-Neoplastic p-Cymene-Based Neutral, Charged Monomeric and Charged Dimeric Type "Piano Stool" Organoruthenium Complexes via PAGE Retardation and Mass Spectrometry Analyses of their Respective Interactions with the MS2 Wild-Type TR-RNA Stem Operator Loop Fragment and Cytotoxic Assessment in the *E. coli* Bacterial Strain ATCC25922", MSc. in Chemical Biology Thesis, School of Chemistry, University of Leeds in Collaboration with the Astbury Research Centre, School of Biology, University of Leeds (Unpublished Work).
- Janes S., Schmidt U., Garrido K.A., Ney N., Concilio S., Zekri M., Caspari T. (2012), "Heat Induction of a Novel Rad9 Variant From a Cryptic Translation Initiation Site Reduces Mitotic Commitment", *Journal of Cell Science*, Publication Manuscript in Press, **Electronic Publication Ahead of Print (13th July 2012)** – See Appendix 6.1, pp.626-663, in this Ph.D. thesis
- Jansen J.G., Fousteri M.I., de Wind N. (2007), "Send in the Clamps: Control of DNA Translesion Synthesis in Eukaryotes", *Molecular Cell*, **28(4)**:522-529
- Jazayeri A., Falck J., Lukas C., Bartek J., Smith G.C., Lukas J., Jackson S.P. (2006), "ATM and Cell Cycle-Dependent Regulation of ATR in Response to DNA Double-Stranded Breaks", *Nature Cell Biology*, **8(1)**:37-45

- Jenster G., van der Korput H.A., Trapman J., Brinkmann A.O. (1995), "Identification of Two Transcription Activation Units in the N-Terminal Domain of the Human Androgen Receptor", *Journal of Biological Chemistry*, **270**(13):7341-7346
- Jiang H.Y., Hickey R.J., Abdel-Aziz W., Tom T.D., Wills P.W., Liu J., Malkas L.H. (2002), "Human Cell DNA Replication is Mediated by a Discrete Multi-Protein Complex", *Journal of Cellular Biochemistry*, **85**(4):762-774
- Jiao Y., Seeger K., Lautrette A., Gaubert A., Mousson F., Guerois R., Mann C., Ochsenbein F. (2012), "Surprising Complexity of the Asf1 Histone Chaperone-Rad53 Kinase Interaction", *Proceedings of the National Academy of Sciences U.S.A.*, **109**(8):2866-2871
- Johnson B.D., Schumacher R.J., Ross E.D., Toft D.O. (1998), "Hop Modulates Hsp70/Hsp90 Interactions in Protein Folding", *Journal of Biological Chemistry*, **273**(6):3679-3686
- Johnson J.L. and Brown C. (2009), "Plasticity of the Hsp90 Chaperone Machinery in Divergent Eukaryotic Organisms", *Cell Stress and Chaperones*, **14**(1):83-94
- Jones C.J. and Wood R.D. (1993), "Preferential Binding of the Xeroderma Pigmentosum Group A Complementing Protein to Damaged DNA", *Biochemistry*, **32**(45):12096-12104
- Jones D.T. and Swindells M.B. (2002), "Getting the Most from PSI-BLAST", *Trends in Biochemical Sciences*, **27**(3):161-164
- Jones D.T. and Ward J.J. (2003), "Prediction of Disordered Regions in Proteins from Position Specific Score Matrices", *Proteins*, **53** (Supplement 6):573-578
- Jones M.E. (1980), "Pyrimidine Nucleotide Synthesis in Animals: Genes, Enzymes and Regulation of UMP Biosynthesis", *Annual Reviews in Biochemistry*, **49**:253-279
- Jones P.A. (2012), "Functions of DNA Methylation: Islands, Start Sites, Gene Bodies and Beyond", *Nature Reviews Genetics*, **13**(7):484-492
- Jones R.L. and Constantinidou A. (2012), "The Efficacy of Caffeine-Potentiated Chemotherapy in Clear Cell Sarcoma", *International Journal of Oncology*, **Electronic Publication Ahead of Print (7th February 2012) DOI:10.1007/510147-012-X**
- Juretić D., Zoranić L., Zucić D. (2002), "Basic Charge Clusters and Predictions of Membrane Protein Topology", *Journal of Chemical Information and Computer Sciences*, **42**(3):620-632
- Kadir R., Bakhrat A., Tokarsky R. Abdu U. (2012), "Localisation of the Drosophila Rad9 protein to the Nuclear Membrane is Regulated by the C-Terminal Region and is Affected in the Meiotic Checkpoint", *PLoS One*, **7**(5):e38010
- Kai M., Furuya K., Paderi F., Carr A.M., Wang T.S. (2007), "Rad3-Dependent Phosphorylation of the Checkpoint Clamp Regulates Repair-Pathway Choice", *Nature Cell Biology*, **9**(6):691-697
- Käll L., Krogh A., Sonnhammer E.L. (2007), "Advantages of Combined Transmembrane Topology and Signal Peptide Prediction: The Phobius Web Server", *Nucleic Acids Research*, **35** (Web Server Issue):W429-W432
- Kang H.Y., Yeh S., Fujimoto N., Chang C. (1999), "Cloning and Characterisation of Human Prostate Coactivator ARA54: A Novel Protein that Associates with the Androgen Receptor", *Journal of Biological Chemistry*, **274**(13):8570-8576

- Kang J., Chen Y., Zhao Y., Yu H. (2007), “Autophosphorylation-Dependent Activation of Human Mps1 is Required for the Spindle Checkpoint”, *Proceedings of the National Academy of Sciences U.S.A.*, **104(51)**:20232-20237
- Kanoh Y., Tamai K., Shirahige K. (2006), “Different Requirements for Association of ATR-ATRIP and 9-1-1 to the Stalled Replication Forks”, *Gene*, **377**:88-95
- Kapelari B., Bech-Otschir D., Heherl R., Schade R., Dumdey R., Dubiel W. (2000), “Electron Microscopy and Subunit-Subunit Interaction Studies Reveal a First Architecture of the COP9 Signalosome”, *Journal of Molecular Biology*, **300(5)**:1169-1178
- Karagöz G.E., Duarte A.M., Ippel H., Uetrecht C., Sinnige T., van Rosmalen M., Hausmann J., Heck A.J., Boelens R., Rüdiger S.G. (2011), “N-Terminal Domain of Hsp90 Triggers Binding to the Co-chaperone p23”, *Proceedings of the National Academy of Sciences U.S.A.*, **108(2)**:580-585
- Karran P. (2000), “DNA Double Strand Break Repair in Mammalian Cells”, *Current Opinion in Genetics and Development*, **10(2)**:144-150
- Kastan M.B. (1999), “Molecular Determinants of Sensitivity to Antitumour Agents”, *Biochimica et Biophysica Acta*, **1424(1)**:R37-R42
- Kato J.Y., Nakamae I., Tomoda K., Fukumoto A., Yoneda-Kato N. (2006), “Preparation and Characterization of Monoclonal Antibodies Against Mouse Jab1/CSN5 Protein”, *Hybridoma (Larchmt.)*, **25(6)**:342-348
- Kaufmann W.K. (1995), “Cell Cycle Checkpoints and DNA Repair Preserve the Stability of the Human Genome”, *Cancer Metastasis Reviews*, **14(1)**:31-41
- Kaufmann W.K., Hefferman T.P., Beaulieu L.M., Doherty S., Frank A.R., Zhou Y., Btyant M.F., Zhou T., Luche D.D., Nikolaishvili-Feinberg N., Simpson D.A., Cordeiro-Stone M. (2003), “Caffeine and Human DNA Metabolism: The Magic and the Mystery”, *Mutation Research*, **532(1-2)**:85-102
- Kaur B. and Doechst P.W. (2000), “Ultraviolet Damage Endonuclease (Uve1p): A Structure and Strand-Specific DNA Endonuclease”, *Biochemistry*, **39(19)**:5788-5796
- Kawano Y., Nagata M., Kohno T., Ichimiya A., Iwakiri T., Okumura M., Arimori K. (2012), “Caffeine Increases the Anti-Tumour Effect of Cisplatin in Human Hepatocellular Carcinoma Cells”, *Biological and Pharmaceutical Bulletin*, **35(3)**:400-407
- Kazlauskas D. and Venclovas C. (2011), “Computational Analysis of DNA Replicases in Double-Stranded DNA Viruses: Relationship with Genome Size”, *Nucleic Acids Research*, **39(19)**:8291-8305
- Kazmirski S.L., Zhao Y., Bowman G.D., O'Donnell M., Kuriyan J. (2005), “Out-of-Plane Motions in Open Sliding Clamps: Molecular Dynamics Simulations of Eukaryotic and Archaeal Proliferating Cell Nuclear Antigen”, *Proceedings of the National Academy of Sciences U.S.A.*, **102(39)**:13801-13806
- Kekebew E., Peng M., Reiff E., Duh Q.Y., Clark O.H., McMillan A. (2006), “Diagnostic and Prognostic Value of Cell-Cycle Regulatory Genes in Malignant Thyroid Neoplasms”, *World Journal of Surgery*, **30(5)**:767-774

Kelly S.O. and Barton J.K. (1999), "Electron Transfer Between Bases in Double Helical DNA", *Science*, **285(5400)**:375-381

Kelly T.J., Nurse P., Forsburg S.L. (1993), "Coupling DNA Replication to the Cell Cycle", *Cold Spring Harbour Symposia on Quantitative Biology*, **58**:637-644

Kemp M.G., Akan Z., Yilmaz S., Grillo M., Smith-Roe S.L., Kang T.H., Cordeiro-Stone M., Kaufmann W.K., Abraham R.T., Sancar A., Unsul-Kacmaz K. (2010), "Tipin-Replication Protein A Interaction Mediates Chk1 Phosphorylation by ATR in Response to Genotoxic Stress", *Journal of Biological Chemistry*, **285(22)**:16562-16571

Kemppainen J.A., Langley E., Wong C.I., Bobseine K., Kelce W.R., Wilson E.M. (1999), "Distinguishing Androgen Receptor Agonists and Antagonists: Distinct Mechanisms of Activation by Medroxyprogesterone Acetate and Dihydrotestosterone", *Molecular Endocrinology*, **13(3)**:440-454

Kerrigan J.E. and Pilch D.S. (2001), A Structural Model for the Ternary Cleavable Complex Formed Between Human Topoisomerase I, DNA and Camptothecin", *Biochemistry*, **40(33)**:9792-9798

Khair L., Chang Y.T., Subramanian L., Russell P., Nakamura T.M. (2010), "Roles of the Checkpoint Sensor Clamp Rad9-RAD1-Hus1 (911)-Complex and the Clamp Loaders Rad17-RFC and Ctf18-RFC in *Schizosaccharomyces pombe* Telomere Maintenance", *Cell Cycle*, **9(11)**:2237-2248

Khong T. and Spencer A. (2011), "Targeting Heat Shock Protein 90 Induces Apoptosis and Inhibits Critical Survival and Proliferation Pathways in Multiple Myeloma", *Molecular Cancer Therapeutics*, **10(10)**:1909-1917

Kilkenny M.L., Doré A.S., Roe M., Nestoras K., Ho J.C.Y., Watts F.Z., Pearl L.H. (2008), "Structural and Functional Analysis of the Crb2-BRCT₂ Domain Reveals Distinct Roles in Checkpoint Signaling and DNA Damage Repair", *Genes and Development*, **22(15)**:2034-2047

Kim A.J., Kim H.J., Jee H.J., Song N., Kim M., Bae Y.S., Chung J.H., Yun J. (2011), "Glucose Deprivation is Associated with Chk1 Degradation Through the Ubiquitin-Proteasome Pathway and Effective Checkpoint Response to Replication Blocks", *Biochimica et Biophysica Acta*, **1813(6)**:1230-1238

Kim G.Y., Mercer S.E., Ewton D.Z., Yan Z., Jin K., Friedman E. (2002), "The Stress-Activated Protein Kinases p38 Alpha and JNK1 Stabilize p21(Cip1) by Phosphorylation", *Journal of Biological Chemistry*, **277(33)**:29792-29802

Kim L.S. and Kim J.H. (2011), "Heat Shock Proteins as Molecular Targets for Breast Cancer Therapeutics", *Journal of Breast Cancer*, **14(3)**:167-174

Kim M-Ae., Kim H-J., Brown A.L., Lee M-Y., Bae Y-S., Park J-I., Kwak J-Y., Chung J.H., Yun J. (2007), "Identification of Novel Substrates for Human Checkpoint Kinase Chk1 and Chk2 Through Genome-Wide Screening Using a Consensus Chk Phosphorylation Motif", *Experimental and Molecular Medicine*, **39(2)**:205-212

Kim R. and Guo J.T. (2010), "Systematic Analysis of Short Internal Indels and Their Impact on Protein Folding", *BMC Structural Biology*, **10**:24

- Kim S.T., Lim D.S., Canman C.E., Kastan M.B. (1999), "Substrate Specificities and Identification of Putative Substrates of ATM Kinase Family Members", *Journal of Biological Chemistry*, **274(53)**:37538-37543
- Kim Y.G. (2002), "Laser-Mediated Production of Reactive Oxygen and Nitrogen Species: Implications for Therapy", *Free Radical Research*, **36(12)**:1243-1250
- King H.A., Cobbold L.C., Willis A.E. (2010), "The Role of IRES Trans-Acting Factors in Regulating Translation Initiation", *Biochemical Society Transactions*, **38(6)**:1581-1586
- Kirichenko A.V. and Rich T.A. (1999), "Radiation Enhancement by 9-Aminocamptothecin: The Effect of Fractionation and Timing of Administration", *International Journal of Radiation, Oncology, Biology, Physics*, **44(3)**:659-664
- Kishi H., Nakagawa K., Matsumoto M., Suga M., Ando M., Taya Y., Yamaizumi M. (2001), "Osmotic Shock Induces G1 Arrest Through p53 Phosphorylation at Ser33 by Activated p38MAPK Without Phosphorylation at Ser15 and Ser20", *Journal of Biological Chemistry*, **276(42)**:39115-39122
- Kitagawa K., Abdulle R., Bansal P.K., Cagney G., Fields S., Hieter P. (2003), "Requirement of Skp1-Bub1 Interaction for Kinetochore-Mediated Activation of the Spindle Checkpoint", *Molecular Cell*, **11(5)**:1201-1213
- Klaassen C.D. (2008), "Casarett and Doull's Toxicology: The Basic Science of Poisons", 7th Edition, McGraw-Hill Medical
- Kleemann R., Hausser A., Geiger G., Mishke R., Burger-Kentischer A., Flieger O., Johannes F.J., Roger T., Calandra T., Kapumiotun A., Grell M., Finkelmeier D., Brunner H., Bernhagen J. (2000), "Intracellular Action of the Cytokine MIF to Modulate AP-1 Activity and the Cell Cycle Through Jab1", *Nature*, **408(6809)**:211-216
- Klugland A. and Lindahl T. (1997), "Second Pathway for Completion of Human DNA Base Excision-Repair: Reconstitution with Purified Protein and Requirement for DNase IV (FEN1)", *The EMBO Journal*, **16(11)**:3341-3348
- Knoepf D.M. *et al* (1999), "How the Cyclin Became a Cyclin: Regulated Proteolysis in the Cell Cycle", *Cell*, **97(4)**:431-434
- Kobayashi A., Hirose T., Yamada T. (2002), "Three Patients with Advanced Nonresectable and Recurrent Gastric Cancer Responding to Chronomodulation Chemotherapy with Tegafur + Cisplatin + Isovornin, Followed by CPT-11 Administration", *Gan To Kagaku Ryoho*, **29(8)**:1439-1445
- Kochetov A.V. (2005), "AUG Codons at the Beginning of Protein Coding Sequences are Frequent in Eukaryotic mRNAs with a Sub-Optimal Start Context", *Bioinformatics*, **21(7)**:837-840
- Kochetov A.V. (2008a), "Alternative Translation Start Sites and Hidden Coding Potential of Eukaryotic mRNAs", *Bioessays*, **30(7)**:683-691
- Kochetov A.V., Ahmad S., Ivanisenko V., Volkova O.A., Kolchanov N.A., Sarai A. (2008b), "uORFs, Reinitiation and Alternative Translation Start Sites in Human mRNA s", *FEBS Letters*, **582(9)**:1293-1297

- Kochetov A.V., Sarai A., Vorob'ev D.G., Kolchanov N.A., (2002), "The Context Organisation of Functional Regions in Yeast Genes with High-Level Expression", *Molekuliarnaia Biologiia*, **36(6)**:1026-1034
- Kohli J. and Nurse P., (1995), "Genetic Nomenclature Guide: *Schizosaccharomyces pombe*", *Trends in Genetics*, **Mar**:9-10
- Kohn K.W. and Pommier Y. (2000), "Molecular and Biological Determination of the Cytotoxic Actions of Camptothecins; Perspective for the Development of New Topoisomerase Inhibitors", *Annals of the New York Academy of Sciences*, **922**:11-26
- Komatsu K., Hopkins K.M., Lieberman H.B., Wang H. (2000a), "*Schizosaccharomyces pombe* Rad9 Contains a BH3-Like Region and Interacts with the Apoptotic Protein Bcl-2", *FEBS Letters*, **481(2)**:122-126
- Komatsu K., Miyashita T., Hang H., Hopkins K.M., Zheng W., Cuddeback S., Yamada M., Lieberman H.B., Wang H-G. (2000b), "Human Homologue of *S. pombe* Rad9 Interacts with BCL-2/BCL-xL and Promotes Apoptosis", *Nature Cell Biology*, **2(1)**:1-6
- Komatsu K., Wharton W., Hang H., Wu C., Singh S., Lieberman H.B., Pledger W.J., Wang H.G. (2000c), "PCNA Interacts with hHus1/hRad9 in Response to DNA Damage and Replication Inhibition", *Oncogene*, **19(46)**:5291-5297
- Kondo T., Wakayama T., Naiki T., Matsumoto K., Sugimoto K. (2001), "Recruitment of Mec1 and Ddc1 Checkpoint Proteins to Double-Strand Breaks Through Distinct Mechanisms", *Science*, **294(5543)**:867-870
- Kondratov R.V. (2007), "A Role of the Circadian System and Circadian Proteins in Ageing", *Ageing Research Reviews*, **6(1)**:12-27
- Kondratov R.V. and Antoch M.P. (2007), "Circadian Proteins in the Regulation of Cell Cycle and Genotoxic Stress Responses", *Trends in Cell Biology*, **17(7)**:311-317
- Koochekpour S. (2010), "Androgen Receptor Signalling and Mutations in Prostate Cancer", *Asian Journal of Andrology*, **12(5)**:639-657
- Kosugi S., Hasebe M., Tomita M., Yanagawa H. (2009), "Systematic Identification of Cell Cycle-Dependent Yeast Nucleocytoplasmic Shuttling Proteins by Prediction of Composite Motifs", *Proceedings of the National Academy of Sciences U.S.A.*, **106(25)**:10171-10176
- Kotsis D.H., Masko E.M., Sigoillot F.D., Di Gregorio R., Guy-Evans H.I., Evans D.R. (2007), "Protein Kinase A Phosphorylation of the Multifunctional Protein CAD Antagonizes Activation by the MAP Kinase Cascade", *Molecular and Cellular Biochemistry*, **301(1-2)**:69-81
- Kristeleit R., Stimson L., Workman P., Aherne W. (2004), "Histone Modification Enzymes: Novel Targets for Cancer Drugs", *Expert Opinion on Emerging Drugs*, **9(1)**:135-154
- Kroemer G. and Pouyssegur J. (2008), "Tumour Cell Metabolism: Cancer's Achilles' Heel", *Cancer Cell*, **13(6)**:472-482
- Kubota Y., Nash R.A., Klungland A., Schlar P., Barnes D.E., Lindahl T. (1996), "Reconstitution of DNA Base Excision-Repair with Purified Human Proteins: Interaction Between DNA Polymerase Beta and the XRCC1 Protein", *The EMBO Journal*, **15(23)**:6662-6670

- Kuga Y., Tanaka T., Okanobu H., Arita M., Yoshimi S., Miwata T., Fujino H., Moriya T., Ohya T. (2011), "A Case of Drug-Induced Interstitial Pneumonia Caused by S-1 and CPT-11 Combination Therapy for Advanced Colon Cancer", *Gan To Kagaku Ryoho (Cancer and Chemotherapy)*, **38(3)**:469-472
- Kühl N.M. and Rensing L. (2000), "Heat Shock Effects on Cell Cycle Progression", *Cellular and Molecular Life Sciences*, **57(3)**:450-463
- Kulkarni A. and Das K.C. (2008), "Differential Roles of ATR and ATM in p53, Chk1 and Histone H2AX Phosphorylation in Response to Hyperoxia: ATR-Dependent ATM Activation", *American Journal of Physiology, Lung Cellular and Molecular Physiology*, **294(5)**:L998-L1006
- Kulkarni P., Rajagopalan K., Yeater D., Getzenberg R.H. (2011), "Protein Folding and the Order/Disorder Paradox", *Journal of Cellular Biochemistry*, **112(7)**:1949-1952
- Kumada K., Yanagida M., Toda T. (1996), "Caffeine-Resistance in Fission Yeast is Caused by Mutations in a Single Essential Gene, *crm1*⁺", *Molecular and General Genetics*, **250(1)**:59-68
- Kumar R. and Singh J. (2006), "A Truncated Derivative of nmt1 Promoter Exhibits Temperature-Dependent Induction of Gene Expression in *Schizosaccharomyces pombe*", *Yeast*, **23(1)**:55-65
- Kumar S. and Carugo O. (2008), "Consensus Prediction of Protein Conformational Disorder from Amino Acid Sequence", *Open Biochemistry Journal*, **2**:1-5
- Kundrat P. and Steward R.D. (2006), "On the Biophysical Interpretation of Lethal DNA Lesions by Ionising Radiation", *Radiation Protection Dosimetry*, **122(1-4)**:169-172
- Kunz C. and Fleck O. (2001), "Role of the DNA Repair Nucleases Rad13, Rad2 and Uve1 of *Schizosaccharomyces pombe* in Mismatch Correction", *Journal of Molecular Biology*, **313(2)**:241-253
- Kusumoto R., Masutani C., Sugawara K., Iwai S., Araki M., Uchida A., Mizukoshi T., Hanaoka F. (2001), "Diversity of the Damage Recognition Step in the Global Genomic Nucleotide Excision Repair in Vitro", *Mutation Research*, **485(3)**:219-227
- Kwok S.F., Solano R., Tsuge T., Chamovitz D.A., Ecker J.R., Matsui M., Deng X.W. (1998), "Arabidopsis Homologs of a c-Jun Coactivator are Present in Both Monomeric Form and in the COP9 Complex and their Abundance is Differentially Affected by the Pleiotropic Cop/Det/Fus Mutations", *The Plant Cell*, **10(11)**:1779-1790
- Kwok S.F., Staub J.S. and Deng X.W. (1999), "Characterization of Two Sub-Units of the Arabidopsis 19S Proteasome Regulatory Complex and Its Possible Interaction with the COP9 Complex", *Journal of Molecular Biology*, **275(1)**:85-95
- Kyriakis J.M. and Avruch J. (1996a), "Protein Kinase Cascades Activated by Stress and Inflammatory Cytokines", *Bioessays*, **18(7)**:567-577
- Kyriakis J.M. and Avruch J. (1996b), "Sounding the Alarm: Protein Kinase Cascades Activated by Stress and Inflammatory Cytokines", *Journal of Biological Chemistry*, **271(40)**:24313-24316
- Kyte J. and Doolittle R.F. (1982), "A Simple Method for Displaying the Hydropathic Character of a Protein", *Journal of Molecular Biology*, **157(1)**:105-132

Lamb J.R., Tugendreich S., Hieter P. (1995), "Tetratricopeptide Repeat Interactions: To TPR or Not to TPR?", *Trends in Biochemical Sciences*, **20(7)**:257-259

Lambert J.R. and Nordeen S.K. (1998), "Steroid-Selective Initiation of Chromatin Remodeling and Transcriptional Activation of the Mouse Mammary Tumour Virus Promoter is Controlled by the Site of Promoter Integration", *Journal of Biological Chemistry*, **273(49)**:32708-32714

Lamont K.R. and Tindall D.J. (2010), "Androgen Regulation of Gene Expression", *Advances in Cancer Research*, **107**:137-162

Langley E., Zhou Z.X., Wilson E.M. (1995), "Evidence for an Anti-Parallel Orientation of the Ligand-Activated Human Androgen Receptor Dimer", *Journal of Biological Chemistry*, **270(50)**:29983-29990

Larsen B.D. and Megeney L.A. (2010), "Parole Terms for a Killer: Directing Caspase3/CAD-Induced DNA Strand Breaks to Co-Ordinate Changes in Gene Expression", *Cell Cycle*, **9(15)**:2940-2945

Larson I.K. and Kastrup J.S. (2002), "Ch.17: Anticancer Drugs" in Kronsgaard-Larsen P., Liljefors T., Madsen U. (2002), "Textbook of Drug Design and Drug Discovery", 3rd Edition, Taylor and Francis, **Ch17**:511-558

Laszlo A. and Fleischer I. (2009), "Heat-Induced Perturbations of DNA Damage Signaling Pathways are Modulated by Molecular Chaperones", *Cancer Research*, **69(5)**:2042-2049

Latif C., Harvey S.H., O'Connell M.J. (2001), "Ensuring the Stability of the Genome: DNA Damage Checkpoints", *The Scientific World Journal*, **1**:684-702

Laurence T.A., Kwon Y., Johnson A., Hollars C.W., O'Donnell M., Camarero J.A., Barsky D. (2008), "Motion of a DNA Sliding Clamp Observed by Single Molecule Fluorescence Spectroscopy", *Journal of Biological Chemistry*, **283(34)**:22895-22906

Laursen L.V., Ampatzidou E., Andersen A.H., Murray J.M. (2003a), "Role for Fission Yeast RecQ Helicase in DNA Repair in G2", *Molecular and Cellular Biology*, **23(10)**:3692-3705

Laursen L.V., Bjergbaek L., Murray J.M., Andersen A.H. (2003b), "RecQ Helicases and Topoisomerase III in Cancer and Aging", *Biogerontology*, **4(5)**:275-287

Lavoie J.N., Rivard N., L'Allemain G., Pouysségur J. (1996), "A Temporal and Biochemical Link Between Growth Factor-Activated MAP Kinases, Cyclin D1 Induction and Cell Cycle Entry", *Progress in Cell Cycle Research*, **2**:49-58

Leach F.S., Nicolaides N.C. Papadopoulos N., Liu B., Jen J., Parsons R., Peltomaki P., Sistonen P., Aaltonen L.A., Nyström-Lahti M., Guan X-Y., Zhang J., Meltzer P., Yu J-Y., Kao F-T., Chen D.J., Cerosaletti K.M., Fournier K.R.E., Todd S., Lewis T., Leach R.J., Naylor S.L., Weissenbach J., Mecklin J-P., Järvinen H., Petersen G.M., Hamilton S.R., Green J., Jass J., Watson P., Lynch H.T., Trent J.M., de la Chapelle A., Kinzler K.W., Vogelstein B. (1993), "Mutations of mutS Homolog in Hereditary Nonpolyposis Colorectal Cancer", *Cell*, **75(6)**:1215-1225

Lee C.C. (2005), "The Circadian Clock and Tumor Suppression by Mammalian Period Genes", *Methods in Enzymology*, **393**:852-861

Lee D.J., Wynveen A., Korneyshev A.A., Leikin S. (2010), "Undulations Enhance the Effect of Helical Structure on DNA Interactions", *Journal of Physical Chemistry B*, **114(35)**:11668-11680

- Lee D.K. and Chang C. (2003), "Molecular Communication Between Androgen Receptor and General Transcription Machinery", *Journal of Steroid Biochemistry and Molecular Biology*, **84(1)**:41-49
- Lee J., Kumagai A., Dunphy W.G. (2001), "Positive Regulation of Wee1 by Chk1 and 14-3-3 Proteins", *Molecular Biology of the Cell*, **12(3)**:551-563
- Lee J., Kumagai A., Dunphy W.G. (2003), "Claspin, A Chk1-Regulatory Protein, Monitors DNA Replication on Chromatin Independently of RPA, ATR and Rad17", *Molecular Cell*, **11(2)**:329-340
- Lee J., Kumagai A., Dunphy W.G. (2007), "The Rad9-Hus1-Rad1 Checkpoint Clamp Regulates Interaction of TopBP1 with ATR", *Journal of Biological Chemistry*, **282(38)**:28036-28044
- Lee J.H. and Paull T.T. (2004), "Direct Activation of the ATM Protein Kinase by the Mre11/Rad50/Nbs1 Complex", *Science*, **304(5667)**:93-96
- Lee K.Y. and Myung K. (2008), "PCNA Modifications for Regulation of Post-Replication Repair Pathways", *Molecules and Cells*, **26(1)**:5-11
- Lee M. and Nurse P. (1988), "Cell Cycle Control Genes in Fission Yeast and Mammalian Cells", *Trends in Genetics*, **4(10)**:287-290
- Lee M.W., Hirai I., Wang H-G. (2003), "Caspase-3-Mediated Cleavage of Rad9 During Apoptosis", *Oncogene*, **22(41)**:6340-6346
- Lee S.H., Oshige M., Durant S.T., Raslia K.K., Williamson E.A., Ramsay H., Kwan L., Nickoloff J.A., Hromas R. (2005), "The SET Domain Protein Metnase Mediates Foreign DNA Integration and Links Integration to Non-Homologous End-Joining Repair", *Proceedings of the National Academy of Sciences U.S.A.*, **102(50)**:18075-18080
- Le Gall T., Romero P., Cortese M.S., Uversky V.N., Dunker A.K. (2007), "Intrinsic Disorder in the Protein Data Bank", *Journal of Biomolecular Structure and Dynamics*, **24(4)**:303-428
- Leloupe C., Hopkins K.M., Wang X., Zhu A., Wolgemuth D.J., Lieberman H.B. (2010), "Mouse Rad9b is Essential for Embryonic Development and Promotes Resistance to DNA Damage", *Developmental Dynamics*, **239(11)**:2837-2850
- Lemaire M., Froment C., Boutros R., Mondesert O., Nebreda A.R., Monsarrat B., Ducommun B. (2006), "CDC25B Phosphorylation by p38 and MK-2", *Cell Cycle*, **5(15)**:1649-1653
- Le Page S., Kwiatkowski F., Paulin C., Mohamed F., Pezet D., Chipponi J., Benhamed M., Gilly F.N., Glehen O. (2006), "In Vitro Thermochemotherapy of Colon Cancer Cell Lines with Irinotecan Alone and Combined with Mitomycin C", *Hepatogastroenterology*, **53(71)**:693-697
- Leung-Pineda V., Ryan C.E., Piwnicka-Worms H. (2006), "Phosphorylation of Chk1 by ATR is Antagonized by a Chk1-Regulated Protein Phosphatase 2A Circuit", *Molecular and Cellular Biology*, **26(20)**:7529-7538
- Leupold U. (1958), "Studies on Recombination in *Schizosaccharomyces pombe*", *Cold Spring Harbor Symposia on Quantitative Biology*, **23**:161-170

Lévi F., Karaboué A., Gorden L., Innominato P.F., Saffroy R., Giacchetti S., Hauteville D., Guettier C., Adam R., Bouchahda M. (2011), “Cetuximab and Circadian Chronomodulated Chemotherapy as a Salvage Treatment for Metastatic Colorectal Cancer (mCRC): Safety, Efficacy and Improved Secondary Surgical Resectability”, *Cancer Chemotherapy and Pharmacology*, **67(2)**:339-348

Lévi F. and Okyar A. (2011), “Circadian Clocks and Drug Delivery Systems: Impact and Opportunities in Chronotherapeutics”, *Expert Opinion in Drug Delivery*, **8(12)**:1535-1541

Lévi F. and Schibler U. (2007), “Circadian Rhythms: Mechanisms and Therapeutic Implications”, *Annual Review of Pharmacology and Toxicology*, **47**:593-628

Levine R.L., Hoogenraad N.J., Kretchmer N. (1971), “Regulation of Activity of Carbamoyl Phosphate Synthetase From Mouse Spleen”, *Biochemistry*, **10(20)**:3694-3699

Li D.Q., Oshiro K., Khan M.N., Kumar R. (2010), “Requirement of MTA1 in ATR-Mediated DNA Damage Checkpoint Function”, *Journal of Biological Chemistry*, **285(26)**:19802-19812

Li G.M. (2008), “Mechanisms and Functions of DNA Mismatch Repair”, *Cell Research*, **18(1)**:85-98

Li G.M. and Modrich P. (1995), “Restoration of Mismatch Repair to Nuclear Extracts of H6 Colorectal Tumor Cells by a Heterodimer of Human MutL Homologs”, *Proceedings of the National Academy of Sciences U.S.A.*, **92(6)**:1950-1954

Li J., Fu J., Toumazou C., Yoon H.G., Wong J. (2006), “A Role of the Amino-Terminal (N) and Carboxyl-Terminal (C) Interaction in Binding of Androgen Receptor to Chromatin”, *Molecular Genetics and Metabolism*, **20(4)**:776-785

Li J., Richter K., Buchner J. (2011), “Mixed Hsp90-Cochaperone Complexes are Important for the Progression of the Reaction Cycle”, *Nature Structural Molecular Biology*, **18(1)**:61-66

Li L., Lou Z., Wang L. (2011), “The Role of FKBP5 in Cancer Aetiology and Chemoresistance”, *British Journal of Cancer*, **104(1)**:19-23

Li N., Banin S., Ouyang H., Li G.C., Courtois G., Shiloh Y., Karin M., Rotman G. (2001), “ATM is Required for IKappaB Kinase (IKKk) Activation in Response to DNA Double Strand Breaks”, *Journal of Biological Chemistry*, **276(12)**:8898-8903

Li S., Liu X., Ascoli M. (2000), “p38JAB1 Binds to the Intracellular Precursor of the Lutropin/Choriogonadotropin Receptor and Promotes Its Degradation”, *Journal of Biological Chemistry*, **275(18)**:13386-13393

Lieberman H.B. (2006), “Rad9, An Evolutionary Conserved Gene with Multiple Functions for Preserving Genomic Integrity”, *Journal of Cellular Biochemistry*, **97(4)**:690-697

Lieberman H.B. (2008), “DNA Damage, Repair and Response Proteins as Targets for Cancer Therapy”, *Current Medicinal Chemistry*, **15(4)**:360-367

Lieberman H.B., Bernstock J.D., Broustas C.G., Hopkins K.M., Leloup C., Zhu A. (2011), “The Role of RAD9 in Tumourigenesis”, *Journal of Molecular Cell Biology*, **3(1)**:39-43

- Lieberman H.B., Hopkins K.M., Lavery M., Chu H.M. (1992), "Molecular Cloning and Analysis of *Schizosaccharomyces pombe rad9*: A Gene Involved in DNA Repair and Mutagenesis", *Mol Gen Genet*, **232(3)**:367-376
- Lieberman H.B., Hopkins K.M., Nass M., Demetrick D., Davey S. (1996), "A Human Homolog of the *Schizosaccharomyces pombe rad9+* Checkpoint Control Gene, *Proceedings of the National Academy of Sciences U.S.A.*, **93(24)**:13890-13895
- Lieberman H.B. and Zhu A. (2010), "Rad9 as a Diagnostic, Prognostic and Therapeutic Tool for Prostate Cancer", *United States Patent Application Publication*, **US Patent No.: 2010/0168202A1** [<http://www.freshpatents.com/-dt20100701ptan20100168202.php>]
- Lim D.S., Kim S.T., Xu B., Maser R.S., Lin J., Petrini J.H., Kastan M.B. (2000), "ATM Phosphorylates p95/Nbs1 in an S-Phase Checkpoint Pathway", *Nature*, **404(6778)**:613-617
- Lim H.W., Kim S.J., Park E.H., Lim C.J. (2007), "Overexpression of a Metacaspase Gene Stimulates Cell Growth and Stress Response in *Schizosaccharomyces pombe*", *Canadian Journal of Microbiology*, **53(8)**:1016-1023
- Lin K., Simossis V.A., Taylor W.R., Heringa J. (2005), "A Simple and Fast Secondary Structure Prediction Method Using Hidden Neural Networks", *Bioinformatics*, **21(2)**:152-159
- Lin S.J., Wardlaw C.P., Morishita T., Miyabe I., Chahwan C., Caspari T., Schmidt U., Carr A.M., Garcia V. (2012), "The Rad4(TopBP1) ATR-Activation Domain Functions in G1/S Phase in a Chromatin-Dependent Manner", *PLoS Genetics*, **8(6)**:e1002801
- Lindling R., Russell R.B., Neduva V., Gibson T.J. (2003), "Exploring Protein Sequences for Globularity and Disorder", *Nucleic Acids Research*, **31(13)**:3701-3708
- Lindsey-Boltz L.A., Wauson E.M., Graves L.M., Sancar A. (2004), "The human Rad9 Checkpoint Protein Stimulates the Carbamoyl Phosphate Synthetase Activity of the Multifunctional Protein CAD", *Nucleic Acids Research*, **32(15)**:1-7
- Linger J.G. and Tyler J.K. (2007), "Chromatin Disassembly and Reassembly During DNA Repair", *Mutation Research*, **618(1-2)**:52-64
- Liu C., Powell K.A., Mundt K., Wu L., Carr A.M., Caspari T. (2003), "COP9/Signalosome Sub-Units and Pcu4 Regulate Ribonucleotide Reductase by Both Checkpoint-Dependent and -Independent Mechanisms", *Genes and Development*, **17(9)**:1130-1140
- Liu C., Pouliot J.J., Nash H.A. (2002), "Repair of Topoisomerase I Covalent Complexes in the Absence of the Tyrosyl-DNA Phosphodiesterase Tdp1", *Proceedings of the National Academy of Sciences U.S.A.*, **99(23)**:14970-14975
- Liu F-H., Wu S-J., Hu S-M., Hsiao C.D., Wang C. (1999), "Specific Interaction of the 70kDa Heat Shock Cognate Protein with the Tetratricopeptide Repeats", *Journal of Biological Chemistry*, **274(48)**:34425-34432
- Liu G., Myers S., Chen X., Bissler J., Sinden R., Leffak M. (2012), "Replication Fork Stalling and Checkpoint Activation by a PKD1 Locus Mirror Repeat Homopurine-Homopyrimidine (Pu-Py) Tract", *Journal of Biological Chemistry*, **6TH August 2012: Electronic Publication Ahead of Print**

- Liu J., Guo L., Cheng G., Wang Y. (2008), "Characterisation and Anti-Tumour Activity of Triethylene Tetramine: A Novel Telomerase Inhibitor", *Biomedicine and Pharmacotherapy*, **62(7)**:480-485
- Liu J., Perumal N.B., Oldfield C.J., Su E.W., Uversky V.N., Dunker A.K. (2006), "Intrinsic Disorder in Transcription Factors", *Biochemistry*, **45(22)**:6773-6888
- Liu J., Tan H., Rost B. (2002), "Loopy Proteins Appear Conserved in Evolution", *Journal of Molecular Biology*, **322(1)**:53-64
- Liu J., Towle M.J., Cheng H., Saxton P., Reardon C., Wu J., Murphy E.A., Kuznetsov G., Johannes C.W., Tremblay M.R., Zhao H., Pesant M., Fang F.G., Vermeulen M.W., Gallagher B.M. Jr., Littlefield B.A. (2007), "In Vitro and In Vivo Anticancer Activities of Synthetic (-)-Laulimalide, a Natural Marine Product Microtubule Stabilizing Agent", *Anticancer Research*, **27(3B)**:1509-1518
- Liu L.F., Desai S.D., Li T-K., Mao Y., Sun M., Sim S-P. (2000), "Mechanism of Action of Camptothecin", *Annals of the New York Academy of Sciences*, **922**:1-10
- Liu L.J., Baxter J.R., Wang M.Y., Harper B.L., Tasaka F., Kohda K. (1990), "Induction of Covalent DNA Modifications and Micronucleated Erythrocytes by 4-Nitroquinoline-1-Oxide in Adult and Fetal Mice", *Cancer Research*, **50(19)**:6192-6198
- Liu N., Schild D., Thelen M.P., Thompson L.H. (2002), "Involvement of Rad51C in Two Distinct Protein Complexes of Rad51 Paralogs in Human Cells", *Nucleic Acids Research*, **30(4)**:1009-1015
- Liu Q., Kaneko S., Yang L., Feldman R.I., Nicosia S.V., Chen J., Cheng J.Q. (2004), "Aurora-A Abrogation of p53 DNA Binding and Transactivation Activity by Phosphorylation of Serine 215", *Journal of Biological Chemistry*, **279(50)**:52175-52182
- Liu S., Song N., Zou L. (2012), "The Conserved C Terminus of Claspin Interacts With Rad9 and Promotes Rapid Activation of Chk1", *Cell Cycle*, **11(14)**: epub ahead of print
- Liu S.T., van Deursen J.M., Yen T.J. (2003), "The Role of Mitotic Checkpoint in Maintaining Genomic Stability", *Current Topics in Developmental Biology*, **58**:27-51
- Liu Y., Fang Y., Shao H., Lindsey-Boltz L., Sancar A., Modrich P. (2010), "Interactions of Human Mismatch Repair Proteins with MutSalpha and MutLalpha with Proteins of the ATR-Chk1 Pathway", *Journal of Biological Chemistry*, **285(8)**:5974-5982
- Liu Y., Kvaratskhelia M., Hess S., Qu Y., Zou Y. (2005), "Modulation of Replication Protein A Function by Its Hyperphosphorylation-Induced Conformational Change Involving DNA Binding Domain B", *Journal of Biological Chemistry*, **280(38)**:32775-32783
- Livnah Z., Ziv O., Shachar S. (2010), "Multiple Two-Polymerase Mechanisms in Mammalian Translesion DNA Synthesis", *Cell Cycle*, **9(4)**:729-735
- Llopis J., Westin S., Ricote M., Wang Z., Cho C.Y., Kurokawa R., Mullen T.M., Rose D.W., Rosenfeld M.G., Tsien R.Y., Glass C.K., Wang J. (2000), "Ligand-Dependent Interactions of Coactivators Steroid Receptor Coactivator-1 and Peroxisome Proliferator-Activated Receptor Binding Protein with Nuclear Hormone Receptors Can Be Imaged in Live Cells and are Required for Transcription", *Proceedings of the National Academy of Sciences U.S.A.*, **97(8)**:4363-4368

- Loegering D., Arlander S.J., Hackbarth J., Vroman B.T., Roos-Mattjus P., Hopkins K.M., Lieberman H.B., Karnitz L.M., Kaufmann S.H. (2004), "Rad9 Protects Cells From Topoisomerase Poison-Induced Cell Death", *Journal of Biological Chemistry*, **279(18)**:18641-18647
- Longhese M.P., Bonetti D., Guerini I., Manfrini N., Clerici M. (2009), "DNA Double-Strand Breaks in Meiosis: Checking Their Formation, Processing and Repair", *DNA Repair (Amst.)*, **8(9)**:1127-1138
- Longhese M.P., Bonetti D., Manfrini N., Clerici M. (2010), "Mechanisms and Regulation of DNA End Resection", *The EMBO Journal*, **29(17)**:2864-2874
- Longhese M.P. (2006), "The Cellular Response to Chromosome Breakage", *Molecular Microbiology*, **60(5)**:1099-1108
- Longhese M.P. (2008), "DNA Damage Response at Functional and Dysfunctional Telomeres", *Genes and Development*, **22(2)**:125-140
- Longhese M.P., Paciotti V., Frascini R., Zaccarini R., Plevari P., Lucchini G. (1997), "The Novel DNA Damage Checkpoint Protein Ddc1p is Phosphorylated Periodically During the Cell Cycle and in Response to DNA Damage in Budding Yeast", *The EMBO Journal*, **16(17)**:5216-5226
- Longhese M.P., Paciotti V., Neecke H., Lucchini G. (2000), "Checkpoint Proteins Influence Telomere Silencing and Length Maintenance in Budding Yeast", *Genetics*, **155(4)**:1577-1591
- Longley M.J., Pierce A.J., Modrich P. (1997), "DNA Polymerase Delta is Required for Human Mismatch Repair in Vitro", *Journal of Biological Chemistry*, **272(16)**:10917-10921
- López-Contreras A.J. and Fernandez-Capetillo O. (2010), "The ATR Barrier to Replication-Born DNA Damage", *DNA Repair (Amst.)*, **9(12)**:1249-1255
- Lopez-Girona A., Furnari B., Mondesert O., Russell P. (1999), "Nuclear Localization of Cdc25 is Regulated by DNA Damage and a 14-3-3 Protein", *Nature*, **397(6715)**:172-175
- Loros J.J., Dunlap J.C., Larrondo L.F., Shi M., Belden W.J., Gooch V.D., Chen C.H., Baker C.L., Mehra A., Colot H.V., Schwerdtfeger C., Lambreghts R., Collopy P.D., Gamsby J.J., Hong C.I. (2007), "Circadian Output, Input and Intracellular Oscillators: Insights Into the Circadian Systems of Single Cells", *Cold Spring Harbor Symposia on Quantitative Biology*, **72**:201-214
- Lovejoy C.A., Xu X., Bansbach C.E., Glick G.G., Zhao R., Ye F., Sirbu B.M., Titus L.C., Shyr Y., Cortez D. (2009), "Functional Genomic Screens Identify CINP as a Genomic Maintenance Protein", *Proceedings of the National Academy of Sciences U.S.A.*, **106(46)**:19304-19309
- Low C.P., Shui G., Liew L.P., Butlner S., Madeo F., Dawes I.K., Wenk M.R., Yang H. (2008), "Caspase-Dependent and -Independent Lipotoxic Cell Death Pathways in Fission Yeast", *Journal of Cell Science*, **121(Pt.16)**:2671-2684
- Low C.P. and Yang H. (2008), "Programmed Cell Death in Fission Yeast *Schizosaccharomyces pombe*", *Biochimica et Biophysica Acta*, **1783(7)**:1335-1349
- Lu A.L., Bai H., Shi G., Chang D.Y. (2006), "MutY and MutY Homologs (MYH) in Genome Maintenance", *Frontiers in Bioscience*, **11**:3062-3080
- Lu A.L., Li X., Gu Y., Wright P.M., Chang D.Y. (2001), "Repair of Oxidative DNA Damage: Mechanisms and Functions", *Cell Biochemistry and Biophysics*, **35(2)**:141-170

- Lu Y.P., Lou Y.R., Peng Q.Y., Nghiem P., Conney A.H. (2011), “Caffeine Decreases Phospho-Chk1 (Ser317) and Increases Mitotic Cells with Cyclin B1 and Caspase 3 in Tumors from UVB-Treated Mice”, *Cancer Prevention Research*, **4(7)**:1118-1125
- Luche D.D. and Forsburg S.L. (2009), “Cell Cycle Synchrony for Analysis of *S. pombe* DNA Replication”, *Methods in Molecular Biology*, **521**:437-448
- Luncsford P.J., Chang D.Y., Shi G., Bernstein J., Madabushi A., Patterson D.N., Lu A.L., Toth E.A. (2010), “A Structural Hinge in MutY Homologues Mediates Catalytic Activity and Rad9-Rad1-Hus1 Checkpoint Complex Interactions”, *Journal of Molecular Biology*, **403(3)**:351-370
- Luo J., Solimini N.L., Elledge S.J. (2009), “Principles of Cancer Therapy: Oncogene and Non-Oncogene Addiction”, *Cell*, **136(5)**:823-837
- Lupas A., Van Dyke M., Stock J. (1991a), “Predicting Coiled Coils From Protein Sequences”, *Science*, **252(5009)**:1162-1164
- Lupas A., Van Dyke M., Stock J. (1991b), “Predicting Coiled Coils From Protein Sequences”, *Science*, **252(5010)**:1162-1164
- Lydall D. (2009), “Taming the Tiger by the Tail: Modulation of DNA Damage Responses by Telomeres”, *EMBO Journal*, **28(15)**:2174-2187
- Lydall T. and Weinert T. (1995), “Yeast Checkpoint Genes in DNA Damage Processing: Implications for Repair and Arrest”, *Science*, **270(5241)**:1488-1491
- Lygeros J., Koultroumpas K., Dimopoulos S., Legouras I., Kouretas P., Heichinger C., Nurse P., Lygerou Z. (2008), “Stochastic Hybrid Modeling of DNA Replication Across a Complete Genome”, *Proceedings of the National Academy of Sciences U.S.A.*, **105(34)**:12295-12300
- Lyne R., Burns G., Mata J., Penkett C.J., Rustici G., Chen D., Langford C., Vetrie D., Bähler J. (2003), “Whole-Genome Microarrays of Fission Yeast: Characteristics, Accuracy, Reproducibility and Processing of Array Data”, *BMC Genomics*, **4(1)**:27
- Mahalingham D., Swords R., Carew J.S., Nawrock S.T., Ballah K., Giles F.J. (2009), “Targeting Hsp90 for Cancer Therapy”, *British Journal of Cancer*, **100(10)**:1523-1529
- Maia A.F., Feijão T., Vromans M.J., Sunkel C.E., Lens S.M. (2010), “Aurora B Kinase Cooperates with CENP-E to Promote Timely Anaphase Onset”, *Chromosoma*, **119(4)**:405-413
- Mailand N., Falck J., Lukas C., Syljuåsen R.G., Welcker M., Bartek J., Lukas J. (2000), “Rapid Destruction of Human Cdc25A in Response to DNA Damage”, *Science*, **288(5470)**:1425-1429
- Majka J., Binz S.K., Wold M.S., Burgers P.M.J. (2006), “Replication Protein A Directs Loading of the DNA Damage Checkpoint Clamp to 5'-DNA Junctions”, *Journal of Biological Chemistry*, **281(38)**:27855-27861
- Maki K., Inoue T., Onaka A., Hashizume H., Somete N., Kobayashi Y., Murakami S., Shigaki C., Takahashi T.S., Masukata H., Nagakawa T. (2011), “Abundance of Pre-Replicative Complexes (Pre-RCs) Facilitates Recombinational Repair Under Replication Stress in Fission Yeast”, *Journal of Biological Chemistry*, **286(48)**:41701-41710
- Maldonado M. and Kapoor T.M. (2011), “Constitutive Mad1 Targeting to Kinetochores Uncouples Checkpoint Signalling from Chromosome Biorientation”, *Nature Cell Biology*, **13(4)**:475-482

- Maloney A. and Workman P. (2002), "HSP90 as a New Therapeutic Target for Cancer Therapy: The Story Unfolds", *Expert Opinion on Biological Therapy*, **2(1)**:3-24
- Malumbres M. and Barbacid M. (2007), "Cell Cycle Kinases in Cancer", *Current Opinion in Genetics and Development*, **17(1)**:60-65
- Mandal A.K., Lee P., Chen J.A., Nillegoda N., Heller A., DiStasio S., Oen H., Victor J., Nair D.M., Brodsky J.L., Caplan A.J. (2007), "Cdc37 has Distinct Roles in Protein Kinase Quality Control that Protect Nascent Chains from Degradation and Promote Post-Translational Maturation", *Journal of Cell Biology*, **176(3)**:319-328
- Mangelsdorf D.J., Thummler C., Beato M., Henlich P., Schutz G., Umesono K., Blumberg B., Kastner P., Mark M., Chambon P., Evans R. (1995), "The Nuclear Receptor Superfamily: The Second Decade", *Cell*, **83(6)**:835-839
- Maniwa Y., Yoshimura M., Bermudez V.P., Yuki T., Okada K., Kanomata N., Ohbayashi C., Hayashi Y., Hurwitz J., Okita Y. (2005), "Accumulation of hRad9 Protein in the Nuclei of Non-Small Cell Lung Carcinoma Cells", *Cancer*, **103(1)**:126-132
- Maniwa Y., Yoshimura M., Bermudez V.P., Okada K., Kanomata N., Ohbayashi C., Nishimura Y., Hurwitz J., Okita Y. (2006), "His239Arg SNP of hRAD9 is Associated with Lung Adenocarcinoma", *Cancer*, **106(5)**:1117-1122
- Manke I.A., Lowery D.M., Nguyen A., Yaffe M.B. (2003), "BRCT Repeats as Phosphopeptide-Binding Modules Involved in Protein Targeting", *Science*, **302(5645)**:636-639
- Manke I.A., Nguyen A., Lim D., Stewart M.Q., Elia A.E., Yaffe M.B. (2005), "MAPKAP Kinase-2 is a Cell Cycle Checkpoint Kinase that Regulates the G2/M Transition and S Phase Progression in Response to U.V. Irradiation", *Molecular Cell*, **17(1)**:37-48
- Maranon J. and Sorrain O.M. (1978), "Semi-Emperical CND/O2 Calculation of the Electronic Structure of the DNA Molecule I: Ground-State Potential Curvies: Tunnelling and Tautomeric Equilibrium in the NH----N and O----H-N Bonds of the Adenine-Thymine Base-Pair", *Journal of Theoretical Biology*, **74(1)**:11-22
- Marcelli M., Stenoien D.L., Szafran A.T., Simeoni S., Agoulnik I.U., Weigel N.L., Moran T., Mikic I., Price J.H., Mancini M.A. (2006), "Quantifying Effects of Ligands on Androgen Receptor Nuclear Translocation, Intranuclear Dynamics and Solubility", *Journal of Cellular Biochemistry*, **98(4)**:770-788
- Maresca T.J. and Salmon E.D. (2009), "Intrakinetochore Stretch is Associated with Changes in Kinetochore Phosphorylation and Spindle Assembly Checkpoint Activity", *Journal of Cell Biology*, **184(3)**:373-381
- Maresca T.J. and Salmon E.D. (2010), "Welcome to a New Kind of Tension: Translating Kinetochore Mechanics Into a wait-Anaphase Signal", *Journal of Cell Science*, **123(Pt.6)**:825-835
- Marnett L.J. and Plastaras J.P. (2001), "Endogenous DNA Damage and Mutation", *Trends in Genetics*, **17(4)**:214-221
- Marnett L.J., Riggins J.N., West J.D. (2003), "Endogenous Generation of Reactive Oxidants and Electrophiles and Their Reactions with DNA and Protein", *The Journal of Clinical Investigation*, **111(5)**:583-593

Marquardt J.U., Seo D., Gomez-Quiroz L.E., Uchida K., Gillen M.C., Kitade M., Kaposi-Novak P., Conner E.A., Factor V.M., Thorgeirsson S.S. (2012), “Loss of c-Met Accelerates Development of Liver Fibrosis in Response to CCl₄ Exposure Through Deregulation of Multiple Molecular Pathways”, *Biochimica et Biophysica Acta*, **1822(6)**:942-951

Martinez E., Palhan V.B., Tjernberg A., Lyman E.S., Gamper A.M., Kundu T.K., Chait B.T., Roeder R.G. (2001), “Human STAGA Complex is a Chromatin-Acetylating Transcription Coactivator that Interacts with Pre-mRNA Splicing and DNA Damage-Binding Factors *In Vivo*”, *Molecular and Cellular Biology*, **21(20)**:6782-6795

Martinkova E., Dontenwill M., Frei E., Stiborova M. (2009), “Cytotoxicity of and DNA Adduct Formation by Ellipticine in Human U87MG Glioblastoma Cancer Cells”, *Neuro Endocrinology Letters*, **30 (Supplement 1)**:60-66

Martins E.A. and Meneghini R. (1990), “DNA Damage and Lethal Effects of Hydrogen Peroxide and Menadione in Chinese Hamster Cells: Distinct Mechanisms are Involved”, *Free Radical Biology and Medicine*, **8(5)**:433-440

Maskaleris T., Lialiaris T., Triantaphyllidis C. (1998), “Induction of Cytogenetic Damage in Human Lymphocytes *In Vitro* and of Antineoplastic Effects in Erlich Ascites Tumour Cells *In Vivo* Treated by Methotrexate, Hyperthermia and/or Caffeine”, *Mutation Research*, **422(2)**:229-236

Massie C.E., Adryan B., Barbossa-Morais N., Lynch N.G., Tran M.G., Neal D.E., Mills I.G. (2007), “New Androgen Receptor Genomic Targets Show an Interaction with the ETS1 Transcription Factor”, *EMBO Reports*, **8(9)**:871-878

Masson J.Y., Tarsounas M.C., Stasiak A.Z., Stasiak A., Shah R., McIlwraith M.J., Benson F.E., West S.C. (2001), “Identification and Purification of Two Distinct Complexes Containing the Five RAD51 Paralogs”, *Genes and Development*, **15(24)**:3296-3307

Masuda Y., Piao J., Kamiya K. (2010), “DNA Replication-Coupled PCNA Mon-Ubiquitination and Polymerase Switching in a Human *In Vitro* System”, *Journal of Molecular Biology*, **396(3)**:487-500

Matias P.M., Donner P., Coelho R., Thomaz M., Peixoto C., Macedo S., Otto N., Joschko S., Scholz P., Wegg A., Basler S., Schafer M., Egner U., Carrondo M.A. (2000), “Structural Evidence for Ligand Specificity in the Binding Domain of the Human Androgen Receptor: Implications for Pathogenic Gene Mutations”, *Journal of Chemical Biology*, **275(34)**:26164-26171

Matsumoto H., Hamada N., Takahashi A., Kobayashi Y., Ohnishi T. (2007), “Vanguard of Paradigm Shift in Radiation Biology: Radiation-Induced Adaptive and Bystander Responses”, *Journal of Radiation Research*, **48(2)**:97-106

Matsumoto S., Shimmoto M., Kakusho N., Yokoyama M., Kanoh Y., Hayano M., Russell P., Masai H. (2010), “Hsk1 Kinase and Cdc45 Regulate Replication Stress-Induced Checkpoint Responses in Fission Yeast”, *Cell Cycle*, **9(23)**:4627-4637

Matsumoto Y. and Kim K. (1995), “Excision of Deoxyribose Phosphate Residues by DNA Polymerase Beta During DNA Repair”, *Science*, **269(5224)**:699-702

Matsuoka S., Huang M., Elledge S.J. (1998), “Linkage of ATM to Cell Cycle Regulation by the Chk2 Protein Kinase”, *Science*, **282(5395)**:1893-1897

- Matsuoka S., Rotman G., Ogawa A., Shiloh Y., Tamai K., Elledge S.J. (2000), "Ataxia Telangiectasia-Mutated Phosphorylates Chk2 *In Vivo* and *In Vitro*", *Proceedings of the National Academy of Sciences U.S.A.*, **97(19)**:10389-10394
- Matzke M.A., Mittelstein-Schied O., Matzke A.J. (1999), "Rapid Structural and Epigenetic Changes in Polyploid and Aneuploid Genomes", *Bioessays*, **21(9)**:761-767
- Maya R., Balass M., Kim S.T., Shkedy D., Leal J.F., Shifman O., Moas M., Buschmann T., Ronai Z., Shiloh Y., Kastan M.B., Katzir E., Oren M. (2001), "ATM-Dependent Phosphorylation of Mdm2 on Serine 395: Role in p53 Activation by DNA Damage", *Genes and Development*, **15(9)**:1067-1077
- McBride W.H., Iwamoto K.S., Syljuasen R., Pervan M., Pajonk F. (2003), "The Role of the Ubiquitin/Proteasome System in Cellular Responses to Radiation", *Oncogene*, **22(37)**:5755-5773
- McCann J., Dietrich F., Rafferty C., Martin A.O. (1993), "A Critical Review of the Genotoxic Potential of Electric and Magnetic Fields", *Mutation Research*, **297(1)**:61-95
- McClellan J.A., Boubliková P., Palecek E., Lilley D.M. (1990), "Superhelical Torsion in Cellular DNA Responds Directly to Environmental and Genetic Factors", *Proceedings of the National Academy of Sciences U.S.A.*, **87(21)**:8373-8377
- McClendon A.K., Rodriguez A.C., Osheriff N. (2005), "Human Topoisomerase IIalpha Rapidly Relaxes Positively Supercoiled DNA: Implications for Enzyme Action Ahead of Replication Forks", *Journal of Biological Chemistry*, **280(47)**:39337-39345
- McDonald E., Workman P., Jones K. (2006), "Inhibitors of the HSP90 Molecular Chaperone: Attacking the Master Regulator in Cancer", *Current Topics in Medicinal Chemistry*, **6(11)**:1091-1107
- McDowell C.L., Bryan-Sutton R., Obermann W.M. (2009), "Expression of Hsp90 Chaperone [Corrected] Proteins in Human Tumour Tissue", *International Journal of Biological Macromolecules*, **45(3)**:310-314
- McGowan C.H. (2003), "Running into Problems: How Cells Cope with Replicating Damaged DNA", *Mutation Research*, **532(1-2)**:75-84
- McGuffin L.J. (2008), "Intrinsic Disorder Prediction from the Analysis of Multiple Protein Fold Recognition Models", *Bioinformatics*, **24(16)**:1798-1804
- McGuffin L.J., Bryson K., Jones D.T. (2000), "The PSI-PRED Protein Structure Prediction Server", *Bioinformatics*, **16(4)**:404-405
- McHugh P.J., Spanswick V.J., Hartley J.A. (1998), "Repair of DNA Interstrand Cross Links: Molecular Mechanisms and Clinical Relevance", *Lancet Oncology*, **2(8)**:483-490
- Mckenna N.J. and O'Malley B.W. (2002), "Combinational Control of Gene Expression by Nuclear Receptors and Coregulators", *Cell*, **108(4)**:465-474
- McKinnon P.J. and Caldecott K.W. (2007), "DNA Strand Break Repair and Human Genetic Disease", *Annual Review of Genomics and Human Genetics*, **8**:37-55
- McLaughlin F. and La Thangue N.B. (2004), "Histone Deacetylase Inhibitors Open New Doors in Cancer Therapy", *Biochemical Pharmacology*, **68(6)**:1139-1144

- McVey M. and Lee S.E. (2008), “MMEJ Repair of Double-Strand Breaks (Directors Cut): Deleted Sequences and Alternative Endings”, *Trends in Genetics*, **24(11)**:529-538
- Medhurst A.L., Warmerdam D.O., Akerman I., Verwaven E.H., Kanaar R., Smits V.A., Lakin N.D. (2008), “ATR and Rad17 Collaborate in Modulating Rad9 Localisation at Sites of DNA Damage”, *Journal of Cell Science*, **121(Pt.23)**:3933-3940
- Meister P., Taddei A., Vernis L., Poidevin M., Gasser S.M., Baldacci G. (2005), “Temporal Separation of Replication and Recombination Requires the Intra-S Checkpoint”, *Journal of Cell Biology*, **168(4)**:537-544
- Melo J.A., Cohen J., Toczyski D.P. (2001), “Two Checkpoint Complexes are Independently Recruited to Sites of DNA Damage *In Vitro*”, *Genes and Development*, **15(21)**:2809-2921
- Melo J. and Toczyski D. (2002), “A Unified View of the DNA Damage Checkpoint”, *Current Opinion in Cell Biology*, **14(2)**:237-245
- Mellon I., Spivak G., Hanawalt P.C. (1987), “Selective Removal of Transcription-Blocked DNA Damage from the Transcribed Strand of the Mammalian DHFR Gene”, *Cell*, **51(2)**:241-249
- Meng L., Gabai V.L., Sherman M.Y. (2010), “Heat Shock Transcription Factor HSF1 has a Critical Role in Human Epidermal Growth Factor Receptor 2-Induced Cellular Transformation and Tumorigenesis”, *Oncogene*, **29(37)**:5204-5213
- Meng L., Hunt C., Yaglom J.A., Gabai V.L., Sherman M.Y. (2011), “Heat Shock Protein Hsp72 Plays an Essential Role in Her2-Induced Mammary Tumorigenesis”, *Oncogene*, **30(25)**:2836-2845
- Mercer W.E. (1998), “Checking on the Cell Cycle”, *Journal of Cellular Biochemistry: Supplement*, **(30-31)**:50-54
- Michaelson R.J., Rosenstein S., Weinert T. (2005), “A Telomeric Repeat Sequence Adjacent to a DNA Double-Stranded Break Produces an Anti-Checkpoint”, *Genes and Development*, **19(21)**:2546-2459
- Michel B., Boubakri H., Baharoglu Z., LeMasson M., Lestini R. (2007), “Recombination Proteins and Rescue of Arrested Replication Forks”, *DNA Repair (Amst.)*, **6(7)**:967-980
- Midic U., Oldfield C.J., Dunker A.K., Obradovic Z., Uversky V.N. (2009), “Protein Disorder in the Human Diseaseome: Unfoldomics of Human Genetic Diseases”, *BMC Genomics*, **10 (Supplement 1)**: S12
- Miller M.L. and Blom N. (2009), “Kinase-Specific Prediction of Protein Phosphorylation Sites”, *Methods in Molecular Biology*, **527**:299-310
- Mishra P.C. and Mishra R.N. (1976), “Electronic Structure of Adenine and Possibility of Proton Tunnelling in the A-T Base-Pair of DNA”, *Indian Journal of Biochemistry and Biophysics*, **13(4)**:357-360
- Mitchison J.M. (1990), “The Fission Yeast *Schizosaccharomyces pombe*”, *Bioessays*, **12(4)**:189-191

- Miwa S., Kitamura S., Shirai T., Hayashi K., Nishida H., Takeuchi A., Nojima T., Tsuchiya H. (2010), “Desmoplastic Small Round Cell Tumour Successfully Treated with Caffeine-Assisted Chemotherapy: A Case Report and Review of the Literature”, *Anticancer Research*, **30(9)**:3769-3774
- Mizianty M.J., Zhang T., Xue B., Zhou Y., Dunker A.K., Uversky V.N., Kurgan L. (2011), “*In Silico* Prediction of Disorder Content Using Hybrid Sequence Representation”, *BMC Bioinformatics*, **12(1)**:245
- Moehren U., Denayer S., Podvinec M., Verrijdt G., Claessens F. (2008), “Identification of Androgen-Selective Androgen-Response Elements in the Human Aquaporin-5 and Rad9 Genes”, *Biochemistry Journal*, **411(3)**:679-685
- Moffatt N.S., Bruinsma E., Uhl C., Obermann W.M., Toft D.O. (2008), “Role of the Co-Chaperone Tpr2 in Hsp90 Chaperoning”, *Biochemistry*, **47(31)**:8203-8213
- Mohamed F., Marchettini P., Stuart O.A., Urano M., Sugarbaker P.H. (2003), “Thermal Enhancement of New Chemotherapeutic Agents at Moderate Hyperthermia”, *Annals of Surgical Oncology*, **10(4)**:463-468
- Mohan A., Oldfield C.J., Radivojac P., Vacic V., Cortese M.S., Dunker A.K., Uversky V.N. (2006), “Analysis of Molecular Recognition Features (MoRFs)”, *Journal of Molecular Biology*, **362(5)**:1043-1059
- Mohan A., Uversky V.N., Radivojac P. (2009), “Influence of Sequence Changes and Environment on Intrinsically Disordered Proteins”, *PLoS Computational Biology*, **5(9)**:e1000497
- Moore C.L., Huang M.H., Robbenolt S.A., Voss K.R., Combs B., Gamblin T.C., Goux W.J. (2011), “Secondary Nucleating Sequences Affect Kinetics and Thermodynamics of Tau Aggregation”, *Biochemistry*, **50(50)**:10876-10886
- Mollapour M., Tsutsumi S., Neckers L. (2010), “Hsp90 Phosphorylation, Wee1 and the Cell Cycle”, *Cell Cycle*, **9(12)**:2310-2316
- Mollapour M., Tsutsumi S., Donnelly A.C., Beebe K., Tokita M.J., Lee M.J., Lee S., Morra G., Bourbouli D., Scroggins B.T., Colombo G., Blagg B.S., Panaretou B., Stetler-Stevenson W.G., Trepel J.B., Piper P.W., Prodromou C., Pearl L.H., Neckers L. (2010), “Swe1 Wee1-Dependent Tyrosine Phosphorylation of Hsp90 Regulates Distinct Facets of Chaperone Function”, *Molecular Cell*, **37(3)**:333-343
- Mollapour M., Tsutsumi S., Kim Y.S., Trepel J., Neckers L. (2011), “Casein Kinase 2 Phosphorylation of Hsp90 Threonine 22 Modulates Chaperone Function and Drug Sensitivity”, *Oncotarget*, **2(5)**:407-417
- Montecucco A. and Biamonti G. (2007), “Cellular Responses to Etoposide Treatment”, *Cancer Letters*, **252(1)**:9-18
- Morgan D.O. (1997), “Cyclin Dependent Kinases: Engines, Clocks and Microprocessors”, *Annual Review of Cell and Developmental Biology*, **13**:261-291
- Morales V., Giamarchi C., Chailleux C., Moro F., Marsaud V., Le Ricousse S., Eichard-Foy H. (2001), “Chromatin Structure and Dynamics: Functional Implications”, *Biochimie*, **83(11-12)**:1029-1039

- Mordes D.A. and Cortez D. (2008), "Activation of ATR and Related PIKKs", *Cell Cycle*, **7(18)**:2809-2812
- Mordes D.A., Glick G.G., Zhao R., Cortez D. (2008), "TopBP1 Activates ATR Through ATRIP and a PIKK Regulatory Domain", *Genes and Development*, **22(11)**:1478-1489
- Moreno S., Hayles J., Nurse P. (1989), "Regulation of the Cell Cycle Timing of Mitosis", *Journal of Cell Science*, (**Supplement 12**):1-8
- Moreno S., Klar A., Nurse P. (1991), "Molecular Genetic Analysis of Fission Yeast *Schizosaccharomyces pombe*", *Methods in Enzymology*, **194**:795-823
- Morgan D.O. (1997), "Cyclin-Dependent Kinases: Engines, Clocks and Microprocessors", *Annual Review of Cell and Developmental Processes*, **13**:261-291
- Mori M., Ishida H., Tatibana M. (1976), "Aggregation States and Catalytic Properties of the Multienzyme Complex Catalysing the Initial Steps of Pyrimidine Biosynthesis in Rat Liver", *Biochemistry*, **14(12)**:2622-2630
- Morimoto R.I. (2012), "The Heat Shock Response: Systems Biology of Proteotoxic Stress in Aging and Disease", *Cold Spring Harbor Symposia on Quantitative Biology*, **76**:10637-10843
- Morris M.C., Heitz A., Mery J., Heitz F., Divita G. (2005), "An Essential Phosphorylation-Site Domain of Human Cdc25C Interacts with Both 14-3-3 and Cyclins", *Journal of Biological Chemistry*, **275(37)**:28849-28857
- Morrow C.J., Tighe A., Johnson V.L., Scott M.I., Ditchfield C., Taylor S.S. (2005), "Bub1 and Aurora B Cooperate to Maintain BubR1-Mediated Inhibition of APC/CCdc20", *Journal of Cell Science*, **118(Pt.16)**:3639-3652
- Mosser D.D., Caron A.W., Bourget L., Merlin A.B., Sherman M.Y., Morimoto R.I., Massie B. (2000), "The Chaperone Function of Hsp70 is Required for Protection Against Stress-Induced Apoptosis", *Molecular and Cellular Biology*, **20(19)**:7146-7159
- Mullenders L.H. and Berneburg M. (2001), "Photoimmunology and Nucleotide Excision Repair: Impact of Transcription Coupled and Global Genome Excision Repair", *J. Photochem. Photobiol. B*, **65(2-3)**:97-100
- Mundt K.E., Porte J., Murray J.M., Brikos C., Christensen P.U., Caspari T., Hagan I.M., Millar J.B., Simanis V., Hoffmann K., Carr A.M. (1999), "The COP9/Signalosome Complex is Conserved in Fission Yeast and Has a Role in S-Phase", *Current Biology*, **9(23)**:1427-1430
- Mundt K.E., Liu C., Carr A.M. (2002), "Deletion Mutants in COP9/Signalosome Sub-Units in Fission Yeast *Schizosaccharomyces pombe* Display Distinct Phenotypes", *Molecular Biology of the Cell*, **13(2)**:493-502
- Munoz M.J., Bejarano E.R., Daga R.R., Jimenez J. (1999), "The Identification of Wos2, a p23 Homologue that Interacts with Wee1 and Cdc2 in the Mitotic Control of Fission Yeasts", *Genetics*, **153(4)**:1561-1572
- Munoz M.J. and Jimenez J. (1999), "Genetic Interactions Between Hsp90 and the Cdc2 Mitotic Machinery in the Fission Yeast *Schizosaccharomyces pombe*", *Molecular and General Genetics*, **261(2)**:242-250

- Murray J.M., Carr A.M., Lehmann A.R., Watts F.Z. (1991), "Cloning and Characterisation of the *rad9* Repair Gene from *Schizosaccharomyces pombe*", *Nucleic Acids Research*, **19(13)**:3525-3531
- Murthy A.E., Bernardis A., Church D., Wasmuth J., Gusella J.F. (1996), "Identification and Characterization of Two Novel Tetratricopeptide Repeat-Containing Genes", *DNA Cell Biology*, **15(9)**:173-177
- Musacchio A. and Hardwick K.G. (2002), "The Spindle Checkpoint: Structural Insights Into Dynamic Signalling", *Nature Reviews Molecular Cell Biology*, **3(10)**:731-741
- Mu D., Park C.H., Matsunaga T., Hsu D.S., Reardon J.T., Sancar A. (1995), "Reconstitution of Human DNA Repair Excision Nuclease in a Highly Defined System", *Journal of Biological Chemistry*, **270(6)**:2415-2418
- Myers J.S. and Cortez D. (2006), "Rapid Activation of ATR by Ionising Radiation Requires ATM and Mre11", *Journal of Biological Chemistry*, **281(14)**:9346-9350
- Nabetani A., Yokoyama O., Ishikawa F. (2004), "Localisation of hRad9, hHus1, hRad1 and hRad17 and Caffeine-Sensitive DNA Replication at the Alternative Lengthening of Telomere-Associated Promyelocytic Leukaemia Body", *Journal of Biological Chemistry*, **279(24)**:25849-25857
- Nair S.S., Subba-Reddy N., Hareesha K. (2011), "Exploiting Heterogeneous Features to Improve *In Silico* Prediction of Peptide Status – Amyloidogenic or Non-Amyloidogenic", *BMC Bioinformatics*, **12 (Supplement 13)**:S21
- Nair U., Bartsch H., Nair J. (2007), "Lipid Peroxidation-Induced DNA Damage in Cancer-Prone Inflammatory Diseases: A Review of Published Adduct Types and Levels in Humans", *Free Radical Biology and Medicine*, **43(8)**:1109-1120
- Nakagawa H., Saito H., Ikegami Y., Aida-Hyugaji S., Sawada S., Ishikawa T. (2006), "Molecular Modelling of New Camptothecin Analogues to Circumvent ABC G2-Mediated Drug Resistance in Cancer", *Cancer Letters*, **234(1)**:81-89
- Nakamura J., La D.K., Swenberg J.A. (2000), "5'-Nicked Apurinic/Apyrimidinic Sites are Resistant to Beta Elimination by Beta Polymerase and are Persistent in Human Cultured Cells after Oxidative Stress", *Journal of Biological Chemistry*, **275(8)**:5323-5328
- Nakaya R., Takaya J., Onuki T., Moritani N., Nozaki N., Ishimi Y. (2010), "Identification of Proteins that May Directly Interact with Human RPA", *Journal of Biochemistry*, **148(5)**:539-547
- Nakayama K.I. and Nakayama K. (2006), "Ubiquitin Ligases: Cell Cycle Control and Cancer", *Nature Reviews Cancer*, **6(5)**:369-381
- Namiki Y. and Zou L. (2006), "ATRIP Associates with Replication Protein A-Coated ssDNA Through Multiple Interactions", *Proceedings of the National Academy of Sciences U.S.A.*, **103(3)**:580-585
- Nasim A. and Hannan M.A. (1993), "Cellular Recovery, DNA Repair and Mutagenesis – A Tale of Two Yeasts", *Mutation Research*, **289(1)**:55-60
- Nasmyth K., Nurse P., Fraser R.S. (1979), "The Effect of Cell Mass on the Cell Cycle Timing and Duration of S-Phase in Fission Yeast", *Journal of Cell Science*, **39(1)**:215-233

- Navadgi-Patel V.M. and Burgers P.M. (2009), “The Unstructured C-Terminal Tail of the “9-1-1” Clamp Subunit Ddc1 Activates Mec1/ATR via Two Distinct Mechanisms”, *Molecular Cell*, **36(5)**:743-753
- Navadgi-Patel V.M. and Burgers P.M. (2011), “Cell Cycle-Specific Activators of the Mec1/ATR Checkpoint Kinase”, *Biochemical Society Transactions*, **39(2)**:600-605
- Nazareth L.V., Stenoien D.L., Bingman III W.E., James A.J., Wu C., Zhang Y., Edwards D.P., Mancini C., Marcelli M., Lamb D.J., Weigel N.L. (1999), “A C619Y Mutation in the Human Androgen Receptor Causes Inactivation and Mislocalization of the Receptor with Concomitant Sequestration of SRC-1 (Steroid Receptor Coactivator 1)”, *Molecular Endocrinology*, **13(12)**:2065-2075
- Nemajerova A., Mena P., Fingerle-Rowson G., Moll U.M., Petrenko O. (2007), “Impaired DNA Damage Checkpoint Response in MIF-Deficient Mice”, *The EMBO Journal*, **26(4)**:987-997
- Newman J.R., Wolf E., Kim P.S. (2000), “A Computationally Directed Screen Identifying Interacting Coiled Coils From *Saccharomyces cerevisiae*”, *Proceedings of the National Academy of Sciences U.S.A.*, **97(24)**:13203-13208
- Neznanov N., Komarov A.P., Neznanova L., Stanhope-Baker P., Gudkov A.V. (2011), “Proteotoxic Stress Targeted Therapy (PSTT): Induction of Protein Misfolding Enhances the Anti-Tumour Effect of the Proteasome Inhibitor Bortezomib”, *Oncotarget*, **2(3)**:209-221
- Ng C.E., Bussey A.M., Raaphorst G.P. (1996), “Sequence of Treatment is Important in the Modification of Camptothecin-Induced Cell Killing by Hyperthermia”, *International Journal of Hyperthermia*, **12(5)**:663-678
- Nguyen D., Steinberg S.V., Ronalt E., Chagnon S., Gottlieb B., Pinsky L., Trifiro M., Mader S. (2001), “A G577R Mutation in the Human AR P Box Results in Selective Decreases in DNA Binding and in Partial Androgen Insensitivity Syndrome”, *Molecular Endocrinology*, **22(11)**:2373-2382
- Ni Bhriain N., Dorman C.J., Higgins C.F. (1989), “An Overlap Between Osmotic and Anaerobic Stress Responses: A Potential Role for DNA Supercoiling in the Co-Ordinate Regulation of Gene Expression”, *Molecular Microbiology*, **3(7)**:933-942
- Nicholson D.W. (1999), “Caspase Structure, Proteolytic Substrates and Function During Apoptotic Cell Death”, *Cell Death and Differentiation*, **6(11)**:1028-1042
- Nickens K.P., Patierno S.R., Ceryak S. (2010), “Chromium Genotoxicity: A Double-Edged Sword”, *Chemico-Biological Interactions*, **188(2)**:276-288
- Nicolaides N.C., Papadopoulos N., Liu B., Wei Y.F., Carter K.C., Ruben S.M., Rosen C.A., Haseltine W.A., Fleischmann R.D., Fraser C.M., Adams M.D., Venter C., Dunlop M.G., Hamilton S.R., Petersen G.M., de la Chapelle A., Vogelstein B., Kinzler K.W. (1994), “Mutations of Two Homologues in Hereditary Non-Polyposis Colon Cancer”, *Nature*, **371(6492)**:75-80
- Nie J., Liu L., He F., Fu X., Han W., Zhang L. (2012), “CKIP-1: A Scaffold Protein and Potential Therapeutic Target Integrating Multiple Signaling Pathways and Physiological Functions”, *Ageing Research Reviews*, **Electronic Publication Ahead of Print (31st July 2012)**
- Niida H. and Nakanishi M. (2006), “DNA Damage Checkpoints in Mammals”, *Mutagenesis*, **21(1)**:3-9

- Nikjoo H., Uehara S., Wilson W.E., Hoshi M., Goodhead D.T. (1998), "Track Structure in Radiation Biology: Theory and Applications", *International Journal of Radiation Biology*, **73(4)**:355-364
- Niknafs B. (2011), "Induction of Apoptosis and Non-Apoptosis in Human Breast Cancer Cell Line (MCF-7) by Cisplatin and Caffeine", *Iranian Biomedical Journal*, **15(4)**:130-133
- Nishi K., Yoshida M., Horinouchi S., Beppu T. (1993), "Mayting of Fission Yeast Occurs Independently of the *pmd1*⁺ Gene Product, a Structural Homologue of Budding Yeast STE6 and Mammalian P-Glycoprotein", *Archives of Microbiology*, **160(2)**:162-165
- Nishi K., Yoshida M., Nishimura M., Nishikawa M., Horinouchi S., Beppu T. (1992), "A Leptomycin B Resistance Gene of *Schizosaccharomyces pombe* Encodes a Protein Similar to the Mammalian P-Glycoproteins", *Molecular Microbiology*, **6(6)**:761-769
- Nitani N., Nakamura K., Nakagawa C., Matsukata H., Nakagawa T. (2006), "Regulation of DNA Repair Machinery in Mrc1 in Fission Yeast", *Genetics*, **174(1)**:155-165
- Nitiss J.L. and Wang J.C. (1996), "Mechanisms of Cell Killing by Drugs that Trap Covalent Complexes Between DNA Topoisomerases and DNA", *Molecular Pharmacology*, **50(5)**:1095-1102
- Norbury C. and Nurse P. (1990), "Controls of Cell Proliferation in Yeast and Mammals", *Ciba Foundation Symposium*, **150**:177-183
- Norland P. and Reichard P. (2006), "Ribonucleotide Reductases", *Annual Review of Biochemistry*, **75**:681-706
- Nozoe T., Yasuda M., Honda M., Imutsuka S., Korenaga D. (2007), "Experimental Evidence for the Efficacy of Combined Therapy of CPT-11 and Hyperthermia for Squamous Cell Carcinoma of the Esophagus", *Hepatogastroenterology*, **54(80)**:2272-2275
- Nunez M.E., Hall D.B., Barton J.K. (1999), "Long Range Oxidative Damage to DNA: Effects of Distance and Sequence" *Chemical Biology*, **6(2)**:85-87
- Nurse P. (1977), "Cell Cycle Controls in Fission Yeast" [Proceedings], *Biochemical Society Transactions*, **5(4)**: 1191-1193
- Nurse P. (1997a), "Checkpoints Come of Age", *Cell*, **91(7)**:865-867
- Nurse P. (1997b), "Regulation of the Eukaryotic Cell Cycle", *European Journal of Cancer*, **33(7)**:1002-1004
- Nurse P. (2001), "Interview, Sir Paul Nurse, Ph.D. Nobel Prize for Medicine Winner", *Medscape General Medicine*, **33(4)**:4
- Nurse P.M. (2002a), "Cyclin-Dependent Kinases and Cell Cycle Control (Nobel Lecture)", *ChemBiochem: A European Journal of Chemical Biology*, **3(7)**:569-603
- Nurse P.M. (2002b), "Nobel Lecture: Cyclin-Dependent Kinases and Cell Cycle Control", *Bioscience Reports*, **22(5-6)**:478-499

- Nurse P. (2009), "The Cell Cycle and Beyond: An Interview with Paul Nurse. Interview by Jim Smith", *Disease Models and Mechanisms*, **2(3-4)**:113-115
- Nyberg K.A., Michelson R.J., Putnam C.W., Weinert T.A. (2002), "Toward Maintaining the Genome: DNA Damage and Replication Checkpoints", *Annual Review of Genetics*, **36**:617-656
- Oakley G.G. and Patrick S.M. (2010), "Replication Protein A: Directing Traffic at the Intersection of Replication and Repair", *Frontiers in Bioscience*, **15**:883-900
- O'Donovan A., Davies A.A., Moggs J.G., West S.C., Wood R.D. (1994), "XPG Endonuclease Makes the 3' Incision in Human DNA Nucleotide Excision Repair", *Nature*, **371(6496)**:432-435
- Ohtsuka K. and Hata M. (2000), "Mammalian HSP40/DNAJ Homologs: Cloning of Novel cDNAs and a Proposal for Their Classification and Nomenclature", *Cell Stress and Chaperones*, **5(2)**:98-112
- Okuya M., Kurosawa H., Kikuchi J., Furukawa Y., Matsui H., Aki D., Matsunaga T., Inukai T., Goto H., Sugita K., Arisaka O., Look A.T., Inaba T. (2010), "Up-Regulation of Survivin by the E2A-HLF Chimera is Indispensable for the Survival of t(17;19)-Positive Leukemia Cells", *Journal of Biological Chemistry*, **285(3)**:1850-1860
- Oldfield C.J., Cheng Y., Cortese M.S., Brown C.J., Uversky V.N., Dunker A.K. (2005), "Comparing and Combining Predictors of Mostly Disordered Proteins", *Biochemistry*, **44(6)**:1989-2000
- Olsen B.B., Fritz G., Issinger O.G. (2012), "Characterization of ATM and DNA-PK Wild-Type and Mutant Cell Lines Upon DSB Induction in the Presence and Absence of CK2 Inhibitors", *International Journal of Oncology*, **40(2)**:592-598
- Olsson G., Czene S., Jenssen D., Harms-Ringdahl M. (2004), "Induction of Homologous Recombination in the HPRT Gene of V79 Chinese Hamster Cells in Response to Low- and High-Let Irradiation", *Cytogenetic and Genome Research*, **104(1-4)**:227-231
- Ordóñez E., Thiyagarajan S., Cook J.D., Stemmler T.L., Gil J.A., Mateos L.M., Rosen B.P. (2008), "Evolution of Metal(loid) Binding Sites in Transcriptional Regulators", *Journal of Biological Chemistry*, **283(37)**:25706-25714
- Orth M., Mayer B., Rehm K., Rothweiler U., Heidmann D., Holak T.A., Stemmann O. (2011), "Shugoshin is a Mad1/Cdc20-Like Interactor of Mad2", *The EMBO Journal*, **30(14)**:2868-2880
- O'Shea C.C. (2005), "Viruses: Seeking and Destroying the Tumour Program", *Oncogene*, **24(52)**:7640-7655
- Oshima J. (2000), "The Werner Syndrome Protein: An Update", *Bioessays*, **22(10)**:894-901
- Osman F., Dixon J., Barr A.R., Whitby M.C. (2005), "The F-Box DNA Helicase Fbh1 Prevents Rhp51-Dependent Recombination Without Mediator Proteins", *Molecular and Cellular Biology*, **25(18)**:8084-8096
- Osman F. and McCready S. (1998), "Differential Effects of Caffeine on DNA Damage and Replication Cell Cycle Checkpoints in the Fission Yeast *Schizosaccharomyces pombe*", *Molecular and General Genetics*, **260(4)**:319-334

- Overgaard K. and Overgaard J. (1974), "Radiation Sensitizing Effect of Heat", *Acta Radiological Therapy and Physical Biology*, **13**:501-511
- Pabla N., Ma Z., McIlhatton M.A., Fishel R., Dong Z. (2011), "hMSH2 Recruits ATR to DNA Damage Sites for Activation During DNA Damage-Induced Apoptosis", *Journal of Biological Chemistry*, **286**(12):10411-10418
- Paek A.L. and Weinert T. (2010), "Choreography of the 9-1-1 Checkpoint Complex: DDK Puts a Check on the Checkpoints", *Molecular Cell*, **40**(4):505-506
- Painter R.B. (1978), "Inhibition of DNA Replicon Initiation by 4-Nitroquinoline-1-Oxide, Adriamycin and Ethyleneimine", *Cancer Research*, **38**(12):4445-4449
- Palazzi M., Maluta S., Dall'oglio S., Romano M. (2010), "The Role of Hyperthermia in the Battle Against Cancer", *Tumorigenesis*, **96**:902-910
- Palermo C., Hope J.C., Freyer G.A., Rao H., Walworth N.C. (2008), "Importance of a C-Terminal Conserved Region of Chk1 for Checkpoint Function", *PLoS One*, **3**(1):e1427
- Pallas A.G. and Karamouzis M.V. (2010), "DNA Repair Pathways and Their Implication in Cancer Treatment", *Cancer Metastasis Reviews*, **29**(4):677-685
- Palombo F., Gallianari P., Iaccarino I., Lettieri T., Hughes M., D'Arrigo A., Truong O., Hsuan J.J., Jiricny J. (1995), "GTBP, a 160-Kilodalton Protein Essential for Mismatch-Binding Activity in Human Cells", *Science*, **268**(5219):1912-1914
- Palombo F., Iaccarino I., Nakajima E., Ikejima M., Shimada T., Jiricny J. (1996), "hMutSbeta, a Heterodimer of hMSH2 and hMSH3, Binds to Insertion/Deletion Loops in DNA", *Curr. Biol.*, **6**(9):1181-1184
- Pandita R.K., Sharma G.G., Laszlo A., Hopkins K.M., Davey S., Chakhparonian M., Gupta A., Wellinger R.J., Zhang J., Powell S.N., Roti Roti J.L., Lieberman H.B., Pandita T.K. (2006), "Mammalian Rad9 Plays a Role in Telomere Stability, S- and G2- Phase-Specific Cell Survival and Homologous Recombinational Repair", *Molecular and Cellular Biology*, **26**(5):1850-1864
- Pandita T.K. (2006), "Role of Mammalian Rad9 in Genomic Stability and Ionising Radiation Response", *Cell Cycle*, **5**(12):1289-1291
- Pankratz D.G. and Forsburg S.L. (2005), "Meiotic S-Phase Damage Activates Recombination Without Checkpoint Arrest", *Molecular Biology of the Cell*, **16**(4):1651-1660
- Pantazis P., Chatterjee D., Han Z., Wyche J. (1999), "Modulation of 9-Nitrocamptothecin-Induced Apoptosis by Hyperthermia in Human Leukaemia HL-60 Cells", *Anticancer Drugs*, **10**(3):317-322
- Pantelias G.E. and Terzoudi G.I. (2011), "A Standardized G2-Assay for the Prediction of Individual Radiosensitivity", *Radiotherapy and Oncology*, **101**(1):28-34
- Papadopoulos J.S. and Agarwala R. (2007), "COBALT: Constraint-Based Alignment Tool for Multiple Protein Sequences", *Bioinformatics*, **23**(9):1073-1079
- Papadopoulos N., Nicolaidis N.C., Wei Y.F., Ruben S.M., Carter K.C., Rosen C.A., Haseltine W.A., Fleischmann R.D., Fraser C.M., Adams M.D. *et al* (1994), "Mutation of a MutL Homolog in Hereditary Colon Cancer", *Science*, **263**(5153):1625-1629

Papp B., Pal C., Hurst L.D. (2003), “Dosage Sensitivity and the Evolution of Gene Families in Yeast”, *Nature*, **424(6945)**:194-197

Park M.J., Park J-H., Hahm S-H., Ko S.I., Lee Y.R., Chung J.H., Sohn S.Y., Cho Y., Kang L-W., Han Y.S. (2009), “Repair Activities of Human 8-Oxoguanine DNA Glycosylase are Stimulated by the Interaction with Human Checkpoint Sensor Rad9-Rad1-Hus1 Complex”, *DNA Repair (Amst.)*, **8(10)**:1190-1200

Pastink A., Eeken J.C., Lohman P.H. (2001), “Genomic Integrity and the Repair of Double-Strand DNA Breaks”, *Mutation Research*, **(480-481)**:37-50

Pecorino L. (2008), “Molecular Biology of Cancer: Mechanisms, Targets and Therapeutics”, 2nd Edition, Oxford University Press

Pedram A., Razandi M., Evinger A.J., Lee E., Levin E.R. (2009), “Estrogen Inhibits ATR Signalling to Cell Cycle Checkpoints and DNA Repair”, *Molecular Biology of the Cell*, **20(14)**:3374-3389

Peng C.Y., Graves P.R., Thoma R.S., Wu Z., Shaw A.S., Piwnica-Worms H. (1997), “Mitotic and G2 Checkpoint Control: Regulation of 14-3-3 Protein Binding by Phosphorylation of Cdc25C on Serine-216”, *Science*, **277(5331)**:1501-1505

Peng K., Radivojac P., Vucetic S., Dunker A.K., Obradovic Z. (2006), “Length-Dependent Prediction of Protein Intrinsic Disorder”, *BMC Bioinformatics*, **7**:208

Peng K., Vucetic S., Radivojac P., Brown C.J., Dunker A.K., Obradovic Z. (2005), “Optimizing Long Intrinsic Disorder Predictors with Protein Evolutionary Information”, *Journal of Bioinformatics and Computational Biology*, **3(1)**:35-60

Perego P., Cossa G., Tinelli S., Corna E., Carenini N., Gatti L., De Cesare M., Ciusani E., Zunino F., Luisson E., Canevari S., Zaffaroni N., Beretta G.L. (2012), “Role of Tyrosyl-DNA Phosphodiesterase I and Inter-Players in Regulation of Tumor Cell Sensitivity to Topoisomerase I Inhibition”, *Biochemical Pharmacology*, **83(1)**:27-36

Pereira N.A. and Song Z. (2008), “Some Commonly Used Caspase Substrates and Inhibitors Lack the Specificity Required to Monitor Individual Caspase Activity”, *Biochemical and Biophysical Research Communications*, **377(3)**:873-877

Pérez-Castro A.J. and Freire R. (2012), “Rad9B Responds to Nucleolar Stress Through ATR and JNK Signalling and Delays the G1-S Transition”, *Journal of Cell Science*, **125 (Pt.5)**:1152-1164

Perez de Castro L., de Cárcer G., Malumbres M. (2007), “A Consensus of Mitotic Cancer Genes: New Insights into Tumour Cell Biology and Cancer Therapy”, *Carcinogenesis*, **28(5)**:899-912

Perrodou E., Chica C., Poch O., Gibson T.J., Thompson J.D. (2008), “A New Protein Linear Motif Benchmark for Multiple Sequence Alignment Software”, *BMC Bioinformatics*, **9**:213

Perry J. and Kleckner N. (2003), “The ATRs, ATMs and TORs are Giant HEAT Repeat Proteins”, *Cell*, **11(22)**:151-155

Petermann E., Helleday T., Caldecott K.W. (2008), “Claspin Promotes Normal Replication Fork Rates in Human Cells”, *Molecular Biology of the Cell*, **19(6)**:2373-2378

- Pfander P. and Diffley J.F. (2011), “Dpb11 Coordinates Mec1 Kinase Activation with Cell Cycle-Regulated Rad9 Recruitment”, *The EMBO Journal*, **30(24)**:4897-4907
- Pichierri P. (2007), “Interplay Between WRN and the Checkpoint in S Phase”, *Italian Journal of Biochemistry*, **56(2)**:130-140
- Pichierri P., Ammazalorso F., Bignami M., Franchitto A. (2011), “The Werner Syndrome protein: Linking the Replication Checkpoint Response to Genome Stability”, *Aging*, **3(3)**:311-318
- Pichierri P., Nicolai S., Cignolo L., Bignami M., Franchitto A. (2012), “The RAD9-RAD1-HUS1 (9-1-1) Complex Interacts with WRN and is Crucial to Regulate its Response to Replication Fork Stalling”, *Oncogene*, **31(23)**:2809-2823
- Pichierri P., Rosselli F., Franchitto A. (2003), “Werner’s Syndrome Protein is Phosphorylated in an ATR/ATM-Dependent Manner Following Replication Arrest and DNA Damage Induced During the S Phase of the Cell Cycle”, *Oncogene*, **22(10)**:1491-1500
- Pichiorri F., Palumbo T., Suh S.S., Okamura H., Trapasso F., Ishii H., Huebner K., Croce C.M. (2008), “Fhit Tumor Suppressor: Guardian of the Genome”, *Future Oncology*, **4(6)**:815-824
- Pirzio L.M., Pichierri P., Bignami N., Franchitto A. (2008), “Werner Syndrome Helicase Activity is Essential in Maintaining Fragile Site Stability”, *Journal of Cell Biology*, **180(2)**:305-314
- Podgomik R., Strey H.H., Rau D.C., Parsegian V.A. (1995), “Watching Molecules Crowd: DNA Double Helices Under Osmotic Stress”, *Biophysical Chemistry*, **57(1)**:111-121
- Pommier Y. and Kohn K.W. (2003), “Cell Cycle and Checkpoints in Oncology: New Therapeutic Targets”, *Medecine Sciences (Paris)*, **19(2)**:173-186
- Pommier Y. (2006), “Topoisomerase I Inhibitors: Camptothecins and Beyond”, *Nature Reviews Cancer*, **6(10)**:789-802
- Post S., Weng Y.C., Cimprich K., Chen L.B., Xu Y., Lee E.Y. (2001), “Phosphorylation of Serines 635 and 645 of Human Rad17 is Cell Cycle Regulated and is Required for G(1)/S Checkpoint Activation in Response to DNA Damage”, *Proceedings of the National Academy of Sciences U.S.A.*, **98(23)**:13102-13107
- Pourquier P. and Langsiaux A. (2011), “Molecular Determinants of Response to Topoisomerase I Inhibitors”, *Bulletin du Cancer*, **98(11)**:1287-1298
- Povirk L.F. (2006), “Biochemical Mechanisms of Chromosomal Translocations Resulting from DNA Double-Strand Breaks”, *DNA Repair (Amst.)*, **5(9-10)**:1199-1212
- Prasad B.D., Goel S., Krishna P. (2010), “In Silico Identification of Carboxylate Clamp Type Tetratricopeptide Repeat Protein in *Arabidopsis* and Rice as Putative Co-Chaperones of Hsp90/Hsp70”, *PLoS One*, **5(9)**:e12761
- Prasad R., Beard W.A., Strauss P.R., Wilson S.H. (1998), “Human DNA Polymerase Beta Deoxyribose Phosphate Lyase: Substrate Specificity and Catalytic Mechanism”, *Journal of Biological Chemistry*, **273(24)**:15263-15270
- Prise K.M., Gillies N.E., Michael B.D. (1998a), “Evidence for Hypoxic Fixation Reaction Leading to the Induction of SSB and DSB in Irradiated DNA”, *International Journal of Radiation Biology*, **74(1)**:53-59

- Prise K.M., Newman H.C., Folkard M., Michael B.D. (1998b), “A Study of DNA Fragmentation Patterns in Cells Irradiated with Charged Particles: Evidence for Non-Random Distributions”, *Physica Medica*, **14 (Suppl. 1)**:20-23
- Pryce D. and McFarlane R.J. (2009), “The Meiotic Recombination Hotspots of *Schizosaccharomyces pombe*”, *Genome Dynamics*, **5**:1-13
- Puddu F., Piergiovanni G., Plevani P., Muzi-Falconi M. (2011), “Sensing Replication Stress and Mec1 Activation Through Two Independent Pathways Involving the 9-1-1 Complex and DNA Polymerase ϵ ”, *PLoS Genetics*, **7(3)**:e1002022
- Puntervoll P., Linding R., Gemünd C., Chabanis-Davidson S., Mattingsdal M., Cameron S., Martin D.M., Ausiello G., Brannetti B., Costantini A., Ferré F., Manselli V., Via A., Cesareni G., Diella F., Superti-Furga G., Wyrwicz L., Ramu C., McGuigan C., Gudavalli R., Letunic I., Bork P., Rychlewski L., Küster B., Helmer-Citterich M., Hunter W.N., Aasland R., Gibson T.J. (2003), “ELM Server: A New Resource for Investigating Short Functional Sites in Modular Eukaryotic Proteins”, *Nucleic Acids Research*, **31(13)**:3525-3630
- Qiu Y. and Davidson J.N. (2000), “Substitutions in the Aspartate Transcarbamoylase Domain of Hamster CAD Disrupt Oligomeric Structure”, *Proceedings of the National Academy of Sciences U.S.A.*, **97(1)**:97-102
- Querol-Audí J., Yan C., Xu X., Tsutakawa S.E., Tsai M-S., Tainer J.A., Cooper P.K., Nogales E., Ivanov I. (2012), “Repair Complexes of FEN1 Endonuclease, DNA and Rad9-Hus1-Rad1 are Distinguished from their PCNA Counterparts by Functionally Important Stability”, *Proceedings of the National Academy of Sciences U.S.A.*, **109(22)**:8528-8533
- Quevedo O., Garcia-Luis J., Matos-Perdomo E., Aragón L., Machín F. (2012), “Nondisjunction of a Single Chromosome Leads to Breakage and Activation of DNA Damage Checkpoint in G2”, *PLoS Genetics*, **8(2)**:e1002509
- Qu M., Yang B., Tao L., Yates J.R. 3rd, Russell P., Dong M.Q., Du L.L. (2012), “Phosphorylation-Dependent Interactions Between Crb2 and Chk1 are Essential for DNA Damage Checkpoint”, *PLoS Genetics*, **8(7)**:e1002817
- Rabkin C.S. and Janz S. (2008), “Mechanisms and Consequences of Chromosomal Translocation”, *Cancer Epidemiology, Biomarkers and Prevention*, **17(8)**:1849-1851
- Radivojac P., Iakoucheva I.M., Oldfield C.J., Obradovic Z., Uversky V.N., Dunker A.K. (2007), “Intrinsic Disorder and Functional Proteomics”, *Biophysical Journal*, **92(5)**:1439-1456
- Radivojac P., Obradovic Z., Smith D.K., Zhu G., Vucetic S., Brown C.J., Lawson J.D., Dunker A.K. (2004), “Protein Flexibility and Intrinsic Disorder”, *Protein Science*, **13(1)**:71-80
- Rajendra R., Gounder M.K., Saleem A., Schellens J.H., Ross D.D., Bates S.E., Sinko P., Rubin E.H. (2003), “Differential Effects of the Breast Cancer Resistance Protein on the Cellular Accumulation and Cytotoxicity of 9-Aminocamptothecin and 9-Nitrocamptothecin”, *Cancer Research*, **63(12)**:3228-3333
- Rajkowitsch L., Chen D., Stampfl S., Semrad K., Waldsich C., Mayer O., Jantsch M.F., Konrat R., Bläsi U., Schroeder R. (2007), “RNA Chaperones, RNA Annealers and RNA Helicases”, *RNA Biology*, **4(3)**:118-130

- Raman M., Chen W., Cobb M.H. (2007), "Differential Regulation and Properties of MAPKs", *Oncogene*, **26(22)**:3100-3112
- Ramsey A.J., Russell L.C., Chinkers M. (2009), "C-Terminal Sequences of Hsp70 and Hsp90 as Non-Specific Anchors for Tetratricopeptide Repeat (TPR) Proteins", *The Biochemical Journal*, **423(3)**:411-419
- Ramsey A.J., Russell L.C., Whitt S.R., Chinkers M. (2007), "Overlapping Sites of Tetratricopeptide Repeat Protein Binding and Chaperone Activity in Heat Shock Protein 90", *Journal of Biological Chemistry*, **275(23)**:17857-17862
- Rao K.V., Samikkannu T., Dakshayani K.B. Zhang X., Sathaye S.S., Indap M.A., Nair M.P. (2012), "Chemopreventative Potential of an Ethyl Acetate Fraction from Curcuma Longa is Associated with Upregulation of p57Kip2 and Rad9 in the PC-3M Prostate Cancer Cell Line", *Asian Pacific Journal of Cancer Prevention*, **13(3)**:1031-1038
- Rao M.S. and Reddy J.K. (1991), "An Overview of Peroxisome Proliferator-Induced Hepatocarcinogenesis", *Environmental Health Perspectives*, **93**:205-209
- Rappas M., Oliver A.W., Pearl L.H. (2010), "Structure and Function of the Rad9-Binding Region of the DNA-Damage Checkpoint Adaptor TopBP1", *Nucleic Acids Research*, **39(1)**:313-324
- Ravi D., Muniyappa H., Das K.C. (2008), "Caffeine Inhibits U.V.-Mediated NF-kappaB Activation in A2058 Melanoma Cells: An ATM-PKCdelta-p38 MAPK-Dependent Mechanism", *Molecular and Cellular Biochemistry*, **308(1-2)**:193-200
- Reardon M.A. and Weber G. (1985), "Increased Carbamoyl-Phosphate Synthetase II Concentration in Rat Hepatomas: Immunological Evidence", *Cancer Research*, **45(9)**:4412-4415
- Reddy J.K. and Rao M.S. (1989), "Oxidative DNA Damage Caused by Persistent Peroxisome Proliferation: Its Role in Hepatocarcinogenesis", *Mutation Research*, **214(1)**:63-68
- Redinbo M.R., Stewart L., Kuhn P., Champoux J.J., Hol W.G. (1998), "Crystal Structure of Human Topoisomerase I in Covalent and Non-Covalent Complexes with DNA", *Science*, **279(5356)**:1504-1513
- Redlack M.J. and Miller J.A. (2011), "Targeting PI3K/Akt/Hsp90 Signalling Sensitizes Gastric Cancer Cells to Deoxycholate-Induced Apoptosis", *Digestive Diseases and Sciences*, **56(2)**:323-329
- Regairaz M., Zhang Y.W., Fu H., Agama K.K., Tata N., Agrawal S., Aladjem M.I., Pommier Y. (2011), "Mus 81-Mediated DNA Cleavage Resolves Replication Forks Stalled by Topoisomerase I-DNA Complexes", *Journal of Cell Biology*, **195(5)**:739-749
- Reha-Krantz L.J., Siddique M.S., Murphy K., Tam A., O'Carroll M., Lou S., Schulz A., Boone C. (2011), "Drug-Sensitive DNA Polymerase δ Reveals a Role for Mismatch Repair in Checkpoint Activation in Yeast", *Genetics*, **189(4)**:1211-1224
- Rein R. and Harris F.E. (1964), "Proton-Tunneling in Radiation-Induced Mutation", *Science*, **146(3644)**:649-650
- Reinhardt H.C., Aslanian A.S., Lees J.A., Yaffe M.B. (2007), "p53-Deficient Cells Rely on ATM- and ATR- Mediated Checkpoint Signaling Through the p38MAPK/MK2 Pathway for Survival After DNA Damage", *Cancer Cell*, **11(2)**:175-189

- Reinhardt H.C. and Yaffe M.B. (2009), "Kinases that Control the Cell Cycle in Response to DNA Damage: Chk1, Chk2 and MK2", *Current Opinion in Cell Biology*, **21(2)**:245-255
- Reiser V., D'Aquino K.E., Ee L.S., Amon A. (2006), "The Stress-Activated Mitogen-Activated Protein Kinase Signaling Cascade Promotes Exit from Mitosis", *Molecular Biology of the Cell*, **17(7)**:3136-3146
- Remerowski M.L., Kellenbach E., Boelens R., van der Marel G.A., van Boom J.H., Maler B.A., Yamamoto K.R., Kaptein R. (1991), "1H NMR Studies of DNA Recognition by the Glucocorticoid Receptor: Complex of the DNA Binding Domain with a Half-Site Response Element", *Biochemistry*, **30(50)**:11620-11624
- Ruhlmann C.H. and Hersteddt J. (2012), "Fosaprepitant for the Prevention of Chemotherapy-Induced Nausea and Vomiting", *Expert Review of Anticancer Therapy*, **12(2)**:139-150
- Ribar B., Izumi T., Mitra S. (2004), "The Major Role of Human AP-Endonuclease Homolog Apn2 in Repair of Abasic Sites in *Schizosaccharomyces pombe*", *Nucleic Acids Research*, **32(1)**:115-126
- Rich T.A. and Kirichenko A.V. (2000), "Camptothecin Dose, Schedule and Timing of Administration for Clinical Radiation Sensitization", *Annals of the New York Academy of Sciences*, **922**:334-339
- Rich T.A., Shelton C.H. 3rd, Kirichenko A., Straume M. (2002), "Chronomodulated Chemotherapy and Irradiation: An Idea Whose Time Has Come?", *Chronobiology International*, **19(1)**:191-205
- Richard D.J., Bolderson E., Khanna K.K. (2009), "Multiple Human Single-Stranded DNA Binding Proteins Function in Genome Maintenance: Structural, Biochemical and Functional Analysis", *Critical Reviews in Biochemistry and Molecular Biology*, **44(2-3)**:98-116
- Richardson K.S. and Zundel W. (2005), "The Emerging Role of the COP9 Signalosome in Cancer", *Molecular Cancer Research*, **3(12)**:645-653
- Riggs D.L., Cox M.B., Cheung-Flynn J., Prapapanich V., Carrigan P.E., Smith D.F. (2004), "Functional Specificity of Co-Chaperone Interactions with Hsp90 Client Proteins", *Critical Reviews in Biochemistry and Molecular Biology*, **39(5-6)**:279-295
- Robinson M.J. and Cobb M.H. (1997), "Mitogen-Activated Protein Kinase Pathways", *Current Opinion in Cell Biology*, **9(2)**:180-186
- Roche P.J., Hoare S.A., Parker M.G. (1992), "A Consensus DNA-Binding Site for the Androgen Receptor", *Molecular Endocrinology*, **6(12)**:2229-2235
- Rochette-Egly C. (2003), "Nuclear Receptors: Integration of Multiple Signalling Pathways Through Phosphorylation", *Cellular Signalling*, **15(4)**:355-366
- Rodriguez-Menocal L. and D'Urso G. (2004), "Programmed Cell Death in Fission Yeast", *FEMS Yeast Research*, **5(2)**:111-117
- Rodriguez M., Yu X., Chen J., Songyang Z. (2003), "Phosphopeptide Binding Specificities of BRCA1 COOH-Terminal (BRCT) Domains", *Journal of Biological Chemistry*, **278(52)**:52914-52918
- Romero P., Obradovic Z., Li X., Garner E.C., Brown C.J., Dunker A.K. (2001), "Sequence Complexity of Disordered Protein", *Proteins*, **42(1)**:38-48

- Ronald S., Sunavala-Dossabhoj G., Adams L., Williams B., De Benedetti A. (2011), “The Expression of Tousled Kinases in CaP Cell Lines and its Relation to Radiation Response and DSB Repair”, *The Prostate*, **71(13)**:1367-1373
- Roos-Mattjus P., Vroman B.J., Burtelow M.A., Rauen M., Eapen A.K., Karnitz L.M. (2002), “Genotoxin-Induced Rad9-Hus1-Rad1 (9-1-1) Chromatin Association is an Early Checkpoint Signaling Event”, *Journal of Biological Chemistry*, **277(46)**:43809-43812
- Roos-Mattjus P., Hopkins K.M., Oestreich A.J., Vroman B.T., Johnson K.L., Naylor S., Lieberman H.B., Karnitz L.M. (2003), “Phosphorylation of Human Rad9 is Required for Genotoxin-Activated Checkpoint Signaling”, *Journal of Biological Chemistry*, **278(27)**:24428-24437
- Roots R., Holley W., Cahtterjee A., Irizarry M., Kraft G. (1990), “The Formation of Strand Breaks in DNA After Hi-LET Irradiation: A Comparison of Data from *In Vitro* Cellular Systems”, *International Journal of Radiation Biology*, **58(1)**:55-69
- Rosenfeld M.G., Lunyak V.V., Glass C.K. (2006), “Sensors and Signals: A Coactivator/Corepressor/Epigenetic Code for Integrating Signal-Dependent Programs of Transcriptional Response”, *Genes and Development*, **20(11)**:1405-1428
- Rossi M.L., Ghosh A.K., Bohr V.A. (2010), “Role of Werner Syndrome Protein in Protection of Genome Integrity”, *DNA Repair (Amst.)*, **9(3)**:331-344
- Roussel M.F. (1999), “The INK4 Family of Cell Cycle Inhibitors in Cancer”, *Oncogene*, **18(38)**:5311-5317
- Routledge K.E., Tartaglia G.G., Platt G.W., Vendruscolo M., Radford S.E. (2009), “Competition Between Intramolecular and Intermolecular Interactions in an Amyloid-Forming Protein”, *Journal of Molecular Biology*, **389(4)**:776-786
- Ruoslahti E. and Rajotte D. (2000), “An Address System in the Vasculature of Normal Tissues and Tumours”, *Annual Review of Immunology*, **18**:813-827
- Russell P., Moreno S., Reed S.I. (1989), “Conservation of Mitotic Controls in Fission and Budding Yeasts”, *Cell*, **57(2)**:295-303
- Russell R. (2008), “RNA Misfolding and the Action of Chaperones”, *Frontiers in Bioscience*, **13**:1-20
- Rybaczek D. and Kowalewicz-Kulbat M. (2011), “Premature Chromosomal Condensation Induced by Caffeine, 2-Aminopurine, Staurosporine and Sodium Metavanadate in S-Phase Arrested HeLa Cells is Associated with a Decrease in Chk1 Phosphorylation, Formation of Phospho-H2AX and Minor Cytoskeletal Rearrangements”, *Histochemistry and Cell Biology*, **135(3)**:263-280
- Rylander M.N., Feng Y., Zimmermann K., Diller K.R. (2010), “Measurement and Mathematical Modeling of Thermally-Induced Injury and Heat Shock Protein Expression Kinetics in Normal and Cancerous Prostate Cells”, *International Journal of Hyperthermia*, **26(8)**:748-764
- Sabatinos S.A. and Forsburg S.L. (2010), “Molecular Genetics of *Schizosaccharomyces pombe*”, *Methods in Enzymology*, **470**:759-795

- Saber A., Nakahara M., Sale J.E., Kikuchi K., Arakawa H., Buerstedde J-M., Yamamoto K., Takeda S., Sonoda E. (2008), "The 9-1-1 DNA Clamp is Required for Immunoglobulin Gene Conversion", *Molecular and Cellular Biology*, **28(19)**:6113-6122
- Sabisz M. and Skladanowski A. (2008), "Modulation of Cellular Response to Anticancer Treatment by Caffeine: Inhibition of Cell Cycle Checkpoints, DNA Repair and More", *Current Pharmaceutical Biotechnology*, **9(4)**:325-336
- Sack J.S., Kish K.F., Wang C., Attar R.M., Kiefer S.E., An Y., Wu G.Y., Scheffler J.E., Salvati M.E., Krystek Jr S.R., Weinmann R., Einspahr H.M. (2001), "Crystallographic Structures of the Ligand-Binding Domains of the Androgen Receptor and Its T877A Mutant Complexed with the Natural Agonist Dihydroxytestosterone", *Proceedings of the National Academy of Sciences U.S.A.*, **98(9)**:4904-4909
- Saito Y., Gopalan B., Mhashilkar A.M., Roth J.A., Chada S., Zumstein L., Ramesh R. (2003), "Adenovirus-Mediated PTEN-Treatment Combined with Caffeine Produce a Synergistic Therapeutic Effect in Colorectal Cancer Cells", *Cancer Gene Therapy*, **10(11)**:803-811
- Sakai Y., Furuichi M., Takahashi M., Mishima M., Iwai S., Shirakawa M., Nakabeppu Y. (2002), "A Molecular Basis for the Selective Recognition of 2-Hydroxy-dATP and 8-Oxo-dGTP by Human MTH1", *Journal of Biological Chemistry*, **277(10)**:8579-8587
- Sakurai H., Mitsuhashi N., Tamaki Y., Akimoto T., Murata O., Kitamoto Y., Maebayashi K., Ishikawa H., Hayakawa K., Niibe H. (1999), "Interaction Between Low Dose-Rate Irradiation, Mild Hyperthermia and Low-Dose Caffeine in a Human Lung Cancer Cell Line", *International Journal of Radiation Biology*, **75(6)**:739-745
- Saleem A., Edwards T.K., Rasheed Z., Rubin E.H. (2000), "Mechanisms of Resistance to Camptothecins", *Annals of the New York Academy of Sciences*, **922**:46-55
- Saleh A., Srinivasula S.M., Balkin L., Robbins P.D., Alnemri E.S. (2000), "Negative Regulation of the Apsf-1 Apoptosome by Hsp70", *Nature Cell Biology*, **2(8)**:476-483
- Salk D. (1985), "In Vitro Studies of Werner Syndrome Cells; Aberrant Growth and Chromosome Behaviour", *Basic Life Sciences*, **35**:419-426
- Samuel J.M., Fournier N., Simanis V., Millar J.B. (2000), "Spo12 is a Multicopy Suppressor of MCS3 that is Periodically Expressed in Fission Yeast", *Molecular and General Genetics*, **264(3)**:306-316
- Sancar A., Lindsey-Boltz L.A., Unsul-Kacmaz K., Linn S. (2004), "Molecular Mechanisms of Mammalian DNA Repair and the DNA Damage Checkpoints", *Annual Review of Biochemistry*, **73**:39-85
- Sanchez-Ruiz J.M. (2010), "Protein Kinetic Stability", *Biophysical Chemistry*, **148(1-3)**:1-15
- Sanchez Y., Wong C., Thoma R.S., Richman R., Wu Z., Piwnicka-Worms H., Elledge S.J. (1997), "Conservation of the Chk1 Pathway in Mammals: Linkage of DNA Damage to Cdk Regulation Through Cdc25", *Science*, **277(5331)**:1497-1501
- Sandhu K.S. (2009), "Intrinsic Disorder Explains Diverse Nuclear Roles of Chromatin Remodelling Proteins", *Journal of Molecular Recognition*, **22(1)**:1-8

- Sar F., Lindsey-Boltz L.A., Subramanian D., Croteau D.L., Hutsell S.Q., Griffith J.D., Sancar A. (2004), "Claspin is a Ring-Shaped DNA-Binding Protein with High Affinity to Branched DNA Structures", *Journal of Biological Chemistry*, **279(38)**:39289-39295
- Sarkaria J.N., Busby E.C., Tibbetts R.S., Roos P., Taya Y. et al (2000), "Inhibition of ATM and ATR Kinase Activities by the Radiosensitizing Agent, Caffeine", *Cancer Research*, **59**:4375-4382
- Savitsky K., Bar-Shira A., Gilad S., Rotman G., Ziv Y., Vanagaite L., Tagle D.A., Smith S., Uziel T., Sfez S. (1995), "A Single Ataxia Telangiectasia Gene With a Product Similar to PI-3 Kinase", *Science*, **268(5218)**:1749-1753
- Savvidis C. and Koutsilieris M. (2012), "Circadian Rhythm Disruption in Cancer Biology", *Molecular Medicine*, **Electronic Publication Ahead of Print (17th July 2012)**
- Schaeffer L., Moncollin V. Roy R., Staub A., Mezzina M., Sarasin A., Weeda G., Hoeijmakers J.H., Egly J.M. (1994), "The ERCC2/DNA Repair Protein is Associated with the Class II BTF2/TFIIH Transcription Factor", *The EMBO Journal*, **13(10)**:2388-2392
- Schaeffer L., Roy R., Humbert S., Moncollin V., Vermeulen W., Hoeijmakers J.H., Chambon P., Egly J.M. (1993), "DNA Repair Helicase: A Component of BTF2 (TFIIH) Basic Transcription Factor", *Science*, **260(5104)**:58-63
- Schärer O.D. and Jiricny J. (2001), "Recent Progress in the Biology, Chemistry and Structural Biology of DNA Glycosylases", *Bioessays*, **23(3)**:270-281
- Schellens J.H.M., Maliepaard M., Scheper R.J., Scheffer G.L., Jonker J.W., Smit J.W., Beijnen J.H., Schinkel A.H. (2000), "Transport of Topoisomerase I Inhibitors by the Breast Cancer Resistant Protein", *Annals of the New York Academy of Sciences*, **992**:188-194
- Schellmann N., Deckert P.M., Bachran D., Fuchs H., Bachran C. (2010), "Targeted Enzyme Prodrug Therapies", *Mini Reviews in Medicinal Chemistry*, **10(10)**:887-904
- Scherer S.J., Maier S.M., Seifert M., Hanselmann R.G., Zang K.D., Muller-Hermelink H.K., Angel P., Welter C., Scharl M. (2000), "p53 and c-Jun Functionally Synergize in the Regulation of the DNA Repair Gene hMSH2 in Response to U.V.", *Journal of Biological Chemistry*, **275(48)**:37469-37473
- Schild D., Lio Y.C., Collins D.W., Tsomondo T., Chen D.J. (2000), "Evidence for Simultaneous Protein Interactions Between Human Rad51 Paralogs", *Journal of Biological Chemistry*, **275(22)**:16443-16449
- Schlessinger A., Punta M., Yachdav G., Kajan L., Rost B. (2009), "Improved Disorder Prediction by Combination of Orthogonal Approaches", *PLoS One*, **4(2)**:e4433
- Schlessinger A., Yachdav G., Rost B. (2006), "PROFbval: Predict Flexible and Rigid Residues in Proteins", *Bioinformatics*, **22(7)**:891-893
- Schmitt E., Boutros R., Froment C., Monsarrat B., Ducommun B., Dozier C. (2006), "CHK1 Phosphorylates CDC25B During the Cell Cycle in the Absence of DNA Damage", *Journal of Cell Science*, **119(Pt20)**:4269-4275
- Schoenmakers E., Alen P., Verrijdt G., Peeters B., Verhoeven G. Rombauts W., Claessens F. (1999), "Differential DNA Binding by the Androgen and Glucocorticoid Receptors Involves the Second Zn-Finger and a C-Terminal Extension of the DNA-Binding Domains", *Biochemical Journal*, **341(Pt.3)**:515-521

- Schoenmakers E., Verrijdt G., Peeters B., Verhoeven G. Rombauts W., Claessens F. (2000), "Differences in DNA Binding Characteristics of the Androgen and Glucocorticoid Receptors Can Determine Hormone-Specific Responses", *Journal of Biological Chemistry*, **275(16)**:12290-12297
- Schroeder D.F., Gahutz M., Maxwell B.B., Cook R.K., Kan J.M., Alonso J.M., Ecker J.R., Chory J. (2002), "De-etiolated 1 and Damaged DNA Binding Protein 1 Interact to Regulate *Arabidopsis* Photomorphogenesis", *Current Biology*, **12(17)**:1462-1472
- Schülke P., Wochnik G.M., Lang-Rollin I., Gassen N.C., Knapp R.T., Berning B., Yassouridis A., Rein T. (2010), "Differential Impact of Tetratricopeptide Repeat Proteins on the Steroid Hormone Receptors", *PLoS One*, **22(5)**:e11717
- Schulte-Frohlinde D., Simic M.G., Gerner H. (1990), "Laser-Induced Strand Break Formation in DNA and Polynucleotides", *Photochemistry and Photobiology*, **52(6)**:1137-1151
- Schweicheimer C. (2004), "The COP9 Signalosome (CSN): An Evolutionary Conserved Proteolysis Regulator in Eukaryotic Development", *Biochimica et Biophysica Acta*, **1695(1-3)**:45-54
- Seeley T.W., Wang L., Zhen J.Y. (1999), "Phosphorylation of Human MAD1 by the BUB1 Kinase *In Vitro*", *Biochemical and Biophysical Research Communications*, **257(2)**:589-595
- Seno J.D. and Dynlacht J.R. (2004), "Intracellular Redistribution and Modification of Proteins of the Mre11/Rad50/Nbs1 DNA Repair Complex Following Irradiation and Heat Shock", *Journal of Cellular Physiology*, **199(2)**:157-170
- Serino G., Tsuge T., Kwok S., Matsui M., Wei N., Deng X.W. (1999), "*Arabidopsis cop8* and *fus4* Mutations Define the Same Gene that Encodes Sub-Unit 4 of the COP9 Signalosome", *The Plant Cell*, **11(10)**:1967-1980
- Shackleford T.J., Zhang Q., Tian L., Vu T.T., Korapati A.L., Baumgartner A., Le X.F., Liao W.S., Claret F.X. (2011), "Stat3 and CCAAT/Enhancer Binding Protein beta (C/EBP-beta) Regulate Jab1/CSN5 Expression in Mammary Carcinoma Cells", *Breast Cancer Research*, **13(3)**:R65
- Shalom S. and Don J. (1999), "TLK: a Novel Evolutionary Conserved Murine Serine/Threonine Kinase Encodes Multiple Testes Transcripts", *Molecular Reproduction and Development*, **52(4)**:392-405
- Shangary S., Brown K.D., Adamson A.W., Edmonson S., Ng B., Pandita T.K., Yalowich J., Taccioli G.E., Baskaran R. (2000), "Regulation of DNA-Dependent Protein Kinase Activity by Ionizing Radiation – Activated Abl Kinase is an ATM-Dependent Process", *Journal of Biological Chemistry*, **275(39)**:30163-30168
- Shanware N.P., Trinh A.T., Williams L.M., Tibbetts R.S. (2007), "Coregulated Ataxia Telangiectasia-Mutated and Casein Kinase Sites Modulate Camp-Response Element-Binding Protein-Coactivator Interactions in Response to DNA Damage", *Journal of Biological Chemistry*, **282(9)**:6283-6291
- Sharma R.A., Gescher A., Plastaras J.P., Leuratti C., Singh R., Gallacher-Horley B., Offord E., Marnett L.J., Steward W.P., Plummer S.M. (2001), "Cyclooxygenase-2, Malondialdehyde and Pyrimidopurine Adducts of Deoxyguanosine in Human Colon Cells", *Carcinogenesis*, **22(9)**:1557-1560

- She Q.B., Bode A.M., Ma W.Y., Chen N.Y., Dong Z. (2001), “Resveratrol-Induced Activation of p53 and Apoptosis is Mediated by Extracellular-Signal-Regulated Protein Kinases and p38 Kinase”, *Cancer Research*, **61(4)**:1604-1610
- She Q.B., Chen N., Dong Z. (2000), “ERKs and p38 Kinase Phosphorylate p53 Protein at Serine 15 in Response to U.V. Radiation”, *Journal of Biological Chemistry*, **275(27)**:20444-20449
- Shechter D., Costanzo V., Gautier J. (2004), “ATR and ATM Regulate the Timing of DNA Replication Origin Firing”, *Nature Cell Biology*, **6(7)**:648-655
- Shell S.M., Hess S., Kvaratskhelia M., Zou Y. (2005), “Mass Spectrometric Identification of Lysines Involved in the Interaction of Human Replication Protein A with Single-Stranded DNA”, *Biochemistry*, **44(3)**:971-978
- Shepherd G.M. (2003), “Hypersensitivity Reactions to Chemotherapeutic Drugs”, *Clinical Reviews in Allergy and Immunology*, **24(3)**:253-262
- Sherman M.Y. (2011), “Proteotoxic Stress Targeted Therapy (PSTT)”, *Oncotarget*, **2(5)**:356-357
- Sherman M.Y., Meng L., Stampfer M., Gabai V.L., Yaglom J.A. (2011), “Oncogenes Induce Senescence with Incomplete Growth Arrest and Suppress the DNA Damage Response in Immortalized Cells”, *Aging Cells*, **10(6)**:949-961
- Sherr C.J. and Roberts J.M. (1999), “CDK Inhibitors: Positive and Negative Regulators of G1-Phase Progression”, *Genes and Development*, **13(12)**:1501-1512
- Shi G., Chang D.Y., Cheng C.C., Guan X., Venclovas C., Lu A.L. (2006), “Physical and Functional Interactions Between MutY Glycosylase Homologue (MYH) and Checkpoint Proteins Rad9-Rad1-Hus1”, *The Biochemical Journal*, **400(1)**:53-62
- Shieh S.Y., Ahn J., Tamai K., Taya Y., Prives C. (2000), “The Human Homologs of Checkpoint Kinases Chk1 and Cds1 (Chk2) Phosphorylate p53 at Multiple DNA Damage-Inducible Sites”, *Genes and Development*, **14(6)**:289-300
- Shikata M., Ishikawa F., Kanoh J. (2007), “Tel2 is Required for Activation of the Mrc1-Mediated Replication Checkpoint”, *Journal of Biological Chemistry*, **282(2)**:5346-5355
- Shiloh Y. (1997), “Ataxia-Telangiectasia and the Nijmegen Breakage Syndrome: Related Disorders but Genes Apart”, *Annual Review of Genetics*, **31**:635-662
- Shim E.Y., Hong S.J., Oum J.H., Yanez Y., Zhang Y., Lee S.E. (2007), “RSC Mobilizes Nucleosomes to Improve Accessibility of Repair Machinery to the Damaged Chromatin” *Molecular and Cellular Biology*, **27(5)**:1602-1613
- Shimizu K., Muraoka Y., Hirose S., Tomii K., Noguchi T. (2007), “Predicting Mostly Disordered Proteins by Using Structure-Unknown Protein Data”, *BMC Bioinformatics*, **8**:78
- Shin M.H., Yuan M., Zhang H., Margolick J.B., Kai M. (2012), “ATM-Dependent Phosphorylation of the Checkpoint Clamp Regulates Repair Pathways and Maintains Genomic Stability”, *Cell Cycle*, **11(9)**:1796-1803
- Shiomi Y., Shinozaki A., Nakada D., Sugimoto K., Usukura J., Obuse C., Tsurimoto T. (2002), “Clamp and Clamp Loader Structures of Human Checkpoint Protein Complexes: Rad9-1-1 and Rad17-RFC”, *Genes and cells*, **7(8)**:861-868

Shiromizu T., mGoto H., Tomono Y., Bartek J., Totsukawa G., Inoko A., Nakanishi M., Matsumura F., Inagaki M. (2006), "Regulation of Mitotic Function of Chk1 Through Phosphorylation at Novel Sites by Clin-Dependent Kinase 1 (Cdk1)", *Genes to Cells*, **11(5)**:477-485

Shoaf W.T. and Jones M.E. (1973), "Uridylic Acid Synthesis in Ehrlich Ascites Carcinoma: Properties, Subcellular Distribution and Nature of Enzyme Complexes of the Six Biosynthetic Enzymes", *Biochemistry*, **12(21)**:4039-4051

Shuck S.C., Short E.A., Turchi J.J. (2008), "Eukaryotic Nucleotide Excision Repair: From Understanding Mechanisms to Influencing Biology", *Cell Research*, **18(1)**:64-72

Siam R., Dolan W.P., Forsburg S.L. (2004), "Choosing and Using *Schizosaccharomyces pombe* Plasmids", *Methods*, **33(3)**:189-198

Sidorova J.M. (2008), "Roles of the Werner Syndrome RecQ Helicase in DNA Replication", *DNA Repair (Amst.)*, **7(11)**:1776-1786

Sierant M.L., Archer N.E., Davey S.K. (2010), "The Rad9A Checkpoint Protein is Required for Nuclear Localization of the Claspin Adaptor Protein", *Cell Cycle*, **9(3)**:548-556

Sigoillot F.D., Berkowski J.A., Sigoillot S.M., Kotsis D.H., Guy H.I. (2003), "Cell Cycle-Dependent Regulation of Mammalian Pyrimidine Biosynthesis", *Journal of Biological Chemistry*, **278(5)**:3403-3409

Sigoillot E.D., Evans D.R. and Guy H.I. (2002a), "Autophosphorylation of the Mammalian Multi-Functional Protein that Initiates *de Novo* Pyrimidine Biosynthesis", *Journal of Biological Chemistry*, **277(27)**:24809-24817

Sigoillot E.D., Evans D.R. and Guy H.I. (2002b), "Growth-Dependent Regulation of Mammalian Pyrimidine Biosynthesis by the Protein Kinase A and MAPK Signaling Cascades", *Journal of Biological Chemistry*, **277(18)**:15745-15751

Sigoillot F.D., Kotsis D.H., Masko E.M., Bame M., Evans D.R., Evans H.I. (2007), "Protein Kinase C Modulates the Up-Regulation of the Pyrimidine Biosynthetic Complex, CAD, by MAP Kinase", *Frontiers in Bioscience*, **12**:3892-3898

Sigoillot F.D., Kotsis D.H., Serre V., Sigoillot S.M., Evans D.R., Guy H.I. (2005), "Nuclear Localization and Mitogen-Activated Protein Kinase Phosphorylation of the Multifunctional Protein CAD", *Journal of Biological Chemistry*, **280(27)**:25611-25620

Sigoillot F.D., Sigoillot S.M., Guy H.I. (2004), "Breakdown of the Regulatory Control of Pyrimidine Biosynthesis in Human Breast Cancer Cells", *International Journal of Cancer*, **109(4)**:491-498

Sigurdsson S., Van Komen S., Bussen W., Schild D., Albala J.S., Sung P. (2001), "Mediator Function of the Human Rad51B-Rad51C Complex in Rad51/RPA-Catalyzed DNA Strand Exchange", *Genes and Development*, **15(24)**:3308-3318

Sijbers A.M., de Laat W.L., Ariza R.R., Biggerstaff M., Wei Y.P., Moggs J.G., Carter K.C., Shell B.K., Evans E., de Jong M.C., Rademakers S., de Rooij J., Jaspers N.G., Hoijsmakers J.H., Wood R.D. (1996a), "Xeroderma Pigmentosum Group F Caused by a Defect in Structure-Specific DNA Repair Endonuclease", *Cell*, **86(5)**:811-822

- Sijbers A.M., van der Spek P.J., Odijk H., van der Berg J., van Duin M., Westerveld A., Jaspers N.G., Bootsma D., Hoejmackers J.H. (1996b), "Mutational Analysis of the Human Nucleotide Excision Repair Gene ERCC1", *Nucleic Acids Research*, **24(17)**:3370-3380
- Sillerud L.O. and Larsen R.S. (2005), "Design and Structure of Peptide and Peptidomimetic Antagonists of Protein-Protein Interaction", *Current Protein and Peptide Science*, **6(2)**:151-169
- Sillje H. and Nigg E. (2001), "Identification of Human Asf1 Chromatin Assembly Factors as Substrates of Tousled-Like Kinases", *Current Biology*, **11(13)**:1068-1073
- Simko M. (2007), "Cell Type Specific Redox Status is Responsible for Diverse Electromagnetic Field Effects", *Current Medicinal Chemistry*, **14(10)**:1141-1152
- Simons J.W. (1999), "Genetic, Epigenetic, Dysgenetic and Non-Genetic Mechanisms in Tumorigenesis II: Further Delineation of the Rate Limiting Step", *Anticancer Research*, **19(6A)**:4781-4789
- Sinclair D.A. and Oberdoerffer P. (2009), "The Ageing Epigenome: Damaged Beyond Repair?", *Ageing Research Reviews*, **8(3)**:189-198
- Sing K.K., Nurmohamed S., Davey S.K., Jia Z. (2007), "Tricistronic Cloning, Over-expression and Purification of the Human Rad9-Hus1-Rad1 Complex", *Protein Expression and Purification*, **54(2)**:204-211
- Sinn B., Tallen G., Schroeder G., Grassl B., Schulze J., Budach V., Tinhofer I. (2010), "Caffeine Confers Radiosensitization of PTEN-Deficient Malignant Glioma Cells by Enhancing Ionizing Radiation-Induced G1 Arrest and Negatively Regulating Akt Phosphorylation", *Molecular Cancer Therapeutics*, **9(2)**:480-488
- Sipickzi M., Heyer W-D., Kholi J. (1989), "Preparation and Regeneration of Protoplasts and Spheroblasts for Fusion and Transformation of *Schizosaccharomyces pombe*", *Current Microbiology*, **12(3)**:169-173
- Sleigh M.J. (1976), "The Mechanism of DNA Breakage by Phleomycin *In Vitro*", *Nucleic Acids Research*, **3(4)**:891-901
- Slijepcevic P. (2006), "The Role of DNA Damage Response Proteins at Telomeres: An Integrative Model", *DNA Repair (Amst.)*, **5(11)**:1299-1306
- Slijepcevic P. and Al-Wahiby S. (2005), "Telomere Biology: Integrating Chromosomal End Protection with DNA Damage Response", *Chromosoma*, **114(4)**:275-285
- Slupphaug G., Kavli B., Krokan H.E. (2003), "The Interacting Pathways for Prevention and Repair of Oxidative DNA Damage", *Mutation Research*, **531(1-2)**:231-251
- Smirnova E., Toueille M., Markkanen E., Hübscher U. (2005), "The Human Checkpoint Sensor and Alternative DNA Clamp Rad9-Rad1-Hus1 Modulates the Activity of DNA Ligase I, a Component of the Long-Patch Base Excision Repair Machinery", *The Biochemical Journal*, **389(Pt.1)**:13-17
- Smith D.F. (2004), "Tetratricopeptide Repeat Co-Chaperones in Steroid Receptor Complexes", *Cell Stress and Chaperones*, **9(2)**:109-111

- Smith E.M., Lin J.M., Meissner R.A., Allada R. (2008), "Dominant-Negative CK2alpha Induces Potent Effects on Circadian Rhythmicity", *PLoS Genetics*, **4(1)**:e12
- Smith G.C., Cary R.B., Lakin N.D., Hann B.C., Teo S.H., Chen D.J., Jackson S.P. (1999), "Purification and DNA Binding Properties of the Ataxia-Telangiectasia Gene Product ATM", *Proceedings of the National Academy of Sciences U.S.A.*, **96(20)**:11134-11139
- Smith J., Tho L.M., Xu N., Gillespie D.A. (2010), "The ATM-Chk2 and ATR-Chk1 Pathways in DNA Damage Signaling and Cancer", *Advances in Cancer Research*, **108**:73-112
- Smits V.A., Warmerdam D.O., Martin Y., Friere R. (2010), "Mechanisms of ATR-Mediated Checkpoint Signalling", *Frontiers in Bioscience*, **15**:840-853
- Sobol R.W., Horton J.K., Kuhn R., Gu H., Singhal R.K., Prasad R., Rajewsky K., Wilson S.H. (1996), "Requirement of Mammalian DNA Polymerase Beta in Base-Excision Repair", *Nature*, **379(6561)**:183-186
- Sobol R.W., Prasad R., Evenski A., Baker A., Yang X.P., Horton J.K., Wilson S.H. (2000), "The Lyase Activity of the DNA Repair Protein Beta-Polymerase Protects from DNA-Damaged-Induced Cytotoxicity", *Nature*, **405(6788)**:807-810
- Sohn S.Y. and Cho Y. (2009), "Crystal Structure of the Human Rad9-Hus1-Rad1 Clamp", *Journal of Molecular Biology*, **390(3)**:490-502
- Solier S., Barb J., Zeeberg B.R., Varma S., Ryan M.C., Kohn K.W., Weistein J.N., Munson P.J., Pommier Y. (2010), "Genome-Wide Analysis of Novel Splice Variants Induced by Topoisomerase I Poisoning Shows Preferential Occurrence in Genes Encoding Splicing Factors", *Cancer Research*, **70(20)**:8055-8065
- Song W., Levin D.S., Varkey J., Post S., Bermudez V.P., Hurwitz J., Tomkinson A.E. (2007), "A Conserved Physical and Functional Interaction Between the Clamp Loader and DNA Ligase I of Eukaryotes", *Journal of Biological Chemistry*, **282(31)**:22721-22730
- Song W., Pascal J.M., Ellenberger T., Tomkinson A.E. (2009), "The DNA Binding Domain of Human DNA Ligase I Interacts with Both Nicked DNA and the DNA Sliding Clamps, PCNA and hRad9-hRad1-hHus1", *DNA Repair (Amst.)*, **8(8)**:912-919
- Sonoda E., Takata M., Yamashita Y.M., Morrison C., Takeda S. (2001), "Homologous DNA Recombination in Vertebrate Cells", *Proceedings of the National Academy of Sciences U.S.A.*, **98(15)**:8388-8394
- Sordet O., Redon C.E., Guirouilh-Brabat J., Smith S., Solier S., Douarre C., Conti C., Nakamura A.J., Das B.B., Nicolas E., Kohn K.W., Bonner W.M., Pommier Y. (2009), "Ataxia Telangiectasia Mutated Activation by Transcription- and Topoisomerase I- Induced DNA Double-Strand Breaks", *EMBO Reports*, **10(8)**:887-893
- Sorensen C.S., Syljuasen R.G., Lukas J., Bartek J. (2004), "ATR, Claspin and the Rad9-Rad1-Hus1 Complex Regulate Chk1 and Cdc25A in the Absence of DNA Damage", *Cell Cycle*, **3(7)**:941-945
- Southwood D.R. and Agard D.A. (2011), "Client-Loading Conformation of the Hsp90 Molecular Chaperone Revealed in the Cryo-EM Structure of the Human Hsp90:Hop Complex", *Molecular Cell*, **42(6)**:771-781

Speit G., Hochsattel R., Vogel W. (1984), "The Contribution of DNA Single-Strand Breaks to the Formation of Chromosome Aberrations and SCEs", *Basic Life Sciences*, **29 (Pt.A)**:229-244

Spirek M., Benko Z., Carnecka M., Rumpf C., Cipak L., Batova M., Marova I., Nam M., Kim D.U., Park H.O., Hayles J., Hoe K.L., Nurse P., Gregan J. (2010), "S. pombe Genome Deletion Project: An Update", *Cell Cycle*, **9(12)**:2399-2402

Spradling A., Ganetsky B., Hieter P., Johnston M., Olson M., Orr-Weaver T., Rossant J., Sanchez A., Waterston R. (2006), "New Roles for Model Genetic Organisms in Understanding and Treating Human Disease: Report from the 2006 Genetics Society of America Meeting", *Genetics*, **172(4)**:2025-2032

Spriggs K.A., Bushell M., Mitchell S.A., Willis A.E. (2005), "Internal Ribosome Entry Segment-Mediated Translation During Apoptosis: The Role of IRES-Trans-Acting Factors", *Cell Death and Differentiation*, **12(6)**:585-591

Spyropoulos I.C., Liakopoulos T.D., Bagos P.G., Hamodrakas S.J. (2004), "TMRPres2D: High Quality Visual Representation of Transmembrane Protein Models", *Bioinformatics*, **20(17)**:3258-3260

Srivastava D.K., Berg B.J., Prasad R., Molina J.T., Beard W.A., Tomkinson A.E., Wilson S.H. (1998), "Mammalian Abasic Site Base Excision Repair: Identification of the Reaction Sequence and Rate Determining Steps", *Journal of Biological Chemistry*, **273(33)**:21203-21209

Stasiak A.Z., Larquet E., Stasiak A., Muller S., Engel A., Van Dyck E., West S.C., Egelman E.H. (2000), "The Human Rad52 Protein Exists as a Heptameric Ring", *Curr. Biol.*, **10(6)**:337-340

Stennicke H.R., Renatus M., Meldal M., Salvesen G.S. (2000), "Internally Quenched Fluorescent Peptide Substrates Disclose the Subsite Preferences of Human Caspases 1, 3, 6, 7 and 8", *The Biochemical Journal*, **350(Pt.2)**:563-568

Stern R., Rose J.A., Friedman R.M. (1974), "Phleomycin-Induced Cleavage of Deoxyribonucleic Acid", *Biochemistry*, **13(2)**:307-312

Stewart Z.A., Westfall M.D., Pietenpol J.A. (2003), "Cell Cycle Deregulation and Anti-Cancer Therapy", *Trends in Pharmacological Sciences*, **24(3)**:139-145

Stiborová M., Borek-Dohalská L., Aimová D., Kotrbová V., Kukacková K., Janouchová K., Rupertová M., Ryslavá H., Hudecek J., Frei E. (2006), "Oxidation Pattern of the Anticancer Drug Ellipticine by Hepatic Microsomes – Similarity Between Human and Rat Systems", *General Physiology and Biophysics*, **25(3)**:245-261

Stiborová M., Sejbal J., Borek-Dohalská L., Aimová D., Poljaková J., Forsterová K., Rupertová M., Wiesner J., Hudecek J., Wiessler M., Frei E. (2004), "The Anticancer Drug Ellipticine Forms Covalent DNA Adducts, Mediated by Human Cytochromes P450, Through Metabolism to 13-Hydroxyellipticine and Ellipticine N2-Oxide", *Cancer Research*, **64(22)**:8374-8380

St Onge R.P., Besley B.D., Park M., Casselman R., Davey S. (2001), "DNA Damage-Dependent and -Independent Phosphorylation of the hRad9 Checkpoint Protein", *Journal of Biological Chemistry*, **276(45)**:41898-41905

St Onge R.P., Besley B.D.A., Pelley J.L., Davey S. (2003), "A Role for the Phosphorylation of hRad9 in Checkpoint Signaling", *Journal of Biological Chemistry*, **278(29)**:26620-26628

- Strahl B.D. and Allis D. (2000), "The Language of Covalent Histone Modifications", *Nature*, **403(6765)**:41-45
- Strauss B., Scudiero D., Henderson E. (1975), "The Nature of the Alkylation Lesion in Mammalian Cells", *Basic Life Sciences*, **5A**:13-24
- Strekowski L., Chandrasekaran S., Wang Y.H., Edwards W.D., Wilson W.D. (1986), "Molecular Basis for Anticancer Drug Amplification: Interaction of Phleomycin Amplifiers with DNA", *Journal of Medicinal Chemistry*, **29(7)**:1311-1315
- Stucki M., Pascucci B., Parlanti E., Fortini P., Wilson S.H., Hubscher U., Dogliotti E. (1998), "Mammalian Base Excision Repair by DNA Polymerases Delta and Epsilon", *Oncogene*, **17(7)**:835-843
- Su C.T., Chen C.Y., Ou Y.Y. (2009), "Protein Disorder Prediction by Condensed PSSM Considering Propensity for Order or Disorder", *BMC Bioinformatics*, **7**:319
- Subramani S. (1991), "Radiation Resistance in *Schizosaccharomyces pombe*", *Molecular Microbiology*, **5(10)**:2311-2314
- Sugimara T. and Ushijima T. (2000), "Genetic and Epigenetic Alterations in Carcinogenesis", *Mutation Research*, **462(2-3)**:235-246
- Sugiura R. (2002), "Functional Analysis of Calcineurin-Mediated Signalling Pathway Using Fission Yeast as a Model System", *Nippon Yakurigaku Zasshi*, **119(3)**:155-161
- Sugiyama Y., Tomoda K., Tanaka T., Arata Y., Yoneda-Kato N., Kato J. (2001), "Direct Binding of the Signal-Transducing Adaptor Grb2 Facilitates Down-Regulation of the Cyclin-Dependent Kinase Inhibitor p27Kip1", *Journal of Biological Chemistry*, **276(15)**:12084-12090
- Sukhanova M.V., D'Herin C., Auffret van der Kemp P., Koval V.V., Boiteux S., Lavrik O.I. (2011), "Ddc1 Checkpoint Protein and DNA Polymerase ϵ Interact with Nick-Containing DNA Repair Intermediates in Cell Free Extracts of *Saccharomyces cerevisiae*", *DNA Repair (Amst.)*, **10(8)**:815-825
- Sukina E.N., Moskalenko I.P., Svinarenko A.V., Sorochan P.P., Prokhach N.E., Nikiforova N.A., Gromakova I.A. (2012), "The Prospects for the Use of Chronomodulated Chemo- and Radiotherapy in Oncology", *Kl'nicheskaiia Meditsina*, **90(2)**:9-13
- Sun M., Duann P., Lin C.T., Zhang H., Liu L.F. (2000), "Rapid Chromatin Reorganisation Induced by Topoisomerase I-Mediated DNA Damage", *Annals of the New York Academy of Sciences*, **992**:340-342
- Sun T.P. and Shieh S.Y. (2009), "Human FEM1B is Required for Rad9 Recruitment and Chk1 Activation in Response to Replication Stress", *Oncogene*, **28(18)**:1971-1981
- Sun W., Nandi S., Osman F., Ahn J.S., Jakovleska J., Lorenz A., Whitby M.C. (2008), "The FANC Ortholog Fml1 Promotes Recombination at Stalled Replication Forks and Limits Crossing Over During DNA Double Strand Break Repair", *Molecular Cell*, **32(1)**:118-128
- Sunavala-Dossabhoy G., Balakrishnan S.K., Sen S., Nuthalapaty S., De Benedetti A. (2005), "The Radioresistant Kinase TLK1B Protects the Cells by Promoting Repair of Double-Strand Breaks", *BMC Molecular Biology*, **6**:19

- Sunavala-Dossabhoy G. and De Benedetti A. (2009), "Tousled Homolog, TLK1, Binds and Phosphorylates Rad9: TLK1 Acts as a Molecular Chaperone in DNA Repair", *DNA Repair (Amst.)*, **8(1)**:87-102
- Sunavala-Dossabhoy G., Li Y., Willimas B., De Benedetti A. (2003), "A Dominant Negative Mutant of TLK1 Causes Chromosome Missegregation and Aneuploidy in Normal Breast Epithelial Cells", *BMC Molecular Biology*, **4**:16
- Supino R., Scovassi A.I., Croce A.C., Bo L.D., Favini E., Corbelli A., Farina C., Misiano P., Zunino P. (2009), "Biological Effects of New Vacuolar H⁺-ATPase Inhibitor in Colon Carcinoma Cell Lines", *Annals of the New York Academy of Sciences*, **1171(1)**:606-616
- Suzuki A., Tsutomi Y., Akahane K., Araki T., Miura M. (1998), "Resistance to Fas-Mediated Apoptosis: Activation of Caspase 3 is Regulated by Cell Cycle Regulator *p21WAF1* and *IAP* Gene Family ILP", *Oncogene*, **17(8)**:931-939
- Suzuki A., Tsuomi Y., Miura M., Akahane K. (1999), "Identification of Binding Domain with *p21* and *ILP* and Inactivation Machinery by *p21*", *Oncogene*, **18(5)**:1239-1244
- Takata M., Sasaki M.S., Sonoda E., Fukushima T., Morrison C., Albala J.S., Swagemakers S.M., Kanaar R., Thompson L.H., Takeda S. (2000), "The Rad51 Paralog Rad51B Promotes Homologous Recombinational Repair", *Mol. Cell. Biol.*, **20(17)**:6476-6482
- Takeishi Y., Ohashi E., Ogawa K., Masai H., Obuse C., Tsurimoto T. (2010), "Casein Kinase 2-Dependent Phosphorylation of Human Rad9 Mediates the Interaction Between Human Rad9-Hus1-Rad1 Complex and TopBP1", *Genes to Cells*, **15(7)**:761-771
- Tan A.L.C., Rida P.C., Surana U. (2005), "Essential Tension and Constructive Destruction: The Spindle Checkpoint and Its Regulatory Links with Mitotic Exit", *The Biochemical Journal*, **386(Pt.1)**:1-13
- Tan Z.J. and Chen S.J. (2006), "Ion-Mediated Nucleic Acid Helix-Helix Interactions", *Biophysical Journal*, **91(2)**:518-536
- Tanaka N. (1983), "Study of New Antineoplastic Antibiotics Based on Newly Discovered Action Mechanisms", *Gan To Kagaku Ryoho. Cancer and Chemotherapy*, **10(4 Pt.2)**:1094-1106
- Tanaka K. (2010), "Multiple Functions of the S-Phase Checkpoint Mediator", *Bioscience, Biotechnology and Biochemistry*, **74(12)**:2367-2373
- Tanaka Y., Maniwa Y., Bermudez V.P., Doi T., Nishio W., Ohbavashi C., Okita Y., Hurwitz J., Hayashi Y., Yoshimura M. (2010), "Single Nucleotide Polymorphisms in DNA Damage Repair Pathways and Lung Cancer Risk", *Cancer*, **116(4)**:896-902
- Tao W. and Levine A.J. (1999), "P19(ARF) Stabilizes p53 by Blocking Nucleo-Cytoplasmic Shuttling of Mdm2", *Proceedings of the National Academy of Sciences U.S.A.*, **96(12)**:6937-6941
- Tapia-Alveal C., Calonge T.M., O'Connell M.J. (2009), "Regulation of Chk1", *Cell Division*, **4**:8
- Taricani L., Shanahan F., Pierce R.H., Guzi T.J., Parry D. (2010), "Phenotypic Enhancement of Thymidylate Synthetase Pathway Inhibitors Following Ablation of NEIL1 DNA Glycosylase/Lyase", *Cell Cycle*, **9(24)**:4876-4833

- Tartaglia G.G. and Vendruscolo M. (2008), “The Zyggregator Method for Predicting Protein Aggregation Propensities”, *Chemical Society Reviews*, **37(7)**:1395-1401
- Tartaglia G.G. and Vendruscolo M. (2010), “Proteome-Level Interplay Between Folding and Aggregation Propensities of Proteins”, *Journal of Molecular Biology*, **402(5)**:919-928
- Tatibana M. and Ito K. (1969), “Control of Pyrimidine Biosynthesis in Mammalian Tissues I: Partial Purification and Characterization of Glutamine-Utilizing Carbamyl Phosphate Synthetase of Mouse Spleen and Its Tissue Distribution”, *Journal of Biological Chemistry*, **244(19)**:5403-5413
- Taylor E.M., Cecillon S.M., Bonis A., Chapman J.R., Povrik L.F., Lindsay H.D. (2009), “The Mre11/Rad50/Nbs1 Complex Functions in Resection-Based DNA End-Joining in *Xenopus Laevis*”, *Nucleic Acids Research*, **38(2)**:441-454
- Taylor M., Moore K., Murray J., Aves S.J., Price C. (2011), “Mcm10 Interacts with Rad4/Cut5(TopBP1) and its Association with Origins of DNA Replication is dependent on Rad4/Cut5(TopBP1)”, *DNA Repair (Amst.)*, **10(11)**:1154-1163
- Tempel K. and von Zallinger C. (1997), “Caffeine Interactions: DNA Repair Enzymes and Nucleic Acid Synthesis”, *Zeitschrift für Naturforschung C. Journal of Biosciences*, **52(7-8)**:466-474
- Teoule R. (1987), “Radiation-Induced DNA Damage and Its Repair”, *International Journal of Radiation Biology and Related Studies in Physics, Chemistry and Medicine*, **51(4)**:573-589
- Thornberry N.A., Rano T.A., Peterson E.P., Rasper D.M., Timkey T., Garcia-Calvo M., Houtzager V.M., Nordstrom P.A., Roy S., Vaillancourt J.P., Chapman K.T., Nicholson D.W. (1997), “A Combinatorial Approach Defines Specificities of Members of the Caspase Family and Granzyme B”, *Journal of Biological Chemistry*, **272(29)**:17907-17911
- Thornton G., Wilkinson C.R., Toone W.M., Jones N. (2005), “A Novel Pathway Determining Multiple Drug Sensitivity in *Schizosaccharomyces pombe*”, *Genes to Cells*, **10(10)**:941-951
- Thornton T.M. and Rincon M. (2009), “Non-Classical p38 MAP Kinase Functions: Cell Cycle Checkpoints and Survival”, *International Journal of Biological Sciences*, **5(1)**:44-51
- Tian L., Peng G., Parant J.M., Leventaki V., Drakos E., Zhang Q., Parker-Thornburg J., Shackelford T.J., Dai H., Lin S.Y., Lozano G., Rassidakis G.Z., Claret F.X. (2010), “Essential Roles of Jab1 in Cell Survival, Spontaneous DNA Damage and DNA Repair”, *Oncogene*, **29(46)**:6125-6137
- Tsiatsiani L., Van Breusegem F., Gallois P., Zavalov A., Lam E., Bozhkov P.V. (2011), “Metacaspases”, *Cell Death and Differentiation*, **18(8)**:1279-1288
- Tibbetts R.S., Brumbaugh K.M., Williams J.M., Sarkaria J.N., Cliby W.A., Shieh S.Y., Taya Y., Prives C., Abraham R.T. (1999), “A Role for ATR in the DNA Damaged-Induced Phosphorylation of p53”, *Genes and Development*, **13(2)**:152-157
- Timbrell J.A. (2008), “Principles of Biochemical Toxicology”, 4th Edition, Informa Healthcare
- Toda T., Shimanuki M., Saka Y., Yamano H., Adachi Y., Shirakawa M., Kyogoku Y., Yanagida M. (1992), “Fission Yeast *pap1*-Transcription is Negatively Regulated by an Essential Nuclear Protein Crm1”, *Molecular and Cellular Biology*, **12(12)**:5474-5484

Toda T., Shimanuki M., Yanagida M. (1991), "Fission Yeast Genes that Confer Resistance to Staurosporine Encode an AP1-Like Transcription Factor and Protein Kinase Related to Mammalian ERK1/MAP2 and Budding Yeast Fos3 and KSS1 Kinases", *Genes and Development*, **5(1)**:60-73

Tomasz M. and Palom Y. (1997), "The Mitomycin Bioreductive Antitumour Agents: Cross-Linking and Alkylation of DNA as the Molecular Basis of Their Activity", *Pharmacology and Therapeutics*, **76(1-3)**:73-87

Tomoda K., Kato J.Y., Tatsumi E., Takahashi T., Matsuo Y., Yoneda-Kato N. (2005), "The Jab1/COP9 Signalosome Sub-complex is a Downstream Mediator of Bcr-Abl Kinase Activity and Facilitates Cell Cycle Progression", *Blood*, **105(2)**:775-783

Tomoda K., Kubota Y., Arata Y., Mori S., Maeda M., Tanaka T., Yoshida M., Yoneda-Kato N., Kato J.Y. (2002), "The Cytoplasmic Shuttling and Subsequent Degradation of p27Kip1 Mediated by Jab1/CSN5 and the COP9 Signalosome Complex", *Journal of Biological Chemistry*, **277(3)**:2302-2310

Tomoda K., Kubota Y., Kato J. (1999), "Degradation of the Cyclin-Dependent-Kinase Inhibitor p27Kip1 is Instigated by Jab1", *Nature*, **398(6723)**:160-165

Tomoda K., Yoneda-Kato N., Fukumoto A., Yamanaka S., Kato J.Y. (2004), "Multiple Functions of Jab1 are Required for Early Embryonic Development and Growth Potential in Mice", *Journal of Biological Chemistry*, **279(41)**:43013-43018

Tompa P. and Csermely P. (2004), "The Role of Structural Disorder in the Function of RNA and Protein Chaperones", *FASEB Journal*, **18(11)**:1169-1175

Tompa P., Fuxreiter M., Oldfield C.J., Simon I., Dunker A.K., Uversky V.N. (2009), "Close Encounters of the Third Kind: Disordered Domains and the Interactions of Proteins", *Bioessays*, **31(3)**:328-355

Tompa P. and Kovacs D. (2010), "Intrinsically Disordered Chaperones in Plants and Animals", *Biochemistry and Cell Biology*, **88(2)**:167-174

Toone W.M., Kuge S., Samuel M., Morgan B.A., Toda T., Jones N. (1998), "Regulation of the Fission Yeast Transcription Factor Pap1 by Stress: Requirement of the Nuclear Export Factor Crm1 (Exportin) and the Stress-Activated MAP Kinase Sty1/Spc1", *Genes and Development*, **12(10)**:1453-1463

Touaille M., El Andaloussi N., Frouin I., Freire R., Funk D., Shevelev I., Funk D., Shevelev I., Friederich-Heineken E., Villani G., Hottiger M.O., Hubscher U. (2004), "The Human Rad9/Rad1/Hus1 Damage Sensor Clamp Interacts with DNA Polymerase Beta and Increases its DNA Substrate Utilisation Efficiency: Implications for DNA Repair", *Nucleic Acids Research*, **32(11)**:3316-3324

Trigg J., Gutwin K., Keating A.E., Berger B. (2011), "Multicoil2: Predicting Coiled Coils and Their Oligomerization States From Sequence in the Twilight Zone", *PLoS One*, **6(8)**:e23519

Trovato A., Chiti F., Maritan A., Seno F. (2006), "Insight Into the Structure of Amyloid Fibrils From the Analysis of Globular Proteins", *PLoS Computational Biology*, **2(12)**:e170

Trovesi C., Falcattoni M., Lucchini G., Clerici M., Longhese M.P. (2011), "Distinct CDK1 Requirements During Single-Strand Annealing, Non-Crossover and Crossover Recombination", *PLoS Genetics*, **7(8)**:e1002263

- Trujillo K.M., Yuan S.S., Lee E.Y., Sung P. (1998), “Nuclease Activities in a Complex of Human Recombination and DNA Repair Factors Rad50, Mre11 and p95”, *Journal of Biological Chemistry*, **273(34)**:21447-21450
- Trumpp A. and Wiestler O.D. (2008), “Mechanisms of Disease: Cancer Stem Cells – Targeting the Evil Twin”, *Nature Clinical Practice Oncology*, **5(6)**:337-347
- Truss M. and Beato M. (1993), “Steroid Hormone Receptors: Interaction with Deoxyribonucleic Acid and Transcription Factors”, *Endocrine Reviews*, **14(4)**:459-479
- Tsai S.Y., Carlstedt-Duke J., Weigel N.L., Dahlman K., Gustafsson J.A., Tsai M.J., O’Malley B.W. (1988), “Molecular Interactions of Steroid Hormone Receptor with Its Enhancer Element: Evidence for Receptor Dimer Formation”, *Cell*, **55(2)**:361-369
- Tse A.N., Sheikh T.N., Alan H., Chou T.C., Schwartz G.K. (2008), “90-kDa Heat Shock Protein Inhibition Abrogates the Topoisomerase I Poison-Induced G2/M Checkpoint in p53-Null Tumor Cells by Depleting Chk1 and Wee1”, *Molecular Pharmacology*, **75(1)**:124-133
- Tseng B.S., Tan L., Kapoor T.M., Funabiki H. (2010), “Dual Detection of Chromosomes and Microtubules by the Chromosomal Passenger Complex Drives Spindle Assembly”, *Developmental Cell*, **18(6)**:903-912
- Tsukahara T., Tanno Y., Watanabe Y. (2010), “Phosphorylation of the CPC by Cdk1 Promotes Chromosome Biorientation”, *Nature*, **467(7316)**:719-723
- Tubbs J.L., Pegg A.E., Tainer J.A. (2007), “DNA Binding, Nucleotide Flipping and the Helix-Turn-helix Motif in Base Repair by O6-Alkylguanine-DNA Alkyltransferase and Its Implications for Cancer Chemotherapy”, *DNA Repair (Amst.)*, **6(8)**:1100-1115
- Turi T.G. and Rose J.K. (1995), “Characterization of a Novel *Schizosaccharomyces pombe* Multidrug Resistance Transporter Conferring Brefeldin A Resistance”, *Biochemical and Biophysical Research Communications*, **213(2)**:410-418
- Turner B.M. (2002), “Cellular Memory and the Histone Code”, *Cell*, **111(3)**:285-291
- Turowec J.P., Duncan J.S., Gloor G.B., Litchfield D.W. (2011), “Regulation of Caspase Pathways by Protein Kinase CK2: Identification of Proteins with Overlapping CK2 and Caspase Consensus Motifs”, *Molecular and Cellular Biochemistry*, **356(1-2)**:159-167
- Tuteja N. and Tuteja R. (2001), “Unraveling DNA Repair in Human: Molecular Mechanisms and Consequences of Repair Defect”, *Critical Reviews in Biochemistry and Molecular Biology*, **36(3)**:261-290
- Ueda S., Takeishi Y., Ohashi E., Tsurimoto T. (2012), “Two Serine Phosphorylation Sites in the C-Terminus of Rad9 are Critical for 9-1-1 Binding to TopBP1 and Activation of the DNA damage Checkpoint Response in HeLa Cells”, *Genes to Cells, Electronic Publication Ahead of Print*
- Umar A., Boyer J.C., Kunkel T.A. (1994), “DNA Loop Repair by Human Cell Extracts”, *Science*, **266(5186)**:814-816
- Umesono K. and Evans R.M. (1989), “Determinants of Target Gene Specificity for Steroid/Thyroid Hormone Receptors”, *Cell*, **57(7)**:1139-1146

- Unger T., Juven-Gershon T., Moallem E., Berger M., Vogt Sionov R., Lozano G., Oren M., Haupt Y. (1999), "Critical Role for Ser20 of Human p53 in the Negative Regulation of p53 by Mdm2", *The EMBO Journal*, **18(7)**:1805-1814
- Unsal-Kacmaz K., Chastain P.D., Qu P.P., Minoos P., Cordeiro-Stone M., Sancar A., Kaufmann W.K. (2007), "The Human Tim/Tipin Complex Co-Ordinates an Intra-S Checkpoint Response to U.V. that Slows Replication Fork Displacement", *Molecular and Cellular Biology*, **27(8)**:3131-3142
- Unsal-Kacmaz K., Makhov A.M, Griffith J.D., Sancar A. (2002), "Preferential Binding of ATR Protein to UV-Damaged DNA", *Proceedings of the National Academy of Sciences U.S.A.*, **99(10)**:6673-6678
- Unsal-Kacmaz K., Mullen T.E., Kaufmann W.K., Sancar A. (2005), "Coupling of Human Circadian and Cell Cycles by the Timeless Protein", *Molecular and Cellular Biology*, **25(8)**:3109-3116
- Unsal-Kacmaz K. and Sancar A. (2004), "Quarternary Structure of ATR and Effects of ATRIP and Replication Protein A on its DNA Binding and Kinase Activities", *Molecular and Cellular Biology*, **24(3)**:1292-1300
- Uversky V.N. and Dunker A.K. (2010), "Understanding Protein Non-Folding", *Biochimica et Biophysica Acta – Proteins and Proteomics*, **1804(6)**:1231-1264
- Uversky V.N., Gillespie J.R., Fink A.L. (2000), "Why are 'Natively Unfolded' Proteins Unstructured Under Physiologic Conditions?", *Proteins*, **41(3)**:415-427
- Uversky V.N., Oldfield C.J., Dunker A.K. (2008), "Intrinsically Disordered Proteins in Human Diseases: Introducing the D2 Concept", *Annual Review of Biophysics*, **37**:215-246
- Uversky V.N., Oldfield C.J., Midic U., Xie H., Vucetic S., Xue B., Iakoucheva L.M., Obradovic Z., Dunker A.K. (2009), "Unfoldomics of Human Diseases: Linking Protein Intrinsic Disorder with Diseases", *BMC Genomics*, **10 (Supplement 1)**:S7
- Uversky V.N., Radivojac P., Iakoucheva I.M., Obradovic Z., Dunker A.K. (2007), "Prediction of Intrinsic Disorder and Its Use in Functional Proteomics", *Methods in Molecular Biology*, **408**:69-92
- Vacic V, Uversky V.N., Dunker A.K., Lonardi S. (2007), "Composition Profiler: A Tool for Discovery and Visualization of Amino Acid Composition Differences", *BMC Bioinformatics*, **8**:211
- Vargas-Roig L.M., Gago F.E., Tello O., Aznar J.C., Ciocca D.R. (1998), "Heat Shock Protein Expression and Drug Resistance in Breast Cancer Patients Treated with Induction Therapy", *International Journal of Cancer*, **79(5)**:468-475
- Vasquez K.M., Christensen J., Li L., Finch R.A., Glazer P.M. (2002), "Human XPA and RPA DNA Repair Proteins Participate in Specific Recognition of Triplex-Induced Helical Distortions", *Proceedings of the National Academy of Sciences U.S.A.*, **99(9)**:5848-5853
- Vásquez-Novelle M.D., Mirchenko L., Uhlmann F., Petronczki M. (2010), "The 'Anaphase Problem': How to Disable the Mitotic Checkpoint When Sisters Split", *Biochemical Society Transactions*, **38(6)**:1660-1666
- Vaziri C. (2010), "Linking Cdc7 with the Replication Checkpoint", *Cell Cycle*, **9(24)**:4787

- Vazquez-Pianzola P. and Suter B. (2012), “Conservation of the RNA Transport Machineries and Their Coupling to Translation Control Across Eukaryotes”, *Computational and Functional Genomics*, **Electronic Publication Ahead of Print**
- Vekhoff P., Duca M., Guianvarc’h D., Benhida R., Arimondo P.B. (2012), “Sequence-Specific Base-Pair Mimics are Efficient Topoisomerase IB Inhibitors”, *Biochemistry*, **51(1)**:43-51
- Venclovas C. and Thelen M.P. (2000), “Structure-Based Predictions of Rad1, Rad9, Hus1 and Rad17 Participation in DNA Sliding Clamp and Clamp-Loading Complexes”, *Nucleic Acids Research*, **28(13)**:2481-2493
- Ventikaraman A.R. (2001), “Functions of BRCA1 and BRCA2 in the Biological Response to DNA Damage”, *Journal of Cell Science*, **114(Pt.20)**:3591-3598
- Ventikaraman A.R. (2002), “Cancer Susceptibility and the Functions of BRCA1 and BRCA2”, *Cell*, **108(2)**:171-182
- Verbeek B., Southgate T.D., Gilham D.E., Margison G.P. (2008), “O6-Methylguanine-DNA Methyltransferase Inactivation and Chemotherapy”, *British Medical Bulletin*, **85**:17-33
- Verrijdt G., Tanner T., Moehren U., Callewaert L., Haelens A., Claessens F. (2006), “The Androgen Receptor DNA-Binding Domain Determines Androgen Selectivity of Transcriptional Response”, *Biochemical Society Transactions*, **34(Pt.6)**:1089-1094
- Vigneron S., Prieto S., Bernis C., Labbé J.C., Castro A., Lorca T. (2004), “Kinetochore Localization of Spindle Checkpoint Proteins: Who Controls Whom?”, *Molecular Biology of the Cell*, **15(10)**:4584-4596
- Vlach J., Hennecke S., Amati B. (1997), “Phosphorylation-Dependent Degradation of the Cyclin-Dependent Kinase Inhibitor p27Kip1”, *The EMBO Journal*, **16(17)**:5334-5344
- Vogelstein B., Lane D., Levine A.J. (2000), “Surfing the p53 Network”, *Nature*, **408(6810)**:307-310
- Volkmer E. and Karnitz L.M. (1999), “Human Homologs of *Schizosaccharomyces pombe* rad1, hus1 and rad9 Form a DNA Damage-Responsive Protein Complex”, *Journal of Biological Chemistry*, **274(2)**:567-570
- Vucetic S., Brown C.J., Dunker A.K., Obradovic Z. (2003), “Flavors of Protein Disorder”, *Proteins*, **52(4)**:573-584
- Vucetic S., Xie H., Iakoucheva L.M., Oldfield C.J., Dunker A.K., Obradovic Z., Uversky V.N. (2007), “Functional Anthology of Intrinsic Disorder: 2. Cellular Components, Domains, Technical Terms, Developmental Processes and Coding Sequence Diversities Correlated with Long Disordered Regions”, *Journal of Proteome Research*, **6(5)**:1899-1916
- Walker G.M. (1982), “Cell Cycle Specificity of Certain Antimicrotubular Drugs in *Schizosaccharomyces pombe*”, *Journal of General Microbiology*, **128(1)**:61-71
- Walter J. and Newport J. (2000), “Initiation of Eukaryotic DNA Replication: Origin Unwinding and Sequential Chromatin Association of Cdc45, RPA and DNA Polymerase α ”, *Molecular Cell*, **5(4)**:617-627

- Walworth N., Davey S., Beach D. (1993), "Fission Yeast Chk1 Protein Kinase Links the Rad Checkpoint Pathway to Cdc2", *Nature*, **363(6427)**:368-371
- Wandlinger S.K., Richter K., Buchner J. (2008), "The Hsp90 Chaperone Machinery", *Journal of Biological Chemistry*, **283(27)**:18473-18477
- Wang L., Hsu C.L., Ni J., Wang P.H., Yeh S., Keng P., Chang C. (2004), "Human Checkpoint Protein hRad9 Functions as a Negative Coregulator to Repress Androgen Receptor Transactivation in Prostate Cancer Cells", *Molecular and Cellular Biology*, **24(5)**:2202-2213
- Wang T.J., Liu Z.S., Zeng Z.C., Du S.S., Qiang M., Zhang S.M., Zhang Z.Y., Tang Z.Y., Wu W.Z., Zeng H.Y. (2010), "Caffeine Enhances Radiosensitization to Orthotopic Transplant LM3 Hepatocellular Carcinoma *In Vivo*", *Cancer Science*, **101(6)**:1440-1446
- Wang W., Guan J., Hu B., Weiss R.S., Iliakis G., Wang Y. (2004), "Involvement of Hus1 in the Chain Elongation Step of DNA Replication After Exposure to Camptothecin or Ionizing Radiation", *Nucleic Acids Research*, **32(2)**:767-765
- Wang W., Lindsey-Boltz L.A., Sancar A., Bambara R.A. (2006), "Mechanism of Stimulation of Human DNA Ligase I by the Rad9-Rad1-Hus1 Checkpoint Complex", *Journal of Biological Chemistry*, **281(30)**:20865-20872
- Wang X., McGowan C.H., Zhao M., He L., Downey J.S., Fearn C., Wang Y., Huang S., Han J. (2000), "Involvement of the MKK6-p38gamma Cascade in Gamma Radiation-Induced Cell Cycle Arrest", *Molecular and Cellular Biology*, **20(13)**:4543-4552
- Wang Y., Cortez D., Yazdi P., Neff N., Elledge S.J., Qin J. (2000), "BASC, A Super Complex of BRCA1-Associated Proteins Involved in the Recognition and Repair of Aberrant DNA Structures", *Genes and Development*, **14(8)**:927-939
- Warbrick E. (1998) "PCNA Binding Through a Conserved Motif", *Bioessays*, **20(3)**:195-199
- Warbrick E. (2000), "The Puzzle of PCNA's Many Partners", *Bioessays*, **22(11)**:997-1006
- Warbrick E. (2006), "A Functional Analysis of PCNA-Binding Peptides Derived from Protein Sequence, Interaction Screening and Rational Design", *Oncogene*, **25(20)**:2850-2859
- Ward I.M. and Chen J. (2001), "Histone H2AX is Phosphorylated in an ATR-Dependent Manner in Response to Replicational Stress", *Journal of Biological Chemistry*, **276(51)**:47759-47762
- Ward J.J., McGuffin L.J., Bryson K., Buxton B.F., Jones D.T. (2004), "The DISOPRED Server for the Prediction of Protein Disorder", *Bioinformatics*, **20(13)**:2138-2139
- Warmerdam O., Kanaar R., Smits V.A. (2010), "Differential Dynamics of ATR-Mediated Checkpoint Regulators", *Journal of Nucleic Acids*, **pii**:319142-319158
- Warnick C.T., Dabbas B., Ford C.D., Strait K.A. (2001), "Identification of a p53 Response Element in the Promoter Region of the hMSH2 Gene Required for Expression in A2780 Ovarian Cancer Cells", *Journal of Biological Chemistry*, **276(29)**:27363-27370
- Wassmann K., Liberal V., Benezra R. (2003), "Mad2 Phosphorylation Regulates its Association with Mad1 and the APC/C", *The EMBO Journal*, **22(4)**:797-806

- Watson A.T., Garcia V., Bone N., Carr A.M., Armstrong J. (2008), "Gene Tagging and Replacement Using Recombinase-Mediated Cassette Exchange in *Schizosaccharomyces pombe*", *Gene*, **407(1-2)**:63-74
- Weber J.D., Taylor L.J., Roussel M.F., Sherr C.J., Bar-Sagi D. (1999), "Nucleolar Arf Sequesters Mdm2 and Activates p53", *Nature Cell Biology*, **1(1)**:20-26
- Wegele H., Müller L., Buchner J. (2004), "Hsp70 and Hsp90: A Replay Team for Protein Folding", *Reviews of Physiology, Pharmacology and Biochemistry*, **151**:1-44
- Wegele H. Wandlinger S.K., Schmid A.B., Reinstein J., Buchner J. (2006), "Substrate Transfer from the Chaperone Hsp70 to Hsp90", *Journal of Molecular Biology*, **356(3)**:802-811
- Wei N. and Deng X.W. (2003), "The COP9 Signalosome", *Annual Review of Cell and Developmental Biology*, **19**:261-286
- Wei N., Serino G., Deng X.W. (2008), "The COP9 Signalosome: More Than a Protease", *Trends in Biochemical Sciences*, **33(12)**:592-600
- Wei N., Tsuge T., Serino G., Dohmae N., Takio K., Matsui M., Deng X.W. (1998), "The COP9 Complex is Conserved Between Plants and Mammals and is Related to the 26S Proteasome Regulatory Complex", *Current Biology*, **8(16)**:919-922
- Wiebauer K. and Jiricny J. (1990), "Mismatch-Specific Thymine DNA Glycosylase and DNA Polymerase Beta Mediate the Correction of G.T Mispairs in Nuclear Extracts from Human Cells", *Proceedings of the National Academy of Sciences U.S.A.*, **87(15)**:5842-5845
- Wiese C., Collins D.W., Albala J.S., Thompson L.H., Kronenberg A., Schild D. (2002), "Interactions Involving the Rad51 Paralogs Rad51C and XRCC3 in Human Cells", *Nucleic Acids Research*, **30(4)**:1001-1008
- Wies E., Schoen H., Victor A., Spix C., Ludwig M., Schneider-Raetzke B., Kohlschmidt N., Bartsch O., Gerhold-Ay A., Boehm N., Grus F., Haaf T., Galetzka D. (2011), "Reduced mRNA and Protein Expression of the Genomic Caretaker RAD9A in Primary Fibroblasts of Individuals with Childhood and Independent Second Cancer", *PLoS One*, **6(10)**:e25750
- Weinberg R.A. (2006), "The Biology of Cancer", 1st Edition, Garland Science
- Wilczynski J., Duechler M., Czyz M. (2011), "Targeting NF- κ B and HIF1 Pathways for the Treatment of Cancer: Part II", *Archivum Immunologicae et Therapine Experimentalis (warsz)*, **59(4)**:301-307
- Williams R.M., Obradovic Z., Mathura V., Braun W., Garner E.C., Young J., Takayama S., Brown C.J., Dunker A.K. (2001), "The Protein Non-Folding Problem: Amino Acid Determinants of Intrinsic Order and Disorder", *Proceedings of the Pacific Symposium on Biocomputing: Januray 2001, Hawaii*, **3-7**:89-100
- Williamson E.A., Rasila K.K., Corwin L.K., Wray J., Beck B.D., Severns V., Mobarak C., Lee S.H., Nickoloff J.A., Hromas R. (2008), "The SET and Transposase Domain Protein Metnase Enhances Chromosomal Decatenation: Regulation by Automethylation", *Nucleic Acids Research*, **36(18)**:5822-5831
- Whitesell L. and Lindquist S.L. (2005), "HSP90 and the Chaperoning of Cancer", *Nature Reviews Cancer*, **5(10)**:761-772

- Wilson D.M. 3rd and Barsky D. (2001), “The Major Human Abasic Endonuclease: Formation, Consequences and Repair of Abasic Lesions in DNA”, *Mutation Research*, **485(4)**:283-307
- Wolffe A.P. and Hayes J.J. (1999), “Chromatin Disruption and Modification”, *Nucleic Acids Research*, **27(3)**:711-720
- Wolf E., Kim P.S., Berger B. (1997), “MultiCoil: A Program for Predicting Two- and Three-Stranded Coils”, *Protein Science*, **6(6)**:1179-1189
- Wong C.I., Zhou Z.X., Sar F., Wilson E.M. (1993), “Steroid Requirement for Androgen Receptor Dimerization and DNA Binding: Modulation by Intramolecular Interactions Between the NH₂-Terminal and Steroid-Binding Domains”, *Journal of Biological Chemistry*, **268(25)**:19004-19012
- Wood V. and Bähler J. (2002), “Website Review: How to Get the Best from Fission Yeast Genome Data”, *Computational and Functional Genomics*, **3(3)**:282-288
- Wood V., Gwilliam R., Rajadream M.A., Lyne M., Lyne R., Stewart A., Sgouros J., Peat N., Hayles J., Baker S., Basham D., Bowman S., Brooks K., Brown D., Brown S., Chillingworth T., Churcher C., Collins M., Connor R., Cronin A., Davis P., Feltwell T., Fraser A., Gentles S., Goble A., Hamlin N., Harris D., Hidalgo J., Hodgson G., Holroyd S., Hornsby T., Howarth S., Huckle E.J., Hunt S., Jagles K., James K., Jones L., Jones M., Leather S., McDonald S., McLean J., Mooney P., Moule S., Mungall K., Murphy L., Niblett D., Odell C., Oliver K., O’Neil S., Pearson D., Quail M.A., Rabbinowitsch E., Rutherford K., Rutter S., Saunders C., Seeger K., Sharp S., Skelton J., Simmonds M., Squares R., Squares S., Stevens K., Taylor K., Taylor R.G., Tivey A., Walsh S., Warren T., Whitehead S., Woodward J., Volckaert G., Aert R., Robben J., Grymonprez B., Weltjens I., Vanstreels E., Rieger M., Schäfer M., Müller-Auer S., Gabel C., Fuchs M., Dusterhoft A., Fritz C., Holzer E., Moestl D., Hilbert H., Borzym K., Langer I., Beck A., Lehrach H., Reinhardt R., Pohl T.M., Eger P., Zimmermann W., Wedler H., Wambutt R., Purnelle B., Goffeau A., Cadieu E., Dréano S., Gloux S., Lelaure V., Mottier S., Galibert F., Aves S.J., Xiang Z., Hunt C., Moore K., Hurst S.M., Lucas M., Rochet M., Gaillardin C., Tallada V.A., Garzon A., Thode G., Daga R.R., Cruzado L., Jimenez J., Sánchez M., del Ray I., Benito J., Dominguez A., Revuelta J.L., Moreno S., Armstrong J., Forsburg S.L., Cerutti L., Lowe T., McCombie W.R., Paulsen I., Potashkin J., Shpakovski G.V., Ussery D., Barrell B.G., Nurse P. (2002), “The Genome Sequence of *Schizosaccharomyces pombe*”, *Nature*, **415(6874)**:871-880
- Wootton J.C. and Federhen S. (1993), “Statistics of Local Complexity in Amino Acid Sequences and Sequence Databases”, *Computational Chemistry*, **17**:149-163
- Workman P. (2002), “Pharmacogenomics in Cancer Drug Discovery and Development: Inhibitors of the Hsp90 Molecular Chaperone”, *Cancer Detection and Prevention*, **26(6)**:405-410
- Workman P. (2003a), “Overview: Translating Hsp90 Biology into Hsp90 Drugs”, *Current Cancer Drug Targets*, **3(5)**:297-300
- Workman P. (2003b), “The Opportunities and Challenges of Personalized Genome-Based Molecular Therapies for Cancer: Targets, Technologies and Molecular Chaperones”, *Cancer Chemotherapy and Pharmacology*, **52 (Supplement 1)**:S45-S56
- Workman P. (2004) “Drug Discovery Strategies: Technologies to Accelerate Transition from Target to Drug”, *Journal of Chemotherapy*, **(Supplement 4)**:13-15
- Workman P. (2005), “New Cancer Drugs on the Horizon”, *Future Oncology*, **1(3)**:315-318
- Workman P., Clarke P.A., Raynaud F.I., van Montford R.C. (2010), “Drugging the PI3 Kinome: From Chemical Tools to Drugs in the Clinic”, *Cancer Research*, **70(6)**:2146-2157

- Wrabl J.O., Gu J., Liu T., Schrank T.P., Whitten S.T., Hilser V.J. (2011), "The Role of Protein Conformational Fluctuations in Allostery, Function and Evolution", *Biophysical Chemistry*, **159(1)**:129-141
- Wray J., Williamson E.A., Chester S., Farrington J., Sterk R., Weinstock D.M., Jasin M., Lee S.H., Nickoloff J.A., Hromas R. (2010), "The Transposase Domain Protein Metnase/SETMAR Suppresses Chromosomal Translocations", *Cancer Genetics and Cytogenetics*, **200(2)**:184-190
- Wray J., Williamson E.E., Royce M., Shaheen M., Beck B.D., Lee S.H., Nickoloff J.A., Hromas R. (2009a), "Metnase Resistance to Topoisomerase II Inhibitors in Breast Cancer Cells", *PLoS One*, **4(4)**:e5323
- Wray J., Williamson E.A., Sheema S., Lee S.H., Libby E., Willman C.L., Nickoloff J.A., Hromas R. (2009b), "Metnase Mediates Chromosome Decatenation in Acute Leukaemia Cells", *Blood*, **114(9)**:1852-1858
- Wu X., Shell S.M., Zou Y. (2005), "Interaction and Co-Localization of Rad9/Rad1/Hus1 Checkpoint Complex with Replication Protein A in Human Cells", *Oncogene*, **24(29)**:4728-4735
- Wu X., Wilson T.E., Lieber M.R. (1999), "A Role for FEN-1 in Non-Homologous DNA End Joining: The Order of Strand Annealing and Nucleolytic Processing Events", *Proceedings of the National Academy of Sciences U.S.A.*, **96(4)**:1303-1308
- Wurth L. (2012), "Versatility of RNA-Binding Proteins in Cancer", *Computational and Functional Genomics*, **epub ahead of print**
- Xiang S-L., Kumano T., Iwasaki S.I., Sun X., Yoshioka K., Yamamoto K.C. (2001), "The J-Domain of Tpr2 Regulates its Interaction with the Proapoptotic and Cell Cycle Checkpoint Protein, Rad9", *Biochemical and Biophysical Research Communications*, **287(4)**:932-940
- Xie H., Vucetic S., Iakoucheva L.M., Oldfield C.J., Dunker A.K., Uversky V.N., Obradovic Z. (2007a), "Functional Anthology of Intrinsic Disorder: 1. Biological Processes and Functions of Proteins with Long Disordered Regions", *Journal of Proteome Research*, **6(5)**:1882-1898
- Xie H., Vucetic S., Iakoucheva L.M., Oldfield C.J., Dunker A.K., Obradovic Z., Uversky V.N. (2007b), "Functional Anthology of Intrinsic Disorder: 3. Ligands, Post-Translational Modifications and Diseases Associated with Intrinsically Disordered Proteins", *Journal of Proteome Research*, **6(5)**:1917-1932
- Xu M., Bai L., Gong Y., Xie W., Hang H., Jiang T. (2009), "Structure and Functional Implications of the Human Rad9-Hus1-Rad1 Cell Cycle Checkpoint Complex", *Journal of Biological Chemistry*, **284(31)**:20457-20461
- Xu X., Vaithiyalingam S., Glick G.G., Mordes D.A., Chazin J., Cortez D. (2008), "The Basic Cleft of RPA70N Binds Multiple Checkpoint Proteins Including Rad9 to Regulate ATR Signalling", *Molecular and Cellular Biology*, **28(24)**:7345-7353
- Yagita K., Yamanaka I., Koinuma S., Shigeyoshi Y., Uchiyama Y. (2009), "Mini Screening of Kinase Inhibitors Affecting Period-Length of Mammalian Cellular Circadian Clock", *Acta Histochemica et Cytochemica*, **42(3)**:89-93
- Yamaguchi S., Decottignies A., Nurse P. (2003), "Function of Cdc2p-Dependent Bub1p Phosphorylation and Bub1p Kinase Activity in the Mitotic and Meiotic Spindle Checkpoint", *The EMBO Journal*, **22(5)**:1075-1087

- Yamasaki H., Omori Y., Zaidan-Daigli M.L., Mironov N., Mesnil M., Krutovskikh V. (1999), "Genetic and Epigenetic Changes of Intracellular Communication Genes During Multi-Stage Carcinogenesis", *Cancer Detection and Prevention*, **23(4)**:273-279
- Yan Y. and Michael W.M. (2009a), "TopBP1 and DNA Polymerase-Alpha Directly Recruit the 9-1-1 Complex to Stalled Replication Forks", *Journal of Cell Biology*, **184(6)**:793-804
- Yan Y. and Michael W.M. (2009b), "TopBP1 and DNA Polymerase Alpha-Mediated Recruitment of the 9-1-1 Complex to Stalled Replication Forks: Implications for a Replication Restart-Based Mechanism for ATR Checkpoint Activation", *Cell Cycle*, **8(18)**:2877-2884
- Yang D.Y., Chang T.C., Shen S.Y. (2007), "Interaction between Human Telomerase and a Carbazole Derivative: A Molecular Dynamics Simulation of a G-Quadruplex Stabilizer and Telomerase Inhibitor", *Journal of Physical Chemistry A*, **111(38)**:9224-9232
- Yang X., Wood P.A., Hrushesky W.J. (2010), "Mammalian TIMELESS is Required for ATM-dependent CHK2 Activation and G2/M Checkpoint Control", *Journal of Biological Chemistry*, **285(5)**:3030-3034
- Yao N.Y., Hurwitz J., O'Donnell M. (2000), "Dynamics of β and Proliferating Cell Nuclear Antigen Sliding Clamps in Traversing DNA Secondary Structure", *Journal of Biological Chemistry*, **275(2)**:1421-1432
- Yao N.Y. and O'Donnell M. (2008), "Replisome Dynamics and Use of DNA Trombone Loops to By-Pass Replication Blocks", *Molecular Biosystems*, **4(11)**:1075-1084
- Yap T.A., Sandhu S.K., Workman P., de Bono J.S. (2010), "Envisioning the Future of Early Anti-Cancer Drug Development", *Nature Reviews Cancer*, **10(7)**:514-523
- Yarmola E.G., Zarudnaya M.I., Lazurkin YuS (1985), "Osmotic Pressure of DNA Solutions and Effective Diameter of the Double Helix", *Journal of Biomolecular Structural Dynamics*, **2(5)**:981-993
- Yasuhira S. (2009), "Redundant Roles of Srs2 Helicase and Replication Checkpoint in Survival and rDNA Maintenance in *Schizosaccharomyces pombe*", *Molecular Genetics and Genomics*, **281(5)**:497-509
- Yee A.S., Paulson E.K., McDevitt M.A., Rieger-Christ K., Summerhayes I., Berasi S.P., Kim J., Huang C.Y., Zhang X. (2004), "The HBP1 Transcriptional Repressor and the p38 MAP Kinase: Unlikely Partners in G1 Regulation and Tumor Suppression", *Gene*, **336(1)**:1-13
- Yeh S. and Chang C. (1996), "Cloning and Characterisation of a Specific Coactivator ARA70, for the Androgen Receptor in Human Prostate Cells", *Proceedings of the National Academy of Sciences U.S.A.*, **93(11)**:5517-5521
- Yi F., Doudevski I., Regan L. (2010), "HOP is a Monomer: Investigation of the Oligomeric State of the Co-Chaperone HOP", *Protein Science*, **19(1)**:19-25
- Yin H. and Hamilton A.D. (2005), "Strategies for Targeting Protein-Protein Interactions with Synthetic Agents", *Angewandte Chemie International Edition*, **44(27)**:4130-4163
- Yin L., Locovei A.M., D'Urso G. (2008), "Activation of DNA Damage Checkpoint in Mutants Defective in DNA Replication Initiation", *Molecular Biology of the Cell*, **19(10)**:4374-4382

- Yin Y., Zhu A., Jin Y.J., Liu Y-X., Zhang X., Hopkins K.M., Lieberman H.B. (2004), "Human RAD9 Checkpoint Control/Proapoptotic Protein Can Activate Transcription of p21", *Proceedings of the National Academy of Sciences U.S.A.*, **101(24)**:8864-8869
- Yokota M., Ikeda H., Kawamoto K., Ito T., Ogasahara K. (2010), "A Case of Irinotecan-Induced Interstitial Pneumonia During Treatment of Recurrent Colon Cancer", *Gan To Kagaku Ryoho (Cancer and Chemotherapy)*, **37(8)**:1611-1614
- Yoshida K., Komatsu K., Wang H-G., Kufe D. (2002), "c-Abl Tyrosine Kinase Regulates the Human Rad9 Checkpoint Protein in Response to DNA Damage", *Molecular and Cellular Biology*, **22(10)**:3292-3300
- Yoshida K., Wang H-G., Miki Y., Kufe D. (2003), "Protein Kinase C δ is Responsible for Constitutive and DNA Damage-Induced Phosphorylation of Rad9", *The EMBO Journal*, **22(6)**:1431-1441
- Yoshizawa-Sugata N. and Masai H. (2007), "Human Tim/Timeless Interacting Protein, Tipin, is Required for Progression of S Phase and DNA Replication Checkpoint", *Journal of Biological Chemistry*, **282(4)**:2729-2740
- You Z., Kong L., Newport J. (2002), "The Role of Single-Stranded DNA and Polymerase Alpha in Establishing the ATR, Hus1 DNA Replication Checkpoint", *Journal of Biological Chemistry*, **277(30)**:27088-27093
- Young J.C., Obermann W.M.J., Hartl F.U. (1998), "Specific Binding of Tetratricopeptide Repeat Protein to the C-Terminal 12kDa Domain of Hsp90", *Journal of Biological Chemistry*, **273(29)**:18007-18010
- Yu A.M. and McVey M. (2010), "Synthesis-Dependent Microhomology-Mediated End-Joining Accounts for Multiple Types of Repair Junctions", *Nucleic Acids Research*, **38(17)**:5706-5717
- Yudkovsky Y., Shteinberg M., Listovsky T., Brandeis M., Hershko A. (2000), "Phosphorylation of Cdc20/Fizzy Negatively the Mammalian Cyclosome/APC in the Mitotic Checkpoint", *Biochemical and Biophysical Research Communications*, **271(2)**:299-304
- Yue M., Singh A., Wang Z., Xu X.J. (2011), "The Phosphorylation Network for Efficient Activation of DNA Replication Checkpoint in Fission Yeast", *Journal of Biological Chemistry*, **286(26)**:22864-22874
- Yuki T., Maniwa Y., Doi T., Okada K., Nishio W., Hayashi Y., Okita Y. (2008), "DNA Damage Sensor Protein hRad9: A Novel Molecular Target for Lung Cancer Treatment", *Oncology Reports*, **20(5)**:1047-1052
- Yu L.P., Lou Y.R., Peng Q-Y., Nghiem P., Conney A.H. (2011), "Caffeine Decreases Phospho-Chk1 (Ser 317) and Increases Mitotic Cells with Cyclin B1 and Caspase 3 in Tumours from UVB-Treated Mice", *Cancer Prevention Research (Phila.)*, **4(7)**:1118-1125
- Zagar T.M., Higgins K.A., Miles E.F., Vujaskovic Z., Dewhirst M.W., Clough R.W., Prosnitz L.R., Jones E.L. (2010), "Durable Palliation of Breast Cancer Chest Wall Recurrence with Radiation Therapy, Hyperthermia and Chemotherapy", *Radiotherapy and Oncology*, **97(3)**:535-540
- Zakrzewska K., Lavery R., Pullman A., Pullman B. (1980), "The Electrostatic Potential and Steric Accessibility of Reactive Sites Within Z-DNA", *Nucleic Acids Research*, **8(17)**:3917-3932

Zambelli B., Musiani F., Ciurli S. (2012), "Metal Ion-Mediated DNA-Protein Interactions", *Metal Ions in Life Sciences*, **10**:135-170

Zawacka-Pankau J., Krachulec J., Grulkowski I., Bielawski K.P., Selivanova G. (2008), "The p53-Mediated Cytotoxicity of Photodynamic Therapy of Cancer: Recent Advances", *Toxicology and Applied Pharmacology*, **232(3)**:487-497

Zeng C.W., Zhang X.J., Lin K.Y., Ye H., Feng S.Y., Zhang H., Chen Y.Q. (2012), "Camptothecin Induces Apoptosis in Cancer Cells via miR-125b Mediated Mitochondrial Pathways", *Molecular Pharmacology*, **Electronic Publication Ahead of Print**

Zhan Q., Antinore M.J., Wang X.W., Carrier F., Smith M.L., Harris C.C., Fornace A.J. Jr. (1999), "Association with Cdc2 and Inhibition of Cdc2/Cyclin B1 Kinase Activity by the p53-Regulated Protein GADD45", *Oncogene*, **18(18)**:2892-2900

Zhang C., Zhang C.X., He Y., Hang H. (2008), "Phosphorylation Sites on Tyr28 and the C-Terminus of Rad9 are Required for Inhibition of Premature Chromosomal Condensation Across the Entire S Phase", *Cellular Physiology and Biochemistry*, **22(1-4)**:295-306

Zhang H., Zhang T., Chen K., Shen S., Ruan J., Kurgan L. (2009), "On the Relation Between Residue Flexibility and Local Solvent Accessibility in Proteins", *Proteins*, **76(3)**:617-636

Zhang L., Tie Y., Tian C., Zing G., Song Y., Zhu Y., Sun Z., He F. (2006), "CKIP-1 Recruits Nuclear ATM Partially to the Plasma Membrane Through Interaction with ATM", *Cellular Signalling*, **18(9)**:1386-1395

Zhang Y. and Calderwood S.K. (2011), "Autophagy, Protein Aggregation and Hyperthermia: A Mini-Review", *International Journal of Hyperthermia*, **27(5)**:409-414

Zhao H. and Piwnicka-Worms H. (2001), "ATR-Mediated Checkpoint Pathways Regulate Phosphorylation and Activation of Human Chk1", *Molecular and Cellular Biology*, **21(13)**:4129-4139

Zhao H., Rybak P., Dobrucki J., Traganos F., Darzynkiewicz Z. (2012), "Relationship of DNA Damage Signaling to DNA Replication Following Treatment with DNA Topoisomerase Inhibitors Camptothecin/Topotecan, Mitoxantrone or Etoposide", *Cytometry Part A: The Journal of the International Society for Analytical Cytology*, **81(1)**:45-51

Zhao H., Tanaka K., Nogochi E., Nogochi C., Russell P. (2003), "Replication Checkpoint Protein Mrc1 is Regulated by Rad3 and Tel1 in Fission Yeast", *Molecular and Cellular Biology*, **23(22)**:8395-8403

Zhao S., Weng Y.C., Yuan S.S., Lin Y.T., Hsu H.C., Lin S.C., Gerbino E., Song M.H., Zdzienicka M.Z., Gatti R.A., Shay J.W., Ziv Y., Shiloh Y., Lee E.Y. (2000), "Functional Link Between Ataxia Telangiectasia and Nijmegen Breakage Syndrome Gene Products", *Nature*, **405(6785)**:473-477

Zheng L., Jia J., Finger D., Guo Z., Zer C., Shen B. (2010), "Functional Regulation of FEN1 Nuclease and Its Link to Cancer", *Nucleic Acids Research*, **39(3)**:781-794

Zheng Q.Z., Zheng X.M., Xu Y., Cheng K., Jiao Q.C., Zhu H.L. (2010), "Synthesis, Biological Evaluation and Molecular Docking Studies of 2-Chloropyridine Derivatives Possessing 1,3,4-Oxadiazole Moiety as Potential Anti-Tumour Agents", *Bioorganic and Medicinal Chemistry*, **18(22)**:7836-7841

Zheng R., Shi Y., Jia Z., Zhao C., Zhang Q., Tan X. (2010), “Fast Repair of DNA Radicals”, *Chemical Society Reviews*, **39(8)**:2827-2834

Zhou B.B., Chaturvedi P., Spring K., Scott S.P., Johanson R.A., Mishra R., Mattern M.R., Winkler J.D., Khanna K.K. (2000), “Caffeine Abolishes the Mammalian G(2)/M DNA Damage Checkpoint by Inhibiting Ataxia-Telangiectasia-Mutated Kinase Activity”, *Journal of Biological Chemistry*, **275(14)**:10342-10348

Zhou B.B. and Elledge S.J. (2000), “The DNA Damage Response: Putting Checkpoints in Perspective”, *Nature*, **408(6811)**:433-439

Zhou C., Seibet V., Geyer R., Rhee E., Lyapina S., Cope G., Deshaies R.J., Wolf D.A. (2001), “The Fission Yeast COP9/Signalosome is Involved in Cullin Modification by Ubiquitin-Related Ned8p”, *BMC Biochemistry*, **2**:7

Zhou L. and Watts F.Z. (2005), “Nep1: A *Schizosaccharomyces pombe* Deneddylation Enzyme”, *The Biochemical Journal*, **389(Pt.2)**:307-314

Zhuang Z. and Ai Y. (2010), “Processivity Factor of DNA Polymerase and its Expanding Role in Normal and Translesion DNA Synthesis”, *Biochimica et Biophysica Acta*, **1804(5)**:1081-1093

Zhu A., Zhang C.X., Lieberman H.B. (2008), “Rad9 has a Functional Role in Human Prostate Carcinogenesis”, *Cancer Research*, **68(5)**:1267-1274

Zou L. and Elledge S.J. (2003), “Sensing DNA Damage Through ATRIP Recognition of RPA-ssDNA Complexes”, *Science*, **300(5625)**:1542-1548

Zou L., Liu D., Elledge S.J. (2003), “Replication A-Mediated Recruitment and Activation of Rad17 Complexes”, *Proceedings of the National Academy of Sciences U.S.A.*, **100(24)**:13827-13832

Zou Y., Liu Y., Wu X., Shell S.M. (2006), “Functions of Human Replication Protein A (RPA): From DNA Replication to DNA Damage and Stress Responses”, *Journal of Cellular Physiology*, **208(2)**:267-273

Zu T., Gibbens B., Doty N.S., Gomes-Pereira M., Huguet A., Stone M.D., Mragolis J., Peterson M., Markowski T.W., Ingram A., Nan Z., Forster C., Low W.C., Schoser B., Somia N.V., Schmechel S., Bitterman P.B., Gourdon G., Swanson M.S., Moseley M., Ranum L.P. (2011), “Non-ATG-Initiated Translation Directed by Microsatellite Expansions”, *Proceedings of the National Academy of Sciences U.S.A.*, **108(1)**:260-265

REFERENCES – Utilised Internet Website Resources

Bioinformatics Server Sites and Tools

- BETASCAN Server Site – <http://groups.csail.mit.edu/cb/betascan/betascan.html>
- cNLS Mapper Server Site – http://nls-mapper.ieb.keio.ac.jp/cgi-bin/NLS_Mapper_form.cgi
- COBALT – http://www.ncbi.nlm.nih.gov/tools/cobalt/cobalt.cgi?/link_loc=BlastHomeAd
- COILS (Coiled-Coil Predictor) – http://www.ch.embnet.org/software/COILS_form.html
- DisCon Server – <http://biomine.ece.ualberta.ca/DisCon/>
- DisEMBL 1.5 Server – <http://dis.emble.de/>
- DISOPRED – <http://bioinf.cs.ucl.ac.uk/disopred>
- DISpro – <http://www.ics.uci.edu/~baldig/dispro.html>
- DISProt (Data Base of Protein Disorder) – <http://www.disprot.org/>
- EBI Bioinformatics Tools Server – <http://www.ebi.ac.uk/Tools>
- ELM (Protein Eukaryotic Linear Motif Database) Server – <http://elm.eu.org/>
- EMBL Bioinformatic Tools Server – <http://embl.org/>
- EMBOSS Pairwise Alignment Tool Server – <http://artedi.ebc.uu.se/programs/pairwise.html>
- ExpASy Proteomics Server – <http://www.expasy.org/>
- GlobProt 2.3 Server – <http://globprot.embl.de/>
- IUPred Server – <http://www.iupred.enzym.hu/>
- Jemboss Alignment Editor – <http://emboss.sourceforge.net/Jemboss/jae.html>
- Kyte-Doolittle Hydrophathy Plot Server – <http://gcat.davidson.edu/rakarnik/kyte-doolittle.htm>
- MARCOIL (Coiled-coil Predictor) – <http://toolkit.tuebingen.mpg.de.marcoil>
- metaPrDOS – <http://prdoc.hgc.jp/cgi-bin/meta/top.cgi>
- MultiCoil (Coiled-Coil Predictor) – <http://groups.csail.mit.edu/cub/multicoil/cgi-bin/multicoil.cgi>
- MultiCoil2 Server – <http://groups.csail.mit.edu/cub/multicoil/cgi-bin/multicoil2.cgi>
- Netphos 2.0 and 3.1b Server – <http://www.cbs.dtu.dk/services/Netphos>
- NetphosK Server – <http://www.cbs.dtu.dk/services/NetphosK>
- PHOBIUS (Transmembrane-Spanning Domain Predictor) Server – <http://phobius.sbc.su.se/>

Bioinformatics Server Sites and Tools (Continued)

PolyView3D (Protein Structural Visualisation Software) – <http://www.cchmc.org/polyview3d.html>

POODLE-S – <http://mbs.cbrc.jp/poodle/poodle-s.html>

PrDOS Server – <http://www.prdos.hgc.jp/cgi-bin/top.cgi>

PROFbval – <http://www.rostlab.org/services/profbval>

Protein Calculator 3.3 (Scripps Institute) Server – <http://www.scripps.edu/~cdputnam/putcalc.html>

Protein Secondary Structure Tools Main Server – http://molbiol.tools.ca_secondary_structure.htm

PSI-BLAST – <http://www.ebi.ac.uk/Tools/sss/psiblast>

PSIPRED – <http://www.bioinf.cs.ucl.ac.uk/psipred/>

REAL-SPINE3 – <http://www.sparks.informatics.iupui.edu/RealSPINE3.0/realspine3.0.html>

REPPER (Coiled-Coil Predictor) – <http://toolkit.tuebingen.mpg.de/repper>

SPLIT 4.0 (Transmembrane-Spanning Domain Predictor) Server – <http://split.pmfst.hr/split/4/>

TANGO (Prediction of Potential Aggregation Regions/Sequences in Proteins) – <http://tango.crg.es/>

TMPred Server – http://www.ch.embnet.org/software/TMPRED_form.html

TMRpres2D Server – <http://bioinformatics.biol.uoa.gr/TMRpres2D>

Vienna RNA Secondary Structure Folding Server – <http://rna.tbi.univie.ac.at/>

YASPIN (Protein Coil, Helix, Strand Motif Content) – <http://www.ibi.vu.nl/programs/yaspin/www>

ZYGGREGATOR Server – <http://www-vendruscolo.ch.cam.ac.uk/zyggregator.php>

Gene/Protein Sequence and Expression Profile Information

GeneCards – <http://www.genecards.org>

GeneDB – <http://www.genedb.org/homepage>

Pombase – <http://old.genedb.org/genedb/pombe>

Pombe Gene Index – <http://www.genedb.org/genedb/pombe/index.jsp>

Pombe Gene Registry – <http://www.genedb.org/genedb/pombe/geneRegistry.jsp>

RCSB PDB (Protein Structure Data Bank) – <http://www.pdb.org/>

Schizosaccharomyces Group Data-Base

http://www.broadinstitute.org/annotation/genome/schizosaccharomyces_group/MultiHome.html

SRS (Sequence Retrieval Site) – <http://www.srs.ebi.ac.uk>

TPR Motif Sequence – <http://www.ncbi.nlm.nih.gov/structure/cdd/cddsrv.cgi?uid=194311>

Uniprot – <http://www.uniprot.org/>

Wellcome Trust Sanger Institute – <http://www.sanger.ac.uk/resources>

Instrumentation Information and Laboratory Service Suppliers

ÄKTATMFPLCTM System Manual – http://www.medmicro.wisc.edu/labs/mcfall-ngai/manuals/acktafplc_manual.pdf

Applied Biosystems Life Technologies Inc. – <http://www.appliedbiosystems.com>

Eurofins MWG Operon – <http://www.eurofinsdna.com>

Literature “Search Engine” Information Data-Bases

American Cancer Society – <http://www.cancer.org/>

International Agency for Research on Cancer (IARC) – <http://www.iarc.fr/>

ISI Web of Knowledge – <http://wok.mimas.ac.uk>

Nobel Prize Award Records – http://www.nobelprize.org/nobel_prizes_medicine/laureates/2001

PubCrawler – <http://pubcrawler.gen.tcd.ie/>

PubMed – <http://www.ncbi.nlm.nih.gov/pubmed>

SciFinder – <http://www.cas.org/SCIFINDER/SCHOLAR/index.html>

Scopus – <http://www.scopus.com/home.url>

Web of Science – http://thomsonreuters.com/products_services/science/science-products/a-z/web-of-science

World Health Organisation (WHO) – <http://www.who.int/en/>

Patents on Strategic Anti-Cancer Therapeutic Manipulation of Human Rad9

<http://www.freepatentsonline.com./7384761.html>

<http://www.freshpatents.com/-dt20100701ptan20100168202.php>

Base Sequence-Predictive Secondary RNA Structure Modelling

Nelson N. and Istrail S. (2012), “RNA Structure and Prediction”, Computational Molecular Biology (BIO502) Module Lecture Notes – <http://tuvalu.edu/~pth.ma.html>

S. pombe Information: Experimental Protocols, Plasmids and Strain Libraries

Bioneer Haploid and Diploid *S. pombe* Strain Libraries – <http://pombe.bioneer.co.kr>
[http://eng.bioneer.com/products/spombe_home.html]

Cold Spring Harbor Laboratory On-Line Protocols – <http://cshprotocols.cshlp.org>

EUROSCARF – <http://www.uni-frankfurt.de/fb15/mikro/euroscarf/>

Forsburg S. *S. pombe* Information Site – <http://www-rfc.edu/~forsberg/cclecture.html>

Nurse P. “Fission Yeast Handbook” – http://biosci.osu.edu/~nile/nurse_lab_manual.pdf

PombeWeb – <http://www-bcf.usc.edu/~forsberg/pombeweb.html>